K.H. OLSEN
(Editor)

PUBLICATION NO. 264 OF THE INTERNATIONAL LITHOSPHERE PROGRAM

CONTINENTAL RIFTS: EVOLUTION, STRUCTURE, TECTONICS

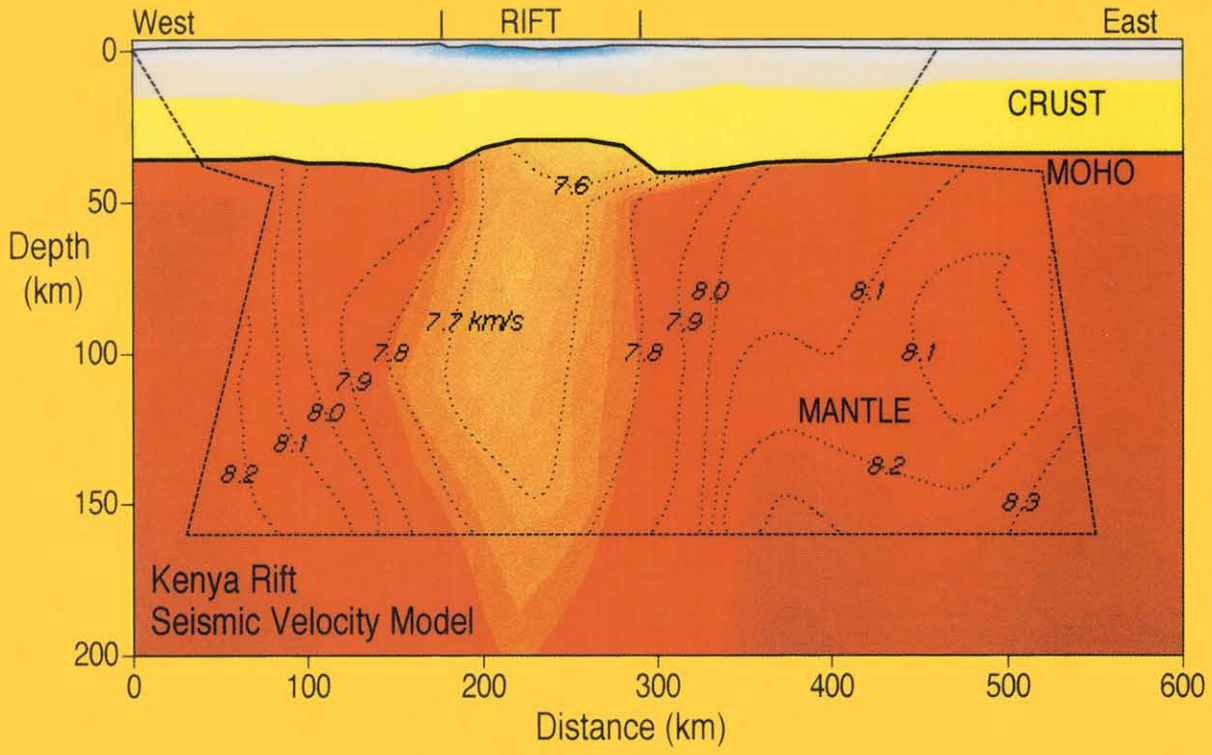

DEVELOPMENTS IN GEOTECTONICS 25

ELSEVIER

Developments in Geotectonics 25

CONTINENTAL RIFTS: EVOLUTION, STRUCTURE, TECTONICS

Edited by
K.H. OLSEN
GCS International
1029 187th Place, SW, Lynnwood, WA 98036, U.S.A.

Publication No. 264 of the International Lithosphere Program

1995
ELSEVIER
Amsterdam – Lausanne – New York – Oxford – Shannon –Tokyo

ELSEVIER SCIENCE B.V.
Sara Burgerhartstraat 25
P.O. Box 211, 1000 AE Amsterdam, The Netherlands

ISBN: 0 444 89566 3 (hardbound)
ISBN: 0 444 89567 1 (paperback)

This book is printed on acid-free paper.

Printed in The Netherlands.

Developments in Geotectonics 25

CONTINENTAL RIFTS: EVOLUTION, STRUCTURE, TECTONICS

FURTHER TITLES IN THIS SERIES

1. *J. Aubouin* - GEOSYNCLINES

2. *R.W. Van Bemmelen* - GEODYNAMIC MODELS

3. *A. Sugimura and S. Uyeda* - ISLAND ARCS

4. *A.R. Ritsema* (Editor) - THE UPPER MANTLE

5. *C. Lomnitz* - GLOBAL TECTONICS AND EARTHQUAKE RISK

6. *X. Le Pichon, J. Francheteau and J. Bonnin* - PLATE TECTONICS

7. *R.W. Girdler* (Editor) - EAST AFRICAN RIFTS

8. *S. Mueller* (Editor) - THE STRUCTURE OF THE EARTH'S CRUST

9. *N. Pavoni and R. Green* (Editors) - RECENT CRUSTAL MOVEMENTS

10. *S.W. Carey* - THE EXPANDING EARTH

11. *A.M. Johnson* - STYLES OF FOLDING

12. *M.H.P. Bott* (Editor) - SEDIMENTARY BASINS OF CONTINENTAL MARGINS AND CRATONS

13. *C.A. Whitten, R. Green and B.K. Meade* (Editors) - RECENT CRUSTAL MOVEMENTS, 1977

14. *M.N. Toksöz, S. Uyeda and J. Francheteau* (Editors) - OCEANIC RIDGES AND ARCS

15. *C.E. Keen* (Editor) - CRUSTAL PROPERTIES ACROSS PASSIVE MARGINS

16. *P. Vyskocil, R. Green and H. Mälzer* (Editors) - RECENT CRUSTAL MOVEMENTS, 1979

17. *J.H. Illies* (Editor) - MECHANISM OF GRABEN FORMATION

18. *E.V. Artyshkov* - GEODYNAMICS

19. *P. Morgan and B.H. Baker* (Editors) - PROCESSES OF CONTINENTAL RIFTING

20. *P. Vyskocil, A.M. Wassef and R. Green* (Editors) - RECENT CRUSTAL MOVEMENTS, 1982

21. *F.-C. Wezel* (Editor) - THE ORIGIN OF ARCS

22. *W. Manspeizer* (Editor) - TRIASSIC-JURASSIC RIFTING
Continental Breakup and the Origin of the Atlantic Ocean
and Passive Margins, Part A and Part B

23. *D.M. Fountain, R. Arculus and R.W. Kay* - CONTINENTAL LOWER CRUST

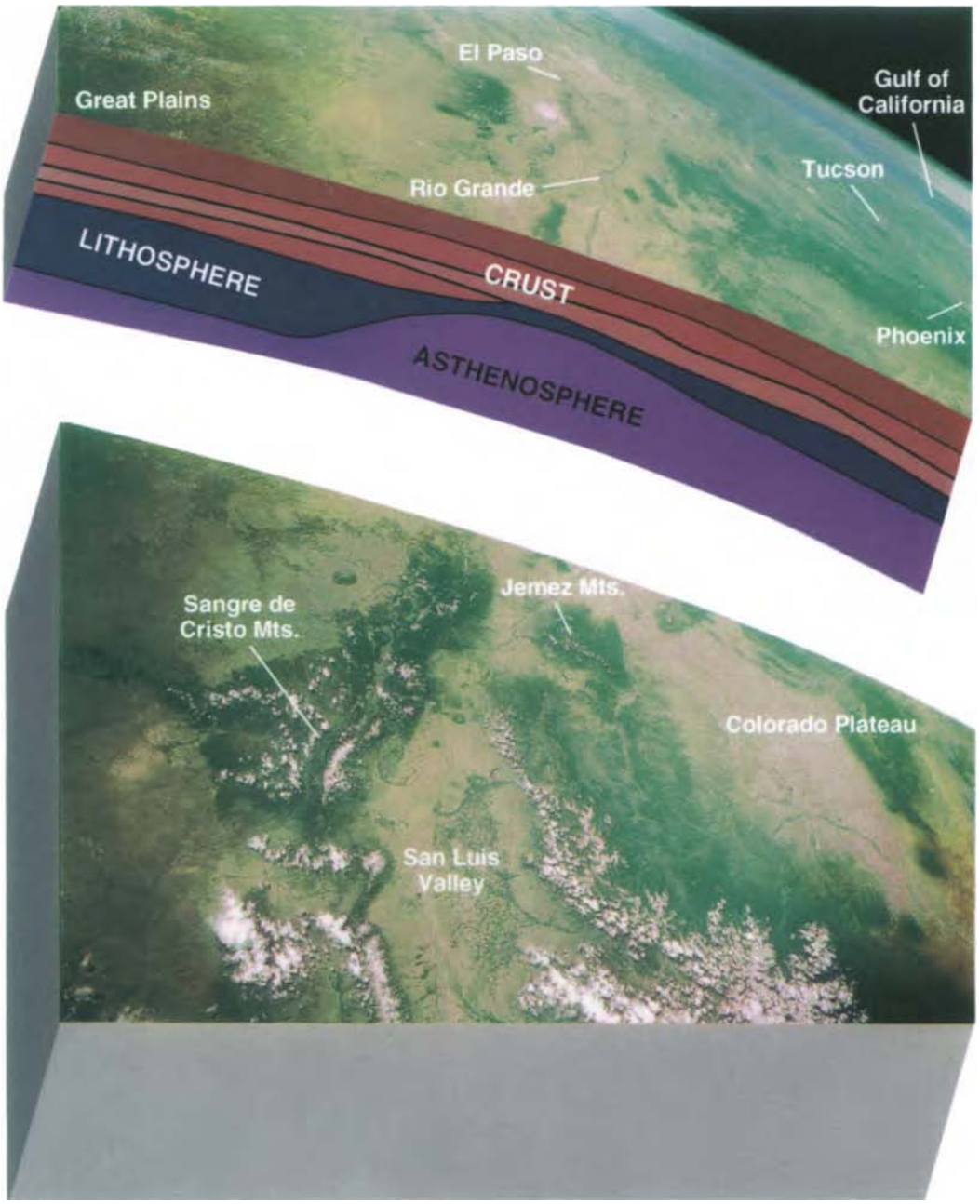

Frontispiece: This spectacular photograph shows a southward view of the Rio Grande rift from the southern San Luis Valley of Colorado to the bolsons of west Texas and Chihuahua (near top), a distance of over 700 km. The Sangre de Christo Mountains, part of the Southern Rocky Mountains, and the Great Plains lie east of the rift. The gypsum dunes of White Sands National Monument are prominent near the middle of the upper (southern) block. The Colorado Plateau lies west of the of the northern and central segments of the rift. Farther south and west, the Basin and Range Province stretches across southern New Mexico, southern Arizona and northern Mexico to the Gulf of California and Baja California, visible near the Earth's limb. The cross section showing crustal layers and upper mantle structure (see color Plate 6–9 of Chapter 6, "The Rio Grande Rift"), is constructed through Albuquerque, New Mexico. At this latitude (35°10'N), the vertical and horizontal scales are approximately the same. For conventional map views of the area see Figure 6–1 and Color Plate 7–1. This photograph is number STS40-151-23, taken with the Linhof camera from the Space Shuttle Columbia on 7 June 1991, at a nominal altitude of 287 km.

Preface

Continental rifting and associated processes of lithospheric extension have been among the most active research frontiers in the Earth sciences over the past four decades. These subjects cover a wide range of interconnected fundamental processes occurring in an important part of the Earth for mankind—the continental crust and lithosphere—and have captured the interest and attention of researchers from a wide spectrum of disciplines in the solid-earth sciences. These disciplines range from classical field geology through newly developed techniques and capabilities for seismological and electromagnetic probing of the Earth, to sophisticated and realistic dynamical modeling with high-speed supercomputers. For more than 30 years, working groups and study committees composed of international researchers focusing on the problems of the Earth's rift zones have been organized under the aegis of programs promoting international cooperative research in the geosciences, such as the International Upper Mantle Project, the Geodynamics Project, and the International Lithosphere Program.

Rifting and lithospheric extensional tectonics have been the subjects of vigorous research and discovery, and, as such, have been extensively discussed and debated at meetings and symposia, and in many books, technical monographs, and special issues of research journals documenting the rapid and continuing progress in these fields. So why publish yet another book on the subject? Despite the extensive literature, the authors of this book felt that a multidisciplinary overview of continental rifting with a principal focus on lithospheric-scale processes would be significantly useful for students and experienced researchers alike in assessing the current state of knowledge and in serving as a framework for future research.

This multi-authored book was prepared by a working group of geoscientists from Europe and North America who had been individually active in rift research problems since the late 1960s. Although some members of the group had long been in personal and professional contact regarding rift research problems, the authors strongly felt a need for more extended discussions with other colleagues from various rifts around the world and for detailed comparisons of data and interpretations beyond the exchange of research papers or brief individual discussions. In the early 1980s, the time was ripe to take a fresh look at research opportunities in many fields due to the development and increased availability of greatly improved geophysical instrumentation and analysis technology. (In the United States, these initiatives have now evolved into the IRIS-PASSCAL Consortium.) Also, about 1980, several of the authors began the process of planning and seeking funds for a major international research program to delineate in detail the deep lithospheric structure of the Kenya segment of the East African rift system—a system long considered to be the world's type continental rift. Ironically, the Kenya rift had almost no modern deep geophysical data available because the costs and logistics of modern research programs were beyond the resources of any single national research group. To plan a comprehensive multidisciplinary program for East Africa, it was necessary to review and reevaluate the results of recent deep crustal and lithospheric-scale research for a wide variety of other continental rift systems. Ultimately, the organization, funding, and field operations for the Kenya rift program (known as the Kenya Rift International Seismic Project, or KRISP) were successfully carried out with results currently being published. This book features a synthesis of key results of the ongoing KRISP program.

About 1984, an informal, "grass-roots" study group was initiated to compare individual research results and to explore in greater depth the apparent differences and similarities in the interpretations from various rift systems. The group became known as the CREST working group, an acronym of Continental Rifts: Evolution, Structure, and Tectonics, which not surprisingly became the title of this book. In organizing CREST, the group was faced with a

dilemma. On the one hand, it was extremely important to include as wide a representation of multidisciplinary expertise as possible, as well as first-hand researchers from a variety of major rift systems. Conversely, the number of participants had to be limited to maintain the continuity and efficiency of working members for several one-to-two-week-long workshops over the several years that would be necessary to complete planned objectives. The problem was that at least 50 to 100 active researchers who could be expected to make valuable contributions came to mind, but such numbers were counterbalanced by the sobering realization that the organizing, scheduling, and funding problems for such an extended-duration working group would be insurmountable. (The organizational complexity and "entropy" of any long-duration working group probably is proportional to something like exp(+n!), where n is the number of participants! We possibly should apologize to many of our colleagues who may have felt left out—but, on the other hand, they were spared a great deal of hard work!) Although perhaps appearing somewhat arbitrary, in the end the nucleus of the CREST group was created mainly from the principals involved in organizing the KRISP project. The survivors of this selection and the much longer-than-bargained-for CREST working and writing process are listed on following pages.

The main workshop activities of the group were accomplished during five intensive discussion and writing sessions held near Karlsruhe, Germany in 1987, 1989, and 1990 (hosted by the Institute for Petrology-Geochemistry and the Institute for Geophysics of Karlsruhe University) and at Los Alamos, New Mexico in 1987 and 1988 (hosted by the Los Alamos National Laboratory branch of the University of California's Institute of Geophysics and Planetary Physics [IGPP]). Each of the five major workshops lasted between one and two weeks and were convened in comparatively isolated surroundings without the usual daily academic and work distractions. The workshops began by formulating the general objectives and style of the book, identifying topics requiring special attention, and assembling the sub-teams of authors to be responsible for specific chapters. Workshops were a mixture of informal but vigorous discussion and debate, interspersed with periods devoted to planning, outlining, and preliminary drafting of several chapters. The various stages of draft chapters and proposals were circulated among all members for critical comments and suggestions. In a few instances, "guest" authors were invited to participate to achieve better balance and completeness. Although this book may focus more on review than on new research, all authors firmly agreed that the entire book should meet the standards of final external peer-review.

This book attempts to present an overview of the present state of understanding and knowledge of the processes of continental rifting from a multidisciplinary, lithospheric-scale perspective. The authors have tried to structure the chapters on each rift system in approximately the same synoptic sequence, so as to facilitate inter comparisons by the reader. The book should complement its many predecessors by attempting a more "unified" picture, with fewer possible omissions and imbalances than the usual somewhat 'random' collection of volunteered papers. In initial stages of planning for the book, an ideal list of rift systems and discussion topics were outlined almost double what survived. As with many long-term cooperative studies of this nature, the initial enthusiasm of the members surpassed abilities to devote as much time and effort to the project as might have been wished for when faced with other important responsibilities, commitments, and deadlines. Nevertheless, the authors feel the book succeeds in presenting the status of a representative majority of the continental rift systems that have been at the forefront of recent research. Although the entire effort took longer than anticipated, there were several "spin-off" technical papers along the way that resulted directly from the CREST collaboration. Because of external time constraints on various authors, individual chapters were completed over a period of more than one year. We recognize that in any complex, rapidly advancing subject such as this, one can never hope to be completely up-to-date, but we nevertheless hope that students and active researchers will find our efforts of value in advancing new efforts and understandings.

Although we may take some satisfaction that much of the time and effort spent by the authors of this book were driven primarily by deep personal

and professional interest, we could not have achieved the result without some financial support. Early discussions with, and a proposal to, the Division of Earth Sciences of the U.S. National Science Foundation (NSF) resulted in a modest grant from the Continental Geodynamics Program office mainly to help defray travel expenses for U.S. members. Dr. Leonard Johnson, NSF Program Director for Continental Geodynamics, also kindly arranged for the International Programs office of NSF to contact the NSF-equivalent funding agencies of several European countries to encourage financial support for European CREST members. Thus, it turned out for most members that their 'additional' participation in CREST activities was approved and partly financed by their respective national funding organizations as a component of already-funded research grants provided by the various national lithospheric studies programs. In special instances, occasional travel assistance was supplemented by a participant's university department. CREST members thus wish to gratefully acknowledge support from the following institutions and agencies: The German Research Society (Deutsche Forschungsgemeinschaft); The National Environmental Research Council, The Royal Society, the departments of geology of Durham University and Leicester University in the U.K.; The Norwegian Research Council for Science and the Humanities (Norsk Allmenvitenskapelig Forskningsrad) and University of Oslo in Norway; The Swiss National Science Foundation and the Swiss Federal Institute of Technology (ETH); The U.S. National Science Foundation and the Institute of Geophysics and Planetary Physics (IGPP)/Los Alamos Branch.

Because the CREST project was a somewhat unconventional experiment in international research collaboration, we sometimes wondered if it would ever be completed successfully. For their continuing and steadfast interest, encouragement, enthusiasm, and advice over the years, we are especially grateful to four friends and colleagues: Particularly for his efforts in helping launch the project, we thank Dr. L.E. Johnson, National Science Foundation, Division of Earth Sciences and Director of the Continental Geodynamics Program. Professor Karl Fuchs, Geophysical Institute, University of Karlsruhe, and President of the Inter–Union Commission on the Lithosphere (ICL) during 1985–1990, made many valuable suggestions as to how we could merge our objectives with those of the International Lithosphere Program (ILP). In the matter of coordination with ILP activities, we also acknowledge the help and advice of Dr. Peter Ziegler, Binningen, Switzerland, who was Chairman of Working Group 3 ("Intraplate Phenomena") of the Inter–Union Commission on the Lithosphere (ICL–WG–3), 1985–1990. Although the CREST project was an independent group and not a formal component of ILP, several CREST members also served as participants in ILP working groups. Last, but certainly not least, we would like to express our deep appreciation to Dr. Charles F. ("Chick") Keller of Los Alamos National Laboratory, Director of the Institute of Planetary Physics (IGPP) of the University of California, Los Alamos branch. Not only did he provide travel support for the Los Alamos members, and organizational and funding help for the meetings held at Los Alamos, but he has expressed continued encouragement and interest in seeing the CREST book come to fruition. May others be as fortunate in their 'choice' of an enlightened research grant administrator.

The editor would like to express his thanks to the authors for devoting so much time and care to this project. Although we all initially expected it would only take a "year or so," I wish to express my appreciation for the patience and perseverance shown by all. The editor would especially like to thank his friend and valued colleague, Dr. Scott Baldridge, not only for technical discussions, but also for sharing his enthusiasm and ideas for improving the organization and style of the book.

Kenneth H. Olsen
Lynnwood, Washington
July 1995

This Page Intentionally Left Blank

The CREST International Research Group

RAINER ALTHERR	*Mineralogisches-PetrographischesInstitut, Universität Heidelberg, Im Neuenheimer Feld 236, D-69120 Heidelberg, Germany*
W. SCOTT BALDRIDGE	*Geology/Geochemistry, EES-1, MS-D462, Los Alamos National Laboratory, Los Alamos, NM 87545, U.S.A.*
MARTIN H. P. BOTT	*Department of Geological Sciences, University of Durham, Science Laboratories, South Road, Durham, DH1 3LE, United Kingdom*
LAWRENCE W. BRAILE	*Department of Earth and Atmospheric Sciences, Purdue University, West Lafayette, IN 47907, U.S.A.*
VOLKER HAAK	*Geoforschungszentrum Potsdam, Telegrafenberg, Potsdam, D-14470, Germany*
WILLIAM J. HINZE	*Department of Earth and Atmospheric Sciences, Purdue University, West Lafayette, IN 47907, U.S.A.*
G. RANDY KELLER	*Department of Geological Sciences, University of Texas at El Paso, El Paso, TX 79968, U.S.A.*
M. AFTAB KHAN	*Department of Geology, University of Leicester, University Road, Leicester, LE1 7RH, United Kingdom.*
PAUL MORGAN	*Department of Geology, Northern Arizona University, P.O. Box 4099, Flagstaff, AZ 86011, U.S.A.*
STEPHAN MUELLER	*Institut für Geophysik, ETH - Hönggerberg, Zürich, CH-80903, Switzerland*
ELSE-RAGNHILD NEUMANN	*Mineralogical-Geological Museum, University of Oslo, Sarsgate 1, Oslo-5, N-0562, Norway*
KENNETH H. OLSEN	*GCS International, 1029 187th Place SW, Lynnwood, WA 98036* Formerly: *Geophysics, ESS-3, Los Alamos National Laboratory, Los Alamos, NM 87545, U.S.A.*
CLAUS PRODEHL	*Geophysikalisches Institut, Universität Karlsruhe, Hertzstrasse 16, Bau 42, D-76187, Karlsruhe, Germany*

GEORGE A. THOMPSON *Department of Geophysics, Stanford University, Stanford, CA 94305, U.S.A.*

RICHARD F. WENDLANDT *Department of Geology, Colorado School of Mines, Golden, CO 80401, U.S.A.*

List of Collaborating Authors

DAVID J. ALLEN	*Exxon Exploration Company, P.O. Box 4778, Houston, Texas 77210, USA*
DIANE I. DOSER	*Department of Geological Sciences, University of Texas at El Paso, El Paso, TX 79968, USA.*
GEORGE R. JIRACEK	*Department of Geological Sciences, San Diego State University, San Diego, California 92182 USA*
JOHN MARIANO	*Exxon Exploration Company, P.O. Box 4778, Houston, Texas 77210, USA*
TOM PARSONS	*United States Geological Survey, MS 999, 345 Middlefield Road, Menlo Park, California 94025, USA*
ERIC D. WENDLANDT	*Montgomery Watson, 365 Lennon Lane, Walnut Creet, California 94598, USA*

This Page Intentionally Left Blank

List of peer reviewers

We greatly appreciate the efforts of our colleagues below who made time in their busy schedules to provide thoughtful peer-reviews of the chapters of this book:

Dr. J. Ansorge	*ETH, Honggerberg, Switzerland*
Dr. R. E. Denison	*University of Texas at Dallas, USA*
Dr. A. B. Dickas	*University of Wisconsin at Superior, USA*
Dr. J. D. Fairhead	*University of Leeds, England*
Dr. J.-I. Faleide	*University of Oslo, Norway*
Dr. C. Froidevaux	*Ecole Normale Superieure, France*
Dr. J. C. Green	*University of Minnesota at Duluth, USA*
Dr. N. J. Kusznir	*University of Liverpool, England*
Dr. J. McCarthy	*United States Geological Survey, USA*
Dr. W. D. Mooney	*United States Geological Survey, USA*
Dr. A. Myhre	*University of Oslo, Norway*
Dr. A. Nyblade	*Pennsylvania State University, USA*
Dr. F.V. Perry	*Los Alamos National Laboratory, USA*
Dr. B. Sundvoll	*University of Oslo, Norway*
Dr. G. A. Thompson	*Stanford University, USA*
Dr. G. WoldeGabriel	*Los Alamos National Laboratory, USA*
Dr. P.E. Wannamaker	*University of Utah, USA*
Dr. H. Zeyen	*University of Karlsruhe, Germany*

Dr. P. Ziegler	*Binningen, Switzerland*
Dr. M. L. Zoback	*United States Geological Survey, USA*

Contents

This Page Intentionally Left Blank

Part I.

Introduction and Overview

This Page Intentionally Left Blank

Chapter 1

Introduction: Progress in understanding continental rifts

K.H. Olsen and P. Morgan

1.1. Terminology and classifications

1.1.1 Definition – What is a rift?

Early studies defined rifts as major elongate tectonic depressions bounded by normal faults, with no implication for the mode of development or for the mechanism of formation of these depressions (e.g., Gregory, 1896, 1921; see also Élie de Beaumont, 1827, 1830, 1844, 1847; Suess, 1880, 1891; de Martonne, 1897; de Lapparent, 1898; Uhlig, 1907, 1912; Obst, 1913; Verweke, 1913, Krenkel, 1922; Willis, 1928, 1936). After many years of debate concerning compressional versus extensional modes for their origin (e.g., Krenkel, 1922; Willis, 1936; Bullard, 1936), rifts are now generally accepted to be extensional features, although they may be associated with earlier, contemporaneous, or later compression. Morphologically, they are well defined as elongate depressions bounded by normal faults (e.g., Mohr, 1982; Ramberg and Morgan, 1984; Rosendahl, 1987). However, the common association of rifts with volcanism, high heat flow, anomalous crust and upper mantle structure, and seismicity provides compelling evidence that rifts are not confined to upper crustal levels, but that they are linked to dynamic processes in the lithosphere and asthenosphere. The term *taphrogenesis*, introduced by Krenkel (1922) to ascribe an extensional origin to the East African Rift, is essentially synonymous with rifting in modern usage.

Burke (1977) defined rifts as zones along which the entire lithosphere has ruptured in extension. This definition was used in modified form by the American Geological Institute (AGI) Glossary of Geology, which defines *rift* in a tectonic context as: "(a) A long, narrow continental trough that is bounded by normal faults; a graben of regional extent. It marks a zone along which the entire lithosphere has ruptured under extension. Cf: *paar*. (b) A belt of strike-slip faulting of regional extent" (Bates and Jackson, 1980). The subject of this book falls basically under the first of these definitions, but to clarify and define the scope of the following chapters some elaboration and modification of this definition is required. (Note that AGI definition [a] invites comparison with the term, paar, which will be elaborated upon below when discussing the basic contrasts between oceanic rift valleys and continental rifts.)

The Burke/AGI definition incorporates the fundamental interactions associated with rifting, but in most rifts no simple tests exist to define *rupture*, which we take to mean a complete breaking through of the lithosphere. Models of rock deformation suggest that the lower crust and/or the lower lithospheric mantle more likely deform in a ductile manner (e.g., Lynch and Morgan, 1987), and that lithospheric rupture may not occur until dike intrusion progresses to a stage of sea-floor spreading, i.e., until all crustal extension is accommodated by the intrusion of new, mantle-derived basaltic crust. Perhaps a more realistic definition of rifts therefore should emphasize

the *modification in extension* of the entire lithosphere. Lithospheric deformation may not be uniformly distributed in a vertical column (e.g., Wernicke, 1985), but the entire lithosphere must be involved in the deformation to meet the criteria used here to define a rift.

For the purposes of this book, we have modified the definition of a *continental rift* to be "an elongate tectonic depression associated with which the entire lithosphere has been modified in extension." A *rift system* is defined as a tectonically interconnected series of rifts. These definitions implicitly include the *transient* thermal as well as the *permanent* structural/compositional modification of the lithosphere during extension. Note that not included in the strict interpretation of this definition are: (1) small extensional features, or simple grabens, in which the entire lithosphere is not modified by extension, (2) highly extended terranes (HETs), in which no elongate tectonic depression is formed, or (3) rifted passive continental margins, where the initial tectonic depression develops into an ocean basin. The reason that these features are different from continental rifts, narrowly defined above, may be in part governed by the magnitude of extension; e.g., a small absolute amount of extension, perhaps less than 5% extension over a 100-km-wide zone, may be insufficient to modify the entire lithosphere, and thus results only in one or a few simple grabens. On the other hand, a large extensional strain, perhaps greater than 100% extension, may require such extensive lithospheric modification that the elongate tectonic depression appears to be lost.

We recognize the arbitrariness of this limited definition of rift, and that the processes responsible for all these tectonic features may be similar. Indeed, they may all represent different stages in a spectrum of lithospheric extension. Therefore, in this book we discuss in some detail examples of both HETs and rifted passive margins. There are several reasons for this: (a) Definitions and classifications adopted here should be used mainly as idealized models to aid understanding of fundamental *processes*. (b) "True" continental rifts, HETs, and rifted passive margins are arguably genetically related varieties of continental extensional structures, but often it may not be possible to distinguish between them by morphological and/or near-surface geological data alone. Extensive, detailed deep geophysical investigations may be required before clear-cut differentiation is possible. (c) Often—but not always—specific rifts, HETS, or rifted margins may have developed as stages in an evolutionary sequence and a careful study of their similarities and differences contributes to the fundamental understanding of larger aspects of continental extension.

1.1.2. Closely related extensional structures

The terms *graben* and *rift valley* are not necessarily synonymous. The classical definition of rift valley incorporated essentially the same criteria now used for graben: "an elongate, relatively depressed crustal block bounded by faults on its long sides". Indeed, two of the oldest known examples of continental rifts, the Rhinegraben segment of the Central European rift system and the Oslo Graben, historically were first recognized and so named because of their graben-like topographic features. Rift valley grabens (or more commonly, half-grabens, most of which display alternating polarity along the length of the rift) are the dominant surface expression of many continental rifts and typically have widths on the order of 20–50 km—a scale characteristic of the thickness of the brittle upper continental crust. In contrast, *simple grabens* are minor structural depressions, usually having scales of a few meters to a few km, and are created by small near-surface extensional strains rather than by deeper lithospheric strain.

Highly extended terranes are characterized by upper crustal extension of the order of 100%, perhaps an order of magnitude greater than is typical in rifts. This extension is typically associated with the formation of broad, shallow basins (e.g., McKenzie, 1978), in contrast to the relatively deep, narrow basins characteristic of rifts. In places, HETs are exposed in domal uplifts, with minor or no associated basins, but it is not clear whether these uplifts are primary or secondary features associated with extension (e.g., Okaya and Thompson, 1985, 1986). In addition, HETs do not always appear to be associated with major modification of the crust and lithosphere (Keller et al., 1990). It is possible that interactions between the crust and mantle are distributed

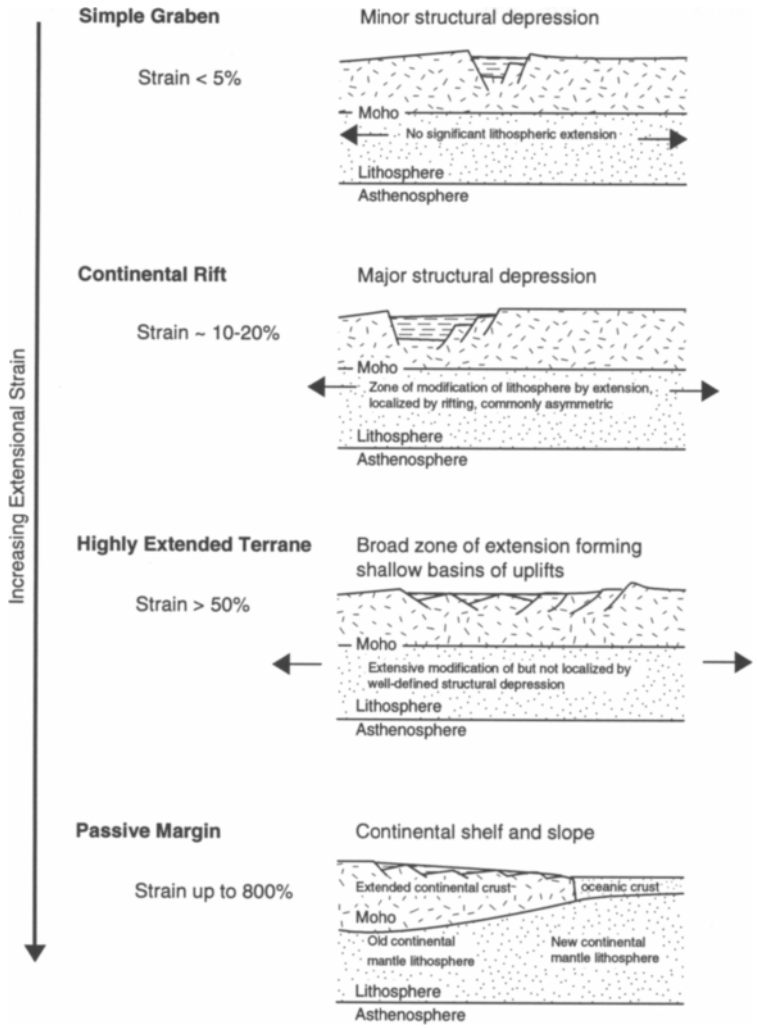

Fig. 1–1. Major terrane styles associated with continental extension.

over a wider area in HETs than in rifts, and therefore do not result in prominent geophysical anomalies and volcanic signatures. Alternatively, individual basins within HETs may be associated with through–going crustal or lithospheric shears, which offset deep extension from shallow extension (Wernicke, 1985). Continental rift extension may be superposed upon HET, as has apparently occurred in two phases of Neogene extension in much of the Western U. S. (e.g., Morgan et al., 1986). This superposition may make the crustal signature of HET difficult to identify through the superposed rift signature. Whatever the reasons for the differences among HETs and rifts, however, both structural features are obviously genetically related through extension, but they have generally been studied in isolation of each other because of their superficial differences.

Passive continental margins, the products of successful continental separation, are heterogeneous, and examples can be found which support their ori-

TABLE 1–1
Terms commonly used to describe continental rifts.

Term	Short definition	Suggested References
Continental rift	Elongate tectonic depression associated with which the entire lithosphere has been modified in extension.	This book
Rift system	Tectonically interconnected series of rifts.	This book
Modern rift	Rift tectonically and/or magmatically active, and/or with remaining transient thermal phenomena.	Morgan and Ramberg (1987)
Paleorift	Dead (or dormant) rift with no remaining transient thermal phenomena.	Neumann and Ramberg (1978); Ramberg and Neumann (1978); Morgan and Ramberg (1987)
Failed arm	Branch of a triple junction not developed into an ocean basin.	Burke and Dewey (1973); Burke (1977, 1980)
Aulacogen	Paleorift in ancient platform that has been reactivated by compressional deformation.	Shatsky and Bogbanov (1961); Milanovsky (1981)
Active rifting	Rifting in response to thermal upwelling of the asthenosphere.	Neumann and Ramberg (1978); Sengor and Burke (1978); Baker and Morgan (1981)
Passive rifting	Rifting in response to remote stress field.	Morgan and Baker (1983); Ramberg and Morgan (1984)

gins as continental rifts or as HETs. As these contrasting examples can sometimes be found along strike from each other on the same margins, a close relationship between rifts and HETs is suggested. Perhaps the fundamental difference between rifts and HETs is simply the magnitude of extension, i.e., HETs are high-strain rifts. However, the interpretation that some rifts develop into continental margins without passing through the HET stage suggests that magnitude of extension is not the only basic difference between rifts and HET. We are drawn to the conclusion that rifts and HETs represent different modes of extension, but that a continuum between these modes exists. This continuum is represented by along–strike variations in volcanic and structural styles of passive continental margins.

The definitions of major extensional features are illustrated in Figure 1–1. A more comprehensive and detailed terminology of the architecture of continental rifts has been developed by Rosendahl (1987), primarily for use in describing the shallow structure of rifts. As the focus of this volume is predominantly in the understanding of rifts on a lithospheric scale, Rosendahl's detailed terminology is not adopted here, but it is recommended for detailed studies of upper crustal rift structure.

Important terms associated with continental rifts are summarized and defined in Table 1–1. Many features characteristic of continental rifts appear to be associated with transient thermal phenomena related to the processes of lithospheric extension, and this gives a primary division of rifts into *modern rifts* and *paleorifts*. A *modern rift* is defined as a rift which

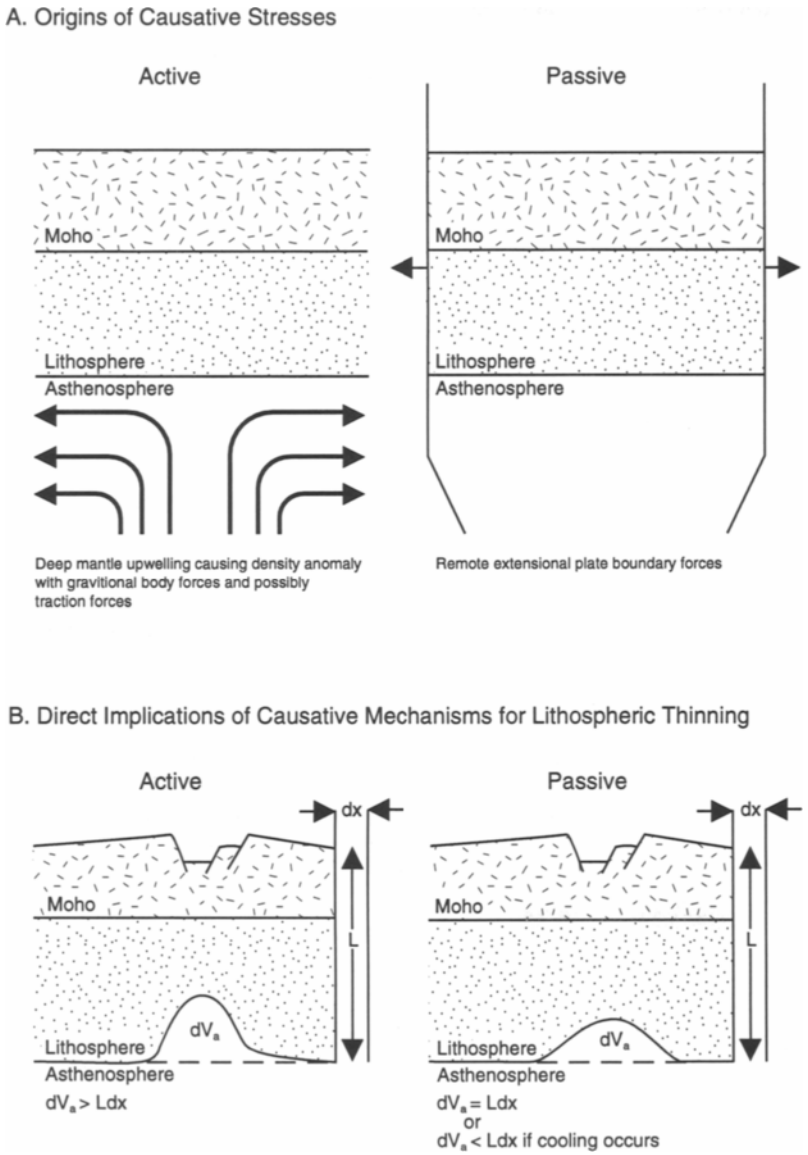

Fig. 1–2. Highly simplified end–member models of the causative or initiating mechanisms of continental rifting.

has active extension-related tectonic or magmatic activity, and/or has transient thermal phenomena (high surface heat flow, thermal uplift, shallow Curie isotherm, low upper mantle seismic velocities, etc.) remaining from extensional perturbation of the lithosphere (Ramberg and Morgan, 1984). A *paleorift* (sometimes also called a "fossil" rift) is defined as a dead (or dormant) rift with no remaining transient thermal phenomena (Neumann and Ramberg, 1978; Ramberg and Neumann, 1978; Ramberg and Morgan, 1984). Two further subdivisions of *paleorift* are useful: A *failed arm*, which is

a *paleorift* which formed as a branch of a ridge–ridge–ridge (three–spreading–arm) triple junction, but which did not develop into an ocean basin (Burke and Dewey, 1973; Burke, 1977, 1980); an *aulacogen* which is a *paleorift* in an ancient platform that has been reactivated at some stage in its history by compression (Shatsky and Bogbanov, 1961; Milanovsky, 1981).

The causal or initiating mechanisms of continental rifting have long been in the minds of rift geoscientists (e.g., Élie de Beaumont, 1827; Suess, 1891, 1904–1909) and have often been described by two end-member models, *active rifting* and *passive rifting* (Neumann and Ramberg, 1978; Sengör and Burke, 1978; Baker and Morgan, 1981; Morgan and Baker, 1983). *Active rifting* is defined as rifting in response to a thermal upwelling of the asthenosphere, where the causative stresses for rifting are directly or indirectly associated with lateral thermal density variations in the lithosphere and the underlying asthenosphere. In *active rifting* the lithosphere is thermally thinned by heating and absorption into the asthenosphere, in addition to necking in response to extension, and hence the volume of asthenosphere rising into the lithosphere exceeds the volume of lithosphere displaced laterally by extension. All modern rifts are of Cenozoic age, i.e. younger than 65 million years (50-100 m.y. is approximately the time scale for a large thermal perturbation, or 'pulse,' at the depth of the continental lithosphere to exponentially decay due to conductive heat transfer processes). *Passive rifting* is defined as rifting in response to a regional stress field, usually assumed to originate from remote plate boundary forces. In *passive rifting*, the lithosphere is thinned only in response to extension. These two contrasting causative mechanisms are illustrated in Figure 1–2a, and the most direct implications of the two model mechanisms for evolution of the lithosphere/asthenosphere boundary are shown in Figure 1–2b.

The causal mechanisms of rifting are not the only mechanisms responsible for the final lithospheric structure resulting from rifting. A number of secondary processes may modify the lithosphere in response to active or passive lithospheric thinning. Some of these processes are illustrated in Figure 1–3. Secondary convection may occur at the base of the lithosphere in zones of lithospheric thinning as a result of the lateral density instability created by the juxtaposition of the hotter lower-density asthenosphere with cooler higher-density lithosphere in the zone of lithospheric necking (Keen, 1985; Buck 1986; Moretti and Froidevaux, 1986). Alternatively, this same density anomaly may cause delamination of the mantle portion of the lithosphere (Bird, 1979; Turcotte and Emerman, 1983). These two processes both tend to thin the lithosphere, and to broaden the zone of thinned lithosphere in addition to thinning caused by the primary stress field. Upwelling of the asthenosphere and lithosphere and heating of the lithosphere preceding and during rifting commonly result in generation of significant volumes of mantle-derived magmas which are added to the crust. The chemistry of the mantle lithosphere may also be modified by this process. Volumetric strain relations associated with crustal and lithospheric extension may be significantly modified by this process.

1.1.3. "Pseudorifts" and other thermo–tectonic structures with only some rift–like characteristics

Several types of major thermo-tectonic features display some rift-like characteristics suggestive of a genetic association with continental rifts and sometimes may be confused with rifts. However, many of these are not generally classified as rifts because they fail to meet one or both of the two principal criteria distinctive of 'true' rifts as defined in section 1.1.1: (1) a *major extensional depression,* and (2) significant *modification of the entire thickness of the lithosphere.* As noted previously, this category possibly should include highly extended terranes and passive margins, but, because of their close relationship with basic rifting processes and evolution, we have felt it necessary to discuss these above (Fig. 1–1, and section 1.1.2.) as well as in greater detail in later chapters. Three of the more clear–cut members of the "pseudorift" category include pull-apart basins, volcano-tectonic depressions, and continental flood basalt provinces (Fig. 1–4). The other sometimes misclassified members of this category are the so–called oceanic rifts. Unfortunately, due to lack of space, detailed discussions of examples of these

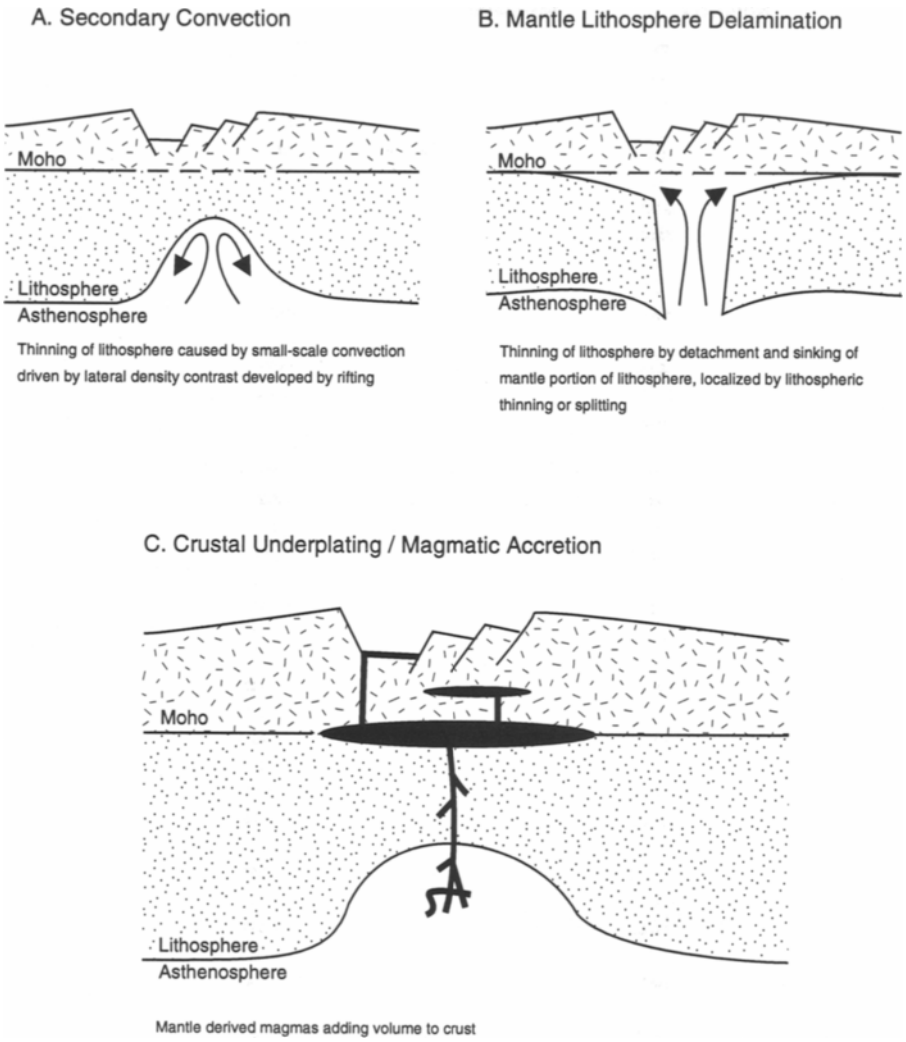

Fig. 1–3. Secondary processes modifying the lithosphere in response to lithospheric thinning.

latter pseudorift structures cannot be included in this book even though this would considerably broaden our general understanding of rifts and rifting processes. However, brief summaries of a few basic characteristics are given below.

Pull-apart basins (sometimes called 'rhombochasms,' or 'rhombograben') customarily are distinguished from rifts primarily through the axis of extension associated with the system. In a rift the axis of extension is roughly perpendicular to the axis of the structural depression, whereas for a pull-apart basin, the axis of extension is parallel or sub-parallel to the axis of the depression. These two structures also originate in contrasting tectonic environments: Rifts are associated with an extensional stress field; pull-apart basins are associated with *en*

echelon offsets in transform faults where the offset has the same sense as the fault displacement (Fig. 1–4). Thus, pull-apart structures commonly occur in regions of predominantly transform faulting such as the San Andreas fault system, the Gulf of California, and the Dead Sea. However, from the criteria adopted in this book, the key factor distinguishing pull-apart basins from true rifts is not so much the orientation of the extension axis but rather that these features are not through-going, lithospheric-scale structures. Again, as in discussions above regarding fine distinctions between grabens, rifts, and HETS, we must reemphasize that the brief definitions adopted here are in some ways arbitrary and that some large tectonic features may be difficult to classify due to present incomplete knowledge of associated deep lithospheric structure. Some would argue that, in the Dead Sea transform system for instance, the large basins of the Gulf of Elat (Aqaba) may be true rift basins, but this cannot yet be proven because of the uncertainty about the deep lithospheric structure beneath these basins.

Volcano-tectonic depressions are typically associated with the migration of major volcanic centers which leads to major magmatic modification of the crust and subsidence of the surface. In this case, surface subsidence is due chiefly to post-magmatic-event lithospheric cooling, widespread collapse of large calderas, and surface loading by the extensive volcanic flows rather than to extensional stresses in the crust and/or lower lithosphere. There is no major extension either parallel or perpendicular to the depression and usually no apparent thinning of the underlying crust. A well known example is the Eastern Snake River Plains region of Idaho which is the track of the 15 m.y. migration of the mantle hot-spot now underlying the Yellowstone area.

Continental flood basalt provinces are the principal continental members of immense crustal emplacements of predominately mafic extrusive and intrusive rocks known as Large Igneous Provinces (LIPs) that have been erupted over relatively short spans of geological time (Coffin and Eldholm, 1994). Both continental and oceanic varieties are commonly attributed to mantle plumes or hotspots, but many details are poorly understood at present. Oceanic LIPs appear to originate by processes other than "normal," steady–state seafloor spreading at midocean ridges. Oceanic LIP examples include oceanic plateaus, ocean basin flood basalts, volcanic passive margins, submarine ridges, and seamount groups. Continental flood basalt provinces (Macdougall, 1988; 1992) are generally vast, laterally extensive volcanic plateaus which are commonly associated with a regional extensional stress field as evidenced by dikes and vent alignments, but lack obvious major *elongate tectonic* depressions. Depressions within these provinces are generally due to gravitational loading by the extensive surface flows. Although continental flood basalt provinces are not usually included as a common branch of rift-to-ocean evolution, they undoubtedly are products of continental extension and often appear in obvious close associations with rift systems, highly extended terranes, and other manifestations of continental breakup. Examples are the Columbia River Plateau extending northward from the Basin and Range province, the Ethiopian Flood Basalt Province embracing the Afar triple-rift junction where the East African Rift system joins the Red Sea and Gulf of Aden sea-floor spreading zones, and the Jurassic-Cretaceous basalts of South America, Southern Africa, and Antarctica associated with the breakup of Gondwana. Because huge volumes of basalt cover such vast continental areas, detailed geophysical and geological exploration of the structure and history of the underlying crust and lower lithosphere in these areas has been slow and difficult. Thus, many possible similarities and associations between rifting processes and continental flood volcanism are masked and remain unclear.

A fundamental distinction exists between "*oceanic rifts*" and continental rifts. In the early days of development of concepts of ocean–floor spreading and the plate tectonics paradigm, it was recognized that the world-girdling mid-oceanic ridge system was clearly associated with, and obviously connected to, major rift valley systems on the continents (e.g., Heezen, 1960, 1969; Girdler, 1964). This global "fracture pattern" became popularly known as the "World Rift System." The initial discovery of mid-ocean ridges in the Atlantic and Indian Oceans was based chiefly on bathymetric observations and focused on what appeared to be a tectonically active,

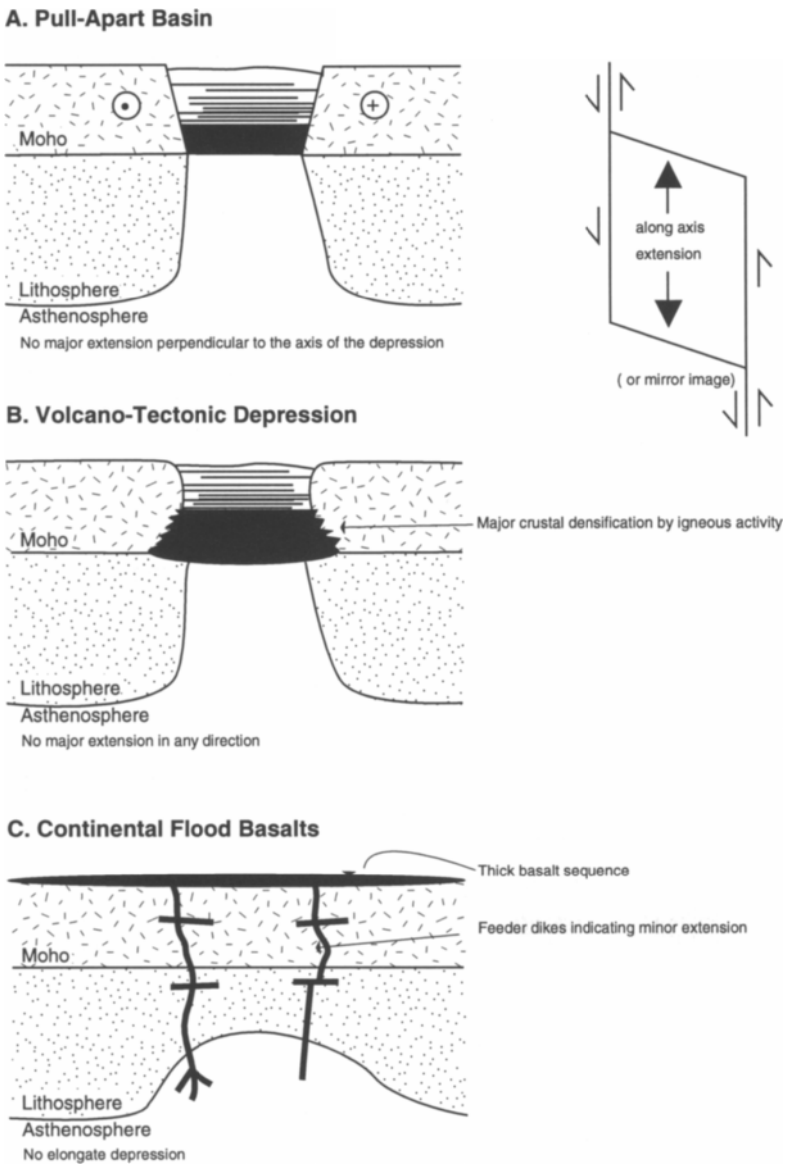

Fig. 1–4. Other tectonic and magmatic structures with rift-like characteristics.

continuous, median valley along the ridge crests. Subsequent research has considerably broadened understanding of extensional tectonism and volcanism of oceanic lithosphere as contrasted with the somewhat different and considerably more complex continental extensional processes. In current usage, *oceanic rifts* are commonly understood to be the troughs along the crests of the mid-ocean ridges where new *oceanic* crust is generated from mantle-derived magmas during sea-floor spreading. In a

sense, the walls of oceanic rift valleys are not faults bounding a down-dropped block of pre-existing crustal rock (as in definitions which emphasize morpho-tectonic criteria, particularly graben-like characteristics, for continental rifts), but rather are more akin to volcanic crater rims which contain upwelling lavas. Thus, oceanic rifts more closely fit within the AGI Glossary definition of *paar*: "A depression produced by the moving–apart of crustal blocks rather by subsidence within a crustal block. It is floored with upper-mantle igneous rocks and is essentially devoid of crustal material. Examples are the Gulf of California and the Dead Sea. Entymol: Hebrew." (Bates and Jackson, 1980).

1.2. Significance of continental rifts

There are a number of important reasons for studying rift zones and rifting processes:

1) Rifting is one of two fundamental tectonic process affecting the continents, the other being collision;

2) Rifting causes permanent modification of the continental lithosphere and may be important in adding material to the lithosphere and in recycling continental mantle lithosphere back into the convecting upper mantle;

3) Through igneous processes, rifting provides a 'window' into the physical-chemical state of the mantle;

4) A variety of natural resources are associated with rift environments;

5) Rifts can be the sites of natural hazards such as earthquakes and volcanism.

It is generally accepted that rifts represent the initial stage of continental breakup and the start of the Wilson cycle of plate tectonics (ocean opening and closing). Plate tectonics requires that new extensional plate boundaries be formed throughout geologic time in order to maintain a multi-plate regime in dynamic equilibrium with subduction zones. These new extensional plate boundaries form preferentially in continental lithosphere because it is weaker than oceanic lithosphere with a similar geotherm (Vink et al., 1984; Lynch and Morgan, 1987), and plate tectonics has placed a new emphasis on continental rifts as the possible sites of incipient lithospheric separation and new oceans. Highly extended terranes, which share many of the characteristics of rifts but which may fall outside the narrow definition of rifts above may also be forerunners of new oceans. Suture zones are the counterparts of rifts in the process of convergence (Burke et al. 1977; Dewey, 1977).

Rifting is associated with permanent modification of the continental crust, and perhaps the whole thickness of the continental lithosphere, even where extension does not progress to continental separation. Magmatic activity in some rifts adds a significant volume of mantle-derived basaltic intrusive and extrusive material to the continental crust, resulting in a crust that is not thinned in proportion to the amount of extension. Additional processes for interactions between the subcontinental lithosphere and the convecting upper mantle have been suggested. These are topics of much current research—particularly by numerical modeling techniques—but may be difficult to quantify because interpretations of possible evidence (e.g., isotope ratios, lithosphere-asthenospheric structures inferred from seismic tomography studies) may still lack adequate spatial resolution. Lithospheric thinning exclusively by ductile processes and consequent asthenospheric upwelling does not transfer material from the lithosphere to the asthenosphere, but "second-order" exchanges at the boundary layer (small-scale convection, lithospheric melting, underplating, "delamination" of the subcrustal lithosphere, and other possible forms of subcrustal lithospheric stoping) indeed probably contribute to recycling of the lithosphere. Rates and the quantitative significance of sub-rift interactions to the global lithospheric-asthenospheric recycling (material-exchange) budget remain unknown. Certainly the reverse process probably happens; as asthenosphere moves upward and cools, it is converted to lithosphere.

Through igneous processes, rifts and other major magmatic systems provide an opportunity to study the chemical composition, physical conditions, and evolution of the sub-continental mantle. Detailed interpretations of geochemical and isotopic characteristics, including radiometric ages, of both extrusive and intrusive rocks provide unique insights

into rifting processes, in part by helping to delineate regional variations in upper mantle properties which may be invisible to geophysical techniques. Xenoliths entrained in magmatic rocks represent samples of the continental lithosphere and provide direct access to portions of this lithosphere.

Several economically important resources are often generated as a direct consequence of both thermal and structural processes of rift evolution. Some resources are formed within rifts, whereas others are created in earlier geological environments and are only later exposed or transported to the near-surface as a consequence of rifting. Largely thermally-associated resources include geothermal energy and mineral deposits of hydrothermal/magmatic origin, such as molybdenum, some hydrothermal copper, and magmatic copper-nickel deposits. Sedimentary rift basins provide nearly-ideal habitats (reservoirs) for hydrocarbon resources, and extensive evaporite deposits are characteristically found in basins associated with the late stages of rifting just prior to continental splitting (e.g., Afar). Increasingly, *groundwater* is becoming a critical resource, especially for developing large urban population centers. Rifts can affect or even control regional hydrology in very significant ways. For example, the Albuquerque basin in arid New Mexico is one of the largest and deepest sedimentary basins within the Rio Grande rift (Chapter 6). The porous, syn-rift Neogene sediments of the Albuquerque basin have a total pore-fluid volume of about 1900 km^3 (equivalent to 12,000 *billion* barrels (bbl.)[1.2×10^{13}], or 1,500 *million* acre-feet. [1.5×10^9].), which represents an extremely large hydrological resource (Birch, 1982). Lake Baikal, the principal rift valley at the heart of the Baikal rift system (Chapter 8), contains ~7400 km^3, approximately one-fifth of the Earth's *fresh surface* water.

Rift-related hazards are consequences of enhanced tectonic and/or magmatic activity in rift areas. Volcanic hazards may include explosive volcanism at large intermediate-to-silicic volcanoes and fissure flows within and on the flanks of rifts. Earthquakes result from the abrupt failure of the lithosphere in the extensional and trans-tensional settings of rifts. The amount of elastic energy that can be stored in the lithosphere to be released in an earthquake is related to the thermal structure of the lithosphere, and a weak inverse correlation exists between the seismic energy release and the amount of volcanism—larger earthquakes typically being associated with non-volcanic rift segments. One still puzzling aspect of rift-related seismicity is the fact that some paleorifts, such as the New Madrid rift (not treated in this book) in the central U.S.A., appear to be closely associated with potentially dangerous earthquake zones (Johnston, 1989; Johnston and Kanter, 1990). This seismicity is possibly due to reactivation of buried faults and old zones of weakness that resulted from extensive crustal modification due to the ancient rifting event. A variation on this hypothesis is that now-cold massive igneous intrusions or mafic residues in the deep crust, emplaced during ancient rifting, may help localize contemporary deep crustal stresses and zones of seismic energy release.

1.3. Some historical highlights of continental rift studies

As has been alluded to previously in this chapter, the early recognition of continental rifts as major tectonic features and the development of many recognizably modern concepts and ideas about their character can be traced back to the early 1800s. As yet there has been no in-depth study specifically focused on the historical development of observations and theories of rifting—although rifting sometimes receives attention in historical treatments of plate tectonics, seafloor spreading, and continental drift (e.g., Hallam, 1973; Wood, 1985). Rosendahl (1987) and Mohr (1991) briefly sketch the origins of several major concepts, terminology, and theories developed by early rift pioneers principally in the East African rift system. Mohr's (1991) list of references is particularly useful not only because it is arranged in chronological order of publication, but also because he attempts to include a more balanced selection of "early" (~pre-1960) papers published in languages other than English. Drake and Girdler (1982) give an overview history of rift studies before 1970 that particularly emphasizes oceanic rifts.

Some historical background to the development of concepts and ideas on processes of rifting is presented by Ruppel (1995).

The structural geologist, Bailey Willis (1857–1949), longtime professor of geology at Stanford University and vigorous opponent of Wegnerian ideas of continental drift, made a wide-ranging tour of East Africa in 1929–30 and published an extensive discussion and interpretation of his observations (Willis, 1936). Willis, in the first chapterr of his 1936 book (partially reprinted in Quennell, 1982), traces the history of ideas on rift valley formation from the early 1800s up to 1930, and supports his discussion with key quotations (in English translation) from original papers published by the chief pioneers of rift studies in both East Africa and the Rheingraben area of central Europe. Willis' 1936 discussion is probably the best single English–language summary of pre–1930 ideas and debates about continental rifting, although, inevitably, it is colored by his own opinions and preconceptions in regard to causative mechanisms. (At this point late in his career, Willis had come to favor mainly compressional mechanisms for the origin and development of rift valleys.) As our main objective in this section is to set the stage for an overview of progress in continental rift research since about 1960, we can provide here only the briefest sketch of the accomplishments and key concepts by the more prominent rift investigators prior to 1930. Thus, students of the history of rift research in this early period are here largely on their own but can profitably begin their searches guided by the excellent bibliographies listed in Willis (1936), Rosendahl (1987), Mohr (1991), and the two reprint volumes by Quennell (1982, 1985).

While the recognition of the basic morphology of rifts and of rifting as an important process in the development of the Earth's surface features is usually credited largely to the publications and syntheses of Suess (1891, 1904–1909) and of Gregory (1896, 1921) on the East African system, many key ideas and concepts had been derived in the early nineteenth century from interpretations in the Rheingraben. Léonce Élie de Beaumont (1798–1874) was an exact contemporary of Charles Lyell and one of the first European geologists to propose a global tectonic synthesis emphasizing mountain building processes (Greene, 1982). By 1836, he had recognized that the Vosges and Schwarzwald form an arched uplift broken along its crest by a subsided block underlying the upper Rhine valley (Élie de Beaumont, 1827, 1841, 1844). Later European workers, including de Lapparent (1887, 1898) and especially Suess (1891) elaborated on the Rhinegraben structure. Indeed, it was Suess who first proposed the term "graben" in an early (~1883) German edition of his 4-volume treatise, *The Face of the Earth* (Suess 1904–1909).

As pointed out by Mohr (1991), for geographic and historical reasons the Afar depression of Ethiopia and the Ethiopian Plateau were explored and geologically investigated earlier (beginning ~1830) than the true rift valleys to the south (in present-day Kenya, Tanzania, Malawi, etc.). However, it was not until deeper explorations into East Africa, notably by Richard Burton and John Hanning Speake beginning in the western rift area in 1857, by Joseph Thompson and Gustav Fischer in the central region of present-day Kenya, and especially by the Hungarian Count Samuel Teleki in the Lake Baringo–Lake Turkana area during 1887-88, that it was realized that many of the great lakes of the region were confined in "long, narrow troughs." This observation eventually led Suess to term such downfaulted valleys as *Bruche* (= fractures, breaks; note this German term is closer in meaning to the English term, "rift" than is "graben"), and to relate them to the "graben" type of structure observed in the Rhine valley. It was Eduard Suess (1831–1914), a Viennese professor of geology justly famous for his monumental treatises on world geology (Suess 1904–1909) as well as the structure of the Alps, who provided what is considered the classic foundation paper on the geology of rift valleys (Suess, 1891), but the remarkable fact is that Suess himself never visited East Africa nor directly observed the spectacular geology that he described so perceptively (Mohr, 1991; 1992)! The outline of this astonishing story is that the second–in–command of Teleki's 1887–1888 expedition to East Africa was Ludwig Ritter von Höhnel, an Austrian naval officer with a talent for perceptive and diligent scientific observation. On his return to Europe, von Höhnel first published a geographical account and then collaborated extensively

with Suess and the petrologist August Rosiwal to extensively update the geological knowledge of East Africa (von Höhnel et al. 1891). This, in turn, inspired Suess to undertake the masterful review and synthesis of the geology of the entire graben system of eastern Africa from the Zambesi via Afar to Palestine (Seuss, 1891), which was to have a profound influence on so many students of the Earth to follow.

The Scotsman John W. Gregory (1864–1932) probably more than anyone else is responsible for first making the African rift valleys scientifically famous and for establishing many of the basic field concepts still used in continental rift studies. Deeply impressed by Suess' 1891 monograph, the 28-year-old Gregory, then employed at the British Museum of Natural History, in late 1882 was asked on very short notice to be the naturalist for a private British expedition to the one as yet unexplored part of the Rift Valley between Lake Rudolph (now Lake Turkana) and the Red Sea. Gregory, delayed awaiting approvals for a leave of absence and to collect essential scientific equipment, joined the already departed expedition in Aden. The original expedition soon failed due to poor planning and logistics, last minute changes in point of entry and area of investigation, and illness and even some deaths of expedition members in the unhealthy territory. To recover from this disaster, Gregory organized his own detachment and during March–August 1893 lead an energetic investigation of the central part of the Kenyan rift (Gregory, 1894). Gregory confirmed in the field and further elaborated upon many of Suess' geological ideas as well as reported his experiences with the natives and observations of the fauna and flora of the region in a popular travelogue–format book, *The Great Rift Valley* in 1896 (Gregory, 1896). After a quarter century of teaching, lecturing, and pioneering geological explorations in many other parts of the world, Gregory returned to the Kenyan rift in 1919 for further, mainly geological studies. The result was a comprehensive and clearly reasoned treatment of the geology and petrology of Kenya and surrounding territories leading to his classic book, *The Rift Valleys and Geology of East Africa* (Gregory 1921; see also Gregory 1920; 1923).

A listing of the more important and productive geological pioneers in East African rift system during the first half of the 20th–century must include C. Uhlig, E. Krenkel, F. Dixey, B. Willis, R.B. McConnell, and B. Baker (for more references see, e.g.: Willis 1936; Rosendahl 1987; Mohr 1991; Quennell 1982, 1985). Krenkel (1922, 1924) first set forth detailed field arguments ascribing a tensile origin for the East African rift and coined the term *taphrogenesis* for this process. Hans Cloos (1939) usually receives the credit for experimentally establishing the mechanical validity for tensile origins of rifts through clay modeling studies, although the basic idea had been extensively discussed by Élie de Beaumont, Suess, Gregory, and others. Only by 1936 was it possible for Edward Bullard to apply the first significant geophysical study—gravity surveys in the East Africa rift area (Bullard, 1936; Girdler, 1964)—to begin to better understand the subsurface structures of rifts. Arthur Holmes in his textbooks (1944, 1965) not only synthesized much of the early work to present the basic picture of the East African rift system that is in use today, but also outlined many unsolved problems that subsequent researchers have pursued in other continental rifts as well as the East African system.

Most prominent 19th and early 20th century Earth scientists concerned with questions of global geodynamics—including Élie de Beaumont, Suess, and Harold Jeffreys (1929)—almost universally rejected extensional mechanisms as the ultimate driving forces for large-scale rifting. Instead, they attempted to fit abundant observational evidence for extensional deformation into global models in which extensional regions were secondary consequences (e.g., geosynclines) of complex, but net-compressional, interactions on a perpetually contracting outermost layer (crust) of an Earth cooling by conduction. Alternative theories, including expanding Earth theories such as that advocated by Holmes (1965), still were unable to account satisfactorily for non-uniform patterns of zones of tectonic deformation, nor could they begin to explain the episodic nature of tectonism during the Earth's history (Ruppel, 1995). By about 1950, however, there were an increasing number of key studies proposing new mechanisms and interpretations—notably the clay

modeling results of Cloos (1939) and the gravity–isostasy analysis of Venning Meinesz (1950)—that began to tip the balance away from compressional theories towards extensional mechanisms. But undoubtedly the deciding factor leading to the modern plate-tectonic interpretations was the massive accumulation of ocean-floor geophysical data in the 1950s that forced widespread recognition of large-scale crustal extension on a nearly world-wide basis.

The style of rift studies underwent a major change after the Second World War (WW II). Prior to 1945, field studies were pursued principally by individuals or small groups using classical methods of geologic mapping and petrologic techniques. Gravity measurements were sparse and radioactive dating was in its infancy. Since rifts were recognized principally by their topography, active Cenozoic rift systems constituted most of the known examples. Principal investigators were mostly academics or were employed by local or national geologic surveys and often devoted major portions of—or entire—careers to a single rift. For those interested in large-scale regional or global generalizations and theoretical "modeling," inductive methods of reasoning tended to dominate.

After WW II, an interdisciplinary team approach to certain problems in the Earth sciences became more common. Coordinated interdisciplinary teams gathered massive data sets over large regions of both land and sea, and often at a global-scale. At first, a great deal of this work was of a reconnaissance nature. This comparatively well-funded "big science" style, characteristic of the latter half of the 20th-century, was due largely to the unparalleled prestige and power that science and technology derived from the development of radar, nuclear weapons, and similar rapid technological advances during the war. Mainly as a result of wartime developments, many new instruments became available (including magnetometers, gravimeters, echo sounders, seismic instruments and new types of seismic energy sources, radio navigation aids, electronic equipment for probing the atmosphere and ionosphere) which allowed rapid accumulation of chiefly *geophysical* data that were to shed new light on a wide variety of problems. Oceanographers were the among the first to benefit from the new technologies and soon launched into a detailed exploration of the ocean floors, which were virtually unknown before 1940. With the additional spur to research deriving from the International Geophysical Year (IGY) (1957-1958), by 1960 oceanographers had succeeded in constructing greatly detailed physiographic maps of the sea floor comparable to those available for the continents (e.g., see Hallam [1973] for a general review, Drake and Girdler [1982] for aspects focusing on rift studies). Perhaps the most remarkable result of the postwar ocean floor topographic work was the discovery of a world-wide undersea mountain range with a seismically active median rift valley along its crest that was clearly connected to major continental rift systems such as the East African–Red Sea system and to extensional structures in the Western United States (e.g., Heezen, 1960, 1969; Girdler, 1958, 1964; Illies, 1969; Drake and Girdler, 1982). The recognition of this "world rift system" with its continental and oceanic interconnections has been one of the central elements in the development of subsequent global tectonic theories.

The highly successful IGY was, however, principally devoted to global studies of the Earth's atmosphere, hydrosphere, and ionosphere particularly in relation to the polar regions. In order to build upon the new spirit of international cooperation and to extend the new instrumental and analytical capabilities to studies of the solid earth, the Russian geologist/geophysicist, V.V. Beloussov, at the 1960 General Assembly of the International Union of Geodesy and Geophysics (IUGG) in Helsinki, proposed organization of an International Upper Mantle Project (IUMP, or UMP). The goals of the UMP were to apply cooperative techniques pioneered during the IGY to a detailed investigation by all possible methods (i.e., a *coordinated, interdisciplinary study*) of the Earth's upper mantle. By the next IUGG General Assembly in Berkeley in 1963, a 7-person international "steering" bureau, the Upper Mantle Committee (UMC), was in place and ten disciplinary Working Groups (e.g., seismology, physics and chemistry, gravity and geodesy, deep drilling, etc.) had been set up to help coordinate the wide scope of UMC plans (Båth 1964). Several countries also formed national UMP committees to further coordi-

nate national efforts in support of the project. The IUMP was designed to expire at the end of the 1960s, but the basic coordinating committee and working group structure has been adopted and improved for various successor projects such as the International Geodynamics Program (also known as the Inter-Union Commission on Geodynamics—IUCG) (1970–1980) and the International Lithosphere Program (ILP) (1980–1990). Upon review by the International Council of Scientific Unions [ICSU], the formal closing date for ILP has now been extended through the 1990s.

One of the first orders-of-business of the UMC in 1963 was to recommend three broad problems which should receive special emphasis for international studies:

(1) Study of continental margins and island arcs.

(2) *Study of the world-wide rift system.*

(3) Gravity earth-tide studies of viscosity and mechanical behavior of the upper mantle.

The inclusion of item (2) was the direct result of the great public as well as scientific interest in the seafloor mapping discoveries of the 1940s and 1950s, and the feeling that coordinated studies of the spectacular East African rift system using newly-available research tools on land would yield results of comparable significance to the oceanic studies. From the start it was recognized that oceanic and continental rifts were different in several important characteristics, so, over time, field projects and topical research conferences tended to separate into two loosely-linked communities. With financial assistance from UNESCO, the first of many international "rift-seminars" was convened in Nairobi in April 1965 (Anonymous, 1965a; 1965b). The 1965 Nairobi conference summarized the status of knowledge of the East African rift system and suggested a broad program for future research (Anonymous 1965a); detailed reviews of regional and disciplinary topics were presented in an accompanying report (Anonymous 1965b). With the encouragement of the UMC, two more symposia dealing with a more world-wide selection of rifts soon followed (Irvine 1966; Knopoff et al. 1969). During the late 1960s, the long-running research program in the Rhinegraben was initiated and began to be reported collectively in IUMP-sponsored publications (e.g., Rothe 1967; Illies and Mueller 1970) as well as in many separate journal articles. Thus, the IUMP established a pattern—particularly in the area of rift research—which has been successfully followed in subsequent decades by its successors, the Geodynamics Program and the ILP: These international unions serve the important functions of encouraging broadly-based international cooperation in research and providing forums for topical seminars and for publication of volumes of collected contributions which supplement individual research papers. For more than 30 years now, rift research has remained one of the principal areas recommended for international studies by the working groups and coordinating committees of the IUMP, IUCG, and ILP.

1.4. A bibliography of major recent monographs and compilations on rifting

In this section, we attempt to provide a bibliographical listing of significant collected works on rifting published since the beginnings of IUMP-style multi-disciplinary research, but organized on a regional and topical basis. This list is evidence of the great intensification of rift studies during the past 30 years, but it is sobering to realize that these symposia volumes represent only the "tip of the iceberg." Probably at least an equal volume of individual papers of significance to rifts and rifting processes is widely scattered throughout the world scientific literature.

Many key references have been published during the past three decades which have focused upon rift-related studies. In this abbreviated bibliography, we are concerned mainly with collected papers and symposia proceedings published together in single volumes. Although most of these can be found in the reference lists of the individual chapters of this book, their collection here may serve as a convenient and more concise guide intended especially for students and researchers new to the field. As noted above, there are also many important individual papers widely scattered throughout the literature which are more difficult to tabulate *en masse*. Serious students may wish to start searching for topics of particular

individual interest by scanning the reference citations and lists in the other chapters of this and similar recent books.

Recent overviews and semi-popular articles. Shorter introductions to rifts and rifting processes have appeared in encyclopedias and annual review-type publications devoted to the Earth-sciences. In this category we note the articles by Burke (1977, 1980), Ramberg and Morgan (1984), Quenell (1987), Bond and Kominz (1988), Rosendahl (1989a, 1989b), Williams (1989), Olsen (1992), and Ruppel (1995). Semi-popular articles for more general audiences include Bonatti (1987), White and McKenzie (1989), and Baldridge and Olsen (1989).

Surprisingly, there exists no satisfactory recent comprehensive listing—nor published global map—showing all continental rifts currently recognized or under study. Indeed, one of the important lessons from rift studies over the past 30 years is that continental rifts are very numerous and have developed within a range of plate-tectonic settings (but dominantly extensional). Rifts are found on all continents and range in age from Archean to Recent. Probably there are more than two hundred proven and postulated significant continental and intercontinental (e.g., the Red Sea) rift structures on Earth—and new candidates are added yearly. Burke et al. (1978) compiled a still-useful, continent-by-continent, "reconnaissance" survey and global map of candidate continental rifts which included bibliographies of then-available publications for each. Ramberg and Morgan (1984) modify the Burke et al. map and present expanded views of rift systems within selected continental areas. Milanovsky (1983) suggests that structural and evolutionary styles of global rifting have varied at different epochs of Earth history.

Collections with a global perspective. Many of the rifting conferences and seminars sponsored by IUMP, IUCG, and ILP have been documented by volumes of collected papers. These publications include conference proceedings edited by Irvine (1966), Knopoff et al. (1969), Neumann and Ramberg (1978), Ramberg and Neumann (1978), Illies (1981), Ramberg and Morgan (1984), and Ramberg, et al. (1987), and the final report of the IUCG Working Group 4 on "Continental and Oceanic Rifts", edited by Palmason (1982). More recently, this sequence has continued with Froidevaux and Tan (1987), Manspeizer (1988), Lucchitta and Morgan (1990), Gangi (1991), Brunnacker and Taieb (1992), and Ziegler (1992a, 1992b, 1992c). In this category should be added several books dealing more generally with fundamental processes important in rifting such as extensional tectonics: Mayer (1987), Coward et al. (1987), and Cloetingh et al. (1994); and magmatism in extensional continental settings: Basaltic Volcanism Study Project (1981), Leeman and Fitton (1989), Kampunzu and Lubala (1991), Storey et al. (1992), and Pritchard et al. (1993).

Individual grabens and rift systems have been featured in special volumes of various research journals; we subdivide them somewhat arbitrarily as follows:

The Rhinegraben and associated Central European rift system. Beginning with Upper Mantle Project-related reports, these include: Rothe and Sauer (1967), Illies and Mueller (1970), and Illies and Fuchs (1975).

The East African rift system and other, older rifts on the African continent. See Anonymous (1965a, 1965b), Baker et al. (1972), Girdler (1972), Bishop (1978), Anonymous (1980), Frostick et al. (1986), Rosendahl et al. (1989), and Prodehl et al. (1994).

The Red Sea and Gulf of Suez. Although the Red Sea–Gulf of Suez system, a nascent ocean basin, is not discussed in this book due to lack of space, there exists an extensive literature on this important component of the Afro-Arabian rift complex: Falcon et al. (1970), Gass (1978), Bonatti (1988), Le Pichon and Cochran (1988), Makris et al. (1991), and Altherr (1992).

The Afar region. Although the Afar region is often classified as a part of the Afro-Arabian complex, it occupies a unique transition region between continental and oceanic styles of rifting. It thus has been the subject of intense multi-disciplinary studies documented by Pilger and Rösler (1975, 1976).

The Dead Sea. Similarly to the Afar region, the Dead Sea rift is considered to be a part of the Afro–Arabian system, but it also possesses some extremes of tectonic style that has attracted numerous geological and geophysical investigations seemingly out of proportion to its size: Freund and Garfunkel (1981), Ben–Avraham (1987), Kovach and Ben–Avraham (1990).

The Baikal rift. There are a number of Russian–language monographs dealing with the Baikal system of rifts, but we restrict this listing to more readily available English language collections: Logatchev and Mohr (1978), Logatchev and Zwart (1990). Since the mid–1980s, a number of international cooperative field study projects have been initiated between geoscientists of the Former Soviet Union and Western scientists in order to better address the important Baikal system in relation to other major world rift systems. See Lipman et al. (1989) for a preliminary multi–disciplinary comparison of the Baikal and the Rio Grande rift systems.

The Oslo Graben. Historically, the Oslo region was the first paleorift to be recognized. Books include Ramberg (1976), and Dons and Larsen (1978), but works edited by Neumann and Ramberg (1978), Ramberg and Neumann (1978), Neumann (1990) also contain many papers devoted to this system.

The Midcontinent Rift system and other North American paleorifts. In recent years, several largely-buried paleorift systems in central and eastern North America have been recognized and intensively studied mainly by geophysical means. The Midcontinent Rift system stretching from the Lake Superior region into Kansas and perhaps Texas is probably the most impressive of these. Collected papers on this region appear in volumes edited by Steinhart and Smith (1966), Wold and Hinze (1982), Gibb et al. (1994), and Ojakangas et al. (1995).

The Rio Grande rift. Books and special journal issues include: Riecker (1979), Baldridge et al. (1984), Keller (1986), and Keller and Cather (1994). A detailed field guide to the entire Rio Grande rift was edited by Hawley (1978).

The Basin and Range province. There is an extensive geological and geophysical literature on the Basin and Range province. The key collected volumes emphasizing rift studies are: Smith and Eaton (1978), Newman and Goode (1979), and Wernicke (1990).

The intra-continental North Sea basin. See Ziegler (1990), and Blundell and Gibbs (1990).

Passive margins. Thematic books and special journal issues containing collections of papers dealing with passive (rifted, extensional) margins often also include papers on *active* (compressional) margins, especially subduction zones. Significant collections dealing with continental margins in general include: Burk and Drake (1974), Bott (1976), Bally (1979), Watkins et al. (1979), Scrutton (1982), Morton and Parson (1988), Raleigh (1989), Sheridan and Grow (1988), and Barr (1992).

Yet, despite the very great progress during the past three decades in both theoretical and field studies reflected by these extensive bibliographies, there is still a surprising lack of consensus about many fundamental questions related to rifting, such as: the relationship of continental rifts to continental margins (why do some extensional features continue to the oceanic stage whereas others stop in the continental rift stage); what is the significance of different volumes and compositions of magmatism in rifts; are there any predictable trends to rift evolution; and how are the causal mechanisms of rifting related in detail to plate tectonics and mantle convection? Many of these questions may not have a single answer. Existing compilations of rift studies, although very impressive and useful, do not yet provide clear answers to most of these basic questions.

1.5. Purpose of this book

This book focuses upon a worldwide selection of continental rifts including the "major four" late Cenozoic rifts, the East African, the Central European, Baikal, and the Rio Grande rifts. We recognize that within the rather strict definitions adopted in this book, 'true' rifts occupy a small portion of

the spectrum of continental extensional features. While not wishing to de-emphasize the importance of other types of extensional features, we have confined our principal discussion to continental rifts in order to place a finite boundary on the scope of this book. We believe our chosen set of representative rifts offers as broad an overview as possible, because these rifts comprise the most intensely studied examples of their class and because the authors have considerable first-hand research experience in these specific systems. As our main goal is an improved understanding of the fundamental *lithospheric* processes of rifting, we have focused primarily on deep structures and processes associated with rifting, and have not attempted to elaborate upon near-surface geological details and upper crustal extensional styles for which there is a large and rapidly growing literature—particularly for petroleum exploration applications (e.g., Katz [1991]; Nelson et al. [1992]; Landon [1994]; Lambiase [1994]). A few other noteworthy examples of tectonic studies of rift development that concentrate upon details of surface faulting, basin evolution, and stratigraphy include: Courtillot (1982), Ebinger et al. (1987), Burgess et al. (1988), Ebinger (1989a, 1989b), and Rosendahl et al. (1992).

Geological, geochemical, and geophysical data have been compiled from selected rift zones in as uniform a format as possible in order to present a unified comparison of these rifts. Some discussion of highly extended terranes, passive margins, and other geologic terranes with rift-like characteristics are included for comparative purposes. These comparisons are made in order to contribute to an improved understanding of the basic processes of rifting. These processes include the initiating and terminating mechanisms of rifting, the response of the lithosphere to rifting, and the relationships among rifts, highly extended terranes, and passive continental margins.

The organization of this book is designed to be of use to general students of tectonics, to research workers interested in specific rifts, and to geoscientists interested in continental rifting as a global geological process. Before data for specific rifts are presented, Chapter 2 examines the causal or initiating mechanisms of rifting, and the five subchapters of Part II give brief discussions of important aspects of the principal geological, geochemical, and geophysical methods by which continental rifts are investigated—including the inherent uncertainties or limitations of these methods. Understanding the basic techniques as well as their limitations is an essential need precisely because investigation of continental rifting is such an *interdisciplinary* endeavor. Few, if any, individuals are likely to possess the training and experience required to fully understand all techniques. Our own experiences as a Working Group are that we have often struggled with each others' terminology, experience, and viewpoints while attempting to share hypotheses, models, understandings, and conclusions about complex processes. We hope that inclusion of these short "tutorials" may provide insight into, and convenient references about, techniques outside one's own area of expertise.

Continental rifts are divided into modern rifts and paleorifts in Parts III and IV, respectively. Modern rifts selected for detailed presentation include three major segments of the Central European rift system in Chapter 4 (the Massif Central-Rhone-Limagne system in south-central France, the Rhinegraben proper, and the Rhenish Massif-Lower Rhine section in northwestern Europe). As noted above, several important characteristics of continental rifts were first recognized in the Rhinegraben area early in the nineteenth century. Chapter 5 treats the East African rift system, with primary focus on the Kenya (Gregory) rift, which has been the area of much recent deep geophysical research. Again, as sketched in the historical section above, the East African rift system was the locale where continental rifting as an important global process was first recognized at the end of the nineteenth century and the early decades of the this century. It is perhaps ironic that the East African system, long considered to be the type continental rift after the pioneering geological efforts of Suess and Gregory, has had to wait for nearly a full century until large-scale, multidisciplinary geophysical research efforts could be brought to bear on its mysteries. The Rio Grande rift, the site of considerable research by U.S. rift scientists over the past two decades is discussed in Chapter 6. Chapter 7 summarizes the important Basin and Range prov-

ince, including the highly extended terranes of this zone. The Baikal rift in southeastern Siberia is overviewed in Chapter 8. Because of new opportunities for cooperative research between rift specialists in Russia and the 'Western' nations, we would not be surprised if the Baikal rift system became the center of many of the exciting new discoveries and insights in rift research over the next couple of decades.

The importance of paleorifts is that they display the entire range of processes associated with lithospheric extension, and are typically eroded to deeper crustal levels. Several examples of paleorift systems are discussed in Part IV. The Oslo graben (Chapter 9) was the cradle of many important concepts in mineralogy, geochemistry, and igneous and metamorphic petrology even before it was recognized as a paleorift. The U. S. Midcontinent rift system (Chapter 10) is an ancient rift that was discovered by its geophysical signature. It displays some of the Earth's most intense and sharply defined regional gravity anomalies which are caused by massive volumes of *extrusive* mafic rocks constituting nearly two thirds of the thickness of the crust. Some examples of one of the possible 'end-points' of continental rift evolution, rifted passive margins, are treated in Chapter 11—including aspects of the North Sea rift zone. The Southern Oklahoma aulacogen (Chapter 12) serves as our type example of aulacogens. The Central and West African rift system (Chapter 13) was created as part of the complex process that led to the separation of Africa and South America in the Early Cretaceous. The Central and West African rift system has been widely accepted as a classic example of a failed arm of a "RRR" triple junction and is the locale of major petroleum deposits.

A book attempting to overview the status of a complex, highly active area of modern scientific research, such as the processes of continental rifting, cannot claim to be even close to being uniformly up-to-date in all areas treated. Nor can it hope to forecast reliably—even for the near future—key topics that may lead to breakthroughs in our understanding of rifting processes during the coming decade. However, in Chapter 14 of Part V, we briefly discuss a few broad topics pertaining chiefly to fundamental processes of continental rifting worldwide which still challenge our understanding.

1.6. References

Altherr, R., (Editor), 1992. The Afro-Arabian rift system (special section). Tectonophysics, 204: 1–110.

Anonymous, 1965a. Report of the UMC/UNESCO Seminar on the East Africa Rift System (I.U.M.P. Sci. Rept. No. 6). University Press, Nairobi, 145 pp.

Anonymous, 1965b. Report on the Geology and Geophysics of the East Africa Rift System (I.U.M.P. Sci. Rept. No. 6). University Press, Nairobi, 117 pp.

Anonymous, 1980. Geodynamic Evolution of the Afro–Arabia Rift Systems – International Meeting Rome 1979. Accademia Nazionale dei Linceii, Rome. Atti No. 47, 705 pp.

Baker, B.H., P.A. Mohr, and L.A.J. Williams, 1972. Geology of the Eastern Rift System of Africa. Geol. Soc. America, Special Paper 136, 67 pp.

Baker, B.H., and P. Morgan, 1981. Continental rifting: progress and outlook. Eos, Trans. Am Geophys. Un., 62: 585–586.

Baldridge, W.S., P.W. Dickerson, R.E. Riecker, and J. Zidek (Editors), 1984. Rio Grande Rift: Northern New Mexico. New Mexico Geol. Soc. Guidebook, 35th Field Conf. 380 pp.

Baldridge, W.S., and K.H. Olsen, 1989. The Rio Grande rift. Amer. Scientist, 77: 240–247.

Bally, A.W. (Editor), 1979. Continental Margins, Geological and Geophysical Research Needs and Problems. National Academy of Sciences, Washington, 302 pp.

Barr, D. (Editor), 1992. Passive continental margin subsidence (special section). J. Geol. Soc. London, 149: 803–854.

Basaltic Volcanism Study Project, 1981. Basaltic Volcanism on the Terrestrial Planets. Pergamon, New York. 1286 pp.

Bates, R.L., and J.A. Jackson (Editors), 1980. Glossary of Geology (2nd Ed.). American Geological Institute, Falls Church, 751 pp.

Båth, M., 1964. Seismology in the Upper Mantle Project. Tectonophysics, 1: 261–271.

Ben–Avraham, Z (Editor), 1987. Sedimentary basins within the Dead Sea and other rift zones (special issue). Tectonophysics, 141: 1–275.

Birch, F.S., 1982. Gravity models of the Albuquerque basin, Rio Grande rift, New Mexico. Geophysics, 47: 1185–1197.

Bird, P., 1979. Continental delamination and the Colorado Plateau. J. Geophys. Res., 87: 10557–10568.

Bishop, W.W., 1978. Geological Background to Fossil Man – Recent Research in the Gregory Rift Valley, East Africa. Geol. Soc. Lond., Scottish Academic, Edinburgh, 585 pp.

Blundell, D.J., and A.D. Gibbs (Editors), 1990. Tectonic Evolution of the North Sea Rifts. Clarendon, Oxford. 272 pp.

Bonatti, E., 1987. The rifting of continents. Sci. Amer., 256 (March 1987): 74–81.

Bonatti, E. (Editor), 1988. Zabargad Island and the Red Sea rift (special issue). Tectonophysics, 150: 1–251.

Bond, G.C., and M.A. Kominz, 1988. Evolution of thought on passive continental margins from the origin of geosynclinal theory (~1860) to the present. Geol. Soc. Am. Bull., 100: 1909–1933.

Bott, M.H.P. (Editor), 1976. Sedimentary basins of continental margins and cratons (special issue). Tectonophysics, 36: 1–314.

Brunnacker, K., and M. Taieb (Editors), 1992. Graben, Geology and Geomorphogenesis (special issue). Z. Geomorph., Supplementband 42: 1–226.

Buck, W.R., 1991. Modes of continental lithospheric extension. J. Geophys. Res., 96: 20161-20178.

Bullard, E.C., 1936. Gravity measurements in East Africa. Phil. Trans. Roy. Soc. Lond., 235: 445–531.

Burgess, C.F., B.R. Rosendahl, S. Sander, C.A. Burgess, J Lambiase, S. Derksen, and N. Meader, 1988. The structural and stratigraphic evolution of Lake Tanganyika: A case study of continental rifting. In: W. Manspeizer, (editor), Triassic–Jurassic Rifting – Continental Breakup and the Origin of the Atlantic Ocean and Passive Margins, Part B, Elsevier, Amsterdam, pp. 859–881.

Burk, C.A., and C.L. Drake (Editors), 1974. The Geology of Continental Margins. Springer-Verlag, New York, 1009 pp.

Burke, K., 1977. Aulacogens and continental breakup. Ann. Rev. Earth Planetary Sci., 5: 371–396.

Burke, K., 1980. Intracontinental rifts and aulacogens. In: Panel on Continental Tectonics (Editors), Continental Tectonics, National Academy of Sciences Studies in Geophysics, Washington, DC., pp. 42–49.

Burke, K., and J.F. Dewey, 1973. Plume generated triple junctions: key indicators in applying plate tectonics to old rocks. J. Geol. 81: 406–433.

Burke, K., J.F. Dewey, and W.S.F. Kidd, 1977. World distribution of sutures — the sites of former oceans. Tectonophysics, 40: 69–99.

Burke, K., L. Delaro, J.F. Dewey, A. Edelstein, W.S.F. Kidd, K.D. Nelson, A.M.C. Sengör, and J. Stroup, 1978. Rifts and Sutures of the World. NASA contract rept. #NAS5–24094, Goddard Space Flight Center, Greenbelt, 238 pp.

Cloetingh, S., O. Eldholm, B.T. Larsen, R.H. Gabrielsen, and W. Stassi (Editors). Dynamics of extensional basin formation and inversion (special issue). Tectonophysics, 240: 1–341.

Cloos, H., 1939. Hebung, Spaltung, Vulkanismus. Geol. Rundsch. 30: 401–527, 637–640.

Coffin, M.F., and O. Eldholm, 1994. Large igneous provinces: Crustal structure, dimensions, and external consequences. Revs. Geophys, 32: 1–36.

Courtillot, V., 1982. Propagation rifts and continental breakup. Tectonics, 1: 239–250.

Coward, M.P., J.F. Dewey, and P.L. Hancock (Editors), 1987. Continental Extensional Tectonics. Geol. Soc. Sp. Publ. No. 28, Blackwell, Oxford, 637 pp.

de Lapparent, A. 1887. Conference sur le sens des mouvements de l'ecoree terrestre. Bull. Soc. Geol. Fr. erd Ser. 15: 220

de Lapparent, A. 1898. Soulivements et Affaissements. Rev. Questions Sci., 14: 5–33.

de Martonne, E., 1897. Die hydrographie des oberen Nilbeckers. Z. Ges. Erdkd., 32: 315.

Dewey, J.F., 1977. Suture zone complexes: a review. Tectonophysics, 40: 53–77.

Dons, J.A., and B.T. Larsen (Editors), 1978. The Oslo Paleorift – A Review and Guide to Excursions. Norges Geol. Under., No. 337, 199 pp.

Drake, C.L., and R.W. Girdler, 1982. History of rift studies. In: G. Pálmason (Editor), Continental and Oceanic Rifts, AGU Geodynamics Ser., 8: 5–15.

Ebinger, C.J., 1989a. Geometric and kinematic development of border faults and accommodation zones, Kivu-Rusizi rift, Africa. Tectonics, 8: 117–133.

Ebinger, C.J., 1989b. Tectonic development of the western branch of the East African rift system. Geol. Soc. Am. Bull., 101: 885–903.

Ebinger, C.J., B.R. Rosendahl, and D.J. Reynolds, 1987. Tectonic model of the Malawi rift, Africa. Tectonophysics, 141: 215–235.

Élie de Beaumont, Léonce, 1827. Observations geologiques. Ann. Mines, 2: 5–82.

Élie de Beaumont, Léonce, 1830. Memoire. Ann. Sci. Nat. Vol. 18–19.

Élie de Beaumont, Léonce, 1841. Explication de la Carte Géologique de la France. Vol. I, "Les Vosges."

Élie de Beaumont, Léonce, 1844. Note sur le rapport qui existe le refroidissement progressif de la masse du globe terrestre et celui de la surface. C. R. Acad. Sci. Paris 19: 1327–1331.

Élie de Beaumont, Léonce, 1847. Note sur les systemes de montagnes les plus anciens de l'Europe. Bull. Soc. Geol. Fr. 2nd ser., 4: 864–991.

Falcon, N.L., I.G. Gass, R.W. Girdler, and A.S. Laughton (Editors), 1970. Structure and evolution of the Red Sea and the nature of the Red Sea, Gulf of Aden and Ethiopian Rift junction (special issue). Philos. Trans., Roy. Soc. London, A267: 1–417.

Freund, R., and Z. Garfunkel (Editors), 1981. The Dead Sea rift (special issue). Tectonophysics, 80: 1–303.

Froidevaux, C., and Tan Tjong Kie (Editors), 1987. Deep internal processes and continental rifting (special issue). Tectonophysics, 133: 165–331.

Frostick, L.E., R.W. Renaut, I. Reid, and J.J. Tiercelin (Editors), 1986. Sedimentation in the African Rifts. Geol. Soc. Spec. Pub. 25, Blackwell, Oxford, 382 pp.

Gangi, A.F. (Editor), 1991. World Rift Systems. Tectonophysics, 197: 99–392.

Gass, I.C. 1978. Crustal and mantle processes: Red Sea case study. Open University, Milton Keynes, 142 pp.

Gibb, R.A., W.J. Hinze, and M.D. Thomas (Editors), 1994, Potential field studies of continental rifts: the Great Lakes region (special section). Can. J. Earth Sci., 31: 617–720.

Girdler, R.W., 1958. The relationship of the Red Sea to the East African rift system. Geol. Soc. London Quart. J. 114: 79–105.

Girdler, R.W., 1964. Geophysical studies of rift valleys. Phys. Chem. Earth, 5: 121–156.

Girdler, R.W. (Editor), 1972. East African rifts (special issue). Tectonophysics, 15: 1–179.

Greene, M.T., 1982. Geology in the Nineteenth Century. Cornell Univ. Press, Ithaca and London, 324 pp.

Gregory, J.W., 1894. Contributions to the physical geography of British East Africa. Geogr. J. Lond. 4: 290–315.

Gregory, J.W., 1896. The Great Rift Valley. Murray, London, 422 pp.

Gregory, J.W., 1920. The African rift valleys. Geogr. J. Lond. 54: 13–47.

Gregory, J.W., 1921. The Rift Valleys and Geology of East Africa. Seeley, Service, London, 479 pp.

Gregory, J.W., 1923. The structure of the Great Rift Valley. Nature 112: 514–516.

Hallam, A., 1973. A Revolution in the Earth Sciences, From Continental Drift to Plate Tectonics. Clarendon, Oxford, 127 pp.

Hawley, J.W. (Editor), 1978. Guidebook to Rio Grande rift in New Mexico and Colorado. New Mexico Bureau Mines Mineral Res., Circ. 163: 241 pp.

Heezen, B.C., 1960. The rift in the Ocean floor. Sci. Amer., 203: 98–110

Heezen, B.C., 1969. The World Rift System: an introduction to the symposium. Tectonophysics, 8: 269–280.

Hinze, W.J., Allen, D.J., Braile, L.W., and Mariano, J., 1995, Overview of the Midcontinent Rift system:. In: R.W. Ojakangas, A.B. Dickas, and J.C. Green (Editors), Late Precambrian and Cambrian Rifting in Middle North America. Geol. Soc. Am. Spec. Pap., in press.

Holmes, A., 1944. Principles of Physical Geology (1st ed.). Nelson, London. 532 pp.

Holmes, A., 1965. Principles of Physical Geology (2nd ed.). Ronald Press, New York.1288 pp.

Illies, J.H., 1969. An inter continental belt of the World Rift System. Tectonophysics, 8: 5–29.

Illies, J.H. (Editor), 1981. Mechanism of graben formation (special issue). Tectonophysics, 73: 1–266.

Illies, J.H., and St. Mueller (Editors), 1970. Graben Problems. International Upper Mantle Project, Scient. Rept. 27. Schweizerbart, Stuttgart. 316 pp.

Illies, J.H., and K. Fuchs (Editors), 1974. Approaches to Taphrogenesis. Inter-Union Commission of Geodynamics, Scientific Rept. 8. Schweizerbart, Stuttgart. 460 pp.

Irvine, T.N. (Editor), 1966. The World Rift System (1965 International Upper Mantle Project Symposium). Geological Survey of Canada paper no. 66-14. Ottawa. 471 pp.

Jeffreys, H., 1929. The Earth: It's Origin, History and Physical Constitution (2nd ed.). Macmillian, New York, 346 pp.

Johnston, A.C., 1989. The seismicity of 'stable continental interiors'. In: S. Gregersen and P.W. Basham (Editors), Earthquakes at North-Atlantic Passive Margins: Neotectonics and Postglacial Rebound, NATO ASI Series vol., 266, Kluwer, Dordrecht, pp. 299-327.

Johnston, A.C., and Kanter, L.R., 1990. Earthquakes in stable continental crust. Sci. Amer., 262: 68-75.

Kampunzu, A.B., and R.T. Lubala (Editors), 1991. Magmatism in Extensional Structural Settings. Springer–Verlag, Berlin, pp.

Katz, B.J., 1991. Lacustrine Basin Exploration–Case Studies and Modern Analogs. Am. Assoc. Petroleum Geol., Mem. 50, AAPG, Tulsa. 340 pp.

Keen, C.E., 1985. The dynamics of rifting: deformation of the lithosphere by active and passive driving forces. Geophys. J. R. astron. Soc., 80: 95–120.

Keller, G.R. (Editor), 1986. The Rio Grande Rift (special section). J. Geophys. Res., 91(B6): 6142–6345.

Keller, G.R., and S.M. Cather (Editors), 1994. Basins of the Rio Grande rift: Structure, Stratigraphy and Tectonic Setting. Geol. Soc. Am. Spec. Pap., 291, 308 pp.

Keller, G.R., P. Morgan, and W.R. Seager, 1990. Crustal structure, gravity anomalies and heat flow in the southern Rio Grande rift and their relationship to extensional tectonics. Tectonophysics, 174: 21–37.

Knopoff, L., B.C. Heezen, and G.J.F. MacDonald (Editors), 1969. The World Rift System (special issue). Tectonophysics, 8: 267–577.

Krenkel, E., 1922. Die Bruchzonen Ostafrikas: Tektonik, Vulkanismus, Erdbeben und Schwereanomalien. Borntrager, Berlin, 184 pp.

Krenkel, E., 1924. Die Bruchzonen Ostafrikas. Geol. Rundsch. 14: 209–232.

Kovach, R.L., and Z. Ben–Avraham (Editors), 1990. Geologic and tectonic processes of the Dead Sea rift zone (special issue). Tectonophysics, 180: 1–137.

Lambiase, J.J. (Editor), 1994. Hydrocarbon Habitat in Rift Basins. Geol. Soc. Sp. Publ. No. 80, Geological Society Publishing House, Bath, 371 pp.

Landon, S.M., 1994. Interior Rift Basins. Am. Assoc. Petroleum Geol., Mem. 59, AAPG, Tulsa. 276 pp.

Leeman, W.P., and J.G. Fitton, 1989. Magmatism associated with lithospheric extension (special section). J. Geophys. Res., 94: 7682–7986.

Le Pichon, X., and J.R. Cochran, 1988. The Gulf of Suez and Red Sea rifting (special issue). Tectonophysics, 153: 1–320.

Lipmann, P.W., N.A. Logatchev, Y.A. Zorin, C.E. Chapin, V. Kovalenko, and P. Morgan, 1989. Intracontinental rift comparisons: Baikal and Rio Grande rift systems. Eos, Trans. Am. Geophys. Un. 70 (no. 19): 578–579, 586–588.

Logatchev, N.A., and P. Mohr (Editors), 1978. Geodynamics of the Baikal rift zone (special issue). Tectonophysics, 45: 1–105.

Logatchev, N.A., and H.J. Zwart (Editors), 1990. Intracontinental mountainous terranes: Geological and geophysical aspects (special issue). J. Geodynamics, 11: 275–396.

Lucchitta, I., and P. Morgan (Editors), 1990. Heat and detachment in continental extension (special issue). Tectonophysics, 174: 1–206.

Lynch, H.D., and P. Morgan, 1987. The tensile strength of the lithosphere and the localization of extension. In: M.P. Coward, J.F. Dewey, and P.L. Hancock (Editors), Continental Extensional Tectonics, Geol. Soc. Sp. Publ. No. 28, Blackwell, Oxford, pp. 53–65.

Macdougall, J.D., (Editor), 1988. Continental Flood Basalts. Kluwer, Dordrecht, 341 pp.

Macdougall, J.D., 1992. Continental flood basalts. In: W.A. Nierenberg (Editor), Encyclopedia of Earth System Science. Academic, San Diego. Vol. 1: 609–613.

Makris, J., P. Mohr, and R. Rihm (Editors), 1991. Red Sea: Birth and early history of a new oceanic basin. Tectonophysics, 198(2–4): 129–468.

Manspeizer, W., (Editor), 1988. Triassic–Jurassic Rifting – Continental Breakup and the Origin of the Atlantic Ocean and Passive Margins, Parts A and B, (2 Vols.), Elsevier, Amsterdam, 1000 pp.

Mayer, L. (Editor), 1986. Extensional Tectonics of the Southwestern United States: A Perspective on Processes and Kinematics. Geol. Soc. Am. Spec. Pap., 208, 122 pp.

McKenzie, D., 1978. Some remarks on the development of sedimentary basins. Earth Planet. Sci. Lett., 40: 25–32.

Milanovsky, E.E., 1981. Aulacogens of ancient platforms: problems of their origin and tectonic development. Tectonophysics, 73: 213–248.

Milanovsky, E.E., 1983. Major stages of rifting evolution in the Earth's history, Tectonophysics, 94: 599–607.

Moretti, I. and Froidevaux, C., 1986. Thermomechanical models of active rifting. Tectonics, 5: 501-511.

Mohr, P., 1982. Musings on continental rifts. In: G. Pálmason (Editor), Continental and Oceanic Rifts, AGU Geodynamics Ser., 8: 293–309.

Mohr, P., 1991. The discovery of African rift geology: A summary. In: A.B. Kampunzu and R.T. Lubala (Editors), Magmatism in Extensional Structural Settings. Springer–Verlag, Berlin, pp. 11–22.

Mohr, P., 1992. A continental rift centenary. Geology, 20: 94–95.

Morgan, P., and B.H. Baker, (Editors), 1983. Processes of Continental Rifting (special issue). Tectonophysics, 94: 680 pp.

Morgan, P., W.R. Seager, and M.P. Golombeck, 1986. Cenozoic thermal, mechanical and tectonic evolution of the Rio Grande rift. J. Geophys. Res., 91: 6263–6276.

Morton, A. C. and Parson, L. M. (Editors), 1988. Early Tertiary volcanism and the opening of the NE Atlantic. Geol. Soc. London Spec. Publ., 39, 477 pp.

Nelson, R.A., T.L. Patton, and C.K. Morley, 1992. Rift-segment interaction and its relation to hydrocarbon exploration in continental rift systems. Am. Assoc. Petroleum Geol. Bull., 76: 1153–1169.

Neumann, E.–R., and I.B. Ramberg (Editors), 1978. Petrology and Geochemistry of Continental Rifts. Riedel, Dordrecht, 296 pp.

Neumann, E.–R. (Editor), 1990. Rift zones in the continental crust of Europe–geophysical, geological and geochemical evidence: Oslo–Horn graben (special issue). Tectonophysics, 178: 1–126.

Newman, G.W., and H.D. Goode (Editors), 1979. Basin and Range Symposium and Great Basin Field Conference. Rocky Mountain Assoc. Geologists, Denver. 662 pp.

Obst, E., Der östliche Abschnitt der grossen östafrikanischen Storungszone. Mitt. Geogr. Ges. Hamburg, 28: 187.

Ojakangas, R.W., A.B. Dickas, and J.C. Green (Editors), 1995. Late Precambrian and Cambrian Rifting in Middle North America. Geol. Soc. Am. Spec. Pap., in press.

Okaya, D.A., and G.A. Thompson, 1985. Geometry of Cenozoic extensional faulting: Dixie Valley, Nevada. Tectonics, 4: 107–125.

Okaya, D.A., and G.A. Thompson, 1986. Involvement of deep crust in extension of Basin and Range Province. Geol. Soc. Am. Spec. Pap., 208: 15–22.

Olsen, K.H., 1992. Continental rifting. In: W.A. Nierenberg (Editor), Encyclopedia of Earth System Science. Academic, San Diego. Vol. 1: 627–641.

Pálmason, G. (Editor), 1982. Continental and Oceanic Rifts, AGU Geodynamics Ser. v. 8, Am. Geophys. Un., Washington, 309 pp.

Pilger, A., and A. Rösler (Editors), 1975. Afar Depression of Ethiopia. Inter-Union Commission of Geodynamics, Scientific Rept. 14. Schweizerbart, Stuttgart. 416 pp.

Pilger, A., and A. Rösler (Editors), 1976. Afar Between Continental and Oceanic Rifting. Inter-Union Commission of Geodynamics, Scientific Rept. 16. Schweizerbart, Stuttgart. 216 pp.

Pritchard, H.M., T. Alabaster, N.B.W. Harris, and C.R. Neary (Editors), 1993. Magmatic Processes and Plate Tectonics. Geol. Soc. Sp. Publ. No. 76, Geological Society Publishing House, Bath, 526 pp.

Prodehl, C., G.R. Keller, and M.A. Khan (Editors), 1994. Crustal and upper mantle structure of the Kenya rift (special issue). Tectonophysics, 236, 483 pp.

Quennell, A.M. (Editor), 1982. Rift Valleys: Afro-Arabian. Benchmark series in geology, Vol. 60, Hutchinson Ross, Stroudsburg, 419 pp.

Quennell, A.M. (Editor), 1985. Continental Rifts. Benchmark series in geology, Vol. 90, Van Nostrand Reinhold, New York, 349 pp.

Quennell, A.M., 1987. Rift valleys. In: C.K. Seyfert (Editor), The Encyclopedia of Structural Geology and Plate Tectonics, Van Nostrand Reinhold, New York, pp. 671–688.

Raleigh, C.B. (Editor), 1989. Margins: A Research Initiative for Interdisciplinary Studies of Processes Attending Lithospheric Extension and Convergence. National Academy of Sciences, Washington, 285 pp.

Ramberg, I.B., 1976. Gravity Interpretation of the Oslo Graben and Associated Igneous Rocks. Norges Geol. Under., No. 325, 194 pp.

Ramberg, I.B., E.E. Milanovsky, and G. Qvale (Editors), 1987. Continental Rifts—Principal and Regional Characteristics. Tectonophysics, 143: 252 pp.

Ramberg, I. B., and Morgan, P., 1984. Physical characteristics and evolutionary trends of continental rifts. Proceedings of the 27th Internat. Geol. Congress, 7: 165-216.

Ramberg, I.B., and E.-R. Neumann (Editors), 1978. Tectonics and Geophysics of Continental Rifts. Riedel, Dordrecht, 444 pp.

Riecker, R.E. (Editor), 1979. Rio Grande Rift: Tectonics and Magmatism. American Geophysical Union, Washington. 438 pp.

Rosendahl, B.R., 1987. Architecture of continental rifts with special reference to East Africa. Ann. Rev. Earth Planet. Sci., 15: 445–503.

Rosendahl, B.R., 1989a. Continental rifting: Types and rates. In: D.E. James (Editor). The Encyclopedia of Solid Earth Geophysics. Van Nostrand Reinhold, New York,. pp 97–104.

Rosendahl, B.R., 1989b. Continental rifts: Structural traits. In: D.E. James (Editor). The Encyclopedia of Solid Earth Geophysics. Van Nostrand Reinhold, New York,. pp 104–126.

Rosendahl, B.R., J.J.W. Rogers, and N.M. Rach (Editors), 1989. African Rifting (special issue). J. African Earth Sciences, v. 8 (nos. 2/3/4), pp. 135–629.

Rosendahl, B.R., E. Kilembe, and K Kaczmarick, 1992. Comparison of the Tanganyika, Malawi, Rukwa and Turkana rift zones from analyses of seismic reflection data. Tectonophysics 213: 235–256.

Rothe, J.P., and K. Sauer (Editors), 1967. The Rhinegraben Progress Report 1967. Abh. geol. Landesamt Baden–Württemberg, Freiburg im Breslau, Vol 6, 148 pp.

Ruppel, C., 1995. Retrospectives, perspectives, and prospectives on rifting processes. J. Geophys. Res., in press.

Scrutton, R. A., (Editor), 1982. Dynamics of passive margins. Geodynamics Series., vol. 6, American Geophysical Union, Washington, DC., 200 pp.

Sengör, A.M.C., and K. Burke, 1978. Relative timing of rifting and volcanism on Earth and its tectonic implications. Geophys. Res. Lett., 5: 419–421.

Shatsky, N.S., and A.A.Bogdanov, 1961. An international tectonic map of Europe, scale 1:2,500,000. Izv. Akad. Nauk SSSR, Ser. Geol. 1961 (4). (in Russian).

Sheridan, R.E. and J.A. Grow (Editors), 1988. The Geology of North America, vol. I-2, The Atlantic continental margin: U. S. Geological Society of America, Boulder, Colorado, 610 pp.

Smith, R.B., and G.P. Eaton (Editors), 1978. Cenozoic Tectonics and Regional Geophysics of the Western Cordillera. Geol. Soc. Am., Memoir 152, 388 pp.

Steinhart, J.S., and T.J. Smith (Editors), 1966. The Earth Beneath the Continents. Amer. Geophys. Un., Geophysical Monograph 10, AGU, Washington. 663 pp.

Storey, B.C., T. Alabaster, and R.J. Pankhurst (Editors), 1992. Magmatism and the Causes of Continental Break-up. Geol. Soc. Sp. Publ. No. 68, Geological Society Publishing House, Bath, 404 pp.

Suess, E., 1880. Über die vermeintlichen säcularen Schwankungen einzelner Theile der Erdoberfläche. Verh. K. K. Geol. Reichanst. Wien, 180 pp.

Suess, E., 1891. Die Brüche des östlichen Afrika. In: Beitrage zur geologischen Kenntniss des östlichen Afrika: Denkschriften Kaiserlichen Akademie Wissenschaften, Wien, Mathematisch–Naturwissen Klasse, 58: 555–584.

Suess, E., 1904–1909. The Face of the Earth. Translated by H.B.C. Sollas, Vol. 1, 1904, 604 pp.; Vol. 2, 1905, 556 pp.; Vol. 3, 1906, 400 pp.; Vol. 4, 1909, pp. Clarendon, Oxford. (First published in German as Das Anlitz der Erde, Vol. 1 1883; vol. 2, 1888; vol. 3, 1901; vol. 4, 1904).

Turcotte, D.L., and S.H. Emmerman, 1983. Mechanisms of active and passive rifting. Tectonophysics 94: 39–50.

Uhlig, C., 1907. Der sogenannte grösse östafrikanische Graben zwischen Magad (Natron–See) und Lawa ja Mwerie (Manjara–See). Geogr. Z., 13: 478–505.

Uhlig, C. 1912. Beitrage zur Kenntniss der Geologie und Petrographie Ost–Afrikas. Centralbl. Mineral. 1912: 565.

van Verweke, L., 1913. Die Entstehung des Mittelrheintales und der mittelrheinischen Gebirge. Mitt. Gesellsch. Erdkunde. Kolonialwesen. Strassburg, Vol. 4.

Vening Meinesz, F.A., 1950. Les grabens africains, résultat de compression ou de tension dans la croûte terrestre? Bull. Inst. R. Colonial Belge, 21: 539–552.

Vink, G., W.J. Morgan, and Wu-Ling Zhao. 1984. Preferential rifting of continents: a source of displaced terranes. J. Geophys. Res., 89: 10072–10076.

von Höhnel, L., A. Rosiwal, F. Toula, and E. Suess, 1891. Beitrage zur geologischen Kenntniss des östlichen Afrika: Denkschriften Kaiserlichen Akademie Wissenschaften, Wien, Mathematisch–Naturwissen Klasse, 58: 447–584.

Watkins, J.S., L. Montadert, and P.W. Dickerson (Editors), 1979. Geological and Geophysical Investigations of Continental Margins. AAPG Memoir 29. Am. Assoc. Petroleum Geologists, Tulsa, 479 pp.

Wernicke, B., 1985. Uniform-sense normal simple shear of the continental lithosphere. Can. J. Earth Sci., 22: 108-125.

Wernicke, B.P. (Editor), 1990. Basin and Range Extensional Tectonics Near the Latitude of Las Vegas, Nevada. Geol. Soc. Am., Memoir 176, 511 pp.

White, R.S., and D.P. McKenzie, 1989. Volcanism at rifts. Sci. Amer., 261 (July 1989): 44–59.

Williams, L.A.J., 1989. Rift valley volcanism. In: D.R. Bowes (Editor). The Encyclopedia of Igneous and Metamorphic Petrology. Van Nostrand Reinhold, New York,. pp 513–518.

Willis, B., 1928. The Dead Sea problem: rift valley or ramp valley. Geol. Soc. America Bull., 39: 452–490.

Willis, B., 1936. East African Plateaus and Rift Valleys. Carnegie Inst. Washington Pub. 470, Washington, DC, 358 pp.

R.J. Wold, and W.J. Hinze, (Editors), 1982. Geology and Tectonics of the Lake Superior Basin. Geol. Soc. Am. Memoir 156, 280 pp.

Wood, R.M., 1985. The Dark Side of the Earth. Allen and Unwin, London, 246 pp.

Ziegler, P., 1990. Geological Atlas of Western and Central Europe, 2nd Ed. Shell Int. Pet. Mij., distributed by Geol. Soc. Publ. House, Bath, 239 pp + maps.

Ziegler, P. (Editor), 1992a. Geodynamics of rifting, Volume 1. Case history studies on rifts: Europe and Asia (special issue). Tectonophysics, 208: 1–363.

Ziegler, P. (Editor), 1992b. Geodynamics of rifting, Volume II. Case history studies on rifts: North and South America and Africa (special issue). Tectonophysics, 213: 1–284.

Ziegler, P. (Editor), 1992c. Geodynamics of rifting, Volume III. Thematic discussions (special issue). Tectonophysics, 208: 1–253.

Chapter 2

Mechanisms of rifting: Geodynamic modeling of continental rift systems

M. H. P. Bott

2.1. Introduction

This chapter focuses on modeling of the geodynamics of continental rifting and associated plateau uplift. Over thirty years ago the central problem was to determine whether rifting was compressive or extensional in origin. It is now firmly established from earthquake mechanisms and geological evidence that the present-day plate-interior major rift structures are extensional. It has also been recognized that the modern rift systems are associated with major anomalous structures beneath the lithosphere. These include *both* thinning of the lithosphere with upwelling of the asthenosphere, *and* regions of anomalously low P-velocity and density within the asthenosphere possibly extending down to the top of the mantle transition zone at 400 km depth.

The central problem nowadays is to establish how continental rifting and its associated structures are initiated. Following on from this, we are confronted with the following problems concerning the development of rift systems:

(1) How does the anomalous upper mantle beneath the lithosphere form and develop?

(2) How does the tensional stress system originate?

(3) How does the lithosphere become thinned?

(4) What is the mechanics of the extensional deformation of the lithosphere, and particularly how does the rifting occur?

(5) How do flank uplifts form?

There are widely differing hypotheses on these problems and it is important to seek critical evidence from geology (history of development and present structure) and geophysics (structure of the crust and underlying mantle).

2.2. Initiation

The mechanism of initiation of rifting is the central problem. Proposed mechanisms fall into two groups, active and passive (Sengör and Burke, 1978), illustrated in Figure 2–1. In the passive hypothesis, lithospheric tension of distant origin causes failure of the continental lithosphere and consequent development of the anomalous underlying upper mantle. In the active hypothesis, the anomalous upper mantle develops first by some form of convective upwelling, and the doming, volcanism and extension are consequent. Either way, gross lithospheric failure is involved. Kusznir and Park (1984) have shown that this can readily take place for realistic models of the continental lithosphere and realistic levels of deviatoric tension provided that the lithosphere is relatively hot and thin.

The *passive hypothesis* depends on the primary occurrence of a sufficiently large deviatoric tension in the lithosphere to cause gross lithospheric failure. The tension is not of local origin, being attributable to a mechanism external to the rift region. The lithosphere fails in tension and finite extension occurs. Vertical movements then occur according to

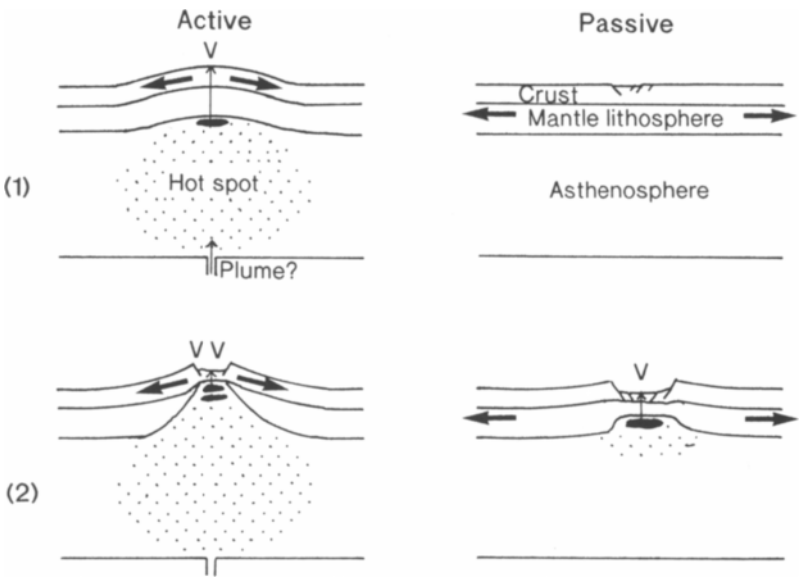

Fig. 2–1. Idealized diagrams comparing the active and passive hypotheses for initiation of continental rifting. (1) shows the initial stage for both hypotheses, and (2) shows a subsequent stage of development. The stippling indicates hot, low density regions of the sub-lithospheric upper mantle; V denotes volcanism.

the McKenzie (1978) theory of sedimentary basin formation, in response to gross thinning of the lithosphere and upwelling of the asthenosphere. Instantaneous crustal thinning by stretching and faulting causes local subsidence, and accompanying rise of the asthenosphere and heating of the lithosphere causes uplift. Subsidence outweighs uplift except where the ratio of lithospheric to crustal thickness exceeds about 7.0, that is the crust is less than about 16 km thick for normal lithosphere or the lithosphere is thicker than about 250 km for normal continental crust. Subsequently, slow thermal subsidence occurs as the lithosphere cools and thickens.

There are various modifications of the passive hypothesis as follows: (1) A finite rate of extension (Jarvis and McKenzie, 1980) increases the subsidence during the stretching stage and decreases the subsequent thermal subsidence; (2) faulting and flexural effects modify the basin geometry (Watts et al., 1982); (3) allowing for lateral heat flow causes slight transient flank uplift and reduces the thermal subsidence (Watts et al, 1982); (4) different amounts of extension of the upper and lower lithosphere alters the balance between stretching and thermal subsidence, and in particular greater extension of the lower lithosphere can explain anomalously high observed thermal subsidence (Royden and Keen, 1980); (5) small-scale convection in the asthenosphere beneath the stretched part of the lithosphere can further thin the lithosphere and also widen the asthenospheric upbulge provided that the viscosity is less than 10^{20} Pa s, thus simulating the effect of differential stretching (Keen, 1987); (6) the stretched region of the upper crust may be offset from the ductile stretching of the lower crust and mantle part of the lithosphere, such as in the simple shear model of Wernicke (1985), or in a more complicated manner involving detachments as reviewed by Lister et al. (1991).

The passive hypothesis with its modifications explains the formation of passive margins segments away from hot spot regions (see Chapter 11), and certain rift structures possibly such as those of the

North Sea and the Gulf of Suez. In these examples, overall subsidence occurs in the stretched region as predicted, with the possibility of small flank uplifts developing as a result of lateral heat conduction or small scale convection as discussed later. However, it is not obvious how the passive hypothesis can account for modern continental rifts associated with doming or plateau uplift or epeirogenic uplift such as western North America, East Africa or Baikal. The underlying anomalous low density regions below the lithosphere which support the regional doming are very much larger than would be expected for simple lithospheric stretching.

The *active hypothesis* explains volcanism, plateau uplift and rifting primarily as a consequence of the formation of an anomalously hot and low density region in the underlying upper mantle - a hot spot. This may result from a narrow plume originating below 400 km depth. Once the anomalous upper mantle has formed, processes proceed as follows. Upwelling gives rise to partial fusion which causes volcanism. Doming occurs as the anomalous low density region develops. Thus doming and/or volcanism should be the first detectable events. The uplifted dome and its deep isostatic compensation give rise to local deviatoric tension in the lithosphere. As the lithosphere thins by heating up, the stress becomes concentrated into the relatively thin strong layer near the surface, with consequent stretching and faulting. The local tensional stress may be supplemented by regional stresses such as are caused by plate boundary forces.

Magma generation in passive rifting occurs as a result of decompression melting in asthenospheric material which upwells as the lithosphere thins by stretching, according to the mechanism of McKenzie and Bickle (1988). Magma generation in active rifting probably predominantly occur as a result of decompression melting in the upper part of the rising plume or other diapiric upwelling within the hot upper mantle. It may also occur at a later stage as in passive rifting, although the McKenzie-Bickle mechanism may have been overemphasized in discussion of active rifting.

Both hypotheses leave underlying problems unanswered. The passive hypothesis requires a sufficiently large tension to cause relatively strong normal sea-level continental lithosphere to fail; possible sources of tension are discussed later. The active hypothesis requires the initial development of the underlying hot spot as discussed in the next section. Compromises between both types of origin seem possible (see below).

The most obvious test of the initiating mechanism is evaluation of the geological history of evolution of the region. Where active mechanisms apply, volcanism should be the first detectable event and the development of a low density mantle with some initial surface uplift should precede rifting; from the onset, the affected stretched region and its flanks should exhibit uplift rather than subsidence, except that the base of the rift depressions may subside below sea level as the rift develops as a result of sediment loading. On the other hand, passive mechanisms require the faulting to precede the volcanism and regional vertical movements, and the stretched region should exhibit subsidence at all stages even without sediment loading, except for local flank uplifts.

It needs to be emphasized that the active and passive hypotheses apply only to the initiation of rift systems, and not to their subsequent development when complicated interaction of processes may occur. Even for initiation, these end-member hypotheses may be too simple. For example, although the Baikal rift system is generally regarded by former Soviet Union workers as of active initiation, nevertheless northwest-southeast deviatoric tension in the plate probably contributed to the initiating stress system. An even more complicated initiation scenario probably applies to the Rio Grande rift and the Basin and Range system as discussed in Chapters 6 and 7.

2.3. Origin of anomalously hot upper mantle (hot spots)

Uplifted continental (and oceanic) swells are the isostatic response to the development of a hot, low density upper mantle beneath, often termed a hot spot. Hot spots (or hot regions) occur where the upper mantle extending from the base of the lithosphere (about 100 km depth) possibly to the top of

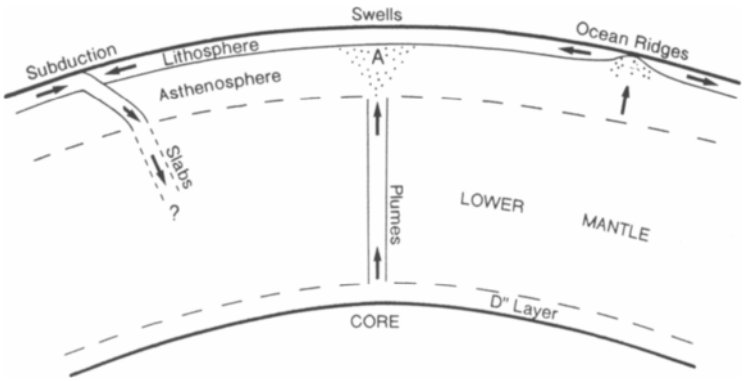

Fig. 2–2. Idealized sketch of the plume hypothesis of mantle convection of Loper (1985), showing the development of a relatively wide hot spot region marked A in the sub-lithospheric upper mantle above the narrow plume.

the mantle transition zone (about 400 km depth) is anomalously hot by the order of 100 K average or more. Taking the volume coefficient of thermal expansion to be 2.7×10^{-5} K^{-1}, the reduction in density for 100 K is about 10 kg/m^3. Assuming the thermal anomaly to extend from 100–400 km depth, this would give rise to a surface uplift of about 900 m on land or 1300 m at sea assuming the hot region is wide enough for local Airy isostasy to apply. If the hot spot is significantly narrower than about 1000 km, the flexural strength of the lithosphere will resist the uplift and cause it to be somewhat less than above. The direct effect of the raised temperature at the base of the lithosphere is to thin the lithosphere and raise the heat flow by about 10 per cent, but this will take about 60 My to become established by thermal conduction, so the effects would not be seen in the early stages of evolution. However, a hot spot may give rise to more extreme local thinning of the lithosphere by other processes as discussed in section 2.6.

The thermal input to the upper mantle required to produce a hot spot is much larger than is generally realized. Taking the specific heat at constant pressure to be 1.25 kJ/kg K, the heat input per square meter required for 100 K rise between 100 and 400 km depths is 1.25×10^{14} J. This is sufficient to supply heat flow of 80 mW/m^2 for 50 My.

How does a hot spot originate? Some sort of convective upwelling in the mantle is the main possibility, but this could be local convection in the upper mantle or deep uprising from the lower mantle. Upper mantle convection would only be expected to redistribute the heat input by thermal conduction from beneath and it is difficult to see how a large heat input could occur by conduction from below over a short time period. The plume hypothesis originating with Morgan (1971) is perhaps the most attractive idea because the heat input into the upper mantle carried by a plume rising from the lower mantle can best account for the rapid input of heat needed to explain development of hot spots over periods of 10 My or less. A useful recent review dealing with plumes and hotspot volcanism has been given by Duncan and Richards (1992).

The concept of plumes rising from a hot boundary layer just above the core-mantle boundary has received much theoretical and experimental support (e.g., Loper and Stacey, 1983; Christensen, 1984; Nataf et al., 1984), and a promising view of gross mantle convection based on plumes rising to form asthenospheric hot spots has been proposed by Loper (1985). This model, which also involves asthenospheric upwelling beneath ocean ridges and a return flow by deeply subducting slabs, is illustrated in Figure 2–2. Thus the plume itself is quite

narrow but the laterally diverging head of heated material in the asthenosphere may have a diameter of over 1000 km.

Hot spots may develop in the upper mantle in back-arc regions above subducting oceanic lithosphere, as a result of upward release of water and/or magma from the top of the subducting slab. The low density upper mantle and thinned lithosphere may give rise to extensional structures such as rifting in some back-arc regions. This type of hot spot may be relevant to the Basin and Range extensional structures and the Rio Grande rift.

2.4. Origin of lithospheric tension

Extensional rifting implies horizontal deviatoric tension. Upper crustal deviatoric tension of the order of 100 MPa is required to produce sediment filled graben of several kilometers thickness (Bott, 1976). Various sources of the tension have been suggested, but the only two types of stress system which appear to be adequate to explain ongoing rifting are lithospheric stress of distant origin appropriate to the passive hypotheses and local loading stress (buoyancy stress) resulting from an underlying low density upper mantle appropriate to an active origin.

The earliest suggestion was that *bending stress* resulting from flexural regional doming would give rise to tension in the upper part of the elastic lithosphere and compression in the lower part. However, Illies (1970) and others have demonstrated that there is insufficient extension available to explain the observed graben subsidence. This "keystone" hypothesis is now generally regarded as inadequate. However, bending stresses resulting from acute bending of the elastic layer caused by faulting may give rise locally to massive brittle failure, greatly reducing the effective elastic thickness of the layer (Marsden et al., 1990).

Another early suggestion appealed to *membrane stress* in the lithosphere (Turcotte, 1974). This is caused by changes in the radii of curvature of a plate as it migrates toward the equator or toward the pole on the surface of a spheroidal Earth. Oxburgh and Turcotte (1974) suggested that the East African rift system may have developed as a result of membrane stress in the African plate as it moved northwards toward the equator. However, other rift systems which have moved away from the equator (Rio Grande, Rhinegraben, Baikal) could not be explained in this way. Further, membrane stress like bending stress is unrenewable and it is doubtful whether there is sufficient extension available. This was an interesting suggestion, but has not been much taken up, probably for the above reasons.

2.4.1. Extensional stress of distant origin (passive hypotheses)

The two main types of renewable tectonic extensional stress of distant origin which have been suggested are convective drag on the base of the lithosphere caused by major cellular convection currents, and plate interior stress caused by plate boundary forces. The distinction between them depends on the style of convection which occurs in the mantle.

Drag on the base of the lithosphere caused by upwelling and diverging convective motion in the underlying upper mantle gives rise to tension above the rising currents and compression above the sinking currents. For example, Nataf et al. (1981), suggested that large scale upper mantle circulation induced by horizontal thermal gradients may cause broad continental extension which may give rise to rifting and break-up. However, plates are probably driven by boundary forces such as ridge push and subduction pull (Forsyth and Uyeda, 1975), when underside drag opposes plate motion and ceases to be relevant as a source of plate interior tension. However, underside drag associated with local advective motion redistributing hot spot material may be a significant factor, as discussed in the next section.

Plate boundary forces give rise to stresses within plate interiors. Notably slab pull and trench suction acting on subducting and overriding plates at subduction zones can give rise to tension (Forsyth and Uyeda, 1975). This may have been an important source of tension in continental lithosphere in past times when subduction was occurring on both sides of a large continental mass such as Pangaea in the early Mesozoic. It may have been an important fac-

tor in continental splitting including the development of rifts prior to passive margin formation. However, at the present time, most normal continental regions appear to be in compression (Zoback et al., 1989), although the stress system in the eastern part of the Eurasian plate is influencing the present development of the Baikal rift system and may have been important at the initiation of this system as described in Chapter 8. Similarly, well-documented changes in regional stresses have influenced the development of the Rhinegraben (Chapter 4). Plate boundary irregularities may give rise to local tension, such as in the vicinity of a bend in a transform fault (e.g. Dead Sea rift) or opposite a sharp bend in the trend of an ocean ridge where the resulting tension may give rise to a failed-arm type of rift (e.g. Benue rift in Nigeria, Chapter 13).

2.4.2 Local extensional stresses caused by hot spots (active hypothesis)

The sub-lithospheric loading caused by anomalously low density upper mantle, normally of thermal origin, gives rise to substantial local deviatoric extensional stress in the strong elastic core of the lithosphere above. This type of stress system as associated with isostatically compensated crustal thickness variation was originally independently recognized by Artyushkov (1973) and by Bott (1971; Bott and Dean, 1972). Bott and Kusznir (1979) and Bott (1992) have shown that such a stress system caused by an anomalous low density upper mantle below the lithosphere can be concentrated into the upper strong part of the continental lithosphere of the uplifted region to produce tension adequate to cause rifting. Tension of this type *must* occur in the crust of continental rift systems associated with updoming, even if their initiation was passive. The problem is to determine whether this is the primary source of the tension (active origin) or not (passive origin).

The mechanism of sub-lithospheric loading is demonstrated in Figure 2–3 which shows a model of an incipient hot spot which gives rise to isostatic doming of 880 m amplitude and also causes deviatoric extensional stress of about 75 MPa in the 20–km–thick strong upper part of the lithosphere. The anomalous principal stresses and shear stresses are shown separately below. The increased normal compressional stress acting on the base of the elastic layer gives rise to the flexural isostatic uplift and contributes a small amount towards the extensional stress in the elastic layer. The most significant contribution to the extensional stress, however, is the outward drag on the base of the elastic layer exerted by the buoyancy driven flow caused by the low density sub-lithospheric load.

Substantial crustal thickening may also give rise to local deviatoric tension and thus to graben formation. Some high plateaus such as Tibet are due to crustal thickening, where the topography and its compensating root give rise to tension (e.g. Froidevaux and Ricard, 1987). Graben formation occurs in this situation as the gravitational energy associated with the compensated uplift is progressively released.

2.4.3. Discussion

Plate boundary forces and local sub-lithospheric loading provide the two most promising explanations of the extensional stress characteristic of continental rift systems. Plate boundary forces are appropriate to rifting associated with passive margin formation and to some of the prominent Mesozoic rifting such as that of the North Sea. Stress resulting from the local sub-lithospheric loading associated with hot spots and surface swells, possibly supplemented by regional plate stress, is most appropriate to some of the present-day uplifted continental rift systems. Lastly, it is important to recognize that the different types of stress system may be superimposed, and in particular stresses caused by (1) topography and density-depth distribution, (2) plate boundary stress systems, and (3) bending and thermal stresses probably combine to cause the actual stresses in most rift systems.

2.5. Modeling lithospheric extension

Thinning of the lithosphere as it extends is an essential feature of the passive mechanism and may also be relevant to active rift formation. Insight into the mechanism of simple lithospheric extension has been obtained by continuum modeling, particularly

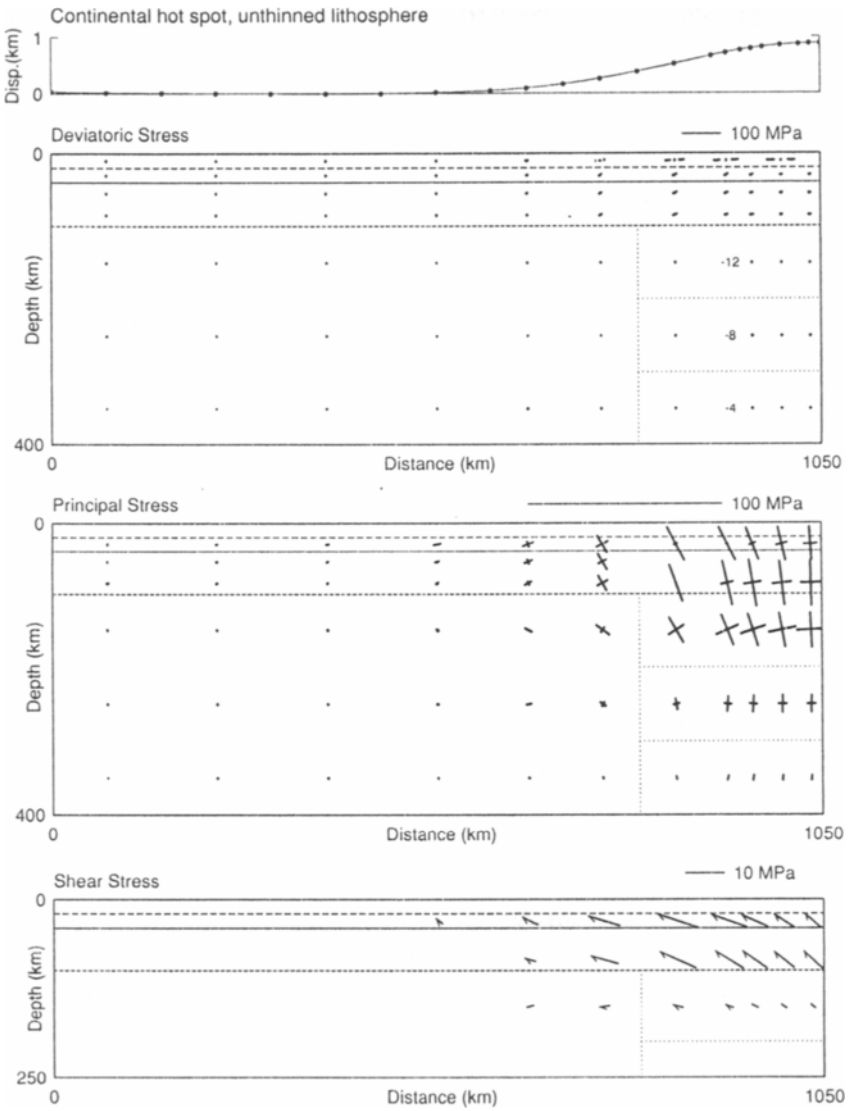

Fig. 2–3. The isostatic surface uplift, deviatoric stresses, anomalous principal pressures and shear stresses caused by a sub-lithospheric region of anomalously low density in the upper mantle, representing a sub-continental hot spot. The deformation and stresses caused by the sub-lithospheric load have been computed by finite element analysis. The right edge of the model is a plane of symmetry, the whole structure being 2100 km wide. The thick broken lines with a dot at the center denote tension and unbroken lines denote compression, with only the nearest to horizontal stress being shown. A solid line denotes the base of the crust and dashed lines denote the base of the elastic upper crust and of the lithosphere. The assumed viscosities are 1023 Pa s for the lower lithosphere and 10^{21} Pa s for the asthenosphere down to 400 km depth. Anomalous densities are in kg/m^3. Further details of the modeling are given by Bott (1992).

following on from the McKenzie (1978) model of basin formation. This type of modeling falls short of reality in that the brittle regions of the lithosphere are treated as a plastic continuum, so that major faults

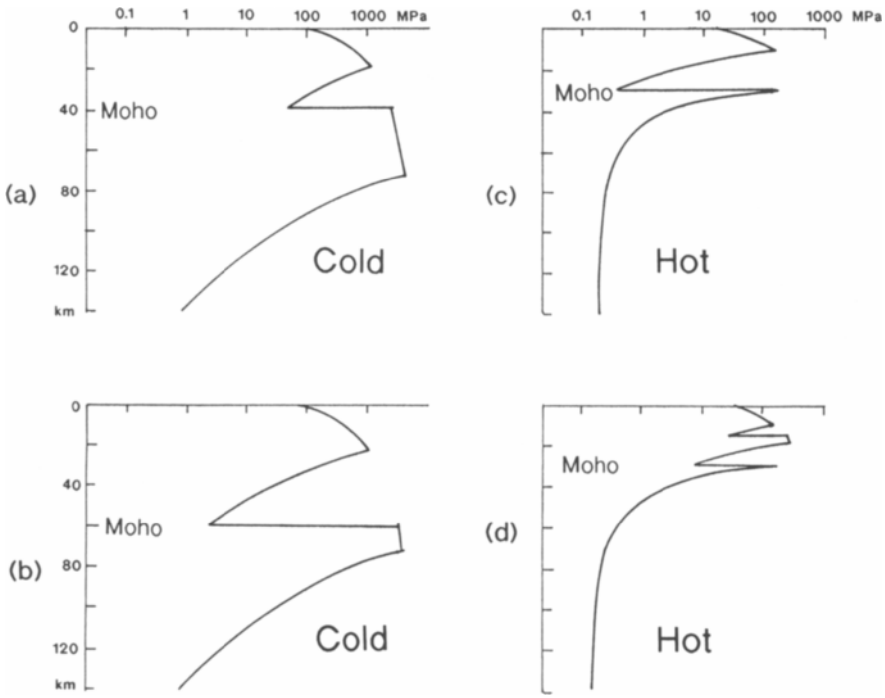

Fig. 2–4. Rheological profiles of the continental lithosphere for cold shield type lithosphere under compression and hot tectonic type of lithosphere under tension, adapted from Ranalli and Murphy (1987). All profiles show strong brittle regions in the upper crust and in the uppermost mantle. Models (a) to (c) assume a granitic quartz-dominated rheology for the crust and an olivine-dominated rheology for the upper mantle, but model (d) includes a lower crustal layer of basic to intermediate composition with plagioclase-dominated rheology. Model (b) has a much thicker crust than model (a).

in the upper crust cannot be included. However, insight is gained into several aspect of extension including temporal and spatial evolution. The two main approaches which have been used are the thin sheet approximation and two-dimensional modeling using numerical methods such as finite element.

The lithosphere-asthenosphere boundary marks the junction between relatively strong and cool lithosphere from the hotter and much weaker asthenosphere, and it is consequently a gradational boundary. It is usually defined by an arbitrary isotherm near to the temperature of onset of partial fusion, such as 90 per cent of the absolute melting temperature.

In simplest terms, the rheology of the continental lithosphere can be summarized in terms of four zones in downward succession as follows: (1) upper crust with quartz-dominant rheology which fails by brittle fracture, with strength increasing with depth according to Byerlee's law; (2) lower crust where the temperature may be high enough for power-law viscous flow to occur; (3) uppermost mantle with olivine-dominant rheology where brittle failure may occur as in the upper crust if the temperature is not too high; and (4) ductile mantle lithosphere at higher temperature deforming by power-law viscous flow. Thus there may be two strong zones in the upper crust and the uppermost mantle separated by a weak zone in the lower crust. A further strong brittle zone may occur within the crust if quartz gives way downwards to a plagioclase dominant rheology. The strong zone in the uppermost mantle is of particular significance in rifting studies as under cool conditions

it offers the greatest resistance to extension. Some examples of rheological profiles of the strength of the continental mantle are shown in Figure 2–4.

The strength of the lithosphere may be defined as the yield strength integrated with respect to depth across its thickness. Apart from the mineralogy, the two factors which influence the lithospheric strength are the temperature-depth profile and the crustal thickness. Higher temperatures and thicker crust both lead to reduced strength. When the applied tectonic force exceeds the lithospheric strength, wholesale lithospheric failure (Kusznir and Park, 1984, 1987) takes place. As the applied force increases further, extension takes place at a finite rate depending on the effective viscosity.

The thin sheet approximation (e.g. England, 1983; Houseman and England, 1986; Sonder and England, 1989; Buck, 1991) assumes that the stretched lithosphere is wide compared to its thickness and that the strain rate is uniform across the thickness of the lithosphere. A rheological profile is constructed for the assumed crustal thickness and geothermal profile. The tectonic force required to give rise to a specified strain rate can then be determined from the rheological profile. Interpolation allows the rate of extension to be determined as a function of applied tectonic force.

There are three main processes which affect the temporal evolution of lithospheric stretching. *First*, the lithosphere becomes thinner and therefore weaker; in absence of opposing effects, this would lead to accelerating thinning producing a narrow rift zone and possibly leading to continental break-up. *Second*, following the adiabatic temperature perturbation on instant stretching, the lithosphere cools as the temperatures re-equilibrate, increasing the strength after sufficient time for the cooling to be effective because weak lower crustal material is replaced by strong olivine-rich upper mantle. *Third*, the changing density-depth distribution as the lithosphere and crust thin produces local loading (buoyancy) stresses which modify the tectonic force causing the deformation. Crustal thinning reduces the extensional tectonic force and thus opposes the stretching. On the other hand, the rise of the low density asthenosphere as stretching proceeds has the opposite effect and enhances the deformation. The crustal effect dominates if the crust is anomalously thick but the asthenospheric effect dominates if the lithosphere is anomalously thick.

The second and the third processes may cause the extending lithosphere to strengthen more rapidly than it is being weakened due to thinning. Such strain hardening may cause the stretching to cease, either terminating the rift zone activity or causing it to migrate laterally to form a wide rift zone. England and his co-workers (papers cited above) and Kusznir and Park (1987) have emphasized the role of thermal effects in opposing stretching and giving rise to wide rift zones. For rapid stretching of 10^{-14} s^{-1} (0.316 Ma^{-1}) or faster, the thermal strengthening is subordinate, producing a narrow rift zone. For slow stretching of 10^{-16} s^{-1} (0.003 Ma^{-1}), cooling is effective possibly leading to lateral migration of stretching to form a wide rift zone. In contrast, Buck (1991) emphasized the importance of buoyancy stresses in controlling formation of narrow or wide rift zones.

An alternative approach to the modeling of extending lithosphere is by two-dimensional modeling of a cross section using analytical or numerical (finite element) methods (e.g. Fletcher and Hallet, 1983; Zuber and Parmentier, 1986; Braun and Beaumont, 1987; Bassi, 1991; Christensen, 1992). This approach makes it possible to study the development of a necking instability resulting from a local weakness such as a small crustal thickening. For instance, Zuber and Parmentier (1986) used a lithospheric model consisting of a strong layer which deforms plastically, overlying a weaker viscous layer, to show how an instability grows to form a rift zone associated with lithospheric thinning. They predicted that the rift zone should be about four times the width of the brittle layer.

An interesting application of the two-dimensional methods is to study multiple necking. In most continental rift systems, there is a single zone of lithospheric failure, or possibly two zones as in East Africa. A more complicated system of lithospheric failures applies to the Basin and Range region of western North America. This was modeled by Fletcher and Hallet (1983) as a series of uniformly spaced regions of lithospheric necking, which are developed if a relatively strong and brittle plastic surface layer is underlain by a viscous lower lithospheric layer

which deforms by power law creep (n=3). They showed that the spacing of the lithospheric failures is 25–60 km for a 10 km thick upper brittle layer. This gives good agreement with the spacing of the basins and ranges as observed. The phenomenon was named "lithospheric boudinage" by Ricard and Froidevaux (1986).

Lithospheric boudinage associated with more complicated rheological distributions has been studied by Ricard and Froidevaux (1986). Zuber et al. (1986) showed that instability at two wavelengths occurred for a lithosphere consisting of a strong upper crust and a strong upper mantle separated by a weak lower crust. Applied to the Basin and Range structure, these more complicated models suggest that the upper crust extends by boudinage with a wavelength of about 40 km, and the upper mantle part of the lithosphere extends by boudinage at a spacing of 150–200 km, with the Moho remaining undisturbed. However, this may not be a good example of normal continental rifting where stretching is much less.

2.6. Thinning of the lithosphere without extension

The asthenospheric upbulge beneath modern rift systems such as East Africa is much larger than can be explained by simple stretching consistent with observed upper crustal extension. This indicates that the lithosphere can be thinned by processes other than extension. A number of mechanisms have been suggested and some of these have been reviewed in detail by Neugebauer (1987). Widening of an existing anomalous asthenospheric upbulge by secondary convection is discussed in section 2.8.

Some mechanisms other than stretching which have been suggested for thinning the lithosphere are as follows:

(1) *Thermal conduction models:* this mechanism involves heating of the lithosphere by thermal conduction from a hot spot below which may move. Models may assume either a high temperature boundary condition at the base of the lithosphere or a high heat flux into it. Crough and Thompson (1976) modeled the lithospheric thinning by the upward migration of a specified isotherm used to mark the boundary. Spohn and Schubert (1983) assumed a 5–10 times greater than normal heat flux into the base of the lithosphere and found a time constant of about 10 My for thinning. The problem with this type of mechanism is that conduction is a very slow process for transferring heat through the lithosphere, and unrealistically high temperature or heat influx at the base is required to account for observed rates of thinning (Neugebauer, 1987).

(2) *Magma injection models*: the lithosphere is heated by magma injection from the underlying partially fused asthenosphere, with associated stretching to accommodate the dikes. This can produce rapid uplift, but Mareschal (1983) has pointed out that the amount of magma required is of the order of 30 per cent by volume to cause even 1 km of uplift.

(3) *Diapiric penetration models*: these involve diapiric upwelling of the relatively low density and low viscosity asthenosphere into the mantle part of the lithosphere, driven by buoyancy forces. There have been a number of suggestions, including the following. Mareschal (1983) demonstrated the feasibility on a realistic time scale but used an unrealistically large density contrast of 200 kg/m^3 between lithosphere and asthenosphere. Turcotte and Emerman (1983) assumed the impingement of a fluid mantle plume on the base of the lithosphere, but found a rather long time scale for the erosion of the lithosphere. Neugebauer (1983) showed that diapiric thinning could occur over about 1 My for more realistic density values, but took rather low values of 10^{18} and 10^{22} Pa s for the viscosity of the asthenosphere and lithosphere respectively. Yuen and Fleitout (1985) assumed a convective plume in the asthenosphere which raised the temperature at the base of the lithosphere by 240 K, and used temperature and pressure dependent viscosity to model thinning of the lithosphere and uplift occurring over a time span of the order of 20 My (see also Fleitout et al., 1986). Moretti and Froidevaux (1986) incorporated non-Newtonian viscosity with a power law of 3 in the mantle and of 7 in the crust (to simulate brittle fracture) to model thinning of the lithosphere and crust in active rifting, with the structure characteristically developing over about 20 My. In all these models,

the time-scale is possibly rather long compared to the observed one unless one or more of the assumptions are extreme.

(4) *Magma-driven diapiric model*: Neugebauer and Reuter (1987) modeled the upward migration of a pool of low density magma below the lithosphere resulting from the buoyancy effects of the magma body and of the associated asthenospheric upbulge, and showed that very rapid time-scales of the development of the lithospheric thinning resulted.

There have thus been recent advances in understanding some possible mechanisms of lithospheric thinning by thermal and diapiric processes, although further improvements in the modeling are needed. The most promising type of model involves diapiric upwelling, progressive conversion of lithosphere to asthenosphere according to a realistic temperature and pressure dependent viscosity, and the buoyant effect of magma. For comparison of the models with observations, we need to know more about the actual time-scale of the thinning, presumably from the evidence provided by igneous rocks. At present, these models are difficult to test.

2.7. Mechanisms of crustal faulting and graben formation

The earliest extensional hypothesis was the wedge subsidence concept as developed by Vening Meinesz (1950). A downward narrowing wedge of continental crust bounded by normal faults dipping at about 60° sinks into the underlying fluid mantle until it reaches isostatic equilibrium, with rim uplifts forming by flexure of the crust outside the faults. Flexure theory predicts a characteristic width of the graben of about 40 km for a 30 km thick elastic crust overlying a fluid upper mantle, and with additional sediment loading subsidence of order of 2 km was calculated. The principal objection to this original form of the wedge subsidence hypothesis is that the predicted root of deep crust projecting into the mantle below the rift has not been observed in seismic experiments, rather the opposite in many regions where the crust is observed to thin.

A modification of the wedge subsidence hypothesis worked out by Bott (1976) proposed that the fault-bounded wedge applies to the brittle upper part of the continental crust, with accompanying ductile stretching and thinning of the lower part of the crust. Calculations were based on the assumption that subsidence will cease when a state of minimum potential (gravitational plus strain) energy is attained. It was shown that significant subsidence depends on low effective friction on the faults. The maximum attainable subsidence increases with the applied deviatoric tension and with the narrowness of the graben. Thus a 30–km–wide graben with sediment loading has a maximum subsidence of about 5 km for a deviatoric tension of 100 MPa. When maximum subsidence is approached, further extensional activity would need to migrate laterally, giving a form of strain hardening additional to those discussed in section 2.5.

The effectiveness of the wedge subsidence mechanism has been demonstrated by finite element analysis (Fig. 2–5), as described by Bott (1992) where further detail is given. This model is driven by deviatoric tension in the upper crust produced by a low density underlying upper mantle (hot spot) with asthenospheric upbulge reaching the base of the crust. Superimposed on the regional swell of 1.7 km elevation produced in absence of faulting, the graben subsidence is 3 km without sediment loading and flank uplift is 1 km. With sediment loading, subsidence above 8 km would occur. This model and others described by Bott (1992) emphasize the importance of a relatively low viscosity structure below the fault wedge to permit it to move sufficiently rapidly.

It is now known that upper crustal extension is normally asymmetrical, with dominance of the half-graben rather than the symmetrical sinking wedge. Half-grabens have been associated with listric faulting and/or shallow detachment faults. However, the general mechanical principles worked out for symmetrical wedges should also apply in principle to half grabens and their evolution.

In the Wernicke (1985) model of crustal extensional faulting, upper crustal asymmetrical faulting passes down into a detachment surface which allows the extension of the ductile part of the lithosphere

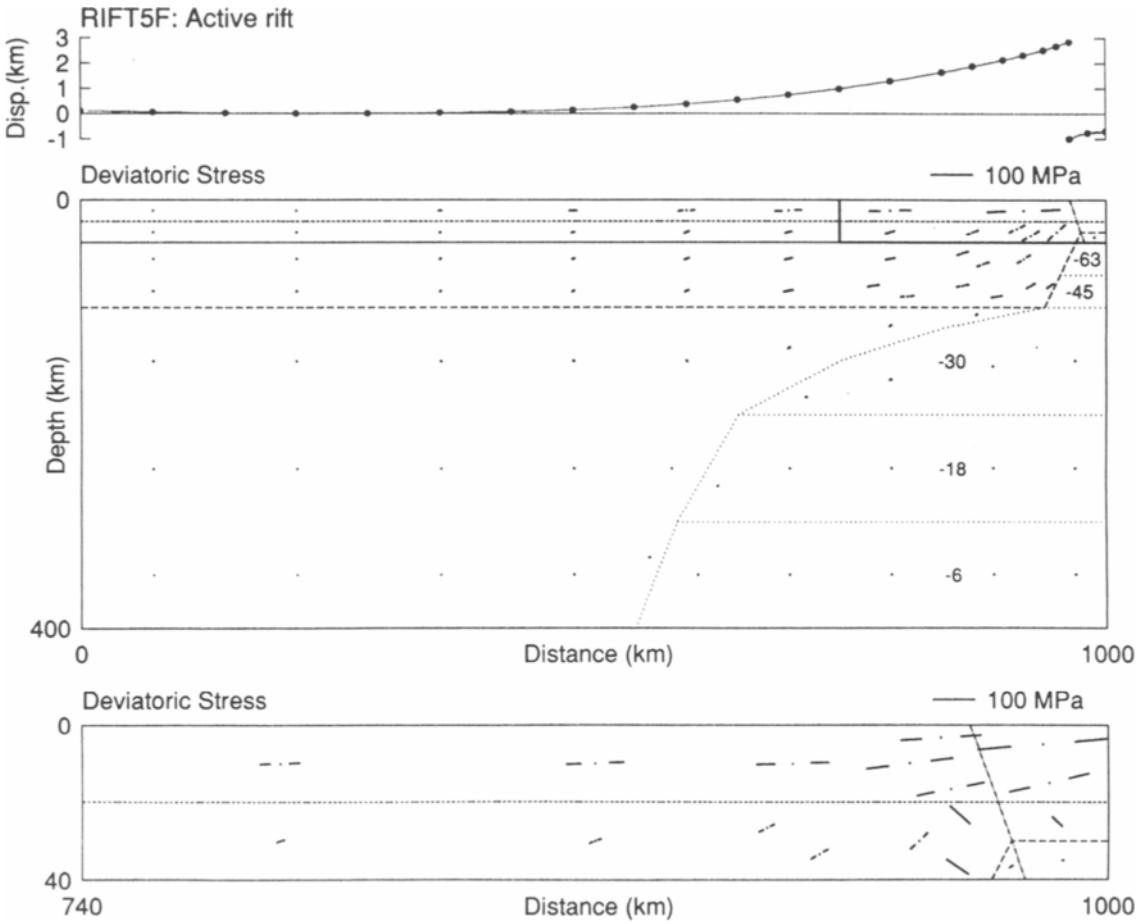

Fig. 2–5. Finite element model of an active rift with low density upper mantle appropriate to a hot spot and an asthenospheric upwelling extending into the crust. The vertical displacement profile and the deviatoric stresses are shown for the left half of a symmetrical model 2100 km wide. A fault bounds a symmetrical graben; The fault displacement of about 3 km subsidence and 1 km flank uplift is superimposed on the broad domal uplift of 1.7 km. Sediment loading has been excluded, but would increase the subsidence by about a factor of three. An enlargement of the central region is shown below. Anomalous densities are in kg/m^3 and other mechanical properties are as in Fig. 2–3. For further details see Bott (1992).

(lower crust and mantle) to be offset from the surface rift structure. A series of more complicated styles of asymmetrical upper crustal extension linked to pure shear deformation of the underlying crust and lithosphere have been documented by Lister et al. (1991), and these are discussed further in Chapter 11. As far as existing evidence indicates, the crustal and lithospheric thinning associated with those main modern rift systems which have been adequately studied (Kenya rift, Baikal, Rio Grande, Rhinegraben) appears to underlie, or nearly underlie, the zone of rifting, rather than being significantly offset, with asymmetrical extension of the upper crust almost directly overlying pure shear thinning of the underlying crust and uppermost mantle.

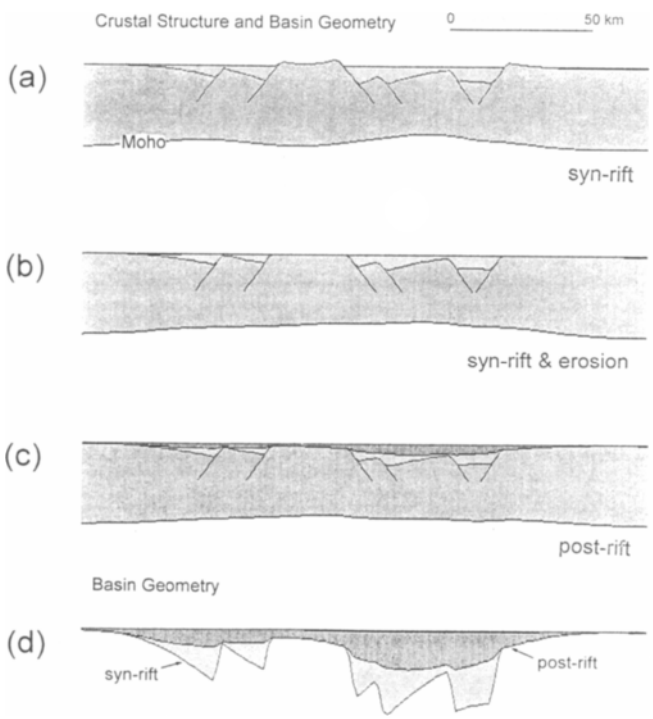

Fig. 2–6. A synthetic example of the use of the flexural cantilever method of basin modeling: (a) Syn-rift basin geometry and crustal structure resulting from imposed fault displacements of various polarities and an underlying balanced crustal structure. Flexural isostatic equilibrium in response to the crustal and sediment loads assumes the faults are locked. The thickness of the flexing elastic layer is taken as 3 km. (b) Syn-rift basin geometry and crustal structure after erosion and flexural isostatic rebound. (c) After 250 Ma of thermal subsidence and post-rift sediment loading. (d) As (c) but with vertical exaggeration of basin geometry. Reproduced from Kusznir and Ziegler (1992) with permission.

The flexural cantilever method introduced by Kusznir et al. (1991) makes it possible to model the flexural and thermal response of the continental lithosphere to planar faulting of the upper crust and distributed pure shear ductile deformation of the lower crust and mantle. The first stage is to impose the observed pattern of fault displacements and stretching on the upper crustal layer. It is assumed that extension by faulting in the upper crust is exactly balanced at depth by plastic deformation. The method models the long term flexural isostatic equilibrium resulting from thinning of the crust by faulting and plastic deformation, from evolving thermal loads, from sediment fill and from erosional unloading. The model is able to predict typical observed basin geometry and subsidence history if it is assumed that plastic pure shear deformation affects a region of 75 to 125 km width for each fault and that the flexing elastic layer is only about 2 to 5 km thick. The method has been applied to the evolution of the Viking Graben by Marsden et al. (1990). A synthetic example is shown in Figure 2–6 to illustrate how the method works.

The flexural cantilever method imposes the observed total fault motion and thus cannot model the process of fault growth. Co-seismic slip on faults can be fitted to observed geodetic data on footwall uplift and hangingwall subsidence using an elastic dislocation model (Mansinha and Smylie, 1971). As an example, Stein and Barrientos (1985) used this

method to model the observed ground displacement profile occurring on the Lost River fault in the Basin and Range province during the Borah Peak earthquake of 1983. They showed that the data better fitted a high angle planar fault than a listric fault.

2.8. Flank uplifts

The earliest explanation of flank uplifts was by upbending of the "elastic lithosphere" on one or both sides of the subsiding rift wedge. This idea was first applied by Vening Meinesz (1950) to a crustal rift block, but equally well applies to wedge subsidence of the brittle upper crustal layer and to half grabens. The cross-sectional shape of the uplift is defined by flexure theory, with the maximum uplift adjacent to the rift faults and an exponentially decaying elevation away from the rift. The occurrence of such flexural flank uplifts is in excellent agreement with geological observations and this mechanism is clearly of much importance despite the neglect of it in continuum models of extension. However, such flank uplift may be much less conspicuous when extension is dominated by shallow dipping faults and detachment surfaces.

Flank uplift can additionally arise from buoyancy forces resulting from local regions of anomalously low density beneath the immediate rift zone. The flexural rigidity of the upper crust distributes the isostatic uplift to include the flank regions. The width and prominence of the flank uplift increases with the flexural rigidity. Some mechanisms by which such flank uplifts are produced are briefly summarized below, the first two being most relevant to active rifting and the others to passive rifting.

Flank uplifts can be produced by buoyancy forces associated with a low density asthenospheric upbulge associated with thinning of the lithosphere without stretching. This will produce doming of the rift zone and its flanks; because of the reduced flexural rigidity of the thinned lithosphere, such doming will be shorter in wavelength than that produced by an upper mantle hot spot beneath lithosphere of normal thickness. Maximum elevation occurs adjacent to the rift faults as in the elastic upbending models.

Diapiric upwelling of the asthenosphere may cause redistribution of mass within the ductile lower crust as well as gross stretching of the crust, thinning the lower crust beneath the rift zone by outward flow, so that slightly thickened crust occurs beneath the flanks. This effect is shown in some of the centrifuge mechanical models of rifting (Mulugeta, 1985). The flexural isostatic response to the thickened crust will be to cause rim uplifts which may reach maximum elevation at some distance from the faults.

Flank uplifts can be caused in passive rifting, and intensified in active rifting, by the effect of small scale convection widening the region of thinned lithosphere. Keen (1985, 1987), Buck (1986) and Fleitout et al. (1986) modeled the effect of small scale convection in thinning the lithosphere and particularly in widening the asthenospheric bulge produced by passive extension, and found that significant effects could be produced over time periods of around 10 Ma. Flexural uplift occurs in response to the buoyancy of the widened region of low density asthenosphere. This type of mechanism explains the formation of flank uplifts which develop significantly later than the onset of the upper crustal extension and rifting, such as those bordering the Gulf of Suez (Steckler, 1985).

A further mechanism of relevance to passive rifting, recently modeled by Chéry et al. (1992), results from lack of local isostatic equilibrium during lithospheric extension. In particular, the Moho is characteristically deeper than its local isostatic level immediately after stretching. The flexural response of the strong upper crustal layer to the anomalous low density at the base of the crust gives rise to flank uplifts whose width and prominence depends on the flexural rigidity.

In conclusion, it is emphasized that flank uplifts may commonly be the combined effect of a broad swell associated with an underlying hot spot, a shorter wavelength uplift associated with an asthenospheric upbulge and footwall flexural uplift associated with major faulting. Other mechanisms described above may also contribute.

2.9. Summary and conclusions

This chapter has summarized some theoretical studies relevant to the geodynamics of continental rifting omitting the petrological intricacies of magma genesis and ascent. Hypotheses for the initiation of rift structures depend on the primary source of extensional stress which initiates the faulting. The *passive hypothesis* attributes the primary extension to plate interior deviatoric tension of distant origin, such as might be produced by the trench suction plate boundary force, with volcanism and vertical movement being a secondary response to lithospheric extension. The *active hypothesis* attributes volcanism, doming and faulting to the influence of an underlying hot upper mantle (hot spot) which may be generated by a plume. Finite element modeling is used to show that quite a small upper mantle hot spot gives rise to substantial deviatoric tension in the strong regions of the lithosphere. The present stress regime, probably applicable during the Tertiary, indicates low-lying continental regions are subject to compression rather than tension; consequently the active hypothesis may be relevant to the Tertiary rift systems, whereas the passive hypothesis may have been dominant during the more tensional stress regime of the Mesozoic.

Failure of the continental lithosphere in extension has been modeled by the thin sheet approximation and also by numerical methods such as finite element. The thin sheet approximation uses realistic rheology but cannot include major faults, treating brittle regions as plastic. Such modeling has demonstrated that strain hardening may affect the lithosphere as it progressively thins as a result of cooling (if the extension rate is slow) and/or evolving buoyancy effects. In general, rapid extension may cause necking and produces narrow rift zones whereas slow extension gives rise to widening rift zones as strain hardening encourages the active zone to migrate laterally. Lithospheric boundinage may occur where the deformation is periodic. Thinning of the lithosphere may also take place without stretching as a result of conversion to asthenosphere; a number of mechanisms have been proposed based on thermal, magmatic and diapiric processes.

Modeling of graben formation normally assumes a relatively simple rheological structure of the lithosphere beneath the faulted upper crust. Despite the predominance of asymmetrical half grabens, modeling of symmetrical grabens has been useful in demonstrating there is a limit to maximum subsidence which depends on the magnitude of the applied tension. A finite element model is presented in Figure 5 which shows that subsidence enhanced by sediment loading can reach at least 8 km in response to the local deviatoric tension resulting from an underlying low density (hot spot) upper mantle of realistic densities, demonstrating the feasibility of the active hypothesis. The flexural cantilever approach is a further method of modeling the thermal and flexural evolution of realistic rift structures which is illustrated in Figure 6.

Flank uplifts are characteristic of most rift zones. The simplest explanation is in terms of elastic upbending of the footwall of the rift faults. Other processes which can enhance flank uplifts include small scale convection widening the zone of lithospheric thinning, upthrust caused by a diapiric upbulge of the asthenosphere and lack of local isostatic equilibrium during lithospheric extension.

Acknowledgements: I am grateful to Professor N.J. Kusznir for reading through the manuscript and giving a number of helpful suggestions. He also kindly provided Figure 2–6.

2.10 References

Artyushkov, E.V., 1973. Stresses in the lithosphere caused by crustal thickness inhomogeneities. J. Geophys. Res., 78: 7675–7708.

Bassi, G., 1991. Factors controlling the style of continental rifting: insights from numerical modeling. Earth Planet. Sci. Lett., 105: 430–452.

Bott, M.H.P., 1971. The Interior of the Earth. First edition, Edward Arnold, London, 316 pp.

Bott, M.H.P., 1976. Formation of sedimentary basins of graben type by extension of the continental crust. Tectonophysics, 36: 77–86.

Bott, M.H.P., 1992. Modeling the loading stresses associated with active continental rift systems. Tectonophysics, 215: 99–115.

Bott, M.H.P. and Dean, D.S., 1972. Stress systems at young continental margins. Nature, Phys. Sci., 235: 23–25.

Bott, M.H.P. and Kusznir, N.J., 1979. Stress distributions associated with compensated plateau uplift structures with application to the continental splitting mechanism. Geophys. J. R. Astron. Soc., 56: 451–459.

Braun, J. and Beaumont, C., 1987. Styles of continental rifting: results from dynamic models of lithospheric extension. Mem. Can. Soc. Pet. Geol., 12: 241–258.

Buck, W.R., 1986. Small-scale convection induced by passive rifting: the cause for uplift of rift shoulders. Earth Planet. Sci. Lett., 77: 362–372.

Buck, W.R., 1991. Modes of continental lithospheric extension. J. Geophys. Res., 96: 20161–20178.

Chéry, J., Lucazeau, F., Daignières, M. and Vilotte, J.P., 1992. Large uplift of rift flanks: a genetic link with lithospheric rigidity? Earth Planet. Sci. Lett., 112: 195–211.

Christensen, U., 1984. Instability of a hot boundary layer and initiation of thermo-chemical plumes. Ann. Geophysicae, 2: 311–320.

Christensen, U.R., 1992. An Eulerian technique for thermomechanical modeling of lithospheric extension. J. Geophys. Res., 97: 2015–2036.

Crough, S.T. and Thompson, G.A., 1976. Numerical and approximate solutions for lithospheric thickening and thinning. Earth Planet. Sci. Lett., 31: 397–402.

Duncan, R.A. and Richards, M.A., 1991. Hotspots, mantle plumes, flood basalts, and true polar wander. Rev. Geophys., 29: 31–50.

England, P., 1983. Constraints on extension of continental lithosphere. J. Geophys. Res., 88: 1145–1152.

Fleitout, L., Froidevaux, C. and Yuen, D., 1986. Active lithospheric thinning. Tectonophysics, 132: 271–278.

Fletcher, R.C. and Hallet, B., 1983. Unstable extension of the lithosphere: a mechanical model for Basin-and-Range structure. J. Geophys. Res., 88: 7457–7466.

Forsyth, D. and Uyeda, S., 1975. On the relative importance of the driving forces of plate motion. Geophys. J. R. Astron. Soc., 43: 163–200.

Froidevaux, C., 1986. Basin and Range large-scale tectonics: constraints from gravity and reflection seismology. J. Geophys. Res., 91: 3625–3632.

Froidevaux, C. and Ricard, Y., 1987. Tectonic evolution of high plateaus. Tectonophysics, 134: 227–238.

Houseman, G. and England, P., 1986. A dynamical model of lithosphere extension and sedimentary basin formation. J. Geophys. Res., 91: 719–729.

Illies, H., 1970. Graben tectonics as related to crust-mantle interaction. In: J.H. Illies and S. Mueller (Editors), Graben problems, International Upper Mantle Project, Sci. Rep. 27: Schweitzerbart, Stuttgart, 4–26.

Jarvis, G.T. and McKenzie, D.P., 1980. Sedimentary basin formation with finite extension rates. Earth Planet. Sci. Lett., 48: 42–52.

Keen, C.E., 1985. The dynamics of rifting: deformation of the lithosphere by active and passive driving forces. Geophys. J. R. Astron. Soc., 80: 95–120.

Keen, C.E., 1987. Dynamical extension of the lithosphere during rifting: some numerical model results. In: K. Fuchs and C. Froidevaux (Editors), Composition, structure and dynamics of the lithosphere-asthenosphere system. Geodynamics Series, Am. Geophys. Union, 16: 189–203.

Kusznir, N.J., Marsden, G. and Egan, S.S., 1991. A flexural-cantilever simple-shear/pure-shear model of continental lithosphere extension: application to Jeanne d'Arc basin, Grand Banks and Viking graben, North Sea. In: A.M. Roberts, G. Yielding and B. Freeman (Editors), The Geometry of Normal Faults. Geol. Soc. London Spec. Publ., 56: 41–60.

Kusznir, N.J. and Park, R.G., 1984. Intraplate lithosphere deformation and the strength of the lithosphere. Geophys. J. R. Astron. Soc., 79: 513–538.

Kusznir, N.J. and Park, R.G., 1987. The extensional strength of the continental lithosphere: its dependence on geothermal gradient, and crustal composition and thickness. In: M.P. Coward, J.F. Dewey and P.L. Hancock (Editors), Continental Extensional Tectonics. Geol. Soc. London Spec. Publ., 28: 35–52.

Kusznir, N.J. and Ziegler, P.A., 1992. The mechanics of continental extension and sedimentary basin formation: a simple-shear/pure-shear flexural cantilever model. Tectonophysics, 215: 117–131.

Lister, G.S., Etheridge, M.A. and Symonds, P.A., 1991. Detachment models for the formation of passive continental margins. Tectonics, 10: 1038–1064.

Loper, D.E., 1985. A simple model of whole-mantle convection. J. Geophys. Res., 90: 1809–1836.

Loper, D.E. and Stacey, F.D., 1983. The dynamical and thermal structure of deep mantle plumes. Phys. Earth Planet. Interiors, 33: 304–317.

Mansinha, L. and Smylie, D.E., 1971. The displacement fields on inclined faults. Bull. Seismol. Soc. Am., 61: 1433-1440.

Mareschal, J.-C., 1983. Mechanisms of uplift preceding rifting. Tectonophysics, 94: 51–66.

Marsden, G., Yielding, G., Roberts, A.M. and Kusznir, N.J., 1990. Application of a flexural cantilever simple-shear/pure-shear model of continental lithosphere extension to the formation of the northern North Sea basin. In: D.J. Blundell and A.D. Gibbs (Editors), Tectonic Evolution of the North Sea Rifts. Oxford University Press, Oxford, pp. 240–261.

McKenzie, D., 1978. Some remarks on the development of sedimentary basins. Earth Planet. Sci. Lett., 40: 25–32.

McKenzie, D. and Bickle, M.J., 1988. The volume and composition of melt generated by extension of the lithosphere. J. Petrol., 29: 625–679.

Morgan, W.J., 1971. Convection plumes in the lower mantle. Nature, 230: 42–43.

Moretti, I. and Froidevaux, C., 1986. Thermomechanical models of active rifting. Tectonics, 5: 501–511.

Mulugeta, G., 1985. Dynamic models of continental rift valley systems. Tectonophysics, 113: 49–73.

Nataf, H. C., Froidevaux, C., Levrat, J.L. and Rabinowicz, M., 1981. Laboratory convection experiments: effect of lateral cooling and generation of instabilities in the horizontal boundary layers. J. Geophys. Res., 86: 6143–6154.

Nataf, H.-C., Hager, B.H. and Scott, R.F, 1984. Convection experiments in a centrifuge and the generation of plumes in a very viscous fluid. Ann. Geophysicae, 2: 303–310.

Neugebauer, H.J., 1983. Mechanical aspects of continental rifting. Tectonophysics, 94: 91–108.

Neugebauer, H.J., 1987. Models of lithospheric thinning. Ann. Rev. Earth Planet. Sci., 15: 421–443.

Neugebauer, H.J. and Reuter, C., 1987. Intrusion of igneous rocks - physical aspects. Geol. Rundschau, 76: 89–99.

Oxburgh, E.R. and Turcotte, D.L., 1974. Membrane tectonics and the East African rift. Earth Planet. Sci. Lett., 22: 133–140.

Ranalli, G. and Murphy, D.C., 1987. Rheological stratification of the lithosphere. Tectonophysics, 132: 281–295.

Ricard, Y. and Froidevaux, C., 1986. Stretching instabilities and lithospheric boudinage. J. Geophys. Res., 91: 8314–8324.

Royden, L. and Keen, C.E., 1980. Rifting process and thermal evolution of the continental margin of eastern Canada determined from subsidence curves. Earth Planet. Sci. Lett., 51: 343–361.

Sengör, A.M.C. and Burke, K., 1978. Relative timing of rifting and volcanism on Earth and its tectonic implications. Geophys. Res. Lett., 5: 419–421.

Sonder, L.J. and England, P.C., 1989. Effects of a temperature-dependent rheology on large-scale continental extension. J. Geophys. Res., 94: 7603–7619.

Spohn, T. and Schubert, G., 1983. Convective thinning of the lithosphere: a mechanism for rifting and mid-plate volcanism on Earth, Venus, and Mars. Tectonophysics, 94: 67–90.

Steckler, M.S., 1985. Uplift and extension at the Gulf of Suez: indications of induced mantle convection. Nature, 317: 135–139.

Stein, R.S. and Barrientos, S.E., 1985. Planar high-angle faulting in the Basin and Range: geodetic analysis of the 1983 Borah Peak, Idaho, earthquake. J. Geophys. Res., 90: 11355-11366.

Turcotte, D.L., 1974. Membrane tectonics. Geophys. J. R. Astron. Soc., 36: 33–42.

Turcotte, D.L. and Emerman, S.H., 1983. Mechanisms of active and passive rifting. Tectonophysics, 94: 39–50.

Vening Meinesz, F.A., 1950. Les grabens africains, résultat de compression ou de tension dans la croûte terrestre?. Bull. Inst. R. Colon. Belge, 21: 539–552.

Watts, A.B., Karner, G.D. and Steckler, M.S., 1982. Lithospheric flexure and the evolution of sedimentary basins. Philos. Trans. R. Soc. London, A, 305: 249–281.

Wernicke, B., 1985. Uniform–sense normal simple shear of the continental lithosphere. Can. J. Earth Sci., 22: 108–125.

Yuen, D.A. and Fleitout, L., 1985. Thinning of the lithosphere by small-scale convective destabilization. Nature, 313: 125–128.

Zoback, M.L., Zoback, M.D., Adams, J., Assumpção, M., Bell, S., Bergman, E.A., Blümling, P., Brereton, N.R., Denham, D., Ding, J., Fuchs, K., Gay, N., Gregersen, S., Gupta, H.K., Gvishiani, A., Jacob, K., Klein, R., Knoll, P., Magee, M., Mercier, J.L., Müller, B.C., Paquin, C., Rajendran, K, Stephansson, O., Suarez, G., Suter, M., Udias, A., Xu, Z.H. and Zhizhin, M., 1989. Global patterns of tectonic stress. Nature, 341: 291–298.

Zuber, M.T, and Parmentier, E.M., 1986. Lithospheric necking: a dynamic model for rift morphology. Earth Planet. Sci. Lett., 77: 373–383.

Zuber, M.T., Parmentier, E.M. and Fletcher, R.C., 1986. Extension of continental lithosphere: a model for two scales of Basin and Range deformation. J. Geophys. Res., 91: 4826–4838.

This Page Intentionally Left Blank

Part II.

Methods of Investigation: Multi-disciplinary Perspectives

This Page Intentionally Left Blank

Chapter 3A

Petrology, geochemistry, isotopes

R.F. Wendlandt, R. Altherr, E.–R. Neumann, and W.S. Baldridge

3A.1. Introduction

The presence of magmatic rocks, a fundamental feature of all continental rift zones, reflects the energy expended in lithospheric extension and upwelling of the asthenosphere. These rocks represent products of the crust and upper mantle, hence carry unique physical and chemical information that cannot be obtained by geophysical techniques. Petrological and geochemical studies of rift–associated igneous rocks can provide information on pressure, temperature, compositions of crust and mantle sources, and processes involved in magma ascent and evolution. Moreover, in contrast to geophysical techniques, which view the present state of the lithosphere, magmatic rocks of different ages potentially record the evolution through time of the mantle and crust beneath rifts.

Magmatic products of continental rifts range from basaltic through intermediate to silicic in composition. Since basaltic magmas are derived from the mantle (the only possibility for deriving basalts from the crust is by complete melting of pre-existing basalt – an unlikely process), these magmatic rocks are of greatest importance in understanding mantle processes. More silicic rocks are useful for understanding crustal processes, since these rocks are generated from and/or acquired their evolved character within the crust.

Occurrences of magmatic rocks are variable both within different parts of a given rift and from one rift to another. This variability, which occurs with respect to the timing, composition, spatial distribution, and volume of igneous products, can limit the application of petrologic techniques to understanding rift evolution. For example, the geographic distribution and volume of magmatic rocks are obvious and fundamental constraints on the usefulness of such rocks for understanding rift processes; information can be obtained only where such rocks occur. Similarly, the occurrence of magmatic rocks is not necessarily uniform in time for any given rift, hence limiting the ability to view different stages in the evolution of a rift. Alternatively, the variations in magmatic occurrences may be related to fundamental processes in the upper mantle or to structural events that are temporally, spatially, and perhaps, thermally discontinuous. Investigations of rift-related igneous rocks, therefore, may provide unique insight into these processes. In this review, we will briefly summarize the principal petrologic techniques that have been applied to igneous rocks in rifts. Our objective is to provide the necessary background for the comparative analysis of rifts that follows.

3A.2. Magma genesis and eruption

Magmas can be derived by a restricted number of fundamental melting mechanisms (Wyllie, 1988) which effectively "move" a source material across its solidus:

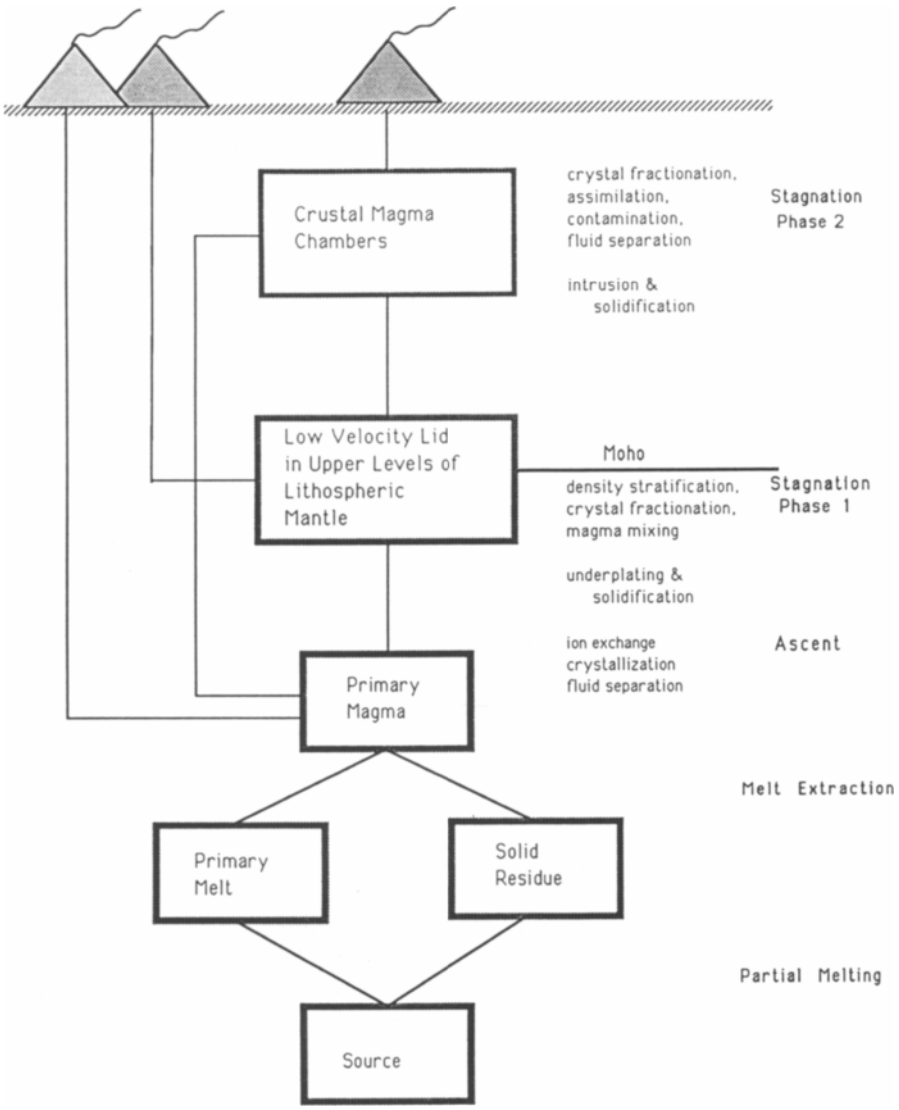

Figure 3A–1. Schematic flow diagram of magma generation and modification processes. Compositional characteristics of primary versus evolved magmas are discussed in the text.

1) increasing temperature at a given depth or through prograde burial metamorphism;

2) modification of source rock composition (perhaps by metasomatic processes) resulting in a decrease in solidus temperature below the ambient temperature;

3) local pressure decrease; and

4) mass transport of material to a lower pressure environment by convective processes.

Production of large amounts of magma by mechanism (1) is mechanistically unlikely because it requires extensive heat transfer by thermal conduction. Mechanism (2) may be appropriate to reconcile small volumes of melt and melts generated by small de-

grees of partial melting but may not be a major process of magma genesis because the fraction of melt that is generated is proportional to the amount of source rock compositional modification that occurs. Mechanism 3 cannot account for large volumes of melt because it requires that either temperatures in the source region be very close to solidus temperatures or that pressure decreases be unrealistically large. Mechanism (4) is the most effective way to obtain large volumes of melt and melts requiring large degrees of partial melting.

A partial melt, representing the fusible or low melting temperature components of a source rock, can be erupted on the surface via any number of possible pathways as shown schematically in Figure 3A–1. A magma extracted from its solid residua that erupts on the surface virtually unchanged in composition is termed "primary". There are no generally accepted criteria for identifying primary magmas, but high Mg/(Mg+Fe) and low SiO_2 values are often used. Occurrences of primary magmas in rift environments are rare but can provide valuable information about P and T of origin and source rock mineralogy if their primary nature can be established. Most often, magma compositions are "evolved" or modified during ascent through the mantle and crust by processes involving mixing (ion exchange processes, assimilation of wallrock or inclusions, magma mixing), crystallization (crystal settling, flotation, or plating on conduit walls), and fluid separation (liquid–fluid, solid–fluid, and liquid–liquid immiscibilities). Evolved magmas are typically characterized by low Mg/(Mg+Fe) and high SiO_2, K_2O, Na_2O, Al_2O_3, and $^{87}Sr/^{86}Sr$. In a given suite of basaltic rocks, we generally consider the rock with highest Mg/(Mg+Fe) ratio to be the most "primitive" (least modified during ascent). In most cases it is difficult to determine if the most primitive rock in a suite represents a primary magma. For the petrologist studying rift volcanism, a detailed understanding of the processes by which a magma is modified involves use of major element, trace element, and isotopic compositions, and application of techniques from both field and experimental petrology.

Removal of melts from mantle source regions and their ascent through the crust result in compositional and physical modifications of these regions (e.g., Johnson, 1991; Wendlandt et al., 1991). For example, residual solid material (mantle or crust) is chemically and mineralogically modified by depletion in volatiles and low melting temperature components during melting and mixing processes and by enrichment in mafic mineral accumulations (cumulates) during crystallization. Continental rift volcanism will alter the lower crust toward more dense and mafic compositions, which will produce attendant changes in crustal velocity structure. The extent of magma and host rock modification during magma ascent is variable and may occur continuously or intermittently when the magma occupies a magma chamber at some intermediate level. Figure 3A–1 arbitrarily depicts two levels of magma stagnation, at the base of the crust and at an upper crustal (shallow) magma chamber. It is well established, however, that magma chambers can form over the range of crustal conditions. In Oslo rift, for example, magma chambers existed both in the deep to intermediate crust (>18 km) and at subsurface levels (1–3 km). Significantly, the proportion of magmas in rifts that never make it to the surface is probably greater than the observed eruptives. The crystallization of these magmas at intermediate depths (above the region of magma genesis) can significantly modify crust composition and physical properties, including density, magnetics, seismic velocity, heat flow, etc.

3A.3. Chemistry of igneous rocks

3A.3.1. Major, Minor, and Trace Elements

The elements constituting a magmatic rock are divided into major, minor, and trace elements according to their abundance. Major elements are those elements which make up the bulk of a rock; their concentrations are given in weight percentages of the respective oxides and a major element occurs normally in quantities above 1 wt%. The major oxides of a magmatic rock typically include SiO_2, TiO_2, Al_2O_3, Fe_2O_3, FeO, MnO, MgO, CaO, Na_2O, K_2O, P_2O_5, H_2O, and CO_2. Minor elements are those elements which occur in magmatic rocks in quantities generally < 1 wt% and > 0.1 wt%. Although, for instance, K and P in rift-related basalts may occur in

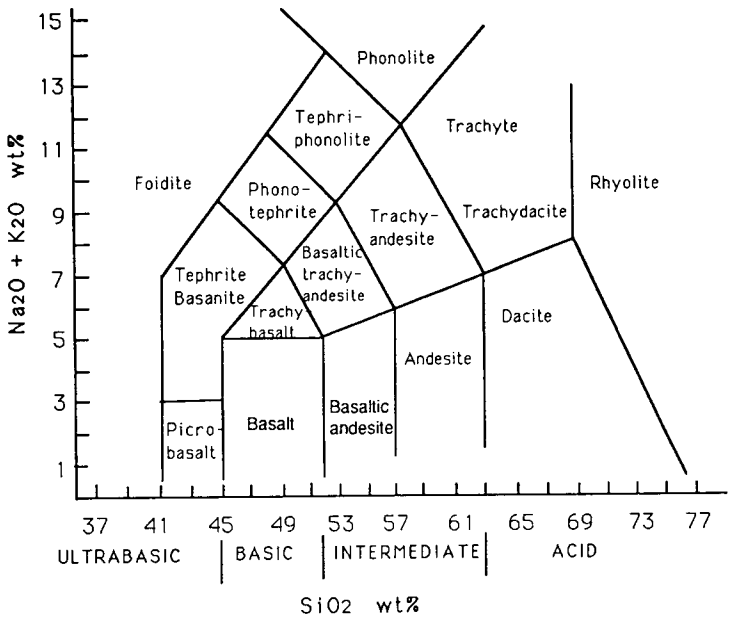

Figure 3A–2. IUGS chemical classification scheme for volcanic rocks based on total alkali (Na_2O and K_2O) and silica (SiO_2) contents.

quantities well below 1 wt.% and, thus, should be regarded as minor elements, they are traditionally listed among the major elements. Trace elements are those that occur at concentrations < 0.1 wt% (1000 ppm). The most important trace elements in igneous petrology (from our present view point) are Cs, Rb, Ba, Th, U, Nb, Ta, Pb, Sr, Zr, Hf, Y, Ni, Cr, Co, Sc, and the rare earth elements (REE, e.g., La, Ce, Nd, Sm, Eu, Gd, Tb, Ho, Tm, Yb, and Lu).

The classification of igneous rocks is based on actual (modal) mineralogy, whenever possible. Where modes cannot be obtained, for example because the rock is too fine-grained or glassy, chemical data are used for classification. For basalts, a fundamental distinction is made between tholeiitic and alkalic compositions. Tholeiitic basalts are those which have enough silica to contain the normative (or theoretically calculated) mineral hypersthene; alkalic basalts, by contrast, contain less SiO_2, hence have normative nepheline or leucite. This distinction is not arbitrary, but rather is based on thermodynamic properties from relevant phase diagrams. Hence these two major basalt types convey fundamental information with regard to the conditions of their formation in the mantle (for example, see Section 3A.5, below). Igneous rock classification used in this volume is that of the International Union of Geological Sciences (IUGS) Subcommission on the Systematics of Igneous Rocks (Streckeisen, 1976, 1979; Le Bas et al., 1986). A simple chemical classification scheme that the IUGS Subcommission recommends for volcanic rocks, based on total alkali ($Na_2O + K_2O$) and silica (SiO_2), is shown in Figure 3A–2.

3A.3.2. Compatible vs. Incompatible Elements

Those elements whose ionic radii and charges are compatible with the crystal structures of the major igneous minerals and which are, therefore, readily incorporated into these minerals are called "compatible". Those elements, alternatively, whose ionic

radii and charges do not allow their ready incorporation into crystal structures are termed "incompatible". Incompatible elements are often subdivided into two subgroups, high field strength (HFS) and low field strength (LFS), based on ionic radius and charge. Elements in the former subgroup (e.g., Zr, Th, U, Nb, etc.) are characterized by high charge and relatively small ionic radius, while those in the latter (e.g., Rb, Sr, Ba, Cs, etc.) are characterized by large radius and low valence. When a mafic to intermediate composition melt is in contact with an igneous mineral, both HFS and LFS elements will preferentially concentrate in the melt. This behavior is described by a distribution coefficient, D, which is defined as the concentration ratio of an element between a mineral assemblage and the melt or fluid. These distribution coefficients are dependent on the specific chemical compositions of the phases as well as on temperature and pressure. Incompatible and compatible elements are characterized by $D < 1$ and $D > 1$, respectively. For any specific igneous system (i.e., a system with coexisting minerals, melt, and possibly, a volatile phase), the elements can be arranged in a "compatibility sequence" which means they are arranged in the order of increasing D.

3A.4. Processes of magmatic evolution

The chemical composition of a particular magmatic rock not only defines its name (Fig. 3A–2) but also reflects its genesis. Some of the important factors which will influence the chemical composition of the final magmatic rock are: the chemical and mineralogical composition of the source rock, the degree of partial melting, the temperature and pressure of melting, the mechanism and extent of melt extraction, crystal fractionation, contamination (as, for example by wall rock assimilation), fluid release and/or exchange with country rocks, and weathering (compare Fig. 3A–1). When dealing with a magmatic rock, the effects of all these processes must be taken into account.

The possibility that the original chemistry of the rock has changed by *weathering* may in most cases be ruled out by careful sampling. Some elements, however, are extremely sensitive to the effects of weathering, including Cs, Ba, F, and Cl, and for these elements, alteration by weathering is still a potential problem.

Contamination by assimilation is a widespread phenomenon. Contamination of basaltic rocks by crustal materials can best be tested by utilizing certain element ratios, for example, K/P, Nb/U, and Ti/Yb, in conjunction with isotope ratios if possible (see below). K and U are enriched and P and Nb are depleted in typical crustal materials and their derivative melts as compared to uncontaminated mantle-derived melts, making the K/P and Nb/U ratios sensitive to assimilation of crustal materials. Crystal fractionation, on the other hand, would simultaneously enrich the melt in K and P or Nb and U, and thus not cause significant changes in the respective element ratios. Conclusions reached from Ti/Yb ratios are not so straightforward: a low Ti/Yb ratio does not necessarily prove that crustal contamination took place, but high Ti/Yb is strong evidence against additions of crustal materials (Hofmann et al., 1986; Leeman and Hawkesworth, 1986; Van Calsteren et al., 1986; Carlson and Hart, 1987).

Most of the magmas which reach the surface have been modified by *crystal fractionation* which can take place at different levels and, hence, might involve different pressure-dependent mineral assemblages. The chemical composition of the erupted lava will reflect this process. For example, a useful indicator of plagioclase fractionation is the presence of negative Eu anomalies visible in chondrite-normalized rare earth element (REE) patterns. These anomalies result because Eu, among the REE, can exist in two oxidation states, Eu^{2+} and Eu^{3+}, and plagioclase preferentially incorporates Eu^{2+} from the melt relative to Eu^{3+} and other REE. Independent of pressure, the net effects of crystal fractionation from a basaltic magma will always be a decrease in $Mg/(Mg+Fe_t)$ and in the contents of other compatible (with respect to the fractionating mineral assemblage) elements similar to Mg, e.g., Ni, Cr, Co. This effect arises because the fractionating assemblage will always be dominated by mafic minerals, including olivine and pyroxenes. If a suite of chemically different magmatic rocks is related by crystal fractionation, one would expect that they define smooth curves in chemical variation diagrams and that their compo-

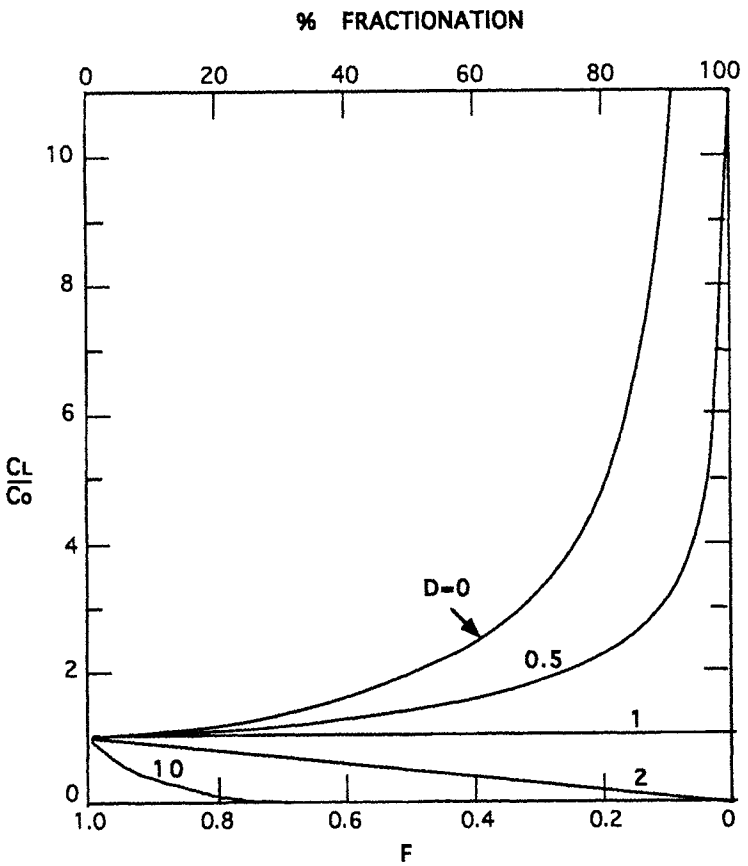

Figure 3A–3. Plot of incompatible (D < 1) and compatible (D > 1) element behaviors during Rayleigh fractional crystallization. C_L/C_O represents the ratio of an element concentration in a daughter melt, C_L, relative to that in the parent melt, C_O. F represents the fraction of melt remaining during crystallization.

sitions can be modeled by subtracting increasing amounts of fractionating mineral assemblages with appropriate mineral compositions. These model calculations require knowledge of the modes of fractionating mineral assemblages and of the distribution coefficients.

Primary magmas derived by partial melting from a normal upper mantle source are expected to have $Mg/(Mg+Fe_t) > 65$, Ni > 250 ppm, and Cr > 300 ppm. For rocks having undergone crystal fractionation that are characterized by lower values, a primary melt composition can be modeled by correcting for the effects of fractionation. During the initial stages of crystal fractionation, the contents of incompatible elements in basaltic to intermediate composition melts are enriched only moderately (Figure 3A–3). In contrast, compatible element concentrations are sensitive to small degrees of crystal fractionation and will initially decrease rapidly as does the ratio $Mg/(Mg+Fe_t)$ (Cox et al., 1979). The approach commonly used in studying suites of related but compositionally varied rocks is to determine the least evolved composition or compositions to which more evolved basalts can be related (i.e., parental melts). Once a primary, or at least the most primitive, melt composition has been established, it

is possible to put constraints on problems like the composition of the mantle source rock, the temperature and pressure conditions of origin, the degree of partial melting, and the mineralogical composition of the solid residue. These problems are, however, related to each other, and cannot be solved independently: If we are interested in the degree of partial melting by which a certain primary melt was generated, it is necessary to make assumptions about the chemical composition of the source and vice versa.

Numerical methods are used to model the evolution of suites of evolved rocks, in which various members are related to each other by assimilation, mixing, and/or fractional crystallization processes (e.g., Langmuir et al., 1977; O'Hara, 1977; DePaolo, 1981; O'Hara and Mathews, 1981; Hagen and Neumann, 1990). These modeling approaches provide insight into crustal processes, including estimates of the extent to which a magma is evolved (i.e., the amount of crystallization that has occurred, or the extent of interaction between magma and surrounding rock during ascent).

3A.5. Experimental studies

Another approach to interpreting basalt compositions lies in comparison with the large volume of data generated from laboratory experiments over a period of more than twenty years. Comparison with experimental petrology can be used to place limits on the depth and temperature of origin of magma, mineralogy and mineral chemistry of source rocks as a function of depth, and eruption path processes. Experiments on a wide range of synthetic and natural materials have permitted the pressure, temperature, and compositional conditions under which melts of various composition are generated or modified to be constrained. Experimental studies cannot, however, constrain bulk composition of the magma source region.

Experimental studies can be conducted using natural or synthetic starting materials that are representative of either source rocks or observed igneous rock compositions. Experiments on source rocks (the "forward" approach) demonstrate possible pressure, temperature, and compositional conditions for which melts can be derived from a presumed source rock. Depending on the assumptions regarding source rock composition, particularly the volatile (water, carbon dioxide, etc.) composition and content that may be present, the observed melt compositions and their physical conditions of origin may (or may not) be reasonably analogous to naturally occurring magmas.

Experiments involving igneous rock compositions (the "inverse" approach) are used to constrain possible source rock mineralogy and the conditions of genesis and evolution for that specific rock composition. For these types of experiments to be meaningful, the genetic history of the composition being studied must be understood, including whether or not the magma in question is primitive or modified by low pressure crystal fractionation or crustal assimilation processes. While the types of information obtained from the forward and inverse approaches differ, the approaches are complementary, and integrating both types of studies provides the best constraints on source conditions.

In principle, a petrogenetic grid can be established, based on experimental studies, in which magma composition is related to a unique range of pressure, temperature, water and carbon dioxide contents, and degree of partial melting conditions in the upper mantle. In practice, the rigorous application of this predictive approach is limited by the uncertainties noted above regarding the compositions of magma, source rocks, the compositional changes that may have occurred to erupted rocks during ascent, and by the incomplete experimental coverage of the range of magma types that occur in rift environments. Sufficient data exist, however, to constrain conditions of origin of major basalt types, tholeiitic and alkalic basalt, that are volumetrically important in many rifts (e.g., Rio Grande, Baikal, Red Sea).

Experiments bearing on the origin of tholeiites indicate genesis at relatively low pressure (less than about 15 kbar) by approximately 5 to 30% partial melting of a spinel lherzolite source composition (Jaques and Green, 1980; Takahashi and Kushiro, 1983). Figure 3A–4 depicts the composition of liquids derived from partial melting of dry lherzolite, a peridotitic rock consisting of olivine, orthopyroxene, clinopyroxene, and an aluminous

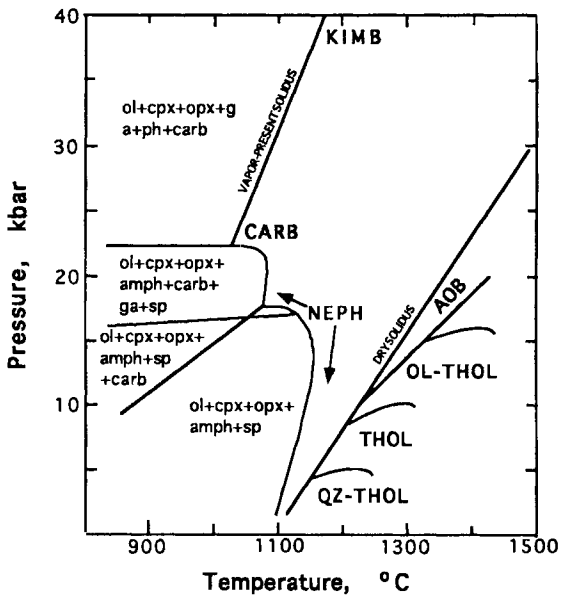

Figure 3A–4. Compositions of liquids derived from partial melting of volatile-absent lherzolite (dry solidus) and from lherzolite containing small amounts of H_2O and CO_2 (modified from Jaques and Green, 1980, Takahashi and Kushiro, 1983, and Olafsson and Eggler, 1983). Abbreviations: ol=olivine, cpx=clinopyroxene, opx=orthopyroxene, amph=amphibole, sp=spinel, ga=garnet, ph=phlogopite, carb=carbonate, AOB=alkali olivine basalt, OL-THOL=olivine tholeiite, THOL=tholeiite, QZ-THOL=quartz tholeiite, KIMB=kimberlite, CARB=carbonatite, and NEPH=nephelinite.

phase such as spinel or garnet. At low pressure (less than about 5 kbar) and for low degrees of partial melting, liquid compositions are relatively enriched in silica (quartz tholeiitic). With increasing pressure up to 15–17 kbar, liquid compositions tend to become less siliceous and more magnesian (olivine tholeiitic). Alkali olivine basalts, on the other hand, can be generated by small degrees of melting (less than several percent) of anhydrous peridotite at pressures in excess of 10 kbar.

Alternatively, small amounts of volatiles, generally H_2O and CO_2, in the magma source region can promote the generation of alkali basalts at lower temperatures than exhibited by dry melting relations. If the mantle contains volatile components, H_2O and CO_2, as conventional wisdom suggests, then the beginning of melting is fundamentally different than for anhydrous conditions. The presence of CO_2 and H_2O stabilizes volatile-bearing minerals at subsolidus conditions in mantle compositions. These volatile-bearing minerals are amphibole at pressures less than about 22 kbar, carbonate (dolomite) and amphibole at intermediate pressures, 17–22 kbar, and carbonate (dolomite or magnesite) at pressures greater than 22 kbar (Fig. 3A–4). A consequence of these minerals is that the beginning of melting of mantle peridotite and the composition of the first formed melt are uniquely defined for a given pressure, temperature, and bulk composition by melting reactions involving these volatile-bearing minerals.

The mantle solidus as determined by Olafsson and Eggler (1983) for a natural spinel lherzolite containing small amounts of H_2O and CO_2 and melt compositions generated near this solidus are also summarized in Figure 3A–4. With increasing pressure, melts become increasingly alkaline and silica-undersaturated. At pressures of about 25–30 kbar, melt compositions are strongly enriched in dissolved carbonate and resemble, in some respects, carbonatites. At still higher pressures, melts are kimberlitic. Because volatile components will be present in trace amounts in mantle source rocks (perhaps several tenths of a

weight percent), only small volumes of melt will be generated near the volatile-present solidus. The continuation of melting at higher temperatures will conform to the volatile-absent phase relations of lherzolite.

The genesis of primary alkali basalts, therefore, can result from small degrees of partial melting involving volatiles at reduced temperature or from very small degrees of partial melting in the absence of volatiles at higher temperatures. Tholeiites are the products of somewhat larger degrees of partial melting, where the effects of small amounts of volatile components on melting relations are diluted. Experimental results predict an overlap in the pressure conditions of origin of these two major basalt types; however, this overlap does not occur when source rock composition (particularly H_2O and CO_2 contents) is constrained. Unfortunately, documentation of basalt composition in rifts rarely reflects the source rock composition to the necessary degree, and therefore, assigning conditions of origin to basalt type is qualitative unless experiments have been conducted on the specific composition in question.

It is important to note, although a detailed discussion is not warranted, that the volcanic record in rift environments is often characterized by a great diversity of magma types, including many volumetrically limited and compositionally extreme types, although tholeiitic and alkalic basalt types may predominate. The compositionally extreme, typically ultra-alkaline, magmas can provide additional information on source rock compositions, conditions of genesis and chemical/thermal processes in the mantle when appropriate experimental constraints are available.

A major gap in our knowledge exists regarding the genesis and significance, with respect to rifting processes, of silicic igneous products. This limitation is particularly apparent in those rift environments where extremely large volumes of relatively silicic material have been emplaced or erupted (e.g., the Oslo Rift and the East African Rift). In East Africa, for example, approximately 50,000 cubic km of flood phonolites and about 25,000 cubic km of flood trachytes have been erupted (Lippard, 1973; Williams, 1982). These volumes require a thermal "trigger" that is significant with respect to the scale of overall rift features. The position of silicic, presumably crust-derived, melts in a petrogenetic grid is undetermined.

3A.6. Isotopes

3A.6.1. Introduction

Because different regimes of the earth have unique major and trace element compositions, they are also characterized by distinctive isotopic compositions. Isotopes of interest for petrological applications include both radiogenic (i.e., formed by radioactive decay processes from another isotope; listed in Table 3A–1) and stable (or non-radiogenic, i.e., not formed by decay from any other isotope). Each element has specific geochemical attributes which makes it a unique tracer of certain petrological processes. In this review, we will limit our discussion to radiogenic isotopic systems.

Generally, radioactive decay systems can be used in two different ways:

1) for direct age determination by measuring the ratio of the parent atom over the daughter atom; and

2) as a tracer of chemical differentiation events in parts of the earth or the solar system based on different geochemical behaviors of parent and daughter atoms.

Better constrained interpretations often result from the integration of measurements of several isotopic systems. For example, when $^{143}Nd/^{144}Nd$ ratios are used in conjunction with $^{87}Sr/^{86}Sr$, the collective result is a very powerful tracer of lithosphere and magma evolution. For a general review of the basics of isotope geochemistry see, for example, Faure (1986).

With respect to rift studies, the decay of ^{40}K to ^{40}Ar is used for dating volcanic rocks whereas the other decay systems are mainly important as geochemical tracers. Dating by Rb–Sr, Re–Os, Sm–Nd, and U–Pb isotopic systems, which are characterized by very long half-lives, is only possible in paleorifts where the igneous rocks are old enough to have accumulated enough daughter isotopes by in situ decay (e.g., Midcontinent Rift)

TABLE 3A–1
Radiogenic isotopic systems used in geochemistry.

Radioactive parent	Decay mechanism	Stable daughter	Approximate half-life (Ga)	Isotope used for normalization
^{40}K	electron capture, β	^{40}Ca, ^{40}Ar	1.3	^{36}Ar
^{87}Rb	β	^{87}Sr	48	^{86}Sr
^{147}Sm	α	^{143}Nd	106	^{144}Nd
^{176}Lu	β	^{176}Hf	33	^{177}Hf
^{187}Re	β	^{187}Os	46	^{186}Os
^{232}Th	α, β	^{208}Pb	14	^{204}Pb
^{235}U	α, β	^{207}Pb	0.7	^{204}Pb
^{238}U	α, β	^{206}Pb	4.8	^{204}Pb

3A.6.2. Isotopes as tracers of geochemical differentiation

It is assumed that about 4.55 Ga ago the mantle was undifferentiated and had homogeneous isotope ratios. The initial isotope ratios as well as the respective parent/daughter element ratios of this so-called primordial mantle are estimated from cosmochemical and geochemical evidence. This assumption allows an estimate of the isotopic composition of the present-day silicate earth (Faure, 1986; DePaolo, 1988). Most geochemists agree on the assumption that the average upper mantle is depleted in incompatible elements as compared to the primordial mantle. This depletion is generally attributed to the formation of the continental crust. Independent mass balances between continental crust, depleted mantle, and primordial mantle based on isotopic and trace element data, indicate that about one-half of the primordial mantle (or perhaps a bit less) has been differentiated to form continental crust and depleted mantle (O'Nions et al., 1979; Jacobsen and Wasserburg, 1979; DePaolo, 1980; Davies, 1981; Allegre et al., 1983; Hofmann et al., 1986). Hence, there should be at least two different chemical and isotopic mantle reservoirs.

Due to differences in incompatibility of the parent and daughter elements, the average depleted mantle should have lower Rb/Sr and Re/Os ratios, but higher Sm/Nd and Lu/Hf ratios than the primordial mantle. In contrast, the average continental crust should be characterized by higher Rb/Sr and Re/Os ratios, and U and Th contents, and lower Sm/Nd and Lu/Hf than the primordial mantle. These incompatibility differences have resulted in characteristic isotopic signatures for the different reservoirs. For example, the upper crust, which is granitic in composition and is believed to have formed through a series of melting processes, is enriched in Rb, U and Th compared to the lower crust and mantle and is also highly enriched in ^{87}Sr (formed by decay from ^{86}Rb) relative to total Sr. Similarly the crust is enriched in ^{206}Pb and ^{207}Pb (formed by decay of U) and ^{208}Pb (formed by decay of Th) and have relatively high $^{206}Pb/^{204}Pb$, $^{207}Pb/^{204}Pb$ and $^{208}Pb/^{204}Pb$ ratios. Parts of the mantle which have been involved in partial melting are relatively depleted in Rb, U, and Th and, therefore, have low Sr and Pb isotopic ratios compared to crustal rocks (e.g. Zartman and Doe, 1981).

For many years it was assumed that oceanic and continental basalts were derived from mixed sources whereby primordial mantle was added to depleted upper mantle from below via mantle plumes. It is now clear, however, that there is no significant direct contribution of the primordial mantle to basaltic magmas (Hofmann et al., 1986). Hence, the enriched isotopic signatures shown by a considerable portion of continental basalts have to be explained by more sophisticated models, including:

1) re-enrichment of formerly depleted mantle occurring by recycling of oceanic crust (altered basalts, sediments) via subduction;

2) isolation of subcontinental lithospheric mantle from mantle convection for long periods of time with enrichment by melt additions from the asthenosphere having different parent/daughter element ratios; and

3) small additions from the lower primordial mantle, which may not have been completely isolated through time, into the upper, more depleted mantle.

As all these processes may have been active during most of the earth's history, a heterogeneous upper mantle has resulted despite the tendency for homogenization by mantle convection. This view is substantiated by recent findings on orogenic lherzolites and on samples of mantle material (xenoliths) brought up by basalts. It is now accepted that the lithospheric mantle is heterogeneous at both a small and a large scale and there is also evidence for large scale heterogeneity in the asthenosphere (e.g., Zindler and Hart, 1986; Hart, 1988). At least 5 isotopic compositions have been identified in basalts and mantle-derived xenoliths (i.e. DMM, PREMA, EM I, EM II, HIMU; see Hart, 1988, for discussion).

An even more complex history has certainly taken place within the continental crust which shows significantly larger ranges in parent/daughter and isotope ratios than the mantle. High grade metamorphic events involving dehydration and partial melting will cause transport of incompatible elements such as Rb, U and Th with fluids and melts from the lower to the upper crust. An old lower crust which has been subjected to repeated high-grade metamorphic events will, therefore, have lower $^{87}Sr/^{86}Sr$, $^{206}Pb/^{204}Pb$, $^{207}Pb/^{204}Pb$, and $^{208}Pb/^{204}Pb$ than the upper crust.

3A.6.3. "Enriched" versus "Depleted" sources

Terms like "enriched" and "depleted", which are used to characterize the ability of a certain mantle source rock to give rise to basaltic melt upon partial melting, are still in use but their meaning has become vague. We know that the mantle can no longer be modeled as a simple two-component mixture (basaltic magma and residual phases). It is now necessary to specify the components in which the mantle is depleted or enriched. For example, a lherzolitic mantle can be enriched in basaltic components but still show low Sr and high Nd isotope ratios that are normally attributed to depleted sources. Such decoupling of trace element and isotopic features may indicate that the enrichment event took place recently.

3A.6.4. Isotopes as tracers of magma sources

The isotopic compositions of magmatic rocks reflect the composition of their source regions and of any subsequent material added either as melt (such as magma mixing) or as solid (such as by crustal contamination). For isotopes of petrologic interest heavier than oxygen (i.e., for the radiogenic isotopes), the isotopes are not fractionated by melting or crystallization processes. In principle, therefore, the isotopic ratio of an uncontaminated melt reflects the isotopic ratio of its source region(s). Similarly, crustal reservoirs can be characterized by either direct sampling of crustal rocks or by analysis of melts generated from these regions. The isotopic compositions of evolved melts are also informative: isotopic ratios are sensitive to processes such as mixing of magmas (assuming different isotopic compositions) and crustal contamination and, thus, are important for modeling of evolution processes.

A major issue of continental rifting is the problem of asthenosphere-lithosphere dynamics or, more specifically, the way in which the lithospheric mantle is thinned. The problem is related to the relative contributions of asthenosphere or pre-rift lithosphere as magma sources. If extension by shear is the dominant process, the subcontinental lithosphere is physically replaced by asthenospheric material and the pre-rift lithospheric will perhaps not contribute to basaltic magmatism except, perhaps, by contamination. If, however, lithospheric thinning is caused by thermal erosion and/or conversion to asthenosphere, basaltic magmas could be derived exclusively from the pre-rift lithosphere or by mixing between asthenospheric and pre-rift lithospheric material. If the subcontinental lithospheric mantle represents a distinct isotopic reservoir contributing to basaltic magmas, then one would expect some systematic variations in magma compositions with tectonic setting (i.e. varying with thickness of underlying litho-

spheric mantle as, for example, rift versus shoulder) or with temporal evolution (i.e. with progressive thinning of the lithosphere).

In general, the following different mantle sources can be involved in the genesis of rift-related basalts: asthenosphere, sub-crustal lithosphere (including former lithosphere converted thermally to asthenosphere), and plumes from the lower portions of the mantle. Whereas there is general agreement on the average isotopic signature of the asthenosphere, any further assignment of certain signatures to either pre-rift lithosphere or plume reservoirs is ambiguous. The continental lithospheric mantle, for example, has been assumed to be either depleted or enriched (reviewed by McDonough, 1990). Only in rifts where mantle-derived xenoliths are abundant can the chemical and isotopic composition of the lithosphere be assessed. These studies may then allow certain isotopic characteristics of basalts to be identified as being derived from either a lithospheric or asthenospheric source (e.g., Menzies and Hawkesworth, 1987).

A potential limitation to the use of isotopes as tracers takes into account the heterogeneity of the mantle. This limitation centers on the possibility that the isotopic composition of a primary basaltic melt depends not only on the average composition of its mantle source but also on the degree of partial melting. Preferential tapping of enriched low melting temperature plumes (Sleep, 1984) may occur at low degrees of partial melting (less than 10%) resulting in a melt isotopic signature that does not necessarily correspond to the average isotopic composition of that portion of the mantle which was involved in the partial melting event. If this controversial mechanism accurately describes partial melting in the mantle, then it may be impossible to distinguish isotopically between enriched blobs in the asthenosphere and/or lithosphere and contributions from mantle plumes.

3A.7. Xenoliths and thermobarometry

Rapidly erupted magmas, exclusively alkaline basaltic varieties, may entrain samples of the mantle and lower crust through which they pass on their way to the surface. These xenoliths are valuable as direct samples of subsurface materials and constrain the nature and evolution of the sampled portions of the lithosphere. Studies of xenoliths can provide information about lithosphere composition (mineralogical and chemical), chemical processes (fluid-rock interactions, enrichment and metasomatism events, mineral equilibration, melt generation), radiometric and model ages, and physical processes (mantle rheology, shearing) occurring at depth. Furthermore, for selected coexisting mineral assemblages in xenoliths, pressure and temperature of equilibration may be estimated from mineral chemistry. These experimentally calibrated geothermometers and geobarometers are potentially powerful constraints on magma source depth and temperature (minimum estimates, of course). Given sufficient number and compositionally (mineralogically) appropriate nodules for analysis, a geotherm (a "trail of magma ascent") and a crustal-mantle stratigraphy can be reconstructed.

Geothermometers and geobarometers can be of several types as discussed by Bohlen and Lindsley (1987). These types include univariant equilibria, multivariant equilibria in which solid solution in one or more phases results in a mineral assemblage being stable over a broad range of pressure and temperature, exchange reactions involving the distribution of two elements (e.g., Fe–Mg, K–Na, Ca–Mg) between coexisting mineral phases, solvus equilibria in which mineral compositional changes across a miscibility gap are temperature dependent, and mineral saturation surfaces in melts. Reliable temperature and pressure estimations require previous experimental calibration, knowledge of phase compositions, and solution models for non-ideal solid solution in minerals. Bohlen and Lindsley emphasize that inadequate solution modeling is the most important source of uncertainty in the application of thermobarometers.

At present, geothermometers are best defined for lherzolitic mineral assemblages including olivine-orthopyroxene-clinopyroxene+/–spinel+/–garnet. The most commonly used geothermometers are based either on chemical exchange reactions or on solvus equilibria.

Geobarometers are typically based on experimentally calibrated changes in the aluminum content of pyroxene that coexists with either plagioclase or aluminous garnet, a multivariant equilibria type of geobarometer. Since the aluminum solubility in pyroxene is a function of both pressure and temperature, an independent estimation of temperature is a prerequisite for estimating pressure. Until recently, reliable calibrations of Al solubility in pyroxene existed only for garnet-bearing assemblages. Recent experimental work, however, has resulted in calibration of a new barometer based on Ca solubility in olivine that can also be used for spinel lherzolites (Kohler and Brey, 1990). This barometer is configured to be used with a recalibration of the two-pyroxene geothermometer (solvus equilibria; Brey and Kohler, 1990).

Reequilibration of mineral compositions in xenoliths after entrainment in melt and during ascent to the surface poses both advantages and disadvantages for the interpretation of temperature and pressure. If compositional reequilibration is extensive, it may preclude reliable estimation of intensive parameters. Alternatively, partial reequilibration may provide information about dynamic changes in the state of the lithosphere. Core-rim thermobarometry of garnet-bearing lherzolites and pyroxenites in the Quaternary eruptive centers of eastern Kenya has been interpreted to document the rapid ascent of lithosphere to pressures greater than approximately 10 kbar (32 km) with a minor corresponding decrease in temperature (about 50°C; Henjes-Kunst, 1989; Henjes-Kunst and Altherr, 1992). Uplift was sufficiently rapid that compositional equilibrium was not attained in the xenoliths. This lithospheric ascent corresponds to a change in geothermal gradient from 9°C/km to 13°C/km (or 60 mW/m^2 to 90mW/m^2).

The limitations to obtaining and using thermobarometric estimations include:

1. Rare occurrences of nodules in certain rift environments that may be related to restrictions in magma age, location, or volume, or to a lack of compositionally suitable host magmas (primary alkaline volcanics);

2. Unraveling contamination and mineral reequilibration associated with nodule incorporation in melt and transport to the surface; and

3. Uncertainties associated with thermobarometer calibration, including both experiments and solution models and with operator application of calibrations.

Despite these limitations, however, thermobarometry studies can provide important constraints for geophysical and dynamic models for continental rift structure and evolution.

3A.8. References

Allegre, C. J., Hart, S.R., and Minster, J.F., 1983. Chemical structure and evolution of the mantle and continents determined by inversion of Nd and Sr isotopic data, I. Theoretical models; II. Numerical experiments. Earth Planet Sci. Lett., 66: 177–190, 191–213.

Bohlen, S.R. and Lindsley, D.H., 1987. Thermometry and barometry of igneous and metamorphic rocks. Ann. Rev. Earth Planet. Sci., 15: 397–420.

Brey, G.P. and Kohler, T.P., 1990. Geothermobarometry in natural four-phase lherzolites, part II. New thermobarometers and practical assessment of existing thermobarometers. J. Petrol., 31: 1353–1378.

Carlson, R.W. and Hart, W.K., 1987. Crustal genesis on the Oregon Plateau. J. Geophys. Res., 92: 6191–6206.

Cox, K.G, Bell, J.D., and Pankhurst, R.J., 1979. Interpretation of Igneous Rocks. London, Allen and Unwin.

Davies, G.F., 1981. Earth's neodymium budget and structure and evolution of mantle. Nature, 290: 208–213.

DePaolo, D. J., 1980. Crustal growth and mantle evolution: Inferences from models of element transport and Nd and Sr isotopes. Geochim. Cosmochim. Acta, 44: 1185–1196.

DePaolo, D.J., 1981. Trace element and isotopic effects of combined wallrock assimilation and fractional crystallization. Earth Planet. Sci. Lett., 53: 189–202.

DePaolo, D.J., 1988. Neodymium Isotope Geochemistry. An Introduction. Springer-Verlag, New York, 187 pp.

Faure, G., 1986. Principles of Isotope Geology. John Wiley and Sons, Inc., Second Edition, 589 pp.

Hagen, H., and Neumann, E.-R., 1990. Modeling of trace-element distribution in magma chambers using open-system models. Computers and Geosciences, 16: 549–586.

Hart, S.K., 1988. Heterogeneous mantle domains: signatures, genesis and mixing chronologies. Earth Planet. Sci. Lett., 90: 273–296.

Henjes-Kunst, F., 1989. Mantle xenoliths in Quaternary basalts from East Africa: Evidences of old lithospheric structures in a young continental rift? Symposium on the Afro-Arabian Rift System, March 6–8, 1989, Karlsruhe, F.R.G., 51–52.

Henjes-Kunst, F., and R. Altherr, 1992. Metamorphic petrology of xenoliths from Kenya and Northern Tanzania and implications for geotherms and lithospheric structures. J. Petrol., 33: 1125–1156.

Hofmann, A. W., Jochum, K.P., Seufert, M. and White, W.M., 1986. Nb and Pb in oceanic basalts: new constraints on mantle evolution. Earth Planet. Sci. Lett., 79: 33–45.

Jacobsen, S.B., and Wasserburg, G.J., 1979. The mean age of mantle and crustal reservoirs. J. Geophys. Res., 84: 7411–7427.

Jaques, A.L. and Green, D.H., 1980. Anhydrous melting of peridotite at 0–15 kb pressure and the genesis of tholeiitic basalts. Contrib. Mineral. Petrol., 73: 287–310.

Johnson, C.M., 1991. Large-scale crust formation and lithosphere modification beneath middle to late Cenozoic calderas and volcanic fields, western North America. J. Geophys. Res., 96: 13485–13507.

Kohler, T.P. and Brey, G.P., 1990. Calcium exchange between olivine and clinopyroxene for natural peridotites from 2 to 60 kb with applications. Geochim. Cosmochim. Acta, 54: 2375–2388.

Langmuir, C.H., Vocke, R.D., Hanson, G.N., and Hart, S.R., 1977. A general mixing equation applied to the petrogenesis of basalts from Iceland and Reykjanes Ridge. Earth Planet. Sci. Lett. 37: 380–392.

Le Bas, M.J., Le Maitre, R.W., Streckeisen, A., and Zanettin, B., 1986. A chemical classification of volcanic rocks based on the total alkali-silica diagram. J. Petrol., 27: 745–750.

Leeman, W.P. and Hawkesworth, C.J., 1986. Open magma systems: trace element and isotopic constraints. J. Geophys. Res. 91, 5901–5912.

Lippard, S.J., 1973. The petrology of phonolites from the Kenya Rift. Lithos, 6: 217–234.

McDonough, W.F., 1990. Constraints on the composition of the continental lithospheric mantle. Earth Planet. Sci. Lett., 101: 1–18.

Menzies, M.A. and Hawkesworth, C.J., 1987. Upper mantle processes and compositions. In, Mantle Xenoliths, (ed. P.H. Nixon), John Wiley & Sons, Ltd., 725–738.

O'Hara, M.J., 1977. Geochemical evolution during fractional crystallization of a periodically refilled magma chamber. Nature, 266: 503–507.

O'Hara, M.J. and Mathews, R.E., 1981. Geochemical evolution in an advancing, periodically replenished, periodically tapped, continuously fractionated magma chamber. J. Geol. Soc. Lond., 138: 237–277.

Olafsson, M. and Eggler, D.H., 1983. Phase relations of amphibole, amphibole-carbonate, and phlogopite-carbonate peridotite: petrologic constraints on the asthenosphere. Earth Planet. Sci. Lett., 64: 305–315.

O'Nions, R.K., Evensen, N.M. and Hamilton, P.J., 1979. Geochemical modeling of mantle differentiation and crustal growth. J. Geophys. Res., 84: 6091–6101.

Sleep, N.H., 1984. Tapping of magmas from ubiquitous mantle heterogeneities: an alternative model to mantle plumes? J. Geophys. Res., 89: 10029–10041.

Streckeisen, A., 1976. To each plutonic rock its proper name. Earth-Sci. Rev., 12: 1–33.

Streckeisen, A., 1979. Classification and nomenclature of volcanic rocks, lamprophyres, carbonatites, and melilitic rocks: recommendations and suggestions of the IUGS Subcommission on the Systematics of Igneous Rocks. Geology, 7: 331–335.

Takahashi, E. and Kushiro, I., 1983. Melting of a dry peridotite at high pressures and basalt magma genesis. Am. Mineral., 68: 859–879.

Van Calsteren, P.W.C., Harris, N.B.W., Hawkesworth, C.J., Menzies, M.A. and Rogers, N.W., 1986. Xenoliths from southern Africa: a perspective on the lower crust. In: The Nature of the Lower Continental Crust, J.B. Dawson, D.A. Carswell, J. Hall, and K.H. Wedepohl (Eds.), Blackwell Scientific, Oxford, pp. 351–362.

Wendlandt, R.F., Baldridge, W.S., and Neumann, E.-R., 1991. Modification of lower crust by continental rift magmatism. Geophys. Res. Lett., 18: 1759–1762.

Williams, L.A.J., 1982. Physical aspects of magmatism in continental rifts. In, Continental and Oceanic Rifts, ed., G. Palmason, Geodynamics Series Vol. 8, Published by AGU and GSA, 193–222.

Wyllie, P.J., 1988. Solidus curves, mantle plumes, and magma generation beneath Hawaii. J. Geophys. Res., 93: 4171–4181.

Zartman, R.E. and Doe, B.R., 1981. Plumbotectonics – the model. Tectonophysics, 75: 135–162.

Zindler, A. and Hart, S.K., 1986. Chemical geodynamics. Ann. Rev. Earth Planet. Sci., 14: 493–571.

Chapter 3B

Seismic techniques

L.W. Braile, G.R. Keller, S. Mueller, and C. Prodehl

3B.1. Introduction

Seismic techniques have been of great value in studies of continental rifts because they provide a relatively detailed image of lithospheric structure, including indications of seismic velocities which can be used to infer crust and upper mantle characteristics such as composition and temperature. Ideally, modern seismic studies are capable of excellent resolution to depths of several tens of kilometers. However, hundreds of instruments and a coordinated program of near-vertical angle of incidence (i.e., reflection), wide angle (i.e., refraction), and passive (i.e., earthquake) recordings are required to accurately resolve all significant structural and velocity anomalies from the surface to depths of greater than 100 km in the upper mantle. Therefore, because of limitations in instrumentation and funding, no truly complete lithospheric scale seismic study has been undertaken. Less ambitious programs have provided and will continue to provide valuable but somewhat lower resolution information.

Resolution is a major consideration when discussing seismic data. However, there is such a variety of seismic techniques that general statements about resolution are difficult. As a practical matter, resolution refers to the ability of a measurement to detect the presence of some feature and the accuracy to which this feature can be located. In rift zones, seismic measurements are often called upon to determine such things as the thickness of the crust, subsurface geometry of basins and faults, magnitudes of velocity anomalies in the crust and upper mantle, and the nature of earthquake activity.

In seismology, resolution is related to both data quality and physical laws. The quality of a data set is usually considered to be a function of the strength of the signal relative to noise (usually expressed as signal-to-noise ratio) and the number and/or density of measurements which is primarily dependent on the numbers of sources and receivers and their relative spacing. Examples of the importance of the quantity of measurements would be the need for redundant measurements in teleseismic and surface wave studies and the need for closely-spaced readings in reflection and refraction studies. Up to a point, the more data available, the higher the resolution.

However, physical laws limit the resolution of even a perfect data set. The Earth strongly attenuates high frequencies so that signals which penetrate deeply into the Earth will be relatively low frequency in nature. The effects of this phenomena can be demonstrated using reflection and refraction signals. An estimate of resolution can be obtained by applying the equation $V = f\lambda$ (velocity = frequency × wavelength). A typical crustal velocity is 6 km/s, and a typical peak frequency of a signal penetrating deeply into the crust is 10 Hz, resulting in a typical (peak frequency) wavelength of 0.6 km. The rule of thumb often used is that features smaller than 1/4 of a wavelength cannot be detected. Thus, such data could not detect features smaller than about 150 m in thick-

ness. In crustal reflection and refraction studies, signals that penetrate to the Moho have peak frequencies of about 5 to 20 Hz resulting in theoretical resolution limits of 300 to 75 m. These estimates are in fact optimistic (the resolution estimates can be thought of as measures of the ability to detect and provide *relative* depth control on fine velocity structure), and it would be hard to argue that any existing data in continental areas can resolve the *absolute* position of the Moho to better than ±1 km.

In this chapter, we consider the capabilities and limitations of seismic methods and seismic data in studies of continental rifts. Substantial structural and velocity variations are expected, and are commonly observed, in continental rifts because of the effects of extension (faulting, basin formation, crustal thinning), magmatism (intrusion and volcanism), and high heat flow (reduction in seismic velocities caused by high temperatures) associated with the rifting process. We begin with a brief description of seismic methods which have been used in rift studies, followed by a review of seismic properties of rocks emphasizing effects of temperature. Finally, we utilize the extensive crustal velocity data which are available for North America to identify characteristic crustal properties associated with continental rifts. Various seismic methods which have been applied to studies of the crust and upper mantle are illustrated schematically in Figure 3B–1. A comparison of the main characteristics of these methods is shown in Table 3B–1 and the principal advantages and limitations of the methods are listed in Table 3B–2. Recently, Mooney (1989) has also provided a useful review of seismic methods for determining crust and upper mantle structure.

Fig. 3B–1. Schematic diagrams illustrating various seismic methods which are commonly used to study Earth's crust and uppermost mantle. These diagrams illustrate seismic wave propagation and associated data types for 2-D models, although the methods can also be applied to 3-D velocity structures. x = distance. z = depth, V = velocity. A. Near-vertical incidence reflection raypaths. Multiple sources and receivers are used to record large numbers of seismograms which are processed to produce a seismic reflection record section which is an approximate image of subsurface structure. Reflections are produced by interfaces. B. Raypaths for refracted (head wave) arrivals which provide travel-time curves which are interpreted to derive velocity and thickness values of the layers. Homogeneous velocities and plane layers represent the simplest case, although the method can resolve velocity gradients and can recognize dipping layers if more than one source location or recording direction is available. C. Two-dimensional velocity variations and representative raypaths from multiple sources to receivers which provide travel-time information necessary to derive a detailed image of velocity variations by simultaneous inversion (e.g., Zelt and Smith, 1992; Hughes and Luetgert, 1992; Braile et al., 1994). D. Representative seismic raypaths for teleseismic arrivals with various azimuths and (generally near-vertical) angles of incidence. Travel-time differences (residuals or delay times) can be used to determine velocity variations (V) within blocks or other appropriately-defined regions within the model. E. Raypaths, earthquake source locations, and receivers (squares on surface) utilized in travel-time inversion methods which simultaneously calculate 2-D (or 3-D) velocity models and earthquake location (latitude, longitude, depth) parameters and origin time. Compressional, shear or both compressional and shear arrivals can be included. Because of the large number of unknown parameters (velocity, location and origin time variables) and the need for adequate raypath coverage, large numbers of stations and earthquake sources are necessary for an effective inversion. F. Schematic diagram illustrating the various raypaths (multiples and converted phases; P = compressional waves, S = shear waves) and resulting seismogram at the surface receiver (square) recorded from a single teleseismic source traveling at near-vertical angle of incidence upwards through a layered velocity model generally corresponding to the Earth's crust. Waveform modeling which compares the observed seismogram with a theoretical seismogram calculated from the model and a source wavelet is used to adjust model (and source) parameters until a satisfactory match of observed and theoretical seismograms is achieved. G. Schematic diagram illustrating surface wave propagation through a velocity model. Plane wavefronts (vertical dashed lines) represent lines of equal phase for surface waves propagating from the source. Amplitudes of the surface waves decrease with depth. Surface wave propagation is dispersive; phase or group velocities vary with wave period. Amplitude versus depth curves (amplitudes relative to the vertical solid line) are shown for two periods (LP = long period, SP = short period) for two modes (F = fundamental mode, 1st = first higher mode) of surface wave propagation. Seismograms display dispersed surface wave signals for propagation through the (two-station) seismograph array. Modeling of the dispersion properties of the seismograms using group and phase velocity analysis (Dziewonski and Hales, 1972; Kovach, 1978) or waveform modeling (Lerner-Lam and Jordan, 1983; Sneider, 1988; Nakanishi, 1993) is used to determine the 2-D or 3-D variation in seismic velocities (primarily shear-wave velocities) between and beneath the stations or seismograph array. H. Earthquake location and mechanism (fault plane solution) deduced from seismogram recordings from arrays or networks of seismograph stations (squares). Observations are used to infer 3-D fault geometry, earthquake slip directions and stress directions. Arrows indicate relative stresses indicated by the (vertical plane) focal sphere diagram.

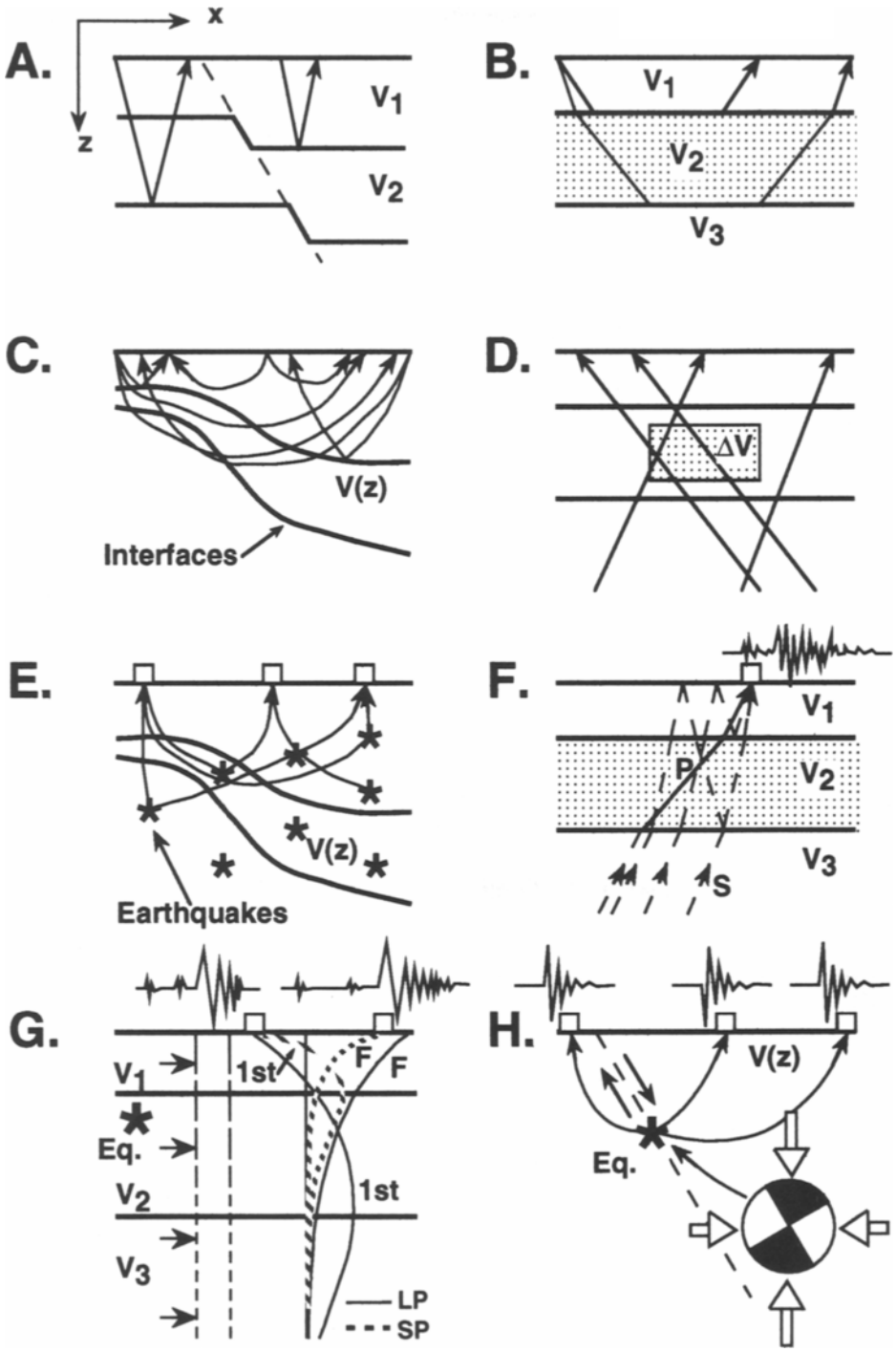
A.
x
z
V1
V2
B.
V1
V2
V3
C.
V(z)
Interfaces
D.
ΔV
E.
V(z)
Earthquakes
F.
V1
P
V2
V3
S
G.
V1
1st
F
F
Eq.
V2
1st
V3
LP
SP
H.
V(z)
Eq.

Table 3B–1.
Comparison of Typical Characteristics of Seismic Techniques for Crustal Velocity Structure Studies (modified from Braile and Chiang, 1986)

Method	Typical Station Spacing	Frequency / Wavelength	Angle of Incidence / Phase Velocity	Processing	Interpretation	Model Complexity	Useful References
Reflection Profiling	0.03-0.20 km	10-30 Hz / 0.2-0.6 km	< 10° / > 10 km/s	statics, CDP stack, deconvolution, migration	velocity analysis, geologic interpretation of record section	2D, some 3D	Brown, 1986; Klemperer and Luetgert, 1987; Matthews and Smith, 1987; Yilmaz, 1987; Mooney, 1989
Refraction, Wide-Angle Reflection Profiling	0.2-10 km	1-20 Hz / 0.3-6 km	40°-90° / 5-10 km/s	statics, bandpass filtering	travel-time, amplitude and synthetic seismogram modeling	1D and 2D	Mueller and Landisman, 1971; Braile and Smith, 1975; Cerveny et al., 1977; Mooney, 1989; Zelt and Smith, 1992; Nowack and Braile, 1993
Teleseismic Delay Times, Receiver Functions, Converted Phases	10-50 km	0.2-2 Hz / 3-30 km	< 20° / > 20 km/s	statics, cross correlation, deconvolution	travel-time inversion, transfer function modeling and inversion	2D for delay times, primarily 1D for receiver functions and converted phases	Jordan and Frazer, 1975; Aki, Christoffersson and Husebye, 1976; Taylor and Owens, 1984; Owens, Zandt and Taylor, 1984; Davis et al., 1993; Iyer and Hirahara, 1993
Local and Regional Earthquakes	10-100 km	2-50 Hz / 0.1-3 km	0°-90° / 2-∞ km/s	station corrections, filtering, phase identification	hypocenter, origin time and velocity model inversion	1D, 2D or 3D	Crosson, 1976; Benz and Smith, 1984; Kissling, 1988; Iyer and Hirahara, 1993; Thurber, 1993
Suface Wave Dispersion	50-1000 km	0.02-0.2 Hz/ 15-200 km	90° / 2-4 km/s	frequency-time analysis, group and phase velocity determination	modeling and inversion of dispersion curves, wave-form modeling	1D, 2D or 3D with regionali-zation schemes	Dziewonski and Hales, 1972; Kovach, 1978; Lerner-Lam and Jordan, 1983; Sneider, 1988; Nakanishi, 1993

Table 3B–2.
Summary of Advantages and Limitations of Seismic Techniques for Crustal Velocity Structure Studies (modified from Braile and Chiang, 1986)

Method	Principal Limitations	Principal Advantages
Reflection Profiling	- Narrow frequency band - Data quality dependent on near-surface conditions - Limited resolution of deep crustal velocities - Processing requires velocity information - Dependent on presence of relatively sharp interfaces - Coherent or random noise may mask true reflections	- High resolution - 2-D and 3D structural interpretation - Processing and data redundancy can enhance S/N - Complete coverage possible - Provides a direct image of the subsurface
Refraction, Wide-Angle Reflection Profiling	- Relatively large station spacing - Horizontal averaging of velocity structure - Complex modeling required for 2-D or 3-D interpretation - Low resolution because of frequency of sources and horizontal averaging	- Relatively broadband signal - Good S/N possible due to refl./refr. coefficients and use of first arrivals - Good velocity information determined - Data from deep crust and upper mantle generally obtained - Both P and S velocities may be determined - Travel-time, amplitude and waveform modeling using synthetic seismograms
Teleseismic Delay Times, Receiver Functions, Converted Phases	- Relatively large station spacing and long wavelength limit resolution - Limited azimuth and distance ranges to sources - Ambiguity of interpretation caused by near-vertical raypaths - Effect of lateral heterogeneity for receiver function studies	- Single station or small array technique - Both P and S velocities may be determined - 2-D or 3-D interpretations possible with multiple stations - Deep crust and upper mantle velocities may be determined to depths of 200 km or more - Earthquake sources, relatively easy field operation - Waveform modeling using synthetic seismograms
Local and Regional Earthquakes	- Large number of unknowns - velocity model, hypocenter locations, origin time - Spatial distribution of earthquakes may not produce good raypath coverage - Large volume of data required - Depth range of model dependent on maximum depth of events	- 2-D and 3-D interpretation - Both P and S velocities may be determined - Passive technique, network operation - Large volume of data available
Surface Wave Dispersion	- Large source required - Station locations not optimum - Low resolution because of long wavelengths, large station spacing, and horizontal averaging - 1-D average model between stations	- Large depth of penetration - Not dependent on existence of interfaces in velocity - Can detect low velocity layers - Cost-effective technique - Sensitive to S-wave velocity structure - 2-D and 3-D interpretation possible

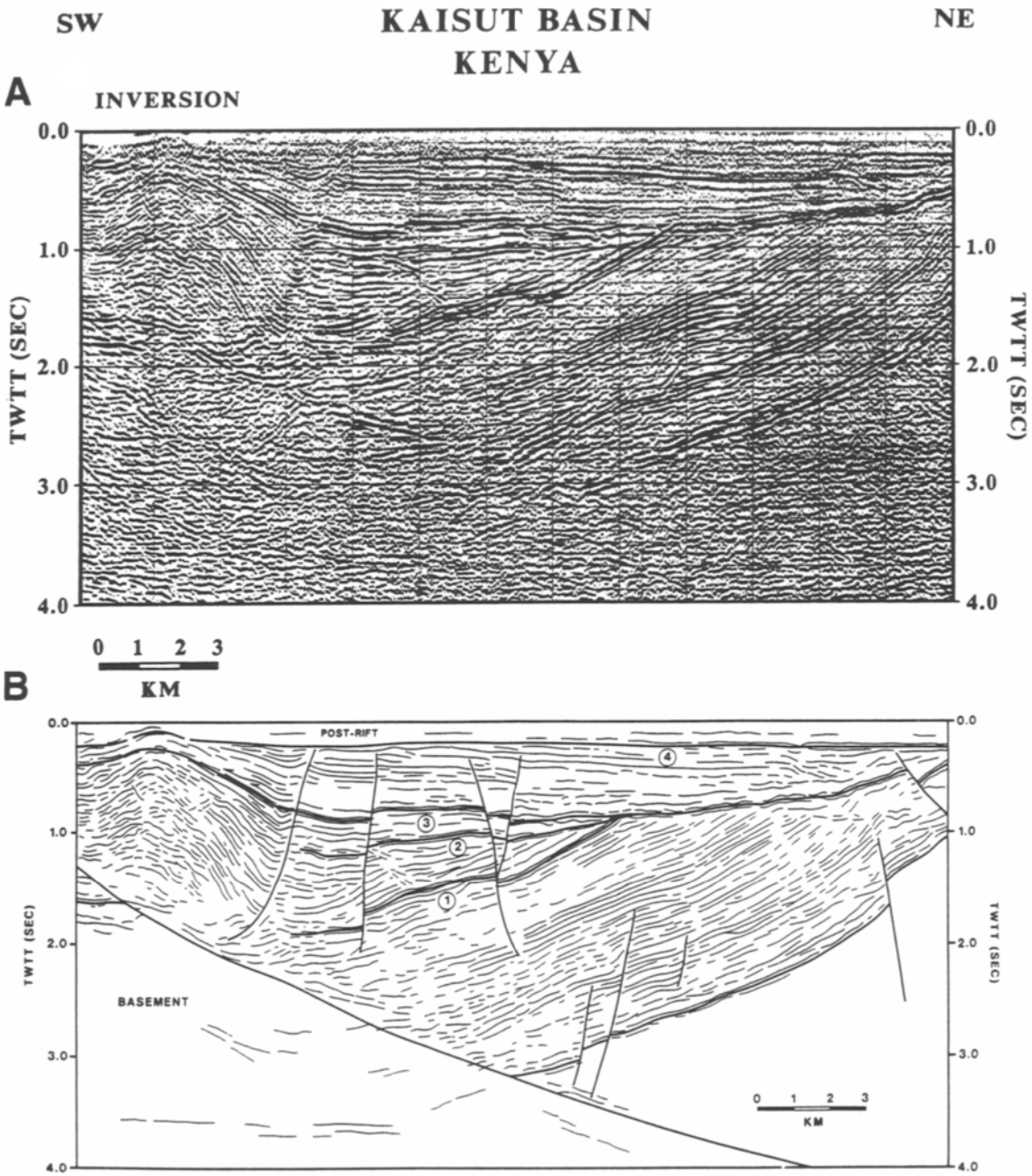

Fig. 3B–2. Seismic reflection record section from the Kaisut Basin of Kenya (from Bosworth and Morely, 1994). TWTT = two-way travel-time. A. Seismic reflection record section. B. Interpreted line drawing of A showing inferred unconformities (numbers 1–4), rift-related (reflections between the basement and unconformity number 4) and post-rift sedimentary rocks, and basement.

An additional characteristic of modern seismic studies is that, increasingly, multiple methods and multiple types of data for the same location are being utilized in an effort to improve resolution, de-

crease the ambiguity of interpretations, and provide information on additional rock properties such as shear-wave velocity, Poisson's ratio, density, electrical properties, seismic attenuation and anisotropy. For example, results of coincident refraction and reflection studies have recently been presented by Mooney and Brocher (1987), Holbrook (1990), Holbrook et al. (1991, 1992a) and Levander et al. (1994). The East African rift system has recently been extensively studied utilizing multiple seismic and other geophysical and geological methods (Prodehl et al., 1994; Braile et al., chapter 5 of this volume) resulting in a substantially-improved understanding of the late-Cenozoic rifting event and its effects in east Africa.

3B.2. Reflection Profiling

During the past 15 years, seismic reflection profiling has received a great deal of attention in lithospheric studies. This technique has been the primary exploration tool of the oil industry for about 50 years. However, reflection data (especially on land) have become widely available in the academic community only since about 1980. A classical reflection survey is designed to record only near-vertical, P-wave reflections (Fig. 3B–1A). Thus, the distance from the source to the most distant receiver is a fraction of the intended maximum depth of penetration. The source is often Vibroseis, a truck-mounted apparatus which vibrates over a carefully controlled sweep of frequencies, rather than an explosion. The popularity of the reflection profiling technique is based on the fact that, in the best of circumstances, the resulting record sections look like vertical cross-sections of the Earth which are easy to interpret, and that the relatively high frequency of the source and dense coverage of seismograms can provide a high resolution image. The major effort after the field work is in data processing which, if successful, makes the interpretation straightforward. The reflection data are displayed as time sections usually in a 2-D plane. Reflected and diffracted energy from outside of this plane can produce complex and possibly misleading images. Furthermore, velocity determination and subsequent conversion of two-way times to depth become more difficult with increasing depth because of the near-vertical incidence of raypaths in reflection data acquisition.

Two main factors tend to pose potential problems to data quality in reflection surveys. As a practical matter, data quality subjectively refers to the clarity of the image presented in the record section. The first of these factors is surprisingly simple and is the large variation in the near-surface seismic velocity. Compensation for these variations is called the static correction which attempts to make small time shifts in the data in order to improve alignments during processing. The other problematical factor is the presence of complicated subsurface geometries and velocity heterogeneity. Migration (e.g., Yilmaz, 1987) is a processing procedure whose goal is to produce record sections in which distortions caused by structure are unraveled. Accurate migration requires a knowledge of velocity, and velocity determinations require reasonable knowledge of geometry (i.e., an accurate migration).

Crustal reflection profiling in rift zones has been very successful in delineating shallow (0 to ~ 20 km) fault structures, the geometries of rift basins, including grabens, associated with extension, and seismic characteristics of the lower crust and the crust-mantle boundary or Moho (Hale and Thompson, 1982; Braile and Chiang, 1986; Jarchow and Thompson, 1989; Mooney and Meissner, 1992). A summary of crustal studies using deep reflection profiling is contained in Brown (1986). Examples of crustal reflection profiling in rift zones include experiments in the Basin and Range province (Allmendinger et al., 1983; Hauge et al., 1987), the Rio Grande rift (Brown et al., 1980), the East African rift (Rosendahl, 1987), and the Anza rift in East Africa (Bosworth and Morley, 1994). An example of a seismic reflection record section is shown in Figure 3B–2. The record section provides a detailed image of fault structures and basin geometry and, with the addition of geological data, can provide the basis for interpretation of the tectonic history of a rift.

3B.3. Refraction (Wide Angle) Profiling

The seismic refraction technique as classically practiced has provided much of the data available on crustal thickness and uppermost mantle P-wave velocities. However, many of these results have assumed overly-simple Earth models (Fig. 3B–1B). In the seismic refraction technique, the distance from the source to the most distant receiver is several times the intended maximum depth of penetration. Elementary texts on seismic exploration leave the impression that only critically-refracted waves that travel along interfaces (i.e., head waves) are interpreted in such studies. When employed to study crustal structure, the term refraction survey is in fact a misnomer because many reflected phases are also interpreted. It is better to think of such surveys as wide-angle experiments because they stress the interpretation of waves which intersect interfaces at angles greater than a few degrees, often greater than the critical angle. However, wide-angle surveys yield results which are not straight-forward to interpret. The strength of such surveys is the resolution possible in determining velocities. The weakness is ambiguities which arise when complex structures are encountered. The first step in interpreting wide-angle seismic data is the correlation of the observed phases. This subjective task may be difficult for secondary arrivals. To facilitate such a correlation, all seismograms along a profile are usually arranged into a record section according to their distance from the shotpoint using reduced travel times. The reduced travel time (Tr) is defined as the observed travel time (T) minus distance (D) divided by the reduction velocity (Vr): $Tr = T - D/Vr$. For the investigation of compressional (P) waves propagating in the crust, $Vr = 6$ km/s is a suitable and widely-used reduction velocity, while for the investigation of the uppermost mantle, 8 km/s is normally used for P-wave studies. The second step, after the correlation of the recorded seismic waves, is the inversion of the observed time-distance data T(D) into velocity-depth functions V(z). The simplest case occurs when the correlated travel-time curves are straight-line segments. Under the assumption that the Earth's crust and upper mantle consist of layers with constant velocities separated by discontinuities at which the velocity increases discontinuously from V(i) to V(i+1), formulas have been developed to calculate layer velocities, depth, and dip of the corresponding layers (e.g., Bullen and Bolt, 1985; Officer, 1958; Perrier, 1973; Steinhart and Meyer, 1961). Curved segments can occur in first as well as in later arrivals. When later arrivals are fitted by concave travel time curves, they can be interpreted as reflections from first-order discontinuities. Computer methods have been developed to simultaneously model reflection and refraction arrivals from a number of sources to multiple receivers (Fig. 3B–1C). These methods, sometimes known as seismic travel-time inversion (Zelt and Smith, 1992), are similar to seismic tomography, but utilize backscattered rather than transmitted energy (Nowack and Braile, 1993). An example of a travel-time inversion for data from the Kenya rift is shown in Figure 3B–3. Additional discussion of wide-angle seismic methods and examples of applications are included in Holbrook (1990) and Holbrook et al. (1992b).

In order to include the analysis of observed amplitudes and waveforms and thus check the reliability of the velocity-depth models obtained by travel-time studies, synthetic seismogram techniques using ray theoretical and reflectivity methods have been developed (e.g., Fuchs and Mueller, 1971; Kind, 1976; Cerveny et al., 1977; Kennett, 1983). These methods assume an elastic half space consisting of homogeneous, horizontal and isotropic layers. In the reflectivity method (Fuchs, 1968), the complete wave field is computed, including all shear waves, converted phases (P to S or vice versa), multiple phases, etc. In the ray method, the wave field

Fig. 3B–3. Crustal seismic model and seismic raypaths representing the data and model parameters used in travel-time inversion. Seismic data are from the KRISP90 experiment in Kenya (Braile et al., 1994). The travel-time data consisted of refracted and wide-angle reflected arrivals recorded at seismographs along the 450 km profile from shotpoints at VIC, KAP, BAR, TAN, BAS, and CHF. A. Velocity model for the shallow crust derived by inversion of refracted arrivals corresponding to raypaths shown in B. C. Derived velocity model (numbers in model are seismic compressional wave velocities in km/s) and raypaths for deep crust and uppermost mantle travel times across the Kenya rift.

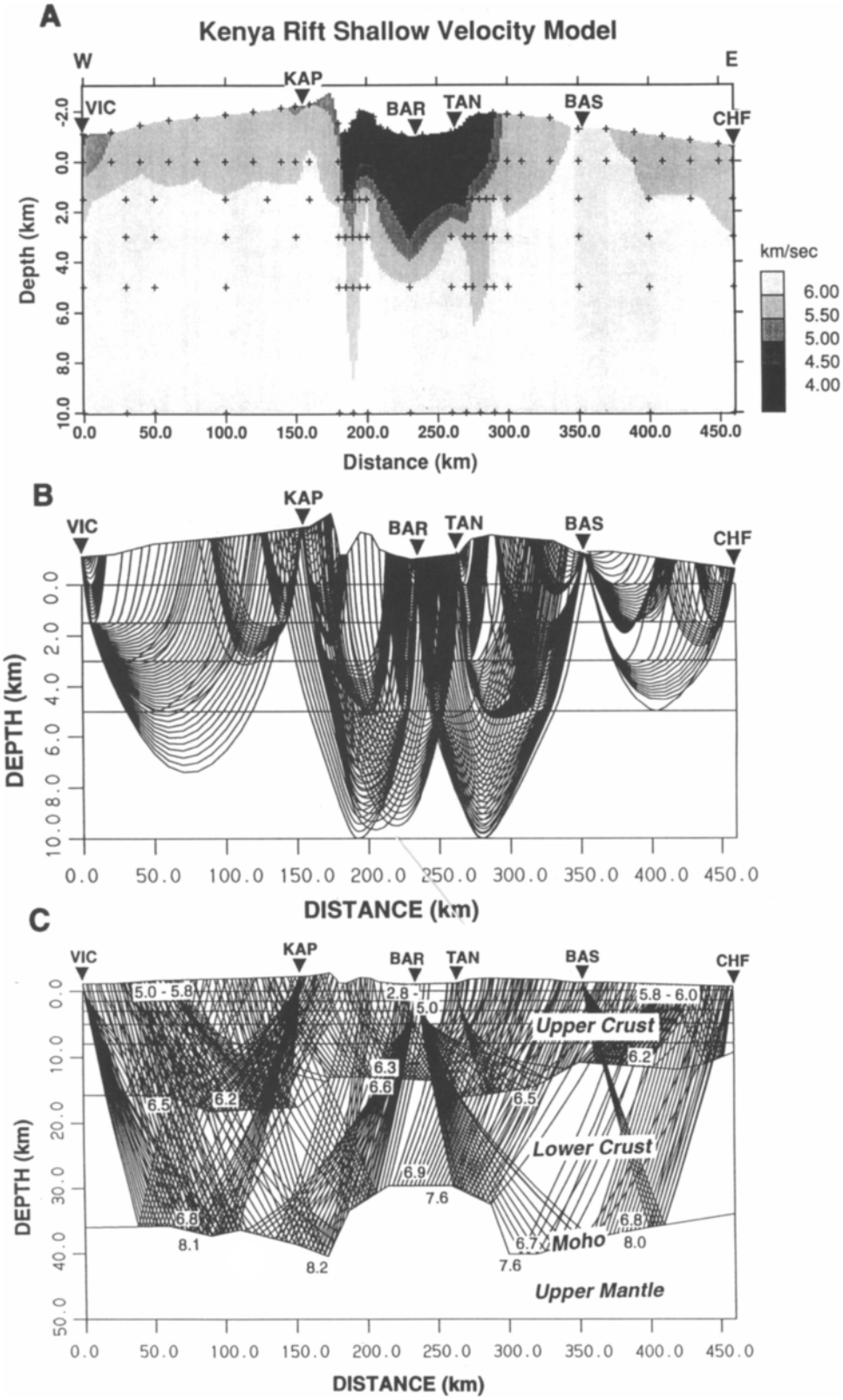
A
Kenya Rift Shallow Velocity Model
W
E
KAP
VIC
BAR
TAN
BAS
CHF
Depth (km)
-2.0
0.0
2.0
4.0
6.0
8.0
10.0
0.0
50.0
100.0
150.0
200.0
250.0
300.0
350.0
400.0
450.0
Distance (km)
km/sec
6.00
5.50
5.00
4.50
4.00
B
KAP
VIC
BAR
TAN
BAS
CHF
DEPTH (km)
0.0
2.0
4.0
6.0
8.0
10.0
0.0
50.0
100.0
150.0
200.0
250.0
300.0
350.0
400.0
450.0
DISTANCE (km)
C
VIC
KAP
BAR
TAN
BAS
CHF
5.0 - 5.8
2.8 - 5.0
5.8 - 6.0
Upper Crust
6.2
6.3
6.6
6.5
6.2
6.5
Lower Crust
6.9
7.6
6.8
8.1
8.2
6.7
Moho
7.6
6.8
8.0
Upper Mantle
DEPTH (km)
0.0
10.0
20.0
30.0
40.0
50.0
0.0
50.0
100.0
150.0
200.0
250.0
300.0
350.0
400.0
450.0
DISTANCE (km)

is separated into elementary waves corresponding to groups of kinematically analogous waves. For a system of homogeneous and parallel layers, elementary seismograms can be computed exactly from ray theory (Mueller, 1970). However, numerical tests have shown that an approximate ray method (Cerveny et al., 1977) yields satisfactory results in most applications.

The reflectivity method at present can only be applied to one-dimensional velocity-depth distributions. For the ray method, however, programs have been developed which allow the calculation of travel times and amplitudes for rays traveling through laterally inhomogeneous structures (e.g., Cerveny and Psencik, 1984; Cerveny, 1985). A combination of 1D and 2D-modeling and interpretation procedures is usually most effective.

In the last few years wide-angle interpretation procedures have not only been applied to P-wave observations, but also to S-wave data which in many cases can be correlated reliably on modern, three-component data sets. In addition, off-line recordings have also been analyzed (e.g., Milkereit et al., 1986).

Another procedure to investigate data sets which are not obtained as observations along profiles but by three-dimensional arrays, is the time-term method, which has been successfully employed by Bamford (1973, 1977). Here, delay times for a particular phase are calculated and the deviations from an average are interpreted as changes in depth to a particular discontinuity. Under certain assumptions this method also allows for investigation of velocity variations at a particular boundary and possible systematic azimuthal variations. For southern Germany and the western United States, Bamford (1973) and Bamford et al. (1979) have predicted the presence of anisotropy beneath the Moho using this method.

In special workshops of the Commission on Controlled Source Seismology of the International Association of Seismology and Physics of the Earth's Interior the different interpretation techniques have been applied by various authors to the same data sets and the results have been compared (Ansorge et al., 1982; Mooney and Prodehl, 1984; Finlayson and Ansorge, 1984). These results provide useful insights into the differences in velocity models produced by various interpretation methods.

3B.4. Teleseismic Techniques

Seismic reflection and refraction techniques are termed "active" in that they involve manmade sources controlled during the experiment. Natural seismic events (earthquakes) also provide a wide variety of information on lithospheric structure and involve "passive" monitoring, usually for extended periods of time. Teleseismic techniques utilize signals from distant sources that arrive at the receivers at near-vertical angles of incidence (Fig. 3B–1D). The travel times of such waves are compared to those for standard, average Earth models. In order to correct for source location errors and deviations from the assumed average Earth model that are not in the area of interest, a reference (base) station is usually established which is outside the primary area of interest. The travel time to this station is used as a reference and travel-time differences with respect to this station (relative residuals) or delay times are the actual observations which are analyzed. The spatial pattern of relative residuals contains information on the shape and magnitude of velocity anomalies under the seismic network. Profiles or 2-D arrays of stations can be employed. Such studies in modern rifts have found that P-waves arrive 1–2 seconds late (Fairhead and Reeves, 1977; Nolet and Mueller, 1982; Davis et al., 1984, Parker et al., 1984; Savage and Long, 1985; Achauer et al., 1988; Green et al., 1991; Green and Meyer, 1992; Davis et al., 1993; Slack et al., 1994). An example of data and modeling of teleseismic delay-time data for the Kenya rift is shown in Figure 3B–4.

Fig. 3B–4. Teleseismic modeling applied to the KRISP85 and 90 data for the Kenya rift (Slack et al., 1994). A. Average relative travel-time residual (in seconds) for teleseismic raypaths used in delay-time inversion to determine upper mantle compressional wave velocities. Station locations are shown by the X and late (positive) and early (negative) arrivals are indicated by the circle and square symbols. B. Upper mantle velocity model used to fit the travel time residuals in A. Velocities below the derived smooth surface are 7.5% lower than above the surface (modified from Slack et al., 1994). Distances are in km. The (0,0) location is the center of the seismograph array.

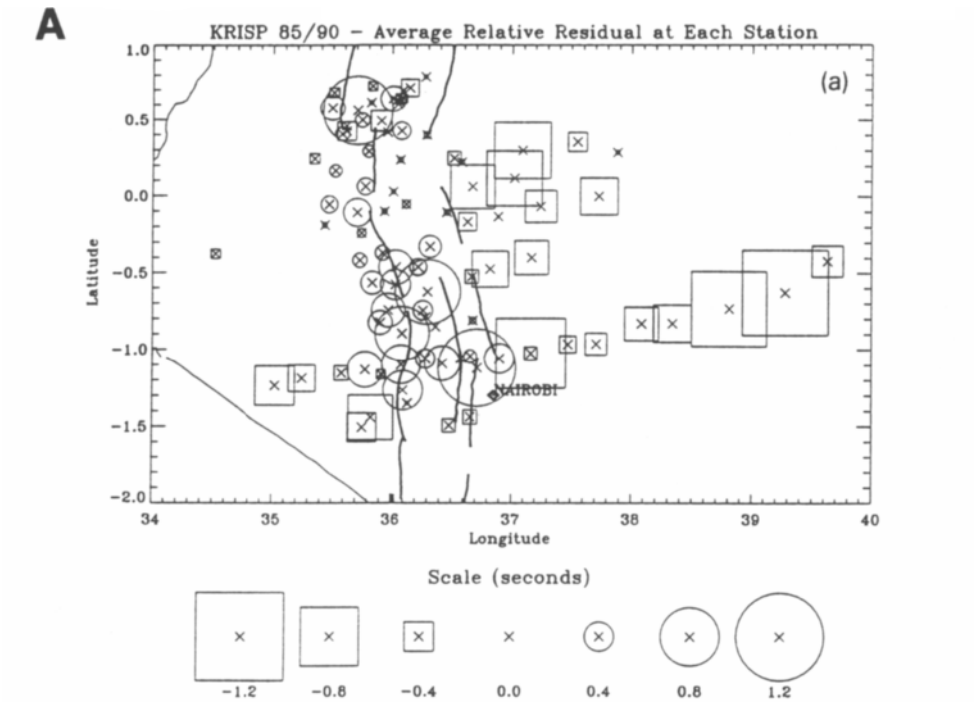
A
KRISP 85/90 – Average Relative Residual at Each Station
(a)
Latitude
Longitude
NAIROBI
Scale (seconds)
-1.2
-0.8
-0.4
0.0
0.4
0.8
1.2

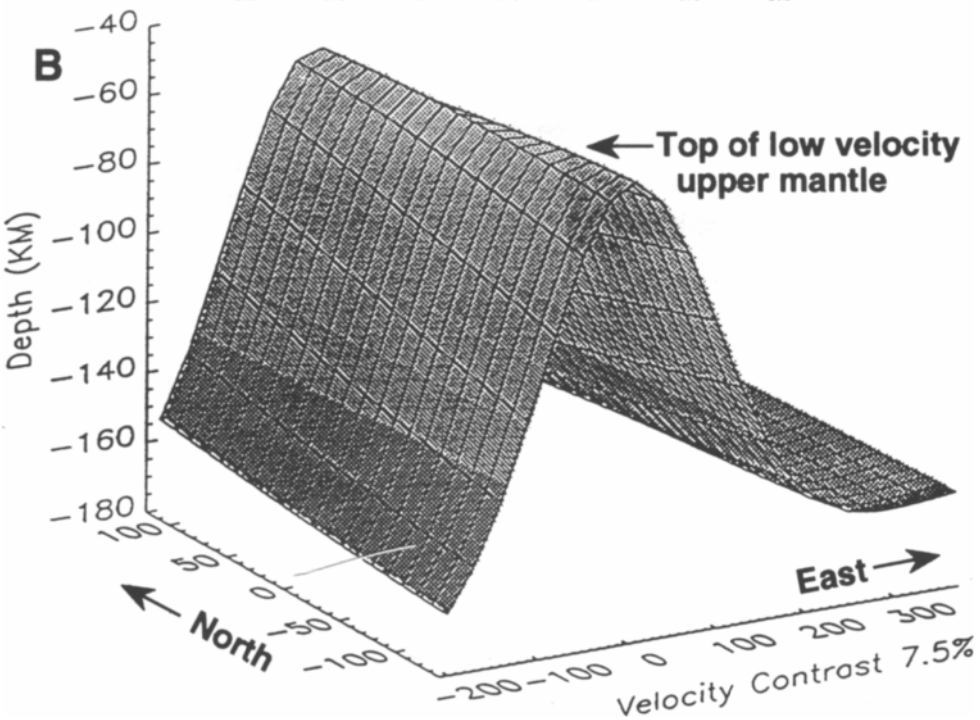
B
Top of low velocity upper mantle
Depth (KM)
North
East
Velocity Contrast 7.5%

In the absence of independent controls, teleseismic studies involve a velocity contrast-volume ambiguity similar to the density contrast-volume ambiguity encountered in gravity studies. With crustal models from reflection and refraction studies as constraints, teleseismic data provide a major source of relatively detailed information about the upper mantle. However, resolution is usually only a few 10's of km in upper mantle studies. Both P-wave and S-wave velocity variations can be analyzed and attenuation (Q^{-1}) variations have also been derived (Slack et al., 1994). On a smaller scale, the teleseismic approach can be effectively utilized to study 3D-features such as magma chambers (Iyer, 1984; Sanford and Einarsson, 1982; Achauer et al., 1986). For quantitative modeling of the P-residuals, a three-dimensional inversion technique developed by Aki et al. (1976, 1977) is used. In this technique, the Earth under the seismic array is divided into rectangular blocks. The starting model is a stack of homogeneous, plane, parallel layers overlying a standard Earth. The velocities in the blocks are then perturbed resulting in travel-time changes within each block, which, when summed along the raypath produces a result equivalent to the observed residuals. Thus, for events from many azimuths recorded at the stations of the network, a series of linear equations is generated relating the observed residuals and the perturbation in each block. The equations are usually solved using a damped least-squares inversion technique. The final results are in percentages of velocity perturbations for each block (Iyer, 1984).

In addition to the analysis of travel time anomalies, recent studies of broadband data (e.g., Owens et al., 1984; 1987) show that the careful analysis of teleseismic waveforms (receiver functions) can provide reasonably detailed data on crustal structure. In the receiver function method, waveform information contained in the seismogram is analyzed by comparing time- or frequency-domain synthetic data (calculated for an initial layered velocity model) with the observed seismograms. The modeling procedure may involve trial-and-error comparisons or an automated (inversion) technique. Usually, shear-wave signals and their S to P conversions and multiple reflections (Fig. 3B–1F) within the crust or other lithospheric layers are included in the analysis. Multicomponent recordings are usually necessary, at least partially so that source wavelet effects can be removed. Averaging of several seismograms or using the average of seismograms from a small array of receivers can improve the stability of the inversion procedure and resolution of the derived model. Because the method requires only a single 3-component seismic station, it is very cost-effective. However, 2- and 3-dimensional velocity variations, if present, may limit the accuracy and applicability of this technique.

3B.5. Studies of Local and Regional Earthquakes

Local and regional earthquakes provide information about Earth structure in a variety of ways. The resolution attainable is heavily dependent on the distribution of stations and sources. Data from networks of seismographs can be interpreted in terms of crustal phases and analyzed in a fashion similar to refraction data (e.g., Mitchell and Hashim, 1977). Waveforms of body waves can also yield information about crustal structure (e.g., Wallace, 1986).

Data from dense networks such as exist in southern California lend themselves to tomographic analysis of both crustal (Hearn and Clayton, 1986a, b; Walck and Clayton, 1987) and upper mantle (Humphreys et al., 1984) structure. The tomographic approach requires a high density of both recording stations and recorded signals corresponding to relatively uniform raypath coverage.

An interesting approach to determining structure within an array is to invert simultaneously for Earth structure and earthquake hypocenters (Fig. 3B–1E). Thus, the search is for the combination of 3D-Earth model and earthquake locations which is optimal in a least-squares sense (e.g., Benz and Smith, 1984; Roecker et al., 1987; Shedlock and Roecker, 1987; Kissling, 1988).

3B.6. Analysis of Surface Waves

Surface waves are fundamentally different from body waves (P and S) in that they are dispersed (i.e., the velocity varies with period) and travel along the

surface of the Earth. The depth of penetration is proportional to the wavelength. Thus, long period waves penetrate deeper, encountering faster material and in turn travel faster. A useful rule-of-thumb is: the maximum depth (in km) for which a surface wave is capable of resolving velocity structure is on the order of the longest period (in seconds) for which data are available (greater depth penetration occurs for higher mode surface waves). For example, dispersion results which extend to periods of 50 s can resolve the velocity structure to a depth of about 50 km. The pattern of dispersion (group or phase velocity versus period) is modeled (Fig. 3B–1G) in terms of horizontal layered Earth models to determine average velocity structure between the source and a single station or between two or more stations. Kovach (1978) provides a review of these waves and their analysis.

Surface waves have relatively low resolution (usually ±3–5 km for Moho depths, for example) but are important because they are primarily sensitive to variations in shear wave velocity (Der et al., 1970). The 2-D and 3-D variations of velocity with period (dispersion) can be analyzed using the dispersion curves or waveform modeling with synthetic seismograms to determine Earth structure (Lerner-Lam and Jordan, 1983; Nakanishi, 1993) and Q^{-1} (Burton, 1974) although the procedures are complicated. Measurements in rift zones have indicated relatively low shear velocities in the crust and the upper mantle (Mueller and Bonjer, 1976; Sinno and Keller, 1986) beneath rifts.

3B.7. Seismicity Studies

Studies of earthquakes in rifts also provide useful information that is not directly related to seismic velocity structure. The most commonly used results from earthquake studies are focal mechanisms and the determination of spatial and temporal variations in seismicity which indicate characteristics of faulting and extension (or other deformation). Focal mechanisms are a major source of data on stress orientations (e.g., Zoback and Zoback, 1980). However, stress orientations inferred from focal mechanisms have an accuracy of about ±15°. Furthermore, if only P-wave first motions are used in the focal mechanism determination, there are two nodal planes which could be the actual fault plane. This ambiguity is removed if S-wave polarizations and/or surface wave analysis are included in the determination. Detailed source studies involving waveform modeling provide a means to compare deep-seated processes to surface faulting (e.g., Doser, 1986). If an area is instrumented densely enough (a seismic network or array) to accurately determine hypocenters, three-dimensional plots or hypocentral cross-sections can be constructed which allow the attitude of active fault planes to be delineated (Fig. 3B–1H).

3B.8. Seismic velocities in rift zones – Information from laboratory studies of rock properties

Seismic studies of rift zones provide information on the seismic velocity structure of the crust and upper mantle. Interpretation of these velocity determinations is facilitated by comparisons with the velocity structure of other regions and with statistical summaries, and by consideration of seismic velocity measurements on rock samples in the laboratory. In this section, we briefly review the available information on seismic velocity studies from laboratory data and their implications for the interpretation of the crustal structure of rifts. Only velocity measurements for crystalline rocks which may be important constituents of the continental crust and upper mantle will be considered. Furthermore, only compressional velocity measurements will be discussed because only limited shear-wave velocity information on the crustal structure of continental rifts is available.

A large number of laboratory velocity measurements on rocks have been published beginning with the early work of Birch and Bancroft (1938), Birch (1943, 1958, 1960, 1961), Hughes and Cross (1951), and Hughes and Maurette (1956, 1957). Compilations of laboratory velocity data are contained in papers by Press (1966) and Christensen (1989a). A recent review of the composition and laboratory seismic velocity determinations of continental crustal

Table 3B.3.
References for rock properties data in Figures.

Figure	Data	References
3B.5	Vp-SiO_2	1, 2, 6, 12, 13, 17, 19, 21, 22, 23
3B.6	dVp/dP	1, 2, 3, 4, 5, 6, 7, 8, 9, 11, 12, 13, 18, 19, 21, 22, 23, 25, 27, 28, 29, 30, 31
3B.7	dVp/dT	5, 9, 10, 14, 15, 16, 20, 21, 22, 23, 24, 26, 29, 30, 31, 32
3B.8	Anisotropy	1, 2, 4, 6, 7, 8, 9, 11, 12, 13, 17, 18, 19, 20, 21, 22, 25, 26, 27, 28, 29
3B.9	Vp-Density	1, 2, 3, 4, 6, 7, 8, 9, 11, 12, 13, 17, 18, 19, 21, 22, 23, 25, 26, 27, 28, 29, 30

References:

1. Birch, 1960; 1961
2. Burke and Fountain, 1990
3. Christensen, 1974
4. Christensen, 1978
5. Christensen, 1979
6. Christensen, 1989a
7. Christensen and Fountain, 1975
8. Chroston and Brooks, 1989
9. Chroston and Evans, 1983
10. Fielitz and Clausthal-Zellerfeld, 1971
11. Fountain, 1976
12. Fountain and Christensen, 1989
13. Fountain et al., 1990
14. Hughes and Cross, 1951
15. Hughes and Maurette, 1956
16. Hughes and Maurette, 1957
17. Jackson and Arculus, 1983
18. Kern, 1978
19. Kern, 1982
20. Kern and Fakhimi, 1975
21. Kern and Richter, 1981
22. Kern and Schenk, 1985
23. Kern and Schenk, 1988
24. Kroenke et al., 1976
25. McDonough and Fountain, 1988
26. Meissner and Fakhimi, 1977
27. Mooney and Christensen, 1994
28. Padovani et al., 1982
29. Peselnick and Nicolas, 1978
30. Peselnick et al., 1977
31. Ramananantoandro and Manghnani, 1978
32. Spencer and Nur, 1976

rocks is presented by Fountain and Christensen (1989) along with an extensive list of references on rock properties. Holbrook et al. (1992a) have recently provided a compilation of lower crustal rock properties data including P- and S-velocities, density, anisotropy, and Poisson's ratio. Christensen and Wepfer (1989) provide a discussion of laboratory methods for measuring rock velocities and limitations of those methods.

In our compilation of laboratory values of rock properties, we have collected available data from published literature (see sources of data listed in Table 3B–3) on compressional wave velocity, composition (a few chemical components such as percentage SiO_2, percentage Fe_2O_3 + MgO, have been tabulated), density, the pressure derivative of velocity (dVp/dP), the temperature derivative of velocity (dVp/dT), and the percentage of anisotropy. For each rock sample, we have classified the rock as upper crustal, lower crustal, or upper mantle, following the descriptions and classifications (which are based on the field location of the collected rock sample, its composition, and the presence of pressure and temperature range indicators provided by mineralogy and metamorphic grade) given by the authors of the laboratory studies. Although not all types of data exist for each sample, our compilation contains information for over 400 rock samples which are inferred to be representative of the Earth's continental crust and the uppermost mantle and which have been analyzed in rock properties laboratories.

It is well known that the seismic velocity of rocks is a function of confining pressure, pore pressure, temperature, anisotropy and composition. Because continental rift zones are sites of magmatic activity and anomalous heat flow, we expect that the most important factors controlling crustal seismic velocity variations in rifts are composition and temperature. Magmatic intrusions into the crust in rifts and depletion of associated upper mantle source regions could result in significant compositional variations which might be evidenced by seismic velocity anomalies. However, the volumes of extrusive or intrusive rocks must be substantial if measured crustal velocities are to be significantly affected by this mechanism (Humphreys and Dueker, 1994). Thermal metamorphism caused by the anomalously high crustal temperatures and the resulting higher metamorphic grade, may be important in rift zones. Laboratory measurements show that the velocities of rocks varies strongly as a function of bulk chemical composition and metamorphic grade which affects the petrologic content. In general, the velocity is inversely correlated with total SiO_2 content, and directly correlated with $FeO+Fe_2O_3+MgO$ content and with increasing metamorphic grade (Christensen, 1965; Holbrook et al., 1992a). For crystalline igneous rocks, the seismic velocity varies systematically according to SiO_2 content and therefore rock type as shown in Figure 3B–5. Note that the velocities for the laboratory rock samples plotted in Figure 3B–5 do not include the effect of temperature. At depths of about 20 km (~ 600 MPa pressure), *in situ* velocities will be reduced by about 0.2 to 0.5 km/s depending on rock type, and temperature-depth curves which are associated with specific heat-flow provinces. Further analyses of the depth (pressure) and temperature effects on velocity are presented below.

At low confining pressures (less than about 200 MPa), corresponding to depths of about 0 to 5 km in the crust, seismic velocity is strongly influenced by pressure because of the closing of cracks and pore spaces. At higher pressures, velocity varies approximately linearly with confining pressure with a derivative of approximately 2.7×10^{-4} km/s/MPa (Fig. 3B–6). Because the effect of pressure on rock velocity is relatively constant for a wide range of rock

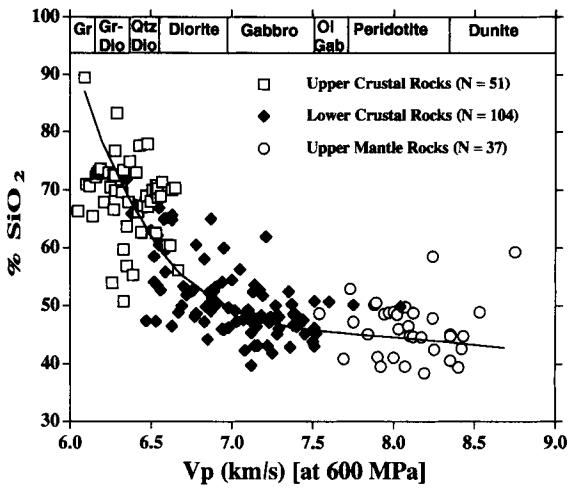

Fig. 3B–5. Laboratory-measured compressional wave velocities (Vp) for rock samples representative of crustal and uppermost mantle rocks plotted versus percentage of SiO_2 in the samples. Data sources are listed in Table 3B–3. The rock types (Gr = granite, Gr-Dio = granodiorite, Ol Gab = olivine gabbro) shown at the top of the diagram correspond to the velocity ranges (corrected to 600 Mpa) calculated for the crust and upper mantle rock types by Christensen (1965). N = number of samples. The line through the data represents approximate relationship of Vp and SiO_2 percentage based on the laboratory measurements on the rock samples.

types, it is possible to account for the pressure effect with reasonable confidence in interpretation and results for all rock types (upper crustal, lower crustal and upper mantle) have been combined in our compilation (Fig. 3B–6). In certain environments, pore pressure may be an important factor controlling the seismic velocity of rocks. High pore pressures in the crust can lead to significantly reduced seismic velocities (Christensen, 1989b). A more extensive discussion of these effects is contained in Fountain and Christensen (1989).

Temperature has a strong effect on seismic velocity and should be an important factor in controlling the crustal and upper mantle velocity structure of continental rifts where thermal anomalies are pronounced. Increased temperatures nearly always produce lower compressional wave velocities in rocks which are likely constituents of the continental crust and upper mantle. A compilation of laboratory ve-

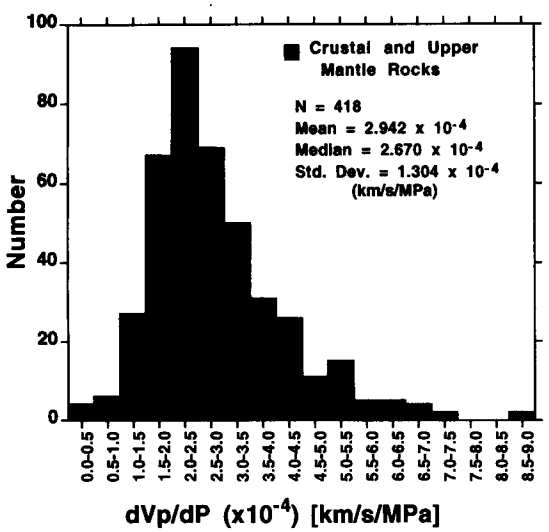

Fig. 3B–6. Histogram of pressure derivative (dVp/dP, compressional wave velocity as a function of pressure) data for crustal and upper mantle rock samples. Derivatives are calculated from confining pressure measurements in the range of 200–1000 MPa. Data sources are listed in Table 3B–3. A summary of statistics is given in Table 3B–4.

locity measurements of the temperature derivative (dVp/dT) is illustrated in histogram form in Figure 3B–7. Median values of the temperature derivatives for the three rock types shown (Table 3B–4) vary from about –3.9 to –5.4 × 10^{-4} km/s/°C. Such values indicate that temperature anomalies of a few hundred degrees will produce observable velocity anomalies.

For example, ultramafic rocks in the uppermost mantle in a high heat flow region could easily be at a temperature that is 500°C higher than in an area of normal heat flow. This temperature difference would cause the compressional wave velocity to be decreased by about 0.27 km/s, assuming a derivative of –5.4 × 10^{-4} km/s/°C appropriate for ultramafic rocks (Table 3B–4). Because the crustal thickness in high heat flow regions is often substantially less than in normal continental areas, it is also necessary to consider the pressure effect. Using the pressure derivative of 2.67 × 10^{-4} km/s/MPa (Fig. 3B–6 and Table 3B–4) and an average crustal density of 2.9 g/cm^3, the pressure effect becomes 7.4 × 10^{-3} km/s/km as a function of depth. Thus, a 10 km thinner crust would result in an expected decrease in upper mantle seismic velocity of 0.074 km/s. Combining the pressure and temperature effects, upper mantle rocks in a high heat flow region with a thin crust may have a contrast in seismic velocity of about –0.35 km/s. Therefore, upper mantle beneath cratons with seismic velocity of 8.0 km/s may be the same rock composition as 7.65 km/s mantle beneath a high heat flow region. The suggestion that temperature in the mantle is a primary control on P_n velocity has been made based on statistical analysis of North American P_n velocity data (Black and Braile, 1982).

Intrusion into the crust is an efficient mechanism to transfer heat to the crust and may result in significant compositional heterogeneity. Mafic intrusions into the lower crust could produce no significant seismic velocity anomaly (velocity of hot intruded material is approximately equal to the velocity of the surrounding lower crust) while the intrusion and crust are still hot (during and within a few million years of a rifting and magmatic event), while after sufficient time for cooling, the intrusion may have a higher than normal velocity. Even after cooling, the relatively small velocity contrast between

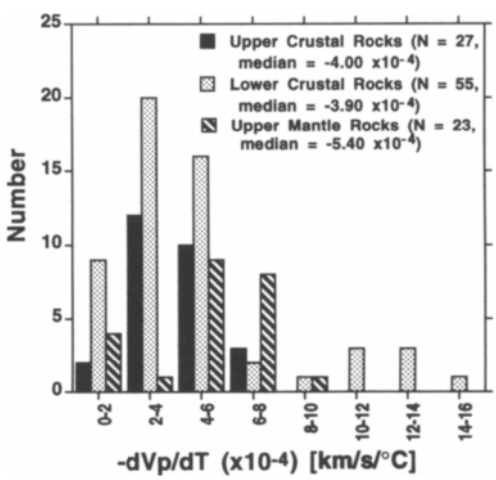

Fig. 3B–7. Histograms of the temperature derivative (dVp/dT, compressional wave velocity as a function of temperature) for laboratory samples of upper crustal, lower crustal and upper mantle rocks. Data sources are listed in Table 3B–3. A summary of statistics is given in Table 3B–4.

Table 3B-4.
Rock properties statistical summaries.

Figure	Property*	Units	Number of Samples	Mean	Median	Standard Deviation
3B.6	dVp/dP	km/s/MPa	418	$2.942\ 10^{-4}$	$2.670\ 10^{-4}$	$1.304\ 10^{-4}$
3B.7	dVp/dT (u.c. rocks)	km/s/°C	27	$-4.192\ 10^{-4}$	$-4.000\ 10^{-4}$	$1.529\ 10^{-4}$
	dVp/dT (l.c. rocks)	km/s/°C	55	$-4.816\ 10^{-4}$	$-3.900\ 10^{-4}$	$3.423\ 10^{-4}$
	dVp/dT (u.m. rocks)	km/s/°C	23	$-5.030\ 10^{-4}$	$-5.400\ 10^{-4}$	$2.003\ 10^{-4}$
3B.8	Anisotropy (u.c. rocks)	%	102	4.137	2.700	3.864
	Anisotropy (l.c. rocks)	%	164	4.935	3.200	4.890
	Anisotropy (u.m. rocks)	%	74	4.642	3.900	3.045

*Vp = compressional wave velocity, P = pressure, T = temperature, u.c. = upper crust, l.c. = lower crust, u.m. = upper mantle.

intruded mafic rocks and "normal" low crustal velocities may cause the intrusions to be undetectable on the basis of seismic velocities from crustal seismic data. Mafic intrusions into the upper crust will normally produce substantial velocity anomalies.

Observations of outcrops and laboratory measurements indicate that most rocks are anisotropic (Fountain and Christensen, 1989). However, in continental regions, significant anisotropy (greater than a few percent) has rarely been observed in large-scale experiments and it is likely that in most parts of the continental crust, isotropy (or at least transverse isotropy) is a reasonable approximation considering the inherent averaging of velocities over many wavelengths of the propagation path. A compilation of laboratory-measured anisotropy data for the compressional wave velocity of upper crustal, lower crustal and upper mantle rock types is shown in Figure 3B–8. A statistical summary of the data is given in Table 3B–4 and the sources of data are listed in Table 3B–3. The median anisotropy for the three rock types is relatively small (2.7 to 3.9%), although some significantly larger (> 10%) values of anisotropy have been observed, and the medians increase slightly from upper crust to lower crust to upper mantle rock types. The measured anisotropy of a rock layer or volume in crustal and upper mantle studies may be significantly lower (or even zero) than the laboratory samples if anisotropic directions are not consistently aligned. Anisotropies of less than 1–2% are extremely difficult to (statistically) resolve from analysis of crustal seismic data. Nevertheless, under appropriate circumstances, it is likely to observe at least small anisotropy in continental crustal seis-

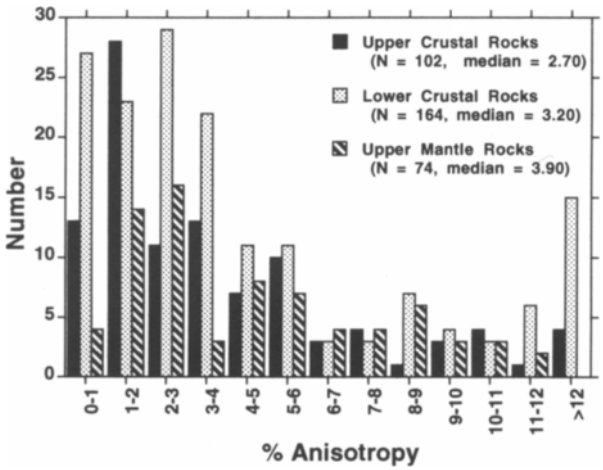

Fig. 3B–8. Histograms of percentage of compressional wave velocity anisotropy for laboratory samples of upper crustal, lower crustal and upper mantle rocks. Data sources are listed in Table 3B–3. A summary of statistics is given in Table 3B–4.

mic studies. Such observations have been reported (e.g., Bamford, 1977; Bamford et al., 1979). Furthermore, anisotropy can be a possible explanation for discrepancies between reflection (near-vertical raypaths) and refraction and wide-angle (near-horizontal raypaths) observations of velocity for data at the same location. Refraction and reflection data can be simultaneously modeled to determine anisotropy (Boztepe and Braile, 1994).

Crustal and upper mantle models interpreted from seismic data are commonly checked and refined by computing the gravity response of equivalent density models. Velocity-density relations are used, at least initially, to estimate appropriate densities in the crust and upper mantle of the density model. Velocity-density data from laboratory measurements of rock properties often display a linear relation although substantial scatter, and, therefore, ambiguity in interpretation, is also observed (Barton, 1986). Furthermore, the velocity-density data from laboratory measurements are observed at relatively low pressures and temperatures and may not be appropriate for predicting density of molten or nearly-melted materials such as could be present in crustal intrusions and in anomalously hot upper mantle. From our rock properties compilation, we have computed the velocity-density relations shown in Figure 3B–9.

3B.9. Crustal seismic velocity structure of continental rifts - a statistical analysis of data from North America

A recently completed compilation of crustal seismic models for the North American continent (Braile et al., 1989; Mooney and Braile, 1990) provides data for comparison of seismic properties of rift areas with other regions of the continental crust. The North American data set is particularly suited to a statistical analysis and comparative studies because a reasonably large number of crustal models have been determined and the North American continent consists of a wide range of age and types of geologic provinces that include both modern and paleorifts. Although unable to provide detailed information relative to any particular rift or geographic area, a statistical analysis of crustal models has the advantage of illuminating general characteristics and trends, "smoothing out" random variations and discrepant points, and emphasizing representative values. A complete listing of the sources of models in the crustal structure compilation, a discussion of the procedures, assumptions and limitations of the data and compilation methods, and some statistical analysis of the continent-wide data is contained in Braile et al. (1989) and Mooney and Braile (1989).

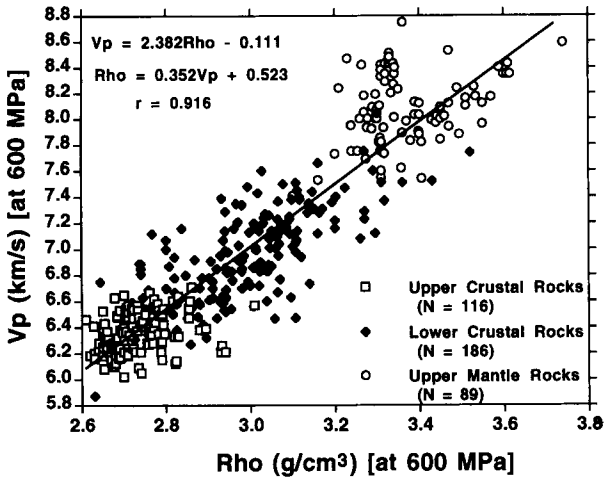

Fig. 3B–9. Plot of compressional wave velocity (Vp) versus density (Rho) for laboratory samples of upper crustal, lower crustal, and upper mantle rocks. Data sources are listed in Table 3B–3. The line and associated equations were derived by a least squares (linear) fit to the data. r = correlation coefficient for the fit.

The crustal velocity structure compilation for North America consists of tabulations of the crustal thickness (Hc), upper mantle compressional wave velocity (P_n), and the average compressional wave velocity of the crystalline crust ($\overline{Vp}$). The crustal structure information is derived from seismic models from 247 seismic studies for continental North America. As an example of the utility of these data, a contour diagram of the North American crustal thickness (Hc) data is shown in Figure 3B–10 with physiographic provinces identified and the locations of selected rifts and other tectonic features illustrated. The data are organized by province for ease of location of individual profiles on maps and to facilitate subsequent analysis of parts of the data set.

The crustal seismic parameters for North America have been separated into rift and non-rift areas. The rift zones include modern rifts (Rio Grande, Basin and Range and Salton Trough), paleorifts (Midcontinent Rift and New Madrid rift), and the Coastal Plain which is the passive continental margin formed by rifting of the Atlantic and Gulf of Mexico oceans in the Mesozoic and is, therefore, technically, part of a paleorift. However, the data for the Coastal Plain are considered separately because they display a distinct distribution for at least one of the statistical parameters. Unfortunately, the number of data points for the paleorift category is relatively small and thus the inferences using statistics based on these data must be interpreted cautiously. A small number of data points representing the Cenozoic volcanic provinces (a "rift-like" feature) are included in the North America minus rifts category. The data for the remainder of North America are considered as a group to be representative of the (mostly) "normal" continental crust. Examples of representative crustal velocity models for rift and non-rift provinces for North America are shown in Figure 3B–11. Crustal models for the "normal" continental crust (largely the North American craton), modern and paleorift zones, the coastal plain, and Cenozoic volcanic provinces are shown for comparison. A relatively thin crust and low upper mantle velocity characterize the modern rift models from North America. The crustal models for the rift areas and average North America (Fig. 3B–11), and the contrasts between these models (primarily crustal thickness and P_n velocity differences) are very similar to the rift and off-rift crustal models which were determined for the Kenya rift area in east Africa (Braile et al., 1994). The paleorift models display anomalous upper crustal structure (as

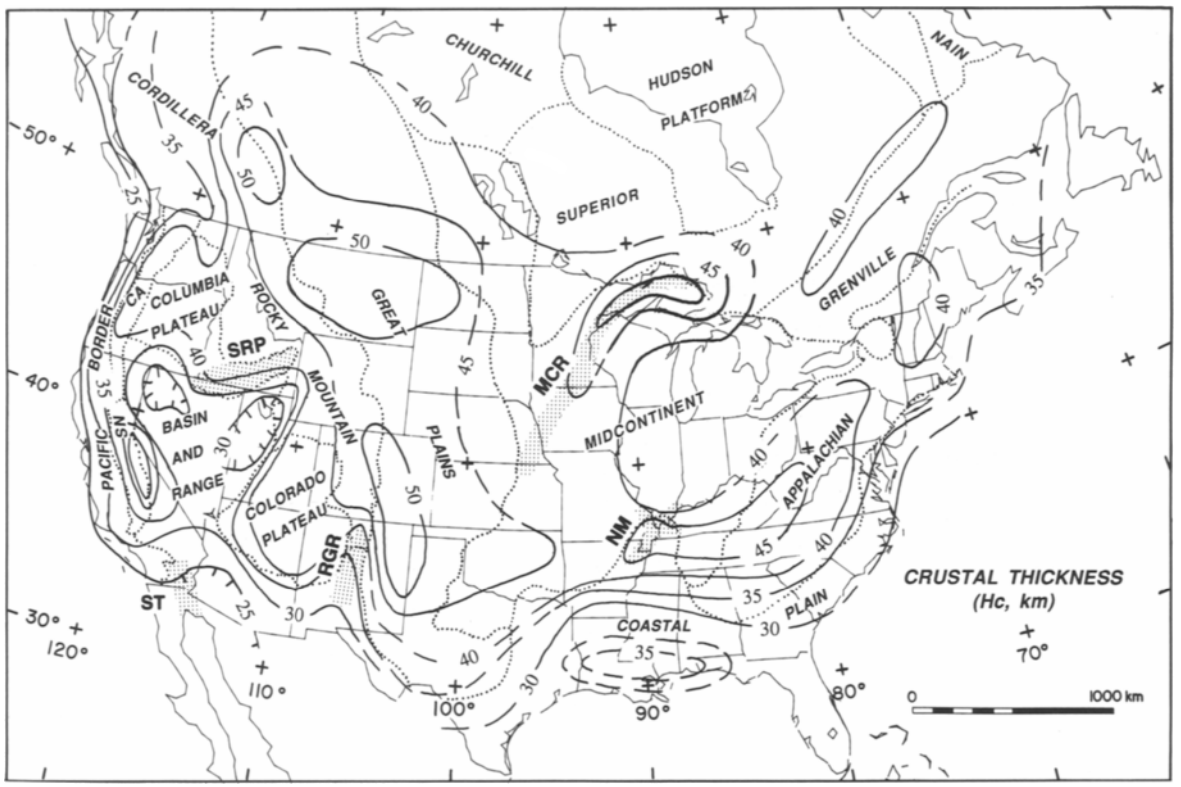

Fig. 3B–10. Contour map of crustal thickness data for North America (Braile et al., 1989). Contour interval is 5 km. Physiographic provinces are indicated by the dotted lines (CA=Cascade Range, SN=Sierra Nevada). Specific rifts are also indicated: NM=New Madrid, MCR=Mid-Continent, RGR=Rio Grande, ST=Salton Trough. The Snake River Plain Cenozoic volcanic terrain is indicated by SRP.

compared with the average North America crustal models) and contain a high-velocity lower crustal layer.

Data for four of the groups of geologic province types (modern) rifts, paleo-rifts, coastal plain and remainder of North America are displayed in histograms in Figures 3B–12 to 3B–14. Simple statistics for the data sets are listed in Table 3B–6.

Crustal thickness histograms for the rift and non-rift regions of North America are shown in Figure 3B–12. The crustal thickness distributions for the provinces are very distinct. When the rift provinces data are removed from the North American compilation, the distribution, which is bimodal (Braile et al., 1989), becomes nearly Gaussian (Fig. 3B–12). The difference in the mean values of crustal thickness for the active rift and "normal" continental crust suggests that crustal thinning during rifting is about 9 km. This thinning could be accomplished by uplift and erosion of part of the upper crust, extension (by normal faulting or ductile stretching), migration of the Moho by phase transition, subcrustal "erosion" (intrusion into and assimilation by melting of lower crustal material by the upper mantle), or a combination of these processes. The coastal plain (passive continental rift margin) data also display a thinner than normal crust. However, the North American paleorifts are characterized by an anomalously thick crust—about 8 km thicker than the normal continental crust. Presumably, these paleorifts

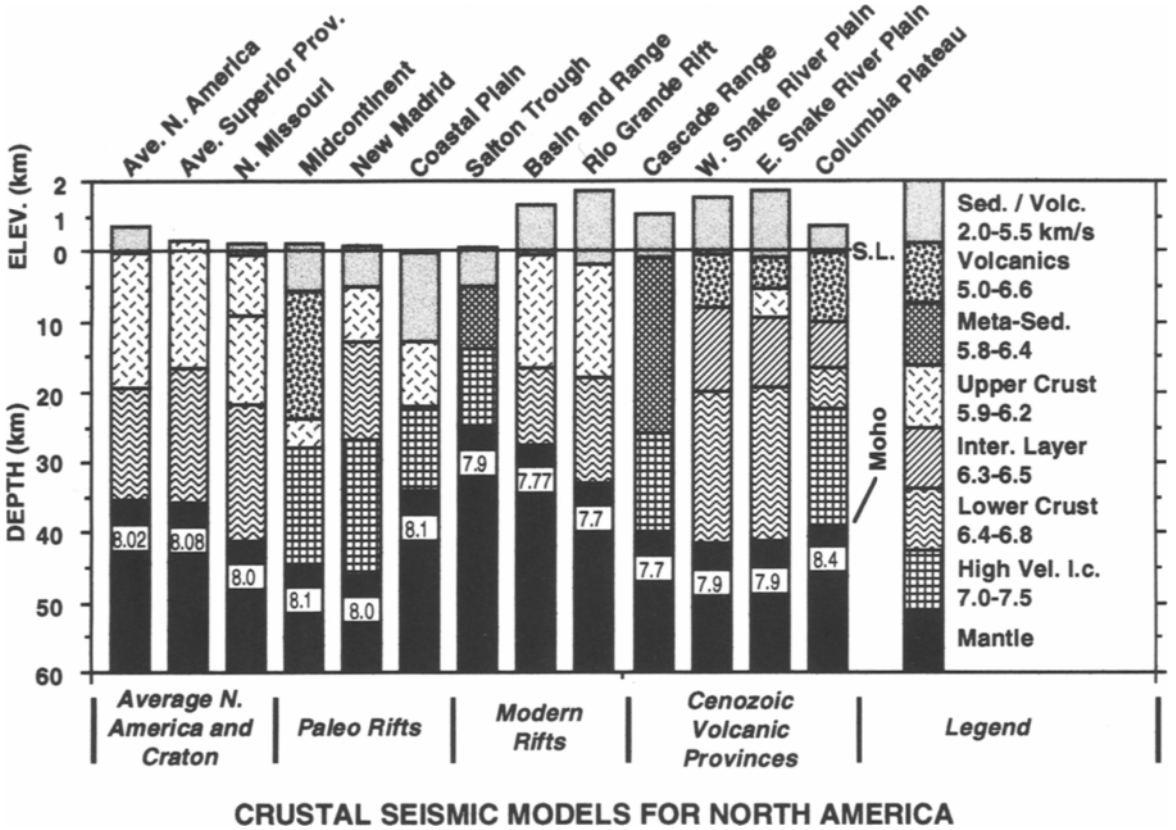

Fig. 3B–11. Selected crustal seismic models for North America. Models are grouped as follows: Average North America and craton models, paleorift, modern rift, and Cenozoic volcanic provinces. Numbers are compressional wave velocities in km/s. ELEV. = elevation above sea level (S.L.); Sed./Volc. = sedimentary and volcanic rocks; Meta-Sed. = meta-sedimentary rocks; Inter.Layer = intermediate layer; High Vel l.c. = high-velocity lower crustal rocks. Sources of models are listed in Table 3B–5.

experienced thinning of their original crust during rifting, but their crusts have thickened subsequently by subsidence and volcanic or sedimentary accumulation or by intrusion into the crust or underplating. Two of the North American paleorifts show evidence of having been thickened by these mechanisms (Ginzburg et al., 1983; Allen et al., Chapter 10 of this volume).

Histograms for the P_n (uppermost mantle) velocity for the North American rift and non-rift areas are shown in Figure 3B–13. The P_n distribution for the non-rift areas displays a strong peak with a mean value of 8.05 km/s. Modern rift areas are characterized by a significantly low P_n velocity (mean = 7.77 km/s). However, this Pn velocity difference is consistent with variations in velocity due to temperature variations in the upper mantle as suggested by Black and Braile (1982). The depth difference (modern rifts compared with normal continental crust, 9 km) and temperature difference (estimated to be about 500°C) at the Moho combine to predict a P_n velocity decrease of 0.34 km/s in rift zones caused by combined pressure and temperature effects (see previous section). This anomaly is very close to the 0.28 km/s observed P_n difference. The coastal plain and paleorift areas have slightly higher than normal P_n velocity. Considering the standard errors of the mean value statistics, the paleorift data are only

Table 3B–5.
Seismic Crustal Models for North America.

Velocity Model	Reference	Remarks
1. Average North America	Braile et al., 1989	Average of structure from 247 refraction studies
2. Average Superior Province	Braile, 1989	Average of 11 Superior Province Models
3. N. Missouri	Stewart, 1968	
4. Midcontinent Rift	Behrendt et al., 1988; Hinze et al., 1990; Allen et al., Chapter 10 of this volume,	Lower crustal velocity beneath rift is uncertain
5. New Madrid Rift	Ginzburg et al., 1983	
6. Coastal Plain	Trehu et al., 1989	Passive continental margin near continental shelf-slope break
7. Salton Trough	Fuis et al., 1984 Mooney and Weaver, 1989	
8. Basin and Range	Braile et al., 1989	Average Basin and Range model
9. Rio Grande Rift	Baldridge et al., 1984	
10. Cascade Range	Leaver et al., 1984	
11. Western Snake River Plain	Hill and Pakiser, 1966 Fauria, 1981	Intermediate velocity layer of Fauria's model included
12. Eastern Snake River Plain	Braile et al., 1982	
13. Columbia Plateau	Catchings et al., 1988	

marginally anomalous in P_n velocity. The P_n data for the coastal plain regions indicate that the P_n velocity is substantially higher for these areas as compared to that beneath 'normal' crust. However, it is likely that at least a large part of the difference in mean P_n velocities between normal North American crust and the coastal plain is caused by differences in the depth to the Moho (and, therefore, pressure differences) and differences in temperature. For example, the crustal thickness histogram (Fig. 3B–12) suggest a difference in depth to Moho of about 10 km between normal continental crust (~ 38 km) and

Table 3B–6.
Statistics for North American Crustal Seismic Data.

Data Set Region	Number of Observations	Mean Value	Std. Error	Std. Deviation	Units
Crustal Thickness (Hc)					
Non-rift Areas	260	37.8	0.6	9.8	km
Modern Rifts	42	29.1	0.6	4.1	km
Paleorifts	10	46.2	1.3	4.2	km
Coastal Plain	25	28.2	1.5	7.3	km
Upper Mantle Velocity (Pn)					
Non-rift Areas	242	8.05	0.04	0.21	km/s
Modern Rifts	44	7.77	0.02	0.12	km/s
Paleorifts	10	8.11	0.02	0.07	km/s
Coastal Plain	24	8.19	0.04	0.17	km/s
Average Crustal Velocity ($\overline{V}p$)					
Non-rift Areas	198	6.46	0.02	0.23	km/s
Modern Rifts	29	6.29	0.04	0.24	km/s
Paleorifts	7	6.67	0.04	0.12	km/s
Coastal Plain	21	6.40	0.07	0.31	km/s

coastal Plain regions (~ 28 km). Temperature differences at the Moho between the normal and Coastal Plain crusts may be approximately 350°C. Using these differences in confining pressure and temperature and appropriate estimates of pressure and temperature derivatives (Table 3B–4), we estimate that the P_n velocity variation caused by pressure and temperature conditions (the thinner crust, and therefore lower pressure, implies a 0.07 km/s *lower* P_n velocity, whereas the lower estimated temperature at the Moho in the coastal plain implies a 0.19 km/s *higher* P_n velocity as compared to "normal" continental crust) would be about 0.12 km/s, thus approximately accounting for the observed (0.14 km/s) difference.

Histograms for the average seismic compressional wave velocity for the North American continental crust are shown in Figure 3B–14 for the rift and non-rift regions. The average crustal velocity ($\overline{V}p$) has been suggested by Smithson et al. (1981) to be indicative of average composition of the crust. However, $\overline{V}p$ is also affected by temperature and pressure variations. In high heat flow environments, the

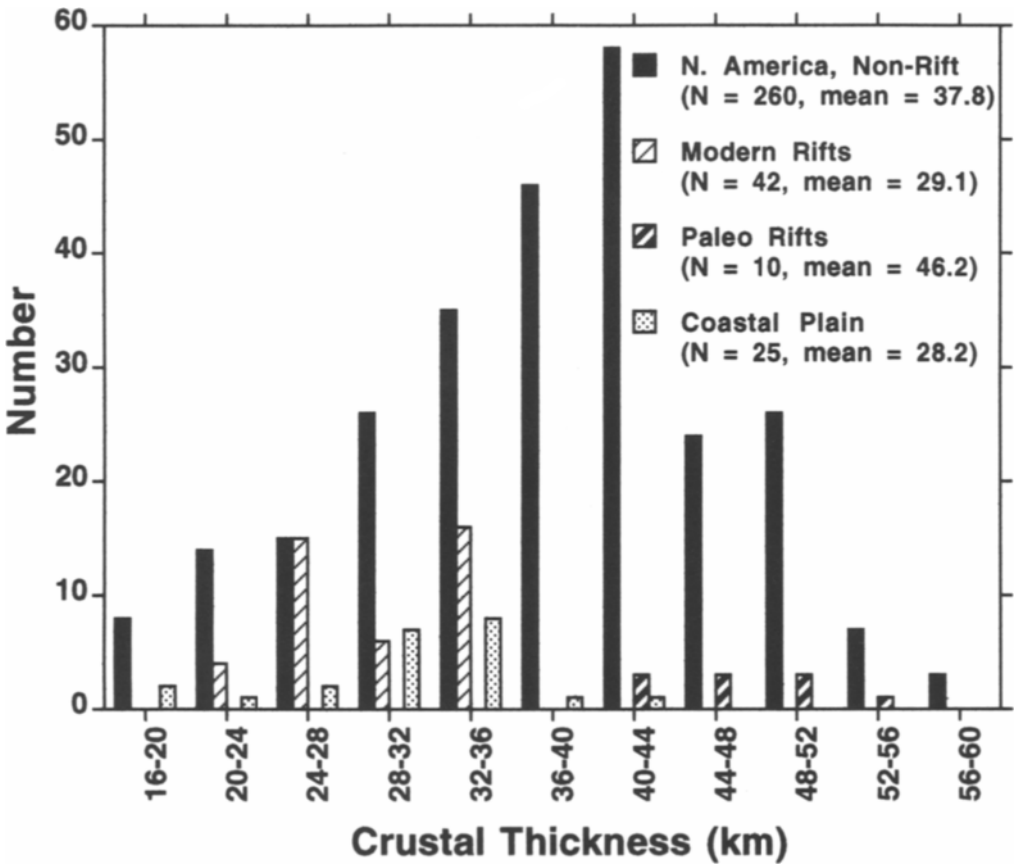

Fig. 3B–12. Histograms of crustal thickness data (Braile et al., 1989) for modern rift, paleorift, coastal plain and the non-rift continental crust of North America. Statistical values are given in Table 3B–6.

temperature effect may be significant and may account for much of the observed variations in $\overline{V}p$. For North America, there is a strong correlation of $\overline{V}p$ with thermal age of provinces similar to the effect observed by Black and Braile (1982) for P_n velocity. These results can be most simply interpreted as an effect of cooling of the crust (and lithosphere) with time after a thermal event and that the observed $\overline{V}p$ variations are primarily controlled by temperature. The $\overline{V}p$ histograms (Fig. 3B–14) indicate that modern rift regions are characterized by anomalously low $\overline{V}p$ —probably as a temperature effect. $\overline{V}p$ data for the paleorifts indicate a distinct anomaly. The $\overline{V}p$ data are significantly higher than for the 'normal' crust. However, because there are insignificant temperature or pressure differences between the normal North American crust and the paleorift crust, the difference cannot be attributable to pressure and temperature effects. (The small difference in crustal thickness, and therefore confining pressure in the crust, between the normal and paleorift provinces could only account for a very small fraction of the observed $\overline{V}p$ differences). Therefore, we conclude that, the crust in paleorifts has been intruded by high-velocity and high-density material (and some lower velocity upper crustal material is replaced by higher velocity rocks) at some stage in the formation of the paleorifts. This process, which may also involve "underplating" (Furlong and Fountain, 1986; Holbrook et al., 1992a), along with cooling with age, probably contributes to the subsidence and thickening of the crust in paleorifts and accounts for the

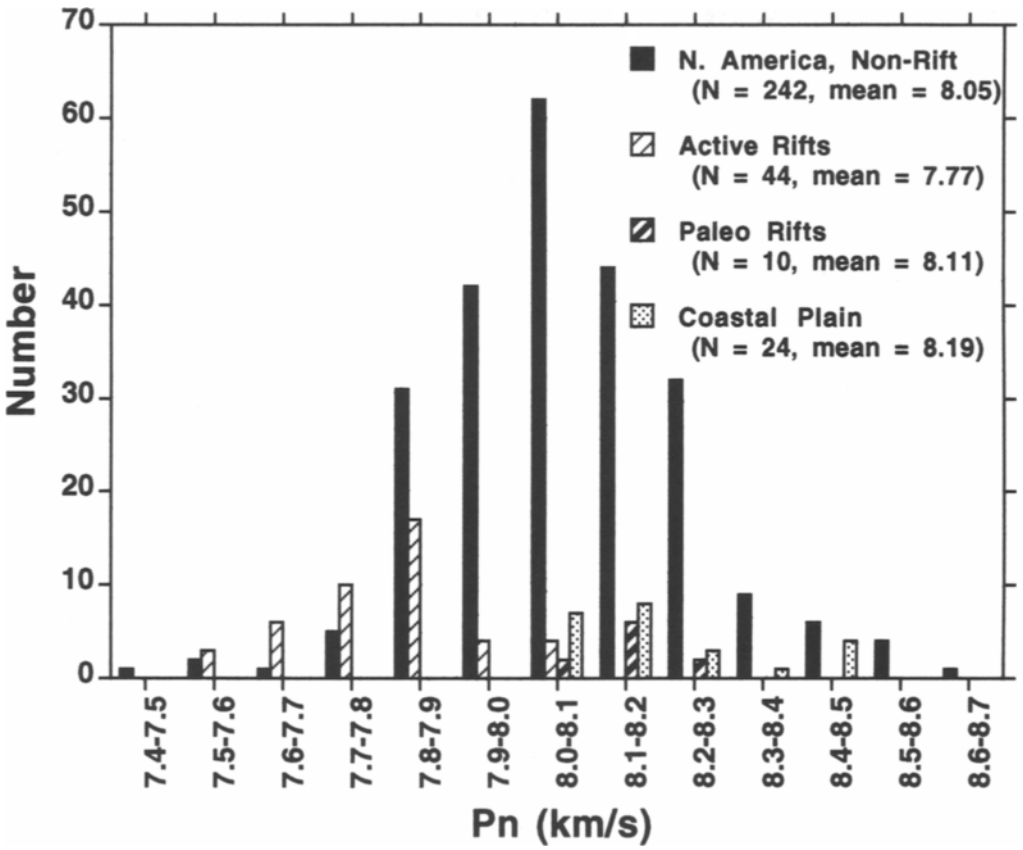

Fig. 3B–13. Histograms of P_n velocity data (Braile et al., 1989) for modern rift, paleorift, coastal plain and the non-rift continental crust of North America. Statistical values are given in Table 3B–6.

observed differences in $\overline{V}p$ between paleorifts and normal continental crust. Because the coastal plain region is a paleorift, one might expect higher than normal average crustal velocity. However, this is not observed. Possible explanations include pressure and temperature effects (because there is a substantial difference in crustal thickness) and difficulties in correctly estimating $\overline{V}p$ in the coastal plain region. The temperature and pressure effects on $\overline{V}p$ for the coastal plain can easily be estimated and do not suggest a major difference. However, the temperature in the crust of the coastal plain region could be different than is currently predicted by heat flow models because of the complicated lateral variations in crustal structure. An additional problem in estimating $\overline{V}p$, which is more prevalent in coastal plain areas, is separating the thick sedimentary section (some of which may have seismic velocities very close to those of the upper crust) from the crystalline crust in the calculation of $\overline{V}p$. Mis-identifying some of the sedimentary section as crystalline crust would have the effect of lowering the $\overline{V}p$ data. Similarly, because the passive margins grade laterally into oceanic crust, some oceanic crustal velocities may be included in the $\overline{V}p$ calculations, thus increasing the values.

Comparing the data for the rift and non-rift areas of North America in the three sets of histograms (Figs. 3B–12, 3B–13, and 3B–14), the crustal structure parameters (crustal thickness, P_n and $\overline{V}p$) for the modern rift regions are all significantly lower than for the normal continental crust. The results are

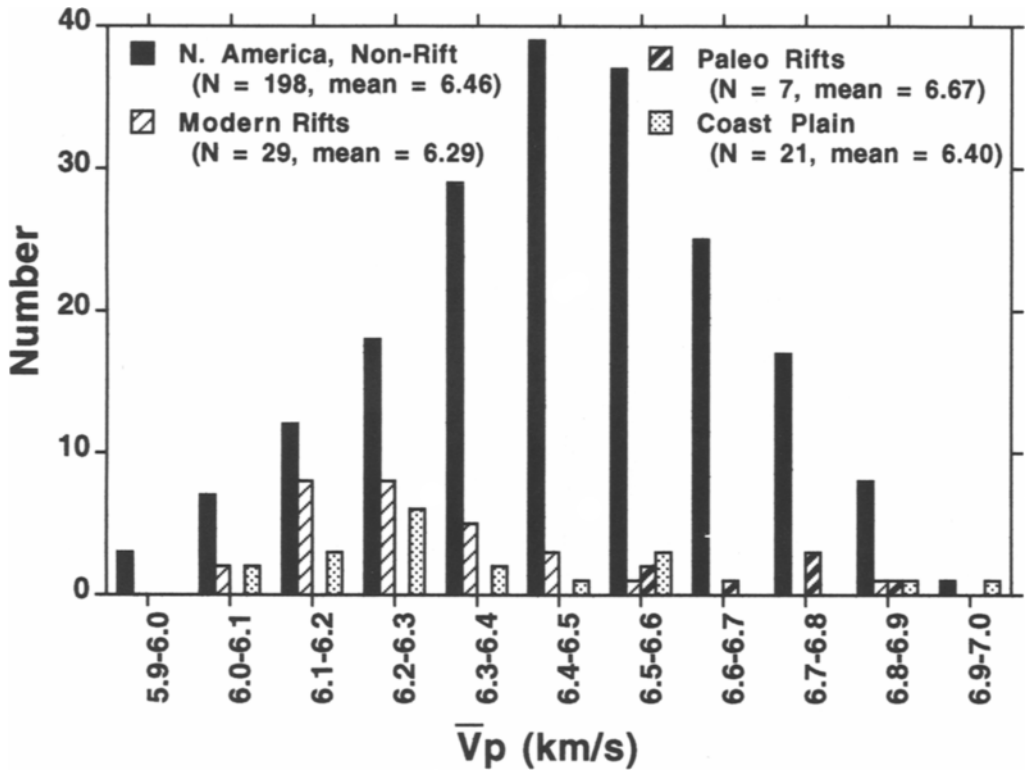

Fig. 3B–14. Histograms of $\overline{V}_p$ (average velocity of the crystalline crust) data (Braile et al., 1989) for modern rift, paleorift, coastal plain and the non-rift continental crust of North America. Statistical values are given in Table 3B–6.

consistent with a thinning of the crust during rifting which averages about 9 km and with crustal and upper mantle velocity variations which are predicted by the estimated temperature differences. For paleorifts, the three crustal parameters are higher than normal, although the P_n velocity is only slightly high and the difference may not be significant. The crustal thickness and $\overline{V}p$ data for paleorifts suggest that the crust is thickened and intruded with higher velocity material at some time in the process of rift development. The coastal plain data are less clear, but do show a thinned crust of approximately normal $\overline{V}p$. The crustal thickness and velocity statistics for paleorifts and the observation that North American paleorifts (Midcontinent rift, New Madrid rift, coastal plain) have been areas of substantial subsidence, suggest that the crustal thickening and increase in $\overline{V}p$ is a response to cooling with age after the main extensional (active rifting) event and associated magmatism. Except for the intrusions into the crust in the paleorifts, the seismic velocity variations in rift and non-rift areas could be explained by temperature effects alone. No significant compositional variations are required to match the seismic data. Of course, compositional variations which do not involve significant volume fractions of the crust would not be detected. Furthermore, large compositional variations related to rifting (intrusion into the crust, depletion of certain mantle elements) could occur and not be visible in the statistical data of the crustal parameters if the variations do not involve significant changes in seismic velocity or density.

3B.10. Conclusions

Many different seismic methods are available for application to studies of the structure, physical properties and processes of continental rifts. Each method has its own capabilities and limitations in terms of the depth range of investigation, degree of resolution attainable, and the physical properties determined. A reasonably accurate and complete image of the structure of continental rifts will generally require application of multiple seismic methods. At present, shear-wave velocity, anisotropy, and Poisson's ratio data from continental rift areas are relatively sparse. Integration of the results of seismic studies with information from other geophysical and geological data will also be important to a full understanding of the rifting process and its effects on the continental crust and upper mantle. An analysis of available data on rock properties indicates the importance of consideration of the effects of pressure and temperature in interpretation of seismic velocity models. Substantial differences in heat flow (and therefore temperature), crustal thickness (and therefore pressure in the lower crust and uppermost mantle), and composition (caused by magmatism) have been observed in well-studied continental rifts. These differences will generally be reflected in significant seismic velocity anomalies. Continental rift areas which have been extensively-studied, including some areas of North America and east Africa, display significant crust and upper mantle seismic velocity variations caused by late-Cenozoic rifting. Similarities between the crustal velocity structures observed in North America and east Africa suggest common characteristics of the stable continental crust and the processes and effects of continental rifting.

3B.11. References

Achauer, U., Greene, L., Evans, J.R., and Iyer, H.M., 1986. Nature of the magma chamber underlying the Mono Craters area, eastern California, as determined from teleseismic travel time residuals. J. Geophys. Res., 91: 13,873–13,891.

Achauer, U., Dahlheim, H.A., and Davis, P.M., 1988. A teleseismic study of the East African rift. 13th Gen. Ass. Europ. Geophys. Soc. (Bologna 1988), Ann. Geophys. Spec. Issue, p.11.

Aki, K., Christofferson, A., and Husebye, E.S., 1976. Three-dimensional seismic structure of the lithosphere under Montana LASA. Bull. Seism. Soc. Am., 66: 501–524.

Aki, K., Christofferson, A., and Husebye, E.S., 1977. Determination of the three-dimensional seismic structure of the lithosphere. J. Geophys. Res., 82: 277–296.

Allmendinger, R.W., Sharp, J.W., von Tish, D., Serpa, L., Kaufman, S., Oliver, J., and Smith, R.B., 1983. Cenozoic and Mesozoic structure of the eastern Basin and Range from COCORP seismic-reflection data. Geology, 11: 532–536.

Ansorge, J., Prodehl, C., and Bamford, D., 1982. Comparative interpretation of explosion seismic data. J. Geophys., 51: 69–84.

Baldridge, W.S., Olsen, K.H., and Callender, J.F., 1984. Rio Grande rift, problems and perspectives. New Mexico Geol. Soc., 35th Field Conf. Guidebook: pp. 1–12.

Bamford, D., 1973. Refraction data in western Germany - a time-term interpretation. Z. Geophys., 39: 907–927.

Bamford, D., 1977. P_n velocity anisotropy in a continental upper mantle. Geophys. J. R. astr. Soc., 49: 29–48.

Bamford, D., Jentsch, M., and Prodehl, C., 1979. P_n anisotropy studies in northern Britain and the eastern and western United States. Geophys. J. R. astr. Soc., 57: 397–430.

Barton, P.J., 1986. The relationship between seismic velocity and density in the continental crust - a useful constraint?. Geophys. J. R. astr. Soc., 87: 195–208.

Behrendt, J.C., and 7 others, 1988. Crustal structure of the Midcontinent rift system: Results from GLIMPCE deep seismic reflection profiles. Geology, 16: 81–85.

Benz, H.M., and Smith, R.B., 1984. Simultaneous inversion for lateral velocity variations and hypocenters in the Yellowstone region using earthquake and refraction data. J. Geophys. Res., 89: 1208–1220.

Birch, F., 1943. Elasticity of igneous rocks at high temperatures and pressures. Geol. Soc. Am. Bull., 54: 263–286.

Birch, F., 1958. Interpretation of the seismic structure of the crust in light of experimental studies of wave velocities in rocks. In: Benioff, H., (ed.): *Contribution in Geophysics in Honor of Beno Gutenberg*. New York, Pergamon Press: pp. 158–170.

Birch, F., 1960. The velocity of compressional waves in rocks to 10 kilobars, Part 1. J. Geophys. Res., 65: 1085–1102.

Birch, F., 1961. The velocity of compressional waves in rocks to 10 kilobars, Part 2. J. Geophys. Res., 66: 2199–2224.

Birch, F. and Bancroft, D., 1938. Elasticity and internal friction in a long column of granite. Bull. Seismol. Soc. Am., 28: 243–254.

Black, P.R., and Braile, L.W., 1982. P_n velocity and cooling of the continental lithosphere. J. Geophys. Res., 87: 10557–10568.

Bosworth, W., and Morley, C.K., 1994. Structural and stratigraphic evolution of the Anza rift, Kenya. Tectonophysics, 236: 93–115.

Boztepe, E.A., and Braile, L.W., 1994. Kinematic inversion for the 2-D horizontal and vertical qP-wave velocities and depths to interfaces applied to the TACT seismic profile, southern Alaska. Geophys. J. Int., 119: 529–547.

Braile, L.W., 1989. Crustal structure of the continental interior. In: Pakiser, L.C., and Mooney, W.D., (eds.): *Geophysical Framework of the Continental United States*. Geol. Soc. Am. Memoir 172, Boulder, Colorado: pp. 285–315.

Braile, L.W., and Smith, R.B., 1975. Guide to the interpretation of crustal refraction profiles. Geophys. J. R. astr. Soc., 40: 145–176.

Braile, L.W., Smith, R.B., Ansorge, J., Baker, M.R., Sparlin, M.A., Prodehl, C., Schilly, M.M., Healy, J.H., Mueller, St., and Olsen, K.H., 1982. The Yellowstone-Snake River Plain seismic profiling experiment: Crustal structure of the eastern Snake River Plain. J. Geophys. Res., 87: 2597–2609.

Braile, L.W., and Chiang, C.S., 1986. The continental Mohorovicic discontinuity: Results from near-vertical and wide-angle seismic reflection studies. In: Barazangi, M., and Brown, L., (eds.): *Reflection Seismology: A Global Perspective*. Geodynamics Series, 13, AGU: 257–272.

Braile, L.W., Hinze, W.J., von Frese, R.R.B., and Keller, G.R., 1989. Seismic properties of the crust and upper-most mantle of the conterminous United States and adjacent Canada. In: Pakiser, L.C., and Mooney, W.D., (eds.): *Geophysical Framework of the Continental United States*. Geol. Soc. Am. Memoir 172, Boulder, Colorado: pp. 655–680.

Braile, L.W., Wang, B., Daudt, C.R., Keller, G.R., and Patel, J.P., 1994. Modeling the 2-D seismic velocity structure across the Kenya rift. Tectonophysics, 236: 251–269.

Brown, L.D., 1986. Aspects of COCORP deep seismic profiling. In: Barazangi, M., and Brown, L., (eds.): *Reflection Seismology: A Global Perspective*. Geodynamics Series 13, AGU: 209–222.

Brown, L.D., Chapin, C.E., Sanford, A.R., Kaufman, S., and Oliver, J., 1980. Deep structure of the Rio Grande rift from seismic reflection profiling. J. Geophys. Res., 85: 4773–4800.

Bullen, K.E., and Bolt, B.A., 1985. *An Introduction to the Theory of Seismology* (4th rev. ed.). Cambridge University Press, Cambridge, England: 499 pp.

Burke, M.M., and Fountain, D.M., 1990. Seismic properties of rocks from an exposure of extended continental crust - new laboratory measurements from the Ivrea Zone. Tectonophysics, 182: 119–146.

Burton, R.W., 1974. Estimations of Q^{-1} from seismic Rayleigh waves. Geophys. J. R. astr. Soc., 36: 167–189.

Catchings, R.D., and 20 others, 1988. The 1986 PASSCAL Basin and Range lithospheric seismic experiment. Eos Trans AGU, 69: 593–598.

Cerveny, V., 1985. Ray synthetic seismograms for complex two-dimensional and three-dimensional structures. J. Geophys., 58: 2–26.

Cerveny, V., Molotkov, I.A., and Psencik, I., 1977. *Ray method in seismology*. Univerzita Karlova, Praha: 214 pp.

Cerveny, V., and Psencik, I., 1984. SEIS 83 – numerical modelling of seismic wave fields in 2-D laterally varying layered structures by the ray method. In: Engdahl, E.R., (ed.): *Documentation of Earthquake Algorithms*. World Data Center (A) for solid earth geophysics, Boulder, Colorado: Rep. SE-35, pp. 36–40.

Christensen, N.I., 1965. Compressional wave velocities in metamorphic rocks at pressures to 10 kilobars. J. Geophys. Res., 70: 6147–6164.

Christensen, N.I., 1974. Compressional wave velocities in possible mantle rocks to pressures of 30 kilobars. *J.* Geophys. Res., 79: 407–412.

Christensen, N.I., 1978. Ophiolites, seismic velocities and oceanic crustal structure. *Tectonophysics*, 47: 131–157.

Christensen, N.I., 1979. Compressional wave velocities in rocks at high temperatures and pressures, critical thermal gradients, and crustal low-velocity zones. *J.* Geophys. Res., 84: 6849–6857.

Christensen, N.I., 1989a. Seismic velocities. In: Carmichael, R.S., (ed.): *Practical Handbook of Physical Properties of Rocks and Minerals*. CRC Press, Boca Raton, Florida: pp. 429–546.

Christensen, N.I., 1989b. Pore pressure, seismic velocities and crustal composition. In: Pakiser, L.C., and Mooney, W.D., (eds.): *Geophysical Framework of the Continental United States*. Geol. Soc. Am. Memoir 172, Boulder, Colorado, pp. 783–798.

Christensen, N.I., and Fountain, D.M., 1975. Constitution of the lower continental crust based on experimental studies of seismic velocities in granulite. Bull. Geol. Soc. Am., 86: 227–236.

Christensen, N.I., and Wepfer, W.W., 1989. Laboratory techniques for determining seismic velocities and attenuations, with applications to the continental lithosphere. In: Pakiser, L.C., and Mooney, W.D., (eds.): *Geophysical Framework of the Continental United States*. Geol. Soc. Am. Memoir 172, Boulder, Colorado: pp. 91–102.

Chroston, P.N., and Evans, C.J., 1983. Seismic velocities of granulites from the Sieland Petrographic Province, N. Norway: Implications for Scandinavian lower continental crust. J. Geophys., 52: 14–21.

Chroston, P.N., and Brooks, S.G., 1989. Lower crustal seismic velocities from Lofoten-Vesteralen, North Norway. Tectonophysics, 157: 251–269.

Crosson, R.S., 1976. Crustal structure modeling of earthquake data. 1. Simultaneous least squares estimation of hypocenter and velocity parameters. 2. Velocity structure of the Puget Sound region. J. Geophys. Res., 81: 3036–3054.

Davis, P.M., Parker, E.C., Evans, J.R., Iyer, H.M., and Olsen, K.H., 1984. Teleseismic deep sounding of the velocity structure beneath the Rio Grande rift. In: Baldridge, W.S., Dickerson, P.W., Riecker, R.E., and Zidek, J., (eds.): *Rio Grande Rift: Northern New Mexico*. New Mexico Geol. Soc., Socorro: pp. 29–38.

Davis, P.M., Slack, P., Dahlheim, H.A., Green, W.V., Meyer, R.P., Achauer, U., Glahn, A., and Granet, M., 1993. Teleseismic tomography of continental rift zones. In: Iyer, H.M., and Hirahara K., (eds.): *Seismic Tomography: Theory and Practice*. Chapman & Hall, London: 397–439.

Der, Z., Masse, R., and Landisman, M., 1970. Effects of observational errors on the resolution of surface waves at intermediate distances. J. Geophys. Res., 75: 3399–3409.

Doser, D.I., 1986. Earthquake processes in the Rain-Bow Mountain-Fairview Peak-Dixie Valley, Nevada, region 1954–1959. J. Geophys. Res., 91: 12,572–12,586.

Dziewonski, A.M., and Hales, A.L., 1972. Numerical analysis of dispersed seismic waves. Methods and Computational Physics, 11: 39–85.

Fairhead, J.D., and Reeves, C.V., 1977. Teleseismic delay times, Bouguer anomalies and inferred thickness of the African lithosphere. Earth Planet. Sci. Lett., 36: 63–76.

Fauria, T.J., 1981. Crustal structure of the northern Basin and Range and western Snake River Plain: A ray-trace travel-time interpretation of the Eureka, Nevada to Boise, Idaho, seismic refraction profile. Unpub. M.S. Thesis, Purdue University, West Lafayette, IN, 91 pp.

Fielitz, K. and Clausthal-Zellerfeld, 1971. Elastic wave velocities in different rocks at high pressure and temperatures up to 750°C. Zeitschrift fur Geophysik, 37: 943– 1056.

Finlayson, D.M., and Ansorge, J.(eds.), 1984. Workshop Proceedings: *Interpretation of Seismic Wave Propagation in Laterally Heterogeneous Structures*. Bur. Min. Resourc., Geol. & Geophys., Canberra: Rep.258, 207 pp.

Fountain, D.M., 1976. The Ivrea-Verbano and Strona-Ceneri Zones, northern Italy: A cross-section of the continent crust - new evidence from seismic velocities of rock samples. Tectonophysics, 33: 145– 165.

Fountain, D.M. and Christensen, N.I., 1989. Composition of the continental crust and upper mantle: A review. In: Pakiser, L.C., and Mooney, W.D., (eds.): *Geophysical Framework of the Continental United States*. Geol. Soc. Am. Memoir 172, Boulder, Colorado: pp. 711– 742.

Fountain, D.M., Salisbury, M.H., and Percival, J., 1990. Seismic structure of the continental crust based on rock velocity measurements from the Kapuskasing Uplift. J. Geophys. Res., 95: 1167– 1186.

Fuchs, K., 1968. The reflection of spherical waves from transition zones with arbitrary depth-dependent elastic moduli and density. J. Phys. Earth 16 (Special Issue): 27– 41.

Fuchs, K., and Mueller, G., 1971. Computation of synthetic seismograms with the reflectivity method and comparison with observations. Geophys. J. R. astr. Soc., 23: 417– 433.

Fuis, G.S., Mooney, W.D., Healy, J.H., McMechan, G.A., and Lutter, W.J., 1984. A seismic refraction survey of the Imperial Valley region, California. J. Geophys. Res., 89: 1165–1189.

Furlong, K.P., and Fountain, D.M., 1986. Continental crustal underplating: Thermal considerations and seismic-petrologic consequences. J. Geophys. Res., 91: 8285– 8294.

Ginzburg, A., Mooney, W.D., Walter, A.W., Lutter, W.J., and Healy, J.H., 1983. Deep structure of northern Mississippi Embayment: Am. Assoc. Petrol. Geol. Bull., 67: 2031– 2046.

Green, W.V., and Meyer, R.P., 1992. Array observations of PKP phases across the Kenya Rift: Implications for structure and tectonics. Tectonophysics, 204: 41– 58.

Green, W.V., Achauer, U., and Meyer, R.P., 1991. A three-dimensional image of the crust and upper mantle beneath the Kenya rift. Nature, 354: 199– 203.

Hale, L.D., and Thompson, G.A., 1982. The seismic reflection character of the continental Mohorovicic discontinutiy. J. Geophys. Res., 87: 4525– 4635.

Hauge, T.A., Allmendinger, R.W., Caruso, C., Hauser, E.C., Klemperer, S.L., Opdyke, S., Potter, C.J., Sanford, W., Brown, L., Kaufman, S., and Oliver, J., 1987. Crustal structure of western Nevada from COCORP deep seismic-reflection data. Geol. Soc. Am. Bull., 98: 320– 329.

Hearn, T.M., and Clayton, R.W., 1986a. Lateral velocity variations in southern California. I. Results for the upper crust from Pg waves. Bull. Seismol. Soc. Am., 76: 511– 520.

Hearn, T.M., and Clayton, R.W., 1986b. Lateral velocity variations in southern California. II. Results for the lower crust from P_n waves. Bull. Seismol. Soc. Am., 76: 511– 520.

Hill, D.P., and Pakiser, L.C., 1966. Crustal structure between the Nevada test site and Boise, Idaho, from seismic-refraction measurements. In: Steinhart, J.S., and Smith, T.J., (eds.): *The Earth Beneath the Continents*. Am. Geophys. Un. Geophys. Mono. 10: 291-419.

Hinze, W.J., Braile, L.W., and Chandler, V.W., 1990. A geophysical profile of the southern margin of the Midcontinent Rift System in western lake Superior. Tectonics, 9: 303– 310.

Holbrook, W.S., 1990. The crustal structure of the northwestern Basin and Range Province, Nevada, from wide-angle seismic data. J. Geophys. Res., 95: 21,843– 21,869.

Holbrook, W.S., Catchings, R.D., and Jarchow, C.M., 1991. Origin of deep crustal reflections: Implications of coincident seismic refraction and reflection data in Nevada. Geology, 19: 175– 179.

Holbrook, W.S., Mooney, W.D., and Christensen, N.I., 1992a. The seismic velocity structure of the deep continental crust. In: Fountain, D.M., Arculus, R., and Kay, R., (eds.): *Continental Lower Crust*. Elsevier, Amsterdam: 1– 43.

Holbrook, W.S., Purdy, G.M., Collins, J.A., Sheridan, R.E., Musser, D.L., Glover, L., III., Talwani, M., Ewing, J.I., Hawman, R., and Smithson, S.B., 1992b. Deep velocity structure of rifted continental crust, U.S. mid-Atlantic margin, from wide-angle reflection/refraction data. Geophys. Res. Lett., 19: 1699– 1702.

Hughes, D.S. and Cross, J.H., 1951. Elastic wave velocities in rocks at high pressures and temperatures. Geophysics, 16: 577– 593.

Hughes, D.S. and Maurette, C., 1956. Variation of elastic wave velocities in granites with pressure and temperature. Geophysics, 21: 277– 284.

Hughes, D.S. and Maurette, C., 1957. Variation of elastic wave velocities in basic igneous rocks with pressure and temperature. Geophysics, 22: 23– 31.

Hughes, S., and Luetgert, J.H., 1991. Crustal structure of the southeastern Grenville Province, northern New York State and eastern Ontario. J. Geophys. Res., 97: 17,455– 17,479.

Humphreys, E., Clayton, R.W., and Hager, B.H., 1984. A tomographic image of mantle structure beneath southern California. Geophys. Res. Lett., 11: 625– 627.

Humphreys, E., and Dueker, K.G., 1994. Physical state of the western U.S. upper mantle. J. Geophys. Res., 99: 9635– 9650.

Iyer, H.M., 1984. Geophysical evidence for the locations, shapes and sizes, and internal structures of magma chambers beneath regions of Quaternary volcanism. Phil. Trans. R. Soc. Lond., A 310: 473–510.

Iyer, H.M., and Hirahara, K., 1993. *Seismic Tomography: Theory and Practice*. Chapman & Hall, London: 842 pp.

Jackson, I., and Arculus, R.J., 1984. Laboratory wave velocity measurements on lower crustal xenoliths from Calcutteroo, South Australia. Tectonophysics, 101: 185–197.

Jarchow, C.M., and Thompson, G.A., 1989. The nature of the Mohorovicic discontinuity. Ann. Rev. Earth Planet. Sci., 17: 475–506.

Jordan, T.H., and Frazer, L.N., 1975. Crustal and upper mantle structure from Sp phases. J. Geophys. Res., 80: 1504–1518.

Kennett, B.L.N., 1983. *Seismic wave propagation in stratified media*. Cambridge University Press, Cambridge, England: 341 pp.

Kern, H., 1978. The effect of high temperature and high confining pressure on compressional wave velocities in quartz-bearing and quartz-free igneous and metamorphic rocks. Tectonophysics, 44: 185–203.

Kern, H., 1982. P- and S-wave velocities in crustal and mantle rocks under the simultaneous action of high confining pressure and high temperature and the effect of the rock microstructure. In: Schreyer, W., (ed.): *High Pressure Researches in Geosciences*. E. Schweizerbart'sche Verlagsbuchhandlung, Stuttgart: pp. 15–45.

Kern, H. and Fakhimi, M., 1975. Effect of fabric anisotropy on compressional-wave propagation in various metamorphic rocks for the range 20–700°C at 2 kbars. Tectonophysics, 28: 227–244.

Kern, H. and Richter, A., 1981. Temperature derivatives of compressional and shear wave velocities in crustal and mantle rocks at 6 kbar confining pressure. J. Geophys., 49: 47–56.

Kern, H. and Schenk, V., 1985. Elastic wave velocities in rocks from a lower crustal section in southern Calabria (Italy). Phys. Earth Planet. Inter., 40: 147–160.

Kern, H., and Schenk, V., 1988. A model of velocity structure beneath Calabria, southern Italy, based on laboratory data. Earth Planet. Sci. Lett., 87: 325–337.

Kind, R., 1976. Computation of reflection coefficients for layered media. J. Geophys., 42: 191–200.

Kissling, E., 1988. Geotomography with local earthquake data. Rev. Geophys., 26: 659–698.

Klemperer, S.L., and Luetgert, J.H., 1987. A comparison of reflection and refraction processing and interpretation methods applied to conventional refraction data from coastal Maine. Seis. Soc. Am. Bull., 77: 614–630.

Kovach, R.L., 1978. Seismic surface waves and crustal and upper mantle structure. Rev. Geophys. Space Phys., 16: 1–13.

Kroenke, L.W., Manghnani, M.H., Rai, C.S., Fryer, P., and Ramananantoandro, R., 1976. Elastic properties of selected ophiolitic rocks from Papua New Guinea: Nature and composition of oceanic lower crust and upper mantle. Tectonophysics, 407–421.

Leaver, D.S., Mooney, W.D., and Kohler, W.M., 1984. Seismic refraction study of the Oregon Cascades. J. Geophys. Res., 89, 3121–3134.

Lerner-Lam, A.L., and Jordan, T.J., 1983. Earth structure from fundamental and higher-mode waveform analysis. Geophys. J. R. astr. Soc., 75: 759–797.

Levander, A., Fuis, G.S., Wissinger, E.S., Lutter, W.J., Oldow, J.S., and Moore, T.E., 1994. Seismic images of the Brooks Range fold and thrust belt, Arctic Alaska, from an integrated seismic reflection/refraction experiment. Tectonophysics, 232: 13–30.

Matthews, D., and Smith, C., (eds.), 1987. *Deep Seismic Profiling of the Continental Lithosphere*, v. 89. J. R. astr. Soc. Special Issue: 1–447.

McDonough, D.T., and Fountain, D.M., 1988. Reflection characteristics of a mylonite zone based on compressional wave velocities of rock samples. Geophys. J., 93: 547–558.

Meissner, R. and Fakhimi, M., 1977. Seismic anisotropy as measured under high-pressure, high-temperature conditions. Geophys. J. R. astr. Soc., 49: 133–143.

Milkereit, B., Bittner, R., and Meissner, R., 1986. Off-line acquisition of crustal reflection and refraction data. Geophys. Res. Lett., 13: 1161–1164.

Mitchell, B.J., and Hashim, B.M., 1977. Seismic velocity determinations in the New Madrid seismic zone: A new method using local earthquakes. Bull. Seismol. Soc. Am., 67: 413–424.

Mooney, W.D., 1989. Seismic methods for the determining earthquake source parameters and lithospheric structure. In: Pakiser, L.C. and Mooney, W.D., (eds.): *Geophysical Framework of the Continental United States*. Geol. Soc. Am. Mem. 172: 11–34.

Mooney, W.D., and Braile, L.W., 1989. The seismic structure of the continental crust and upper mantle of North America. In: Bally, A., and Palmer, P., (eds.): *The Geology of North America: An Overview*. Geol. Soc. Am., Boulder, CO, 39–52.

Mooney, W.D., and Brocher, T.M., 1987. Coincident seismic reflection/refraction studies of the continental lithosphere: A global review. Rev. Geophys., 25: 723–742.

Mooney, W.D., and Meissner, R., 1992. Multi-genetic origin of crustal reflectivity: A review of seismic reflection profiling of the continental lower crust and Moho. In: Fountain, D.M., Arculus, R., and Kay, R.W., (eds.): *Continental Lower Crust*, Elsevier, Amsterdam, 45–79.

Mooney, W.D., and Prodehl, C. (eds.), 1984. Proceedings of the 1980 Workshop of the International Association of Seismology and Physics of the Earth's Interior on the seismic modelling of laterally varying structures: *Contributions Based on Data from the 1978 Saudi Arabian Refraction Profile*. U.S. Geol. Survey Circular, 937: 158 pp.

Mooney, W.D., and Weaver, C.S., 1989. Regional crustal structure and tectonics of the Pacific Coastal States: California, Oregon and Washington. In: Pakiser, L.C., and Mooney, W.D., (eds.): *Geophysical Framework of the Continental United States*. Geol. Soc. Am. Mem. 172: 129–161.

Mooney, W.D., and Christensen, N.I., 1994. Composition of the crust beneath the Kenya rift. Tectonophysics, 236: 391–408.

Mueller, G., 1970. Exact ray theory and its application to the reflection of elastic waves from vertically inhomogeneous media. Geophys. J. R. astr. Soc., 21: 261–283.

Mueller, S., and Landisman, M., 1971. An example of the unified method of interpretation for crustal seismic data. Geophys. J. R. astr. Soc., 23: 365–371.

Mueller, St., and Bonjer, K.P., 1973. Average structure of the crust and upper mantle in East Africa. Tectonophysics, 20: 283–293.

Nakanishi, I., 1993. Surface wave tomography: Velocity and Q. In: Iyer, H.M., and Hirahara K., (eds.): *Seismic Tomography: Theory and Practice*. Chapman & Hall, London: 92–132.

Nolet, G., and Mueller, St., 1982. A model for the deep structure of the East African rift system from simultaneous inversion of teleseismic data. Tectonophysics, 84: 151–178.

Nowack, R.L., and Braile, L.W., 1993. Refraction and wide-angle reflection tomography: Theory and results. In: Iyer, H.M., and Hirahara, K., (eds.): *Seismic Tomography: Theory and Practice*. Chapman & Hall, London: 733–763.

Officer, C.B., 1958. *Introduction to the Theory of Sound Transmission*. McGraw Hill, New York: 284 pp.

Owens, T.J., Zandt, G., and Taylor, S.R., 1984. Seismic evidence for an ancient rift beneath the Cumberland Plateau, TN: A detailed analysis of broadband teleseismic P-waveforms. J. Geophys. Res., 89: 7783–7795, 1984.

Owens, T.J., Taylor, S.R., and Zandt, G., 1987. Crustal structure at regional seismic test network stations determined from inversion of broadband teleseismic P waveforms. Bull. Seismol. Soc. Am., 77: 631–662.

Padovani, E.R., Hall, J., and Simmons, G., 1982. Constraints on crustal hydration below the Colorado Plateau from V_p measurements on crustal xenoliths. Tectonophysics, 84: 313–328.

Parker, E.C., Davis, P.M., Evans, J.R., Iyer, H.M., and Olsen, K.H., 1984. Upwarp of anomalous asthenosphere beneath the Rio Grande rift. Nature, 312: 354–356.

Perrier, G., 1973. La croute terrestre. In: Coulomb, J., and Jobert, G., (eds.): *Traite de geophysique interne*, v.I: Sismologie et pesanteur. Masson et Cie., Paris: 229–281.

Peselnick, L. and Nicholas, A., 1978. Seismic anisotropy in an ophiolite peridotite: Application to oceanic upper mantle. J. Geophys. Res., 83: 1227–1235.

Peselnick, L., Lockwood, J.P., and Stewart, R., 1977. Anisotropic elastic velocities of some upper mantle xenoliths underlying the Sierra Nevada Batholith. J. Geophys. Res., 82: 2005–2010, 1977.

Press, F., 1966. Seismic velocities. In: Clark, S.P., (ed.): *Handbook of Physical Constants*. Geol. Soc. Am. Mem. 97: 195–218.

Prodehl, C., Keller, G.R., and Khan, M.A. (eds.), 1994. Crustal and Upper Mantle Structure of the Kenya Rift. Tectonophysics, 236: 483 pp.

Ramananantoandro, R. and Manghnani, M.H., 1978. Temperature dependence of the compressional wave velocity in an anisotropic dunite: Measurements to 500C at 10 kbar. Tectonophysics, 47: 73–84.

Roecker, S.W., Yeh, Y.H., and Tsai, Y.B., 1987. Three-dimensional P and S wave velocity structures beneath Taiwan: Deep structure beneath an arc-continent collision. J. Geophys. Res., 92: 10,547–10,570.

Rosendahl, B.R., 1987. Architecture of continental rifts with special reference to East Africa. Ann. Rev. Earth Planet. Sci., 15: 445–503.

Sanford, A.R., and Einarsson, P., 1982. Magma chambers in rifts, in G. Palmason (ed.), Continental and oceanic rifts. American Geophys. Union, Geodynamics Series, 8: 147–168.

Savage, J.E.G., and Long, R.E., 1985. Lithospheric structure beneath the Kenya dome. Geophys. J. R. astr. Soc., 82: 461–477.

Shedlock, K.M., and Roecker, S.W., 1987. Elastic wave velocity structure of the crust and upper mantle beneath the north China basin. J. Geophys. Res., 92: 9327–9350.

Sinno, Y.A., and Keller, G.R., 1986. A Rayleigh wave dispersion study between El Paso, Texas and Albuquerque, New Mexico. J. Geophys. Res., 91: 6168–6174, 1986.

Slack, P.D., Davis, P.M., Kenya Rift International Seismic Project (KRISP) Teleseismic Working Group, 1994. Attenuation and velocity of P-waves in the mantle beneath the East African Rift, Kenya. Tectonophysics, 236: 331–358.

Smithson, S.B., Johnson, R.A., and Wong, Y.K., 1981. Mean crustal velocity: A critical parameter for interpreting crustal structure and crustal growth. Earth Planet. Sci. Lett., 53: 323–332.

Snieder, R., 1988. Large-scale waveform inversions of surface waves for lateral heterogeneity: 1. Theory and numerical examples. J. Geophys. Res., 93: 12,055–12,065.

Spencer, J.W., Jr. and Nur, A.M., 1976. The effect of pressure, temperature and pore water on velocities in Westerly granite. J. Geophys. Res., 81: 899–904.

Steinhart, J.S., and Meyer, R.P., 1961. *Explosion Studies of Continental Structure*. Carnegie Inst. of Washington Publ. 622: 409 pp.

Stewart, S.W., 1968. Crustal structure in Missouri by seismic-refraction methods. Seismol. Soc. Am. Bull., 58: 291–323.

Taylor, S.R., and Owens, T.J., 1984. Inversion of receiver transfer functions for crustal structure. Earthquake Notes, 55: 5–12.

Trehu, A.M., Klitgord, K.D., Sawyer, D.S., and Buffler, R.T., 1989. Regional investigations of crust and upper mantle—Atlantic and Gulf of Mexico continental margins. In: Pakiser, L.C., and Mooney, W.D., (eds.): *Geophysical Framework of the Continental United States*. Geol. Soc. Am. Mem. 172: 349–382.

Thurber, C.H., 1993. Local earthquake tomography: Velocities and Vp/Vs – theory. In: Iyer, H.M., and Hirahara K., (eds.): *Seismic Tomography: Theory and Practice*. Chapman & Hall, London: 563–583.

Walck, M.C., and Clayton, R.W., 1987. P wave velocity variations in the Coso region, California, derived from local earthquake travel times. J. Geophys. Res., 92: 393–405.

Wallace, T.C., 1986. Inversion of long period regional body waves for crustal structure. Geophys. Res. Lett., 13: 749–752.

Yilmaz, O., 1987. *Seismic Data Processing, Investigations in Geophysics Series*, vol. 2. Society of Exploration Geophysicists, Tulsa, OK: 526 pp.

Zelt, C.A., and Smith, R.B., 1992. Seismic travel-time inversion for 2-D crustal velocity structure. Geophys. J. Int., 108: 16–34.

Zoback, M.L., and Zoback, M., 1980. State of stress in the conterminous United States. J. Geophys. Res., 85: 6113–6156.

Chapter 3C

Potential field methods

M.H.P. Bott and W.J. Hinze

3C.1. Introduction

Potential field methods, specifically the gravity and magnetic exploration methods, have been used extensively in the study of continental rifts, both modern and ancient. *Gravity studies* have provided an important input to rift studies since the pioneering studies of Bullard (1936) and Vening Meinesz (1950). Subsequently, gravity has been used to delineate hidden rifts, to determine the shape of rift troughs, including the nature of faulting, to investigate crustal and upper mantle structure in association with explosion and earthquake seismology, and to ascertain the isostatic state of rifts, including flexural studies. *Magnetic surveys*, although not as widely used as gravity in rift studies, reveal basement and igneous structure, map hidden rifts, and have been used to estimate the depth to the Curie point isotherm. This short review aims to discuss the applicability and limitations of these methods.

3C.2. The gravity method

The lateral variations of the Earth's gravitational field can be determined either by measuring the vertical component of gravitational attraction using a gravity meter or by using satellites to determine the variation in geoid height which is proportional to the anomalous gravitational potential. Gravity measurements have been used for nearly all continental rift studies, although the satellite determined geoid field is a good indicator of broad mantle structure such as plume heads associated with rifts. Both surface gravity and satellite measurements reflect the ellipsoidal shape and rotation of the Earth and lateral deviations from the ellipsoid involving surface topography and lateral density inhomogeneities within the Earth. Geoid anomalies can be calculated from gravity anomalies and vice versa, but the geoid is less sensitive to short wavelengths derived primarily from near-surface, local geologic sources and more sensitive to long wavelengths.

Relative gravity measurements can be made to an accuracy of a small fraction of a milliGal (1 mGal = 10^{-5} m s^{-2}), which is more than adequate for rift studies. Raw gravity measurements need to be related to the world gravity network, then corrected for planetary gravity variations related to latitude using the International Gravity Formula and for station elevation, before they can be used for interpretation. Elevation corrections include the *free air correction*, allowing for decrease of the Earth's gravity with height above sea level or other datum, the *Bouguer correction* correcting for the attraction of material from the station to sea level assuming it to be a uniform slab, and the *terrain correction* which accommodates for lateral variations in topographical height. Other minor corrections such as for tidal variation of gravity and deviation of the geoid from the ellipsoid are sometimes applied to specialized gravity surveys.

The *free air anomaly* is obtained when the latitude and free air corrections alone are made; the free air anomaly reflects the vertical component of the gravitational attraction of both the topography above datum and lateral variations of density below it, and is useful in flexural studies and for marine work. The *Bouguer anomaly* is determined when the Bouguer and terrain corrections are also applied; the Bouguer anomaly reflects lateral variations in density, eliminating the direct effects of topography. It is the most useful type of anomaly for modeling in terms of postulated mass distributions. An *isostatic anomaly* is calculated by subtracting the predicted gravity effect of theoretical subsurface mass variations related to surface topography according to a specific hypothesis (e.g., Airy or Pratt) from the Bouguer anomaly. This anomaly can be used to test the model suggested by the isostatic hypothesis as well as providing a broader indication of the degree to which simple isostasy applies.

3C.3. Interpreting gravity anomalies

The first step in interpreting a local gravity (or magnetic) anomaly is to separate the local residual anomaly from the regional anomaly. There are then three main approaches to the interpretation of a residual anomaly: (1) the *indirect method* (or modeling) whereby a theoretical model of the subsurface is fitted to the observed anomaly by a process of trial and error; (2) the *parametric method* which aims to fit a simple geometric shape to an anomaly, such as a slab or a sphere in gravity or a dike in magnetics; this approach can be used to place limits, such as maximum possible depth to top of the body causing an anomaly; and (3) the *direct method* whereby potential field operations such as upward continuation are carried out. The indirect method is by far the most widely used approach in the interpretation of gravity anomalies over continental rifts, although direct methods have also been used especially in flexural studies.

Gravity modeling makes repeated use of the forward problem of calculating the gravity anomaly of an arbitrary two- or three-dimensional body. An initial geologic model is hypothesized and its anomaly is computed by standard techniques and compared with the observed anomaly. The shape and/or density distribution is repeatedly adjusted until an acceptable fit is obtained by trial and error. This process can be carried out automatically using a variety of inversion techniques such as non-linear optimization. The main problem with the indirect method is that in absence of other information on the source body, the resulting model can never be unique. Other models can also be constructed to give equally good fits. This problem is minimized by constraining the proposed geologic model with collateral information from magnetic and seismic data and drill hole logs. Furthermore, ambiguity in interpretation can be overcome provided that adequate assumptions can be made. For example, if the density contrast across a single interface and its depth at one point can both be specified, as in the case of the floor of the sediment filled trough, then the shape of the interface can be mapped from the gravity anomaly it causes. However, errors in the observed anomaly will lead to errors in the mapping, and horizontal resolution is limited to wavelengths not much shorter than the depth of the interface. If constraints are inadequate to ensure uniqueness as above, it may be necessary to compute a range of possible models consistent with the observations.

A simple application of the indirect method (modeling) relevant to rift studies is to obtain the subsurface shape of the floor of an outcropping sedimentary graben of specified density contrast with the basement (which may vary with depth) from the gravity anomaly it causes. Sedimentary troughs are characterized by large negative local anomalies (several tens of milliGals) with steep marginal gradients. Such anomalies of shallow origin do not extend more than a few kilometers beyond the edges of the trough. In continental rift regions, the deeper crustal and mantle anomalies are of longer wavelength and can be approximately removed without serious error. In the past, such gravity interpretations have been important in indicating the large thickness of low density sediments characteristic of rift troughs and confirming that they are bounded by normal faults (e.g., Girdler, 1964; Zorin, 1971; Kahle and Werner, 1980; Keller et al., 1991). However, the gravity method

has now been mainly superseded by seismic reflection studies for investigating the internal structure and subsurface shape of rift troughs.

Gravity modeling has also been effectively used to assess crustal and upper mantle structure beneath continental rift systems. The short wavelength effect of shallow structure such as sediment filled troughs needs first to be removed (or incorporated in the model). The Bouguer anomaly can then be interpreted in terms of variation in Moho depth, density anomalies within the crust above the Moho, and lateral variations in the density of the upper mantle. Characteristically, the Moho beneath an active rift system shallows as a result of crustal stretching, there may be dense intrusions within the crust (e.g., Searle, 1970), and the broad domal uplift characteristic of active continental rifts is commonly supported by a hot, low density region in the upper mantle usually associated with a plume head. Although the crustal anomalies are generally of shorter wavelength than the upper mantle anomalies, the separation of the two contributions cannot be done uniquely. The best approach is to use explosion seismology to define the crustal thickness and its variation, and to use the gravity anomaly to refine the crustal model and to determine the mantle anomaly, assuming a realistic density contrast. Gravity interpretation is thus complementary to teleseismic seismology in determining the anomalous upper mantle which characteristically underlies active rift systems. Of importance in relating the gravity to the seismic data are empirical relationships between density and P-wave velocity, although these break down when partial fusion is involved. An early example of the use of gravity to infer crustal and mantle structure beneath the East African rift system is given by Baker and Wohlenberg (1970). A more recent evaluation of the gravity anomaly of the central East African rift system (Nyblade and Pollack, 1992) shows that the anomaly is caused not only by the rift-related modifications to the crust and upper mantle, but also by regional pre-rift crustal sources associated with an ancient suture. Numerous other examples of the use of gravity modeling to investigate the crustal structure of modern continental rifts and to speculate on mechanisms for rifting from the models exist in the geophysical literature. Recent examples are the studies of ten Brink et al. (1993) in the Dead Sea basin and Burov et al. (1994) in the north Baikal rift zone.

A further important use of the gravity method in rift studies is to assess the state and mechanism of isostasy. Other geophysical methods cannot give this information. The most obvious application is in discussion of the long wavelength negative Bouguer anomalies which occur over the broad domal uplifts associated with many of the present rift systems. Thus, the East African Plateau is 1300 km wide, about 1200 m high on average, and has a negative Bouguer anomaly peaking at about –200 mGal over the eastern rift system. The negative Bouguer anomaly represents the low density isostatic support for the elevated topography (e.g., Girdler and Sowerbutts, 1970; Fairhead, 1976). The isostatic support is demonstrably not caused by crustal thickening and must be attributed to a substantial low density region in the underlying upper mantle which is thought to originate as a result of the thermal effects of a plume head.

At shorter wavelengths in rift regions such as East Africa, the correlation between gravity and topography is less obvious. This is because at shorter wavelengths the surface and internal loads can be wholly or partly supported by the strength of the elastic lithosphere, so that flexural compensation occurs which is dependent on wavenumber. Ebinger et al. (1989) have analyzed the flexural equilibrium of subregions of the East African rift system to determine the variations of effective elastic plate thickness within the region. In order to carry out this analysis, both topography and gravity are transformed to the wavenumber domain using the two-dimensional fast Fourier transform. The coherence between topography and gravity can then be determined as a function of wavenumber. The results can then be compared with theoretical models and thus the best fitting elastic plate thickness can be determined. The resulting elastic plate thickness was found to be above 65 km in the stable cratonic regions and within the range of 21 to 36 km below the active Ethiopian, Kenya and western rift systems. Intermediate values were obtained in uplifted regions which are un-

faulted. The thinning of the elastic plate in the regions of active rifting is attributable to the raised temperatures in the crust and lithosphere.

Gravity studies have also had an important role in identifying and studying the crustal structure of ancient rifts (Keller et al., 1983). These rifts are commonly characterized by a present-day thickened crust probably as a result of underplating during the rifting process which results in a broad negative gravity anomaly. This negative, at least in part, is counteracted by the positive gravity anomaly associated with pervasive mantle-derived intrusions into the lower crust over a region that extends well beyond the limits of the surface graben. Such is the case in the New Madrid Rift which coincides with the axis of the Mississippi Embayment. The resulting broad positive anomaly is marked by an axial negative gravity anomaly caused by the less-dense sedimentary rocks of the hidden graben beneath the Embayment sediments (Hildenbrand, 1985). Still other ancient rifts, such as the Midcontinent Rift Systems of central North America (Hinze et al., 1992) are profound positive gravity anomalies due to mantle-derived mafic volcanic rocks that fill the grabens and spill out beyond the margins. The interpretation of these gravity anomalies is far from unique, but reflection seismic studies over the past few decades (Zhu and Brown, 1986; Chandler et al., 1989; Hinze et al., 1990) show that the volcanic rocks of the rifts contain numerous reflection events and thus these seismic data can be used to constrain the gravity interpretation. Allen et al. (1992) have shown that the 1100 Ma old Midcontinent Rift centered on Lake Superior is a broad topographic high which is isostatically compensated by an underplated crust or depleted upper mantle associated with this ancient rifting event. The topographic feature is believed to be a vestige of a broad domal uplift that originated at the time of rifting which was associated with a mantle plume.

3C.4. The magnetic exploration method

Lateral variations of the geomagnetic field on a scale of less than a few thousand kilometers are caused by variations in the magnetite (and related minerals) content in rocks within the outermost 50 km shell of the Earth, and can thus be used for geological purposes. Most modern mapping of the geomagnetic field for exploration purposes makes use of aeromagnetic surveying and total field anomalies are normally measured for simplicity. Ground surveys can be carried out for follow up detail or for other local exploration purposes. The geomagnetic field at long wavelengths can be determined by satellite magnetometry.

The geomagnetic total field value varies from about 20,000 nT (nannoTesla) at low latitudes to about 60,000 nT in the vicinity of the poles. The common instrument for measuring total field anomalies is the proton precession magnetometer which measures absolute values. It has a typical accuracy of about 1 nT which is adequate for most purposes. More sensitive alkali vapor magnetometers can improve the accuracy by over an order of magnitude for precision surveying.

Magnetometer observations need to be corrected for short period variations of the geomagnetic field caused by ionospheric currents and associated induced currents within the Earth. This is best done by setting up a base station to record the variations within the survey area. Correction for the long wavelength variations with latitude and longitude, which include the dipole and non-dipole fields which originate within the core and in vicinity of the core-mantle boundary, can be made by subtracting the International Geomagnetic Reference Field (IGRF) from the observed total field value. The IGRF is updated every five years to account for the secular variation in the geomagnetic field. There is a small decrease of the field with height, but the correction is only applied for high precision work. The resulting magnetic anomalies reflect lateral variation in the magnetic polarization within the outermost shell of the Earth, extending down to the depth of the Curie point temperature (50 km or less), beneath which the rocks are effectively non-magnetic.

3C.5. Interpretation of magnetic anomalies

Magnetic interpretation methods are closely similar in many ways to those used for gravity interpretation. This is because both gravity and magnetic anomalies can be derived from scalar potential fields which satisfy Laplaces's equation. However, magnetic interpretation is generally more complicated in that the basic gravitational unit is a point mass (monopole) whereas the basic magnetic unit is a dipole. This means that the causative magnetic bodies are not as closely related to the anomalies they cause as they are in gravity. Consequently the process of modeling (indirect method) is less straightforward to apply, although this can be overcome by using non-linear computer inversion techniques. A further complication in magnetics is that the direction of magnetization is not necessarily along the direction of the present Earth's field, due to the presence of remanent as well as induced magnetization. The parametric method is widely used for interpretation of anomalies in terms of dikes, and the direct methods such as upward continuation apply to magnetics as well as to gravity.

Magnetic anomalies are nearly all caused by the presence of magnetite and related minerals in rocks, although the presence of a few other minerals such as pyrrhotite locally also give rise to significant anomalies. As most sedimentary rocks (with occasional exceptions) do not contain significant amounts of magnetite or other magnetic minerals, these rocks are usually effectively non-magnetic. Igneous rocks, especially those of mafic and ultramafic composition, are typically more strongly magnetic and may possess strong remanent magnetization reflecting the field direction at the time of formation. Metamorphic rocks are variably magnetic and as a result the pattern of magnetic anomalies generally reveals the basement strike direction even when overlain by sediments. In such a situation, the depth to the magnetic basement can be estimated using simple parametric methods or by using the Fourier spectrum.

Magnetic surveys have been carried out in continental rift zones, although the significance of the resulting interpretations falls far short of the contribution from gravity. An example is the application to the Baikal rift zone (Novoselova, 1978). Here the magnetic anomalies mainly (although not entirely) reflect the structure of the pre-rift basement rocks. The sedimentary rift troughs generally correspond to negative magnetic anomalies (reflecting their weak magnetization?). Local anomalies occur over the rift basalts. The magnetic anomalies here also indicate that the magnetic layer above the Curie point temperature is thinned as a result of raised temperatures. The upwarped Curie isotherm beneath the Rio Grande Rift (Mayhew, 1982) has also been mapped with satellite magnetic anomaly data. These satellite data have also been used to map aulacogens (e.g., Longacre et al., 1982). Magnetic anomaly data have been used to map the sinistral strike-slip motion on the Dead Sea Rift by evaluating the displacement of magnetic anomalies across the rift (Hatcher et al., 1981). Further, the buried New Madrid Rift has been mapped by the attenuated magnetic anomaly pattern over the graben and the marginal magnetic anomalies associated with rift-related intrusives (Hildenbrand, 1985). Magnetic anomalies have been especially useful in mapping buried segments of the Midcontinent Rift System (Hinze et al., 1966; King and Zietz, 1971) because of the strong remanent magnetization of the associated mafic volcanic rocks. More recently (Chandler et al., 1989; Mariano and Hinze, 1994) have successfully modeled the complex remanent magnetization of the volcanic rocks of the Midcontinent Rift in combination with gravity and seismic reflection data leading to improved structure and stratigraphic interpretation of the grabens of the rift.

3C.6. References

Allen, D.J., Hinze, W.J., and Cannon, W.F., 1992. Drainage, topographic, and gravity anomalies in the Lake Superior region: Evidence for a 1100 Ma mantle plume. Geophys. Res. Lett., 19: 2119–2122.

Baker, B.H., and Wohlenberg, J., 1970. Structure and evolution of the Kenya Rift Valley. Nature, 229: 538–542.

Bullard, E.C., 1936. Gravity measurements in East Africa. Philos. Trans. R. Soc. London Ser. A, 235: 445–531.

Burov, E.B., Houdry, F., Diament, M., and Deverchue, J., 1994. A broken plate beneath the North Baikal rift zone revealed by gravity modeling. Geophys. Res. Lett., 21: 129–132.

Chandler, V.W., McSwiggen, P.L., Morey, G.B., Hinze, W.J., and Anderson, R.L., 1989. Interpretation of seismic reflection, gravity and magnetic data across the Middle Proterozoic

Midcontinent Rift System in western Wisconsin, eastern Minnesota, and central Iowa. Am. Assoc. Pet. Geol. Bull., 73: 261–275.

Ebinger, C.J., Bechtel, T.D., Forsyth, D.W., and Bowin, C.O., 1989. Effective elastic plate thickness beneath the East African and Afar Plateaus and dynamic compensation of the uplifts. J. Geophys. Res., 94: 2883–2901.

Fairhead, J.D., 1976. The structure of the lithosphere beneath the eastern rift, East Africa, deduced from gravity studies. Tectonophysics, 30: 269–298.

Girdler, R.W., 1964. Geophysical studies of rift valleys. Physics Chem. Earth, 5: 121–156.

Girdler, R.W., and Sowerbutts, W.T.C., 1970. Some recent geophysical studies of the rift system in E. Africa. J. Geomagn. Geoelectr., 22: 153–163.

Hatcher, R.D., Jr., Zietz, I., Regan, R.D., Abu-Ajamieh, M., 1981. Sinistral strike-slip motion of the Dead Sea Rift: Confirmation from new magnetic data. Geology, 9: 458–462.

Hildenbrand, T.G., 1985: Rift structure of the Northern Mississippi Embayment from analysis of gravity and magnetic data. J. Geophys. Res., 90: 12607–12622.

Hinze, W.J., O'Hara, N.W., Trow, J.W., and Secor, G.B., 1966. Aeromagnetic studies of eastern Lake Superior. In: J.S. Steinhart and T.J. Smith (Ed.). The Earth Beneath the Continents. Am. Geophys. Union Geophys. Monogr., 10: 95–110.

Hinze, W.J., Braile, L.W., and Chandler, V.W., 1990. A geophysical profile of the southern margin of the Midcontinent Rift System in western Lake Superior. Tectonics, 9: 303–310.

Hinze, W.J., Allen, D.J., Fox, A.J., Sunwoo, D., Woelk, T., and Green, A.G., 1992, Geophysical investigations and crustal structure of the North American Midcontinent Rift System. Tectonophysics, 213, 17–32.

Kahle, H.-G., and Werner, D., 1980. A geophysical study of the Rhinegraben-II. Gravity anomalies and geothermal implications. Geophys. J.R. astron. Soc., 62: 631–647.

Keller, G.R., Lidiak, E.G., Hinze, W.J., and Braile, L.W., 1983. The role of rifting in the tectonic development of the Midcontinent, U.S.A. Tectonophysics, 94: 391–412.

Keller, G.R., Khan, M.A., Morgan, P., Wendlandt, R.F., Baldridge, W.S., Olsen, K.H., Prodehl, C., and Braile, L.W., 1991. A comparative study of the Rio Grande and Kenya rifts. Tectonophysics, 197: 355–371.

King, E.R., and Zietz, I., 1971. Aeromagnetic study of the Midcontinent Gravity High of central United States. Geol. Soc. Am. Bull., 82: 2187–2208.

Longacre, M.B., Hinze, W.J., and von Frese, R.R.B., 1982. A satellite magnetic model of northeastern South American aulacogens. Geophys. Res. Lett., 9: 318–321.

Mariano, J., and Hinze, W.J., 1994. Gravity and magnetic models of the Midcontinent Rift in eastern Lake Superior. Can. J. Earth Sci., 31: 661–674.

Mayhew, M.A., 1982. Application of satellite magnetic anomaly data to Curie isotherm mapping. J. Geophys. Res., 87: 4846–4854.

Novoselova, M.R., 1978. Magnetic anomalies of the Baikal rift zone and adjacent areas. Tectonophysics, 45: 95–100.

Nyblade, A.A., and Pollack, H.N., 1992. A gravity model for the lithosphere in western Kenya and northeastern Tanzania. Tectonophysics, 212: 257–267.

Searle, R.C., 1970. Evidence from gravity anomalies for thinning of the lithosphere beneath the rift valley in Kenya. Geophys. J.R. astron. Soc., 21: 13–21.

ten Brink, U.S., Ben-Avrahan, Z., Bell, R.E., Hassouneh, M., Coleman, D.F., Andreasen, G., Tibor, G., and Coakley, B., 1993. Structure of the Dead Sea pull-apart basin from gravity analyses. J. Geophys. Res., 98: 21877–21894.

Vening Meinesz, F.A., 1950. Les grabens africains, résultat de compression ou de tension dans la croûte terrestre? Bull. Inst. R. Colonial Belge, 21: 539–552.

Zhu, T., and Brown, L., 1986. Consortium for continental reflection profiling Michigan surveys: Reprocessing and results. J. Geophys. Res., 91: 11477–11495.

Chapter 3D

Heat flow in rifts

P. Morgan

3D.1. Discussion

There is a superficial similarity in heat flow data from most Cenozoic continental rifts (Morgan, 1982). They are characterized by a large scatter in data, which typically range from near zero heat flow, to values in excess of 150 mWm^{-2}. Older rifts are generally characterized by more uniform thermal regimes, although anomalies located in the rifts, of the order of ± 20% background, have been reported. To understand the significance of these data it is important to appreciate the factors which contribute to surface heat flow.

Heat flow data are a determination of near-surface conductive heat flow. Temperature data are usually collected in near-vertical bore holes, or in near-vertical probe penetrations of lake sediments, and hence essentially only the vertical component of heat flow is determined. This restriction is not generally important, except in regions of high relief or major subsurface structure, because, to a first approximation, the earth's surface is isothermal and isotherms are subparallel to the surface. Significant local departures from this approximation, and the effects of changes in local surface conditions (climatic changes, erosion and sedimentation), are generally compensated by individual data corrections (e.g., Jaeger, 1965). The most important limitation of heat flow data for analysis of rift processes is that the data represent only the near-surface conductive heat flow.

The surface heat flow pattern in rift zones represents a number of components: 1) heat generated by radioactive decay of unstable isotopes in the crust; 2) heat conducted into the crust from the underlying mantle; 3) heat refracted in the crust by thermal conductivity structure; 4) heat advected into the crust by magmatism; 5) heat advected within the crust by tectonic deformation; and 6) heat redistributed in the uppermost crust by ground water flow. The first three of these components comprise the surface heat flow in stable regions, and it is important to recognize that heat flow in stable regions can vary by a factor of two or three, primarily due to variations in 1) (Morgan, 1984). If paleo-rifts are defined as rifts in which all transient thermal anomalies have decayed (Morgan and Ramberg, 1987), their heat flow anomalies are due to components 1) and 3), perhaps spatially controlled by the rift structures. By this definition, paleo-rift thermal structure would be expected in rifts which have not experienced tectonic or magmatic activity for at least the past 65 to 250 Ma (Morgan, 1984). In young rift zones, additional surface heat flow anomalies may be expected due to a combination of increased heat flow from the underlying mantle, and some combination of components 4) to 6). To understand rift evolution, it is important to be able to separate deep from shallow thermal sources for the surface heat flow. Some of this separation may be made by integration of other data sets with surface heat flow, e.g., surface, seismic or electro-

magnetic evidence for magmatism associated with elevated heat flow. This section, however, deals only with the thermal aspects of this problem.

The first task in analysis of heat flow data associated with rifting is to determine whether or not an anomalous heat source is associated with rifting. Although surface heat flow anomalies may be associated with the rift, the spatially averaged heat flow from the rift may be indistinguishable from the spatially averaged regional heat flow adjacent to the rift. If the rift floor and rift flank average heat flow values are indistinguishable, we must conclude that either no significant deep thermal source is associated with rifting, or that the thermal source is younger than the characteristic time for thermal conduction to produce a surface anomaly for the source depth. This characteristic time varies as the square of source depth, and varies from about 17 Ma for the base of a 30 km thick crust, to about 65 Ma for the base of a 100–km–thick lithosphere (Lachenbruch and Sass, 1977). Thus, lack of an average surface heat flow anomaly associated with a rift is not alone diagnostic of the presence or absence of a heat flow source at depth.

Spatial averaging of surface heat flow data is not a trivial task, primarily due to incomplete, and/or spatially aliased coverage of the data. Bore holes are rarely drilled specifically for heat flow measurements, and are generally sited for alternative economic reasons, such as oil, mineral, or water exploration or production. An adequate data set may not therefore exist for reliable spatial averaging. If the data set is inadequate, other indications of anomaly source depth must be used.

Information concerning the source of surface heat flow anomalies can be obtained from the magnitude of the anomaly, and/or the spatial association of the anomaly with other surface features (or from association with other geological or geophysical data sets if available). Heat flow in stable regions typically averages from about 40 to 55 mWm^{-2}. Heat flow may be as low as about 30 mWm^{-2} in mafic terranes with little crustal radiogenic heat production, up to about 100 mWm^{-2} in terranes with a thick, high heat-production component of granitic plutons. Thus, heat flow inside the range 30 to 100 mWm^{-2} cannot, on its own, be unambiguously recognized as diagnostic of a deep thermal perturbation. However, heat flow values less than about 25 mWm^{-2} are only expected where there is downward advection of heat. Heat flow values in excess of 125 mWm^{-2} yield steady-state conductive predictions of the geotherm that exceed the crustal solidus above the Moho, and can only be explained by transient thermal models, and/or models with crustal heat sources or advection.

If anomalous local heat flow is evident, its source may be evident through an examination of the spatial relationship of the anomaly with other features in the rift. High heat flow spatially associated with young volcanism is an obvious example of an advective crustal heat source. Less obvious, but very common, is the spatial redistribution of heat by ground water flow. This redistribution can occur in rifts with significant thermal anomalies, such as the Rio Grande rift (Morgan et al., 1986), or to produce localized anomalies in rifts without significant thermal anomalies, such as the Baikal rift (Lysak, 1984) and the Rhinegraben (Clauser, 1987). These local anomalies of shallow origin give the Baikal rift and the Rhinegraben a superficial thermal signature that is similar to the rifts with significant anomalies of deeper origin (cf. Morgan, 1982). Great care must be taken to determine the sources of the anomalies before extrapolations are made about the deep thermal structure of rift zones.

Thermal anomalies resulting from, or accompanying tectonic deformation within the lithosphere have been used to constrain the mode of rifting and deep processes in rifting (e.g., Lachenbruch and Sass, 1978; McKenzie, 1978). These anomalies are the most important anomalies to isolate when considering rifting models, but the complex time-space interactions of deep thermal sources with the surface (Morgan, 1983), and the masking of these anomalies by more shallow sources, generally make these anomalies alone poor constraints upon models of rifting processes (Morgan and Baker, 1983; Ramberg and Morgan, 1984). Combined with other geological and geophysical information, however, they can place important constraints upon the processes of rifting.

3D.2. References

Clauser, C., 1987. Conductive and convective heat flow in the northern Upper Rhinegraben – can they be separated? International Union of Geodesy and Geophysics, XIX General Assembly, Vancouver, Canada, August 9–22, 1987, Abstracts, v. 1, U8-18: 77.

Jaeger, J. C., 1965. Application of the theory of heat conduction to geothermal measurements. In: W. H. K. Lee (ed.), Terrestrial Heat Flow, American Geophysical Union, Geophysical Monograph 7: 7–23.

Lachenbruch, A. H., and J. H. Sass, 1977. Heat flow and the thermal regime of the crust. In: J. G. Heacock (ed.), The Earth's Crust, Its Nature and Physical Properties, American Geophysical Union, Geophysical Monograph 20: 626–675.

Lachenbruch, A. H., and J. H. Sass, 1978. Models of an extending lithosphere and heat flow in the Basin and Range province. In: R. B. Smith and G. P. Eaton (eds.), Cenozoic Tectonics and Regional Geophysics of the Western Cordillera, Geological Society of America, Memoir 152: 209–250.

Lysak, S. V.,1984. Terrestrial heat flow in the south of East Siberia. Tectonophysics, 103:205–215.

McKenzie, D. P., 1978. Some remarks on the development of sedimentary basins. Earth Planet. Sci. Lett., 40: 25–32.

Morgan, P., 1982. Heat flow in rift zones. In: G. Palmasson (ed.), Continental and Oceanic Rifts, Geological Society of America and American Geophysical Union, Geodynamics Series, 8: 107–122.

Morgan, P., 1983. Constraints on rift thermal processes from heat flow and uplift, Tectonophysics, 94: 277–298.

Morgan, P., 1984. The thermal structure and thermal evolution of the continental lithosphere. Phys. Chem. Earth., 15: 107–193.

Morgan, P. and B. H. Baker, 1983. Introduction – processes of continental rifting. Tectonophysics, 94: 1–10.

Morgan, P., and I. B. Ramberg, 1987. Physical changes in the lithosphere associated with thermal relaxation after rifting, Tectonophysics, 143: 1–11.

Morgan, P., V. Harder, and T. H. Giordano, 1986. Heat and fluid flow in the Rio Grande rift: a possible modern thermal analogue of a Mississippi Valley type ore-forming system. In: R. W. Nesbitt and I. Nichol (eds.), Geology in the Real World—the Kingsley Dunham Volume, Inst. Mining and Metallurgy, 295–305.

This Page Intentionally Left Blank

Chapter 3E

Practical magnetotellurics in a continental rift environment

G.R. Jiracek, V. Haak, and K.H. Olsen

3E.1. Introduction

It is no exaggeration to say that surface measurements of deep electrical resistivity may hold the key to understanding how continental rifts develop. This is so because low resistivities detected in the mid-to-lower crust in rift zones reflect conditions that control the strain rate, and therefore, the style and extent of tectonic deformation. Although low resistivities in active continental rifts probably are associated with fluids (either water and/or magma), it is their origin, their accumulation, and their influence that are critical. For example, is the strength of the lithosphere (and its brittle-ductile profile with depth) dominantly controlled by accumulations of high pressure H_20–$C0_2$ pore fluids, and, if so, what are the origins of these fluids? By better defining the depth and lateral extent of conductive occurrences in the crust and by carefully contrasting them with other geophysical measurements, important constraints on deep physical conditions will follow. Attempts at such syntheses are not new, e.g., Garland (1975), Hermance (1982), Haak and Hatton (1986), and Keller (1989) have made this effort, but it is clear that many new correlations are very important (e.g., Jodicke, 1992; Jones, 1992; Hyndman et al., 1993; Jiracek, 1995) and others will be forthcoming as research continues.

In this contribution we provide a self-contained but brief overview of the principal technique used to derive the deep subsurface distribution of electrical resistivity—namely the magnetotelluric (MT) method. MT exploration of the Earth has evolved to the status of a mature science during the past two decades with the advent of digital instrumentation, real-time processing, and sophisticated, robust analysis techniques showing increasing promise for interpreting complex, three-dimensional (3-D) electrical structures in the Earth. MT and other geoelectromagnetic methods are probably the least understood of geophysical techniques. This results in the humorous expectation among MT practitioners of the "MT (empty) stare", a look on colleagues' faces when the conversation turns to MT results.

Magnetellurics is the recording and study of naturally occurring electric and magnetic fields at the Earth's surface. The object of MT is to map the electrical properties of the Earth from the surface to many tens of km and to relate these geoelectric properties to the physical state and the tectonic processes that deform the Earth. There are many everyday examples of electromagnetic (EM) radiation such as radio waves, microwaves, and visible light itself (Fig. 3E–1). These common phenomena are at frequencies much higher than those used in most MT applications and, except for celestial light sources, the examples above are of man-made origin. There are several electromagnetic geophysical techniques that use transmitted energy from man-made sources (so-called *active sources*). Indeed, there are forms of MT that use controlled sources; however, to probe deep into the Earth, much more powerful energy sources at low frequencies are required. The sun is the major *passive source* for this application. A dis-

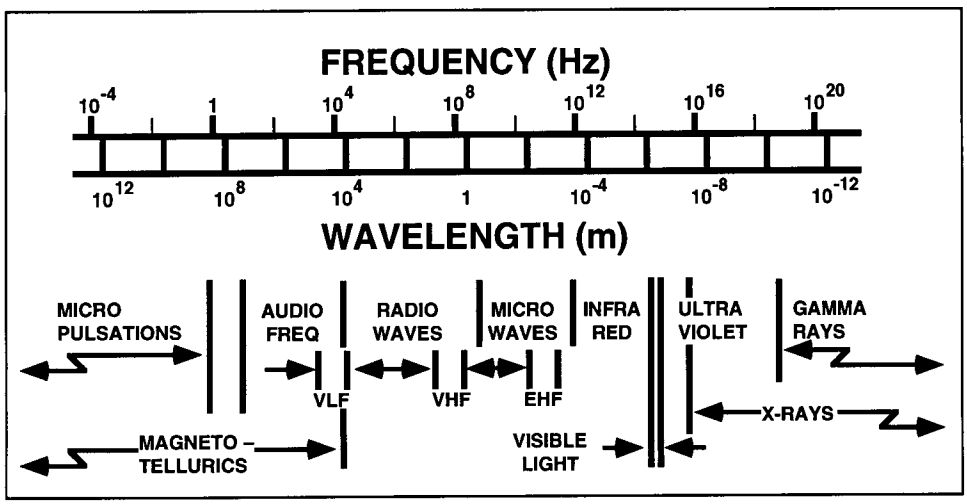

Fig. 3E–1. Twenty-four decades of the electromagnetic spectrum. Abbreviations, VLF, VHF, and EHF designate very low frequency, very high frequency, and extremely high frequency bands, respectively. The magnetotelluric frequency range extends from about 10^{-4} to 10^{+4} Hz.

advantage of a passive source is that it cannot be controlled by the experimenter. For example, MT measurements must depend on the uncertain energy levels in solar emissions.

When EM fields from any source encounter an obstacle such as the Earth, some energy penetrates (transmits) and some reflects. The reflected waves constructively and destructively interfere with the incident waves, and the transmitted waves are attenuated before they reflect from subsurface discontinuities. The Earth is a much better electrical conductor than air so the total electric field measured at the surface by MT is nearly zero because there is near cancellation of the incident field by the reflected field. The magnitude of the reflected electric field is a very large proportion (nearly 100%) of the incident field. The consequence is that the transmitted electric field is only a tiny fraction of the incident field. Fortunately this fraction is not zero, otherwise there would be no MT method. As it is, the wave propagation mechanism changes at the Earth's surface from that which dominates in an insulator (the air) to that which dominates in a conductor (the Earth). The technical description of this change embraces the end member processes of EM propagation, namely displacement currents and conduction currents, respectively. This chapter discusses the physics of these consequences and how they are used in practice to apply the MT method. In the first sections below, we try to provide a non-specialist geoscientist with a working knowledge of the MT method and its terminology. Then, these basic MT principles are applied both to synthetic and to actual continental rift data in order to illustrate the value and limitations of the method. Finally, we address the ultimate question of what derived resistivity values may mean through a discussion of possible connections between the geoelectric results and the rheology of continental rifts. The focus will be on findings from the lithosphere (mainly the crust) where excellent data have been accumulated during the last 15 years. Results from deeper—in the asthenosphere—are equally important, and historically were the first to be reported. However, most recent MT studies have targeted the crust where correlations with other geophysical data have been particularly rewarding.

3E.2. Magnetotelluric measurements

The MT method is a relatively new geophysical technique. The first paper on MT was written less than 50 years ago by the distinguished Soviet academician, A.N. Tikhonov (1950). Even so, the fundamentals of the method are a direct consequence of the classical electromagnetic (EM) theory established more than 100 years ago by the work of Ampere, Faraday, and Maxwell. Tikhonov's (1950) seminal contribution was to show that, at low frequencies, the spatial derivative of the horizontal component of the Earth's magnetic field (**H**) is proportional to the orthogonal component of the electric field (**E**) [**vector** quantities are shown in **boldface**]. He used previously published diurnal **H** data from magnetic observatories at Tucson, Arizona, USA, and from Zui, USSR, to estimate the thickness and electrical conductivity of the crust at these sites. The first western paper on MT was published by Cagniard (1953) in which he developed the formulas relating **E** and **H** on the surface of a layered medium with an incident plane wave. The works of Tikhonov and Cagniard form the basis of one-dimensional (1-D) MT analysis and this is often referred to as the *Tikhonov-Cagniard model.*

The practicality of the Tikhonov-Cagniard model of MT was soon challenged by Wait (1954), who argued that the proportionality between orthogonal **E** and **H** fields at the Earth's surface was valid only if the source fields do not vary appreciably over a characteristic distance called the *skin depth* (skin depth will be rigorously defined later). Madden and Nelson (1964) came to the defense of the Tikhonov-Cagniard model by showing that when the source's horizontal wavelength is much greater than the skin depth, as it is for the Earth, the model remains valid. Later, Dmitriev and Berdichevsky (1979) further proved that the horizontal magnetic field components need not be uniform, but can vary linearly over a layered earth.

Magnetotelluric source fields can be classified as originating either from lightning or from solar activity. Roughly speaking, fields below a frequency of 1 Hz are caused by the Sun; above 1 Hz, fields are due to worldwide thunderstorm activity. Fields due to solar activity result from complex interactions between the solar wind (charged particles ejected from the Sun) and the Earth's magnetosphere. In particular, the continuous and irregular pulsations of the solar wind change the shape and size of the magnetosphere and cause it to vibrate like an extraterrestrial jello. The resulting complex hydromagnetic waves are a major source of MT energy in a broad frequency band between 1 and about 10^{-4} Hz (Fig. 3E–1). Energy in hydromagnetic waves is transformed into propagating electromagnetic waves after passing through the electrically conductive, anisotropic ionosphere. This interaction forms large horizontal sheets of current in the ionosphere. Indeed, current systems of the daily variation are literally of hemispherical proportions.

Electromagnetic energy from lightning discharges around the world propagates in an atmospheric waveguide formed by the Earth and the ionosphere. This waveguide has resonance frequencies where energy is enhanced; e.g., the first Schumann resonance at 7.8 Hz has a wavelength equal to the circumference of the Earth. At frequencies of about 2 kHz, the waveguide is absorbing and energy in the natural electromagnetic spectrum is very low.

The physics of the interactions of the solar wind with the Earth's magnetosphere/ionosphere and the propagation of energy from distant lightning discharges is the subject of considerable research. Clear introductory discussions appear in Rokityansky (1982) and Vozoff (1991). From the standpoint of applying the MT method, there must be sufficient energy in the MT frequency band (Fig. 3E–1) and the incident plane wave assumption of the Tikhonov-Cagniard model must be valid. The latter is a fundamental assumption in applying the MT method; its validity depends on the location, size, and complexity of the source fields and their distances from the observation site. For example, a location at high magnetic latitudes (auroral latitudes) on the Earth's surface would be inappropriate during times of intense magnetic storms, but a mid-latitude site might be acceptable at the same time. Measurements taken during nearby thunderstorm activity would not meet the plane wave criterion, whereas waves from distant lightning can be properly treated as incident plane waves.

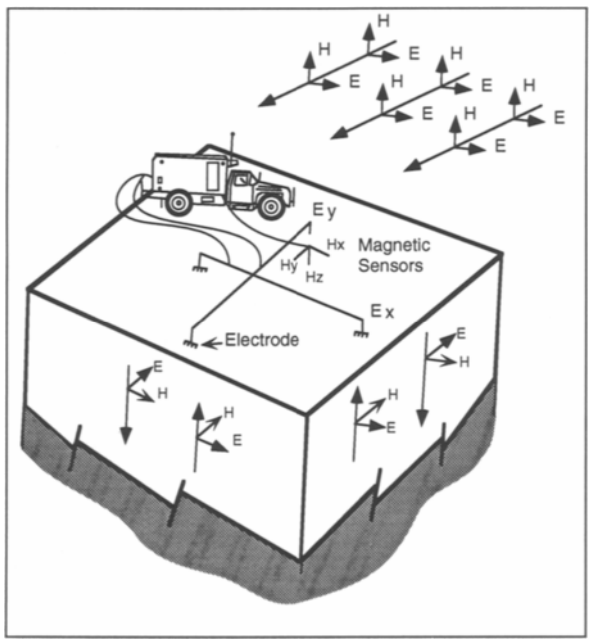

Fig. 3E–2. Magnetotelluric field layout with schematic incident, reflected, and transmitted propagating electromagnetic fields (redrawn from Sternberg et al., 1984).

The **E** and **H** fields measured at the surface of the Earth are samples of a stochastic (random) process since the solar wind and lightning activity are random variables of time and space. Therefore, the collection of all possible field measurements is unknown and infinite since we have no exact spatial-temporal knowledge of the underlying processes. Thus, at first it appears that the best one could hope for with such measurements would be statistical estimates of desired quantities. For example, only statistical probabilities can be used to describe the finite, known samples in the process of throwing a single die with six faces. If such were the case with MT measurements, the method would be of very limited value. What is needed to derive deterministic quantities is a measure—or measures—that when recorded now are the same as they were in the past or as they will be in the future. Clearly, the **E** and **H** fields themselves do not satisfy this property which is called *statistical stationarity*. Fortunately, there are such quantities in the MT case; they are the spectral ratios of the **E** to **H** field components. The "trick" therefore, that enables practical use of the MT method is to take time measurements of **E** and **H**, convert them into their frequency representations, and then compute the E/H ratios. The conversion from time to frequency domain measurements is usually done by Fourier transforming via a computer algorithm such as the Fast Fourier Transform (FFT).

Physical measurements of the **E** and **H** fields are commonly made as shown schematically in Figure 3E–2. Orthogonal, horizontal **E** fields are recorded by measuring the time-varying potential differences (voltages) between two nonpolarizing electrodes at the surface of the Earth. The ratio of these voltages divided by the horizontal distances (typically a few 100 m) are approximations of the E_x and E_y time-varying fields. Three perpendicular components of magnetic fields are normally obtained using induction coils which yield the time derivatives of the magnetic x, y, and z fields. Upon integration, one obtains the required H_x, H_y, and H_z time-varying fields. Magnetic fields can be measured directly by SQUID (Superconducting Quantum Interference Device) magnetometers, as was common in the late 1970s and early 1980s, but more recently, the development of highly sensitive, low noise induction coils has largely replaced SQUID measurements.

3E.3. Basic magnetotelluric principles

Simple manipulation of Maxwell's equations (Faraday's and Ampere's laws) together with the constitutive relations for a homogeneous linear isotropic medium yields the general electromagnetic (EM) *wave equation* for the time-varying vector **E** field in charge-free regions (e.g., Ward and Hohmann, 1988),

$$\nabla^2\mathbf{E} = \mu\left(\sigma\frac{\partial\mathbf{E}}{\partial t} + \varepsilon\frac{\partial^2\mathbf{E}}{\partial t^2}\right). \qquad (1)$$

Here, μ is the magnetic permeability (in henrys/m, H/m), σ is the electric conductivity (in siemens/m, S/m), and ε is the electric permittivity (in farads/m, F/m); these are the physical quantities that describe the EM properties of a material. In most geophysical EM applications, μ can be assumed to have its free space value, μ_o, and, as we shall soon see, the permittivity term in Eq. 1 can be neglected. This

places the ultimate emphasis on the conductivity as the principal diagnostic electrical parameter for the Earth. For purely traditional reasons geophysicists usually report the reciprocal of the conductivity which is the resistivity, ρ. Resistivity units are ohm-meters (ohm-m) since the siemen and the ohm are reciprocal units. Because, for practical reasons mentioned earlier, we want the **E** and **H** values as functions of frequency, it is convenient to immediately write the equivalent of the wave equation in the frequency domain. This is obtained by Fourier time transforming Eq. 1 to yield

$$\left(\nabla^2 + k^2\right)\mathbf{E}(x,y,z,\omega) = 0 \; . \tag{2}$$

This is called the *Helmholtz equation* where **E** is now a function of the angular frequency ω, equal to $2\pi f$, where f is frequency in hertz (Hz). The factor k is called the complex *propagation "constant"* or *wave number* in the medium,

$$k = \omega\left[\left(\varepsilon - i\frac{\sigma}{\omega}\right)\mu\right]^{1/2} . \tag{3}$$

The corresponding wave and Helmholtz equations for the vector **H** field are exactly as in Eqs. 1 and 2 upon substitution of **H** for **E**. Some researchers use the magnetic induction, **B**, instead of **H** via the constitutive relation $\mathbf{B} = \mu\mathbf{H}$.

We are now prepared to state the two major assumptions of the MT method. These are:

• *Quasistatic approximation*

The *quasistatic approximation* results from assuming that the σ term in k (Eq. 3) dominates over the ε term. That is, $\sigma >> \omega\varepsilon$. Physically, this states that electrical *conduction currents* are always very much larger than electrical *displacement currents*. Conduction currents are the familiar type as in household wiring which give rise to so-called ohmic loss or heating. Displacement currents are loss-free, temporal variations in **E** fields which explain how an EM field (e.g., light) can propagate through a vacuum. The quasistatic approximation states that the Earth behaves as a *good conductor (poor insulator)* at the frequencies used in MT. An important consequence of the quasistatic approximation is that the complex propagation constant, k, now has real and imaginary parts of identical magnitude, i.e.,

$$\begin{aligned} k &= \left(-i\,\sigma\mu\omega\right)^{1/2} = \left(\sigma\mu\omega\right)^{1/2} e^{-i\pi/4} \\ &= \left(\frac{\sigma\mu\omega}{2}\right)^{1/2} - i\left(\frac{\sigma\mu\omega}{2}\right)^{1/2} . \end{aligned} \tag{4}$$

The wave equation (Eq. 1) now has only a first partial time derivative term. Physically, it becomes a *diffusion equation* of the same form that governs the diffusion of heat through a solid. Electrical conductivity in the Earth measured by MT is mainly due to ionic fluids such as saline water or magma. The dominant conduction currents proceed by the diffusion of ions through these fluids.

• *Normally incident plane wave approximation*

In the above preliminary discussion of MT source fields, it was stated that the Tikhonov-Cagniard model assumes that a plane wave is incident upon the Earth's surface. We now add the requirement that the plane wave be normally incident. This is certainly not true of waves from all sources which are superimposed to form the resultant at a given measurement site at a given time. However, because the Earth is such a good conductor (i.e., the quasistatic approximation holds), all waves, irrespective of their incoming directions are refracted very nearly vertically (normally) into the Earth. This condition, which is the essence of Madden and Nelson's (1964) defense of the Tikhonov-Cagniard model, validates the second assumption and greatly simplifies computer modeling of the MT response of the Earth.

3E.3.1. Homogeneous half-space

With a plane wave normally incident on a homogeneous half-space, the **E** and **H** fields are constant in direction and magnitude over planes perpendicular to the vertical, downward +z, direction of propagation. Taking **E** in the x direction and **H** in the y direction, the Helmholtz equation becomes an ordinary differential equation with solution

$$E_x(z) = E_0 e^{\pm ikz} . \tag{5}$$

Here, E_0 is a constant which is the magnitude of E_x at z = 0. The minus sign is chosen in the exponent to insure that the fields decrease with propagation in the +z direction in the Earth. Therefore, in a ho-

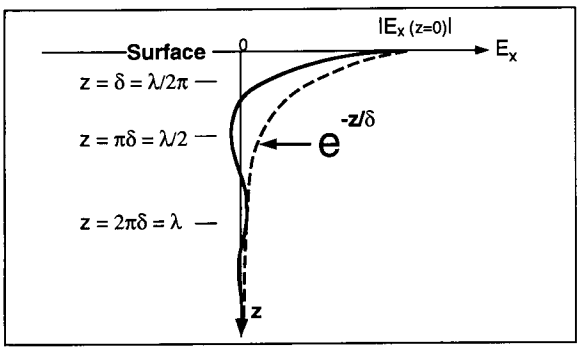

Fig. 3E–3. Exponential attenuation of sinusoidal variation of E_x as a function of propagation in the +z direction. E_x magnitudes are approximately 37%, 4%, and 0.2% of the surface value at depths of a skin depth, δ, a half wavelength, $\lambda/2$, and one wavelength, λ, respectively.

mogeneous medium both the **E** and the **H** fields decrease exponentially, and at a depth equal to 1/|Imk| the field amplitudes are reduced to 1/e of their values at z = 0. This depth, where the field decreases to about 37% of the surface value, is called the *skin depth*, δ,

$$\delta = \sqrt{\frac{2}{\sigma\mu\omega}}. \qquad (6)$$

In practical units, this equation becomes

$$\delta \approx 0.5\sqrt{\rho T} \ \text{[km]} \qquad (7)$$

after substituting $4\pi \times 10^{-7}$ henries/m for μ_o and $\omega = 2\pi/T$, where T is the period of the incident field. SI units are used on the right side of Eq. 7, i.e., ρ in ohm-m and T in s, but the resulting units of δ are km. The skin depth, Eq. 7, is probably the most widely employed practical equation in MT since it is used to give a rough estimate of the depth of exploration. However, the skin depth equation is strictly true only for a homogeneous half-space and the real Earth is never so simple. Figure 3E–3 illustrates the spatial attenuation expressed by the skin depth and how δ relates to the wave length, λ, of the downward propagating wave. Since the real and imaginary parts of k have equal magnitudes (Eq. 4), and Re $k = 2\pi/\lambda$ for any propagating wave, this means that $l = 2p\delta$. Furthermore, since the *phase velocity* of a propagating wave is defined as $v = \lambda f$, then v is equal to $2\pi\delta f$. Shortly, some representative values for δ, λ, and v will be calculated, but first we consider the "trick", a parameter called the characteristic impedance, that allows the MT method to work.

As mentioned earlier, it is the spectral (frequency domain) ratios of the fields that are invariant (stochastically stationary) in MT. These ratios are the MT response of the Earth, and in the case appropriate to Eq. 5, we define the *characteristic impedance*, Z, of a medium as the spectral ratio $E_x(\omega)/H_y(\omega)$. Since the dimensions of **E** and **H** are V/m and A/m, respectively, we see that this spectral ratio has units of impedance, namely ohms. Using the expression for E_x (Eq. 5) and Maxwell's "curl-of-E" equation (i.e., Faraday's law) with an exp(+$i\omega t$) time dependency yields

$$Z(\omega) = \frac{E_x(\omega)}{H_y(\omega)} = \frac{\omega\mu_0}{k}. \qquad (8)$$

The characteristic impedance of free space (σ = 0, $\mu_0 = 4\pi \times 10^{-7}$ H/m, and $\varepsilon_0 = (1/36\pi) \times 10^{-9}$ F/m), is the well-known result, $Z_0 = (\mu_0/\varepsilon_0)^{1/2} \sim 376.6$ ohms. It is also very illustrative to calculate the characteristic impedance and other parameters for a typical MT situation on a continental land surface. Consequently, with T = 100 s and ρ = 100 ohm-m, Eqs. 7, 8, and subsequent discussion following Eq. 7 yield

$$\text{Re}\, Z = \text{Im}\, Z \sim 0.002 \text{ ohms}$$
$$\delta \sim 50 \text{ km}$$
$$\lambda \sim 310 \text{ km}$$
$$v \sim 3 \text{ km/s}.$$

At this same frequency the wavelength in free space is $3 \times 10^{+7}$ km, or over 2000 times the diameter of the Earth!

We now explore the useful extensions of the concept of characteristic impedance to surface measurements where the Earth is homogeneous, 1-D, and finally, multi-dimensional.

3E3.2. Measurements at the surface of a homogeneous half-space

Figure 3E–4a schematically depicts a plane wave normally incident upon a homogeneous half-space; the wave number k can be considered as a vector

pointed in the direction of propagation. Superscripts ^{i}, ^{r}, and ^{t} denote incident, reflected, and transmitted **E** and **H** fields, respectively. Applying the boundary conditions that tangential **E** and **H** fields must be continuous across the boundary (surface of the Earth) it is straightforward (e.g., Ward and Hohmann, 1988) to show that the *transmission coefficient* is given by

$$T(\omega) = \frac{E_x^t}{E_x^i} = \left(\frac{2Z_1}{Z_0 + Z_1} \right), \tag{9}$$

and the *reflection coefficient* is

$$R(\omega) = \frac{E_x^r}{E_x^i} = \left(\frac{Z_1 - Z_0}{Z_1 + Z_0} \right). \tag{10}$$

Z_0 and Z_1 are the *characteristic impedances* of free space and the homogeneous half-space, respectively. Similar equations can be derived for the transmitted and reflected **H** fields. For example, the reflection coefficient for the **H** field is $\{(Z_0 - Z_1)/(Z_0 + Z_1)\}$. Reflection and transmission coefficients are very important because they describe the amplitude and phase of the reflected and transmitted fields. Those familiar with linear systems will recognize Eq. 9 and Eq. 10 as the frequency domain representations of a linear system in which $T(\omega)$ and $R(\omega)$ take on the roles of *system response functions* or *transfer functions*. Note, also, that $Z(\omega)$ in Eq. 8 is a system response function relating an input $H_y(\omega)$ to an output $E_x(\omega)$. Because MT measurements are made at the surface of the Earth we need to calculate the total **E** and **H** fields at z = 0. This can be done using the field representations either above (medium 0) or below (medium 1) the surface and letting z = 0. Of course, the total **E** or **H** fields above z = 0 have both an incident and reflected component. The result of these manipulations when expressed as the ratio E/H at z = 0 is called the *surface impedance*, Z_s,

$$Z_S = \frac{\text{Total } E_x \text{ at } z = 0}{\text{Total } H_y \text{ at } z = 0} = Z_1 . \tag{11}$$

This important result states that the surface impedance of a homogeneous half-space equals the characteristic impedance of the medium. The surface impedance is a complex function of frequency, and applying Eqs. 3 and 8, we find

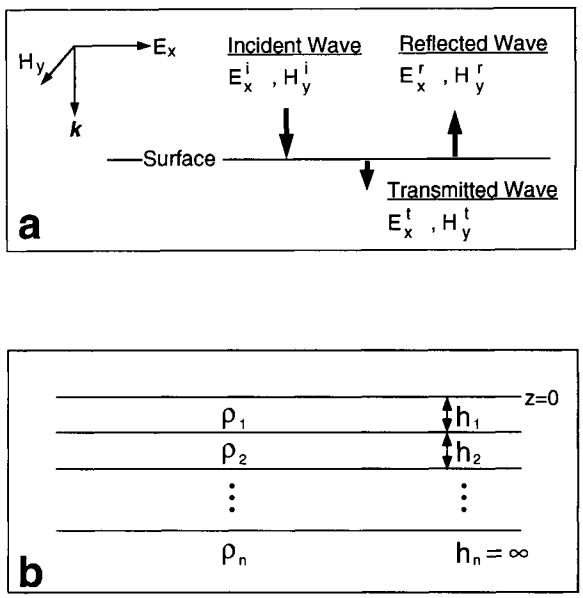

Fig. 3E–4.(a) Normally incident, reflected, and transmitted, plane waves at surface of a homogeneous half-space. E_x, H_y, and the vector propagation "constant", ***k***, form a right-handed orthogonal set. (b) N-layered, 1-D Earth model.

$$\begin{aligned} Z_S &= \left\{ \frac{\omega\mu_0\rho}{2} \right\}^{1/2} (1+i) \\ &= (\omega\mu_0\rho)^{1/2} e^{i\pi/4} \\ &= |Z_S| e^{i\phi_Z} . \end{aligned} \tag{12}$$

It is customary to express surface impedance in terms of its phase, ϕ_z, and another quantity called the apparent resistivity. Solving for ρ in Eq. 12, a complex quantity is avoided by defining a real quantity, the *apparent resistivity*, ρ_a, as

$$\rho_a = \frac{1}{\omega\mu_0} |Z_S|^2 . \tag{13}$$

The apparent resistivity, ρ_a, and the phase of the surface impedance, ϕ_z, as functions of frequency (or period) are the MT response parameters most commonly used in data presentations and interpretations.

For the case of a homogeneous half-space, these quantities are equal to the to the true resistivity, ρ and an impedance phase of 45° (from Eq. 12).

Physical understanding of electromagnetic reflection and transmission phenomena is enhanced by considering the approximate **E** and **H** relationships at the surface of a homogeneous half-space with Earth-like properties. The characteristic impedance of the Earth (~0.002 ohms in the sample calculation above) is very much smaller than that of the overlying atmosphere (nearly free space at 376.6 ohms). In this case, the reflection coefficient (Eq. 10) is nearly equal to –1. A reflection coefficient of –1 means that there is total reflection with a phase change of π; therefore, there would be total cancellation of the incident electric field. If this were exactly the case, there would be zero transmission (T = 0) and the MT method would be of no value for probing the Earth. Similar manipulation of the equations as done here for **E** fields can be done for **H** fields, yielding the result that the reflection coefficient for **H** (given the discussion following Eq. 10) is nearly +1. This means that the total **H** field at the surface of a homogeneous half-space is nearly twice the amplitude of the incident **H** field. With the **E** field approaching zero and the **H** field twice its incident value at the surface of the Earth, it is not surprising that the ratio of the two (the surface impedance) is a very small quantity.

3E.3.3. Layered earth

The surface impedance of an arbitrary n-layered, 1-D earth (Fig. 3E–4B) can be found by solving the 2n equations obtained by applying the boundary conditions on continuity of tangential **E** and **H** fields at n interfaces (e.g., Wait, 1970). The important features of this solution can be gleaned by examining the simplest case where n = 2. In this situation the surface impedance is given by

$$Z_S = Z_1 \frac{Z_2 + Z_1 \tanh(ik_1h_1)}{Z_1 + Z_2 \tanh(ik_1h_1)} . \qquad (14)$$

The apparent resistivity is, as always, given by Eq. 13. The response (ρ_a and ϕ_z as functions of T) for this case are directly dependent on the behavior of the tanh functions. There are four asymptotic relations that contain the essential physics of the response. These are:

1. For *high* frequencies (*short* periods) and/or *large* h_1, the response is that of the *top* layer. This can be seen by noting that $\tanh(ik_1h_1) \rightarrow 1$, and Eq. 14 becomes $Z_s \sim Z_1$ so $\rho_a \rightarrow \rho_1$.

2. For *low* frequencies (*long* periods) and/or *small* h_1, the response is that of the *bottom* layer, i.e., the basement. That is, $\tanh(ik_1h_1) \rightarrow 0$, and Eq. 14 becomes $Z_s \sim Z_2$ so $\rho_a \rightarrow \rho_2$.

The remaining two asymptotic relations require us to make the so-called *"thin-layer"* approximation. This approximation hinges on the smallness of the argument ik_1h_1 of the tanh function so that the function can be replaced simply by its argument. The product k_1h_1 is small if the skin depth (δ_1 = 1/ |Im k_1|) is large compared to h_1. Thus, the thickness of a thin layer is small compared to its skin depth, and since $\delta = 2\pi\lambda$, a thin layer is one that is thin compared to the wavelength in the layer. *This approximation is virtually always obeyed at long periods in MT.* Applying these limits to Eq. 14 yields:

3. For *highly conductive basement*, a *thin resistive upper layer* ($\rho_2 << \rho_1$) is manifested by its *thickness only*, independent of its exact electrical properties. Mathematically, as $\rho_2 \rightarrow 0$, $|Z_2| << |Z_1|$, and

$$Z_S \approx i\omega\mu_0 h_1 , \qquad (15)$$

with $\rho_a \approx \omega\mu_0 h_1^2$ So ρ_a depends only on the value of h_1, the thickness of the layer overlying the conductive basement.

4. For *highly resistive basement, a thin conductive upper layer is manifested by its h/ρ quotient only* (S_1 in this case). *Neither ρ or h can be resolved separately.* Mathematically: as $\rho_2 \rightarrow \infty$,, $|Z_2| >> |Z_1|$ and Eq. 14 reduces to

$$Z_S \approx \omega\mu_0 \frac{1}{ik_1^2 h_1} = \frac{1}{S_1} , \qquad (16)$$

with $\rho_a \approx 1/\omega\mu_0 S_1^2$. S_1 defines the *conductance* of the layer, which is h_1/ρ_1. That is, when $\rho_2 >> \rho_1$, ρ_a depends on the h_1/ρ_1 quotient or the conductance of the layer overlying the resistive basement.

It is very important to note that points 3 and 4 above not only apply to the first layer of a two-layer sequence; they apply to highly conductive and highly resistive layers *anywhere in an arbitrary, layered*

sequence as long as the buried layers are thin. This simple fact provides enormous practical limitations on the resolution of MT measurements. Indeed, only when the layers are thick can we separate ρ and h in the conductive case and resolve ρ in the resistive case.

Plots of log ρ_a and linear ϕ_z versus log T (called *MT sounding curves*) are the most widely used presentations of MT data, and are the recommended plotting conventions (Hobbs, 1992). Figure 3E–5 illustrates the asymptotic relations 1 through 4 above for two-layer models where the basement is either perfectly resistive or perfectly conductive. In both cases, ρ_a curves are asymptotic at short periods to ρ_1, the true resistivity of the top layer. The oscillations in the curves at intermediate periods are due to constructive and destructive interference of waves reflected from the top and bottom of the first layer. This is a highly attenuated version of what in optics literature is called "the quarter-wave effect." This phenomenon is well-understood in the MT case (e.g., Zhdanov and Keller, 1994), yet it was improperly attributed to an "artifact" by Spies and Eggers (1986). The lack of true one-dimensionality in the real Earth and measurement errors result in these oscillations being rarely observed in actual MT field data.

Rewriting the apparent resistivity relations given after Eqs. (15) and (16) in terms of period, T, and taking logarithms, we have

$$\log\rho_a = -\log T + \log\left(2\pi\mu_0 h_1^2\right), \qquad (17)$$

and

$$\log\rho_a = +\log T - \log\left(2\pi\mu_0 S_1^2\right). \qquad (18)$$

These are the logarithmic representations of asymptotic relations 3 and 4 above. Eqs. (17) and (18) are clearly equations of straight lines on log–log MT sounding curves with slopes equal to –1 and +1, respectively. Thus, the sounding curves in Figure 3E–5 have a slope of –45° when the basement is highly conductive and a slope of +45° when the basement is highly resistive. These straight lines in MT sounding plots were named *"h-lines"* and *"S-lines"*, respectively, by Russian researchers (Berdichevsky and Dmitriev, 1976). These descending and ascending branches can be used directly to calculate h_1, the *depth to the conductive basement*, and the *conductance, S_1, above a resistive basement* using

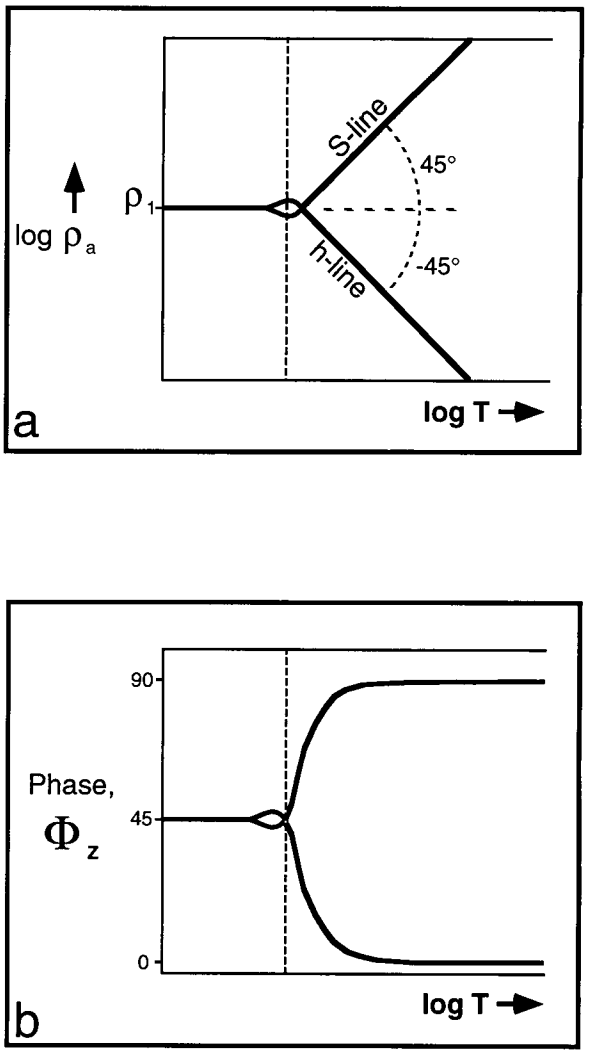

Fig. 3E–5. Two-layer MT sounding curves of (a) log apparent resistivity, ρ_a and (b) impedance phase, ϕ_z versus log period, T. Shown are the limiting cases of perfectly resistive and perfectly conductive basement which produce S-line and h-line, respectively. All other two-layer MT sounding curves would lie within these limiting cases.

$$h_1 = \left(\frac{T\rho_a}{2\pi\mu_0}\right)^{1/2} \approx 357\,(T\rho_a)^{1/2} \quad \text{[m]}, \qquad (19)$$

and

$$S_1 = \left(\frac{T}{2\pi\mu_0\rho_a}\right)^{1/2} \approx 357\left(\frac{T}{\rho_a}\right)^{1/2} \quad \text{[S]}. \qquad (20)$$

Convenient coordinate values at which to apply Eqs. 19 and 20 on actual ρ_a sounding curves are at ρ_a = 1 ohm-m, which means that observed h and S trends must sometimes be extrapolated.

Although the above relations are derived for a simple two-layer Earth, it is of utmost importance to appreciate that these relations hold approximately for highly conductive or highly resistive layers no matter how many overlying layers there are. This means that steeply descending branches (~h–lines) can be used to calculate the *total depth* to *any* highly conducting layer. Similarly, steeply ascending branches (~S–lines) can be used to calculate the *total conductance* above *any* highly resistive layer, i.e., $h_1/\rho_1 + h_2/\rho_2 + \ldots$ In practice, a highly conductive layer closely produces an h-line when its conductance is very much greater than the total conductance of all overlying layers. A consequence of this observation is the so-called *screening effect*, i.e., the response of highly conductive layers, at the surface or at depth, will prevent the detection of deeper conductive occurrences unless they are of much greater conductance than the overlying layers. A resistive layer closely produces an S-line when its thickness is very much greater than the total thickness of all overlying layers. Thus, we are again reminded that a thin *conductive* layer is manifested by its *conductance* (point 3 above) and a thin *resistive* layer is manifested by its *thickness* (point 4 above). Later in the *Introduction to magnetotelluric interpretation* section (§ 3E.4), we will illustrate the practical application of the four asymptotic relations above to both actual and synthetic data.

The complex surface impedance measured on a layered Earth can be shown to be a so-called *minimum phase function*. In this case the real and imaginary parts of Z_s are not independent; this leads to interrelations between the values of ρ_a and ϕ_z which are expressed by a Hilbert transform pair. A very useful approximate relation has been known for some time in the Russian literature (e.g., Vanyan et al., 1967) and has been applied to MT analysis by Boehl et al. (1977). It is

$$\phi_z(T) \approx \frac{\pi}{4} - \frac{\pi}{4}\frac{d(\log\rho_a)}{d(\log T)}. \qquad (21)$$

Applying this relation, we expect the phase of Z_s to be 45° at maxima and minima (and flat portions) of ρ_a log–log sounding curves. The impedance phase is 90° and 0°, corresponding to an h-line and an S-line, respectively. These features are evident in the ϕ_z sounding curves presented in Figure 3E–5. The failure of the relationship in Eq. (21) to hold (including impedance phase values outside the 0° to 90° range) is often taken as evidence for a three-dimensional (3-D) earth. The relationship (Eq. 21) seems to hold for most (perhaps all) two-dimensional (2-D) structures, although we are not aware of any proof of this assertion.

3E.3.4. Multi-dimensional earth

At the surface of a multi-dimensional (2-D or 3-D) earth or an anisotropic 1-D earth, the simple linear relation between E_x and H_y given in Eq. (11) no longer holds. The Tikhonov-Cagniard model needs revision. A solution to this dilemma was proposed by Madden and Nelson (1964) who postulated that the E_x and E_y fields depend on both the H_x and H_y fields. That is,

$$\begin{aligned} E_x(\omega) &= Z_{xx}(\omega)H_x(\omega) + Z_{xy}(\omega)H_y(\omega) \\ E_y(\omega) &= Z_{yx}(\omega)H_x(\omega) + Z_{yy}(\omega)H_y(\omega) \end{aligned} \qquad (22)$$

or in tensor notation

$$\begin{bmatrix} E_x \\ E_y \end{bmatrix} = \begin{bmatrix} Z_{xx} & Z_{xy} \\ Z_{yx} & Z_{yy} \end{bmatrix} \begin{bmatrix} H_x \\ H_y \end{bmatrix}$$

or, (23)

$$\mathbf{E} = \overline{\overline{\mathbf{Z}}}\,\mathbf{H}\,.$$

Here, the four impedance elements form a 2 by 2 *impedance tensor*, $\overline{\overline{\mathbf{Z}}}$ The field relationships of Eqs. (22) and (23) are still linear, but now each equation represents a two-input/single-output linear system (Reddy and Rankin, 1974). But, an immediate problem arises when attempting to solve Eq. (22) for the

four impedance values. Namely, the system is underdetermined since there are only two equations in four unknowns (Z_{xx}, Z_{xy}, Z_{yx}, Z_{yy}).

The four impedance elements can be determined if one can obtain four independent equations of the form of Eq. (22). This can be accomplished if two different source polarizations are used. In practice, however, because both **E** and **H** fields contain noise, it is statistically desirable to have many polarizations contributing to the recordings. This allows averaging to reduce the effects of noise. The result is an overdetermined system since there are now more equations than unknowns. Sims et al. (1971) developed techniques to derive least-squares estimates of the tensor impedance elements that minimize the sums of the squared differences between the measured and predicted **E** fields.

The main problem with impedance elements estimated in this manner is that they contain autopowers (products of identical field components, one a complex conjugate) that are always biased by measurement noise. This problem can be reduced considerably by a technique called *remote reference MT* first suggested by Gamble et al. (1979). Remote reference MT uses H_x and H_y fields recorded simultaneously at two separate sites, one called the base and the other called the remote site. A substitution of the remote complex conjugate magnetic components for the base complex conjugate magnetic components can now be made when solving the impedance equations. This works well provided the desired MT signal is correlated between the base and remote sites but the noise is not; this is often the case between sites separated by only a few kilometers. For example, noise caused by wind vibrating the sensors may be totally different at the two sites while the MT signal due to large-scale ionospheric sources is highly correlated over large distances. In a recent MT survey in Italy, an electric train power distribution system produced noise correlated over tens of kilometers so the base and remote sites had to be separated by hundreds of km. Nevertheless, the desired MT signals were correlated testifying to the validity of one of the basic MT assumptions, that of normally incident plane waves.

3E.3.5. Two-dimensional earth

Now consider the MT response of a two-dimensional earth. Taking the invariant (or strike) direction to be the y-coordinate of a 2-D earth will define the *geoelectric strike direction*. For this coordinate choice, $\partial/\partial y = 0$, and Maxwell's electromagnetic equations separate into two independent modes or polarizations. The component of the electric field, E_y, parallel to the geoelectric strike direction defines *E-polarization*; the component of electric field perpendicular to the geoelectric strike direction defines the *H-polarization*. The terms E- and H-polarization are those recommended by the international EM induction community (Hobbs, 1992). Alternative specifications of *transverse electric (TE)* and *E-parallel* are also commonly used to designate E-polarization. These terms relate to the orientation of E_y transverse (perpendicular) to the geoelectric plane of symmetry and its parallel relationship to the geoelectric strike direction, respectively. *Transverse magnetic (TM)* and *H-parallel* are corresponding terms used interchangeably for H-polarization. The E- and H-polarizations each has only three EM field components. For E-polarization, where E_y is assumed, H_x and H_z are derived from Maxwell's equations. Correspondingly, for H-polarization, where H_y is assumed, E_x and E_z are derived from Maxwell's equations.

In the perfect 2-D case, only two impedances are needed to completely describe the tensor impedance. That is, the 2 by 2 impedance tensor in Eq. (23) reduces to

$$\overline{\overline{\mathbf{Z}}} = \begin{bmatrix} 0 & Z_{xy} \\ Z_{yx} & 0 \end{bmatrix} \tag{24}$$

where

$$Z_{yx} = -E_y/H_x, \quad Z_{xy} = E_x/H_y, \tag{25}$$

and the diagonal elements of the impedance tensor are zero.

As in Eqs. 22 and 23, the first subscript refers to the electric field component; therefore, Z_{yx} and Z_{xy} are the impedance elements for the E-and H-polarizations, respectively. The corresponding apparent resistivities are calculated using Eq. 11 where Z_{yx} and Z_{xy} are substituted for Z_s.

In the 1-D (or homogeneous) case the impedance response of the Earth is described by two numbers (parameters) at each sample period since Z_s is a complex quantity. The two separate complex impedance elements in the 2-D case (Eq. 25) yield four parameters in the impedance description. Actually, there are five parameters since the orientation of the rectangular coordinate system must also be included.

In actual field practice, the orthogonal measuring axes (Fig. 3E–2) rarely coincide with directions exactly parallel and perpendicular to the geoelectric strike. Consequently, the coordinate system must be rotated either physically or computationally to off-diagonalize the impedance tensor to the form of Eq. 24. This is expressed computationally by a standard coordinate transformation or rotation by some angle. If the Earth were perfectly two-dimensional, there would be a specific angle where Z_{xx} and Z_{yy} would be identically zero. Since the actual Earth is never exactly two-dimensional, some other scheme must be used to determine an approximate or quasi 2-D earth geometry. Most schemes either minimize some combination of the diagonal components of the impedance tensor or maximize a combination of the off-diagonal elements, usually in a least squares sense. This analysis is often called a *Swift analysis* (Swift, 1967). For a perfectly 2-D earth, the Swift analysis yields two directions called the *principal directions*; one is the *geoelectric strike direction* and the other direction perpendicular to the strike is the *geoelectric dip direction*. In an ideal 2-D earth, identical principal directions would be calculated at all measurement sites and at all sounding periods.

The importance of the basic Swift analysis cannot be overemphasized since it has been the dominant MT processing scheme for over 25 years. The analysis always produces principal directions, but they represent quasi 2-D geoelectric strike and dip directions. In nature, the directions always vary at different periods and from site to site in violation of a perfect 2-D earth. Swift (1967) presented indices called *skew* and *ellipticity* to quantify the degree of violation. Even so, the most common presentations of MT data are those parameters appropriate for a perfect 2-D case. Namely, apparent resistivity and impedance phase are presented as functions of period for the two principal directions. These values are designated E-polarization, TE, or E-parallel and H-polarization, TM, or H-parallel, even though such designations are strictly true only for a perfect 2-D geometry.

The rotation of the tensor impedance elements to achieve principal directions even in a 2-D situation does not actually distinguish the E-polarization direction from the H-polarization direction since there is a 90° ambiguity in the rotation. This ambiguity is eliminated by using the fact that only the E-polarization gives rise to a vertical magnetic field. Swift (1967) defined a complex parameter called the *tipper* function which describes a linear relation between the vertical and horizontal magnetic fields. Consequently, in the multi-dimensional case,

$$H_z = T_x H_x + T_y H_y \,. \tag{26}$$

The term, *tipper*, is ascribed to T. Madden (Vozoff, 1972) who visualized the horizontal magnetic field over a 1-D earth as being tipped into the vertical by the effects of lateral inhomogeneities. The coordinate directions of the tipper can be rotated just as the impedance tensor can be. For a 2-D earth, the tipper can thus be expressed as a function of only one principal direction, the dip direction. The easiest way to understand the concept of the tipper function is to use the "right-hand rule" as learned in introductory physics. Assuming that the right thumb points in the direction of geoelectric strike, the right-hand fingers curl in a circular manner about the thumb. The direction of the thumb is that of current (or E_y) in the strike direction. The pattern of the fingers represents both the H_x and H_z magnetic field directions set up by the current flow. Therefore, where the y-direction is the strike direction of a 2-D Earth, the current flow along strike produces the H_x and H_z magnetic fields; the tipper relation quantifies the relation between the magnetic field components. This discussion presents the essential physical nature of the E-polarization, which has only the field components E_y, H_x, and H_z. Another way of presenting the relation between the vertical and horizontal magnetic fields is to treat the tipper as a complex vector (Tx, Ty). This permits the definitions of in-phase and out-of-phase *induction vectors* or *induction arrows* (Schmucker, 1970) as functions of frequency and location.

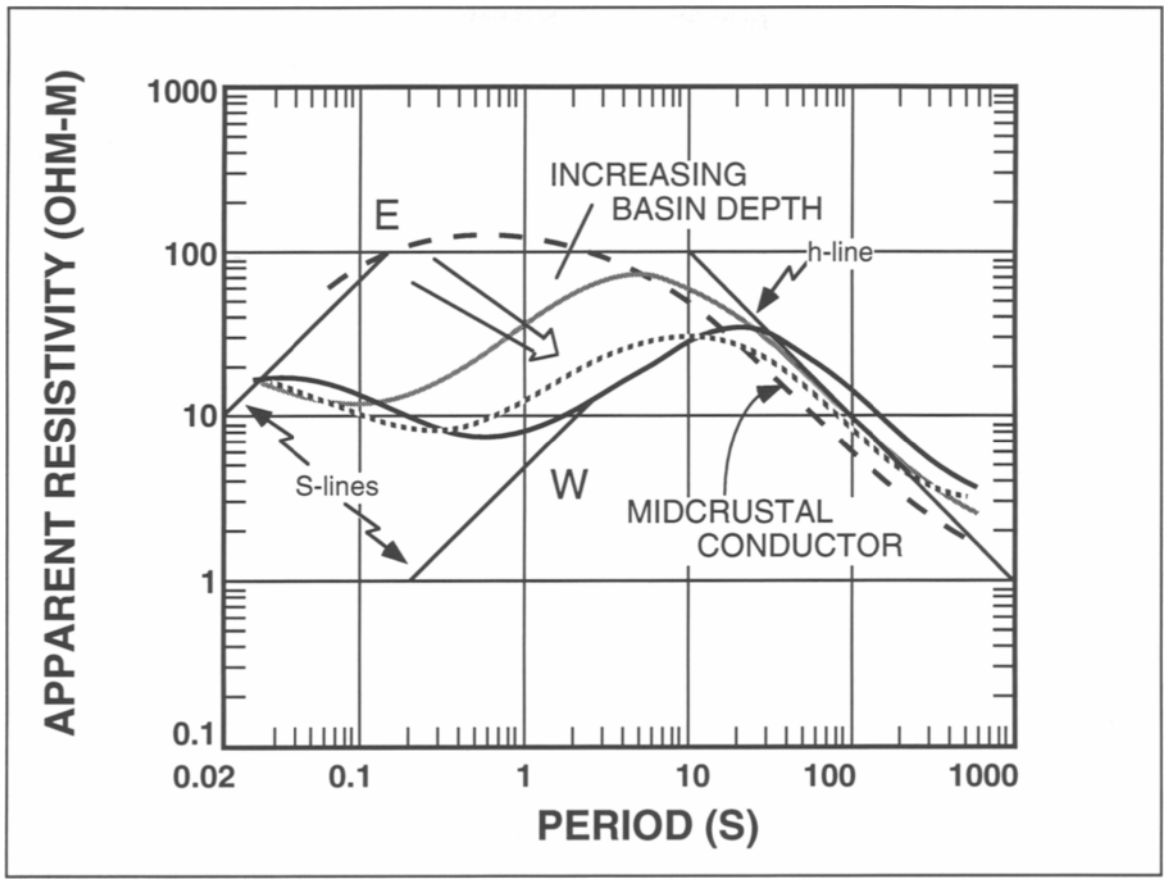

Fig. 3E–6. Sequence of E-polarization apparent resistivity versus period MT sounding curves from the Rio Grande rift. Ascending branches (near S-lines) from 0.1 to 10 s period indicate increasing basin depth from east to west; h-lines at periods >10 s mark the response of a midcrustal conductor. The h-line drawn yields a depth of 11 km to this conductor; the S-lines drawn yield a range of basin conductance from 15 to 200 S.

3E.4. Introduction to magnetotelluric interpretation

3E.4.1. One-dimensional interpretation

The principles of 1-D MT interpretation are detailed in the previous discussion in *Layered earth* (§ 3E.3.3) under the Basic magnetotelluric principles section. These principles are illustrated in Figure 3E–6, which contains four smoothed MT sounding curves across a portion of the Rio Grande rift near Santa Fe, New Mexico (Jiracek et al., 1987; Biehler et al., 1991). The very fact that the curves vary across the rift basin violates the 1-D assumption. But, as shown in the next section, some multi-dimensional MT curves (especially E-polarization curves from a 2-D conductive surface environment) may yield a reasonable 1-D estimate of the vertical section beneath a recording site. The curves presented in Figure 3E–6 are such examples. There are four obvious layers expressed in these soundings. Data at periods shorter than 1 s reflect an increasingly conductive (lower resistivity) water-saturated, basin-fill with a fresh water layer overlying a saline water zone. Be-

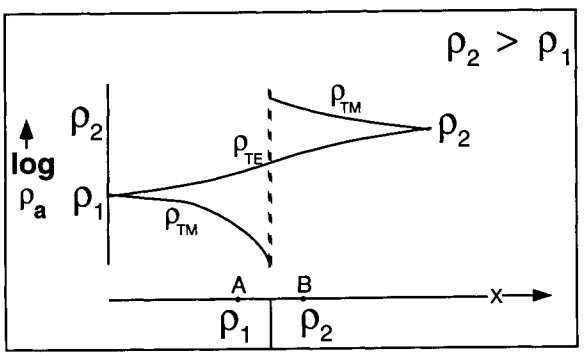

Fig. 3E–7. Variation of TE and TM apparent resistivities versus distance at a single period across a vertical contact. ρ_{TE} varies smoothly within the range of ρ_1 and ρ_2; ρ_{TM} is discontinuous with values far outside the range of ρ_1 and ρ_2.

low these two layers is a resistive (>100 ohm-m) basement of relatively dry granitic composition, like that of the mountains bounding the rift (Biehler et al., 1991). Finally, there is a very prominent midcrustal conductive zone whose bottom is not resolved by the 800 s period data. Applying the four asymptotic relations from the *Layered earth* section we find: (1) The top layer resistivity is about 20 ohm-m; (2) The deepest layer resistivity is 2–3 ohm-m; (3) The depth (using Eq. (19)) to the top of the midcrustal conductor is about 11 km using the h-line in Fig. 3E–6; and (4) The total conductance (using Eq. (20) and the S-lines drawn in Fig. 3E–6) above the resistive basement varies progressively east to west across the basin from about 15 to 200 S. Since the MT results are virtually identical at the shortest periods, i.e., the resistivity variations above the basement are laterally continuous, the change in conductance reflects increasing basin depth. The variations in the positions of the h lines revealing the midcrustal conductor are thought to arise from 3-D (along strike) variations rather than any significant changes in the depth to conductor. All of the above geoelectric features are highly consistent with seismic and gravity interpretations (Biehler et al., 1991) except for the midcrustal conductor. This strong electrical feature, which is thought to be caused by important geochemical phenomena in the crust (section § 3E.5), is not sensed by any other geophysical method.

3E.4.2. Two-dimensional interpretation

The most important characteristics of 2-D MT apparent resistivity sounding curves are realized by understanding the variations in E- and H- polarization results on either side of a simple geoelectric contact. Figure 3E–7 depicts such a contact with ρ_1 representing the more conductive quarter-space to the left of resistive quarter-space ρ_2. The physics of the response of this 2-D model at the two measurement sites A and B is profoundly different for the two polarizations.

E-polarization

All three EM field components in E-polarization (E_y, H_x, and H_z) are continuous across all boundaries so the fields vary smoothly across geologic contacts. Therefore, the apparent resistivity, which is proportional to E_y/H_x (Eqs. 11 and 13) is smoothly varying across a contact. Figure 3E–7 illustrates this behavior as measured at a constant arbitrary period. The ρ_{TE} curve would be sharper at arbitrarily shorter periods compared to a smoother curve at longer periods. This behavior is characteristic of the *inductive effect*, which controls the frequency response of the E-polarization. This effect depends on the time derivative of the magnetic flux (Faraday's law of induction) so it diminishes at lower frequencies. Note that the ρ_{TE} response in Figure 3E–7 does not lie outside the range defined by ρ_1 and ρ_2.

H-polarization

In H-polarization, H_y and E_z are continuous across a contact but E_x is discontinuous. The discontinuity in E_x follows from the continuity of the normal component of the current density, **J**. The definition of **J** results in continuity of the quotient E_x/ρ in the model in Figure 3E–7. The electric field discontinuity at a contact is due to electric charge accumulation on the contact which is the underlying cause of the *galvanic effect* (Berdichevsky and Dmitriev, 1976). The galvanic effect produces the discontinuous behavior of

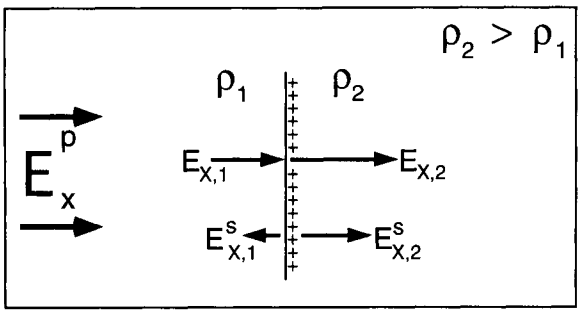

Fig. 3E–8. Primary electric field, E^P, normally incident on 2-D contact schematically showing surface charge accumulation, secondary electric fields, $E^S_{x,1}$ and $E^S_{x,2}$, and total electric fields, $E_{x,2}$ and $E_{x,1}$. The secondary electric fields from the + charges subtract from the primary field on the conductive side (ρ_1) and add to the primary electric field on the resistive side (ρ_2), resulting in $E_{x,2} > E_{x,1}$.

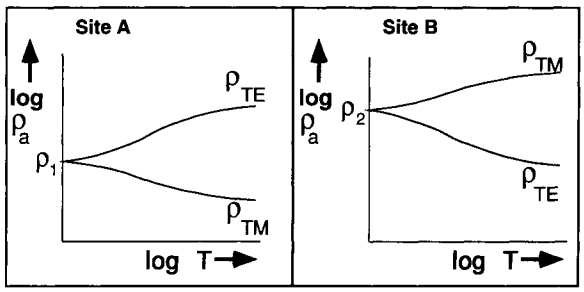

Fig. 3E–9. Schematic MT apparent resistivity sounding curves at sites A and B in Fig. 3E–7. Curve for ρ_{TE} is above that for ρ_{TM} on the conductive side of the contact and ρ_{TM} is above ρ_{TE} on the resistive side.

the ρ_{TM} results shown in Figure 3E–7 with values falling far outside the range of ρ_1 and ρ_2. The discontinuity in ρ_{TM} ($\propto |E_x/H_y|^2$) is identical to the square of the $E_{x,2}/E_{x,1}$ discontinuity discussed above because there is no change in H_y along the surface in the 2-D case. This emphasizes the dominant role played by electric field discontinuities in H-polarization apparent resistivity responses. It can be shown (e.g., Kaufman, 1985) that electric charges form anywhere there exists a component of electric field in the direction of a change in resistivity. The charges are the source of *secondary electric fields* that modify the initial (or *primary*) *electric fields*. The resulting *total* (primary plus secondary) *electric fields* are those that appear in the continuity relations for the normal component of **J**. Figure 3E–8 graphically shows these relations for a primary electric field perpendicular to a 2-D resistivity contrast. The secondary field directions and magnitudes on each side of the contact are schematically those required for a total field increase on the resistive side and the opposite on the conductive side of the boundary. The determination of the surface charge polarity is made by recalling that the secondary electric field directions must be consistent with the direction that a hypothetical positive test charge would move. Those directions are directed away from a positively charged boundary as depicted in Figure 3E–8.

In Figure 3E–7, note that at locations sufficiently removed from the contact, neither ρ_{TE} or ρ_{TM} responses sense the contact. This horizontal distance is approximately one skin depth (Vozoff, 1991). The curves sketched in Figure 3E–7 graphically present the major characteristic differences between E- and H-polarization MT apparent resistivity results. Namely, that E-polarization (TE) values plot above H-polarization (TM) results on the conductive side of a contact and, vice versa on the resistive side of a 2-D contact. This realization, along with a basic geologic knowledge of the survey area, can be of enormous value when first trying to understand MT observations.

The characteristics emphasized above at a single period, of course, transfer to the sounding curves at various measurement sites. Such apparent resistivity sounding curves for two sites, one on either side of the contact in Figure 3E–7, are presented in Figure 3E–9. Two major characteristics of these soundings are: (1) both curves converge to the true resistivities at each site location at the shortest periods, and otherwise; (2) ρ_{TE} is above ρ_{TM} on the conductive side of the contact (site A), and vice versa on the resistive side of the contact (site B).

A convenient way to display many MT sounding curves along a profile is in so-called *pseudosection* form. A pseudosection is a plot of contours of equal

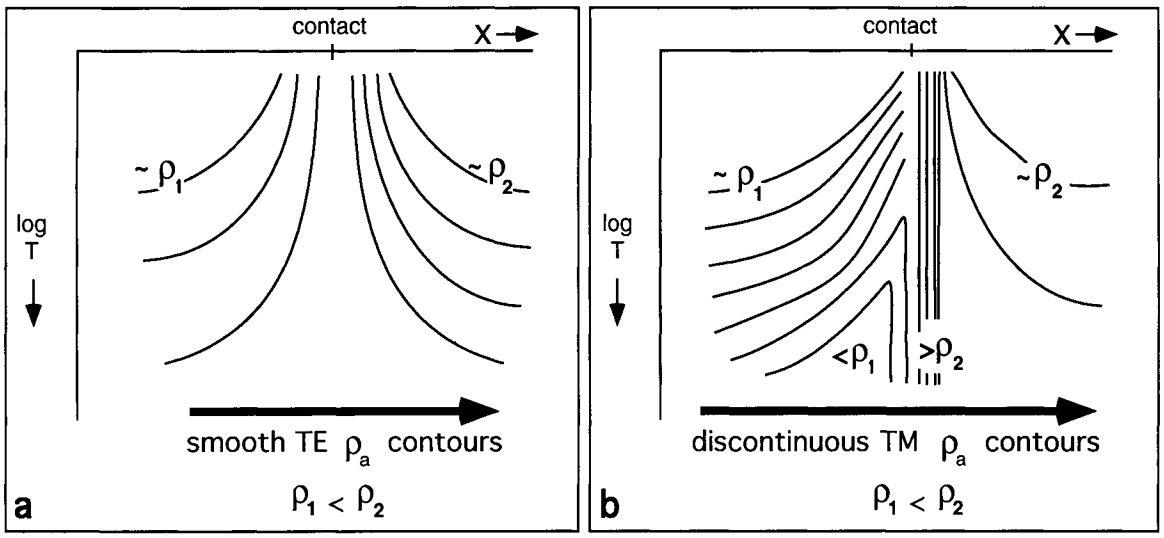

Fig. 3E–10. Representative pseudosections of (a) TE, and (b) TM, apparent resistivity (ρ_a) across a vertical contact in Figure 3E–7. Horizontal location of contact is marked by ρ_a vertical contours especially in TM case where values are discontinuous.

apparent resistivity, or impedance phase, where the horizontal axis is linear horizontal distance (e.g., in km) and the vertical axis is the log of the period (Fig. 3E–10). Since the shorter period data plot at the top of the graph and the longer period data at the bottom, apparent resistivity pseudosections give a rough idea of the true-resistivity geoelectric section. However, the term 'pseudo' is highly appropriate for such plots since they can be very misleading. For example, the discontinuous behavior of the ρ_{TM} data across a simple contact (Figure 3E–7) plots as a false intrusive-like conductive zone on the low resistivity side of a contact (Fig. 3E–10b). Such false behavior does have a beneficial aspect since sharp vertical contours are good indicators of the positions of lateral boundaries, especially in ρ_{TM} pseudosections (Fig. 3E–10).

To illustrate the above 2-D MT considerations, a hypothetical geologic-geoelectric continental rift model depicted in Figure 3E–11 is used. Figure 3E–12 contains the MT apparent resistivity sounding curves for sites 1 and 2 at locations in the conductive basin and on a neighboring resistive flank (Fig. 3E–11), respectively. Plotting both soundings on the same graph allows a clear comparison of the two major characteristics emphasized above. Namely, 1) the curves converge to the true resistivities (10 and

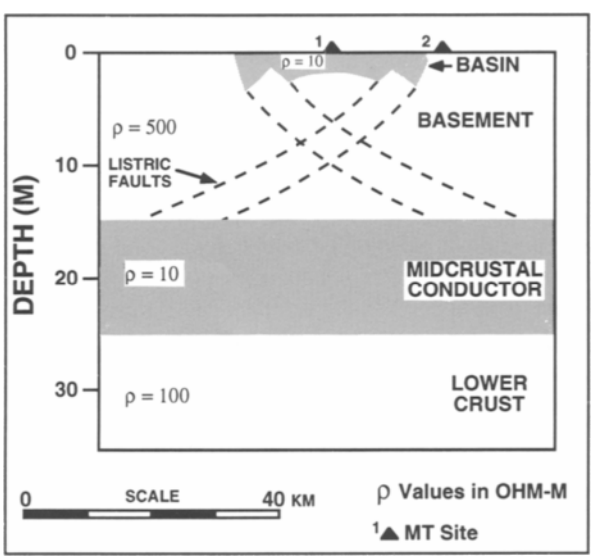

Fig. 3E–11. Hypothetical 2-D geologic-geoelectric continental rift model with conductive 10 ohm-m basin bounded by listric faults, 500 ohm-m basement, 10 ohm-m midcrustal conductor from 15 to 25 km depth, and 100 ohm-m lower crust.

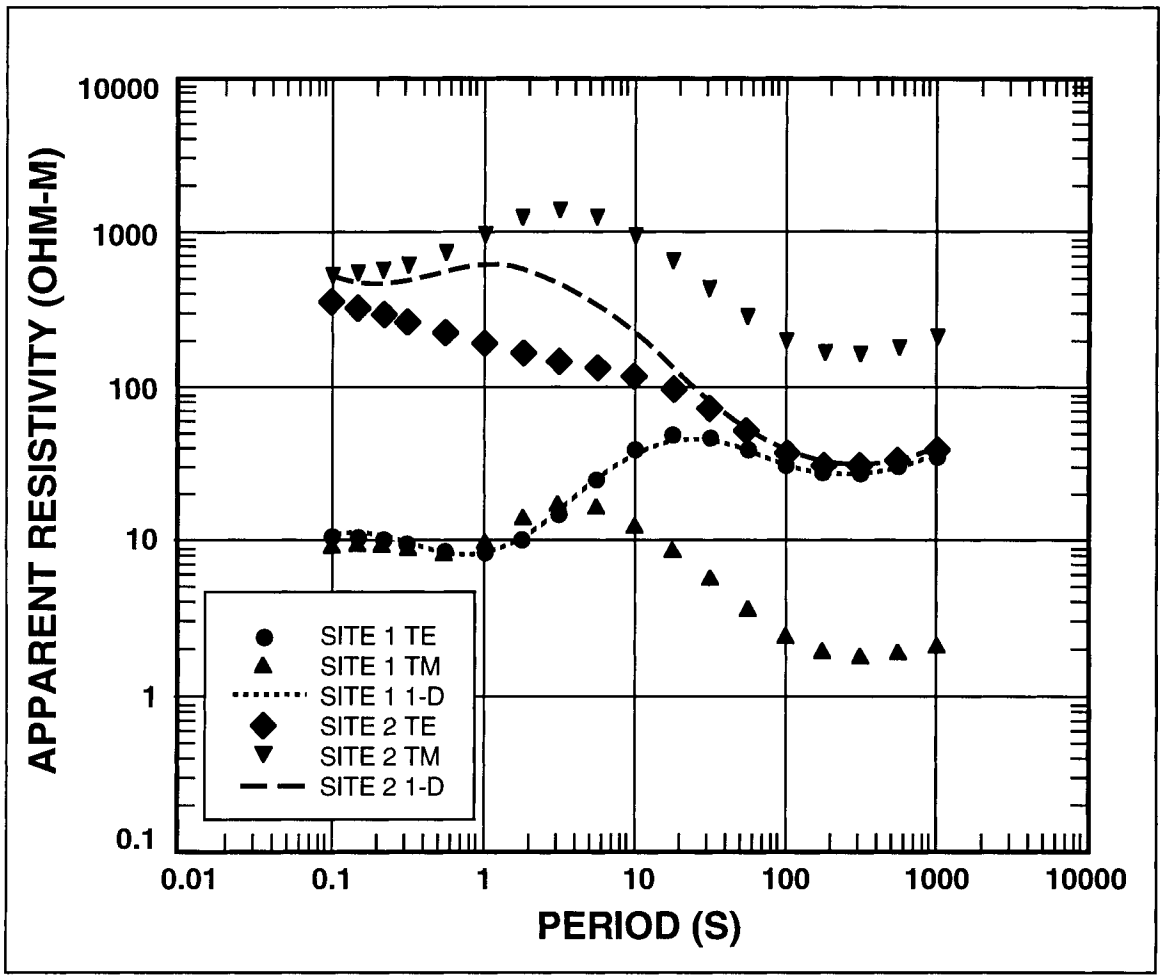

Fig. 3E–12. Synthetic apparent resistivity MT sounding curves at sites 1 and 2 within and outside the conductive rift basin shown in Fig. 3E–11. ρ_{TE} curve virtually equals 1-D curve appropriate for vertical section below conductive site 1. ρ_{TE} curve agrees with 1-D curve appropriate for vertical section below resistive site 2 only at long periods.

500 ohm-m, respectively) at the shortest periods and 2) ρ_{TE} is above ρ_{TM} at site 1 and vice versa at site 2. Imprinted on these observations are the effects of skin depth, and a 10 ohm-m midcrustal conductive zone from 15 to 25 km depth. The latter is expressed as descending branches on all curves especially from 10 to 100 s period. It is very instructive to compare the 2-D curves with the 1-D results calculated at each site as if a layered Earth with the same vertical section is assumed. These results (Fig. 3E–12) show how closely the TE curve on the conductive side (site 1 in the basin) matches the 1-D curve. This is not true for results at resistive site 2 adjacent to the basin except at the longer periods. Note that all curves in Figure 3E–12 begin to rise at the longest periods shown; this is the response to a more resistive (100 ohm-m) lower crust (Fig. 3E–11).

Although 2-D Earth models can be constructed with very complicated responses that require careful attention to vertical and horizontal skin depth considerations, the simple features discussed above are surprisingly useful in initial interpretations.

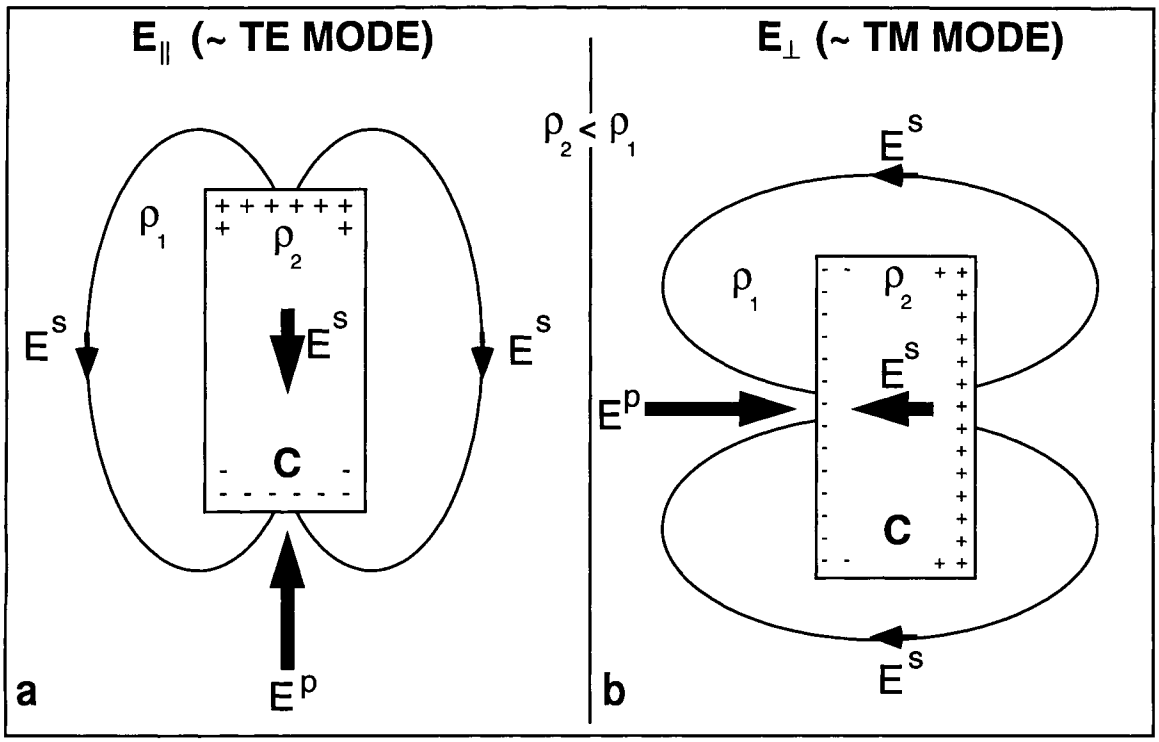

Fig. 3E–13. Plan view of primary electric field, E^P, normally incident on ends of 3-D conductive (C) body schematically showing dipolar surface charge accumulation and secondary electric fields, E^s. The secondary electric fields subtract from E^P over the conductive body and along its sides but add to E^P off the ends of the body in both the ~TE (a) and ~TM (b) cases. The macroscopic effect is current channeling into the conductive body (Jiracek, 1990).

3E.4.3. Three-dimensional interpretation

The MT response of 3-D Earth structures is dominated by galvanic effects because electric field components in the directions of resistivity changes occur in all directions. Now, whereas the impedance description of 1-D and 2-D Earths required 2 and 5 parameters, respectively, the 3-D Earth requires 8. These are the real and imaginary parts of each of the full 4 tensor impedance elements (Eq. 23). To illustrate the major 3-D effects, it is sufficient to present two simple examples. Both examples use 3-D rectangular blocks, one conductive and one resistive.

Electric field distortion

Figure 3E–13 presents a map view of a 3-D rectangular body that is conductive relative to a surrounding layered host. A primary electric field is sketched both parallel and perpendicular to the long axis of the body. These cases are designated $E_{||}$ and $E_{\perp}$, respectively, in Figures 3E–13a and 3E–13b. There are no strict designations of E-polarization and H-polarization for the 3-D case, hence, terms ~TE mode and ~TM mode are used in Figure 3E–13. Included schematically in the two examples in Figure 3E–13 are the galvanic charge distributions and resulting secondary electric field variations, E^s. The polarity of the charges is such to cause a secondary field opposing the primary field in the conductive

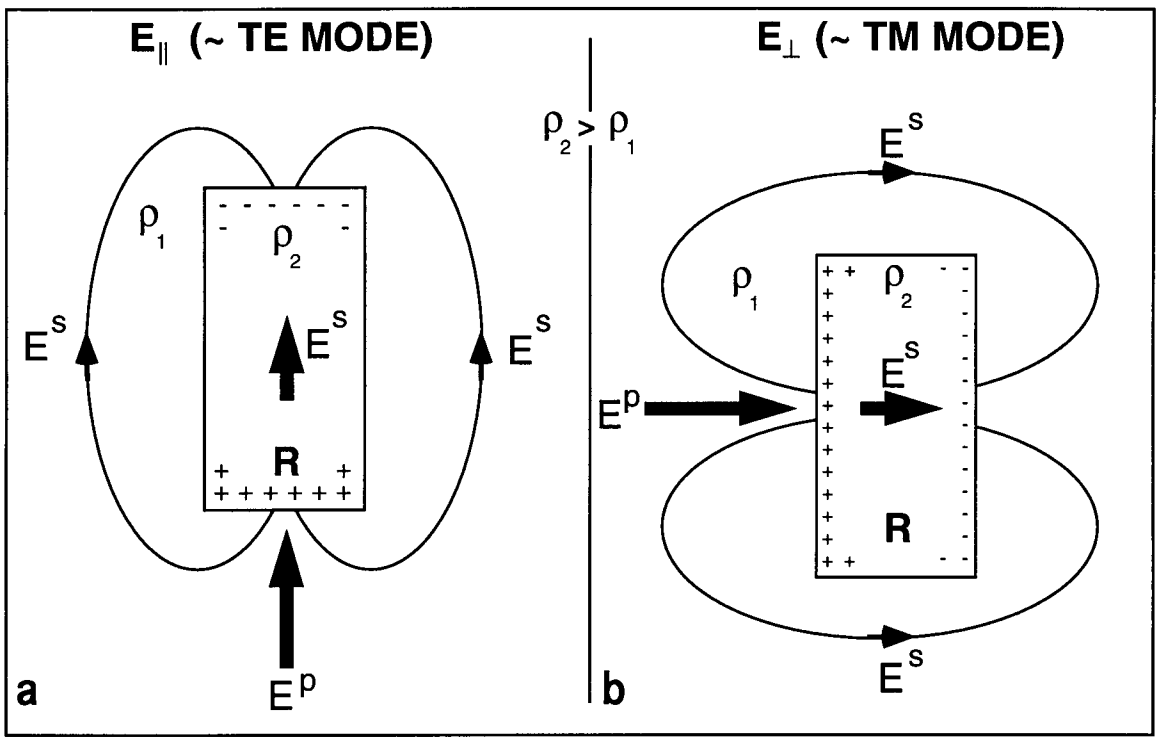

Fig. 3E–14. Plan view of primary electric field, E^P, normally incident on ends of 3-D resistive (R) body schematically showing dipolar surface charge accumulation and secondary electric fields, E^s. The secondary electric fields add to E^P over the resistive body and along its sides but subtract from E^P off the ends of the body in both the ~TE (a) and ~TM (b) cases. The macroscopic effect is current deflection around the resistive body (Jiracek, 1990).

body. Only then can the total electric field decrease in a conductive body as required to preserve the continuity of normal current density. Even though the total **E** is decreased in a conductor it is important to realize that the current is enhanced. This expected increase of current in good conductors is called *current channeling.*

For clarity, some details are omitted in Figure 3E–13 since the sketches are meant to show only the major features. The important result is that there are galvanic charges and H-polarization-like effects for both polarizations of the electric field. By simply estimating the sense of the vectorial addition of the primary and secondary electric fields depicted in Figure 3E–13, one can make a good guess of what the resulting total **E** field patterns will be. For example, the total field is reduced directly over the body and along its sides, whereas the fields are enhanced off the ends of the conductor. The overall, total effect is that of current channeling into conductive inhomogeneties (Jiracek, 1990).

Figures 3E–14a and 3E–14b present the situations opposite to those in Figure 3E–13, namely those of a relatively resistive 3-D inclusion. Now the secondary field must be additive to the primary field in the resistive body. This single consideration enables the sketches in Figure 3E–14 to be made. From these it is clear that the total electric field is enhanced directly over the body and along its sides, but, it is diminished off the ends. Now the current channeling is around the outside of the resistive body, an effect called *current deflection.*

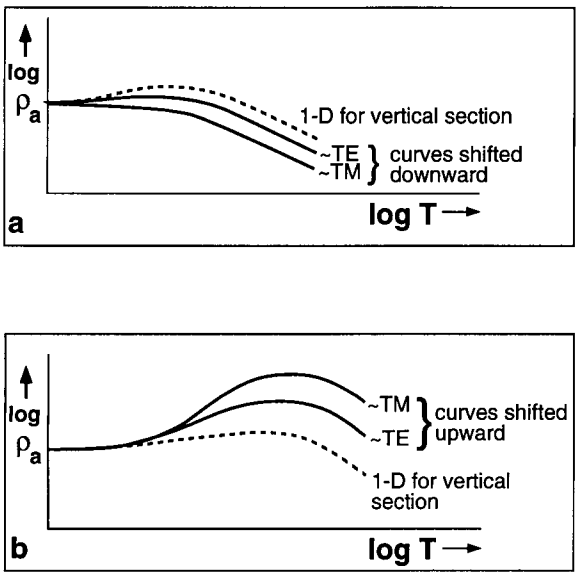

Fig. 3E–15. Schematic apparent resistivity MT sounding curves over 3-D conductive (a) and resistive bodies (b) in Fig. 3E–14 compared to curves appropriate to 1-D section in which bodies are embedded. Both ~TE and ~TM sounding curves are static shifted downward over the conductive body and they are static shifted upward over the resistive body.

Distortion of apparent resistivity curves

An understanding of the galvanic electric field distortions alone often enables one to estimate the surface effects on 3-D MT sounding curves even though the apparent resistivity calculation (Eq. 13) includes both the electric and the magnetic fields. This is so because the 3-D galvanic magnetic field distortion is determined by a volume integral of the current distortion, which is small for near-surface bodies of small volume. In these cases, the apparent resistivity results are dominated by electric field variations. They are shifted upward where the total electric fields are enhanced and are shifted downward where total electric fields are depressed. These observations explain why the ~TE and ~TM apparent resistivity curves directly over isolated conductive and resistive bodies are shifted as shown in Figures 3E–15a and 3E–15b, respectively. The results are sketched in comparison to an apparent resistivity sounding curve appropriate to a 1-D Earth with the same vertical properties as the 3-D case. This shows that the 3-D sounding curves are shifted downward at sites located over surface conductors and upward over resistors. However, at sites off to the side of a conductive body, for example, the ~TE curves would be shifted up and the ~TM curves would be lowered. These conclusions follow from scrutiny of the sketches in Figures 3E–13a and 3E–13b.

Where the shifting up or down of the apparent resistivity sounding curves is frequency (period) independent, the constant shift is referred to as a *static shift*. The shift is constant or static when the primary electric field is uniform over the extent of the body, the galvanic magnetic effects are inconsequential, and the inductive (TE-like) effects are negligible. These requirements are always met for small 3-D bodies below some frequency value, therefore, above some arbitrarily long period. As frequency decreases, the increased skin depth in the host rock eventually results in a quasi-uniform charging field over the depth extent of the body. At high frequencies the field is stronger at the top of a body, therefore, the body is charged more at the top. Such a variation with frequency does not produce a static shift. Inductive effects, since they depend on a time derivative, always decrease with decreasing frequency.

The question of whether or not magnetic field galvanic distortion can be neglected depends on the overall volume of the current channeling and/or current deflection as mentioned earlier. An informed discussion of this topic has been recently presented by Chave and Smith (1994) where they confirm that such distortion is frequency dependent. Therefore, galvanic magnetic effects or significant inductive response from 3-D bodies oppose static shift. Still, it is clear to all MT practitioners that there is a surprising recurrence of static shifts in MT sounding data. In fact, static shifts are probably the leading contemporary problem in magnetotelluric processing and modeling. Therefore, it is not unexpected that many schemes have been devised to address the problem of static shift (a review of techniques appears in Jiracek, 1990). However, no method is com-

pletely successful without auxiliary data. In actual situations different static shifts from different scales of inhomogeneities in the vicinity of a measurement site all superimpose.

Several well-formulated proposals have appeared in recent years to partially address the 3-D galvanic distortion problem (e.g., Groom and Bahr, 1992; Chave and Smith, 1994). The details of these are beyond the scope of this discussion. However, since this is one of the most active research areas in MT, the main theme of these techniques is briefly presented here. Namely, the measured (distorted) impedance tensor is mathematically expressed in terms of a background (regional) impedance multiplied by tensor distortion terms. The desired regional impedance is assumed to be either 1-D or 2-D; the distortion tensors allow for 3-D electric and magnetic distortions. The latter are complex and frequency dependent; the former are real, frequency independent (static) distortions. Both distortions are location dependent. In practice, a low frequency assumption is usually invoked wherein the wavelengths inside and outside the inhomogeneities are large compared the size of the 3-D scatterer. This, and the neglect of the magnetic distortion, produces real, frequency independent electric field distortion tensor elements (Larsen, 1977; Wannamaker et al., 1984; Zhang et al., 1987; Bahr, 1988; Groom and Bailey, 1989). Galvanic (current channeling) magnetic effects have been included in 3-D MT distortion formalisms by Groom and Bailey (1991), Zhang et al. (1993), and Chave and Smith (1994). All of the tensor distortion schemes perform tensor decomposition to attempt to retrieve a pure, undistorted regional impedance tensor. Unfortunately, an indeterminacy remains for each method that requires the independent knowledge of the regional impedance tensor for at least one frequency.

3E.5. Mid-to-lower crustal conductive zones

3E.5.1. Introduction

It has been argued recently (Hyndman et al., 1993) that the deep crust is conductive everywhere. However, there is a trend for tectonically active areas to have shallower (midcrustal) conductive zones that are better developed than in stable areas. That continental rifts have such features was recognized early on, e.g., by Schmucker (1964) in the Rio Grande rift. Jiracek et al. (1979) emphasized this observation for four rifts (Rio Grande, Baikal, East Africa, and the Rhinegraben) by concluding that they are characterized by zones of < 50 ohm-m at depths of 10–30 km. Jones (1992) summarized an additional 10 years of data and correctly states that no single conductivity model fits all rifts. In fact, there are still arguments about whether or not there is a crustal conductor directly beneath the Rhinegraben or just under its eastern shoulder (Schmucker and Tezkan, 1988; Jones, 1992; Mareschal et al., 1994). For other young continental rifts the question is not if, but why, there are conductive zones. Naturally, the next question is what are the consequences?

The question of why the mid-to-lower continental crust is conductive is truly a "hot topic" as evidenced by a barrage of recent papers on the subject. Jones (1992) has a very complete summary as do Hyndman et al. (1993). There has also been a major effort to relate the conductive occurrences with crustal seismic reflectors and refractors (Gough, 1986; Jones, 1987; Hyndman, 1988; Hyndman and Klemperer, 1989; Hyndman and Shearer, 1989; Merzer and Klemperer, 1992). The intent of this contribution to be a practical assessment of MT in a continental rift environment demands a brief review of some of these recent results. This will be done in an overview manner; the reader is strongly urged to consult the above references for more details.

3E.5.2. Sources of crustal conductors

There are really only three possible sources for crustal conductive zones. These are water, magma, and conductive minerals such as graphite. Because graphite is much more conductive ($\rho = 10^{-5}$ ohm-m; Duba and Shankland, 1982) than highly saline water (10^{-2} ohm-m minimum; Nesbitt, 1994) which is in turn more conductive than magma (about 0.5 ohm-m; Hermance, 1979), it requires much less graphite to produce a conductive zone. Temperatures in the lower crust are above the critical temperature (374°C for pure H_2O) so the term *aqueous fluid* is preferred instead of water since liquid and gaseous H_2O are

indistinguishable. After early interpretations that conductive zones, especially in rift environments, were caused solely by magma (e.g., Pedersen and Hermance, 1978; Banks and Beamish, 1979) the favored explanations have become aqueous fluids or conductive minerals, mainly graphite (Hermance and Pedersen, 1980; Jiracek et al., 1983; Jodicke, 1993; Hyndman et al., 1993; Katsube and Mareschal, 1993). As stressed by Jones (1992), there is no single cause for the enhanced crustal conductivities since different effects operate in different tectonic environments and at different depths.

For H_2O to accumulate in the crust, there must be both a source and a capping mechanism. Sources include deep circulating meteoric water, crustal devolatization by metamorphic reactions, and fluids released from mantle derived magmas crystallizing higher up in the lithosphere. Newton (1990) emphasized that emplacement of mantle-derived magmas in the lower crust contributes greatly to the thermal and volatile budgets in highly extensional regimes such as rifts. The magma volatile content is mainly H_2O and CO_2 (Wilson, 1989), the solubility of which decrease as the magma migrates upward. The fate of ascending volatiles depends on pressure, temperature, time, and whether crustal melting or retrograde metamorphism occurs (Thompson and Connolly, 1990). H_2O is very soluble in granitic melts and retrograde metamorphism moves water into hydrated minerals that are resistive (Olhoeft, 1981). A theoretical reason to expect trapping of aqueous fluids in cracks at the brittle-ductile transition in the crust has been presented by Bailey (1990). The argument is that vertical fluid transport is rapid in the ductile crust but that it slows abruptly at the brittle-ductile transition. The resulting overpressure would induce horizontal fractures in which water would accumulate. Bailey's (1990) hypothesis is especially appealing since the coincidence of the depth to the top of crustal conductive zones and the brittle-ductile transition has been reported by several studies (e.g., Jiracek et al., 1983; 1987; Hyndman et al., 1993). However, Bailey's (1990) mechanism would operate most effectively where the principal regional stress is horizontal (compressional) rather than vertical as it is in extensional rift environments.

The question of whether graphite, or other conductive minerals exist in the deep crust must also address the sources and accumulation processes (Hyndman et al., 1993). The source of graphite is usually thought to be from the reduction of CO_2-rich fluids. CO_2 itself is a nonconducting fluid. Even though the amount of graphite needed to produce a conductive zone is small, there must be a connected film (Katsube and Mareschal, 1993) on regional scales. Intergranular graphite films are suggested to explain low resistivities in a 10 km deep borehole in Germany (Jodicke, 1992; Haak et al., 1991) and in the deep Precambrian shield of Canada (Katsube and Mareschal, 1993). Duba et al. (1994) emphasize that a suite of conductive accessory minerals (ilmenite, magnetite, pyrite, pyrrhotite) including graphite were measured in the German drill cores. A graphite explanation is not usually invoked in conductive rift settings because a continuous supply of deep fluids is expected. Also, there appears to be a strong correlation with temperature which is not expected for graphite. Graphite is often used as an explanation where a conducting zone doesn't have a corresponding seismic signature. This would be the consequence for thin graphite films but it is also expected for very low water fractions (~1 %). Such levels of connected water saturation result in orders of magnitude change in electrical conductivity but corresponding changes in seismic velocities are very small (Watanabe, 1993).

3E.5.3. Intergranular aqueous fluid–dihedral angle control

New experimental data (Holness, 1993) suggest that enhanced electrical conductivity of deep metamorphic rocks is caused by water-saturated, low-porosity continental crust which has profound rheological implications. These data concern the interconnectivity of intergranular (not fracture-controlled) fluids as a function of pressure and temperature in the ductile crustal environment. Results from Holness (1993) are simplified schematically in Figure 3E–16a where the concept of dihedral angle is also sketched (Fig. 3E–16b). The dihedral angle or wetting angle (Brenan, 1991) is the angle subtended by intersecting grain walls at pore corners in a re-

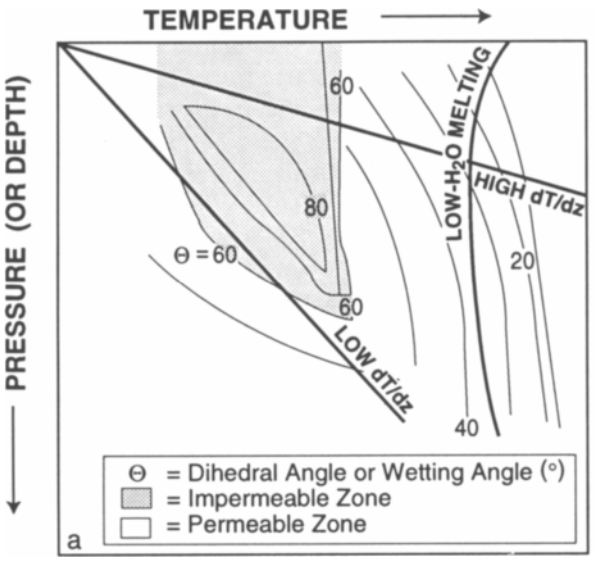

SCHEMATIC SINGLE GRAIN WATER DISTRIBUTION	DEEP CRUSTAL PROPERTIES		
	WATER	ELECTRICAL	RHEOLOGICAL
Θ ≥ 60°	ISOLATED	RESISTIVE	LOW STRAIN RATE
Θ ≤ 60°	CONNECTED	CONDUCTIVE	HIGH STRAIN RATE

b

Fig. 3E–16.(a) Schematic pressure, temperature, dihedral angle plot for crustal conditions. Pattern of dihedral angle contours follows those of quartzite–H_2O system presented by Holness (1993). Shaded region is where aqueous fluids reside in isolated pores and the rock is impermeable to fluid flow (θ>60°). At dihedral angles θ<60° the rock has an interconnected fluid phase and is permeable to grain-edge fluid flow. High and low dT/dz geothermal gradients illustrate situations where interconnected aqueous fluid would be trapped beneath an impermeable cap (shaded region). Notice that for various values of high dT/dz, the depth to the trapped fluid would vary but the temperature would be nearly constant following an isotherm. (b) Schematic single grain aqueous fluid distribution as a function of value of dihedral angle (60°<θ<60°); table of implications in deep crustal metamorphic rocks.

crystallized rock at equilibrium conditions. The values of dihedral angle define the 3-D continuity, therefore, interconnectivity of the grain-edge porosity. Interconnectivity can only exist if the angle is less than a critical value which is about 60° for 1% porosity (Hyndman, 1988). Total grain-edge wetting is achieved at 0° dihedral angle. Dihedral angle implications on crustal conductivity have been discussed (e.g., Hyndman, 1988; Marquis and Hyndman, 1992). However, the data were not adequate to define a pressure (depth)-temperature-dihedral angle plot as was done by Holness (1993). The published plot is for a pure quartzite-H_2O equilibrium system where the wet melting temperature is about 1100°C. Presumably this temperature would be near 640°C for a wet crust of granitic composition. Therefore, actual pressure and temperature values have been omitted in Figure 3E–16a since the major features of a plot embracing the ductile portion of the crust are what we want to emphasize. Two hypothesized geothermal gradients are sketched in Figure 3E–16a. These illustrate that two regions of fluid connectivity may exist in the ductile crust under an impermeable cap (θ >60°). For high geothermal gradients, fluid interconnectivity would occur at a near-constant temperature irrespective of the actual value of the geothermal gradient. The temperature is defined by the near-vertical contour of θ = 60°, which is almost parallel to the rock melting curve (Fig. 3E–16a). For lower geothermal gradients, the region of interconnectivity is at lower temperature nearer the brittle-ductile transition. The temperature at the top of the zone would vary considerably depending on the intersection of the geothermal gradient with the non vertical θ = 60° contour. Note that if the geothermal gradient is very low, the

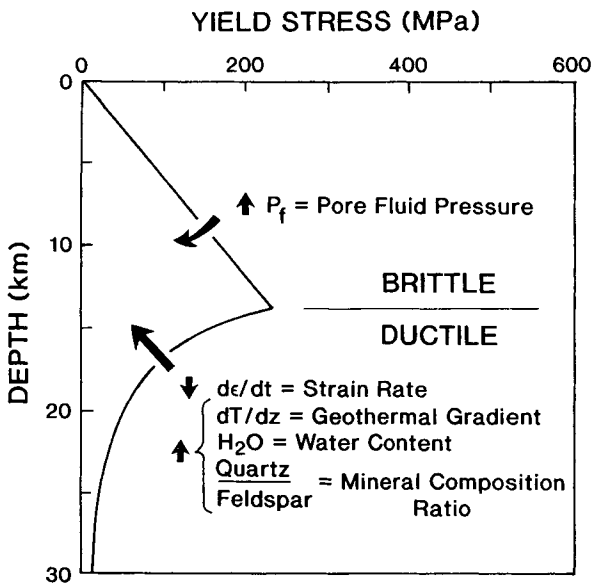

Fig. 3E–17. Synoptic diagram of crustal rheological behavior showing the effects of increasing pore fluid pressure in the brittle regime; and decreasing strain rate and increasing geothermal gradient, water content, and quartz/feldspar ratio in the ductile portion of the crust (redrawn from Sibson, 1984).

dihedral angle would be <60° throughout the entire region (depth range) plotted and there would be no impermeable cap. This would be the case of continuous dewatering of the crust even with a continuous source of deep aqueous fluid.

The dihedral angle considerations above present two situations where deep crustal conductive zones would have sharp upper boundaries. One, where the geothermal gradients are high, dictates that the depth to the conductive zone would be an isotherm. In the other case, at lower geothermal gradients, a deeper conductive zone would be at lower temperatures. More experimental results, such as those presented by Holness (1993) on actual rock/fluid assemblages expected throughout the crust, are needed to confirm or reject these expectations. Such a confirmation has just appeared (Holness, 1995) which presents results at 4 kbar pressure for the quartz-H_2O–CO_2 system with trace amounts of feldspar. Watson and Brenan (1987) reported on dihedral angle measurements performed principally on dunite and quartzite with CO_2–H_2O and solutes of NaCl and other salts. Their results are appropriate to conditions in the deep crust and upper mantle (950–1105°C temperature and 1 GPa pressure) with a low percentage of aqueous brine solution. The major findings were that the effect of saline solutions was to decrease the dihedral angle to as low as 40° for the quartz-fluid system but there was no change in the high dihedral angle ($\theta >> 60°$) in dunite with, or without, salts. This implies that aqueous solutions are more likely to be interconnected in the ductile crust if the aqueous solution is saline but not so in the mafic mantle. The latter result agrees with a similar study reported on clinopyroxene-rich rocks (Watson and Lupulescu, 1993).

3E.5.4. Consequences of intergranular aqueous fluid

Watson and Brenan (1987) suggest that it is tempting to conclude that the dihedral angle-controlled fluid distributions apply to any conditions in the Earth where recrystallization has occurred, i.e, any pressure-temperature condition above the lowest metamorphic grade. In the case of a rift environment we must first ask whether or not the crust is in the required mechanical and chemical equilibrium. In fact, brittle fracturing occurs in active areas, such as rifts, even in the ductile regions of the crust as a result of tectonic stresses and igneous intrusions. These transient events deviate from static equilibrium but for rocks hot enough to undergo rapid plastic deformation, it is likely that equilibrium pore geometries develop rapidly (Brenan, 1991). For equilibrium wetting to occur, its rate must exceed the rate of ductile rock deformation; this is always the expected situation (Watson and Brenan, 1987).

It is clear from many experimental results (e.g., Kronenberg and Tullis, 1984; Cooper and Kohlstedt, 1986) that a connected fluid phase decreases the strength (the viscosity) of the rock and enhances the strain rate. The strength of the crust has the general profile depicted in Figure 3E–17 but there are several interdependent factors (Sibson, 1984) that can perturb it. In the ductile portion of the crust an increase in the geothermal gradient, water content, or quartz content will decrease the strength and the brittle-ductile transition will migrate upward. More

locally, a zone of interconnected water within the ductile region will facilitate increased pressure solution creep which enhances the strain rate. Experimentally, this effect is large where grain wetting occurs in olivine-basalt partial melts (Cooper and Kohlstedt, 1986). The process involves the diffusion of dissolved minerals along grain boundaries from regions of higher stress (at asperities) where the solubility is high to regions of low stress where the solubility is low (Turcotte and Schubert, 1982). This diffusion requires fluid interconnectivity.

Since an interconnected aqueous film has orders of magnitude higher conductivity compared to that of isolated pockets of H_2O, the connection with rheology as outlined above strongly suggests that the mapping of deep conductive zones is an indirect measurement of strain levels in the crust (Fig. 3E–15b). Thus, we made the assertion in our *Introduction* (§ 3E.1) that measurements of deep electrical resistivity may hold the key to understanding how continental rifts deform. The association of electrical resistivity with dihedral angle wetting is dependent on both pressure and temperature (Fig. 3E–16a) as well as rock type and fluid composition so the consequences are very far reaching. Therefore, we eagerly await more data relating the consequences of interconnected aqueous fluids in the crust with tectonic processes and geophysical properties, including electrical resistivity.

Acknowledgments. The most insightful discussions on the magnetotelluric method appear in notes that have never been published. Some of the best of these were done by U. Schmucker and P. Weidelt, F. Bostick, and the late G. Hohmann. The "theory section" of this contribution has benefited greatly from informally distributed Xerox copies of these works; in particular, one of us (GRJ) has subscribed to the approach learned at the University of California-Berkeley under the tutelage of S.H. Ward and H.F. Morrison and from fellow students including Jerry Hohmann. Much of this contribution comes from a condensation of notes used at San Diego State University and at the SAGE program (Summer of Applied Geophysical Experience). We thank more than 400 students who have critically reviewed the notes and have led to continual changes and corrections. The writing of much of this was accomplished at the Los Alamos National Laboratory (LANL), Institute of Geophysics and Planetary Physics where GRJ was on sabbatical leave in 1994. The hospitality of the staff and director of the Institute, C.F. Keller, are warmly appreciated. Discussions with LANL petrologists W.S. Baldridge and D. Hickmott on the implications of dihedral angle wetting were very helpful. A careful critical review by P.E. Wannamaker is very much appreciated.

3E.6. References

Bahr, K., 1988. Interpretation of the magnetotelluric impedance tensor: regional induction and local telluric distortion. J. Geophys., 62: 119–127.

Bailey, R.C., 1990. Trapping of aqueous fluids in the deep crust. Geophys. Res. Lett., 17: 1129–1132.

Banks, R.J. and Beamish, D., 1979. Melting in the crust and upper mantle beneath the Kenya Rift: evidence from Geomagnetic Deep Sounding experiments. J. Geol. Soc. London, 136: 225–233.

Berdichevsky, M.N. and Dmitriev, V.J., 1976. Basic principles of interpretation of magnetotelluric sounding curves. In: A. Adam (Editor), Geoelectric and Geothermal Studies, KAPG Geophys. Monogr., Academiai Kiado, Budapest, 164–22.

Biehler, S., Ferguson, J., Baldridge, W.S., Jiracek, G.R., Aldern, J.L., Martinez, M., Fernandez, R., Romo, J., Gilpin, B., Braile, L.W., Hersey, D.R., Luyendyk, B.P. and C.L. Aiken, 1991. A geophysical model of the Española Basin, Rio Grande rift, New Mexico. Geophysics, 56: 340–353.

Boehl, J.E., Bostick, F.X, Jr. and Smith, H.W., 1977. An application of the Hilbert transform to the magnetotelluric method: Elec. Geophys. Res. Lab. Rept., Univ. Texas, Austin, 98 pp.

Brenan, J., 1991. Development and maintenance of metamorphic permeability: implications for fluid transport. In: D. M. Kerrick (Editor), Contact Metamorphism. Mineral. Soc. Amer., Reviews in Mineralogy, 26: 291–319.

Cagniard, L., 1953. Basic theory of the magnetotelluric method of geophysical prospecting. Geophysics, 18: 605–635.

Chave. A.D. and Smith, J.T., 1994. On electric and magnetic galvanic distortion tensor decomposition. J. Geophys. Res., 99: 4669–4682.

Cooper, R.F. and Kohlstedt, D.L., 1986. Rheology and structure of olivine-basalt melts. J. Geophys. Res., 91: 9315–9323.

Dmitriev, V.I. and Berdichevsky, M.N., 1979. The fundamental model of magnetotelluric sounding: Proc. IEEE, 67: 1034–1044.

Duba, A.L. and Shankland, T.J., 1982. Free carbon and electrical conductivity in the Earth's mantle. Geophys. Res. Lett., 9: 1271–1274.

Duba, A., Helkamp, S., Meurer, W., Nover, G. and Will, G., 1994. Evidence from borehole samples for the role of accessory minerals in lower-crustal conductivity. Nature, 367:59–61.

Gamble, T.B., Goubau, W.M. and Clarke, J., 1979. Magnetotellurics with a remote reference. Geophysics, 44: 53–68.

Garland, G.D., 1975. Correlation between electrical conductivity and other geophysical parameters. Phys. Earth Planet. Interiors, 10: 220–230.

Gough, D.I., 1986. Seismic reflectors, conductivity, water and stress in the continental crust. Nature, 323: 143–144.

Groom, R.W., and Bailey, R.C., 1989. Decomposition of magnetotelluric impedance tensor in the presence of local three-dimensional galvanic distortion. J. Geophys. Res., 94: 1913–1925.

Groom, R.W., and Bailey, R.C., 1991. Analytic investigations of the effects of near-surface three-dimensional galvanic scatterers on MT tensor decompositions. Geophysics, 56: 496–518.

Groom, R.W. and Bahr, 1992. Corrections for near surface effects: Decomposition of the magnetotelluric impedance tensor and scaling corrections for regional resistivities: A tutorial. Surv. Geophys., 13: 341–379.

Haak, V. and Hutton, V.R.S., 1986. Electrical resistivity in continental lower crust. In: J.B. Dawson, D.A. Carswell, J. Hall and K.H. Wedepohl (Editors), The Nature of the Lower Continental Crust. Geol. Soc. London, Spec. Publ., 24: 35–49.

Haak, V., Stoll, J. and Winter, H., 1991. Why is the electrical resistivity around the KTB hole so low?. Phys. Earth Planet. Inter., 66: 12–23.

Hermance, J.F., 1979. The electrical conductivity of materials containing partial melt: A simple model from Archie's law. Geophys. Res. Lett., 6: 613–616.

Hermance, J.F., 1982. Magnetotelluric and geomagnetic deep-sounding studies in rifts and adjacent areas: constraints on the physical processes in the crust and upper mantle. In: Special Volume on Continental and Oceanic Rifts, International Commission on Geodynamics. Am. Geophys. Union, Washington, DC, 8: pp. 169–192.

Hermance, J.F. and Pedersen, J., 1980. Deep structure of the Rio Grande rift: A magnetotelluric interpretation. J. Geophys. Res., 85: 3899–3912.

Hobbs, B.A., 1992. Terminology and symbols for use in studies of electromagnetic induction in the earth. Surv. Geophys., 13: 489–515.

Holness, M. B., 1993. Temperature and pressure dependence of quartz-aqueous fluid dihedral angles: the control of adsorbed H_2O on the permeability of quartzites. Earth Planet. Sci. Lett., 117: 363–377.

Holness, M.B., 1995. The effect of feldspar on quartz-H_2O–CO_2 dihedral angles at 4 kbar, with consequences for the behavior of aqueous fluids in migmatites. Contrib. Mineral. Petrol., 118: 356–364.

Hyndman, R.D., 1988. Dipping seismic reflectors, electrically conductive zones, and trapped water in the crust over a subducting plate. J. Geophys. Res., 93: 13,391–13,405.

Hyndman, R.D. and Klemperer, S.L., 1989. Lower-crustal porosity from electrical measurements and inferences about composition from seismic velocities. Geophys. Res. Lett., 16: 255–258.

Hyndman, R.D. and Shearer, P.M., 1989. Water in the lower continental crust: modelling magnetotellurics and seismic reflection results. Geophys. J. Int., 98: 343–365.

Hyndman, R.D., Vanyan, L.L., Marquis, G. and Law, L.K., 1993. The origin of electrically conductive lower continental crust: saline water or graphite?. Phys. Earth Planet. Inter., 81: 325–344.

Jiracek, G.R., 1990. Near-surface and topographic distortions in electromagnetic induction. Surv. Geophys., 11: 163–203.

Jiracek, G.R., 1995. Geoelectromagnetics charges on. In: U.S. National Report to International Union of Geodesy and Geophysics, 1991–1994, Amer. Geophys. Union, in press.

Jiracek, G.R., Ander, M.E. and Holcombe, H.T., 1979. Magnetotelluric soundings of crustal conductive zones in major continental rifts. In: Robert E. Riecker (Editor), Rio Grande Rift: Tectonics and Magmatism. Am. Geophys. Union, Washington DC, pp. 209–222.

Jiracek, G.R., Gustafson, E. and Mitchell, P.S., 1983. Magnetotelluric results opposing magma origin of crustal conductors in the Rio Grande rift. Tectonophysics, 94: 299–326.

Jiracek, G.R., Rodi, W.L. and Vanyan, L.L., 1987. Implications of magnetotelluric modeling for the deep crustal environment in the Rio Grande rift. Phys. Earth Planet. Inter., 45: 179–192.

Jodicke, H., 1992. Water and graphite in the earth's crust—an approach to interpretation of conductivity models, Surv. Geophys., 13: 381–407.

Jones, A.G., 1987. MT and reflection: an essential combination. Geophys. J.R. Astron. Soc., 89: 7–18.

Jones, A.G., 1992. Electrical conductivity of the continental lower crust, In: The Continental Lower Crust, edited by D.M. Fountain, R.J. Arculus, and R.W. Kay, Elsevier, New York, pp. 81–143.

Katsube, T.J. and Mareschal, M., 1993. Petrophysical model of deep electrical conductors: graphite lining as a source and its disconnection due to uplift. J. Geophys. Res., 98: 8019–8030.

Kaufman, A.A., 1985. Tutorial: Distribution of alternating electrical charges in a conducting medium, Geophys. Prosp., 33: 171–184.

Keller, G.V., 1989. Electrical structure of the crust and upper mantle beneath the United States, Part 2, Survey of data and interpretation. In: L.C. Pakiser and W.D. Mooney (Editors), Geophysical Framework of the Continental United States, Geol. Surv. Amer. Mem. 172, Boulder, Colorado, 425–446.

Kronenberg, A.K. and Tullis, J., 1984. Flow strengths of quartz aggregates: Grain size and pressure effects due to hydrolytic weakening. J. Geophys. Res., 89: 4281–4297.

Larsen, J.C., 1977. Removal of local surface conductivity effects from low frequency mantle response curves. Acta Geod. Geophys. Mont., 12: 183–186.

Madden, T. and Nelson, P., 1964. A defense of Cagniard's magnetotelluric method: Project NR-371-401. Geophys. Lab., MIT, 41 pp.

Mareschal, M., Jouanne, V., Menvielle, M., Chouteau, M., Grandis, H. and Tarits, P., 1993. Magnetotelluric observations over the Rhine graben, France: A simple impedance tensor analysis helps constrain the dominant electric features. Phys. Earth Planet. Inter.,

Marquis, G. and Hyndman, R.D., 1992. Geophysical support for aqueous fluids in the deep crust: seismic and electrical relationships. Geophys. J. Int., 110: 91–105.

Merzer, A.M. and Klemperer, S.L., 1992. High electrical conductivity in a model lower crust with unconnected, conductive, seismically reflective layers. Geophys. J. Int., 108: 895–905.

Newton, R.C., 1990. Fluids and shear zones in the deep crust. Tectonophysics, 182: 21–37.

Olhoeft, G.R., 1981. Electrical properties of granite with implications for the lower crust. J. Geophys. Res., 86: 931–936.

Pedersen, J. and Hermance, J.F., 1978. Evidence for molten material at shallow to intermediate crustal levels beneath the Rio Grande rift at Santa Fe (abs.), EOS Trans. AGU, 59: 390.

Reddy, I.K. and Rankin, D., 1974. Coherence functions for magnetotelluric analysis. Geophysics, 39: 312–320.

Rokityansky, I.I., 1982. Geoelectromagnetic Investigation of the Earth's Crust and Mantle. Springer-Verlag, New York, 381 pp.

Schmucker, U., 1964. Anomalies of geomagnetic variations in the southwestern United States. J. Geomagn. Geoelectr., 15: 192–221.

Schmucker, U., 1970. Analysis of geomagnetic variations in the southwestern United States. Bull. Scripps Inst. Oceangr., 13: 165 pp.

Schmucker, U. and Tezkan, B., 1988. 10 Jahre elektromagnetische Tiefenforschung im Rheingraben -eine Zusam-menfassung mit Ausblick auf neuere Ergebnisse. In: V. Haak and J. Homilius (Editors), Protokoll über das 12. Kolloquium "Elektromagnetische Tiefenforschung". Königstein im Taunus, 1–3 March, pp. 17–34.

Sibson, R.H., 1984. Roughness at the base of the seismogenic zone: Contributing factors. J. Geophys. Res., 89: 5791–5799.

Sims, W.E. Bostick, F.X., Jr. and Smith, H.W., 1971. The estimation of magnetotelluric impedance tensor elements from measured data. Geophysics, 36: 938–942.

Spies, B.R. and Eggers, D.E., 1986. The use and misuse of apparent resistivity in electromagnetic methods. Geophysics, 51: 1462–1471.

Sternberg, B.K., Buller, P.L., Kisabeth, J.L. and Mehreteab, E., 1984. Electrical methods for hydrocarbon exploration: II. Magnetotelluric (MT) method. In: Unconventional Methods in Exploration for Petroleum and Natural Gas. S. Methodist Univ. Press., 220–230.

Swift, C.M., Jr., 1967, A Magnetotelluric Investigation of an Electrical Conductivity Anomaly in the Southwestern United States. Ph.D. Thesis, Massachusetts Institute of Technology, Cambridge, Mass.

Thompson, A.B. and Connolly, J.A.D., 1990. Metamorphic fluids and anomalous porosity in the lower crust. Tectonophysics, 182: 47–55.

Tikhonov, A.N., 1950. Determination of the electrical characteristics of the deep strata of the earth's crust. Dok. Akad. Nauk., USSR, 73: 2, 295–297.

Turcotte, D.L. and Schubert, G., 1982. Geodynamics: Applications of Continuum Physics to Geological Problems. John Wiley, New York, 450 pp.

Vanyan, L.L., 1967. Electromagnetic depth soundings. Consultants Bureau, New York, 200 pp.

Vozoff, K., 1972. The magnetotelluric method in the exploration of sedimentary basins. Geophysics, 37: 9891–141.

Vozoff, K., 1991, The magnetotelluric method. In: Nabighian, M.N. (Editor), Electromagnetic Methods in Applied Geophysics, 2, B. Soc. Explor. Geophys., 641–711.

Wait, J.R., 1954, On the relation between telluric currents and the earth's magnetic field. Geophysics, 19: 281–289.

Wait, J.R., 1970. Electromagnetic Waves in Stratified Media. 2nd ed., Pergamon Press, New York.

Wannamaker, P.E., Hohmann, G.W., and Ward, S.H., 1984. Magnetotelluric responses of three-dimensional bodies in layered earths. Geophysics, 49: 1517–1533.

Ward, S.H. and Hohmann, G.W., 1988. Electromagnetic theory for geophysical applications. In: Nabighian, M.N., (Editor), Electromagnetic Methods in Applied Geophysics–Theory, 1. Soc. Explor. Geophys., 131– 311.

Watanabe, T., 1993, Effects of water and melt on seismic velocities and their application to characterization of seismic reflectors. Geophys. Res. Lett., 20: 2933–2936.

Watson, E.B. and Brenan, J.M., 1987. Fluids in the lithosphere, 1. Experimentally determined wetting characteristics of $C0_2$–H_20 fluids and their implications for fluid transport, host-rock physical properties and fluid inclusion formation. Earth planet. Sci. Lett., 85: 497–515.

Watson, E.B. and Lupulescu, A., 1993. Aqueous fluid connectivity and chemical transport in clinopyroxene-rich rocks. Earth Planet. Sci. Lett., 117: 279–294.

Wilson, M., 1989. Igneous Petrogenesis. Unwin Hyman, London, 466 pp.

Zhang, P., Roberts, R.G. and Pederson, L.B., 1987. Magnetotelluric strike rules. Geophysics, 52: 267–278.

Zhang, P., Pedersen, L.B., Mareschal, M. and Choteau, M.,1993. Channeling contribution to tipper vectors: A magnetic equivalent to electric distortion. Geophys. J. Int., 113: 693–700.

Zhdanov, M.S. and Keller, G., 1994. The Geoelectrical Methods in Geophysical Prospecting. Elsevier, Amsterdam, 900 pp.

This Page Intentionally Left Blank

Part III.

Modern Rifts

This Page Intentionally Left Blank

Chapter 4

The European Cenozoic rift system

C. Prodehl, St. Mueller, and V. Haak

4.1. Introduction

4.1.1. Description and Location

The European Cenozoic Rift system (ECRS) traverses the lithosphere of western and central Europe extending from the Mediterranean to the North Sea over a distance of some 1100 km (Fig. 4–1). It is a continuous system of rift structures from the Rhône depression in southeastern France to the Leine graben in northern Germany and through the Lower Rhine Embayment in western Germany into the central graben in the North Sea. Also the Eger graben of the Bohemian Massif is viewed as part of the European Cenozoic rift system (Ziegler, 1992), but will not be discussed in this contribution. This rift system evolved in the Alpine foreland during late Eocene to Recent times. Its development is contemporaneous with the main and late Alpine orogenic phases (Ziegler, 1992).

Southwards, off the mainland of France, the Cenozoic rift system continues through the Gulf of Lions into the Spanish Valencia trough. Ziegler (1992) discusses the possible southwestern prolongation of the Cenozoic European rift system into the western Mediterranean Sea, i.e. the Valencia trough (Banda and Santanach, 1992) and the grabens of Corsica-Sardinia, which were formed when they were still attached to the Provence (Illies, 1975b). The European Cenozoic Rift system continues southwestward across the Alboran Sea to the Rif fold belt into the Atlas ranges. The southern continuation of the rift system through the Mediterranean Sea and beyond, however, will not be discussed in this chapter.

In southern France the rift starts in the Rhône depression. While the Rhône valley in southeastern France is not well developed as a graben, the Limagne graben, west of the Rhône valley, is a very significant rift structure which traverses the Massif Central and is flanked by volcanic chains. Further north, the Bresse-Saône graben system continues from the Rhône valley and separates the Massif Central of France from the Franco-Swiss Jura and the Alpine orogenic belt. Both the Limagne graben and the Bresse-Saône graben system terminate against the Burgundy transform fault system, which links the grabens of southeastern France with the Rhinegraben near Basel.

The Rhinegraben (Fig. 4–1) between Basel and Frankfurt is the central segment of the European Cenozoic rift system and has been the most thoroughly investigated (Rothé and Sauer, 1967, Illies and Mueller, 1970, Illies and Fuchs, 1974, Fuchs et al., 1987). It extends as an almost linear feature for about 300 km from Basel to Frankfurt. In contrast to the Massif Central region, the Rhinegraben and its surroundings is almost devoid of volcanic activity. The only well known and prominent volcanic feature is the Kaiserstuhl volcano in its southern part.

At the northern end of the Rhinegraben, at a triple junction near Frankfurt (Ziegler, 1992), the rift system splits up: to the north it follows the Hessen de-

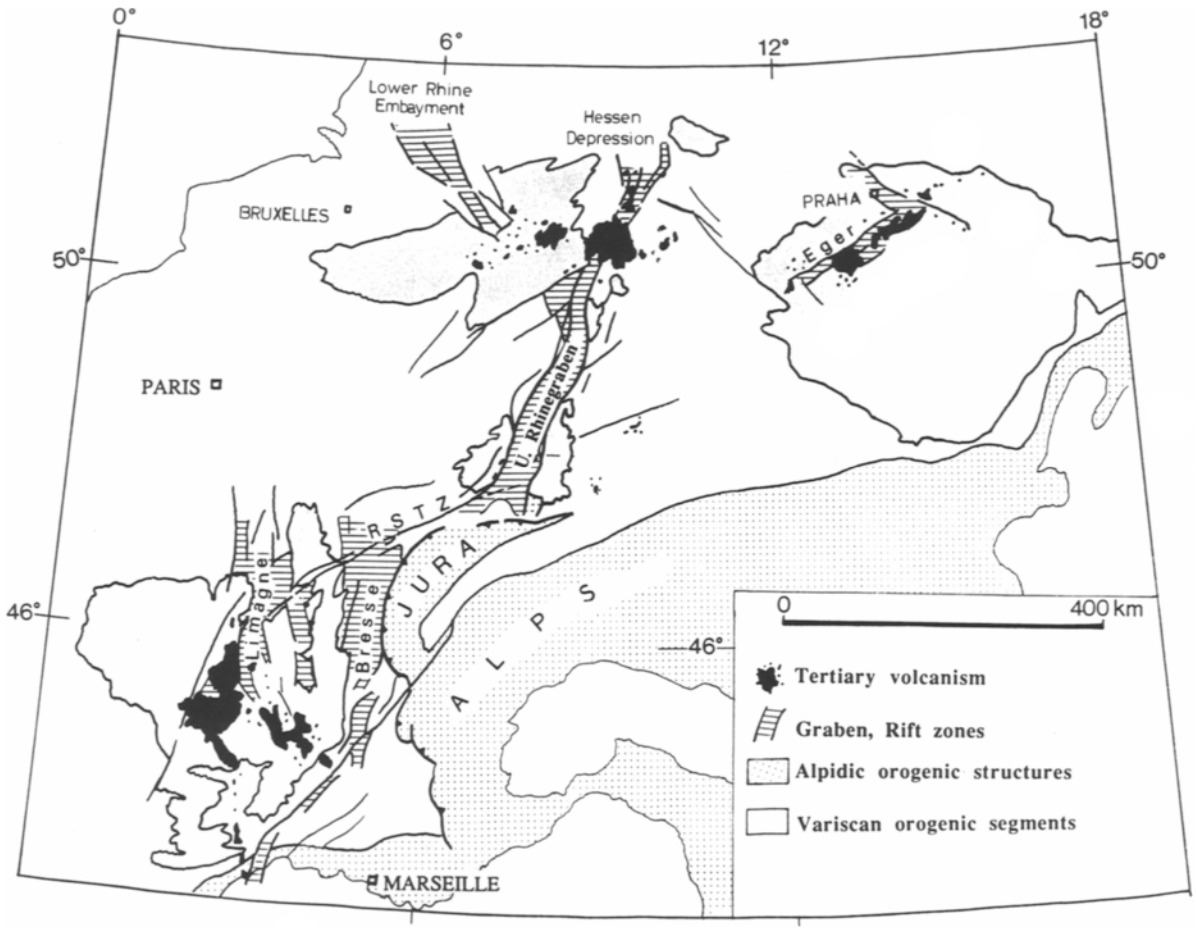

Fig. 4–1. The European Cenozoic rift system between the North Sea and the Mediterranean Sea (after Echtler et al., 1994, fig. 1).

pression and the Leine graben near Göttingen and seems then to disappear beneath the young sediments of the North German Plain. The other branch of the rift system has been more active in recent times. It continues from the northern end of the Rhinegraben near Frankfurt northwestward through the Rhenish Massif (Fuchs et al., 1983) into the Lower Rhine embayment (referred to as Ruhr graben by Ziegler, 1992) and from there can be traced into the North Sea.

All parts of the rift system show an asymmetric structure; in addition the Rhinegraben is characterized by a north-south segmentation. The regional stress field in central Europe has undergone a systematic variation since upper Miocene times and has changed the kinematics of this rift system (Müller et al., 1992) and its volcanic activity.

4.1.2. Recognition as a rift

As early as 1836 the French scientist Élie de Beaumont studied the steep escarpments of the Vosges mountains and of the Black Forest and suggested that the flat plain along the river Rhine (with the Kaiserstuhl volcano) was the surface of a subsided crustal block which had been downthrown along converging major faults, thereby causing the uplift of the adjacent "graben" shoulders. In a subsequent

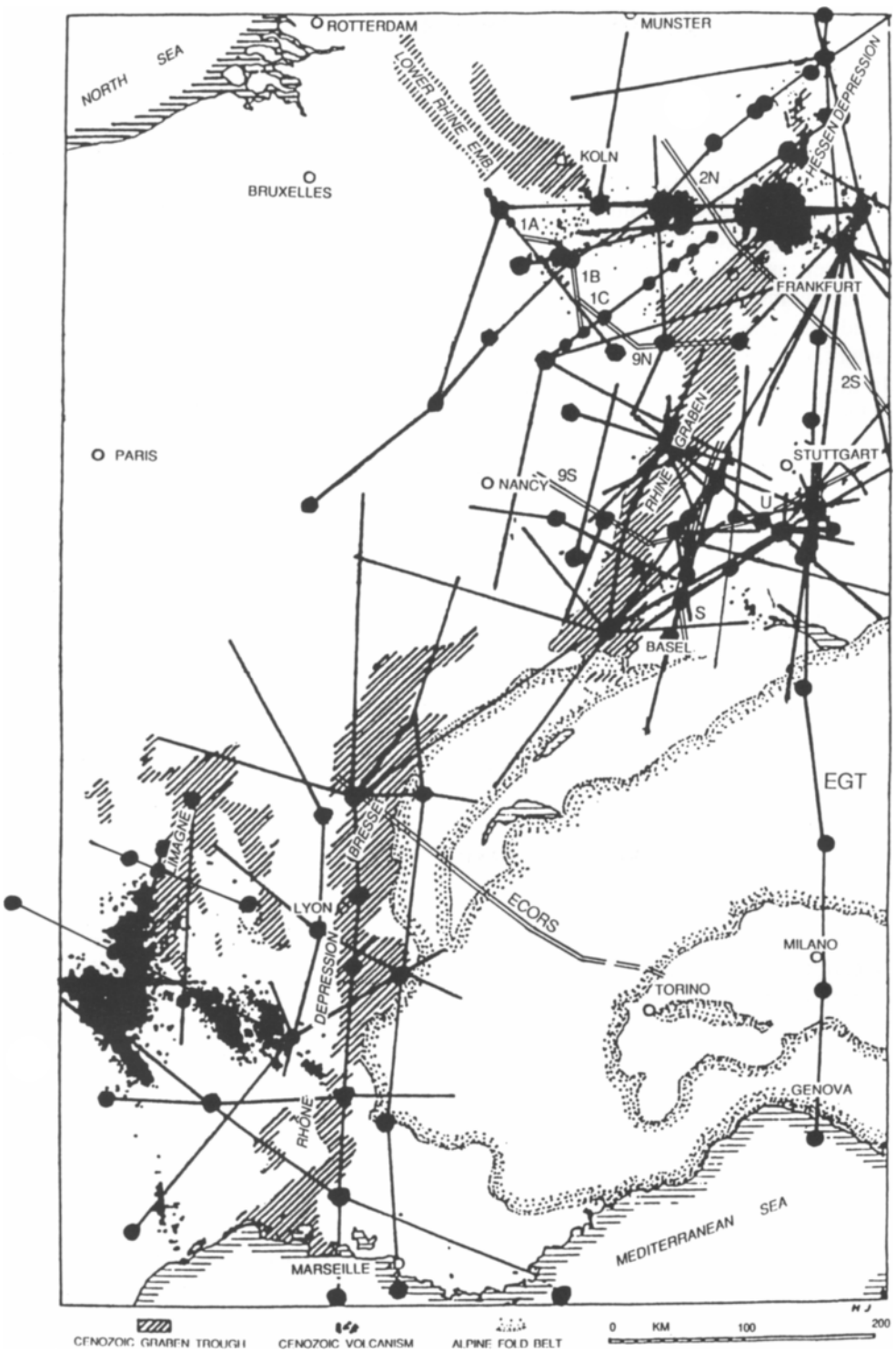

Fig. 4–2. Location map of explosion seismology surveys of the European Cenozoic rift system up to 1987. Base map showing Cenozoic graben troughs and Cenozoic volcanism from Illies (1973, fig. 1).

publication, he was the first to outline the elements of a concept describing "modern rifts" (Élie de Beaumont, 1841).

The significant physiography of continental grabens is expressed by a partial parallelism of the framing fault scarps. This is seen most clearly in the Rhinegraben, but can also be viewed in the Central Massif of France along the Limagne graben and the Rhône–Saône valleys, as well as, to a certain extent, along the Lower Rhenish embayment between Bonn and Köln. An individual average width of 30–40 km between both master faults seems to be a specific attribute of nearly all graben segments. This regularity is maintained by sharp curves of the main trend. Thus, a change in the direction of one escarpment is closely followed by a corresponding change on the opposite side, causing the "woodcut-like" contours of graben systems (Illies, 1974a).

Other typical peculiarities of a graben are its tensional features and internal block tectonics as well as the seismo-tectonic activity parallel to the graben axis. Taphrogenesis is additionally influenced by erosional processes along the elevated graben shoulders and the consequent transport of debris into the graben depressions. Several thousand meters of sedimentary infill deposited in the fault troughs correspond to proportional denudations of the elevated flanks (Illies, 1974a).

The European Cenozoic rift system is pierced by many volcanic plugs and is partially covered by flood basalts (Fig. 4–2), especially in the Hessen depression and the Central Massif of France (Illies, 1970, 1973). Geophysical investigations have revealed anomalous physical properties of crust and mantle, such as high heat flow, moderate seismicity, thinned crust, and anomalous upper-mantle structure, which may be related to the magmatic activity.

4.1.3. Regional tectonic framework

The Cenozoic rifts of southeastern France strike essentially parallel to the front of the western Alps and transect the structural grain of the Late Paleozoic Variscan fold belt at a steep angle (Ziegler, 1992). Localization of individual grabens can be related to tensional reactivation of Late Variscan fracture systems. These grabens are linked by NE trending sinistral transform faults which may represent reactivated Permo-Carboniferous fracture systems (Ziegler, 1992). Subsidence of these grabens began during the Eocene, accompanied partly by strong volcanic activity.

A sinistral NE-striking transform fault system forms the structural connection of the Limagne and Bresse grabens of south-central France with the southern end of the Rhinegraben. The NNE-trending Rhinegraben shows a difference in the evolution of the southern and the northern parts (Roll, 1979). Rifting started with graben subsidence in the southern Rhinegraben about 45 Ma under an extensional stress regime in the foreland of the Alps (Illies and Greiner, 1979) (Fig. 4–3). The maximum horizontal extensional stress rotated from NNE–SSW to a NNW–SSE to NW–SE direction at about 20 Ma (Ahorner, 1975; Illies, 1975a, b, Meier, 1989, Meier and Eisbacher, 1991). Since that time, the graben has experienced transpression. Graben subsidence ceased in the southern Rhinegraben (Villemin and Coletta, 1990) and was followed by mid-Miocene updoming of the Vosges - Black Forest complex (Laubscher, 1987). The doming was accompanied by volcanic activity in the Kaiserstuhl area within the graben and in the Hegau and Urach volcanic fields to the east (Lippolt et al., 1974).

As an unstable block on the perimeter of the Alpine collision front, the Rhenish Massif is wedged between the Rhinegraben and the Lower Rhine embayment. Uplift of the Rhenish Massif of at least 150 m was accompanied by widespread volcanism in the western Eifel and the Neuwied basin. From the southern rim of the Taunus and Hunsrück to the Westerwald and Eifel a belt of earthquake epicenters and a grid of faults, partially still active and indicating mild neotectonics, traverse the Rhenish Massif in the direction of the maximum horizontal compressive stress axis (Illies and Fuchs, 1983). Near Bonn, active graben tectonics begins again, however, different from the Rhinegraben now under tension corresponding to the new direction of the axis. The Lower Rhine embayment continued to subside during Miocene to Recent times, some faults forming considerable steps. This graben feathers out to the northwest and gradually loses its identity (Ziegler, 1992).

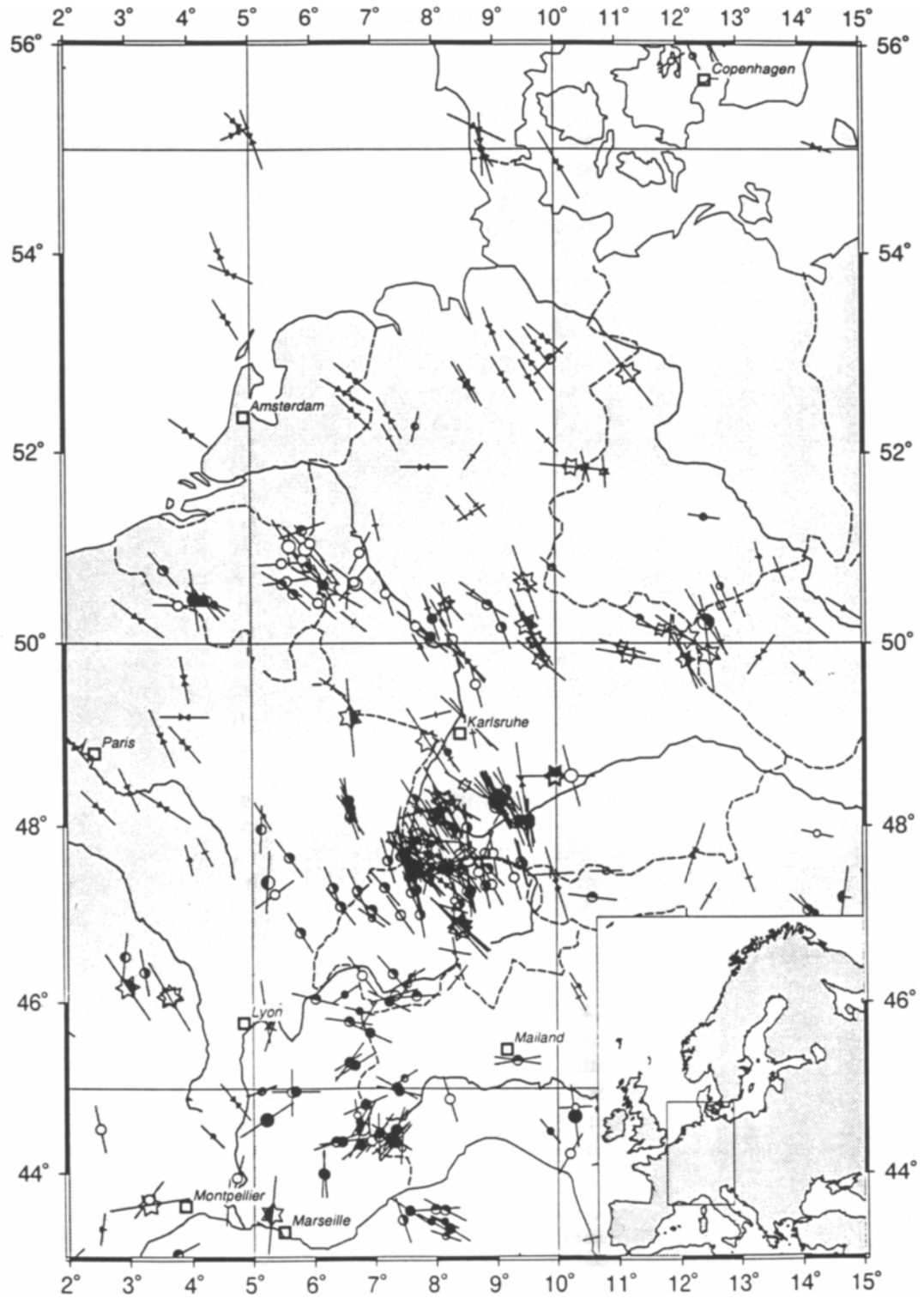

Fig. 4–3. Stress map of central Europe (from B. Müller pers. comm., 1994)

4.2. Significance

As in most rift systems around the world, there has been commercial interest for some time in exploring and exploiting the natural resources of the graben troughs. Hot springs near the edge of the graben shoulders became the site of Roman settlements. The area of Pechelbronn in the Alsace in the Rhinegraben is known for its oil wells since 1498; it is one of the oldest oil fields in Europe. Thousands of boreholes have since penetrated into the sedimentary graben fill of the Rhinegraben, with the deepest borehole reaching a depth of 3336 m, in particular exploring the chances for geothermal energy exploitation. Many shafts for mining potassium salt, asphalt, ligurite and iron ore have been sunk into the graben and precious metal ores have been mined in the exposed flanks of the graben since the Middle Ages. Immeasurable geophysical investigations have aided in the understanding of the structural features in and around the graben.

The seismicity of this Cenozoic rift system is moderate compared to other continental graben systems. Although the historical seismic record covers about 1000 years, no great earthquake has been documented. The strongest event with an estimated intensity of IX occurred in 1356 and destroyed the city of Basel at the southern end of the Rhinegraben (Bonjer et al., 1984). In modern times, mainly the Hohenzollerngraben, located to the east between the Rhinegraben and the Urach volcanic field, has been the site of relatively strong earthquakes (Schneider, 1971, Illies, 1982). Occasionally, earthquakes with intensities of VII–VIII causing minor damage are felt in the Lower Rhine embayment (van Eck et al., 1993).

Since the beginning of modern crustal and upper-mantle investigations, the Rhinegraben and the grabens of the French Massif Central have been sites of intensive research. The crustal and upper-mantle structure has been investigated predominantly by seismic methods with observation and interpretation techniques varying through time, and results have been published by various authors. Figure 4–2 shows the seismic-refraction lines observed from 1966 to 1989 to investigate the crustal and upper-mantle structure of the rift system and its surroundings.

A review of the crustal and upper-mantle structure beneath the European Cenozoic rift system up to 1978 was published by Prodehl (1981). Since then, new data—in particular, seismic-reflection surveys—became available (e.g., Aichroth et al., 1992, Bergerat et al., 1990, Brun et al., 1991, 1992, Gajewski, 1989, Lüschen et al., 1989, Wenzel et al., 1991) and were subsequently reviewed by Prodehl et al. (1992). In that publication, emphasis was put on two transects through the central part of the rift system, one traversing the southern Rhinegraben from the Vosges Mountains to the Black Forest (see AA' in Fig. 4–9 and Fig. 4–17), the other one traversing the Rhenish Massif and the Hessen depression (BB' in Fig. 4–9 and Fig. 4–25). These transects are part of a series of transects through major rift structures of the world which have been compiled for this volume.

4.A. The southern section of the Central European rift in south-central France

4.A3. Geological information

4.A3.1. Introduction

Superimposed on old Hercynian structures, the volcanic provinces together with intersecting graben structures form the southern part of the European Cenozoic rift system (ECRS) which developed in western Europe since Oligocene time. The Limagne graben is the most prominent segment of this Massif Central graben system. To the east, the Rhone depression separates the Massif Central from the Alps, and the Bresse-Saone graben system, at the western margin of the Franco-Swiss Jura, continues to the north-northeast, but terminates against the Burgundy transform fault system which links the grabens of southeastern France with the Rhinegraben. The development of the Central European graben system in Cenozoic times reveals that the recent story of the Massif Central in the Variscan belt is connected with geological convulsions associated with the Alpine orogeny, thus showing the complex nature of its geodynamical evolution.

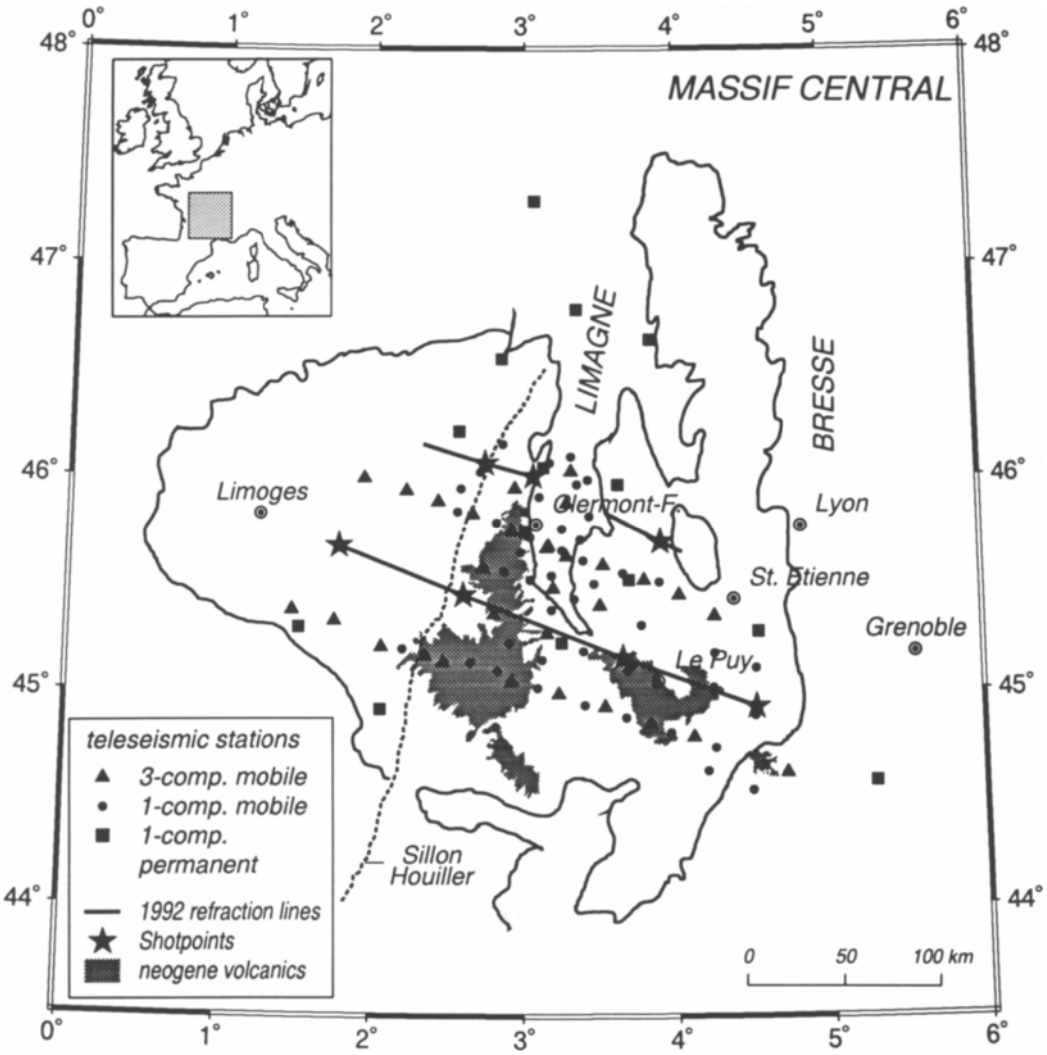

Fig. 4–4. Simplified geologic map of the Central Massif of France showing neovolcanic provinces and graben areas and location of seismic-refraction profiles.

4.A3.2. Sedimentary record

The Cenozoic rifts of southeastern France strike essentially parallel to the deformation front of the western Alps and transect the structural grain of the Late Paleozoic Variscan fold belt at a steep angle (Ziegler, 1992).

The French Massif Central is part of the late Paleozoic Hercynian fold belt. Similar to the Rhenish Massif and the Vosges-Black Forest area, it is a pre-Triassic peneplain reactivated since Jurassic times. After a major Jurassic transgression covering most of the peneplain, at the beginning of the Oligocene a new phase of significant fracturing occurred when large subsidence trenches developed as the basin of Limagne d'Allier, the basins of Montbrison and Roanne, Forez, Le Puy, and others within the Massif (Roques, 1971). Also, large subsided areas developed surrounding the Massif Central, including the Paris basin to the northwest, the Aquitaine basin

to the southwest, the Languedoc to the southeast, and the Rhône and Bresse depressions to the east and northeast. Volcanic activity began at this time in the Limagne and later migrated westwards. Simultaneously the whole Massif Central rose and tilted from east to west. In Quaternary times, volcanic activity migrated back to the east and concentrated on the western marginal fault of the Limagne, with the most recent volcanoes being only 2500 years old (Hirn and Perrier, 1974).

The Burgundy trough has been an area of strong sedimentation during most of the Permian and Mesozoic times (Boigk and Schöneich, 1974). At certain periods, between the crystalline blocks of the Massif Central and the western Alps a marine connection from Southwest Germany to the Mediterranean has been inferred in the contour maps of Boigk and Schöneich (1974) through today's Bresse and southern Rhône depressions.

The Limagne region consists of the Limagne d'Allier, also named more simply the Limagne graben, and the Montbrison and Roanne basins, both separated by the Forez horst. The two depressions join in the region of Moulins. Oligocene sediments become progressively thinner towards north and vanish near Nevers (Fig. 4–4). The average thickness of the sediments shows strong asymmetries, being greater in the western than in the eastern part of the Limagne graben. The greatest depth to the basement is about 2.5 km and occurs just north of Clérmont-Ferrand, near the western master fault (see Fig. 2 of Hirn and Perrier, 1974; Morange et al., 1971). To the south, towards Brioude, the basement rises and a complex faulted area shows alternating outcrops of crystalline rocks and Oligocene sediments which are not affected by erosion. It is not known how far the original sedimentary cover extended.

The Bresse and Limagne grabens began to develop simultaneously with the Rhinegraben, with parallel orientations 150-km-apart from each other. Illies (1973) suggests that the three graben segments terminate at the same major transverse geotectonic feature: the so-called Burgundy transfer zone, a sinistral northeasterly striking transform fault system following paths of weakness in the Hercynian basement. Contini and Théobald (1974) studied the transition between the Rhine and the Saône rift valleys in detail and observed two tectonic stages: the first is a reactivation of Permo-Carboniferous fracture systems and can be recognized in the Hercynian basement and its Triassic cover, the second tectonic stage is manifested in the deposition of post-Triassic sediments. Illies (1973, 1974c) explains the southern extension of the Rhinegraben by the graben zones of eastern France in the early Tertiary, prior to the folding of the Swiss Jura in Pliocene times, as caused by the rotation of the strain ellipsoid when the Rhinegraben, dilatational during Oligocene and Miocene, changed into a shear graben in Upper Pliocene and Pleistocene times.

Subsidence of the Saône, Bresse, and Limagne grabens began during the middle Eocene. The Bresse graben experienced its most rapid subsidence in Oligocene times along convergent main faults and along synthetic and antithetic shear zones with a main strike direction of N20°E. Syn-rift deposits of lacustrine shales and carbonates and fringing clastics, were followed by an evaporitic sequence and distal marine incursions (Blès et al., 1989, Illies, 1974c, Ziegler, 1992). By the early Miocene, marine connections between the Alpine foreland basin and the Paris and Northwest European basins were blocked by the thermal uplift of the Massif Central and the Rhenish Massif (Ziegler, 1992). After a time of decreased and partly interrupted subsidence of the Bresse and Limagne grabens in the Miocene, possibly in connection with the thermal doming of the Massif Central and the Vosges-Black Forest dome, combined with wrench-related upwarping of the Burgundy area, the kinematics of the Bresse graben changed in the Pliocene. The eastern border fault zone was overridden by west-vergent folds of the Swiss Jura, and the extensional tectonics changed into a compressional regime. At present, the Bresse and Limagne grabens are being uplifted.

Due to the changes in the regional stress field (Blès and Gros, 1991) during the late Miocene and Plio-Pleistocene, the Bresse valley rift started to develop differently from the Rhinegraben. The highly asymmetric sedimentary fill of the Bresse graben reaches a maximum thickness of about 5 km (Bergerat et al., 1990; Truffert et al., 1990).

4.A3.3. Igneous activity

Taphrogenesis in the grabens of southeastern France was connected with intensive volcanism producing primitive mafic alkaline magmas (Wilson and Downes, 1992). The main activity concentrated in the Auvergne, west of the Limagne graben. Here, from north to south are aligned the range of small volcanoes forming the Chaîne des Puys, the great stratovolcano of Mont Dore, the basalt lava plateau of the Cézallier, the central volcano of the Cantal and the basaltic plateau of the Aubrac (de Goer and Mergoil, 1971; Jung, 1946; Rutten, 1969). Another large volcanic district is the Velay in the southeastern prolongation of the Limagne graben.

The evolution with time can be reconstructed on the basis of recent K-Ar dating (Briot and Harmon, 1989; Werling, 1992). After the initiation of rifting in the Eocene, about 40 Ma, basaltic volcanism began within the Limagne graben in the Lower Miocene, about 19 Ma. In the upper Miocene, from 11–12 Ma onwards, the volcanism on the western flank started in the Cantal and Aubrac as well as in the Causses to the south and in the Velay to the southeast. The main activity, however, occurred in the Pliocene between 5 Ma and 2 Ma. Almost all provinces of the western flank (Petite Chaîne de la Sioule, Mont Dore, Cézallier and Cantal), those in the southeastern prolongation of the Limagne graben (Devès, Velay and Coiron), and the southernmost volcanic provinces (Escandorgue and Languedoc), were active at that time. Recent volcanism occurred in the Chaîne des Puys to the northwest and in the Vivarais to the southeast. Evidently, there is no systematic connection between age of the volcanism and its geographic distribution with relation to the Limagne graben system (Werling, 1992).

With the exception of the lava plateaus, the composition of the volcanics varies widely. Jung (1946) has defined groups depending on their alkalinity. Brousse (1971) defines fourteen magmatic regions on the basis of petrology, space, and time.

4.A3.4. Xenolith studies

In the Massif Central xenoliths have been found in great numbers within volcanic rocks of Oligocene-to-Recent age (Downes and Leyreloup, 1986; Nicolas et al., 1987; Werling, 1992). Besides well equilibrated xenoliths, it is those showing strongly zoned mineral alignments documenting pressure and temperature changes, which enable reconstruction of the spatial and temporal development of the thermal state of the lithosphere underneath the Massif Central (Altherr, oral comm., Werling, 1992). Studying mineral zoning of ortho- and clinopyronenites of non-equilibrated xenoliths, many samples document simple heating and cooling processes, but in others, rather complex developments also are seen where an older cooling process has been overprinted by a younger heating event. In general, a systematic relation between mineral zonation and age of eruption evidently does not exist. According to Werling (1992) it is unlikely that the phenomenon of an older cooling process is connected with tectonic processes during rifting, but more probably should be attributed to processes during extension of the lithosphere at the Variscan orogeny in Upper Carboniferous-to-Permian times.

The alkali basalts of the Massif Central contain almost exclusively Mg-rich spinel-lherzolithes and spinel-harzburgites which are rich in Mg and Cr, while garnet lherzolithes are very rare. During partial melting processes within the mantle, the Cr/(Cr+Al)$^{-}$ and the Mg/(Mg+Fe^{2+})-ratios in the restite increase, while at the same time, a gradual depletion of basaltic components such as Al, Ca, Fe, and Ti occurs (Werling, 1992). Nicolas et al. (1987) interpret the orthopyroxene-clinopyroxene-spinel clusters in the xenoliths as having crystallized from magma pockets which are, themselves, formed on the sites of garnets. This melting occurred when the local geothermal gradient crossed the solidus in the garnet lherzolithe field during asthenospheric upwelling.

Downes and Leyreloup (1986) describe in detail a systematic study of granulitic xenoliths found in the Tertiary and Quaternary volcanics of the Massif Central, which include immature metasediments and calc-alkaline meta-igneous suites. According to

Downes and Leyreloup (1986), this indicates the formation of the crust in an island-arc or continental margin environment. The meta-igneous lithologies of the lower crustal xenoliths in the Massif Central range from ultramafic pyroxenites and hornblendites, through granulites, to intermediate and silicic charnockites and form about 60% of the xenolith population, while the remaining lower crustal xenoliths are metasedimentary granulites (Downes, 1993). More recent studies by Werling (1992) result in a temperature range between 650°C and 1210°C. The estimated pressures and temperatures of equilibrated xenoliths of the various volcanic provinces of differing ages align well along the continental "steady state" model geotherm of 85–90 mWm^{-2} of Chapman (1986).

The primitive mafic-alkaline magmas within the European Cenozoic rift system are regarded by Wilson and Downes (1992) as the closest approach to mantle-derived primary magma compositions which were erupted through variably thinned lithosphere and which have experienced a complex Phanerozoic history of deformation and magmatism in both subduction and extensional tectonic settings. According to Nicolas et al. (1987), in the Massif Central the asthenospheric upwarp above 70-km-depth appears in a number of 10 km diapiric intrusions.

4.A4. Geophysical surveys and results

4.A4.1. Seismic studies

Following various seismic investigations in the 1950s and 1960s (see, e.g., Labrouste, 1970), detailed seismic investigations of crustal and uppermantle structure in the southern section of the central European rift system and in the Massif Central of France began in 1970 with modernized equipment and were carried out during various field campaigns between 1970 and 1992 (Figs. 4–2 and 4–4).

In 1970 several parallel, mostly north-south trending, reversed seismic-refraction profiles were recorded parallel to the main tectonic structures of the Massif Central (Fig. 4–2 and 4–4; Hirn, 1976; Hirn and Perrier, 1974; Perrier and Ruegg, 1973). In 1971, a long-range profile through France from the Bretagne to the Mediterranean Sea near Toulon traversed the Massif Central between Limoges and Arles (Hirn et al., 1973; Sapin and Prodehl, 1973). Based on these data and confirmed by later investigations, the structure of the Hercynian crust of the Massif Central outside the graben and volcanic zones is rather uniform and is very similar to the crust of other Hercynian areas in Europe (Prodehl, 1984). Two intracrustal reflectors near 10 and 20 km depth can be recognized in the seismic-refraction data, and the Moho is a rather flat boundary at about 30 km depth (Hirn, 1976). However, due to the neotectonic events during Tertiary and Quaternary times leading to taphrogenesis and volcanic activity, the original Hercynian crust of the Massif Central has been heavily disrupted in many places.

Two of the reversed profiles of 1970 were recorded along the axis of the Limagne graben (Hirn and Perrier, 1974) and along the volcanic zone Chaîne des Puys – Mont Dore – Cantal (Perrier and Ruegg, 1973). Under the Limagne graben, a strong reflector within the uppermost crust is seen at 3 km depth. The existence of velocity inversions in the upper crust—which reaches to a depth of 16–19 km—were not evident from existing data, but neither could they be ruled out. The dominant feature of the crust under the Limagne graben was a strong reflector at 24 km depth. Hirn and Perrier (1974) emphasized that there is fair evidence that this discontinuity is underlain by a layer with velocity increasing gradually from 7.5 km/s to about 8.4 km/s at 40 km depth and that fairly well-developed phases can be recognized in the data which have evidently traveled below this depth with a velocity greater than 8.4 km/s. Under the volcanic region west of the Limagne graben, Perrier and Ruegg (1973) found also a reflector at 23 km depth, on top of a layer having a velocity increasing from about 7.2 to 8.4 km/s at 45 km depth. Further west, a "normal" Hercynian crust of 30 km thickness is seen. The result of these investigations was summarized by Perrier and Ruegg (1973) in a cross section (Fig. 4–5) which was also checked by gravity modeling.

In 1972 a special survey covered the Bresse and Rhône graben system (Michel, 1978; Michel et al., 1977), which was supplemented in 1976. Contrary to the Rhône graben, the Bresse graben was traversed only by several unreversed lines in westerly and

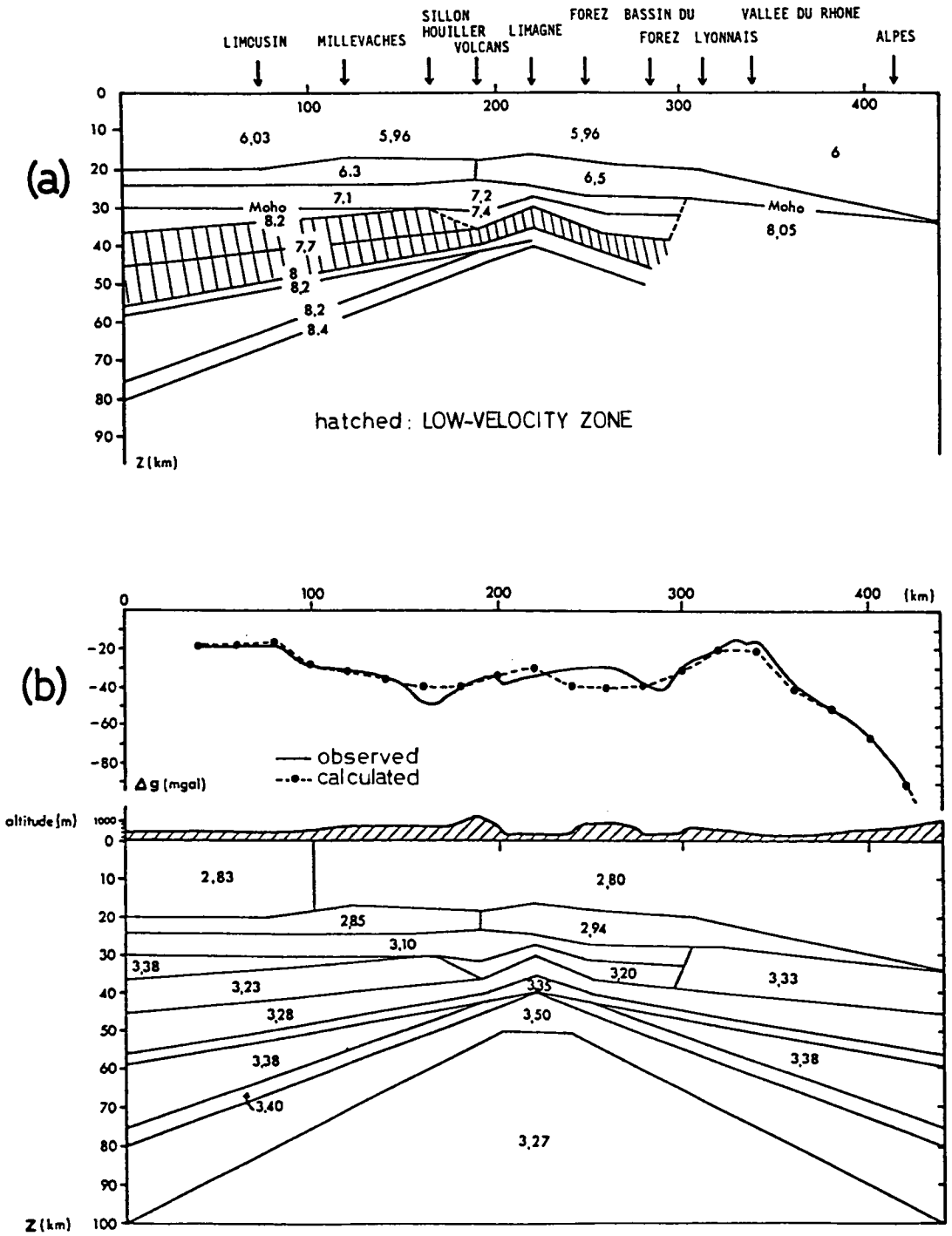

Fig. 4–5. (a) Crustal cross section through the Central Massif of France at the latitude of Clermont-Ferrand (from Perrier and Ruegg, 1973, fig. 63). (b) Gravity model through the Central Massif of France at the latitude of Clérmont-Ferrand (from Perrier and Ruegg, 1973, fig. 64).

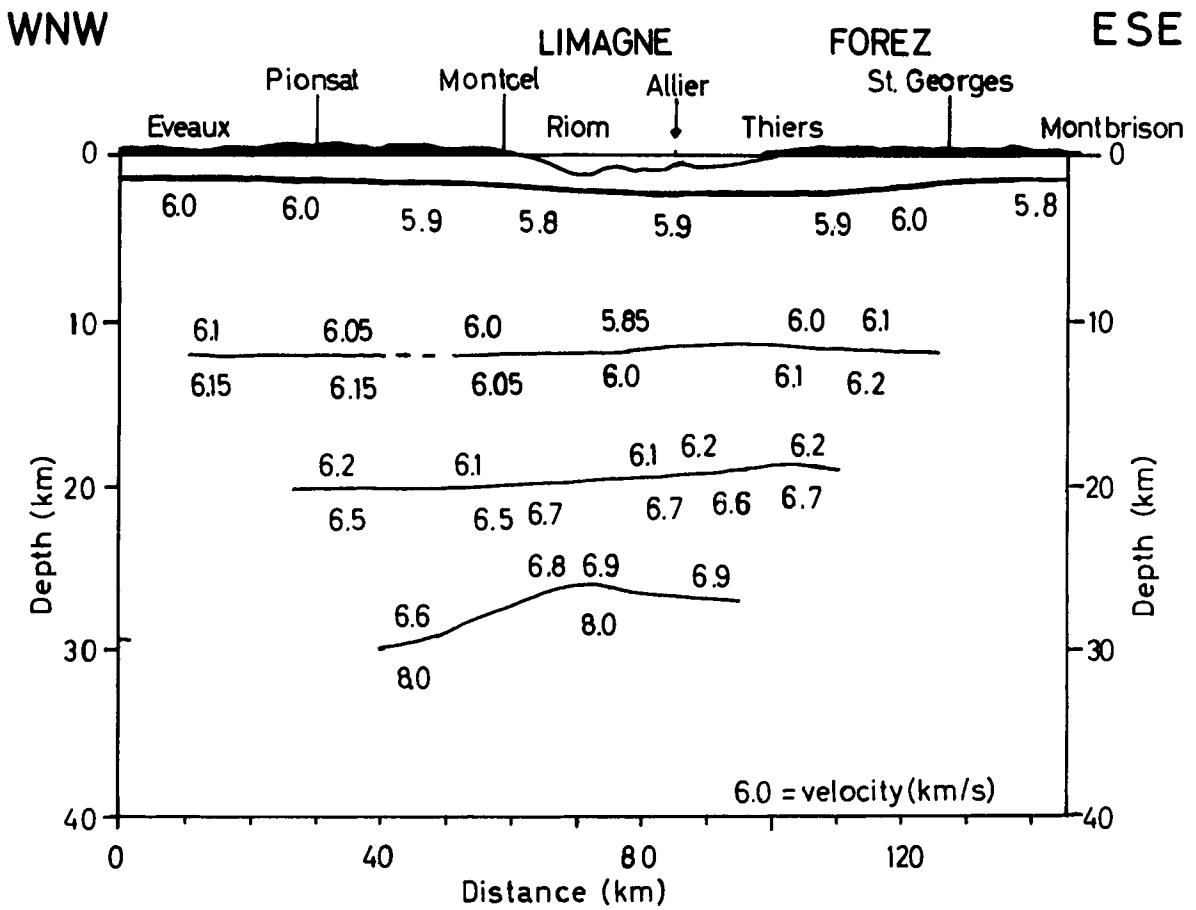

Fig. 4–6. Crustal section across the Limagne graben approximately 30 km north of Clérmont-Ferrand (from Landes, 1994)

north-northeasterly directions. Some of these shots were also used to record unreversed lines into the Swiss Jura (Egloff, 1979). However, the Bresse graben is the only part of the southern European Cenozoic rift system that was investigated in some detail by the ECORS programme. In 1987 a detailed seismic-reflection line was recorded from the western Alps through the Jura and Bresse grabens to the eastern edge of the Massif Central near Tournus (Fig. 4–2; Bergerat et al., 1990; Bois et al., 1991).

In general, the axis of minimum crustal thickness follows approximately the direction of the northern Bresse and, north of the city of Dôle, seems to bend to the northwest. For profiles running from the northern Rhône graben into the Swiss Jura mountains, Egloff (1979) found depths of 27–29 km, and his Moho depth contour map indicates a gradual increase in crustal thickness from 26 km in the northwest of the Swiss Jura mountains to 30 km at their eastern border. Based on the ECORS profile through the Jura Mountains and Bresse basin (Bergerat et al., 1990; Bois et al., 1991; Truffert et al., 1990), the Moho rises from 29 km depth beneath the Jura border to 27 km at the edge of the Massif Central. The highly asymmetric sedimentary fill of the Bresse graben is underlain by a rather transparent upper crust with some easterly dipping reflectors. From the Massif Central to the center of the sedimentary basin, the thickness of the crystalline upper crust is reduced

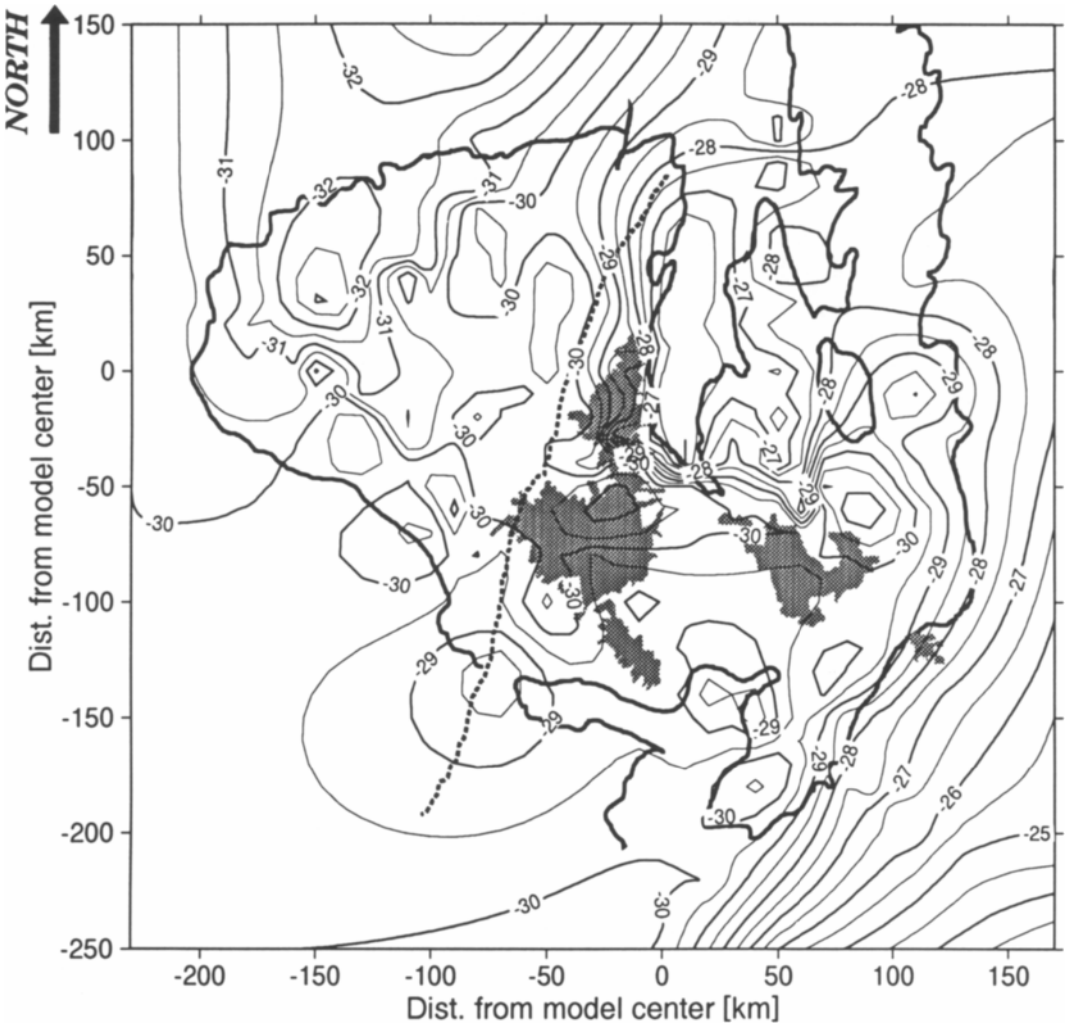

Fig. 4–7. Moho map for the area of the Massif Central (from Bauer, in prep., 1995)

from 17.5 to 13 km. The top of the 10 km thick laminated lower crust parallels the Moho, but is rather difficult to define in detail (Bergerat et al., 1990).

In the southern Rhône Valley and on its flanks, in the Cévennes to the west, and in the Alps to the east, three longitudinal and two transverse profiles have been recorded (Fig. 4–2; Michel et al., 1977; Sapin and Hirn, 1974; Sapin and Prodehl, 1973). Compared to the structure of the surrounding Hercynian crust, the velocity-depth structure of the lines within the graben area show characteristic differences. To the west, under the Cévennes, some fine structure of the middle crust is revealed, while to the east, the Moho dips rapidly towards the Alps and reflections from intermediate boundary zones cannot be correlated in the data. The velocity of the uppermost mantle immediately beneath the Moho is 8.1–8.2 km/s at the border of the Cévennes to the southern Rhône graben, but under the graben area proper, where crustal thickness is reduced, upper-mantle phases cannot be correlated. Under the axis of the southern Rhône valley, sediments may reach almost 10 km thickness. Thus, the thickness of the crystalline crust here is reduced to about 15 km compared to about

22–23 km thickness for the crystalline crust of the southern Rhinegraben. This reduction in thickness is primarily attributed to the upper part of the crust, the "granitic" layer (Sapin and Hirn, 1974). The similarity of the thinned crystalline crust of maximum 15 km thickness, with 10 km and more overlying sediments, is a feature which is also found under other basins with a very thick sedimentary cover like Northern Germany (Prodehl, 1981, 1984, Aichroth et al., 1992, Reichert, 1993).

The joint teleseismic – seismic refraction investigation of 1991–92 (Granet et al., 1994; Stoll et al., 1994; Zeyen et al., 1994) has led to a new understanding of the geophysical data obtained hitherto. The detailed teleseismic and seismic-refraction investigations of 1991–92 in the Massif Central centered around the Limagne graben, and followed detailed petrological field studies of xenoliths in the young volcanic areas surrounding the southern part of the Limagne graben described above (Werling, 1992).

In late 1992, a special seismic refraction survey was carried out (Fig. 4–4) in the central part of the Massif Central. About 150 mobile seismographs simultaneously recorded 7 borehole shots along two WNW–ESE traverses, 70-km-apart, across the southern Limagne graben (Landes, 1994; Novak, 1993; Zeyen et al., 1994). The 150-km-long northern profile crosses the Limagne graben north of Clérmont-Ferrand and traverses crystalline basement rocks just north of the Chaîne des Puys on the west side of the graben, as well as the horst of Forez to the east of the graben. Due to unfavorable noise conditions, however, stations were not deployed in the graben proper. The southern profile of 230 km length is centered at the southern termination of the Limagne graben. It crosses the young volcanic fields of the Cézallier in the west and the Velay/Devès in the east.

Particular aims of this seismic-refraction survey were firstly, to study the effect of rifting and volcanism on the structure of the Hercynian crust; and secondly, to obtain absolute velocities, i.e. to calibrate the crust and uppermost mantle in an area where teleseismic tomography studies and petrological xenolith investigations had been carried out as well.

Surprisingly, in spite of the fact that the southern profile crosses the southernmost tip of the Limagne graben and various young volcanic areas, this line revealed a rather homogeneous crustal structure. Following a Pg-phase indicating a basement velocity of 6.0 km/s, two well-defined wide-angle reflections provide clear evidence of an intermediate crustal boundary at about 17–18 km and the Moho at 29–30 km depth. However, in the area of the Velay/Devès volcanic fields the intermediate crustal reflections are masked by strong signal-induced noise possibly originating from reverberations generated within the near-surface volcanic edifices. The Pn-phase on this line was only recorded east-to-west, but not reversed. Based on the flat crustal structure defined by a series of wide-angle P_MP reflections, the unreversed velocity of 7.9–8.0 km/s is assumed to be a true velocity (Novak, 1993). The fan observations underneath the Limagne graben to the north suggest that the Moho rises to about 26 km, but the sub-Moho velocity remains high (8.0–8.1 km/s), while the Moho stays at 29 km depth below the western flank of the graben (Zeyen et al., 1994). For the northern profile a low, unreversed Pn-velocity of 7.5 km/s is interpreted as an apparent velocity and the resulting two-dimensional crustal model provides an asymmetric structure. The least depth to Moho of 26 km is located near the western border of the Limagne graben proper (Fig. 4–6). Towards west, the crust thickens rather abruptly to 30 km; to the east the increase in depth is more gradual, 28 km depth being obtained under the horst of Forez. Figure 4–7 shows an updated contour map of the depth to Moho for the area of the Massif Central using all data presently available (Bauer, in prep., 1995). The internal crustal structure under the graben area consists of an upper crust with two layers of only slightly varying velocity of about 6.1 and 6.2 km/s, with an intermediate boundary at about 12 km depth, and a lower crust with 6.6–6.8 km/s below 20 km depth (Landes, 1994; Zeyen et al., 1994; H. Zeyen, A. Hirn, M. Landes, and O. Novak, in preparation).

The analysis of xenoliths had supplied information on the petrological composition as well as on the p–T conditions and the petrologically predicted seismic velocities in the source regions of the lower

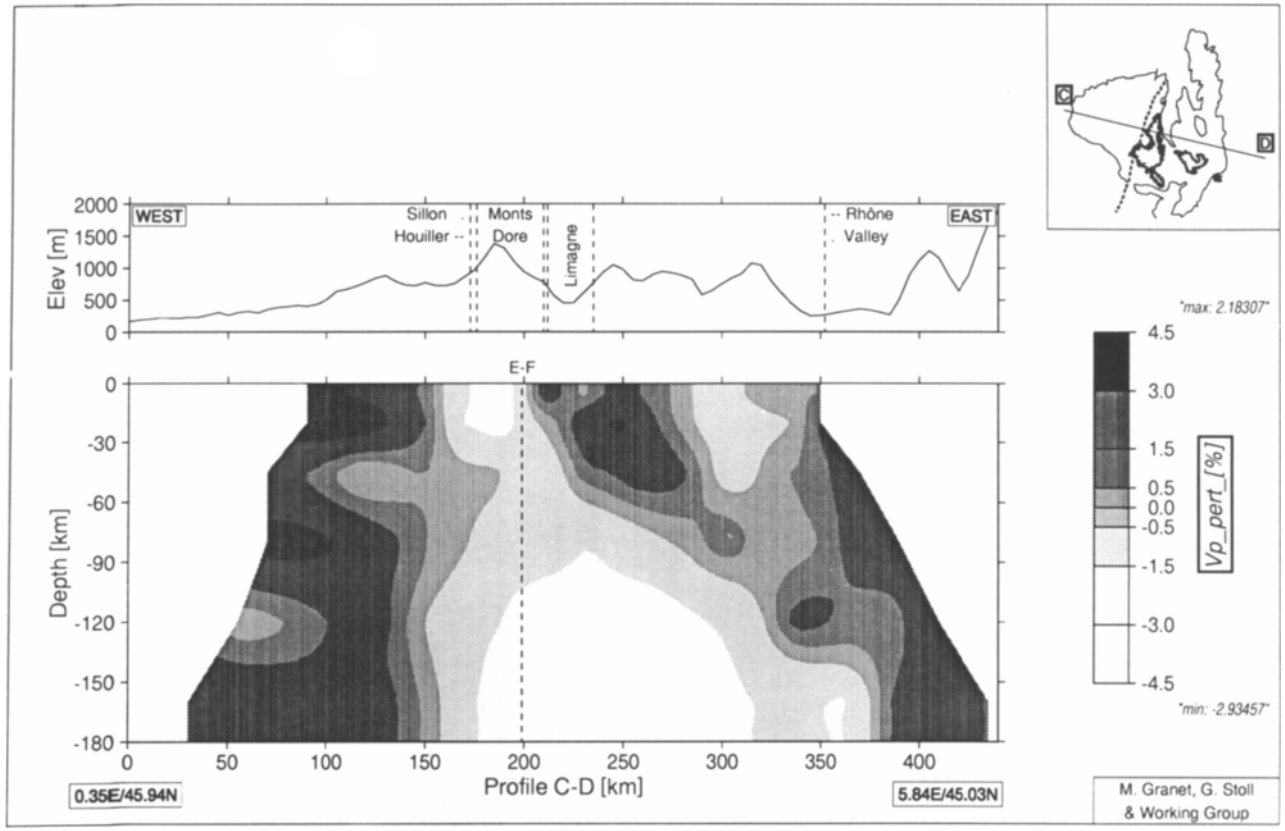

Fig. 4–8. Tomographic cross section through the Massif Central between Limoges and St. Étienne traversing Mont Dore and the southern Limagne graben south of Clérmont-Ferrand (from Granet et al., 1994, fig. 7b)

lithosphere. In order to study the velocity structure of the lithosphere-asthenosphere system beneath this volcanic area, a teleseismic network of 80 mobile short-period seismographs was installed to supplement the existing permanent 14-station-network. The aperture of the array was about 300 km in the E–W direction, and 270 km in the N–S direction. This joint array covered the central part of the Massif Central and recorded more than 120 teleseismic events over a period of 7 months (Granet et al., 1994; Stoll et al., 1994). Inversion of P-wave traveltime residuals of teleseismic events recorded by this dense array yielded a detailed tomographic image of the 3-dimensional velocity structure beneath the Massif Central to about 180 km depth. The relative velocity variations in lateral direction range in average from about +1% to –2.5%, which corresponds to velocity variations of about 0.25–0.3 km/s.

The three-dimensional model (Fig. 4–8) displays strong heterogeneities of the lithosphere down to 60 km depth. Surprisingly, it does not show any evidence of velocity anomalies which could directly be associated with taphrogenesis of the Limagne graben proper. However, the model suggests a strong correlation between volcanic provinces and the location of negative travel time perturbations. Two areas with reduced velocities may be interpreted as a thermal signal visible today and indicating a magma ascent during the Oligocene which followed zones of extended lithospheric fracturing inherited from the Hercynian orogeny and reactivated during the Oligocene. The weakest velocity perturbations are seen between 60 and 100 km depth. The corresponding change in the velocity pattern is interpreted by Granet et al. (1994) as evidence for a smooth transition between lithosphere and asthenosphere, which at the same time defines the thickness of the lithosphere. Below 100 km depth an extended zone of reduced velocities covers a large area in depth and width. The authors interpret this result as evidence for a plume-type structure now in its cooling phase.

4.A4.2. Gravity

Based on a gravimetric study carried out in 1953 by the Companie Générale de Géophysique, Morange et al. (1971) have published a Bouguer contour map of the Limagne graben and surroundings. Compared to average values of –10 to –20 mgal on the western flank, the Bouguer gravity values in the graben proper average between –30 to –40 mgal, but also indicate the existence of various basins. In general the Bouguer gravity decreases from north to south between Moulins and Clérmont-Ferrand and rises again further south. A minimum of –55 mgal is observed near Riom north of Clérmont-Ferrand, near the western edge of the graben.

Interpreting the long-wave length Bouguer gravity anomalies of the 1:1,000,000-scale map of France, Autran et al. (1976) define the Vosges-Auvergne block by a general low Bouguer gravity. Weber (1980) interprets this block as an area of high metamorphism. The greatest negative anomaly occurs south of the Auvergne, with values below –45 mgal, which according to Weber is caused by a crustal thickening of the area surrounding the thinned crust of the Limagne and adjacent young volcanic chains. Following Hirn and Perrier (1974), the entire Massif Central is under compensated, the mean isostatic anomaly being 25 mgal for a depth of compensation of 30 km (Airy).

After correcting for both the sediments and Moho effects, the Limagne graben does not appear as an outstanding graben feature in the gravity data. Rather, a gravity low of –70 mgal remains for the whole region where volcanic activity has occurred (Stoll et al., 1994). As discussed in detail in connection with the teleseismic investigations, the areas of volcanic activity are strongly related to the areal extent of the teleseismic velocity anomalies. Furthermore, the Bouguer gravity minimum can be compensated directly by the teleseismic low-velocity areas. Stoll et al. (1994) used the 3-dimensional tomography model of the Massif Central by Granet et al. (1994) discussed elsewhere in this paper to constrain a 3-dimensional density model using a linear velocity/density relation for solid rocks. They then calculated the 3-D Bouguer gravity of this model with an interactive computer program to model 3-dimensional density structures. The result is a remarkable fit indicating that no—or only small amounts of—partial melt can be expected under the Limagne graben area. A more detailed investigation

of anomalous crustal effects on the Bouguer gravity field is presently being carried out by Bauer (in prep., 1995).

4.A4.3. Magnetic anomalies

The most prominent magnetic features of the aeromagnetic map are related to volcanic structures (Aubert and Perrier, 1971). From a 3-dimensional inversion of aeromagnetic data covering Mont Dore, Bayer and Cuer (1981) deduce the presence of a deep magnetic source which can be related to an intrusive body in a fractured basement, or to sedimentary formations older than Mont Dore volcanism.

Magnetic anomalies also seem to be associated with the pre-Hercynian and Hercynian border zones (Weber, 1980). The main feature of the aeromagnetic map in the Massif Central is the strong relief associated with the Paleozoic Sillon Houiller fault zone between Clérmont-Ferrand and Aurillac. According to Aubert and Perrier (1971) this strong relief can be associated with a deep magnetic layer which underlies all the local anomalies connected with the volcanic structures. North of the Vichy and Moulins anomalies, the anomalies of the total magnetic field computed for a height of 13 km indicate that the Massif Central extends to the northeast as far as the south of Alsace (Aubert and Perrier, 1971). Comparing gravity and magnetic maps, Aubert and Perrier (1971) point out apparent large structural anomalies in which the difference in values east and west of the Sillon Houiller fault zone, together with some amphibolite–rich areas, are the most prominent features.

4.A4.4. Seismicity

France is in a marginal position in relation to the principal peri-Mediterranean seismic zones, but has nevertheless experienced several destructive earthquakes and many significant shocks. However, the main seismic activity is concentrated near the frontiers, i.e. part of the Pyrenees, Alps and the Rhine *sensu lato*, while for the Massif Central region only little activity is shown in the seismicity maps (Fourniguet et al., 1981). Fourniguet et al. (1981) point out that the seismicity shows no clear alignment of events between the Rhine and the Bresse grabens.

The recent seismicity of the Massif Central has been monitored in detail since 1960 when a modern seismic network was installed at the geophysical observatory of Clérmont-Ferrand. Present earthquake activity is much less than in the Rhinegraben region and seems to be confined to the Limagne graben proper. The dominant seismicity is observed west of the graben in the area of the Chaîne des Puys, while another cluster of activity is observed at the southern end of the graben around Brioude (Dorel, oral comm., 1994, Nicolas et al., 1990). Weak seismicity is also observed in the southern Rhône valley (Nicolas et al., 1990).

4.A4.5. Stress pattern

Blès et al. (1989) have investigated the different stages of brittle deformation of the Massif Central basement and the surrounding sedimentary cover from the end of the Hercynian orogeny to the end of the Tertiary, using structural analysis and particularly microtectonic methods. The prevailing compressional tectonic regime of the Stephanian was followed by a series of extensional periods at Permian-Triassic, Early and Middle Jurassic, and Late Jurassic to Cretaceous times. Normal faults which formed during these extensional periods have strongly influenced the distribution of emerging continental areas and sedimentary basins.

From 75 Ma (Campanian) to the Present, the distribution of stresses was controlled by the convergence of Africa and Europe. Blès et al. (1989) distinguish several tectonic episodes in the Massif Central. N-S compression dominated during the Eocene. In the Late-Eocene-Oligocene, general E–W extension was responsible for graben genesis in mainly N–S strike directions synchronous with the formation of the Rhinegraben, and particularly in the center of the Massif and at its eastern and southeastern borders (Müller et al., 1992). Finally, during the Alpine orogeny and during the evolution of the Jura thrust belt at the end of the Miocene, compression varying from NW–SE to E–W prevailed in the northern and southern parts of the Massif.

The deformation of Neogene and Quaternary deposits in the Rhône valley proves that the Middle to Upper Miocene molasse of the east side of the Rhône valley was affected by E–W compression, but that Pliocene sands and clays show only small normal faults caused by E–W to NE–SW extension (Blès and Gros, 1991).

Analysis of faults in post-Late Miocene basalt flows indicates a normal faulting stress regime with an S_{Hmin} orientation of N78°E and vertical offsets of Quaternary basalt flows along N–NNW trending faults and ongoing seismicity are signs of some degree of continuing subsidence (Müller et al., 1992). Available focal mechanism data (Nicolas et al., 1990), hydraulic fracturing measurements (Cornet and Burlet, 1992) and over-coring data indicate a combination of normal and strike-slip faulting (Müller et al., 1992).

4.A4.6. Heat flow

The heat flow map of France (Vasseur, 1982) shows a broad maximum (100–110 mWm^{-2}) of elevated heat flow along the European Cenozoic rift system. One high of 110 mWm^{-2} runs along the Bresse graben through northeastern France and may continue into the Landau area of the Rhinegraben. Another high of ~110 mWm^{-2} is indicated in the area of the southern Rhône valley.

The most prominent 110 mWm^{-2} anomaly on the map, however, is observed above the Massif Central proper and is of much larger extent. Compared to a continental average of 64 mWm^{-2}, this anomaly with an average heat flow ~105 ± 13 mWm^{-2} is easily comparable with other tectonic active regions like the Basin and Range province (Lucazeau and Bayer, 1982) and is discussed in detail by Lucazeau and Bayer (1982) and Lucazeau et al. (1984). The authors conclude that the radioactive components of the crust and the mantle cannot account for the entire surface anomaly. By removing the integrated radioactive contribution from the surface heat flow, Lucazeau et al. (1984) obtain a residual anomaly with an amplitude of 25–30 mWm^{-2} involving a smaller area close to the Cenozoic Limagne graben and the adjacent volcanic area. The authors interpret this mantle heat flow anomaly as a transient component related to a mantle diapir ascending beneath the Massif Central since the Oligocene, a result which is in good agreement with the results and interpretation of recent teleseismic studies (Granet et al., 1994, Stoll et al., 1994). Lucazeau et al. (1984) describe a kinematic model for a thermal diapir in the mantle which has a width of 40 km, starting at a depth of 150 km and ascending with a velocity of 1 cm per year. For this diapir they assume the following scenario: Before the Oligocene, the lithosphere was stable, as at present in Brittany. During the Oligocene (30 Ma) stretching of the lithosphere initiates a diapiric process. From the Miocene (20 Ma) to the Pliocene (5 Ma), the mantle diapir progressively rises. At the same time, widespread volcanism develops. When the diapir reaches the Moho, the less dense and more rigid crust stops the ascent and causes a lateral extension of the diapir at Moho depth. The resulting pressure at the base of the crust is supposed to be responsible for the crustal doming. According to the teleseismic model of Granet et al. (1994), some component of partial melting must be assumed in order to explain all features of the topography, gravity, teleseismic data, and the geothermal observations.

Consequently, according to Lucazeau et al. (1984), the origin of the high heat flow values in the Massif Central can be explained by a three-component model: (1) The crust of Hercynian type explains a high crustal component of 50–60 mWm^{-2} due to radioactive heat production.(2) Recent Cenozoic activity of the lithosphere is accompanied by the rise of a mantle diapir as described above, resulting in a heat-flow component of 25–30 mWm^{-2}. (3) The remaining part of the heat flow of 35 mWm^{-2} is slightly higher than the heat flow of a typical cratonic mantle (26–28 mWm^{-2}), and may be related to a residual thermal effect associated with the Hercynian orogeny (300 Ma) and/or to different estimations of paleoclimatic effects (Lucazeau et al. (1984).

4.A4.7. Geodetic data

Fourniguet et al. (1981) reviewed the available data and hypotheses and compiled a tectonic map which, in addition to the seismotectonic field, takes into account age and structures of ancient massifs,

and the basement geology of sedimentary basins. The map emphasizes fracturing by indicating the age and direction for the main movement whenever possible. For parts of France, the neotectonic data were completed by comparative studies of the NGF 1885–1895 leveling and the IGN 1963–1969 first-order network elevations. The map shows that the Tertiary troughs (Rhinegraben, Bresse, Limagne) are subsiding although they are not considered to be very active zones.

4.A5. Structure and interpretation

4.A5.1. Introduction

As mentioned above, interpretation of the recently obtained seismic-refraction and teleseismic data has not yet been fully completed, and therefore summarizing publications are still in preparation (e.g., H. Zeyen, A. Hirn, M. Landes, and O. Novak, in preparation; G. Stoll, in preparation). Therefore it does not seem appropriate to construct a transect for the southern part of the European Cenozoic rift system on the basis of the presently available published and unpublished results. However, except for some minor details in the region of the southern Limagne graben, the older Moho contour map compiled by Prodehl et al. (1992; Fig. 4–29) probably will not be changed very much compared with the new Moho map being compiled by Bauer (Fig. 4–7; Bauer, in prep., 1995).

4.A5.2. Near-surface rift structures

For the graben areas many borehole data are available which have been used to compile thickness contour maps for various paleogeographic times (Boigk and Schöneich, 1974). For the Bresse graben, descriptions accompanying the corresponding geological maps of France (e.g., 1:50,000-scale quadrangles for Lons-Le-Saunier and for Châlon-sur-Saône) give many details on boreholes (for references see also Boigk and Schöneich, 1974). The ECORS line through the Bresse graben (Bois et al., 1991, Fig. 4) demonstrates the strong asymmetry of the graben fill, which reaches maximum values of about 5 km and shows a rather transparent crystalline upper crust whose thickness decreases from ~18 km under the edge of the Massif Central in the west to 13 km under the basin center. A similar asymmetry is also shown in the contour map of basement depths of the Limagne graben which Morange et al. (1971) compiled from borehole data, shallow seismic-reflection results, and a Bouguer gravity map (using an average density of 2.3 g/cm^3). Depths to basement are generally shallow and do not exceed 2.5 km. The thickness of the upper crust here is about 16–19 km (Hirn and Perrier, 1974), and the authors point out that velocity reductions may only be minor if they exist at all.

The sedimentary basin of the southern Rhône Valley seems to differ from the other graben sections. In the center of the Rhône depression, the cross sections of Sapin and Hirn (1974) show sedimentary layers with up to 10 km thickness. Thicknesses and mean velocities of the sedimentary sequences were taken from stratigraphic indications in boreholes, deep seismic logging, geophysical prospecting results, and Pg-arrival delays. Sapin and Hirn (1974) point out that the basement of the southern Rhône Valley is much more depressed relative to its flanks than for the Limagne and the Rhinegrabens. The underlying upper crystalline crustal layer with velocities varying regionally between 6.07 and 6.12 km/s was identified in the western part of the southern Rhône Valley. Its thickness ranges from 8 km near the graben axis, where it is overlain by 8–10 km sediments, to more than 20 km under the adjacent Massif Central.

4.A5.3. Deep crust

Various Moho maps, published for different parts of the European Cenozoic rift system and adjacent areas (Edel et al., 1975, Egloff, 1979, Hirn, 1976, Zeis, 1988, Zeis et al., 1990), have been merged into a joint Moho depth contour map (Prodehl et al., 1992, Fig. 3, reproduced below as Fig. 4–29). For the southern Rhône Valley and the Rhinegraben, crustal thinning of about 20% is seen in comparison to the surrounding areas (Edel et al., 1975, Hirn, 1976), while the new data indicate less thinning for the Limagne graben (<15%) and no thinning at all for the Chaîne des Puys. For the northern Rhône and

Bresse graben system, the seismic data indicate a reduction in crustal thickness of only 10% in comparison with the structure beneath the flanking plateau de Langres in the west and the Swiss Jura Mountains in the east (Michel, 1978). The crustal thickness shown in this map for the Limagne graben and its surroundings has been confirmed by new data obtained in 1992. Under the central Limagne graben a decrease in crustal thickness has been identified by Landes (Landes, 1994; Zeyen et al., 1994). However, beyond the southern end of the Limagne graben, a more rapid increase of crustal thickness to near 30 km has been found (Novak, 1993; Zeyen et al., 1994), as indicated in the new Moho contour map for the Massif Central (Fig. 4–7; Bauer, in prep., 1995). Also, the formerly assumed thinning of the crust west of the volcanic areas of the Chaîne des Puys, Mont Dore, Cézallier and Cantal could not be confirmed by the new data set.

Under the southern Rhône valley the depth to Moho, normally about 30 km, is partly reduced to 24–25 km. Considering the different tectonic development, it is not surprising that the structure underneath the flanks to the west and to the east differs considerably. Underneath the southern Rhône depression, the total crustal thickness is reduced to 24–25 km and also the intermediate boundary between upper and lower crust rises towards the center of the valley, overlain by a sedimentary cover nearly 10-km-thick. The Moho dips gently from the Rhône valley to the west to about 30 km depth under the Massif Central and more rapidly to the east towards the Alps (Hirn, 1976; Sapin and Hirn, 1974).

4.A5.4. Upper mantle

Perrier and Ruegg (1973) have summarized their results in an east-west cross section (Fig. 4–5). "Normal" uppermost mantle immediately beneath the Moho, with velocities ~8 km/s, is present in the west under the Limousin and Millevaches areas as well as east of the Bassin du Forez, but evidently disappears in between. Another interesting feature is the low-velocity subcrustal lithosphere which appears as an inversion only where "normal" upper mantle material is present. According to Perrier and Ruegg (1973), a high velocity layer of 8.4 km/s rises to depths of less than 50 km under the Limagne graben, and resembles the high velocities found by Ansorge et al. (1979) beneath the Rhinegraben area at depths below 40 km.

The anomalously low upper-mantle velocities seen in the earlier investigations are only partly confirmed where the Limagne graben proper is clearly expressed as a depression, but only if the observed apparent velocity of 7.4 km/s on the 1992 northern profile is interpreted as a true velocity—in contrast to the interpretation by Landes (1994) and Zeyen et al. (1994). Normal crustal thickness near 30 km and upper-mantle velocities typical for undisturbed Variscan crust are evidently not affected by the young volcanic activity and prevail near the termination of the Limagne graben.

Interpretation of the recent teleseismic data reveals large velocity differences of almost 3–4% between undisturbed Hercynian areas and the tectonically reactivated areas of the Limagne graben and surrounding young volcanic zones (Fig. 4–8). The upper two layers of the teleseismic model down to 60 km depth show two low-velocity zones beneath the main volcanic complexes. In contrast, between 60 and 180 km depth, the entire south central part of the Massif Central is underlain by an approximately –3% broad low-velocity structure which is interpreted by Granet et al. (1994) as a plume-type structure in a cooling stage. According to Granet et al. (1994), the thickness of the lithosphere is limited to about 70–80 km. This is consistent with the lithospheric thickness proposed by Babuska and Plomerova (1992). The position of the anomalous low-velocity regions in the lower lithosphere beneath the volcanic areas is supported by the Bouguer gravity data. Stoll et al. (1994) compare the seismic

Fig. 4–9. Map of central Europe with simplified geology and location of recent seismic surveys. Base map from Aichroth et al. (1992). Key: EGT = European Geotraverse refraction line (x = shotpoints E to K), 1A ... 9S = DEKORP seismic-reflection lines. Other seismic-reflection lines: S = Black Forest, U = Urach geothermal area, KTB = German continental deep drillhole (Kontinentale Tief-Bohrung). Geographic areas: EI = Eifel, HU = Hunsrück, KR = Kraichgau, LG = Leine graben, OD = Odenwald, PF = Pfälzerwald, RH = Rhön, SP = Spessart, TA = Taunus, VO = Vogelsberg, WE = Westerwald.

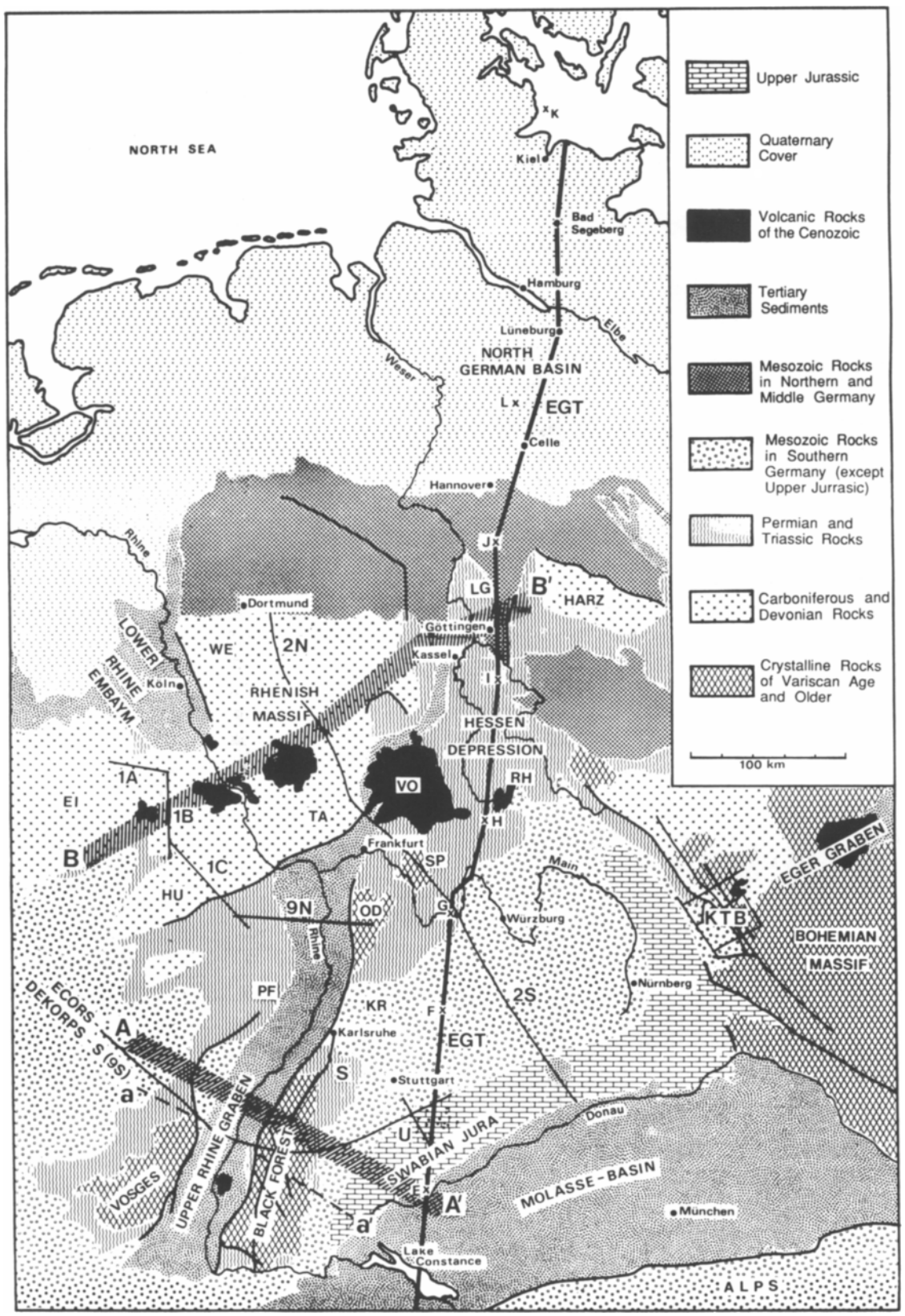
NORTH SEA
Kiel
K
Bad Segeberg
Hamburg
Lüneburg
Elbe
Weser
NORTH GERMAN BASIN
L
EGT
Celle
Hannover
J
Rhine
LG
B'
HARZ
Dortmund
Göttingen
Kassel
I
WE
2N
LOWER RHINE EMBAYM
Köln
RHENISH MASSIF
HESSEN DEPRESSION
VO
RH
H
1A
EI
1B
TA
B
1C
Frankfurt
SP
Main
EGER GRABEN
HU
9N
OD
G
Würzburg
KTB
BOHEMIAN MASSIF
Rhine
PF
KR
2S
Nürnberg
ECORS - DEKORPS
A
F
Karlsruhe
EGT
S
Stuttgart
a
U
Donau
SWABIAN JURA
UPPER RHINE GRABEN
BLACK FOREST
VOSGES
E
A'
MOLASSE-BASIN
a'
München
Lake Constance
ALPS
Upper Jurassic
Quaternary Cover
Volcanic Rocks of the Cenozoic
Tertiary Sediments
Mesozoic Rocks in Northern and Middle Germany
Mesozoic Rocks in Southern Germany (except Upper Jurrasic)
Permian and Triassic Rocks
Carboniferous and Devonian Rocks
Crystalline Rocks of Variscan Age and Older
100 km

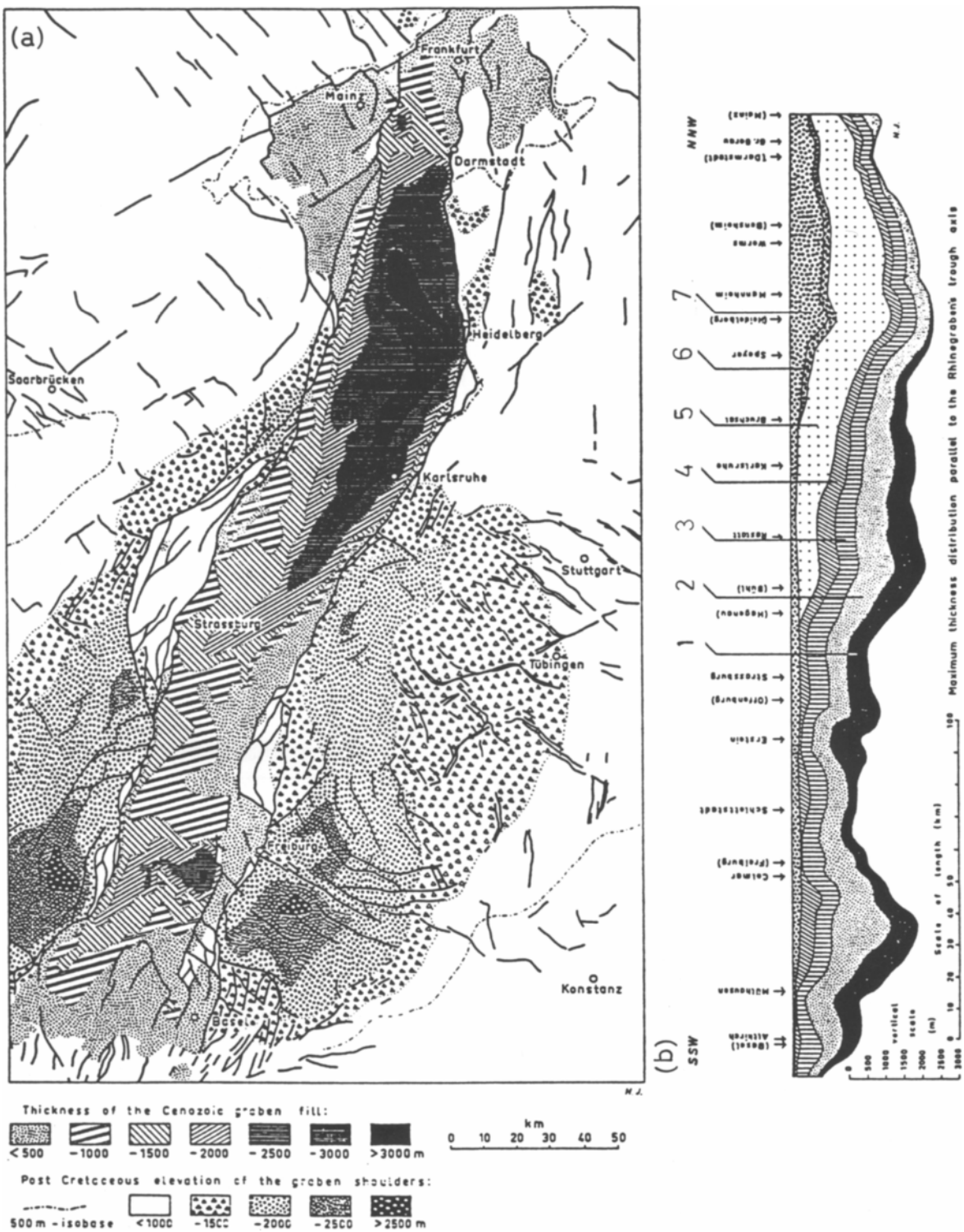
(a)
Frankfurt
Mainz
Darmstadt
Heidelberg
Saarbrücken
Karlsruhe
Stuttgart
Strasbourg
Tübingen
Freiburg
Konstanz
Basel
(b)
NNW
SSW
Maximum thickness distribution parallel to the Rhinegraben's trough axis
Thickness of the Cenozoic graben fill:
< 500
- 1000
- 1500
- 2000
- 2500
- 3000
> 3000 m
km
0 10 20 30 40 50
Post Cretaceous elevation of the graben shoulders:
500 m - isobase
< 1000
- 1500
- 2000
- 2500
> 2500 m

tomography image directly with the observed Bouguer gravity anomalies and conclude that no or only a small amount of partial melt in the mantle beneath the Limagne graben and its surroundings is needed to match the amplitudes of the Bouguer anomaly field with the modeled velocity variations.

4.B. The Rhinegraben

4.B3. Geologic information

4.B3.1. Introduction

The most conspicuous segment of the European Cenozoic rift system is the Rhinegraben in southwestern Germany (Fig. 4–1 and 4–9) which extends from Basel in northwestern Switzerland to Frankfurt. The axis of the Rhinegraben is roughly oriented in a north-northeasterly direction. The length of the graben between Basel and Frankfurt amounts to approximately 310 km, while its width averages 36 km. In its southern part, the Rhinegraben is bordered by the Vosges mountains in the west and by the Black Forest in the east. The rift flanks are less elevated in the central part (Saverne and Kraichgau regions), whereas to the north (the Pfälzerwald in the west and the Odenwald in the east) they again form higher shoulders (Fig. 4–10a).

4.B3.2. Sedimentary record

The upper crust of the modern-day Rhinegraben area is composed of three different units: the Hercynian (Variscan) basement, the superimposed Mesozoic cover, and the Cenozoic sedimentary fill at the top. The Hercynian basement is exposed by erosion in the Vosges mountains, the Black Forest, the Odenwald, and parts of the Pfälzerwald. It consists of Precambrian gneisses, folded Paleozoic sediments, and granites as well as volcanic rocks mostly of Carboniferous age. Locally, parts of the Lower Permian are folded.

The general strike of the fold axes and the intrusive masses follows a northeasterly (Hercynian) direction oblique to the axis of the Rhinegraben. In the north, near Frankfurt, the visible Rhinegraben structure is truncated by the Hunsrück-Taunus fault zone, active since Paleozoic times, while in the south, near Basel, the graben proper is offset by an east-west trending fault associated with a canyon-like trough filled with Upper Paleozoic sediments. Parallel to and accompanying the young north-northeasterly oriented border faults of the graben, there are zones of blasto-mylonites, granitic dikes, fissure intrusions and shear zones. Most of these lineaments have been subjected to left-lateral strike-slip movements. According to Edel and Fluck (1989), the present picture of the Rhenish Shield basement, seen in outcrops and boreholes in the Rhinegraben area, is mainly the result of late Visean-early Namurian structural features and is represented by a linear arrangement of magmatic bodies and the distribution of strike-slip and thrust faults.

Since Upper Permian time, the cratonic basement has remained stable, but underwent uniform epeirogenic subsidence with subsequent sedimentary depositions. Based on published seismic data, Edel (1975) has compiled a depth contour map of the Hercynian basement for the southern Rhinegraben. The distribution of Triassic and Lower Jurassic strata indicates a maximum thickness of about 1.5 km for the entire Mesozoic cover (Fig. 4–10b), but does not show any relation to the future graben structure. The Mesozoic sedimentary units encompass all series ranging from Upper Permian to Jurassic. This formation is not folded, but shows signs of intensive dislocations by vertical movements, flexures, and faulting. Boigk and Schöneich (1970) have compiled contour maps of distribution and thickness of the various Mesozoic layers for the Rhinegraben area and a subsequent publication by the same authors (Boigk and Schöneich, 1974) extends these paleo-

Fig. 4–10. (a) Thickness distribution of sedimentary fill of the Rhinegraben and contours of simultaneous flank uplift (from Illies, 1974b, Fig. 1). (b) Cross section of the Rhinegraben showing its sedimentary fill (from Illies, 1974b, fig. 2). Stratigraphic key: 1 = Lymnaea marls, 2 = Pechelbronn beds, 3 = Grey beds, 4 = Niederroedern beds, 5 = Aquitanium, 6 = Upper Miocene, 7 = Plio-Pleistocene.

geographic contour maps from the Rhinegraben through the Bresse-Rhône graben areas to the Mediterranean Sea.

The uppermost layer is the filled sedimentary trough of the Rhinegraben which comprises a temporal sequence spanning the period from Middle Eocene to Quaternary. For the southern part of the graben, Doebl (1970) has published detailed isopach maps and an isobath contour map of the base of the Tertiary. The isobath map was subsequently redrawn for the entire Rhinegraben (Doebl and Olbrecht, 1974). Development of the trough started with irregular flat depressions in Lower to Middle Eocene time. Initial syn-rift deposits consist of lacustrine shales and carbonatites and fringing clastics, followed by an evaporitic sequence (Ziegler, 1992). Stronger depressions followed in the Upper Eocene, particularly in the south. During latest Eocene and early Oligocene, marine incursions reached the Rhinegraben from the West Alpine foreland basin (e.g. Sittler, 1969; Doebl and Teichmüller, 1979).

During the Tertiary the area of greatest depression migrated gradually northward to the area around Mannheim (Figs. 4–10b and 4–11). After a break in Miocene times, the deepening process continued and is probably still active today. During the Oligocene, rifting reached the Rhenish Massif. This led to the development of a narrow sea-way linking the Alpine foreland basin with the Northwest European basin via the Rhine and Leine grabens (Vinken, 1988). These marine connections remained intermittently open until the late Oligocene when brackish conditions were established in the Rhinegraben. Uplift of the southern Rhinegraben-Vosges-Black Forest dome started during the late middle Miocene (Laubscher, 1987). At about this time, the southern parts of the Rhinegraben ceased to subside (Villemin and Coletta, 1990). In contrast, the northern parts of the Rhinegraben continued to subside during the Miocene, resulting in a deposition of up to 1500 m of mainly shales and sands (Illies, 1974a, Sittler, 1969, von Eller and Sittler, 1974, Roll, 1979). During the Pliocene and Pleistocene, further uplift of the Vosges and the Black Forest flanks was paralleled by slow intermittent subsidence of the southern Rhinegraben, resulting in a relatively thin cover of the Oligocene sediments by Quaternary gravels. The northern parts of the graben continued to subside and Pliocene-Pleistocene deposits here reach thicknesses up to 1000 m (Ziegler, 1992). In total, since Eocene times the graben has been filled with nearly 19,000 km^3 of sediments (Roll, 1979). Most of these sediments have been derived from the denudation of the graben flanks the volume of which has been estimated by Roll to amount to ~27,000 km^3.

4.B3.3. Igneous activity

Rift valley volcanism started in the Rhinegraben area as early as 80 Ma with pipes, dikes, necks, diatremes, and occasional flows, which lasted until 13 Ma (Fig. 4–2). The volcanics erupted almost exclusively along faults in the highlands bordering the graben area. With the exception of the Kaiserstuhl which lies on the intersection of the north-south-striking main fault and the northeast-southwest-striking Bonndorf graben fault system, the main graben fault is free of volcanics (Lippolt et al., 1974). The Miocene Kaiserstuhl complex is the only area with shallow-level fractionation of the graben-related volcanism (Keller, 1990). To the east, southeast of Stuttgart (Fig. 4–2), the so-called Swabian volcano (Geyer and Gwinner, 1968, Mäussnest, 1974a) has perforated the Mesozoic cover with more than 300 volcanic conduits between 16–11 Ma, while numerous eruptions of the Hegau, west of Lake Constance (Fig. 4–2), covered the time period between 15 and 7 Ma and produced some highly visible, but deeply eroded, volcanic edifices (Geyer and Gwinner, 1968, Schreiner, 1984). The nearest major volcanic eruptions to the north start again in the Vogelsberg which is already part of the Hessen depression (to be described in the next section). The Tertiary volcanism of the Rhinegraben area is dominated by highly undersaturated primitive magmas of the alkali-basaltic series. Olivine-melilitites and olivine-nephelinites are primary compositions. They likely originated at ~100 km depth in a garnet-lherzolite mantle. Degrees of partial melting are very low. According to geochemical and isotopic criteria, asthenospheric mantle is the most likely source of these magmas (Keller, 1990). Between 16 and 8 Ma melilite-ankaratrite and phonolites predominate in the Kaiserstuhl and Hegau (Lippolt et al., 1974).

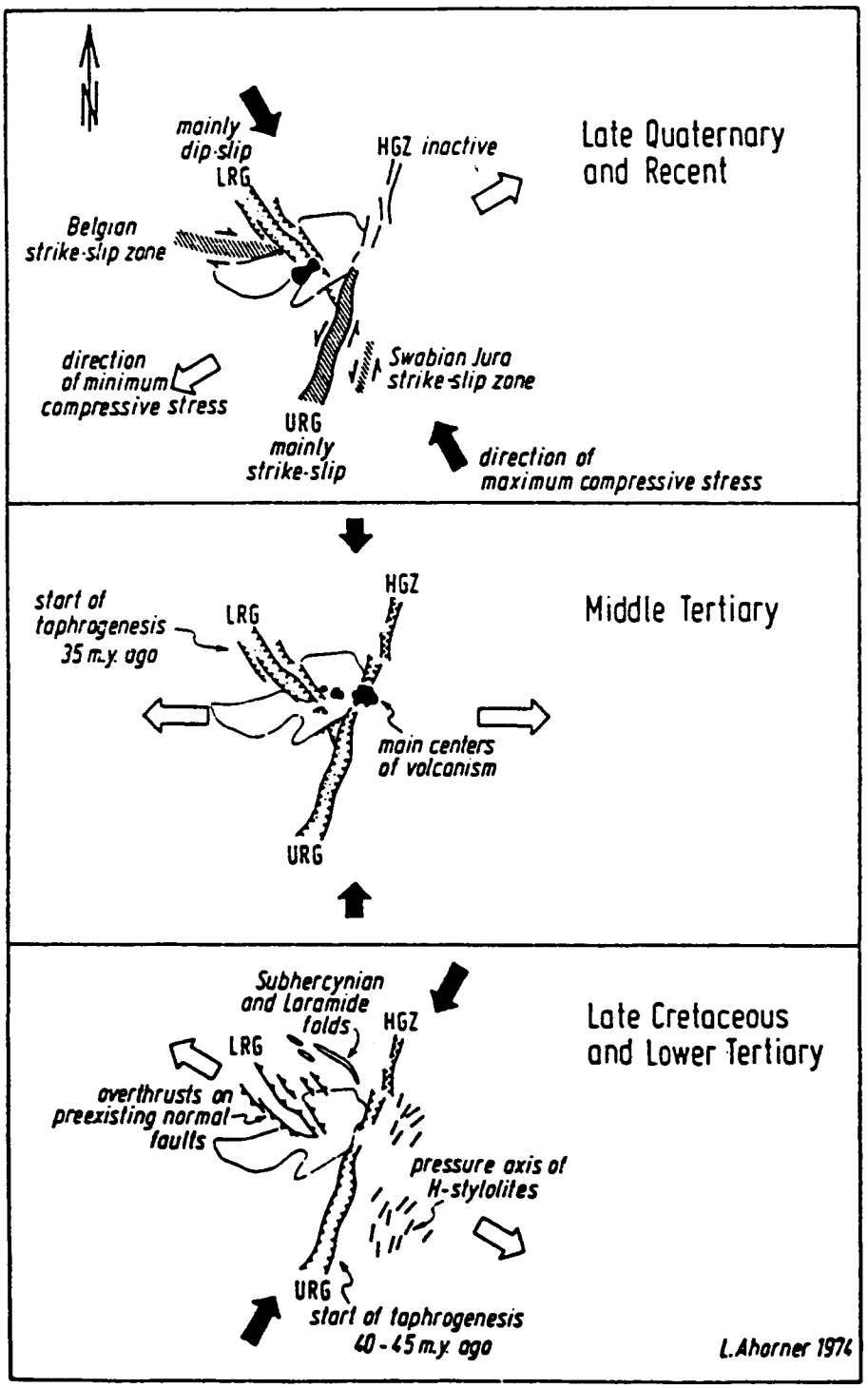

Fig. 4–11. Rotating stress field and the tectonic evolution of the Rhinegraben system showing stress field at 40 Ma, 20 Ma, and Recent (from Illies, 1974c, fig. 2).

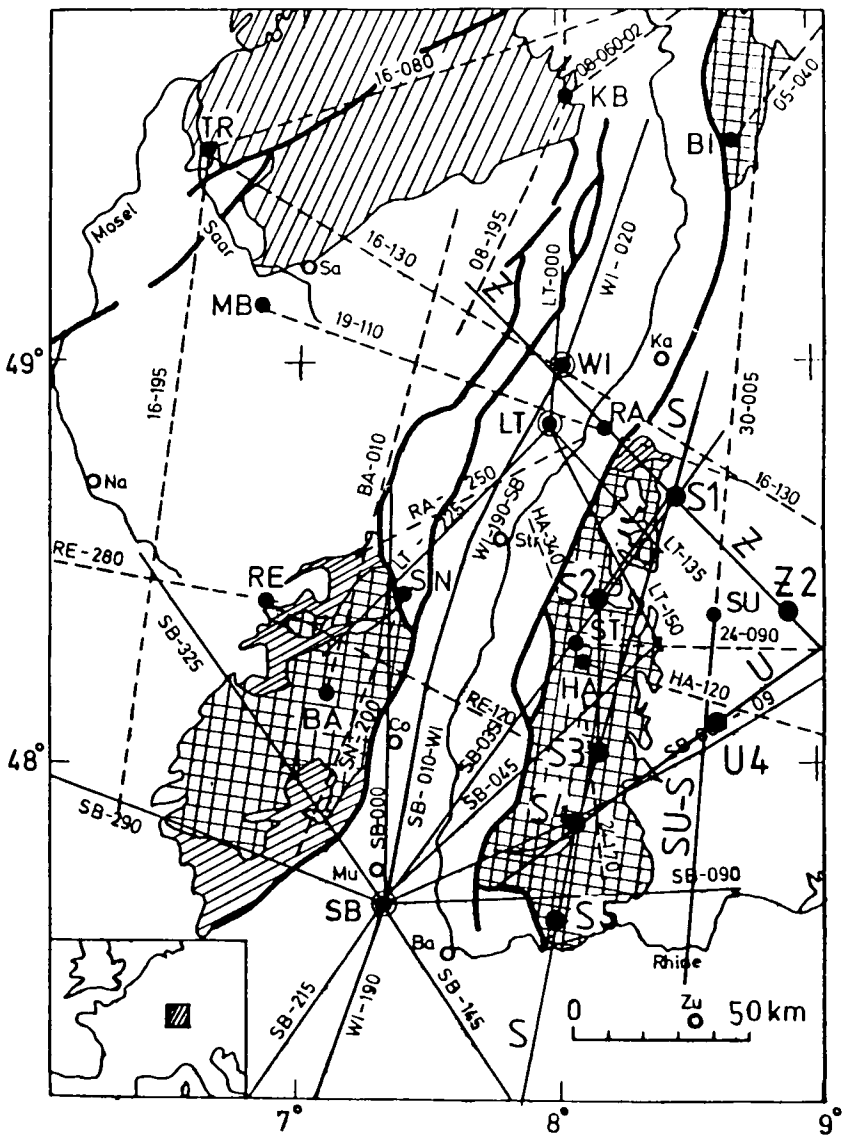

Fig. 4–12. Location map of seismic-refraction profiles in the central and southern Rhinegraben before 1987 (extended from Edel et al., 1975, fig. 1).

4.B3.4. Xenolith studies

Crustal xenoliths were found in the Urach and Hegau volcanic areas, but not in the Rhinegraben proper. They include medium-to-high-grade metasedimentary and felsic-to-mafic meta-igneous rocks. Also present are pyroxenites and hornblendites (Sachs, 1988). A model crustal profile has been proposed by Mengel et al. (1991) based on calculated or measured P-wave velocities of xenoliths and depth-V_P relationships, and has been superimposed on a seismic cross section along the European Geotraverse (Franke et al., 1990b, Prodehl and Aichroth, 1992). The resulting crustal model

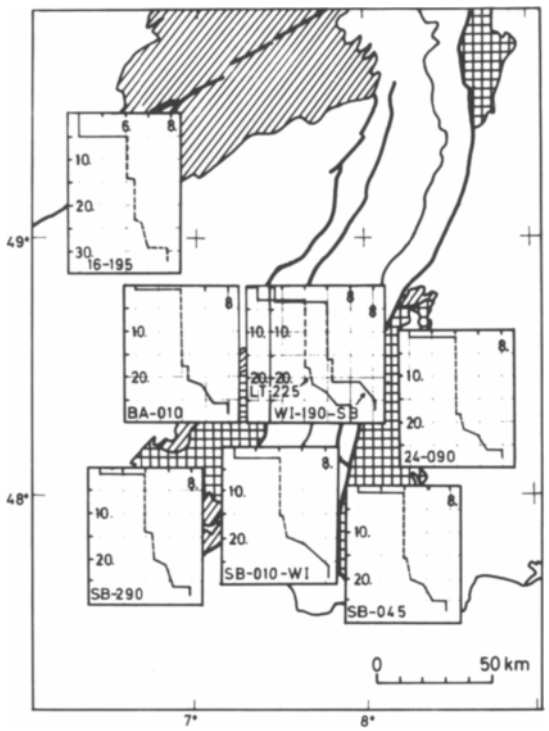

Fig. 4–13. Map of the central and southern Rhinegraben showing velocity-depth distributions for the corresponding profiles (for location see Fig. 4–12). The velocity-depth functions are representative for the area in which they have been plotted (from Edel et al., 1975, fig. 15).

beneath the Hegau and Urach areas consists largely of metasediments with subordinate felsic meta-igneous rocks. As most of the metasedimentary samples seem to be depleted in felsic components, the authors suggest intracrustal differentiation by partial melting. The mafic and ultramafic xenoliths of both areas differ in their mineralogy and chemical composition from the samples found in the Rhenish Massif area and thus seem to reflect a contrasting style of crustal evolution. Glahn et al. (1992) discuss in detail the petrological composition of crust and upper mantle of the Urach area in a joint interpretation of their teleseismic and xenolith investigations.

4.B4. Geophysical surveys and results

4.B4.1. Seismic studies

The first evidence for an anomalously thin crust beneath the southern Rhinegraben was indicated by Rothé and Peterschmitt (1950) by analysis of seismic records from large explosions near Haslach in the central Black Forest. However, a systematic geophysical investigation of the Rhinegraben rift system was not started until 1965 when an international program was initiated (Rothé and Sauer, 1967).

Synoptic interpretations of all available seismic-refraction measurements up to 1972 were based primarily on quarry blast recordings supplemented by deep crustal reflection observations (Schulz, 1957;

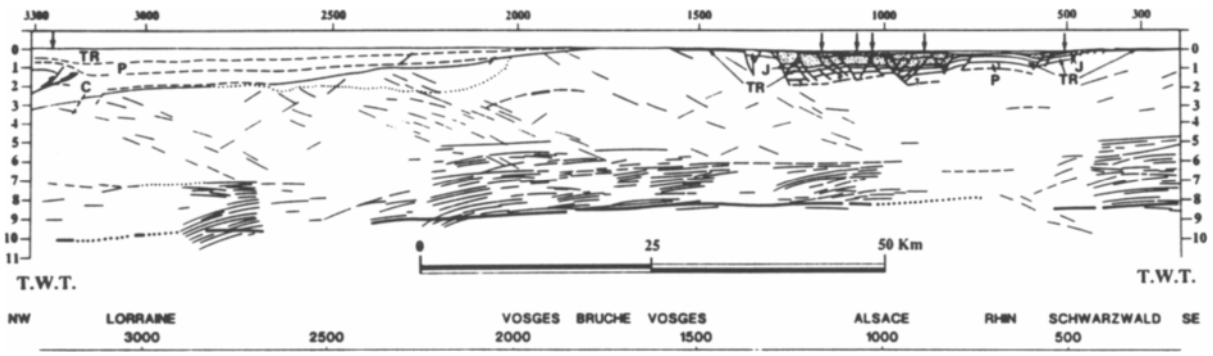

Fig. 4–14. Seismic-reflection line drawing of the ECORS/DEKORP-S line (from Brun et al., 1991). For location, see 9S in Figure 4–9.

Demnati and Dohr, 1965; Dohr, 1967, 1970), and led to the following results (Ansorge et al., 1970; Meissner et al., 1970; Mueller, 1970; Mueller et al., 1969, 1973):

(1) A low-velocity zone was found in the upper part of the crust under the western flank of the Rhinegraben which widens considerably as the center of the graben is approached.

(2) The presence of an intermediate high-velocity layer (also termed "cushion") was postulated in the depth range of the crust-mantle transition whose dimensions, however, could not be delineated with data available at that time.

(3) The width of the Rhinegraben rift system, i.e. of the "modified" lithospheric structure beneath the rift, was estimated to be about 200 km. In comparison, the morphological graben which is offset from the center of the rift system has an average width of only 36 km.

(4) The most conspicuous feature of the rift was its asymmetry, both with regard to the sedimentary infill of the graben and the crustal structure, indicating that the rifting process must have started at the eastern margin of the graben. It seemed as if the asymmetry reached to depths of 18 to 20 km.

(5) The depth of earthquake foci determined by macro- and microseismic methods did not exceed 12 km beneath the graben proper, while under the eastern flank of the rift, focal depths of 6 to 8 km seemed to prevail. These observations confirmed the above-mentioned asymmetry and would place the hypocenters close to the "roof" of the crustal low-velocity zone.

(6) Prominent echoes arriving at about 7.0 to 9.5 seconds two-way traveltime (TWT) were identified in crustal reflection work, providing evidence for a lamellar structure in the depth interval between about 18–20 and 25 km, i.e. within the lower crust immediately below the crustal low-velocity zone.

After this exploratory phase, the first specially designed seismic-refraction experiment was performed in the southern part of the Rhinegraben in 1972 (Rhinegraben Research Group, 1974; Edel et al., 1975; Prodehl et al., 1976).

The most important explosion source for the 1972 seismic-refraction experiment was a shotpoint near Steinbrunn (SB) at the southern end of the Rhinegraben near Basel (Figs. 4–2 and 4–12), where a series of borehole shots was observed fan-like along various profiles into the Rhinegraben, into its eastern and western flanks, and along the Franco-Swiss Jura towards the southwest (Egloff, 1979).

In 1984, within the framework of the Deep Continental Drilling Program (KTB), a second very detailed seismic survey was carried out in the Black Forest along a north-south line using seismic-refraction as well as reflection techniques (Fuchs et al., 1987; Gajewski and Prodehl, 1987; Gajewski, 1989; Lüschen et al., 1987, 1989).

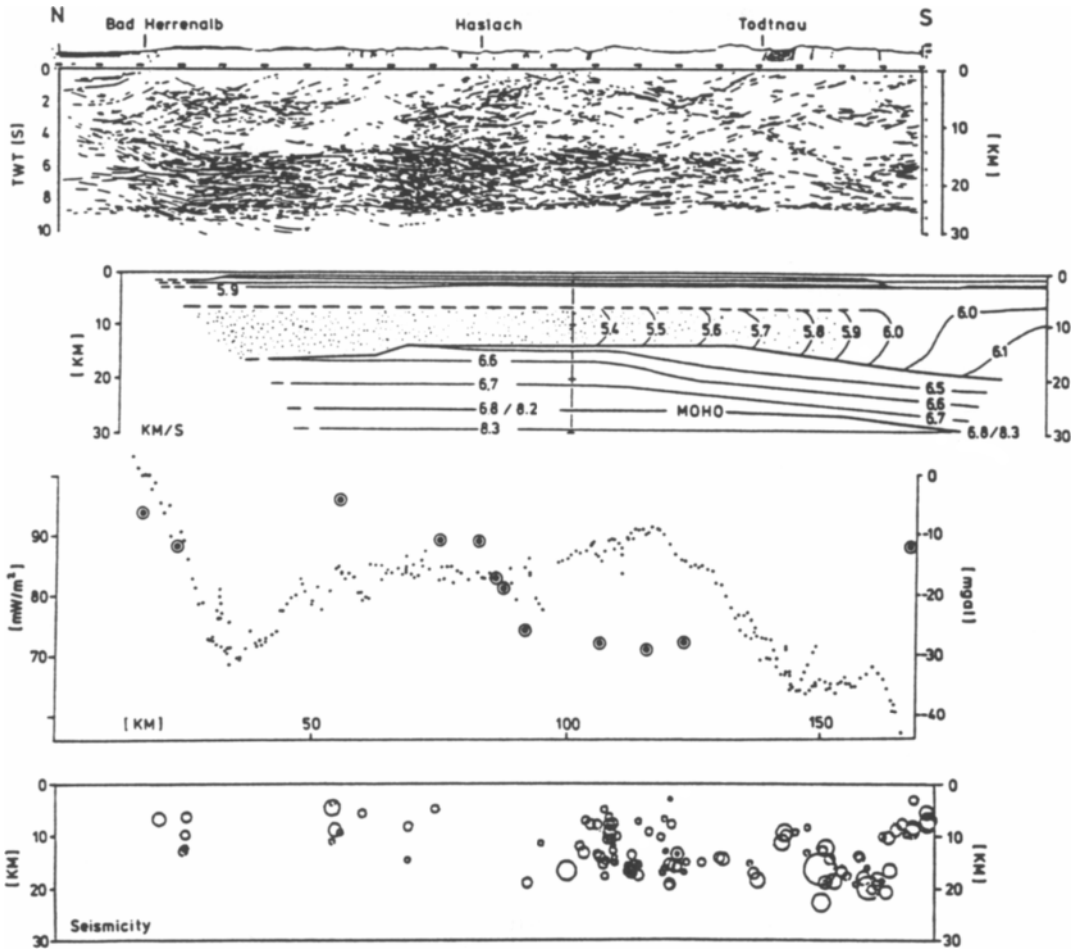

Fig. 4–15. Crustal model of the Black Forest and Swiss Jura, derived from a compilation of geophysical data (from Lüschen et al., 1987, 1989). From top to bottom: structural data from a Vibroseis seismic-reflection survey, velocity model, Bouguer gravity anomaly (small dots) and heat flow (large dots), seismicity distribution (magnitudes between 1 and 5, projected within a strip of ±10 km width). The transect of Figure 4–17 crosses this line near Haslach.

In the northern part of the graben area, no modern seismic-refraction surveys have been completed, and for all compilations of crustal structure, only the older quarry blast observations recorded prior to 1972 are available (Meissner et al., 1970, 1976b; Meissner and Vetter, 1974).

High-resolution seismic-reflection lines through the Rhinegraben were enabled by a cooperative project of ECORS and DEKORP. In the fall of 1988, two ECORS-DEKORP seismic-reflection lines (9S and 9N in Figs. 4–2 and 4–9) were recorded across the Rhinegraben (see Fig. 4–14; Brun et al., 1991, 1992, Gutscher, 1991, Wenzel et al., 1991). Two short seismic-reflection lines were added in 1990 and 1991 in the transition from the Black Forest to the Dinkelberg block at the southern end of the Rhinegraben, NE of Basel (Echtler et al., 1994).

Using existing data recorded by the permanent local network stations that were installed around the Rhinegraben by the Universities of Karlsruhe in Germany, Strasbourg in France, and Zürich in Switzerland, in order to study the seismicity of the gra-

ben (see section 4.B4.4 – Seismicity), various seismic tomography studies have been made (Wenderoth, 1978, Raikes and Bonjer, 1983, Koch, 1993a, b). However, because of the small number and the wide spacing of the available permanent stations, these studies lack the details that have been achieved by the specially arranged teleseismic surveys using portable equipment described in the following paragraphs.

Within the graben proper, the location of the ECORS-DEKORP line coincides with the location of a teleseismic cross section through the southern Rhinegraben area (Fig. 4–9) which was installed in 1988 and 1989. The array consisted of a dense network of short-period stations that covered essentially two parallel lines of about 200 km length across the southern Rhinegraben between Strasbourg and the Kaiserstuhl volcano (Glahn and Granet, 1992, Glahn et al., 1993). A depth range of about 100 km was achieved.

The area of the Swabian Volcano to the east of the Rhinegraben was traversed by several seismic surveys, most of which, however, did not reach into the Rhinegraben proper. In 1978, the Urach geothermal area was the goal of a multidisciplinary research effort (Hänel, 1982) which also comprised detailed seismic reflection (Bartelsen et al., 1982), refraction (Jentsch et al, 1982, Gajewski and Prodehl, 1985) and teleseismic (Glahn et al., 1992) investigations. The detailed Black Forest investigation of 1984 (Gajewski and Prodehl, 1987) also comprised two lines from the Rhinegraben to the east: (1) a NW–SE line through the northern Black Forest and Hohenzollerngraben into the Molasse Basin, and (2) a SW–NE-line through the southern Black Forest and along the Swabian Jura (Gajewski et al., 1987). The area was further traversed by the European Geotraverse (Fig. 4–2 and 4–9; Aichroth et al., 1992, Prodehl and Aichroth, 1992). Finally, the teleseismic survey in the Urach geothermal area recorded more than 300 teleseismic events (Glahn et al., 1992) achieving a depth penetration of about 70 km using a mobile array of digital short-period stations between 1985 and 1987.

The most prominent phase seen in the seismic-refraction data is interpreted as P_MP, i.e. the wide-angle reflection from the crust-mantle boundary, also known as phase P_R by Ansorge et al. (1970), phase 1 by Edel et al. (1975) or phase c by Gajewski and Prodehl (1987). Another strong reflected phase, referred to as phase P_C by Ansorge et al. (1970), phase 2 by Edel et al. (1975) and phase b by Gajewski and Prodehl (1985, 1987), is also observed on many profiles. It is identified as a wide-angle reflection from the top of the lower crust or, in the classical terminology, from the top of the Conrad discontinuity, which beneath the Black Forest and the Swabian Volcano, coincides with the bottom of a mid-crustal low-velocity zone. The relative amplitudes of both phases vary systematically. In profiles crossing the flanks of the Rhinegraben or located entirely outside the graben, the P_MP reflection (phase 2) shows the strongest amplitudes and the intermediate reflection (phase 1) is less well developed. Within the graben, phase 2 is dominant and phase 1 is either hidden by the coda of the high-amplitude phase 2 or is too weak to be recognized. As a consequence, in the resulting crustal models (Fig. 4–13), the Moho appears either as a first-order discontinuity (strong phase 1 = P_MP) beneath the flanks, or as a broad transition zone (dominant phase 2) beneath the graben proper.

The most detailed and accurate crustal model pertains to the eastern flank of the southern graben, underneath the Black Forest (Fig. 4–15), based on the combined seismic reflection and refraction survey carried out as pre-site surveys for possible KTB drilling sites. Combined interpretation of refraction and reflection data in the Black Forest has revealed an additional feature of the lower crust: a fine structure showing thin layers of alternating high and low velocities. The possible existence of such a lamination of the lower crust was proposed earlier by Fuchs (1970), Meissner (1967, 1973), and Mueller et al. (1969, 1973), but could only be proven quantitatively with the aid of detailed amplitude-distance observations together with the computational modeling of synthetic seismograms using the reflectivity method (Deichmann and Ansorge, 1983; Sandmeier and Wenzel, 1986; Wenzel et al., 1987). In order to model also lateral changes of the properties of the laminated lower crust, Gajewski and Prodehl (1987) applied the ray method, in which, however, some simplifications had to be introduced.

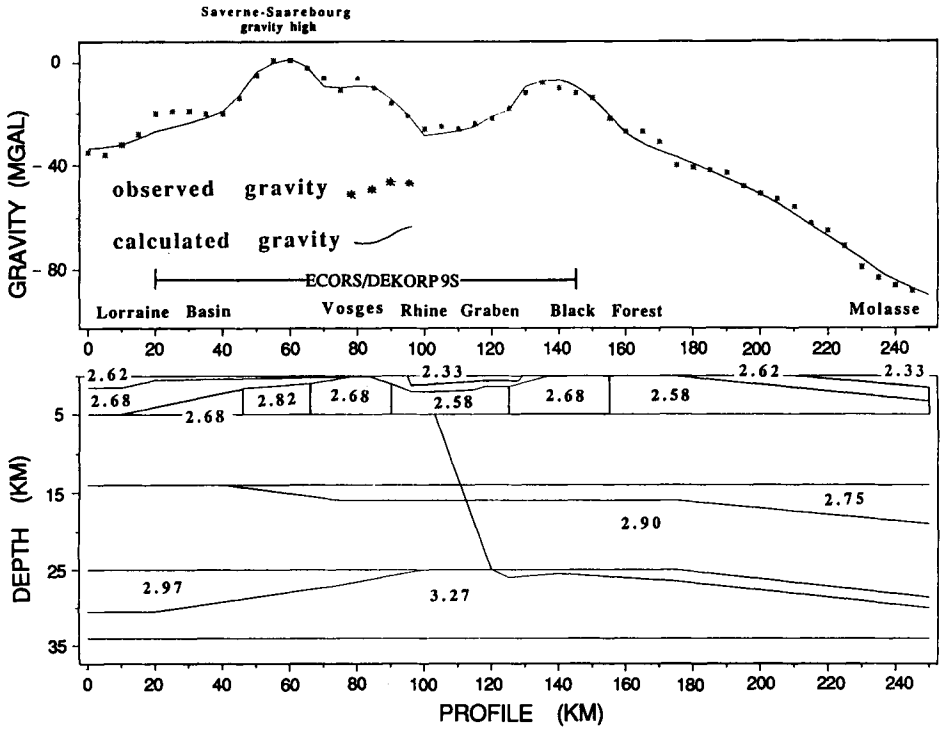

Fig. 4–16. Gravity model along the ECORS/DEKORP-S line (from Prodehl et al., 1992, fig. 7). For location, see 9S in Figure 4–9.

The recent ECORS-DEKORP-S seismic-reflection profile (Fig. 4–14), crossing the southern Rhinegraben (9S in Figs. 4–2 and Fig. 4–9; Brun et al., 1991), shows a sharply defined Moho at the base of a layered lower crust, decreasing in depth from 8.5 s two-way traveltime (TWT) under the Black Forest to 8 s under the Rhinegraben and then progressively descending northwestward to 10 s at the northwestern end of the profile in Lorraine, to the west of the Vosges mountains-Pfälzerwald. Here, as well as under the Black Forest, the highly reflective lower crust is well defined with a 3 s TWT mean thickness which progressively decreases to 2 s TWT and less below the graben, with a somewhat asymmetric shape.

In the northern Rhinegraben (profile DEKORP-ECORS-9N), the thickness of the lower crust decreases from 5.5.s TWT in the Saar-Nahe depression, west of the graben, where a distinct Variscan heritage of thrusting, extension, and rhyolitic volcanism is evident, to 3.5 s TWT in the east beneath the uplifted Odenwald. At the same time the reflection signature changes, indicating in the west a reduced reflectivity between reflections originating from the mid-crustal and the Moho level as compared to a distinctly layered lower crust in the east. The Moho rises from west to east from 10.5s to 8.7 s TWT (Wenzel et al., 1991).

4.B4.2. Gravity

Magnetic and gravimetric data of the Upper Rhenish Shield basement in the Vosges, the Upper Rhine segment of the Rhinegraben, and the Black Forest were correlated by Edel and Fluck (1989) with geological observations on outcrops and in boreholes. The resulting map demonstrates a contrast between a "heavy" and "magnetic" Saxothuringian basement, characterized by Paleozoic units metamorphosed to varying degrees and intruded by Early

Carboniferous basites, and the "lighter" Moldanubian, consisting mainly of gneisses and granites.

Bouguer gravity data provide valuable information on the shallow and deep crustal structure particularly when integrated with data from seismic refraction and reflection surveys (Kahle and Werner, 1980; Setto and Meissner, 1987; Truffert et al., 1990; Wagener and Götze, 1989; Gutscher, 1991; Rousset et al., 1993).

Interpreting the Bouguer gravity map of Germany compiled by Grosse and Conrad (1990), Grosse et al. (1990) attributed the Rhinegraben minimum largely to the Tertiary sedimentary fill of the graben as suggested by the steep gradients. From a detailed Bouguer anomaly map, which was compiled in the context of the ECORS-DEKORP project, Rousset and Bayer (1990) constructed a residual anomaly map by subtracting the effects of the Tertiary graben fill, the Moho depth variations and the deeper mantle anomalies. The resultant map gives a picture of the crustal density variations. It should be noted that in the map of Grosse et al. (1990) additional positive axes are indicated along both flanks of the graben.

Figure 4–16 gives an integrated 250 km long profile which extends from the Lorraine Basin through the Rhinegraben to the Molasse Basin south of Lake Constance, and parallels the ECORS-DEKORP 9S reflection line (Fig. 4–9). This profile shows that the Rhinegraben is marked by a gravity low of about –30 mGal which is flanked by relative highs of –5 mGal in the Vosges and –10 mGal in the Black Forest. Towards the SE, in the Molasse Basin the Bouguer gravity anomaly drops below –80 mGal. The Moho structure was taken from available seismic data. Total crustal thickness is 30 km in the NW below the Lorraine Basin, thins rapidly to 25 km below the Rhinegraben, and increases progressively towards the SE as the Alps are approached, reaching 32 km south of Lake Constance.

In agreement with Grosse et al. (1990) and Rousset and Bayer (1990), the gravity cross section presented in Figure 4–16 does not require a thermal mantle anomaly as was suggested by earlier investigations (Kahle and Werner, 1980). Kahle and Werner interpreted a pronounced Bouguer anomaly of about 100 mgal, which could not be compensated by the Mesozoic sedimentary graben fill, as evidence of a deep-seated thermal anomaly beneath the graben.

Elevated P-wave velocities in the lowermost crust of 6.7–7.4 km/s (Lüschen et al., 1987, Edel et al., 1975), combined with a high Poisson's ratio of 0.25–0.28 (Holbrook et al., 1987, 1988) suggest a predominantly mafic, dense lower crust (2.9–3.0 g/cm^3). The resulting, moderate density contrast at the crust-mantle boundary of 0.3 g/cm^3 provides a good fit with the observed Bouguer values in southwestern Germany for both 2-D and 3-D gravity calculations. Such a small density contrast contradicts the presence of a large, low-density body as previously suggested by Kahle and Werner (1980).

The Lorraine basin gravity minimum is due to a local increase in crustal thickness and the presence of moderately dense Mesozoic and Late Paleozoic sediments. The Saverne-Saarebourg gravity high is interpreted (based on its short wavelength) as being caused by upper crustal crystalline units of an intermediate to mafic composition (e.g., gneisses, granodiorites, diorites, and gabbros), which outcrop locally within the Saxothuringian zone in the Pfälzerwald and in the Odenwald (Edel and Fluck, 1989). The Rhinegraben minimum can be largely explained by the 1.0–1.5 km of Tertiary fill overlying 1 km of Mesozoic pre-rift sediments. However, some contribution from lateral compositional heterogeneities in the crystalline basement is also required, which can be correlated with Variscan granites outcropping in the northern Black Forest and the south-central Vosges.

Rousset et al. (1993) have computed a similar density model along the ECORS-DEKORP-9S line. They emphasize the striking contrast in the upper crust between the dense and shallow structures of Barrandian or Cadomian origin located in the Saxothuringian domain (northwestern part of the seismic line in Lorraine) and the abundant low-density granites in the Moldanubian domain (eastern part of the seismic line in the central Black Forest). Their model also highlights the main seismic results: an uplift of the Moho from 32 km west of, to 25 km beneath, the graben and a thinning and deepening of the denser lower crust. They attribute the thinning of the crust to the time before Cenozoic rifting be-

gan, based on the long-wavelength character of the crustal thinning. In this way, they also explain the 27–29 km depths under the Moldanubian domain of southern Germany (e.g., Gajewski and Prodehl, 1985, 1987; Zeis et al., 1990) with a pre-Tertiary thinning of the Hercynian crust.

4.B4.3. Magnetic anomalies

Edel and Fluck (1989) identified highly magnetic bodies in the northern Vosges as andesites and basalts (Bruche valley) and micro-diorites and diorites (Champ du Feu Massif), and they correlate gabbros and diorites in the Odenwald with a large NE–SW trending magnetic anomaly seen in the aeromagnetic map of Germany north of Mannheim (Eberle, 1973).

During many years of elaborate fieldwork, Mäussnest (1973, 1974a, b) systematically mapped basaltic eruptions on the eastern flank of the Rhinegraben, comprising in particular the volcanic provinces of the Hegau, the Swabian Jura and the Kraichgau. During these investigations various basaltic features hidden under the sedimentary cover (dikes, small volcanoes) had been discovered. In the Black Forest and the Kaiserstuhl area similar fieldwork and their interpretation had been undertaken (e.g., Greiner and Sittig, 1971; Hahn and Pucher, 1982).

The transect of Figure 4–17b shows a profile of aeromagnetic observations across the Rhinegraben. A "pearl-string" of small magnetic anomalies in southern Germany is correlated by Franke et al. (1990b) with the Saxothuringian/Moldanubian boundary. The cross section makes use of a map of aeromagnetic anomalies compiled by Eberle (1973) for western Germany.

4.B4.4. Seismicity

The seismicity of the Rhinegraben has been studied by a network of varying station-density since the mid-1960s and seismicity maps have been prepared spanning various time periods (Bonjer, 1992, Bonjer et al., 1984, 1989, Gelbke, 1978, Wilhelm et al., 1989). In comparison with other continental graben systems, the seismicity of the Rhinegraben is low and varies considerably with time. In the middle section of the graben, between Strasbourg and Karlsruhe, seismic activity is rather moderate. Higher levels of activity are monitored in the northern and southern sections as shown in published seismicity maps and in depth-distribution sections across the Rhinegraben area and along the axes of the Rhinegraben and the Black Forest (Bonjer et al., 1984, Wilhelm et al., 1989, Koch, 1993a, b).

Of particular interest is an east-west variation across the graben area; the number of earthquakes as well as the focal depth increases from west towards east, as can be noted in depth distribution profiles across the graben (Bonjer et al., 1984, Wilhelm et al., 1989, Koch, 1993b). This asymmetry in the seismicity pattern is particularly clear in the southernmost graben. In general, the greatest depth of events is limited to 16 km, but in the Dinkelberg block at the southeastern edge of the Rhinegraben, NE of Basel, and in the adjacent southern Black Forest, particularly deep hypocenters of more than 20 km depth have been determined (Bonjer, 1992, Faber et al., 1994). In the Vosges Mountains and the graben proper, focal depths of 16 km are not exceeded (Bonjer, 1992, Bonjer et al., 1984, 1989, Gelbke, 1978). Also the apparent evidence of seismic gaps of 4–6 km width recognized along the eastern master fault zone has been discussed (Gelbke, 1978, Koch, 1993b).

An exceptionally high level of seismic activity occurs in the area of the Hohenzollerngraben located to the east between the Rhinegraben and the Urach volcano. This area has been the site of relatively strong earthquakes since 1911, which are aligned in an almost N–S direction, oblique to the NW–SE striking graben; the focal mechanisms are of a left-lateral strike-slip mode (Illies, 1982, Schneider, 1971). The earthquake dislocations of the events after 1911, with magnitudes of more than 5, have been estimated to be from 10 to 25 cm (Mälzer, 1988).

4.B4.5. Stress pattern

From stress tensor determinations and investigations of striated microfaults and calcite twin lamellae analyses, Larroque and Laurent (1988) develop a stress field evolution for the southern part of the Rhinegraben from the Eocene to the present. Their model (Larroque and Laurent, 1988, Fig. 18) shows a relatively uniform stress field during the Eocene

with S_{Hmax} approximately N–S which changes to an extensional regime during the Oligocene in the Rhinegraben and its northern branches. Only areas in the southern graben are then still subjected to a compressional regime which could episodically affect infilling in the southern part of the graben. After a period of relative quiescence, a second phase of extension began in early Miocene. In the Miocene, emplacement of the Jura caused a N–S compression in that sector, and heavy sedimentation during the late Oligocene affected only the northern graben. Since the Miocene the regional modern stress field is characterized by a NW to NNW direction of the maximum compressive horizontal principal stress S_{Hmax} oriented N140° (Fig. 4–3), and a left-lateral strike slip faulting regime that was initiated in the Quaternary (Ahorner, 1975, Illies and Greiner, 1978).

Regional compilations of present-day stress indicators in western Europe (Fig. 4–3; Müller et al., 1992, Fig. 11) have outlined a generally uniform maximum compressive horizontal principal stress (S_{Hmax}) orientation of NW–SE direction (Ahorner, 1970, 1975, Illies and Greiner, 1979, Müller et al., 1992). The data obtained in the Rhinegraben show the same trend. The focal mechanism data in the Rhinegraben area indicate a mixture of predominantly strike-slip faulting and normal faulting. All have consistent S_{Hmax} direction of about N150°E, in agreement with the studies of borehole breakouts and hydraulic fracturing in boreholes in the Rhinegraben and its vicinity (Becker et al., 1987, Müller et al., 1992, Plenefisch and Bonjer, 1994).

Fault plane solutions of more than 30 earthquakes (Bonjer et al., 1984) demonstrate that the seismic dislocations take place predominantly as left-lateral strike slip mechanisms in the southern graben area, whereas normal faulting prevails in the north. In the northern graben, Bonjer et al. (1984) have observed that most of the seismic dislocations occur on fault segments striking N30°W whereas in the south a strike of N20°E or N60°W (conjugate direction) is dominant. Furthermore the authors note a clockwise rotation of the principal stress directions from north to south by about 40°.

4.B4.6. Heat flow

Heat flow measurements carried out during the KTB pre-site investigations in the Black Forest range from 70 to 105 mWm^{-2} (Burkhardt et al., 1989, Wilhelm et al., 1989) and also indicate that the flanks of the Rhinegraben are thermally influenced by the taphrogenesis. Compared to the mean heat-flow density of 70 to 81 mWm^{-2} for Germany (Hänel, 1982), values measured in the Rhinegraben range from 70 to 140 mWm^{-2} and indicate the occurrence of significant local thermal anomalies within the rift. These anomalies have widths smaller than 1 km and their intensity increases with depth (Morgan, 1982). Local groundwater circulation certainly contributes significantly to the generation of these anomalies.

Cermak et al. (1991) have compiled all heat flow data measured in western Germany. As most of these values were determined in fairly shallow boreholes of 50–300 m depth, the authors corrected all values for surface topography and for the effect of long-term paleo-climatic changes. The resulting contour map (Cermak et al., 1991, Fig. 2) shows a pronounced heat-flow anomaly of over 100 mWm^{-2} for the Rhinegraben, with an inferred maximum of 120 mWm^{-2} between Karlsruhe and Baden-Baden, and an average of 80–90 mWm^{-2} under the Black Forest and the Swabian Jura to the east.

4.B4.7. Geodetic data

The map of elevation changes (DGK-Arbeitskreis, 1979, Mälzer, 1988, Mälzer and Zippelt, 1986) shows a maximum uplift in the area of the Pfälzerwald, underneath the northwestern shoulder of the Rhinegraben (+ 0.5 mm/yr). Under the northern graben proper and to the east in the Kraichgau region a subsidence is observed which reaches maximum values of –0.8 mm/yr, while the central graben around Karlsruhe is an area of uplift (0.3–0.5 mm/yr). The northern and central Black Forest seems to be a relatively stable block, while the southern Black Forest, south of Badenweiler-Lenzkirch fault zone, may be slightly tilting towards south with subsidences up to 0.5 mm/yr. No data are available for the southwestern Rhinegraben.

A special investigation was carried out in the Hohenzollerngraben. Here, three geodetic test-nets were established, and a preliminary result indicates, for some points, significant displacement vectors up to 4 mm which suggest a relative clockwise rotation against a stabilized field. Also, significant subsidences of 1 mm/yr and greater were observed during a 12 year period which point to recent active vertical kinematics (Mälzer, 1988).

4.B4.8. Electromagnetic studies

Besides seismic methods, electrical resistivity research is a powerful tool to investigate deep crustal and upper-mantle structure. In the Rhinegraben electrical resistivity research started about 20 years ago when electromagnetic methods were still in the early stage of their development. Therefore, some of these early results may be questionable due to poor data quality and/or less sophisticated processing and interpretation methods. Nevertheless, the results of all studies which are available today agree in their general aspects (see, e.g., Wilhelm et al., 1989).

The first magnetotelluric measurement in the Rhinegraben was made by Losecke (1970) at a single site about 20 km north of Karlsruhe. The inferred low-resistivity layer at about 25 km depth, which was widely recognized in the literature as being typical for a rift structure, appeared to be more of an accidental result. Nevertheless, this result was confirmed by subsequent, more detailed magnetotelluric profiles across the Rhinegraben (Scheelke, 1972, 1974), one of which is coincident with the transect in Figure 4–17 discussed below. The final model of the electrical resistivity was obtained by modeling the apparent resistivity and the phases of E- and B-polarizations at periods of 10, 100, and 1000 s at all stations into a 2D-model (Scheelke, 1972, 1974). A very similar resistivity model has been inferred from only electric field measurements (telluric method) by Haak and Reitmayr, 1974). Winter (1974), using the independent geomagnetic depth sounding method along Scheelke's profile 1, derived a model comparable to Scheelke's, resulting in a low-resistivity layer in the crust between 25 and 45 km. Based on the calculation of geomagnetic depth sounding transfer functions, Reitmayr (1975) concluded that this low resistivity "layer" (a conductance of about 400 to 800 S) between 25 and 45 km depths must disappear at a distance about 50 km east of the eastern Rhinegraben border.

A low-resistivity layer between 12 and 15 km depth with a conductance of 650 S has been inferred by Tezkan (1988; see also Berktold, 1989) from a combined interpretation of short-period magnetotellurics and geomagnetic depth sounding data in the Black Forest. He discusses convincingly that this layer cannot continue beneath the Rhinegraben, but seems to be confined to the Black Forest. From a number of 2D-model calculations, Teufel (1986) concludes that this shallow low-resistivity layer should also be limited to a distance about 50 km eastward of the eastern graben border. This agrees with several intensive electromagnetic studies further to the east of the Black Forest, towards (and including) the Urach volcanic area (inactive since 15 Ma), which revealed no pronounced low-resistivity layer anywhere within the crust (Berktold and Kemmerle, 1982, Richards et al., 1982). There does not yet exist any model calculation which combines Tezkan's and Reitmayr's low-resistivity structures.

In the surroundings of the proposed Black Forest-KTB site, controlled-source LOTEM (*L*ong *O*ffset *T*ransient *E*lectro*M*agnetic system) soundings found an electromagnetically determined anomalous 2-km thick low-resistivity layer in the depth range between 7 and 11 km, which could not be resolved by magnetotelluric depth soundings with periods greater than 10 s (Wilhelm et al., 1989). Wilhelm et al. explain such layers of high electrical conductivity by possible horizontal movements of fluids or by a relic of overthrusted, graphite-containing metasediments which have been found among surface rocks.

4.B5. Structure and interpretation

4.B5.1. Introduction

The more recent and more detailed data that have become available since 1972 comprise in particular the addition of high-resolution, near-vertical, and wide-angle seismic-reflection data obtained in the

Rhinegraben area. These data have led to a detailed modeling and a new understanding of the crustal and upper-mantle structure beneath the Rhinegraben and its surrounding flanks.

The transect of Figure 4–17 summarizes the available geophysical data. It extends from Lunéville in northeastern France to Sigmaringen in southwest Germany, crosses the Lorraine basin, the Vosges, the Rhinegraben about 20 km south of Strasbourg, and the Black Forest in a WNW–ESE direction. Further east, the transect bypasses the geothermal anomaly of Urach to the south, and crosses the Swabian Jura in a southeasterly direction between Rottweil and Sigmaringen to end in the Molasse Basin near Saulgau. It should be pointed out that the structures shown in Figure 4–17 have only been observed in the central part of the Rhinegraben and that any generalization may lead to contradictions with data observed further south or north. This is particularly true for the polarity of main faulting evident in seismic-reflection data and for the upper-mantle low-velocity area derived from teleseismic delay time studies.

The seismic data from the Rhinegraben area reflect a strong structural asymmetry that is not only evident in the sedimentary fill but at all crustal levels. The transect clearly shows the laterally varying asymmetric crustal structure, which is well constrained east of the Rhinegraben but less so to the west. A strong decrease in P-wave velocity is seen under the Rhinegraben (ULV) and, shifted to shallower depths, also beneath the Black Forest. Magnetotelluric data obtained in the Black Forest suggest that near the bottom of the seismic low-velocity zone a thin layer of high conductivity is present at 12–15 km depth (Tezkan, 1988). The conductivity anomaly, the seismic velocity inversion, and any other stronger velocity discontinuity disappear further east, and only under the Molasse basin is a minor velocity inversion again indicated.

Information about the upper-mantle structure is scarce. From traveltime residuals, Wenderoth (1978) has deduced an intrusion of asthenospheric material into the lithosphere under the graben proper, which seems to agree with magnetotelluric and geomagnetic depth sounding observations (Scheelke, 1972, 1974; Winter, 1974; Reitmayr, 1975). According to Reitmayr (1975) the mushroom-like updoming of the conductosphere (= asthenosphere) is restricted to the immediate neighborhood of the graben and is not seen about 50 km to the east of the graben (Fig. 4–17). The high upper-mantle velocities derived from long-offset observations of P-wave data for the area east of the Rhinegraben (Ansorge et al., 1979, Stangl, 1983), as well as the generalized updoming of the lithosphere-asthenosphere boundary deduced from seismic surface and body wave studies (Panza et al., 1980), are also shown in the transect.

The transect also includes other geophysical data such as Bouguer anomalies, magnetic anomalies, heat flow, and recent crustal movements, which were taken from appropriate published maps.

Fig. 4–17. Geophysical transect through the southern Rhinegraben from Lunéville, northeastern France, to Sigmaringen, southwestern Germany. For location, see AA' in Figure 4–9.
SOURCES: Ansorge et al., 1970, 1979; Bonjer et al., 1984; Brun et al., 1991; Deichmann and Ansorge, 1983; Demnati and Dohr, 1965; Dohr, 1970; Edel et al., 1975; Emter, 1976; Gajewski et al., 1987; Gajewski and Prodehl, 1985, 1987; Gelbke, 1978; Glahn et al., 1992; Granet, 1986; Kahle and Werner, 1980; Lauer and Peterschmitt, 1970; Liebscher, 1964; Mueller et al., 1969, 1973; Mueller and Peterschmitt, 1981; Panza et al., 1980; Reitmayr, 1975; Scheelke, 1974; Spakman, 1986; Sponheuer, 1969; Stangl, 1983; Tezkan, 1988; Villemin et al., 1986; Wenderoth, 1978; Werner et al., 1982; Winter, 1974; Zucca, 1984.
EXPLANATIONS: 16-095, BA-010, SB-WI, SB-BB = seismic-refraction lines of 1972 and before (Edel et al., 1975); S, SZ, U, K = seismic-refraction lines of 1984 (Gajewski et al., 1987); 6.0 = velocities in km/s; *(18) = earthquake hypocenters after Bonjer et al. (1984, Table 1); LVZ = low-velocity zone with moderate velocity decrease; ULVZ = LVZ with strong velocity decrease; thick bars = steep-angle reflections of surveys before 1968; GDR/dotted bars = steep-angle reflections after Dohr (1970); M = Moho; dashed lines = seismic-refraction boundaries; hatched lines = magnetotelluric boundaries; vertically hatched stripe = lithosphere-asthenosphere boundary from surface and shear wave data (Panza et al., 1980); dotted depth ranges = zones of decreased P-wave velocity (open circles = 1.0–2.2%, dots = less or equal to 1%) in the uppermost mantle from teleseismic tomography studies (simplified from Fig. 4–18 after Glahn et al., 1992).
(a) Bouguer anomalies (from Werner et al., 1982). **(b)** Magnetic anomalies (from Eberle, 1973). **(c)** Heat flow (Hänel, 1983). **(d)** Recent crustal movement (from DGK-Arbeitskreis, 1979). **(e)** Generalized cross section AA' of the lithosphere comprising seismic-refraction, seismic-reflection, teleseismic, and magneto-telluric data.

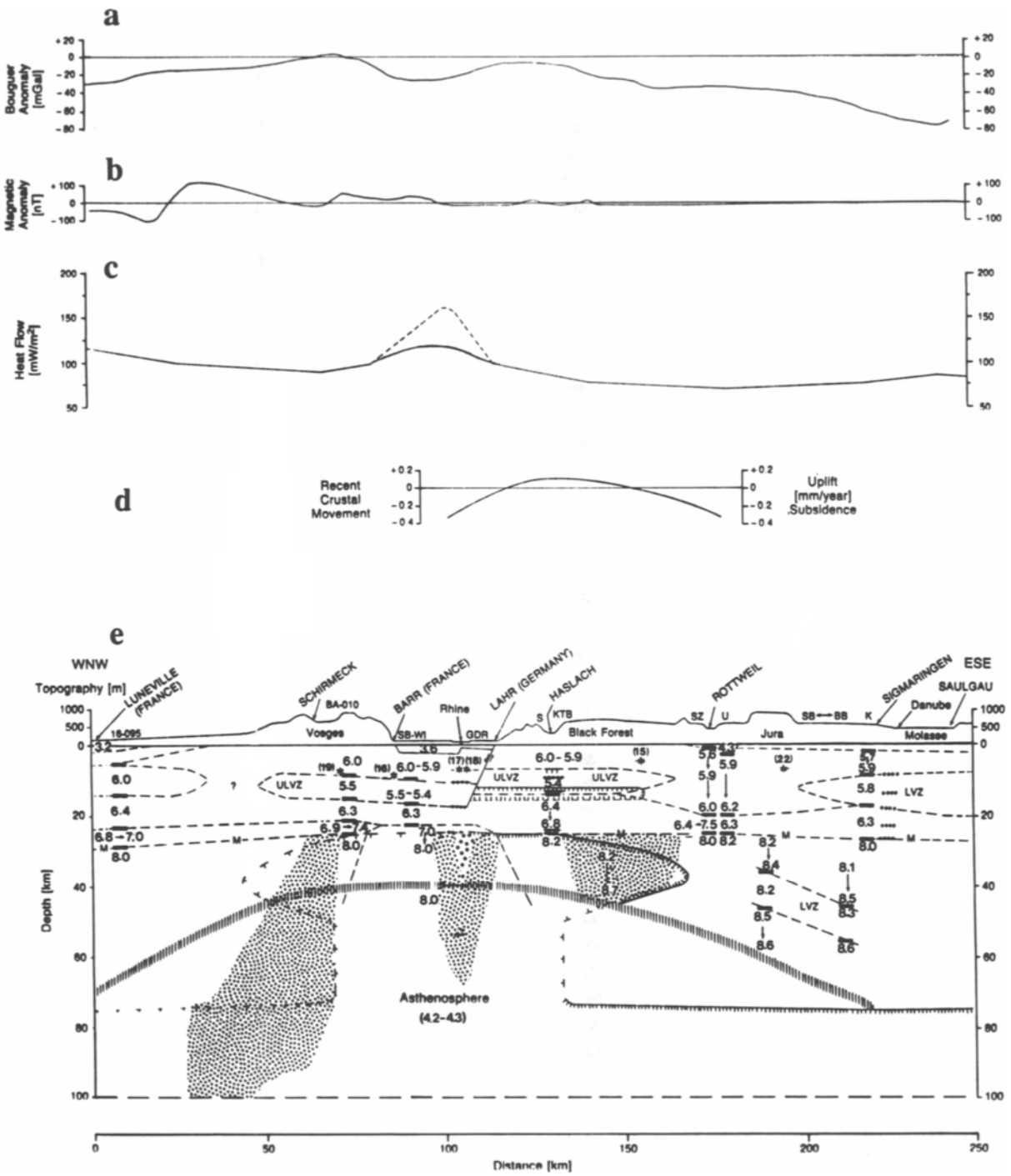
a
Bouguer Anomaly [mGal]
+20
0
-20
-40
-60
-80
b
Magnetic Anomaly [nT]
+100
0
-100
c
Heat Flow [mW/m²]
200
150
100
50
d
Recent Crustal Movement
+0.2
0
-0.2
-0.4
Uplift [mm/year]
Subsidence
e
WNW
ESE
Topography [m]
1000
500
0
LUNEVILLE (FRANCE)
SCHIRMECK
BA-010
BARR (FRANCE)
Rhine
LAHR (GERMANY)
HASLACH
ROTTWEIL
SIGMARINGEN
SAULGAU
Danube
18-095
Vosges
SB-W1
GDR
S
KTB
Black Forest
SZ
U
Jura
SB
BB
K
Molasse
ULVZ
LVZ
Asthenosphere
(4.2-4.3)
Depth [km]
20
40
60
80
100
0
50
100
150
200
250
Distance [km]

4.B5.2. Near-surface rift structures

The asymmetric sedimentary graben fill seen in cross sections (e.g., Illies, 1974b; Fig. 4–10), contour maps of individual layers and depth maps to the base of the Tertiary (Boigk and Schöneich, 1970, 1974; Doebl, 1970; Doebl and Olbrecht, 1974) and the crystalline basement (Edel, 1975) is well imaged in the modern seismic-reflection data (Brun et al., 1992; see, e.g., Fig. 4–14).

Both seismic-reflection lines through the Rhinegraben illustrate the structural asymmetry of the Rhinegraben. In the graben and in the Saverne area an apparent 1.5 s thickening of the upper crust is noted in the reflection section (Brun et al., 1991). The surface asymmetry of the southern Rhinegraben is possibly controlled in the west by a listric master fault. The main subsidence and axis of the graben, as reflected by the thickness of the Tertiary syn-rift sediments, is associated with its western border fault. The Tertiary sediments thin towards the eastern graben margin and are dissected by conjugate normal faults in the central parts of the graben, whereas at its eastern margin they are deformed into a gentle anticline (Brun et al., 1992).

For the profile DEKORP-ECORS-N (Fig. 4–9), Brun et al. (1992) and Wenzel et al. (1991) discuss in detail the change of the polarity of the graben from south to north. In contrast to the southern profile DEKORP-ECORS-S, in this northern profile the graben-bounding master fault is along the eastern flank of the graben. Here the graben also subsided asymmetrically, with the master fault in the east and without significant tilt of the sedimentary fill. Quaternary and Tertiary sediments attain maximum thickness in the east and thin towards the west. The Tertiary graben fill reaches a maximum thickness of 3400 m near the eastern master fault and decreases westward stepwise across two east-dipping normal faults to about 300 m. The dip of the master fault decreases from 55° at shallow depth to 45° at 3000 m depth (Brun et al., 1992). The varying structure seen in the sediments evidently reaches into the basement.

From models based on seismic refraction investigations for the upper crystalline crust the following features can be generalized: The upper crust of the flanks, both beneath the Vosges Mountains in the west and the Black Forest in the east (Fig. 4–15), shows a distinct low-velocity zone from about 8 to 13–15 km depth in which the velocity decreases from about 5.9–6.0 km/s to less than 5.5 km/s. A velocity decrease beneath the graben proper, possibly somewhat less pronounced, is very likely, but cannot be derived from available seismic-refraction data alone because of high-noise problems caused by the sedimentary fill of the graben. Therefore Edel et al. (1975) have simply assumed an average velocity of 6 km/s throughout the upper crust beneath the sediments (Fig. 4–13), although the presence of considerable vertical and horizontal heterogeneities in the upper crust is quite likely. The inclusion of deep-reflection observations from within the Rhinegraben (Demnati and Dohr, 1965; Dohr, 1967, 1970) in a synoptic interpretation required a pronounced low-velocity zone under the graben proper (Mueller et al., 1969, 1973) comparable to the velocity inversion zones found under the flanks of the graben. The high-resolution seismic reflection data in the Black Forest (Lüschen et al., 1987) show essentially a non-reflective upper crust which agrees with the strong velocity inversion derived by Gajewski and Prodehl (1987) from the seismic-refraction data (Fig. 4–15). At a first glance, the velocity inversion seems to be much stronger than that suggested by the data of Edel et al. (1975). However, when viewing the lateral structural variations, it is noted, that the velocity inversion underneath the Black Forest gradually disappears towards south where the line SB-045 intersects the Black Forest line. On the basis of his three-dimensional plot of hypocenters based on observations of the permanent local Rhinegraben seismic network, Koch (1993b) concludes that the lateral extent of the low-velocity zone under the Black Forest must be limited to the Black Forest area only. This has also been recognized by Gajewski et al. (1987) from interpretiation of the seismic-refraction data east of the Black Forest.

4.B5.3. Deep crust

The depth range below 15 km can be divided into two parts: the middle crust with a mean velocity of 6.3–6.5 km/s and the lower crust with 6.8–7.2 km/s,

but these two depth ranges are not always separated by a distinct boundary as, e.g., in the model for the Black Forest (Fig. 4–15).

The apparent "thinning" of the lower crust beneath the graben, possibly caused by subcrustal physicochemical processes, may be the reason why the crust-mantle boundary does not appear as a sharp discontinuity giving rise to strong near-vertical and wide-angle reflections. This is in contrast to the occurrence of numerous reflections originating from the lamellar structure of the lower crust outside the graben. Nevertheless, the well-recorded refracted P_n phase, showing a true velocity of about 8 km/s for the upper mantle underlying the lower crust of the graben, results in the clear definition of the Moho at about 24–25 km depth beneath the southern Rhinegraben (Fig. 4–13; Rhinegraben Research Group, 1974). This discontinuity dips slightly towards the north (Zucca, 1984) and reaches a depth of 27–28 km south of Frankfurt (Meissner and Vetter, 1974, Edel et al., 1975), corresponding to an increase from near 8 s TWT in the south to 8.7 s in the north (Brun et al., 1991, Wenzel et al., 1991). Similar to the attitude of the master fault, the DEKORP-ECORS reflection data reveal deep-reaching asymmetries at all crustal levels. The very detailed seismic-reflection data clearly show that lateral differences occur throughout the crust srof the graben as well, and that these vary considerably in the same way as the near-surface polarity of the graben changes along its trace.

Although the data indicate a 0.5 s step-like offset of the Moho in the eastern part of the graben, the lack of clear reflections within the lower crust does not permit the delineation of a continuous fault from the surface to the top of the mantle (Brun et al., 1991). As the older and newer data and their interpretations evidently contradict each other, the structural features derived from the reflection section in Figure 4–14 have not been transferred onto the transect of Figure 4–17e, which presents an *average* compilation of all available seismic data.

Across the graben, in the east-west direction, the crust-mantle boundary shows an asymmetric behavior. It dips gently to the east from 24–25 km under the graben to 26 km under the Black Forest and 28 km under the Swabian Jura (Ansorge et al., 1970, Mueller et al., 1973, Edel et al., 1975, Bartelsen et al., 1982, Deichmann and Ansorge, 1983, Gajewski and Prodehl, 1985, 1987, Gajewski et al., 1987, Lüschen et al., 1987), while it dips rapidly to about 30 km depth immediately west of the western flank of the Rhinegraben (Rhinegraben Research Group, 1974, Meissner and Vetter, 1974, Edel et al., 1975, Brun et al., 1991, Wenzel et al., 1991).

The apparent "thinning" of the lower crust beneath the graben was also observed along both seismic-reflection lines recorded through parts of the southern Black Forest and the adjacent Dinkelberg block at the southern end of the Rhinegraben northeast of Basel. These profiles were interpreted by Echtler et al. (1992) together with the data of the ECORS-DEKORP-line 9S. Significant differences in thickness of the reflective lower crust and transparent upper crust appear to be related to a differential crustal evolution. A 12–14 km thick lower crust beneath the Black Forest is associated with Permo-Carboniferous re-equilibration of a thickened Variscan orogenic crust. A thinning of the lower crust of about 5 km in the graben and in the Dinkelberg block (a rifted domain in a transitional position between graben and eastern shoulder) corresponds in its extent to upper-crustal faults and is thus interpreted to be related to Cenozoic rifting (Echtler et al., 1994).

Based on the three-component data of the 1984 seismic-refraction survey of southwestern Germany (Gajewski et al., 1987), a detailed interpretation of the S-waves also has been carried out (Holbrook et al., 1987, 1988; Gajewski, 1989; Krammer, 1988). The resulting values for Poisson's ratio are: 0.25 for the uppermost crust, as low as 0.15 within the Black Forest low-velocity zone, and 0.24–0.30 in the lower crust. It is particularly interesting to note that the lamellar structure derived from the P-wave data is *not* seen in the S-wave data. The results of petrological modeling indicate a gneissic/granitic upper crust (Mueller, 1977), high quartz contents in the mid-crustal low-P-velocity zone, and a granulitic lower crust of laterally varying bulk composition, from granodioritic/quartz monzodioritic to gabbroic (Holbrook et al., 1988). Under the assumption that a rather high quartz content of 50% is acceptable for the lower crust, Sandmeier and Wenzel (1990)

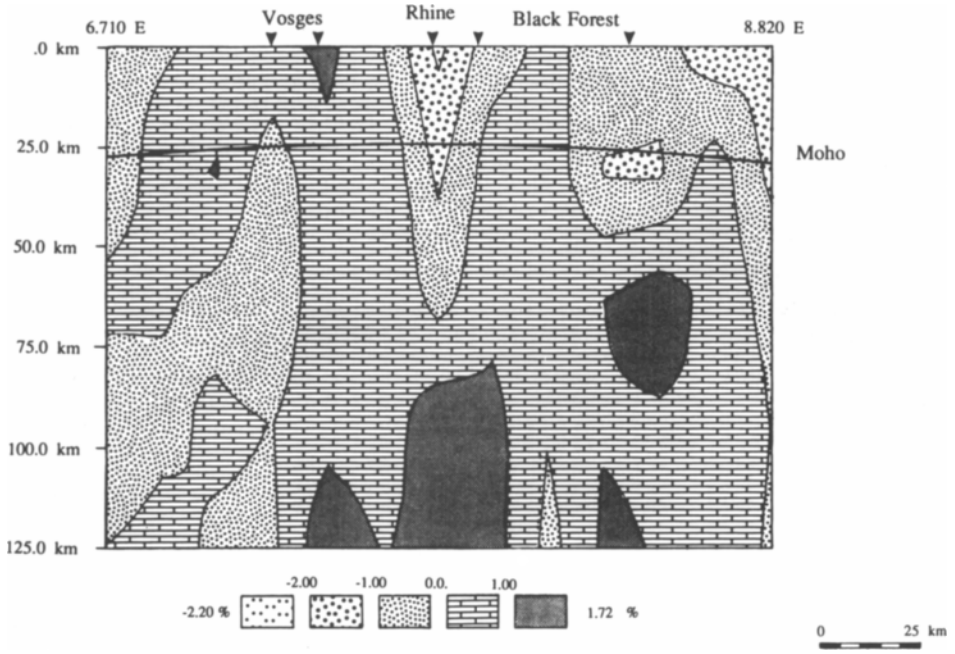

Fig. 4–18. Teleseismic cross section showing smoothed velocity perturbations (in %) of a sediment-corrected model derived from a 3-D inversion (from Glahn et al., 1993, fig. 9a). For location, see AA' in Figure 4–9.

propose a slightly different, purely compositional model for alternating high- and low-velocity lower crustal rock sequences to explain the complex reflectivity for P-waves only.

A specially designed S-wave reflection survey in the Black Forest, however, indicates high reflectivity of the lower crust for S-waves as well (Lüschen et al., 1990) which Lüschen et al. explain by assuming alternating anisotropic and isotropic lamellae.

4.B5.4. Upper mantle

Not only the crust, but also the lower lithosphere shows a highly anomalous behavior. A puzzling feature of S-wave propagation in the uppermost mantle is discussed in detail by Gajewski et al. (1990). On some profiles east of the Rhinegraben a very clear P_n phase is observed, while a corresponding S_n phase cannot be correlated, although the signal-to-noise conditions would definitely permit a detection of such a phase if it were present with comparable energy. On the other hand, Plenefisch et al. (1994) have studied S_n-phases generated from earthquakes. In contrast to seismic-refraction data, earthquakes with deep foci (20–30 km depth) generate clear S_n phases—with one exception: No S_n waves are generated at stations located on the eastern flank (Black Forest and Dinkelberg) by earthquakes with foci from the southwest, i.e. when the waves traverse the southern Rhinegraben, their S_n-component is absorbed. Computation of synthetic seismograms demonstrates that fault plane orientations and sub-Moho velocity gradients and/or a high S-wave attenuation may be the causes for the disappearance of S_n phases.

From reversed observations of seismic events in the Rhön, at the southeastern margin of the Hessen depression, and in the Dinkelberg area close to Basel, Ansorge et al. (1979) determined a true upper-mantle

velocity of 8.6 km/s at a depth of about 40–50 km. An only slightly lower velocity (8.4–8.5 km/s) is reported by the same authors and by Stangl (1983) for the reversed line Steinbrunn–Böhmischbruck, extending from Basel to the northeast through the Black Forest and Swabian-Franconian Jura. This result is supported by high S-wave velocities obtained from the dispersion of Rayleigh waves (Reichenbach and Mueller, 1974; Sprecher, 1976). These observations are in agreement with Koch's (1993b) 3-D hypocenter inversions of earthquake data, which result in generally high P_n velocities of 8.3–8.4 km/s, with the exception of the Kaiserstuhl area where Koch (1993b) finds an exceptionally low P_n velocity of 7.9 km/s. However, this depth range has not been covered by seismic-refraction data. On the other hand, due to the small number of permanent earthquake stations available in the Rhinegraben area, it remains doubtful, how much a tomographic inversion is able to reveal of local details, and in particular to determine absolute velocities.

In contrast to high velocities of more than 8.4 km/s underneath the eastern flank of the Rhinegraben, a velocity of only 8.2 km/s was obtained along an unreversed profile west of the Vosges at the same depth range of 40–50 km. Similar low velocities are found on long-range profiles through western and south-central France (Bottinga et al., 1973, Hirn et al., 1973, 1975). Thus, the properties of the upper mantle appear to be highly anomalous beneath southwestern Germany, whereas on the other side of the Rhinegraben in France, normal velocities are found (Ansorge et al., 1979). Such a change in uppermost-mantle velocities, however, is not indicated in recent teleseismic data (Glahn et al., 1993) which cover the central Rhinegraben area and its flanks to about 100 km away from the graben axis.

From an early study of travel time residuals in a limited area, Wenderoth (1978) deduced that asthenospheric material was injected into the lithosphere beneath the graben. On the basis of the data available today, his findings could be interpreted as a crustal effect; however, they seemed to agree with magnetotelluric and geomagnetic depth sounding observations (Scheelke, 1974, Winter, 1974, Reitmayr, 1975). Panza et al. (1980) concluded from surface and shear wave analysis that the lithosphere-asthenosphere boundary is domed up to about 50 km depth beneath the active Rhinegraben, the Rhenish Massif and the Lower Rhine Embayment.

These earlier conclusions cannot, however, be supported by the results of modern interpretations of large-scale P-delay studies (Babuska et al., 1988, Spakman, 1986), and by recent teleseismic observations carried out in the southern Rhinegraben area during 1989, which extend 100 km to the west and southeast of the graben axis (Glahn et al., 1993). The new 3-D models of Glahn et al. (1993) reveal a rather complicated depth structure of the lower lithosphere (Fig. 4–18) indicating a graben related, NNE–SSW oriented anomaly pattern involving the lower crust, the Moho and the uppermost mantle to a depth of about 65–75 km. Below 70 km, and reaching to at least 140 km depth, E–W oriented structures prevail. Of particular interest is a low-velocity area at 80–120 km depth beneath the central Black Forest. These E–W oriented structures correlate with a regional gravity low of –60 mgal east of the graben (Rousset and Bayer, pers. comm., 1993).

The new teleseismic data do not confirm the presence of an elevated lithosphere-asthenosphere boundary at depths above 75 km; the lithosphere shows a complex velocity structure with small-scale velocity anomalies. A low-velocity region beneath the Moho is seen at the latitude where the transect of Figure 4–17 traverses the Rhinegraben; it is bounded by rather steeply dipping high-velocity zones located under the Vosges and Black Forest. Though of considerable extent, this low-velocity zone, however, can only be interpreted as a localized lower crust - upper mantle feature. It cannot be regarded as a general asthenospheric upwarping, because further south, within the graben as well as underneath its flanks, this low-velocity zone fades out. The region of high sub-Moho velocities underneath the eastern graben flank correlates with the high upper-mantle velocities observed by Ansorge et al. (1979) at 40–50 km depth.

4.C The two northern branches: The Rhenish Massif/lower Rhine embayment and the Hessen depression

4.C3. Geologic information

4.C3.1. Introduction

At its northern end, in the area of Frankfurt, the Central European rift branches into two sections, forming a triple junction (Ziegler, 1992). One branch leads to the north along the eastern edge of the Rhenish Massif through the Hesssen depression and the Leine graben near Göttingen and then disappears under the sediments of the North German Plain. The other branch leads northwestward, traversing the Rhenish Massif where it is more or less hidden along the Rhine river. It appears again as an active rifting feature in the Lower Rhine embayment (Figs. 4–1, 4–2; 4–9, 4–19).

The development of the Lower Rhine embayment as a segment of the European Cenozoic rift system is best demonstrated by the paleogeographic maps of Ziegler (1990, 1992). While rifting in the Hessen depression is seen since Eocene time, clear evidence of taphrogenesis in the Lower Rhine embayment appears there only since Oligocene time. The seismicity maps of Ahorner (1983, see, e.g., Fig. 4–23) show that recent seismic activity is almost completely absent in the Hessen depression, but is very well pronounced on a broad strip from the Rhinegraben through the Rhenish Massif into the Lower Rhine embayment.

The Rhenish Massif is a consolidated block between the Rhinegraben in the south, the Lower Rhine embayment in the northwest, and the Hessen depression in the east (Fig. 4–19). It is part of the Hercynian mountain system of western Europe, and, as such, is part of the Rhenohercynian zone (Murawski et al., 1983; Rutten, 1969; Martin and Eder, 1983). Tertiary to Quaternary volcanism is concentrated in the Westerwald, Eifel, and Siebengebirge and, as mentioned above, in the Hessen depression to the east. Since Mesozoic times the Rhenish Massif has been undergoing uplift, a movement which seems still to be active today (Illies and Fuchs, 1983; Illies et al., 1979).

Within the scope of a priority program of the German Research Society (DFG), "Vertical movements and their causes as exemplified in the case of the Rhenish Massif," the Rhenish Massif was investigated in detail by a broad-scale geoscientific effort (Fuchs et al., 1983). The program comprised geological, geophysical, geodetic, petrological, geochemical, geomorphological, and age-dating surveys. Giese (1983) and Giese et al. (1983) have compiled seismic and magnetotelluric cross sections into an interpretive crustal section and discuss an evolutionary model of the Hercynian crust in the Rhenohercynian and Saxothuringian domain of western Europe.

The "European Geotraverse" (EGT), sponsored by the European Science Foundation as a large-scale international multidisciplinary research program, traversed central Europe on a strip from Genova to Kiel (Blundell et al., 1992, Freeman and Mueller, 1992), running more or less through the Hessen depression. The research enabled experiments on a lithospheric scale, including petrological xenolith investigations and detailed seismic and magnetotelluric profiling (see, e.g., Figs. 4–9, 4–24 and 4–26).

4.C3.2. Sedimentary record

The Rhenohercynian zone today is largely composed of epicontinental and hemipelagic sediments and volcanics. The bulk of the clastic sequences was derived from the Caledonian mountain chains of the British Isles and Scandinavia (Caledonian "molasse"). These sequences, however, only represent the marginal, "miogeosynclinal" part of what was originally a much larger basin, probably of oceanic width (Franke, 1986). Radiolarian cherts, flysch greywackes, and some MORB-type spilites, contained in nappes in the southern parts of the Rhenohercynian zone, possibly represent obducted remnants of the Rhenohercynian ocean basin.

Fig. 4–19. Rhenish Massif between the Rhinegraben in the south and the Lower Rhine embayment in the northwest (from Illies and Fuchs, 1983, fig. 1).

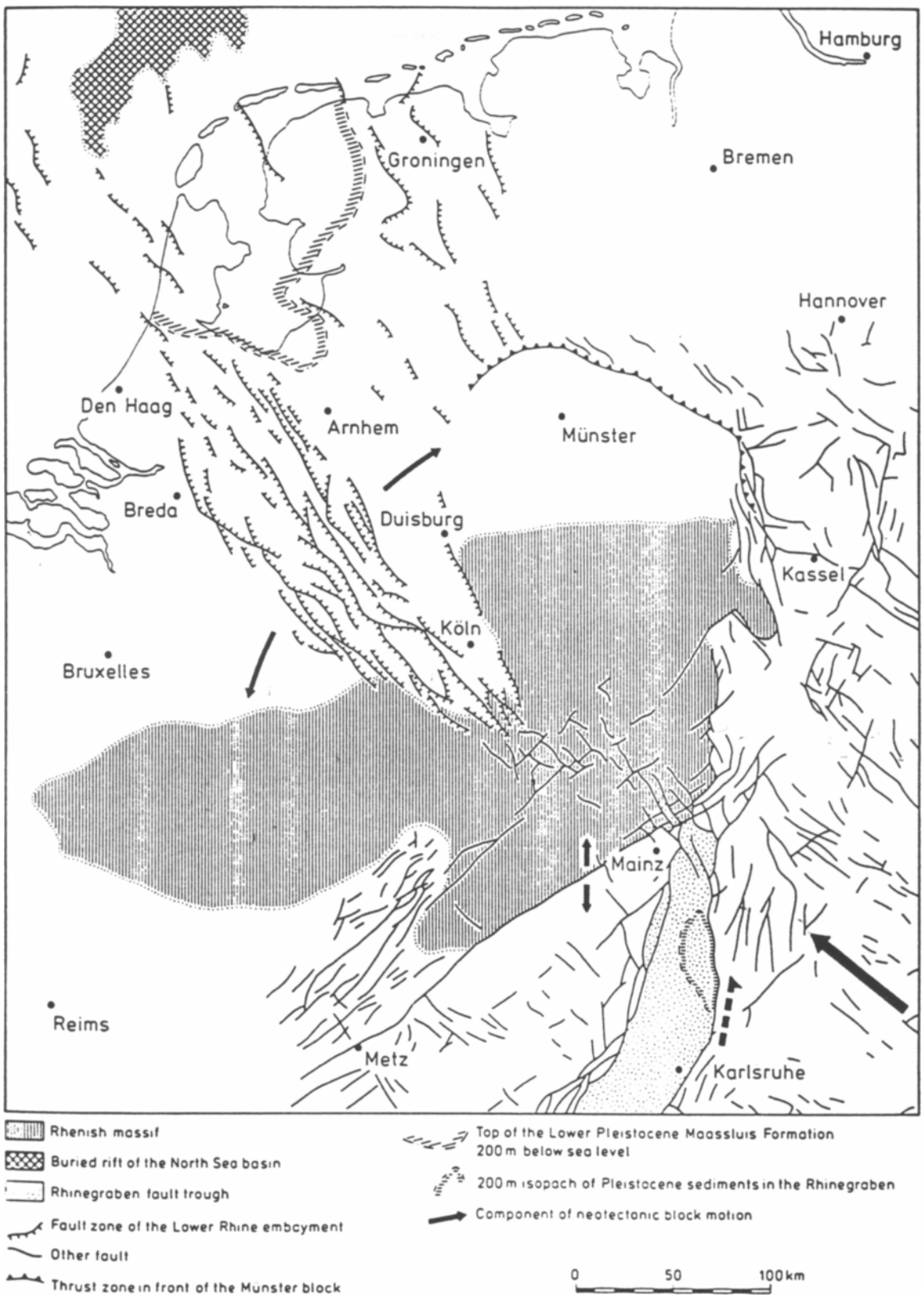
Hamburg
Groningen
Bremen
Hannover
Den Haag
Arnhem
Münster
Breda
Duisburg
Kassel
Köln
Bruxelles
Mainz
Reims
Metz
Karlsruhe
Rhenish massif
Buried rift of the North Sea basin
Rhinegraben fault trough
Fault zone of the Lower Rhine embayment
Other fault
Thrust zone in front of the Münster block
Top of the Lower Pleistocene Maassluis Formation 200 m below sea level
200 m isopach of Pleistocene sediments in the Rhinegraben
Component of neotectonic block motion
0
50
100 km

Today, the Rhenish Massif is wedged between the Rhinegraben and the Lower Rhine embayment (Fig. 4–19). It is an uplifted plateau in which a dense drainage pattern has engraved several generations of erosional land forms. Following Illies et al. (1979), it is composed of a thick series of slates, graywackes, quartzites, limestones, and locally volcanics of mainly Devonian and Lower Carboniferous age. The series, generally some 4,000 m, but locally up to 10,000 m thick, was primarily the infill of the Rhenohercynian geosyncline. The strata were strongly folded and slightly metamorphosed during the Hercynian orogeny between 330 and 300 Ma (Ahrendt et al., 1978), forming a part of the Variscan mountain range. The first phase of uplift and erosion occurred during Upper Carboniferous and Lower Permian. Subsequently, Upper Permian and Mesozoic seas marginally flooded the Massif while its central part remained a flat, emerged plateau. Tertiary marine transgression temporarily reached peripheral sections of the platform, but most of the area was covered by fluvial gravel accumulation (Quitzow, 1959; Löhnertz, 1978). Widespread dominantly basaltic eruptions pierced the Massif during Eocene, Oligocene and Miocene (Cantarel and Lippolt, 1977). Since the Pliocene, the ancestral Rhine and Mosel rivers traversed the platform and their fluvial terraces are preserved today up to 300 m above present river levels. From the Upper Pliocene on, the whole unit was subjected to a regional uplift at varying rates. The uplifted plateau extends over an area of about 100 × 200 km and includes the Rhenish Massif and some smaller marginal areas overlain by outliers of the peripheral Triassic sedimentary cover. The Rhine and Mosel rivers and a dense pattern of their tributaries have cut deep antecedent river valleys during the uplift. Timing and rates of uplift are inferred from a sequence of well dated river terraces (Bibus, 1983; Semmel, 1983).

In contrast to the deeply subsided Rhinegraben, the Lower Rhine embayment, the physically visible continuation of the European Central rift to the northwest, is characterized by a smaller thickness of Tertiary sediments (Teichmüller, 1974). The paleogeographic maps by Ziegler (1990, 1992) demonstrate the history and sedimentary development of the Lower Rhine embayment (named Ruhr Valley graben by Ziegler). Evidence for graben-related activity only starts in Oligocene time. According to Teichmüller (1974), the western margin was the more active one. Late middle Oligocene northwestward rift propagation into the Netherlands is evident from the stratigraphic record of the Lower Rhine embayment (Zagwijn, 1989, Ziegler, 1992). During the Oligocene, the area of the Rhenish Massif and Ardennes corresponded to a low-lying peneplain onto which marine transgressions encroached along tectonic depressions (Ziegler, 1992), while marine connections between the Northwest German basin and the Alpine foreland basin occurred via the Rhine–Leine graben where they remained intermittently open until the early late Oligocene. The Lower Rhine embayment continued to subside during Miocene to Recent times. Its strike is parallel to the present northwest-directed maximum horizontal compressional stress field (Illies and Greiner, 1978; Ahorner et al., 1983, Ziegler, 1992; Eck et al., 1993). The graben feathers out to the northwest and loses its identity before reaching the North Sea (Ziegler, 1992; Zijerveld et al., 1992).

4.C3.3. Igneous activity

The Rhenish Massif contains an enormous abundance of volcanic rocks, with ages reaching from the Middle Cretaceous to the youngest Pleistocene. K-Ar and ^{14}C dating are the main tools for establishing their distribution in time (Fig 4–20; Lippolt, 1983). The oldest post-Permian volcanic rock occurs in the Wittlich basin and has an age of more than 100 Ma. The main volcanic activity of the Rhenish Massif started in the Hocheifel (West Eifel) area during the Upper Eocene, where it continued until the Middle Miocene. Volcanic activity in the Siebengebirge, Westerwald and Rhön occurred during the Upper Oligocene and Lower Miocene. During the Middle Miocene, the Vogelsberg and the northern Hessen volcanic province were active (Lippolt, 1983).

The volcanism of the Rhenish Massif is associated with tectonic events related to the formation of the Rhine rift system. During the Tertiary, the volcanic activity shifted from west (Hocheifel, 46 Ma)

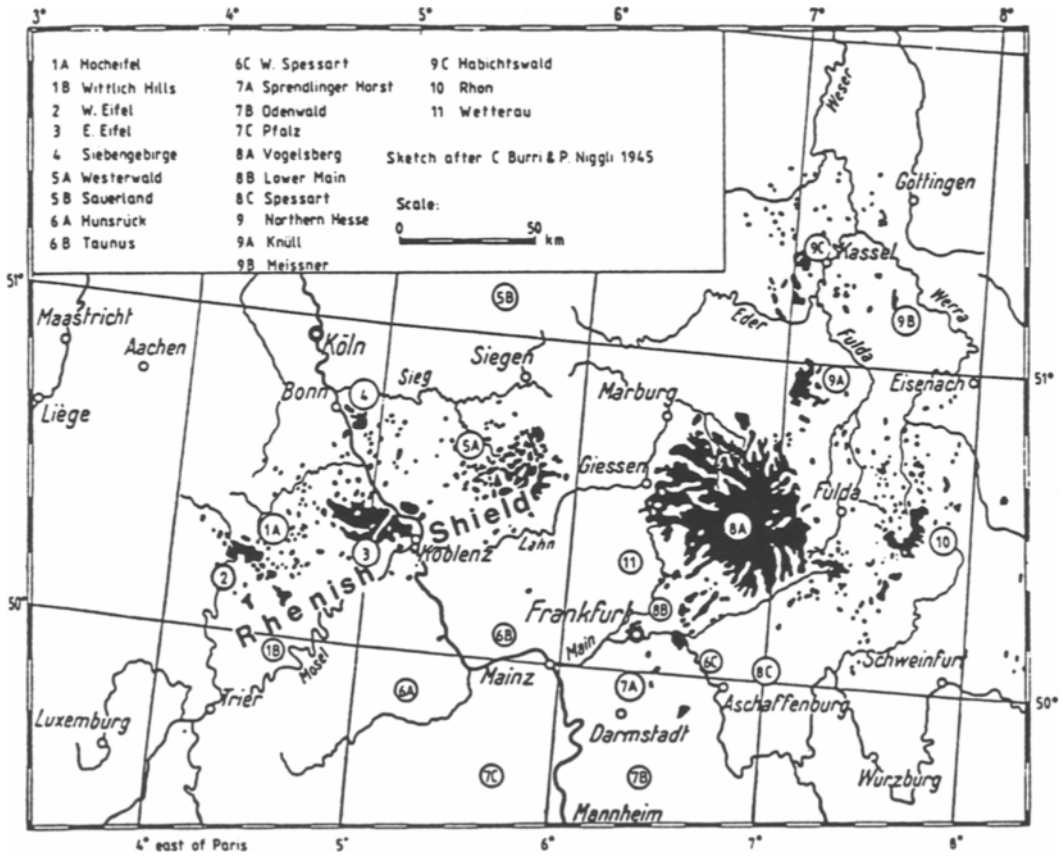

Fig. 4–20. Geographic distribution of volcanic centers in the Rhenish Massif and its surroundings (from Lippolt, 1983, fig. 1).

to east (northern Hessen depression, 20 Ma). The youngest Quaternary volcanism is restricted to two fields west of the Rhine (Seck, 1983).

Two late Quaternary volcanic fields have developed in the West Eifel, covering an area of some 500–600 km^2 with about 220 eruptive centers, and, about 25 km to the east, the smaller East Eifel (Laacher See area) with some 70 volcanic centers distributed over an area of about 400 km^2 (Illies et al., 1979). K–Ar dates and paleomagnetic polarity narrow its time of activity to the interval between 0.7 Ma and about 10,000 a. The well-established sequence of Rhine terraces can be dated in the younger section by its relation to the volcanic rocks, while for the older part one has to rely exclusively on paleomagnetic observations (Lippolt, 1983).

The Eifel volcanic fields, about 0.7 Ma old, formed roughly synchronously with the main Quaternary phase of uplift. The fields (West Eifel and East Eifel) are 50 and 30 km long, elongated in NW–SE direction, and contain about 240 and 90 volcanoes, respectively. The larger West Eifel differs from the East Eifel field by more mafic and silica-undersaturated magmas, greater abundance and larger size of peridotite xenoliths, and near-absence of highly differentiated magmas (Schmincke et al., 1983).

The magmas of the Quaternary volcanic fields in the western central part of the Rhenish Massif appear to have been derived from metasomatically modified mantle sources (Schmincke et al., 1983). NW–SE-oriented pathways may have been largely controlled by the present tensional lithospheric stress field, local N–S and NE–SW orientations possibly being influenced by pre-existing zones of structural weakness in the crust. Volcanic activity coincides broadly with increasing rates of uplift during Quaternary times, but data are insufficient to correlate distinct volcanic and tectonic phases. Quaternary magmas may have been generated in a low-velocity anomaly in the mantle beneath the area (Schmincke et al., 1983).

In the Westerwald, nepheline basanites predominate (von Gehlen and Forkel, 1983). The almost circular Westerwald volcanic province of less than 1000 km^2 has not yet been studied in the same detail as that of the Eifel and the northern Hessen depression. As far as volcanic rocks have been dated (Lippolt, 1983), basaltic and trachytic rocks about 25 Ma old (Oligocene/Miocene) predominate, followed by some eruptions at about 5 Ma (Miocene/Pliocene) in the western part, and finally only a few younger than 1 Ma (Quaternary) close to the Rhine, the latter dates belonging to the Quaternary Eifel province (von Gehlen and Forkel, 1983).

4.C3.4. Xenolith studies

Tertiary and Quaternary alkali basaltic volcanism in western Germany and in France has raised to the earth's surface numerous xenoliths of crustal and upper-mantle rocks. The area between the Alps and the North German Plain includes several thousand individual outcrops of Cenozoic age. In the Rhenohercynian zone xenoliths are found in the northern part of the Hessen depression and in the Eifel volcanic fields. Both localities have been subject to extensive petrological and geochemical investigations (Wörner et al., 1982, Seck, 1983, Seck and Wedepohl, 1983, Stosch et al., 1986, 1992, Mengel and Wedepohl, 1983, Mengel et al., 1991, Mengel and Kern, 1992).

Depleted mantle compositions are observed in peridotite xenoliths. The abundant depleted spinel-peridotite xenoliths sampled from Tertiary and Quaternary alkali basalts in the Eifel, Westerwald, and Hessen depression areas contain on average about 70% olivine. These lherzolites and harzburgites cannot explain the chemical composition of nepheline-bearing basalts except by assuming very low degrees of partial melting of the former rocks (less than 1%). Peridotite xenoliths are mainly equilibrated in the range from 900° to 1150°C related to a depth range of 60–80 km. Coarse grained xenoliths without recrystallization after heavy shearing are abundant in the Hessen depression whereas porphyroclastic peridotites predominate in the volcanic areas of the Rhenish Massif. The latter probably indicate shearing in the border zones of uprising diapirs in the upper mantle. Metasomatically altered peridotites (with about 4% amphibole or phlogopite) occur as xenoliths in basalts from the sampled areas. According to Fuchs and Wedepohl (1983) they may be the source rock for the magmas of the nepheline containing basalts.

Mengel (1992) summarizes the main results on chemical compositions of both localities and discusses the investigations of Mengel et al. (1991), who compiled thermo-barometric estimates for crustal and mantle xenoliths in Germany. Using the temperature-depth relations of Pollack and Chapman (1977), they arrive at thermo-barometric estimates of 900–1000 Mpa and 800°C for mafic granulites, and 700 Mpa, 600°C for medium-to-high-grade metasedimentary rocks which would imply a surface-heat flow of more than 120 mWm^{-2}. But the compilation of regional heat flow patterns for Germany reveals 60–70 mWm^{-2} for the northern Hessen depression and 70–80 mWm^{-2} for the Eifel (Haenel, 1983). Therefore, Mengel (1992) regards it as unlikely that the reported thermo-barometric estimates have any significance for the present thermal conditions in the middle or lower crust. Rather, he assumes that they reflect orogenic processes affecting these crustal segments, presumably during the Variscan orogeny.

From 1000 xenoliths from the Eifel, Voll (1983) deduces the following profile (downwards): 0–5 km = Devonian, 5–15 km = greenschist facies phyllites,

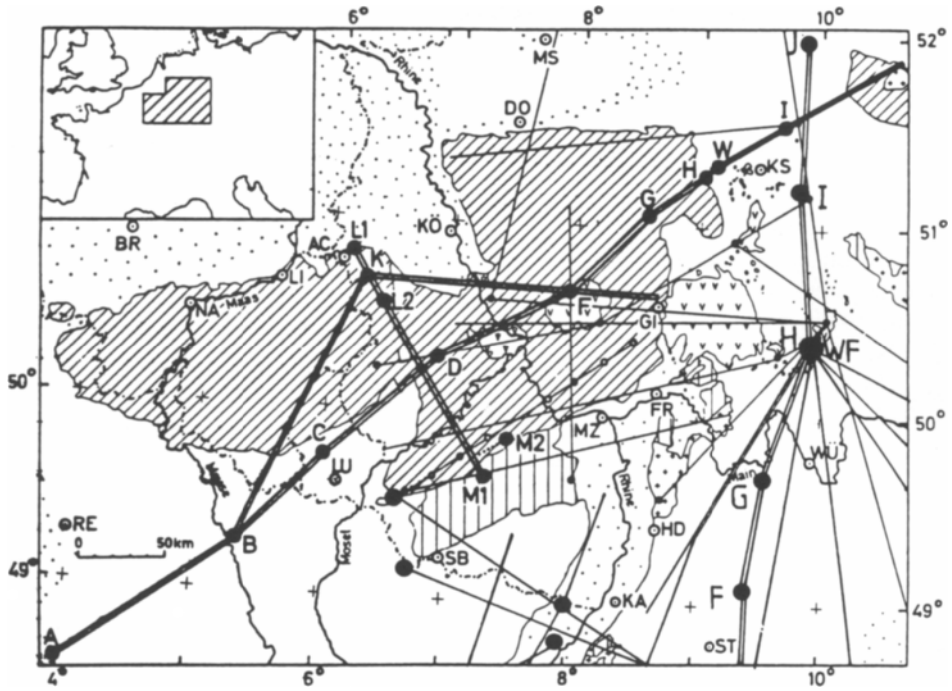

Fig. 4–21. Location map of seismic-refraction profiles in the Rhenish Massif and adjacent areas until 1987 (extended from Mechie et al., 1983, fig. 1).

15–20 km = low amphibolite facies, 20–25/30 km = medium- to high-grade amphibolite facies gneisses. While the upper and mid crustal composition is debated, there is agreement on the amphibolite-facies sequence of the lower crust (Stosch et al., 1992).

While Voll (1983) based his crustal profile solely on the abundance of rock types, Mengel (1992), as an alternative, assumes that all major rock types have been sampled but that the accidental abundance of any rock type does not have any significance. On this basis Mengel et al. (1991) summarized the xenolith lithologies from the northern Hessen depression and the Eifel, and compiled crustal sections in connection with seismic velocity information. According to Mengel et al. (1991) and Stosch et al. (1992), the middle crust between depths of about 10 and 25 km consists mainly of meta-sediments, felsic gneisses and granulites. Meta-sedimentary rock types are particularly abundant in the Eifel at 5 to 15 km depth but less common within the northern Hessen depression xenoliths. At depths between 24 and 26 km, the increase of observed seismic velocity (Aichroth et al., 1992, Mechie et al., 1983) from about 6.8 to 8 km/s (28–34 km) is correlated with the presence of mafic granulites intercalated with eclogites, pyroxenites and hornblendites. Beneath the northern Hessen depression, the granulite layer may grade into a composite eclogite-peridotite layer at the lower part of this transition zone. The crustal rock composition of the northern Hessen depression deduced by Mengel et al. (1991) is included in the interpretive crustal cross section of the European Geotraverse through central Germany (see Fig. 4–26, lower part; Franke et al., 1990b; Prodehl and Aichroth, 1992). Mengel and Kern (1992) discuss the problem that the petrological Moho which they define as the boundary between non-peridotitic crustal rocks and olivine-dominated rocks is not identical with the position of the seismic Moho for the case that mafic rocks are transformed into eclogites at the base of an orogenically thickened crust.

4.C4. Geophysical surveys and results

4.C4.1. Seismic studies

Prior to 1974, a series of profiles based mainly on quarry-blast observations had been recorded (Figs. 4–2 and 4–21), which are described in general by Giese et al. (1976). In addition, special wide- and steep-angle seismic-reflection measurements were carried out in some selected areas (Glocke and Meissner, 1976; Meissner et al., 1976a, 1980, 1983). Some of these early lines also cover part of the Hessen depression to the east (Mooney and Prodehl, 1978; Prodehl and Fuchs, 1986).

Within the program to investigate vertical movements and their origin as exemplified in the Rhenish Massif, a long-range seismic refraction experiment (Fig. 4–21) was carried out in 1978–1979 to determine the velocity structure of the crust and uppermost mantle (Mechie et al., 1982, 1983; Prodehl and Mechie, 1985). In order to avoid known complications, the 1979 long-range refraction survey (Mechie et al., 1982, 1983) avoided crossing major volcanic fields (Fig. 4–21). Some short steep-angle reflection lines were run at the same time across the border zones of the Rhenish Massif in the north (Meissner et al., 1981) and in the south (Meissner et al., 1980).

About 10 years later, two DEKORP steep-angle seismic-reflection lines were recorded through the Rhenish Massif in a NW–SE direction. BELCORP/DEKORP-1 runs west of the Rhine traversing the Aachen thrust, the Eifel north-south zone, the Mosel trough, the Hunsrück, and the Saar-Nahe basin (DEKORP Research Group, 1991). DEKORP 2-N crosses the Münsterland basin, the Carboniferous coal basin at the northern margin of the Rhenish Massif, the Westerwald and the Taunus, but avoids the Tertiary volcanic fields of the Westerwald and the Vogelsberg (Franke et al., 1990a). During the course of these steep-angle measurements, wide-angle reflection data were also obtained (Giese et al., 1990).

The Hessen depression was traversed in the strike direction by the detailed 1986 EGT long-range seismic-refraction line (Galson and Mueller, 1984, 1985; Freeman et al., 1986) between shotpoints H and J (Figs. 4–9 and 4–26; Aichroth et al., 1992; Prodehl and Aichroth, 1992). In 1990, the high-resolution seismic-reflection line DEKORP 3 was recorded, part 3A of which ran also along strike of the Hessen depression, approximately between EGT shotpoints I and J (see Fig. 4–9), but about 30 km west of the European Geotraverse (Heinrichs et al., in preparation).

Already, older data which were reinterpreted by Mooney and Prodehl (1978) clearly displayed that lateral heterogeneities play a major role. Mooney and Prodehl (1978) concluded that the general pattern of arrivals in the seismic-refraction data could be separated into three types, which also has been noted elsewhere (e.g., Giese et al., 1976, Prodehl, 1979, 1984). In type I, only the reflection from the crust-mantle boundary, P_MP, were seen in secondary arrivals. In type II, an earlier second reflected phase, P_IP, could be correlated. Finally, in type III, only the phase P_IP, but not the reflection from the Moho (P_MP) was present. In mapping the areas where those phases could be seen, it appears that the disappearance of the P_MP phase (type III) is restricted to profiles which cross major volcanic fields, such as the Westerwald and Vogelsberg flood basalts. Here the Moho may be heavily disrupted or "smeared" and an intermediate intracrustal boundary at about 20 km depth forms the main reflector for seismic waves, an appearance which had also been found by Edel et al. (1975) for the southern Rhinegraben proper.

Record sections of the 1979 refraction survey show rather uniform high velocities in first arrivals out to distances of more than 100 km, indicating a uniform uppermost crust with rather high velocities of 6.2–6.3 km/s. This is in agreement with a multitude of reflections in the first 2–3 seconds of the DEKORP seismic-reflection data (see, e.g. Fig. 4–22; Franke et al., 1990a; DEKORP Research Group, 1991), some of which can be related to geological structures exposed at the surface such as thrust faults in the eastern Rhenish Massif (Franke et al., 1990a) and the Aachen thrust fault (Faille du Midi), the deep extension of which could be clearly traced in the reflection data underneath the Rhenish Massif (Meissner et al., 1981; DEKORP Research Group, 1991).

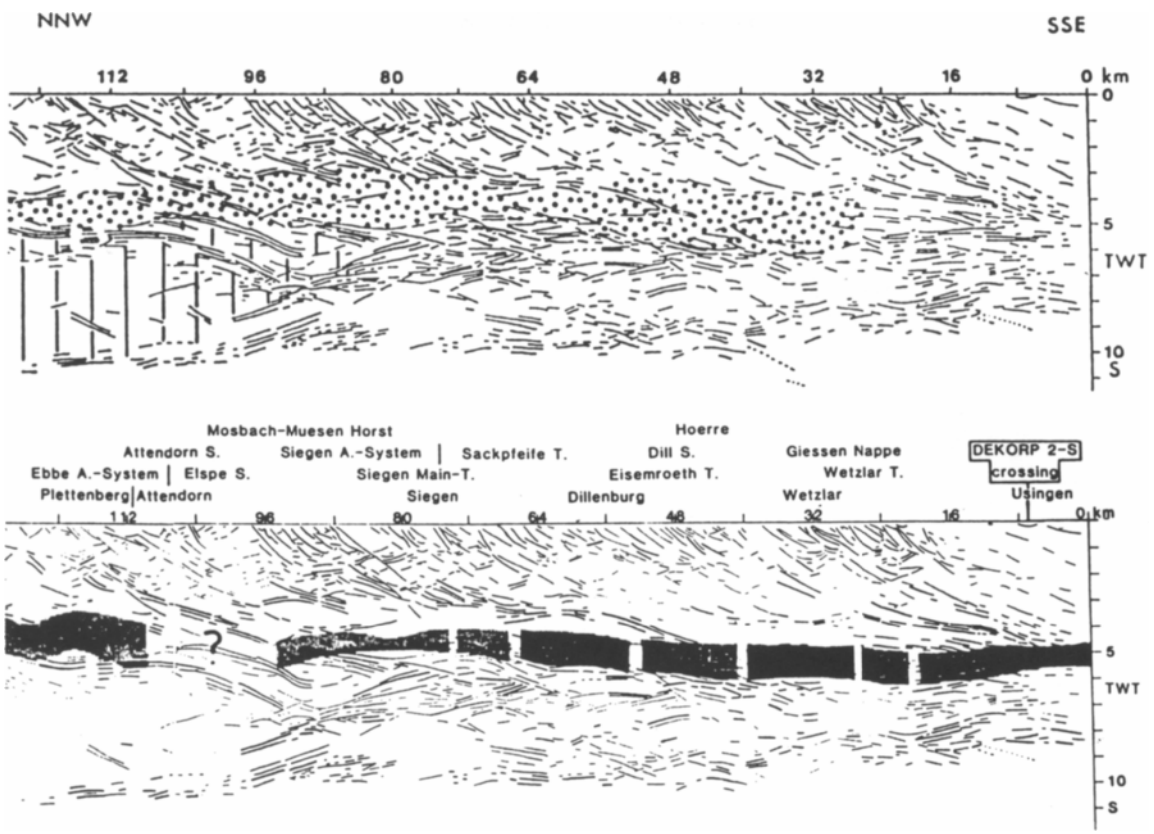

Fig. 4–22. Seismic-reflection observations along DEKORP-2N (compiled from Franke et al., 1990a, and Volbers et al., 1990). *Upper part:* Seismic domains recognized in the Rhenish Massif. Dotted depth range: mid-crustal zone of reduced reflectivity and identified as area of reduced velocity, vertically hatched depth range: transparent domain in the lower crust. *Lower part:* Superposition of the mid-crustal high-conductivity zone on the seismic-reflection data, coinciding to a large part with the area of reduced velocity.

Contrary to the seismic-refraction first-arrival data, strong variations are seen in the secondary-arrival phases (Mechie et al., 1983, Figs. 2 and 3) reflected from the crust-mantle and intracrustal boundaries. In the far southwest, between Reims and Verdun (profiles A and B–SW, i.e., well outside the Rhenish Massif), the phase *c* interpreted as wide-angle reflection from the Moho is seen at 70–120 km distance resulting in a Moho depth of about 30 km, as is typical for Hercynian Europe outside the European Cenozoic rift system. However, when crossing into the Rhenish Massif east of Verdun, starting on profile B–NE, the crust-mantle reflection *c* suddenly is seen at much greater distances, implying a rather rapid increase of crustal thickness to about 37 km. For all subsequent profiles located west of the Rhine (profiles B–NE to D–SW), phase *c* is the reflection from the Moho at about 37 km depth. On the profiles continuing to the east of the Rhine (D–NE, F–SW, and F–NE), the large-amplitude arrivals start at much smaller distances, again at 70–80 km offsets, and evidently have to be interpreted as two separate phases, *c* and *e*, the first one being a reflection from about 30 km and the second one from 37–38 km depth. The resulting model by Mechie et al. (1983) shows a thin layer of mantle material (velocity above 8 km/s) at about 30 km depth. Underneath this thin mantle layer the velocity decreases strongly, and mantle velocities of about 8 km/s are only reached again below 35 km depth

(see transect below, Fig. 4–25). The splitting of the large-amplitude phases c and e becomes less evident on the profiles further to the northeast (shotpoints G and W), but is indicated again on the easternmost section from shotpoint I.

In the DEKORP seismic-reflection data east of the Rhine, the most striking feature is the appearance of an almost structureless middle crust (see, e.g., Fig. 4–22), which is much less prominent west of the Rhine (DEKORP Research Group, 1991). On both lines strong lateral traveltime variations of the bordering reflective areas above and below very clearly show that the middle crust is not homogeneous, but that its structure varies considerably, as is also evident from seismic-refraction data. Strong reflectivity prevails generally in the lower crust, but also here strong variations in reflectivity of the lower 5–10 seconds TWT reflect the heterogeneity of the structure of the lower crust as evidenced earlier by the refraction data.

The seismic-refraction data of the EGT (Aichroth et al., 1992) give evidence for a narrow low-velocity zone (V_p = 5.9 km/s) underneath the Hessen depression, overlying a thin layer with a high velocity (V_p = 6.7 km/s) between shotpoints H and I, and is based in particular on a high-amplitude phase *b*.

The crust-mantle boundary here, in particular between shotpoints H and J underneath the Hessen depression (Aichroth et al., 1992), appears as a several km thick transition zone. Here, phase *c* is disturbed and its critical distance is shifted to a distance greater than 80 km. The special behavior of the Moho in this region may be viewed in context with the Tertiary volcanic activity in the Hessen depression.

The structure of the upper mantle below the Moho has been investigated from several seismological data sets: A teleseismic study in the late 1970s concentrated on the Rhenish Massif and surroundings (Raikes, 1980; Raikes and Bonjer, 1983); and the lithosphere-asthenosphere boundary has been mapped using P-delays (Babuska et al., 1988, 1992) as well as by body shear wave and surface wave studies (Panza et al., 1980).

The observation of teleseismic P-wave residuals within, and in the vicinity of, the Rhenish Massif showed that arrivals within the Massif were up to 0.6 seconds later than those immediately outside. Stations within the Massif also showed delays which were strongly azimuthal-dependent. The major anomaly occurs west of the Rhine, beneath the West Eifel, where modeling shows a velocity decrease of 3–5 % extending from about 50 to 200 km depth. A shallower low-velocity region (less than 60 km depth) seems to be located under the Vogelsberg volcanics at the southern end of the Hessen depression (Raikes, 1980; Raikes and Bonjer, 1983).

4.C4.2. Gravity

Based on incomplete older maps (e.g., Gerke, 1957) and material still unpublished at the present time (e.g. Plaumann, 1987), Jacoby et al. (1983) compiled a Bouguer anomaly contour map for the area of the Rhenish Massif. More recently, Grosse and Conrad (1990) have compiled a Bouguer map of the whole of Germany and adjacent areas, adapting the various maps to the format of the Bouguer maps of the Federal Republic of Germany (Plaumann, 1987). For the area of the European Geotraverse which traverses the Hessen depression, the Bouguer gravity data were compiled in EGT Atlas Map 9 (Freeman and Mueller, 1992).

The major features of the central European Bouguer field are discussed by Grosse et al. (1990, 1992). For the area of the Rhenish Massif and vicinity, Grosse et al. (1990) point out a gravity low of the Massif west of the Rhine, a gravity high of the Hunsrück southern margin, a gravity high of the Massif east of the Rhine, a gravity low in the Münster basin, and a gravity low of the Lower Rhine embayment west of Köln.

The gravity lows of the Lower Rhine embayment and that of the Münster basin to the north of the eastern Rhenish Massif are clearly associated with sediment accumulations. The positive gravity of the Hunsrück southern margin may be caused by steeply inclined phyllites and metavolcanics of the Northern Phyllite Zone (Grosse et al., 1990).

Of particular interest are the contrasting gravity anomalies of the Rhenish Massif west and east of the Rhine (see also Fig. 4–25). Over the eastern Massif anomalies are positive (+10 to +20 mgal) and over the western part they are negative (–10 to –20

ferences exist in detail. Focal regions with large historical earthquakes show, for instance, in general an unusually low level of microseismicity.

The overall seismicity pattern of the Rhenish Massif and Lower Rhine embayment is, according to Ahorner (1983), clearly related to stress-field controlled large-scale block movements along major crustal fracture zones and does not show any direct relationship to plateau uplift, with the exception of some special regions such as the Hohes Venn in the northwest of the Rhenish Massif.

4.C4.5. Stress pattern

Stress directions (Ahorner, 1983, Fig. 7) have been determined from in-situ measurements (Baumann and Illies, 1983) as well as from fault plane solutions of earthquakes which occurred during 1975 and 1982 in Central Europe between the Alps and the North Sea (Ahorner, 1983; Ahorner et al., 1983). Stress directions from fault-plane solutions are in good agreement with the results of in-situ stress measurements. Although the maximum compressive stress shows an average direction of about 145° with respect to North in the whole area, regional differences in the stress directions and the seismotectonic regime are recognizable. For the southern Rhinegraben, the Swabian Jura, and the western Vosges Mountains, strike-slip mechanisms are predominant. In the northernmost Rhinegraben, the Rhenish Massif, and the Lower Rhine embayment, tensional dip-slip dislocations along NW–SE trending fault planes are typical (Ahorner et al., 1983).

The general seismotectonic regime of the Middle Rhine zone between Mainz and Bonn is clearly characterized by extensional rifting along a broad NW–SE trending fracture zone which follows approximately the Rhine, and connects the major seismically active features of the Rhinegraben with those of the Lower Rhine embayment (Fig. 4–3; Ahorner, 1983, Fig. 11). The Rhenish Massif is bisected by this zone into two parts which were pushed away from each other in NE–SW direction (Ahorner, 1983).

The Lower Rhine embayment has an offset of about 20 km westward of the northernmost faults of the Rhinegraben and strikes approximately parallel to the present S_{Hmax} orientation in western Europe (Müller et al., 1992). Quaternary extension perpendicular to its flanks amounts to 100–200 m and has occurred on preexisting rift faults. The Lower Rhine embayment shows a clear predominance of tensional dip-slip dislocations along NW–SE trending fault planes. Active crustal rifting can be followed over a total length of 350 km from Nijmegen in the Lower Rhine embayment to Heidelberg in the northern Rhinegraben (Ahorner, 1975, 1983).

Besides the prevailing tensional dip-slip dislocations which indicate crustal extension in a SW–NE direction, also compressional dip-slip dislocations indicating NW–SE crustal compression have been found in the Taunus and the Hohes Venn. Both stress directions belong to the same general stress regime and are in agreement with in situ stress measurements proving a quite uniform regional stress field for the Rhenish Massif and vicinity (Illies and Greiner, 1979; Baumann and Illies, 1983). Evidently, the mode of seismotectonic dislocations and the overall pattern of seismicity are controlled by the present-day regional stress field within the earth's crust of central Europe (Ahorner, 1975, 1983, Müller et al., 1992).

4.C4.6. Heat flow

Density, specific heat capacity, thermal diffusivity and heat production data have been published by Hänel (1983) for various sedimentary, acid and basic rock samples in western Germany, as well as the thermal conductivity as a function of temperature. New heat-flow density determinations made in shallow boreholes and corrected for the paleoclimatic effect result in a mean heat-flow density for Ger-

Fig. 4–23. Historical seismicity pattern and geological features of the Rhenish Massif (from Ahorner, 1983, fig. 1). Key: 1 = fault zone active during Tertiary time; 2 = fault zone active until Quaternary and Recent time; 3 = thrust fault of Hercynian age; 4 = major Hercynian anticline; 5 = Quaternary volcano; 6 = earthquake swarm; 7 = border line of the Caledonian Brabant massif; 8 = Hainaut basin; 9 = seismic events due to mining activity; 10 = border line of underground salt deposits.

mgal). Jacoby et al. (1983) have attributed these gravity differences exclusively to crustal structure differences, which are clearly seen in the seismic data (Mechie et al., 1983), but the contrasting velocities in the subcrustal lithosphere (Raikes and Bonjer, 1983) may also have some influence on the gravity field.

4.C4.3. Magnetic anomalies

Magnetic anomalies correlate with outcropping volcanic areas in the Eifel, Westerwald and northern Hessen depression. Some anomalies can be attributed to particular structures such as some ore deposits in mining areas, some thrust zones for which magnetic bodies have been modeled, or the Tertiary volcanic centers near Kelberg and in the West Eifel, some of which can also be recognized in the seismic-reflection data of DEKORP (Wonik and Hahn, 1989; DEKORP Research Group, 1991). No immediate correlation of magnetic anomaly patterns with rifting features is evident.

For the area of the European Geotraverse which traverses the Hessen depression, the aeromagnetic anomaly data were compiled in Atlas Map 10 (Freeman and Mueller, 1992). Based on the 1:1,000,000 aeromagnetic map of the total intensity of the Earth's magnetic field for an altitude of 3000 m above m.s.l. (Wonik and Hahn, 1989), Hahn and Wonik (1990) have computed the magnetic relief for the area of the seismic-reflection line DEKORP 2-N. They present the results in form of a depth contour map assuming a two-layer model: an upper layer which is non-magnetic, and a lower layer which is homogeneously magnetized (M = 0.35 A/m) parallel to the ambient field. The depth of this boundary undulates between 6 and 15 km along the seismic line. The depth uncertainty amounts to a few kilometers, that of the magnetization to about –50% to + 150%. The authors conclude that the magnetic relief represents a boundary between two crustal layers that are clearly different regarding their mineral content, which here probably indicates low-grade metamorphism above the boundary and high-grade metamorphism below it. Consequently, the two layers are regarded to be different with respect to origin and diagenesis and the magnetic relief is interpreted as a decollement interface coinciding with a zone of weak seismic reflectivity which may also coincide with the top of the mid-crustal low-velocity zone in the seismic-refraction cross sections.

4.C4.4. Seismicity

Seismicity maps of the northern European Cenozoic rift system clearly show the main activity in the southern and the northern Rhinegraben as well as in the Lower Rhine embayment, while almost no seismic activity is present today in the Hessen depression (Ahorner, 1983; Ahorner et al., 1983). In particular, the Lower Rhine embayment has been the site of destructive historical earthquakes up to the present (Eck et al., 1993). Another active zone north of the Rhenish Massif is the Belgian earthquake zone which trends in an east-west direction and follows the border zone between the Caledonian Brabant Massif and the Hercynian Rhenish Massif (Ahorner, 1983).

A belt of earthquake epicenters traverses the Rhenish Massif (Fig. 4–23) about parallel to the Rhine river (Ahorner, 1975, 1983). In some areas the seismotectonic activity seems to be associated with normal faulting of Pleistocene and sometimes Holocene age. This intra-shield deformation is diffuse because lengths and vertical throws of faults are mostly small. Only the Neuwied basin, centered between both ends of the active rift valleys (northern Rhinegaben and Lower Rhine embayment), shows larger vertical motions up to 300 m (Illies et al., 1979).

Ahorner's (1983) study of earthquake activity in the Rhenish Massif (Fig. 4–23) is based on a detailed investigation of the historical seismicity pattern since 1500 A.D., and on a special microearthquake survey carried out from 1976 to 1982. More than 800 local earthquakes of tectonic origin, ranging in magnitude from M_L = 0 to 4.7, were recorded during the 6-year-study, most of which could be located with reasonable accuracy (±1 km horizontally and ±2 km vertically). Fault plane solutions were derived for events with magnitude greater than M_L = 3. The main features of the historical seismicity pattern are reproduced by the short-term microseismicity study (Ahorner, 1983), although dif-

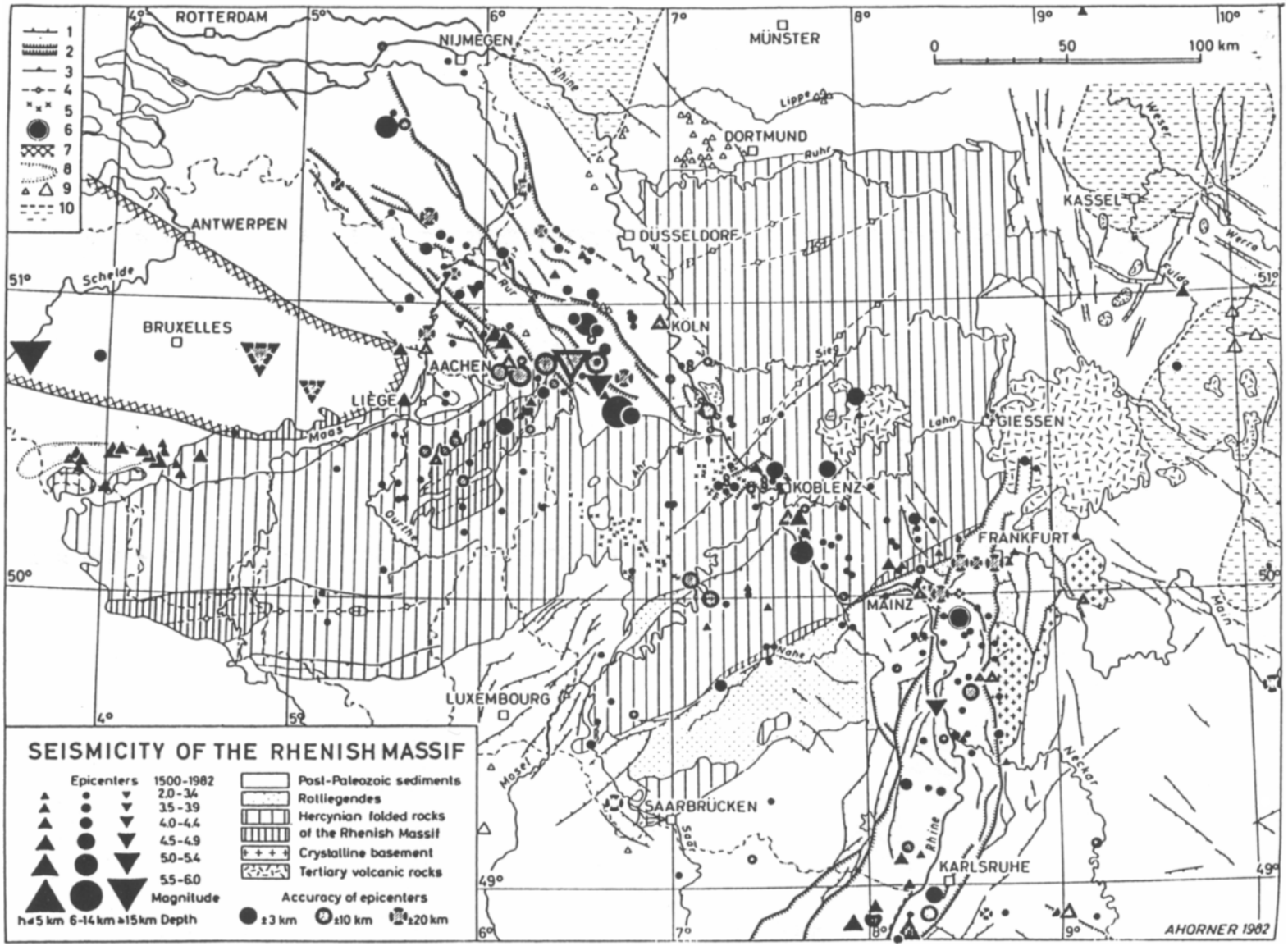
ROTTERDAM
NIJMEGEN
MÜNSTER
DORTMUND
KASSEL
ANTWERPEN
DÜSSELDORF
BRUXELLES
KÖLN
AACHEN
LIÈGE
GIESSEN
KOBLENZ
FRANKFURT
MAINZ
LUXEMBOURG
SAARBRÜCKEN
KARLSRUHE
Rhine
Lippe
Ruhr
Weser
Werra
Fulda
Schelde
Meuse
Sieg
Lahn
Maas
Ahr
Our
Nahe
Moselle
Saar
Neckar
Main
0 50 100 km
AHORNER 1982
SEISMICITY OF THE RHENISH MASSIF
Epicenters 1500-1982
2.0-3.4
3.5-3.9
4.0-4.4
4.5-4.9
5.0-5.4
5.5-6.0
Magnitude
h<5 km 6-14 km ≥15 km Depth
Post-Paleozoic sediments
Rotliegendes
Hercynian folded rocks of the Rhenish Massif
Crystalline basement
Tertiary volcanic rocks
Accuracy of epicenters
±3 km
±10 km
±20 km

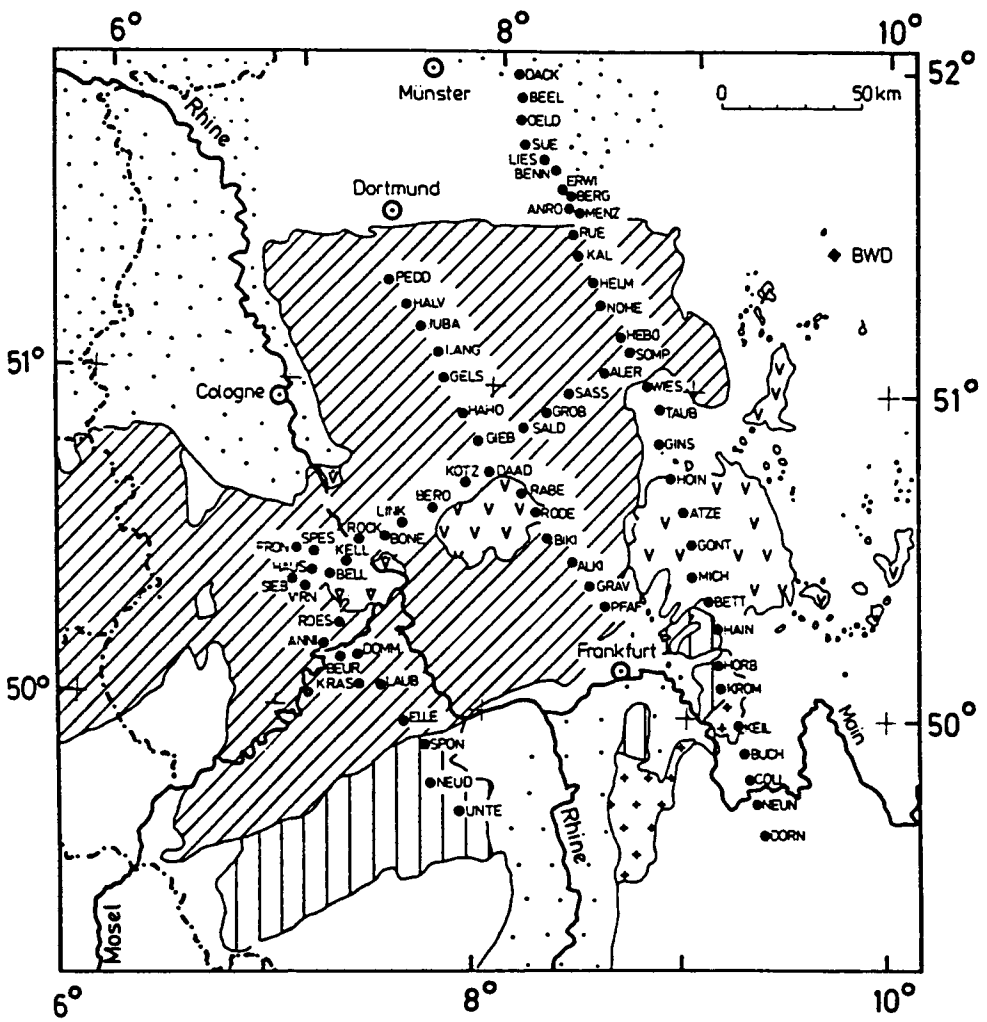

Fig. 4–24. Map of the magnetotelluric surveys in the Rhenish Massif (from Jödicke et al., 1983; fig. 1).

many of 81 mWm^{-2}. Hänel's new heat-flow density map shows a Hercynian trend of the isolines within the Rhenish Massif. Two regions of high heat flow greater than 80 mWm^{-2}, the Westerwald-Taunus area and the region around the Hunsrück-Taunus border fault zone, are clearly separated by a region of relatively low heat flow parallel to the Mosel and Lahn rivers

The same separation is shown on maps of temperature distribution at 10 km and 30 km depth. The mean temperature at 30 km depth in the Rhenish Massif averages to 800°C (Hänel, 1983).

Hänel (1983) discusses also the possible existence of a magma chamber under the Laacher See area (Schmincke et al., 1983) and the absence of a corresponding temperature and heat flow anomaly. He calculates the present temperature in the center and at the top of the proposed magma chamber and the resulting heat flow density at the earth's surface. From these calculations it must be concluded that heat has not yet reached the earth's surface and that any possible surface heat-flow anomaly due to the intrusion, about 10,000 years after emplacement, is therefore zero.

4.C4.7. Geodetic data

The map of height changes (DGK-Arbeitskreis, 1979; Mälzer et al., 1983) is based on a 4000-km-long connected leveling network and contains 4800 releveled points. It shows that the Rhenish Massif is not uplifting as a rigid block but that the present uplift is concentrated in limited areas. West of the Rhine the Massif is predominantly either uplifting or is stable, while east of the Rhine alternating subsidence and uplift trends occur. On both sides of the Rhine near Koblenz an E-W trending area of uplift is observed showing vertical movements of up to 0.6 mm/yr.

In the Lower Rhenish embayment some faults form considerable steps within Pleistocene terrace surfaces. Here, the recent height changes are a multiple of estimated average rates in the Pleistocene (Illies and Fuchs, 1983). In and around the Lower Rhine embayment a continuous taphrogenesis is indicated by the map of height changes (Mälzer et al., 1983). Northeast of the Lower Rhine embayment, uplift of 0.6–0.9 mm/yr occurs in the Bergisches Land. Uplift is not only visible in the Devonian rocks but also in the eastern Quaternary sediments of the embayment. To the west of the Lower Rhine embayment, in the Venn Sattel and northern Eifel, the greatest uplift rates of up to 1.6 mm/yr are observed.

4.C4.8. Electromagnetic methods

A magnetotelluric survey was undertaken in the Rhenish Massif and adjacent areas in 1977–1981 (Fig. 4–24) (Jödicke et al., 1983) and along the 1987/88 DEKORP-2N seismic-reflection line (Volbers et al., 1990) at altogether 150 sites. The earlier survey comprises three parallel lines traversing the Rhenish Massif in a NNW–SSE direction, and one line running from WSW to ENE parallel to the seismic-refraction long-range line (Mechie et al., 1983). The observations were made in the period range of 5–3000 seconds at more than 70 sites along the four profiles. The DEKORP-2N line is near the earlier middle line and was observed with much greater station density, however, natural noise conditions here were less favorable. At its southern end, the easternmost line crosses the Vogelsberg in the southern Hessen depression.

The high conductivity found in the North German sedimentary basin (Haak et al., 1986) ends abruptly at its southern border near Hannover, signifying a corresponding change of crustal structure. Throughout the Rhenish Massif, high-conductivity layers are inferred at depths of the middle and lower crust. Four profiles running from north-northwest to south-southeast show low resistivity layers dipping from north to south to greater depth nearly continuously. In the vicinity of the Rhine on the fifth profile, which coincides with the present transect (Fig. 4–25), the magnetotelluric data could not be processed due to excessive industrial noise.

Preliminary 2-D modeling indicates that there is no major dislocation of this conductor at the southern margin of the Rhenish Massif where it borders the Rhinegraben. In some areas, especially outside the Rhenish Massif proper, an additional increase of conductivity at shallower depths was found (Jödicke et al., 1983).

The discontinuous course of the low resistivity layers, except for that gap on the transect shown below (see Fig. 4–25), does not seem to be created by internal magnetotelluric problems such as, e.g., static shift problems, but is likely to be real. Lohr's (1982) rather closely spaced stations around the Laacher See (Eifel) confirmed the existence and depth of the low-resistivity layer within the crust at the western end of the present transect. Also Bahr (1985) obtained a similar result south of the Laacher See and in the Westerwald.

Bahr (1985) also determined the upper mantle resistivity at two sites, one close to the Rhine, and one in the Westerwald. He applied a particular geomagnetic method which is free of static shift problems. The important aspect of his models is the inference of the upper boundary of the electrical asthenosphere (conductosphere) which appears to be at about 180 km at a station beside the Rhine river and at about 80 km at a station in the Westerwald.

4.C5. Structure and interpretation

4.C5.1. Introduction

The transect of Figure 4–25 is a summary of all available geophysical data. It has been drawn between Luxembourg in the southwest and the Harz Mountains in the northeast and follows approximately the main line of the long-range seismic project of 1979 (Figs. 4–9 and 4–21). The cross section contains essentially seismic information, mainly from seismic-refraction surveys (Mechie et al., 1983; Aichroth et al., 1992; Prodehl and Aichroth, 1992), but where available, also seismic-reflection results (Glocke and Meissner, 1976; Meissner et al., 1976a, 1980, 1983; Franke et al., 1990a; DEKORP Research Group, 1991). Teleseismic traveltime studies (Raikes, 1980; Raikes and Bonjer, 1983) and body shear and surface wave investigations (Panza et al., 1980) have also been incorporated. At some locations results of seismicity and special earthquake studies are available, and the position of hypocenters has been marked (Ahorner, 1983). Zones of increased conductivity have been obtained from magnetotelluric studies for the lower crust as well as for the subcrustal lithosphere (Jödicke et al., 1983, Volbers et al., 1990).

The upper part of the section contains geophysical data which have been mapped during various surveys: Bouguer gravity (Gerke, 1957; Jacoby et al., 1983), aeromagnetics (Eberle, 1973), heat flow (Hänel, 1983) and uplift / subsidence data from repeated detailed geodetic surveys (DGK-Arbeitskreis, 1979; Mälzer et al., 1983).

Magnetic anomalies correlate with outcropping volcanic areas in the Eifel, Westerwald and northern Hessen depression. Model calculations do not show any significant increase over the mean heat-flow density of 70 to 81 mWm^{-2} for Germany (Hänel, 1983). The map of height changes (DGK-Arbeitskreis, 1979) indicates uplift for areas of the eastern Eifel and Westerwald (0.6 mm/yr) and subsidence (–0.4 mm/yr) as well as uplift for the Hessen depression near Kassel (0.5 mm/yr).

4.C5.2. Near-surface rift structures

Throughout the Rhenish Massif, the uppermost part of the crust is rather uniform (Fig. 4–25) characterized by velocities increasing from about 5.1–5.5 km/s near the surface to 6.2–6.3 km/s at about 2–3 km depth. Only in the east, beneath the Hessen depression, is the depth to the crystalline basement for velocities above 6 km/s greater than 5 km. With increasing depth a basement of rather high velocity of about 6.3–6.4 km/s and relative uniformity is encountered; velocities vary only slightly in vertical and horizontal directions. Along the seismic-reflection line DEKORP-2N (Fig. 4–22; Franke et al., 1990a), the upper crust is characterized by a multitude of reflections which relate to stratigraphic and tectonic elements of the Variscan fold belt. Important thrust faults known at the surface can be correlated with prominent reflections east of the Rhine from the Ebbe Anticline southwards. West of the Rhine the Aachen thrust belt (Faille du Midi), in particular, can be followed southwards in the reflection data.

Fig. 4–25. Geophysical transect through the Rhenish Massif and Hessen depression from Luxembourg to the Harz. For location, see BB' in Figure 4–9.
Sources: Ahorner, 1983; Aichroth et al., 1992; DGK-Arbeitskreis, 1979; DEKORP Research Group, 1991; Dürbaum et al., 1967; Eberle, 1973; Franke et al., 1990a; Fuchs et al., 1983; Glocke and Meissner, 1976; Gerke, 1957; Grubbe, 1976; Hänel, 1983; Jacoby et al., 1983; Jödicke et al., 1983; Mälzer et al., 1983; Mechie et al., 1983; Meissner et al., 1976a, 1980, 1983; Mooney and Prodehl, 1978; Prodehl and Fuchs, 1986; Raikes, 1980; Raikes and Bonjer, 1983; Schmincke et al., 1983; Volbers et al., 1990.
Explanations: Sp = shotpoints of 1979 survey (Mechie et al., 1983); dashed bars = steep-angle reflections: DKP2-N = line DEKORP 2N (Franke et al., 1990a); DJN 1967 = local seismic survey (Dürbaum et al., 1967); EGT = European Geotraverse; OCH = Ochtendung fault zone (Ahorner, 1983, fig. 10); vertically hatched depth range = zone of decreased P-wave velocity (larger or equal to 3%) in the uppermost mantle from teleseismic tomography studies (from Raikes, 1980). For further explanation, see Figure 4–17. **(a)** Bouguer anomalies (from Jacoby et al., 1983). **(b)** Magnetic anomalies (from Eberle, 1973). (c) Heat flow (from Hänel, 1983). **(d)** Recent crustal movement (from DGK-Arbeitskreis, 1979). **(e)** Generalized cross section BB' of the lithosphere comprising seismic-refraction, seismic-reflection, teleseismic, and magnetotelluric data

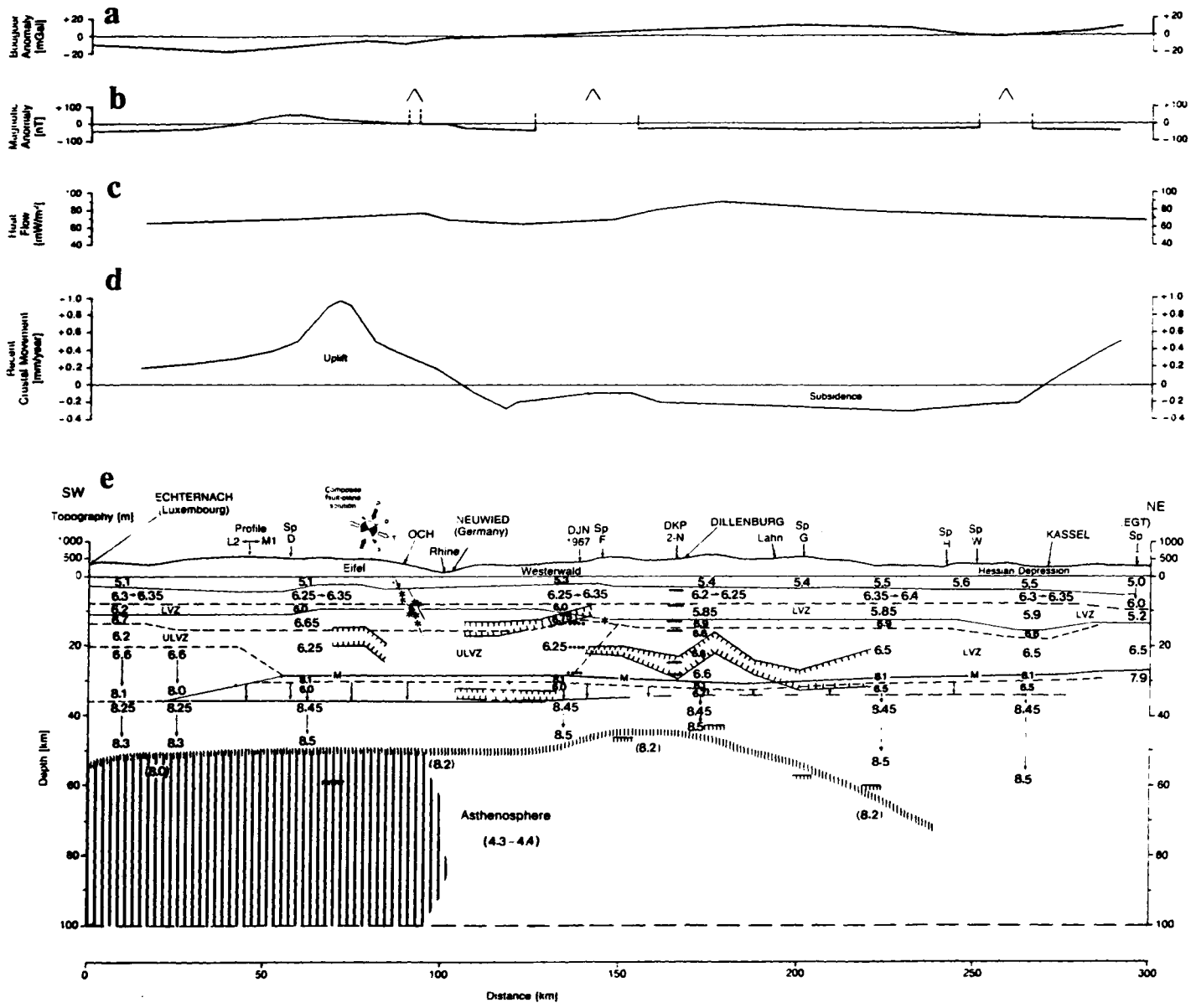
a
b
c
d
e
Uplift
Subsidence
SW
NE
ECHTERNACH
(Luxembourg)
Topography [m]
Profile
L2 — M1
Sp
D
OCH
NEUWIED
(Germany)
Rhine
DJN
1967
Sp
F
DKP
2-N
DILLENBURG
Lahn
Sp
G
Sp
H
Sp
W
KASSEL
EGT)
Sp
Eifel
Westerwald
Hessian Depression
LVZ
ULVZ
M
Asthenosphere
(4.3 - 4.4)
Depth [km]
Distance [km]

At a depth of about 8 km (dashed interface in Fig. 4–25) a velocity inversion is recognized along the entire length of the transect. In the west, this upper-crust low-velocity zone is rather thin and the velocity reversal relatively small, decreasing from about 6.35 km/s to 6.0–6.2 km/s. East of the Rhine, the velocity reversal is greater (6.4 / 5.85 km/s) and the thickness of the low-velocity zone increases to a maximum beneath the Hessen depression. This is in agreement with the data of the European Geotraverse (Aichroth et al., 1992, Prodehl and Giese, 1990).

The DEKORP-2N seismic-reflection line, which crosses the transect near Dillenburg (Fig. 4–25), indicates that the middle crust has a thickness of approximately 3–6 s TWT and displays a considerable relief. It is bounded by levels of high reflectivity, but is in itself relatively transparent (Franke et al., 1990a). This transparent middle crustal layer correlates roughly with a zone of reduced velocity gradient or weak velocity inversion and a remarkably good electrical conductor (EREGT Group, 1990, ERCEUGT Group, 1990, 1992). The strongly reflective levels marking its upper and lower boundary appear as high-velocity lamellae in the refraction data (Aichroth et al., 1992; Mechie et al., 1983).

Immediately west of the Rhine, in the western part of the Neuwied basin, a seismically active fault mapped by Ahorner (1983) is shown on the transect. Hypocenters associated with this fault can be traced to a depth of about 15 km, traversing the upper crust and reaching into a high-velocity middle crustal layer characterized by velocities between 6.6 and 6.7 km/s. This high-velocity zone is thickest (5–6 km) where the suggested northwestern prolongation of the Rhinegraben traverses the Rhenish Massif; eastward it thins and its velocity increases to as much as 6.9 km/s.

4.C5.3. Deep crust

The middle crust, below 12–15 km depth, shows strong vertical and lateral heterogeneity. In the western half of the transect, to some 10 km east of the Rhine, a very strong velocity decrease from 6.7 to 6.2 km/s is postulated. East of the Westerwald volcanic field, where the velocity of the overlying high-velocity zone increases to 6.9 km/s, the lower crust has a velocity of 6.5 km/s; i.e. the velocity contrast between upper and middle crust becomes smaller. Along the European Geotraverse, a similar locally confined high-velocity zone is found at 12 km depth beneath the Hessen depression south of shotpoint I (Fig. 4–9; Aichroth et al., 1992). In the DEKORP-2N profile (Franke et al., 1990a) this thin high-velocity layer can be related to a zone of convergent listric thrust faults giving rise to an anisotropic effect (Giese et al., 1990).

Below the mid-crustal high-velocity zone, the lower crust is characterized by decreased velocities ranging in depth from 15–18 to 30 km. The lower crust corresponds to a zone of increased conductivity as observed in the area of the Eifel and Westerwald. However, under the Neuwied Basin, this high-conductivity zone appears to be absent. Within the lower crustal low-velocity zone, strong lateral velocity changes are observed. Moreover, the anomalous high-conductivity layer appears to change abruptly in depth and disappears altogether towards the Hessen depression.

The DEKORP-2N reflection profile shows that the lower crust is essentially non-reflective in the north, outside the area of Cenozoic volcanic activity, and highly reflective in its southern parts where it passes between the Westerwald and Vogelsberg volcanic centers.

Fig. 4–26. Crustal cross section along the EGT Central Segment between Lake Constance and the Baltic Sea. Depth versus distance is exaggerated 4–1. *Upper part:* Seismic-refraction model. The contour interval of the iso-velocity lines (dashed lines) is 0.1 km/s between shotpoints D and J, and 0.2 km/s between shotpoints J and K. Discontinuous velocity changes are indicated by thick lines with two velocity values, above and below the boundary (from Aichroth et al., 1992; Prodehl and Aichroth, 1992). *Lower part:* Petrological interpretation of the seismic cross section (from Franke et al., 1990b; Prodehl and Aichroth, 1992). The vertical columns indicate locations where xenolith data are available from young volcanic eruptions (Mengel et al., 1991).

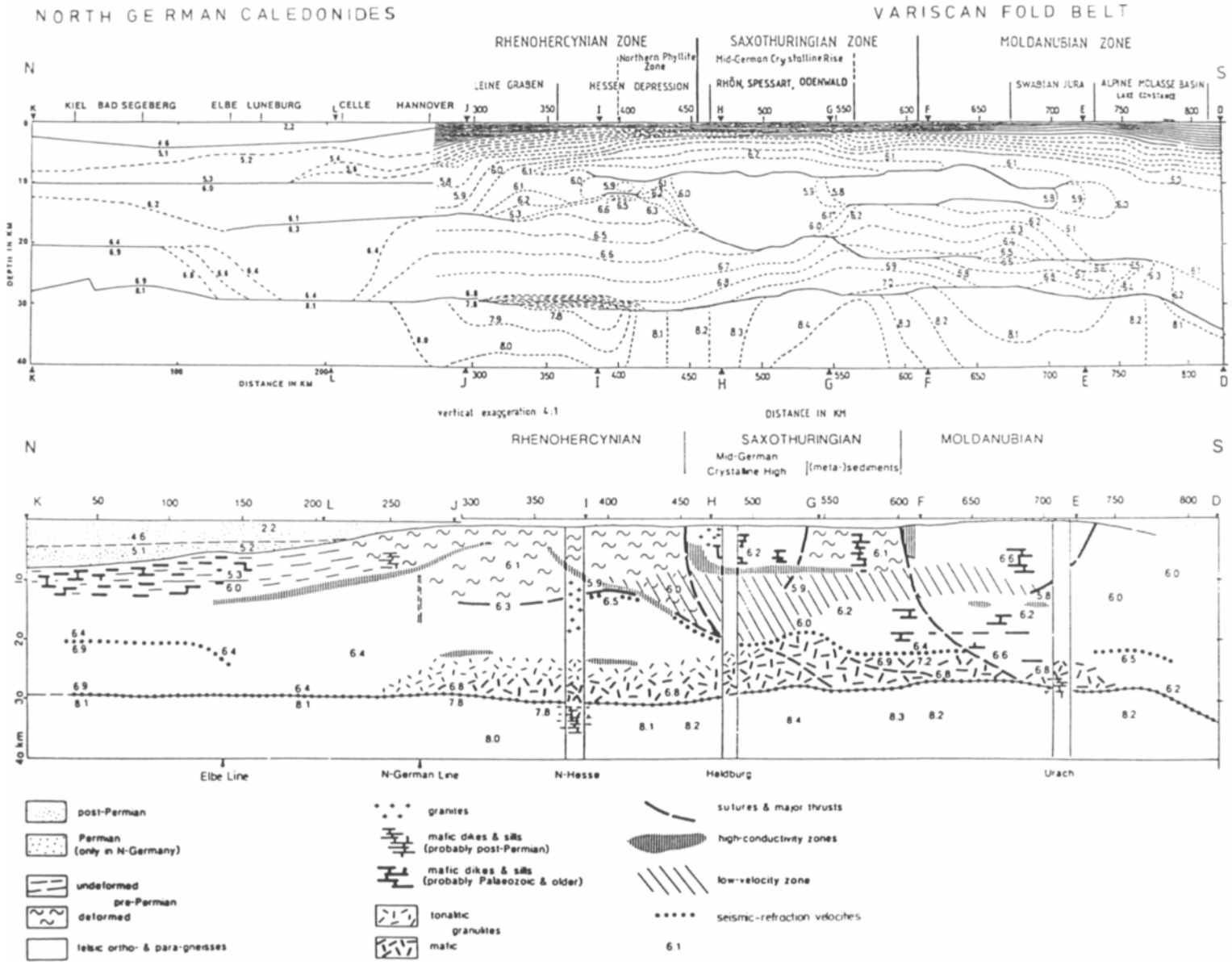
NORTH GERMAN CALEDONIDES
VARISCAN FOLD BELT
RHENOHERCYNIAN ZONE
SAXOTHURINGIAN ZONE
MOLDANUBIAN ZONE
Northern Phyllite Zone
Mid-German Crystalline Rise
LEINE GRABEN
HESSEN DEPRESSION
RHÖN, SPESSART, ODENWALD
SWABIAN JURA
ALPINE MOLASSE BASIN
LAKE CONSTANCE
KIEL
BAD SEGEBERG
ELBE LUNEBURG
CELLE
HANNOVER
N
S
DEPTH IN KM
DISTANCE IN KM
vertical exaggeration 4:1
RHENOHERCYNIAN
SAXOTHURINGIAN
Mid-German Crystalline High
(meta-)sediments
MOLDANUBIAN
40 km
Elbe Line
N-German Line
N-Hesse
Heldburg
Urach
post-Permian
Permian (only in N-Germany)
undeformed pre-Permian
deformed
felsic ortho- & para-gneisses
granites
mafic dikes & sills (probably post-Permian)
mafic dikes & sills (probably Palaeozoic & older)
tonalitic granulites
mafic
sutures & major thrusts
high-conductivity zones
low-velocity zone
seismic-refraction velocities

To the west of the Ardennes/Rhenish Massif block, beyond the transect shown in Figure 4–25, the crust has an average thickness of 30 km. Velocities in the lower crust immediately above the Moho are anomalously low (6.15 km/s). Under the Ardennes and the western Eifel, below 20 km depth, a high-velocity lower crust is found. The Moho occurs at a depth of 37 km (left part of Fig. 4–25; Mechie et al., 1983). Under most of the Rhenish Massif, however, a thin layer with upper-mantle velocities of 8.1 km/s at a depth of 30 km separates a low-velocity lower crust (6.25–6.5 km/s) from a deeper lower-crust-like layer extending from 30 to 35–37 km. The velocity gradually increases from 6.0 km/s under the eastern Eifel and western Westerwald, and further east from 6.5 km/s, to mantle velocities of 8.3–8.5 km/s. An extensive high-conductivity zone seems to exist in this lower-crust-like depth range east of the Rhine at around 35 km depth which, however, cannot be traced continuously, and at near-constant depth level, further to the east. The data of DEKORP-2N define the Moho as the lower limit of reflections (Prodehl and Giese, 1990). It rises from about 11 s TWT in the north to 8.5 s TWT in the south. At the intersection of DEKORP-2N with the transect, reflections can be identified at 30 and around 35 km depth (Fig. 4–25).

At its easternmost end, the long-range line through the Rhenish Massif crosses the Hessen depression. However, due to lack of sufficient recording distances to the northeast, i.e., beyond the Harz Mountains, depth information is restricted to the upper crust. Here, the European Geotraverse supplies the missing information. The north-south cross section of Aichroth et al. (1992) (see Fig. 4–26) shows the Moho at a depth slightly less than 30 km and normal upper-mantle velocities above 8 km/s, but shows no indication of the prominent velocity inversion between 30 and 37 km as seen underneath the Rhenish Massif to the west. Rather, the crust shows here a particular feature not seen prominently under the Rhenish Massif, namely a strong velocity inversion in the upper crust below 10 km depth. Its intensity and thickness is only comparable to that found beneath the Black Forest (Gajewski and Prodehl, 1987). It is noteworthy that the area underlain by the very distinct velocity inversion is characterized by extensive basaltic volcanism at the surface.

4.C5.4. Upper mantle

Under most of the transect the lithosphere-asthenosphere boundary is located at a depth of 45–50 km, as evident from teleseismic P-delay studies and shear body and surface wave analyses. According to Raikes (1980) and Raikes and Bonjer (1983), this anomalous low-velocity upper mantle region is centered under the western Eifel (Fig. 4–25); it may extend to depths of about 200 km, but terminates to the east approximately at the river Rhine. Compared to the average mantle velocities found outside the Rhenish Massif, mantle velocities are here decreased by 3 to 5%. As a possible explanation, it has been suggested that several distinct mantle domains differing in isotope and trace element ratios were affected during partial melting. Concentric zonation in volume erupted, Mg-numbers and, in part, type of xenoliths in the West Eifel might reflect the detachment level of the magmas in the mantle. Uplift and volcanism may be related via ascent of hotter mantle material beneath the area, partial melting being due to decompression (Schmincke et al., 1983).

The map of lithosphere thickness (Panza et al., 1980) shows a broad thinning of the lithosphere from about 90 to less than 50 km along the area of the Rhinegraben and its northwestern branch. Towards the north, along the Hessen depression and its suggested continuation beneath the North German plain the lithosphere seems to have regained its original thickness.

The results of Raikes and Bonjer (1983) generally correlate with the upper-mantle structure derived by Babuska et al. (1988, 1992) and Spakman (1986) who defined a pronounced velocity inversion under the Rhenish Massif, but who could not resolve local details. According to Panza et al. (1980), the lithosphere-asthenosphere boundary dips east of the Lahn area to depths greater than 50 km. The measured shear-velocity contrast, however, is not always sig-

nificant and varies between an increase and a decrease, i.e., from 4.35 km/s in the lower lithosphere versus 4.2–4.4 km/s in the asthenosphere.

4.6. Tectonic evolution of the European Cenozoic rift system

4.6.1. Role of pre-existing geologic features

According to Illies (1978), the regional setting of the Rhinegraben appears mainly basement controlled. In the Rhinegraben area the Paleozoic basement is indicated by a swarm of lineaments, shear zones, and dikes parallel to the NNE trend of the graben. These pre-existing features had mostly formed during the Asturian phase of the Variscan orogeny and had prepared the way for rifting and locally attracted fault progression during the breakup of the graben in Eocene time (Illies, 1978).

This is not only true for the Rhinegraben, but is generally seen in all grabens of western Europe. The European Cenozoic rift system follows a coherent belt of weakness of the basement from southern Norway to southern France, the so-called Mediterranean-Mjösen zone, as already stated by Stille in 1925 and never denied in recent literature (see, e.g., Illies, 1978, and Ziegler, 1992). Localization of individual grabens can be related to tensional reactivation of Late Variscan fracture systems. The grabens are linked by northeast-trending sinistral transform faults that, according to Ziegler (1992), probably also present reactivated Permo-Carboniferous fracture systems.

4.6.2. Origin and Evolution of stress field

According to Illies (1974c) the main features of Rhinegraben tectonics comprise dip-slip faults, tilted blocks, and antithetic block rotations, leading to a crustal dilatation normal to the graben axis of about 5 km. These features imply a tensional state of stress with a horizontal component of the minimum stress direction normal to the graben axis. Thus, a regional paleo-stress field with an average direction of relative maximum stress about 20° (NNE) must be concluded for the beginning of rifting in central Europe in middle Eocene time. This was followed by a period of relative quiescence with stress conditions for which there has been some controversy concerning interpretations by different authors (Müller et al., 1992). A second short phase of extension began in early Miocene (Ahorner, 1975). The average direction of maximum compressive stress today is about 320° (NW) (Fig. 4–3; Illies, 1974c, Müller et al., 1992), as derived from fault plane solutions of earthquakes (e.g., Ahorner, 1975; Bonjer et al., 1984, 1989; Plenefisch and Bonjer, 1994), over-coring measurements (e.g., Baumann and Illies, 1983; Illies and Greiner, 1979), borehole breakouts (e.g., Blümling, 1986, Becker et al., 1987), evaluation of recent crustal movements (e.g. Mälzer, 1988), hydraulic fracturing measurements (Müller et al., 1992), and geological data (e.g., Illies, 1974c). This modern stress field, characterized by a NW to NNW S_{Hmax} direction and a strike-slip faulting regime, began in the Quaternary (Ahorner, 1975; Illies, 1978; Müller et al., 1992). Illies (1974c) connects temporally the sinistral rotation of about 60° for the axes of the strain ellipse relative to the crust of stable Europe with the sedimentation of the Rhinegraben (see Fig. 4–11).

The overall pattern of focal mechanisms within the Rhenish Massif and its vicinity is clearly related to stress-field-controlled block movements along major crustal fracture zones, like the Rhinegraben system, and shows no direct relationship to the uplift of the Massif (Ahorner, 1983). Only in some special regions, e.g., the Hohes Venn in the northwestern part of the Rhenish Massif, where an exceptionally large present-day uplift rate of 1.6 mm/yr has been found by geodetic means, does Ahorner (1983) see some evidence for a causal correlation between seismicity and plateau uplift.

4.6.3. Generalized evolutionary stages

The changing conditions in the plate-tectonic regime along the contact between the African and the European plate have far-reaching implications for intraplate tectonics in stable Europe (Mueller and Kahle, 1993). Following Illies (1975) who schematically sketched three major stages in the evolution of the Mediterranean-Alpine system (Fig. 4–27), Mueller and Kahle (1993) have summarized the general evolution: The first stage (Fig. 4–27a), in late

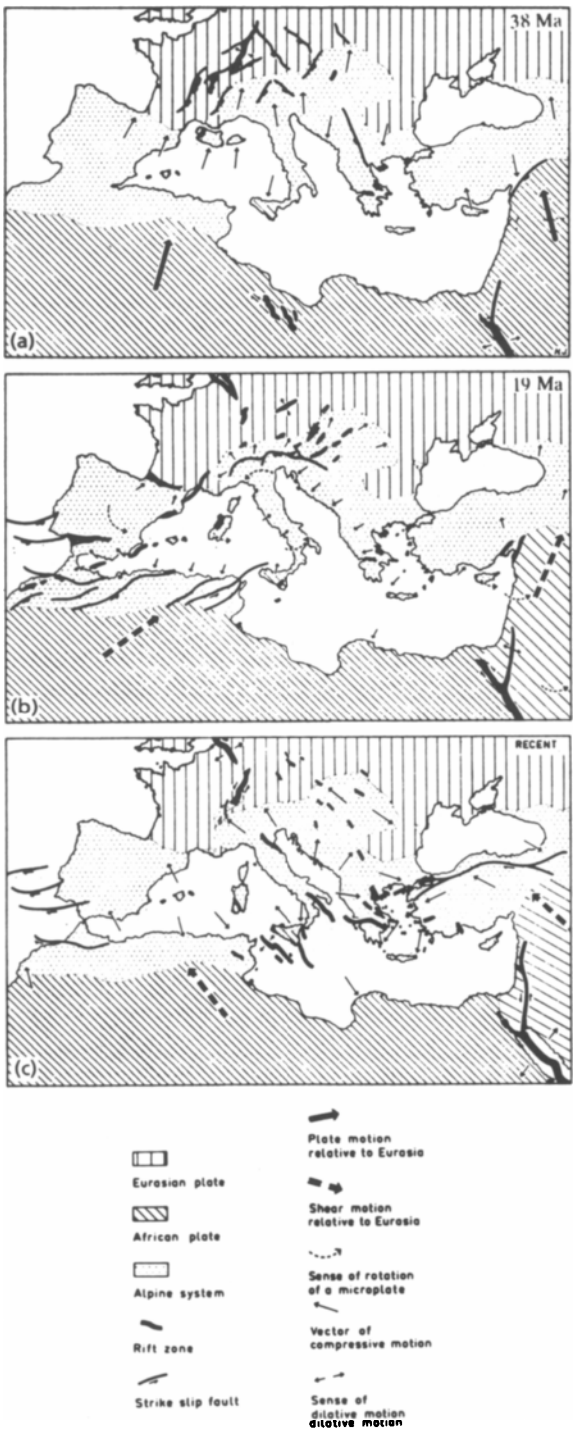

Fig. 4–27. Changing conditions in the plate-tectonic regime along the collision zone between the African and Eurasian plates with implications on intraplate tectonics in Europe and North Africa (after Illies, 1975b. (a) Eocene pattern (about 38 Ma) dominated by a mainly NNE directed compressive deformation. (b) Lower Miocene pattern (about 19 Ma), governed by sinistral shear which conditioned counterclockwise rotations of some interspersed microplates and caused SW–NE oriented orogenic processes. (c) 'Recent' phase (2–0 Ma), favoring dextral strike-slip displacements parallel to the main plate boundary due to a primarily SE–NW oriented compressive stress field.

Eocene (38 Ma ago), is characterized by mainly SSW–NNE directed compressive deformations. This was the phase of maximum folding and overthrusting in the Alps as well as that of most extensive rifting in the western and northern foreland of the arc. In a second stage (Fig. 4–27b), in early Miocene time (~19 Ma), a left-lateral shear motion dominated, causing counterclockwise rotations of some of the lithospheric fragments in the Mediterranean such as the island chain of Corsica and Sardinia and the Apennine peninsula. This stage also favored a SW–NE directed shortening of the lithosphere in a number of orogenic zones around the Mediterranean. In a third stage (Fig. 4–27c), representative of Early Pleistocene(~2 Ma)-to-Recent, right-lateral slip displacements parallel to the plate boundary and a SE–NW-trending compressive push against Europe by the African plate—due to its gradual counterclockwise rotation—are dominant. Both interacting effects produce the stress and motion pattern presently observed in the Mediterranean-Alpine region. Dewey et al. (1989) describe six smoothed and simplified phases of the African motion in the European frame of reference, from 220 Ma to the present (see also Mueller and Kahle, 1993, Table I). The part relevant for the development of the European Cenozoic rift system since the end of Mesozoic times is depicted in Figure 4–28 which also demonstrates the correlation between plate motion and the rotating stress field described above.

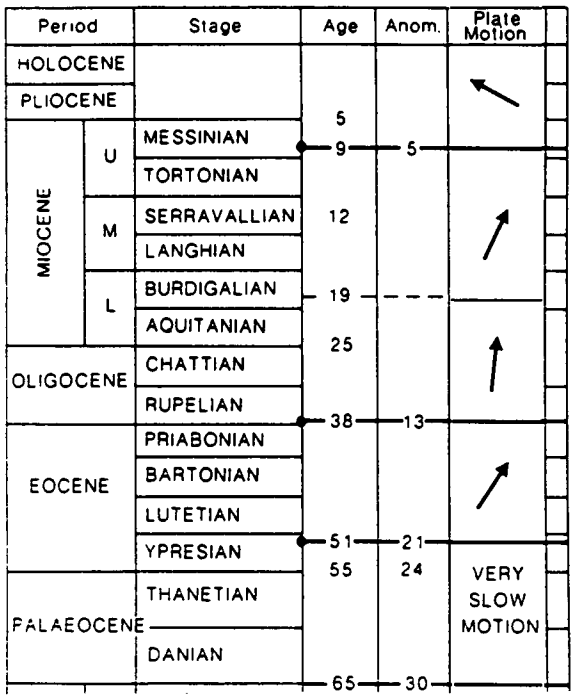

Fig. 4–28. Correlation table showing the general direction of African plate motion with respect to Europe (modified from Mueller and Kahle, 1993, table 1)

Upwelling of mantle material began long before the first indications of rifting and graben formation and, becoming gradually visible at the surface, first signaled imminent changes in the lithosphere-asthenosphere system. In the Early Tertiary, and in some places during the Late Cretaceous, volcanic activity appeared in some areas of the future rift system. At that time the Mesozoic cover was intruded by several groups of volcanic necks and dikes with absolute ages between 70 and 55 Ma. The ascending magma was of a dominantly olivine-nephelinitic composition which must have originated in the upper mantle at depths of 80 to 100 km (corresponding to the "top" of the "undisturbed" asthenosphere in central Europe).

It was only about 25 to 10 Ma later, i.e. in middle Eocene time (45 Ma), that the first surficial changes became apparent. In the Saône, Limagne and Bresse grabens sedimentation commenced during the middle Eocene and in the Rhinegraben in the late Eocene. The formation of the Rhinegraben began in the south with the rifting propagating northward. Magma of about the same composition as the Early Tertiary volcanics was extruded during later volcanic cycles, particularly in Miocene time (18 to 12 Ma), in the Kaiserstuhl and also in the Hegau on the eastern flank.

Gradual subsidence of the graben was largely compensated by simultaneous sedimentation and was accompanied by uplift of the graben shoulders. With the beginning of Lower Miocene the subsidence in the southern graben slowed down after the sediments had reached a thickness of about 2.2 km. Due to uplift of the flanks, substantial erosion took place, which in the Black Forest and Vosges mountains affected a layer of up to 1 km in thickness. The load of sediments denuded from the rift shoulders is of the same order as that deposited in the graben. At that time taphrogenetic processes were still moving further northward, with the most intense activity concentrated in the region of Heidelberg-Mannheim. The framework of the northern trough segment of the Rhinegraben was formed in Plio-Pleistocene time with the sedimentary strata attaining an average thickness of 3.4 km.

A lateral gap with a width about 5 km (more recent results: 5–8 km; R. Altherr, oral communication, 1994) remains open when the vertical movements and the rotations of the tilted blocks are restored (Illies, 1974c). This is the amount by which both flanks of the graben have moved apart horizontally since the Middle Eocene. In addition to vertical movements and tilts, left-lateral strike-slip displacements have taken place in the direction of the graben axis. The amounts of horizontal displacement along strike are, however, rather small in comparison to those of the basement perpendicular to strike.

Further north, the Rhenish Massif was not again covered by the sea after Lower Jurassic time, except for the northern and northwestern margins which were affected by short ingressions during the Upper Cretaceous. The first uplifting movements

took place at the end of the Cretaceous and in the early Tertiary in the northwestern part of the Massif. But in spite of these movements the surface of the entire Massif did not rise much above sea level during the Lower Tertiary. A short marine ingression covered large areas of the western Rhenish Massif in the Middle/Upper Oligocene. The main uplift started at the end of the Oligocene and continued up to the present time (Meyer et al., 1983).

Physiographically, the uplifted block of the Rhenish Massif crosscuts the belt of active rifting. Illies et al. (1979) suggest that incompetent rock material of the upper crust covers an active rift belt underneath and that the tectonically incompetent behavior of the slightly metamorphosed Devonian slates impeded progression of the surficial rift valley.

In terms of regional tectonics the uplifted Rhenish Massif is part of an incoherent mosaic of blocks in the northern foreland of the Alpine fold belt (Illies and Greiner, 1978) which is surrounded by rift valleys and fault troughs. In the west and east, extinct rift segments flank the unit, the Luxembourg embayment and the Hessen depression, respectively. At the southern and northern end, active rift segments, the Rhinegraben and the Lower Rhine embayment, frame the Massif. These active rift segments are linked together seismo-tectonically along a northeast-trending "subplate boundary" which obliquely traverses the Rhenish Massif (Illies and Greiner, 1979).

Illies et al. (1979) interpret the rift-triggered plateau uplift of the Rhenish Massif as a ductile crustal elongation that causes crustal attenuation and the subsequent processes of mantle rise and isostatic rebound. Hidden rift progression evolved in the deeper crust of a unit which surficially marks the missing link with the central European rift belt. Mantle rise and crustal doming substituted here for the physiographic phenomenon of rift valley formation. Rupturally incompetent behavior of the involved rock masses in the upper crust impeded the development of rift type morphostructures.

4.6.4. Reactivation

Geophysical evidence in the Massif Central indicates an updoming of a mantle plume which controls volcanism, heat production, and uplift, but evidently occurs very quietly and at great depth, causing almost negligible seismicity. With the exception of the southern Rhône valley, subsidence and taphrogenesis in the grabens of south-central France is minor.

Young volcanic activity in the Massif Central and in the Eifel as well as present-day seismicity, which is weak in the Massif Central but relatively strong in the southern and northern Rhinegraben and along the northwestern branch of the rift through the Rhenish Massif and Lower Rhine embayment, indicate that rifting has slowed but has not stopped entirely.

The general seismotectonic regime of the Middle Rhine zone between Mainz and Bonn is clearly characterized by extensional rifting along a broad NW–SE trending fracture zone, which follows approximately the course of the Rhine and connects major seismotectonic features of the Rhinegraben with those of the Lower Rhine embayment. The Rhenish Massif is bisected by this zone into two parts which were shifted away from each other in SW–NE direction. From the geological point of view, the hidden zone of active rifting probably consists—even deep underground—not of large pervading fault lines, but of numerous smaller faults, oriented in subparallel or en-echelon configuration. This implies a rather diffuse picture of ruptural deformation of the crust, which might be caused by the slaty composition of the majority of rocks in the upper part of the crust of the Rhenish Massif (Ahorner et al., 1983).

4.7. General conclusions

4.7.1. Key questions and problems

The European Cenozoic rift system is one of the currently active rift systems that evolved on old, stabilized continental crust. It is considered a "passive"

rift system in so far as its evolution was apparently governed by stress-induced lithospheric extension (Ziegler, 1992). Ziegler (1992) describes and discusses a number of models which have attempted to explain the evolution of the Cenozoic rift of central and western Europe, ranging from a hot-spot driven mechanism (Cloos, 1939) through foreland splitting in response to continent-continent collision (Molnar and Tapponnier, 1975; Sengör et al., 1978; Bergerat and Geyssant, 1980; Dewey and Windley, 1988) to a new cycle of plate-reorganization during the late Alpine orogeny. Ziegler (1992) concludes that the evolution of this rift system is governed by the interaction of the Eurasian and African plates and by early phases of a plate-boundary reorganization that may lead to the breakup of the present continental assembly, as suggested by Late Oligocene-early Miocene southward propagation across the west Mediterranean fold belts.

In earlier models of continental rifting a symmetrical shape of the rift-forming structures was assumed which should result in steep flanks and flat morphology of the corresponding graben floor. Recent geophysical investigations in a number of rifts, however, have proved that rifts in general are characterized by strong asymmetries. This is also true for the individual parts of the Cenozoic European rift system, as has been discussed in some detail in the previous sections.

Important elements of many recent investigations of the European Cenozoic rift system comprise:

- earthquakes: their depth distribution and their focal mechanisms,
- recent crustal movements,
- direction of stress,
- temperature-depth distribution,
- basin infill and denudation of the flanks,
- properties of the brittle upper crust, in particular of possible velocity inversions
- properties of the ductile lower crust: structure and the nature of its lamellar structure,
- petrological composition of the crust and upper mantle,
- the role of the uppermost mantle,
- anisotropy.

Geophysical investigations confirm a strong asymmetry of the individual grabens in various parameters:

- sedimentary fill
- volcanic activity
- stress distribution
- gravity
- earthquake distribtion in quantity and in depth
- crustal and upper-mantle structure

The sedimentary fill of the individual grabens is highly asymmetric, as has been discussed in detail above for the Rhinegraben (e.g., Illies, 1974b), the Bresse graben (e.g. Bois et al., 1991), the Limagne graben (Morange et al., 1971) and the southern Rhône valley (Sapin and Hirn, 1974).

There is a significant difference in volcanic activity between individual sections of the European Cenozoic rift system. Increased activity is recorded in the Massif Central and in the Rhenish Massif area including the Hessen depression, while the central portion, the Rhinegraben proper is almost devoid of volcanic fields.

A significant gravity signature is seen for the Rhinegraben and the Limagne graben, although, the magnitudes are quite different. For the Rhinegraben only ~20 mGal differences between graben and flanks are observed, which some authors explain as caused by the sedimentary fill only. For the Limagne graben and surrounding areas of the Massif Central, up to 80 mGal contrasts are observed (Stoll et al., 1994).

Earthquake activity shows a rather peculiar pattern. Present-day activity concentrates in the Lower Rhine embayment, in the northern foreland of the Rhenish Massif to the west, in the northern Rhinegraben (e.g., Ahorner, 1983), and in the southern Rhinegraben, while the Hessen depression and the Massif Central show little to no activity. In addition, the southern Rhinegraben shows a characteristic asymmetry in frequency and depth of events (Bonjer et al., 1984, 1989; Bonjer, 1992).

While for the Rhinegraben and the Rhenish Massif areas, the general trend of the stress field does not seem to be related to any rifting features, sparse data in France indicate a possible rotation of the stress field towards the north, which may be an interaction between Alpine orogeny and rifting. It may

not be accidental that the most recent chain of volcanoes, the Chaîne des Puys, is also oriented in a north-south direction.

Heat flow values in the Rhinegraben average about 70 mWm^{-2}, while for the Massif Central the average is between 90 and 100 mWm^{-2}.

Wherever modern seismic data are available, the lower crust under graben and flank areas is characterized by a strong reflectivity. This seems to be a general characteristic inherited from the Variscan orogeny and is interpreted as the presence of alternating high- and low-velocity layers whose thicknesses are estimated to be of the order of only 100 m (Wenzel et al., 1987). For the Massif Central, it has been shown that the statistical abundance of the high-velocity layers increases with depth (Novak, 1993).

The laminated lower crust has been thinned considerably underneath the graben areas proper, particularly beneath the central Limagne graben (Landes, 1994) and the Rhinegraben (Brun et al., 1992; Echtler et al., 1994).

The crust-mantle boundary shows rift-related updoming, although its intensity is quite variable. Under the Massif Central, updoming seems to be limited to the western sides of the Limagne (Landes, 1994) as well as the Bresse grabens proper (Bois et al., 1991). In contrast, under the southern Rhône valley and under the Rhinegraben, the updoming involves wide parts of the shoulders as well, though here also some asymmetry in the shape of the domes is observed; the western flank is more accentuated, while thickening of the crust is more gentle towards the east (Edel et al., 1975; Sapin and Hirn, 1974).

For the Rhinegraben and the volcanic areas of the Rhenish Massif and the Hessen depression, the Moho, normally a first-order discontinuity, seems to be heavily disrupted, although a P_n-velocity within a normal range slightly above 8 km/s is observed almost everywhere. Under the entire Massif Central, recent seismic observations seem to indicate the overall presence of a normal uppermost mantle with velocities ~8 km/s (Landes, 1994; Novak, 1993; Zeyen et al., 1994), in contrast to earlier interpretations (Perrier and Ruegg, 1993; Hirn and Perier, 1974).

There is a clear low-velocity anomaly in the upper mantle beneath the western Rhenish Massif down to 150 km depth, which is not present to the east. Under the Massif Central, there also is a clear correlation between volcanic areas at the surface and low-velocity zones in the uppermost mantle, i.e., between 25–30 km (Moho) and 60 km depth. The deep (60–150 km), large-scale low-velocity anomaly is interpreted as an indication of a postulated mantle plume (Granet et al., 1994). Under the southern Rhinegraben there is no clear indication of a general low-velocity zone in the lower lithosphere underlying the Moho, but localized, smaller-scale low-velocity areas of limited extent do exist (Glahn et al., 1993).

The recent generalized map of lithospheric thickness by Babuska and Plomerova (1992), derived from average P-wave residuals, shows a thin lithosphere of 60–80 km underneath the Rhenish Massif and northern Rhinegraben, while under the Massif Central a normal thickness of 120–140 km is seen. A quantitatively similar result had also been obtained earlier by Panza et al. (1980) from surface and shear wave investigations. This result is certainly in contrast with more recent and more detailed tomographic results by Granet et al. (1994).

4.7.2. Sequence of events

Ziegler (1992) discusses the sequence of evolutionary events in detail. Initial rifting phases during the late Eocene and Oligocene, as well as compressional foreland stresses connected with Pyrenean and Alpine collision zones caused by African plate motion (see Figs. 4–27 and 4–28), may have played a major role in the tensional reactivation of Permo-Carboniferous fracture systems. Such stresses thus controlled the localization of individual grabens such as the Rhône depression, the Limagne and Bresse grabens, the Rhinegraben, the Burgundy transform fault system, the Hessen depression, and the Lower Rhine embayment (Ziegler, 1992).

Repeated changes in the stress field controlled the subsidence of various segments of the European Cenozoic rift system, possibly as an interplay between collision-related foreland compressional and regional tensional stresses as well as rift-induced

thermal uplift. Progressive lithospheric thinning may have caused thermal updoming in the Rhenish Massif and in the Massif Central which started in the early Miocene and continues today. Intrusion of melts into intra-lithospheric levels may have caused uplift of axial grabens and erosion of their sedimentary fill as may be seen in the grabens developed within the Massif Central and the Vosges-Black Forest system.

The late Oligocene-early Oligocene phase of foreland compression coincides with the initial rifting phases of the Rhine, Saône, Bresse, and Limagne grabens. Subsidence of these grabens was governed by a northerly-directed compressional stress field. During the early Oligocene, the Rhinegraben rifting continued northwards through the Hessen depression and Leine graben to the margins of the Northwest European basin. A reduced subsidence rate in mid-Oligocene indicates a temporary relaxation of compressional foreland stresses. During the late Oligocene-early Miocene a second phase of rapid subsidence started in the Rhinegraben, at the same time the Lower Rhine embayment subsided, indicating a northwestward propagation of rifting which continued into Pliocene times. The Limagne and Bresse grabens ceased to subside during the early Miocene, but the subsidence of the Bresse graben was reactivated again during late Miocene and Pliocene.

4.7.3. Lithospheric thinning and rifting

Various contour maps of the Moho, published for different parts of the central European rift system and adjacent areas by different authors (Edel et al., 1975; Egloff, 1979; Zeis, 1988) have been merged into a joint Moho depth contour map (Fig. 4–29).

The pronounced crustal thinning of about 20% in comparison with the surrounding areas (Hirn, 1976), as found for the southern Rhône valley and the Rhinegraben, does not seem to continue along the entire graben system. For the Limagne, northern Rhône-, upper Saône, and Bresse graben systems, seismic data also indicate a reduction in crustal thickness in comparison with the structure beneath the flanking plateau de Langres in the west and the Swiss Jura in the east. However, the difference does not exceed 10% (Michel et al., 1977). For example, Egloff (1979) finds depths of 27–29 km for profiles reaching from the northern Rhône graben into the Swiss Jura, and his Moho depth contour map indicates a gradual increase in crustal thickness from 26 km northwest of the Swiss Jura to 30 km at its eastern border. The axis of minimum crustal thickness follows approximately the direction of the northern Bresse and, north of the city of Dôle, seems to bend towards the northwest.

In conclusion, it is well documented that the crust for the graben areas of the central European rift system differs from the adjacent continental crust. Besides a strong seismic reflection from the crust-mantle boundary, and sometimes replacing it, a strong-amplitude intracrustal phase is evident on many graben profiles indicating a good reflector at about 20 km depth. A highly anomalous crust-mantle transition—confined to the Rhinegraben proper—is superimposed on a regional uplift of the crust-mantle boundary which reaches well beyond the boundaries of the graben. Such a transition zone is also well documented for the graben areas of southeastern France. The updoming of the mantle (Fig. 4–29) which reflects a fairly active stage of taphrogenesis (Menard, 1973) culminates in the southern Rhinegraben and the Limagne graben and, to a certain extent, is also seen under the Vogelsberg and the subsequent Hessen depression. Under the Rhenish Massif, taphrogenesis may have just started or has been severely disturbed by the very strong crustal block of the Rhenish Massif, and therefore may not yet have reached its culmination.

Teleseismic investigations of the Massif Central (Fig. 4–8), the southern Rhinegraben (Fig 4–18), and the Rhenish Massif (Fig. 4–25; Raikes and Bonjer, 1983) provide strong evidence for considerable upper-mantle heterogeneity. Anomalous velocity-depth structure at lower crustal-uppermost mantle level reflect a clear coincidence of two zones of decreased seismic velocities and the presence of volcanic activity which are evident from the surface to a depth of 70 km (Granet et al., 1994). Plume interactions causing mass intrusion, differentiation, or phase transformations may be considered as possible causes for the low-velocity zone below 70 km depth. The graben system and the volcanic provinces of the Massif Central are clearly situated above a region

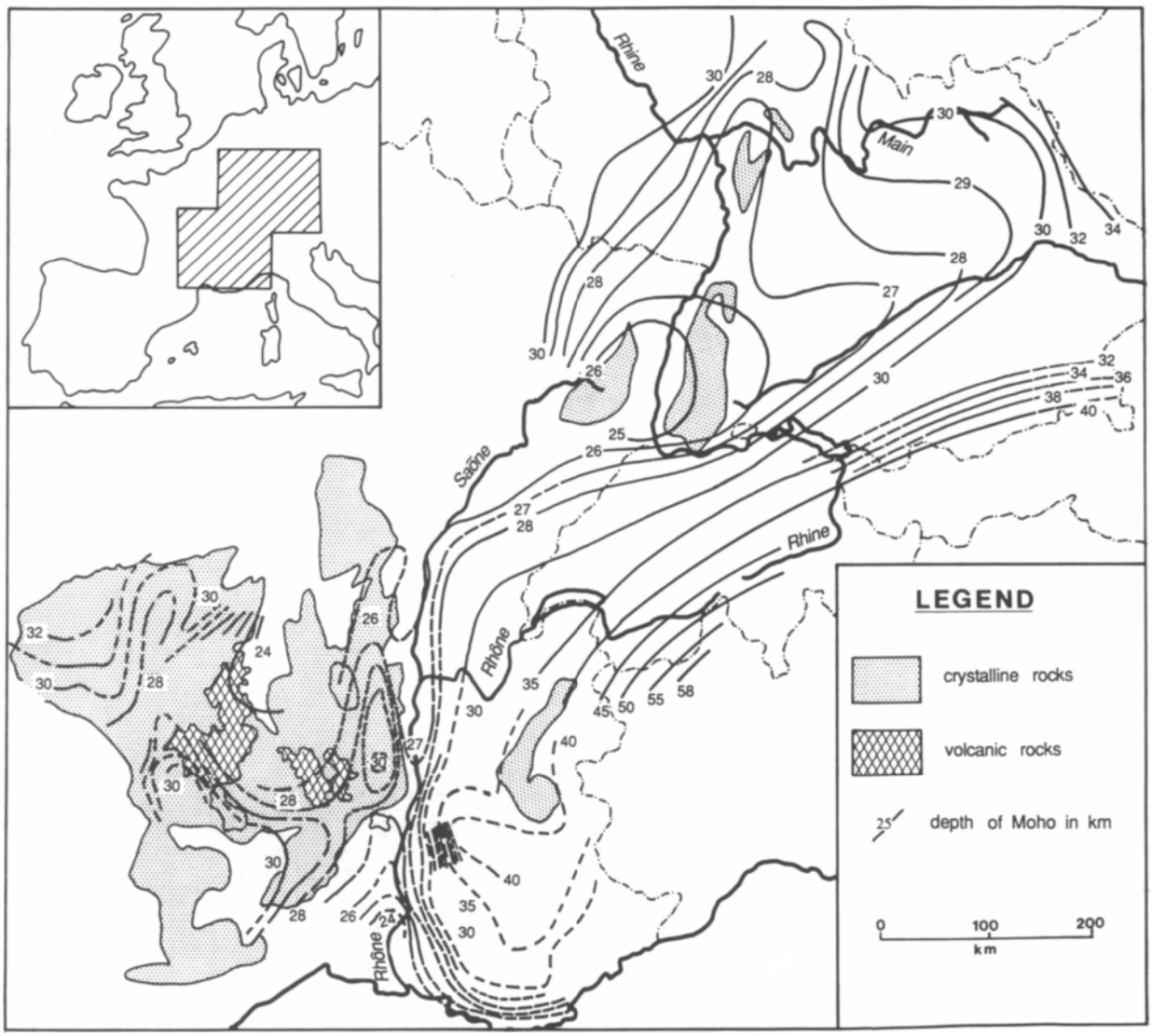

Fig. 4–29. Contour map of the depth to the crust-mantle boundary along the European Cenozoic rift system through southeastern France and southwestern Germany. After Prodehl et al. (1992), compiled from Edel et al. (1975), Egloff (1979), Hirn (1976), Zeis (1988), and Zeis et al. (1989).

of anomalously low-velocity upper mantle (Granet et al., 1994). Here, active upwelling of mantle material is indicated. In contrast, for the southern Rhinegraben, velocity reductions are on the order of a maximum of 2% and areas of decreased velocity cannot be traced over long distances as continuous, graben-related features (Glahn et al., 1993). However, under the western Rhenish Massif there is again a distinct region of strong velocity reduction (3–5%) reaching from 50 to at least 200 km depth, indicative of a unique upwarp of the lithosphere-asthenosphere boundary (Raikes and Bonjer, 1983).

In conjunction with a zone of increased seismicity extending from the northern Rhinegraben along the river Rhine into the Lower Rhine embayment, it seems evident that taphrogenesis has shifted its center of activity away from the southern Rhinegraben towards the Lower Rhine embayment, possibly in connection with a gradual upwarp of asthenospheric material under the western Rhenish Massif. The possible extension of this upwarp to the northwest is unknown. However, such a velocity reversal is definitely not seen under the eastern Rhenish Massif. Fuchs and Wedepohl (1983) discuss this asymmetry of the mantle anomaly in terms of the occurrence of Quaternary volcanism west of the Rhine only.

Acknowledgments. The authors thank U. Achauer, B. Aichroth, K.-P. Bonjer, D. Gajewski, A. Hirn, W.S. Holbrook, M. Landes, E. Lüschen, J. Mechie, B. Müller, O. Novak, R. Stangl, G. Stoll, F. Wenzel and H. Zeyen for valuable discussions and for data and material which were not, or only partly, published at the time of writing. B. Müller supplied the stress map of central Europe. K. Fuchs and J. Ansorge have contributed to this paper by many fruitful discussions. The authors are especially grateful to J. Ansorge and H. Zeyen who carefully reviewed the manuscript. The German Research Society supported the CREST working group by enabling two of the authors (V.H. and C.P.) to participate in the necessary working sessions at Los Alamos, New Mexico.

4.8. References

Ahorner, L., 1970. Seismo-tectonic relations between the graben zones of the Upper and Lower Rhine valley. In: Illies, J.H., and Mueller, St. (Editors): Graben problems. Schweizerbart, Stuttgart: pp. 155–166.

Ahorner, L., 1975. Present-day stress field and seismotectonic block movements along major fault zones in central Europe. In: Pavoni, N., and Green, R. (Editors), Recent crustal movements. Tectonophysics, 29: 233–249.

Ahorner, L., 1983. Historical seismicity and present-day microearthquake activity of the Rhenish Massif, central Europe. In: Fuchs, K., von Gehlen, K., Mälzer, H., Murawski, H., and Semmel, A. (Editors): Plateau uplift - the Rhenish Shield - a case history. Springer, Berlin-Heidelberg: pp. 198–221.

Ahorner, L., Baier, B., and Bonjer, K.-P., 1983. General pattern of seismotectonic dislocation and the earthquake-generating stress field in central Europe between the Alps and the North Sea. In: Fuchs, K., von Gehlen, K., Mälzer, H., Murawski, H., and Semmel, A. (Editors): Plateau uplift - the Rhenish Shield - a case history. Springer, Berlin-Heidelberg: pp. 187–197.

Ahrendt, H., Hunziker, J.C., and Weber, K., 1978. K/Ar-Altersbestimmungen an schwach-metamorphen Gesteinen des Rheinischen Schiefergebirges. Z. Dtsch. Geol. Ges., 129: 229–247.

Aichroth, B., Prodehl, C., and Thybo, H., 1992. Crustal structure along the central segment of the EGT. In: R. Freeman and St. Mueller (Editors), The European Geotraverse, Part 8. Tectonophysics, 207: 43–64.

Ansorge, J., Bonjer, K.-P., and Emter, D., 1979. Structure of the uppermost mantle from long-range seismic observations in southern Germany and the Rhinegraben area. In: Fuchs, K., and Bott, M.H.P. (Editors): Structure and compositional variations of the lithosphere and asthenosphere. Tectonophysics, 56: 31–48.

Ansorge, J., Emter, D., Fuchs, K., Lauer, J.P., Mueller, St., and Peterschmitt, E., 1970. Structure of the crust and upper mantle in the rift system around the Rhinegraben. In: Illies, J.H., and Mueller, St. (Editors): Graben problems. Schweizerbart, Stuttgart: pp. 190–197.

Aubert, M., and Perrier, G., 1971. La structure profonde du Massif Central. In: Symposium sur la géologie, la morphologie, et la structure profonde du Massif Central français. Plein Air Service Éd., Clérmont-Ferrand, pp. 45–69.

Autrant, A., Gérard, A., and Weber, C., 1976. La carte gravimétrique de la France, exemples d'utilisation géologique. Bull Soc. Géol. Fr., 18: 1119–1132.

Babuska, V., Plomerova, J., and Pajdusak, P., 1988. Lithosphere-asthenosphere in central Europe: models derived from P residuals. In: G. Nolet and B. Dost (Editors), Fourth Workshop on the European Geotraverse (EGT) project - the upper mantle. Europ.Science Foundation, Strasbourg, pp. 37–48.

Babuska, V., and Plomerova, J., 1992. The lithosphere in central Europe - seismological and petrological aspects. In: R. Freeman and St. Mueller (Editors), The European Geotraverse, Part 8. Tectonophysics, 207: 141–163.

Bahr, K., 1985. Magnetotellurische Messung des elektrischen Widerstandes der Erdkruste und des oberen Mantels in Gebieten mit lokalen und regionalen Leitfähigkeitsanomalien. Ph.D. Thesis, Univ. Göttingen, 121 pp.

Baier, B., and Wernig, J., 1983. Microearthquake activity near the southern border of the Rhenish Massif. In: Plateau uplift - the Rhenish Shield - a case history. Springer, Berlin-Heidelberg: pp. 222–227.

Bamford, D., 1973. Refraction data in western Germany - a time-term interpretation. Z. Geophys., 39: 907–927.

Bamford, D., 1977. P_n velocity anisotropy in a continental upper mantle. Geophys. J. R. astr. Soc., 49: 29-48.

Banda, E., and Santanach, P., 1992. The Valencia trough (western Mediterranean): an overview. In: P.A. Ziegler (Editor), Geodynamics of rifting. Volume I. Case history studies on rifts: Europe and Asia. Tectonophysics, 208: 183–202.

Bartelsen, H., Lueschen, E., Krey, Th., Meissner, R., Schmoll, J., and Walther, Ch., 1982. The combined seismic reflection - refraction investigation of the Urach geothermal anomaly. In: Hänel, R. (ed.): The Urach geothermal project (Swabian Alb, Germany). Schweizerbart, Stuttgart: pp. 247–262.

Bauer, C., 1995. Schweremodellierung von 3-D-Strukturen er Erdkruste im Französischen Zentralmassiv unter Einbeziehung seismischer und geologischer Informationen. Diploma Thesis, Univ. Karlsruhe, in prep.

Baumann, H., and Illies, J.H., 1983. Stress field and strain release in the Rhenish Massif. In: Fuchs, K., von Gehlen, K., Mälzer, H., Murawski, H., and Semmel, A. (Editors): Plateau uplift - the Rhenish Shield - a case history. Springer, Berlin-Heidelberg: pp. 177–186.

Bayer, R., and Cuer, M., 1981. Inversion tri-dimensionelle des données aéromagnetiques sur le massif volcanique du Mont Dore: implications structurales et géothermiques. Ann. Géophys., 37: 347–365.

Becker, A., Blümling, P., and Müller, W.H., 1987. Recent stress field and neotectonics in the Eastern Jura Mountains, Switzerland. Tectonophysics, 135: 277–288.

Bergerat, F., and Geyssant, J., 1980. La fracturation tertiaire de l'Europe du Nord: résultat de la collision Afrique - Europe. C.R. Acad. Sci. Paris. Ser. D, 390: 1521–1524.

Bergerat, F., Mugnier, J.-L., Guellec, S., Truffert, C., Cazes, M., Damotte, B., and Roure, F., 1990. Extensional tectonics and subsidence of the Bresse basin: an interpretation from ECORS data. Mém. Soc. Géol. France, N.S., 156: 145–156.

Berktold, A., 1989. Electrical resistivity studies at the KTB location Schwarzwald. In: R. Emmermann and J. Wohlenberg (Editors), The German Continental Deep Drilling Program (KTB) - site selection studies in the Oberpfalz and Schwarzwald. Springer, Berlin-Heidelberg, pp. 385–408.

Berktold, A., and K. Kemmerle, 1982. Distribution of electrical conductivity in the Urach geothermal area, a magnetotelluric and geomagnetic depth sounding investigation. In: R. Hänel (ed.), The Urach Geothermal Project, Schweizerbart, Stuttgart, pp. 289-300.

Bibus, E., 1983. Distribution and dimension of young tectonics in the Neuwied basin and the lower middle Rhine. In: Fuchs, K., von Gehlen, K., Mälzer, H., Murawski, H., and Semmel, A. (Editors): Plateau uplift - the Rhenish Shield - a case history. Springer, Berlin- Heidelberg: pp. 55–61.

Blès, J.L., and Gros, Y., 1991. Stress field changes in the Rhône valley from the Miocene to the present. Tectonophysics, 194: 265–277.

Blès, J.L., Bonigoly, D., Castaing, C., and Gros, Y., 1989. Successive post-Variscan stress fields in the European plate (French Massif Central and its borders): comparison with geodynamic data. Tectonophysics, 169: 79–111.

Blümling, P., 1986. In-situ Spannungsmessung in Tiefbohrungen mit Hilfe von Bohrlochrandausbrüchen und die Spannungsverteilung in der Kruste Mitteleuropas und Australiens. Ph.D.Thesis, Univ. Karlsruhe, 135 pp.

Blundell, D., Freeman, R., and Mueller, St. (Editors), 1992. A continent revealed - The European Geotraverse. Cambridge Univ. Press, 275 pp.

Boigk, H., and Schöneich, H., 1970. Die Tiefenlage der Permbasis im nördlichen Teil des Oberrheingrabens. In: Illies, J.H., and Mueller, St. (Editors), Graben problems. Schweizerbart, Stuttgart: 45–55.

Boigk, H., and Schöneich, H., 1974. Perm, Trias und älterer Jura im Bereich der südlichen Mittelmeer-Mjösen-Zone und des Rheingrabens. In: Illies, J.H., and Fuchs, K. (Editors), Approaches to Taphrogenesis. Schweizerbart, Stuttgart: 60–71.

Bois, C., and ECORS Scientific Parties, 1991. Post-orogenic evolution of the European crust studied from ECORS deep seismic profiles. In: Meissner, R., Brown, L., Dürbaum, H.-J., Franke, W., Fuchs, K., and Seifert, F. (Editors), Continental lithosphere: deep seismic reflections. Am. Geophys. Un., Geodyn. Ser., 22, Washington, D.C., pp. 59–68.

Bonjer, K.-P., 1992. The southern part of the Upper Rhinegraben area: Seismicity and seismic dislocation pattern at the eastern masterfault system. SFB-Berichtsband 1990-1992, pp. 985–1031.

Bonjer, K.-P., Faber, SD., and Apopei, I., 1989. Seismizität als Zugang zu räumlichen und zeitlichen Anomalien der Spannungen in der Lithosphäre. SFB-Berichtsband 1987-1989, pp. 65–138.

Bonjer, K.-P., Gelbke, C., Gilg, B., Rouland, D., Mayer-Rosa, D., and Massinon, B., 1984. Seismicity and dynamics of the upper Rhinegraben. J. Geophys., 55: 1–12.

Bortfeld, R.K., Gowin, J., Stiller, M., Baier, B., Behr, H.-J., Heinrichs, T., Dürbaum, H.J., Hahn, A., Reichert, C., Schmoll, J., Dohr, G., Meissner, R., Bittner, R., Milkereit, B., and Gebrande, H., 1985. First results and preliminary interpretation of deep reflection seismic recordings along profile DEKORP-2-south. J. Geophys., 57: 137–163.

Bottinga, Y., Hirn, A., and Steinmetz, L., 1973. Implications de l'existence d'un canal à moindre vitesse sous Moho. Bull. Soc. Géol. Fr., (7), 15: 500–505.

Brey, G:P:, and Köhler, T.P., 1990. Geothermobarometry in four phase lherzolithes II. New thermometers and practical assessment of existing thermometers. J. Petrol., 31: 1353–1378.

Briot, D., and Harmon, R.S., 1989. Relationships between isotopes and geologic settings in volcanics from the Massif Central. Terra abstracts, 1: 343.

Brousse, R., 1971. Magmatologie du volcanisme néogène et quaternaire du Massif Central. In: Symposium sur la géologie, la morphologie, et la structure profonde du Massif Central français. Plein Air Service Éd., Clérmont-Ferrand, pp. 377–478.

Brun, J.-P., Gutscher, M.-A., and the ECORS-DEKORP teams, 1992. Deep crustal structure of the Rhine Graben from DEKORP-ECORS seismic reflection data: a summary. In:

P.A. Ziegler (Editor), Geodynamics of Rifting, Volume I. Case history studies on rifts: Europe and Asia. Tectonophysics, 208: 139–147.

Brun, J.-P., Wenzel, F., and the ECORS-DEKORP team, 1991. Crustal scale structure of the southern Rhine Graben from ECORS - DEKORP seismic reflection data. Geology, 19: 758–762.

Burkhardt, H., Haack, U., Hahn, A., Honarmand, H., Jäger, K., Stiefel, A., Wägerle, P., and Wilhelm, H., 1989. Geothermal investigations in the KTB locations Oberpfalz and Schwarzwald. In: R. Emmermann and J. Wohlenberg (Editors), The German Continental Deep Drilling Program (KTB) - site selection studies in the Oberpfalz and Schwarzwald. Springer, Berlin-Heidelberg, pp. 433–480.

Cantarel, P., and Lippolt, H.J., 1977. Alter und Abfolge des Vulkanismus der Hocheifel. Geol. Paläontol. Monatsh., 1977: 600–612.

Cermak, V., Bodri, L., Schulz, R., and Tanner, B., 1991. Crustal temperatures along the central segment of the European Geotraverse. In: R. Freeman, Huch, M., and St. Mueller (Editors), The European Geotraverse, Part 7. Tectonophysics, 195: 241–251.

Chapman, D.S., 1986. Thermal gradients in the continental crust. In: Dawson, J.B., Carswell, D.A., Hall, J., and Wedepohl, K.H. (Editors), The nature of the lower continental crust. Geol. Soc. Spec. Publ., no. 24, pp. 63–70.

Cloos, H., 1939. Hebung - Spaltung - Vulkanismus: Elemente einer geometrischen Analyse irdischer Großformen. Geol. Rdsch., 30: 405–527.

Contini, D., and Théobald, N., 1974. Relations entre le Fossé Rhönan et le Fossé de la Saône. Tectonique des régions sous-vosgiennes et préjurassiennes. In: Illies, J.H., and Fuchs, K. (Editors): Approaches to taphrogenesis. Schweizerbart, Stuttgart: pp. 310–321.

Cornet, F.H., and Burlet, D., 1992. Stress field determinations in France by hydraulic tests in boreholes. In: Zoback, M.L. (ed.), The world stress map project. J. Geophys. Res., 97: 11,829–11849.

Deichmann, N., and Ansorge, J., 1983. Evidence for lamination in the lower continental crust beneath the Black Forest (Southwestern Germany). J. Geophys., 52: 109–118.

DEKORP Research Group, 1991. Results f the DEKORP 1 (BELCORP-DEKORP) deep seismic reflection studies in the western part of the Rhenish Massif. Geophys. J. Int., 106: 203–227.

Demnati, A., and Dohr, G., 1965. Reflexionsseismische Tiefensondierungen im Bereich des Oberrheingrabens und des Kraichgaus. Z. Geophys., 31: 229–245.

Dewey, J.F., and Windley, B.F., 1988. Palaeocene - Oligocene tectonics of NW Europe. In: A.C. Morton and L.M. Parson (Editors), Early Tertiary volcanism and the opening of the NE Atlantic. Geol. Soc. London Spec. Publ., 39: 25–31.

Dewey, J.F., Helman, M.L., Turco, E., Hutton, D.H.W., and Knott, S.D., 1989. Kinematics of the western Mediterranean. In: Coward, M.P., Dietrich, D., and Park, R.G. (Editors), Alpine Tectonics. Spec. Publ. Geol. Soc. Lond., 45: 265–283.

DGK-Arbeitskreis, 1979. On the "Map of height changes in the Federal Republic of Germany - status 1979", scale 1 : 1,000,000. Allg. Vermessungsnachr., 86: 362–363.

Doebl, F., 1970. Die tertiären und quartären Sedimente des südlichen Rheingrabens. In: Illies, J.H., and Mueller, St. (Editors), Graben problems. Schweizerbart, Stuttgart: 56–66.

Doebl, F., and Olbrecht, W., 1974. An isobath map of the Tertiary base in the Rhinegraben. In: Illies, J.H., and Fuchs, K. (Editors), Approaches to taphrogenesis. Schweizerbart, Stuttgart: 71–72.

Doebl, F., and Teichmüller, R., 1979. Zur Geologie und heutigen Geothermik im mittleren Oberrhein-Graben. Fortschr. Geol. Rheinld. Westf., 27: 1–17.

Dohr, G., 1967. Beobachtungen von Tiefenreflexionen im Oberrheingraben. In: Rothé, J.P., and Sauer, K. (Editors): The Rhinegraben progress report 1967. Abh. Geol. Landesamt Baden-Württemberg 6: pp. 94–95.

Dohr, G., 1970. Reflexionsseismische Messungen im Oberrheingraben mit digitaler Aufzeichnungstechnik und Bearbeitung. In: Illies, J.H., and Mueller, St. (Editors): Graben problems. Schweizerbart, Stuttgart: pp. 207–218.

Downes, H., 1993. The nature of the lower continental lower crust of Europe: petrological and geochemical evidence from xenoliths. In: Snieder, R., Cermak, V., and Poupinet, G., Structure and evolution of the European lithosphere and upper mantle. Phys. Earth Planet. Inter., 79: 195–218.

Downes, H., and Leyreloup, A., 1986. Granulite xenoliths from the French Massif Central - petrology, Sr and Nd isotope systematics and model age estimates. In: Dawson, J.B., Carswell, D.A., Hall, J., and Wedepohl, K.H. (Editors), The nature of the lower continental crust. Geol. Soc. Spec. Publ., no. 24, pp. 319–330.

Dürbaum, H.-J., Fritsch, J., and Nickel, H., 1967. Deep seismic sounding in the eastern part of the Rhenish Massif. Proceedings 9th Gen. Ass. Europ. Seismol. Comm. (Copenhagen 1966). Akademisk Forlag, Kobenhavn: pp. 265–271.

Eberle, D., 1973. Aeromagnetische Karte der Bundesrepublik Deutschland. Bundesanst.f.Bodenf., Hannover: scale 1 : 1,000,000.

Echtler, H., Lüschen, E., and Mayer, G., 1994. Lower crustal thinning in the Upper Rhinegraben: Implications for recent rifting. Tectonics, 13: 342–353.

Eck, T. van, Ahorner, L., and Paulssen, H., 1993. The earthquake of the century in northwestern Europe: The Roermond, The Netherlands, earthquake of April 13, 1992. Earthquakes and volcanoes, 24: 15–26.

Edel, J.B., 1975. Structure de la croûte terrestre sous le fossé Rhénan et ses bordures. Thèse, Univ.Strasbourg, 207 pp.

Edel, J.B., and Fluck, P., 1989. The upper Rhenish Shield basement (Vosges, Upper Rhinegraben and Schwarzwald): main structural features deduced from magnetic, gravimetric, and geological data. Tectonophysics, 169: 303–316.

Edel, J.B., Fuchs, K., Gelbke, C., and Prodehl, C., 1975. Deep structure of the southern Rhinegraben area from seismic refraction investigations. J. Geophys., 41: 333–356.

Egloff, R., 1979. Sprengseismische Untersuchungen der Erdkruste in der Schweiz. Ph.D.thesis, ETH Zuerich: 167 pp.

Élie de Beaumont, L., 1841. Les Vosges. In: Élie de Beaumont, L., and Dufrénoy, P.A., Explicaton de la carte géologique de la France. Vol. 1: Paris.

Eller, J.-P. von, and Sittler, C., 1974. Les Vosges et le Fossé Rhénan. In: Debelmas, J. (ed.), Géologie de la France. Vol. 1: Vieux Massifs et Grands Bassins Sédimentaires. Doin Edition, Paris, pp. 63–104.

Emter, D., 1976. Seismic results from southwestern Germany. In: Giese, P., Prodehl, C., and Stein, A. (Editors): Explosion seismology in central Europe - data and results. Springer, Berlin-Heidelberg: pp. 283–289.

ERCEUGT Group, 1990. The lateral and vertical distribution of electrical resistivity of the central segment of the European Geotraverse. In: R. Freeman, P. Giese, and St. Mueller (Editors), The European Geotraverse: integrative studies - results from the 5th Earth Science Study Centre. Europ. Science Foundation, Strasbourg, pp. 163–167.

ERCEUGT Group, 1992. An electrical resistivity crustal section from the Alps to the Baltic Sea (central segment of the EGT). In: R. Freeman and St. Mueller (Editors), The European Geotraverse, Part 8. Tectonophysics, 207: 123–139.

EREGT Group, 1990. An electrical resistivity transect from the Alps to the Baltic Sea (Central Segment of the EGT). In: R. Freeman and St. Mueller (Editors), Proceedings of the 6th EGT Workshop: Data compilation and synoptic interpretation. European Science Foundation, Strasbourg, pp. 299–313.

Faber, S., Bonjer, K.-P., Brüstle, W., and Deichmann, N., 1994. Seismicity and structural complexity of the Dinkelberg block, southern Rhine Graben. Geophys. J. Int., 116: 393–408.

Fourniguet, J., Vogt, J., and Weber, C., 1981. Seismicity and recent crustal movements in France. Tectonophysics, 71: 195–216.

Franke, W., 1986. Development of the central European Variscides - a review. In: Freeman, R., Mueller, St., and Giese, P. (Editors): Proceedings of the Third Workshop on the European Geotraverse (EGT) project - the central segment. Europ. Science Foundation, Strasbourg: pp. 65–72.

Franke, W., Bortfeld, R.K., Brix, M., Drozdzewski, G., Dürbaum, H.J., Giese, P., Janoth, W., Jödicke, H., Reichert, C., Scherp, R., Schmoll, J., Thomas, R., Thünker, M., Weber, K., Wiesner, M.G., and Wong, H.K., 1990a. Crustal structure of the Rhenish Massif: results of the deep seismic reflection lines DEKORP 2-North and 2-North-Q, 1990a. Geol. Rdsch. 79: 523–566.

Franke, W., Giese, P., Grosse, S., Haak, V., Kern, H., Mengel, K., and Oncken, O., 1990b. Geophysical imagery of geological structures along the central segment of the EGT. In: R. Freeman, P. Giese and St. Mueller (Editors), The European Geotraverse: integrative studies - results from the 5th Earth Science Study Centre. Europ. Science Foundation, Strasbourg, pp. 177–186.

Freeman, R., and Mueller, St. (Editors), A continent revealed - The European Geotraverse - Atlas of compiled data. Cambridge Univ. Press, 73 pp. and 14 maps.

Freeman, R., Mueller, St., and Giese, P. (Editors), 1986. Proceedings of the Third Workshop on the European Geotraverse (EGT) project - the central segment. Europ. Science Foundation, Strasbourg: 260 pp.

Frey, F.A., Green, D.H., and Roy, S.D., 1978. Integrated models of basalt petrogenesis: a study of quartz-tholeiites to olivine melilitites from Southern Eastern Australia. J. Petrol., 19: 463–513.

Fuchs, K., 1970. On the determination of velocity-depth distributions of elastic waves from the dynamic characteristics of the reflected wave field. Z. Geophys., 36: 531–548.

Fuchs, K., Bonjer, K.-P., Gajewski, D., Lueschen, E., Prodehl, C., Sandmeier, K.-J., Wenzel, F., and Wilhelm, H., 1987. Crustal evolution of the Rhinegraben area. 1.Exploring the lower crust in the Rhinegraben rift by unified geophysical experiments. Tectonophysics, 141: 261–275.

Fuchs, K., von Gehlen, K., Mälzer, H., Murawski, H., and Semmel, A. (Editors), 1983. Plateau uplift - The Rhenish Shield - a case history. Springer, Berlin- Heidelberg: 411 pp.

Fuchs, K., and Wedepohl, K.H., 1983. Relation of geophysical and petrological models of upper mantle structure of the Rhenish Massif. In: Fuchs, K., von Gehlen, K., Mälzer, H., Murawski, H., and Semmel, A. (Editors): Plateau uplift - the Rhenish Shield - a case history. Springer, Berlin- Heidelberg: pp. 352–363.

Gajewski, D., 1989. Compressional- and shear-wave velocity models of the Schwarzwald derived from seismic refraction data. In: R. Emmermann and J. Wohlenberg (Editors), The German Continental Deep Drilling Program (KTB) - site selection studies in the Oberpfalz and Schwarzwald. Springer, Berlin-Heidelberg, pp. 363–383.

Gajewski, D., Fuchs, K., Sandmeier, K.-J., and Stangl, R., 1990. Constraints on composition of the uppermost continental mantle from P_n and S_n observations. Geophys. J. Int., 103: 497–507.

Gajewski, D., Holbrook, W.S., and Prodehl, C., 1987. A three-dimensional crustal model of southwest Germany derived from seismic refraction data. Tectonophysics, 142: 49–70.

Gajewski, D., and Prodehl, C., 1985. Crustal structure beneath the Swabian Jura, SW Germany, from seismic refraction investigations. J. Geophys., 56: 69–80.

Gajewski, D., and Prodehl, C., 1987. Seismic refraction investigation of the Black Forest. Tectonophysics, 142: 27–48.

Galson, D.A., and Mueller, St. (Editors), 1984. Proceedings of the First Workshop on the European Geotraverse (EGT) project - the northern segment. Europ. Science Foundation, Strasbourg: 169 pp.

Galson, D.A., and Mueller, St. (Editors), 1985. Proceedings of the Second Workshop on the European Geotraverse (EGT) project - the southern segment. Europ. Science Foundation, Strasbourg: 267 pp.

Gehlen, K. von, and Forkel, W., 1983. Tertiary volcanism in the Westerwald mountains. In: Fuchs, K., von Gehlen, K., Mälzer ,H., Murawski, H., and Semmel, A. (Editors): Plateau uplift - the Rhenish Shield – a case history. Springer, Berlin-Heidelberg: p. 133.

Gelbke, C., 1978. Lokalisierung von Erdbeben in Medien mit beliebiger Geschwindigkeits-Tiefen-Verteilung unter Einschluß späterer Einsätze und die Hypozentren im Bereich des südlichen Oberrheingrabens von 1971-1975. Ph.D. thesis, Univ. Karlsruhe: 188 pp.

Gerke, K., 1957. Die Karte der Bouguer-Isanomalen von Westdeutschland. Dtsch. Geodät. Komm. B: 46, I: scale 1 : 1,000,000.

Geyer, O.F., and Gwinner, M.P., 1968. Einführung in die Geologie von Baden-Württemberg, 2nd. ed. Schweizerbart, Stuttgart, 228 pp.

Giese, P., 1983. The evolution of the Hercynian crust - some implications to the uplift problem of the Rhenish Massif. In: Fuchs, K., von Gehlen, K., Mälzer ,H., Murawski, H., and Semmel, A. (Editors): Plateau uplift - the Rhenish Shield – a case history. Springer, Berlin-Heidelberg: pp. 303–314.

Giese, P., Jödicke, H., Prodehl, C., and Weber, K., 1983. The crustal structure of the Hercynian mountain system - a model for crustal thickening by stacking. In: Martin, H., and Eder, F.W. (Editors), 1983. Intracontinental fold belts - case studies in the Variscan belt of Europe and the Damara belt in Namibia. Springer, Berlin-Heidelberg: pp. 405–426.

Giese, P., Ibbeken, S., Baier, B., and Schulze-Frereichs, K., 1990. Accompanying seismic refraction investigations along the profile DEKORP-2-North. Geol. Rdsch., 79: 567–579.

Giese, P., Prodehl, C., and Stein, A. (Editors), 1976. Explosion seismology in central Europe - data and results. Springer, Berlin-Heidelberg: 429 pp.

Glahn, A., and Granet, M., 1992. 3-D structure of the lithosphere beneath the southern Rhine Graben area. In: P.A. Ziegler (Editor), Geodynamics of Rifting, Volume I. Case history studies on rifts: Europe and Asia. Tectonophysics, 208: 149–158.

Glahn, A., Granet, M., and the Rhine Graben Teleseismic Group, 1993. Southern Rhine Graben: Small wavelength tomographic study and its implication for the dynamic evolution of the graben. Geophys. J. Int., 113: 399–418.

Glahn, A., Sachs, P.M., and Achauer, U., 1992. A teleseismic and petrological study of the crust and upper mantle beneath the geothermal anomaly Urach/SW-Germany. Phys. Earth Planet. Inter., 69: 176–206.

Glocke, A., and Meissner, R., 1976. Near-vertical reflections recorded at the wide-angle profile in the Rhenish Massif. In: Giese, P., Prodehl, C., and Stein, A. (Editors): Explosion seismology in central Europe - data and results. Springer, Berlin-Heidelberg: pp. 252–256.

Goer, A. de, and Mergoil, J., 1971. Structure et dynamique des édifices volcaniques tertiaires et quaternaires. In: Symposium sur la géologie, la morphologie, et la structure profonde du Massif Central français. Plein Air Service Éd., Clérmont-Ferrand, pp. 345–376.

Granet, M., 1986. A teleseismic study of the Upper Rhinegraben area: array mislocation diagram and 3-D inversion. J. Geophys., 59: 119–128.

Granet, M., Stoll, G., Dorel, J., Achuer, U., Poupinet, G., and Fuchs, K., 1994. New constraints on the geodynamical evolution of the Massif Central (France): a mantle plume hypothesis from teleseismic tomography. Geophys. J. Int., in press.

Greiner, G., and Sittig, E., 1971. Erdmagnetische Messungen in der Baden-Badener Senke. Jber. u. Mitt. oberrh. geol. Ver., N.F., 53: 263–274.

Grosse, S., Behr, H.J., Edel, J.B., and Heinrichs, T., 1992. The gravity field along the central segment of the EGT. In: R. Freeman and St. Mueller (Editors), The European Geotraverse, Part 8. Tectonophysics, 207: 97–121.

Grosse, S., and Conrad, W., 1990. Map of the Bouguer field of Germany and conterminous areas. In: R. Freeman, P. Giese and St. Mueller (Editors), The European Geotraverse: integrative studies - results from the 5th Earth Science Study Centre. Europ. Science Foundation, Strasbourg, pp. 131–133.

Grosse, S., Conrad, W., Behr, H.J., and Heinrichs, T., 1990. Major gravity axes and anomalies in central Europe. In: R. Freeman, P. Giese and St. Mueller (Editors), The European Geotraverse: integrative studies - results from the 5th Earth Science Study Centre. Europ. Science Foundation, Strasbourg, pp. 135–146.

Grubbe, K., 1976. Seismic-refraction measurements along two crossing profiles in northern Germany and their interpretation by a ray-tracing method. In: Giese, P., Prodehl, C., and Stein, A. (Editors): Explosion seismology in central Europe - data and results. Springer, Berlin-Heidelberg: pp. 268–282.

Gutscher, M.-A., 1991. Gravity interpretation along seismic-reflection profile DEKORP-9N (northern Rhine Graben). Terra Nova, 3: 166–174.

Haak, V., 1985. Anomalies of the electrical conductivity in the earth's crust and upper mantle. In: K.-H. Hellwege (Editor in Chief), Landolt Börnstein New Series: Numerical data and functional relationships in science and technology. Group V, Volume 2b: K. Fuchs and H. Soffel (Editors), Physical properties of the interior of the earth, the moon and the planets, Springer, Berlin-Heidelberg, pp. 397–436.

Haak, V., Berktold, A., Jödicke, H., Knödel, K., and Losecke, W., 1986. The distribution of electrical conductivity along the central segment of the EGT. In: Freeman, R., Mueller, St., and Giese, P. (Editors): Proceedings of the Third Workshop on the European Geotraverse (EGT) project - the central segment. Europ. Science Foundation, Strasbourg: pp. 117–126.

Haak, V., and Reitmayr, G., 1974. The distribution of electrical resistivity in the Rhinegraben area as determined by telluric and magnetotelluric methods. In: J.H. Illies and K. Fuchs (Editors): Approaches to taphrogenesis. Schweizerbart, Stuttgart: pp. 366–369.

Hänel, R. (ed.), 1982. The Urach geothermal project (Swabian Alb, Germany). Schweizerbart, Stuttgart: 419 pp.

Hänel, R., 1983. Geothermal investigations in the Rhenish Massif. In: Fuchs, K., von Gehlen, K., Mälzer, H., Murawski, H., and Semmel, A. (Editors): Plateau uplift - the Rhenish Shield - a case history. Springer, Berlin-Heidelberg: pp. 228–246.

Hahn, A., and Pucher, R., 1982. Die magnetischen Anomalien des Oberrheins. Geol. Jb., E23: 81–96.

Hahn, A., and Wonik, T., 1990. Preliminary interpretation of the magnetic anomalies in the area of the seismic reflection profile DEKORP 2-N. Geol. Rdsch. 79: 603–610.

Hirn, A., 1976. Sondages sismiques profonds en France. Bull. Soc. Géol. Fr., 18: 1065–1071.

Hirn, A., and Perrier, G., 1974. Deep seismic sounding in the Limagnegraben. In: Illies, J.H., and Fuchs, K. (Editors): Approaches to taphrogenesis. Schweizerbart, Stuttgart: pp. 329–340.

Hirn, A., Steinmetz, L., Kind, R., and Fuchs, K., 1973. Long range profiles in western Europe - II. Fine structure of the lower lithosphere in France (southern Bretagne). Z. Geophys., 39: 363–384.

Hirn, A., Prodehl, C., and Steinmetz, L., 1975. An experimental test of models of the lower lithosphere in Bretagne (France). Ann. Géophys., 31: 517–530.

Holbrook, W.S., Gajewski, D., and Prodehl, C., 1987. Shear-wave velocity and Poisson's ratio structure of the upper lithosphere in southwest Germany. Geophys. Res. Lett., 14: 231–234.

Holbrook, W.S., Gajewski, D., Krammer, A., and Prodehl, C., 1988. An interpretation of wide-angle shear-wave data in Southwest Germany: Poisson's ratio and petrological implications. J. Geophys. Res., 93: 12,081–12,106.

Illies, J.H., 1970. Graben tectonics as related to crust-mantle interactions. In: Illies, J.H., and Mueller, St. (Editors): Graben problems. Schweizerbart, Stuttgart: pp. 4–27.

Illies, J.H., 1973. The Rhine Graben rift system - plate tectonics and transform faulting. Geophys. Surv., 1: 27–60.

Illies, J.H., 1974a. Taphrogenesis, introductory remarks. In: Illies, J.H., and Fuchs, K. (Editors): Approaches to taphrogenesis. Schweizerbart, Stuttgart: pp. 1–13.

Illies, J .H., 1974b. Taphrogenesis and plate tectonics. In: Illies, J.H., and Fuchs, K. (Editors): Approaches to taphrogenesis. Schweizerbart, Stuttgart: pp. 433–460.

Illies, J.H., 1974c. Intra-Plattentektonik in Mitteleuropa und der Rheingraben. Oberrhein. geol. Abh., 23: 1–24.

Illies, J.H., 1975a. Recent and paleo-intraplate tectonics in stable Europe and the Rhinegraben rift system. Tectonophysics, 29: 251–264.

Illies, J.H., 1975b. Intraplate tectonics in stable Europe as related to plate tectonics in the Alpine system. Geol. Rdsch., 64: 677–699.

Illies, J.H., 1978. Two stages Rhinegraben rifting. In: Ramberg, I.B., and Neumann, E.-R. (Editors), Tectonics and geophysics of continental rifts. D. Reidel Publ. Comp., Dordrecht, Holland, pp. 63–71.

Illies, J.H., 1982. Der Hohenzollerngraben und Intraplatten-Seismizität infolge Vergitterung lamellärer Scherung mit einer Riftstruktur. Oberrhein. geol. Abh., 31: 47–78.

Illies, J.H., and Fuchs, K. (Editors), 1974. Approaches to Taphrogenesis. Schweizerbart, Stuttgart: 460 pp.

Illies, J.H., 1975. Intraplate tectonics in stable Europe as related to plate tectonics in the Alpine system. Geol. Rdsch., 64: 677–699.

Illies, J.H., and Fuchs, K., 1983. Plateau uplift of the Rhenish Massif - introductory remarks. In: Fuchs,K., von Gehlen, K., Mälzer, H., Murawski, H., and Semmel, A. (Editors): Plateau uplift - the Rhenish Shield - a case history. Springer, Berlin-Heidelberg: pp. 1–8.

Illies, J.H., and Greiner, G., 1978. Rhinegraben and the Alpine system. Geol. Soc. Am. Bull., 89: 770–782.

Illies, J.H., and Greiner, G., 1979. Holocene movement and state of stress in the Rhinegraben rift system. In: Whitten, C.A., Green, R., and Meade, B.K. (Editors), Recent crustal movements, 1977. Tectonophysics, 52: 349–359.

Illies, J.H., and Mueller, St. (Editors), 1970. Graben problems. Schweizerbart, Stuttgart: 316 pp.

Illies, J.H., Prodehl, C., Schmincke, H.-U., and Semmel, A., 1979. The Quaternary uplift of the Rhenish Shield in Germany. Tectonophysics, 61: 197–225.

Jacoby, W.R., Joachimi, H., and Gerstenecker, C., 1983. The gravity field of the Rhenish Massif. In: Fuchs, K., von Gehlen, K., Mälzer, H., Murawski, H., and Semmel, A. (Editors): Plateau uplift - the Rhenish Shield - a case history. Springer, Berlin- Heidelberg: pp. 247–258.

Jentsch, M., Bamford, D., Emter, D., and Prodehl, C., 1982. A seismic-refraction investigation of the basement structure in the Urach geothermal anomaly, Southern Germany. In: Hänel, R. (ed.): The Urach geothermal project. Schweizerbart, Stuttgart: pp. 231–245.

Jödicke, H., Untiedt, J., Olgemann, W., Schulte, L., and Wagenitz, V., 1983. Electrical conductivity structure of the crust and upper mantle beneath the Rhenish Massif. In: Fuchs, K., von Gehlen, K., Mälzer, H., Murawski, H., and Semmel, A. (Editors): Plateau uplift - the Rhenish Shield - a case history. Springer, Berlin- Heidelberg: pp. 288–302.

Jung, J., 1946. Géologie de l'Auvergne et de ses confins bourbonnais et limousins. Mém. pour servir à l'explication de la Carte Géol. Fr., Paris, 372 pp.

Kahle, H.-G., and Werner, D., 1980. A geophysical study of the Rhinegraben - II. Gravity anomalies and geothermal implications. Geophys. J. R. astr. Soc., 62: 631–647.

Keller, J., 1990. Volcanism in the southern Rhinegraben. In: Symposium on Rhine-Rhône Rift System, ICL-WG3 Symp. (23-24 March 1990). Abstracts. Geol. Inst. Univ. Basel, p. 20.

Koch, M., 1993a. Simultaneous inversion for 3-D crustal structure and hypocentres including direct, refracted and reflected phases - II. Application to the northern Rhine Graben / Rhenish Massif region, Germany. Geophys. J. Int., 112: 413–428.

Koch, M., 1993b. Simultaneous inversion for 3-D crustal structure and hypocentres including direct, refracted and reflected phases - III. Application to the southern Rhine Graben seismic region, Germany. Geophys. J. Int., 112: 429–447.

Krammer, A., 1988. Auswertung und Interpretation seismischer Scher- und Wechselwellen am Beispiel eines Refraktionsprofils im Schwarzwald. Diploma Thesis, Geophys. Inst., Univ. Karlsruhe, 132 pp.

Labrouste, H.Y., 1970. Rapport préliminaire sur les grands profils seismiques en France. Europ. Seismol. Comm., Acad. Sci. USSR, vol. 1, pp. 405–442.

Landes, M., 1994. Untersuchung der Krustenstruktur des zentralen Limagne-Grabens (Frankreich). Diploma Thesis, Geophys. Inst., Univ. Karlsruhe, in preparation.

Larroque, J.M., and Laurent, Ph., 1988. Evolution of the stress field pattern in the south of the Rhine Graben from the Eocene to the present. Tectonophysics, 148: 41–58.

Laubscher, M., 1987. Die tektonische Entwicklung der Nordschweiz. Eclogae Geol. Helv., 80: 287–303.

Lauer, J.P., and Peterschmitt, E., 1970. Ondes réfléchies des explosions des Bagenelles et de St. Nabor (Vosges, France). Proceedings 10th Gen. Ass. Europ. Seismol. Comm. (Leningrad 1968), Acad. Sciences USSR, Moscow: vol. I, pp. 444–453.

Liebscher, H.-J., 1964. Deutungsversuche für die Struktur der tieferen Erdkruste nach reflexionsseismischen und gravimetrischen Messungen im deutschen Alpenvorland. Z.Geophys., 30: 51–96 and 115–126.

Lippolt, H.J., Todt, W., and Horn, P., 1974. Apparent potassium-argon ages of lower Tertiary Rhinegraben volcanics. In: Illies, J.H., and Fuchs, K. (Editors): Approaches to taphrogenesis. Schweizerbart, Stuttgart: 213–221.

Lippolt, H.J., 1983. Distribution of volcanic activity in space and time. In: Fuchs, K., von Gehlen, K., Mälzer, H., Murawski, H., and Semmel, A. (Editors): Plateau uplift - the Rhenish Shield - a case history. Springer, Berlin-Heidelberg: pp. 112–120.

Löhnertz, W., 1978. Zur Altersstellung der tiefliegenden fluviatilen Tertiärablagerungen der SE-Eifel (Rheinisches Schiefergebirge). N. Jahrb. Geol. Paläontol. Abh., 156: 179–206.

Lohr, U., 1982. Ergebnisse magnetotellurischer Messungen im Gebiet des Laacher Sees. Ph.D. Thesis, Univ. Braunschweig, 195 pp.

Losecke, W., 1970. Ergebnisse magnetotellurischer Messungen bei Speyer. In: J. H. Illies and St. Mueller (Editors), Graben Problems, Schweizerbart, Stuttgart, pp. 242–243.

Lucazeau, F., and Bayer, R., 1982. Évolution thermique et géodynamique du Massif Central français depuis l'Oligocène. Ann. Géophys., 38: 405–429.

Lucazeau, F., Vasseur, G., and Bayer, R., 1984. Interpretation of heat flow data in the French Massif Central. Tectonophysics, 103: 99–119.

Lüschen, E., Wenzel, F., Sandmeier, K.-J., Menges, D., Rühl, Th., Stiller, M., Janoth, W., Keller, F., Söllner, W., Thomas, R., Krohe, A., Stenger, R., Fuchs, K., Wilhelm, H., and Eisbacher, G., 1987. Near-vertical and wide-angle seismic surveys in the Black Forest, SW Germany. J. Geophys. 62: 1–30.

Lüschen, E., Wenzel, F., Sandmeier, K.-J., Menges, D., Rühl, Th., Stiller, M., Janoth, W., Keller, F., Söllner, W., Thomas, R., Krohe, A., Stenger, R., Fuchs, K., Wilhelm, H., and Eisbacher, G., 1989. Near-vertical and wide-angle seismic surveys in the Schwarzwald. In: R. Emmermann and J. Wohlenberg (Editors), The German Continental Deep Drilling Program (KTB) - site selection studies in the Oberpfalz and Schwarzwald. Springer, Berlin-Heidelberg, pp. 297–362.

Lüschen, E., Nolte, B., and Fuchs, K., 1990. Shear-wave evidence for an anisotropic lower crust beneath the Black Forest, southwest Germany. Tectonophysics, 173: 483–493.

Mälzer, H., 1988. Regional and local kinematics in SW-Germany by geodetic methods - geophysical and geological interpretation. J. Geodynamics, 9: 141–151.

Mälzer, H., and Zippelt, K., 1986. Kriechende Spannungsumwandlungen: Rezente vertikale und horizontale Bewegungen. SFB-Berichtsband 1984-1986, pp. 47–97.

Mälzer, H., Hein, G., and Zippelt, K., 1983. Height changes in the Rhenish Massif: determination and analysis. In: Fuchs, K., von Gehlen, K., Mälzer, H., Murawski, H., and Semmel, A. (Editors): Plateau uplift - the Rhenish Shield - a case history. Springer, Berlin- Heidelberg: pp. 164–176.

Mäussnest, O., 1973. Magnetische Feldmessungen im Hegau-Vulkangebiet unter besonderer Berücksichtigung der basaltischen Gänge. Oberrhein. geol. Abh., 22: 87–101.

Mäussnest, O., 1974a. Die Eruptionspunkte des Schwäbischen Vulkans. Z. Dtsch. Geol. Ges., 125: 23–54, 227–352.

Mäussnest, O., 1974b. Der paleozäne Basalt-Vulkanismus im Raum des Unteren Neckars. In: Illies, J.H., and Fuchs, K. (Editors): Approaches to Taphrogenesis. Schweizerbart, Stuttgart: pp. 222–226.

Martin, H., and Eder, F.W. (Editors), 1983. Intracontinental fold belts - case studies in the Variscan belt of Europe and the Damara belt in Namibia. Springer, Berlin-Heidelberg: 945 pp.

Mechie, J., Prodehl, C., and Fuchs, K., 1983. The long-range seismic refraction experiment in the Rhenish Massif. In: Fuchs, K., von Gehlen, K., Mälzer, H., Murawski, H., and Semmel, A. (Editors): Plateau uplift - the Rhenish Shield - a case history. Springer, Berlin- Heidelberg: pp. 260–275.

Mechie, J., Prodehl, C., Fuchs, K., Kaminski, W., Flick, J., Hirn, A., Ansorge, J., and King, R., 1982. Progress report on Rhenish Massif seismic experiment. Tectonophysics, 90: 215–230.

Meier, L., 1989. Ein Modell für die Tiefenstruktur und Kinematik im Bereich des nördlichen Rheingrabens. Ph.D.Thesis, Univ. Karlsruhe, 146 pp.

Meier, L., and Eisbacher, G.H., 1991. Crustal kinematics and deep structure of the northern Rhine Graben, Germany. Tectonics, 10: 621–630.

Meissner, R., 1967. Zum Aufbau der Erdkruste, Ergebnisse der Weitwinkelmessungen im bayerischen Molassebecken, Teil 1 und 2. Gerlands Beitr. Geophys., 76: 211–254 and 295–314.

Meissner, R., 1973. The Moho as a transition zone. Geophys. Surv., 1: 195–216.

Meissner, R., Bartelsen, H., Glocke, A., and Kaminski, W., 1976a. An interpretation of wide-angle measurements in the Rhenish Massif. In: Giese, P., Prodehl, C., and Stein, A. (Editors): Explosion seismology in central Europe – data and results. Springer, Berlin-Heidelberg: pp. 245–251.

Meissner, R., Bartelsen, H., and Murawski, H., 1980. Seismic reflection and refraction studies for investigating fault zones along the Geotraverse Rhenoherzynikum. Tectonophysics, 64: 59–84.

Meissner, R., Bartelsen, H., and Murawski, H., 1981. Thin-skinned tectonics in the northern Rhenish Massif. Nature, 290: 399–401.

Meissner, R., Berckhemer, H., and Glocke, A., 1976b. Results from deep-seismic sounding in the Rhine-Main area. In: Giese, P., Prodehl, C., and Stein, A. (Editors): Explosion seismology in central Europe - data and results. Springer, Berlin-Heidelberg: pp. 303–312.

Meissner, R., Berckhemer, H., Wilde, R., and Poursadeg, M., 1970. Interpretation of seismic refraction measurements in the northern part of the Rhinegraben. In: Illies, J.H., and Mueller, St. (Editors): Graben problems. Schweizerbart, Stuttgart: pp. 184–190.

Meissner, R., Springer, M., Murawski, H., Bartelsen, H., Flueh, E.R., and Dürschner, H., 1983. Combined seismic reflection - refraction investigations in the Rhenish Massif and their relation to recent tectonic movements. In: Fuchs, K., von Gehlen, K., Mälzer, H., Murawski, H., and Semmel, A. (Editors): Plateau uplift - the Rhenish Shield - a case history. Springer, Berlin- Heidelberg: pp. 276–287.

Meissner, R., and Vetter, U., 1974. The northern end of the Rhinegraben due to some geophysical measurements. In: Illies, J.H., and Fuchs, K. (Editors): Approaches to taphrogenesis. Schweizerbart, Stuttgart: pp. 236–243.

Menard, H.W., 1973. Epeirogeny and plate tectonics. EOS, Trans. Am. Geophys. Un., 54: 1244–1255.

Mengel, K., 1992. Evidence from xenoliths for the composition of the lithosphere. In: Blundell, D., Freeman, R., and Mueller, St. (Editors), A continent revealed - The European Geotraverse. Cambridge Univ. Press, pp. 91–102.

Mengel, K., and Kern, H., 1992. Evolution of the petrological and seismic Moho - implications for the continental crust-mantle boundary. Terra Nova, 4: 109–116.

Mengel, K., Sachs, P.M., Stosch, H.G., Wörner, G., and Loock, G., 1991. In: R. Freeman, M. Huch and St. Mueller (Editors), The European Geotraverse, Part 7. Tectonophysics, 195: 271–289.

Mengel, K., and Wedepohl, K.H., 1983. Crustal xenoliths from the northern Hessian depression. In: Fuchs, K., von Gehlen, K., Mälzer, H., Murawski, H., and Semmel, A. (Editors): Plateau uplift - the Rhenish Shield - a case history. Springer, Berlin- Heidelberg: pp. 332–335.

Michel, B., 1978. La croûte entre vallée du Rhin et vallée du Rhône: interprétation de profils sismiques et résultats structuraux. Thèse, Univ. Paris VII, 133 pp.

Michel, B., Hirn, A., Ansorge, J., and Prodehl, C., 1977. Profils sismiques dans la region Morvan - Vosges - Jura. 5e Reun. Annu. Sci. Terre (Rennes 1977) (abstr.).

Molnar, P., and Tapponnier, P., 1975. Cenozoic tectonics of Asia: effect of continental collision. Science 189: 419–426.

Mooney, W.D., and Prodehl, C., 1978. Crustal structure of the Rhenish Massif and adjacent areas; a reinterpretation of existing seismic-refraction data. J. Geophys., 44: 573–601.

Morange, A., Heritier, F., and Villemin, J., 1971. Recherches d'hydrocarbures en Limagne. In: Symposium sur la géologie, la morphologie, et la structure profonde du Massif Central français. Plein Air Service Éd., Clérmont-Ferrand, pp. 295–308.

Morgan, P., 1982. Heat flow in rift zones. In: G. Palmason (Editor), Continental and oceanic rifts. Am. Geophys. Un., Geodyn. Ser., 8: 107–122.

Mühlen, W. von zur, 1956. Ergebnisse der "Steinbruch-Seismik" im Siegerland, Kraichgau und in Hessen/Unterfranken. Geol. Jahrb., 71: 569–594.

Müller, B., Zoback, M.L., Fuchs, K., Mastin, L., 1992. Regional patterns of tectonic stress in Europe. In: Zoback, M.L. (ed.), The world stress map project. J. Geophys. Res., 97: 11,783-11,803.

Mueller, St., 1970. Geophysical aspects of graben formation in continental rift systems. In: Illies, J.H., and Mueller, St. (Editors): Graben problems. Schweizerbart, Stuttgart: pp. 27–37.

Mueller, St., 1977. A new model of the continental crust. In: J.G. Heacock (ed.), The earth's crust. Am. Geophys. Un., Geophys. Monogr., 20: 289–317.

Mueller, St., and Kahle, H.-G., 1993. Crust-mantle evolution, structure and dynamics of the Mediterranean-Alpine region. In: Smith, D.E., and Turcotte, D.L. (Editors), Contributions of space geodesy to geodynamics: crustal dynamics.. Am. Geophys. Un., Geodyn. Ser., 23: 249–298.

Mueller, St., and Peterschmitt, E., 1981. Detailed crustal structure from deep-seismic sounding and near-earthquake studies. PAGEOPH, 119: 1192–1196.

Mueller, St., Peterschmitt, E., Fuchs, K., and Ansorge, J., 1969. Crustal structure beneath the Rhinegraben from seismic refraction and reflection measurements. Tectonophysics, 8: 529–542.

Mueller, St., Peterschmitt, E., Fuchs, K., Emter, D., and Ansorge, J., 1973. Crustal structure of the Rhinegraben area. In: Mueller, St.(ed.): The structure of the earth's crust, based on seismic data. Tectonophysics, 20: 381–392.

Murawski, H., Albers, H.J., Bender, P., Berners, H.-P., Dürr, St., Huckriede, R., Kauffmann, G., Kowalczyk, G., Meiburg, P., Müller, R., Muller, A., Ritzkowski, S., Schwab, K., Semmel, A., Stapf, K., Walter, R., Winter, K.-P., and Zankl, H., 1983. Regional tectonic setting and geological structure of the Rhenish Massif. In: Fuchs, K., von Gehlen, K., Mälzer, H., Murawski, H., and Semmel, A. (Editors): Plateau uplift - the Rhenish Shield - a case history. Springer, Berlin- Heidelberg: pp. 9–38.

Nicolas, A., Lucazeau, F., and Bayer, R., 1987. Peridotite xenoliths in Massif Central basalts, France: textural and geophysical evidence for asthenospheric diapirism. In: Nixon, P.H. (ed.), Mantle xenoliths. J. Wiley and Sons, Chichester, pp. 563–574.

Nicolas, M., Santoir, J.P., and Delpech, P.Y., 1990. Intraplate seismicity: new seismotectonic data in western Europe. Tectonophysics, 179: 27–53.

Novak, O., 1993. Integrierte geophysikalisch-petrologische Interpretation des obersten Mantels und der unteren Kruste im Bereich des südlichen Limagnegrabens (Frankreich). Diploma Thesis, Geophys. Inst., Univ. Karlsruhe, 100 pp.

Panza, C.F., Mueller, St., and Calganile, G., 1980. The gross structure of the lithosphere-asthenosphere system in Europe from seismic refraction surface and body waves. PAGEOPH, 118: 1200–1213.

Perrier, G., and Ruegg, J.C., 1973. Structure profonde du Massif Central français. Ann. Geophys., 29: 435–502.

Pflug, R., 1982. Bau und Entwicklung des Oberrheingrabens. Wiss. Buchges., Darmstadt, 145 pp.

Plaumann, S., 1987. Karte der Bouguer-Anomalien in der Bundesrepublik Deutschland 1 : 1,500,000. Geol. Jahrb., E, 40: 3–7.

Plenefisch, T., and Bonjer, K.-P., 1994. The stress tensor in the Rhinegraben area derived from earthquake focal mechanisms. Geologie en Mijnbouw, in press.

Plenefisch, T., Faber, S., and Bonjer, K.-P., 1994. Investigations of S_n- and P_n-phases in the area of the upper Rhinegraben and northern Switzerland. Geophys. J. Int., in press.

Pollack, H.N., and Chapman, D.S., 1977. On the regional variation of heat flow, geotherms and lithospheric thickness. Tectonophysics, 38: 279–296.

Prodehl, C., 1979. Crustal structure of the western United States – a reinterpretation of seismic-refraction measurements from 1961 to 1963 in comparison with the crustal structure of central Europe. U.S. Geol. Survey Prof. Paper 1034, 74 pp.

Prodehl, C., 1981. Structure of the crust and upper mantle beneath the central European rift system. In: Freund, R., and Garfunkel, Z. (Editors): The Dead Sea rift. Tectonophysics, 80: 255–269.

Prodehl, C., 1984. Structure of the earth's crust and upper mantle. In: K.-H. Hellwege (Editor in Chief), Landolt Börnstein New Series: Numerical data and functional relationships in science and technology. Group V, Volume 2a: K. Fuchs and H. Soffel (Editors), Physical properties of the interior of the earth, the moon and the planets, Springer, Berlin-Heidelberg, pp. 97–206.

Prodehl, C., and Aichroth, B., 1992. Seismic investigations along the European Geotraverse in Central Europe. In: H. Kern and Y. Gueguen (Editors), Structure and composition of the lower continental crust. Terra nova, 4: 14–24.

Prodehl, C., Ansorge, J., Edel, J.B., Emter, D., Fuchs, K., Mueller, St., and Peterschmitt, E., 1976. Explosion-seismology research in the central and southern Rhinegraben - a case history. In: Giese, P., Prodehl, C., and Stein, A. (Editors): Explosion seismology in central Europe - data and results. Springer, Berlin-Heidelberg: pp. 313–328.

Prodehl, C., and Fuchs, K., 1986. Rifting in central Europe. In: Freeman, R., Mueller, St., and Giese, P. (Editors): Proceedings of the Third Workshop on the European Geotraverse (EGT) project - the central segment. Europ. Science Foundation, Strasbourg: pp. 189–194.

Prodehl, C., and Giese, P., 1990. Seismic investigations around the EGT in Central Europe. In: R. Freeman, P. Giese, and St. Mueller (Editors), The European Geotraverse: integrative studies - results from the 5th Earth Science Study Centre. Europ. Science Foundation, Strasbourg, pp. 77–97.

Prodehl, C., and Mechie, J., 1985. Crustal structure of the northern Eifel from seismic-refraction investigations. N. Jahrb. Geol. Palaeont. Abh., 171: 453–457.

Prodehl, C., Mueller, St., Glahn, A., Gutscher, M., and Haak, V., 1992. Lithospheric cross sections of the European Central rift system. In: P.A. Ziegler (Editor), Geodynamics of Rifting, Volume I. Case history studies on rifts: Europe and Asia. Tectonophysics, 208: 113–138.

Quitzow, H.W., 1959. Hebung und Senkung am Mittel- und Niederrhein während des Jungtertiärs und Quartärs. Fortschr. Geol. Rheinl. Westfalen, 4: 389–400.

Raikes, S.A., 1980. Teleseismic evidence for velocity heterogeneity beneath the Rhenish Massif. J. Geophys., 48: 80–83.

Raikes, S.A., and Bonjer, K.-P., 1983. Large-scale mantle heterogeneity beneath the Rhenish Massif and its vicinity from teleseismic P-residuals measurements. In: Fuchs, K., von Gehlen, K., Mälzer, H., Murawski, H., and Semmel, A. (Editors): Plateau uplift - the Rhenish Shield - a case history. Springer, Berlin-Heidelberg: pp. 315–331.

Reichenbach, H., and Mueller, St., 1974. Ein Krusten-Mantel-Modell für das Riftsystem um den Rheingraben, abgeleitet aus der Dispersion von Rayleigh-Wellen. In: Illies, J.H., and Fuchs, K. (Editors): Approaches to taphrogenesis. Schweizerbart, Stuttgart: pp. 348–354.

Reichert, C., 1993. Ein geophysikalischer Beitrag zur Erkundung der Tiefenstruktur des Nordwestdeutschen Beckens längs des refraktionsseismischen Profils NORDDEUTSCHLAND 1975/76. Geol. Jb., E50: 3–87.

Reitmayr, G., 1975. An anomaly of the upper mantle below the Rhine Graben, studied by the inductive response of natural electromagnetic fields. J. Geophys., 41: 651–658.

Rhinegraben Research Group for Explosion Seismology, 1974. The 1972 seismic refraction experiment in the Rhinegraben - first results. In: Illies, J.H., and Fuchs, K. (Editors): Approaches to taphrogenesis. Schweizerbart, Stuttgart: pp. 122–137.

Richards, M. L., U. Schmucker, and E. Steveling, , 1982. Electrical conductivity in the Urach geothermal area, a geomagnetic induction study using pulsations. In: R. Hänel (ed.), The Urach Geothermal Project, Schweizerbart, Stuttgart, pp. 301–311.

Roll, A., 1979. Versuch einer Volumenbilanz des Oberrheintalgrabens und seiner Schultern. Geol. Jahrb., A52: 82 pp.

Roques, M., 1971. Structure géologique du Massif Central. In: Symposium sur la géologie, la morphologie, et la structure profonde du Massif Central français. Plein Air Service Éd., Clérmont-Ferrand, pp. 17–32.

Rothé, J.P., and Peterschmitt, E., 1950. Etude séismique des explosions d'Haslach. Ann. Inst. Phys. Globe Strasbourg, 5(3): 3–28.

Rothé, J .P., and Sauer, K. (Editors), 1967. The Rhinegraben progress report 1967. Abh. Geol. Landesamt Baden-Wuerttemberg, 6: 146 pp.

Rousset, D., and Bayer, R., 1990. Nouvelles cartes gravimetriques du sud du Fossé Rhénan. C. R. Acad. Sci. Paris, 310: 199–206.

Rousset, D., Bayer, R., Guillon, D., and Edel, J.B., 1993. Structure of the southern Rhine Graben from gravity and reflection seismic data (ECORS-DEKORP program). Tectonophysics, 221: 135–153.

Rutten, M.G., 1969. The Geology of Western Europe. Elsevier, Amsterdam: 520 pp.

Sachs, P.M., 1988. Untersuchungen zum Stoffbestand der tieferen Lithosphäre an Xenolithen südwestdeutscher Vulkane. Ph.D. Thesis, Univ. Stuttgart, 249 pp.

Sandmeier, K.-J., and Wenzel, F., 1986. Synthetic seismograms for a complex model. Geophys. Res. Lett., 13: 22–25.

Sandmeier, K.-J., and Wenzel, F., 1990. Lower crustal petrology from wide-angle P- and S-wave measurements in the Black Forest. Tectonophysics, 173: 495–505.

Sapin, M., and Hirn, A., 1974. Results of explosion seismology in the southern Rhône valley. Ann. Géophys., 30: 181-202.

Sapin, M., and Prodehl, C., 1973. Long-profiles in western Europe - I. Crustal structure between the Bretagne and the Central Massif of France. Ann. Géophys., 29: 127–145.

Scheelke, I., 1972. Magnetotellurische Messungen im Rheingraben und ihre Deutung mit zweidimensionalen Modellen. Gamma, 20. Inst. Geophys. Techn. Univ. Braunschweig: 199 pp.

Scheelke, I., 1974. Models for the resistivity distribution from magnetotelluric soundings. In: Illies, J.H., and Fuchs, K. (Editors): Approaches to Taphrogenesis. Schweizerbart, Stuttgart: pp. 362–365.

Schmincke, H.-U., Lorenz, V., Seck, H.A., 1983. The Quaternary Eifel volcanic fields. In: Fuchs, K., von Gehlen, K., Mälzer, H., Murawski, H., and Semmel, A. (Editors): Plateau uplift - the Rhenish Shield - a case history. Springer, Berlin- Heidelberg: pp. 139–151.

Schneider, G., 1971. Seismizität und Seismotektonik der Schwäbischen Alb. Enke, Stuttgart, 79 pp.

Schreiner, A., 1984. Hegau und westlicher Bodensee. Sammlung geologischer Führer, 62. Borntraeger, Berlin-Stuttgart, 93 pp.

Schulz, G., 1957. Reflexionen aus dem kristallinen Untergrund des Pfälzer Berglandes. Z. Geophys., 23: 225–235.

Seck, H.A., 1983. Eocene to recent volcanism within the Rhenish Massif and the northern Hessian depression - summary. In: Fuchs, K., von Gehlen, K., Mälzer, H., Murawski, H., and Semmel, A. (Editors): Plateau uplift - the Rhenish Shield - a case history. Springer, Berlin- Heidelberg: pp. 153–162.

Seck, H.A., and Wedepohl, K.H., 1983. Mantle xenoliths in the Rhenish massif and the northern Hessian depression. In: Fuchs, K., von Gehlen, K., Mälzer, H., Murawski, H., and Semmel, A. (Editors): Plateau uplift - the Rhenish Shield - a case history. Springer, Berlin- Heidelberg: pp. 343–351.

Semmel, A., 1983. The early Pleistocene terraces of the upper middle Rhine and its southern foreland - questions concerning their tectonic interpretation. In: Fuchs, K., von Gehlen, K., Mälzer, H., Murawski, H., and Semmel, A. (Editors): Plateau uplift - the Rhenish Shield - a case history. Springer, Berlin- Heidelberg: pp. 49–54.

Sengör, A.M.C., Burke, K., and Dewey, J.F., 1978. Rifts at high angles to orogenic belts: tests for their origin and the upper Rhine Graben as an example. Am. J. Sci., 278: 24–40.

Setto, I., and Meissner, R., 1987. Support from gravity modelling for seismic interpretation. Annales Geophysicae, 5B: 389–394.

Sittler, C., 1969. The sedimentary trough of the Rhine Graben. Tectonophysics, 8: 543–560.

Spakman, W., 1986. The upper mantle structure in the central European-Mediterranean region. In: Freeman, R., Mueller, St., and Giese, P. (Editors): Proceedings of the Third Workshop on the European Geotraverse (EGT) project - the central segment. Europ. Science Foundation, Strasbourg: pp. 215–221.

Sponheuer, W., 1969. Die Verteilung der Herdtiefen in Mitteleuropa und ihre Beziehung zur Tektonik. In: Stiller, H. (ed.): Seismologische Arbeiten aus dem Institut für Geodynamik. Veröff. Inst. f. Geodynamik, Jena. Akademie-Verlag, Berlin. Reihe A, Heft 13: pp. 82–103.

Sprecher, Ch., 1976. Die Struktur des oberen Erdmantels in Zentraleuropa aus Dispersionsmessungen an Rayleigh-Wellen. Ph.D. Thesis, ETH Zürich, no. 5864, 156 pp.

Stangl, R., 1983. Geschwindigkeits-Tiefen-Verteilungen von P-Wellen im oberen Mantel Süddeutschlands, die mit Laufzeit- und Amplituden-Beobachtungen auf zwei gegengeschossenen Lang-profilen verträglich sind. Diploma thesis, Geophys. Inst., Univ. Karlsruhe: 159 pp.

Stille, H., 1925. Rheinische Gebirgsbidung im Kristianagebiet und in Westdeutschland. Abh. Preuß. Geol. L.-A., N.F. 95: 110.

Stoll, G., Fuchs, K., Granet, M., Achauer, U., and Bayer, R., 1994. The structure beneath Massif Central from teleseismic tomography and Bouguer gravity (abstr.). Ann. Geophys., 12: C33.

Stosch, H.-G., Lugmair, G.W., and Seck, H.A., 1986. Geochemistry of granulite-facies lower crustal xenoliths: implications for the geological history of the lower continental crust beneath the Eifel, West Germany. Geol. Soc. Lond. Spec. Publ., 24: 309–317.

Stosch, H.-G., Schmucker, A., and Reys, Ch., 1992. The nature and geological history of the deep crust under the Eifel, Germany. Terra Nova, 4: 53–62.

Teichmüller, R., 1974. Die tektonische Entwicklung der Niederrheinischen Bucht. In: Illies, J.H., and Fuchs, K. (Editors): Approaches to taphrogenesis. Schweizerbart, Stuttgart: pp. 269–285.

Teufel, U, , 1986. Die Verteilung der elektrischen Leitfähigkeit in der Erdkruste unter dem Schwarzwald, ein Beispiel für Möglichkeiten und Grenzen der Interpretation von Audio-Magnetotellurik, Magnetotellurik, Erdmagnetischer Tiefensondierung. Ph.D. Thesis, University of München.

Tezkan, B., 1988. Electromagnetic sounding experiments in the Schwarzwald central gneiss massif. J. Geophys., 62: 109–118.

Truffert, C., Burg, J.-P., Cazes, M., Bayer, R., Damotte, B., and Rey, D., 1990. Structures crustales sous le Jura et la Bresse: constraintes sismiques et gravimétriques le long des profils ECORS Bresse - Jura et Alpes II. Mém. Soc. Géol. France, N.S., 156: 157–164.

Vasseur, G., 1982. Synthèse des résultats du flux géothermique en France. Ann. Géophys., 38: 189–201.

Villemin, T., Alvarez, F., and Angelier, J., 1986. The Rhinegraben: extension, subsidence, and shoulder uplift. Tectonophysics, 128: 47–59.

Villemin, T., and Coletta, B., 1990. Subsidence in the Rhine Graben: a new compilation of borehole data. In: Symposium on Rhine-Rhône Rift System, ICL-WG3 Symp. (23-24 March 1990). Abstracts. Geol. Inst. Univ. Basel, p. 31.

Vinken, R. (ed.), 1988. The Northwest European Tertiary Basin. Results of the Int. Geol. Correlation Program No.124. Geol. Jahrb., A-100: 508 pp.

Volbers, R., Jödicke, H., and Untiedt, J., 1990. Magnetotelluric study of the earth's crust along the deep seismic reflection profile DEKORP 2-N. Geol. Rdsch., 79: 581–601.

Voll, G., 1983. Crustal xenoliths and their evidence for crustal structure underneath the Eifel volcanic district. In: Fuchs, K., von Gehlen, K., Mälzer, H., Murawski, H., and Semmel, A. (Editors): Plateau uplift - the Rhenish Shield - a case history. Springer, Berlin- Heidelberg: pp. 336–342.

Wagener, M., and Götze, H.J., 1989. Regional three dimensional gravity investigations in the Black Forest, Southwest Germany. Tectonophysics, 157: 13–23.

Weber, C., 1980. Apports de la gravimétrie et du géomagnétisme. In: Autran, A., and Dercourt, J., Évolutions géologiques de la France. Mém. BRGM no. 107, pp. 28–31.

Wedepohl, K.H., 1986. Xenoliths from the upper mantle and lower crust in W-Germany. In: Freeman, R., Mueller, St., and Giese, P. (Editors): Proceedings of the Third Workshop on the European Geotraverse (EGT) project - the central segment. Europ. Science Foundation, Strasbourg: pp. 161–166.

Wenderoth, R., 1978. Laufzeitanomalien teleseismischer P-Wellen im Gebiet des Oberrheingrabens. Diploma thesis, Geophys. Inst., Univ. Karlsruhe: 170 pp.

Wenzel, F., Brun, J.-P., and the ECORS-DEKORP Working Group, 1991. A deep reflection seismic line across the northern Rhine Graben. Earth Planet. Sci. Lett., 104: 140–150.

Wenzel, F., Sandmeier, K.-J., and Waelde, W., 1987. Properties of the lower crust from modeling refraction and reflection data. J. Geophys. Res., 92: 11,575–11,583.

Werling, F., 1992. Die Druck-Temperatur-Entwicklung der unteren Lithosphäre im Bereich des känozoischen französischen Riftsystems, abgeleitet aus der Mineralchemie peridotitischer, pyroxenitischer und granulitischer Xenolithe. Berichtsband für 1990-1992, SFB 108 der Universität Karlsruhe, pp. 1077–1099.

Werner, D., Kahle, H.-G., Ansorge, J., and Mueller, St.,1982. Mass displacement and geothermics within the upper mantle of the Rhinegraben rift system: a model to interpret data from gravity and seismology. In: Palmason, G. (ed.): Continental and oceanic rifts. Am. Geophys. Un., Geodyn.Ser., 8: 283–292.

Wilhelm, H., Berktold, A., Bonjer, K.-P., Jaeger, K., Stiefel, A., and Strack, K.-M., 1989. Heat flow, electrical conductivity and seismicity in the Black Forest crust, SW Germany. In: Mereu, R.F., Mueller, S., and Fountain, D.M., Properties and processes of earth's lower crust. Geophys. Monogr. Ser. 51, Am. Geophys. Un., Washington, D.C., pp. 215–234.

Wilson, M., and Downes, H., 1992. Mafic alkaline magmatism associated with the European Cenozoic rift system. In: P.A. Ziegler (Editor), Geodynamics of Rifting, Volume I. Case history studies on rifts: Europe and Asia. Tectonophysics, 208: 173–182.

Winter, R., 1974. A model for the resistivity distribution from geomagnetic depth soundings. In: Illies, J.H., and Fuchs, K. (Editors): Approaches to taphrogenesis. Schweizerbart, Stuttgart: pp. 369–375.

Wörner, G., Schmincke, H.U., and Schreyer, W., 1982. Crustal xenoliths from the Quaternary Wehr volcano (East Eifel). N. Jb. Mineral. Abh., 144: 29–55.

Wonik, T., and Hahn, A., 1989. Karte der Magnetfeldanomalien Bundesrepublik Deutschland, Luxembourg, Schweiz und Österreich (westlicher Teil) 1:1,000,000. Geol. Jahrb., E, 43: 21 pp.

Zagwijn, W.H., 1989. The Netherlands during the Tertiary and the Quaternary: a case history of Coastal Lowland evolution. Geol. Mijnbouw, 57: 577–588.

Zeis, St., 1988. Interpretation refraktionsseismischer Profile zur Ermittlung der Krustenstruktur auf der Sueddeutschen Grossscholle. Diploma thesis, Geophys. Inst., Univ. Karlsruhe: 155 pp.

Zeis, St., Gajewski, D., and Prodehl, C., 1990. Crustal structure of Southern Germany from seismic-refraction data. Tectonophysics, 176: 59–86.

Zeyen, H., Landes, M., Novak, O., Sobolev, S., Dryad, L., and Hirn, A., 1994. Lithospheric modeling in the northern Massif Central (France) (abstr.). Ann. Geophys., 12: C34.

Ziegler, P.A., 1988. Evolution of the Arctic - North Atlantic and the western Tethys. Am. Assoc. Pet. Geol. Mem., 43: 198 pp.

Ziegler, P.A., 1990. Geological atlas of western and central Europe. 2nd ed., Shell Internationale Petroleum Mij., distributed by Geol. Soc. Publ. House, Bath, 238 pp. and 56 encl.

Ziegler, P.A., 1992. European Cenozoic rift system. In: P.A. Ziegler (Editor), Geodynamics of Rifting, Volume I. Case history studies on rifts: Europe and Asia. Tectonophysics, 208: 91–111.

Zijerveld, L., Stephenson, R., Cloetingh, S., Duin, E., and Van den Berg, M.W., 1992. Subsidence analysis and modelling of the Roer Valley Graben (SE Netherlands). In: P.A. Ziegler (Editor), Geodynamics of rifting. Volume I. Case history studies on rifts: Europe and Asia. Tectonophysics, 208: 159–171.

Zucca, J.J., 1984. The crustal structure of the southern Rhinegraben from re-interpretation of seismic-refraction data. J. Geophys., 55: 13–22.

Chapter 5

The East African rift system

L.W. Braile, G.R. Keller, R.F. Wendlandt, P. Morgan, and M.A. Khan

5.1. Introduction

Over the years, various workers have divided the East African rift system (EARS) into segments in a variety of ways. Rosendahl (1987) provides a useful historical perspective on early studies of the EARS. This large and classic rift system ultimately needs to be explained with an integrated model of its structure, origin, and evolution. However, in spite of a number of recent studies, we are a long way from having the data necessary to formulate such a model. In this review, primarily because of the differences in magmatic histories and in topographic expressions, we will employ the common division of the rift system into two branches; the western branch that we will call the Western rift and which extends from Lake Mobutu (Albert) on the north to Lake Malawi on the south (Plate 5–1), and the eastern branch consisting of two distinct rift zones: the Kenya or Gregory rift and the Ethiopian rift which we will consider to include southern Afar (Plate 5–1). As emphasized by Rosendahl (1987), these branches can be divided into at least six rift zones excluding Ethiopia and Afar. Because our goal is a broader view of the EARS, we will restrict ourselves to the terms Western, Kenya, and Ethiopian rifts (Plate 5–1). Each of these features is a complex rift zone in itself and has been the object of many studies. The EARS can be thought of a part of the even larger Afro–Arabian rift zone which includes the Red Sea and the Dead Sea rift zone. The Red Sea and Dead Sea rift zones have been the subject of several recent volumes (e.g., Ben-Avraham, 1987; Makris et al., 1991; Altherr, 1992; Ziegler, 1992) and will not be treated here specifically.

The topographic and fault characteristics of the modern EARS are evident in the topographic map shown in Plate 5–1. Regionally, the EARS corresponds to a topographically high continental area with average elevations generally greater than 1000 m. Locally, the rift valleys of the EARS are narrow (about 70 to 150 km) topographic lows bordered by uplifted "rift shoulders." Traces of the primarily-extensional faults further delineate the rifts (Plates 5–1 and 5–2).

5.2. Significance

The East African rift system is generally considered to be the classic example of a continental rift. Gregory (1896, 1921) conducted early, definitive studies of this rift system, and it is usually the standard to which other rifts are compared (e.g., Logatchev et al., 1983; Keller et al., 1991). Rosendahl (1987) briefly summarizes early studies and reminds us that even Gregory and his contemporaries (e.g.. Suess, 1891; de Martonne, 1897; de Lapparent, 1898) were influenced by early work in the Rhinegraben by workers such as Élie de Beaumont (1827, 1847). In addition, classic studies of the East African rift system such as Krenkel (1922),

Willis (1936), Cloos (1939) and Holmes (1944) contain substantial insight concerning what are often considered to be "modern" problems.

There are several characteristics of the EARS that make it particularly useful for studying continental rifting. Rift-related volcanism, faulting and topographic relief are well-exposed in the EARS. A variety of tectonic styles, reflected in grabens and half-grabens, transverse fault zones and accommodation zones, and influences of pre-existing geologic structures, are present in the rift system. Because of its age, the EARS records a particularly significant stage of continental rifting in which rifting of the African craton began about 15 to 40 million years ago (age of initiation varies with location) and the rift system continues to be active today. Finally, several areas of the EARS are relatively well-studied with surface geological, geochemical, and shallow and deep geophysical surveys.

5.3. Geological framework

5.3.1. Overview

Only regional geologic maps (1:20,000,000 scale geologic map of the world; 1:5,000,000 scale geologic map of Africa, Choubert and Fauve-Muret, 1990) exist for the entire EARS. Individual countries have had geologic mapping efforts of which Kenya's is probably the most notable, and has resulted in a series of 1:250,000 scale maps. Hackman et al. (1990) present a synthesis of what has been learned about north-central Kenya by this effort. Much geologic mapping has been centered on the rifted areas and specific scientific and practical problems, and has generally not resulted in uniform-coverage geologic maps in the classic quadrangle sense. The surrounding Precambrian terranes have also attracted considerable geologic and economic interest, but studies in these areas have usually been very detailed and local in nature.

5.3.2. Igneous activity

The difference in the volume of magmatic products extruded in the eastern and western branches of the EARS is striking. There have been many discussions and estimates of the actual volumes (e.g., Baker et al., 1972; Williams, 1982; Karson and Curtis, 1989; and Mohr, 1989; MacDonald, 1994). Recently, Mohr (1992) compared the initial flood volcanism in the Ethiopian, Kenya, and Western rifts, and estimated that these volumes were 400,000 km^3 (including Afar and Yemen), 220,000 km^3, and 100,000 km^3 respectively. Volume estimates for the Western rift vary widely ranging from 2000 km^3 (Barberi et al., 1982) to 100,000 km^3 (Mohr, 1992). However, it is clear that volume of rift-related volcanics in the Ethiopian and Kenya rifts are far greater than in the Western rift. The large volume of flood basalts in Ethiopia (primarily in Afar) is consistent with the suggestion that the original crust has been largely replaced by magmatic products (Mohr, 1989). In Kenya, there are significant volumes of phonolites in addition to flood basalts. However, the Kenya Rift International Seismic Project (KRISP) results do not suggest wholesale reorganization of the crust. There is an anomalous lower crustal layer which could be underplated material and may have been involved in the generation of the phonolites (Hay and Wendlandt, 1995; Hay et al., 1995a, 1995b).

5.3.2.1. Western rift

Volcanism in the Western rift occurs in four isolated Miocene to recent volcanic provinces including, from north to south, the Toro-Ankole, Virunga, S. Kivu, and Rungwe regions. These provinces are limited in areal extent and volcanic productivity and represent the only significant centers of volcanic activity over a distance of approximately 1200 km. The onset of volcanic activity in these districts progressed from north to south, commencing at approximately 12.6 Ma in the Virunga Province (Bellon and Pouclet, 1980), 10 Ma at S. Kivu (Pasteels et al., 1989), and 7 Ma at Rungwe (Ebinger et al., 1989b). The earliest volcanism in the northernmost Toro-Ankole province has not been established. Ebinger (1989a) interprets the onset of volcanism to be prior to or concurrent with faulting and rift basin development in the Western rift. Active volcanism is controlled by faults and fissures parallel to basin border faults and by crosscutting transfer faults at intersections of rift segments (Ebinger, 1989b).

Compositions of all lavas in the western rift are characterized by high incompatible element and volatile contents. Eruptives in the Toro-Ankole and Virunga provinces are extremely potassic and silica-undersaturated (Bell and Powell, 1969; Demant et al., 1994; De Mulder et al., 1986; Rogers et al., 1992), in contrast to the Kenya rift where sodic volcanism is characteristic, and to the Ethiopia rift where tholeiitic to weakly alkaline eruptives are typical. Carbonatites and leucite- and kalsilite-bearing lavas are reported from both the Toro-Ankole and Virunga provinces (Bell and Powell, 1969; Sahama, 1960, 1973). Lavas from the S. Kivu province are much less alkaline, consisting of tholeiite, alkali basalt, basanite, melilite nephelinite, and lesser amounts of trachyte (Auchapt et al., 1987; Marcelot et al., 1989; Pasteels et al., 1989). Auchapt et al. (1987) identify three volcanic cycles in the South Kivu province: a pre-rift stage (70–7 Ma) characterized by the eruption of quartz tholeiites and olivine tholeiites, an early rifting stage (7.8–1.9 Ma) characterized by alkali basalts, and the most recent stage (14 Ka–Recent) involving eruption of transitional to alkalic basalt. The Rungwe province is characterized by the presence of olivine basalt, alkali basalt, basanite, and nephelinite, along with phonolite and trachyte lavas (Ebinger et al., 1989b; Furman, 1990, 1992).

5.3.2.2. Kenya rift

Lavas of the Kenya rift are dominantly sodic and alkaline. Compositions range from carbonatite to nephelinite, basanite, alkali basalt, and transitional basalt with extensive volumes of more evolved and felsic eruptives. The total volume of volcanic rocks in the Kenya rift is approximately 230,000 km^3 (Williams, 1982). A general migration of volcanism from north to south and from west to east and progressions from strongly alkaline to less alkaline magmatism and from mafic to more evolved and felsic compositions are noteworthy aspects of Kenya rift magmatic evolution. Excellent discussions of temporal-spatial-compositional variations of volcanism associated with the Kenya rift are provided by Williams (1982) and Baker (1987). Keller et al. (1991) summarize the relationship between volcanism and tectonic evolution of the Kenya rift.

The age of earliest rift-related igneous activity is conjectural, but may be represented by the emplacement of kimberlite diatremes in northern Tanzania at about 45–40 Ma (Nixon, 1973; Wendlandt and Morgan, 1982) and, subsequently, by the eruption of alkali basalts in northern Kenya (Turkana) and a carbonatite near the Uganda-Kenya border at approximately 30 Ma (Williams, 1982). Subsequent volcanism (23–4 Ma) was localized in broad downwarps that eventually became the sites of half-graben and graben structures.

Early-middle Miocene volcanism involved the eruption of strongly silica-undersaturated lavas of nephelinite-phonolite-carbonatite affinity in eastern Uganda and western Kenya and approximately 35,000 km^3 of alkaline flood basalts, primarily in northern Kenya (Williams, 1982). These mafic eruptives were followed by approximately 50,000 km^3 of flood phonolite (Lippard, 1973), erupted during late Miocene (14–11 Ma), which filled and overflowed the rift structure existing at this time. Flood phonolite eruptives are concentrated primarily in southern Kenya (Williams, 1970, 1972; Baker et al., 1971, 1972; King and Chapman, 1972). Younger volcanism was variable in composition, but included the eruption of approximately 25,000 km^3 of flood trachytes and ignimbrites from about 5–2 Ma (Baker et al., 1972; Williams, 1972, 1982), overspilling the rift a second time. During Quaternary time, basaltic volcanism shifted away from the central rift region to the east, approximately 150–250 km into the Marsabit area, to the Mt. Kilimanjaro region, and northeast of Mt. Kenya. Other Quaternary volcanic activity includes the eruption of trachytic calderas along the rift valley floor.

5.3.2.3. Ethiopian rift

The Ethiopian rift is characterized by largely bimodal magmatism, transitional basalts that straddle the tholeiitic-alkaline boundary and younger (Upper Miocene-Pliocene to Recent) trachyte-pantellerite ignimbrites and lavas. Mohr (1983) estimates that Tertiary lavas emanating from fissures

and producing plateaus may comprise as much as 300,000 km^3. Although volcanism started earlier, peak eruption volumes associated with the rift occurred during the period 32–21 Ma (Mohr and Zanettin, 1988). Magmatism is ongoing and includes < 1 Ma basalt, rhyolite, and lesser amounts of intermediate volcanics concentrated along the rift axes.

The Akobo basalts in southwest Ethiopia have been dated as Eocene, 49–47 Ma (Davidson and Rex, 1980). However, these volcanics were erupted significantly before the initiation of rifting in the Middle Miocene in southern and southwestern Ethiopia (WoldeGabriel et al., 1991). In the main Ethiopian rift, WoldeGabriel et al. (1990) recognize six episodes of volcanic activity starting in mid-Oligocene or earlier, all of which involve the eruption of transitional basalts. In Afar, volcanism started during late Oligocene-early Miocene (ca. 25 Ma) with a second episode in late Miocene (7 Ma) and oceanic crust development from Pliocene to present.

WoldeGabriel (1987) and Hart et al. (1989) present geochemical and isotopic evidence that the mantle sources of basalts were heterogeneous, including both enriched and depleted mantle, as well as ocean island basalt (OIB)-type mantle source. Hart et al. (1989) determined that initial magmas were derived from an enriched, subcontinental lithospheric mantle, but that with time, increasing contributions from depleted asthenosphere are observed.

5.3.2.4. Comparisons/Contrasts

Volcanic activity occurred initially in the Ethiopian rift (ca. 49 Ma), followed by the Kenya rift (ca. 30–24 Ma), and most recently in the Western rift (12 Ma). In the Western rift, the onset of volcanic activity progressed from north to south. Oligocene volcanism in Kenya occurred in the Turkana area but may have significantly preceded rifting. Beginning about 21 Ma in northern Kenya and about 10–12 Ma in southern Kenya, volcanism was localized in fault-bounded rift structures. In the last 4 Ma, basaltic volcanism has shifted east away from the rift axis. In all three East African rift segments, volcanism appears to have generally preceded or in some cases have been contemporaneous with major rift faulting (e.g. Ebinger, 1989a, b). The most extensive volume of volcanics was in Ethiopia, followed by Kenya. These rifts contain perhaps an order of magnitude more volcanic material than observed in the longer Western rift. Felsic rocks represent a significant proportion of the total volume of volcanic material in the Ethiopian and Kenya rifts. In contrast, felsic lavas are much less abundant in the Western rift.

5.4. Geophysical surveys and results

Because of recent efforts by the Kenya Rift International Seismic Project (KRISP), Project PROBE of Duke University, and the Institute of African Geosciences at the University of Leeds, there has been a major increase in the amount of geophysical data in the Western and Kenya rifts. These data, when added to earlier results in the Ethiopian rift (Berckhemer et al., 1975; Ruegg, 1975; Makris and Ginzburg, 1987), provide a much improved, although far from complete, picture of lithospheric structure and tectonic evolution of the EARS.

5.4.1. Kenya rift

The Kenya rift (Plates 5–1 and 5–2) has been the focus of the greatest number and variety of geophysical studies. Swain et al. (1994) provide a review of studies prior to 1989, the beginning of the major KRISP effort in 1989–90 (KRISP Working Party, 1991). A series of papers contained in a special volume edited by Prodehl et al. (1994a) present the results of the KRISP 90 seismic experiments. In terms of crustal structure, the most surprising result of the KRISP experiments was the large variation along the rift axis. As shown in Figure 5–1, the crust thins from about 35 km at the apex of the Kenya dome to about 20 km at Lake Turkana. Most of this thinning occurs in the lowermost crustal layer which Keller et al. (1994) interpret as being dominantly underplated material. Hay and Wendlandt (1995) summarize the geochemical data which support this interpretation and argue that this layer probably formed early in the evolution of the rift and then acted as the source of the voluminous flood phonolites.

The KRISP 90 refraction and teleseismic data provide an opportunity to examine the velocity structure of the Kenya rift from the surface to about 160

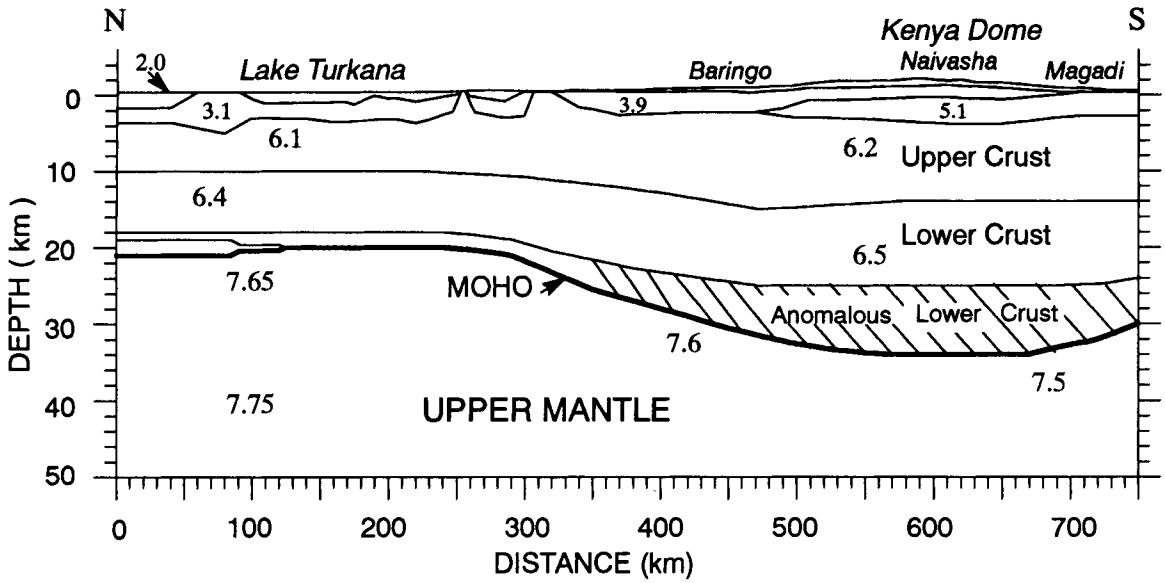

Fig. 5–1. Axial line (north to south, corresponding to deployments A, B, and C in Plate 5–2) seismic velocity model of the Kenya rift (Mechie et al., 1994). Numbers are interpreted seismic compressional-wave velocities in km/s.

km depth. To simultaneously view the shallow (crustal) and deep (uppermost mantle) structure, we have combined the KRISP 90 cross line interpretation (Braile et al., 1994) for the upper 40 km depth range, with the teleseismic upper mantle velocity model (40 to 160 km depth range) of Slack et al. (1994). The crustal model consists of compressional wave velocity structure derived by travel-time modeling of refraction and wide-angle reflection arrivals from surface explosive sources along an approximately west-east profile (dashed line near equator on Plate 5–1 and deployment D on Plate 5–2). The teleseismic velocity model (Slack et al., 1994) for the upper mantle consists of velocity values representing differences (in percent) relative to a "standard mantle" velocity-depth curve. The velocity differences were computed by simultaneous inversion of multiple delay times (residuals) of P-wave arrivals recorded at the surface for raypaths from many distant earthquakes. The teleseismic receiver arrays operated during the KRISP 85 (KRISP Working Group, 1987) and KRISP 90 experiment were located in the region extending 200 km south of the refraction profile (deployment D, Plate 5–2). The teleseismic delay times were corrected for the travel-time effects of the variable velocities and thicknesses of crustal layers so that the teleseismic model represents only mantle velocity structure. Because the upper mantle velocity model derived from the teleseismic data consists of velocity variations rather than actual velocities, we have combined the crustal and upper mantle models by converting the mantle velocity differences to actual velocities using the upper mantle velocities just below the Moho that were derived by the refraction modeling as control (Mechie et al., 1994; Braile et al., 1994; Prodehl et al., 1994b). Using P_n velocities from refraction and the average uppermost mantle teleseismic velocity variations within the rift (7.6 km/s and –4% respectively) we calculated that teleseismically derived velocity differences, which averaged +1.7% in the region immediately beneath the Moho under the eastern flank of the rift, correspond to a velocity of 8.06 km/s. This value is very close to the 8.04 km/s velocity for the mantle beneath the Moho in the worldwide averaged *iasp91* Earth model of Kennett and Engdahl (1991) and is close to a typical value for a cratonic region. For example, averages of P_n veloci-

ties for seismic studies in the midcontinent and shield regions of North America yield a value of about 8.1 km/s (Braile, 1989). A small velocity gradient with depth (approximately 0.00015 km/s/km above 120 km depth and 0.0028 km/s/km below 120 km depth), consistent with the *iasp91* model, was also added to the mantle velocities derived from the teleseismic model velocity differences. The crustal and mantle velocity values were then gridded, smoothed and contoured to provide a consistent P wave velocity model (Plate 5–3) of the crust and uppermost mantle across the Kenya rift. The most striking feature of the crust and uppermost mantle velocity model is the relatively narrow (100–200 km) anomalous region and the vertical alignment of the rift valley (defined by topography and boundary faults, and the sedimentary and volcanic fill which extends to depths of greater than 5 km), the mantle upwarp (crustal thinning of about 10 km), and the underlying anomalously low velocity upper mantle. This alignment suggest that the rifting processes at the surface and within the crust (uplift, extensional faulting, graben formation, volcanism, igneous intrusion in the lower crust, and shallowing of the Moho) are the response to the hot (and therefore anomalously low-velocity) upper mantle beneath the rift. The interpreted crustal and uppermost mantle velocity structure also displays a high degree of symmetry. The crustal thinning across the rift is abrupt, and the narrow and steep-sided nature of the mantle anomaly provide evidence that it is young.

Gravity anomalies in the Kenya and Western rifts have been the object of much interest since the early work of Bullard (1936). Swain et al. (1994) summarize the studies in Kenya and a recent study in the western rift (Upcott et al., 1995) summarizes much of the gravity work in that area. The source of both the short and long wavelength anomalies has been debated often, and many studies have focused on the role of intrusions in the crust. An interesting new interpretation stresses the importance of the suture between the Tanzanian craton and Mozambique belt (Nyblade and Pollack, 1992). This anomaly is obscured on the profile illustrated in Figure 5–2, but its location has been highlighted. The seismic results from Kenya provide the control necessary to present a clearer picture of the implications of the gravity anomalies. The nearly 200 mGal gravity anomaly which is observed along the axial seismic profile (Plate 5–2) can be explained almost completely by the axial variation in crustal thickness (Fig. 5–1), (Mechie et al., 1994). To investigate the anomalies observed across the rifts, a regional Earth model along the equator extending across the Kenya and Western rifts was prepared (Fig. 5–2). This model shows that the local axial gravity maxima is narrow and is due largely to intra-rift basement structure. There is no need for an axial dike, but Swain (1992) shows that there may be a slight densification of the crust in the axial area caused by intrusions. The seismic model (Plate 5–3) also shows slightly higher values in the middle and upper crust within the rift (Braile et al., 1994). Otherwise, the combined seismic and gravity data are satisfied by the model shown in Figure 5–2 which shows thinning of the mantle lithosphere to be much larger than thinning of the crust. The thinned lithosphere under the Lake Victoria region represents a deeper-seated anomaly (e.g., Ebinger et al., 1989a).

5.4.2. Western Rift

In the Western rift, the area of Lakes Tanganyika, Rukwa, and Malawi has been the focus of much recent attention because extensive seismic reflection data in these lakes have been published and analyzed in detail. Project PROBE collected data for Lakes Tanganyika and Malawi, and data for Lake Rukwa were collected as part of a program led by Amoco in collaboration with the Tanzanian Petroleum Devel-

Fig. 5–2. Regional earth model derived for a gravity profile across the equator from 25°W to 41°W longitudes. Numbers indicate densities in g/cm3. A variety of near-surface geological bodies are included in order to match the short wavelength component of the gravity field. All depths on this model are referenced to a surface elevation of ~1 km, not sea level which is the reference for the KRISP seismic models. Dashed line indicates tie to the KRISP 90 axial line (Fig. 5–1). The interpreted position of the suture between the Tanzanian Craton and the Mozambique Belt is shown following Nyblade and Pollack (1992). Upper crustal densities in the Kenya rift valley are slightly (0.01–0.02 g/cm^3) higher than in adjacent areas following Swain (1992). K = Mt. Kenya. Modified from Hay et al. (1995b) and Simiyu and Keller (in preparation),

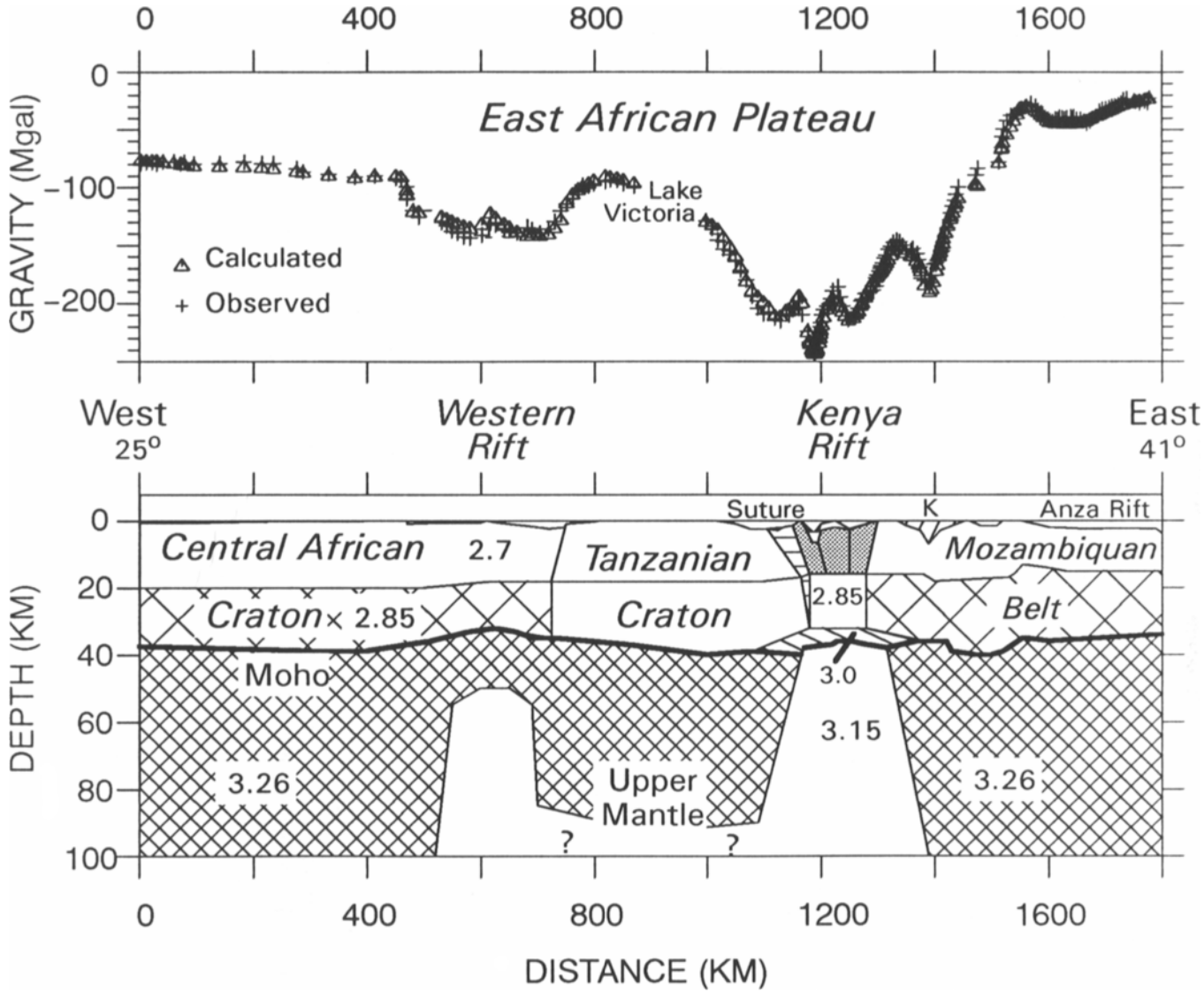
0
400
800
1200
1600
GRAVITY (Mgal)
0
-100
-200
East African Plateau
Lake Victoria
Calculated
Observed
West
25°
Western Rift
Kenya Rift
East
41°
Suture
K
Anza Rift
Central African Craton
2.7
× 2.85
Tanzanian Craton
2.85
Mozambiquan Belt
Moho
3.0
3.15
3.26
Upper Mantle
?
?
3.26
DEPTH (KM)
0
20
40
60
80
100
0
400
800
1200
1600
DISTANCE (KM)

opment Corporation. Rosendahl et al. (1992) summarized the results from these three lakes and compared them to Project PROBE results from Lake Turkana in the northern Kenya rift. These efforts have yielded an excellent picture of the shallow structure (0 to about 10 km depth) in the area of these lakes.

Although these seismic reflection studies provide an excellent view of the structure of the uppermost portion of the crust, data on deeper structure in the western rift are extremely sparse (e.g., Prodehl and Mechie, 1991). This deficiency seems particularly crucial because of the large differences between the western and eastern arms of the EARS and the significance of deeper crustal and upper mantle variations which are visible in the Kenya rift (Plate 5–3). There are no deep seismic reflection or refraction data available for the Western rift, and no broad-band passive seismic recordings which could provide constraints on deep structure are available, although an effort is underway to obtain such data in Tanzania (Andrew Nyblade, personal communication, 1994). Bram (1975) used earthquake recordings to construct two low-resolution profiles of seismic arrivals. These data did indicate crustal thinning beneath the Western rift but the interpretations are crude by modern standards. Nolet and Mueller (1982) used a variety of seismic data to derive a regional model of the Western rift lithosphere. Their model has to be considered an average over a broad area (1°S to 10°N latitudes) and contains a 35 km thick crust and low upper mantle velocities to a depth of 140 km, perhaps similar to those observed for the Kenya rift.

5.4.3. Ethiopian rift

Knowledge of deeper structure is much better for the Ethiopian rift than for the Western rift. Here the seismic studies of Berckhemer et al. (1975) and Ruegg (1975) provide a good picture of crustal and, to some extent, uppermost mantle structure. Makris and Ginzburg (1987) reinterpreted these early data with modern methods and integrated the results with gravity. The resulting crustal models (Fig. 5–3) and contours of crustal thickness attest to major modification of the crust during rifting. Velocities near 6.0 km/s appear only in about the upper 5 km (beneath the sedimentary and volcanic layer) of the crust within Afar, and velocities of about 6.9 km/s are reached at depths of only ~ 10 km (Fig. 5–3). The thinned crust beneath the Ethiopian rift and Afar is underlain by an anomalous upper mantle (Fig. 5–3) with low compressional seismic velocities (7.4 to 7.8 km/s) which Makris and Ginzburg (1987) infer to be caused by high temperature in the mantle. On the adjacent Ethiopian plateau, a typical continental crustal velocity structure was observed by Berckhemer et al. (1975), Bonjer et al. (1970), Herbert and Langston (1985), and Makris and Ginzburg (1987) (Fig. 5–3). It would appear that the transition from relatively thick crust (~40 km) to thinned, rifted crust is as abrupt in Ethiopia as it is in Kenya. However the velocity structure in the Kenya rift does not show evidence of the large extension and thinning of the continental crust and pervasive modification by magmatism implied by the Ethiopian rift and Afar crustal seismic models (Fig. 5–3). Lower crustal seismic velocities in the Ethiopian rift and Afar are about 6.9 km/s and the lower crustal layer is present at a relatively shallow depth (about 10 km) as compared to the lower crust of Kenya (Fig. 5–1 and Plate 5–3). Significant crustal thinning has apparently occurred in the Lake Turkana area of the Kenya rift (Fig. 5–1) but lower crustal seismic velocities (about 6.4 km/s) are not unusually high. Mohr (1989) suggests that new igneous material has replaced the bulk of the original Afar crust and the geophysical data appear to support this view.

5.4.4. Other Geophysical Data

Morgan (1982), Nyblade et al. (1990), and Wheildon et al. (1994) provide overviews of heat flow in East Africa. There are of course many high values related to volcanic activity. Nyblade et al. (1990) show that the Tanzanian craton (between the Western and Kenya rifts, Plate 5–1) is associated with low heat flow. Wheildon et al. (1994) argue that the overall conductive heat flow in Kenya is low and that high values are caused by advection of heat (magmatism) into the crust. The lack of a thermal

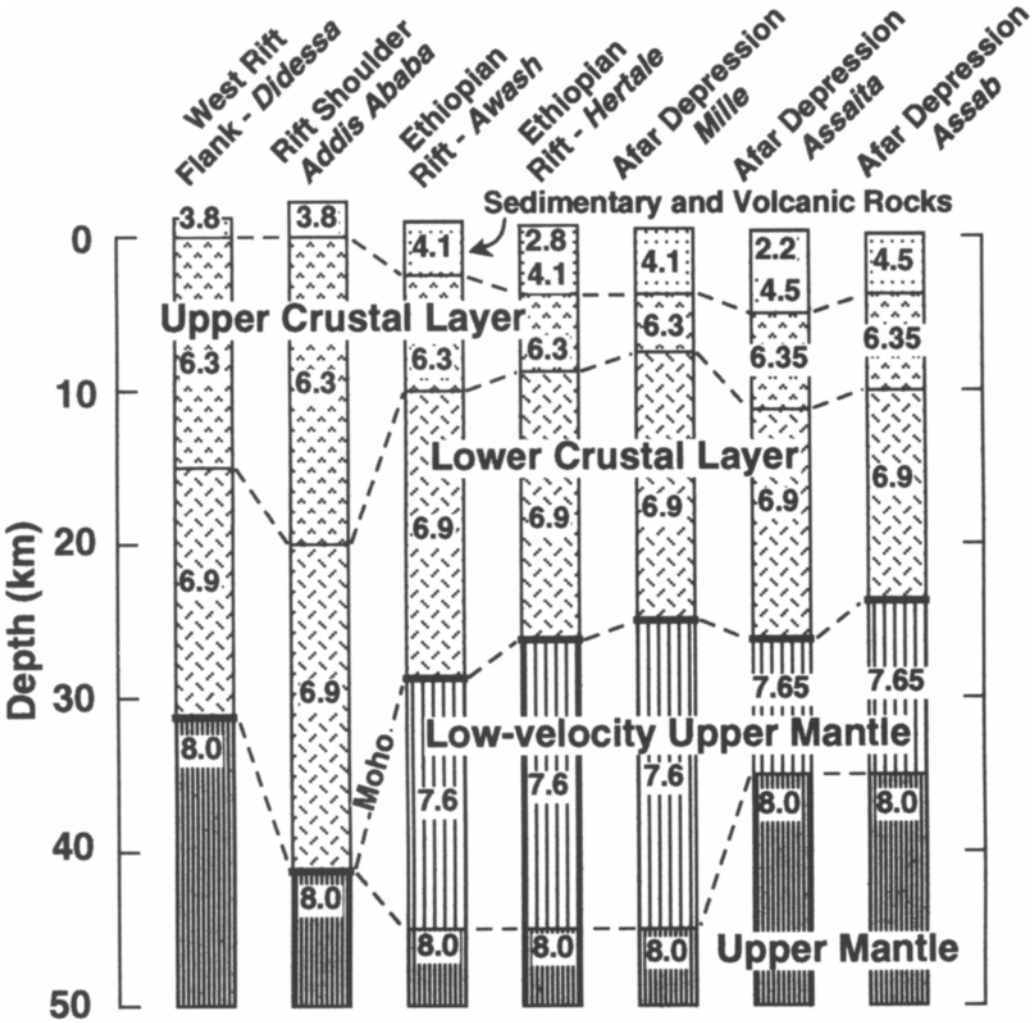

Fig. 5–3. Crust and uppermost mantle seismic velocity models for the Ethiopian Rift and Afar areas. Original models are from Makris and Ginzburg (1987). Numbers in the crustal models are seismic compressional wave velocities in km/s. The velocity value shown for each layer is the average velocity for layers in which a velocity gradient was interpreted in the original (Makris and Ginzburg, 1987) models.

signature of the rifting from conduction attests to the youthfulness of the tectonic activity because the heat pulse has yet to reach the surface.

Large (M>5.5) earthquakes are rare in the EARS, but there have been many studies of local seismicity from microearthquake networks (e.g., Rykounov et al., 1972; Maasha and Molnar, 1972; Maasha, 1975; Bungum and Nnko, 1984; Pointing and Maguire, 1990; Young et al, 1990; Tongue et al, 1992, 1994). Wohlenberg (1969) and Fairhead and Stuart (1982) provide reviews of seismicity from a regional perspective. There are many interesting details revealed by these studies, but from a larger perspective the level of seismicity seems moderate and probably lower than for the Baikal rift zone (Doser and Yarwood, 1991). A recent (1990–91) sequence of large events occurred in southern Sudan. Girdler and McConnell (1994) suggest that these events indicate

that the Western rift extends 350 km north of Lake Mobutu (Albert), (Plate 5–1). Several of the larger events have occurred at depths of 20–40 km which is rare in modern rift zones where the high heat flow and magmatism suggests that brittle behavior should be restricted to the upper crust. Many studies in rift zones have found a cessation of seismicity at about 15 km which has been interpreted to be the depth of the brittle-to-ductile transition. The deep events in East Africa have been the object of numerous investigations (Shudofsky, 1985; Shudofsky et al., 1987; Jackson and Blenkinsop, 1993; Doser and Yarwood, 1994; Nyblade and Langston, 1995), and it is difficult to determine if their foci are in the lower crust or in the upper mantle. These focal mechanisms are consistent with the regional stress field of approximately E–W extension. However, their depth has implications for the composition of the crust, the nature of faulting, and crustal heat production. The lower crust/uppermost mantle must be composed of material which exhibits brittle behavior under the P–T conditions that can be inferred; crust penetrating faults are implied if surface faults are projected down to the hypocenters of the deep events; and excess heat production in the upper crust would help resolve the contradiction between high surface heat flow and brittle behavior in the lower crust/upper mantle (Nyblade and Langston, 1995).

5.5. Basin structure

Project PROBE and recent petroleum exploration efforts have provided numerous seismic reflection studies of uppermost crustal structure in the Western rift and in the central and northern portion of the Kenya rift (e.g., Rosendahl, 1987; Rosendahl et al., 1992; Ebinger, 1989a, b; Dunkelman et al., 1988; Morley, 1992; Morley, et al., 1992; Strecker and Bosworth, 1991; Chorowicz, and Sorlien, 1992). These studies have shown that typical rift basins are related to asymmetrical half-grabens and grabens which reverse polarity along the rift zones. The regions between individual structures are often structurally complex, transfer (accommodation) zones. Seismic reflection data show that individual basins contain as much as 7 km of sedimentary and volcanic fill (Morley et al., 1992).

In the space available here, it is not possible to address adequately all of the detailed structural arguments which have been made possible by the availability of these seismic reflection data and the additional work that this effort has spawned. The following is an attempt to highlight a few major points. The detailed studies in the Western rift show that fault zones which bound the basins are complex, but that the main bounding fault zone is associated with an elevated flank which can be interpreted as a footwall uplift (e.g., Kusznir and Ziegler, 1992). There are both planar and listric faults present, but Rosendahl et al. (1992) suggest that the listric faults may be pre-Cenozoic in age. Ebinger (1989a) observes that the deep earthquakes may suggest steeply-dipping planar faults that penetrate the crust. The stress regime in the EARS has been the subject of some debate (e.g., Ebinger, 1989a; Rosendahl et al., 1992). Ebinger (1989a) argues for the importance of E–W extension while Rosendahl et al. (1992) argue for NW–SE directed extension. In either case, the sinuous nature of the Western rift in particular would produce zones of shearing and transtension. For Kenya, Strecker et al. (1990) and Bosworth et al. (1992) present evidence that the stress field rotated from E–W to NW–SE during the Pleistocene. The complex patterns of faulting in the Western rift (e.g., Rosendahl et al., 1992, Plate 5–2) would seem to be consistent with a changing stress field. Finally, the migration of faulting is an important question which is still open. In the Western rift, some faults seem to grow both to the north and south to produce linked but segmented basins, and there is a tendency for the basins to narrow with time (Ebinger, 1989a). However, various workers have also reported N–S and E–W migrations of tectonism and volcanism. Considering the major axial variations in lithospheric structure revealed by the KRISP project and our lack of knowledge of deep structure in the Western rift, it probably is premature to draw generalizations about migration of tectonism in the EARS as a whole.

The Ethiopian rift and Afar have been the focus of many structural studies. However, no seismic reflection data are available to help understand how surface structures continue at depth. Mohr (1978) provides a thorough review of studies up to the late 1970s. Exposures are good in the area although many structures are covered by volcanics. However, in the rifted areas, extremely complex patterns of faulting are found. Mohr (1987) and WoldeGabriel et al. (1990) have studied the main Ethiopian rift and found structures similar to those found in the Western and Kenya rifts. In particular, both studies found evidence for axial changes in polarity of the faulting. WoldeGabriel et al. (1990) point out differences with the rifts to the south and found evidence for two stages of rift development with half-grabens eventually developing into grabens. Southern Ethiopia and its connection with the Kenya rift has been studied by Moore and Davidson (1978), Davidson and Rex (1980), WoldeGabriel and Aronson (1987) and Ebinger and Ibrahim (1994). Here the rift widens and becomes diffuse. Also, the interaction of several phases of extension cause complexity (Ebinger and Ibrahim, 1994). However, structures in southern Ethiopia appear to continue into Kenya east of Lake Turkana.

There have been numerous studies of the role of older structures in the development of the EARS. On a large scale, the Kenya and Western rifts generally follow the boundaries of the Tanzanian Craton, an Archean feature. Studies in Kenya show that the rift structures are often controlled by the boundary (collisional zone) between the Tanzanian craton and the Proterozoic Mozambique belt (e.g., Smith and Mosley, 1993; Hetzel and Strecker, 1994). For example shear zones in Precambrian rocks control the change of orientation in the rift's western margin near Lake Baringo. However, Ebinger (1989a) argues that many major faults in the Western rift are not controlled by older structures.

In the eastern branch of the rift system, rift structures occur in broad and complex regions in Afar, southern Ethiopia, northern Kenya, and northern Tanzania. These areas are topographically low, and Morley et al. (1992) and Hendrie et al. (1994) show that at least northern Kenya is an area where extension is high, on the order of 35–40 km. This value is

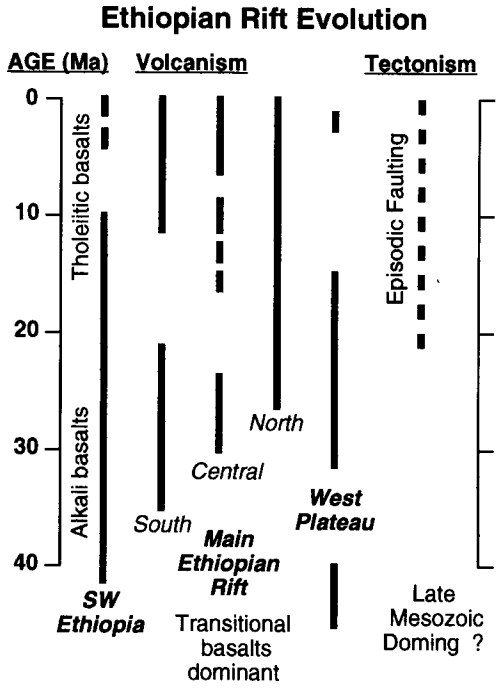

Fig. 5–4. Schematic diagram illustrating the volcanic and tectonic evolution of the Ethiopian Rift during the last 40 million years.

significantly greater than the extension of 10 km or less found in central Kenya (Strecker and Bosworth, 1991) and in the Western rift (Ebinger, 1989a, b; Rosendahl et al., 1992).

The role of uplift in rift evolution is a particularly important question. There seems to be agreement that an early phase of uplift occurred throughout the EARS. However, the volcanic activity has constructed topography, and tectonism has probably produced foot-wall uplifts which complicate efforts to study uplift caused by deep-seated processes such as mantle plumes. Ebinger et al. (1989b) have analyzed uplift across the Western and Kenya rifts and present convincing arguments that the entire region including the Lake Victoria stable block must be held up by dynamic processes in the upper mantle. There seems little doubt that a plume has caused uplift of the Ethiopian plateau. Nyblade and Robinson (1994) present an interpretation that uplift along the EARS

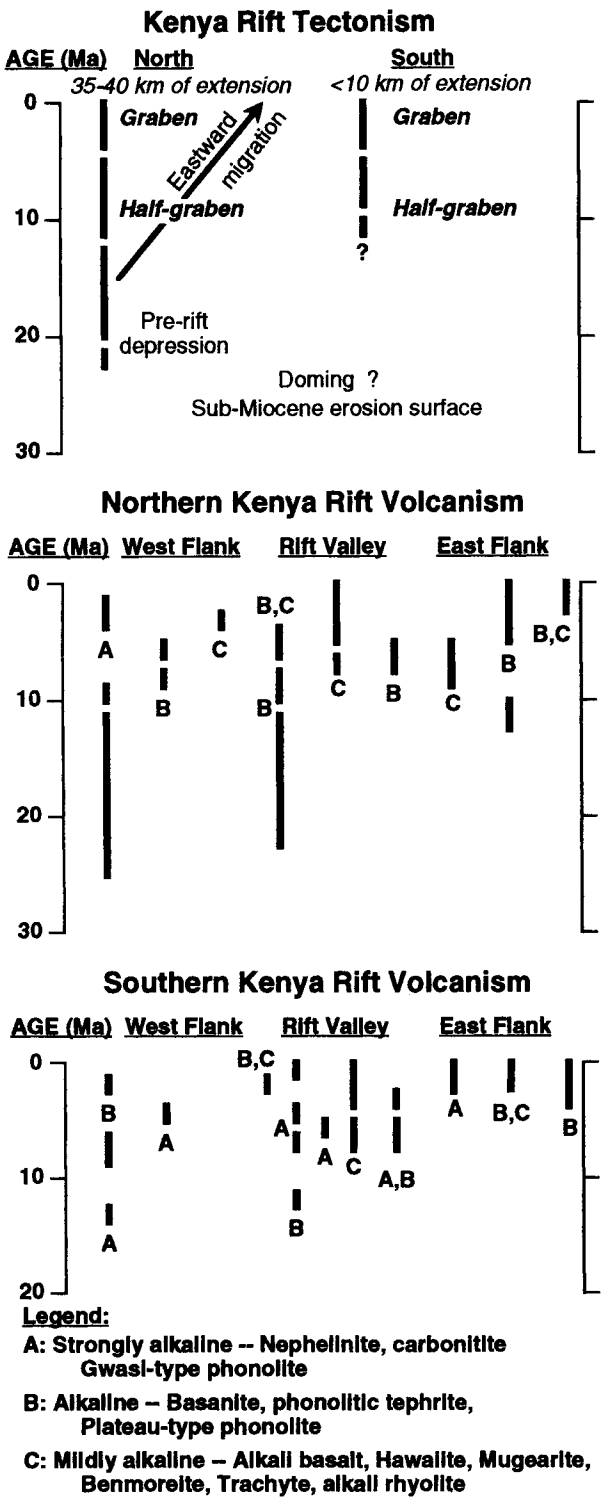

is related to a large mantle anomaly that extends from the Mid-Atlantic ridge across southern Africa and north to Ethiopia.

The crustal structure data from the KRISP project document that along-axis crustal thinning correlates with the south to north increase in extension, and the decrease in elevation from central to northern Kenya (Mechie et al., 1994; Keller et al, 1994). In the Western rift, there are no seismic data that clearly constrain deep crustal structure, but gravity studies indicate that the zone of crustal thinning is narrow (e.g., Upcott et al., 1995). Ebinger (1989a) argues that the zone of crustal thinning in the Western rift is narrow because there are few faults in the flank areas, the accommodation zones do not extend into the flank areas, and there is a lack of volcanic centers along the flanks. There are not sufficient constraints to discuss along-axis variations in crustal structure in the Western rift.

Outside of Kenya, our main source of data on upper mantle structure is studies of long wavelength gravity anomalies (e.g., Fairhead, 1976; Brown and Girdler, 1980; Banks and Swain, 1978; Ebinger et al., 1989a, 1991). Within Kenya there have been several seismic studies of deep structure (e.g., Maguire and Long, 1976; Savage and Long, 1985; Herbert and Langston, 1985; Davis, 1991; Achauer et al., 1994; Slack et al., 1994). These studies show that, even to depths of about 150 km, the zone of reduced velocities is not a great deal wider than the rift valley itself (Plate 5-3).

A major point that can be drawn from the studies of crustal and upper mantle structure is that the deeper structures appear symmetrical. The KRISP results show that the area of thinnest crust is centered on the rift valley as is the region of low velocities in the upper mantle (Plate 5-3). This observation does not favor the simple shear model of a lithosphere-penetrating detachment (Bosworth, 1987).

Fig. 5-5. Schematic diagram illustrating the volcanic and tectonic evolution of the Kenya Rift during the last 30 million years.

5.6. Evolution

The Ethiopian, Western, and Kenya rifts are considered to be part of a large rift system because they share some broad similarities in timing and are related in a geographic sense. However, these rifts are distinct entities each with its own tectonic and magmatic evolution. The evolution of the Ethiopian rift and southern Afar has been summarized by WoldeGabriel et al. (1990) and Mohr (1978). Ebinger (1989a) presented a scheme for the evolution of the Western rift; and Hackman et al. (1990), Keller et al. (1991), Morely et al. (1992), and Smith (1994) have recently summarized the evolution of the Kenya rift. We will draw heavily on these analyses in our effort to review the overall evolution of the EARS.

In any evolutionary scheme, most of Afar has to be considered an extreme case (Prodehl and Mechie, 1991), because the crust there is composed almost entirely of new magmatic material (Mohr, 1992). Primarily Miocene volcanism occurred on the Ethiopian plateaus flanking Afar, but in Afar, volcanism, and possibly faulting, began at about 25 Ma. Beginning about 4 Ma, extensive basaltic volcanism covered most of Afar and obscured the geologic record of events. Since that time, the history of northern and eastern Afar is more a story of sea-floor spreading than continental rifting.

In the main Ethiopian rift and its flanking plateaus, volcanism began in the mid-Oligocene or earlier (Fig. 5–4). WoldeGabriel et al. (1990) found evidence for six episodes of volcanism but no evidence for lateral migration of volcanism from the flanks to the rift valley such as is observed in Kenya (e.g., Baker, 1987). They also found structural evidence for pre-middle Oligocene uplift and faulting primarily because pre-Tertiary rocks outcrop in the escarpment bounding the rift valley on the west. Faulting in this rift has occurred in stages so that initial half grabens had produced a largely symmetrical graben structure by 3.5 Ma.

Although there is still much to be learned, the Kenya rift is the most intensively studied segment of the EARS and, thus, we have considerable information on timing of events there. However, the extensive volcanism covers much of the geologic record having completely filled the rift valley on

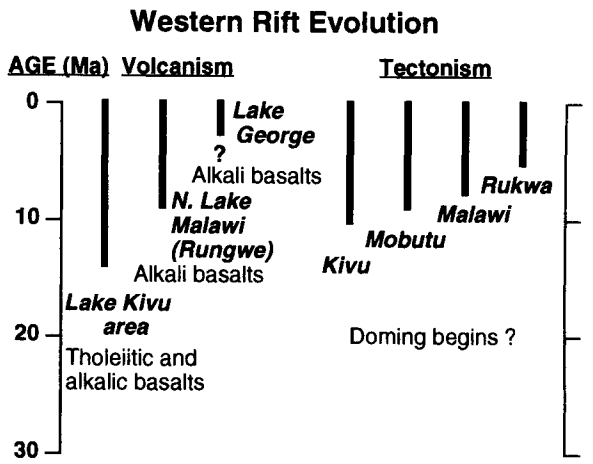

Fig. 5–6. Schematic diagram illustrating the volcanic and tectonic evolution of the Western Rift during the last 30 million years.

occasion (e.g., Williams, 1982). Nonetheless, the complexity of the evolution shown in Figure 5–5 is due in part to our improved state of knowledge of this region. For example, Bellieni et al. (1987) have used the volcanic record to infer a detailed evolution for the Lake Turkana area in northern Kenya. In addition, Morley et al. (1992) used a variety of geological and geophysical data to document the evolution of the northern portion of the Kenya rift.

Smith (1994) reviewed the geomorphic, stratigraphic, and fission-track evidence concerning uplift of the Kenya topographic dome. He concludes that an uplift of <1 km occurred prior to volcanism. Geologic evidence only constrains the timing to be post-Cretaceous in age but Smith (1994) argues that the main phase of uplift took place during the period of 40–21 Ma. A pre-rift depression formed in the early Miocene, but clear development of half grabens did not occur until about 12 Ma. From the Pleistocene to Recent, there has been a tendency for the zone of faulting and volcanism to migrate toward the center of the rift valley. The main phase of tectonism was Plio-Pleistocene (<5 Ma) in age. Volcanism initiated earlier in northern Kenya than in the Kenya dome area (Fig. 5–5). The age of the initiation of volcanism generally becomes younger southward from the Turkana region (28–33 Ma),

through the Kenya dome region (16–20 Ma), into Tanzania (<10 Ma). Beginning in the Quaternary, a series of young volcanoes developed along the rift valley axis, but there are also impressive off-axis volcanoes (Mounts Elgon, Kenya and Kilimanjaro, and the Chyulu Hills).

The Western rift generally appears to be younger than the Kenya rift. Doming began at about 20 Ma and volcanism began at about 12 Ma in the north and at about 7 Ma in the south (Ebinger, 1989a), (Fig. 5–6). The volcanism has continued to the present. The development of the many basins in the Western rift began concurrently with or prior to the volcanism. Through time, the border faults propagated to both the north and the south resulting in the linkage of many basins which were initially separate features. The basins have tended to narrow with time due to hanging wall collapse (Ebinger, 1989a). As in the area of the Kenya topographic dome, the main phase of tectonism occurred in the last 5 Ma.

5.7. Conclusions

The East African rift system displays dramatic surficial, crustal and upper mantle contrasts, some of which have been delineated in detail by geological and geophysical studies. In the Kenya rift, where there is the greatest amount of deep structural information largely from seismic studies, the rift is relatively narrow (about 100-km-wide) at the surface, and crustal thinning and anomalously low upper mantle velocities are confined to a relatively narrow zone directly beneath the rift (Plate 5–3). Crustal models derived from recent seismic studies in the Kenya rift show no evidence for major intrusions into and densification of the crust beneath the rift as had been inferred primarily on the basis of gravity models. The Kenya rift also displays striking east-west symmetry, at least at the latitude of the KRISP 90 seismic survey. Along-rift (north-south) variations in volcanism, structural style and crustal and upper mantle seismic velocities in the Kenya rift are substantial and may be at least partially related to the Kenya dome (Plate 5–2).

The presence of zones of very low seismic velocity in the (hot) upper mantle directly beneath rifts and associated crustal thinning suggest that active mantle processes are the primary cause of rifting in Kenya and Ethiopia. The timing of magmatic and tectonic events in the Cenozoic evolution of the EARS also supports this conclusion. For example, broad uplift, followed by the initiation of volcanic activity, generally preceded significant extension and the development of the fault-bounded rift valleys of the EARS.

The EARS provides classic examples of continental rifts in Ethiopia, Kenya and the Western rift. However, there are strong similarities between these rifts and other continental rifts such as the Rio Grande rift and the Baikal rift. In contrast, Afar, which is topographically low and characterized by a highly-extended and intruded crust, appears to be transitional to oceanic crust or rifted-ocean-margin crust.

Based on our examination of rift structure, magmatism and geological evolution of the East African rift system, we suggest the following generalizations related to continental rifting:

(1) Rifts, which are relatively narrow geologic features in their surface expression (rift valleys, grabens), may be underlain by a relatively narrow, hot, upper mantle upwarp. However, regionally extensive continental rifting, such as in east Africa, may be manifested by broad areas of high elevation, magmatism, tectonism and thinned lithosphere.

(2) Axial variations along rifts and differences between rifts even within the same system (e.g. the Western rift and the Kenya rift in the EARS), can be significant. These variations are reflected in structural style (near–surface faulting), volumes and compositions of intrusive and extrusive igneous activity, amount of extension, and timing of magmatic and tectonic events.

Despite substantial increases in geological and geophysical information about the EARS and continental rifts in general, there are many questions which remain. An explanation for the substantial variations in structural style and crustal velocity structure along rifts and within a rift system is one

of the outstanding problems. Additional questions related to the structure and geological evolution of continental rifts include:

(1) What is the cause of deep (lower crust and sub-Moho) earthquakes which are sometimes observed in continental rifts?

(2) What is the role of strike-slip faulting in rift development and the influence of transverse faults and pre-existing structure on rift segmentation and along-axis variations in rift style?

Finally, understanding the detailed mechanism of how deep (upper mantle) processes cause near-surface continental rifting will require additional studies, particularly on the third (depth) and fourth (time) dimensions of continental rifts.

Acknowledgements. Phil Slack and Paul Davis kindly provided a preprint of their 1994 KRISP paper. We are grateful to many colleagues whose knowledge and insight helped develop this paper. Manfred Strecker, Andrew Nyblade, Jim Mechie, Elizabeth Anthony, Bill Bosworth, Chris Morley, Cindy Ebinger, and Chris Swain were particularly helpful. Andy Nyblade, Walter Mooney, Scott Baldridge and G. WoldeGabriel provided useful comments on the manuscript. In addition to CREST project funding, this work was supported by NSF grant EAR–9316868 to GRK, and by NSF grants for the KRISP 90 project.

5.8. References

Achauer, U., and the KRISP Teleseismic Working Group, 1994. New ideas on the Kenya rift based on the inversion of the combined data sets of the 1985 and 1989-90 seismic tomography experiments. In: C. Prodehl, G.R. Keller, and M.A. Khan (Editors), Crustal and upper mantle structure of the Kenya rift, Tectonophysics, 236: 305–329.

Altherr, R. (Editor), 1992. The Afro-Arabian Rift System, Tectonophysics, 204: 1–110.

Auchapt, A., Dupuy, C., Dostal, J., and Kanika, M., 1987. Geochemistry and petrogenesis of rift-related volcanic rocks from South Kivu (Zaire), J. Volcanol. Geotherm. Res., 31: 33–46.

Baker, B.H., 1987. Outline of the petrology of the Kenya rift alkaline province. In: J.G. Fiton and B.G.J. Upton (Editors), Alkaline Igneous Rocks, Geol. Soc. London Spec. Publ. 30: 293–311.

Baker, B.H., Williams, L.A.J., Miller, J.A., and Fitch, F.J., 1971. Sequence and geochronology of the Kenya rift volcanics, Tectonophysics, 11: 191–215.

Baker, B.H., Mohr, P.A., and Williams, L.A.J., 1972. Geology of the East Africa rift system, Geol. Soc. America Spec. Paper, 136, 67 pp.

Banks, R.J. and Swain, C.J., 1978. The isostatic compensation of East Africa, Proc. R. Soc. London, Ser. A, 364: 331–352.

Barberi, F., Santacroce, R., and Varet, J., 1982. Chemical aspects of rift magmatism. In: G. Palmason (Editor), Continental and Oceanic Rifts. Geodynamics Ser. 8: 223–258.

Bell, K., and Powell, J.L., 1969. Strontium isotopic studies of alkalic rocks: The potassium-rich lavas of the Birunga and Toro-Ankole regions, East and Central Equatorial Africa, J. Petrol., 10: 536–572.

Bellieni, G., Visentin, E.J., Piccirillo, E.M., and Zanettin, B., 1987. Volcanic cycles and magmatic evolution in northern Turkana (Kenya). Tectonophysics, 143: 161–168.

Bellon, H., and Pouclet, A., 1980. Datations K-Ar de quelques laves du Rift-ouest de l'Afrique Centrale: Implications sur l'evolution magmatique et structurale, Geol. Rund., 69: 49–62.

Ben-Avraham, Z. (Editor), 1987. Sedimentary basins within the Dead Sea and other rift zones. Tectonophysics, 141: 1–275.

Berckhemer, H., Baier, B., Bartelsen, H., Behle, A., Burckhardt, H., Gebrande, H., Makris, J., Menzel, H., Miller, H., and Vees, R., 1975. Deep seismic soundings in the Afar region and on the highland of Ethiopia. In: A. Pilger and A. Rosler (Editors), Afar Depression of Ethiopia. Schweizerbart, Stuttgart, pp. 89-107.

Bonjer, K.-P., Fuchs, K., and Wohlenberg, J., 1970. Crustal structures of the East African rift system from spectral response ratios of long period body waves. Z. Geopysik, 36: 287-297.

Bosworth, W., 1987. Off axis volcanism in the Gregory rift, East Africa: implications for models of continental rifting. Geology, 15: 397-400.

Bosworth, W., Strecker, M.R. and Blisniuk, P.M., 1992. Integration of East African paleostress and present-day stress data: Implications for continental stress field dynamics. J. Geophys. Res., 97: 11851–11865.

Braile, L.W., 1989. Crustal structure of the continental interior, In: Pakiser, L.C., and Mooney, W.D. (Editors), Geophysical Framework of the continental United States, Geol. Soc. Amer. Memoir 172: 285–315.

Braile, L.W., Wang, B., Daudt, C.R., Keller, G.R., and Patel, J.P., 1994. Modelling the 2-D seismic velocity structure across the Kenya rift. In: C. Prodehl, G.R. Keller, and M.A. Khan (Editors), Crustal and upper mantle structure of the Kenya rift. Tectonophysics, 236: 251–269.

Bram, K., 1975. Zum Aufbau der Kruste und des oberen Mantels im Bereich des westlichen Grabens des ostafrikanischen Grabensystems und im östlichen Zaire-Becken. Ergebnisse einer Untersuchung der Raumwellen von Nah-Erdbeben. Geophys. Abh., Inst. Geophysik, Freie Univ. Berlin, 4: 65 pp.

Brown, C. and Girdler, R.W., 1980. Interpretation of African gravity and its implication for the breakup of the continents, J. Geophys. Res., 85: 6443–6455.

Bungum, H., and Nnko, A.A., 1984. Seismicity and tectonics of the Stiegler's Gorge area, Tanzania. J. Geophys, Res., 89: 1874–1888.

Bullard, E. C., 1936. Gravity measurements in East Africa, Phil. Trans. R. Soc. A., 235, 287–297.

Chorowicz, J., and Sorlien, C., 1992. Oblique extensional tectonics in the Malawi rift, Africa. Geol. Soc. Am. Bull., 104: 1015–1023.

Choubert, G., and A. Faure-Muret (General Coordinators, International Geological Mapping Bureau), International Geological Map of Africa. 1:5,000,000 scale, Commission for the Geological Map of the World and UNESCO, 6 sheets, 1990.

Cloos, H., 1939. Hebung, Splatung, Vulkanismus. Geol. Rundsch. 30: 403–527, 637–640.

Coussement, C., Gente, P., Rolet, J., Tiercelin, J.-J., Wafula, M., and Buku, S., 1994. The North Tanganyika hydrothermal fields, East African Rift system: their tectonic control and relationship to volcanism and rift segmentation. Tectonophysics, 237: 155–173.

Davidson, A., and Rex, D., 1980. Age of volcanism and rifting in southwestern Ethiopia. Nature, 283: 657–658.

Davis, P.M., 1991. Continental rift structures and dynamics with reference to teleseismic studies of the Rio Grande and East African rifts. In: A.F. Gangi (Editor), World rift systems. Tectonophysics, 197: 307-325.

de Lapparent, A., 1898. Soulivements et Affaissements. Rev. Questions Sci. 14: 5–33.

Demant, A., Lestrade, P., Lubala, R.T., Kampunzu, A.B., and Durieux, J., 1994. Volcanological and petrological evolution of Nyiragongo volcano, Virunga volcanic field, Zaire. Bull. Volcanol., 56, 47–61.

de Martonne, E., 1897. Die hydrographie des oberen Nilbeckers. Z. Ges. Erdkd. 32: 315.

De Mulder, M., Hertogen, J., Deutsch, S., and Andre, L., 1986. The role of crustal contamination in the potassic suite of the Karisimbi volcano (Virunga, African Rift Valley), Chem. Geol., 57: 117–136.

Doser, D.I. and Yarwood, D.R., 1991, Strike-slip faulting in continental rifts: examples from Sabukia, east Africa (1928) and other regions, Tectonophysics, 197: 213–224.

Doser, D.I., and Yarwood, D.R., 1994. Deep crustal earthquakes associated with continental rifts. Tectonophysics, 229: 123–131.

Dunkelman, T.J., Karson, J.A., and Rosendahl, B.R., 1988. Structural style of the Turkana rift, Kenya, Geology, 16: 258-261.

Ebinger, C.J., 1989a. Tectonic development and the western branch of the East African rift system, Geol. Soc. of Am. Bull., 101: 885–903.

Ebinger, C.J. 1989b. Geometric and kinematic development of border faults and accommodation zones, Kivu-Rusizi rift, Africa, Tectonics, 8: 117–133.

Ebinger, C.J., Bechtel, T.D., Forsyth, D.W., and Bowin, C., 1989a. Effective elastic plate thickness beneath the East African and Afar plateaux and dynamic compensation of the uplifts. J. Geophys. Res., 94: 2893–2901.

Ebinger, C.J., Deino, A.L., Drake, R.E., and Tesha, A.L., 1989b. Chronology of volcanism and rift basin propagation: Rungwe volcanic province, East Africa. J. Geophys. Res., 94: 15,785–15,803.

Ebinger, C.J., and Ibrahim, A., 1994. Multiple episodes of rifting in central and East Africa: A re-evaluation of gravity data. Geol. Rundsch., 83: 689–702.

Ebinger, C.J., Karner, G.D. and Weissel, J.K., 1991. Mechanical strength of extended continental lithosphere: constraints from the Western rift system, East Africa. Tectonics, 10: 1239–1256.

Élie de Beaumont, L., 1827. Observations geologiques. Ann. Mines 2: 5–82.

Élie de Beaumont, L., 1847. Note sur les systemes de montagnes les plus anciens de l'Europe. Bull soc. Geol. Fr. 2nd. Ser. 4: 864–991.

Fairhead, J.D., 1976. Structure of the lithosphere beneath the Eastern rift, East Africa, deduced from gravity studies. Tectonophysics, 30: 269–298.

Fairhead, J.D., and Stuart, G.W., 1982. The seismicity of the East African rift system and comparison with other continental rifts. In: (Editor) Continental and Oceanic Rifts, by G. Palmason (Editor), AGU Geodynamics Series 8, Washington D.C., pp. 41–61.

Furman, T., 1990. Magmatism and continental rift propagation at Rungwe, Tanzania: Petrogenetic constraints, Eos Trans., 71: 1678.

Furman, T., 1992. Alkalic lavas from the Rungwe volcanic province, Tanzania: Trace element signature of the mantle source, Eos Trans., 73: 329–330.

Girdler, R.W., and McConnell, D.A., 1994. The 1990 to 1991 Sudan earthquake sequence and the extent of the East African rift system. Science, 264: 67–70.

Gregory, J.W., 1896. The Great Rift Valley. John Murray, London, 405 pp.

Gregory, J.W., 1921. The Rift Valleys and Geology of East Africa. Seeley, London, 479 pp.

Hackman, B.D., Charsley, J.J., Key, R.M., and Wilkinson, A.F., 1990. The development of the East African rift system in north-central Kenya. Tectonophysics, 184: 189–211.

Hart, W.K., WoldeGabriel, G., Walter, R.C., and Mertzman, S.A., 1989. Basaltic volcanism in Ethiopia: Constraints on continental rifting and mantle interactions, J. Geophys. Res., 94: 7731–7748.

Hay, D.E., and Wendlandt, R.F., 1995. The origin of Kenya rift plateau-type flood phonolites: Results of high-pressure/high-temperature experiments in the systems phonolite-H_2O and phonolite-H_2O-CO. J. Geophys. Res., 100: 401–410.

Hay, D.E., Wendlandt, R.F., and Wendlandt, E.D., 1995a. The origin of Kenya rift plateau-type flood phonolites: Evidence from geochemical studies for fusion of lower crust modified by alkali basaltic magmatism. J. Geophys. Res., 100: 411–422.

Hay, D.E., Wendlandt, R.F., and Keller, G.R., 1995b. The origin of Kenya rift plateau-type flood phonolites: Integrated petrologic and geophysical constraints on the evolution of the crust and upper mantle beneath the Kenya Rift. J. Geophys. Res., 100: 10,549–10,557.

Hendrie, D.B., Kusnir, N.J., Morley, C.K., and Ebinger, C.J., 1994. Cenozoic extension in northern Kenya: A quantitative model of rift basin development in the Turkana region. In: C. Prodehl, G.R. Keller, and M.A. Khan (Editors), Crustal and upper mantle structure of the Kenya rift. Tectonophysics, 236: 409–438.

Herbert, L., and Langston, C.A., 1985. Crustal thickness estimates at AAE (Addis Ababa, Ethiopia), and NAI (Nairobi, Kenya) using P-wave conversion. Tectonophysics, 111: 299-327.

Hetzel R. and Strecker, M.R., 1994. Late Mozambique Belt structures in Western Kenya and their influence on the evolution of the Cenozoic Kenya rift. J. Struct. Geol., 16: 189–201.

Holmes, A., 1944. Principles of Physical Geology. London: Nelson, 532 pp. 1st ed.

Jackson, J.A. and Blenkinsop, T., 1993. The Malawi earthquake of 10 March, 1989: Deep faulting within the East African rift system. Tectonics 12: 1131–1139.

Karson, J.A., and Curtis, P.C., 1989. Tectonic and magmatic processes in the eastern branch of the East African rift and implications for magmatically active continental rifts. J. African Earth Sci., 8: 431–453.

Keller, G.R., Khan, M.A., Morgan, P., Wendlandt, R.F., Baldridge, W.S., Olsen, K.H., Prodehl, C., and Braile, L.W., 1991. A comparative study of the Rio Grande and Kenya rifts. In: A.F. Gangi (Editor), World rift systems. Tectonophysics, 197: 355-372.

Keller, G.R., Mechie, J., Braile, L.W., Mooney, W.D. and Prodehl, C., 1994. Seismic structure of the uppermost mantle beneath the Kenya Rift. In: C. Prodehl, G.R. Keller and M.A. Khan (Editors), Crustal and upper mantle structure of the Kenya rift. Tectonophysics, 236: 201–216.

Kennett, B.L.N. and Engdahl, E.R., 1991. Traveltimes for global earthquake location and phase identification. Geophys. J. Int., 105: 429–465.

King, B.C., and Chapman, G.R., 1972. Volcanism of the Kenya rift valley, Phil. Trans. R. Soc. Lond. A., 271: 185–208.

Krenkel, E., 1922. Die Bruchzonen Ostafrikas. Berlin: Gebr. Borntraeger. 184 pp.

KRISP Working Group, 1987. Structure of the Kenya rift from seismic refraction. Nature, 325 (no. 6101): 239-242.

KRISP Working Party, 1991. Large-scale variation in lithospheric structure along and across the Kenya Rift. Nature, 354: 223-227.

Kusznir, N.J. and Ziegler, P.A., 1992. The mechanics of continental extension and sedimentary basin formation: a simple-shear flexural cantilever model. In: P.A. Ziegler (Editor), Geodynamics of Rifting, Volume III. Thematic discussions. Tectonophysics, 215: 117–132

Lippard, S.J., 1973. The petrology of phonolites from the Kenya rift. Lithos, 6: 217–234.

Logatchev, N.A., Zorin, Y.A., and Rogozhina, V.A., 1983. Baikal rift: Active or passive? - Comparison of the Baikal and Kenya rift zones. Tectonophysics, 94: 223-240.

Maasha, N., 1975. The seismicity of the Ruwenzori region in Uganda, J. Geophys. Res., 80, 1485–1496.

Maasha, N., and P. Molnar, 1972. Earthquake fault parameters and tectonics in Africa. J. Geophys. Res., 77: 5731–5743.

Macdonald, R., 1994. Petrological evidence regarding the evolution of the Kenya rift valley. In: C. Prodehl, G.R. Keller and M.A. Khan (Editors), Crustal and upper mantle structure of the Kenya rift. Tectonophysics, 236: 373–390.

Maguire, P.K.H., and Long, R.E., 1976. The structure of the western flank of the Gregory rift (Kenya), Part I. The Crust, Geophys. J. R. Astr. Soc., 44: 661-675.

Makris, J. and Ginzburg, A., 1987. The Afar Depression: transition between continental rifting and sea-floor spreading. Tectonophysics, 141: 199-214.

Makris, J., Mohr, P., and Rihm, R., 1991. Red Sea: Birth and Earth History of a New Oceanic Basin. Tectonophysics, 198: 1–468.

Marcelot, G., Dupuy, C., Dostal, J., Rancon, J.P., and Pouclet, A., 1989. Geochemistry of mafic volcanic rocks from the Lake Kivu (Zaire and Rwanda) section of the western branch of the African Rift, J. Volcanol. Geotherm. Res., 39, 73–88.

Mechie, J., Keller, G.R., Prodehl, C., Gaciri, S., Braile, L.W., Mooney, W.D., Gajewski, D. and Sandmeier, K.-J., 1994. Crustal structure beneath the Kenya Rift from axial profile data. In: C. Prodehl, G.R. Keller and M.A. Khan (Editors), Crustal and upper mantle structure of the Kenya rift. Tectonophysics, 236: 179–200.

Mohr, P., 1978. Afar. Ann. Rev. Earth. Planet. Sci. 6: 145–172.

Mohr, P., 1983. Ethiopian flood basalt province, Nature, 303: 577–583.

Mohr, P., 1987. Patterns of faulting in the Ethiopian rift valley. Tectonophysics, 143: 169–179.

Mohr, P., 1989. The nature of the crust under Afar: New igneous, not stretched continental. Tectonophysics, 167: 1–11.

Mohr, P., 1992. Nature of the crust beneath magmatically active continental rifts. Tectonophysics, 213: 269–284.

Mohr, P., and Zanettin, B., 1988. The Ethiopian flood basalt province. In Continental Flood Basalts, edited by J.D. Macdougall, Kluwer Academic Publishers, 63–110.

Moore, J.M. and A. Davidson, 1978. Rift structure in southern Ethiopia. Tectonophysics, 46: 159–173.

Morgan, P., 1982. Heat flow in rift zones. In: G. Palmason (Editor), Continental and Oceanic Rifts, Geodynamics Series v. 8, American Geophysical Union, Washington, D.C., pp. 107–122.

Morley, C.K., 1992. Variable extension in Lake Tanganyika. Tectonics, 7: 785–801.

Morley, C.K., Wescott, W.A., Stone, D.M., Harper, R.M., Wigger, S.T., and Karanja, F.M., 1992. Tectonic evolution of the northern Kenyan rift. J. Geol. Soc. Lond., 149: 333-348.

Nixon, P.H., 1973. Kimberlitic volcanoes in East Africa, Overseas Geol. Miner. Resour., 41: 119–138.

Nolet, G. and Mueller, S., 1982. A model for the deep structure of the East African rift system from simultaneous inversion of teleseismic data. Tectonophysics, 84: 151–178.

Nyblade, A.A., and Langston, C.A., 1995. East African earthquakes below 20 km depth and their implication for crustal structure. Geophys. J. Int., in press.

Nyblade, A.A., and Pollack, H.N., 1992. A gravity model for the lithosphere in western Kenya and northeastern Tanzania. Tectonophysics, 212: 257–267.

Nyblade, A.A., Pollack, H.N., Jones, D.L., Podmore, F., and Mushayandebvu, M., 1990. Terrestrial heat flow in East and Southern Africa. J. Geophys. Res. 95: 17,371–17,384.

Nyblade, A.A., and Robinson, S.W., 1994. The African Superswell, Geophys. Res. Lett., 21: 765–768.

Pasteels, P., Villeneuve, M., De Paepe P, and Klerkx, J., 1989. Timing of the volcanism of the southern Kivu province: Implications for the evolution of the western branch of the East African rift system. Earth Planet. Sci. Lett., 94: 353–363.

Pointing, A.J., and Maguire, P.K.H., 1990. A seismic model for the crust in northern Kenya derived from local earthquake data. J. African Earth Sci., 11: 401-409.

Prodehl, C., and Mechie, J., 1991. Crustal thinning in relationship to the evolution of the Afro-Arabian rift system - a review f seismic-refraction data. In: Makris, J., P. Mohr, and R. Rihm, (Editors), Red Sea: Birth and early history of a new oceanic basin. Tectonophysics, 198: 311-327.

Prodehl, C., Keller, G.R., and Khan, M.A., (Editors) 1994a. Tectonophysics, Special vol. 236, Elsevier.

Prodehl, C., Jacob, B., Thybo, H., Dindi, E. and Stangl, R., 1994b. Crustal structure on the northeastern flank of the Kenya rift. In: C. Prodehl, G.R. Keller, and M.A. Khan (Editors), Crustal and upper mantle structure of the Kenya rift. Tectonophysics, 236: 271–290.

Rodgers, N.W., DeMulder M. and Hawkesworth, C.J., 1992. An enriched mantle source for potassic basanites: evidence from Karasimbi volcano, Virunga volcanic province, Rwanda. Contrib. Min. Petrol., 11: 543–556.

Rosendahl, B.R., 1987. Architecture of continental rifts with special reference to East Africa. Ann. Rev. Earth Planet. Sci., 15: 445–503.

Rosendahl, B.R., Reynolds, D.J., Lorber, P.M., Burgess, C.F., McGill, J., Scott, D., Lambiase, J.-J., and Derksen, S.J., 1986. Structural expressions of rifting: lessons from Lake Tanganyika, Africa. In: L.E. Frostick, R.W. Renaut, I. Reid, and J.-J. Tiercelin (Editors), Sedimentation in the African Rifts. Geol. Soc. London Spec. Publ., 25: 29–43.

Rosendahl, B.R., Kilembe E., and Kaczmarick, K., 1992. Comparison of the Tanganyika, Malawi, Rukwa and Turkana rift zones from analyses of seismic reflection data. Tectonophysics, 213: 235–256.

Ruegg, J.C., 1975. Main results about the crustal and upper mantle structure of the Djibouti region (T.F.A.I.). In: A. Pilger and A. Rösler (Editors), Afar Depression in Ethiopia. Schweizerbart, Stuttgart, pp. 120-134.

Rykounov, L.N., Sedov, V.V., Savrina, L.A. and Bourmin, V.J., 1972. Study of microearthquakes in the rift zones of East Africa, In: R.W. Girdler, (Editor), East African rifts, Tectonophysics, 15: 123–130.

Sahama, Th.G., 1960. Kalsilite in the lavas of Mt. Nyiragongo (Belgium Congo), J. Petrol., 1: 146–171.

Sahama, Th.G., 1973. Evolution of the Nyiragongo magma, J. Petrol., 14: 33–48.

Savage, J.E.G., and Long, R.E., 1985. Lithospheric structure beneath the Kenya dome. Geophys. J., 82: 461–477.

Shudofsky, G.N., 1985. Source mechanisms and focal depths of East African earthquakes using Rayleigh wave dispersion and body-wave modeling. Geophys. J.R. Astr. Soc., 83: 563–614.

Shudofsky, G.N., Cloetingh, S., Stein, S., and Wortel, R., 1987. Unusually deep earthquakes in East Africa: constraints on the thermo-mechanical structure of a continental rift system. Geophys. Res. Lett., 14: 741–744.

Slack, P.D. and Davis, P.M. and the KRISP Teleseismic Working Group, 1994. Attenuation and velocity of P-waves in the mantle beneath the East African rift, Kenya. In: C. Prodehl, G.R. Keller, and M.A. Khan (Editors), Crustal and upper mantle structure of the Kenya rift. Tectonophysics, 236: 331–358.

Smith, M., 1994. Stratigraphic and structural constraints on mechanisms of active rifting in the Gregory rift, Kenya. In: C. Prodehl, G.R. Keller, and M.A. Khan (Editors), Crustal and upper mantle structure of the Kenya rift. Tectonophysics, 236: 3–22.

Smith, M., and Mosley, P., 1993. Crustal heterogeneity and basement influence on the development of the Kenya Rift, East Africa. Tectonics, 12: 591–606.

Strecker, M.R., and Blisniuk, P.M., and Eisbacher, G.H., 1990. Rotation of extension direction in the central Kenyan rift. Geology, 18: 299–302.

Strecker, M.R., and Bosworth, W. 1991. Quaternary stress-field change and rifting processes in the East African Gregory Rift. Eos Transactions Am. Geophys. Un, 71: 17–22.

Suess, E., 1891. Die Brüeche des ostlichen Afrikas. Denkschr. Akad. Wiss. Wien 553: 1–580.

Swain, C.J., 1992. The Kenya rift axial gravity high: a re-interpretation. In: R. Altherr (Editor), The Afro-Arabian rift system. Tectonophysics, 204: 59-70.

Swain, C.J., Maguire, P.K.H., and Khan, M.A., 1994, Geophysical experiment and models of the Kenya rift before 1989. In: C. Prodehl, G.R. Keller, and M.A. Khan (Editors). Crustal and upper mantle structure of the Kenya rift. Tectonophysics, 236: 23–32.

Tongue, J.A., Maguire, P.K.H., Young, P.A.V., 1992. Seismicity distribution from temporary earthquake recording networks in Kenya. Tectonophysics, 204: 71–79.

Tongue, J.A., Maguire, P.K.H., and Burton, P., 1994. An earthquake study in the Lake Baringo basin of the central Kenya rift. In: C. Prodehl, G.R. Keller, and M.A. Khan (Editors), Crustal and upper mantle structure of the Kenya rift, Tectonophysics, 236: 151–164.

Upcott, N.M., Mukasa, R.K., Ebinger, C.J., and Karner, G.D., 1995. Along-axis segmentation and isostasy in the Western rift, East Africa. J. Geophys. Res., in press.

Wendlandt, R.F. and Morgan, P., 1982. Lithospheric thinning in East Africa. Nature, 298: 734–736.

Wheildon, J., Morgan, P., Williamson, K.H., Evans, T.R., and Swanberg, C.A., 1994. Heat flow in the Kenya rift zone. In: C. Prodehl, G.R. Keller, and M.A. Khan (Editors), Crustal and upper mantle structure of the Kenya rift. Tectonophysics, 236: 131–149.

Williams, L.A.J., 1970. The volcanics of the Gregory Rift Valley, East Africa, Bull. Volcanol., 439–465.

Williams, L.A.J., 1972. The Kenya Rift volcanics: A note on volumes and chemical composition. In East African Rifts, edited by R.W. Girdler, Tectonophysics, 15: 83–96.

Williams, L.A.J., 1982. Physical aspects of magmatism in continental rifts, Am. Geophys. Un., Geodyn. Ser., 8: 193-222.

Willis, B., 1936. East African Plateaus and Rift Valleys. Washington, DC: Carnegie Inst. 358 pp.

Wohlenberg, J., 1969. Remarks on the seismicity of East Africa between 4°N–12°S and 23°E–40°E. Tectonophysics, 8: 567–577.

WoldeGabriel, G., 1987. Volcanotectonic history of the central sector of the Main Ethiopian Rift: A geochronological, geochemical and petrological approach (Ph.D. Thesis), Case Western Reserve University, 410 pp.

WoldeGabriel, G., and Aronson, J.L., 1987. Chow Bahir rift: A "failed" rift in southern Ethiopia. Geology, 15: 430–433.

WoldeGabriel, G., Aronson, J.L., and Walter, R.C., 1990. Geology, geochronology, and rift basin development in the central sector of the Main Ethiopia Rift. Geological Society of America Bulletin, 102: 439–458.

WoldeGabriel, G., Yemane, T., Suwa, G., White, T., and Asfaw, B., 1991. Age of volcanism and rifting in the Burji-Soyoma area, Amarco Horst, southern Main Ethiopian Rift: geo- and biochronologic data. J. African Earth Sci., 13: 437–447.

Young, P.A.V., Maguire, P.K.H., Laffoley, N. d'A, and Evans, J.R., 1991. Implications of distribution of seismicity near Lake Bogoria in the Kenya rift. Geophys. J. Int., 105: 665–674.

Ziegler, P.A. (Editor), 1992. Geodynamics of Rifting, Volume II. Case History Studies on Rifts: North and South America and Africa. Tectonophysics, 213: 1–284.

This Page Intentionally Left Blank

Chapter 6

The Rio Grande Rift

W.S. Baldridge, G.R. Keller, V. Haak, E. Wendlandt, G.R. Jiracek, and K.H. Olsen,

6.1 Introduction

The Rio Grande rift is part of a broad region of the western United States, including the Basin and Range province, that has undergone lithospheric thinning and crustal extension during the middle to late Cenozoic (Plate 6–1). The entire region is included in the Cordillera of western North America. The present extensional setting of the rift is generally related to plate boundary forces acting along the southwestern edge of the North American plate, a transform boundary along which right-lateral slip occurs.

In contrast to the present tectonic setting, initial extension c. 30 Ma began in a back-arc or intra-arc setting during east-dipping subduction of the Farallon plate beneath the North American plate (e.g., Snyder et al., 1976; Dickinson and Snyder, 1979; Livaccari, 1979; Eaton, 1979, 1982; Dickinson, 1981; Engebretson et al., 1984; Glazner and Bartley, 1984). This age corresponds with the earliest deposition of sediments in broad extensional basins, but this earlier extensional event is distinct in style and extension directions from the later, rift-style extension. Without the later extension event, it is unlikely that the early event would have resulted in an important continental rift. The spatial association between these two events, however, suggests some genetic relation.

Extension throughout the Basin and Range and Rio Grande rift is superimposed on structures formed during a late Cretaceous to early Tertiary compressional orogenic event, the Laramide orogeny, which gave rise to basement-cored uplifts and broad thin-skin-style thrust sheets. The rift as a whole follows a zone of crustal deformation formed during the Laramide (of middle Eocene age, c. 50–40 Ma, in New Mexico) and Ancestral Rocky Mountains (Pennsylvanian; approximately 300 Ma) orogenic events (e.g., Chapin and Seager, 1975; Lucas, 1984). It cuts across a regional northeast-trending structural grain of the Precambrian basement.

Because of the complex pre-rift Cenozoic history, basins of the rift commonly include a significant thickness of early Tertiary sediments deposited in Laramide foreland-style basins. Consequently, displacements on rift-bounding faults are difficult to interpret in terms of rift-related offset because observed structural offsets on pre-Cenozoic marker horizons may be composite offsets of Laramide compression and middle to late Cenozoic extension. All of these events are thus important in the context of the formation of the rift basins and their sediments, but, as discussed below, only the latest extension event meets the usual criteria for rifting.

Historical Note

The Rio Grande rift was first characterized as a morphological depression (the Rio Grande depression) extending from Colorado through New Mexico (Bryan, 1938). For more than 20 years, Bryan and his students and colleagues conducted a vigorous research program on various stratigraphic, structural,

and geomorphic problems related to the rift (e.g., Bryan, 1938; Wright, 1946; Stearns, 1943; 1953a, b, c). The term "rift" was first applied to the Rio Grande depression by Kelley (1952, 1977) in an analogy to what was then commonly referred to as the San Andreas rift (San Andreas fault). The term "rift" conveyed Kelley's hypothesis that formation of the Rio Grande rift involved a major component of strike-slip offset parallel to the rift axis. In the 1960's several regional studies included the Rio Grande rift (see references in Chapin, 1979). Chapin (1971) established more or less the present definition of the rift in Colorado, New Mexico, west Texas, and Chihuahua, and outlined its characteristic features. Additional studies emphasizing the uniqueness of the rift relative to adjacent tectonic provinces were presented by Decker and Smithson (1975) and Cordell (1978). The international scientific community was largely unaware of the rift until an international conference was convened in Santa Fe, New Mexico, in October of 1978. The volume published as a result of this conference (Riecker, 1979) established the Rio Grande rift as a major Cenozoic continental rift. Since then, many general and topical studies have been carried out by numerous investigators from a large number of institutions (e.g., Baldridge et al., 1984; Keller, 1986; Olsen et al., 1987; Baldridge et al., 1991; Keller et al., 1991).

6.2. Regional setting

The Rio Grande rift extends as a series of interconnected, asymmetrical basins from Leadville, Colorado, to Big Bend, Texas, and Chihuahua, Mexico, a distance of more than 1000 km (Fig. 6–1). From central Colorado to southern New Mexico the rift occupies part of the axis of a broad, subcontinental-scale uplift, at least 2500 km in breadth and 1300 km in length. The uplift, including the Colorado Plateau and western Great Plains, was likened in physiography and scale to a mid-oceanic ridge and named the Alvarado (continental) ridge by Eaton (1986, 1987). The crestal region of this mammoth uplift, in places exceeding 4.2 km in elevation, was defined by Eaton (1986) as the tectonic (in contrast with the physiographic) southern Rocky Mountains.

The northern rift, occurring along the central part of the Alvarado ridge, is a distinctive tectonic and physiographic feature separating the Colorado Plateau on the west slope of the ridge from the Great Plains, part of the stable North American craton, on the east slope (e.g., Chapin and Seager, 1975; Cordell, 1978; Baldridge et al., 1983, 1984; Olsen et al., 1987). The southern rift, lying along the axis of the southern Alvarado ridge and farther south in west Texas and northern Mexico, is physiographically similar to and essentially contiguous with the adjacent Basin and Range province in southern New Mexico and northern Mexico. The southern rift arguably can be distinguished from the larger Basin and Range province by a variety of geological and geophysical features, including higher heat flow, numerous Quaternary faults, thin crust, and greater basin size and depth (e.g., Seager and Morgan, 1979; Sinno et al., 1986). A more important distinction, however, is its axial position with respect to the Alvarado ridge.

Over much of its length the deep basins of the rift are part of a broader region of late Cenozoic extensional deformation, characterized by large crustal blocks separated by steeply dipping normal faults (Baldridge et al., 1983). In central New Mexico, west of Albuquerque and Socorro, this region is more than 200 km wide, extending southwestward across the physiographic Colorado Plateau to Springerville, Arizona, and possibly beyond (Fig. 6–1). It constitutes a transition zone along the southeastern Colorado Plateau, though differing in its physiography and amount of structural offset from the more familiar transition zone of the southwestern Plateau (Mogollon rim). The style and timing of structural deformation of this region are similar to that of the main rift basins, but the magnitude of structural relief is much less; vertical offsets on normal faults probably do not exceed a few hundred meters.

The transition zone along the southeastern margin of the Plateau is separated from the less deformed "core" of the Plateau to the northwest by a broadly linear, northeast-trending array of late Cenozoic volcanic fields, commonly referred to as the Jemez zone (or lineament). The Jemez zone very likely corresponds to a major boundary or zone of weakness in the lithosphere. However, it is not an expres-

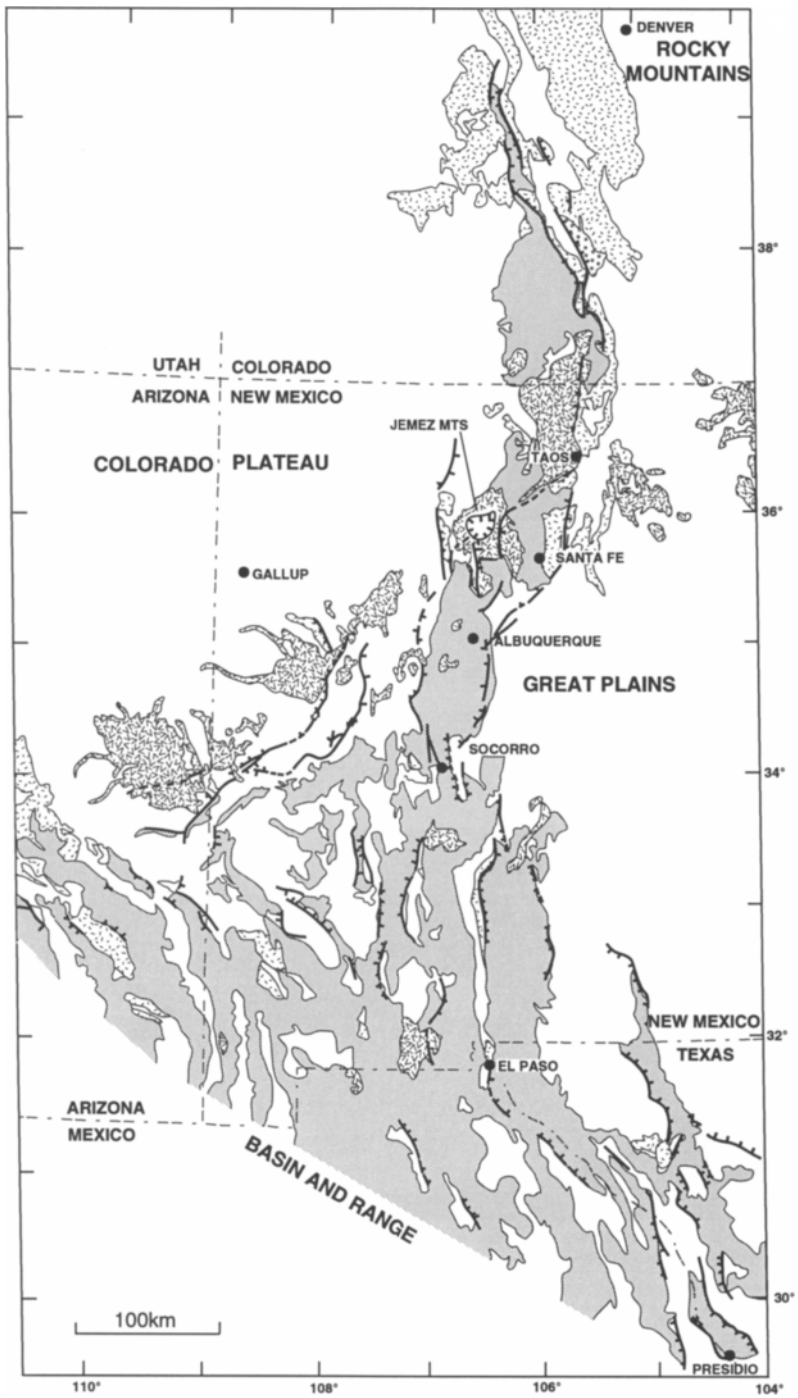

Fig. 6–1. Tectonic map of Rio Grande rift. Shaded pattern is Miocene to Quaternary sediments and sedimentary rocks of middle to late Cenozoic basins. "V" pattern is volcanic rocks younger than 15 Ma. Dashed pattern is Precambrian rocks of uplifts. Modified from Baldridge et al. (1984).

sion of a fault or fracture zone and does not seem to correspond to any single, simple structure in the upper crust (Baldridge et al., 1983).

South of the Colorado Plateau, the massive pre- and early syn–rift Mogollon-Datil volcanic field, which overlies a composite upper crustal intrusion of batholithic proportions (Elston, 1984), is similarly deformed. Narrow, deep grabens near Datil, Reserve, and Silver City, around the periphery of the volcanic field, are separated from the larger, main basins of the rift by a region approximately a hundred kilometers wide in which extensional deformation formed only shallow grabens.

Recognition that this broader zone of deformation is tectonically, though not physiographically, part of the Rio Grande rift significantly expands the definition by Chapin (1971). In addition, reactivation of preexisting structures during late Cenozoic extension occurred over an even broader area, e.g., in the Texas Panhandle over 300 km east of the rift (Budnick, 1987). In west Texas, Quaternary fault scarps are observed over a wide area (Muehlberger et al., 1978), also suggesting that the effects of rifting were broad.

6.3. Cenozoic evolution

The tectonic evolution of the Rio Grande rift is complicated by the fundamental change in the western margin of the North American plate from subduction to transform faulting that occurred during the late Cenozoic. Subduction occurred for at least 100 m.y. prior to extension. Laramide compressional deformation, during which crustal thickening occurred and which lasted until about 40 Ma in New Mexico (Seager and Mack, 1986), was derived presumably from coupling of the shallow subducting plate with the overlying North American plate. Following the Laramide orogeny and lasting until about 20 Ma, a major period of magmatism occurred, characterized by intermediate magmas spread widely throughout the southwestern U.S. and northern Mexico. During this event the lithosphere was thermally weakened, allowing later extension to occur (Morgan and Golombek, 1984; Morgan et al., 1986).

Cenozoic extensional deformation in New Mexico and eastern Arizona occurred in two phases: late Oligocene-early Miocene and middle Miocene-Holocene (e.g., Baldridge et al., 1980; Seager et al., 1984). The earlier phase resulted in formation of broad, relatively shallow basins bounded, in part at least, by low-angle faults. Crustal extension may have been as great as 30–50%. The style of deformation and the fact that extension closely followed, and partially overlapped with, widespread mid-Tertiary magmatism suggest that the lithosphere was relatively hot and the brittle-ductile transition relatively shallow (Morgan and Golombek, 1984; Morgan et al., 1986). In the southeastern Plateau and central rift area, crustal extension began about 31 Ma and lasted about 9 Ma (Aldrich et al., 1986). The latter phase of deformation, part of the classical "basin and range extensional event" which effected most of the western United States (Shafiqullah et al., 1980; Eaton, 1982), resulted in formation of a north-northeast-trending series of asymmetrical grabens—the Rio Grande rift—and in a broad "transition zone" along the southeastern and southern margins of the Colorado Plateau (Fig. 6–1). Grabens were generally narrow and bounded by steep faults, suggesting that the lithosphere was cooler and that the brittle-ductile transition was deeper than in the previous extensional event (Morgan et al., 1986). The transition zone is characterized by normal faults which tend to be oriented in east-northeast or north-northeast directions and form long fault zones approximately concentric to the Plateau margin (Fig. 6–1). Offsets along these faults, however, are not great compared to axial rift grabens and probably do not exceed a few hundred meters. The northern rift, because of its position between the Colorado Plateau and the Great Plains (part of the continental craton), is a well-defined morpho-tectonic feature. The Colorado Plateau has acted as a semi-independent microplate since at least the late Permian, resisting break-up except along its margins (Steiner, 1988). The southern rift, where the earliest and most extension has occurred, is physiographically indistinguishable from the adjacent Basin and Range province.

The timing of uplift which accompanied Cenozoic extension is poorly constrained, and only two elevation points are firmly established: (1) widespread Cretaceous marine shales and littoral sandstones indicate that this area was at or near sea level at this time, and (2) the present elevation of the rift floor, which ranges from <1219 m in southern New Mexico to approximately 3000 m in central Colorado (near Leadville). An erosion surface of Eocene age, which is recognized widely throughout the southern Rocky Mountains, provides a topographic datum (Scott, 1975; Epis and Chapin, 1975).

6.4. Pre-rift sedimentary rocks

The Cordilleran region of the U. S., including the area of the Rio Grande rift, lay near the Paleozoic western margin of the North American craton. Large parts of the region were below sea level throughout most of the Paleozoic, resulting in widespread deposition of carbonate and sandstone shelf sediments. For example, in southern New Mexico, Cambrian through Devonian sediments consist of carbonate, sandstone, and minor shale. The central part of the rift area was effected by an elongate ridge-like structure, the transcontinental arch, that stretched from northern Mexico to the Lake Superior region of Canada. This structure remained above sea level during much of the early to middle Paleozoic. Thus, throughout the central rift area, early and middle Paleozoic strata are missing from the section. By the end of the Devonian the transcontinental arch was no longer a dominant structure. Hence, in the Mississippian the entire rift area was covered by thick and laterally extensive shallow marine limestone.

Beginning in the late Paleozoic and extending into the Mesozoic, much of the interior of the craton was emergent, and a steeply dipping subduction zone was present along the western margin of North America. Thus, the Cordilleran region was subject to frequent marine transgressions and regressions and diverse sedimentation. Deformation in the Pennsylvanian, probably caused by collision along the southern margin of the craton with South America, effected a broad zone from Texas to Wyoming (Kluth and Coney, 1981). Sedimentary rocks of the late Paleozoic and much of the Mesozoic (Triassic and Jurassic) consist of interbedded red beds, dune sandstone, shallow marine strata, and, adjacent to late Paleozoic uplifts, arkosic sandstone. Triassic and Jurassic rocks are absent from central and southern New Mexico.

East- to northeast-directed compression resulting from convergence along the western margin of North America affected much of the Cordilleran region from the late Jurassic to the early Tertiary. In the late Cretaceous a major inland seaway (a back-arc basin), extending from the Arctic to the Gulf of California, developed between the emergent craton to the east and a growing uplift to the west. In the rift area thick units of black shale and sandstone, interbedded with transgressive terrigenous sediments, were deposited. General emergence of the area near the end of the Cretaceous was contemporaneous with compressional deformation of the Laramide orogeny, which near the eastern margin of the Cordillera continued into the middle Eocene. By the late Eocene a regional peneplane was developed across Laramide uplifts. Since the Laramide event, the entire Cordillera has remained above sea level. Tertiary sedimentation in the rift area is characterized generally by continental basinal deposits, including interbedded epi- and pyroclastic rocks.

6.5. Geology of the rift

6.5.1. Geological Maps

Geologic maps of Colorado, New Mexico, and Texas at a scale of 1:500,000 and larger are available from the U.S. Geological Survey, the New Mexico Bureau of Mines and Mineral Resources, and the Texas Bureau of Economic Geology. Geologic and tectonic maps of portions of the rift have been published by Kelley and Wood (1946), Woodward et al. (1975, 1978), Kelley (1977, 1978), Tweto (1978), Baldridge et al. (1983), and Henry and Price (1985).

In Mexico, the data available are much less satisfactory. A geologic map of the State of Chihuahua is available through the El Paso Geological Society. However, detailed mapping is sparse, and fundamental questions such as the extent of Quaternary faulting and young volcanism are incompletely known.

6.5.2. Structure

Two generations of structures are recognized in the Rio Grande rift: (1) an early generation related to a late Oligocene-early Miocene (c. 30–20 m.y. ago) event, and (2) a later generation related to a middle or late Miocene-Holocene event (Baldridge et al., 1980; Seager et al., 1984; Morgan et al., 1986). Early generation basin-marginal faults are poorly exposed, if at all, and are only locally recognized in flank uplifts where they occur as systems of closely-spaced low-angle normal faults. This early, low-angle faulting involved both domino-style and listric faulting. It may also have involved detachment faulting. Domino-style faulting involves structural offset along fault planes which were initially high-angle and were later rotated with continued extension to a shallow angle (Chamberlain, 1983; Baldridge et al., 1984; Morgan et al., 1986; Olsen et al., 1987). In addition, some rotation toward a low-angle position may have occurred as modern ranges were uplifted and tilted. Many early rift basins trended northwestward, parallel to early extensional structures in Nevada (Zoback and Thompson, 1978). In the rift, this trend may suggest that bounding structures were controlled by preexisting Laramide structural grain or by a northeast-southwest extension direction, or both (e.g., Seager et al., 1984; Lipman, 1981).

Many outcrops of early sediments are located high on the flanks of the rift, outside the modern grabens. Their position indicates that they were originally deposited in broad basins and were subsequently uplifted relative to the modern grabens (Stearns, 1953a; Chapin and Seager, 1975).

The modern rift basins acquired their form during the middle or late Miocene-Holocene extension event. Individual basins are typically asymmetrical, with one or both sides bounded by steeply dipping faults or by zones several kilometers wide in which numerous steeply dipping faults are closely spaced (Callender and Zilinski, 1976; Vernon and Riecker, 1989; Russell and Snelson, 1990, 1994; Biehler et al., 1991). The main basins are complex in detail, and are themselves divided by intrabasin horsts and grabens (Cordell, 1976; Lipman and Mehnert, 1979; Keller et al., 1984; Lozinsky, 1989). In the northern and central rift, the sense of basin asymmetry ("polarity") characteristically alternates between adjacent basins across transfer faults or complex structural zones of distributed strain ("accommodation zones"), which transfer fault offsets to adjacent grabens. For example, the greatest vertical offset of the San Luis basin occurs along its eastern margin (Lipman and Mehnert, 1979). The Española basin dips toward the west (Biehler et al., 1991). The deep Albuquerque-Belen basin, which appears on the surface to consist of a single sedimentary basin, actually comprises two oppositely-hinged structural basins. The northern basin (Albuquerque basin) dips to the east, the southern basin (Belen basin) dips to the west (Russell and Snelson, 1990, 1994).

The dominant component of offset on bounding faults is vertical, with offset of pre-Tertiary units exceeding 10 km in some basins (Lozinsky, 1989). Total thickness of Cenozoic fill alone, however, is not an accurate measure of offset on rift-bounding faults, since early Tertiary units (Eocene and Oligocene) predate rifting. Horizontal components of offset along rift-bounding or intrarift faults are more difficult to establish because of the lack of suitable marker units. A component of horizontal offset is recognized along rift-marginal and intrarift faults of the central rift (e.g., Woodward and DuChene, 1975; Muehlberger, 1979; Steinpress, 1981; Aldrich, 1986; Wachs et al., 1988; Baldridge et al., 1990; Hayden and Mawer, 1991). The full extent of lateral offset along rift faults has possibly not yet been recognized, largely because of the lack of suitable markers and of detailed analysis.

6.5.3. Kinematics

Kelley (1979, 1982) proposed that formation of the rift involved left-lateral transcurrent motion along the rift axis, based on offset of Jurassic wedge edges, en echelon right lateral offset of rift basins, and structural ramps between en echelon border faults. However, wedging out of Jurassic edges may be an erosional phenomenon (Chapin and Cather, 1981).

Muehlberger (1979) suggested that the Española basin comprises a rhombohedrally shaped crustal block (Española block) which underwent counter-

clockwise rotation about a vertical axis in response to left slip along the axis of the rift. Rotation of the block resulted in uplift at the acute ends of the block and topographic lows at the obtuse ends. Brown and Golombek (1985, 1986) postulated from paleomagnetic data that the Española block underwent 17.8°±11.4° of counterclockwise rotation since 5 m.y. ago. This model has several major uncertainties, including the fact that (1) the Española block as defined by Muehlberger (1979) is almost certainly not a single major crustal block, but rather is cut by numerous faults (Kelley, 1978; Vernon and Riecker, 1989; Biehler et al., 1991); and (2) the amount of rotation determined from paleomagnetic studies is small (6–13° above statistical error) and hence very sensitive to small errors in correction of inclinations due to tectonic deformation at sampling sites. Subsequent paleomagnetic studies by Salyards et al. (1991) do not support a single block undergoing counterclockwise rotation.

Alternative models for the structure of the rift are suggested by many recent field and experimental studies of extensional terranes (Gibbs, 1984; Wernicke, 1985; Bosworth, 1985, 1987; Bosworth et al., 1986; Rosendahl, 1987; McClay and Ellis, 1987; Ellis and McClay, 1988). These studies show that rift basins may be related to low angle listric or detachment faults, or ductile shear zones, at depth. One side of an extensional basin is typically bounded by a single major "breakaway" fault, which is arcuate in plan view and may become listric with depth, with the other side hinged. Basins are typically strongly asymmetric. Shoulder uplift and tilting adjacent to the major listric bounding fault result from unloading and uplift of the footwall. Adjacent basins hinged on opposite sides are bounded by transfer (strike slip) faults or by complex zones of distributed deformation (accommodation zones). These models predict rotations about vertical axes, but observed rotations are local, involve both clockwise and counter-clockwise motion, and are related to the lateral faults.

Recent studies in the central Rio Grande rift suggest that these models may apply to the rift. For instance, the oppositely-hinged Albuquerque and Belen basins are separated by an accommodation zone (Lozinsky, 1988, 1989; Russell and Snelson, 1990, 1994). The Belen basin is bordered by a system of major east-facing, low-angle normal faults forming a west-dipping basin (Russell and Snelson, 1990, 1994). The western margin of the basin (essentially the eastern edge of the Colorado Plateau) has undergone isostatic uplift of the footwall block, forming a flanking uplift. South of the Belen basin, the rift is a broader zone of extension formed by three east-facing, nested half-grabens (Fig. 6–2) (Lewis and Baldridge, 1994). The arrangement of these half-grabens suggests that they sole into an east-dipping detachment.

6.5.4. Syn–rift sediments

Basin fill of the Rio Grande rift (Fig. 6–3, Plate 6–2) is entirely of nonmarine origin, consisting dominantly of late Oligocene to Holocene sediments and sedimentary rocks with minor volumes of interbedded volcanic and tuffaceous rocks (Chapin, 1988). Except for the Española basin (see below), synrift sedimentary and volcanic deposits from Oligocene age to entrenchment of the Rio Grande drainage in the middle Pleistocene are collectively called the Santa Fe Group (e.g., Chapin, 1988). Sedimentary fill mainly comprises broad, coalescing alluvial-fan deposits that grade basinward into fine-grained alluvial-plain and playa deposits. These latter units establish that during much or most of its history the rift consisted of a series of closed basins. Freshwater lacustrine deposits are present in the San Luis, Española, and Albuquerque-Belen basins. Eolian sands and sandstones are locally present in some basins. After establishment of the axial Rio Grande drainage in the Pliocene (e.g., Bachman and Mehnert, 1978) piedmont deposits adjacent to the uplifted rift flanks interfingered with axial river sands and gravels. These axial river deposits and their intertonguing piedmont facies are known by a variety of names in different parts of the rift (Chapin, 1988). In the Española basin, clays and fine-grained sands indicate that the Rio Grande was locally dammed by lava flows (Manley, 1976; Waresbach and Turbeville, 1990).

In comparison with other basins of the rift, the Española basin underwent unusually deep dissection following establishment of axial drainage, exposing

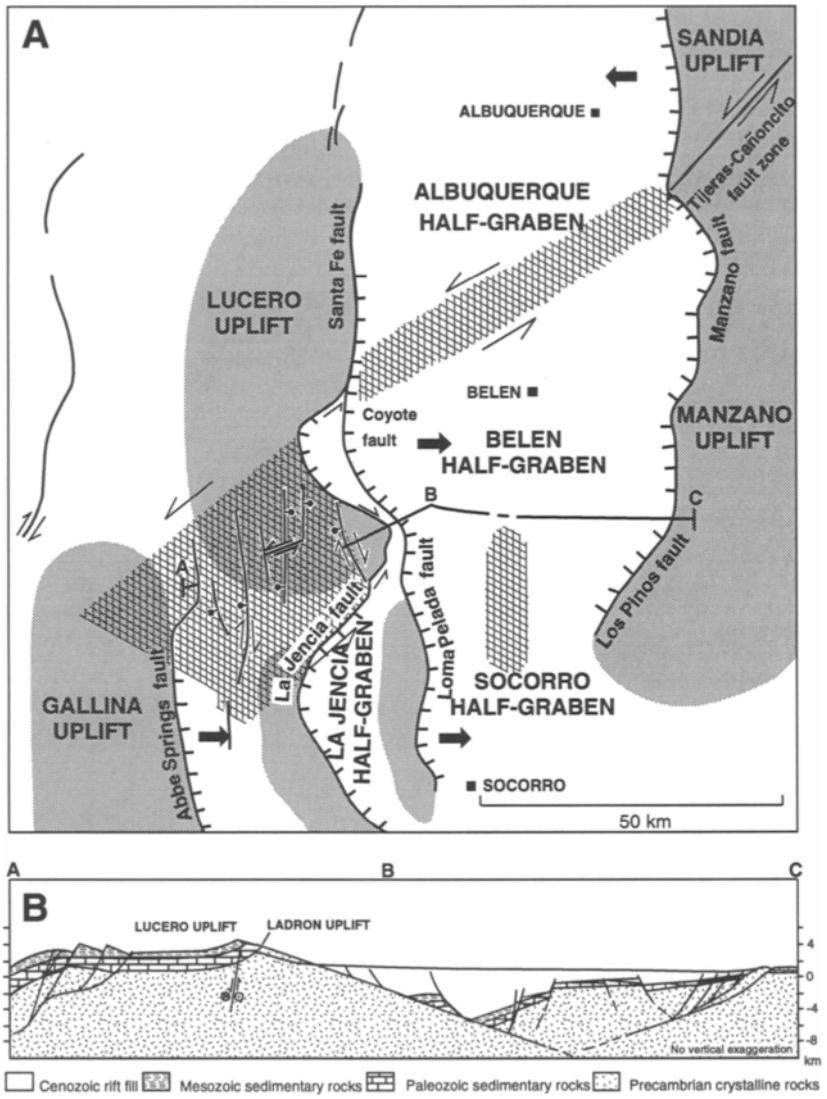

Fig. 6–2. A. Tectonic map of the Albuquerque-Belen basin, showing geometry of linked and nested half-grabens, tilted block uplifts, and accommodations zones. Hachured lines indicate bounding faults of half-grabens; hachures on downthrown side. Shaded areas indicate uplifts. Cross-hatched pattern indicates accommodation zones. Broad, double-barbed arrows indicate direction of dip of underlying detachment. Small, single-barbed arrows indicate sense of strike-slip offset on faults. Large, single-barbed arrows indicate sense of shear in accommodation zones. B. Cross section along profile C–C'–B' in A, above. Both diagrams modified from Lewis and Baldridge (1994).

a complete range of pre- and synrift basin fill sediments and volcanic rocks. It is one of the few locations within any Cenozoic continental rift where well exposed prerift and synrift basin fill has been studied thoroughly enough to allow detailed paleogeographic reconstruction of nearly the entire Cenozoic (Ingersoll et al., 1990). Dispersal patterns, petrofacies analysis, K–Ar ages, and chemical analyses of volcanic clasts allow characterization of three major petrofacies in the northern Española basin,

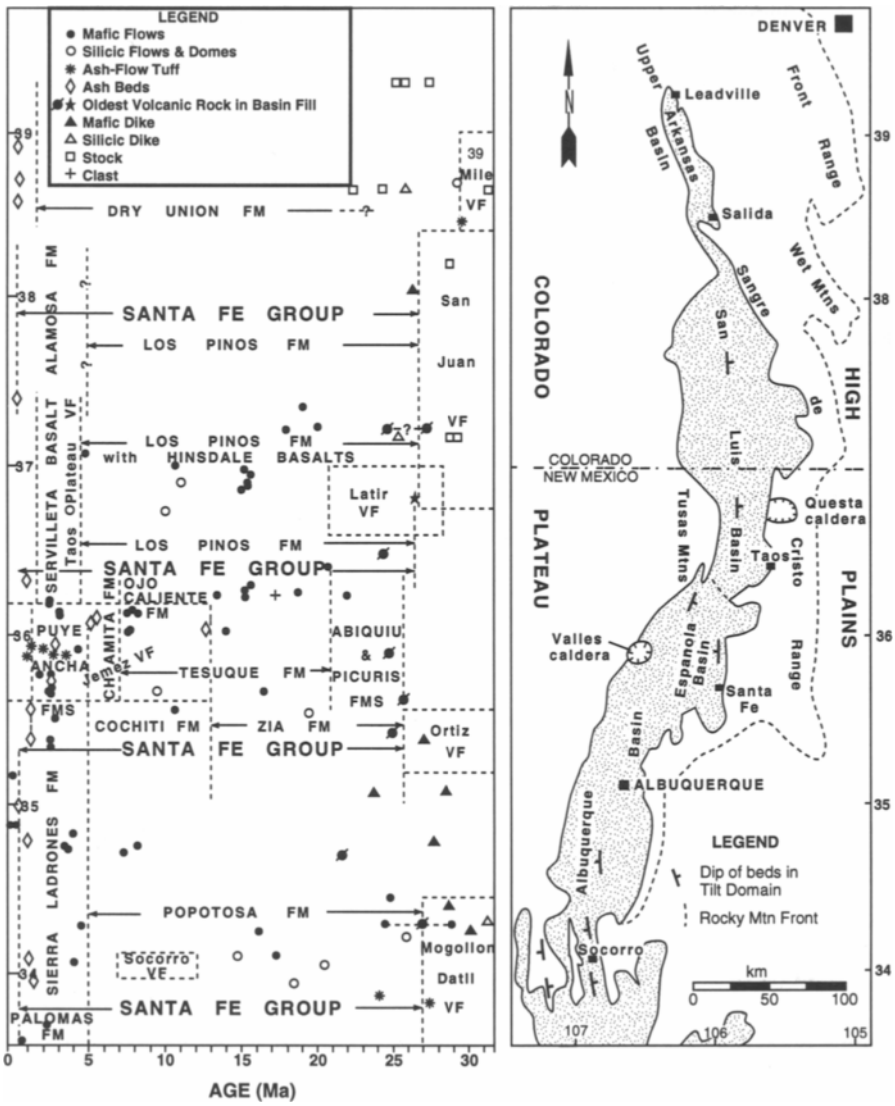

Fig. 6–3. Summary of stratigraphic nomenclature and age constraints for axial basins of the northern and central Rio Grande rift. Modified from Chapin (1988).

each associated with a separate and distinctive volcanic center and each encompassing an array of local formations (Plate 6–2), within the late Oligocene to Pliocene basin fill. The earliest rift deposits (Oligocene to early Miocene) consist of volcaniclastic aprons spread over pre-existing topography, with little evidence of syndepositional faulting. Their source areas included the San Juan and Latir volcanic fields formed during the magmatic event which immediately preceded rifting. Some of the early units now crop out on the flanks of the rift, outside the modern basins. Their position indicates that they were originally deposited in broad basins and were subsequently uplifted relative to the modern basins (Stearns, 1953a; Chapin and Seager, 1975). In middle and late Miocene time the broad, southward-slop-

ing volcaniclastic aprons in the northern basin interfingered with, and were buried by, fanglomerates dominated by clasts of Precambrian rocks derived from flank uplift along (predominantly) the eastern side of the basin (e.g., Galusha and Blick, 1971; Cavazza, 1986; Ingersoll et al., 1990). In this basin, the term Santa Fe Group refers only to basin fill of Miocene age (Plate 6–2).

Adjacent to the southern Española and eastern Santo Domingo basins, a similar, north- to west-sloping alluvial fan developed in the late Oligocene from eruptive centers in the Ortiz Mountains and Cerrillos Hills, and underlies Miocene and later rift fill in much of the southern Española basin (Stearns, 1953a, c; Kautz et al., 1981; Biehler et al., 1991).

6.5.5. Magmatism

The volume of magmatic rocks associated with the Rio Grande rift is small compared with rifts such as the Kenya rift (Chapter 5), yet these rocks convey unique information about thermal, compositional, and tectonic processes involved in rifting.

6.5.5.1. Late Oligocene to Early Miocene

The largest volumes of magmatic rocks are associated primarily with the northern and southern parts of the rift, and preceded and/or accompanied initial extension. Examples include the San Juan volcanic field in southwestern Colorado (Lipman et al., 1978, 1989), the Latir volcanic field in north-central New Mexico (Lipman et al., 1986; Johnson and Lipman, 1988; Johnson et al., 1989, 1990), the Mogollon-Datil volcanic field in southwestern New Mexico (Elston et al., 1976; Elston, 1984; McIntosh et al., 1992; Davis and Hawkesworth, 1993), and the Trans-Pecos magmatic province of west Texas (e.g., Barker, 1979; Price et al., 1986). The San Juan and Mogollon-Datil areas include numerous overlapping calderas and doubtless overlie large composite plutons in the upper crust (Elston et al., 1976; Elston, 1984). Other, smaller igneous areas occur along the length of the rift from northern Colorado southward into Mexico (Steven, 1975; Baldridge et al., 1984).

Compositions of magmatic rocks associated with this earlier (middle Tertiary) phase of rifting are dominantly high-K calc-alkaline intermediate to silicic. In general, compositions evolved from calc-alkaline intermediate to more alkaline and silicic types with time (Lipman et al., 1989; Davis and Hawkesworth, 1993). Few basaltic lavas reached the surface during this phase of magmatism. Instead, large volumes of basaltic andesites are characteristic. In the southeastern Colorado Plateau and Rio Grande rift areas, basaltic andesites typically have $^{87}Sr/^{86}Sr = 0.705–0.708$, but occasionally range to >0.71 (Bikerman and Bell, 1986; Abitz, 1989; Davis et al., 1989; Baldridge et al., 1991; Davis and Hawkesworth, 1993). These basaltic andesites are part of the SCORBA ("southern cordilleran basaltic andesites") suite that extends from the southwestern United States into western Mexico (Cameron et al., 1989). In eastern Chihuahua, the SCORBA suite has $^{87}Sr/^{86}Sr = 0.704–0.705$ and $\varepsilon_{Nd} = +2$ to -2, which are similar to isotopic values for Pliocene-Holocene alkali basalts (Perry et al., 1987, 1988, and references therein) from the least-extended portions of the Rio Grande rift region. These isotopic values are interpreted to represent "enriched" lithospheric mantle that has not yet been displaced by upwelling asthenospheric mantle associated with major lithospheric extension (Perry et al., 1987, 1988). Higher values of $^{87}Sr/^{86}Sr$ almost certainly indicate that magmas have significantly interacted with crustal rocks (Lipman et al., 1989). Total volume of the prerift and early rift magmatism in the Rio Grande rift region is on the order of several hundred thousand cubic kilometers (Lipman et al., 1989).

The middle Tertiary magmatism in the region of the Rio Grande rift was part of or closely related to a very widespread magmatic event that preceded and accompanied extension throughout the western United States (of which early extension in the Rio Grande rift was a part). In the middle Tertiary (approximately 40–20 Ma), huge volumes of magmas, dominantly of intermediate to silicic composition, were emplaced throughout the region now occupied by the Basin and Range province and Rio Grande rift, and along the margins of the Colorado Plateau. This magmatism, a consequence of subduction of the Farallon plate, may have thermally weakened the lithosphere, allowing it to be broken by extension. If not part of the widespread mid-Tertiary magmatic event, early magmatism in the region of the rift was

at least closely related to it in that genesis of magmas may have been triggered by rifting of already heated lithosphere. Therefore, middle Tertiary magmatism cannot be simply related to the modern basins of the rift or to the present tectonic setting. Early magmatism is related to rifting (lithospheric extension) only insofar as the definition of rifting is expanded to include the events leading up to lithospheric extension.

6.5.5.2. Middle Miocene to Holocene

Regional distribution. Following a minimum in eruption rates 17-22 Ma, magmatism resumed in the Rio Grande rift and throughout the transition zone. Middle Miocene to Holocene volcanism, which was associated with extension of the rift-Basin and Range region, was widespread, though not voluminous, and was particularly concentrated around the margins of the Colorado Plateau (Luedke and Smith, 1978). Major volcanism occurred earliest in the Jemez volcanic field (c. 14 Ma), centered on the bounding faults of the rift (Gardner et al., 1986; Heiken et al., 1990), and in the White Mountains volcanic field (c. 9 Ma) in eastern Arizona (Nealey, 1989), both of which are central volcanoes comprised dominantly of intermediate lavas.

These volcanoes partially define a north-northeast trending array of volcanic centers referred to as the Jemez zone (or Jemez lineament) (Mayo, 1958; Laughlin et al., 1982). Individual volcanic fields are associated with local structures, generally oriented N-S to NNE-SSW, rather than east-northeast parallel to the trend of the Jemez zone. Vents are typically aligned along, or parallel to, faults. The trend of the Jemez zone as a whole has a well-defined structural expression only where it crosses the Rio Grande rift (Baldridge et al., 1983; Aldrich, 1986). Although the zone has been compared to the Snake River plains–Yellowstone trend and inferred to mark a hot spot track (Suppe et al., 1975), numerous K–Ar dates do not substantiate any systematic progression of ages along the zone (Laughlin et al., 1976; Lipman, 1980). The Jemez zone may correspond to a boundary between the essentially undeformed core of the Plateau to the northwest, which has resisted Cenozoic breakup, and a transition zone to the southeast (Baldridge et al., 1983; Aldrich et al., 1986) which has undergone extension during formation of the rift and Basin and Range province. About 5 Ma, eruption of lava, mainly basalts from small shield cones and from cinder or spatter cones aligned along fissures, became widespread throughout the rift area and continued into the Holocene.

Currently, much effort is being expended in developing new techniques, including surface exposure dating using buildup of cosmogenic ^{3}He and ^{36}Cl, U-series disequilibria, and $^{40}Ar/^{39}Ar$, and in renewed application of classical techniques such as ^{14}C on charcoal beneath flows to dating of very young flows (Anthony, 1993). Recent results indicate that volcanism in the southern rift is as young as 10–17 ka (Carrizozo flow and Potrillo volcanic field, respectively; Leavy, 1987; Anthony and Poths, 1992), and that youngest volcanism in the Zuni-Bandera volcanic field (McCartys flow) is ~3 ka (Laughlin et al., 1994). For reasons not well understood, most of the eruptive activity since 5 Ma has taken place along the Jemez lineament rather than along the axis of the rift.

General petrological features. Late Miocene to Holocene magmatism is characterized by the following general features. (1). A wide range of magma types is present, from basalts to high-silica rhyolites. The greatest volume of intermediate to silicic volcanic rocks is associated with the Jemez volcanic field (Heiken et al., 1990). (2). Basaltic compositions encompass a spectrum of both hypersthene (hy)- and nepheline (ne)-normative compositions, but, in contrast to many other continental rifts, subalkaline compositions are volumetrically dominant. Different compositions are typically erupted in close spatial and temporal proximity. (3). All basaltic compositions are at least slightly evolved, with $Mg/(Mg+Fe^{2+})<68$. (4). Compositional evolution is controlled dominantly by low pressure fractionation (<10 kbar); significant polybaric fractionation has not been documented. (5). Magmatic compositions reflect multiple parents which cannot be related to each other by fractionation of observed phenocrysts or by crustal contamination. (6). Compositions of the basalts, as well as of more evolved magmas, typically reflect variable degrees of crustal contamination. Although crystal fractionation appears to re-

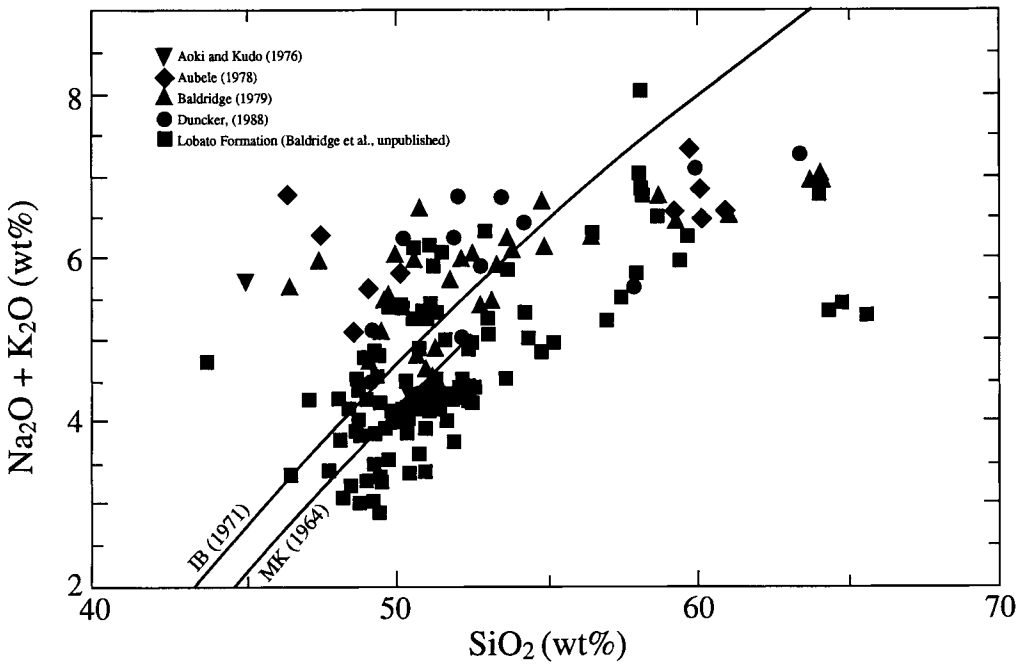

Fig. 6–4. (Na_2O+K_2O) vs. SiO_2 for basalts and related intermediate rocks from the Jemez volcanic field and related Cerros del Rio, El Alto, and Santa Ana Mesa volcanic fields. Lines labeled MK (1964) and SIB (1971) divide the fields of alkali-olivine basalts (above) from tholeiitic basalts (below), based on MacDonald and Katsura (1964) and Irvine and Baragar (1971), respectively. The classification of Irvine and Baragar (1971) yields a much better fit to the normative mineralogy.

main the dominant process in the evolution of intermediate and silicic magmas, effects of both magma mixing and crustal contamination are documented (Perry et al., 1990, 1993).

The greatest volumes of basaltic rocks within the Rio Grande rift, the Taos Plateau volcanic field (>200 km^3; Lipman and Mehnert, 1979; Dungan et al., 1986), and the Jemez volcanic field (>70 km^3), are subalkaline in composition. Basalts of the Taos field (Servilleta basalts) are distinctive in their relatively low alkali content (K_2O ~0.7 wt. %; Na_2O+K_2O generally 3–4 wt. %) and incompatible trace elements, implying large amounts of melting at shallow depths (uppermost mantle). They are also petrographically distinctive, typically characterized by diktytaxitic texture and cylindrical vesicle pipes. These "low-alkali" tholeiites seem to be unique to the Rio Grande rift and immediately adjacent regions. Basaltic rocks from the Taos field contain strong petrographic and geochemical evidence for assimilation of lower crustal rocks (Dungan et al., 1986). A range of other rock types from "silicic alkalic basalt" and andesite, to high-silica rhyolite is also present in the Taos field, whose origins reflect combined effects of low-pressure crystal fractionation, magma mixing, and crustal contamination processes (Lipman and Mehnert, 1978; Dungan et al., 1986; McMillan and Dungan, 1988).

Basalts from the Jemez volcanic field include a range of hy- and ne-normative compositions (Fig. 6–4). In contrast to the Servilleta basalts, hy-normative (subalkaline) basalts from the Jemez field are characterized by higher alkali contents ($Na_2O + K_2O$ >5%), intermediate between those of the low-alkali tholeiites and alkali olivine basalts. Although classified as tholeiites according to Yoder and Tilley (1962), their trace-element and isotopic compositions are most closely related to the ne-normative, alkali olivine basalts. These "high-alkali" or "transitional," hy-normative basalts, and the ne-norma-

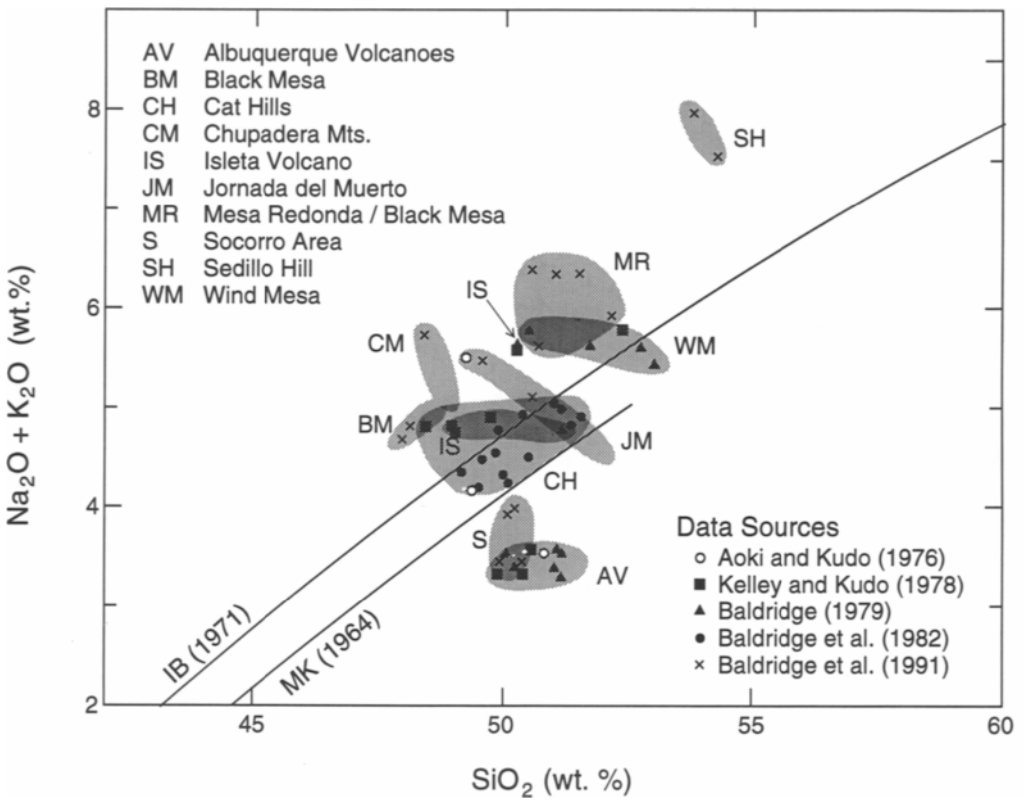

Fig. 6–5. (Na_20+K_20) vs. SiO_2 for selected basaltic rocks from the central Rio Grande rift. Lines labeled MK (1964) and IB (1971) are same as for Fig. 6–4.

tive basalts to which they are related, are similar in composition to late Cenozoic basaltic rocks widely distributed throughout the rift and western U.S. (Fig. 6–5). The presence of quartz xenocrysts in many of the basaltic units implies significant crustal contamination.

In the central and southern Rio Grande rift, volcanism is less sustained and less voluminous. A range of hy- and ne-normative compositions (Fig. 6–5) was erupted in numerous small volcanic fields, many of which comprise only a single compositional type (Baldridge et al., 1991; Anthony et al., 1992). Most of the hy-normative types are similar to the high-alkali, sub-alkaline group of the Jemez volcanic field. Exceptions are the small volumes of Servilleta-type, low-alkali tholeiitic basalts of the Albuquerque Volcanoes (Kelley and Kudo, 1978; Baldridge, 1979a), and some flows erupted in the Zuni-Bandera and Lucero areas (Renault, 1970; Baldridge et al., 1987). Examples of high-alkali, hy-normative basalts from the central and southern rift are the Jornado del Muerto field and the Carrizozo flows (Renault, 1970; Baldridge et al., 1991; Anthony et al., 1992). Major examples of ne-normative volcanic rocks include the Elephant Butte and Potrillo volcanic fields (Renault, 1970; Hoffer, 1976; Anthony et al., 1992). No pattern to the geographic distribution of the compositional groups is evident, with both major magma types occurring in the axis of the rift (Anthony et al., 1992).

Timing. In recent years, progress has been made in resolving episodes of magmatism within the general middle Miocene to Holocene time frame. On the transition zone of the Colorado Plateau and in the central rift, volcanism occurred in two phases separated by a minimum 6–4 Ma (Baldridge et al., 1987; Aldrich et al., 1986). This timing is also compatible with major basaltic volcanism in the Jemez volcanic field, which occurred <13–9 and 3–2 Ma (Goff et al., 1989). However, large volumes of dacites and andesites were erupted during the interval 6–4 Ma, possibly reflecting the transfer of heat and mass into the crust by continued basaltic magmatism. Thus, the absence in the Jemez field of basalts erupted 6–4 Ma may not indicate that basaltic magmas were not generated, only that they were unable to reach the surface. Similar timing relations do not appear to hold in the northern rift (Taos Plateau volcanic field) or on the Great Plains (Ocaté and Raton–Clayton areas), where numerous basaltic flows were erupted during this interval.

Basalts erupted in the Lucero volcanic area of the transition zone underwent a slight but systematic compositional shift with time (Baldridge et al., 1987). Miocene volcanism consisted exclusively of alkali olivine basalts. In contrast, the first phase of Pliocene volcanism (4–3 m.y. ago) included significant volumes of tholeiitic basalts. The most recent volcanism (1.1–0 m.y. ago) consisted of both tholeiitic rocks (much lower in alkalis than the previous phase), erupted from a single shield volcano, and a suite of high-alkali, ne-normative basalts (Baldridge et al., 1987, 1991). No comparably long record exists for other basaltic areas of the rift or transition zone to determine whether such a systematic shift toward more tholeiitic compositions exist in other areas, but certainly many of the youngest (less than 1.5 m.y. old) basaltic rocks throughout the area are tholeiitic (Perry et al., 1987). In the Springerville volcanic field, basaltic lavas erupted 2.1–0.3 Ma progressed from tholeiitic toward more alkalic compositions with decreasing age. Alkali olivine basaltic volcanism migrated eastward with time (Condit et al., 1989).

Petrogenetic model. The dominant controls on the compositions of parental basaltic magmas associated with rifting are probably the depth and amount of partial melting; the mineralogy of the source (partially a function of depth); and fractional crystallization and wall-rock contamination en route to the surface. The degree of enrichment of the source area(s), measured particularly by trace elements and the isotopic ratios of long-lived radionuclides, is an important but secondary feature in controlling magma compositions. Volatile phases (mainly H_20 and CO_2) can critically affect magma compositions, but parental magmas of the rift do not in general appear to be especially volatile-rich.

Lipman and Mehnert (1975) proposed a model invoking diapirism of asthenospheric mantle to explain the compositions of basalts associated with the rift in northern New Mexico (Taos Plateau volcanic field). Beneath the axis of the rift, where upwelled asthenosphere was shallowest, tholeiitic melts were generated; in contrast, beneath the flanks of the rift where depth to upwelled asthenosphere was greater, alkalic magmas were produced. Although the mantle source of basalts of the Taos volcanic field are now thought to lie within ancient continental lithosphere (see below), this model is largely correct in inferring depth of magmagenesis.

The wide range of magma types in close spatial and temporal proximity and the generally small volumes of magmas that are characteristic of many volcanic fields imply that melts form as independent, isolated batches, even within relatively small volumes of the upper mantle. This model suggests that melting occurs locally in regions of the mantle where temperature exceeds a "critical isotherm." Melting may be nucleated in regions of local enrichments of volatile or other low-melting-point phases in a compositionally heterogeneous mantle. The exact depth at which melting occurs, and the amount of partial melting, are the dominant controls on magma composition. Once formed, crystallization in all basalts occurs dominantly at pressures <10 kbar (i.e., within the crust), where the liquidus phases for all compositions are the same or similar. Hence, basalts are not substantially diversified from each other by crystal fractionation processes.

Mantle source regions. The general enrichment in HREEs and LILEs that is characteristic of all basaltic magmas (alkalic and tholeiitic) of the rift suggests derivation of all of the magmas from enriched

mantle sources. The enriched sources may comprise (1) ancient, enriched subcontinental lithosphere, which in the region of the Rio Grande rift ranges from about 1.8 to 1.1 Ga in age, or (2) an enriched asthenospheric source such as ocean island basalt (OIB)-type asthenosphere. An OIB-type mantle source may reflect the existence of deep mantle upwelling such as such as a plume or hot spot. A major challenge to petrogenetic modeling of the rift basalts, then, lies in distinguishing between these two enriched mantle sources. In either case, a progression in trace-element and/or isotopic composition of basalts with time might be expected as lithospheric extension proceeds.

A model for mantle source regions was proposed by R. N. Thompson and colleagues (Leat et al., 1988, 1989, 1990; Gibson et al., 1991), who postulated, mainly from La, Yb, Ta, and K, that Oligocene to Quaternary basalts from the northern rift (Colorado) were derived from both lithospheric and asthenospheric sources. They interpreted that olivine basalts with OIB-like trace-element compositions were derived from an OIB-source asthenosphere, and that minettes were derived from continental lithosphere. A third group of lavas with high La/Ta and generally low LIL/HFS was derived from subduction-modified lithosphere. Their interpretation of an asthenospheric source was based, in part, on the explicit assumption that the similarity to oceanic island basalts in trace-element compositions (especially Ta/Yb and La_N/Yb_N) implied a similar (asthenospheric) source. They recognized that crustal contamination played a secondary role in modifying magma compositions.

Trace elements may not discriminate well between subcrustal lithosphere and OIB-type asthenosphere, however, since both sources are enriched relative to MORB mantle sources. Also, trace element compositions of basalts are very sensitive to multiple processes, including inhomogeneities in the mantle source(s), small differences in the amounts of partial melting, fractional crystallization, and crustal contamination. Isotopic data from several areas in the northern rift (Perry et al., 1987; McMillan and Dungan, 1988) indicate that substantial contamination of basalts (especially tholeiitic basalts) by both lower and upper crust occurs, the effect of which on trace elements must be significant but has not been well quantified. Finally, none of the basalts from the northern rift have the very depleted isotopic signatures that characterize alkalic basalts in the southern rift and Basin and Range province, and *none* fall in the field of OIBs.

A petrogenetic model for late Miocene to Holocene basaltic rocks, developed by Perry et al. (1987, 1988), was based mainly on the correlation of Sr and Nd isotopic compositions of alkalic basalts with tectonic setting and upper mantle geophysical properties. Alkalic, rather than tholeiitic, basalts are most appropriate for interpretation of mantle sources because (1) they commonly contain mantle-derived xenoliths (next section), (2) and typically display little or no evidence for crustal contamination. In regions which have undergone at least moderate lithospheric extension, such as the southern Rio Grande rift and Basin and Range province, isotopic compositions are characterized by "depleted" values ($^{87}Sr/^{86}Sr = 0.7030–0.7033$; $\varepsilon_{Nd} = +7$ to $+8$), similar to some ocean island basalts (see Chap. 3A for discussion of "enriched" and "depleted"). In contrast, isotopic compositions from unextended areas, such as the Great Plains, are relatively enriched (although still slightly depleted relative to chondritic values), with $^{87}Sr/^{86}Sr$ typically 0.7040–0.7045 and $\varepsilon_{Nd} = 0$ to $+2$. Uncontaminated alkalic basalts from the northern rift also have enriched isotopic values. In the transition zone along the southeastern Colorado Plateau, isotopic compositions are intermediate between these extreme values. This correlation was interpreted to indicate that the upper mantle beneath the rift region is composed of two distinct geochemical reservoirs that, prior to lithospheric extension, corresponded to ancient lithospheric mantle and to asthenosphere, part of the convecting upper mantle. Intermediate values, such as along the transition zone, reflect mixing between these two end members in the source regions of the basaltic melts. This model agrees with subsequent isotopic work in the Basin and Range province (Fitton et al., 1991).

Thus, it appears, from isotopic data, that all of the Quaternary basalts of the northern rift (including and northward from the Jemez volcanic field) were derived from a continental lithospheric source. In the northern rift (e.g., Cerros del Rio and Jemez

fields), where the amount of lithospheric extension is least, geochemically defined and geophysically defined lithospheric mantle do not correspond. Here, ε_{Nd} values (+0.2 to +2.2) of alkali basalts indicate that these basalts were derived from enriched mantle and that relatively little replacement of enriched mantle by depleted mantle has occurred. Yet low P_n velocities (approximately 7.7 km/s) and low mantle densities (3.22 g/cm^3), modeled from gravity data, indicate that asthenosphere here extends upward to near the base of the crust (approximately 35 km). It is likely that beneath the northern rift, enriched lithospheric mantle has been "thermally thinned" and converted to asthenosphere, retaining its geochemical properties, rather than being displaced by isotopically depleted asthenosphere. Thus, a zone of partially melted former lithosphere may form a carapace above upwelling, true depleted asthenosphere (Perry et al., 1988).

The geochemistry of basaltic rocks also provides constraints on the evolution of mantle processes associated with rifting. Isotopic compositions of alkalic basalts from the transition zone underwent a shift with time during the late Miocene to Pliocene. ε_{Nd} values of basalts erupted 7–8 Ma are slightly more enriched (+3.2 to +4.2) than those of basalts erupted 4.3–0.8 Ma (+5.5 to +6.6), suggesting that the isotopic composition of the source area changed during the minimum in eruptive activity 6–4 Ma. This isotopic shift is interpreted as a displacement of lithosphere by asthenosphere and a shallowing of the lithosphere/asthenosphere boundary with late Miocene-Pliocene uplift and reactivation of rifting (Perry et al., 1988). In the central and southern rift, where extension is greater, preliminary studies (McMillan and Dickin, 1991) indicate that lithospheric thinning occurred earlier (c. 10 Ma).

6.5.6. Xenolith Studies

Suites of crustal and mantle xenoliths hosted in volcanic rocks are abundant in the Rio Grande rift and Colorado Plateau transition zone. As actual samples of the deeper lithosphere, these xenoliths provide important constraints on the major and trace element composition, thermal state, and age of the crust and mantle beneath the rift. If equilibration pressures and temperatures can be estimated for the xenoliths, information about the change of chemical composition, density and temperature with depth in the lithosphere can be used to better parameterize and interpret geophysical imaging data. In addition, the characterization of xenoliths from host magmas of different ages may document temporal changes in the lower crust and upper mantle during the evolution of rifting.

6.5.6.1. Mantle xenoliths

Although many mantle xenolith localities exist throughout the Rio Grande rift region, the classical locality of Kilbourne Hole maar, located in the southern rift near the Mexican border, is the most diverse and well-studied.

Mantle xenoliths from Kilbourne Hole include Group I and II lherzolites, as well as composite spinel lherzolite-spinel pyroxenite xenoliths. Less common types are clinopyroxenite, kaersutite-bearing pyroxenites, and wehrlite (Carter, 1970; Irving, 1980). Group I spinel lherzolites, believed to be parental to basalt magmas, are most abundant, recording temperatures of 900–1050°C and deriving from 40–80 km depth (Bussod, 1981). These xenoliths have heterogeneous trace element and isotopic compositions, yet most show chemical and Nd-Sr isotopic affinities with MORB-type, depleted mantle (Roden et al., 1988). This was initially interpreted as a sampling of preserved ancient oceanic lithosphere (Reid and Woods, 1978), yet the isotopic data are more compatible with asthenosphere (depleted mantle) which upwelled during lithospheric extension (Perry et al., 1987).

The spinel lherzolites are fertile with respect to the major element constituents of basalt, but have depleted incompatible trace element abundances. This suggests that the mantle below the rift has undergone at least one depletion event (partial melt/fluid extraction). In some samples, isotopic heterogeneity and $^{143}Nd/^{144}Nd$ which are unsupported by present-day $^{147}Sm/^{144}Nd$ indicates that there has also been a relatively recent enrichment in incompatible elements. Although age relationships in mantle xenoliths are often difficult to interpret, this enrichment probably occurred less than 750 Ma ago (Roden

et al., 1988). The enrichment may be due to mixing, melting, and metasomatism associated with upwelling mantle beneath the rift (Roden et al., 1988).

The Group II pyroxenite xenoliths and pyroxenite portions of the composite xenoliths have been modeled as dikes and crystal cumulates associated with the host magma (Irving, 1980). Incompatible element enrichment and isotopic equilibration occurs in the Kilbourne Hole lherzolite wallrock adjacent to pyroxenite dikes, yet is confined to centimeter scale areas (Roden et. al, 1988).

Other xenolith localities include Abiquiu, Cieneguilla, and Elephant Butte (Plate 6–3) in the northern and central Rio Grande rift, and Mt. Taylor, Black Range, Cerro Negro, the Lucero volcanic area, and Bandera Crater in the Colorado Plateau transition zone. Inclusion types found in these localities are spinel lherzolites, harzburgite, pyroxenites, and a diverse megacryst assemblage (Laughlin et al., 1971; Fodor, 1978; Baldridge, 1979b; Warren et al., 1979). Spinel lherzolites from the Rio Grande rift north of Kilbourne Hole also unequivocally represent mantle conditions, yielding equilibration temperatures of 935–1030°C at pressures of 14–20 kbar. When corresponding pressure and temperature estimates of crustal granulites from the same locality are made, a best-fit geothermal gradient of 20–30°C/km is defined for this portion of the Rio Grande rift (Baldridge, 1979b; Warren et al., 1979).

6.5.6.2. Crustal Xenoliths

Crustal xenoliths from the Rio Grande rift can be used to constrain the composition and age of the lower crust, as well as to evaluate the possibility of rift-related processes such as large-scale magmatic underplating. Crustal lithologies represented in xenoliths from the Rio Grande rift differ markedly from those of the adjacent, thicker and stable crust of the Colorado Plateau (Wendlandt et al., 1993). Whereas xenoliths from the unrifted Colorado Plateau lithosphere include eclogites, granulites, and high-grade hydrous assemblages, the Rio Grande rift crustal suites are dominated by anhydrous, granulite-facies rocks.

The Kilbourne Hole crustal xenolith suite is once again the most well-studied. Sampling of other xenolith localities within the Rio Grande rift and Colorado Plateau transition zone, however, indicate that the Kilbourne Hole xenolith compositions may not be representative of the entire region. For instance, granulite-facies xenoliths at Kilbourne Hole include siliceous paragneisses interpreted as tectonically-underplated sediments from a Proterozoic subduction zone (Reid et al., 1989). However, other lower crustal xenolith suites from the Rio Grande rift and transition zone do not include this metasedimentary component and are dominated by mafic, metaigneous granulites.

The metapelitic granulites from Kilbourne Hole maar have been the subject of numerous studies. These garnet-bearing xenoliths are compositionally heterogeneous (banded), and believed to be representative of in-situ lower crustal conditions (Padovani and Carter, 1977a; E. R. Padovani and M. R. Reid, in Pallister, 1989). Their major and trace element compositions are similar to those of an average shale, indicating a sedimentary protolith and a lack of extensive chemical modification during residence in the lower crust. Although evidence of localized decompression melting exists, these lower crustal xenoliths seem not to have suffered significant partial melt extraction (Padovani and Carter, 1977b; Wandless and Padovani, 1985). The relatively pristine nature of these rocks is further indicated by metasedimentary $^{18}O/^{16}O$ values, arguing against extensive exchange with mantle fluids (James et al., 1980).

Isotopic age relationships in the metapelites have been determined using the compositional banding of the samples. Rb-Sr and Pb isotope systematics of separated layers from these xenoliths indicate a 1.6 Ga metamorphic or stabilization age for the lower crust in this region. This Proterozoic basement age agrees well with metamorphic ages of exposed basement rocks in south-central New Mexico (Condie and Budding, 1979), and is somewhat younger than crust-formation ages for lower crustal xenoliths from the unrifted Colorado Plateau (Wendlandt et al., 1993). Metapelitic granulites are in isotopic equilibrium on a mineral scale, however, and approximately zero age Rb-Sr internal isochrons suggest

recent reheating. Temperatures above the blocking temperatures of the constituent minerals are likely to have been attained concomitant with crustal thinning associated with Rio Grande rift development (E. R. Padovani and M. R. Reid, in Pallister, 1989).

The existence of a significant metapelitic lower crustal component in the Kilbourne Hole suite underscores the potential role of non-magmatic processes in crustal growth and evolution. A significant volume of metapelitic compositions in the lower crust could have important implications for heat production, heat flow, seismic velocity and chemical composition of the crust. Despite evidence for loss of U during metamorphism, the Kilbourne Hole xenoliths have retained high K and Th concentrations and thus are capable of higher heat production than is normally assumed for lower crust. The necessary mantle heat flux contribution could thus be significantly reduced if these heat-producing metapelites form a significant component of the lower crust (E. R. Padovani and M. R. Reid, in Pallister, 1989). The seismic velocities of the metapelitic xenoliths are anisotropic due to their foliation, yet are on the whole less than the seismic velocity determined for lower crustal levels of the southern Rio Grande rift. Mafic lithologies with higher seismic velocities may be required to make up the velocity difference in the lower crust in this region (Reid et al., 1989).

Other lower crustal xenolith localities in the Rio Grande rift (even those relatively near Kilbourne Hole) are dominated by mafic lithologies (Plate 6–4), with some retaining igneous textures (Baldridge, 1979b; Warren et al., 1979). This lack of metasedimentary xenoliths may suggest that the crust beneath Kilbourne Hole is not representative of that beneath the entire Rio Grande rift.

Magmatic underplating, or the rejuvenation of lower crust by mantle-derived magmas, has been recognized as a potentially significant process beneath continental rifts. Thermometric data from Kilbourne Hole crustal and mantle xenoliths have recently been used to develop a thermal evolution model of the southern Rio Grande rift. Bussod and Williams (1991) modeled the thermal consequences of massive intrusion of basaltic dikes and sills into a pre-rift, thermally stable lower crust and upper mantle. They envisioned large-scale mafic intrusion 20–30 Ma ago into a region from 25–45 km in depth, accompanied by large-scale partial melting, metasomatism, and recrystallization. This model is consistent with observed bimodal volcanism in the Rio Grande rift region, and with the relatively recent isotopic equilibration of minerals in granulite facies lower crustal xenoliths. After intrusion ceased, conductive cooling from this thermal event could account for the present surface heat flow of 82 mW/m^2 (Bussod and Williams, 1991). In some cases, metaigneous lower crustal xenoliths may actually represent younger underplated mafic magmas that have assimilated variable amounts of the preexisting lower crust. This magmatism may or may not be expressed at the surface. Determining the emplacement or crystallization ages of the magmas is critical, but difficult, because the mafic lithologies normally do not contain minerals suitable for dating by the U-Pb isotope method. Nd and Sr isotopic compositions have recently been used, however, to place constraints on the crustal residence time of two-pyroxene granulites from the Elephant Butte area in the central Rio Grande rift. These rocks, which are inferred to have been derived from the lower crust, have crustal residence times (i.e., Nd model ages) that are significantly younger than accepted crustal ages determined for the central rift region (approximately 1.7 Ga). The Sr and Nd isotopic compositions and the T_{DM} ages of 0.84–0.93 Ga are interpreted to be the result of mixing between older, Proterozoic-age lower crust and Cenozoic underplated mafic magmas. An assimilation-fractional crystallization (AFC) model constrained by the isotopic data indicates that the rift granulites could be produced by contamination of an underplating alkalic basaltic melt with 30–35% felsic components of the lower crust (Wendlandt, 1992).

6.6. Geophysical surveys and results

6.6.1. Seismic Refraction

Seismic refraction studies (Fig. 6–6) provide a general picture of crustal thickness in the region of the Rio Grande rift. Most existing refraction profiles have station spacings greater than 5 km, thus limiting lateral resolution of deep crustal structures,

Fig. 6–6. Index of existing seismic refraction profiles for the Rio Grande rift. Modified from Sinno et al. (1986).

and only one is truly reversed. However, many of the profiles cross each other, providing an internally consistent picture of crustal structure. For example, Schneider and Keller (1994) interpreted the profiles in west-central New Mexico (a and b, Fig. 6–6) in an integrated analysis with gravity data. Adams and Keller (1994) extended these results across the rift by using gravity modeling to tie the seismic results of Stewart and Pakiser (1962), Olsen et al. (1979), Sinno et al. (1986), and Roberts et al. (1991) to the seismic profiles interpreted by Schneider and Keller (1994). The resulting picture, discussed further in section 6.7.1, shows that the region of crustal thinning associated with the central portion of the rift is wider than the physiographic expression and that the transitions in crustal structure at the rift margins are relatively gradual. In the southern portion of the rift, the partially reversed and interlocking refraction profiles of Sinno et al. (1986) correlate very well with the regional gravity anomalies in the area (Ramberg et al., 1978; Daggett et al., 1986), and delineate a broad zone of crustal thinning which distinguishes the rift from the adjacent Basin and Range. To the north, in the region of Albuquerque, Santa Fe, and the Jemez Mountains (35°–36° N), seismic control is limited to a very low resolution refraction

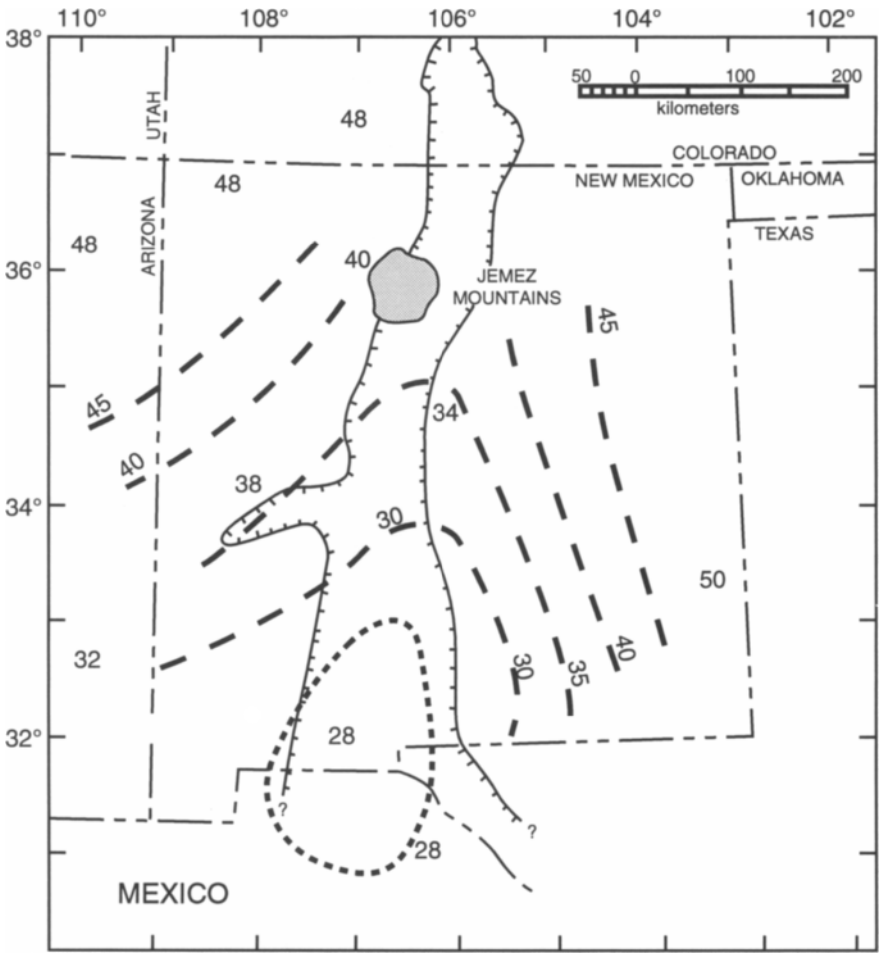

Fig. 6–7. Contour map of crustal thickness in the area of the southern Rio Grande rift. Contours are depth to Moho, in kilometers; datum is sea level. Modified from Keller et al. (1990).

profile which recorded the GASBUGGY nuclear explosion (Toppozada and Sanford, 1976), to an unreversed refraction profile in the rift (Olsen et al, 1979), and to a receiver function study at Albuquerque (Murphy, 1991). These results indicate a distinct thinning of the crust beneath the rift, but the width of the zone of thinned crust cannot be determined from the seismic data alone. The segment of the rift north of the Jemez Mountains is essentially unstudied by crustal-scale refraction profiles. Combining the refraction profiles with independent constraints from gravity studies, surface wave analyses, and teleseismic studies, allows interpretation of crustal thickness (Fig. 6–7). In most of the New Mexico portion of the rift, this map is probably a good representation of the general crustal structure because it is consistent with a broad range of data. The paucity of reversed refraction profiles is a bigger problem in defining the true velocity of the upper mantle than in defining general crustal thickness values. The refraction results indicate that the velocity of the uppermost mantle (P_n) is approximately

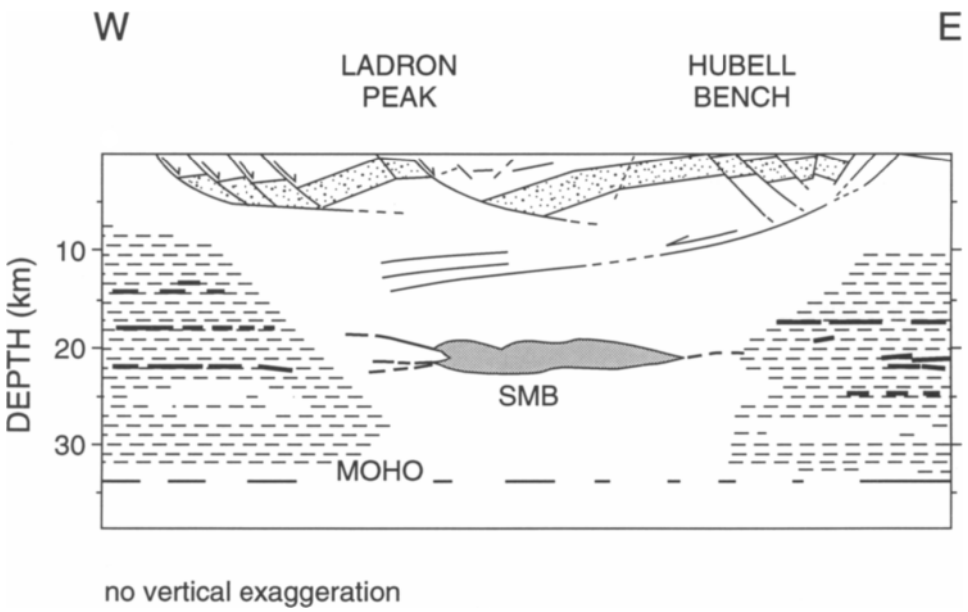

Fig. 6–8. Cross section across the southern Albuquerque basin, from COCORP seismic reflection profiling. Stippled pattern represents pre-rift sedimentary rocks; SMB indicates Socorro magma body. Modified from DeVoogd et al. (1988).

7.7 km/s; this value is fairly well constrained in southern New Mexico by the reversed and interlocking profiles of Sinno et al. (1986).

Studies of regional earthquake phases in northern New Mexico (Murdock and Jaksha, 1981) indicate that the average mantle lithosphere velocity is about 8.0 km/s. However, this result does not rule out a narrow low velocity region under the rift. Our lack of knowledge of the crustal structure of the northern portion of the Rio Grande rift is a major barrier to fully understanding the formation of the rift.

6.6.2. Seismic Reflection

Deep seismic reflection profiling in the Rio Grande rift was conducted by COCORP in the southern part of the Albuquerque-Belen basin (Brown et al., 1979, 1980), and subsequently reinterpreted by Cape et al. (1983), Wu (1986), and deVoogd et al. (1986, 1988). DeVoogd et al. (1986, 1988) interpreted the Moho, marked by a discontinuous reflection at 11–12 s (two-way travel time), at a depth of 33–34 km, which corresponds to the M–discontinuity as mapped by Olsen et al. (1979) from refraction data. A strong reflector at about 7 s correlates with the mid-crustal magma chamber detected through earthquake studies (Sanford et al., 1973, 1977, 1979; Rinehart et al., 1979). DeVoogt at al. (1988) also inferred west-dipping detachment faulting at a depth of 5–14 km beneath the basin (Fig. 6–8).

A large amount of seismic reflection data obtained by the petroleum industry has been released for basin studies in the rift (Keller and Cather, 1994). Davis and Stoughton (1979), Kluth and Schaffenaar (1994), and Brister and Gries (1994) used reflection data provided by Amoco to determine the deep structure of the San Luis basin in southern Colorado (Fig. 6–1). This feature is a major, complex rift basin which contains significant volumes of pre-rift Tertiary rocks. Keller et al. (1986) used a long reflection profile provided by Exxon to demonstrate the sub–surface extent of Laramide uplifts and basins in the southern New Mexico portion of the rift. Figuers

(1987) included a seismic reflection line in his detailed structural analysis of the northern Franklin Mountains, near El Paso. The structure of the Huerco bolson southeast of El Paso was delineated by Collins and Raney (1994). Black (1984) presented industry reflection data in the Española basin area and interpreted complicated compressional structure beneath the basin. A limited amount of reflection data for an area north of Santa Fe was obtained by the SAGE geophysics program (Biehler et al., 1991), who reinterpreted the data of Black (1984) in terms of extensional structures and erosional unconformities. Barrow and Keller (1994) documented that the Estancia basin east of Socorro (Fig. 6–1) was only slightly influenced by rifting.

High-quality, oil–industry, seismic reflection data (Russell and Snelson, 1990, 1994) for the Albuquerque-Belen basin demonstrate that the basin consists of two separate asymmetrical sub-basins of opposite structural polarity that were downdropped along low–angle to listric normal faults. The northern (Albuquerque) sub-basin was downdropped along a major west-dipping system of listric normal faults, and the southern (Belen) sub-basin along a system of major east-dipping low-angle faults. The sub-basins are separated by a complex, oblique-trending structural zone that accommodates the differential extension and polarity change between the basins (Fig. 6–2).

6.6.3. Surface Wave Dispersion

The analysis of surface wave dispersion is a useful but low-resolution means of determining average earth structure along a particular propagation path. Surface waves are most sensitive to variations in shear wave velocity and are thus a valuable source of information on this difficult-to-measure parameter. Rayleigh waves are the most often studied surface wave. The world standard (WWSSN) seismograph stations at El Paso, Texas (EPT), and Albuquerque, New Mexico (ALQ), are ideally situated for an analysis of Rayleigh wave dispersion along the Rio Grande rift. Data for this path, as well as some complementary data, were analyzed by Keller et al. (1979a) and Sinno and Keller (1986). The results of these studies were in good agreement with crustal structure determination from refraction data, suggesting the presence of high values (0.29) of Poisson's ratio in the upper mantle. The phase velocities measured were very similar to those for the East African rift path Nairobi, Kenya, to Addis Ababa, Ethiopia (Knopoff and Schlue, 1972).

Schlue et al. (1986) measured Rayleigh wave phase velocities along a short path across the central portion of the rift. Their results indicated an average upper crustal shear velocity of 3.33 km/s and two low velocity layers.

6.6.4. Teleseismic Data

Travel time anomalies and waveform studies for phases (usually P-waves) from distant earthquakes provide a valuable source of information on velocity structure, particularly at sub-Moho depths. P-wave travel time anomalies across the central Rio Grande rift were studied by Davis et al. (1984), Parker et al. (1984), Spence and Gross (1990), Davis (1991), Davis et al. (1993), and Slack (1994). Slack (1994) presented the most complete analysis to date of teleseismic data for the central and northern Rio Grande rift, including the U.S. Geological Survey data of Spence and Gross (1990). P- and S-wave travel time delays of up to 1.5 s were recorded by stations within the central rift compared to stations on stable, undisturbed lithosphere of the Great Plains. These delays correspond to velocity reductions of up to 8% within the uppermost mantle. The absolute velocity reduction and the correlation with S-wave delays imply that temperatures in the mantle are very close to the solidus of peridotite, consistent with but not requiring the presence of partial melt. Tomographic models image a low-velocity body at depths of 35 to 255 km beneath the rift and adjacent areas. At depths of 35 to 90 km, the velocity (thermal) anomaly is greatest west of the rift, beneath the southeastern Colorado Plateau transition zone (Plate 6–5). Between 90 and 200 km, an anomaly is still present beneath the transition zone, but is not as pronounced. Below 200 km the overall anomaly is less distinct, with the greatest velocity reduction centered beneath the axis of the rift. The teleseismic data are tentatively interpreted to be consistent with a two-stage evolution for the rift (see above). In the

earlier phase (Oligocene to early Miocene), the rift opened in an east-west direction. The velocity reduction observed at depths >200 km is presumed to reflect an associated, axially symmetrical thermal anomaly, which subsequently has largely decayed away. The anomalous low-velocity body presently underlying the transition zone between the core of the Colorado Plateau and the rift may reflect processes resulting from the modern (late Miocene to present) regional stress field (extension axis oriented northwest-southeast).

In a separate study, teleseismic P-wave relative arrival-time data for the Jemez volcanic field (see above) were inverted to image velocity anomalies beneath the Valles caldera (Lutter et al., 1995). Results confirm the existence, inferred in previous studies, of a mid-crustal low-velocity region beneath the caldera in the depth range 8–13 km (below sea level). This feature, of about 6 km lateral extent, is inferred to be the expression of a remnant magma chamber remaining from Pleistocene caldera-forming ignimbrite eruptions. A less well-constrained lower crust/upper mantle low-velocity anomaly is also imaged, and tentatively thought to reflect thermal effects of basaltic magmas ponded at the crust-mantle interface.

6.6.5. Gravity Data

Through the efforts of the U.S. Geological Survey, the University of Texas at Dallas, and the University of Texas at El Paso, a good data base of gravity readings is available for the entire Rio Grande rift area, including Mexico (Aiken et al., 1988). An overall Bouguer anomaly map of the rift has been published (Cordell et al., 1982), and more detailed (1:500,000) Bouguer and residual Bouguer anomaly maps of the State of New Mexico are also available (Keller and Cordell, 1984; Aiken et al., 1978). A detailed gravity map for part of the Española basin is presented by Biehler et al. (1991), and many other local studies have employed gravity data effectively to study basin geometry.

The Bouguer gravity field in the area of the rift is complicated by the presence of large regional elevation variations which are not all directly related to the rifting process. These elevation changes, and large older crustal features such as early Tertiary batholiths, produce regional gravity anomalies which approach 200 mGals. The most obvious gravity anomalies associated with the rift are the gravity lows which correlate with the basins (Plate 6–6). These anomalies have proven invaluable in providing a generalized picture of the structure of the basins (e.g., Cordell, 1978; Ramberg et al., 1978; Keller et al., 1984; Adams and Keller, 1994).

These studies have generally shown that the subsurface structure of the basins is much more complex than their physiographic expression would suggest. Many sub-basins and buried horst blocks exist and many features are asymmetrical. In every basin, there are drill holes which increase the confidence in gravity interpretations. The gravity studies do not suggest any obvious regular variation in the structure of individual basins along the rift. For example, basins with at least 3 km of rift fill are found in southern Colorado (San Luis basin) and near El Paso, Texas (Hueco and Mesilla basins). However, gravity data agree with the physiographic expression in showing a north to south widening of the rift.

Cordell (1982) evaluated the major components of the rift's gravity field, observing the classic picture of three components first described in East Africa (Fairhead, 1976). A long wavelength gravity low is associated with a broad zone of low seismic velocities in the upper mantle (e.g., Davis et al., 1993) which is interpreted as evidence for lithospheric thinning. Crustal thinning and/or mafic additions to the crust produce an intermediate-wavelength gravity high, which is illustrated in the wavelength filtered map shown in Plate 6–7. In the southern portion of the rift, Daggett et al. (1986) documented the close correspondence of this anomaly to crustal thinning shown by seismic data. In northern New Mexico, this anomaly becomes very obscure, suggesting that the zone of crustal thinning is narrowing to the north as proposed by Cordell (1982). As discussed above, the last major component of the gravity field is the short-wavelength low associated with the basins.

6.6.6. Aeromagnetic Data

An extensive data base of aeromagnetic measurements for the Rio Grande rift area primarily provides information on older structures. Cordell (1984) compiled a digital data base for New Mexico and published a 1:500,000-scale map of the state. An aeromagnetic map for Colorado has been published (Zietz and Kirby, 1972a, b), but is not in digital form. Keller et al. (1985) compiled a data base for west Texas and conducted an integrated analysis with gravity data. Himes (1968) studied aeromagnetic data in the northern part of the State of Chihuahua, Mexico. De Angelo and Keller (1988) digitized these data and merged them with data from New Mexico, Arizona, and west Texas. Their work showed a strong northwest fabric to the magnetic anomalies in southern New Mexico, which is due to pre-rift structures and may be as old as Precambrian. As north-south-trending rift structures extend southward from central New Mexico, they appear to be deflected to a northwest trend (De Angelo and Keller, 1988). The magnetic anomalies show that this deflection may be a local response to a zone of weakness which is not related to the rift.

Cordell (1976) analyzed aeromagnetic anomalies in the central rift, noting a correlation between gridded patterns in the magnetic anomalies and in the patterns of faulting. This correlation indicates basement control of rift bounding faults. Anomalies in northern New Mexico were analyzed by Cordell and Keller (1984) and were found to mostly be due to pre-rift structures and volcanic rocks. A prominent northeast trending anomaly was offset along north-trending discontinuities which could be strike-slip faults.

6.6.7. Heat Flow

Heat flow data delineate a major geothermal anomaly associated with the Rio Grande rift and adjacent Basin and Range province (Reiter et al., 1975, 1979, 1986; Decker and Smithson, 1975; Seager and Morgan, 1979; Smith and Jones, 1979; Swanberg, 1979; Taylor, 1981; Reiter and Tovar, 1982; Clarkson and Reiter, 1984; Decker et al. 1984, 1988). Although regional trends are clear, a large scatter in the data makes the construction of contour maps somewhat subjective (e.g., compare Reiter et al., 1975; Swanberg, 1979; Sass et al., 1981).

Decker and Smithson (1975) suggested that the southern Rio Grande rift is characterized by a heat flow of approximately 100 mW/m^2. A crustal conductive geotherm calculated from this value is consistent with lower crustal xenolith data on pressures and temperatures (Padovani and Carter, 1977a; Seager and Morgan, 1979). This conductive geotherm cannot be extrapolated far below the Moho, however, before it exceeds the mantle solidus, indicating convective heat transfer in the upper mantle beneath the rift and perhaps also a component of advective heat transfer into the crust. To the north, the rift is associated with a clearly defined heat flow high. Conductive geotherms calculated from these data exceed the crustal solidus above the Moho, requiring advective heat transfer into the crust (Clarkson and Reiter, 1984; Decker et al., 1984, 1988; Morgan and Golombek, 1984; Cook et al., 1978). Scatter in the heat flow data in the rift is primarily a result of groundwater flow in the rift basins, with a possible contribution from upper crustal magmatic activity (Morgan et al., 1986).

Reduced heat flow data (i.e, corrected for upper crustal radioactivity) suggest that the southern Rio Grande rift is thermally distinct from the adjacent Basin and Range province, the latter being characterized by a more stable and predictable thermal regime (Morgan et al., 1986; Blackwell, 1978). Reduced heat flow data from the northern Rio Grande rift confirm the inference from the surface heat flow values that an advective component of heat into the crust beneath the rift must be present (Decker et al., 1984; 1988).

6.6.8. Electromagnetic Techniques

Earliest measurements of transient geomagnetic variations across the Rio Grande rift were recorded in 1960 by Schmucker (1964). These yielded a pronounced reversal of the vertical component of magnetic field between Las Cruces and Cornudas, New Mexico, indicating a relatively shallow concentration of electrical currents under the Rio Grande valley. The anomaly (first called the "Texas anomaly")

was modeled (Schmucker, 1970) using a perfect conductor smoothly rising from 200 km to a depth of 100 km between the two sites. Schmucker (1970) also considered a step-like structure, wherein the conductive horizon deepens from 180 km west of the Rio Grande to 360 km to the east, when fitting his data. The step-like geometry was favored by Swift (1967), who made the first magnetotelluric (MT) measurements in the area. However, he (as did Porath and Gough, 1971) placed a step from ≥100 ohm-m to ≤60 ohm-m material in the depth range from 35 km east to 140 km west of the rift. Gough (1974) demonstrated the nonuniqueness of the absolute depth determinations from the data. Also, Swift (1967) cautioned that his model was only diagrammatic, since he had only two control points, one on either side of the rift, together with Schmucker's (1970) earlier measurements. Weidelt (1975) used Schmucker's geomagnetic transfer functions to calculate a resistivity model by a new inversion method, using cells which were 90 km in horizontal and 40 km in vertical extent. The final model showed a 40 km deep low-resistivity zone between Las Cruces and Orogrande, with a resistivity of 10 to 15 ohm-m. The conductance (conductivity-thickness product) of this block was calculated to be 3000–4000 S.

The geomagnetic-variation array studies of Porath and Gough (1971), which covered the whole of New Mexico with a relatively large station spacing, found no clear continuation of the rift anomaly to the north except near Albuquerque. Towle (1980), with a more detailed geomagnetic variation study, demonstrated a conductor in the central rift area between Albuquerque and Socorro, New Mexico. A model which yielded a satisfactory fit to his data indicated a shallow conductor beneath the rift at 15 km depth, and a deeper conductor at 35 km extending 100 km toward the east and west. Such a conductor is at least indicated in the data of Porath and Gough (1971) by the reversal of the geomagnetic induction arrows near Albuquerque.

The first comprehensive MT soundings were made in the Rio Grande rift in the 1970's, initially for geothermal exploration in the Jemez Mountains (Wilt et al., 1976; Hermance, 1979a). Despite generally poor data quality, these studies showed that anomalously low resistivity was present in the middle to lower crust. The conductive anomalies were initially interpreted as evidence for magma in the crust (Pedersen and Hermance, 1976; 1978; Pedersen, 1980). Since seismic data compellingly supported the presence of a magma body in the crust near Socorro (Sanford et al., 1977), Hermance and Pedersen (1980) postulated that such a body (or one "generically related") extended the full length of the rift. Hermance and Pedersen's (1980) conclusions were based on MT soundings at El Paso, Texas, and Santa Fe, New Mexico. The conductive layer was modeled at a depth of 21–28 km (perhaps approximately 20 km; Keshet and Hermance, 1986) under El Paso and at 10–17 km under Santa Fe. The El Paso result is compatible with Schmucker's (1964; 1970) deeper sensing geomagnetic variation data. More recent MT sounding confirm that a conductor at 10–15 km depth does extend under the full width of the rift at the approximately latitude of Santa Fe (Jiracek et al., 1987; Rodriquez et al., 1987; Biehler et al., 1991; Jiracek et al., 1993).

In comparing the result of MT studies in the Rio Grande rift, Baikal rift, East African rift, and the Rhinegraben, Jiracek et al. (1979) showed that all were characterized by anomalously low resistivity (high conductivity) at depths less than 30 km, i.e., in the crust. However, their MT soundings over the 20-km-deep "Soccoro magma body" revealed a depth to a conductive horizon of 10 km rather than the expected 20 km. This depth was confirmed by more extensive MT studies (Jiracek et al., 1983, 1987; Mitchell and Jiracek, 1983; Mitchell, 1983) along the COCORP seismic profile (Brown et al., 1980), 40 km north of Socorro. Given the disparity between the depth to magma and to the electrical conductor, Jiracek et al. (1983) argued against magma as the source of the crustal conductors in the Rio Grande rift. Instead, they proposed that a conductive horizon occurs near the brittle-ductile transition, where an impermeable cap traps pore water beneath. Earthquake focal depths in the Socorro area (Sanford et al., 1979) indicate the coincidence of the thickness of the seismogenic (brittle) crust with the depth to the conductive zone. Bailey (1990) described a mechanism by which aqueous fluids might accumulate at the brittle-ductile transition.

Neither two-dimensional (2-D) modeling (Jiracek et al., 1983, 1987) nor three-dimensional (3-D) basin modeling (Gustafson, 1986) reveals a highly conducting layer in the crust in the immediate vicinity of Socorro. This dilemma resulted in the suggestion by Jiracek et al., 1983) that active, shallow magma injection (evidenced by recurring swarms of earthquakes) destroys the integrity of the fluid-trapping, impermeable cap. Thus, they concluded, water is released, leaving a relatively resistive crust since the injected amounts of magma are slight. The relative resistive nature of the crust beneath Socorro is at odds with a recent geomagnetic variation profile run 10 km south of Socorro by Hermance and Neumann (1991). Hermance and Neumann (1991) point out that geomagnetic variation measurements use only magnetic fields, which are less contaminated by surficial (small) features than are the telluric (electric) fields used in MT. However, large-scale variations in basin shapes also produce highly distorted magnetic fields, as was shown by Gustafson (1986) to be expected in the Socorro area. Therefore, the 2-D modeling of both Jiracek et al. (1983, 1987) and Hermance and Neumann (1991) are suspect in the complex 3-D structural setting of Socorro. Gustafson's (1986) 3-D modeling requires a crustal conductor 40 km north of, but not beneath, Socorro.

Whether or not a highly conductive crustal zone directly beneath Socorro exists, it seems certain that the intracrustal electrical conductor in the Rio Grande rift does not coincide with a contemporary magma zone. The Socorro magma body is modeled (Brocher, 1981) as a series of partially molten magma pods, each 30–40 m in thickness. Therefore, even if a full basaltic melt with a resistivity of 0.5 ohm-m (Hermance, 1979b) is assumed, it is unlikely that the integrated conductance is more than a few 100 S. Such a target would not be detected by electromagnetic measurements because of the high conductance, screening effect of the rift fill (see Section 3.5). The conductances of the highly conductive zones modeled by the various researchers 40 km north of Socorro, at El Paso, and near Santa Fe exceed 1000 S in each case, thus they are well-resolved by MT soundings.

MT soundings crossing the eastern and western boundaries of the Rio Grande rift have exposed a distinct asymmetry. Ander (1981) presented MT profiles in Arizona and western New Mexico, some of which extended into the rift. These results west of Socorro and west of the Jemez Mountains extend the crustal conductor beyond the rift itself well into the Basin and Range province. The intracrustal conductor is significantly attenuated, or not present, under the Colorado Plateau west of the northern part of the rift (Ander, 1981; Pedersen and Hermance, 1981). This is similar to both measurements of the eastern boundary of the rift with the Great Plains province. These are along the profile 40 km north of Socorro (Jiracek et al., 1983, 1987) and east of Santa Fe (unpublished data collected by one of us (GRJ) in 1993) . In both cases there is a very sharp rift boundary electrical signature. Jiracek et al. (1983, 1987) show the transition under the central rift-bounding Manzano Mountains to be a deepening of the conductor from 10 km to about 25 km with a five-fold decrease in its conductance. An even larger depth increase (15 to 40 km) is detected east of Santa Fe, near Las Vegas, New Mexico. These depths to the conductive zone in and adjacent to the Rio Grande rift are inversely correlated with heat flow (Reiter et al., 1978; Clarkson and Reiter, 1984). Such a correlation with deep geothermal wells (down to 4.5 km) is strongly evident in the Jemez Mountains along the western side of the Rio Grande rift (Jiracek et al., 1993). This has resulted in speculation by the authors that the depth to the crustal conductor in this region of the rift marks the depth to an isotherm that may be higher (approximately 500–600°C) than the brittle-ductile transition (350–400°C) in silicic crust.

6.6.9. Seismicity

The Rio Grande rift region has been known to be seismically active for many years (e.g., Reid, 1911). Instrumental studies began in 1960, and early review articles were written by Sanford et al. (1972, 1979). The most active area in this century has been between Socorro and Albuquerque, New Mexico (Fig. 6–9). The largest events in this area occurred during a swarm which extended from July 1906 to January 1907. Two of these events reached Intensity VIII.

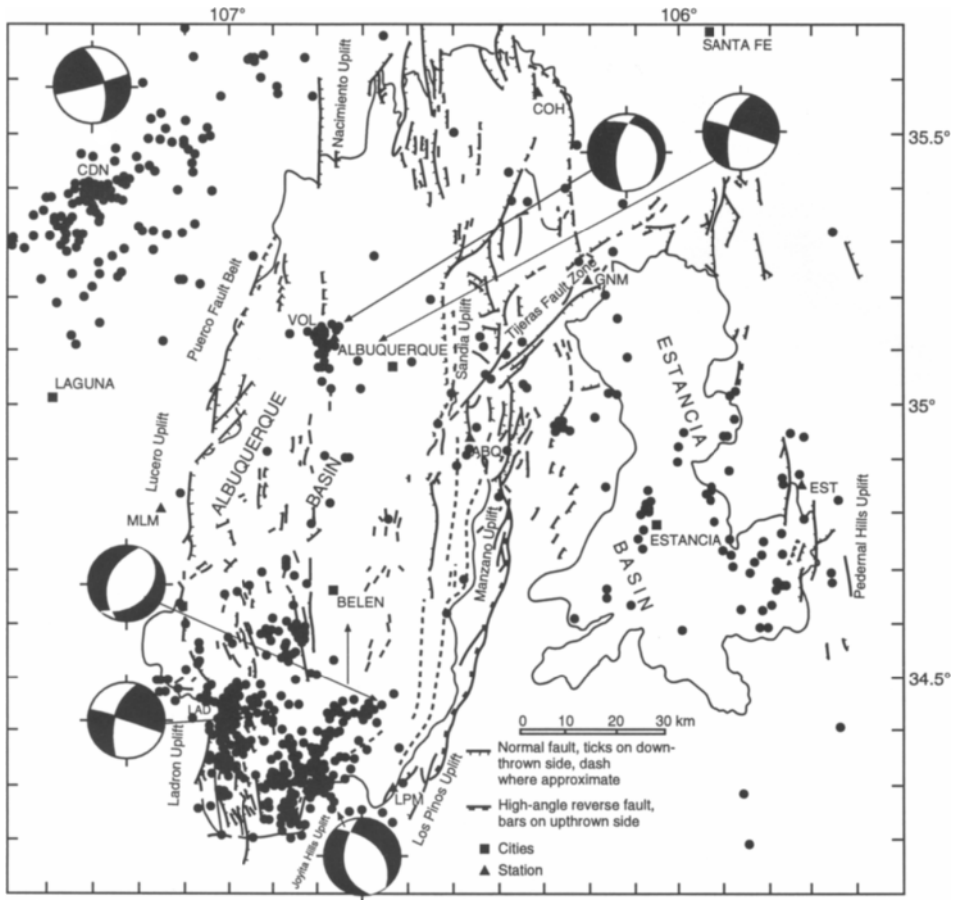

Fig. 6–9. Earthquake epicenters in central New Mexico for the period January 1976 through November 1981, undifferentiated with respect to magnitude. Focal mechanism diagrams are lower hemisphere projections with compressional quadrants shaded. Modified from Sanford et al. (1991).

Studies of the seismicity in this area revealed unusual reflected S-wave phases which suggested the presence of a magma chamber (Sanford et al., 1973, 1977, 1979; Rinehart et al., 1979) at mid-crustal depths which correlated with an amplitude anomaly in reflection (Brown et al., 1979, 1980) and refraction (Olsen et al., 1979) data. Recent earthquakes in the Albuquerque area were studied by Jaksha and Sanford (1986). Their focal mechanisms indicated WNW-ESE extension with a mixture of strike-slip and normal faulting.

Seismicity in the northern New Mexico portion of the rift (Plate 6–8) came under investigation through studies by Los Alamos National Laboratory beginning in 1972. The western boundary of the rift near Española was found to be particularly active (Sanford et al., 1979; Cash and Wolff, 1984).

Seismicity data in the southern portion of the rift are scarce. A seismograph station has been operating in El Paso since the early 1960's and was upgraded to WWSSN status in 1977. Seismicity along the easternmost portion of the rift in west Texas was

monitored between 1977 and 1981 and discussed by Dumas et al. (1980) and Dumas (1981). A large (M 6.4) earthquake occurred in this area in 1931 (Byerly, 1934a, b). Doser (1987) suggested the earthquake occurred along the western boundary of a graben which can be considered the easternmost rift structure in the area. Her results indicated a northwest-trending direction of extension and a roughly equal mix of dip-slip and strike-slip faulting.

Another very large event occurred in northeasternmost Sonora, Mexico, near Douglas, Arizona, in 1887 (Sbar and DuBois, 1984). This event created a fault scarp 76 km long with a maximum height of 4.5 – 5.1 m. Its location is about 100 km west of the accepted western boundary of the rift, but at this latitude the rift widens and becomes diffuse, much as the Kenyan portion of the East African rift widens as it passes southward into Tanzania. These seismic studies, along with studies of Quaternary fault scarps (Muehlberger et al., 1978; Machette, 1986, 1987), attest to the continuing tectonic activity of the rift. In general, this activity is moderate and characterized by swarms of events. Focal mechanisms generally indicate E-W extension (Fig. 6–9), although many local variations occur (Sanford et al., 1979; Doser, 1987).

6.6.10. Stress Measurements

Studies of paleostress and contemporary stress indicators (Zoback and Zoback, 1980) indicate that the middle Tertiary was a time of ENE-WSW extension in the western U.S. The stress direction rotated about 45° to WNW-ESE extension in the late Tertiary (e.g., Zoback et al., 1981). Although local complications occur, this pattern generally holds for the Rio Grande rift area (Aldrich et al., 1986; Henry and Price, 1986). Focal mechanism studies (e.g., Sanford et al., 1979; Jaksha and Sanford, 1986; Doser, 1987) indicate that strike-slip movements are locally important along the rift.

6.6.11. Recent Crustal Movements

Ongoing tectonic activity in the Rio Grande rift has been investigated through the analysis of leveling data. The Socorro, New Mexico, area has been of particular interest (Reilinger and Oliver, 1976; Reilinger et al., 1980; Larsen et al., 1986). The most recent results (Larsen et al., 1986) indicate an average uplift rate of 0.23 cm/yr from 1912 to 1951 and of 0.18 cm/yr from 1951 to 1980. Geomorphic evidence suggests an uplift rate of 0.18 cm/yr over the past 20,000 years (Ouchi, 1983). This uplift has been attributed to the inflation of the mid-crustal magma chamber in the area (Reilinger and Oliver, 1976). Larsen et al. (1986) showed that the uplift as well as the observed flanking areas of subsidence could be modeled with deflating spherical sources at 19 or 35 km feeding an inflating sill at 19 km. At a rate of 0.2 cm/yr, 40 m of uplift could occur in 20,000 years, which seems a reasonable value if the inflation is equally young. If extrapolated over a million years, this rate would yield 2 km of uplift, which seems unlikely. Savage et al. (1980) measured horizontal strain in the area and found weak evidence for a slight horizontal contraction.

Significant vertical movements have also been observed in west Texas (Reilinger et al., 1980; Ni et al., 1981) in areas which are probably associated with the rift.

6.7. Structure of the lithosphere

6.7.1. Crust

Moho depths are primarily derived from seismic refraction studies, which indicate that the crust beneath the axis of the Rio Grande rift is moderately thinned compared to adjacent crust (Olsen et al., 1979; Cooke et al., 1979; Sinno et al., 1986). At 35° N latitude, Moho depth beneath the rift axis (Albuquerque-Belen basin) is about 33 km compared to 45 km under the Colorado Plateau near the Arizona-New Mexico border and 50 km under the Great Plains (Olsen et al., 1979). The depth to the Moho decreases to less than 30 km beneath the southern rift (Sinno et al., 1986). Beneath the rift reflected phases indicate that two major crustal layers are present (Plates 6–9, 6–10). An additional layer is present at the base of the crust beneath the Great Plains east of the rift. In general, the upper crust, to a depth of 15–18 km, is characterized by V_p ~6.0 km/s and V_s ~3.5 km/s. This depth corresponds generally to the maximum depth of most earthquake foci,

and may represent the brittle-ductile transition in rheological properties. Beneath the axis of the rift, the lower crust is characterized by V_p ~6.5 km/s and V_s ~3.7 km/s. Increased temperature in the rift could explain the difference between the V_p value and the higher (~6.8 km/s) values observed at similar depths in adjacent area. Because of its high seismic velocity (V_p = 7.1 km/s), lower crust east of the rift is assumed to be of gabbroic/mafic granulite composition. Nothing is known of its age, and no xenolith localities are recognized by which to sample its lithology.

Because very few detailed deep seismic profiling and gravity studies have been completed in the segment of the rift north of the New Mexico-Colorado border, details of crustal structure there are not well constrained. For comparison with transects presented in Plate 6–9, Plate 6–10, and in Figure 6-11, Figure 6–10 presents a preliminary interpretation of a crustal cross section for the latitude of Alamosa, Colorado based mainly on available geological, gravity, aeromagnetic and heat flow data.

In the central rift (Socorro area), earthquake studies (Sanford et al., 1973, 1977, 1979; Rinehart et al., 1979) indicate the presence of a tabular magma chamber at a depth of about 19–20 km. A strong seismic reflector at about 7 s correlates with this magma body (Fig. 6–11). This body extends over an area of about 1700 km^2.

The compressional velocity in the lower crust beneath the rift (6.4–6.5 km/s) is substantially less than lower crustal velocities (6.7–7.1 km/s) under the flanks both to the east and west.

Gravity data provide a strong constraint on crustal structure. Most workers recognize three main components in the gravity field (Plate 6–9). The first is a very long (>500) wavelength gravity low resulting from lithospheric thinning, i.e., lower density asthenosphere replacing higher density lithosphere, beneath a broad region including the Colorado Plateau and western Great Plains (e.g., Thompson and Zoback, 1979; Ander, 1981). The second is a much narrower axial gravity high (Decker and Smithson, 1975; Cordell, 1976, 1978; Ramberg et al., 1978) which in the southern portion of the rift has been shown by seismic data to result primarily from crustal thinning (Daggett et al., 1986). Cordell (1982) has shown that this anomaly narrows from south to north suggesting that extension in the rift also decreases from south to north. The last component of the gravity field is the series of short-wavelength lows which are due to the large thickness of fill in the rift basins. In the Albuquerque basin, drilling has shown the rift-related fill to exceed 4 km in thickness. In this basin, as well as others, Eocene (Laramide) sediments and Oligocene (pre-rift) volcanic rocks locally form a significant thickness of older basin fill. However, gravity modeling efforts integrated with seismic and drilling data (Mattick, 1967; Cordell, 1976; Ramberg et al., 1978; Birch, 1982; Daggett, 1982; Cape et al., 1983; Wen, 1983; Gilmer et al., 1986; Adams and Keller, 1994) attest to the fact that the Rio Grande rift is associated with a generally large amount of sedimentary fill.

Near El Paso, Santa Fe, and Socorro, the inferred depth to the boundary between upper and lower crustal layers (Conrad discontinuity) beneath the rift axis correlates generally with regions of low electrical resistivity (Hermance and Pedersen, 1980; Towle, 1980; Rodriguez, 1987; Hermance and Neumann, 1991; Biehler et al, 1991). Though these regions were originally interpreted as an indication of magma (Hermance and Pederson, 1980), a more likely interpretation seems to be the presence of hydrous fluids trapped beneath an impermeable layer within the brittle-ductile transition (Jiracek et al., 1983, 1987).

6.7.2. Mantle

6.7.2.1. From Physical Studies

Upper mantle P_n velocities beneath the axis of the rift are estimated to be 7.6–7.7 km/s, although no truly reversed refraction profile exists along the rift. These low P_n velocities beneath the rift axis are conventionally interpreted as asthenospheric values. In contrast, upper mantle velocities adjacent to the rift are typically 8.0–8.2 km/s (Olsen et al., 1979; Sinno et al., 1986; Stewart and Pakiser, 1962; Wolf and Cipar, 1993). A simple interpretation of these data implies that beneath the axis of the rift, asthenosphere extends approximately (i.e., within the resolution of the seismic technique) to the base of the

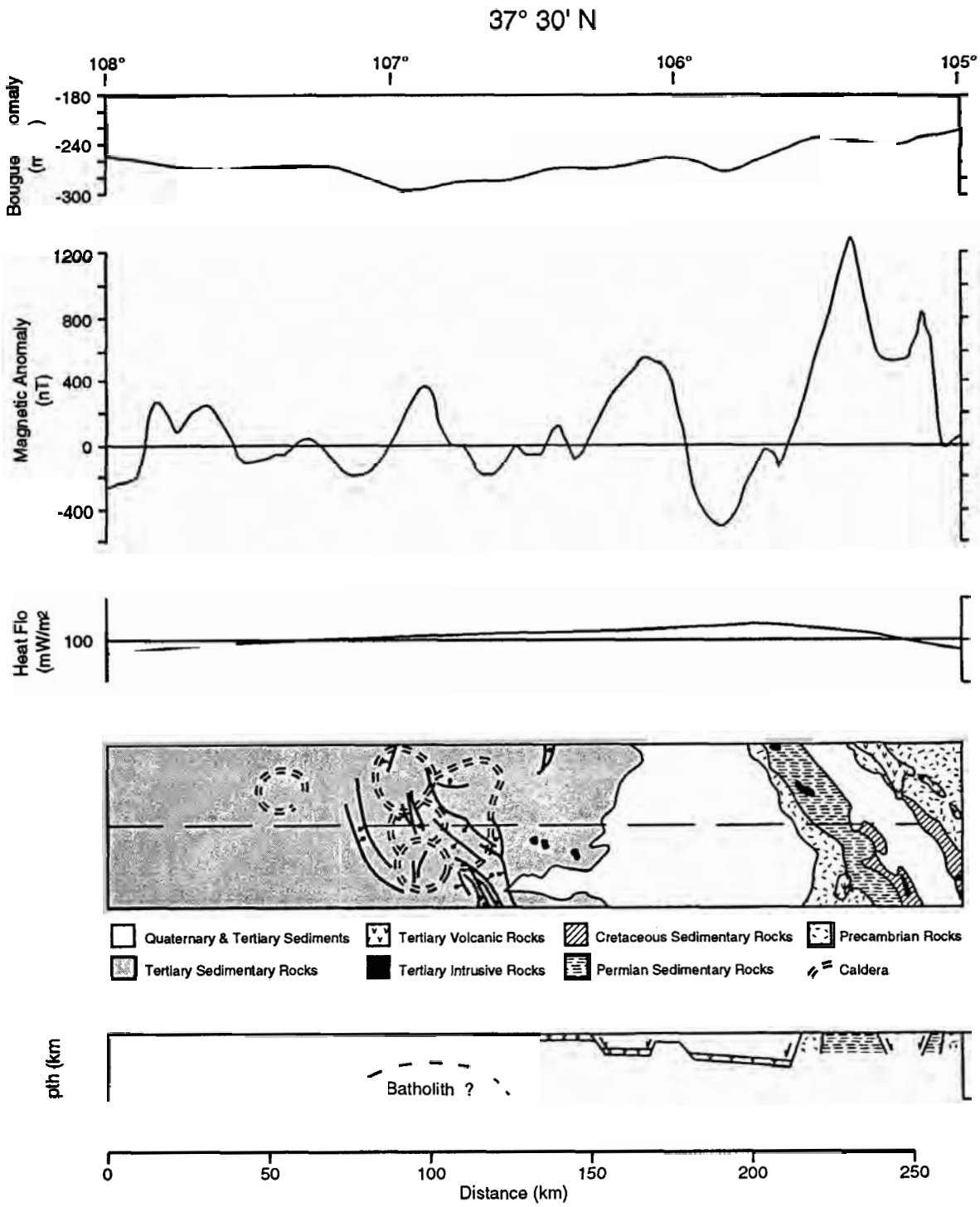

Fig. 6–10. Gravity, magnetic, and heat flow profiles, geological strip map. and crustal transect across the Rio Grande rift at 37°30'N, near Alamosa, Colorado.

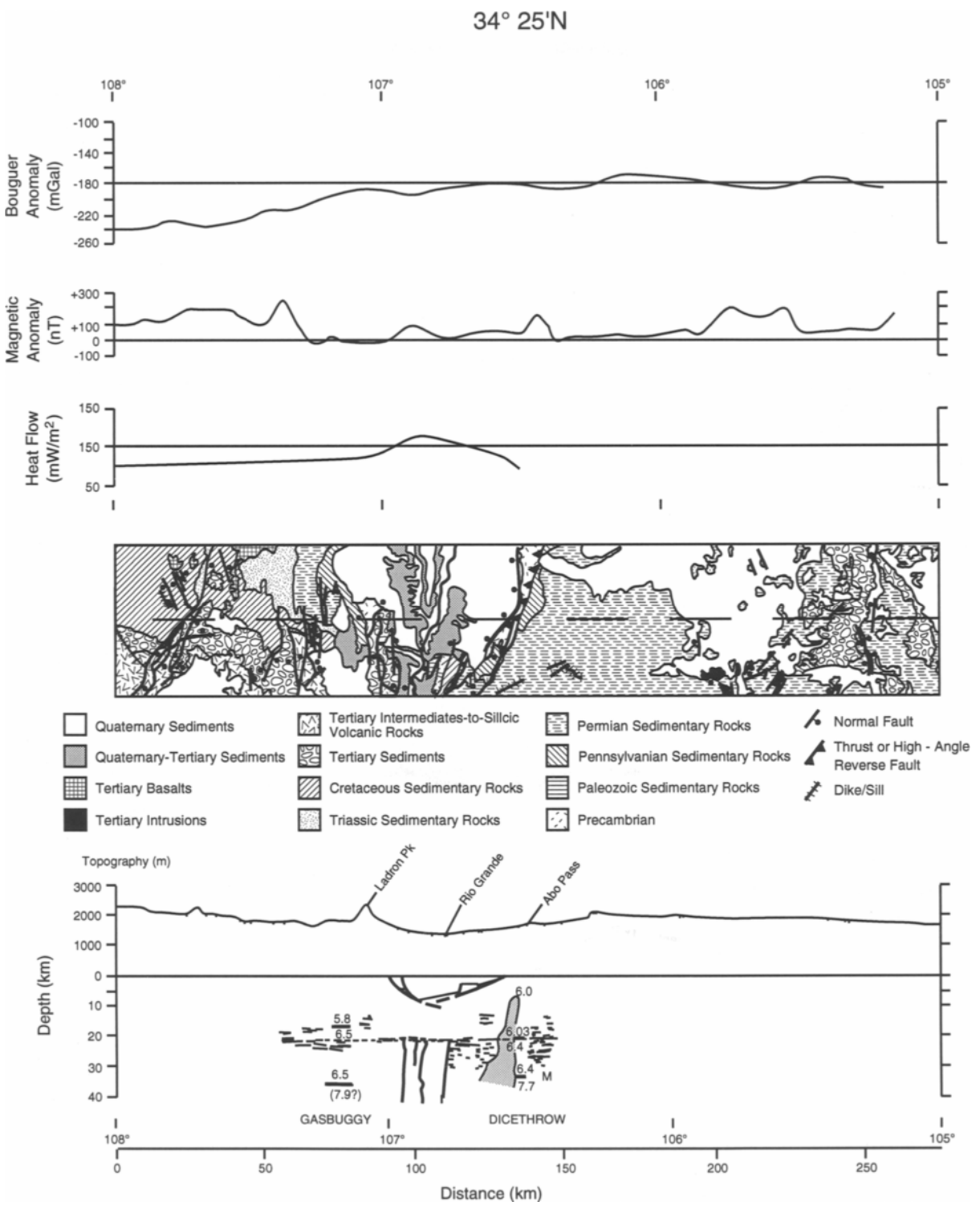

Fig. 6–11. Gravity, magnetic, and heat flow profiles, geological strip map, and lithospheric transect through the Rio Grande rift at 34°25'N, near Socorro, New Mexico, showing inferred crustal magma chamber.

crust (e.g., Olsen et al., 1987). Studies of regional phases (Keller et al., 1979a, b) do suggest that higher velocity (about 8.0 km/s) material may underlie the region of lower velocity (Murdock and Jaksha, 1981).

In contrast, teleseismic P-wave delays indicating a velocity contrast of up to –8% beneath the axis of the rift were interpreted by Davis (1991) and Davis et al. (1993) to indicate that the lithosphere extends to a depth of approximately 70 km beneath the rift compared to 200 km several hundred kilometers away. This interpretation would allow for a substantial "lid" of mantle lithosphere to be present beneath the rift. Part of the reason that teleseismic techniques yield different results regarding lithospheric thickness beneath the rift than existing explosion refraction surveys is the lower vertical resolution of teleseismic techniques. The P_n velocities from the refraction studies also need confirmation by reversed profiles. In general, however the different results from the different techniques has not been satisfactorily addressed.

6.7.2.2. From Isotopic Studies

Isotopic studies of basaltic rocks can directly measure only the compositions of the source regions. However, when correlated with certain physical characteristics (gravity, heat flow, seismic velocities) and with the geologic history of different tectonic provinces, isotopic compositions can be used to infer whether magma sources originate in asthenospheric or lithospheric mantle (see section 6.5.5.2). Based on inferred depth of generation of tholeiitic and alkalic basalts, late Cenozoic basaltic magmas from the northern Rio Grande rift and Great Plains originated in lithospheric mantle, and those from the southern rift and Basin and Range province in asthenospheric mantle. Basalts from the transition zone of the southeastern Colorado Plateau (east-central Arizona and west-central New Mexico) originated from a mixture of lithospheric and asthenospheric sources. Assuming from petrologic studies that alkalic basalts are generated from 50–70 km provides a means of estimating the depth of the lithosphere/asthenosphere boundary (e.g., Plate 6–8).

6.7.2.3. Thinning Processes

Various mechanisms for thinning the lithosphere beneath the rift are possible. A general model of delamination of the lithospheric mantle was proposed by Bird (1979) as a mechanism for lithospheric thinning in regions undergoing extension. Delamination would place asthenosphere directly against the base of the crust, which would be expected to generate large volumes of melt derived from the lower crust. Since no evidence exists for major crustal melting, delamination is not a likely mechanism in the Rio Grande rift.

Thermal thinning, i.e., in situ partial melting of lithosphere, was proposed by Perry et al. (1987, 1988) to reconcile the disparate observations of an isotopically enriched source of basaltic melts (interpreted as subcrustal lithosphere) with low seismic P_n velocities (representing asthenosphere) in the northern Rio Grande rift (see above). Essentially, it was envisioned that upwelling asthenosphere was overlain by a thin (few kilometers) "carapace" of mantle lithosphere containing a small amount of partial melt, formed as heat is advected from the underlying asthenosphere. Since the carapace of "lithosphere" contains partial melt, it is characterized by low seismic velocities and is indistinguishable from seismic "asthenosphere." Yet both regions can be distinguished isotopically. This carapace is probably thin (few kilometers). At any give depth it is a transient feature. In situ melting of subcrustal lithosphere is probably not an effective mechanism for major lithospheric thinning in geologically short time periods due to the slow rate of conductive heat transfer, unless material is displaced laterally by rising asthenosphere, a process referred to as convective thinning by Spohn and Schubert (1983). The effectiveness of convective thinning is limited by the ability of material to be displaced laterally.

Erosion of the base of the lithosphere (Perry et al., 1987, 1988) may also contribute to lithospheric thinning in regions of extension. The lithosphere/asthenosphere contact is likely to be irregular, especially if more enriched, volatile-rich regions of the lower lithosphere are preferentially melted by heat advected by the convecting asthenosphere. Any downward-projecting irregularities in the boundary

may be removed by lateral movement of the underlying convecting mantle. Erosion may be accomplished in part by secondary convection that is set in motion by extension (Buck, 1986; Moretti and Froidevaux, 1986). Both convective thinning and sub-lithospheric erosion could be geochemically significant as a means for recycling of enriched subcrustal mantle in the globally convecting asthenosphere.

Acknowledgements. This work is a compilation of data and ideas from many sources, some as yet unpublished. We thank our colleagues on the CREST project for many stimulating discussions and ideas. L. House provided the figure of relocated earthquake epicenters from the Jemez Mountains-Española basin area (Plate 6–8) from unpublished sources. We thank E. Y. Anthony for contributing to the petrology of the southern rift. K. Reid aided in the preparation of Figs. 6–4 and 6–5. We thank G. A. Thompson and M. L. Zoback for valuable comments on an early draft of this manuscript. F. V. Perry reviewed portions of the manuscript. W. S. Baldridge and K. H. Olsen acknowledge the support of the Institute of Geophysics and Planetary Physics (Los Alamos National Laboratory branch) of the University of California and National Science Foundation grant EAR-8617315 to L. W. Braile (Purdue University). G. R. Keller acknowledges the support of Air Force Office of Scientific Research Contract F49620-92-J-0438. Support for E. Wendlandt was provided by the Los Alamos National Laboratory branch of the University of California's Institute of Geophysics and Planetary Physics.

6.8. References

Abitz, J. A., 1989. Geology and petrogenesis of the northern Emory Caldera, Sierra County, New Mexico. Ph.D. Dissertation, University of New Mexico, Albuquerque, N.M., 174 pp.

Adams, D. C., and Keller, G. R., 1994. Crustal structure and basin geometry in south-central New Mexico. Geological Society of America, Spec. Paper, 291: 241–255..

Aiken, C. L. V., Laughlin, A. W. and F.A. West, 1978. Residual Bouguer gravity anomaly map of New Mexico. Los Alamos Nat. Lab., Pub. LA07466-MAP, 1:500,000.

Aiken, C. L. V., Schellhorn, R.W., and de la Fuente, M.F., 1988. Gravity of northern Mexico. In: K.F. Clark et al. (Editors), Stratigraphy, Tectonics, and Resources of Part of Sierra Madre Occidental Province, Mexico. El Paso Geol. Soc. Guidebook, pp. 119–134.

Aldrich, M. J., Jr., 1986. Tectonics of the Jemez lineament in the Jemez Mountains and Rio Grande rift. J. Geophys. Res., 91: 1753–1762.

Aldrich, M. J, Jr., Chapin, C. E., and Laughlin, A. W., 1986. Stress history and tectonic development of the Rio Grande rift, New Mexico. J. Geophys. Res., 91: 6199–6211.

Ander, M. E., 1981. Geophysical study of the crust and upper mantle beneath the Rio Grande rift and adjacent Great Plains and Colorado Plateau. Los Alamos Nat. Lab. Rep. LA-8676, 218 pp.

Anthony, E. Y., 1993. Dating techniques for Quaternary lavas. Eos, Trans. Am. Geophys. Union, 74: 350.

Anthony, E. Y., and Poths, J. 1992. ^{3}He surface exposure dating and magma dynamics, the Potrillo volcanic field, Rio Grande rift, New Mexico. Geochim. Cosmochim. Acta, 56: 4105–4108.

Anthony, E. Y., Hoffer, J. M., Waggoner, W. K., and Chen, W., 1992. Compositional diversity in late Cenozoic mafic lavas in the Rio Grande rift and Basin and Range province, southern New Mexico. Geol. Soc. Am. Bull., 104: 973–979.

Aoki, K., and Kudo, A. M., 1976. Major-element variations of late Cenozoic basalts of New Mexico. N. M. Geol. Soc., Spec. Publ., 5: 82–88.

Bachman, G. O., and Mehnert, H. H., 1978. New K-Ar dates and the late Pliocene to Holocene geomorphic history of the central Rio Grande region, New Mexico. Geol. Soc. Am. Bull., 89: 283–292.

Bailey, R. C., 1990. Trapping of aqueous fluids in the deep crust. Geophys. Res. Lett., 17: 1129–1132.

Baldridge, W.S., 1979a. Petrology and petrogenesis of Plio-Pleistocene basaltic rocks from the central Rio Grande rift, New Mexico, and their relation to rift structure. In: R. E. Riecker (Editor), Rio Grande Rift: Tectonics and Magmatism. Am. Geophys. Union, Spec. Publ., pp. 323–353.

Baldridge, W.S., 1979b. Mafic and ultramafic inclusion suites from the Rio Grande Rift (New Mexico) and their bearing on the composition and thermal state of the lithosphere. J. Volcanol. and Geotherm. Res., 6: 319–351

Baldridge, W. S., Damon, P. E., Shafiqullah, M., and Bridwell, R. J., 1980. Evolution of the central Rio Grande rift, New Mexico: New potassium-argon ages. Earth Planet. Sci. Lett., 51: 309–321.

Baldridge, W. S., Perry, F. V., and Gladney, E. S., 1992. Petrology and geochemistry of the Cat Hills volcanic field, central Rio Grande rift, New Mexico. Geol. Soc. Am. Bull., 93: 635–643.

Baldridge, W. S., Bartov, Y., and Kron, A., 1983. Geologic map of the Rio Grande rift and southeastern Colorado Plateau, New Mexico and Arizona (1:500,000). Supplement to: R. E. Riecker (Editor), Rio Grande Rift: Tectonics and Magmatism, Am. Geophys. Union, Spec. Publ.

Baldridge, W. S., Olsen, K. H., and Callender, J. F., 1984. Rio Grande rift: Problems and perspectives. N. M. Geol. Soc., Field Conf. Guideb., 35: 1–12.

Baldridge, W. S., Perry, F. V., and Shafiqullah, M., 1987. Late Cenozoic volcanism of the southeastern Colorado Plateau: I. Volcanic geology of the Lucero area, New Mexico. Geol. Soc. Am. Bull., 99: 463–470.

Baldridge, W. S., and Olsen, K. H., 1989. The Rio Grande rift. Am. Sci., 77: 240–247

Baldridge, W. S., Gardner J. N., and Reneau, S. L., 1990. Transfer faulting in the central Rio Grande rift: Oblique slip on the Pajarito fault system. Eos, Trans. Am. Geophys. Union, 71: 1584.

Baldridge, W. S., Perry, F. V., Vaniman, D. T., Nealey, L. D., Leavy, B. D., Laughlin, A. W., Kyle, P., Bartov, Y., Steinitz, G., and Gladney, E. S., 1991. Middle to late Cenozoic magmatism of the southeastern Colorado Plateau and central Rio Grande rift (New Mexico and Arizona, USA): A model for continental rifting. Tectonophysics, 197: 327–354.

Barker, D. S., 1979. Cenozoic magmatism in the Trans-Pecos province: Relation to the Rio Grande rift, In: R. E. Riecker (Editor), Rio Grande Rift: Tectonics and Magmatism. Am. Geophys. Union, Spec. Publ., pp. 382–392.

Barrow, R., and Keller, G. R., 1994. An integrated geophysical study of the Estancia basin, central New Mexico. Geological Society of America, Special Paper 291: 171–186.

Biehler, S., Ferguson, J., Baldridge, W. S., Jiracek, G. R., Aldern J.L., Martinez, M., Fernandez, R., Romo, J., Gilpin, B., Braile, L. W., Hersey, D. R., Luyendyk, B. P., and Aiken, C. L., 1991. A geophysical model of the Espaola basin , Rio Grande rift, New Mexico. Geophys., 56: 340–353.

Bikerman, M., and Bell, K., 1986. Isotopic Sr and Nd study of the Mogollon-Datil volcanic rocks, New Mexico (abstr.), Geol. Soc. Am., Abstr. Prog., 18: 541.

Birch, F. S., 1982. Gravity models of the Albuquerque basin, Rio Grande rift, New Mexico. Geophys., 47: 1185–1197.

Bird, P., 1979. Continental delamination and the Colorado Plateau. J. Geophys. Res., 84: 7561–7571.

Black, B. A., 1984. Structural anomalies in the Espaola basin. N. M. Geol. Soc., Field Conf. Guideb. 35: 59–62.

Blackwell, D. D., 1978. Heat flow and energy loss in the western United States. In: R. B. Smith and G. P. Eaton (Editors), The Structure and Physical Properties of the Earth's Crust. Am. Geophys Union, Geophys. Monogr., 14, pp. 169–184.

Bosworth, W., 1985. Geometry of propagating continental rifts. Nature, 316: 625–627.

Bosworth, W., 1987. Off axis volcanism in the Gregory rift, East Africa: Implications for models of continental rifting. Geology, 15: 397–400.

Bosworth, W., Lambiase, J., and Keislar, R., 1986. A new look at Gregory's rift: The structural style of continental rifting. Eos, Trans. Am. Geophys. Union, 67: 577+.

Brister, B. S., and Gries, R. R., 1994. Tertiary stratigraphy and tectonic development of the Alamosa basin (northern San Luis basin), Rio Grande rift, south-central Colorado. Geol. Soc. Am., Special Paper, 291: 39–58.

Brocher, T. M., 1981, Geometry and physical properties of the Socorro, New Mexico, magma bodies. J. Geophys. Res., 86: 9420–9432.

Brown, L. D., Krumhansl, P. A., Chapin, C. E., Sanford, A. R., Cook, F. A., Kaufman, S., Oliver, J. E., and Schilt, F. S., 1979. COCORP seismic reflection studies of the Rio Grande rift, In: R. E. Riecker (Editor), Rio Grande Rift: Tectonics and Magmatism. Am. Geophys. Union, Spec. Publ., pp. 169–184.

Brown, L. D., Chapin, C. E., Sanford, A. R., Kaufman, S., and Oliver, J., 1980. Deep structure of the Rio Grande rift from seismic reflection profiling. J. Geophys. Res., 85: 4773–4800.

Brown, L. L., and Golombek, M. P., 1985. Tectonic rotations within the Rio Grande rift: Evidence from paleomagnetic studies. J. Geophys. Res., 90: 790–802.

Brown, L. L., and Golombek, M. P., 1986. Block rotations in the Rio Grande rift, New Mexico. Tectonics, 5: 423–438.

Bryan, K., 1938. Geology and ground-water conditions of the Rio Grande depression in Colorado and New Mexico. In: Regional Planning, Pt. 6, Rio Grande Joint Investigation in the Upper Rio Grande Basin, Natl. Res. Comm., 1, part 2, sec. 1, pp. 197–225.

Buck, W. R., 1986. Small-scale convection induced by passive rifting: The cause for uplift of rift shoulders. Earth Planet. Sci. Lett., 77: 362–372.

Budnick, R. T., 1987. Late Miocene reactivation of Ancestral Rocky Mountain structures in the Texas Panhandle: A response to Basin and Range extension, Geology, 15: 163–166.

Bussod, G., 1981. Thermal and kinematic history of mantle xenoliths from Kilbourne Hole, NM. M. S Thesis, University of Washington, Seattle, Wash.

Bussod, G. Y. A., and Williams, D. R., 1991. Thermal and kinematic model of the southern Rio Grande Rift: Inferences from crustal and mantle xenoliths from Kilbourne Hole, New Mexico, Tectonophy., 197: 373–389.

Byerly, P., 1934a. The Texas earthquake of August 16, 1931. Bull. Seis. Soc. Am., 24: 81–99.

Byerly, P., 1934b. The Texas earthquake of August 16, 1931. Bull. Seis. Soc. Am., 24: 303–324.

Callendar, J. F., and Zilinsky, R. E., 1976. Kinematics of Tertiary and Quaternary deformation along the eastern edge of the Lucero uplift, central New Mexico. N. M. Geol. Soc. Spec. Publ., 6: 53–61.

Cameron, K. L., Nimz, G. J., and Kuentz, D., 1989. Southern cordilleran basaltic andesite suite, southern Chihuahua, Mexico: A link between Tertiary continental arc and flood basalt magmatism in North America. J. Geophys. Res., 94: 7817–7840.

Cape, C. D., McGeary, S., and Thompson, G. A., 1983. Cenozoic normal faulting and the shallow structure of the Rio Grande rift near Socorro, New Mexico. Geol. Soc. Amer. Bull, 94: 3–14.

Carter, J. L., 1970. Mineralogy and chemistry of the earth's mantle based on the partial fusion-partial crystallization model. Geol. Soc. Am. Bull, 81: 2031–2034.

Cash, D. J., and Wolff, J. J., 1984. Seismicity of the Rio Grande rift in northern New Mexico, 1973–1983. N. M. Geol. Soc., Field Conf. Guideb., 35: 25–28.

Cavazza, W., 1986. Miocene sediment dispersal in the central Española basin, Rio Grande rift, New Mexico, U.S.A. Sediment. Geol., 51: 119–135.

Chamberlin, R. M., 1983. Cenozoic domino-style crustal extension in the Lemitar Mountains, New Mexico: A summary. N. M. Geol. Soc., Field Conf. Guideb., 34: 111–118.

Chapin, C. E., 1971. The Rio Grande rift, part I: Modifications and additions. N. M. Geol. Soc., Field Conf. Guideb., 22: 191–202.

Chapin, C. E., 1979. Foreword, In: R. E. Riecker, R. E. (Editor), Rio Grande Rift: Tectonics and Magmatism. Am. Geophys. Union, Spec. Publ., pp. v–vii.

Chapin, C. E., 1988. Axial basins of the northern and central Rio Grande rifts. In: L. L. Sloss (Editor), Sedimentary Cover—North American Craton: U.S., Geol. Soc. Am., Decade North Am. Geol., D-2: 165–170.

Chapin, C. E., and Seager, W. R., 1975. Evolution of the Rio Grande rift in the Socorro and Las Cruces areas. N. M. Geol. Soc., Field Conf. Guideb., 26: 191–201.

Chapin, C. E., and Cather, S. M., 1981. Eocene tectonics and sedimentation in the Colorado Plateau—Rocky Mountains area. Ariz. Geol. Soc. Digest, 14: 173–198.

Clarkson, G., and Reiter, M., 1984. Analysis of terrestrial heat flow profiles across the Rio Grande rift and southern Rocky Mountains in northern New Mexico. N. M. Geol. Soc., Field Conf. Guideb., 35: 39–44.

Collins, E. W., and Raney, J. A., 1994. Tertiary and Quaternary tectonics of the Hueco bolson, Trans-Pecos Texas and Chihuahua, Mexico. Geol. Soc. Am., Special Paper, 291: 265–282.

Condie, K. C., and Budding, A. J., 1979. Geology and geochemistry of Precambrian rocks, central and south-central New Mexico. N. M. Bur. Mines Miner. Res., Mem. 35, 58 pp.

Condit, C. D., Crumpler, L. S., Aubele, J. C., and Elston, W. E., 1989. Patterns of volcanism along the southern margin of the Colorado Plateau: The Springerville field. J. Geophys. Res., 94: 7975–7986.

Cook, F. A., Decker, E. R., and Smithson, S. B., 1978. Preliminary transient heat flow model of the Rio Grande rift in southern New Mexico. Earth Planet. Sci. Lett., 40: 316–326.

Cook, F. A., McCullar, D. B., Decker, E. R., and Smithson, S. B., 1979. Crustal structure and evolution of the southern Rio Grande rift. In: R. E. Riecker (Editor), Rio Grande rift: Tectonics and Magmatism. Am. Geophys. Union, Spec. Publ., pp. 195–208.

Cordell, L., 1976. Aeromagnetic and gravity studies of the Rio Grande graben in New Mexico between Belen and Pilar, N. M. Geol. Soc., Spec. Publ. 6: 62–70.

Cordell, L., 1978. Regional geophysical setting of the Rio Grande rift. Geol. Soc. Am. Bull., 89: 1073–1090.

Cordell, L., 1982. Extension in the Rio Grande rift. J. Geophys. Res., 87: 8561–8569.

Cordell, L., 1984. Composite residual total intensity aeromagnetic map of New Mexico. Nat. Ocean. Atmos. Admin., Nat. Geophys. Data Center Map, 1:500,000.

Cordell, L., Keller, G. R., and Hildenbrand, T. G., 1982. Bouguer gravity map of the Rio Grande rift, Colorado, New Mexico, and Texas. U. S. Geol. Surv., Map GP-949, 1:1:000,000.

Cordell, L., and Keller, G. R., 1984. Regional structural trends inferred from gravity and aeromagnetic data in the New Mexico-Colorado border region. N. M. Geol. Soc., Guideb., 35: 21–23.

Daggett, P. H., 1982. An integrated geophysical study of the crustal structure of the southern Rio Grande rift. Ph.D. Thesis, New Mexico State University, Las Cruces, New Mexico, 197 pp.

Daggett, P. H., Keller, G. R., Morgan, P., and Wen, C. L., 1986. Structure of the southern Rio Grande rift from gravity interpretations. J. Geophys. Res., 81: 6147–6167.

Davis, J., and Hawkesworth, C., 1993. The petrogenesis of 30-20 Ma basic and intermediate volcanics from the Mogollon-Datill volcanic field, New Mexico, USA. Contrib. Mineral. Petrol., 115: 165–183.

Davis, J. M., Hawkesworth, C. J., and Elston, W. E., 1989. Oligocene to Miocene magmatic transitions in the Mogollon-Datil volcanic field, New Mexico, USA. N. M. Bur. Mines Miner. Res., Bull., 131, 67 pp.

Davis, P. M., 1991. Continental rift structures and dynamics with reference to teleseismic studies of the Rio grande and East African rifts. Tectonophysics, 197: 309–325.

Davis, P. M., Parker, E. C., Evans, J. R, Iyer, H. M., and Olsen, K. H., 1984. Teleseismic deep sounding of the velocity structure beneath the Rio Grande rift. N. M. Geol. Soc., Field Conf. Guideb., 35: 29–38.

Davis, P. M., Slack, P., Dahlheim, H. A., Green, W. V., Meyer, R. P., Achauer, U., Glahn, A., and Granet, M., 1993. Teleseismic tomography of continental rift zones. In: H. M. Iyer and K. Hirahara (Editors), Seismic tomography—Theory and Practice, Chapter 15, Chapman and Hall, 848 pp.

Davis, T. L, and Stoughton, D., 1979. Interpretation of seismic reflection data from the northern San Luis Valley, south-central Colorado. In: R. E. Riecker (Editor), Rio Grande Rift: Tectonics and Magmatism, Am. Geophys. Union, Spec. Publ., pp. 185–194.

De Angelo, M. V., and Keller, G. R., 1988. Geophys ical anomalies in southwestern New Mexico. N. M. Geol. Soc., Field Conf. Guideb., 39: 71–75.

Decker, E. R., and Smithson, S. B., 1975. Heat flow and gravity interpretation across the Rio Grande rift in southern New Mexico and west Texas. J. Geophys. Res., 80: 2542–2552.

Decker, E. R., Bucher, G. J., Buelow, K. L., and Heasler, H. P., 1984. Preliminary interpretation of heat flow and radio-activity in the Rio Grande rift zone in central and northern Colorado. N. M. Geol. Soc., Field Conf. Guideb., 35: 45–50.

Decker, E. R., Heasler, H. P., Buelow, K. L., Baker, K. H., and Itallin, J. S., 1988. Significance of past and recent heat-flow and radioactivity studies in the southern Rocky Mountains region. Geol. Soc. Am. Bull., 100: 1851–1885.

deVoogd, B., Brown, L.D., and Merey, C., 1986. Nature of the eastern boundary of the Rio Grande rift from COCORP surveys in the Albuquerque basin, New Mexico. J. Geophys. Res., 91: 6305–6320.

deVoogt, B., Serpa, L., and Brown, L., 1988. Crustal extension and magmatic processes: COCORP profiles from Death Valley and the Rio Grande rift. Geol. Soc. Am. Bull., 100, 1550–1567.

Dickinson, W. R., 1981. Plate tectonic evolution of the southern Cordillera. Ariz. Geol. Soc. Digest, 14: 113–135.

Dickinson, W. R., and Snyder, W. S., 1979. Geometry of triple junctions related to San Andreas transform. J. Geophys. Res., 84: 561–572.

Doser, D. I., 1987. The 16 August 1931 Valentine, Texas, earthquake: Evidence for normal faulting in west Texas. Bull. Seismol. Soc. Am., 77: 2005–2017.

Dumas, D. B., 1981. Seismicity of west Texas. Ph. D. Dissertation, U. Texas at Dallas, Richardson, 94 pp.

Dumas, D. B., Dorman, H. J., Latham, G. V., 1980. A reevaluation of the August 16, 1931, Texas earthquake. Bull. Seismol. Soc. Am., 70: 1171–1180.

Dungan, M. A., Lindstrom, M. M., McMillan, N. J., Moorbath, S., Hoefs, J., and Haskin, L. A., 1986. Open system magmatic evolution of the Taos Plateau volcanic field, northern New Mexico 1. The petrology and geochemistry of the Servilleta Basalt. J. Geophys. Res., 91: 5999–6028.

Eaton, G. P., 1979. A plate-tectonic model for late Cenozoic crustal spreading in the western United States. In: R. E. Riecker (Editor), Rio Grande Rift: Tectonics and Magmatism, Am. Geophys. Union, Spec. Publ., pp. 7–32.

Eaton, G. P. 1982. The Basin and Range province: Origin and tectonic significance. Ann. Rev. Earth Planet. Sci., 10: 409–440.

Eaton, G. P., 1986. A tectonic redefinition of the southern Rocky Mountains. Tectonophysics, 132: 163–193.

Eaton, G. P., 1987. Topography and origin of the southern Rocky Mountains and Alvarado ridge. In: M. P. Coward, J. F. Dewey, and P. L. Hancock (Editors), Continental Extensional Tectonics, Geol. Soc. London, Spec. Publ. 28, pp. 355–369.

Ellis, P. G., and McClay, K. R., 1988. Listric extensional fault systems—results of analogue model experiments. Basin Res., 1: 55–70.

Elston, W. E., 1984. Mid-Tertiary ash-flow tuff cauldrons, southwestern New Mexico. J. Geophys. Res., 89: 8733–8750.

Elston, W. E., Rhodes, R. C., Coney, P. J., and Deal, E. G., 1976. Progress report on the Mogollon Plateau volcanic field, southwestern New Mexico, 3, Surface expression of a pluton. N. M. Geol. Soc., Spec. Publ. 5: 3–28.

Engebretson, D. C., Cox, A., and Thompson, G. A., 1984. Correlation of plate motions with continental tectonics: Laramide to basin-range. Tectonics, 3: 115–119.

Epis, R. C., and Chapin, C. E., 1975. Geomorphic and tectonic implications of the post-Laramide, late Eocene erosion surface in the Southern Rocky Mountains. In: Cenozoic History of the Southern Rocky Mountains. Geol. Soc. Am., Mem. 144: 45–74.

Fairhead, J. D., 1976. The structure of the lithosphere beneath the eastern rift, East Africa, deduced from gravity studies. Tectonophysics, 30: 269–298.

Figuers, S. H., 1987. Structural geology and geophysics of the pipeline complex, northern Franklin Mountains, El Paso, Texas. Ph.D. Dissertation, University of Texas at El Paso, El Paso, Texas, 279 pp.

Fitton, J. G., James, D., and Leeman, W. P., 1991. Basic magmatism associated with late Cenozoic extension in the western United States: Compositional variations in space and time. J. Geophys. Res., 96: 13,693–13,711.

Fodor, R. V., 1978. Ultramafic and mafic inclusions and megacrysts in Pliocene basalt, Black Range, New Mexico. Geol. Soc. Am. Bull, 89: 451–459.

Galusha, T., and Blick, J.C., 1971. Stratigraphy of the Santa Fe Group, New Mexico. Am. Mus. Nat. Hist. Bull., 144, 127 pp.

Gardner, J. N., Goff, F., Garcia, S., and Hagan, R. C., 1986. Stratigraphic relations and lilthologic variations in the Jemez volcanic field, New Mexico. J. Geophys. Res., 91: 1763–1788.

Gibbs, A. D., 1984. Structural evolution of extensional basin margins. J. Geol. Soc. London, 141: 609–620.

Gibson, S. A., Thompson, R. N., Leat, P. T., Morrison, M. A., Hendry, G. L., and Dickin, A. P., 1991. The Flat Tops volcanic field. 1. Lower Miocene open-system, multisource magmatism at Flander, Trappers Lake. J. Geophys. Res., 96: 13,609–13,627.

Gilmer, A. L., Mauldin, R. A., and Keller, G. R., 1986. A gravity study of the Jornada del Muerto and Palomas basins. N. M. Geol. Soc., Field Conf. Guideb., 37: 131–134.

Glazner, A. F., and Bartley, J. M., 1984. Timing and tectonic setting of Tertiary low-angle normal faulting and associated magmatism in the southwestern United States, Tectonics, 3: 385–396.

Goff, F., Gardner, J. N., Baldridge, W. S., Hulen, J. B., Nielson, D. L., Vaniman, D., Heiken, G., Dungan, M. A., and Broxton, D., 1989. Excursion 17B: Volcanic and hydrothermal evolution of Valles caldera and Jemez volcanic field. N. M. Bur. Mines Miner. Res., Mem. 46: 381–434.

Gough, D. I., 1974. Electrical conductivity under western North America in relation to heat flow, seismology and structure. J. Geomagn. Geoelec., 26: 105–124.

Gustafson, E. P., 1980. Three-dimensional magnetotelluric response of the Rio Grande rift near Socorro, New Mexico. M. S. Thesis, San Diego State University, San Diego, California.

Hayden, S. N., and Mawer, C. K., 1991. Dextral transtensional deformation along the western margin of the Rio Grande rift, central New Mexico (abstr.). Geol. Soc. Am., Abstr. Prog., 23: 31.

Heiken, G., Goff, F., Gardner, J. N., Baldridge, W. S., Hulen, J. B., Nielson, D. L., and Vaniman, D., 1990. The Valles/Toledo caldera complex, Jemez volcanic field, New Mexico. Annu. Rev. Earth Planet. Sci., 18: 27–53.

Henry, C. D., and Price, J. G., 1985. Summary of the tectonic development of Trans-Pecos Texas. Bur. Econ. Geol., Misc. Map 36 (1:1,000,000), Univ. Texas, Austin, Tex.

Henry, C, D., and Price, J. G., 1986. Early Basin and Range development in Trans-Pecos Texas and adjacent Chihuahua: Magmatism and orientation, timing, and style of extension. J. Geophys. Res., 91: 6213–6224.

Hermance, J. F., 1979a. Toward assessing the geothermal potential of the Jemez Mountains volcanic complex: A telluric–magnetotelluric survey. Los Alamos National Laboratory, Rep. LA7656-MS, 86 pp.

Hermance, J. F., 1979b. The electrical conductivity of materials containing partial melts: A simple model from Archie's law, Geophys. Res. Lett., 6: 613–616.

Hermance, J. F., and J. Pedersen, 1980. Deep structure of the Rio Grande rift, A magnetotelluric interpretation. J. Geophys. Res., 85: 3899–3912.

Hermance, J. F., and Neumann, G. A., 1991. The Rio Grande rift: New electromagnetic constraints on the Socorro magma body. Physics Earth Planet. Int., 66: 101–117.

Himes, D., 1968. Analysis of gravity, magnetic, and surface geologic data, northern Chihuahua, Mexico. M.S. Thesis, Rice Univ., Houston, 78 pp.

Hoffer, J. M., 1976. Geology of Potrillo basalt field, south-central New Meico. N. M. Bur. Mines Mineral. Res., Circ. 149, 30 pp.

Ingersoll, R. V., Cavazza, W., Baldridge, W. S., and Shafiqullah, M., 1990. Cenozoic sedimentation and paleotectonics of north-central New Mexico: Implications for initiation and evolution of the Rio Grande rift. Geol. Soc. Am. Bull., 102: 1280–1296.

Irvine, T. N., and Baragar, W. R. A., 1971. A guide to the chemical classification of the common volcanic rocks. Canad. J. Earth Sci., 8: 523–548.

Irving, A. J., 1980. Petrology and geochemistry of composite ultramafic xenoliths in alkalic basalts and implications for magmatic processes within the mantle. Am. J. Sci., 280A: 329–426.

Jaksha, L. H., and Sanford, A. R., 1986. Earthquakes near Albuquerque, New Mexico, 1976-1981. J. Geophys. Res., 91: 6293–6303.

James, D. E., Padovani, E. R., and Hart, S. R., 1980. Preliminary results on the oxygen isotope composition of the lower crust, Kilbourne Hole maar, New Mexico. Geophys. Res. Lett.: 321–324.

Jiracek, G. R., Ander, M. E., and Holcombe, H. T., 1979. Magneto-telluric soundings of crustal conductive zones in major continental rifts. In: R. E. Riecker (Editor), Rio Grande Rift: Tectonics and Magmatism, Am. Geophys. Union, Spec. Publ., 209–222.

Jiracek, G. R., Gustafson, E., and Mitchell, P. S., 1983. Magneto-telluric results opposing magma origin of crustal conductors in the Rio Grande rift. Tectonophysics, 94: 299–326.

Jiracek, G. R., Rodi, W. L., and Vanyan, L. L., 1987. Implications of magnetotelluric modeling for the deep crustal environment in the Rio Grande rift. Phys. Earth Planet. Int., 45: 179–192.

Jiracek, G. R., Kinn, C. L., Scott, C. L., Curran, S. A., Kuykendall, M. G., 1993. Magnetotelluric mapping of upper crustal isotherms beneath the Valles caldera hydrothermal system. Eos, Trans. Am. Geophys. Union, 74 (Suppl.): 229.

Johnson, C. M., and Lipman, P. W., 1988. Origin of metaluminous and alkaline volcanic rocks of the Latir volcanic field, northern Rio Grande rift, New Mexico. Contrib. Mineral. Petrol., 100: 107–128.

Johnson, C. M., Czamanske, G. K., and Lipman, P. W., 1989. Geochemistry of intrusive rocks associated with the Latir volcanic field, New Mexico, and contrasts between evolution of plutonic and volcanic rocks. Contrib. Mineral. Petrol., 103: 990–109.

Johnson, C. M., Lipman, P. W., and Czamanske, G. K., 1990. H, O, Sr, Nd, and Pb isotope geochemistry of the Latir volcanic field and cogenetic intrusions, New Mexico, and relations between evolution of a continental magmatic center and modifications of the lithosphere. Contrib. Mineral. Petrol., 104: 99–124.

Heywood, C. E., 1992. Isostatic residual gravity anomalies of New Mexico. U.S. Geol. Survey Water Resources Investigation Report 91–4065, 27 pp.

Kautz, P. F., Ingersoll, R. V., Baldridge, W. S., Damon, P. E., and Shafiqullah, M., 1981. Geology of the Espinaso Formation (Oligocene), north-central New Mexico. Geol. Soc. Am. Bull., 92, Part I: 980–983; Part II: 2318–2400.

Keller, G. R., 1986. Introduction to special section on the Rio Grande rift. J. Geophys Res., 91: 6142.

Keller, G. R. and Cordell, L., 1984. Bouguer gravity anomaly map of New Mexico. Nat. Ocean. Atmos. Admin., Nat. Geophys. Data Center Map, 1:500,000.

Keller, G. R., and Cather, S. M. (Editors), 1994, Basins of the Rio Grande rift: Structure, stratigraphy, and tectonic setting. Geol. Soc. Am., Special Paper 291, 308 p.

Keller, G. R., Braile, L. W., and Schlue, J. W., 1979a. Regional crustal structure of the Rio Grande rift from surface wave dispersion measurements. In R. E. Riecker (Editor), Rio Grande Rift: Tectonics and Magmatism, Am. Geophys. Union, Spec. Publ.: 115–126.

Keller, G. R., Braile, L. W., and Morgan, P., 1979b. Crustal structure, geophysical models and contemporary tectonism of the Colorado Plateau. Tectonophysics, 61: 131–147.

Keller, G. R., Cordell, L., Davis, G. H., Peeples, W. J., and White, G., 1984. A geophysical study of the San Luis basin. N. M. Geol. Soc., Field Conf. Guideb., 35: 51–57.

Keller, G. R., Smith, R. A., Hinze, W. J., and Aiken, C. L. V., 1985. A regional gravity and magnetic study of west Texas. Soc. Explor. Geophys., Spec. Pub., Utility of Regional Gravity and Magnetic Anomaly Maps, pp. 198–212.

Keller, G. R., Seager, W. R., and Thompson, S. 1986. A seismic reflection study of part of the southern Jornada del Muerto. N. M. Geol. Soc., Field Conf. Guideb., 37: 139–142.

Keller, G. R., Morgan, P., and Seager, W. R., 1990. Crustal structure, gravity anomalies and heat flow in the southern Rio Grande rift and their relationship to extensional tectonics. Tectonophysics, 174: 21–37.

Keller, G. R., Khan, M. A., Morgan, P., Wendlandt, R. F., Baldridge, W. S., Olsen, K. H., Prodehl, C., and Braile, L. W., 1991. A comparative study of the Rio Grande and Kenya rifts. Tectonophysics, 197: 355–371.

Kelley, V. C., 1952. Tectonics of the Rio Grande depression of central New Mexico. N. M. Geol. Soc., Field Conf. Guideb., 3: 92–105.

Kelley, V. C, 1977. Geology of Albuquerque basin. N. M. Bur. Mines Miner. Res., Mem. 33, 59 pp.

Kelley, V. C., 1978. Geology of Espaola basin, New Mexico. N. M. Bur. Mines Miner. Res., Map 48 (1:125,000).

Kelley, V. C., 1979. Tectonics, middle Rio Grande rift, New Mexico. In: R. E. Riecker (Editor), Rio Grande rift: Tectonics and Magmatism. Am. Geophys. Union, Spec. Publ., pp. 57–70.

Kelley, V. C., 1982. The right-relayed Rio Grande rift, Taos to Hatch, New Mexico. N. M. Geol. Soc., Field Conf. Guideb., 33: 147–151.

Kelley, V. C., and Wood, G. H., 1946. Lucero uplift, Valencia, Socorro, and Bernalillo Counties, New Mexico. U.S. Geol. Surv. Oil and Gas Inves. Prelim. Map, 47.

Kelley, V. C., and Kudo, A. M., 1978. Volcanoes and related basalts of Albuquerque basin, New Mexico. N. M. Bur. Mines Miner. Res., Circ. 156, 30 pp.

Keshet, Y., and Hermance, J. F., 1986. A new regional electrical model for the southern section of the Rio Grande rift and the adjacent Basin and Range and Great Plains. J. Geophys. Res., 91: 6359–6366.

Kluth, C. F., and Coney, P. J., 1981. Plate tectonics of the Ancestral Rocky Mountains. Geology, 9: 10–15.

Kluth, C. F., and Schaftenaar, C. H., 1994. Depth and geometry of the northern Rio Grande rift in the San Luis basin, south-central Colorado. Geol. Soc. Am., Special Paper 291: 27–37.

Knopoff, L., and Schlue, J. W., 1972. Rayleigh wave phase velocities for the path Addis Ababa-Nairobi. Tectonophysics, 15: 157–163.

Larsen, S. C. Reilinger, R. E., and Brown, L., 1986. Evidence of ongoing crustal deformation related to magmatic activity near Socorro, New Mexico. J. Geophys. Res., 91: 6283–6292.

Laughlin, A. W., Brookins, D. G., Kudo, A. M., and Causey, J. D., 1971. Chemical and strontium isotopic investigations of ultramafic inclusions and basalt, Bandera Crater, New Mexico. Geochim. Cosmochim. Acta 35: 107–113.

Laughlin, A. W., Brookins, D. G., and Damon, P. E., 1976. Late Cenozoic basaltic volcanism along the Jemez zone of New Mexico and Arizona (abstr.). Geol. Soc. Am., Abstr. Prog. 8: 598.

Laughlin, A. W., Aldrich, M. J., Jr., Ander, M. E., Heiken, G. H., and Vaniman, D. T., 1982. Tectonic setting and history of late-Cenozoic volcanism in west-central New Mexico. N. M. Geol. Soc., Field Conf. Guideb. 33: 279–284.

Laughlin, A. W., Poths, J., Healey, H. A., Reneau, S., and WoldeGabriel, G., 1994. Dating of Quaternary basalts using the cosmogenic ^{3}He and ^{14}C methods with implications for excess ^{40}Ar. Geology, 22: 135–138.

Leat, P. T., Thompson, R. N., Morrison, M. A., Hendry, G. I., and Dickin, A. P., 1988. Compositionally-diverse Miocene-Recent rift-related magmatism in NW Colorado: Partial melting, and mixing of mafic magmas from 3 different mantle sources. In: M. A. Menzies and K. Cox (Editors), Oceanic and Continental Lithosphere. J. Petrol. Lithosphere Issue: 351–377.

Leat, P. T., Thompson, R. N., Dickin, A. P., Morrison, M. A., and Hendry, G. L., 1989. Quaternary volcanism in northwestern Colorado: Implications for the roles of asthenosphere and lithosphere in the genesis of continental basalts. J. Volcan. Geotherm. Res., 37: 291–310.

Leat, P. T., Thompson, R. N., Morrison, M. A., Hendry, G. L., and Dickin, A. P., 1990. Geochemistry of mafic lavas in the early Rio Grande rift, Yarmony Mountain, Colorado, U.S.A. Chem. Geol., 81: 23–43.

Leavy, B. D., 1987. Surface-exposure dating of young volcanic rocks using the in situ buildup of cosmogenic isotopes. Ph.D. Dissertation, N. M. Inst. Mining Tech., Socorro, New Mexico, 167 pp.

Lewis, C. J., and Baldridge, W. S., 1994. Crustal extension in the Rio Grande rift, New Mexico: Half-grabens, accommodation zones, and shoulder uplifts in the Ladron Peak–Sierra Lucero area. Geol. Soc. Am., Special Paper 291: 135–155.

Lipman, P. W., 1980. Cenozoic volcanism in the western United States: Implications for continental tectonics. In: Studies in Geophysics: Continental tectonics. Nat. Acad. Sci., Washington, D. C., pp. 161–174.

Lipman, P. W., 1981. Volcano-tectonic setting of Tertiary ore deposits, southern Rocky Mountains. In: W. R. Dickinson and W. D. Payne (Editors), Relations of Tectonics to Ore Deposits in the Southern Cordillera, Ariz. Geol. Soc. Digest, 14, 199–214.

Lipman, P. W., and Mehnert, H. H., 1975. Late Cenozoic basaltic volcanism and development of the Rio Grande depression in the southern Rocky Mountains. Geol. Soc. Am., Mem. 144: 119–154.

Lipman, P. W., and Mehnert, H. H., 1979. The Taos Plateau volcanic field, northern Rio Grande rift, New Mexico. In: R. E. Riecker (Editor), Rio Grande Rift: Tectonics and Magmatism, Am. Geophy. Union, Spec. Publ., pp. 289–311.

Lipman, P. W., Doe, B. R., Hedge, C. E., and Steven, T. A., 1978. Petrologic evolution of the San Juan volcanic field, southwestern colorado: Pb and Sr isotopic evidence. Geol. Soc. Am. Bull., 89: 59–82.

Lipman, P. W., Mehnert, H. H., and Naeser, C. W., 1986. Evolution of the Latir volcanic field, northern New Mexico, and its relation to the Rio Grande rift, as indicated by K-Ar and fission-track dating. J. Geophys. Res., 91: 6329–6346.

Lipman, P. W., Logatchev, N. A., Zorin, Y. A., Chapin, C. E., and Kovalenko, V., 1989. Intracontinental rift comparisons—Baikal and Rio Grande rift systems. Eos, Trans. Am. Geophys. Union, 70: 578–579, 586–588.

Livaccari, R. F., 1979. Late Cenozoic tectonic evolution of the western United States. Geology, 7: 72–75.

Lozinsky, R. P., 1988. Stratigraphy, sedimentology, and sand petrology of the Santa Fe Group and pre-Santa Fe Tertiary deposits in the Albuquerque basin, central New Mexico. Ph. D. Dissertation, N. M. Inst. Mining Tech., Socorro, N. M., 235 pp.

Lozinsky, R. P., 1989. Cenozoic basin-fill stratigraphy and depositional history of the Albuquerque basin, central New Mexico, N. M. Geol. Soc., Field Conf. Guideb., 40: 269–272.

Lucas, S. G., 1984. Correlation of Eocene rocks of the northern Rio Grande rift and adjacent areas: Implications for Laramide tectonics. N. M. Geol. Soc., Field Conf. Guideb. 35: 123–128.

Lutter, W.J., Roberts, P.M., Thurber, C.H., Steck, L., Fehler, M.C., Stafford, D.G., Baldridge, W.S., and Zeichert, T.A., 1995, Teleseismic-wave image of crust and upper mantle structure beneath the Valles caldera, New Mexico: Initial rersults from the 1993 JTEX passive array. Geophys. Res. Lett., 22: 505508.

Luedke, R. G., and Smith, R. L., 1978. Map showing distribution, composition and age of late Cenozoic volcanic centers in Arizona and New Mexico. U.S. Geol. Surv., Misc. Geol. Invest., Map I-1091-A.

MacDonald, G. A., and Katsura, T., 1964. Chemical compositon of Hawaiian lavas. J. Petrol., 5: 82–133.

Machette, M. N., 1986. History of Quaternary offset and paleoseismicity along the La Jencia fault, central Rio Grande rift, New Mexico. Bull. Seismol. Soc. Am., 76: 259–272.

Machette, M, N., 1987. Preliminary assessment of paleoseismicity at White Sands Missile Range, southern New Mexico: Evidence for recency of faulting, fault segmentation, and repeat intervals for major earthquakes in the region. U. S. Geol. Survey, Open-file Rep. 87–444, 46 pp.

Manley, K., 1976. The late Cenozoic history of the Espaola basin, New Mexico. Ph.D. Dissertation, U. Colo., Boulder, Colo., 171 pp.

Mattick, R. E., 1967. A seismic and gravity profile across the Hueco bolson, Texas. In: Geological Survey Research 1967, Chap. D: U. S. Geol. Surv., Prof. Paper, 575-D, p. D85–D91.

Mayo, E. B., 1958. Lineament tectonics and some ore districts of the Southwest, Am. Inst. Min. Eng. Trans., 10: 1169–1175.

McClay, K. R., and Ellis, P. G., 1987. Geometries of extensional fault systems developed in model experiments. Geology, 15: 341–344.

McIntosh, W. C., Chapin, C. E., Ratte, J. C., and Sutter, J. F., 1992. Time-stratigraphic framework for the Eocene-Ologocene Mogollon-Datil volcanic field, southwest New Mexico. Geol. Soc. Am. Bull., 104: 851–871.

McMillan, N. J., and Dungan, M. A., 1988. Open system magmatic evolution of the Taos Plateau volcanic field, northern New Mexico: 3. Petrology and geochemistry of andesite and dacite. J. Petrol. 29: 527–557.

McMillan, N. J., and Dickin, A. P., 1991. Magma production during tectonic transition: Development of the Rio Grande rift in S. NM, Eos, Trans. Am. Geophys. Union, 73 (Suppl., Oct. 29): 560–561.

Mitchell, P. S., 1983. Deep magnetotelluric profiling of the southern Albuquerque-Belen basin, New Mexico. M. S. Thesis, San Diego State University, San Diego, California.

Mitchell, P. S., and Jiracek, G. R., 1983. Magnetotelluric soundings along the COCORP seismic profile in the central Rio Grande rift. N. M. Geol. Soc., Field Conf. Guideb., 34: 133–136.

Moretti, I., and Froidevaux, C., 1986. Thermomechanical models of active rifting. Tectonics, 5: 501–511.

Morgan, P., and Golombek, M. P. 1984. Factors controlling the phases and styles of extension in the northern Rio Grande rift. N. M. Geol. Soc., Field Conf. Guideb., 35: 13–19.

Morgan, P., Seager, W. R., and Golombek, M. P., 1986. Cenozoic thermal, mechanical and tectonic evolution of the Rio grande rift. J. Geophys. Res., 91: 6263–6276.

Muehlberger, W. R., 1979. The Embudo fault between Pilar and Arroyo Hondo, New Mexico: An active intracontinental transform fault. N. M. Geol. Soc., Field Conf. Guideb., 30: 77–82.

Muehlberger, W. R., Belcher, R. C., and Goetz, L. K., 1978. Quaternary faulting in Trans-Pecos Texas. Geology, 6: 337–340.

Murdock, J. N., and Jaksha, L. H., 1981. The P wave velocity of the uppermost mantle of the Rio Grande rift region of north central New Mexico. J. Geophys. Res., 86: 7055–7063.

Murphy, B. P., 1991. Determination of shear wave velocity structure in the Rio Grande rift through receiver function and surface wave analysis. Ms. Thesis, University of Texas at El Paso, El Paso, Texas, 117 pp.

Nealey, L. D., 1989. Geology and petrology of the late Cenozoic Mount Baldy trachytic volcanic complex, White Mountains volcanic field, Apache and Navajo Counties, Arizona. Ph.D. Dissertation, Univ. N. Mex., Albuquerque, N. M., 320 pp.

Ni, J., Reilinger, R. E., and Brown, L. D., 1981. Vertical crustal movements in the vicinity of the 1931 Valentine, Texas, earthquake. Bull. Seismol. Soc. Am., 71: 857–864.

Olsen, K. H., Keller, G. R., Stewart, J.W., 1979. Crustal structure along the Rio Grande rift from seismic refraction profiles. In: R. Riecker (Editor), Rio Grande Rift: Tectonics and Magmatism, Am. Geophys. Union, Spec. Publ., pp. 127–143.

Olsen, K. H., Baldridge, W. S., and Callender, J. F., 1987. Rio Grande rift: An overview. Tectonophysics, 143: 119–139.

Ouchi, S., 1983. Effects of uplift on the Rio Grande over the Socorro magma body, New Mexico. N. M. Geol. Soc., Field Conf. Guideb., 34: 54–56.

Padovani, E. R., and Carter, J. L., 1977a. Aspects of the deep crustal evolution beneath south central New Mexico. In: J. G. Heacock, G. V. Keller, J. E. Oliver, and G. Simmons (Editors), The Earth's Crust. Am. Geophys.Union, Geophys. Mono. 20: 19–55.

Padovani, E. R., and Carter, J. L., 1977b. Granulite facies xenoliths from Kilbourne Hole maar, New Mexico, and their bearing on deep crustal evolution (abstr.). 2nd Int Kimb. Conf., Santa Fe, NM.

Pallister, J. S., 1989. Excursion 7A: From silicic calderas to mantle nodules: Cretaceous to Quaternary volcanism, southern Basin and Range province, Arizona and New Mexico. N. M. Bur. Mines Min. Res., Mem. 46: 121–185.

Parker, E. C., Davis, P. M., Evans, J. R., Iyer, H. M., and Olsen, K. H., 1984. Upwarp of anomalous asthenosphere beneath the Rio Grande rift. Nature, 312: 354–356.

Pedersen, J., 1980. A magnetotelluric investigation of the deep electrical structure of the Rio Grande rift and adjacent tectonic provinces. Ph.D Dissertation, Brown University, Providence, Rhode Island.

Pedersen, J., and Hermance, J. F., 1976. Towards resolving the absence or presence of an active magma chamber beneath the southern Rio Grande rift zone (abstr.), Eos, Trans. Am. Geophys Union, 57: 1014.

Pedersen, J., and Hermance, J. F., 1976.. Evidence for molten material at shallow to intermediate crustal levels beneath the Rio Grande rift at Santa Fe (abstr.), Eos, Trans. Am. Geophys. Union, 59:390.

Pedersen, J., and Hermance, J. F., 1981. Deep electrical structure of the Colorado Plateau as determined from magnetotelluric measurements. J. Geophys. Res., 86: 1849–1857.

Perry, F. V., Baldridge, W. S., and DePaolo, D. J., 1987. Role of asthenosphere and lithosphere in the genesis of late Cenozoic basaltic rocks from the Rio Grande rift and adjacent regions of the southwestern United States. J. Geophys. Res., 92: 9193–9213.

Perry, F. V., Baldridge, W. S., and DePaolo, D. J., 1988. Chemical and isotopic evidence for lithospheric thinning beneath the Rio Grande rift. Nature, 332: 432–434.

Perry, F. V., DePaolo, D. J., and Baldridge, W. S., 1993. Neodymium isotopic evidence for decreasing crustal contributions to Cenozoic ignimbrites of the western United States: Implications for the thermal evolution of the Cordilleran crust. Geol. Soc. Am. Bull., 105: 872–882.

Porath, H., and Gough, D. I., 1971. Mantle conductive structures in the Western United States from magnetometer array studies. Geophys. J. Royal Astr. Soc., 22: 261–275.

Price, J. G., Henry, C. D. Parker, D. F., and Barker, D. S., 1986. Igneous geology of Trans-Pecos Texas. Guideb. 23, Tex. Bur. Econ. Geology, 360 pp.

Ramberg, I. B., Cook, F. A., and Smithson, S. B., 1978. Structure of the Rio Grande rift in southern New Mexico and west Texas based on gravity interpretation. Geol. Soc. Am. Bull., 89: 107–123.

Reid, H. F., 1911. Remarkable earthquakes in central New Mexico in 1906 and 1907, Bull. Seismol. Soc. Am., 1: 10–16.

Reid, J. B., and Woods, G. A., 1978. Oceanic mantle beneath the southern Rio Grande rift. Earth Planet. Sci. Lett., 41: 303–317.

Reid, M., Hart, S. R., Padovani, E. R., Wandless, G. A., 1989. Contribution of pelitic sediments to the composition, heat production, and seismic velocity of the lower crust. Earth Planet. Sci. Lett., 95: 367–381.

Reilinger, R. E., and Oliver, J. E., 1976. Modern uplift associated with a proposed magma body in the vicinity of Socorro, New Mexico. Geology, 4: 583–586.

Reilinger, R. E., Oliver, J. E., Brown, L. D., Sanford, A. R., and Balazs, E. I., 1980. New Measurements of crustal doming over the Socorro magma body. Geology, 8: 291–295.

Reiter, M., and Tovar, J. C., 1982. Estimates of terrestrial heat flow in northern Chihuahua, Mexico, based on petroleum bottom hole temperatures. Geol. Soc. Am. Bull., 93: 613–624.

Reiter, M., Edwards, C. L., Hartman, H., and Weidman, C., 1975. Terrestrial heat flow along the Rio Grande rift, New Mexico and southern Colorado. Geol. Soc. Am. Bull., 86: 811–818.

Reiter, M., Shearer, C., and Edwards, C. L., 1978. Geothermal anomalies along the Rio Grande rift in New Mexico. Geol., 6: 85–88.

Reiter, M., Mansure, A. J., and Shearer, C., 1979. Geothermal characteristics of the Rio Grande rift within the southern Rocky Mountains complex 1979. In: R. E. Riecker (Editor), Rio Grande Rift: Tectonics and Magmatism, Am. Geophys. Union, Spec. Pub., pp. 253–267.

Reiter, M., Eggleston, R. E., Broadwell, B. R., and Minier, J., 1986. Terrestrial heat flow estimates from deep petroleum tests along the Rio Grande rift in central and southern New Mexico. J. Geophys. Res., 91: 6225–6245.

Renault, J., 1970. Major-element variations in the Potrillo, Carrizozo, and McCartys basalt fields, New Mexico. N. M. Bur. Mines Miner. Res., Circ. 113, 20 pp.

Riecker, R. E. (Editor), 1979, Rio Grande rift: Tectonics and Magmatism, Am. Geophys. Union, Spec. Publ., 438 p.

Rinehart, E. J., Sanford, A. R., and Ward, R. M., 1979. Geographic extent and shape of an extensive magma body at midcrustal depths in the Rio Grande rift near Socorro, New Mexico. In: R. E. Riecker (Editor), Rio Grande Rift: Tectonics and Magmatism, Am. Geophys. Union, Spec. Pub., pp. 237–251.

Roberts, D. G., Adams, D. C., and Keller, G. R., 1991. A geophysical analysis of crustal structure in the Ruidoso area. N. M. Geol. Soc., Field Conf. Guideb., 42: 191–197.

Roden, M.F., Irving, A. J., and Murthy, V. R., 1988. Isotopic and trace element composition of the upper mantle beneath a young continental rift: Results from Kilbourne Hole, New Mexico. Geochim. Cosmochim. Acta, 52: 461–473.

Rodriguez, J. C., 1987. Two-dimensional magnetotelluric interpretation of the eastern portion of the Española basin, New Mexico, U. S. A. M.S. Thesis, Centro de Investigacion Cientifica y de Educacion Superior de Ensenada, Mexico.

Rosendahl, B. R., 1987. Architecture of continental rifts with special reference to East Africa. Annu. Rev. Earth Planet. Sci., 15: 445–503.

Russell, L. R., and Snelson, S., 1990. Structural style and tectonic evolution of the Albuquerque basin segment of the Rio Grande rift. In: B. Pinet and C. Bois (Editors), The Potential of Deep Seismic Profiling for Hydrocarbon Exploration, Editions Technip, Paris, 175–207.

Russell, L. R., and Snelson, S., 1994. Structure and tectonics of the Albuquerque basin segment of the Rio Grande rift: Insights from reflection seismic data. Geol. Soc. Am., Special Paper 291: 83–112.

Salyards, S. L., Anderson, S., Ni, J., and Aldrich, M. J., 1991. Detailed paleomagnetic sampling and implications for block-size and rotational mechanics in an extending and rotating environment, Espaola basin, New Mexico. Eos, Trans. Am. Geophys. Union, Suppl. Oct. 29: 126.

Sanford, A. R., Budding, A. J., Hoffman, J. P., Alptekin, O. S., Rush, C. A., and Toppozada, T. R., 1972. Seismicity of the Rio Grande rift in New Mexico. N. M. Bur. Mines Miner. Res., Circ. 120.

Sanford, A. R., Alpetkin, O. S., Toppozada, T. R., 1973. Use of reflection phases on microearthquake seismograms to map an unusual discontinuity beneath the Rio Grande rift. Bull. Seismol. Soc. Am., 63: 2021–2034.

Sanford, A. R., Mott, R. P., Schuleski, P. J., Rinehart, E., Caravella, F. J., Ward, R. M., and Wallace, T. C., 1977. Geophysical evidence for a magma body in the crust in the vicinity of Socorro, New Mexico. In: J. G. Heacock (Editor), The Earth's Crust: Its Nature and Physical Properties. Am. Geophys. Union, Geophys. Monograph 20, pp. 385–403.

Sanford, A. R., Mott, R. P., Jr., Shuleski, P. J., Rinehart, E. J., Caravella, F. J., Ward, R. M., and Wallace, T. C., 1979. Geophysical evidence for a magma body in the crust in the vicinity of Socorro, New Mexico. In: R. E. Riecker (Editor), Rio Grande Rift: Tectonics and Magmatism. Am. Geophys. Union, Spec. Publ., pp. 385–403.

Sanford, A. R., Jaksha, L. H., and Cash, D. J., 1991. Seismicity of the Rio Grande rift in New Mexico. In: D. B. Slemmons, E. R. Engdahl, M. D. Zoback, and D. D. Blackwell (Editors), Neotectonics of North America, Decade Map Vol. 1, Geol. Soc. Am., Boulder, Colo., pp. 229–244.

Sass, J. H., Blackwell, D. D., Chapman, D. S., Costain, T. K., Decker, E. R., Lawver, L. W., and Swanberg, C. A., 1981. Heat flow from the crust of the United States. In: Y. S. Touloukian, W. R., Judd, and R. F. Roy (Editors), Physical Properties of Rocks and Minerals, McGraw-Hill, New York: 503–508.

Savage, J. C., Lisowski, M., Prescott, W. H., and Sanford, A. R., 1980. Geodetic measurements of horizontal deformation across the Rio Grande rift near Socorro, New Mexico. J. Geophys. Res., 85: 7215–7220.

Sbar, M. L., and DuBois, S. M., 1984. Attenuation of intensity for the 1887 northern Sonora, Mexico, earthquake. Bull. Seismol. Soc. Am., 74: 2613–2678.

Schlue, J. W., Singer, P. J., and Edwards, C. L., 1986. Shear wave structure of the upper crust of the Albuquerque-Belen basin from Rayleigh wave phase velocities. J. Geophys. Res., 91: 6277–6281.

Schmucker, U. 1964. Anomalies of geomagnetic variations in the southwestern United States. J. Geomagn. Geoelect., 15: 193–221.

Schmucker, U., 1970. Anomalies of geomagnetic variations in the south-western United States. Bull. Scripps Inst. Oceanogr., 13: 33–53.

Schneider, R. V., and Keller, G. R., 1994. Crustal structure of the western margin of the Rio Grande rift and Mogollon-Datil volcanic field, southwestern New Mexico and southeastern Arizona. Geol. Soc. Am., Special Paper 291: 207–226.

Scott, G. R., 1975. Cenozoic surfaces and deposits in the southern Rocky Mountains. In: B. M. Curtis (Editor), Cenozoic History of the Southern Rocky Mountains. Geol. Soc. Am., Mem., 144: 227–248.

Seager, W. R., and Morgan, P., 1979. Rio Grande rift in southern New Mexico, west Texas, and northern Chihuahua. In: R. E. Riecker (Editor), Rio Grande Rift: Tectonics and Magmatism, Am. Geophys. Union, Spec. Publ., pp. 87–106.

Seager, W. R., and Mack, G. H., 1986. Laramide paleotectonics in southern New Mexico. In: J. A. Peterson (Editor), Paleotectonics and Sedimentation in the Rocky Mountain Region. Am. Assoc. Pet. Geol., Mem., 41: 669–685.

Seager, W. R., Shafiqullah, M., Hawley, J. W., and Marvin, R. F., 1984. New K-Ar dates from basalts and the evolution of the southern Rio Grande rift. Geol. Soc. Am. Bull., 95: 87–99.

Shafiqullah, M. Damon, P. E., Lynch, D. J., Reynolds, S. J., Rehrig, W. A., and Raymond, R. H., 1980. K-Ar geochronology and geologic history of southwestern Arizona and adjacent areas, Ariz. Geol. Soc., Digest 12: 201–260.

Sinno, Y. A., and Keller, G. R., 1986. A Rayleigh Wave dispersion study between El Paso, Texas, and Albuquerque, New Mexico. J. Geophys. Res., 91: 6168–7174.

Sinno, Y. A., Daggett, P. H., Keller, G. R., Morgan, P., and Harder, S. H., 1986. Crustal structure of the southern Rio Grande rift determined from seismic refraction profiling. J. Geophys. Res., 91: 6143–6156.

Slack, P. D., Teleseismic investigations of the East African and Rio Grande rifts, University of California, Los Angeles, Ph.D. Dissertation, 1994.

Smith, D.L., and Jones, R. L., 1979. Thermal anomaly in northern Mexico: An extension of the Rio Grande rift? In: R. E. Riecker (Editor), Rio Grande Rift: Tectonics and Magmatism, Am. Geophys. Union, Spec. Pub., 269–278.

Snyder, W. S., Dickinson, W. R., and Silberman, M. L., 1976. Tectonic implications of space-time patterns of Cenozoic magmatism in the western United States, Earth Planet. Sci. Lett., 32: 91–106.

Spence, W., and Gross, R. S., 1990. A tomographic glimpse of the upper mantle source of magmas of the Jemez lineament, New Mexico. J. Geophys. Res., 98: 10,829–10,849.

Spohn, T., and Schubert, G., 1983. Convective thinning of the lithosphere: A mechanism for rifting and mid-plate volcanism on earth, venus, and mars. Tectonophysics, 94: 67–90.

Stearns, C. E., 1943. The Galisteo Formation of north-central New Mexico, J. Geology, 51: 301–319.

Stearns, C. E., 1953a. Tertiary geology of the Galisteo-Tonque area, New Mexico. Geol. Soc. Am. Bull., 64: 459–508.

Stearns, C. E., 1953b. Upper Cretaceous rocks of Galisteo-Tonque area, north-central New Mexico. Am. Assoc. Petrol. Geol., 37: 961–974.

Stearns, C. E., 1953c. Early Tertiary vulcanism in the Galisteo-Tonque area, north-central New Mexico. Am. J. Sci., 251: 415–452.

Steiner, M. B., 1988. Paleomagnetism of the late Pennsylvanian and Permian: A test of the rotation of the Colorado Plateau. J. Geophys. Res. 93: 2201–2215.

Steinpress, M. G., 1981. Neogene stratigraphy and structure of the Dixon area, Espaola basin, north-central New Mexico: Summary. Geol. Soc. Am. Bull., 92: 2553–2671.

Steven, T. A., 1975. Middle Tertiary volcanic field in the southern Rocky Mountains, Geol. Soc. Am., Mem., 144: 75–94.

Stewart, S. W., and Pakiser, L. C., 1962. Crustal structure in eastern New Mexico from the GNOME explosion. Bull. Seismol. Soc. Am., 52: 1017–1030.

Suppe, J., Powell, C., and Berry, R., 1975. Regional topography, seismicity, Quaternary volcanism and the present-day tectonics of the western United States. Am. J. Sci., 275a: 397–436.

Swanberg, C. A., 1979, Chemistry of thermal and non-thermal groundwaters in the Rio Grande rift and adjacent tectonic provinces. In: R. E. Riecker (Editor), Rio Grande Rift: Tectonics and Magmatism, Am. Geophys. Union, Spec. Pub., pp. 279–288.

Swift, C. M., Jr., 1967. A magnetotelluric investigation of an electrical conductivity anomaly in the southwestern United States, Ph. D Dissertation, Mass. Inst. Tech., Cambridge, Mass.

Taylor, B., 1981. Heat flow studies and geothermal exploration in western Trans-Pecos Texas. Ph.D. Dissertation, University of Texas at El Paso, El, Paso, Texas, 326. pp.

Thompson, G. A., and Zoback, M. L., 1979. Regional geophysics of the Colorado Plateau. Tectonophysics 61: 149–181.

Toppozada, T. R., and Sanford, A. R., 1976. Crustal structure in central New Mexico interpreted from the Gasbuggy explosion. Bull. Seismol. Soc. Am., 66: 877–886.

Towle, J. N., 1980. New evidence for magmatic intrusion beneath the Rio Grande rift, New Mexico. Geol. Soc. Am. Bull., 91, Part I: 626–630.

Tweto, O., 1978. Tectonic map of the Rio Grande rift system in Colorado. In: J. W. Hawley (Editor), Guidebook to Rio Grande Rift in New Mexico and Colorado, N. M. Bur. Mines Miner. Res. Circ. 163, Sheet 1.

Vernon, J. H., and Riecker, R. E., 1989. Significant Cenozoic faulting, east margin of the Espaola basin, Rio Grande rift, New Mexico. Geology, 17: 230–233.

Wachs, D., Harrington, C. D., Gardner, J. N., and Maasen, L. W., 1988. Evidence of young fault movements on the Pajarito fault system in the area of Los Alamos, New Mexico. Los Alamos Nat. Lab. Rep. LA-11156-MS, 23 pp.

Wandless, G. A., Padovani, E. R., 1985. Trace element geochemistry of lower crustal xenoliths from Kilbourne Hole maar, New Mexico, Eos, Trans. Am. Geophys. Union, 66, p. 1110.

Waresback, D. B., and Turbeville, B. N., 1990. Evolution of a Plio-Pleistocene volcanogenic-alluvial fan: The Puye Formation, Jemez Mountains, New Mexico. Geol. Soc. Am. Bull., 102: 298–314.

Warren, R. G., Kudo, A. M., and Keil, K., 1979. Geochemistry of lithic and single-crystal inclusions in basalt and a characterization of the upper mantle-lower crust in the Engle basin, Rio Grande rift, New Mexico. In: R. E. Riecker (Editor), Rio Grande Rift: Tectonics and Magmatism. Am. Geophys. Union, Spec. Publ., pp. 393–415.

Weidelt, P., 1975. Inversion of two-dimensional conductivity structures. Phys. Earth Planet. Int., 10: 282–291.

Wen, C.L., 1983. A study of bolson fill thickness in the southern Rio Grande rift, southern New Mexico, west Texas and Chihuahua. M.S. Thesis. University of Texas, El Paso, Texas, 74 pp.

Wendlandt, E., 1992. Isotopic and geochemical studies of continental lithosphere in cratons and active rifts: Xenoliths from the Colorado Plateau and Rio Grande rift regions, Ph.D. Dissertation, University of California, Los Angeles, California, 217 pp.

Wendlandt, E., DePaolo, D. J., and Baldridge, W. S., 1993. Nd and Sr isotopic chronostratigraphy of Colorado Plateau lithosphere: Implications for magmatic and tectonic underplating of the continental crust. Earth Planet. Sci. Lett., 116: 23–43.

Wernicke, B., 1985. Uniform-sense normal simple shear of the continental lithosphere. Can. J. Earth Sci., 22: 108–125.

Wilt, M. J., Lattanner, A., and Meidav, T., 1976. A magnetotelluric-telluric profile survey of the Valles caldera prospect, Sandoval County, New Mexico. Geonics, Inc., Project Rep. 76.118 to Union Oil Co.

Woodward, L. A., and DuChene, H. R., 1975. Geometry of Sierrita fault and its bearing on tectonic development of the Rio Grande rift, New Mexico. Geology, 3: 114–116.

Woodward, L.A., J.F. Callender, and R. E. Zilinski, 1975. Tectonic map of the Rio Grande rift. N. M. Geol. Soc., Map MC-11.

Woodward, L. A., Callender, J. F., Seager, W. R., Chapin, C. E., Gries, J. C., Shaffer, W. L., and Zilinski, R. E., 1978. Tectonic map of Rio Grande rift region in New Mexico, Chihuahua, and Texas. In: J. W. Hawley (Editor), Guidebook to Rio Grande rift in New Mexico and Colorado, N. M. Bur. Mines Miner. Res., Circ. 163, Sheet 2.

Wolf, L. W., and Cipar, J. J., 1993. Through thick and thin: A new model for the Colorado Plateau from seismic refraction data from Pacific to Arizona Crustal Experiment. J. Geophys. Res., 98: 19,881–19,894.

Wright, H. E., Jr., 1946. Tertiary and Quaternary geology of the lower Rio Puerco area, New Mexico. Geol. Soc. Am. Bull., 57: 383–456.

Wu, Z., 1986. Shallow structure of the southern Albuquerque basin (Rio Grande rift), New Mexico, from COCORP seismic reflection data. In: M. Barazangi and L. Brown (Editors), Reflection Seismology: A Global Perspective, Am. Geophys. Union, Geodynamics Series, 14, pp. 293–304.

Yoder, H. S., and Tilley, C. E., 1962. Origin of basaltic magmas: An experimental study of natural and synthetic rock systems. J. Petrol., 3: 342–532.

Zietz, I., and Kirby, J. R., 1972a. Aeromagnetic map of Colorado. U. S. Geol. Surv., Geophys. Invest. Map GP-836, 1:500,000.

Zietz, I., and Kirby, J. R., 1972b. Aeromagnetic map of Colorado. U.S. Geol. Surv., Geophys. Invest. Map GP-880, 1:1,000,000.

Zoback, M. L., and Thompson, G. A., 1978. Basin and Range rifting in northern Nevada: Clues from a mid-Miocene rift and its subsequent offsets. Geology, 6: 111–116.

Zoback, M. L., and Zoback, M. D., 1980. State of stress in the conterminus United States. J. Geophys. Res., 85: 6113–6156.

Zoback, M. L., Anderson, R. E., and Thompson, G. A., 1981. Cainozoic evolution of the state of stress and style of tectonism of the Basin and Range province of the western United States. Phil. Trans Royal Soc. London, 300: 401–434.

This Page Intentionally Left Blank

Chapter 7

The Basin and Range Province

T. Parsons

7.1. Introduction

The Basin and Range province is a broad, highly extended terrane embedded within the North American western Cordillera that extends from Canada, through the western United States, and across much of Mexico. The province roughly occupies the space between the Cascade Ranges and Rocky Mountains in the north and the Sierra Nevada and the Colorado Plateau in the middle, and it engulfs the Sierra Madre Occidental Range in northern Mexico (Fig. 7–1). Seismicity, high heat flow, and recent basaltic volcanism indicate that the Basin and Range province is actively extending. Its descriptive name is derived from a particular (and most recent) mode of extensional block-faulting that left the characteristic pattern of alternating basins and ranges across the province (e.g., Gilbert, 1928). This pattern is especially prominent in the Great Basin, a region of internal drainage that occupies most of the northern Basin and Range province. Estimates of the total crustal extension across the Basin and Range province converge to between 50 and 100% (e.g., Hamilton and Myers, 1966; Zoback et al., 1981; Wernicke, 1992), though it is recognized that this extension is not uniformly distributed across the province, but instead occurs as extreme extension (100–300%) in some areas, and as minor extension (<10%) in others.

The Basin and Range is unlike most continental rifts because of the breadth of extended lithosphere there. At its widest points, the Basin and Range province is more than 900 km across, much wider than continental rifts such as the 100–300 km wide Rio Grande (Chapter 6) and East African (Chapter 5) rifts. Other broadly extended regions of crust are observed, but are usually found beneath sea level, as in the case of the extended crust beneath the North Sea, the Bering Strait, and the South China Sea, or beneath thick basinal sedimentary rocks. In contrast, the northern Basin and Range stands at an average 1.5 km above sea level. Much of the Basin and Range province lies within a rain shadow behind the Sierra Nevada and Cascade Ranges, and the resulting dearth of erosion and sedimentation has preserved excellent exposures of extended crust. Good exposures, combined with the enigmatic nature of actively extending continental crust residing at high elevations, has invited a great deal of study; as of 1992 more than 7200 papers and books have been written under a subject heading of "Basin and Range". An unfortunate sampling bias in many types of geologic and geophysical data towards the Basin and Range province north of the Mexico-United States border causes much of the focus of this chapter to be on the United States Basin and Range, where more is known. Exceptions to this are included where possible, such as the more comprehensive study of Mexican Basin and Range crustal and mantle xenoliths.

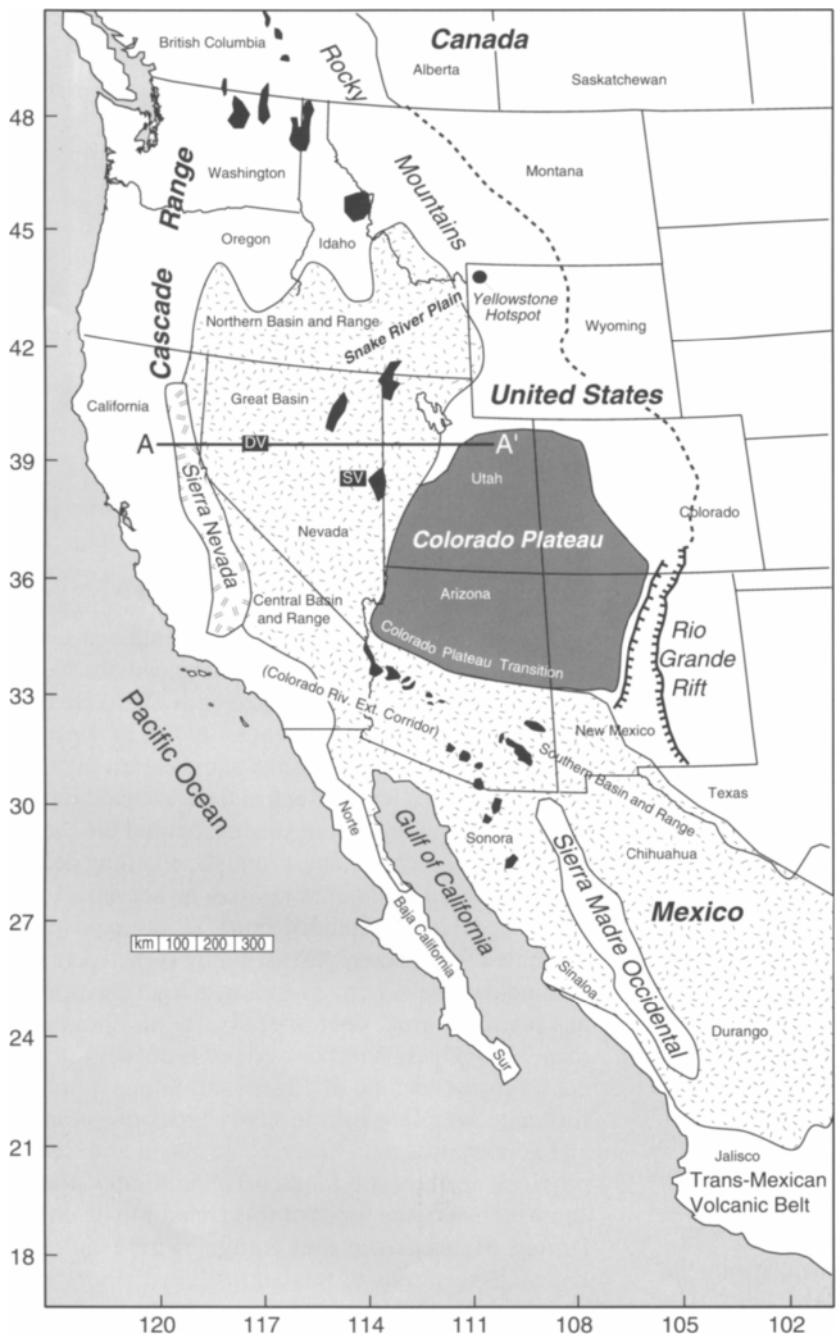

Fig. 7–1. Location of the Basin and Range province (stippled pattern) in relation to other tectonic elements of the North American western Cordillera. The Rio Grande Rift is treated as a separate entity in this study, though is often included as part of the Basin and Range in other regional studies. The black areas are regions of metamorphic core complexes (highly extended terranes; usually on apparent low-angle normal faults), and the patterned area marks the outline of the area traditionally known as the Basin and Range province because of the signature block-faulted topography. Note that a significant part of the Basin and Range area is found in Mexico. A to A' is the location of the cross section shown in Figure 7–15.

7.1.1. Tectonic Cycles in Western North America

Basin and Range extensional structure overprints a long history of tectonism that affected various parts of the western Cordillera (e.g., Conde, 1982). The region has been the locus of many cycles of extensional, compressional, and transform deformation. Late Proterozoic extension created a passive margin along western North America, opening a proto-Pacific basin. This stable continental margin may have persisted until late in the Ordovician Period, when island arcs began to form as a result of convergence and subduction. By Middle Devonian and Mississippian time, the Antler orogeny caused compressional deformation in western North America. By Permian time, back-arc extension caused the formation of linear basins west of the Antler orogenic belt. The Mesozoic Era brought changes in the North American plate drift direction, assembling island arcs together, and moving the trench westward. The Sonoma orogeny was active in the Great Basin, and the great thrust sheets of the Sevier fold and thrust belt that extend from Alaska to Mexico were formed as a result of subduction-generated compressional stresses. By Cretaceous time, an increase in plutonic and volcanic activity created batholiths like those that form the Sierra Nevada. An apparent flattening in the angle of subduction during Late Cretaceous time may have initiated the Laramide orogeny that involved cratonic basement rocks well inboard of the fold and thrust belt, and persisted into the Cenozoic Era, ending abruptly at about 40–50 Ma. "Basin and Range" has become an inclusive term that covers most of the extended crust found in the western Cordillera. A variety of extensional styles were active at various times during the Cenozoic Era, which left their marks across the region, and have come to define the extended province. In general, Cenozoic extensional tectonism is most widely observed in areas of pre-Cenozoic tectonic deformation (e.g., Wernicke, 1992). Middle Cenozoic to Quaternary transform deformation along the western continental margin is partly expressed within the Basin and Range province and links have been suggested between the two deformational patterns (e.g., Zoback et al., 1981; Pezzopane and Weldon, 1993).

7.1.2. Timing and Styles of Basin and Range Extension

The most current interpretation of the Basin and Range province classifies all extensional phases from Eocene time to present as "Basin and Range" extension (e.g., Wernicke, 1992). Two distinct extensional styles are commonly observed across the province: (1) an initial stage of isolated highly extended terranes such as metamorphic core complexes, (regions where mid-crustal rocks are exposed at the surface, exhumed by low-angle normal faults, uplift, and erosion), and (2) a second, later stage of higher-angled block faulting. Highly extended terranes were formed in British Columbia, Canada, and in Washington, Oregon, Idaho, and northern Nevada in the United States during Eocene time. Not all of the Eocene highly extended terranes can be classified as metamorphic core complexes, but they do tend to be localized areas of large-magnitude extension bounded by areas that were not as strongly extended (see Wernicke, 1992, and Axen et al., 1993, for detailed descriptions and locations of these terranes). During Oligocene time, highly extended terranes formed in the Great Basin of eastern Nevada on low-angle detachment faults that may have formed in a back, or intra-arc setting (e.g., Zoback et al., 1981), and clustered along the Proterozoic North American continental edge (e.g., Coney, 1980). Further south, in the southern Basin and Range, the earliest stages of extension began by latest Oligocene time in the southern parts of California and Arizona in the United States, and in Durango, Chihuahua, and Oaxaca, Mexico. By early Miocene time, strong extension had begun on major normal faults across much of Mexico (e.g., Henry and Aranda-Gomez, 1992), and metamorphic core complexes were forming along the Colorado River between California and Arizona (e.g., Howard and John, 1987) and along the southern edge of the Colorado Plateau in southern Arizona (e.g., Rehrig and Reynolds, 1980). A narrow zone of extension between the southern Sierra Nevada and southern Colorado Plateau, sometimes called the central Basin and Range (e.g., Jones et al., 1992; Wernicke, 1992), became active during late Oligocene to early Miocene time, and some of the latest forming metamorphic core complexes are

found in this zone (e.g., Wernicke et al., 1988; Axen et al., 1992). The middle Miocene brought the regionally broadest stage of extension to the northern and southern Basin and Range provinces at about 10 and 13 Ma, respectively (e.g., Zoback et al., 1981). This late stage of relatively small magnitude extension on steeply dipping normal faults caused the characteristic block-faulted basin-range structure that gives the province its name. Widespread block-faulting occurred across much of the western Great Basin and southern Arizona, and the opening of the Gulf of California accompanied normal faulting in Mexico at about 12–10 Ma (e.g., Stock and Hodges, 1989). Pliocene and Quaternary eruptions accompany incipient rifting in the Jalisco block that lies at the southern edge of the Sierra Madre Occidental in Mexico (Wallace at al., 1992) (Fig. 7–1), possibly indicating that the Basin and Range province is growing to the south. Large-magnitude earthquakes shake the Basin and Range province occasionally, and are distributed along its entire length, indicating that extension is widespread and ongoing.

7.2. Significance of the Basin and Range Province in reference to worldwide rifting

Two important questions about the Basin and Range province are: why is so much of the province so high, and why is it so wide? Extension generally leads to isostatic subsidence, yet the northern Basin and Range is a high plateau. Moreover, as can be seen from examination of this book, the vast majority of continental rifts are narrow features, and usually form as one or two chains of elongate basins. The Basin and Range province is made up of hundreds of basins of varying depth, age, and orientation that stretch across several hundred km. The origin of the extensional stresses that caused the straining of the Basin and Range is also subject to question, as is the partitioning of extensional strain. For example, why didn't a narrow rift develop into an ocean basin as a result of strong extensional stresses instead of broadly distributed strain? Does extension of orogenic lithosphere manifest itself differently from extension of cratonic lithosphere? A better understanding of the differences between the Basin and Range province and other continental rift zones may help to explain the conditions that lead to more typical rifting, as well as being important to studies of continental extension.

Internal differences in extensional style within the Basin and Range provide further problems as well as possible clues about the extensional process. For example, the northern part of the province stands one km higher in elevation on average than the southern part (Plate 7–1), even though the crustal thickness and composition are largely similar between the two sub-provinces. This difference is a probable indication of a strongly varying, regionally dependent mantle role in Basin and Range extension. The thickness of the crust is generally uniform across the province despite highly variable surface extension. However, the crust is thinner than adjoining unextended provinces like the Colorado Plateau, Rocky Mountains, and the Sierra Nevada, an indication that crustal pure shear does occur, but on a much broader scale than that of individual basins within the extended province. At an average 30 km thick, the 50–100% extended Basin and Range crust must have either started out thick (>45–60 km) (e.g., Hamilton, 1987), or its thickness was inflated during extension by magmatism and/or lower-crustal flow from outside the province. Magmatism is ubiquitous in Basin and Range extension, and the different patterns of Cenozoic volcanism in the Basin and Range province allow for the cataloging and assessment of the tectonic role of magmatic input into extending lithosphere. Identification of apparent low-angle normal faults in the Basin and Range, whose formation seems to have been confined to particular time intervals in different parts of the province, continues to cause controversy as to whether those faults formed at low angles, or evolved into that orientation. The upper-crustal response to extensional stress changed significantly to more numerous, higher-angle faults during the latest stage of extension. The reasons for this change remain unknown, though many ideas abound. In this chapter I attempt to summarize the current state of knowledge about the Basin and Range province, as well as models for its behavior.

7.3. Geologic Observations

7.3.1. Topography

At an average 1.5 km above sea level, the northern Basin and Range province is unusually elevated for a highly extended province. In general, lithospheric thinning leads to isostatic subsidence, since the buoyant crustal layer is thinned (e.g., Lachenbruch and Morgan, 1990). The southern Basin and Range behaves more typically, and is on average 1 km lower in elevation, with some isolated localities below sea level. The complex tectonism associated with the formation of the continental margin, and later subduction-related orogenies created many inherited topographic features still resolvable in the Basin and Range. The Proterozoic rift that created the western North American continental margin left a thick sequence of sedimentary rocks still present in the eastern Great Basin (e.g., Stewart and Poole, 1974). The Devonian to Mississippian Antler orogeny left an apparent structural division that bisects the northern Basin and Range province into two roughly symmetric sub-provinces (e.g., Eaton et al., 1978). The Sevier fold and thrust belt marks the eastern extent of the Great Basin, but is not observed in the southern Basin and Range. Laramide deformation apparently occurred mostly east of the present-day Basin and Range province, though Laramide structures may be masked by Basin and Range extension (e.g., Dickinson and Snyder, 1979).

Pervasive extension-related topographic variation within the Basin and Range are present at many different scales. The stage of block-fault extension that began in the middle Miocene left behind a series of alternating ranges spaced an average 25–35 km apart, with basins about 10–20 km wide in-between. The typical length-to-width ratio of the ranges is about 4:1 up to 8:1 (Zoback et al., 1981). These basin-range pairs are most pronounced in the Great Basin, but similar structural trends are observed in the southern Basin and Range as well (Fig. 7–2), with the pattern extending across much of Mexico. Block faulted topography overprints the earlier phases of low-angle faulted, domed uplift of mid-crustal rocks (metamorphic core complexes; outlined on Figure 7–1). The eastern Snake River Plain cuts a low topographic swath across the northern Basin and Range (Figs. 7–1,7–2), and marks the track of the Yellowstone hotspot (e.g., Morgan, 1972; Armstrong et al., 1975, Pierce and Morgan, 1992) (Fig. 7–2). Surrounding the low topography of the Snake River Plain is a rugged, actively extending part of the northern Basin and Range province that may be strongly influenced by the Yellowstone hotspot (e.g., Anders and Sleep, 1992; Pierce and Morgan, 1992) (Fig. 7–2). There is a fairly abrupt topographic step between the elevated northern Basin and Range, and lower southern Basin and Range that is located in southern Nevada—approximately between the southern end of the Sierra Nevada and southern Colorado Plateau (Plate 7–1, Fig. 7–2). Like most rifts, much of the Basin and Range province is bounded by high-standing margins, the Sierra Nevada on the west flank, and the Rocky Mountains and Colorado Plateau on the east flank. Seismicity along the margins of the Basin and Range indicates that the rift-flanks may still be rising. The reader is directed to the summary of Mayer (1986) for more detailed discussion of Basin and Range topographic variation.

7.3.2. Sedimentary Record – Two Example Basins

Because of the large number and diverse nature of the basins in the Basin and Range province, the complete sedimentary history of the Basin and Range is beyond the scope of this review. Thus I choose two structurally different, characteristic styles of basin to discuss briefly here; the Spring Valley in eastern Nevada ("SV" on Figure 7–1), which formed during Oligocene time and is associated with the formation of the Snake Range metamorphic core complex, and Dixie Valley in western Nevada ("DV" on Figure 7–1), which formed during later stage middle Miocene high-angle normal faulting. The following summary of Spring Valley is based on studies by Miller et al., (1983), Bartley and Wernicke (1984), Gans et al., (1985), and McCarthy (1986). Spring Valley is located within the Mesozoic Sevier orogenic zone in eastern Nevada, but the Paleozoic section was locally only mildly deformed prior to Tertiary extension. Oligocene normal displacement on the low-angle Snake Range decollement thinned

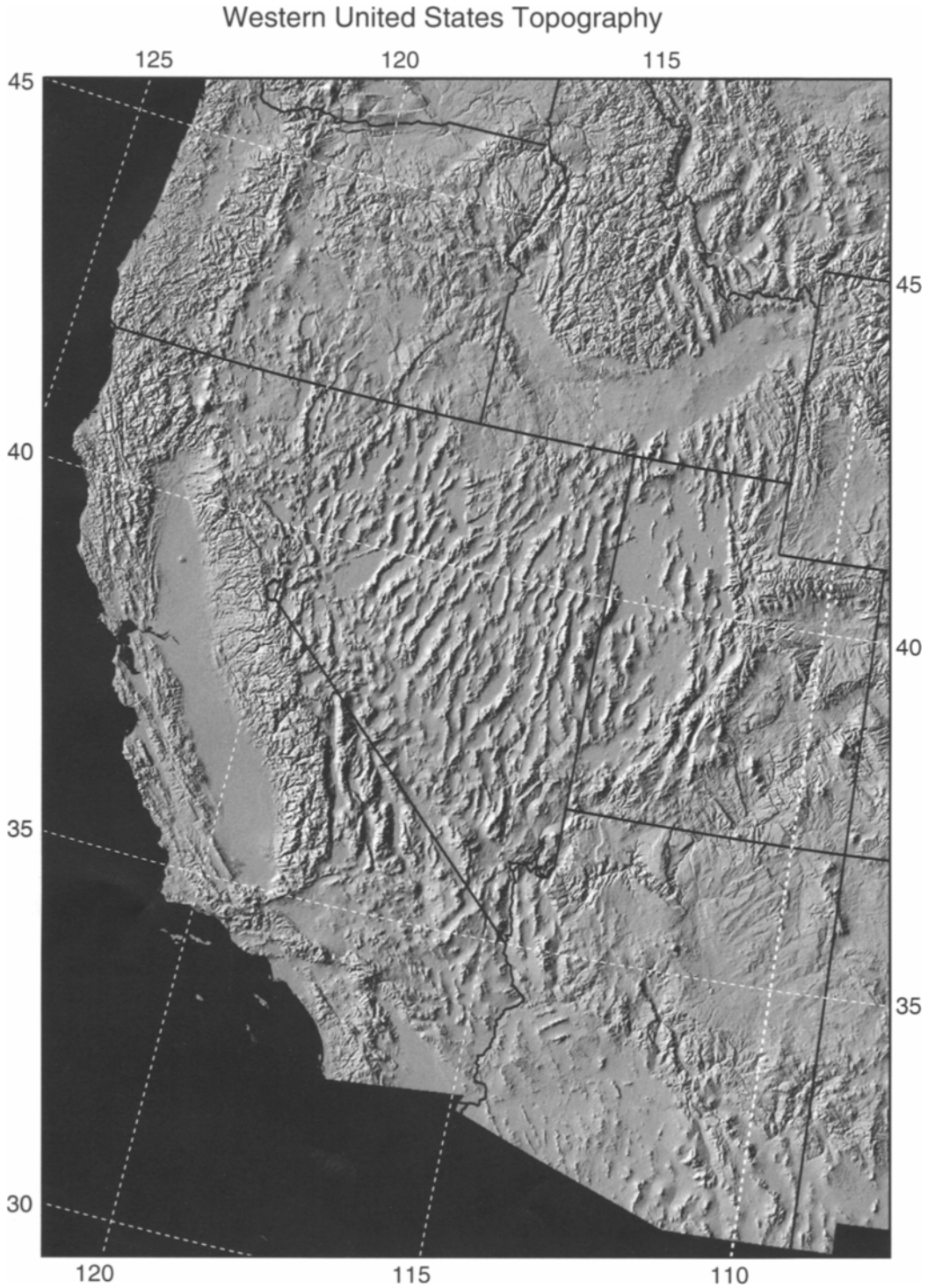
Western United States Topography
125
120
115
45
40
35
30
120
115
110
45
40
35

the Paleozoic section, opened the Spring Valley basin, and elevated Precambrian basement rocks that now core the Snake Range to the east. A well on the east side of the valley penetrated about 1650 m of Tertiary and Quaternary sedimentary rocks overlying 150 m of Paleozoic rocks separated from Precambrian quartzite by the detachment fault at about 1800 m depth. Either later-stage, higher angle normal faulting (Miller et al., 1983; Gans et al., 1985), or rotation of hanging wall blocks on higher angle normal faults that sole into a second detachment beneath the Snake Range decollement (Bartley and Wernicke, 1984), caused a deepening of the western Spring Valley, which contains 3–4 km of Tertiary and Quaternary sediments above a thicker 2 km sequence of Paleozoic rocks.

In contrast, Dixie Valley in western Nevada was formed during the later stage of extension in the Great Basin, when higher-angled block-faulting predominated. The following summary is based on studies by Speed (1976), Thompson and Burke (1973), and Okaya and Thompson (1985). Dixie Valley is an asymmetric, westward-thickening half graben that is controlled on its western side by a ~50° dipping (down to the east) normal fault. Alluvial fan deposits shed from the Stillwater Range fill the upper, western part of the valley, while the rest of the upper section is occupied by a 1-km-thick section of Tertiary lacustrine and playa deposits. Beneath those deposits lies a 500-m-thick section of Tertiary volcaniclastic rocks that rests on Mesozoic basement rocks. Gravity and seismic data show a 3-km total basin depth. Offsets in 12,000-year-old lake-shoreline markers constrain about 1 mm/yr of extension during that time interval, and offsets in an 8-m.y.-old basalt flow constrain a 0.4 mm/yr average extension rate during the past 8 m.y. Large normal-fault earthquakes have occurred as recently as 1954, and continuous microseismicity indicates that extension continues in Dixie Valley. Ongoing deformation has uplifted Tertiary and Quaternary sediments in many places. They preserve a record of the earliest interruption of through-going drainage by block-faulting and formation of basins (Stewart, 1980).

Fig. 7–2. Topography of western North America (Thelin and Pike, 1991) showing the distinctive patterns of block faulting that pervade both the northern and southern Basin and Range province. The eastern Snake River Plain can be seen clearly as a low topographic area in southern Idaho.

7.3.3. Igneous Activity

Synextensional magmatism is nearly always observed as a phase of any Basin-and-Range extensional system. The particular manifestation of magmatism is highly variable across the province: synextensional plutonism from silicic to mafic compositions, dike and sill intrusions of variable compositions, rhyolite and basalt flows, ash flow tuffs, cinder cones, and in some areas, flood basalts are seen as eruptive surface features. The exact relational timing of extensional faulting and associated magmatism is highly variable across the Basin and Range province, and can change with extensional style, timing, and locality. Taylor et al. (1989) found in a transect across the eastern Great Basin that only one of four distinct extensional faulting episodes correlated exactly with nearby volcanic activity, and Best and Christiansen (1991) concluded that extension during peak volcanism in the Great Basin was limited. In contrast, Gans et al. (1989) found cross-cutting relations in the eastern Great Basin indicating that voluminous magmatism slightly predated extension, compared those relations with other parts of the Basin and Range, and concluded that magmatism plays an active role in extension. A close association in space and time between magmatism and metamorphic core complex development has been noted (e.g., Coney, 1980; Glazner and Bartley, 1984; Ward, 1991; Axen et al., 1993). Virtually all examples of low-angle normal faulting within the Basin and Range province, as well as worldwide, have some form of lower-plate intrusive magmatism that can be related to the extensional episode that caused the faulting (Table 7–1). The ubiquitous association of magmatism with low-angle faulting and metamorphic core-complex development has led some authors to suggest a mechanical tie between the processes (e.g., Lister and Baldwin, 1993; Parsons and Thompson, 1993). Further discussion on the mechanics of low-angle normal faulting can be found in Section 7.5.1.

Table 7–1

Core Complex	Associated Lower-Plate Magmatism	Reference
Whipple Mountains- S. Calif.	Mid-Tertiary dike swarms and mafic plutons	(e.g., Davis et al., 1982)
Chemehuevi Mountains- S. Calif.	Mid-Tertiary dike swarms	(e.g., John, 1982)
Homer Mountain-Sacremento Mountains-S. Calif.	Mid-Tertiary dike swarms	(e.g., Spencer, 1985)
Castle Dome Mountains-S. Calif.	Mid-Tertiary dike swarms	(e.g., Logan and Hirsch, 1982)
Black Mountains - S. Calif.	Miocene mafic dikes and plutons	(e.g., Asmerom et al., 1990)
Eldorado Mountains- S. Calif.	Tertiary Mafic-silicic dikes and plutons	(e.g., Anderson, 1971)
Mopah Range - S. Calif.	Cross-cutting Tertiary mafic dikes/low-angle faults	(e.g., Hazlett, 1990)
Buckskin-Rawhide Mountains - Arizona	Tertiary mafic-silicic plutons	(e.g., Bryant and Wooden, 1989)
Santa Catalina-Rincon-Tortolita - Arizona	Mid-Tertiary granite plutons	(e.g., Kieth et al., 1980)
South Mountains - Central Arizona	Mafic and Silicic Mid-Tertiary dikes and plutons	(e.g., Reynolds and Rehrig, 1980)
Pinaleno-Santa Teresa Mountains - Arizona	Mid-Tertiary silicic dike swarms	(e.g., Rehrig and Reynolds, 1980)
Harcuvar Mountains - Arizona	Tertiary Pluton	(e.g., Rehrig and Reynolds, 1980)
Harquahala Mountains - Arizona	Mid-Tertiary silicic dikes and pluton	(e.g., Rehrig and Reynolds, 1980)
Mojave Mountians - W. Arizona	Upper plate (?) Mid-Tertiary mafic-silicic dike swarms	(e.g., Nakata, 1982)
Newberry-Dead Mountains- S. Nevada	Tertiary Mafic-Silicic dikes	(e.g., Simpson in prep.)
Ruby Range - NE Nevada	Mid-Tertiary deep structural granitic intrusions	(e.g., Wickham et al., 1993)
Snake Range - Nevada	Oligocene-Miocene Mafic dikes	(e.g., Lee et al., 1987)
Kettle - Okanogan Domes -E. Washington	Eocene Mafic dike swarms	(e.g., Holder et al., 1990)
Mykonos, Aegean Sea - Greece	Miocene dikes - plutons	(Lee and Lister, 1992)
Cyclades Islands, Aegean Sea - Greece	Coeval magmatism	(Lister et al., 1984)
D'Entrecasteaux Islands - Papua New Guinea	Granodiorite plutons coeval with low-angle detachment	(Hill et al., 1992)

Table 7-1. Compilation of metamorphic core complexes and observed mode and best timing constraints of magmatism in relation to low-angle faulting. Virtually all core complexes have some form of lower-plate intrusive magmatism associated with them.

Because of the huge volume of magmatic activity across the Basin and Range province, I focus here on the broad space-time patterns of magmatic activity that have swept across the province during Tertiary time. The following discussion is based primarily on reviews and studies by Coney and Reynolds (1977), Burke and McKee (1979), Lipman (1980), Zoback et al. (1981), Gans et al. (1989), Armstrong and Ward (1991), Henry and Aranda-Gomez (1992), Jones et al. (1992), and Axen et al. (1993). At the beginning of Tertiary time, magmatism occurred north and south of what is called the Laramide gap

(Fig. 7–3a), an interruption in arc-related magmatism that extended from the middle of Nevada and Utah to the United States-Mexico border, and initiated at about 80 Ma. This gap is thought to relate to low-angle subduction of the Farallon slab, which may have cooled the asthenospheric wedge where melt was generated (e.g., Dumitru et al., 1991), and minor volcanism was shifted eastward into the Rocky Mountains. The beginning of Tertiary time was also associated with the culmination in a decline of magmatic activity that began at 80 Ma. From 65 to 60 Ma, a rapid increase in activity swept through the region north of the Laramide gap, and the beginnings of Eocene extension in southwest Canada and the northwest United States brought increased magmatism between 60 and 55 Ma.

During Eocene time, a gradual southern sweep of extension-related magmatism worked its way from Idaho and Montana south into northern Nevada and Utah. These melts were typically of andesitic and rhyolitic compositions, and probably resulted from heavy contamination of mantle-derived basalts. South of the Laramide magmatic gap in Mexico, the volcanism that occurred during Eocene time was probably subduction-related. By late Eocene and early Oligocene time, a strong shift in extensional magmatic activity to the southern Great Basin occurred, centered in Nevada and Utah, and is referred to as the Great Basin ignimbrite flare-up (Fig. 7–3a). The Laramide gap persisted through Oligocene time, separating an episode of magmatism that swept westward across southeast California and southern Arizona. Independent centers of activity in southern Colorado and eastern Arizona were joined by magmatism associated with the opening of the Rio Grande rift (Fig. 7–3a).

The late Oligocene and early Miocene brought a northward sweep of core complex extension and magmatism from Mexico into the Colorado River extensional corridor, and a closing of the Laramide magmatic gap. The joining of the Nevada and Arizona magmatic centers was associated with a change from primarily intermediate composition melts into a primarily bimodal system predominated by basaltic eruptions. By middle Miocene time, basaltic volcanism dominated most of the active Basin and Range province from Mexico to northern Nevada. A westward shift in magmatic activity, correlated with incipient extension in the western Great Basin, occurred at this time, and a northeastward shift from southern Arizona across the southwest Colorado Plateau margin was also associated with the onset of extension there (Fig. 7–3b). During this period, magmatism appears to have moved into stable areas just prior to the onset of extensional faulting. The Yellowstone hotspot broke through in northern Nevada during middle Miocene time (~17–16 Ma), and created a series of northeast-younging caldera systems as the North American plate tracked over the plume. Extensive flood basalts followed the earlier stages of caldera formation; these basalts continue to erupt across much of the plume track (eastern Snake River plain, Idaho). Formation of the northern Nevada rift, a 500-km-long magmatic feature that extends south from eastern Oregon to southern Nevada, is thought to have resulted from dike injection from the Yellowstone plume (Zoback and Thompson, 1978); and it is possible that the Columbia Plateau flood basalt province is related to the Yellowstone plume as well. The extent to which the Yellowstone plume has affected the extensional magmatic patterns in the Basin and Range province (if at all) remains controversial, and will be further addressed in later sections. Magmatic activity from late Miocene time to the present has migrated away from the regions of strongest middle Miocene activity in central Nevada and southern Arizona, and has concentrated at the outer margins of the Basin and Range province (Fig. 7–3c).

7.3.4 Xenolith Studies

Xenoliths are found in the northern Basin and Range province in the eastern Snake River Plain in Idaho, and in the Great Basin at one locality in central Nevada. In the southern Basin and Range xenoliths are more abundant; localities include Mexico, southern California, and southern Arizona. On the eastern Snake River Plain, Archean lower-crustal xenoliths were brought to the surface by Quaternary basalts, possibly indicating that Archean crust underlies that region (Leeman et al., 1985). Menzies, in a 1989 study that includes xenoliths from central Nevada divides the western United States into mantle

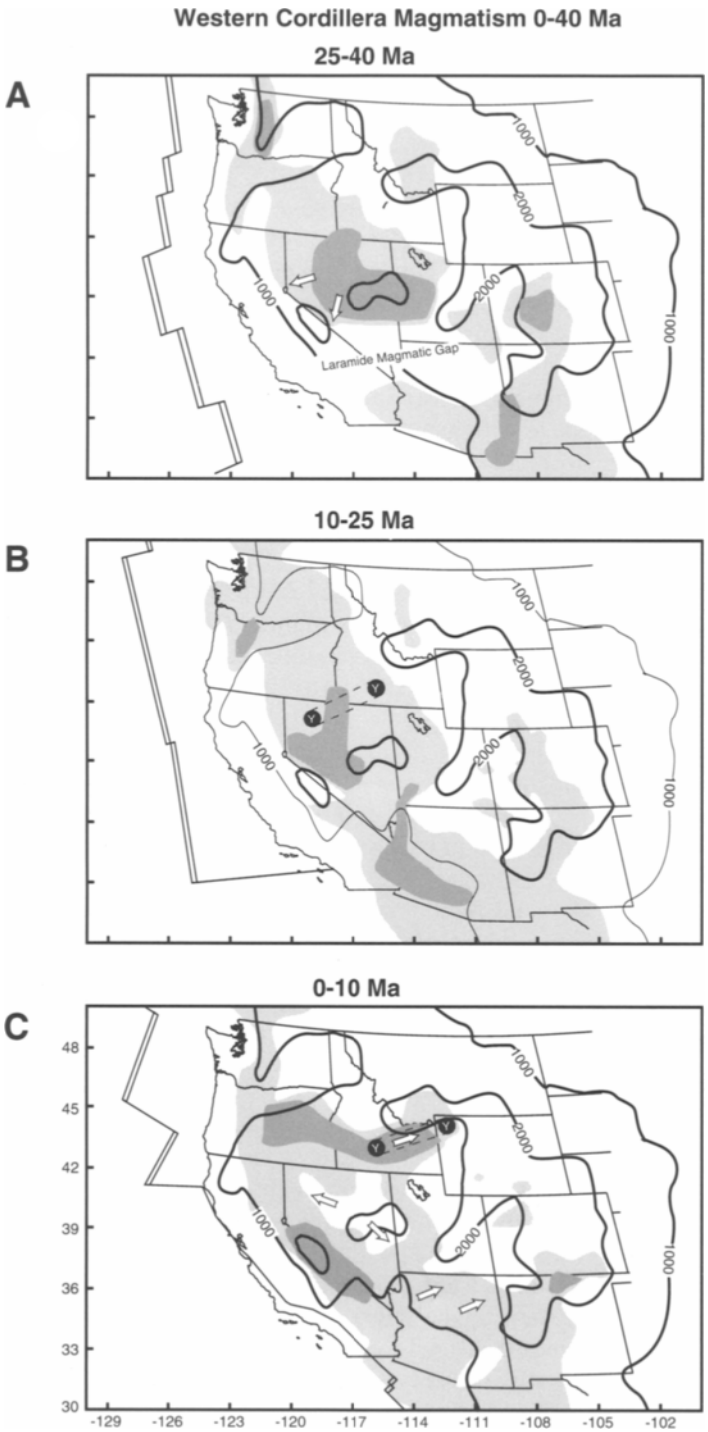

Fig. 7–3. Space-time patterns of magmatic activity in the western United States since Eocene time (after Armstrong and Ward, 1991). The darkest areas correspond to peak activity during the time interval. Large arrows on the continent show the approximate directions of magmatic migration during the time interval, and the smaller arrows show plate motion in the hotspot frame. The approximate locations and motion directions of the subducting Farallon plate are also shown. The inferred location of the Yellowstone plume is shown in windows (b) and (c). Details on the magmatic patterns are discussed in the text. Contour lines are smoothed topography in meters.

domains based on seismic tomography, heat flow, and xenolith thermobarometry. He places the Basin and Range province within an oceanic mantle domain, because of similarities of xenolith isotope-signature to mid-ocean and ocean-island basalts. Upper mantle and lower crustal xenoliths are found in southern California and southern Arizona in Tertiary volcanic rocks. The upper mantle xenoliths are lherzolites and harzburgites, and commonly show evidence for brittle deformation related to multiple stages of intrusive events in the upper mantle and also ductile deformation possibly related to tectonic extension (Wilshire, 1990; Wilshire et al., 1991). Composite xenoliths containing two or more rock types indicate that the crust-mantle boundary is very likely interlayered and has evolved through multiple stages of magmatic intrusion (Wilshire et al., 1991). Lower-crustal xenoliths are also found in southern California and Arizona and consist of mafic and ultramafic gabbros and microgabbros of intrusive origin, indicating that magmatic intrusion has also shaped the lower crust in the region as well as the upper mantle (Wilshire, 1990; McGuire, 1992).

Studies of xenoliths found in Mexico consistently report high-temperature granulite facies rocks from the lower crust and upper mantle beneath northern and central Mexico (Nimz et al., 1986; Ruiz et al., 1988; Hayob, et al., 1989; Roberts and Ruiz, 1989; Rudnick and Cameron, 1991). Upper mantle xenoliths are primarily spinel-lherzolites, and lower-crustal xenoliths are primarily granulites and banded gneisses. All the xenoliths are thought to originate from very near the crust-mantle boundary. Very high metamorphic temperatures up to 950–1100 °C (Hayob et al., 1989) are reported, and highly variable ages suggest that this metamorphism has occurred in many stages from 1.1 Ga to as young as 1 Ma in northern Mexico (Rudnick and Cameron, 1991), and includes a post-Oligocene stage in central Mexico (Hayob et al., 1989). The high-grade metamorphism in the xenoliths from Mexico is suggested to be the result of a regional basaltic underplating event that took place sometime after 30 Ma (Hayob et al., 1989). However, Torgersen (1993) finds that low $^3He/^4He$ ratios, while indicating the presence of some mantle-derived magmas, are in general too low for massive underplating to have occurred.

7.3.5 Isotope Geochemistry, Major and Trace Element Studies

The great abundance of igneous rock generated during Basin and Range extension has led to extensive study of the chemistry and composition of these igneous rocks and inclusions. The isotope and geochemical characteristics of mantle-derived melts can reveal clues about the mantle and crustal columns through which they intrude. Variable lithospheric-mantle ages and compositions can be deduced from isotope ratios in neodymium, strontium, and lead. The origins of basalts from different regions within the Basin and Range province vary from asthenospheric sources with minor lithospheric contamination, to those that include significant components of melted lower crust and/or lithospheric mantle. Glazner and Farmer (1991) point out that subtle crustal contamination by mafic crust can be mistaken for subcontinental mantle-source variability in some instances. However, there is good agreement in the broad isotopic patterns observed across the Basin and Range province and margins, which can be gleaned from the variety of studies of extension-related igneous rocks from the Basin and Range province presented below.

Many researchers have noted extreme variability in the western United States subcontinental mantle based on strontium and neodymium isotope variation. Menzies et al. (1983) suggested that melts from the Basin and Range province tapped a source similar to mid-oceanic ridge basalts, while melts from the Snake River Plain, and Sierra Nevada retained the primary isotopic characteristics of the underlying mantle lithosphere. Lum et al. (1989) tested possible contamination modes against the observations that Snake River Plain magmas have apparent lithospheric sources while central Nevada magmas appear to have asthenospheric sources against possible contamination modes; they concluded that contamination cannot account for the variations and that upwelling asthenosphere beneath the highly extended Great Basin causes the observed differences.

Leeman and Harry (1993) proposed two stages of magmatism in the Great Basin; the first, from 40–5 Ma involved melting of Precambrian-aged mafic veins and pods within the mantle lithosphere, and the second (since 5 Ma) involved melting of upwelling asthenosphere. Fitton et al. (1988) also suggested an asthenospheric source for late Cenozoic Basin and Range basalts, and further note a bilateral symmetry in basalt chemistry from the Great Basin that mirrors the topographic and gravity signatures pointed out by Eaton et al. (1978). They also noted increases in lithospheric-mantle involvement in basalts erupted around the outer margins of the Basin and Range. Regional lower-crustal cooling of about 300 °C from early Oligocene to early Miocene time was concluded to have caused reduced crustal contribution to rhyolite eruptions as inferred from neodymium isotope data (Perry et al., 1993).

Liviccari and Perry (1993) contoured zones of neodymium-depleted mantle model ages in the western United States, and observed that much of the Precambrian mantle lithosphere beneath the northern Basin and Range province has been preserved, although the dominance of asthenospheric sourced Late Cenozoic basalts in the southern Basin and Range caused them to suggest lithospheric removal there. Ormerod et al. (1988) located a roughly north-south oriented lithospheric boundary associated with strong variation in strontium and neodymium ratios in the western Great Basin, near the Sierra Nevada. They also found a second, northward-younging asthenospheric-source component that can be correlated with the trailing edge of the subducted Juan de Fuca plate. Farmer et al. (1989) analyzed isotope ratios in post-10-Ma basalts, and located a boundary in southern Nevada that separates asthenospheric-source basalts in central Nevada from lithospheric-source basalts in southern Nevada. They suggest that the Laramide magmatic gap may have preserved the mantle lithosphere in southern Nevada, as did Liviccari and Perry (1993). Temporal isotope and bulk chemistry variations were used to constrain the depth of magma generation in the same part of southern Nevada, and 50% less thinning of the mantle lithosphere than would be predicted from surface extension was inferred there (Daley and De Paolo, 1992). Further south, the southern Cordillera basaltic andesite province erupted across northern Mexico and southern Arizona from about 32 to 17 Ma and has a typical arc-like trace element signature; stratigraphic analysis indicates these rocks were emplaced in an extensional environment, perhaps constraining initial extension in Mexico to a back- or intra-arc setting (Cameron et al., 1989).

At about 16–17 Ma the Yellowstone plume emerged, and accompanying basaltic volcanism began to dominate in the northern Basin and Range. Interpretations of Neogene Cordilleran basalt compositions vary as to whether or not they are consistent with a mantle plume source; some workers have suggested that they are (e.g., Fitton et al., 1991; Menzies et al., 1991), whereas others have found that isotopic signatures in places are more closely related to the underlying lithosphere (e.g., Lum et al., 1989; Lipman and Glazner, 1991; Bradshaw et al., 1993). A mantle plume acts more as a source of voluminous hot material than as a point source of heat (e.g., Sleep, 1990), and it is likely that conducted heat applied broadly to the lithosphere by a plume head would cause some melting of the existing mantle lithosphere as well as supply more primitive melts directly from the asthenosphere.

7.4. Geophysical Observations

7.4.1. Seismicity

The Basin and Range province is a seismically active region (Fig. 7–4). Nearly as many historical earthquakes greater than magnitude 7 have occurred in the Basin and Range as have along the San Andreas Fault system (e.g., Ryall et al., 1966; Thompson and Burke, 1974). The 1983 M_s 7.3 Borah Peak earthquake that struck just north of the eastern Snake River Plain in Idaho serves as a reminder that the Basin and Range continues to pose a considerable seismic hazard. The following summary of Basin and Range seismicity is based on studies by Thompson and Burke (1974), Smith (1978), Smith and Lindh (1978), Stickney and Bartholomew (1987), Dewey et al. (1989), Smith et al. (1989), and Pezzopane and Weldon (1993). Seismicity in the Basin and Range tends to occur as episodic swarms or clusters of events that strike previously quiescent

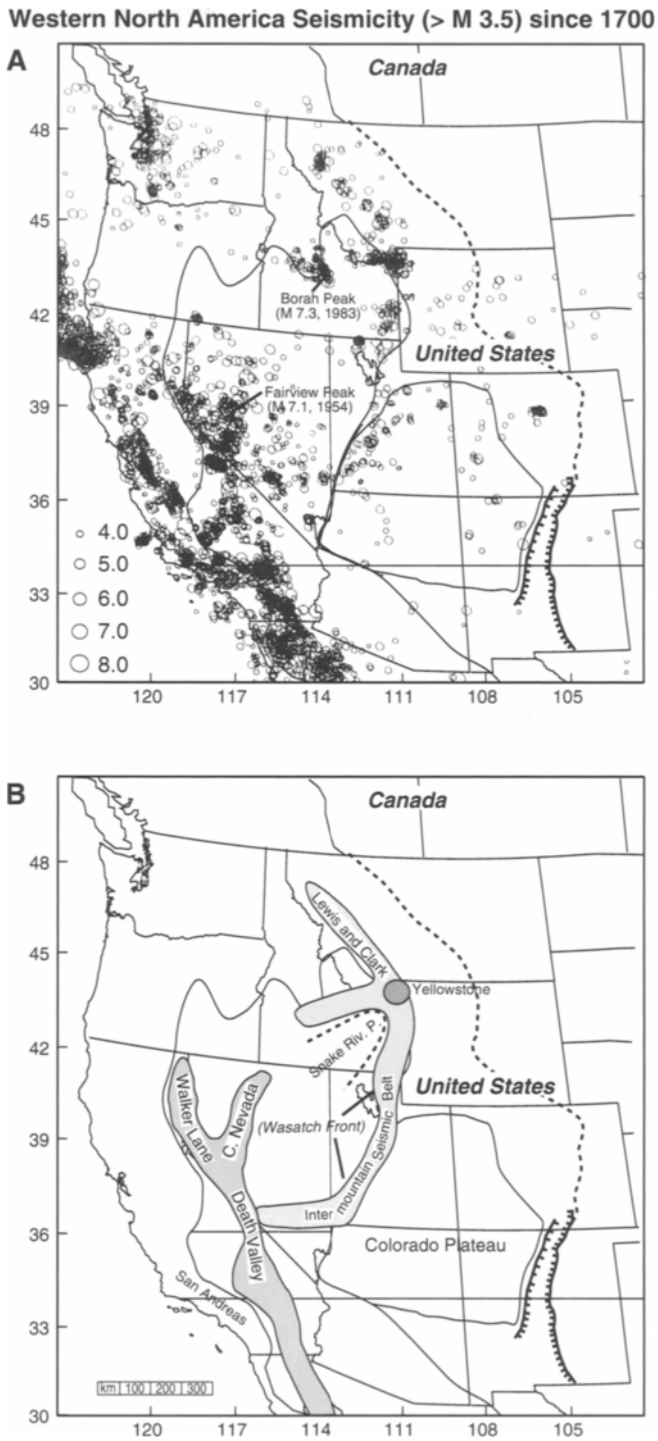

Fig. 7–4. (a) Western North American seismicity (events > M 3.5) since 1700 (after Dewey et al., 1989). (b) The patterns of extensional and oblique seismic strain discussed in the text are outlined in gray below. The dashed line is meant to illustrate the apparent parabolic distribution of seismicity around the eastern Snake River Plain. In general the Basin and Range is most active in the north, especially in the outer margins. Geologic provinces are outlined as indicated on Figure 7–1.

areas, which after some period of activity, return to quiescence. Much like the most recent patterns of magmatism, seismicity in the Basin and Range is most active along its margins (Fig. 7–4). As would be expected in an extensional province, fault-plane solutions show that normal-fault slip dominates, though many oblique and pure strike-slip earthquakes are observed as well. The maximum observed focal depth of earthquakes in the Basin and Range province is about 15 km, although the majority of quakes are shallower. The depth to the brittle-ductile transition is inferred to be at 15 km based on this observation (e.g., Sibson, 1982).

Apart from the widespread, scattered seismicity that occurs across the entire Basin and Range province, there are two broad zones of increased activity along the eastern and western margins of the northern part of the province (Fig. 7–4). Along the eastern margin, the Intermountain seismic belt extends through Utah, eastern Idaho, and western Montana. In southern Utah and Arizona the Intermountain seismic belt is located along the edges and outer margins of the Colorado Plateau. Generally low-level seismicity tends to cluster along the boundaries of the stable Colorado Plateau crustal block, perhaps an indication that its margins are collapsing in extension. To the north, the rising Wasatch Front (Fig. 7–4) marks the boundary between the Basin and Range province and the more stable Rocky Mountains, and has created a zone of active north-south striking subparallel faults. North of the Wasatch Front, the Yellowstone caldera is a center of shallow seismic activity related to the ascent and emplacement of magma in the crust. An apparent parabolic distribution of seismicity distributed around the eastern Snake River Plain in Idaho (e.g., Anders et al., 1989) includes the 1983 Borah Peak earthquake and aftershocks. The interior of the eastern Snake River Plain is virtually aseismic (e.g., Jackson et al., 1993), and it is thought that magmatic strain accommodation of some form may prevent large earthquakes from occurring there (e.g., Parsons and Thompson, 1991; Anders and Sleep, 1992). North of the eastern Snake River Plain, a diffuse zone of intermittent seismicity trends northwest across western Montana, and is associated with a shear zone known as the Lewis and Clark line.

A second zone of seismicity is found along the western boundary of the Basin and Range province. This zone is interrelated to the transform domain along coastal California and Basin and Range extension; oblique slip, transtensional deformation, and extensional transform faulting are commonly mixed with normal faulting along this zone. In the southernmost Basin and Range, seismicity is concentrated along the spreading system in the Gulf of California. Further to the north this seismic belt branches away from the southern end of the San Andreas Fault zone, and crosses southeastern California into Death Valley (Fig. 7–4). The central Nevada seismic belt, consisting primarily of extensional earthquakes, branches northeast away from this zone, and includes recent large earthquakes such as the 1954 M 7.1 Fairview Peak earthquake. The Walker Lane, a complex zone of primarily right-lateral slip, continues in a northwesterly trend along the Sierra Nevada-Basin and Range boundary. Oblique rifting continues along this trend into eastern and central Oregon.

7.4.2 The State of Stress

The state of stress in the Basin and Range province has been determined from earthquake focal mechanisms, hydraulic fracture experiments, recent fault slip indicators, young volcanic alignments, and borehole deformation studies. Some indicators, such as dated volcanic rocks, allow determinations at particular times in the past and focal mechanisms provide information at hypocentral depths. Not surprisingly, the dominant stress state is extensional, with the greatest principal stress oriented near-vertical, the least principal stress oriented broadly east-west, and the intermediate stress oriented broadly north-south (Fig. 7–5). Below, variations and features of the Basin and Range stress field are summarized after studies by Thompson and Zoback (1978), Zoback and Zoback (1980), Zoback (1989), Zoback and Zoback (1989), Mount and Suppe (1992), and Suter et al. (1992). Stress-directions discussed below will be the horizontal component of the least horizontal stress, which is essentially parallel to the extensional strain direction.

Fig. 7–5. Directions of the greatest horizontal stress in the Basin and Range province and Colorado Plateau (after Zoback and Zoback, 1989). The approximate direction of extensional strain is perpendicular to the greatest horizontal stress. The stress directions are variable across the province, changing from west to east. Further discussion can be found in the text.

Stress measurements are sparse in the southern Basin and Range. In central Mexico and along the spreading ridge in the Gulf of California, the least principal stress direction is generally aligned in a northwesterly direction. Along the southern and western edges of the Colorado Plateau, the least-stress directions are aligned radially away from the center of the plateau, a further suggestion that the plateau margin is collapsing gravitationally. The western flank of the Colorado Plateau in Utah shows a northwesterly orientation in the least principal stress (Fig. 7–5), which is parallel to the stresses in the eastern Great Basin, a possible indication of Basin and Range extension encroaching into the plateau. To the north, the margins of the Great Basin show approximately east-west least principal stress directions, whereas the interior of the Great Basin, in the Nevada seismic belt, the least principal stress direction is oriented more northwesterly. North of the Wasatch Front, the least principal stress direction changes again and is oriented more towards the southwest in the region around the eastern Snake River Plain, perhaps as a result of uplift by the Yellowstone plume (e.g., Pierce and Morgan, 1992). In general the variations in stress orientations across the Basin and Range are not well explained, but probably result from variations in crustal rheology and forces applied from outside the domain.

Table 7–2

Strain Rate 1/s	Time Interval	Basis	Location	Reference
3.80E-16 (1cm/800km/yr.)	present	Plate motions and space Geodesy	Northern Basin and Range: Colorado Plateau to Sierra Nevada	1,2,3
3.80E-16 (1cm/800km/yr)	historical earthquakes	Summation of seismic moments	Northern Basin and Range	4,5
6.30E-16 (10.7km/52km/10Ma)	10 Ma +/- 4 my	Lateral and vertical offsets of northern Nevada rift	North-central Nevada	6,7
7.90E-16 (10m/30km/12Ka)	Holocene	Offsets of 12 Ka lake shoreline; 30 km between ridge crests	Dixie Valley, northern Nevada	8
4.10E-16 (3km/30km/8Ma)	8 Ma	Offset of 8 Ma basalt; 30 km between ridge crests	Dixie Valley, northern Nevada	9
2.90E-16 (4m/27km/15Ka)	15 Ka	Two offsets of 15 Ka alluvial surface by Lost River fault; 27 km between ridge crests	Site of 1983 Borah Peak earthquake N of E. Snake River Plain (Thousand Springs segment)	10
8.20E-16 (~14km/80km/7Ma)	7 Ma (age of calderas longitude Lost Riv. Fault)	Dip of faults taken to be 50 degs. and strata 15 degs. Three tilt blocks spanning 80 km.	Three tilt-block ranges N. of E. Snake Riv. Plain (Lost River, Lemhi, and Beaverhead Ranges, ID)	5,11
11.0E-16 to 17.0E-16 (21-34mm/600km/yr)	16 Ma	Migration rate of rhyolitic volcanism less plate motion rate	Track of hotspot from emergence point to Yellowstone, NV and ID	12

Table 7-2. Northern Basin and Range extensional strain rates from Miocene time to present as derived from a variety of methods. Opening has slowed by about 50% since middle and late Miocene time. References: 1. De Mets et al. (1990), 2. Minster and Jordon (1987), 3. Beroza et al. (1985), 4. Eddington et al. (1987), 5. R. B. Smith et al. (1989), 6. Zoback (1978), 7. Zoback (1979), 8. Thompson and Burke (1973), 9. Okaya and Thompson (1985), 10. Scott et al. (1985), 11. Thompson (1960), 12. Rodgers et al. (1990).

7.4.3 Strain Rate from Geodetic and Other Observations

The present and historical extensional strain rate in the Basin and Range province has been determined from a variety of methods including the tracking of geological markers, space geodesy, and summation of earthquake moments (Table 7–2). The most recent (middle Miocene to present) strain rates are best constrained in the northern Basin and Range and converge to an average 6×10^{-16} s^{-1} strain rate over the entire interval. The present-day rate of about 3.8×10^{-16} s^{-1} is slower than the historical average (e.g., Beroza et al., 1985; Minster and Jordon, 1987; Smith et al., 1989; DeMets et al., 1990). Extensional strain in the Basin and Range has to be considered when reconciling the difference between complete relative Pacific-North American plate motion and San Andreas Fault motion. Argus and Gordon (1991) compared very long baseline interferometry (VLBI) data for motions of sub-elements within the western Cordillera with the NUVEL-1 model (DeMets et al., 1990) for Pacific-North American motion. They found that the San Andreas fault motion differs from ideal Pacific-North American relative plate motion and that Basin and Range extension, westward drift of the Sierra Nevada block, and to a lesser extent, compression across the San Andreas fault absorbs the difference. Clark et al. (1987) determined from VLBI data that Basin and Range extension accounts for 9–10 mm/yr of Pacific-North American plate divergence.

7.4.4. Crustal and Upper–Mantle Structure from Seismic Observations

7.4.4.1. Seismic Reflection Profiling in the Basin and Range Province

Deep, whole-crustal seismic reflection data have been collected in the Basin and Range (Fig. 7–6) province along an east-west transect across Nevada at about the latitude 40°N (e.g., Klemperer et al., 1986; Allmendinger et al., 1987; Jarchow et al., 1993), in the Mojave Desert of southern California (e.g., Cheadle et al., 1986), in Death Valley, California (de Voogd et al., 1986; Serpa et al., 1988; Brocher et al., 1993), across the Whipple Mountain metamorphic core complex in southern California (e.g., Flueh and Okaya, 1989), in Dixie Valley, Nevada (Okaya, 1986), and across the southern Basin and Range and Colorado Plateau transition in southern Arizona (e.g., Hauser et al., 1987; Goodwin and McCarthy, 1990; Howie et al., 1991). Vertical-incidence deep-crustal seismic data from the Basin and Range province tend to show such general features as upper-crustal Cenozoic extensional structures that overprint Precambrian, Paleozoic, and Mesozoic structures, all overlying a highly reflective laminated lower crust. Often, upper-crustal reflectivity is absent, and the crust is transparent until the lower-crustal zone of reflectivity is reached (Fig. 7–7). The Moho is typically a bright, high-amplitude series of reflections and/or an abrupt termination of reflectivity and tends to be relatively flat despite the presence of strongly varying topography and surface extension above it.

In the northern Basin and Range, the 40° N Consortium for Continental Reflection Profiling (COCORP) transect showed that the reflective textures changed from diffuse dipping reflections within the province margins in California and Utah into a strong, sub-horizontal pattern of reflectivity in the extended crust of Nevada (e.g., Allmendinger et al., 1987). Similar changes in reflectivity patterns from unextended into extended crust are noted elsewhere, and it is thus thought that the laminated lower-crustal reflectors are generated during the extension process (e.g., McCarthy and Thompson, 1988). Because of the remarkable continuity in reflection character in the Moho across the northern Basin and Range, and the lack of a correlation of Moho structure with upper-crustal tectonic features along the transect, the Moho boundary is thought to be young and to have evolved during Cenozoic extension (Klemperer et al., 1986). Near-vertical incidence data were collected near the COCORP 40° N transect in 1986 as part of the Nevada Program for Array Seismic Studies of the Continental Lithosphere (PASSCAL) experiment, and an extraordinarily bright, high amplitude Moho reflection was observed beneath Buena Vista Valley in northwestern Nevada. Carbonell and Smithson (1991) suggested that the high-amplitude Moho transition might result from interlayered melt zones, and Jarchow et al. (1993) constrain the event to be a single molten sill no greater than 200 m thick. Extended correlation of industry reflection profiles from Dixie Valley in the northern Basin and Range also shows a reflective lower crust and a layered, transitional Moho boundary (Okaya, 1986). Deep reflection profiles from the central Basin and Range in Death Valley show a bright, mid-crustal reflection that is similar to the mid-crustal melt body beneath the Rio Grande rift (see Chapter 6); this reflector is also interpreted as a melt body (de Voogd et al., 1986). However, bright reflections from the lower crust in the nearby Amargosa Desert in southern Nevada are interpreted as shear zones rather than as melt bodies (Brocher et al., 1993).

Deep-crustal reflection data were collected in the California Mojave Desert in the southern Basin and Range province in 1982 by COCORP. These data have a similar texture to the profiles collected at the Basin and Range margins along the 40° N COCORP transect in that they seem to show many preserved pre-Tertiary structures, though the possibility exists that more recent, deep low-angle normal faults were imaged (Cheadle et al., 1986). Further east, deep-crustal data were collected over the Whipple Mountain metamorphic core complex near the Colorado River in southeastern California. These data show ample mid-crustal reflectivity that is interpreted as mylonitized lower-plate rocks beneath the Whipple Mountain detachment fault extending to depth (Flueh and Okaya, 1989). In 1986 COCORP collected vertical-incidence data along a northeast-directed transect that extended from the Colorado River into

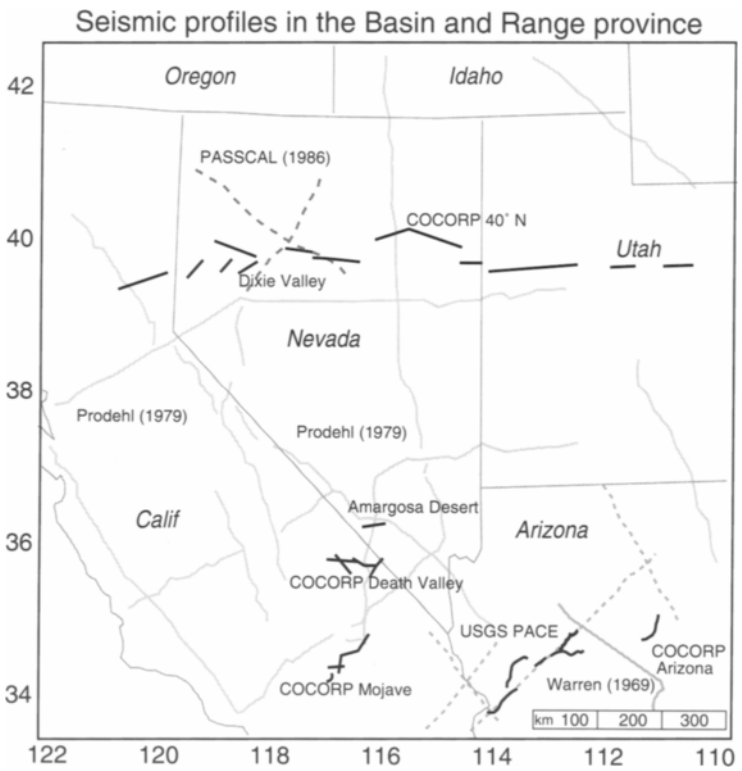

Fig. 7–6. Locations of vertical-incidence and long-offset seismic profiles in the Basin and Range province. Solid black lines are vertical-incidence reflection profiles, while gray lines are long-offset refraction profiles.

the Colorado Plateau of Arizona (Hauser et al., 1987). This transect crossed a variety of extensional provinces from the block-faulted southern Basin and Range, through the Buckskin-Rawhide metamorphic core complex, into the mildly extended Colorado Plateau transition zone (Fig. 7–8). The sections from the southern Basin and Range are similar in appearance to those from the northern Basin and Range in that bright mid-crustal reflectivity is observed above a flat-lying, high amplitude Moho reflection (Hauser et al., 1987). Beneath the Buckskin-Rawhide metamorphic core complex, the mid-crustal reflectivity is fine-scaled and appears disrupted by the extension process (McCarthy and Parsons, 1994). The Colorado Plateau transition zone is actively extending, although the extension is of small magnitude compared with most of the southern Basin and Range. Vertical-incidence data collected in this region by COCORP (Hauser et al., 1987) and Stanford University (Goodwin and McCarthy, 1990; Howie et al., 1991) show preserved intrusive structures of possible Precambrian age in the upper crust, but the middle and lower crust show evidence of recent extensional reworking (Goodwin and McCarthy, 1990; Howie et al., 1991), including a mid-crustal magma body (Parsons et al., 1992a). The reader is directed to Smithson and Johnson (1989) for a more detailed discussion of vertical-incidence studies in the western Cordillera; this discussion also describes numerous shallow to mid-crustal reflection profiles collected in the Basin and Range province that are not discussed here. Also, Mooney and Meissner (1992) compare vertical incidence studies from a variety of extensional provinces worldwide.

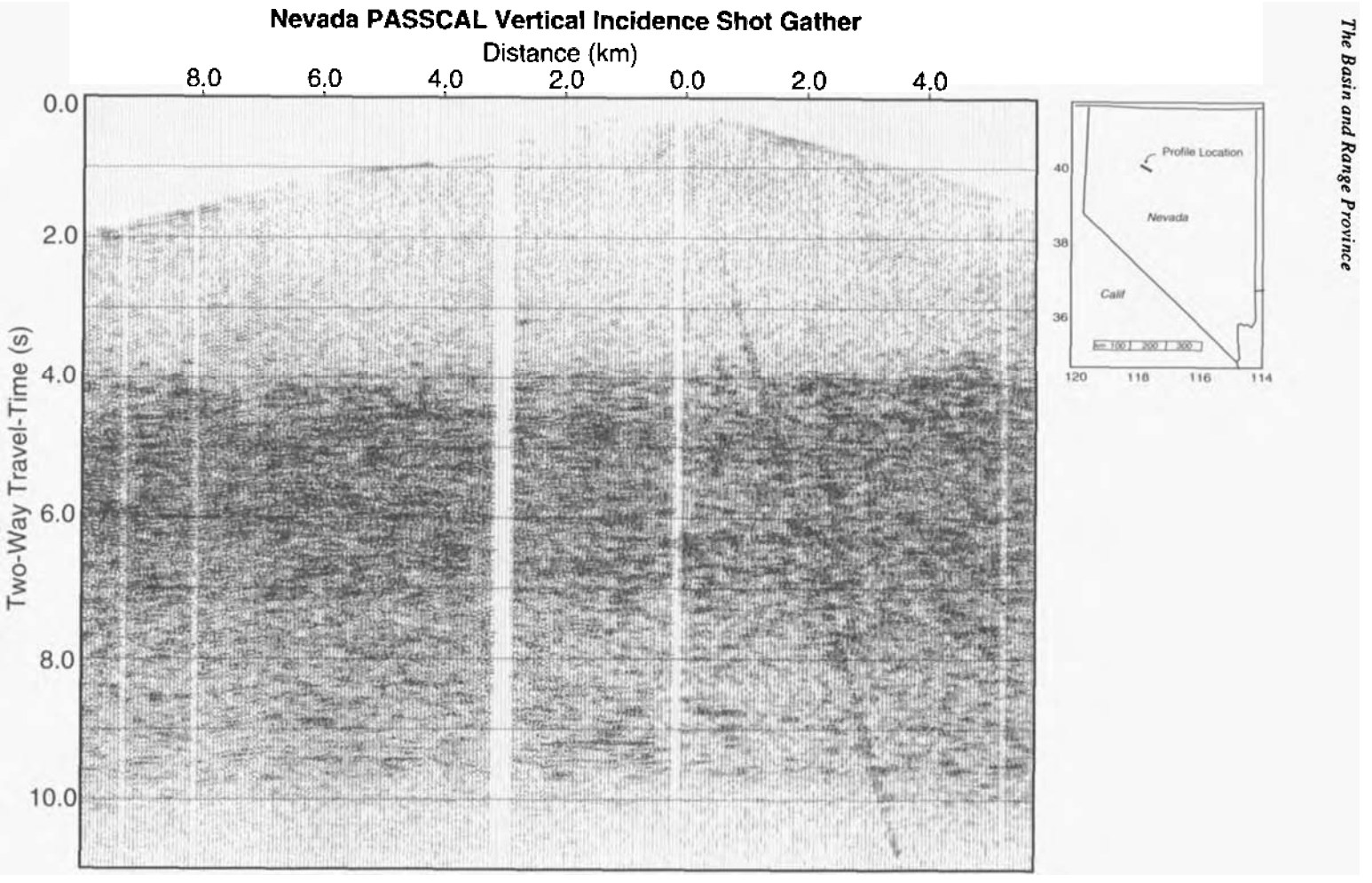

Fig. 7–7. Vertical incidence shot gather from the Nevada PASSCAL experiment in northern Nevada (after Jarchow et al., 1993). A relatively transparent upper crust lies above a highly reflective lower crust. The upper mantle is also transparent to vertical incidence seismic energy. This reflective texture is commonly observed in extended regions worldwide and is inferred to be a direct consequence of the extension process. These reflections were suggested to represent a combination of ductile shear and magmatic intrusions (Holbrook et al., 1991). A still molten horizontal intrusion was found at the Moho (Jarchow et al., 1993).

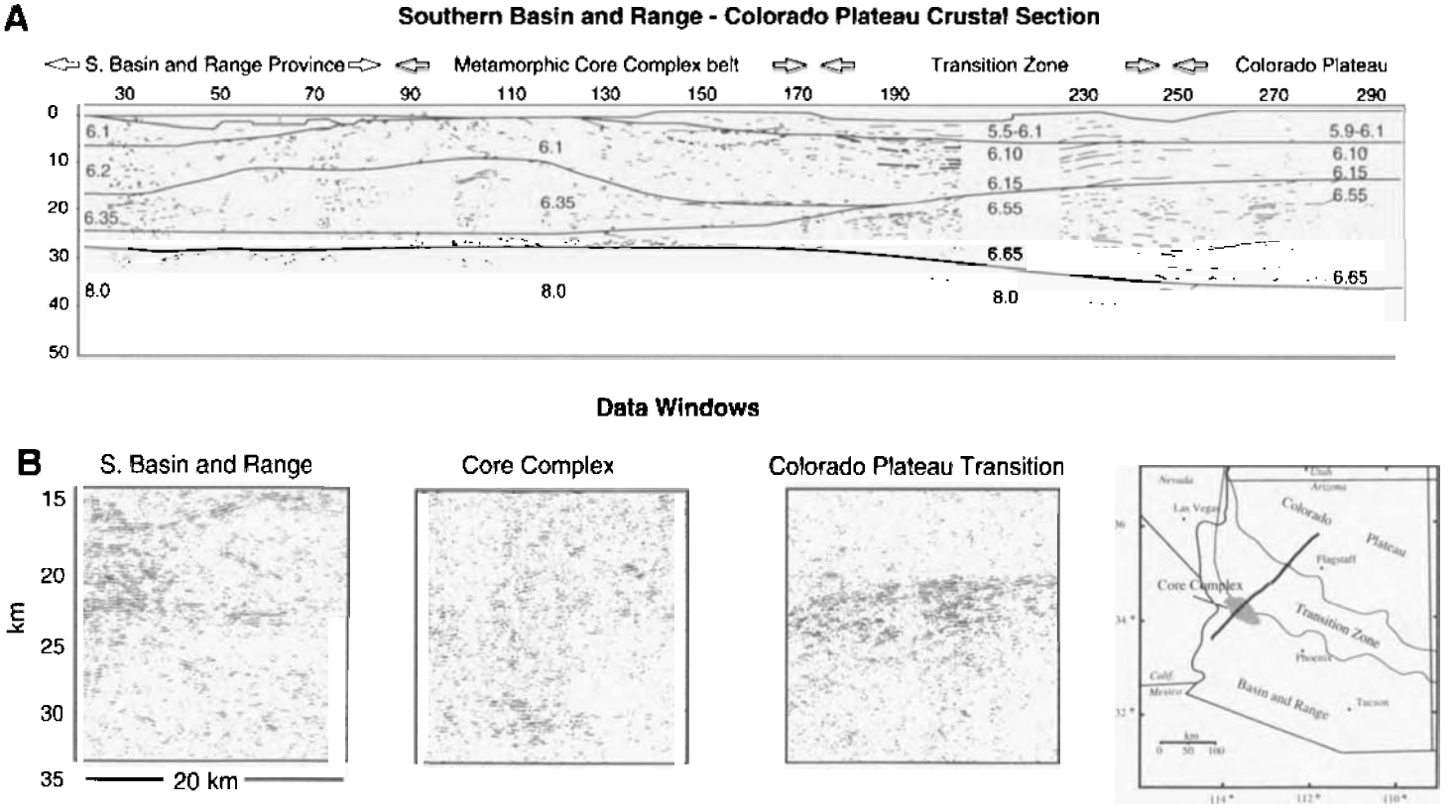

Fig. 7–8. Velocity model from a seismic refraction study in the southern Basin and Range that crossed "typical" Basin and Range crust as well as a metamorphic core complex (McCarthy et al., 1991) combined with line drawings of the COCORP Arizona seismic reflection profiles (after Hauser et al., 1987). Example data windows are shown below of the actual vertical incidence stacks. The southern Basin and range lower crust is highly reflective and is similar to the textures observed in the northern Basin and Range (Fig. 7–7). A thick welt of slow (6.35 km/s) lower crustal material underlies the Buckskin-Rawhide core complex, and reflection data from this area appears choppier and more disrupted than from beneath the typical Basin and Range or Colorado Plateau transition. Up to 4 km of mafic rock could have been added to the lower crust beneath the core complex if it was distributed in thin sheets (McCarthy and Parsons, 1994).

7.4.4.2 Seismic Refraction Studies: The Crustal Velocity Structure of the Basin and Range

Crustal seismic refraction studies in the Basin and Range province have been carried out along very similar transects to the seismic reflection profiles discussed above. Regional refraction profiles that cross Nevada east-west at 39° N, and north-south at about 116° W were carried out in the early 1960's and were reinterpreted by Prodehl (1979). These experiments had large station spacings, and did not provide much detail within the crust, but they were successful in determining the whole-crustal thickness. The wide-angle component of the 1986 Nevada PASSCAL experiment provides more crustal detail in northern Nevada (e.g., Catchings and Mooney, 1989; Benz et al., 1990; Holbrook, 1990). In the southern Basin and Range province, refraction studies were carried out above the Whipple Mountain metamorphic core complex in southeast California (Wilson et al., 1991), in central Arizona from the southern Basin and Range across the Colorado Plateau transition (Warren, 1969) and nearly coincident with the COCORP Arizona reflection profiles, northeast from the Colorado River into the Colorado Plateau (McCarthy et al., 1991).

There is some difference in the interpretations of the Nevada PASSCAL data (Catchings and Mooney, 1989; Holbrook, 1990; Benz et al., 1990), but the broad features are similar; the northern Basin and Range crust is thin, about 30 km thick, and does not vary more than 1–3 km along the profiles. A high velocity layer of varying extent was detected near the base of the crust in all interpretations, and magmatic underplating was suggested as the origin of those high-velocity rocks. Mid-crustal velocities were reported in the 6.0–6.2 km/s range, and have been suggested to be of granitic to granodioritic composition. Low velocity zones (~5.5 km/s) were found in the upper 10 km of crust, and were suggested to be fractured crust (Catchings, 1992) or silicic intrusions, underthrusted sediments, or high temperature zones (Holbrook, 1990). Reinterpretation of the early refraction data collected in the northern Basin and Range (Prodehl, 1979) ties well with the more recent profiles in terms of crustal thickness.

A fascinating result of wide-angle seismic profiling in the southern Basin and Range has been the crustal thickness determinations of the Whipple Mountain and Buckskin-Rawhide metamorphic core complexes in southeastern California (McCarthy et al., 1991; Wilson et al., 1991). Beneath the areas of the locally greatest extension, the crust maintains its thickness. A 10 to 15-km-thick welt of 6.35 km/s crust was identified on two crossing profiles just above a thin higher velocity (6.6 km/s) lower-crustal layer (Fig. 7–8). In addition, The upper-crustal low-velocity layer is thinner beneath the core complexes because mid-crustal rocks were exhumed on low-angle normal faults. The refraction studies of the Whipple Mountain and Buckskin-Rawhide metamorphic core complexes were the beginnings of the U.S. Geological Survey (USGS) Pacific to Arizona Crustal Experiment (PACE). The PACE profiles extend north of the core complexes across the Colorado Plateau transition zone, where the crust gradually thickens to a maximum of 39 km (Fig. 7–8). The zone of 6.35 km/s crust that was present beneath the core complexes is absent beneath the more weakly extended Colorado Plateau transition zone. A similar increasing crustal thickness across the Colorado Plateau transition zone was observed by Warren (1969) on a profile collected further to the east of the PACE transect. Braile et al. (1989), Mooney and Braile (1989), and Pakiser (1989) provide further discussion on the crustal velocity structure of the western United States. A discussion of the regional implications of crustal-structure variation can be found in Section 7.5.2.

7.4.4.3 Upper-Mantle—Velocity Structure from Earthquake-Source Studies

The upper mantle beneath the Basin and Range has been studied using a variety of techniques applied to long and intermediate period seismograms recorded by local, regional, and teleseismic earthquake and large explosive sources. Depending on the source range, receiver density, and phases analyzed, either an averaged one-dimensional velocity profile, or two- and three-dimensional variations in velocity structure are produced. A general result from studies of the Basin and Range province is an aver-

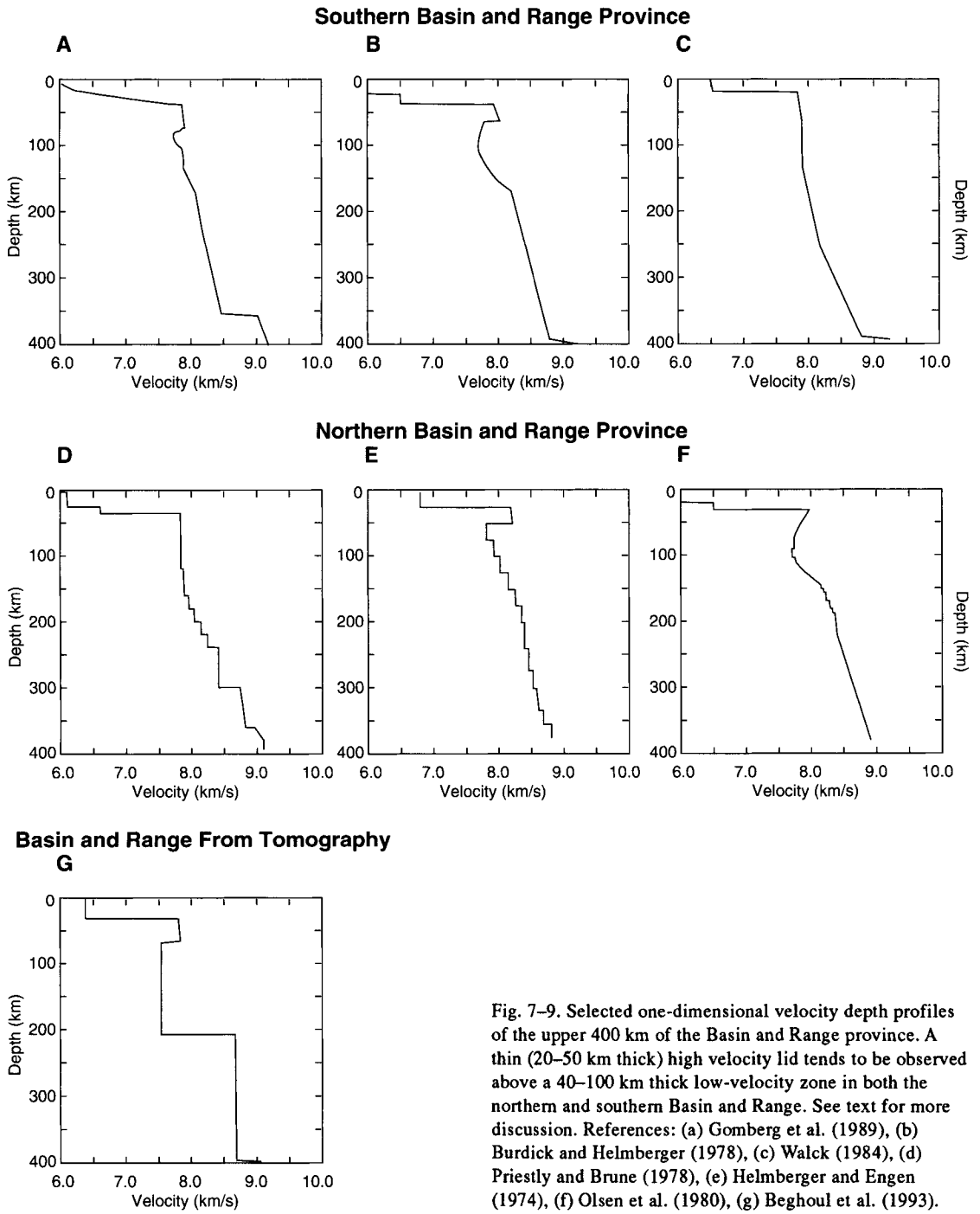

Fig. 7–9. Selected one-dimensional velocity depth profiles of the upper 400 km of the Basin and Range province. A thin (20–50 km thick) high velocity lid tends to be observed above a 40–100 km thick low-velocity zone in both the northern and southern Basin and Range. See text for more discussion. References: (a) Gomberg et al. (1989), (b) Burdick and Helmberger (1978), (c) Walck (1984), (d) Priestly and Brune (1978), (e) Helmberger and Engen (1974), (f) Olsen et al. (1980), (g) Beghoul et al. (1993).

age lower velocity upper mantle as compared with the interior continental craton, including a low velocity zone at or near the top of the upper mantle. The causes of these observations may include a thinner high velocity mantle lithosphere and a hotter, lower velocity asthenosphere than the continental interior. Variability in mantle structure within the Basin and Range province can be generalized to include the identification of the subducting Juan de Fuca slab beneath the northern part of the province and a low velocity asthenosphere connected with the Yellowstone hotspot. Teleseismic shear-wave arrivals in the Basin and Range often show significant splitting between the transverse and radial shear components, which may be the result of tectonic deformation in the mantle lithosphere and upper asthenosphere; thus splitting directions can help in the interpretation of mantle extensional dynamics.

One-dimensional Q or velocity-depth profiles for the Basin and Range crust and upper mantle generated from body and surface waves have been reported by Archambeau et al. (1969), Helmberger and Engen (1974), Burdick and Helmberger (1978), Priestly and Brune (1978), Olsen et al., (1980), Olsen and Braile (1981), Olsen et al., (1983), Walck (1984), Gomberg et al. (1989), and Al-Khatib and Mitchell (1991). The velocity profiles generally show about an 80-km-thick Basin and Range lithosphere overlying a thin low velocity zone, followed by a linear velocity increase with depth (Fig. 7–9). Upper mantle Q values tend to be lowest in the western Basin and Range, where the most recent magmatic and tectonic activity has occurred. One-dimensional shear-wave velocity models are also sensitive to recent volcanic activity, with the slowest low velocity zones recorded on the volcanic plateaus.

Two- and three-dimensional images of portions of the Basin and Range upper mantle have been created through tomographic inversion of direct mantle arrivals from regional sources (e.g., Hearn et al., 1991; Beghoul et al., 1993), and inversion of teleseismic residuals (e.g., Koizumi et al., 1973; Solomon and Butler, 1974; Iyer et al., 1977; Romanowiscz, 1979; Dueker and Humphreys, 1990; Biasi and Humphreys, 1992; Humphreys and Dueker, 1994). Tomographic studies show that the mantle lid beneath the Basin and Range is lower in velocity (< 7.9 km/s) than its margins (> 7.9 km/s). The mantle lid beneath the eastern Snake River Plain (track of the Yellowstone hotspot) is especially slow (< 7.6–7.8 km/s), presumably because of thermal softening of the upper mantle (Hearn et al., 1991). However, P_n velocities determined from controlled-source seismic studies tend to find faster velocities in the uppermost mantle at 8.0 km/s in the Basin and Range (e.g., Catchings and Mooney, 1989; Holbrook, 1990; McCarthy et al., 1991). This discrepancy may result from a shallower sampling by the controlled sources than from earthquake sources. Teleseismic residuals indicate a high velocity body deep beneath the northern and western Basin and Range province that is inferred to be the subducting Juan de Fuca plate or remnants of the Farallon slab (e.g., Koizumi et al., 1973; Solomon and Butler, 1974; Iyer et al., 1977; Romanowiscz, 1979; Biasi and Humphreys, 1992). The shallower velocity structure (< 250 km depth) identified through inversion of P-wave residuals shows northeast-trending low velocity zones beneath the eastern Snake River Plain and the St. George volcanic trend (chain of recent basaltic eruptions that crosses southern Nevada and Utah; Fig. 7–3c); the intervening zones of higher velocity upper mantle beneath central Nevada correspond to areas where magmatic activity peaked during Miocene time (Dueker and Humphreys, 1990; Biasi and Humphreys, 1992; Humphreys and Dueker, 1994). Upper mantle velocities as determined from a variety of methods appear to be slowest beneath areas that have seen tectonic and magmatic activity most recently, those areas near the eastern and western margins of the province.

It is generally agreed that upper mantle shear wave splitting results from tectonically imposed strain fabric in the mantle rocks (e.g., Ribe and Yu, 1991). Preferred alignment of olivine crystals causes the shear waves vibrating parallel to the elongate crystals to arrive faster than those vibrating perpendicular to the preferred-alignment direction. Thus the recorded fast direction is roughly parallel to the strain direction. The origin of the mantle strain is thought to be from internal continental deformation as well as from whole plate motion. Shear-wave splitting results are available from the northern Basin and Range (e.g., Savage and Silver, 1993) and

the southern Basin and Range (e.g., Ruppert, 1992). Results from the northern Basin and Range show a fast direction of N 74° E with a 1 s difference between fast and slow arrivals (split) in the northwestern province, while in the northeastern Basin and Range the fast direction is about 45° different at N 72° W with a 1 s split (Savage and Silver, 1993). A similar variation in the horizontal stress direction from the northwestern to northeastern Basin and Range is observed (e.g., Zoback and Zoback, 1989), but the present-day stress directions do not parallel the fast or slow anisotropy directions. Savage and Silver (1993) suggest this mismatch may be because present day Basin and Range extension is too weak to overprint previous deformation fabric in the mantle. Two anisotropic layers (cumulative 0.7–0.8 s split) were postulated beneath the southern Basin and Range province in southern Arizona: a N 35° W fast direction in the 30–50 km depth interval (parallel to present-day extension) and an additional 80–km-thick zone extending into the asthenosphere with a fast direction oriented N 60° E, roughly parallel to North American plate motion (Ruppert, 1992).

7.4.5 Potential Field Studies

The northern Basin and Range province corresponds to a regional Bouguer gravity low, the boundary of which lies along the topographic edge between the northern and southern Basin and Range (Plate 7–2). The sources of the high topography and low Bouguer gravity in the northern Basin and Range both result from an upper-mantle low-density anomaly (e.g., Eaton et al., 1978). There is a bilateral symmetry in the long-wavelength gravity field of the northern Basin and Range province across a north-south center line (Plate 7–2). This increase in the Bouguer anomaly towards the Basin and Range margins was noted and compared with the outward migration of seismicity and magmatism into the margins by Eaton et al. (1978) and is suggested to result from asthenospheric upwelling beneath the central northern province. Isostatic residual maps have been created (e.g., Simpson et al., 1986; Jachens et al., 1989) that remove mantle effects from the Bouguer gravity so that crustal variations may be examined. These maps show evidence for low-density plutons at the heart of the bilaterally symmetric pattern in the Bouguer gravity map, possibly indicating a genetic link between anomalous upper-mantle and upper-crustal plutonism. Similarly, a large quantity of basalt intruded into the eastern Snake River Plain crust causes a strong positive crustal gravity anomaly in the northern Basin and Range.

Gravity data from the Basin and Range province have been used to address problems involving the extension process. Thompson and McCarthy (1990) pointed out that highly extended terranes such as metamorphic core complexes are not associated with large gravity anomalies, and the crust beneath them tends to be equally thick as less extended crust surrounding them. They suggested that at depth, rocks of equal density must have replaced the 10 km or so of upper crustal rock that was stripped off the top in order to prevent a strong gravity anomaly from being created. They further suggested that the low-density rocks must have been magmatically intruded, because inflow of ductile lower-crustal rocks would have emplaced enough dense material as to generate strong positive gravity anomalies which are not observed. However, Kruse et al. (1991) fit the Bouguer anomaly to a model of ductile lower-crustal flow from beneath the unextended Colorado Plateau to the extended Lake Mead region of the central Basin and Range. The Lake Mead region lies about 1 km lower than the Colorado Plateau and has a similar crustal thickness to the plateau, whereas many metamorphic core complexes are mountainous and are elevated above their surroundings. Thus examination of gravity data seems to indicate that lower-crustal flow and magmatism may operate independently or in concert to maintain crustal thickness during extension, depending on conditions within an individual terrane.

Aeromagnetic data from the Basin and Range provide information about crustal composition and evolution. A "quiet basement zone" extends from southern Nevada into Idaho (Mabey et al., 1978) and is centered along the line of symmetry identified on Bouguer gravity maps. The Snake River Plain stands out as a strong magnetic anomaly, particularly the western arm of the plain. The strength of the magnetic anomaly decreases along the eastern Snake

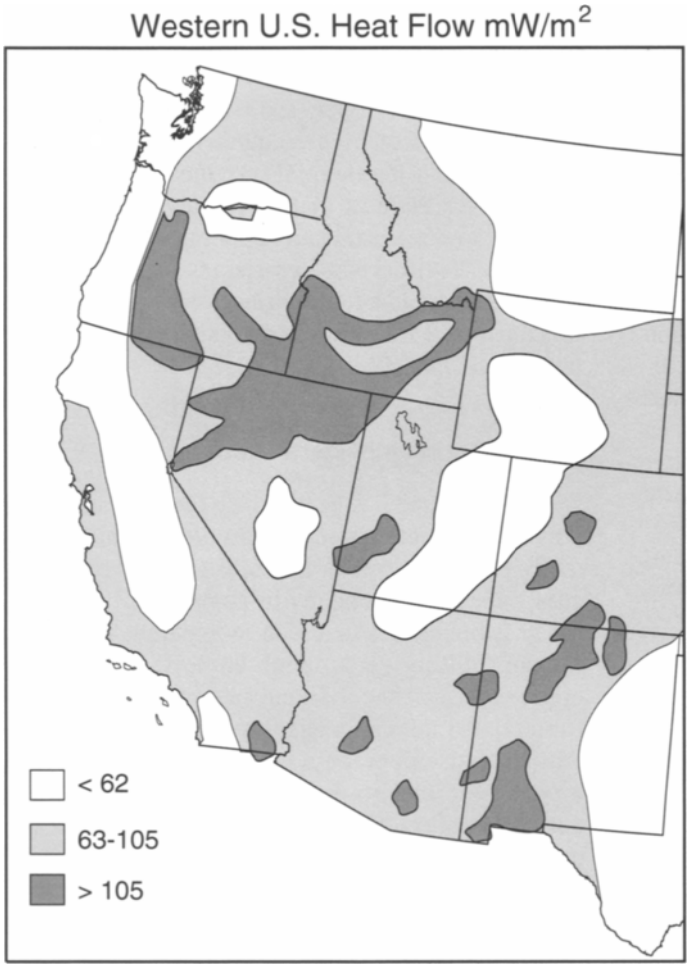

Fig. 7–10. Heat flow in the western United States after Morgan and Gosnold (1989). The darkest areas have the highest surface heat flow, and the lightest are the lowest.

River plain towards the Yellowstone caldera. Blakely and Jachens (1991) note that 46% of the surface area of Nevada has Mesozoic and Cenozoic igneous rocks in the upper 1 km of the crust. They also identify a roughly north-south trending 500-km-long magnetic anomaly across the middle of Nevada that has remained essentially linear since middle Miocene time. This feature has been termed the northern Nevada rift, and may represent a linear series of mafic dike intrusions (Zoback and Thompson, 1978; Zoback et al., 1994). The rift has been used as a marker for post-rift extension at an oblique angle to it (Zoback, 1978; Zoback and Thompson, 1978). The depth to the Curie temperature isotherm was estimated from magnetic anomaly properties in the state of Nevada, and the basal depth of the magnetic sources was observed to be shallowest in regions having the highest heat flow (Blakely, 1988).

7.4.6 Heat Flow and Magnetotelluric Studies

A result of recent tectonic extension and accompanying magmatism in the Basin and Range province has been an increase in surface heat flow relative to other more stable tectonic provinces in the western Cordillera such as the Colorado Plateau,

Sierra Nevada, and Rocky Mountain foreland. Reduced heat flow in the Basin and Range is typically 50–100% higher than the surrounding stable provinces, and in places can be more than 300% greater (e.g., Battle Mountain high, northwestern Nevada) (Lachenbruch, 1978; Lachenbruch and Sass, 1978; Blackwell, 1978, Morgan and Gosnold, 1989). The relative highs and lows in reduced heat flow are shown in Fig. 7–10, though caution should be exercised when making regional interpretations of Basin and Range heat flow contours, as flow of ground water and variable magmatic advection can complicate matters considerably. The source of heat loss through the Basin and Range lithosphere has been suggested to be a direct result of elevation of hotter material closer to the surface caused by lithospheric thinning (e.g., Crough and Thompson, 1976; Lachenbruch and Sass, 1978; Artyushkov and Batsanin, 1984). However, constraints on the timing of extension, heat loss, and the observation that broad, unextended volcanic plateaus can be as hot as the Basin and Range province, leads to the conclusion that advective heat from magmatic sources must play an important combined role with lithospheric thinning in generating heat flow in the Basin and Range (e.g., Morgan and Gosnold, 1989; Mareschal and Bergantz, 1990). The southern Basin and Range province shows very similar heat flow values to the northern Basin and Range, though the metamorphic core complex belt along the Colorado River is relatively cold, while other regions of less pronounced Miocene extension remain hot, perhaps because 10 km of radiogenic upper-crust was stripped off the core complexes during extension (J. H. Sass et al., written communication, 1993).

Magnetotelluric studies in the southern Basin and Range province of southern California and Arizona find a highly conductive zone at depth that begins approximately at the Colorado River and continues to the east (e.g., Keller, 1989; Klein, 1990). A transect paralleling the USGS PACE seismic refraction and COCORP Arizona seismic reflection lines shows a deep zone of conductivity that may correlate with the top of the reflective lower crust and deepens beneath the Colorado Plateau transition (Klein, 1990). In the northern Basin and Range province, an intensive magnetotelluric survey was conducted across the Battle Mountain heat flow high, and high conductivities were observed through the crust at all depths, especially in Dixie Valley and the Carson Sink (Keller, 1989). A mid-crustal zone (~20 km deep) of high conductivity was also observed beneath the thermal province of the eastern Snake River Plain in Idaho (Stanley, 1982). A 70-km-wide lower crustal and upper mantle conductive zone was identified that corresponds with the roughly north-south trend of the northern Nevada Rift, and was attributed to diking and conductive permeable fractures (Chau, 1989).

7.5. Structure and Interpretation

The Basin and Range province presents some key crustal and mantle structural problems that bear directly on the extension and uplift processes. I discuss three such problems in some detail here: (1) the possible causes that lead to apparent low-angle normal faulting versus high-angle faulting in the upper crust, (2) the maintenance of relatively uniform crustal thickness despite strongly varying extension and topography, and (3) the variations in topographic elevation between the southern and northern Basin and Range province despite the nearly uniform crustal thickness and average magnitude of extension in the two sub-provinces.

7.5.1 Low-Angle vs. High-Angle Normal Faulting

Anderson's (1951) theory provided a general framework to describe faulting in relation to the ambient stress field in the Earth's crust. The theory predicts that when the vertical lithostatic load is the greatest principal stress, normal faulting ensues at an angle ~45° to 70° from vertical, when the difference between the horizontal least principal stress and vertical greatest principal stress exceeds the shear strength of the rocks. As more faults are investigated world-wide, it is increasingly clear that Anderson theory alone cannot adequately describe many observed faults. For example, shallow dipping to horizontal fault planes are commonly observed, often with extreme normal displacements. Because these faults are shear failures that respond to the local stress field, apparently either the greatest principal

stress direction deviates from the vertical (e.g., Bartley and Glazner, 1985; Bradshaw and Zoback, 1988; Melosh, 1990), or a steeply dipping fault plane rotates to a more shallow dip after displacement (e.g., Davis, 1983). Reactivation along ancient low-angle fault planes is a less likely explanation because in most cases the shear strength of a plane of weakness improperly oriented to the principal stress axes exceeds that for a new fault in fresh rock along a more favored plane (Sibson, 1985). There is clear evidence that rotation followed by initiation of new fault planes occurs, as in the case at Yerington, Nevada (Proffett, 1977). However, evidence from structural reconstructions indicates that many detachment faults begin and propagate at low angles, including the Whipple Mountains (Yin and Dunn, 1992) and Chemehuevi Mountains of southern California (Miller and John, 1988), the Harcuvar Mountains of central Arizona (Reynolds and Spencer, 1985), and in the Mormon Mountains of Nevada (Wernicke et al., 1985).

The expected pattern for brittle extension with a vertical greatest principal stress is finite motion along steeply dipping fault planes, with a new plane forming when it is no longer efficient to continue motion along the first (much like the middle Miocene episode of block faulting in the Basin and Range province). Historical earthquakes have focal mechanisms that indicate steeply dipping fault planes (>40°) (e.g., Jackson, 1987). When lower angled faults occur, they tend to expose sharp divisions between brittle deformation in the upper plate and ductile deformation in the lower plate; this has invited the suggestion that the low-angle faults represent the brittle-ductile transition (e.g., Gans et al., 1985). Models involving isostatic uplift ("rolling hinge" models) suggest that unloading caused by movement on a normal fault causes upwarp of the footwall, which rotates the initially steep fault plane towards the horizontal (e.g., Heiskanen and Vening Meinesz, 1958; Spencer, 1984; Wernicke and Axen, 1988). Observational evidence suggests that isostatic rebound of local features such as the footwall of a normal fault occurs in the middle crust, rather than involving the whole crust. For example, analysis of gravity data suggests that the load differences between the relatively narrow (~20 km wide) basins and ranges in the western Cordillera of the United States are supported by the strength of the crust (e.g., Eaton et al., 1978; Kruse et al., 1991), which implies that isostatic compensation has occurred by midcrustal shear flow, rather than in the mantle. Seismic reflection profiles from the northern Basin and Range province tend to support that result, showing a flat Moho beneath both basins and ranges (e.g., Klemperer et al., 1986). Footwall rebound should occur equally on every steep normal fault of approximately the same offset, which indicates that the observed variation in dip-angle is likely a consequence of heterogeneities in composition, rheology, or stress distribution.

The stress field and rheology of the upper crust may be influenced towards conditions favoring low-angle normal faulting by magmatism (e.g., Lister and Baldwin, 1993; Parsons and Thompson, 1993). Advected heat from intruded magma could raise the brittle-ductile transition temporarily, and shear along the ductile zone (e.g., Melosh, 1990) or shear stresses imposed directly by the intrusion (Parsons and Thompson, 1993) might cause a rotation in the stress field favoring low-angle faulting. Any model for in-situ low-angle faulting must include some source of shear that drives the faulting, either gravitational as in the case of Gulf of Mexico faults (e.g., Bradshaw and Zoback, 1988), or some other source where topographic inclination is not likely to be a factor, such as in the metamorphic core complexes in the Basin and Range. Furthermore, models for metamorphic core complex development must be consistent with the following observations: (1) the crust beneath core complexes is often as thick as surrounding less extended terranes, (2) core complexes lack strong Bouguer gravity anomalies, thus regardless of its source, the material that maintains crustal thickness beneath the core complexes must be on average the same density as the whole-crustal average, and (3) the exposed core rocks are typically warped upwards into mountainous antiformal structures rather than buried beneath thick sedimentary basins.

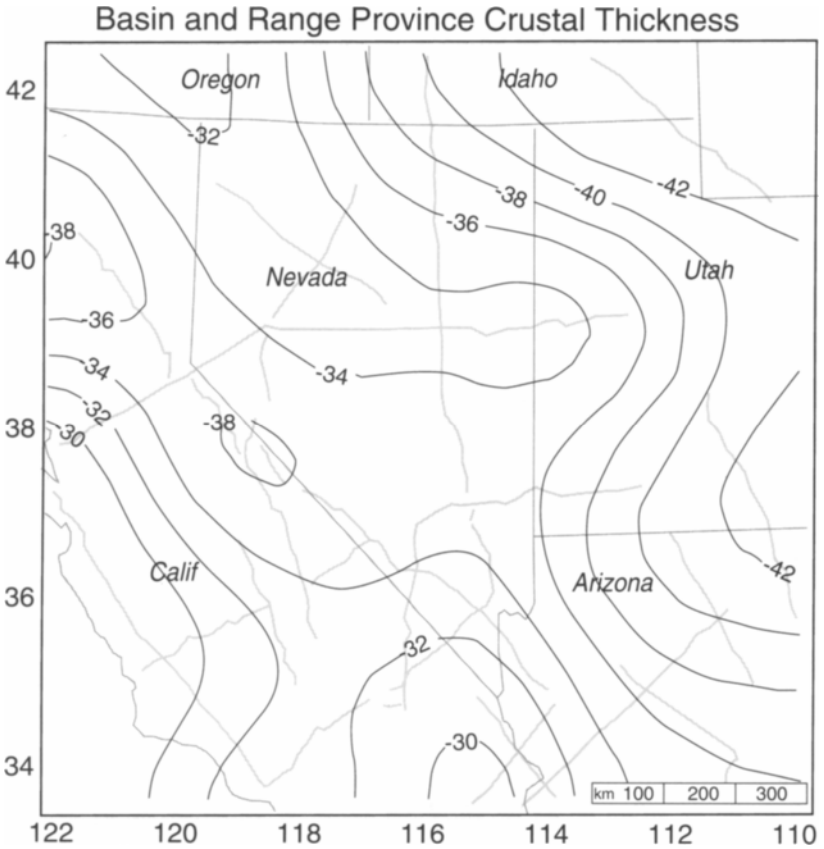

Fig. 7–11. Contour plot of the crustal thickness of the western Cordillera where estimates from seismic refraction profiles are available (Fig. 7–6) (shown as gray lines; Warren, 1969; Prodehl, 1979; Catchings and Mooney, 1989; McCarthy et al., 1991). This plot is similar to compilations by Pakiser (1989) and Jones et al. (1992).

7.5.2 Basin and Range Crustal Extension and Thickness

As the number of seismic refraction studies in the Basin and Range increased, it became clear that the crust within the extended province is remarkably uniform despite strong variation in the timing and magnitude of stretching from terrane to trerrane (Fig. 7–11). Either the pre-Tertiary Basin and Range crust was a minimum of 60 km thick, and up to 120 km thick in places, or crustal material was added during extension. Long-term inter-plate convergence and subduction very likely did increase the crustal thickness of western North America during the Paleozoic and Mesozoic Eras (e.g., Bird, 1984), but it would have to have exceeded the present thicknesses of the Rocky Mountains and Colorado Plateau if the present Basin and Range crustal thickness evolved through closed-system pure shear of the Cordilleran crust. Gans (1987) inferred a 40 to 50 km pre-extension crustal thickness for the northeastern Basin and Range province, and reconciled the estimated 77% surface extension with the present 30–35 km thickness by proposing an open-system mode of extension that included lower-crustal ductile flow and the addition of a 5-km-thick magmatic layer.

The maximum focal depth of earthquakes in the Basin and Range province is about 15 km, an indication that the crustal layer beneath the brittle upper crust responds to regional extensional stresses by aseismic creep, or ductile flow. The high observed surface heat flow indicates that the ductile layer may have increased mobility through heat conducted from the mantle and/or advected by intruding magma. Buck (1991) suggested that lithospheric rheology controls extensional modes. When thermal weakening dominates and lower crustal flow occurs very fast, then core complexes form; otherwise either a wide rift occurs if the lithosphere is moderately hot and weak, or a narrow rift forms if the lithosphere is cold and strong. The role that the ductile layer may play in maintaining crustal thickness during extension is not well constrained, nor is the amount of ductile lower-crustal material that may have been added to the extending Basin and Range crust from more stable unextended terranes such as the Colorado Plateau or the Sierra Nevada. Perhaps some indication may come from the patterns of seismic reflectivity that are commonly observed in the lower crust of extended terranes worldwide. As was shown in Section 7.4.4.1, the lower crust of the Basin and Range province can be highly reflective at vertical incidence (e.g., Figs. 7–7, 7–8). The reflective lower crust does not extend very far into the more stable terranes along the Basin and Range margins such as the Sierra Nevada, the northern and southern Colorado Plateau, or the Mojave block, all regions where pre-Tertiary structures seem to be preserved (e.g., Cheadle et al., 1986; Allmendinger et al., 1987; Howie et al. 1991). If the lower-crustal reflectivity is the result of shearing in the lower crust, and significant flow from stable blocks occurred, than such fabric would be expected beneath those stable blocks. The absence of reflectivity from the bordering stable terranes suggests that significant flow from these regions has not occurred. A further complication in interpreting lower-crustal reflectivity is the strong possibility that at least some of the reflectors are caused by Tertiary magmatic intrusions into the extended crust.

The Moho is an often-suggested locus of magmatic underplating (e.g., Furlong and Fountain, 1986; Matthews and Cheadle, 1986; Bohlen and Mezger, 1989; Bergantz, 1989; Wilshire, 1990). The seismic velocities from the highly reflective lower crust of the northern Basin and Range province are high (7.1–7.3 km/s) in places, and are lower (~6.6 km/s) in other parts, perhaps indicating variable input of mafic magma into the lower crust there (e.g., Holbrook et al., 1991). Lower-crustal velocities tend to be slow in the southern Basin and Range province, though velocity constraints allow up to a 4 km thickness of mafic intrusive rocks if it is distributed within the lower-crustal layer in thin sheets (McCarthy and Parsons, 1994). While underplating or intrusion of distributed horizontal mafic sheets is often suggested as a means to maintain crustal thickness and advect heat into the lower crust to stimulate flow there, little attention is given to how such sheets might be emplaced in an extensional environment that should favor vertical rather than horizontal intrusions. The rheologic boundaries of the lithosphere such as the Moho may be traps where basaltic magma is more likely to orient horizontally because the rheologic differences lead to long term changes in the stress magnitude across them. While the upper-most mantle lid is likely more rigid than the lower crust it is seldom seismogenic in extending regimes. The commonly observed association of extension with magmatism and high heat flow is perhaps an indication that dike intrusion along with some amount of ductile deformation is the means by which upper-mantle extensional strain occurs. The ductile lower crust develops less deviatoric stress and may become over-inflated by dike intrusion as compared with the stronger upper mantle (e.g., Parsons et al., 1992b) (Figure 7–12). Subsequent dikes in the mantle reach the ductile lower crust in which the horizontal stress exceeds the lithostatic load, and the magma is hence forced to intrude horizontally, underplating the Moho. Multiple occurrences of this cycle may be important in the evolution of the lower crust and Moho in extending terranes.

Models of whole-lithospheric extensional flow identify two wavelengths of necking instabilities, a local one at the scale of basin-range spacings that is accommodated by middle and lower crustal flow, and a province-wide thinning of the lithospheric mantle (e.g. Froidevaux, 1986; Zuber et al., 1986). That

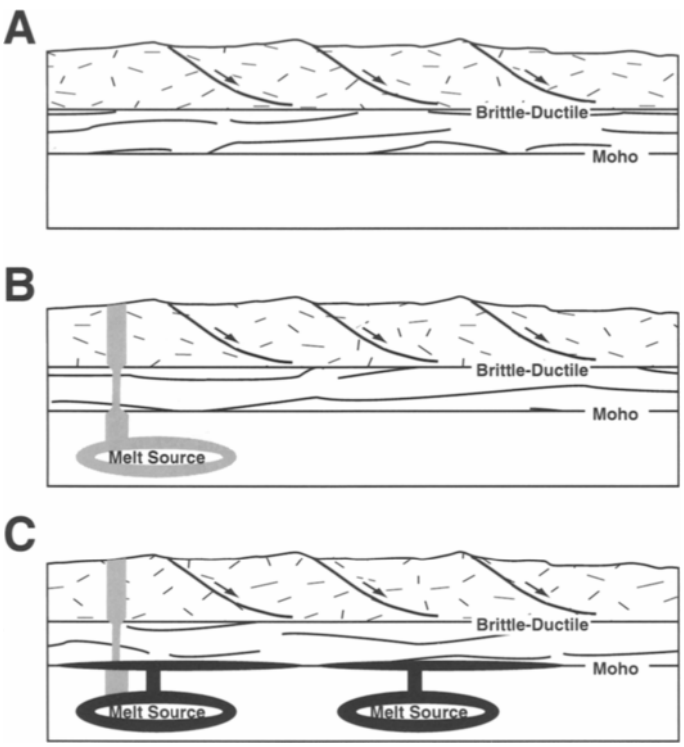

Fig. 7–12. Sequence of events leading to horizontal intrusion and underplating at the crust-mantle boundary. (a) In an extending regime the deviatoric stress (difference of maximum vertical and least horizontal) accumulates in the more brittle upper crust and upper mantle. The more ductile lower crust tends to flow and relax the deviatoric stress before much can accumulate there.(b) A vertical dike initiates, and thins as it crosses the Moho, because of the smaller deviatoric stress. The strain caused by the dike in this case imposes a stress which exceeds the residual deviatoric stress in the lower crust. The dike continues into the brittle upper crust where it widens, and combines with normal faulting to accommodate the deviatoric stress there. (c) A second pulse of dike intrusions form in the mantle and propagate upwards, but the dikes encounter a compressive regime in the lower crust. The melt is induced to intrude horizontally at the crust-mantle boundary because of the new stress conditions there. The second set of dikes accommodates the remaining deviatoric stress in the mantle, which may begin accumulating again with continued extension and the whole cycle may repeat many times. Multiple cycles of this process would cause the lower crust to become more mafic, and would help extending crust to maintain its thickness as well as influence the character of the Moho.

predicted local variability of extensional flow combined with the observed seismic velocity and reflectivity observations can perhaps lead to a unified conclusion. Since it seems that significant flow from outside the Basin and Range province is precluded by the lack of strong patterns of reflectivity in its margins, then the only sources that could have maintained Basin and Range crustal thickness are a thick pre-extension crust, and/or intrusion of magma from the mantle. Furthermore, the variable seismic velocities in the lower crust of the Basin and Range indicate that underplating probably occurs as distributed thin sheets rather than as a thick, contiguous layer. The scale length of lower-crustal reflections from beneath the Basin and Range is typically short (<5 km), perhaps an indication that ductile crustal flow has acted to disrupt the intrusive sheets into small lenses, while also evening out crustal thickness locally, pulling rock from beneath the ranges into the crust beneath the basins. Underplating

as thin sheets is more effective in conducting heat quickly into the lower crust than would be a massive underplated layer. Thus the granulite xenoliths observed from beneath the southern Basin and Range may have been heated by a relatively smaller volume of mafic melt than was proposed by Hayob et al. (1989), which is more consistent with the low observed $^3He/^4He$ ratios (e.g., Torgersen, 1993).

7.5.3 Isostatic Constraints on the Basin and Range Upper Mantle Structure

The mantle beneath the Basin and Range province can be investigated if the thickness and density of the crust are known. If a good estimate of these two parameters can be made, then it is possible to estimate the crustal contribution to uplift and thereby isolate the remaining mantle contribution. There is a strong indication that the southern and northern Basin and Range mantle are behaving quite differently, since the crust in the two regions is similar in thickness and average velocity, while their topographic elevations differ by about a km. If the crustal buoyancy alone cannot float the lithosphere enough to account for the difference in elevations, then a mantle contribution to the northern Basin and Range elevation is indicated. The crustal-thickness information for the western United States from seismic refraction surveys (Fig. 7–11) was combined with information on upper-crustal density variation from a basin-stripped isostatic residual gravity map (Saltus, 1991). These gravity data give an indication of the relative density variation of the upper-crustal basement rocks because the effects of sedimentary basins and regional trends have been removed. Density perturbations of the upper-crustal rocks can be approximated with the relation $\rho \approx \left(g/0.04L_{uc}\right)$ (e.g., Simpson and Jachens, 1989), where g is gravity in mGal, and L_{uc} is an assumed upper-crustal thickness (15 km). Lower-crustal densities are not delimited by the data and were assigned a uniform value of 2.9 g/cm^3; the lower-crustal layer is too thin for even strong density variations within it to cause the large observed mass deficit. Combining the crustal-thickness and upper-crustal density data results in the approximate crustal contribution to uplift across the western Cordillera; this when compared with the topography, indicates the mantle contribution to uplift (Fig. 7–13). Regional isostasy is assumed because the free air gravity anomaly averages zero across the region (e.g., Thompson and Zoback, 1979).

The upper-mantle mass per unit area is found by dividing the study area into a grid of isostatic columns. These columns are calculated using a two-layer isostatic expression with a known crustal layer, and a second mantle layer that extends down to an assumed local iso-density asthenosphere at a depth of ~200 km. The problem can be viewed as a group of 200-km-deep columns each containing the unknown boundary between the lithosphere (of unknown density) and the fixed-density asthenosphere. Since the crust is treated as a known quantity, and the topographic elevation is known, then the mass contained within the lithospheric mantle part of the column required to float it to its individual height can be calculated. The mantle mass per unit area of a given column (ΔM_n) is found by comparing it to a reference column, which is the column in the study area that contains the greatest amount of mass (and hence has the lowest mantle buoyancy), as

$$\Delta M_n = \left(I_n - I_{ref}\right) ,$$

where

$$I_n = \rho_a E_n - \left(\rho_a - \rho_c\right) L_{cn}$$

is a modified form of the isostatic equation (e.g., Lachenbruch and Morgan, 1990). The variable L_{cn} is the thickness of the crust in column n, ρ is density with the a and c subscripts denoting asthenosphere and crust respectively (ρ_a = 3.2 g/cm^3; variation in the fixed asthenosphere density does not affect relative difference between columns), and E_n is topographic elevation .

On the basis of isostatic calculations, Figure 7–13 shows that a broad low-density anomaly underlies the northern Basin and Range province, extending from the Sierra Nevada in the west to the Colorado Plateau in the east. Similar results were achieved by Jones et al. (1992), who used a slightly different method. The peak of the anomaly corresponds approximately to the center of the northern Basin and Range province, with the bulk of the anomaly to the south beneath the central Basin and

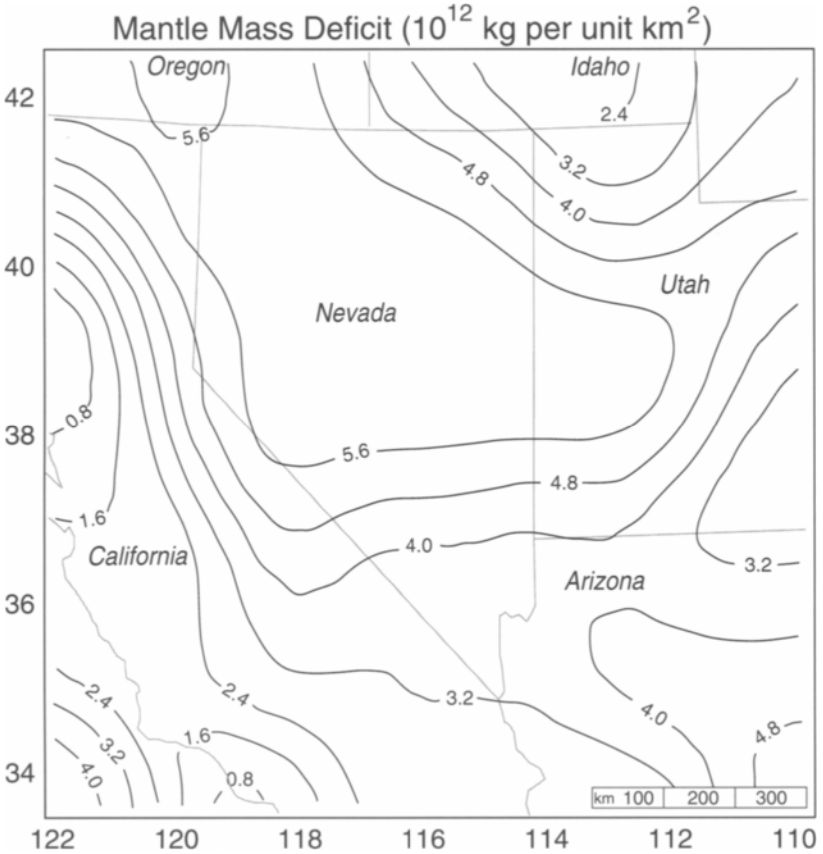

Fig. 7–13. Contour plot of relative variation in upper-mantle mass beneath investigated part of the western Cordillera. Values were calculated using a modified form of the isostatic equation with crustal depth information from seismic-refraction profiles (Fig. 7–11). The free-air gravity anomaly across the region is near zero, which implies that the area is in isostatic equilibrium. The thin crust of the northern Basin and Range province associated with its high elevation requires an underlying low-density upper mantle if isostasy is to be satisfied. The similar crust of the southern Basin and Range is a km lower in elevation, a possible indication that the mantle asthenosphere is different from north to south.

Range. The inferred Yellowstone plume track (eastern Snake River Plain) does not appear as a low-density anomaly on this image because the crust there has been largely replaced by more dense basalt (e.g., Sparlin et al., 1982), which has caused subsidence. The sum of the mantle isostatic mass deficit is ~3.6×10^{18} kg beneath the region investigated. Extension and thinning of the Basin and Range lithosphere allowed the asthenosphere to rise and take its place, causing some of the mass deficit. Earthquake-source methods that measure the variation in lithospheric thickness between the Basin and Range province and the unextended Colorado Plateau converge on a difference in the mantle-lid thickness that ranges between 15 and 50 km across the two provinces (see Section 7.4.4.3 or Iyer and Hitchcock, 1989; Beghoul et al., 1993). If a reasonable density contrast between asthenosphere and lithosphere of 0.05 g/cm^3 is used (e.g., Thompson and Zoback, 1979; Lachenbruch and Morgan, 1990) then the mass deficit caused by lithospheric thinning amounts to ~4.8×10^{17}–1.6×10^{18} kg, or 13%–44% of the total anomaly. If the entire anomaly is attributed to lithospheric thinning over an adiabatic asthenosphere, then a mantle lithospheric layer ~112

km thick would need to have been removed from the Basin and Range province across the study area to account for the entire estimated mass deficit.

The mantle lid as measured in the northern and southern Basin and Range province is very similar (Fig. 7–9), which implies that some other cause of low density mantle besides mantle lithospheric thinning has occurred in the northern Basin and Range. Saltus and Thompson (1993) investigated the topographic difference between the northern and southern Basin and Range using gravity data and found that only half of the isostatic support could possibly come from the crust, while thermal expansion and phase changes were unlikely sources of the density anomaly in the mantle. Instead, they suggested that the Yellowstone plume may be responsible for the low density northern Basin and Range mantle. The possible role of the Yellowstone plume in Basin and Range extension is discussed further in Section 7.6.4.

7.6. Tectonic Evolution: Sources of Basin and Range Extensional Stress

The extensional stresses that caused the opening of the Basin and Range province are the consequences of pre-Tertiary and Tertiary tectonic events. Possibly both passive and active rifting have occurred at various stages of Basin and Range extension. As was discussed briefly in Section 7.1.1, tectonic cycles have worked and reworked the western Cordilleran lithosphere since it was a passive margin in the Proterozoic Eon. It would be difficult to quantify exactly how much the lithosphere was weakened relative to the cratonic interior by those tectonic cycles, but they have very likely defined the breadth of Basin and Range extension, since broad rifting is predicted in weak lithosphere, while narrow, more typical rifting is predicted in cold, strong lithosphere (e.g., Buck, 1991). It is a common coincidence to observe extensional deformation overprinting earlier compressional structure throughout the Basin and Range province (e.g., Coney, 1987; Wernicke, 1992). Many of the sources of extensional stress can be attributed to the varying configurations between the North American and the Pacific, and the now-extinct Farallon, oceanic plates.

7.6.1 North America – Farallon Plate : Back- and Intra-Arc Extension

At about 43 Ma a major global plate reorganization caused a change in the Pacific plate motion relative to North America (e.g., Engebretson et al., 1985). The Farallon plate still intervened between North America and the Pacific plate at this time (Fig. 7–3), and was isolated from the global system by a spreading center between it and the Pacific plate and a subduction zone along the North American plate boundary. The motion of the Farallon plate may also have begun to slow independently of the global system because the Pacific-Farallon spreading ridge drifted east relative to North America, causing the subduction of increasingly younger oceanic lithosphere until a plate with positive buoyancy was forced beneath North America (e.g., Engebretson et al., 1984). The rate of Farallon-North American convergence at 40° N was still at its peak at 50 Ma, but began a rapid decline shortly after that (e.g., Engebretson et al., 1984). Heaton and Kanamori (1984) noted a worldwide tendency for back-arc basins to form behind subduction zones with rapid convergence and low coupling. Thus the suggestion that the early stages of northern Basin and Range province extension that began in southern Canada and the northwestern United States resulted from back-arc extensional stresses (e.g., Zoback et al., 1981) seems valid. Stratigraphic constraints and trace-element signatures of volcanic rocks that erupted at about 30 Ma in northern Mexico indicate that the initial stages of extension there occurred in a back- or intra-arc setting (Cameron et al., 1989). When the Farallon-North American convergence rate slowed because the oceanic slab buoyancy increased, that style of extension seems to have died out in the northern Basin and Range province. The ignimbrite volcanic event in central Nevada, the closing of the Laramide magmatic gap, and associated extension correlates in time with the onset in slowing of the convergence rate between the Farallon and North American plates and a possible change in the angle of subduction. Speculatively, this stage of extension may have been a brief period of active rifting, driven by a sudden burst of magmatism associated with renewed asthenospheric contact beneath Nevada and

Utah after the slab angle steepened. Elston (1984) suggested that an "extensional orogeny" caused the ignimbrite event, and that the subduction of hot, young oceanic lithosphere enhanced the tendency of continental lithosphere to extend towards its margin through thermal input.

7.6.2 Extensional Spreading Resulting from Orogenic Over-thickening

A consequence of unstable over-thickening of continental lithosphere is that it will attempt to spread back out to its pre-compressional thickness. The over-thickened lithosphere can be thought of as storage of potential energy poised to be released. In order for that release to occur, the outer boundaries of the thickened lithosphere must become less confined, to allow room for spreading, or the topographic head must overcome those constraints. Widespread compressional features in the western Cordillera indicate that lithospheric thickening occurred during long-term subduction and reached far inland during the Laramide orogeny, perhaps because of low-angle subduction of the Farallon slab (e.g., Dickinson and Snyder, 1978; Bird, 1984). Coney and Harms (1984) reassembled the Tertiary extension of the Basin and Range assuming extension on the order of 40–60%, and found the pre-extension thickness to be about 40–60 km, similar to thicknesses beneath the Colorado Plateau and Rocky Mountains. Further explanation is required to explain why the over-thickened Basin and Range province lithosphere should have extended so readily while the equally thickened Colorado Plateau and Rocky Mountains have not. Coney (1987) and Sonder et al. (1987) suggested that a softer lithospheric rheology caused by the ignimbrite event may have stimulated lithospheric outflow and allowed preferential spreading in the Basin and Range; they further suggested that this spreading may have been enhanced by decreased compressional stresses applied at the continental margin because of slowing Farallon subduction. Harry et al. (1993) proposed through finite-element modeling that the orogenic over-thickening may have caused upper mantle weakening that focused extensional strain and re-equilibration of lithospheric thickness in the Basin and Range province. They also suggested that the marginal highlands of the Sierra Nevada and Colorado Plateau were outside the regions of upper mantle weakening and hence were not extended.

7.6.3 Basin and Range Rifting as a Result of Pacific - North American Plate Divergence

The global-circuit and hotspot-reference plate reconstruction models (Engebretson et al., 1985; Stock and Molnar, 1988) show that the Pacific plate has drifted to the northwest relative to a reference fixed on the interior of North America since 42 Ma. The rate of longitudinal displacement (the westerly component) has been about 30 km/m.y., depending on the latitude examined. The half spreading rate on the Pacific-Farallon ridge was slightly greater over the same time period, allowing the ridge axis to migrate slowly eastward towards North America. The initial contact of the eastern accreting edge of the Pacific plate with the western edge of the North American plate occurred at 29 Ma just south of the Pioneer fracture zone (Severinghaus and Atwater, 1990). Since then the Pacific plate has moved west by about 10.2° of longitude, which corresponds to slightly over 900 km at the latitude of 38° N. This compares to 8.3° of latitudinal drift during the same time period. The segment of the North American edge at the initial contact point has kept pace with the rapid west drift of the Pacific plate for the last 29 m.y. The Pacific-North American plate boundary evolved in the last 29 Ma from a short simple contact at the subduction interface to the present complex zone, over 2,300 km long, that partly resides within the continent and partly includes a small new ocean in the Gulf of California (Atwater, 1970; Lonsdale, 1991). Atwater (1970) explained the plate boundary evolution in the context of the migrating-triple-junction paradigm. However, Lonsdale (1991) has convincingly shown that long, extinct ridge segments and the corresponding fragments of the Farallon plate are still preserved offshore along most of the Pacific-North American plate boundary, limiting the applicability of the migrating triple junction hypothesis to the Californian system and indicating that the boundary lengthened primarily through a series of plate-capture events. With each

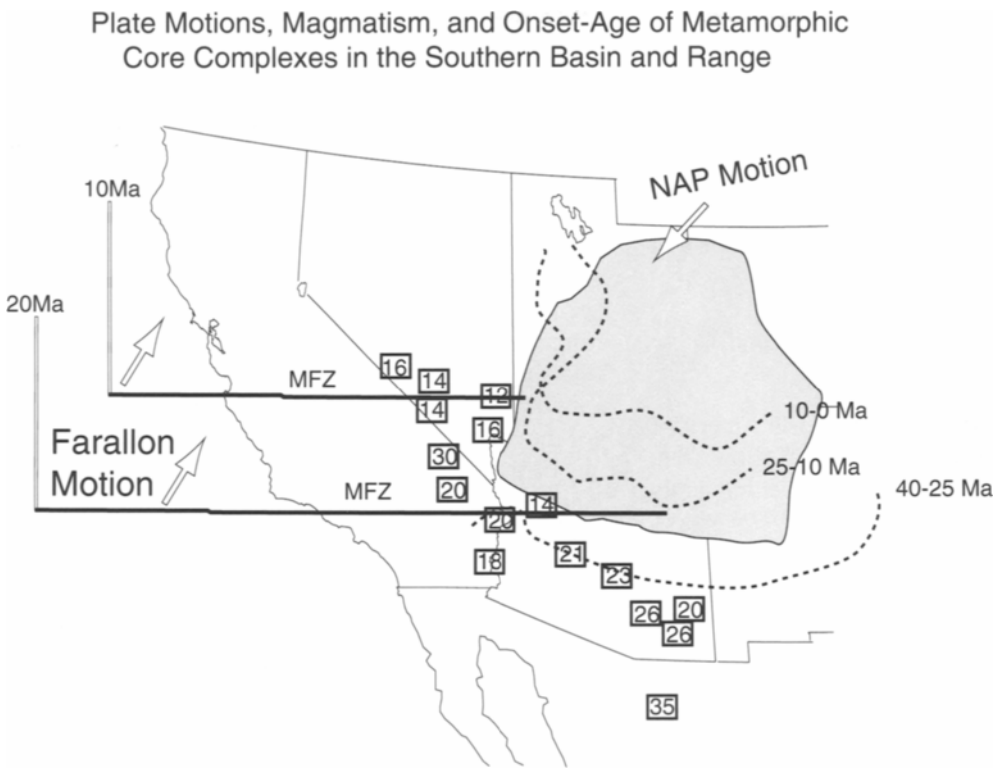

Fig. 7–14. Predicted locations of the coherent Farallon slab shown with the locations and timing of onset of core complex extension and magmatism. The dashed lines mark the local northward extent of magmatic activity with time after Armstrong and Ward (1991), and the boxed numbers are approximate time since core-complex initiation (in Ma) as summarized by Axen et al. (1993). The gray shaded area is the uplifted Colorado Plateau. These tectonic events are part of a broad northwest-younging trend that parallels the continental margin, and seems related to the change in subduction style.

event, a longer segment of the North American continent and the corresponding subducted fragment of the Farallon plate were exposed to the rapid west drift of the Pacific plate. Cordilleran North America expanded westward to fill the burgeoning gap between the rigid Pacific plate and the cratonic interior of North America (e.g., Bohannon and Parsons, submitted, 1994).

Many researchers have noted an apparent tie between the onset of extension in the southern Basin and Range province and the termination of Farallon plate subduction beginning at about 30 Ma (e.g., Atwater, 1970; Engebretson et al., 1984; Glazner and Bartley, 1984; Severinghaus and Atwater, 1990; Ward, 1991; Axen et al., 1993). Axen et al. (1993) and Gans et al. (1989) show a space-time migration of activity in this belt that closely corresponds to the northward progression of the Pacific plate contact zone between 15 and 30 Ma. It began at approximately 30 Ma at precisely the latitude of the initial contact. The space-time migration of the initiation of extension follows the position of the northern limit of the plate contact, and the migration of cessation corresponds well with the northern limit of active spreading taking place south of the Farallon fracture zone (Figure 7–14). By 15 Ma the Pacific-North American contact zone had lengthened to include all of the continental edge from the southern borderland rift of Crouch and Suppe (1993) to the latitude of southern Nevada. Most of the extension that was active in the Basin and Range province up to 15 Ma was taking place somewhere directly inland of

the contact zone (Axen et al., 1993). By 10 Ma that pattern had probably changed somewhat because a large amount of regional extension was taking place in the Great Basin that was north of the inland projection of the Mendocino fracture zone (e.g., Hamilton, 1987; Gans et al., 1989; Wernicke, 1992). The direction of least principal stress (and extensional strain) had rotated about 45° by this time to a more east-west direction (Zoback et al., 1981).

7.6.4 Role of Yellowstone Plume in Basin and Range Extension?

During the past 16–17 m.y., the North American plate has moved southwest over the Yellowstone plume, leaving the Snake River Plain behind as its track (Morgan, 1972; Armstrong et al., 1975, Pierce and Morgan, 1992). The Yellowstone hot spot emerged with a burst of basaltic volcanism that may have formed the Columbia Plateau flood basalts to the northwest and the northern Nevada rift to the southeast (Zoback and Thompson, 1978). Magmatic activity on the eastern Snake River Plain was initially characterized by pulses of silicic volcanism (each of ~2- to 3-m.y. duration) progressing toward the present Yellowstone caldera. Most of the silicic volcanic rocks decrease in age to the northeast (35 to 40 mm/yr) as a result of southwestward plate migration over the plume (Christiansen and Lipman, 1972; Armstrong et al., 1975). Extensive basaltic volcanism followed, covering the plain and persisting through Holocene time (e.g., Luedke and Smith, 1983). Seismic-refraction data indicate that much of the midcrust beneath the plain was replaced by intruded basalt (e.g., Sparlin et al., 1982). The location of the Yellowstone starting plume head and the start of the plume tail is subject to discussion, because it may have encountered the subducting Juan de Fuca plate during its ascent and part of the plume-head material could have been spread westward as far as the Juan de Fuca ridge by the descending plate (R. I. Hill et al., 1992).

While the deep origin of mantle plumes is controversial, their surface expression is dramatic and widely observed. Perhaps the two most ubiquitous manifestations of mantle plumes are voluminous volcanism and a broad regional topographic swell. The typical swell associated with plumes is ~1–2 km of uplift centered across a region ~1000-2000 km in diameter (e.g., Crough, 1983; Sleep, 1990); this uplift is largely the result of isostatic compensation in the asthenosphere and lithosphere and, to a lesser extent, a dynamic pressure gradient of flow in the asthenosphere (below the limit of detection at Hawaii) (Sleep, 1990). The interpreted anatomy of a mantle plume consists of a starting plume head generated during its initial ascent through the mantle, an active plume tail that continues to flow after the starting plume head contacts the lithosphere, and ponded plume-tail material that collects at the base of the lithosphere as the active plume tail continues to flow (e.g., Griffiths and Campbell, 1991). The initial contact of the starting plume head with the lithosphere heats a broad region, because the plume head is much wider than its tail (e.g., Campbell and Griffiths, 1990; Duncan and Richards, 1991). When a hot-spot swell forms in continental lithosphere the uplifted crust may be raised far enough above the level of midplate compression to be in a state of extension, which results in rift formation centered in the swell (e.g., Crough, 1983). The magnitudes of the generated deviatoric stresses fall short of those necessary to cause complete continental breakup (Hill, 1991). The buoyancy and swell associated with the starting plume head tend to move with the lithospheric plate (Sleep, 1990; Griffiths and Campbell, 1991). The heat associated with mantle plumes tends to be contained in the mantle near the plume for a considerable time. For example, Davies (1992) concluded that the thermal anomaly associated with the Hawaiian plume has not waned during its 43-m.y. existence because the swell does not decay monotonically with distance along the volcanic chain as would be the case in a thermal decline with age. That is, the material hotter than the normal mantle adiabat remains ponded below the lithosphere and above normal asthenosphere because of the long time required for heat applied at the base of the lithosphere to conduct to the surface and because secondary convection within the thermal boundary created by plume material is inefficient.

In Section 7.5.3 it was shown that a low-density mantle underlies the northern Basin and Range province. If the Yellowstone plume behaved like the vast

majority of plumes observed worldwide, then it probably had a starting head consisting of hot, lower density mantle compared to the surrounding Basin and Range asthenosphere. The emplacement of such a low-density mantle anomaly would have caused a topographic swell across the northern Basin and Range which may have in turn contributed to gravitational spreading as discussed in Section 7.6.2 and may have extended the Basin and Range province eastward along the plume track (e.g., Anders and Sleep, 1992; Pierce and Morgan, 1992). The increased thermal input from the flux of basaltic volcanism may have also stimulated extension in the vicinity of the plume by reducing the rheologic strength of the lithosphere (e.g., Anders and Sleep, 1992). The Yellowstone plume cannot be suggested as the sole cause of the latest phase of Basin and Range block faulting between 10–13 Ma, because those structures are active far south into Mexico, well out of reach of even a very large plume head. Thus if valid, the plume-head hypothesis may be more directly applicable to the relative topographic difference between the northern and southern Basin and Range.

7.7. Summary

The Basin and Range province defies generalities. There are almost always exceptions to every broad statement that can be made. For example it might be safe to suggest that the episodes of extension on low-angle normal faulting are over and that all present-day extension occurs on high-angle faults; but a seismic reflection survey in southeastern Arizona may have identified a seismogenic low-angle normal fault there (Johnson and Loy, 1992). Thus all the following broad statements and conclusions must be interpreted with the understanding that contradictions may be found at a given locality or in a specific study.

The entire western third of North America is elevated well above sea level regardless of whether it was extended or not, apparently the result of long-term subduction. Extension has widened the zone of high elevation, causing minor subsidence in the northern Basin and Range, and major subsidence, including the opening of a new ocean basin in the southern Basin and Range. Basin and Range extension is largely confined to the orogenic crust of the western Cordillera. Tectonism within the Cordillera probably weakened the lithosphere enough to enable the broad extension that has occurred there, in contrast to the more typical pattern of narrow rifting that is observed worldwide. Also contributing to the atypical breadth and elevation of the extended Basin and Range lithosphere are the time-space varying sources of extensional stresses imposed. A complicated series of events led to the extensional stresses, beginning with back-arc extension that occurred as isolated core complexes in the Pacific Northwest region during Eocene and early Oligocene time. Back-arc extension was probably also the initial style of opening in the southern Basin and Range in Mexico, beginning in middle Oligocene time. In order for a metamorphic core complex to have formed, unusual conditions such as an increased tendency for lower-crustal rocks to flow beneath them, or a change in the stress field must have existed. Both of those conditions could have been met by increased magmatism beneath the complexes, and it may be that subduction-related magmatism localized back-arc extension to those highly extended terranes in the northern Basin and Range during Eocene time.

Over-thickened lithosphere may have been weakened by the orogenic process itself, a flare-up in arc-related magmatism associated with slowing subduction, or heat transferred from the younger, hotter oceanic lithosphere that was subducted beneath it during the latest Eocene. Those factors, combined with decreased convergence at the subduction margin may have allowed the over-thickened Basin and Range lithosphere to return to a more normal thickness. However, the present-day Colorado Plateau is only collapsing very weakly along its outer margins, and is for the most part a stable piece of lithosphere. Thus it would seem that conservation of energy constraints prevent over-thickening alone from driving the Basin and Range lithosphere into the intense extension that has occurred there, unless the lithospheric mantle beneath it was substantially different from that of the rest of the western Cordillera. In other words, gravitational collapse undoubtedly contrib-

uted to some Basin and Range spreading, but outside forces had to act on the lithosphere to stretch it beyond the point of stability.

Such outside forces may have come from the divergence between the Pacific and North American plates. Up until 30 Ma the subducting Farallon plate protected the western Cordillera from the relative northwest motion of the Pacific plate. As the Farallon plate offshore of North America diminished due to continued subduction, the Pacific plate converged on North America. Asthenosphere windows have been suggested to have evolved as the remnants of the Farallon plate sank into the mantle. There is a space problem with such models because the westward drift of the Pacific plate would have quickly exposed such windows to the surface, since the North American plate could never move fast enough to cover the window if it existed at the continental margin. If instead, the Farallon plate was mechanically underplated beneath the North American continental margin as is suggested by seismic refraction studies of the margin (Howie et al., 1993; Brocher et al., 1993), then that preserved slab may have provided the link between the Pacific and North American plates that began to move together after contact (e.g., Stock and Molnar, 1988). The post-30-Ma core complex extension that began in northern Mexico and trended northward with the growing contact between the North American and Pacific plates (Fig. 7–14) then took up the divergence between the two plates. That extension took place primarily in the weak orogenic crust behind the Mesozoic batholiths clustered along the coast, but also may have occurred in the California Continental Borderlands that now lie offshore of southern California. The growing contact between the North American and Pacific plates became partially resolved along the San Andreas transform, which is not however perfectly aligned to take up all the relative motion between the two plates. Thus broad, small-magnitude extensional deformation in the Basin and Range province became necessary in order to take up the remaining relative motion, which may have prompted the latest phase of block faulting across the province. Complicating matters further, the Yellowstone plume emerged during Miocene time, and may have emplaced low-density asthenosphere beneath the northern Basin and Range province, causing its high elevation relative to the southern Basin and Range. The plume may also have made some contribution to extension through the resulting topographic swell, and may have extended the Basin and Range province to the northeast as the continent tracked over it.

Geologic and geophysical probing of the Basin and Range lithosphere indicate a province that is highly variable at the surface, while being far more uniform at depth. This uniformity may be more apparent than real, however, because of the fact that the resolution in methods applied to the deeper study of the lithosphere is quite low as compared with direct examination of the surface. The picture of the lithosphere as it emerges with the present levels of resolution (Fig. 7–15) is a brittle upper-crustal layer that extends by a variety of modes (e.g., high and low-angle faulting, magmatism) overlying a ductile lower-crustal layer that accommodates much of the surface variation in strain by flow that equalizes the thickness of the crust to an average 30 km (± 5 km). The ductile lower-crustal layer is augmented by thin sheets of magma intruded from the mantle that give it increased mobility through advected heat. Similarly, the crust-mantle boundary is interlayered mafic intrusive rocks and mantle peridotites, and has been very hot (granulite facies in the southern Basin and Range), though 300 °C of cooling may have occurred in the north-central Basin and Range lower crust. Magmatism accompanied extension, but the exact timing and relation to extensional faulting remains controversial. The uppermost mantle is a thin high-velocity zone (7.6–8.1 km/s) that is slower than the upper mantle beneath the interior continental craton. Beneath a 20–40 km-thick mantle lid lies a low-velocity (7.5–7.7 km/s) zone of mantle asthenosphere that may range from 40 to 100 km thick. The crustal and upper mantle structures are similar beneath the northern and southern Basin and Range, which implies that the 1 km difference in topographic elevation is at least partly due to a density contrast in the asthenosphere between the two sub-provinces. The chemistry of magma rising through the northern Basin and Range province is consistent with upwelling asthenosphere there, perhaps because the

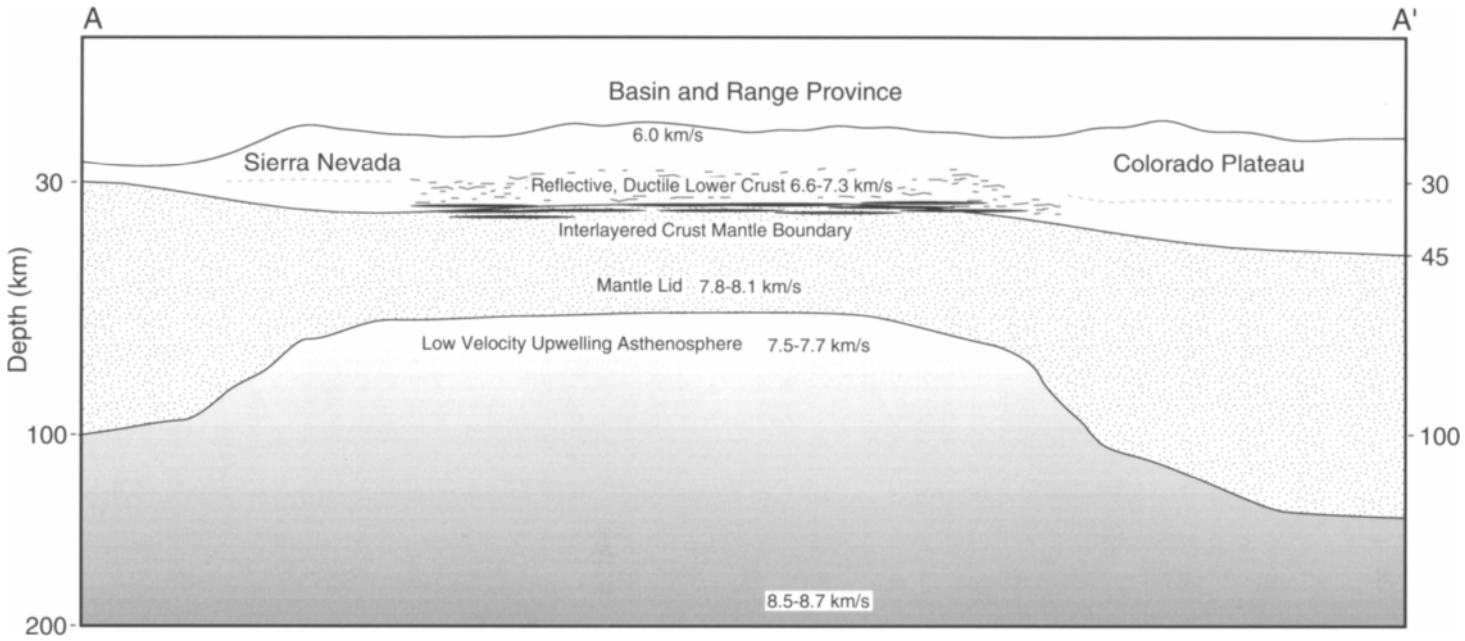

Fig. 7–15. Interpretive lithospheric cross-section (A–A' on Figure 7–1) of the northern Basin and Range province. The crust of the Basin and Range is thinner (30–35 km) than the adjacent Sierra Nevada and Colorado Plateau provinces (40–45 km), and the lower crust is highly reflective, possibly a result of ductile deformation and magmatic intrusions. The lower crustal velocities of the Basin and Range vary from about 6.6 to 7.3 km/s, perhaps because of variable magmatic underplating. Xenoliths from the crust-mantle boundary indicate that the Moho transition is interlayered magmatic intrusions and mantle peridotites. A thinned (30–50 km thick compared with 100–140 km thick beneath the Colorado Plateau and Great Valley) high velocity (7.8–8.1 km/s) mantle lid overlies a lower velocity (7.5–7.7 km/s) asthenosphere.

lithosphere has been thinned relative to the more stable regions surrounding the province, or because of active upwelling from a plume source.

Acknowledgments. Many of the studies and original ideas presented here were pointed out to me and/or shaped through discussions with Bob Bohannon, John Howie, Simon Klemperer, Jill McCarthy, Walter Mooney, Stan Ruppert, Rick Saltus, Bob Simpson, Norm Sleep, George Thompson, and Howard Wilshire. Special thanks to Scott Baldridge, Jill McCarthy, Walter Mooney, Ken Olsen, and George Thompson for helpful, careful, and constructive reviews of the manuscript. Support for this work came from the U.S. Geological Survey Deep Continental Studies Program and the U. S. Geological Survey Branch of Pacific Marine Geology.

7.8. References

Allmendinger, R. W., Hauge, T. A., Hauser, E. C., Potter, C. J., Klemperer, S. L., Nelson, K. D., Knuepfer, P., Oliver, J., 1987. Overview of the COCORP 40° N transect, western United States: The fabric of an orogenic belt. Geol. Soc. Am. Bull., 98: 308–319.

Al-Khatib, H. H., and Mitchell, B. J., 1991. Upper mantle anelasticity and tectonic evolution of the western United States from surface wave attenuation. J. Geophys. Res., 96: 18129–18146.

Anders, M. H., Geissman, J. W., Piety, L. A., and Sullivan, J. T., 1989. Parabolic distribution of circumeastern Snake River Plain seismicity and latest Quaternary faulting, migratory pattern and association with the Yellowstone hotspot. J. Geophys. Res., 94: 1589–1621.

Anders, M. H., and Sleep, N. H., 1992. Magmatism and extension: the thermal and mechanical effects of the Yellowstone hotspot. J. Geophys. Res., 97: 15379–15393.

Anderson, E. M., 1951. The dynamics of faulting and dyke formation. Edinburgh, Oliver and Boyd, 206 pp.

Anderson, R. E., 1971. Thin skin distension in Tertiary rocks of southeastern Nevada. Geol. Soc. Am. Bull., 82: 43–58.

Archambeau, C. B., Flinn, E. A., and Lambert, D. G., 1969. Fine structure of the upper mantle. J. Geophys. Res., 74: 5825–5865.

Argus, D. F., and Gordon, R. G., 1991. Current Sierra Nevada-North American motion from very long baseline interferometry: Implications for the kinematics of the western United States. Geology, 19: 1085–1088.

Armstrong, F.C., Leeman, W.P., and Malde, H.E., 1975. K-Ar dating, Quaternary and Neogene volcanic rocks of the Snake River Plain, Idaho. Am. J. Science, 275: 225–251.

Armstrong, R. L., and Ward, P., 1991. Evolving geographic patterns of Cenozoic magmatism in the North American Cordillera: The temporal and spatial association of magmatism and metamorphic core complexes. J. Geophys. Res. 96: 13201–13224.

Artyushkov, Y. V., and Batsanin, S. F., 1984. Change in the thermal regime of the Earth's crust associated with the approach of anomalous mantle to its lower boundary. Izvestiya, Earth Physics, 20: 887–891.

Asmerom, Y., Snow, J. K., Holm, D. K., Jacobsen, S. B., Wernicke, B. P., and Lux, D. R., 1990. Rapid uplift and crustal growth in extensional environments; an isotopic study from the Death Valley region, California. Geology, 18: 223–226.

Atwater, T. M., 1970, Implications of plate tectonics for the Cenozoic tectonic evolution of North America: Geol. Soc. Am. Bull., 81: 3513–3536.

Axen, G. J., Taylor, W. J., and Bartley, J. M., 1993. Space-time patterns and tectonic controls of Tertiary extension and magmatism in the Great Basin of the western United States. Geol. Soc. Am. Bull.: 105: 56–76.

Bartley, J.F., and Glazner, A.F., 1985. Hydrothermal systems and Tertiary low-angle normal faulting in the southwestern United States. Geology, 13: 562–564.

Bartley, J. M., and Wernicke, B. P., 1984. The Snake Range decollement interpreted as a major extensional shear zone. Tectonics, 3: 647–657.

Beghoul, N., Barazangi, M., and Isacks, B. L.,1993. Lithospheric structure of Tibet and western North America: Mechanisms of uplift and a comparative study. J. Geophys. Res., 98: 1997–2016.

Benz, H. M., Smith, R. B., and Mooney, W. D., 1990. Crustal structure of the northwestern Basin and Range province from the 1986 Program for Array Seismic Studies of the Continental Lithosphere seismic experiment. J. Geophys. Res., 95: 21823–21842.

Bergantz, G. W., 1989. Underplating and partial melting: Implications for melt generation and extraction. Science, 245: 1093–1095.

Beroza, G. C., Jordon, T. H., Minster, J. B., Clark, T. A., and Ryan, J. W., 1985. VLBI vector position data; Application to western U.S. deformation. Eos Trans., 66: 848.

Best, M. G., and Christiansen, E. H., 1991. Limited extension during peak Tertiary volcanism, Great Basin of Nevada and Utah. J. Geophys. Res., 96: 13509–13528.

Biasi, G. P., and Humphreys, E., 1992. P-wave image of the upper mantle structure of central California and southern Nevada. Geophys. Res. Lett., 19: 1161–1164.

Bird, P., 1984. Laramide crustal thickening event in the Rocky Mountain foreland and Great Plains. Tectonics, 3: 741–758, 1984.

Blackwell, D. D., 1978. Heat flow and energy loss in the western United States. In: Smith, R. B., and Eaton, G. P. (Editors), Cenozoic tectonics and regional geophysics of the western Cordillera. Geol. Soc. Am. Mem. 152, pp. 175–208.

Blakely, R. J., 1988. Curie temperature isotherm analysis and tectonic implications of aeromagnetic data from Nevada. J. Geophys. Res., 93: 11817–11832.

Blakely, R. J., and Jachens, R. C., 1991. Regional study of mineral resources in Nevada: Insights from three-dimensional analysis of gravity and magnetic anomalies. Geol. Soc. Am. Bull., 103: 795–803.

Bohlen, S. R., and Mezger, K., 1989. Origin of granulite terranes and the formation of the lowermost continental crust. Science: 326–329.

Bradshaw, G.A., and Zoback, M.D., 1988. Listric normal faulting, stress refraction, and the state of stress in the Gulf Coast Basin. Geology, 16: 271–274.

Bradshaw, T.K., Hawkesworth, C.J., and Gallagher, K., 1993. Basaltic volcanism in the southern Basin and Range: no role for a mantle plume. Earth Planet. Sci. Lett., 116: 45–62.

Braile, L. W., Hinze, W. J., von Frese, R. R. B., and Keller, G. R., 1898. Seismic properties of the crust and uppermost mantle of the coterminous United States and adjacent Canada. In: Pakiser, L. C., and Mooney, W. D. (Editors), Geophysical Framework of the continental United States. Geol. Soc. Am. Mem., 172, pp. 655–680.

Brocher, T. M., Carr, M. D., Fox, K. F. Jr., and Hart, P. E., 1993. Seismic reflection profiling across Tertiary extensional structures in the eastern Amargosa Desert, southern Nevada, Basin and Range province. Geol. Soc. Am. Bull., 105: 30–46.

Brocher, T. M., Holbrook, W. S., ten Brink, U. S., Hole, J. A., and Klemperer, S. L., 1993. Results from wide-angle seismic reflection and refraction profiling of the San Francisco Bay area during BASIX. Geol. Soc. Am. Abstr. Prog., 25: A-310.

Bryant, B., and Wooden, J. L., 1989. Lower-plate rocks of the Buckskin Mountains, Arizona; a progress report. In: Spencer, J. E., and Reynolds, S. J. (Editors), Geology and mineral resources of the Buckskin and Rawhide mountains, west-central Arizona. Bulletin - State of Arizona, Bureau of Geology and Mineral Technology, Geological Survey Branch, 198, pp. 47–50.

Buck, W. R., 1991. Modes of continental lithospheric extension. J. Geophys. Res., 96: 20,161–20,178.

Burdick, L. J., and Helmberger, D. V., 1978. The upper mantle P-velocity structure of the western United States: J. Geophys. Res., 83: 1699–1712.

Burke, D. B., and McKee, E. H., 1979. Mid-Cenozoic volcano-tectonic troughs in central Nevada. Geol. Soc. of Am. Bull., 90: 181–184.

Campbell, I.H., and Griffiths, R.W., 1990. Implications of mantle plume structure for the evolution of flood basalts. Earth Planet. Sci. Lett., 99: 79–93.

Cameron, K. L., Nimz, G. J., Kuentz, D., Niemeyer, S., and Gunn, S., 1989. Southern Cordilleran basaltic andesite suite, southern Chihuahua, Mexico: A link between Tertiary continental arc and flood basalt magmatism in North America. J. Geophys. Res., 94: 7817–7840.

Carbonell, R. and Smithson, S. B., 1991. Crustal anisotropy and the structure of the Mohorovicic discontinuity in western Nevada of the Basin and Range province. In: Mesiner, R. et al. (Editors), Continental lithosphere: Deep seismic reflections. Geodynamics Series, American Geophysical Union, 22, pp. 31–38.

Catchings, R. D., 1992. A relation among geology, tectonics, and velocity structure, western to central Nevada Basin and Range. Geol. Soc. Am. Bull., 104: 1178–1192.

Catchings, R.D., and Mooney, W.D., 1989. Basin and Range crustal and upper mantle structure, northwest to central Nevada. J. Geophys. Res., 96: 6247–6267.

Chau, L. L., 1989. A magnetotelluric of electrical conductivity in the northern Nevada rift zone; implications on Tertiary extension in the central Basin and Range. [M.S. Thesis]. University of California, Riverside, Riverside, California, 132 pp.

Cheadle, M. J., Czuchra, B. L., Byrne, T., Ando, C. J., Oliver, J. E., Brown, L. D., Malin, P. E., and Phinney, R. A., 1986. The deep crustal structure of the Mojave Desert, California, from COCORP seismic reflection data. Tectonics, 5: 293–320.

Christiansen, R. L., and Lipman, P. W., 1972. Cenozoic volcanism and plate tectonic evolution of the western United States, II, Late Cenozoic. Phil. Trans. R. Soc. Lond., 271: 234–249.

Clark, T. A., Gordon, D., Himwich, W. E., Ma, C., Mallama, A., and Ryan, J. W., 1987. Determination of relative site motions in the western United States using Mark III very long baseline interferometry. J. Geophys. Res., 92: 12741–12750.

Conde, K. C., 1982. Plate tectonics and crustal evolution, New York, Pergamon Press. 310 pp.

Coney, P. J., 1980. Cordilleran metamorphic core complexes: An overview. Geol. Soc. Am. Mem., 153: 7–31.

Coney, P. J., 1987. The regional tectonic setting and possible causes of Cenozoic extension in the North American Cordillera. In: Coward, M. P., Dewey, J. F., and Hancock, P. L. (Editors), Continental Extensional Tectonics: Geol. Soc. Lond. Spec. Pub., 28, pp. 177–186.

Coney, P. J., and Harms, T. A., 1984. Cordilleran metamorphic core complexes: Cenozoic extensional relics of Mesozoic compression. Geology, 12: 550–554.

Coney, P. J., and Reynolds, S. J., 1977. Cordilleran Benioff zones. Nature, 270: 403–406.

Crouch, J. K., and Suppe, J., 1993. Late Cenozoic tectonic evolution of the Los Angeles Basin and inner California borderland; a model for core complex-like crustal extension. Geol. Soc. Am. Bull. 105: 1415–1434.

Crough, S.T., 1983. Hotspot swells. Ann. Rev. Earth Planet. Sci., 11: 165–193.

Crough. S. T., and Thompson, G. A., 1976. Thermal model of continental lithosphere, J. Geophys. Res., 81: 4857–4862.

Daley, E. E., and DePaolo, D. J., 1992. Isotopic evidence for lithospheric thinning during extension: Southeastern Great Basin. Geology, 20: 104–108.

Davies, G.F., 1992. Temporal variation of the Hawaiian plume flux: Earth Planet Sci Lett., 113: 277–286.

Davis, G. H.., 1983. Shear-zone model for the origin of metamorphic core complexes. Geology, 11: 342–347.

Davis, G.A., Anderson, J.L., Martin, D.L., Krummenacher, D., Frost, E. G., and Armstrong, R. L., 1982. Geologic and geochronologic relations in the lower plate of the Whipple detachment fault, Whipple Mountains, southeastern California: A progress report. In: Frost, E.G., and Martin, D.L. (Editors), Mesozoic-Cenozoic tectonic evolution of the Colorado River region, California, Arizona, and Nevada. San Diego, California, Cordilleran Publishers, pp. 408–432.

DeMets, C. Gordon, R. G., Argus, D. F., and Stein, S., 1990. Current plate motions: Geophys. J. Int., 101: 425–478.

de Voogd, B., Serpa, L., Brown, L., Hauser, E., Kaufman, S., Oliver, J., Troxel, B., Willemin, J., and Wright, L. A., 1986. Death Valley bright spot: A midcrustal magma body in the southern Great Basin, California? Geology, 14: 64–67.

Dewey, J. W., Hill, D. P., Ellsworth, W. L., and Engdahl, E. R., 1989. Earthquakes, faults, and the seismotectonic framework of the contiguous United States. In: Pakiser, L. C., and Mooney, W. D. (Editors), Geophysical Framework of the continental United States. Geol. Soc. Am. Mem., 172, pp. 541–576.

Dickinson, W. R., and Snyder, W. S., 1978. Plate tectonics of the Laramide Orogeny. Geological Society of America Memoir, 151: 355–366.

Dueker, K., and Humphreys, E., 1990. Upper-mantle velocity structure of the Great Basin. Geophys. Res. Lett., 17: 1327–1330.

Dumitru, T. A., Gans, P. B., Foster, D. A., and Miller, E. L., 1991. Refrigeration of the western Cordilleran lithosphere during Laramide shallow-angle subduction. Geology, 19: 1145–1148.

Duncan, R.A., and Richards, M.A., 1991. Hotspots, mantle plumes, flood basalts, and true polar wander. Rev. Geophys., 29: 31–50.

Eaton, G. P., Wahl, R. R., Protska, H. J., Maybe, D. R., and Kleinkopf, M. D., 1978. Regional gravity and tectonic patterns: Their to late Cenozoic epeirogeny and lateral spreading of the western Cordillera. In: Smith, R. B., and Eaton, G. P. (Editors), Cenozoic tectonics and regional geophysics of the western Cordillera. Geol. Soc. Am. Mem. 152, pp. 51–92.

Eddington, P. K., Smith R. B., and Renggli, C., 1987. Kinematics of Basin-Range intraplate extension. In: Coward, M. P., Dewey, J. F., and Hancock, P. L. (Editors), Continental Extensional Tectonics: Geol. Soc. Lond. Spec. Pub., 28, pp. 371–392.

Elston, W. E., 1984. Subduction of young lithosphere and extensional orogeny in southwestern North America during mid-Tertiary time. Tectonics, 3: 229–250.

Engebretson, D. C., Cox, A., and Gordon, R. G., 1985. Relative motions between oceanic and continental plates in the Pacific basin. Geol. Soc. Am. Spec. Pap., 206, 59 pp.

Engebretson, D. C., Cox, A., and Thompson, G. A., 1984. Correlation of plate motions with continental tectonics: Laramide to Basin and Range. Tectonics, 3: 115–119.

Fitton, J.G., James, D., and Leeman, W.P., 1991. Basic magmatism associated with late Cenozoic extension in the western United States: Compositional variations in space and time. J. Geophys. Res., 96: 13,693–13,712.

Fitton, J. G., James, D., Kempton, P. D., Ormerod, D. S., and Leeman, W. P., 1988. The role of lithospheric mantle in the generation of late Cenozoic basic magmas in the western United States. J. Petrol., Special Lithosphere Issue: 331–349.

Flueh, E. R., Okaya, D. A., 1989. Near vertical and intermediate offset reflection data from west of the Whipple Mountains, SE California. J. Geophys. Res., 94: 625–636.

Froidevaux, C., 1986. Basin and Range large-scale tectonics: constraints from gravity and reflection seismology. J. Geophys. Res., 91: 3625–3632.

Furlong, K. P., and Fountain, D. M., 1986. Continental crustal underplating: Thermal considerations and seismic-petrologic consequences. J. Geophys. Res., 91: 8285–8294.

Gans, P. B., 1987. An open-system, two-layer crustal stretching model for the eastern Great Basin. Tectonics, 6: 1–12.

Gans, P. B., Mahood, G. A., and Schermer, E., 1989. Synextensional magmatism in the Basin and Range Province; A case study from the eastern Great Basin. Geol. Soc. Am. Spec. Pap., 233, 53 pp.

Gans, P. B., Miller, E. L., McCarthy, J., and Oulcott, M. L., 1985. Tertiary extensional faulting and evolving ductile-brittle transition zones in the northern Snake Range and vicinity: New insights from seismic data. Geology, 13: 189–193.

Gilbert, G. K., 1928. Studies of basin-range structure. U. S. Geol. Surv. Prof. Pap., 153: 1–92.

Glazner, A. F., and Bartley, J. M., 1984. Timing and tectonic setting of Tertiary low-angle normal faulting and associated magmatism in the southwestern United States. Tectonics, 3: 385–396.

Glazner, A. F., and Farmer, G. L., 1991. Production of isotopic variability in continental basalts by cryptic crustal contamination. Science, 255: 72–74.

Gomberg, J., Priestly, K., Brune, J., 1989. The compressional velocity structure of the crust and upper mantle of northern Mexico and the border region. Bull. Seismol. Soc. Am., 79: 1496–1519.

Goodwin, E. B., and McCarthy, J., 1990. Composition of the lower crust in west-central Arizona from three-component seismic data. J. Geophys. Res., 95: 20097–20109.

Griffiths, R. W., and Campbell, I. H., 1991. On the dynamics of long-lived plume conduits in the convecting mantle. Earth Planet. Sci. Lett., 103: 214–227.

Hamilton, W. B., 1987. Crustal extension in the Basin and Range Province, Southwestern United States. In: Coward, M. P. , Dewey, J F, Hancock, P L (Editors), Continental extensional tectonics. Geol. Soc. Spec. Pub., 28, pp. 155–176,

Hamilton, W., and Myers, W. B., 1966. Cenozoic tectonics of the western United States. Rev. Geophys., 4: 509–549.

Harry, D. L., Sawyer, D. S., and Leeman, W. P., 1993. The mechanics of continental extension in western North America: implications for the magmatic and structural evolution of the Great Basin. Earth Planet. Sci. Lett., 117: 59–71.

Hauser, E.C., Gephart, J., Latham, T., Brown, L., Kaufman, S., Oliver, J., and Lucchitta, I.,1987. COCORP Arizona transect: Strong crustal reflections and offset Moho beneath the transition zone. Geology, 15: 1103–1106.

Hayob, J. L., Essene, E. J., Ruiz, J., Ortega-Gutierrez, F., and Aranda-Gomez, J. J., 1989. Young high-temperature granulites from the base of the crust in central Mexico. Nature, 342: 265–268.

Hazlett, R.W., 1990, Extension-related Miocene volcanism in the Mopah Range volcanic field, southeastern California. Geol. Soc. Am. Mem., 174: 133–145.

Hearn, T., Beghoul, N., and Barazangi, M., 1991. Tomography of the western United States from regional arrival times. J. Geophys. Res., 96: 16369–16381.

Heaton, T. H., and Kanamori, H., 1984. Seismic potential associated with subduction in the northwestern United States. Bull. Seismol. Soc. Am., 74: 933–941.

Heiskanen, W.A., and Vening Meinesz, F. A.., 1958. The Earth and its gravity field. New York, McGraw-Hill, 470 pp.

Helmberger, D. V., and Engen, G. R., 1974. Upper mantle shear structure. J. Geophys. Res., 79: 4017–4028.

Henry, C. D., Aranda-Gomez, J. J., 1992. The real southern Basin and Range: Mid- to late Cenozoic extension in Mexico. Geology, 20: 701–704.

Hill, E. J., Baldwin, S. L., and Lister, G. S., 1992. Unroofing of active metamorphic core complexes in the D'Entrecasteaux Islands, Papua New Guinea. Geology, 20: 907–910.

Hill, R.I., 1991. Starting plumes and continental breakup. Earth Planet. Sci. Lett., 104: 398–416.

Hill, R. I., Campbell, H., Davies, G. F., and Griffiths, R. W., 1992. Mantle plumes and continental tectonics. Science, 256: 186–192.

Holbrook, W. S., 1990. The crustal structure of the northwestern Basin and Range province, Nevada, from wide-angle seismic data. J. Geophys. Res., 95: 21843–21869.

Holbrook, W. S., Catchings, R. D., and Jarchow, C. M., 1991. Origin of deep reflections: implications of coincident seismic refraction and reflection data in Nevada. Geology, 19: 175–179.

Holder, G.M., Holder, R.W., and Carlson, D.H., 1990. Middle Eocene dike swarms and their relation to contemporaneous plutonism, volcanism, core-complex mylonitization, and graben subsidence, Okanogan Highlands, Washington. Geology, 18: 1082–1085.

Howard, K. A., and John, B. E., 1987. Crustal extension along a rooted system of imbricate low-angle faults: Colorado River extensional corridor, California and Arizona. In: M. P. Coward, J. F. Dewey, and P. L. Hancock (Editors), Continental Extensional Tectonics, Geol. Soc. Spec. Pub., 28: 299–311.

Howie, J. M., Miller, K. C., and Savage, W. U., 1993. Integrated crustal structure across the South Central California Margin: Santa Lucia Escarpment to the San Andreas Fault: J. Geophys. Res., 98: 8173–8196.

Howie, J. M., Parsons, T., and Thompson, G. A., 1991. High-resolution P- and S-wave deep crustal imaging across the edge of the Colorado Plateau, USA: Increased reflectivity caused by initiating extension. In: Mesiner, R. et al. (Editors), Continental lithosphere: Deep seismic reflections. Geodynamics Series, American Geophysical Union, 22, pp. 21–29.

Humphreys, E., Dueker, K. G., 1994. Western U.S upper mantle structure. J. Geophys. Res., 99: pp. 9615–9634.

Iyer, H. M., and Hitchcock, T., 1989. Upper mantle velocity structure in the continental U.S. and Canada. In: Pakiser, L. C., and Mooney, W. D. (Editors), Geophysical Framework of the continental United States. Geol. Soc. Am. Mem., 172, pp. 681–710.

Iyer, H. M., Roloff, J. N., and Croakley, J. M., 1977. P-wave residual measurements in the Battle Mountain heat flow high, Nevada. EOS Trans., 58: 1238.

Jachens, R. C., Simpson, R. W., Blakely, R. J., and Saltus, R. W., 1989. Isostatic residual gravity and crustal geology of the United States. In: Pakiser, L. C., and Mooney, W. D. (Editors), Geophysical Framework of the continental United States. Geol. Soc. Am. Mem., 172, pp. 405–424.

Jackson, J., 1987. Active normal faulting and crustal extension. In: Coward, M. P., Dewey, J F, Hancock, P L (Editors), Continental extensional tectonics. Geol. Soc. Spec. Pub., 28, pp. 3–17.

Jackson, S. M., Wong, I. G., Carpenter, G. S., Anderson, D. M., and Martin, S. M., 1993. Contemporary seismicity in the eastern Snake River Plain, Idaho based on microearthquake monitoring. Bull. Seismol. Soc. Am., 83: 680–695.

Jarchow, C. M., Thompson, G. A., Catchings, R. D, and Mooney, W. D., 1993. Seismic evidence for active magmatic underplating beneath the Basin and Range province, western United States. J. Geophys. Res., 98: 22095–22108.

John, B.E., 1982. Geologic framework of the Chemehuevi Mountains, southeastern California. In: Frost, E.G., and Martin, D.L. (Editors), Mesozoic-Cenozoic tectonic evolution of the Colorado River region, California, Arizona, and Nevada. San Diego, California, Cordilleran Publishers, pp. 317–325.

Johnson, R. A., and Loy, K. L., 1992. Seismic reflection evidence for seismogenic low-angle faulting in southeastern Arizona. Geology, 20: 597–600.

Jones, C. H., Wernicke, B. P., Farmer, G. L., Walker, J. D., Coleman, D. S., McKenna, L. W., and Perry, F. V., 1992. Variations across and along a major continental rift: an interdisciplinary study of the Basin and Range Province, western USA. Tectonophysics, 213: 57–96.

Keith, S.B., Reynolds, S.J., Damon, P.E., Shafiqullah, M., Livingston, D.E., and Pushkar, P., 1980. Evidence for multiple intrusion and deformation within the Santa Catalina-Rincon-Tortolita crystalline complex, southeastern Arizona. In: Crittenden, M.D., et al. (Editors), Cordilleran metamorphic core complexes: Geol. Soc. Am. Mem., 153, pp. 217–268.

Keller, G. V., 1989. Electrical structure of the crust and upper mantle, part 2. In: Pakiser, L. C., and Mooney, W. D. (Editors), Geophysical Framework of the continental United States. Geol. Soc. Am. Mem., 172, pp. 425–446.

Klein, D. P.., 1991. Crustal resistivity structure from magnetotelluric soundings in the Colorado Plateau and Basin and Range provinces, central and west Arizona. J. Geophys. Res., 96: 12313–12331.

Klemperer, S. L., T. A. Hauge, E. C. Hauser, J. E. Oliver, and C. J. Potter, 1986. The Moho in the northern Basin and Range province, Nevada, along the COCORP 40° N seismic-reflection transect. Geol. Soc. Am. Bull., 97: 603–618.

Koizumi, C. J., Ryall, A., and Priestly, K. F., 1973. Evidence for a high-velocity lithospheric plate under northern Nevada. Seismol. Soc. Am. Bull., 63: 2135–2144.

Kruse, S., McNutt, M., Phipps-Morgan, J., Royden, L., Wernicke, B., 1991. Lithospheric extension near Lake Mead, Nevada: A model for ductile flow in the lower crust. J. Geophys. Res., 96: 4435–4456.

Lachenbruch, A. H., 1978. Heat flow in the Basin and Range province and thermal effects of tectonic extension. Pure and Applied Geophysics, 117: 34–50.

Lachenbruch, A. H., and Sass, J. H., 1978. Models of an extending lithosphere and heat flow in the Basin and Range province. In: Smith, R. B., and Eaton, G. P. (Editors), Cenozoic tectonics and regional geophysics of the western Cordillera. Geol. Soc. Am. Mem. 152, pp. 209–250.

Lachenbruch, A. H., and Morgan, P., 1990. Continental extension, magmatism and elevation; formal relations and rules of thumb. Tectonophysics, 174: 39–62.

Lee, J., and Lister, G.S., 1992. Late Miocene ductile extension and detachment faulting, Mykonos, Greece. Geology, 20: 121–124.

Lee, J., Miller, E. L., and Sutter, J. F., 1987. Ductile strain and metamorphism in an extensional tectonic setting; a case study from the northern Snake Range, Nevada, USA. In: Coward, M. P., Dewey, J. F., and Hancock, P. L. (Editors), Continental extensional tectonics. Geol. Soc. Spec. Pub., 28: 267–298.

Leeman, W. P., and Harry, D. L., 1993. A binary source model for extension-related magmatism in the Great Basin, western North America. Science, 262: pp. 1550–1554.

Leeman, W. P., Menzies, M. A., Matty, D. J., and Embree, G. F., 1985. Strontium, neodymium, and lead isotope compositions of deep crustal xenoliths from the Snake River Plain - evidence for Archean basement. Earth Planet. Sci. Lett., 75: 354–368.

Lipman, P. W., 1980. Cenozoic magmatism in the western United States: Implications for continental tectonics. In: Continental Tectonics, Stud. in Geophys., U. S. National Academy of Sciences, Washington, D. C., pp. 161–174.

Lipman, P.W., and Glazner, A.F., 1991. Introduction to middle Tertiary cordilleran volcanism: Magma sources and relations to regional tectonics. J. Geophys. Res., 96: 13193–13200.

Lister, G. S., and Baldwin, S. L., 1993. Plutonism and the origin of metamorphic core complexes. Geology; 21: 607–610.

Lister, G. S., Banga, G., and Feenstra, A., 1984. Metamorphic core complexes of Cordilleran type in the Cyclades, Aegean Sea, Greece. Geology, 12: 221–225.

Liviccari, R. F., and Perry, F. V., 1993. Isotopic evidence for preservation of Cordilleran lithospheric mantle during the Sevier-Laramide orogeny, western United States. Geology, 21: 719–722.

Logan, R.E., and Hirsch, D.D., 1982. Geometry of detachment faulting and dike emplacement in the southwestern Castle Dome Mountains, Yuma County, Arizona. In: Frost, E.G., and Martin, D.L. (Editors), Mesozoic-Cenozoic tectonic evolution of the Colorado River region, California, Arizona, and Nevada. San Diego, California, Cordilleran Publishers, pp. 599–607.

Lonsdale, P., 1991. Structural patterns of the Pacific floor offshore of Peninsular California, In: Dauphin, J. P., and Simoeit, B. R. T. (Editors), Am. Assoc. Petrol. Geol. Mem., 47, Tulsa, OK, USA, pp. 87–143.

Luedke, R.G., and Smith, R.L., 1983. Map showing distribution, composition, and age of late Cenozoic volcanic centers in Idaho, western Montana, west-central South Dakota, and northwestern Wyoming. U.S. Geol. Surv. Misc. Geol. Investig. Map I-1091-C, scale 1:1,000,000.

Lum, C. L., Leeman, W. P., Foland, K. A., Kargel, and Fitton, J. G., 1989. Isotopic variations in continental basaltic lavas as indicators of mantle heterogeneity: Examples from the Western U. S. Cordillera. J. Geophys. Res., 96: pp. 7871–7884.

Mareschal, J., and Bergantz, G., 1990. Constraints on thermal models of the Basin and Range province. Tectonophysics, 174: 137–146.

Matthews, D., and Cheadle, M., 1986. Deep reflections from the Caledonides and Variscides west of Britain, and comparisons with the Himalayas. In: Barazangi, M., and Brown, L. (Editors), Reflection Seismology: A Global Perspective, Am. Geophys. Union, Geodyn. Ser., 13, pp. 5–19.

Mabey, D. R., Zietz, I., Eaton, G. P., and Kleinkopf, M. D., 1978. Regional magnetic patterns of the Cordillera in the western United States. In: Smith, R. B., and Eaton, G. P. (Editors), Cenozoic tectonics and regional geophysics of the western Cordillera. Geol. Soc. Am. Mem. 152, pp. 93–106.

Mayer, L., 1986. Topographic constraints on models of lithospheric stretching of the Basin and Range province, western United States. Geol. Soc. Am. Spec. Pap. 208: 1–14.

McCarthy, J., 1986. Reflection profiles from the Snake Range metamorphic core complex: A window into the mid-crust. In: Reflection Seismology: The Continental Crust. American Geophysical Union, Washington, D. C., Geodyn. Ser. 14, pp. 281–292.

McCarthy, J., and Parsons, T., 1994. Insights into the kinematic Cenozoic evolution of the Basin and Range-Colorado Plateau transition from coincident seismic refraction and reflection data. Geol. Soc. Am. Bull., in press.

McCarthy, J., Larkin, S.P., Simpson, R.W., and Howard, K.A., 1991. Anatomy of a metamorphic core complex: Seismic refraction/wide-angle reflection profiling in southeastern California and western Arizona. J. Geophys. Res., 96: 12,259–12,291.

McCarthy, J., and Thompson, G.A., 1988. Seismic imaging of extended crust with emphasis on the western United States. Geol. Soc. Am. Bull., 100: 1361–1374.

McGuire, A. V., 1992. Gabbroic xenoliths from Wikieup, AZ: Samples of lower crust formed during continental extension: EOS Trans. 73: 548.

Melosh, H. J.., 1990. Mechanical basis for low-angle normal faulting in the Basin and Range province. Nature, 343: 331–335.

Menzies, M.A., Kyle, P.R., Jones, M. and Ingram, G., 1991. Enriched and depleted source components for tholeiitic and alkaline lavas from Zuni-Bandera, New Mexico: Inferences about intraplate processes and stratified lithosphere. J. Geophys. Res., 96: 13,645–13,672.

Menzies, M. A., 1989. Cratonic circumcratonic and oceanic mantle domains beneath the western United States. J. Geophys. Res., 94: 7899–7915.

Menzies, M. A., Leeman, W. P., Hawkesworth, C. J., 1983. Isotope geochemistry of Cenozoic volcanic rocks reveals mantle heterogeneity below western USA. Nature, 303: 205–209.

Miller, E. L., Gans, P. B., and Garing, J., 1983. The Snake Range decollement: An exhumed mid-Tertiary ductile-brittle transition. Tectonics, 2: 239–263.

Miller, J. M. G., and John, B.E., 1988. Detached strata in a Tertiary low-angle normal fault terrane, southeastern California. A sedimentary record of unroofing, breaching and continued slip. Geology, 16: 645–648.

Minster, J. B., and Jordon, T. H., 1987. Vector constraints on western U.S. deformation from space geodesy, neotectonics, and plate motions. J. Geophys. Res., 92: 4798–4804.

Mooney, W. D., and Braile, L. W., 1989. The seismic structure of the continental crust and upper mantle of North America. In: Bally, A. W., and Palmer, A. R. (Editors), The geology of North America; an overview, Vol. A. Geol. Soc. Am., Boulder, CO, USA. pp. 39–52.

Mooney, W. D., and Meissner, R., 1992. Multi-genetic origin of crustal reflectivity: a review of seismic reflection profiling of the continental lower crust and Moho. In: Fountain, D. M., Arculus, R., and Kay, R. W. (Editors), Continental Lower Crust. Amsterdam, Elsevier, pp. 45–79.

Morgan, P., and Gosnold, W. D., 1989. Heat flow and thermal regimes in the continental United States. In: Pakiser, L. C., and Mooney, W. D. (Editors), Geophysical Framework of the continental United States. Geol. Soc. Am. Mem., 172, pp. 493–522.

Morgan, W.J., 1972. Deep mantle convection plume and plate motions: Am. Assoc. Pet. Geol. Bull., 56: 203–312.

Mount, V. S., and Suppe, J., 1992. Present-day stress orientations adjacent to active strike-slip faults: California and Sumatra. J. Geophys. Res., 97: 11995–12013.

Nakata, J. K., 1982. Preliminary report on diking events in the Mojave Mountains, Arizona. In: Frost, E.G., and Martin, D.L. (Editors), Mesozoic-Cenozoic tectonic evolution of the Colorado River region, California, Arizona, and Nevada. San Diego, California, Cordilleran Publishers, pp. 85–89.

Nimz, G. J., Cameron, K. L., Cameron, M., and Morris, S. L., 1986. Petrology of the lower crust and upper mantle beneath southeastern Chihuahua, Mexico. Geof. Int., 25: 85–116.

Okaya, D. A., 1986. Seismic profiling of the lower crust: Dixie Valley, Nevada. In: Reflection Seismology: The Continental Crust. American Geophysical Union, Washington, D. C., Geodyn. Ser. 14, pp. 269–279.

Okaya, D. A., and Thompson, G. A., 1985. Geometry of Cenozoic extensional faulting: Dixie Valley, Nevada. Tectonics, 4: 107–125.

Olsen, K. H., Braile, L., and Johnson, P., 1980. Seismic velocity and Q-structure of the upper mantle lid and low velocity zone for the eastern Great Basin. Geophys. Res. Lett., 12: 1029–1032.

Olsen, K. H., and Braile, L. W., 1981. Seismograms of explosions at regional distances in the western United States: Observations and reflectivity method modeling. In: Husebye, and Mykkeltveit, S. (Editors), Identification of Seismic Sources - Earthquake or Underground Explosion, pp. 453–466.

Olsen, K. H., Braile, L. W., and Stewart, J. N., 1983. Modeling short–period crustal phases (P, Lg) for long–range refraction profiles. Phys. Earth Planet. Int., 31: 334–347.

Ormerod, D. S., Hawkesworth, C. J., Rogers, N. W., Leeman, W. P., and Menzies, M. A., 1988. Tectonic and magmatic transitions in the western Great Basin, USA. Nature, 333: 349–353.

Pakiser, L. C., 1989. Geophysics of the Intermontane system. In: Pakiser, L. C., and Mooney, W. D. (Editors), Geophysical Framework of the continental United States. Geol. Soc. Am. Mem., 172, pp. 235–248.

Parsons, T., and Thompson, G. A., 1991. The role of magma overpressure in suppressing earthquakes and topography: worldwide examples. Science, 253: 1399–1402.

Parsons, T., Howie, J. M., and Thompson, G. A., 1992a. Seismic constraints on the nature of lower crustal reflectors beneath the extending southern Transition Zone of the Colorado Plateau, Arizona. J. Geophys. Res., 97: 12391–12407.

Parsons, T., Sleep, N. H., and Thompson, G. A., 1992b. Host rock rheology controls on the emplacement of tabular intrusions: implications for underplating of extending crust. Tectonics, 11: 1348–1356.

Parsons, T. and Thompson, G. A., 1993. Does magmatism influence low-angle normal faulting? Geology, 21: 247–250.

Perry, F. V., DePaolo, D. J., and Baldridge, W. S., 1993. Neodymium isotopic evidence for decreasing crustal contributions to Cenozoic ignimbrites of the western United States: Implications for the thermal evolution of the Cordilleran crust. Geol. Soc. Am. Bull., 105: pp. 872–882.

Pezzopane, S. K., and Weldon, R. J., II, 1993. Tectonic role of active faulting in central Oregon. Tectonics, 12: 1140–1169.

Pierce, K. L., and Morgan, L. A., 1992. The track of the Yellowstone hot spot: Volcanism, faulting, and uplift. In: Link, P. K. et al. (Editors), Regional geology of eastern Idaho & western Wyoming. Geol. Soc. Am. Mem. 179, pp. 1–53.

Priestly, K., and Brune, J., 1978. Surface waves and the structure of the Great Basin of Nevada and western Utah. J. Geophys. Res., 83: 2265–2272.

Prodehl, C., 1979. Crustal structure of the western United States. U.S. Geol. Surv. Prof. Pap., 1034, 74 pp.

Proffett, J.M., 1977. Cenozoic geology of the Yerington District, Nevada and its implications for the nature of Basin and Range faulting. Geol. Soc. Am. Bull., 88: 247–266.

Rehrig, W. A., Reynolds, S. J., 1980. Geologic and geochronologic reconnaissance of a northwest–trending zone of metamorphic core complexes in southern and western Arizona. In: Crittenden, M. D., et al. (Editors), Cordilleran metamorphic core complexes. Geol. Soc. Am. Mem., 153: 131–157.

Reynolds, S.J., and Rehrig, W.A., 1980. Mid-Tertiary plutonism and mylonitization, South Mountains, central Arizona. In: Crittenden, M. D., et al. (Editors), Cordilleran metamorphic core complexes. Geol. Soc. Am. Mem., 153: 159–176.

Reynolds, S.J., and Spencer, J.E., 1985. Evidence for large-scale transport on the Bullard detachment fault, west-central Arizona. Geology, 13: 353–356.

Ribe, N. M., and Yu, Y., 1991. A theory for plastic deformation and textural evolution of olivine. J. Geophys. Res., 96: 8325–8335.

Roberts, S. J., and Ruiz, J., 1989. Geochemistry of exposed granulite facies terrains and lower crustal xenoliths in Mexico. J. Geophys. Res., 94: 7961–7974.

Rodgers, D. W., Hackett, W. R., and Ore, H. T., 1990. Extension of the Yellowstone plateau, eastern Snake River Plain, and Owyhee plateau. Geology, 18: 1138–1141.

Romanowiscz, B. A., 1979. Seismic structure of the upper mantle beneath the United States by three-dimensional inversion of body wave arrival times. R. Astron. Soc. Geophys. J., 57: 479–506.

Rudnick, R. L., and Cameron, K. L., 1991. Age diversity of the deep crust in northern Mexico. Geology, 19: 1197–1200.

Ruiz, J., Patchett, P. J., Ortega-Gutierrez, F., 1988. Proterozoic and Phanerozoic basement terranes of Mexico from Nd isotopic studies. Geol. Soc. Am. Bull., 100: 274–281.

Ruppert, S. D., 1992. Tectonics of western North America [Ph.D. Thesis]. Stanford University, Stanford, California, 217 pp.

Ryall, A., Slemmons, D. B., and Gedney, L. D., 1966. Seismicity tectonism, and surface faulting in the western United States during historic time. Bull. Seismol. Soc. Am., 56: 1105–1136.

Saltus, R. W., 1993. Why is it downhill from Tonopah to Las Vegas? Geophysical constraints on isostatic support of the Great Basin. EOS Trans., 74: 548.

Saltus, R.W., 1991. Gravity and heat flow constraints on Cenozoic tectonics of the Western United States Cordillera [Ph.D. thesis]: Stanford, California, Stanford University, 245 p.

Savage, M. K., and Silver, P. G., 1993. Mantle deformation and tectonics: constraints from seismic anisotropy in the western United States. Phys. Earth Planet. Int., 78: 201–227.

Scott, W. E., Pierce, K. L., and Hait, M. H. Jr., 1985. Quaternary tectonic setting of the 1983 Borah Peak earthquake, central Idaho. U. S. Geol. Surv. Open File Rep., 85–290: 1–16.

Serpa, L., de Voogd, B., Wright, L., Willemin, J., Oliver, J., Hauser, E., Troxel, B., 1988. Structure of the central Death Valley pull-apart basin and vicinity from COCORP profiles in the southern Great Basin. Geol. Soc. Am. Bull., 100: 1437–1450.

Severinghaus, J., and Atwater, T., 1990. Cenozoic geometry and thermal state of the subducting slabs beneath western North America. In: Wernicke, B. (Editor), Basin and Range Extension. Geol. Soc. Am.. Mem., 176, pp. 1–22.

Sibson, R. H., 1982. Fault zone models, heat flow, and the depth distribution of earthquakes in the continental crust of the United States. Bull. Seismol. Soc. Am., 72: 151–163.

Sibson, R. H.., 1985. A note on fault reactivation. J. Struc. Geol., 7: 751–754.

Simpson, R.W., and Jachens, R.C., 1989. Gravity methods in regional studies. In: Pakiser, L.C., and Mooney, W.D. (Editors), Geophysical framework of the continental United States. Geol. Soc. Am. Mem. 172: 35–44.

Simpson, R. W., Jachens, R. C., Blakely, R. J., and Saltus, R. W., 1986. A new isostatic residual gravity map of the coterminous United States with a discussion on the significance of isostatic residual anomalies. J. Geophys. Res., 91: 8348–8372.

Sleep, N. H., 1990. Hotspots and mantle plumes: Some phenomenology. J. Geophys. Res., 95: 6715–6736.

Smith, R. B., 1978. Seismicity, crustal structure, and intraplate tectonics of the interior of the western Cordillera. In: Smith, R. B., and Eaton, G. P. (Editors), Cenozoic tectonics and regional geophysics of the western Cordillera. Geol. Soc. Am. Mem. 152, pp. 111–144.

Smith, R. B., and Lindh, A. G., 1978. Fault-plane solutions of the western United States: A compilation. In: Smith, R. B., and Eaton, G. P. (Editors), Cenozoic tectonics and regional geophysics of the western Cordillera. Geol. Soc. Am. Mem. 152, pp. 107–109.

Smith, R. B., Nagy, W. C., Julander, K. A. S., Viveiros, J. J., Barker, C. A., and Gants, D. G., 1989. Geophysical framework of the eastern Basin and Range-Colorado Plateau-Rocky Mountain transition. In: Pakiser, L. C., and Mooney, W. D. (Editors), Geophysical Framework of the continental United States. Geol. Soc. Am. Mem., 172, pp. 205–234.

Smithson, S. B., and Johnson, R. A., 1989. Crustal structure of the western U.S. based on reflection seismology. In: Pakiser, L. C., and Mooney, W. D. (Editors), Geophysical Framework of the continental United States. Geol. Soc. Am. Mem., 172, pp. 577–612.

Solomon, S. C., and Butler, R. G., 1974. Prospecting for dead slabs. Earth Planet. Sci. Lett., 21: 421–430.

Sonder, L. J., England, P. C., Wernicke, B. P., and Christiansen, R. L., 1987. A physical model for Cenozoic extension of western North America. In: Coward, M. P., Dewey, J. F., and Hancock, P. L. (Editors), Continental Extensional Tectonics: Geol. Soc. Lond. Spec. Pub., 28, pp. 187–201.

Sparlin, M.A., Braile, L.W., and Smith, R.B., 1982. Crustal structure of the eastern Snake River Plain determined from ray trace modeling of seismic refraction data. J. Geophys. Res., 87: 2619–2633.

Speed, R., 1976. Geology of Humbolt Lopolith and vicinity. Geol. Soc. Am. Map MC-14, Boulder, CO.

Spencer, J.E., 1984. Role of tectonic denudation in warping and uplift of low-angle normal faults. Geology, 12: 95–98.

Spencer, J.E., 1985. Miocene low-angle normal faulting and dike emplacement, Homer Mountain and surrounding areas, southeastern California and southernmost Nevada. Geol. Soc. Am. Bull., 96: 1140–1155.

Stanley, W. E. D., 1982. Magnetotelluric soundings on the Idaho National Engineering Laboratory facility, Idaho. J. Geophys. Res., 87: 2683–2691.

Stewart, J. H., 1980. Geology of Nevada. Nevada Bureau of Mines and Geology Special Publication 4.

Stewart, J. H., and Poole, F. G., 1974. Lower Paleozoic and uppermost Precambrian Cordilleran miogeocline, Great Basin, western United States. In: Dickinson, W. R. (Editor), Tectonics and Sedimentation. Society of Economic Paleontologists and Mineralogists Special Publication, pp. 22, 28–57.

Stickney, M. C., and Bartholomew, M. J., 1987. Seismicity and late Quaternary faulting of the northern Basin and Range province, Montana and Idaho. Bull. Seismol. Soc. Am., 77: 1602–1625.

Stock, J. M., and Hodges, K. V., 1989. Pre-Pliocene extension around the Gulf of California and the transfer of Baja California to the Pacific Plate. Tectonics, 8: 99–115.

Stock, J., and Molnar, P., 1988. Uncertainties and implications of the Late Cretaceous and Tertiary position of North America relative to the Farallon, Kula, and Pacific plates. Tectonics, 7: 1339–1384.

Suter, M., Quintero, O., and Johnson, C. A., 1992. Active faults and the state of stress in the central part of the trans-Mexican volcanic belt, Mexico, 1, The venta de Bravo Fault. J. Geophys. Res., 97: 11983–11994.

Taylor, W. J., Bartley, J. M., Lux, D. R., and Axen, G. J., 1989. Timing of Tertiary extension in the Railroad Valley-Pioche transect, Nevada: Constraints from $^{40}Ar/^{39}Ar$ Ages of volcanic rocks. J. Geophys. Res., 94: 7757–7774.

Thelin, G. P., and Pike, R. J., 1991. Landforms of the conterminous United States. U. S. Geol. Surv. Misc. Investig. Ser., Map I-2206, scale 1:3500000.

Thompson, G. A., 1960. Problem of late Cenozoic structure of the Basin Ranges: Report of the International Geological Congress XXI. Part 18, p. 62–28.

Thompson, G. A., and Burke, D. B., 1974. Regional geophysics of the Basin and Range province. Ann. Rev. Earth Planet. Sci., 2: 213–238.

Thompson, G. A., and Burke, D. B., 1973. Rate and direction of spreading in Dixie Valley, Basin and Range province, Nevada. Geol. Soc. Am. Bull., 84: 627–632.

Thompson, G. A., and McCarthy, J., 1990. A gravity constraint on the origin of highly extended terranes. Tectonophysics, 174: 197–206.

Thompson, G. A., and Zoback, M. L., 1979. Regional geophysics of the Colorado Plateau. Tectonophysics, 61: 149–181.

Torgersen, T., 1993. Defining the role of magmatism in extensional tectonics: Helium 3 fluxes in extensional basins. J. Geophys. Res., 98: 16257–16,269.

Walck, M. C., 1984. The P-wave upper-mantle structure beneath an active spreading centre: the Gulf of California. Geophys. J. R. Astr. Soc., 76: 697–723.

Wallace, P., Carmichael, I. S. E., Righter, K., and Becker, T. A., 1992. Volcanism and tectonism in western Mexico: A contrast of style and substance. Geology, 20: 625–628.

Ward, P., 1991. On plate tectonics and the geologic evolution of southwestern North America: J. Geophys. Res., 96: 12479–12496.

Warren, D. H., 1969. A seismic refraction survey of crustal structure in central Arizona. Geol. Soc. Am. Bull., 80: 257–282.

Wernicke, B., 1992. Cenozoic extensional tectonics of the U. S. Cordillera. In: B. C. Burchfiel, P. W. Lipman, and M. L. Zoback (Editors), The Cordilleran Orogen; conterminous U. S. The Geology of North America Volume G-3, Geol. Soc. Am., Boulder, CO, pp. 553–581.

Wernicke, B., and Axen, G. J.., 1988. On the role of isostasy in the evolution of normal fault systems. Geology, 16: 848–851.

Wernicke, B., Axen, G. J., and Snow, J. K., 1988. Basin and Range extensional tectonics at the latitude of Las Vegas, Nevada. Geol. Soc. Am. Bull., 100: 1738–1757.

Wernicke, B., Walker, J. D.., and Beaufait, M.S., 1985. Structural discordance between Neogene detachments and frontal Sevier thrusts, central Mormon Mountains, southern Nevada. Tectonics, 4: 213–246.

Wickham, S. M., Peters, M. T., Fricke, H. C., and O'Neil, J. R., 1993. Identification of magmatic and meteoric fluid sources and upward- and downward-moving infiltration fronts in a metamorphic core complex. Geology, 21: 81–84.

Wilshire, H. G., 1990. Lithology and evolution of the crust-mantle boundary region in the southwestern Basin and Range province. J. Geophys. Res., 95: 649–665.

Wilshire, H. G., McGuire, A. V., Noller, J. S., and Turrin, B. D., 1991. Petrology of lower crustal and upper mantle xenoliths from the Cima volcanic field, California. J. Petrol., 32: 169–199.

Wilson, J. M., McCarthy, J., Johnson, R. A., and Howard, K. A., 1991. An axial view of a metamorphic core complex: Crustal structure of the Whipple and Chemehuevi Mountains, southeastern California. J. Geophys. Res., 96: 12293–12311.

Yin, A., and Dunn, J.F., 1992. Structural and stratigraphic development of the Whipple-Chemehuevi detachment fault system, southeastern California: Implications for the geometrical evolution of domal and basinal low-angle normal faults. Geol. Soc. Am. Bull., 104: 659–674.

Zoback, M. L., 1989. State of stress and modern deformation of the northern Basin and Range province. J. Geophys. Res., 94: 7105–7128.

Zoback, M. L., 1979. Direction and amount of late Cenozoic extension in north-central Nevada. Geol. Soc. Am. Abs. Prog., 11: 137.

Zoback, M. L., 1978, A detailed study of late Cenozoic deformation in the northern Basin and Range [Ph.D. thesis]: Stanford, California, Stanford University, 247p.

Zoback, M. L., Anderson, R. E., and Thompson, G. A., 1981. Cainozoic evolution of the state of stress and style of tectonism of the Basin and Range province of the western United States. Phil. Trans. R. Soc. Lond., A300: 407–434.

Zoback, M. L., McKee, E. H., Blakely, R. J., and Thompson, G. A., 1994. The northern Nevada rift: Regional tectono-magmatic relations and middle Miocene stress direction. Geol. Soc. Am. Bull., 106: pp. 371–382.

Zoback, M. L., and Thompson, G. A., 1978. Basin and Range rifting in northern Nevada: Clues from a mid-Miocene rift and its subsequent offsets. Geology, 6: 275–284.

Zoback, M. L., and Zoback, M. D., 1989. Tectonic stress field of the continental United States. In: Pakiser, L. C., and Mooney, W. D. (Editors), Geophysical Framework of the continental United States. Geol. Soc. Am. Mem., 172, pp. 523–539.

Zoback, M. L., and Zoback, M. D., 1980. State of stress in the coterminous United States. J. Geophys. Res., 76: 1171–1183.

Zuber, M. T., Parmentier, E. M., and Fletcher, 1986. Extension of continental lithosphere: a model for two scales of Basin and Range deformation. J. Geophys. Res., 91: 4826–4838.

Chapter 8

The Baikal rift system

G. R. Keller, M. H. P. Bott, R. F. Wendlandt, D. I. Doser, and P. Morgan

8.1. Introduction

8.1.1. Description and Location

The Baikal rift system (Fig. 8–1), variously described as being 1800 km (Logatchev, 1984) to 2400 km long (Logatchev and Florensov, 1978), is situated at the boundary between the Siberian Platform (craton) to the northwest and the Caledonian Sayan-Baikal fold belt to the southeast (Fig. 8–2). Lake Baikal, which is the world's most voluminous and probably oldest lake, occupies only the central third of the rift system. This rift system has been the object of intensive study by Soviet scientists for many years (e.g., Florensov, 1969), and good geologic maps have been published for the area (Yanshin, 1980; Khrehov, 1983). Summary accounts of the structure and evolution of this complex rift system are found in the group of papers edited by Logatchev and Mohr (1978) and in more recent papers by Zorin (1981), Logatchev et al. (1983), Logatchev (1984), and Logatchev and Zorin (1987,1992).

Since the mid–1980s, a number international cooperative field study projects have been initiated between Baikal specialists of the (Former) Soviet Union and Western scientists in order to better address the Baikal system in relation to other major rift systems. For example, Lipmann et al. (1989) reports a preliminary multidisciplinary comparison of the Baikal and the Rio Grande rift systems.

The Baikal rift system is composed of fifteen individual topographic depressions which are associated with an approximately 1500–km–long domal uplift (Fig. 8–1) referred to as the Sayan-Baikal uplift by Logatchev and Zorin (1987). The Selenga saddle divides this uplift into the Baikal-Stanavad uplift in the north and the Sayan/Khamar-Daban uplift in the south. However, Ufimtsev (1990) and Windley and Allen (1993) show that the Baikal region is part of a larger uplifted region, the Mongolian plateau. Windley and Allen (1993) suggest that this large uplift and the associated magmatism may due to a mantle plume.

The structural grain of the Precambrian and Lower Paleozoic basement has been a major controlling influence on the geometry of the Baikal rift system (Zamarayev and Ruzhich, 1978). The central portion of Baikal Rift system is almost entirely located on the relatively weak and anisotropic basement of the Sayan-Baikal fold belt. The northeastern end of the rift system penetrates the Aldan Shield. The subvertical crustal boundary between the Siberian Platform and the fold belt forms an abrupt western boundary for the central portion of the rift system and its domal uplift, and in particular runs along the west side of the Lake Baikal depressions.

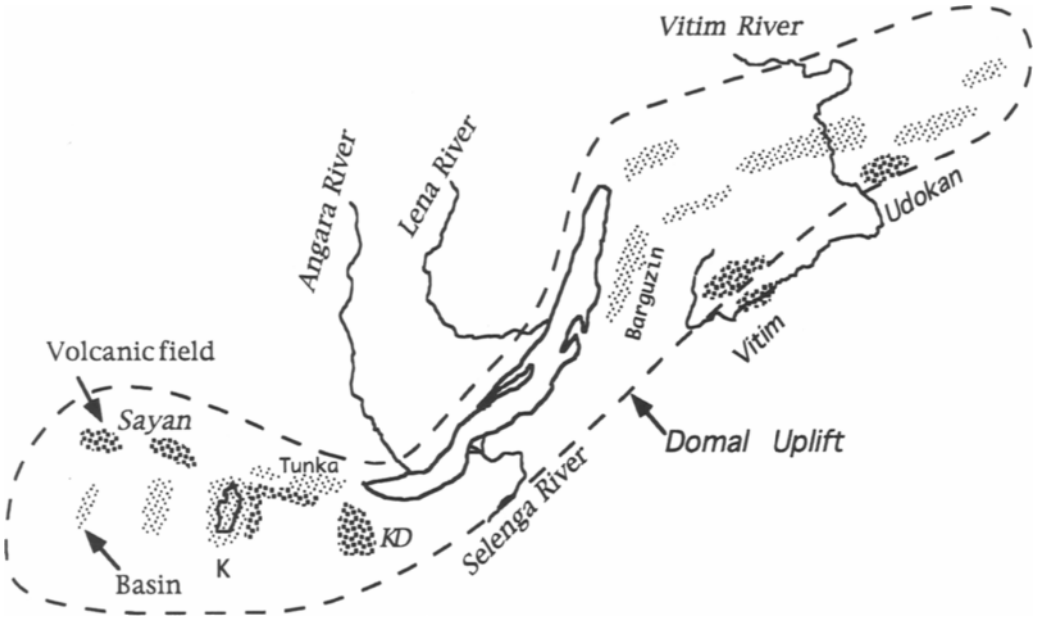

Fig. 8–1. Regional index map showing the major basins and volcanic fields. KD – Khamar-Daban volcanic field, K – Khubsugul basin.

8.2. Significance

Lake Baikal is the deepest lake in the world and contains 20% of the world's fresh water. This rift system is particularly important because of its intraplate location. It is over 2000 km from the nearest plate boundary but it is the most seismically active continental rift in the world today (Doser, 1991 a, b). The lithosphere of this rift may also be anomalously cold (e.g., Ruppel et al., 1993) providing an end member in opposing contrast to the East African rift.

8.3. Geological information

8.3.1. Basin sructure

The fifteen individual topographic depressions in the rift system (Figs. 8–1 and 8–2) are bounded on one or both sides by fault scarps. Most of the related basins are half-graben. The deepest basins are probably the three main ones found within Lake Baikal (Hutchinson et al., 1992, Scholz et al., 1993). The other depressions are up to 100-200 km long and 30-40 km wide (Fig. 8–1). Based on multichannel seismic data, the Selenga delta area (Fig. 8–2) possesses a maximum sediment thickness of over 8 km (Scholz et al., 1993). About 3000 m of sediment was penetrated in a borehole on the Selenga delta, but sediments only as old as Early Oligocene (maybe Eocene) were penetrated (Logatchev and Zorin, 1987). The only other documented well control in the rift is in the Tunka depression (Figs. 8–1 and 8–3), where lower Miocene sediments were penetrated at a depth of 2100 m, and in the Barguzin and Chara basins (Logatchev and Zorin, 1992). Bathymetric, seismic reflection (Hutchinson et al., 1992; Scholz et al., 1993) and gravity data indicates that the four basins in Lake Baikal are related to complex half-graben or tilted graben structures with their major faults close to the west edge of the lake (Fig. 8–3). Seismic and gravity data indicate a maximum sediment thickness of only about 4000 m in the North Baikal basin suggesting it may be younger than the

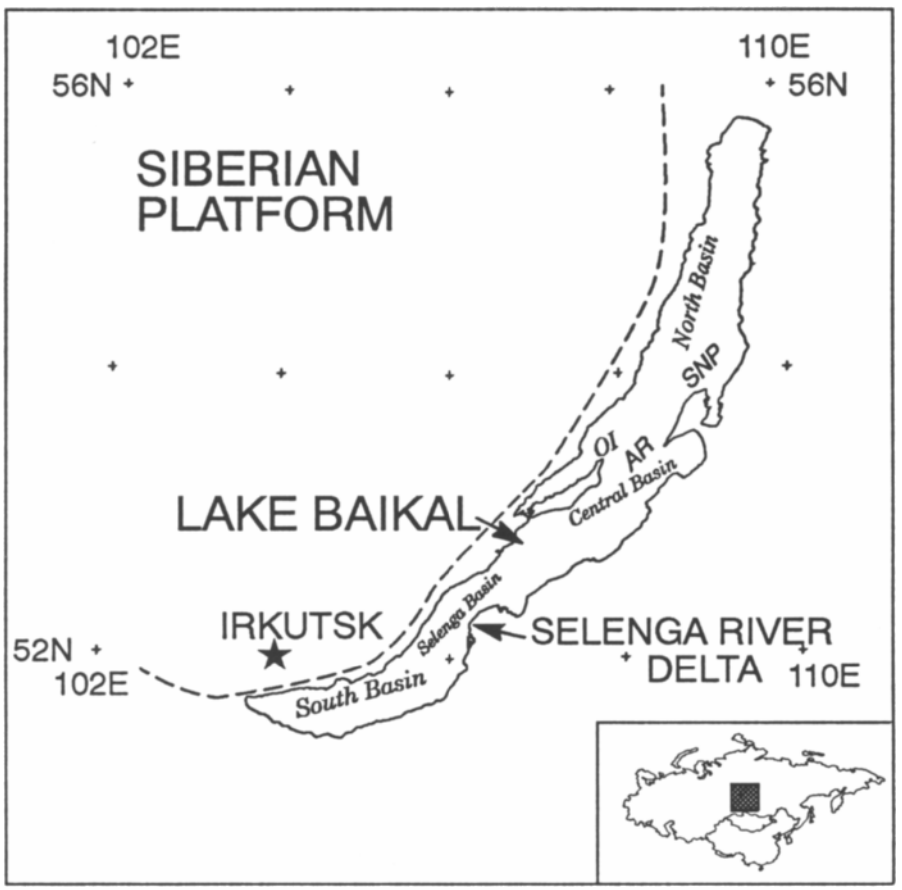

Fig. 8–2. Index map of the Lake Baikal region. OI – Olkhon Island, AR – Academician Ridge, SNP – Svyatoi Nos Peninsula. Dashed line is the approximate boundary of the Siberian platform.

basins to the south. The asymmetry of the basins in the lake is not pronounced and the bounding faults are relatively linear (Sherman, 1992; Balla et al., 1991). Olkhon Island, the submarine Academician ridge, the Ushkanjy Islands, and the Svyatoi Nos Peninsula (Fig. 8–2) form a complex structural high which has some of the characteristics of a zone of accommodation (Rosendahl, 1987). However, any transfer of motion is between faults with the same sense of motion (Hutchinson et al., 1992). A cross-section of the Tunka depression is shown in Figure 8–3 for comparison with the basins within the lake. Logatchev and Zorin (1992) provide structural maps of the major basins outside the lake. These maps are based mostly on gravity inversions and indicate sedimentary fill generally less than 3 km in thickness.

8.3.2. Basin sedimentation

Studies of the sedimentary history of the Baikal region have played an important role in interpretations of rift evolution to date. However, the lack of deep drilling data introduces considerable uncertainties about dating of sedimentary units. A widespread late Cretaceous-Paleogene erosion surface suggests regional uplift of the region prior to the Eocene

(Florensov, 1969; Logatchev and Florensov, 1978). Logatchev and Zorin (1984) proposed a two-stage development of the rift in which subdued uplift from about 35 Ma to about 4 Ma resulted in deposition of fine grained sediments, including coal, in the proto-rift basins. During this period, up to 5000 m of sediment was deposited in the South Baikal basin, but elsewhere these units probably do not exceed 2000 m in thickness.

Rapid uplift from about 4 Ma to present resulted in an abrupt change to deposition of coarse sandstones and conglomerates. A proposed order-of-magnitude increase in strain rate resulted in brittle deformation (at least of the upper crust) during this stage of evolution, rapid deepening of the proto-rift basins, and rift segmentation. Locally, over 5000 m of coarse sediment accumulated in the Selenga delta region during this period.

More explicit information on ages of erosional surfaces, the initiation of sedimentation in proto-rift basins, onset of volcanism and faulting, and sedimentation rates are required to constrain the tectonic evolution of the Baikal rift system. These deficiencies are discussed more thoroughly at a later point in the chapter.

8.3.3. Distribution of volcanics

The three principal areas of volcanic activity are the Sayan/Khamar-Daban, Vitim, and Udokan fields (Fig. 8–1). The predominant mildly alkaline volcanism is mainly found on the uplifted basement of the domal uplifts rather than in the rift depressions, with the exception of the Tunka depression (Fig. 8–3) (Logatchev and Florensov, 1978). A slight displacement of the Vitim and Udokan fields to the southeast of the domal uplift axis is apparent in Figure 8–1. The main phase of volcanism occurred in Miocene to Pliocene time, but possibly started as early as Paleogene in the Tunka depression (Kiselev et al., 1978; Barberi et al., 1982; Kiselev, 1987).

The total volume of volcanic rocks erupted in the Baikal rift system, 5000–6000 km3, is small for a major rift system, being nearly two orders-of-magnitude less than that of the East African rift system (Baker et al., 1972). The largest volume of volcanic products and the longest history of igneous activity occurs, perhaps significantly, in the southwestern region, where fissure-erupted basalt sheets are interbedded at various levels in the Cenozoic sediment succession of the Tunka basin (Paleocene (?) to Quaternary).

The temporal and spatial distributions of volcanic activity are summarized in Kiselev et al. (1978). and Kiselev (1987). The initial volcanism accompanied the development of the proto-rift basins and was concentrated in the southwest (Sayan/Khamar-Daban) and central (Vitim) regions of the Baikal rift (Logatchev and Zorin, 1984; Kiselev et al., 1978). During Pleistocene-Recent time, volcanic activity was initiated in the extreme northeast Udokan field (Fig. 8–1) and continued sporadically elsewhere in the rift system. Kiselev et al. (1978) noted that only the Tunka depression experienced volcanism over an extended time period, accumulating thicknesses of 500-600 m of volcanics. In most other regions, graben development during the rifting stage was characterized by the absence of volcanism.

8.3.4. Compositions of volcanics

Compositions of volcanic products range from tholeiite through transitional to alkaline basalts. On a volumetric basis, alkali olivine basalts are more abundant than tholeiites, trachybasalts, trachytes, and basanites (Gerasimovskiy et al., 1980; Logatchev and Zorin, 1984). Tholeiites are the predominant basalt type in the Tunka depression (Fig. 8–1), although Kiselev et al. (1978) emphasized that normative tholeiites occur in all the volcanic regions to a limited extent. Transitional and alkali basalts are found in all the volcanic fields of the Baikal rift system. There is a general tendency for more alkaline and more evolved magmatic products to occur outside the rift valleys and for the most evolved magmas (mugearites through trachytes) to be located in the Udokan field in the northeast region; however, Kiselev et al. (1978) claimed that hawaiites (slightly differentiated eruptives) are common throughout the region. In summary, the earliest eruptives were tholeiitic and localized in the southwest part of the rift, while more alkaline basalts and intermediate composition volcanics are generally younger (but mainly pre-rifting), distally removed

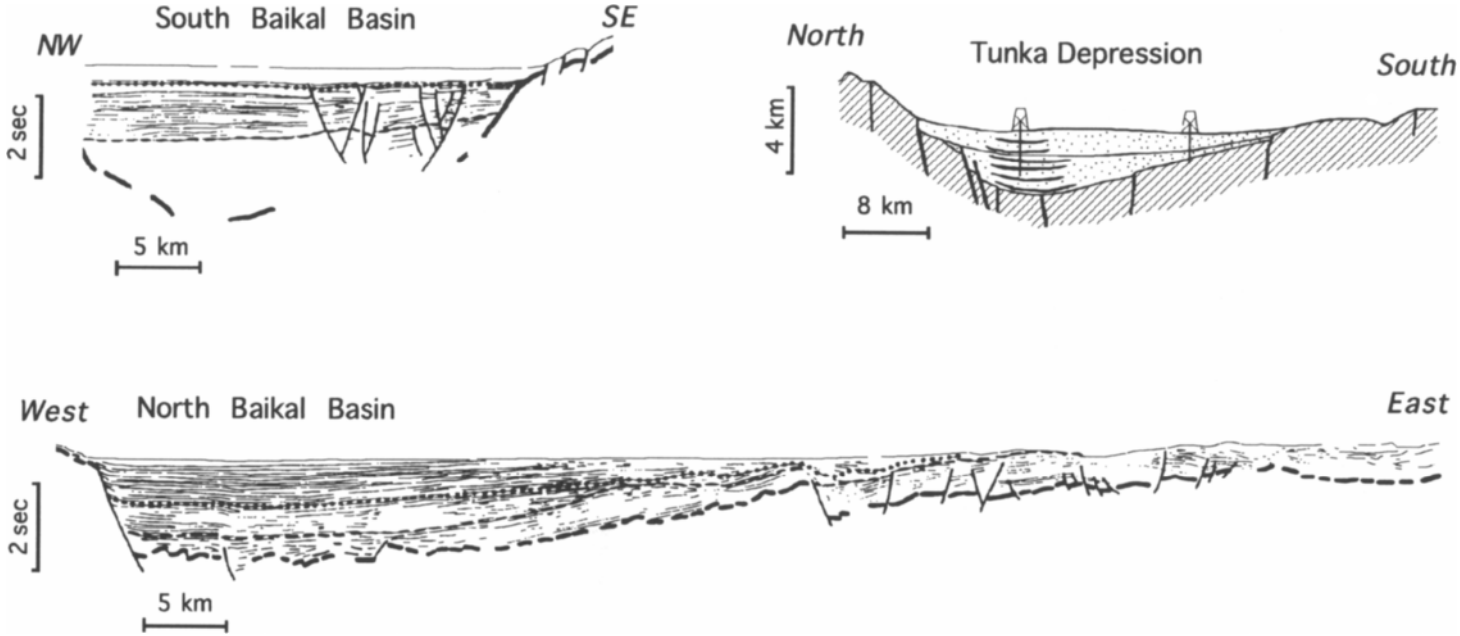

Fig. 8–3. Cross-section of three basins within the Baikal rift zone. Tunka depression after Logatchev and Zorin (1992). Baikal basins after Hutchinson et al. (1992).

from the rift valleys, and become more evolved toward the northeast. No temporal-spatial trends are evident for the alkaline and transitional basalts (Barberi et al., 1982).

Strongly undersaturated magmas are rare although some basanites, nephelinites, and nepheline-rich basanites are found in the Dzhida River basin (southern Khamar-Daban area), Vitim Plateau, and Udokan fields (Fig. 8–1). These strongly undersaturated rocks tend to be young (Quaternary age); Yeskin et al. (1978), however, reported an extrusive melilitite of lower-to-middle Eocene age (52±8 Ma) occurring on the northwest shore of Ushkanjy Island. Potassic alkalic magmas occur in small amounts throughout the Baikal region, but particularly in the extreme southwestern and northeastern regions (Kostyuk, 1983; Kononova et al., 1988; Ionov et al, 1992). These occurrences range in age from Oligocene to Holocene, but are mostly Quaternary.

8.3.5. Xenolith studies

Mantle xenoliths are apparently abundant in Baikal rift-associated volcanics (Kiselev, 1987; Kiselev and Popov, 1992), but there are few systematic studies of their occurrence and provenance. Although spinel facies peridotites are most common, pyrope garnet megacrysts, eclogites, and lherzolites occurring in the potassic alkalic magmas mentioned above (Kostyuk, 1983) suggest pressures and temperatures of origin in excess of 25 kbar and 1300° C. Further constraints on the depth and temperature of origin of basalts associated with the Baikal rift system are provided by Polyakov et al. (1985). These authors estimated conditions of initial basalt genesis of 60-80 km depth (garnet perioditite facies), temperatures of 1200-1300° C, and water contents in the source rock of 0.1 wt%. A megacryst assemblage was estimated to have formed at shallower depths, 45-60 km, and lower temperatures, 900-1200° C. Details on these studies are sketchy.

Xenoliths have recently been collected from the Bartoy volcanoes (Ionov et al., 1992) which are associated with the Khamar-Daban region in relatively close proximity to the rift (Fig. 8–1), the Tariat depression in Mongolia (Preß et al., 1986; Stosch et al., 1986) which is located about 500 km southwest of Lake Baikal, and the Vitim volcanic field (Ionov and Jagoutz, 1989) which also occurs off the rift axis and is underlain by a thick lithosphere section (>100 km; Zorin et al.,1989). The geographic distribution of these localities enable comparison of different mantle regions. Samples from all three locations are interpreted to represent lithospheric mantle. Spinel peridotite xenoliths from the Tariat depression and the Vitim volcanic field are characterized by strong, long-term depletion (2 Ga) of incompatible elements (Stosch et al., 1986) and slight depletion of major elements (Preß et al., 1986) which are probably related to the formation of continental crust. In contrast, spinel lherzolites from the Bartoy volcanoes show evidence of greater thermal variability and isotopic and chemical heterogeneity in the underlying lithosphere, which may be attributed to the volcanoes' close proximity to the Baikal rift and the suture zone separating the Siberian Platform from the Sayan-Baikal fold belt (Ionov et al., 1992).

8.4. Geophysical surveys and results

8.4.1. Seismic studies of crustal and mantle structure

Since the early 1950s, Soviet workers have carried out an extensive program of wide-angle seismic profiling, called Deep Seismic Sounding (DSS), designed to collect data on deep crustal and upper mantle structure throughout northern Eurasia (Egorkin and Pavlenkova, 1981; Pavlenkova and Egorkin, 1983; Egorkin et al. 1987; Ryaboy, 1989; Benz et al. 1992; Belousov et al. 1992a, 1992b). The DSS program is unique and has attracted considerable interest among Western seismologists because about 50 very long profiles have been recorded out to distances of 2000–4000 km by using both large chemical and nuclear explosions as sources (Benz, et al. 1992). Over the same period, numerous more regional-scale profiling studies also were done using more conventional techniques and source-types, often in coordination with the longer profiles. Western specialists have long had considerable difficulty in evaluating the DSS program and its scientific conclusions mainly because the Soviets often published just sketchy *interpretations-only* of crustal and up-

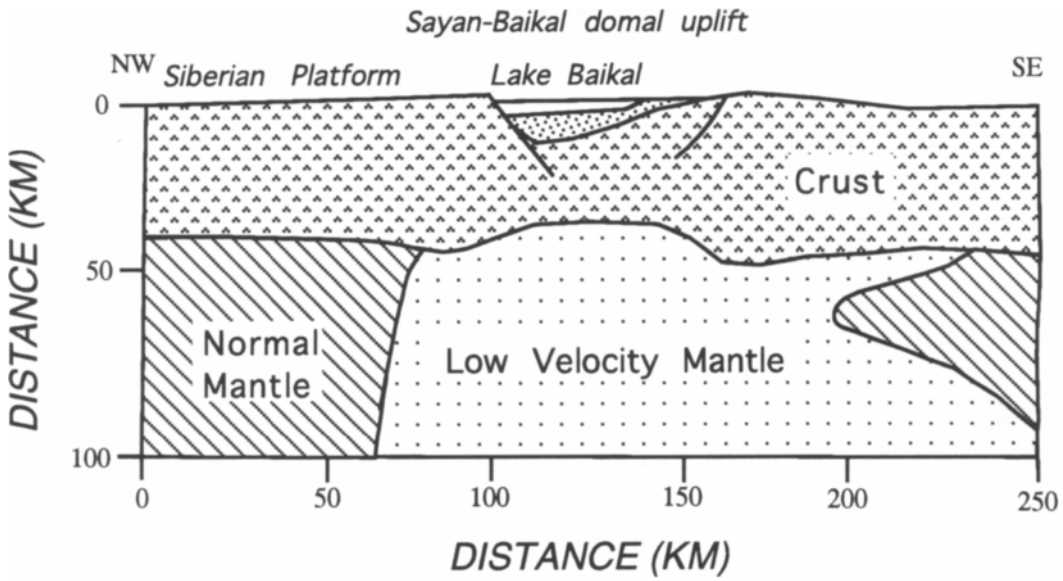

Fig. 8–4. Lithospheric scale cross-section across the south Lake Baikal region (after Logatchev and Zorin, 1987).

per mantle structure, omitting details of techniques, profile coverage and resolutions, and particularly record–section data. Also, much of the DSS literature tended to be widely scattered in Russian language publications difficult to obtain outside the [Former] Soviet Union. However, beginning in 1990, various international agreements with [Former] Soviet seismological organizations is making DSS data more generally available for further analysis by international cooperative working groups, in addition to creating opportunities for new cooperative field studies (Benz, et al. 1992; Belousov et al. 1992a, 1992b).

Although many significant details of DSS and regional surveys covering the Baikal region are not yet available, Olsen (1983) attempted to compile the extent and principal conclusions of those surveys that were published or in progress prior to the mid–1980s. DSS studies in the Baikal region were initiated about 1968 and original descriptions and summaries can be found in Puzyrev et al. (1973, 1978), Krylov et al. (1974, 1975), Krylov and Mishenkin (1984), Puzyrev (1981) and Egorkin et al. (1984, 1987). These studies indicate a crustal thickness of 35–40 km beneath the Siberian Platform to the northwest of Lake Baikal and a similar thickness beneath the Sayan Baikal fold belt to the east of Lake Baikal (Fig. 8–4). A crustal low velocity zone with velocity differential of 0.2-0.3 km/s has been detected beneath the southeastern shore of Lake Baikal. Details of crustal structure in the regions to the southwest and northeast of Lake Baikal appear to be insufficient for assessment of local modifications. A slight overall thickening of the crust to 42–46 km appears beneath the rift flanks along Lake Baikal, but a more extreme localized thinning to 34–35 km occurs beneath central Lake Baikal based on gravity models of the crust in this region which suggests local Airy isostatic compensation of the basins. (Logatchev and Zorin, 1987).

The uppermost mantle beneath the Baikal depression and a narrow flanking zone of similar width to the east of it yields an anomalously low Pn velocity of 7.6–7.8 km/s, with normal Pn of 8.1–8.2 km/s

beneath the Siberian Platform to west and the Sayan-Baikal fold belt further east (Puzyrev et al., 1978). This zone of anomalously low Pn has been interpreted as the top of the asthenosphere which rose as the lithosphere was diapirically thinned at the start of the later stage of evolution of the Baikal rift system (Zorin and Rogozhina, 1978; Zorin, 1981; Zorin and Lepina, 1985). An anomalously low velocity upper mantle extending to depths of several hundred kilometers is indicated by teleseismic P wave delays of about 1.0–1.5 s (Zorin and Rogozhina, 1978; Rogozhina and Kozhevnikov, 1979; Logatchev et al., 1983). This anomalous region is abruptly terminated to the northwest beneath the boundary of the Siberian Platform, but extends to the southeast beneath the Sayan-Baikal region and generally underlies the region of domal uplift (Fig. 8–4). The anomalous upper mantle must extend to 300-400 km depth according to Zorin (1981).

8.4.2. Gravity anomalies

Gravity anomalies have played a major role in interpretations of the deep structure of the Baikal rift system (e.g., Bulmasov, 1960; Stepanov, 1963; Zorin, 1966; Artemjev and Artyushkov, 1971). However, no contour maps have been published except the very regional map of Ruppel et al., (1993) and published profiles usually do not display precise scales in milligals. Recent studies (e.g., Ruppel et al., 1992) suggest that at least regional gravity may soon be available.

Gravity anomalies indicate large local lows (up to 80 mGal amplitude in southern Lake Baikal) with steep gradients over the sediment-filled rift troughs and a regional positive attributed to a thinning of the crust beneath the deeper parts of Lake Baikal (Artemjev and Artyushkov, 1971; Zorin, 1971). Zorin (1981) and Logatchev and Zorin (1987, 1992) reported that gravity and seismically determined Moho depths correlate generally with topography and that local isostatic compensation is important in the region. Logatchev and Zorin (1992) derived a relationship between Moho depth and topography and constructed a contour map of crustal thickness of the Baikal region. On a broader scale, a large scale Bouguer gravity low over the uplifted region indicates isostatic equilibrium associated with the underlying low density upper mantle, mainly associated with the upbulge of the low density asthenosphere which has been assumed to have on average an –0.03 g/cm^3 density contrast (Logatchev et al., 1983).

8.4.3. Magnetic anomalies

Aeromagnetic measurements have recently become one of the major publicly available data sets for the Baikal region. A map constructed by Donald Adams (1993, personal communication) is shown as Figure 8–5. The outline of the Siberian Platform is a particularly striking feature on this map. Aeromagnetic anomalies over the Baikal rift system (Novoselova, 1978) primarily reflect the strike of the Sayan-Baikal basement rocks except over the relatively small areas of Tertiary basalts. The magnetic anomalies along the Baikal rift zone are relatively low and more subdued than over the adjacent regions, especially to the east. This is interpreted by Novoselova (1978) as indicating a thinner and weaker magnetic layer along the rift zone, reflecting the relatively high crustal temperature. The base of the magnetic layer is estimated at 18.5 km where the temperature is about 400° C.

8.4.4. Heat flow studies

The general pattern of heat flow, as summarized by Lysak (1978, 1987, 1992), is as follows. A low average value of 38 mW/m^2 characterizes the adjacent parts of the Siberian Platform. To the east of Lake Baikal, the heat flow of the Sayan-Baikal zone is typically about 50 mW/m^2. Heat flow measurements in the Lake Baikal depressions are much more variable 0–475 mW/m^2) and the mean value is probably about 80 mW/m^2. The greatest variability is in the south of the lake. Variable heat flow also characterizes the other rift depressions to southwest and northeast of the lake.

Lysak (1978), Zorin and Osokina (1984) and Logatchev and Zorin (1987) have modeled the rise in the regional heat flow over the Baikal depression in terms of a hot lower crustal dike with its top at 15 km depth and temperature at 800° C. However, the highly variable heat flow indicates hydrothermal

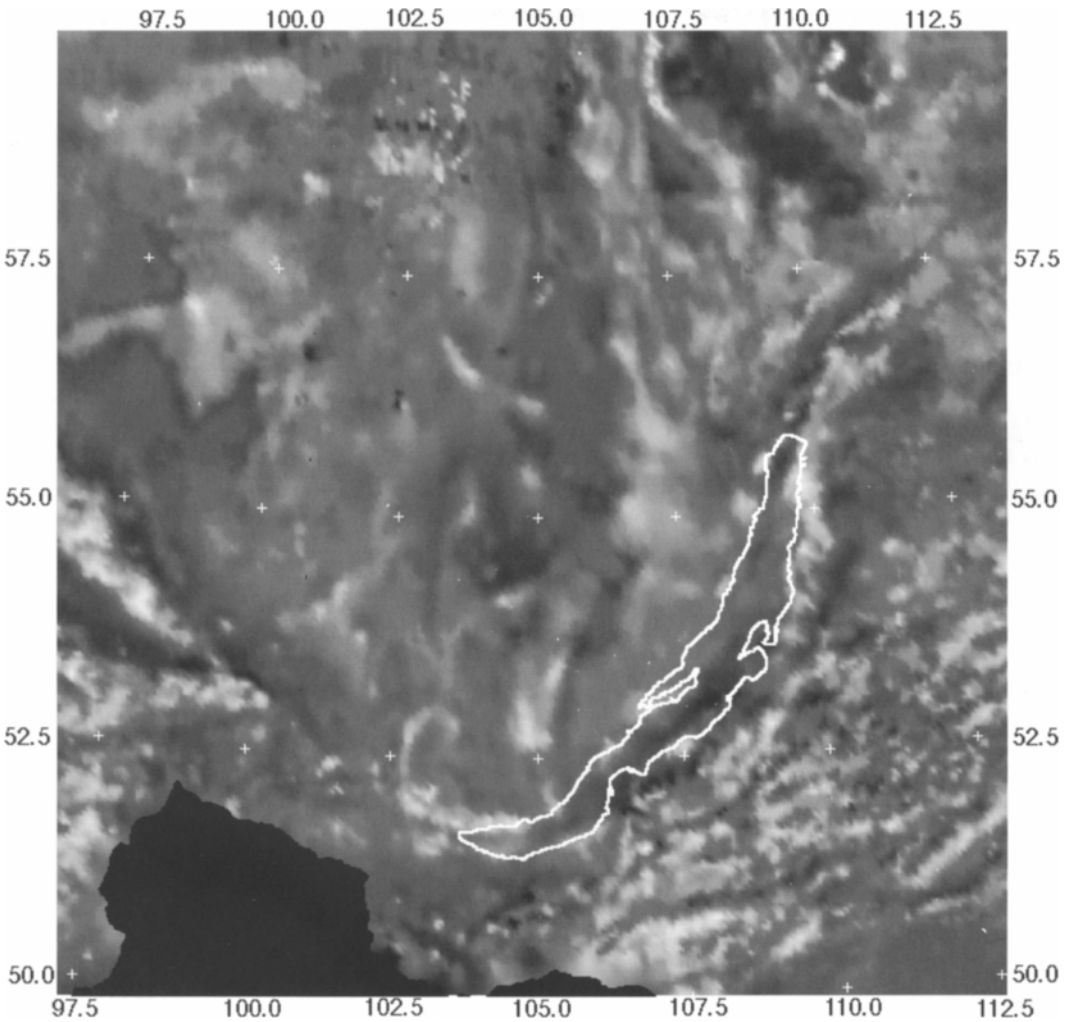

Fig. 8–5. Aeromagnetic anomaly map of the Baikal region. Light areas are highs.

activity (e.g. Shanks and Callender, 1992) with the possibility of smaller igneous intrusions at shallower depth. It also seems possible that the high average heat flow of Lake Baikal can be explained by this activity without need for a wide lower crustal dike-like heat source. Either way, the average crustal temperatures beneath the rift depressions appear to be much higher than beneath the adjacent regions. Anomalously high temperatures within the crust beneath the Baikal depressions are also indicated by the depressed magnetic anomalies (Novoselova, 1978) and by magnetotelluric results (see 8.4.5). Thus the heat flow anomalies associated with the Baikal rift system are almost entirely attributable to

hydrothermal and crustal igneous activity immediately beneath the rift depressions. This is readily understandable, since the original upper mantle hot region beneath continental lithosphere of normal thickness would only marginally increase the geothermal gradient (say 10%) and the asthenospheric upwelling beneath the Baikal rift system depressions only occurred 4 Ma ago which would not be long enough for thermal equilibrium to be established by thermal conduction in the 30–35 km thick crust.

8.4.5. Electromagnetic studies

More than 300 magnetotelluric soundings in the Baikal rift system and adjacent areas had been performed by 1977, and Berdichesvky et al. (1977) described a comprehensive interpretation which was based on a subdivision of the observed types of apparent resistivity curves. Their 1D-model interpretation was based on the average effective apparent resistivity curve for each region. The essential result is the existence of a low resistivity (ca. 10 ohm–m) layer between 15 and 45 km beneath the Baikal region. The maximum conductance (= conductivity times thickness), however, lies about 200 km to the east of Lake Baikal with values up to 2000 S. Berdichevsky et al. (1977) offered an alternative model which consisted of two low resistivity layers, the upper layer between depths of 12 and 20 km, the deeper layer between 35 and 60 km. This model would agree with the seismic model published by Puzyrev and Krylov (1977). Regardless of whether this low resistivity layer is split into two layers or is a single layer beneath the area east of Lake Baikal, it signifies an anomalous crust compared to the Siberian platform crust which has normal or only slightly decreased resistivity. In a more recent magnetotelluric study, Popov (1987; 1990; and personal communication) inferred a rather similar model from his measurements. Moreover, he argues that the low resistivity layer in the crust deepens from 12–14 km in the south to 25–30 km in the northeast, while a deeper low resistivity layer rises from 110 to 60–70 km in the northeast. Berdichevsky et al. (1977) and Popov (1987; 1990; and personal communication) argued that the upper low resistivity layer of their respective models is due to hydrothermal activity, and that the deeper layer is due to partial melting.

8.4.6.Seismicity, focal mechanisms. and stress field

Knowledge of seismicity is mainly based on about 20 seismological stations established in the 1950s and on field studies (Golenetsky and Misharina, 1978; Golenetsky, 1990). Most of the seismic activity occurs along the belt of rift depressions. The adjacent region to the southeast has much more sparse seismicity and the Siberian Platform is virtually aseismic (Golenetsky, 1990). Earthquake epicenters cluster along elongated belts along the strike of the system and often occur along known faults with much weaker activity within the intervening blocks. Most of the small earthquakes have foci within the upper crust, but data are insufficient to establish depth distributions. The magnitude-frequency relationship is normal and there are no indications of any spatial or temporal sequences of large earthquakes. The largest earthquakes (M>7) occur about every 150 years.

Sparse station coverage of the regional seismograph network has meant that few focal depth determinations can be made and that composite focal depth determinations must often be employed due to lack of data for single events. The poor focal depth control makes the quality of many mechanisms doubtful, since inaccurate focal depths can lead to the miscalculation of take-off angles needed in focal mechanism determinations. In order better to determine the changes in focal depth and focal mechanism across the rift, Doser (199la, b) determined the source parameters for pre- and post-1960 earthquakes with magnitude >5.7 using the body waveform modeling technique of Baker and Doser (1988). Focal mechanisms obtained from this analysis are shown in Figure 8–6.

Parfenoy et al. (1987) used gravity, stress field, and seismic studies to argue that the Olekma River (Fig. 8–6) represents the easternmost boundary of the Baikal rift. Waveform modeling of three earthquakes occurring just west of the Olekma River between 1958 and 1967 indicates normal faulting is occurring along faults that parallel the edge of the

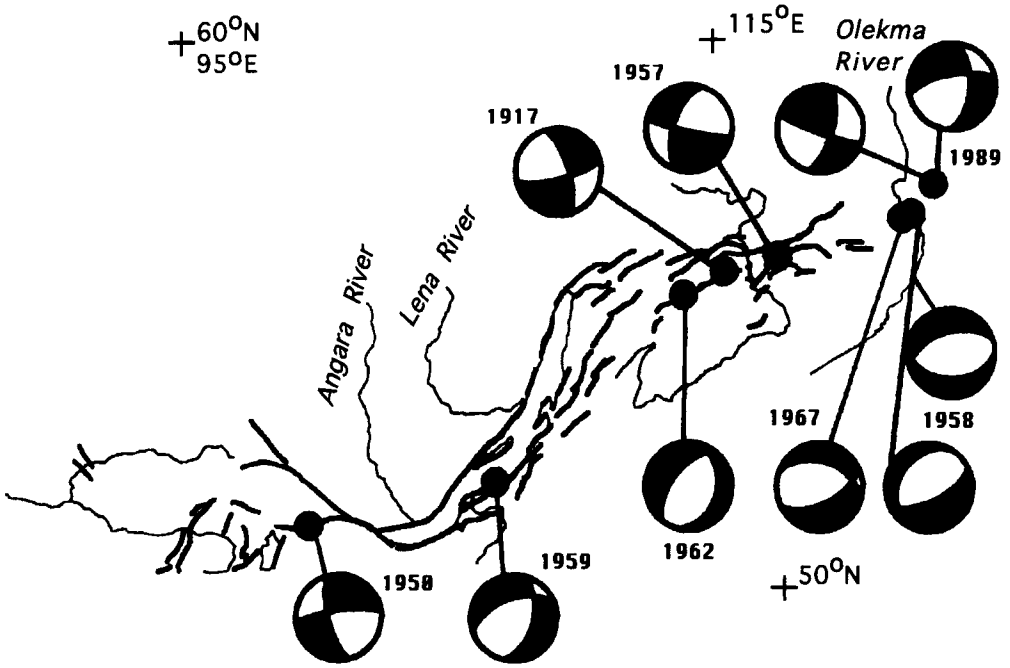

Fig. 8–6. Earthquake focal mechanisms. After Doser (1991 a, b). Year of the events studied are shown.

Siberian craton. Earthquake depths ranged from 6 to 10 km. Analysis of a sequence of earthquakes occurring east of the Olekma River in 1989, however, shows strike-slip faulting, with focal depths as great as 30 km. Thus, the source parameters obtained from body waves support the observation of Parfenoy et al. (1987) that there is a significant change in stress field and crustal structure east of the Olekma River. The deep earthquakes are of particular interest and may be evidence for rift migration (Déverchère et al., 1991; Doser and Yarwood, 1994).

The largest instrumentally recorded earthquake within the rift (magnitude 7.8) occurred in the east central rift in 1957 (Fig. 8–6). The main surface rupture trended east-west and showed left-lateral as well as normal motion. Body waveforms indicate the earthquake was composed of at least three sub-events with focal depths of about 10 km. The focal mechanisms of the sub-events are similar to the observed surface rupture, indicating strike-slip and normal motion along a high angle fault. An attempt was made to model the waveforms of the largest and last sub-event with rupture along a low angle (<30 dip) fault, but no suitable mechanism was found. The north Baikal earthquake of 1917 (magnitude 6.7), occurring about 30 km west of the 1957 event, also has a large component of strike-slip motion, but occurred at a greater depth of 16 km. Thirty kilometers further west, the 1952 Muyakan earthquake occurred on a normal fault at a shallow depth of 5 km.

Historically the central region of Lake Baikal has been the site of significant seismicity. In 1862 an earthquake of about magnitude 7 occurred in the Selenga River delta region, producing 7 to 8 m of subsidence of the northern part of the delta, forming Proval Bay. In 1959, the Srednebaikal earthquake occurred about 10 km northeast of Proval Bay. Waveform modeling of the 1959 event indicates the earthquake occurred along a northeast striking, northwestward dipping, normal fault that bounds the southeastern shore of the lake. A 14 km focal depth

places the earthquake near the top of the low velocity layer mapped along the southeast shore of Lake Baikal. This suggest top of the low velocity layer may signify the bottom brittle-ductile transition zone in this region.

The southwestern portion of the rift system is generally seismically active at the magnitude <5.5 level, with the few earthquakes above this magnitude level occurring prior to 1960. Only the largest event, the 1950 (magnitude 6.7) Mondy earthquake, had sufficient data at teleseismic distances for analysis. Following the earthquake, a series of discontinuous fractures trending northwest was found on a river terrace. Waveform inversions of body wave data give a strike-slip mechanism and a focal depth of 6 km. The mechanism is not consistent with the sense of motion (southwest side up) observed along the river terrace, suggesting the surface fractures may be secondary.

All earthquakes studied occurred on high angle faults (dip > 30°), with all but one event having a dip >50°. This is in agreement with the model of rift development proposed by Artyushkov et al. (1990) that suggests thinning of the crust was not produced by stretching of the upper crust along low angle faults but rather by thinning of the crystalline crust beneath the rift.

Focal depths within the rift system (west of the Olekma River) range from 5 to 16 km. This suggests the base of the seismogenic zone in the region is at about 15 km. East of the Olekma River there must be a significant change in crustal properties since studies of the 1989 earthquake sequence give focal depths of 25 to 30 km for the larger events.

The majority of earthquakes within the Baikal rift system have strikes of 240° to 280° or of 40° to 80°, the general trend of the rift zone and of faults within it. Within the rift system about 50% of the earthquakes exhibit normal faulting (rakes of -60° to -120°). However, the three largest earthquakes in the rift system (1917,1950, 1957) were associated with strike-slip faulting (rakes of -160° to -180° or 0° to -20°). East of the Olekma River both the strike and rake change, indicating a change in stress field.

8.5. Structure and interpretation.

There had been no deep seismic *reflection* studies in the Baikal rift system before 1992 other than relatively shallow penetration studies within the lake (Hutchison et al., 1992). However, a large scale, multi-channel, seismic reflection survey was undertaken on the lake in the fall of 1992, and the initial results were reported by Scholz et al. (1993). As discussed in the section on seismicity, earthquake source studies indicate that high-angle normal faulting with elements of strike slip is predominant in the rift system, and these new data show that the primary border faults of the basins are found along the northwestern shore of the lake and generally have dips >65°. Complex faulting and depositional patterns were found to be associated with the Academician ridge. This feature is clearly a major basement high which separates the northern and central Baikal basins. The high angle faulting suggests minor amounts of extension in agreement with the model of Artyushkov et al (1990). This would suggest that the estimate of 25 km in the South Baikal basin (Logatchev and Zorin, 1987; Zorin and Cordell, 1991) may be high. This estimate was however based on crustal thickness values inferred in large part from the analysis of topography and gravity anomalies.

The extensive DSS work in the region combined with gravity studies provides a regional picture of crustal structure that suggests surprisingly short wave-length variations in crustal thickness beneath Lake Baikal which indicate local isostatic compensation. Logatchev and Zorin (1992) used gravity and topographic data along with seismic results to construct a contour map of crustal thickness. Their results indicate crustal thinning to less than 35 km beneath the lake, some areas of thick (>45 km) crust associated with the flanks, and regional crustal thicknesses of about 40 km. The 1992 work may also ultimately give an improved picture of crustal structure at Moho depths.

The combination of DSS and teleseismic P-wave delay results provide the lithospheric cross-section shown in Figure 8-4. However, very few of these data are available for further study. This cross-section shows that a very large asymmetrical region of

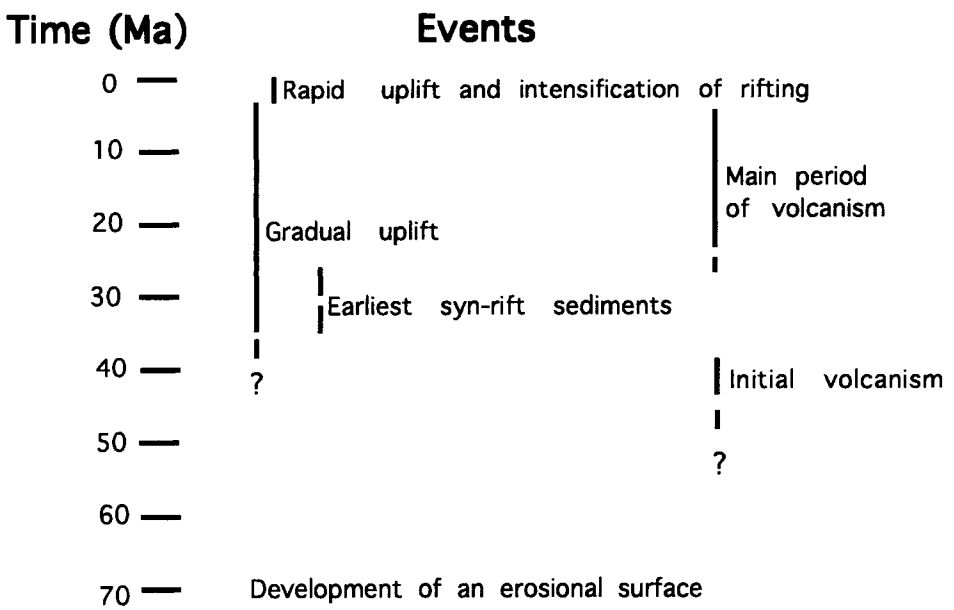

Fig. 8–7. Evolution of the Baikal rift zone

anomalous upper mantle underlies the whole Baikal rift system. It is terminated abruptly at the edge of the Siberian Platform. Zorin et al. (1989) analyzed the lithospheric thickness in the Baikal region using gravity and seismic data. The contour map of lithospheric thickness presented by Logatchev and Zorin (1992) shows the rift zone to be associated with a lithospheric thicknesses of less than 50 km.

8.6. Tectonic evolution

Logatchev and Florensov (1978) and Logatchev and Zorin (1987) described two stages in the evolution of the Baikal rift system. The earlier stage (Oligocene, 30-35 Ma, or earlier, to early Pliocene, 4 Ma) involved subdued uplift and the development of proto-rift depressions, as indicated by the absence of coarse sands and gravels in the sediments. Up to 5000 m of sediments was deposited in the South Baikal depression during this stage of evolution, but the proto Lake Baikal remained shallow since sedimentation kept pace with subsidence. The greatest volume of volcanism in the Baikal rift system occurred during this stage, especially during the Oligocene to Miocene. The earliest volcanic rocks of possible Paleogene age occur in the region of the Tunka depression (Kiselev, 1987).

The later stage occurred over about 4 Ma from early Pliocene to the present, with rapid domal uplift at the onset leading to a greatly increased rate of extension and subsidence. During this time, about 1000 m of predominantly coarse sandstones and conglomerates have been deposited in the young rift depressions. Volcanism continued but much more subdued than earlier. Hutchinson et al. (1992) identified seismic stratigraphic evidence to suggest that the later stage of evolution could be subdivided into two phases.

The evolution deduced from the sedimentary record, structure, and volcanism is shown in Figure 8–7. Although evidence on timing of rifting is limited, the Baikal rift appears to display an interesting

progressive lengthening of the system in both directions from the initial south Baikal depressions, which may have started to form as early as the Paleocene (Fig. 8–1). The adjacent northern Baikal and Tunka depressions were next initiated in the Oligocene to early Miocene. The whole system of rift basins has continued to extend towards the northeast and southwest. The topographic relief and seismicity observed today attests to the fact that this rift zone is still very active.

8.7. Origin and development

Most Russian earth scientists support an active origin for the Baikal rift system (Logatchev and Florensov, 1978; Zorin and Rogozhina, 1978; Zorin, 1981; Logatchev et al., 1983; Artyushkov et al., 1990). The initial structure to form was the anomalous upper mantle beneath the continental lithosphere. This gave rise to the subsequent volcanic and tectonic development of the Baikal rift system. The earlier stage of evolution occurred before and possibly during the thinning of the lithosphere and the later stage followed on from it. The tensile stress system causing the rifting has been attributed to the gravitational body forces associated with the asthenospheric upbulge since the early suggestions of Zorin (1971) and Artyushkov (1972).

An alternative passive hypothesis of origin was proposed by Molnar and Tapponnier (1975) and Tapponnier and Molnar (1979) and is supported by Zonenshain and Savostin (1981) and Kiselev and Popov (1992). They suggested that the Baikal rift system was initiated as a result of the collision of India and Asia 30 m.y. ago. The crucial difficulty of this hypothesis is that the Baikal rift system may have started to form much earlier than 30 m.y. ago. The drilled sediments of the South Baikal depression go back to perhaps late Eocene (>38 Ma) and the base of the succession was not reached. The drill hole was about 3000 m deep and the preliminary interpretations of the recent seismic reflection results would suggest sedimentary thicknesses of on the order of 5 km or more in the area. The volcanic rocks of the Tunka depression may be as old as Paleogene. This does not necessarily rule out a passive hypothesis related to plate phenomena other than the Indian collision. However, the following features of our present knowledge of the Baikal rift system suggest that active processes were also important in the formation of the rift zone: (1) the Baikal rift system developed within continental lithosphere unconnected to any plate boundaries; (2) the volcanism and uplift of the early stage preceded the main rifting and the most intense volcanism preceded the thinning of the lithosphere; (3) the volcanism mainly occurred on the uplifted bordering regions and is notably absent from the rift depressions apart from the Tunka depression; (4) the region of anomalous upper mantle appears to be much larger than could be produced by lithospheric extension of 10-25 km. Recent studies in Mongolia (e.g., Zorin et al., 1990; Ufimtsev, 1990; Khain, 1990; Windley and Allen, 1993) have led to the suggestion that the extension which formed the rift is due to mantle plume related uplift over a large area (Windley and Allen, 1993) or that the rifting may be due to the combination of a plume and the Indian-Asian collision (Khain, 1990). The plume model is consistent with the evidence for an active rifting model but would suggest that the Baikal rift is only part of a larger picture. It will be interesting to see if the plume hypothesis can be tested by future studies.

The present (and past?) tensional stress is strongly oriented in a northwest-southeast direction. The actual stress system which caused the rifting, past and present, may thus be a superposition of a local unidirectional horizontal deviatoric tension produced by the domal uplifts and the supporting low density upper mantle as suggested by Zorin, (1971) and Artjushkov (1972), and a regional stress system related to plate boundary forces producing a maximum horizontal deviatoric tension in the northwest-southeast direction. This regional stress system may be related to subduction at the northwestern margin of the Pacific producing trench suction in a northwest-southeast direction supplemented by compression in the orthogonal direction related to the India-Asia collision. The grain of the Sayan-Baikal basement and the boundary with the Siberian Platform has defined the detailed geometry of the system of rift depressions, with extension perpendicular to strike in the central region of the system but a component

of strike slip motion in some of the outlying districts where the grain is oblique to the present stress system.

An outstanding problem is the time scale of thinning of the lithosphere. Zorin (1981) suggested it occurred over 30 Ma during the early stage of evolution, but the relatively abrupt change from fine to coarse sediments in the Middle Pliocene may suggest a rapid lithospheric thinning 5 m.y. ago (Molnar and Tapponnier, 1975).

8.8. References

Artemjev, M. E., and E. V. Artyushkov, 1971. Structure and isostasy of the Baikal rift and the mechanism of rifting. J. Geophys. Res., 76: 1197–1211.

Artyushkov, E.V., F.A. Letnikov, V.V. Ruzhich, 1990. The mechanism of formation of the Baikal basin, J. of Geodynamics, 11: 277–291.

Artyushkov, E. V., 1972. The origin of great stresses in the crust, Izv. Akad. Nauk SSSR, ser. Fiz Zemli, No. 8: 3–25.

Baker, B. H., P. A. Mohr, and L. A. J. Williams, 1972. Geology of the Eastern Rift System of Africa. Geol. Soc. Amer. Spec. Pap. 136, 67 pp.

Baker, M.R., and D.I. Doser, 1988. Joint inversion of regional and teleseismic earthquake waveforms. J. Geophys. Res., 93: 20372045.

Balla, Z., M.N. Kuzmin, and K.G. Levy, 1991. Kinematics of the Baikal opening: Results of modeling. Annales Tectonicae, 5: 1831.

Barberi, F., R. Santacroce, and J. Varet, 1982. Chemical aspects of rift magmatism. In: G. Palmason (Ed.) Continental and Oceanic Rifts, Am. Geophys. Union Geodynamics Series 8: 223–258.

Belousov, V.V., N.I. Pavlenkova, and G.N. Kvyatkovskaya, (Eds.), 1992a. Structure of the crust and upper mantle of the [Former] Soviet Union, Part I: Integrated geophysical models of the major geostructures of the USSR. International Geol. Rev., 34(3): 213–338.

Belousov, V.V., N.I. Pavlenkova, and G.N. Kvyatkovskaya, (Eds.), 1992b. Structure of the crust and upper mantle of the [Former] Soviet Union, Part II: Generalized geophysical data on the structure of the tectonosphere of the USSR. International Geol. Rev., 34(4): 345–444..

Benz, H.M., J.D. Unger, W.S. Leith, W.D. Mooney, L. Solodilov, A.V. Egorkin, and V.Z. Ryaboy, 1992. Deep seismic sounding in northern Eurasia. Eos, Trans. AGU, 73: 297–300.

Berdichevsky, M. N., L. L. Vanyan, V. A. Kuznetzov, V. T. Levadny, M. M. Mandelbaum, G. P. Nechaeva, B. A. Okulessky, P. P. Shilovsky, I. P. Shpak, 1980. Geoelectrical model of the Baikal region, Phys. Earth Planet Int., 22: 1-11.

Bulmasov, A. P., 1960. Magnetic and gravity fields of Baikal region in connection with its seismicity. Bull. Sov. Seismol. Akad. Nauk SSSR, 10: 49-58 (in Russian).

Déverchère, J., F. Houdry, and M. Diament, 1991. Evidence for a seismogenic upper mantle and lower crust in the Baikal rift. Geophys. Res. Letters, 18: 1099-1102.

Doser, D.I., 1991a. Faulting within the western Baikal rift as characterized by earthquake studies: Tectonophysics, 196: 87-107.

Doser, D.I., 1991b. Faulting within the eastern Baikal rift as characterized by earthquake studies: Tectonophysics, 196: 109–139.

Doser, D.I. and D.R. Yarwood, 1994. Deep crustal earthquakes associated with Continental rifts. Tectonophysics, 229: 123–131.

Egorkin, A.V., and N.I. Pavlenkova, 1981. Studies of mantle structure of the U.S.S.R. territory on long–range seismic profiles. Phys. Earth Planet. Inter., 25: 12–26.

Egorkin, A.V., S.K. Zuganov, and N.M. Chernyshev, 1984. The upper mantle in Siberia. Proceedings 27 Int. Geol. Congr., v. 8 (Geophysics): pp. 29–56, VNU Science Press, Utrecht, The Netherlands.

Egorkin, A.V., S.K. Zuganov, N.I. Pavlenkova, and N.M. Chernyshev, 1987. Results of lithospheric studies from long–range profiles in Siberia. Tectonophysics, 140: 29–47.

Florensov, N. A., 1969. Rifts of the Baikal mountain region. Tectonophysics, 8: 443-456.

Gerasimovskiy, V. I., I. A. Roshchina, and I. D. Shevaleyevskiy, 1980. Chemical compositions of basalts in the Baykal rift zone, Geochem. Int. 17: 1-10.

Golenetsky, S.I., 1990. Problems of the seismicity of the Baikal rift zone. J. Geodynamics, 11: 293-307.

Golonetsky, S. I., and L. A. Misharina, 1978. Seismicity and earthquake focal mechanisms in the Baikal rift zone, Tectonophysics, 45: 71-85.

Hutchinson, D.R., A.J. Golmshtok, L.P. Zonenshain, T.C. Moore, C.A. Scholz and K.D. Klitgord, 1992. Depositional and tectonic framework of the rift basins of Lake Baikal from multichannel seismic data, Geology, 20: 589-592.

Ionov, D.A., and E. Jagoutz, 1989. Isotope behavior of strontiumn and neodymium in minerals of garnet- and spinel-containing peridotite xenoliths of the Vitim Plateau: first data from the USSR. Trans. (Doklady) USSR Acad. Sci., Earth Sci. Sect., 310:232-236.

Ionov, D.A., U. Kramm, and H.-G. Stosch, 1992. Evolution of the upper mantle beneath the southern Baikal rift zone: An Sr-Nd isotope study of xenoliths from the Bartoy volcanoes, Contrib. Minerl. Petrol., 111: 235-247.

Khain, V.E., 1990. Origin of the central Asian mountain belt: Collision or mantle diapirism. J. Geodynamics, 11: 389-394.

Khrenov, P.M. (editor), 1983. Geological Map of the Baikal Region. 27 Geological Convention, CCCP, 1:1,000,000.

Kiselev, A. I., H. A. Golovko, and M. E. Medvedev, 1978. Petrochemistry of Cenozoic basalts and associated rocks in the Baikal rift zone, Tectonophysics, 45: 49-59.

Kiselev, A. I., 1987. Volcanism of the Baikal rift zone, Tectonophysics, 143: 235-244.

Kiselev, A. I., and A. M. Popov, 1992. Asthenospheric diapir beneath the Baikal rift: Petrologic constraints: Tectonophysics, 208: 287-295.

Kononova, V.A., V.A. Pervov, V.I. Drynkin, A.L. Kerzin, and Y.D. Andreyeva, 1988. Rare-earth and rare elements in the Cenozoic basin volcanites of Transbaikalia and Mongolia. Geochem. Internat., 24 (12): 32–46.

Kostyuk, V. P., 1983. The potassic-alkalic magmatism of the Baikal-Aldan Belt, Soviet Geol. and Geophys. 24: 31–38.

Krylov, S.V., S.I. Golenetsky, and G.V. Petrik, 1974. Agreement of seismology and DSS/data on the uppermost mantle structure of the Baikal rift zone (in Russian). Geol. i Geofiz., 15 (12): 12: 61-66.

Krylov, S.V., and B.P. Mishenkin, 1984. Deep structure of the Baikal region from seismic data. Proceedings 27 Int. Geol. Congr., v. 8 (Geophysics): pp. 65–72, VNU Science Press, Utrecht, The Netherlands.

Krylov, S.V., B.P. Mishenskin, Z.F. Mishenkina, G.V. Petrik, and V.S. Seleznev, 1975. Seismic cross-section of the lithosphere in the Baikal rift zone (in Russian). Geol. i Geofiz., 16 (3): 72-83.

Lipmann, P.W., N.A. Logatchev, Y.A. Zorin, C.E. Chapin, V. Kovalenko, and P. Morgan, 1989. Intracontinental rift comparisons: Baikal and Rio Grande rift systems. Eos, Trans. Am. Geophys. Un. 70 (no. 19): 578–588.

Logatchev, N. A., 1984. The Baikal rift system, Episodes, 7: 38-43.

Logatchev, N. A, and N. A. Florensov, 1978. The Baikal system of rift valleys, Tectonophysics, 45: 1-13.

Logatchev, N. A., and P. Mohr (Eds.), 1978. Geodynamics of the Baikal rift zone, Tectonophysics, 45: 1-105.

Logatchev, N.A., Yu. Zorin and V. Rogozhina, 1983. Baikal rift: active or passive? – Comparison of the Baikal and Kenya rift zones, Tectonophysics, 94: 223–240.

Logatchev, N. A., and Yu. Zorin, 1984. Structure and evolutionary stages of the Baikal rift. Tectonics (27th Int. Geol. Congr., Moscow) 7: 251–267.

Logatchev, N.A., and Yu. A. Zorin, 1987. Evidence and causes of the two-stage development of the Baikal rift, Tectonophysics, 143: 225-234.

Logatchev, N.A., and Yu. A. Zorin, 1992. Baikal rift zone: Structure and geodynamics. Tectonophysics, 208: 273-286.

Lysak, S.V., 1978. The Baikal rift heat flow, Tectonophysics, 45: 87-93.

Lysak, S.V., 1987. Terrestrial heat flow of continental rifts: Tectonophysics, 143: 31-41.

Lysak, S.V., 1992. Heat flow variations in continental rifts. Tectonophysics, 208: 309-323.

Molnar, P., and P. Tapponnier, 1975. Cenozoic tectonics of Asia: effects of a continental collision, Science, 189: 419-426.

Novoselova, M. R., 1978. Magnetic anomalies of the Baikal rift zone and adjacent areas, Tectonophysics, 45: 95-100.

Olsen, K.H., 1983. The role of seismic refraction data for studies of the origin and evolution of continental rifts, Tectonophysics, 94:349-370.

Parfenoy, L.M., B.M. Kos'min, and V.S. Imayev, L. Savostin, and P.P. Shirshov, 1987. The tectonic character of the Olekma-Stanovoy seismic zone. Geotectonics, 21: 560–572.

Pavelenkova, N.I., and A.V. Egorkin, 1983. Upper mantle heterogeneity in the northern part of Eurasia. Phys. Earth Planet. Inter., 33: 180–193.

Polyakov, A. I., V. A. Turkov, N. S. Murav'yeva, L. I. Nesmeyanova, and K I. Ignatenko, 1985. The physicochemical conditions in basalt magma production and evolution in the Baykal rift zone. Geochem. Int. 22: 98-113.

Popov, A.M., 1987. On causes of increased electrical resistivity of the crust (on the example of the Baikal area). Geol. Geophys. 12: 57-64 (In Russian).

Popov, A.M., 1990. A deep geophysical study in the Baikal region. Pure Appl. Geophys., 187: 575–587.

Preß, S., G. Witt, H.A. Seck, D. Eonov, and V.I. Kovalenko, 1986. Spinel peridotite xenoliths from the Tariat Depression, Mongolia. I: Major element chemistry and mineralogy of a primitive mantle xenolith suite. Geochim. Cosmochim. Acta, 50: 2587-2599.

Puzyrev, N. N., M. M. Mandelbaum, S. V. Krylov, B. P. Mishenkin, G. V. Krupskaya, G. V. Petrik, 1973. Deep seismic investigations in the Baikal rift zone, Tectonophysics, 20: 85-95.

Puzyrev, N. N., M. M. Mandelbaum, S. V. Krylov, B. P. Mishenkin, G. V. Petrik and G. V. Krupskaya, 1978. Deep structure of the Baikal and other continental rift zones from seismic data, Tectonophysics, 45: 15-22.

Puzyrev, N. N. (Ed.), 1981. Bowels of Lake Baikal from Seismic Data, Nauka, Novosibirsk, 105 pp. (in Russian).

Rogozhina, V. A., and V. M. Kozhevnikov, 1979. Area of anomalous mantle under the Baikal rift, Nauka, Novosibirsk, 102 pp. (in Russian).

Rosendahl, B.R., 1987. Architecture of continental rifts with special reference to East Africa: Annual Rev. Earth Planet. Sci, 15: 445–503.

Ruppel, C., M. Kogan, and M. McNutt, 1993. Implications of new gravity data for Baikal rift zone structure. Geophys. Res. Letters, 20: 1635-1638.

Ryaboy, V.Z., 1989. Upper Mantle Structure Studies by Explosion Seismology in the USSR. Delphic Press, Falls Church, VA, 155 pp.

Scholz, C.A., Klitgord, K.D., Hutchinson, D.R., Ten Brink, U.S., Zonenshain, L.P., Golmshtok, A.Y., and Moore, T.C., 1993. Results of 1992 seismic reflection experiment in Lake Baikal. EOS, Trans. Am. Geophys. Union, 74: 465-470.

Shanks, W.C. and E. Callender, 1992. Thermal springs in Lake Baikal, Geology, 20: 495-497. Sherman, S. I., 1978. Faults of the Baikal rift zone, Tectonophysics, 45: 31-39.

Sherman, S.I., 1992. Faults and tectonic stresses of the Baikal rift zone. Tectonophysics, 208: 297-307.

Stepanov, P. P., 1963. On the application of isostatic corrections, Prikl. Geofiz., 37: 147-153.

Stosch, H.-G., G.W. Lugmair, and V.I. Kovalenko, 1986. Spinel peridotite xenoliths from the Tariat Depression Mongolia. II: Geochemistry and Nd and Sr isotopic composition and their implications for the evolution of the subcontinental lithosphere. Geochim. Cosmochim. Acta, 50: 2601–2614.

Tapponnier, P., and P. Molnar 1979. Active faulting and Cenozoic tectonics of the Tien Shan, Mongolia, and Baykal regions, J. Geophys. Res., 84: 3425-3459.

Ufimtsev, G.F., 1990, Morphotectonics of the Mongolia-Silberian Mountain belt. Journ. Geodynamics, 11: 309-325.

Windley, B.F. and Allen, M.B., 1993. Mongolian plateau: Evidence for a late Cenozoic mantle plume under central Asia. Geology, 21: 295-298.

Yanshin, AL., 1980. Geological Map [of] South Eastern Siberia and Northern Mongolian Autonomous Region. Ministry of Geology, CCCP, 1:1,500,000.

Yeskin, S., A. A. Bukharov, and Yu. A. Zorin, 1978. Cenozoic igneous activity in Lake Baikal. Dokl. Akad. Nauk SSSR, 239: 40–43.

Zamarayev, S. M., and V. V. Ruzhich, 1978. On relationships between the Baikal rift and ancient structures. Tectonophysics, 45: 41-47.

Zonenshain, L. P., and L. Savostin, 1981. Geodynamics of the Baikal rift zone and plate tectonics of Asia. Tectonophysics, 76: 1-45.

Zorin, Yu. A., 1966. On the deep structure of the Baikal depression based on geophysical data, Izv. Akad. Nauk SSSR, Ser. Geol. no. 7: 76-85 (in Russian).

Zorin, Yu., 1971. Recent structure and isostasy of the Baikal rift zone and adjacent area, Nauka, Moscow, 168 pp. (in Russian).

Zorin, Yu., and V. A. Rogozhina, 1978. Mechanism of rifting and some features of the deep-seated structure of the Baikal rift zone, Tectonophysics, 45: 23-30.

Zorin, Yu., V. M. Kozhevnikov, M. R. Novoselova, and E. Kh. Turutanov, 1989. Thickness of the lithosphere beneath the Baikal rift zone and adjacent regions. Tectonophysics, 168: 327-337.

Zorin, Yu., Novoselova, M.R., Turutanov, E. Kh., and Kozhevnikov, V.M., 1990. Structure of the lithosphere of the Mongolian-Siberian mountainous province. Journ. Geodynamics, 11: 327-342.

Zorin, Yu. ,1981. The Baikal rift: an example of the intrusion of asthenospheric material into the lithosphere as the cause of disruption of lithospheric plates, Tectonophysics, 73: 91-104.

Zorin, Yu. , and S. V. Osokina, 1984. Model of the transient temperature field of the Baikal rift lithosphere, Tectonophysics, 103: 193-204.

Zorin, Yu. A., and S. V. Lepina, 1985. Geothermal aspects of development of asthenospheric upwellings beneath continental rift zones, J. Geodynamics, 3:1-22.

Zorin, Yu. A., and L. Cordell, 1991. Crustal extension in the Baikal rift zone. Tectonophysics, 198: 117-121.

This Page Intentionally Left Blank

Part IV.

Paleorifts

This Page Intentionally Left Blank

Chapter 9

The Oslo rift

E.–R. Neumann, K. H. Olsen, and W. S. Baldridge

9.1 Introduction

The large volumes of magmatic rocks interspersed with Paleozoic sedimentary rocks of the Oslo Region were early recognized as an outstanding feature relative to the Precambrian terrain on both sides (e.g. Buch, 1810; Keilhau, 1838). Gradually, it became clear that this Paleozoic province was partly bounded by faults and represented a younger sequence down-faulted relative to the Precambrian basement to the east and west (Kjerulf, 1855; Brøgger, 1883, 1886). Cloos (1939) finally recognized the feature as a graben or rift structure.

We now know that the Oslo Region is only a part of the Oslo rift which extends SSW from lake Mjøsa to the Sorgenfrei-Tornquist Zone (Fig. 9–1), giving a total length of about 400 km. The northern part, the Oslo Graben, is exposed on land, whereas the southern part, the Skagerrak Graben, is submerged. The term Oslo Region refers strictly to the province of Paleozoic rocks (about 200 km long and 35 to 65 km wide) within the Oslo Graben (Dons, 1978). The Oslo rift itself represents only a minor portion of the intricate system of rifts and grabens which formed as the result of repeated rifting in the Skagerrak - North Sea - Norwegian-Greenland Sea and adjacent areas from Carboniferous to Cretaceous time (Ziegler, 1978, 1982, 1988).

The Precambrian basement east and west of the Oslo Graben consists of amphibolite to granulite facies granitic gneisses, metagabbros, and metasedimentary rocks, granites and migmatites formed between 1800–1550 Ma and considerably reworked during the Sveconorwegian orogeny between 1200 and 900 Ma (e.g. Berthelsen, 1980; Skjernaa and Pedersen, 1982). It has been proposed that the Oslo Rift may be localized along an old (1750–1500 Ma) suture zone (Berthelsen, 1980). However, there are major disagreements about the accretion history of southwestern Scandinavia, no model is generally accepted (e.g. Berthelsen, 1980; Gorbatschev et al., 1987). The Skagerrak Graben and its flanks are buried under Mesozoic sedimentary rocks (Ro et al., 1990a, 1990b).

9.2. Significance

The Oslo rift is important because it presents a view into the roots of a very magmatic continental rift system. Oftedahl (1952) estimated the present level of exposure to be 1–3 km beneath the original surface in the northern, and about 3 km in the southern part of the Oslo Graben. Where erosion was greatest, volcanic rocks have been stripped away, leaving the underlying intrusive rocks and structures exposed. However, also some surface features (e.g. intra-rift sediments) are still exposed. In addition, the Oslo rift allows the complete evolutionary history of a rift to be studied. The large quantities of magmatic rocks also represent an important source of information about the chemical character of the upper mantle and lower crust under NW Europe in Permo-Carboniferous time. The Paleozoic province

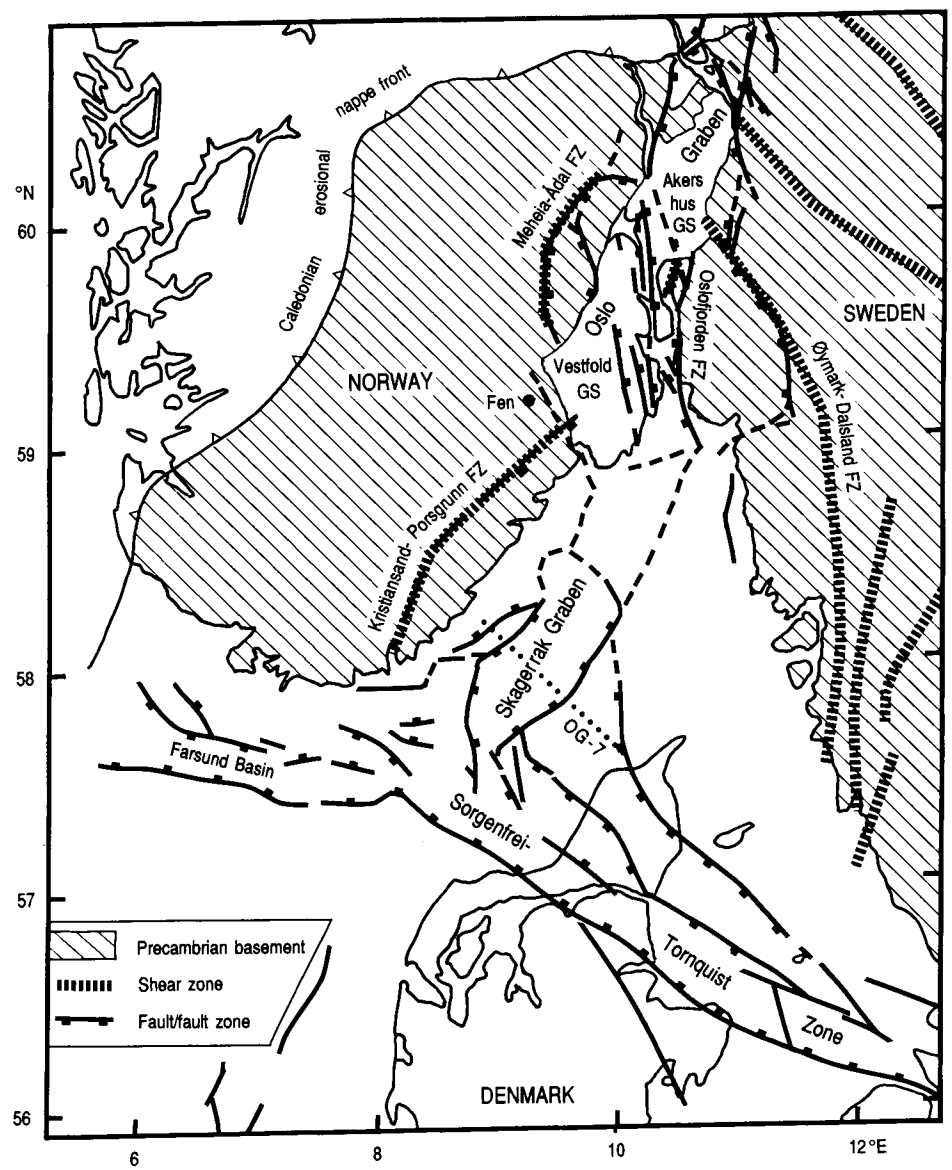

Fig. 9–1. Regional structural map of the Oslo Rift and adjacent areas based on maps by Ramberg et al. (1977), Falkum and Petersen (1980), Ro et al. (1990b), and Buer (1990). FZ: fracture zone, GS: graben segment. The location of the seismic profile OG–7 is shown as a dotted line.

made an important impact on geological thinking as early as the beginning of the 19th century (e.g. von Buch, 1810; Hausmann, 1811–1818; Lyell, 1835), and became a classical province for studies in magmatic and metamorphic petrology and mineralogy (e.g. Brøgger, 1890; Goldschmidt, 1911; Barth, 1945).

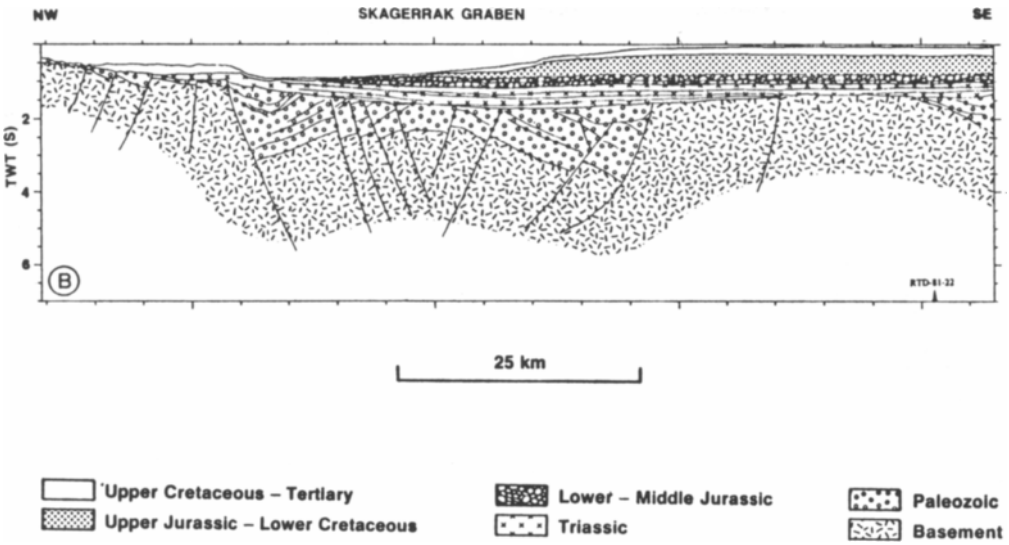

Fig. 9–2. Seismic line drawing of profile OG–7 across the Skagerrak Graben (the location is shown in Fig. 9–1). The figure is reproduced from Ro et al. (1990b) with the permission of the authors.

A considerable number and variety of metallic and non-metallic mineral deposits appear to be genetically related to the rifting processes. Most of these deposits are small, however, but the native silver deposits in the Kongsberg area were previously of considerable economic importance. Reviews of mineralization connected with the Oslo paleorift are given by Ihlen and Vokes (1978), Schønwandt and Petersen (1983), and Ihlen (1986).

9.3. Geological information

9.3.1. Introduction

The Oslo Region has been a classical site for geological, petrological and mineralogical studies for more than 100 years. The geological data set for the on-land part of the Oslo rift is therefore very good. Many of the data and large-scale geological maps of local areas, however, are not easily accessible as they are in Norwegian and are hidden away in old, obscure publications (including master's theses). During the period 1894–1975, a large number of papers on the Oslo Graben were published in the Norwegian Academy of Science series: 'Skr. Norske Vidensk.-Akad. i Oslo, I. Mat.-naturv. Kl.' - including "Studies on the igneous rock complex of the Oslo Region. I–XXV" (1943–1975). A compilation of papers on the Oslo Graben published before 1978 was presented by Dons and Larsen (1978). Revised geological maps of the Oslo Graben and adjacent areas are being published by the Norwegian Geological Survey (NGU). Tectonic and structural maps have been presented by Larsen (1975), Ramberg et al. (1977), Ramberg and Larsen (1978), and Buer (1990).

The Oslo rift consists of a series of graben segments. There appears to be some change in orientation of the boundary faults from north to south. The Oslo Graben comprises two asymmetric graben segments bounded by roughly N–S trending faults, the Vestfold Graben Segment (GS) to the south, and the Akershus GS to the north (Fig. 9–1). Age relations and compositional characteristics of the magmatism are well known (Neumann et al., 1992, and references therein).

The submerged part of the Oslo rift (the Skagerrak Graben) has recently been mapped by seismic reflection profiling (Husebye et al., 1988; Ro et al., 1990a, 1990b). These authors found the Skagerrak Graben to be defined by major, NE–SW trending faults; to the south it turns southeast into the Sorgenfrei-Tornquist Zone. A number of rotated blocks topped by Early Paleozoic sedimentary rocks have been observed within the graben (Fig. 9–2). Small half–grabens with probable Early Paleozoic sediments outside the Skagerrak Graben suggest that a relatively wide area was involved in the rifting process (e.g. Husebye et al., 1988; Ro et al., 1990a, 1990b).

9.3.2. Sedimentary record

The site of the Permian Oslo rift was essentially a cratonic basin during early Paleozoic time (Størmer, 1967; Ramberg, 1976; Bockelie, 1978) in which was deposited a succession of Cambro-Silurian marine sediments and late Silurian red beds (Fig. 9–3; Bjørlykke, 1974; Worsley et al., 1983). The thickness of this sequence increases from about 2500 m in the Oslo Graben to ≤4 km in the southern part of the Skagerrak Graben (Ro et al., 1990a, 1990b). The entire succession was folded during the Caledonide Orogeny and eroded to a peneplain.

Locally the Cambro-Silurian succession is unconformably overlain by Upper Carboniferous and Lower Permian sedimentary rocks (the Asker Group) which underlie Permian lavas (Ramberg and Spjeldnæs, 1976; Henningsmoen, 1978; Olaussen, 1981). Ooides, marine fossils, and strong micritization of fossils found in a conglomerate in the Asker group imply a short, shallow, marine transgression, probably of Upper Carboniferous age (Olaussen, 1981). Sedimentary rocks also occur as thin layers between lava flows (< 10 m), or as fillings in fossil depressions. Large volumes of fanglomerates are preserved on some islands along the Oslofjorden fault zone in the southeastern part of the Oslo Graben. These deposits, which are mainly made up by lava clasts, imply that lavas once existed on the eastern flank of the rift, and that large vertical displacement along the Oslofjorden fault zone took place during the volcanic stage (e.g. Brøgger, 1900; Størmer, 1935; Holtedahl, 1931; Larsen et al., 1978). Laminated siltstones, conglomerates and breccias dominated by magmatic clasts also occur inside some of the cauldrons (e.g. Larsen, 1978). However, all taken together, the volumes of sedimentary rocks deposited in the Oslo Graben during the rifting period are negligible compared to those of magmatic rocks.

Along the boundary faults in the Skagerrak graben, a younger sequence (≤1 km thick) rests unconformably on Lower Paleozoic sedimentary rocks (Fig. 9–2; Ro et al., 1990b). This sequence may represent erosion products derived from the rift shoulders or elevated parts of the rift floor, but the presence of lavas cannot be excluded (Ro et al, 1990b; Ro and Faleide, 1992).

9.3.3. Igneous activity

The magmatic history of the Oslo rift has recently been reviewed by Neumann et al. (1992). The oldest known magmatic activity related to the Oslo rifting event is a series of syenitic sills and doleritic dikes dated to 304–294 Ma (Fig. 9–4) (Sundvoll et al., 1992). The main magmatic period started at 300–290 Ma with basaltic shield volcanism; these basaltic lavas are generally referred to as B_1 (Fig. 9–3). The B_1 lavas range in composition from nephelinite to quartz tholeiite, and show a northward decrease in thickness and alkalinity. The B_1 sequence is overlain by numerous flows of rhomb porphyry (RP) lavas (intermediate composition) inter fingering with basalts. Trachytes and ignimbrites are common towards the top of the lava sequence. The lava sequence reaches a maximum thickness of about 3000 m (Fig. 9–3) (e.g. Oftedahl, 1952; Ramberg and Larsen, 1978). The estimated rate of RP extrusions decrease northwards from about one flow per 250,000 years in the southern, to about one flow per 800,000 years in the central part of the Oslo Graben (Sundvoll et al., 1990).

The extrusive period culminated with the formation of central volcanoes, many of which developed into calderas (Figs. 9–3, 9–4) (e.g. Oftedahl, 1953; Larsen, 1978; Ramberg and Larsen, 1978;

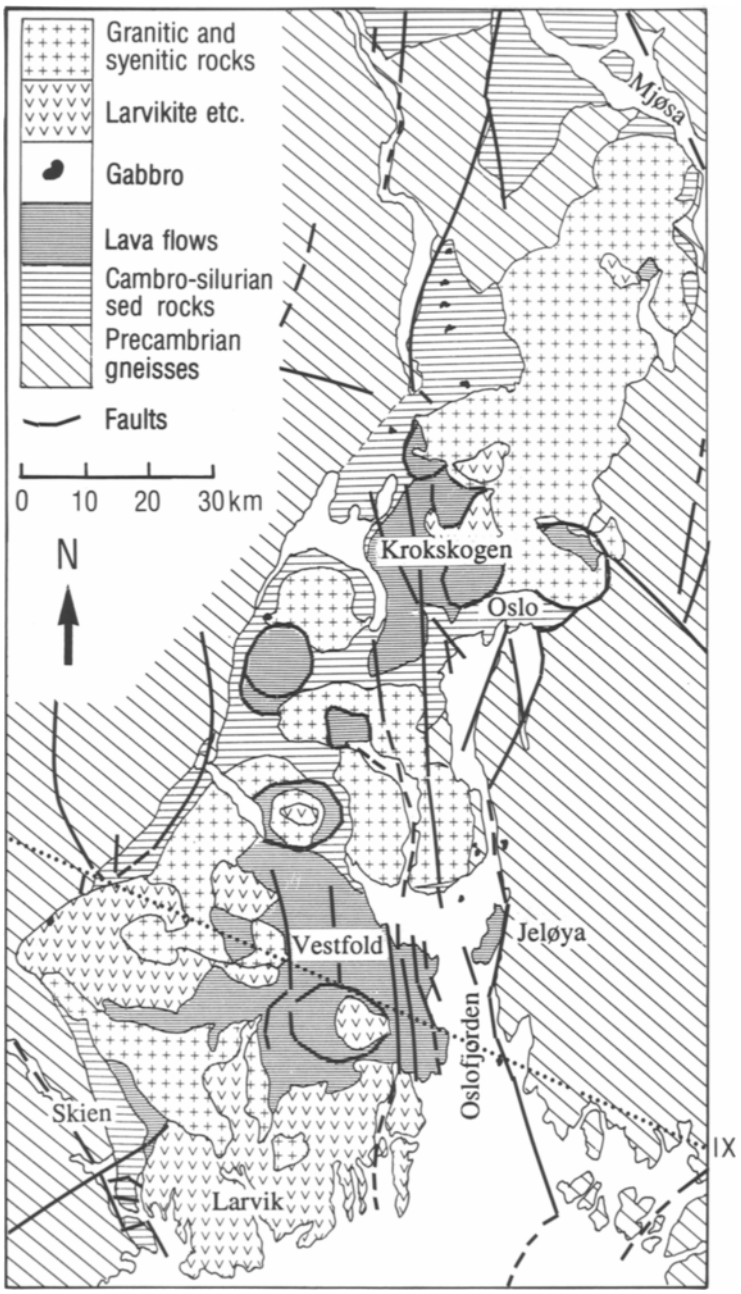

Fig. 9–3. Simplified geological map of the Oslo Graben, based on maps by Oftedahl (1960), Larsen (1975), Ramberg et al. (1977), and Buer (1990). The location of the transect (Fig. 9–11) is shown as a dotted line marked IX.

Schønwandt and Petersen, 1983). The youngest lavas are dated to 268 Ma in the Vestfold, and 243 Ma in the Akershus Graben Segment (Sundvoll et al., 1990).

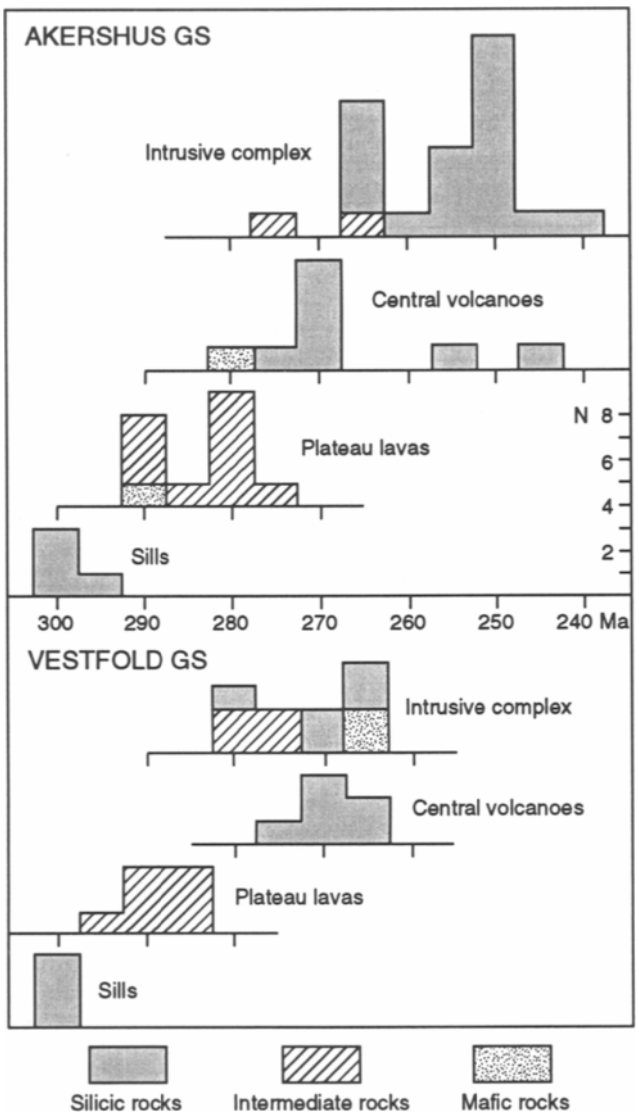

Fig. 9–4. Numbers of age determinations (Rb-Sr ages) plotted against age for the different magmatic stages in the Vestfold and Akershus Graben Segments (northern and southern part of the Oslo Graben, respectively). Sills: syenitic sills, including one dike in the Vestfold GS; plateau lavas: B_1 basalts and rhomb porphyry lavas; central volcanoes: lavas, central intrusions and ring-dikes related to central volcanoes and calderas; Intrusive complex: intrusive complexes. Dotted: basaltic lavas and gabbros; hatched: rhomb porphyry lavas and larvikites; black: syenites and granites. Based on data from Sundvoll and Larsen (1990), and Sundvoll et al. (1990, 1992). See text for further explanation.

The lava sequence was intruded by a number of large, semicircular, composite batholiths of intermediate to silicic composition which are now exposed along the floor of the Oslo Graben (Fig. 9–3) (e.g. Sæther, 1962; Nystuen, 1975; Ihlen and Martinsen, 1986). The intrusions are dated to 277–268 Ma in the southern, and 273–241 Ma in the northern part of the Oslo Graben (Fig. 9–4) (Rasmussen et al.,

1988; Sundvoll et al., 1990; Sundvoll and Larsen, 1990). A number of small layered gabbros were emplaced at the same time (about 266 Ma) (Neumann et al., 1985).

Rift-related magmatism extending far onto the flanks of the main graben system is demonstrated by large N–S trending RP dikes (about 280–270 Ma) exposed west and east of the Oslo Graben and along the coast east and west of the Skagerrak Graben (Sundvoll and Larsen, 1993), and NW–SE trending dikes (300–260 Ma) along the Sorgenfrei-Tornquist Zone in southernmost Sweden (Klingspor, 1976; Sundvoll and Larsen, 1993).

The only ultramafic xenoliths found so far in the Oslo rift are olivine clinopyroxenites hosted by a mildly alkaline basalt within the RP lava sequence at Krokskogen (Neumann et al., 1988a). The olivine clinopyroxenite xenoliths represent cumulates formed at a temperature of about 1100° C and a minimum pressure of 5.5–6 kbar (corresponding to a depth of ≥16–17 km). The clinopyroxene in these xenoliths fall on the Vestfold-Krokskogen mixing trend in Figure 9–5.

The volcanic rocks cover an area of about 1400 km^2, their volume is estimated to be about 300 km^3, of which about 25% are basaltic lavas, 60% intermediate rhomb porphyries and 14% trachytic and rhyolitic flows (Ramberg, 1976). The intermediate to silicic intrusive rocks cover about 5100 km^2 of the rift floor (Fig. 9–3) (Barth, 1945; Ramberg, 1976). Gravity modeling indicates depths from 3–5 to 10–12 km for the silicic bodies (Ramberg, 1976). The depths of the larvikite intrusions are uncertain as their densities are similar to those of the Precambrian country-rocks. Although large masses of both extrusive and intrusive rocks have been removed by erosion, it thus seems clear that felsic to silicic magmas dominated the surface and subsurface magmatism of the Oslo Graben.

The petrology and geochemistry of the magmatic rocks in the Oslo rift have been discussed in a number of recent papers (Neumann et al., 1986, 1988a, 1988b; Neumann 1988; Anthony et al., 1989; Neumann et al., 1990; Sundvoll et al., 1990, 1992; Neumann et al., 1992; Trønnes and Brandon, 1992; Neumann, 1993; Sundvoll and Larsen, 1993). The petrological and geochemical data imply extensive fractionation processes which must have left considerable volumes of cumulate rocks at depth in the crust under the Oslo rift. The densities and seismic velocities (V_P) of these cumulate rocks are estimated to be 2.8–3.5 g/cm^3 and 7.5–8.0 km/s, respectively. Estimates based on petrological modeling, and the observed volumes of different rock types at the surface, suggest that cumulus minerals alone account for a net transfer of at least 2×10^{17} kg of magmatic material from the mantle into the deep crust. Extrusion temperatures of 1270–1340° C have been estimated from whole rock major element compositions in basaltic lavas. This implies that the Oslo rift magmatism was not associated with a large temperature anomaly in the underlying upper mantle, but rather caused by partial melting in a $CO_2 \pm H_2O$–enriched mantle source region(s).

The isotopic compositions of the exposed magmatic rocks are interpreted as the combined result of interaction between two lithospheric mantle sources and contamination at different depths in the crust (e.g. Neumann et al., 1988b; Anthony et al., 1989; Neumann et al., 1990). The earliest, highly alkaline basalts in the Skien area appear to originate in a nearly undepleted mantle reservoir with initial isotopic ratios of ε_{Nd}: about +1, and ε_{Sr}: −10 to −15 (UM in Fig. 9–5). With time, this nearly undepleted reservoir appears to have been progressively overwhelmed by melts derived from a mildly depleted source (MM in Fig. 9–5), giving rise to the mixing trend defined by the Skien basalts (horizontally hatched in Fig. 9–5). The UM reservoir first appeared to be restricted to the southern part of the Oslo Graben, and explained as the possible result of local mantle metasomatism associated with the Fen carbonatite complex (Anthony et al., 1989). There are indications, however, that this source is also present under southernmost Sweden, in which case an association with the Fen complex seems highly unlikely (Sundvoll and Larsen, 1993).

With ε_{Nd} and ε_{Sr} of about (+4, −10), the MM source is similar to the PREMA (prevalent mantle) source proposed by Wörner et al. (1986) to represent an end-member for continental basalts in general. The MM source falls on a ε_{Nd}-time trend for southern Norway, indicating that it must represent a source which has existed in the lower lithosphere under southwest-

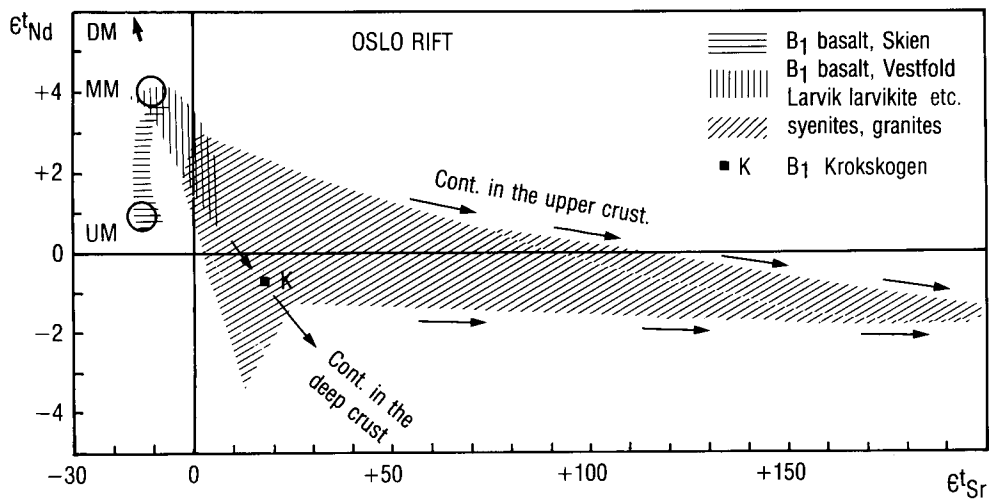

Fig. 9–5. Initial $^{143}Nd/^{144}Nd$ and $^{87}Sr/^{86}Sr$ relations among Permo-Carboniferous magmatic rocks in the Oslo Graben normalized to estimated isotopic ratios for an undepleted, primordial mantle of the same age (data from Neumann et al., 1988, 1990b, 1992; Anthony et al., 1989). The vertically hatched area includes rhomb porphyry lavas and clinopyroxenes in cumulate xenoliths from the Krokskogen area. DM = depleted MORB source; MM = mildly depleted mantle proposed as lithospheric mantle source of mildly alkaline to tholeiitic basalts and intermediate rocks (Neumann et al., 1988, 1990b); UM = very mildly depleted mantle proposed as lithospheric mantle source for the most alkaline lavas in the Skien B_1 sequence (Anthony et al., 1989). See text for further information.

ern Scandinavia for several hundred million years (Mearns, 1986; Mearns et al., 1986). The majority of the mafic to intermediate rocks in the Oslo rift are derived from the MM source, but have suffered different degrees of contamination during residence in lower crustal magma chambers (vertically hatched trend in Fig. 9–5) (Neumann et al., 1988b, 1990, 1992). Trace element and isotopic compositions of the syenitic and granitic rocks indicate that the contribution of old crustal components is quite low (Neumann et al., 1988b; Rasmussen, 1988; Sundvoll et al., 1990; Trønnes and Brandon, 1992). This implies formation either by extensive crystal fractionation of mantle-derived melts, or partial melting of Permian gabbros. The high initial Sr isotopic ratios exhibited by some granitic and syenitic rocks (Fig. 9–5) are typical of contamination in the upper crust (Neumann et al., 1988b; Trønnes and Brandon, 1992).

9.4 Geophysical surveys and results

9.4.1. Seismic crustal studies (reflection, refraction, teleseismic)

Prior to 1980, the land areas of southern Scandinavia were only sparsely covered by modern, high-resolution, seismic refraction and reflection profiles. Since about 1975, large quantities of multichannel seismic reflection data have been collected in the North Sea and Skagerrak by oil companies. Marine profiling technology has recently been used by several national and international scientific working groups for basic tectonic studies of basement, deep crustal, and uppermost mantle structures in the North Sea and Skagerrak (EUGENO-S Working Group 1988; Husebye et al. 1988; Ro et al. 1990a, 1990b). Seismic data for the North Sea rifts are treated extensively in Blundell and Gibbs (1990) and will not be further considered here. Figure 9–6 and

Table 9–1 give details of the seismic profiles and the permanent seismological observatories in southern Scandinavia which have provided various types of seismic data for construction of Moho depths (Fig. 9–7) and lithospheric thickness maps (Calcagnile, 1982; Kinck et al., 1991).

Seismic refraction/wide-angle-reflection data have been used to model variations in crustal thickness and structure in the Oslo rift and adjacent parts of the Precambrian shield. Principal profiles of Figure 9–6 and Table 9–1 relevant to rift structure are: B, D, E3, E4, I, K, L, M, N, and O (Sellevoll and Warrick, 1971; Kanestrøm and Haugland, 1971; Kanestrøm, 1971, 1973, 1977; Tryti and Sellevoll, 1977; Bungum et al., 1980; Cassell et al., 1983; Ro et al., 1990a, 1990b; Kinck et al., 1991). The large-aperture NORSAR seismic array is centered near Lake Mjøsa at the northern end of the Akershus GS of the Oslo rift (Bungum et al., 1971) [the center point of the original, 100-km-diameter, 22-subarray system is designed as NOA in Fig. 9–6]. Because land-based and marine-based surveys employed somewhat different observational and interpretational techniques, and—in this region—were performed essentially in two separated time periods between which seismic profiling technology evolved dramatically, somewhat different aspects of crustal structure tend to be emphasized beneath the land and the marine areas. In evaluating generalizations for the combined Oslo-Skagerrak Graben system, differences and limitations in resolution, types and depths of emphasized structures, etc., between the various data sets should be kept in mind (see also discussion in Chapter 3B and Table 3B–1, Table 3B–2, this book).

The refraction/wide-angle-reflection data of greatest relevance to crustal structure in the center of the Oslo Graben Segment are the profiles of Tryti and Sellevoll (1977), and the area studies of Gundem (1984) who used NORSAR array recordings to model ray paths from selected quarry and road construction blasting in the Oslo Region. Three distinct layers in the crust were well observed: (1) the upper crust from the surface to 15 km depth, in which the P-wave velocity increases from 5.6 to 6.34 km/s; (2) an intermediate layer from 15 km (interpreted to be the 'Conrad' discontinuity) to about 20 km depth, in which the velocity is 6.6 km/s, a value characteristic of 'normal' continental crust; and (3) a 12 km thick high-velocity (7.1 km/s) lower crustal layer from 20 km depth (labeled 'Horizon-I' by Tryti and Sellevoll [1977]) to the Moho at about 32 km. The sub-Moho velocity (P_n-velocity) is 8.07 km/s, and the Moho dips slightly (ca. 1° to 4 °) to the north, reaching a depth of 35 km northeast of Oslo. Both the Conrad and Horizon-I are relatively flat and horizontal. Amplitude analyses indicate that the high-velocity lowermost crustal layer terminates within 10 to 20 km of the outside limits of the Oslo Region, except to the east of the Oslofjorden fault zone where it extends possibly 50 km to the east beneath the Precambrian rocks. Wide-angle reflections from the top of Horizon-I show frequency-dependent interference-like effects, suggesting fine-scale high/low velocity lamination along the upper surface of the lowermost crustal layer. The relatively high velocities and close association with the surface volcanics strongly supports the interpretation that the lowermost crustal layer is a magmatically underplated layer and/or zone of magmatic cumulates and residues ('fossil rift cushion') which developed during the highly magmatic phase of Oslo rift evolution. The seismic interpretation is strongly supported by gravity modeling (Section 9.4.2) and petrological, geochemical, and isotopic evidence (Neumann, 1980; Neumann et al., 1986, 1990; Section 9.5.3).

Gundem (1984) analyzed archival NORSAR array recordings of 12 quarry and road construction blasts in the Oslo area. Gundem's 'profile lines' (not shown on Fig. 9–6) were essentially large-offset (~ 80–100 km), un-reversed, mainly S–to–N profile segments principally traversing the Akershus GS and the neighboring Precambrian flank area immediately to the east. Thus, observed phases were mainly confined to post-critical wide-angle reflections from the Moho (PmP), the Conrad, and sometimes the Horizon-I discontinuities. Furthermore, clustering of the widely offset sources and the NORSAR sub-arrays resulted in reflection turning points in which the crustal reflectors were only illuminated in 'spot-like' areas of ~ 5–10 km diameter intermittently along several general profile azimuths. Nevertheless, amplitudes were well calibrated and some useful infor-

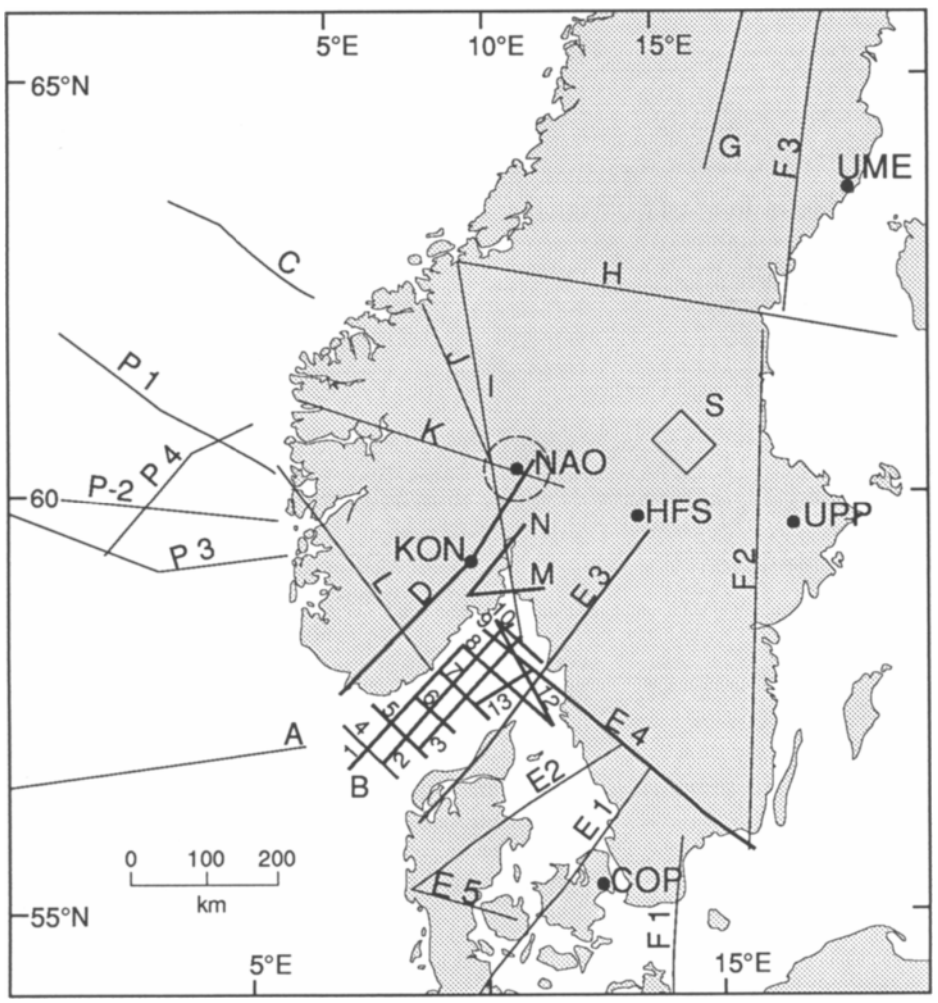

Fig. 9–6. Map showing seismic profiles and seismological observatories (stars) in southern Scandinavia which have been used as sources for crustal structures and lithospheric thickness estimates. Details of profiles and references are given in Table 9–1. Seismological observatories: COP = Copenhagen, HFS = Hagfors, KON = Kongsberg, NOA = NORSAR array center and NORESS, UME = Umeå, UPP = Uppsala. Modified from Kinck et al. (1990).

mation on lateral variations in velocity contrasts of major crustal discontinuities and velocity-depth gradients were derived. Sharp velocity contrasts at the Moho were observed throughout the study area: 6.7/6.8 km/s to 8.1/8.2 km/s in the eastern Precambrian flank, and ~ 7.0 to 7.9/8.1 km/s in the graben. The Conrad discontinuity near 15 km depth is fairly well observed in the Precambrian flank (eastern velocity-depth model of Fig. 9–10), but both the Conrad and the intermediate (Horizon-I) discontinuity are somewhat indistinct and appear considerably more variable in both depth and in sharpness within the graben segment and the graben-flank border regions.

TABLE 9-1

Seismic Reflection and Refraction Profiles in Southern Scandinavia, shown in Figure 9-6.

Map symbol	Name/Area	Type	References
A	Central Graben (North Sea)	Refraction	Barton and Wood, 1984
B1-9,12,13	Skagerrak: RV Mobil Search	Deep reflection (16 s twt surveys)	Husebye et al., 1988; Kinck et al., 1990; Larsson et al.,1990; Lie et al., 1990; Lie and Husebye, 1993
B1-9,12,13	Skagerrak Graben (Oil companies)	Multichannel marine reflection	Ro et al., 1990a, 1990b
C	Møre margin	Expanding Spread	Olafsson, 1988
D	CANOBE/S. Norway	Refraction	Cassell et al., 1983
E1-E5	EUGENO/S. Denmark, Kattegat, SW Sweden	Refraction	EUGENO-S Working Group, 1988; Lund et al., 1987
F1-F3	FENNOLORA,	Refraction	Clowes et al., 1987
F1-F3	FENNOLORA (southern profiles)	Refraction	Guggisberg and Berthelsen, 1987
G	Swedish Lappland	Refraction	Båth, 1984
H	Trondheim-Sundsvall	Refraction	Vogel and Lund, 1971
I*	Oslo–Trondheim	Refraction	Kanestrøm, 1971
J	Otta–Ørsund	Refraction	Mykkeltveit, 1980
K*	Flora–Åsnes	Refraction	Sellevoll & Warrik, 1971
L*	Fedje –Grimstad	Refraction	Sellevoll & Warrik, 1971
M-N	Oslo Rift	Refraction	Tryti and Sellevoll, 1977
O	Larvik - Lysekil	Refraction	Egilson & Husebye, 1991
P1-P4	North Sea Deep Profiles NSDP-84	Reflection	Klemperer, 1988
S	Siljan impact structure	Reflection	Lund et al., 1988; Juhlin & Pedersen, 1987; Dahl-Jensen et al., 1987

* These pre-1971 profiles were reinterpreted by Kværna (1984) using synthetic seismogram modeling techniques.

Early seismic refraction (Weigel et al., 1970) and reflection (Aric, 1968) surveys of the deeper parts of the crust in the Skagerrak in the 1960's were able only to constrain the total crustal thickness between 29 and 32 km and to suggest the presence of intracrustal discontinuities at depths between 12 and 20 km. Concurrent refraction and near-vertical reflection data (EUGENO-S Working Group, 1988) provide crustal structure information mainly for the Precambrian basement in the flank area east of the Skagerrak Graben (Fig. 9–1). The Moho depth increases from about 32 km beneath the mouth of the Oslofjorden to a maximum of 47 km near the intersection of profiles E4 and E2 (Figs. 9–6, 9–7). The thickness of the upper crust (depth to the Conrad velocity discontinuity) increases from 11–12 km in the northern Skagerrak to about 20 km in the southwestern Sweden (EUGENO-S Working Group,

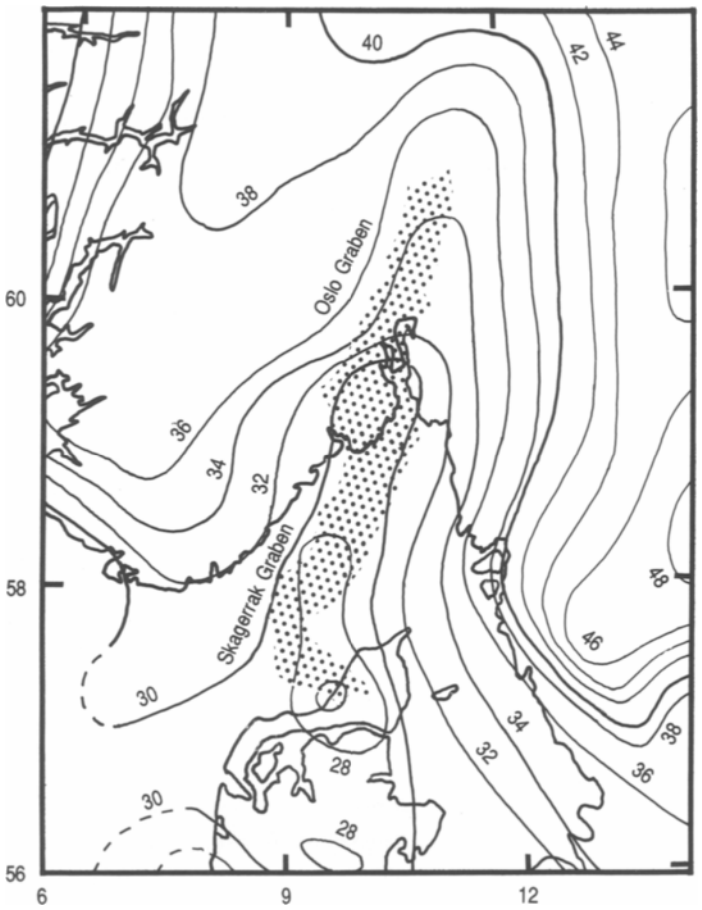

Fig. 9–7. Moho depth below sea level, contour interval 2 km. Dotted area: the general outline of the Oslo Rift. Modified from Kinck et al. (1990).

1988). Closely-spaced (300 m) marine airgun shots along the northwestern end of profile E4 were recorded by land-based recorders in Sweden (Lund et al., 1987). These records yielded high-resolution profiles which could be jointly analyzed and compared by both conventional refraction and reflection stacking techniques. The lower crust beneath the shield is rather reflective but the responsible lower crustal reflectors appear to be less than about 10 km in lateral extent; the upper crust is comparatively transparent. The character of the Moho reflections indicates a narrow but finely layered crust-mantle transition zone (Lund et al., 1987).

Large amounts of marine multichannel seismic reflection data have been collected in the North Sea and Skagerrak by oil companies, including 1739 km of special deep reflection seismic profiles mainly in Skagerrak (B1 through B13, Fig. 9–6) (Husebye et al., 1988; Ro et al., 1990a, 1990b; Larsson and Husebye, 1990; Kinck et al., 1991; Lie and Husebye, 1993). These data show that the Skagerrak Graben is bounded by two northeast trending, opposite polarity faults which appear to become listric with depth. The most prominent structural feature of the Paleozoic sediments and Precambrian basement surface in the center of the Skagerrak Graben is an ap-

parent domal feature more or less symmetrical with respect to the graben axis and with the thickest sediments deposited essentially in two troughs overlying the hanging walls of the flanking normal faults (Ro et al., 1990a, 1990b). It has not yet been determined whether the doming of the basement is mainly a structural accommodation zone between two opposing half-grabens (Rosendahl, 1987) or may be due to a deep magmatic intrusion beneath the graben axis. The Mobil Search reflection data give very good resolution in the deep crust. These data show a general high reflectivity in the lower part of the crust under southeast Norway; the Moho is not a uniformly sharp reflector but usually can be identified by a marked peak in the density of reflective lamina as a function of depth (Fig. 9–8) (Larsson and Husebye, 1990; Kinck et al., 1991). However, under the Skagerrak Graben the reflectivity is weak, this makes it difficult to determine the depth to Moho. The Conrad cannot be observed as a first-order discontinuity (Larsson and Husebye, 1990; Kinck et al., 1991).

9.4.2. Upper mantle structure

In addition to providing fixed recording points for some regional crustal profiling studies (e.g. Cassell et al., 1983; Gundem, 1984; Vogfjord and Langston, 1990), the NORSAR and NORESS arrays with their unique array-processing capabilities have been used to estimate the large-scale structure and physical properties of the crust and upper mantle beneath the arrays. Spectral-ratio analysis of long-period P-waves (see Chapter 3.4) from earthquakes at teleseismic distances was used by Berteussen (1975, 1977) to derive a Moho depth of 32–34 km beneath the northern rift which increases to ~38 km beneath the shield to the west. Moho depth determinations by the spectral-ratio method are fairly reliable, but Berteussen (1977) found that the technique cannot be used with confidence to delineate other finer-scale structures of the crust and upper mantle. The teleseismic spectral-ratio method has also been used with data from the other Fennoscandian seismic observatories to estimate Moho depths beneath the entire shield and the agreement between spectral-ratio and refraction results is generally good (Bungum et al., 1980). Spectral ratio results of 34 km for KON, 45 km for HFS and 31 km for COP were included in the data-base from which the Moho contours on Figure 9–7 are derived.

Large-scale seismic velocity anomalies in the upper mantle to ~600 km depths beneath the Baltic Shield have been studied by three-dimensional, 'tomographic' modeling/inversion techniques (See Chapter 3.4 and Aki et al., 1977) using both teleseismic P-wave delays (Husebye and Hovland, 1982; Husebye et al., 1986), and sub-Moho P_n- and S_n-wave travel-times (Bannister et al., 1991) observed at the Fennoscandian seismic observatories. For Baltic Shield teleseismic studies, resolution constraints of the technique require comparatively large 'computational cell' dimensions which are of the same order as the rift structure itself, and, therefore, finer details of lateral velocity variations in the subcrustal lithosphere and the asthenosphere beneath the entire Oslo-Skagerrak rift system are poorly resolved. Thus, on this scale, the upper mantle beneath the Permian-age Oslo-Skagerrak 'thermal event' does not now appear to be uniquely associated with significant velocity-anomalies down to 600 km (Husebye et al., 1986). A separate technique of analysis of long-period Rayleigh-wave dispersion at the Fennoscandian seismic observatories gives good results for the depth of the lithosphere-asthenosphere transition (~110 km) and for shear-wave velocities in both the mantle 'lid' and the asthenosphere (Calcagnile, 1982). These Rayleigh dispersion results are consistent with those from other shields in that shear-velocities in the lower lithosphere-asthenospheric depth range are comparatively high, indicating relatively low upper mantle temperatures.

The 1987 Mobil Search multichannel deep seismic survey in the Skagerrak employed special long recording windows allowing processing of reflection seismic 'events' with up to 40 s two-way-time (TWT) along one profile. Occasional apparent sub-Moho reflective regions were observed and several of these show characteristics which suggest they are true mantle reflections rather than spurious signals such as scattering or diffraction associated with large faults in the overlying crust, 'ghost' multiples from shallower layered structures, etc. (Lie et al., 1990). The best candidates for mantle reflections are sev-

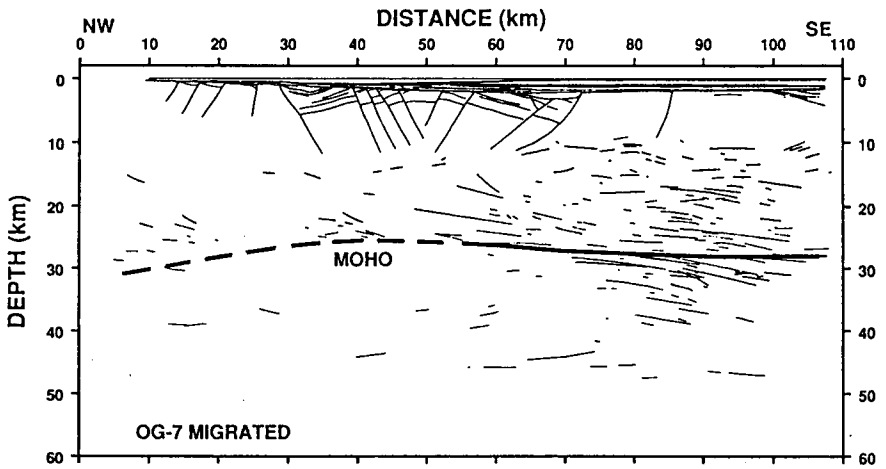

Fig. 9–8. Depth-migrated line drawing of profile OG–7 (Fig. 9–1) reproduced from Ro and Faleide (1992) with the permission of the authors. Reflectivity is weaker in the upper then in the lower crust, some reflectors are also apparent in the uppermost part of the mantle. Moho is defined by a peak in reflectivity.

eral continuous and nearly horizontal reflections between ca. 22 and ca. 29 s TWT (equivalent to ~ 80–110 km in this region—the Moho is at ~ 30 km) which are observed in the southwestern portion of profile OG–13 (Fig. 9–8). The individual reflectors have lengths in the 5–20 km range and are vertically separated by about 10 km. Rayleigh-wave dispersion analysis indicates the base of the lithosphere in this region of Scandinavia to be at 110–120 km (Calcagnile, 1982), about the same as the deepest reflectors observed on B–13. Lie et al. (1990) suggest that both these deep lithospheric reflections and the high reflectivity regions commonly observed in the lower crust may originate in the ductile rheological environments characteristic of both the deep crust and the lower lithosphere.

Where deep seismic reflection data are available, the lower crust is highly reflective and the upper crust is relatively transparent. The Permo-Carboniferous Oslo-Skagerrak rift system approximately bisects the Gothian-Grenvillian age (1700–950 Ma) Sveconorwegian province (Berthelsen, 1987) which underwent strong reworking during the Sveconorwegian orogeny (1200–950 Ma). From plate tectonic interpretations, Berthelsen (1987) and co-workers (EUGENO-S Working Group, 1988) have suggested that the deep Precambrian crustal areas eastward and westward of the rift system constitute two or more distinct structural age provinces. Structural age provinces are differentiated on the basis of their emplacement ages and styles of folding, faulting and metamorphism. However, while a few listric thrusts can be traced through the entire crust (EUGENO-S Working Group, 1988), presently available seismic data by themselves do not appear adequate to definitively delineate suspected deep lateral boundaries of these structural/evolutionary crustal subdivisions.

9.4.3. Gravity

Analyses of Bouguer gravity anomalies have until recently provided the principal geophysical constraints on the deep lithospheric structure of the Oslo paleorift system. Although gravity models are not unique and may vary considerably in fine detail, they can provide a useful series of solutions to aid tectonic interpretation. Data from 5300 gravity stations covering 8500 km^2 of the Oslo Graben and neighboring districts were collected and compiled by Smithson (1961, 1963), Ramberg and Smithson (1971) and Ramberg (1972a, 1972b, 1976). Fifteen

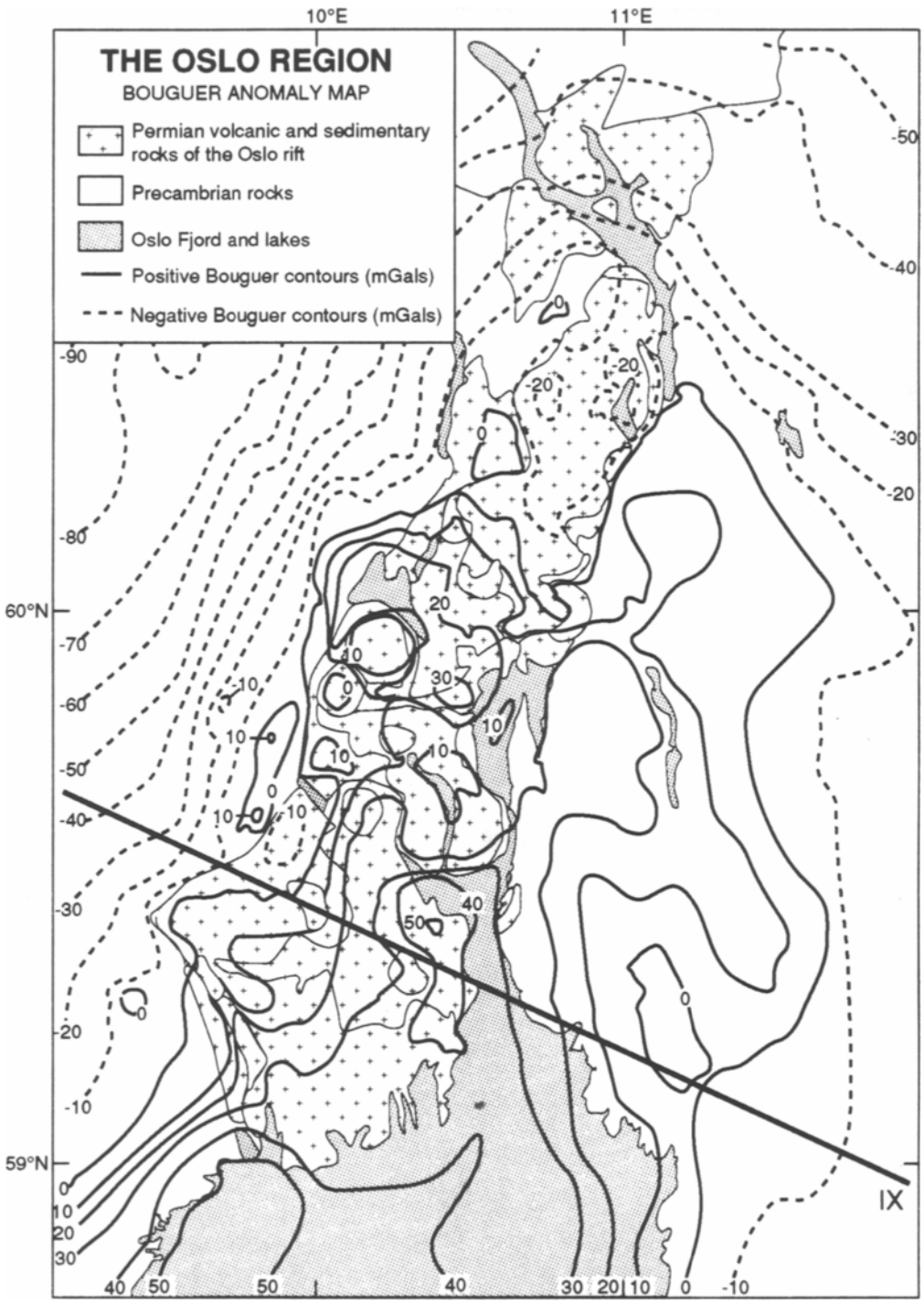

Fig. 9–9. Simplified Bouguer anomaly map for southern Norway after Ramberg (1976). The gravity profiles consistently define a wide (120 km), large positive gravity anomaly that generally follows the Oslo graben but extends about 50 km eastwards of the main graben.

gravity profiles perpendicular to the arbitrary "Oslo rift axis" are shown on the Southern Norway Bouguer Anomaly map of Ramberg (1976) (simplified here as Fig. 9–9). The gravity profiles consistently define a wide (120 km), distinct positive anomaly that generally follows the Oslo Graben but extends about 50 km eastward into Precambrian terrain. The positive gravity anomaly continues in a ESE direction along the Sorgenfrei-Tornquist Zone (Ro and Faleide, 1992).

Ramberg (1972a, 1976) interpreted the positive gravity anomaly to represent the combined effect of a crustal thinning of about 6–10 km along the graben axis and a large body of mafic to ultramafic rocks ($>1.3\times10^{16}$ kg) in the deep to intermediate crust under the graben. Besides the mafic rocks exposed at the surface, the gravity data along our model profile (profile IX of Figs. 9–3 and 9–9) suggest at least one small body of mafic rocks (2.95 Mg/m^3) in the upper crust under the Oslo Graben. A more detailed interpretation of other localized gravity anomalies (intrusives, cauldron subsidence, etc.) within the Oslo igneous province was presented by Ramberg (1976).

The gravity data were reinterpreted by Wessel and Husebye (1987) using a "2 1/2–D" type inversion technique with a calculational crustal model consisting of a large number of rectangular prisms. Wessel and Husebye concluded that the gravity anomaly over the Oslo rift is caused by a body concentrated in the intermediate crust (10–20 km depth), with a lateral density contrast of about +0.06 Mg/m^3 with respect to the country rocks. The anomalous body extends eastwards well outside the graben area, and its size increases southwards.

A shortcoming of the Wessel and Husebye (1987) gravity model is that it is based on one particular interpretation of the residual of the regional gravity field. Their conclusions—particularly in regards to derived depth of density anomalies—therefore may be biased by their *a priori* assumption of the regional gravity anomaly because the regional anomaly is somewhat dependent on the local crustal structure. We therefore present here a revised model for the general large-scale mass distribution that seems more consistent with all available geological, seismic, gravity, petrological, and aeromagnetic data (Olsen et al., 1987; 1989). The features of the gravity field treated by the present calculations are (1) the broad positive anomaly across the Oslo Graben and adjacent areas, (2) the >+30 mGal high along the west side of the Oslofjord, (3) the gravity minimum over the Precambrian Østfold/Bohus granite east of the Oslofjord, and (4) the Telemark and Hardanger highs in central and western Norway.

The gravity model (Fig. 9–10) is calculated with a 2 1/2–dimensional, forward-modeling program. A mean density of 2.75 Mg/m^3 is used for the upper crust (above 15-km-depths) throughout. This agrees well with rock density measurements of Precambrian gneisses and granodiorites of southern Norway (Ramberg, 1976). Outside the graben area a lower crustal layer of density 2.94 is chosen, which is consistent with densities of granulite facies metamorphic rocks of the lower crust (Ramberg and Smithson, 1971). A two-layer crust is assumed here for computational convenience only; some NORSAR seismic data suggest a more complex layering. A density of 3.30 Mg/m^3 is used for the mantle. These assumed lower-crustal and mantle density contrasts, together with the seismically estimated Moho depths (Kinck et al., 1991), account for nearly all the long-wavelength gravity variations which constitute the regional anomaly in southern Norway. Samples of the Østfold/Bohus granite measure 2.63 Mg/m^3, significantly lower than surrounding Precambrian gneiss (Lind, 1967). Measurements of metamorphic rocks of the Jotun, Hardanger and Telemark thrust nappes of the Scandinavian Caledonides average 2.87 Mg/m^3.

The principal feature of our gravity interpretation (shown for Profile IX in Fig. 9–10) is a 90-km-wide massive body which we place at the base of the crust—consistent with the 12-km-thick high-velocity layer observed by seismic profiling in the lowermost crust (Tryti and Sellevoll, 1977) and petrological information (Neumann, 1980, 1988; Neumann et al., 1986, 1990). While we agree with the +0.06 Mg/m^3 density contrast of Wessel and Husebye (1987), we believe the interpretation shown here (i.e. location of the massive body in the *lower* rather than in the *middle* crust) to be more consistent with other data chiefly for three reasons: (1) The Falkum-Orud seismic profile of Tryti and Sellevoll (1977) shows

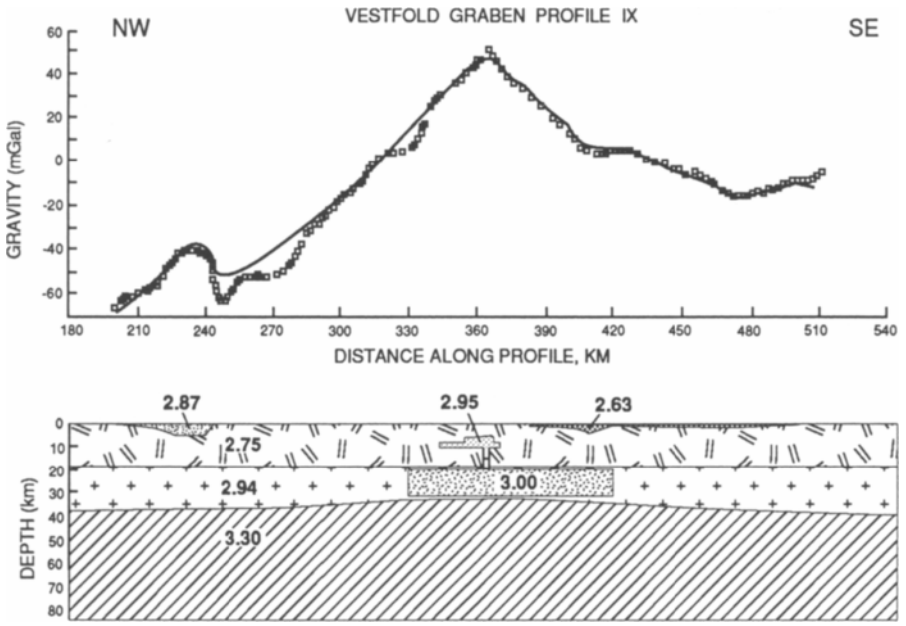

Fig. 9–10. Gravity model along Profile IX across Vestfold Graben calculated with a 2 1/2- dimensional, forward-modeling program. A mean density of 2.75 Mg/m^3 is used for the upper crust (above 15-km-depths) throughout, consistent with density measurements of Precambrian gneisses and granodiorites of southern Norway (Ramberg, 1976). Outside the graben area a lower crustal layer of density 2.94 is assumed, which is consistent with densities of granulite facies metamorphic rocks (Ramberg and Smithson, 1971). A two-layer crust is assumed here for computational convenience only. A density of 3.30 Mg/m^3 is used for the mantle. See text for further discussion.

a high-velocity layer (7.1 km/s) in the lowermost crust beneath the graben and to the east; the regions of high seismic velocity and high density are thus well correlated. (2) The petrogenetic models for the Oslo rift favor crystallization in magma-chambers in the lower crust (P > 5.5 kbars). (3) Combined seismic and gravity data from other continental paleorifts also show dense, high-velocity 'pillows' at the base of the crust.

The shallower dense mass is a basaltic intrusion which we assume to be at about 10 km-depth. Lastly, the Precambrian Østfold/Bohus granite is interpreted as a floored batholith, consistent with field geological evidence.

9.4.4. Magnetic anomalies

Aeromagnetic contour quadrangle maps at scales of 1: 50,000 and 1:250,000 are available for most of southern Norway from the Geological Survey of Norway (NGU). Since about 1985, digitally processed magnetic-anomaly maps in color and shaded relief formats also have been published. The magnetic anomaly map of the Oslo rift is characterized by generally lower intensities and short spatial wavelength (< 5 km) variations in the Precambrian areas, and by much higher intensities and somewhat smoother spatial variations essentially coincident with the magmatic outcrops of the Akershus and the Vestfold Graben Segments. Thus, the Oslo rift igneous rocks with their associated strong magnetic properties dominate the magnetic anomaly maps just as their high densities do for the Bouguer gravity data.

Marine magnetic surveys in the Skagerrak (Sellevoll and Aalstad, 1971; Åm, 1973) have shown intermittent areas of high magnetic intensity, particularly south of Kristiansand and offshore south of the Vestfold GS, but the possible association of these with suspected magmatic intrusions in the crystalline crust has not been confirmed by other geophysical or geological data.

9.4.5. Seismicity

Just as for most other types of geophysical data (heat flow, deep electrical conductivity, and contemporary stress fields), seismicity provides information chiefly on *contemporary* crustal conditions and thus may contribute only indirectly to understanding extinct processes in paleorifts. However, the structural remnants of earlier tectonic and magmatic episodes are preserved within present lithospheric structures and these older structures may still significantly influence zones of relative weakness (faults, fracture zones) and/or localized regions of stress concentration. Thus, earthquake distribution patterns sometimes provide useful clues to supplement interpretation of deeply buried lithospheric structures.

The contemporary seismicity of Scandinavia is typical of intraplate regions, that is, widely scattered and infrequent, intermediate magnitude earthquakes. A synthesis of instrumentally (1955–1987) and macroscopically (1880–1963) located earthquakes in Scandinavia covering the past century (Bungum, 1989) shows that earthquakes are most frequent along the west coast of Norway. The analysis by Bungum (1989) tends to confirm a modest seismicity concentration along the Oslo rift (and perhaps extending into southern Sweden?) that has been suspected for several years (Husebye et al., 1978; Bungum and Fyen, 1979; Bungum et al., 1986). The sparse hypocenter and focal mechanism data for small earthquakes in the Oslo rift seismicity trend show no correlation with surface faults or geological lineaments (Bungum and Fyen, 1979) suggesting little relation to modern plate tectonic or glacial rebound forces. Alternatively, some studies (Sykes, 1978; Johnston, 1989; Johnston and Kanter, 1990) of historic large destructive intraplate earthquakes in now-stable continental interior regions (including the Oslo rift and New Madrid rift) suggest that the majority of these large shocks may be spatially associated with deep mafic and ultramafic plutons developed during paleorifting events. However, stress-field modeling studies attempting to account for such apparent earthquake-pluton-paleorift associations have been unconvincing and so the hypothesis remains unproven.

9.4.6. Heat flow

Heat flow measurements from lakes and drill holes in Norway give an average of 42.8±8.8 mWm^{-2} (1.02±0.21 HFU), implying a temperature of about 250–350° C at the Mohorovicic discontinuity. A small positive heat flow anomaly (< 1.26 HFU) appears to exist in the Oslo Region (Hänel et al., 1974, 1979; Grønlie et al., 1977). These authors interpret this anomaly to reflect the presence of rocks with high thermal heat conductivity and/or high heat production (enhanced concentrations of U, Th and K). Of course, contemporary heat flow data do not give direct information about Permian rifting processes, but may nevertheless provide some useful clues and constraints to help interpret the deep structural modifications of the crust which have resulted from extinct rifting and associated magmatic events.

9.4.7. Electrical properties

Magnetotelluric studies to determine the electrical conductivity structure and possible 'fossil' anomalies of the *crust* specific to the region of the Oslo rift are not yet available. To date, electromagnetic surveys in Scandinavia mainly have been low-frequency studies of the Precambrian interior of the Baltic Shield which emphasize large-scale electrical properties of the lithosphere-asthenosphere transition (Jones, 1982; Hjelt, 1984).

9.5. Structure and interpretation

9.5.1. Introduction

A large number of structural features in the Oslo Graben and adjacent areas have been identified and mapped by a combination of satellite imagery, aerial photographs and surface mapping (Ramberg et al.,

1977; Ramberg and Larsen, 1978; Buer, 1990). In the Skagerrak Graben, seismic reflection profiles have been used to deduce the main structural features.

The Precambrian basement east and west of the Oslo rift is dominated by a NW–SE and NE–SW trending pre-rift fracture pattern, N–S trending features are also present but less frequent (Ramberg et al., 1977; Ramberg and Larsen, 1978). The same directions are also found in a number of major shear zones (Fig. 9–1) (e.g. Skjernaa, 1972; Starmer, 1972, 1985; Falkum and Petersen, 1980; Hageskov, 1981). Many of these shear zones have a history of repeated deformation, starting in Precambrian, and ending in post-Permian time.

9.5.2. Near-surface structures

The age relations between the structural elements of the Oslo Graben and their significance in the evolutionary history of the Oslo rift have been discussed in a series of papers (e.g. Ramberg and Larsen, 1978; Schou-Jensen and Neumann, 1988; Buer, 1990; Sundvoll et al., 1990, 1992). The main conclusions are summarized below.

The oldest structural element in the Oslo Graben is a series syenitic sills which predate all other magmatic activity in the Oslo Region (Ramberg and Morgan, 1984; Sundvoll et al, 1992).

The major structural features in the Oslo Graben are N–S to NNW–SSE trending normal faults (including boundary faults), open extensional fractures of large extent, and dikes (Figs. 9–1, 9–3). NW–SE and NE–SW trending curved and linear faults with minor normal displacement; tensional fractures and dikes are also present, but much less frequent (Ramberg et al., 1977; Ramberg and Larsen, 1978). The vertical displacement along most faults is unknown. An exception is the N–S trending Oslofjorden boundary fault zone along which southern part a vertical displacement of about 3 km has been estimated (Oftedahl, 1952; Ramberg, 1976; Schou-Jensen and Neumann, 1988).

The NNW–SSE to N–S trending faults and dikes are cut by NW–SE and NE–SW trending structures, by ring-dikes, and by syenitic to granitic intrusions. Evidence cited above (sections 9.3.2 and 9.3.3) show that the faults were activated before or during the earliest period of volcanism (about 295 Ma) and that recurrent movements continued throughout the period of B_1 and RP volcanism; the large RP dikes were emplaced during the latest part of this period (about 270–280 Ma; Sundvoll and Larsen, 1993). The total vertical displacement on the Oslofjorden fault zone is estimated to be about 3 km, no estimates are available for the other faults of this system.

Ring-structures associated with the calderas cut the N–S to NNW–SSE trending faults and fractures. However, the NNW–SSE alignment of groups of calderas in the southern and central part of the Oslo Region (Fig. 9–3) is clearly governed by major linear structures.

Structures belonging to the NE–SW and NW–SE systems dissect ring-structures and silicic intrusions.

An integrated stretching model for the Oslo rift (Ro and Faleide, 1992) indicate that the Oslo rift formed in response to stretching of a 100-km-wide area by a β-factor of 1.4–1.6. According to Ro and Faleide (1992), upper crustal extension by faults accounts for a stretching factor of only 1.1–1.2. The discrepancy between total and fault-related stretching is assigned to thermal expansion of the lithosphere and uplift, due to a positive temperature anomaly in the asthenosphere. Regional crustal stretching has been related to dextral strike-slip movement along the Sorgenfrei-Tornquist Zone in Late Paleozoic time (320–300 Ma) (Ro et al., 1990b). A link between the Skagerrak Graben and the Sorgenfrei-Tornquist Zone is supported by structural data (Ro et al., 1990a, 1990b) (Fig. 9–1) and coinciding magmatic activity in the Oslo rift, and dike emplacement along the Sorgenfrei-Tornquist Zone in southern Sweden (300–260 Ma; Sundvoll and Larsen, 1993).

9.5.3. Deep crust and upper mantle

Combined interpretation of the data from all seismic techniques implies moderate crustal thinning beneath the rift area as compared to adjacent parts of the Fennoscandian Shield, with a southwards increase in the degree of thinning (i.e., depth to the Moho decreases southward) along the axial trend of the Oslo-Skagerrak rift system. The crustal model

derived by Cassell et al. (1983) [profile D] shows thinning from 34 km in the adjacent Precambrian Shield to 25–29 km within the northern end of the rift. The most recent Moho depth mapping, which incorporates results from all types of available seismic data (Kinck et al., 1991), resolves an irregular Moho contour with an increase in the crustal thickness from 28–35 km in the rift area, to > 45 km in central and eastern Sweden (Fig. 9–7). This increase in the crustal thickness is accompanied by a general north-northeastwards increase in lithospheric thickness from ~110 km in northern Denmark to > 170 km near the center of the Fennoscandian Shield in the vicinity of the northern Bothnian Bay region (Calcagnile, 1982).

The combined seismic data also indicate some differences in shallower crustal structure between the rift area and the adjacent Precambrian Shield. The Precambrian Shield appears to consist of distinct upper and lower crustal layers each with small or no internal velocity gradients, a Conrad discontinuity at 14–17 km depth (velocity contrast: 0.25–0.40 km/s), and a marked Moho discontinuity (velocity increase from 6.7/6.8 to 8.1/8.2 km/s). Within the Oslo section of the rift system, the Conrad discontinuity seems to be intermittent and less well defined, the lowermost crust beneath the Permian volcanic areas is characterized by a thick (from ~20-km-depth to the Moho at 32 km), massive layer with relatively high (7.0–7.1 km/s) P-wave velocity, and the velocity contrast at Moho is < 0.9 km/s.

Figure 9–11 shows a crustal transect across the Vestfold Graben Segment of the Oslo rift. Transect location is shown in Figure 9–2 and is coincident with gravity profile IX of Ramberg (1976). The top panel shows observed Bouguer gravity anomaly and total magnetic field profiles. The center panel is a crustal cross section based on interpretations of seismic refraction profiles (principally Tryti and Sellevoll, 1977; Cassell et al., 1983; Gundem, 1984) and on the gravity model of Olsen et al. (1987). Bold figures are seismic P-wave velocities in km/s; velocity-depth plots for the un-reversed NE–SW CANOBE and NORSAR profiles approximately perpendicular to the transect are shown projected at the ends of the section. Densities from the gravity interpretation (Olsen et al., 1987; 1989) are in Mg/m^3. The bottom panel is a 50 km wide geological strip map along the transect.

Since the deep levels of the Skagerrak region were surveyed by reflection techniques rather than by refraction profiles, the velocity-versus-depth profiles within the crust are not well determined, but the presence of an intermittent Conrad and a fairly sharp Moho are indicated. For the central Skagerrak Graben, there is no obvious indication from the reflection surveys of the thick, high-velocity, lowermost crustal 'rift pillow' which is so clearly observed seismically beneath the Oslo Graben. However, marine magnetic surveys and sparse dredging and drillhole data suggest that some volcanic and intrusive rocks are also associated with the Skagerrak Graben.

The high-velocity lowermost crustal 'rift pillow' observed by seismic profiling is also reflected by other data. Our gravity interpretation (Fig. 9–10) places, at the base of the crust, a 90-km-wide, massive body with a +0.6 Mg/m^3 density contrast to the Precambrian country rocks. There is extensive petrological and geochemical evidence (Neumann et al., 1992, and references therein) that the excess mass in the deep crust represents dense cumulates and gabbroic rocks formed from mantle-derived magmas in deep crustal magma-chambers. These magmas were also the source for a considerable part of the voluminous volcanic and plutonic rocks of the Oslo igneous province. It seems clear, however, that the magmatic rocks exposed at the surface represent only

Fig. 9–11. Crustal transect across the Vestfold Graben Segment of the Oslo rift. Transect location is shown in Figure 10.2 and is coincident with gravity profile IX of Ramberg (1976). The top panel shows observed Bouguer gravity anomaly and total magnetic field profiles. The center panel is a crustal cross section based on interpretations of seismic refraction profiles (principally Tryti and Sellevoll, 1977; Cassell et al., 1983; Gundem, 1984) and on the gravity model of Olsen et al. (1987). Bold figures are seismic P-wave velocities in km/s; velocity-depth plots for the unreversed NE–SW CANOBE and NORSAR profiles approximately perpendicular to the transect are shown projected at the ends of the section. Densities from the gravity interpretation (Olsen et al., 1987) are in Mg/m^3. The bottom panel is a 50 km wide geological strip map along the transect.

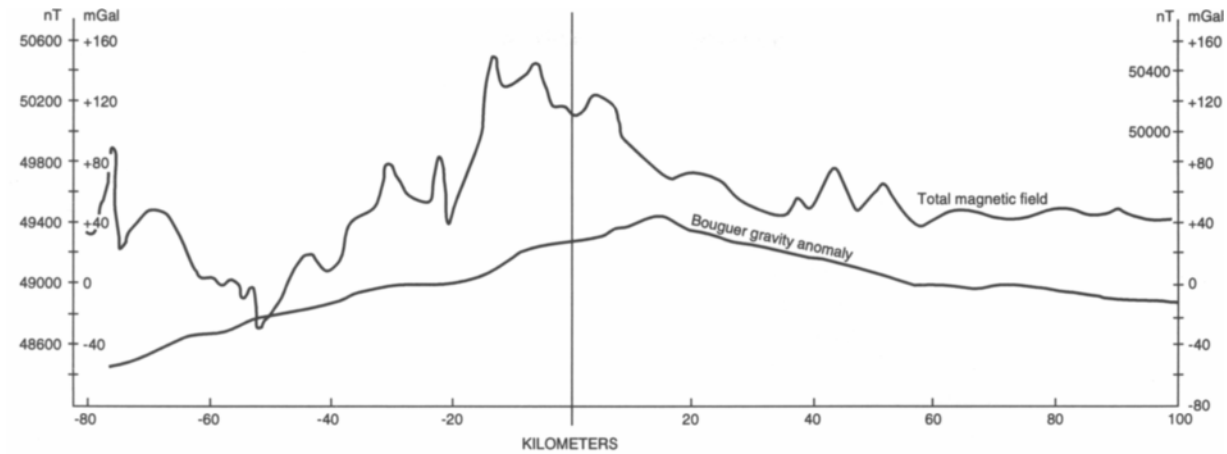
nT
mGal
50600
+160
50200
+120
49800
+80
49400
+40
49000
0
48600
-40
50400
50000
Total magnetic field
Bouguer gravity anomaly
-80
-60
-40
-20
20
40
60
80
100
KILOMETERS

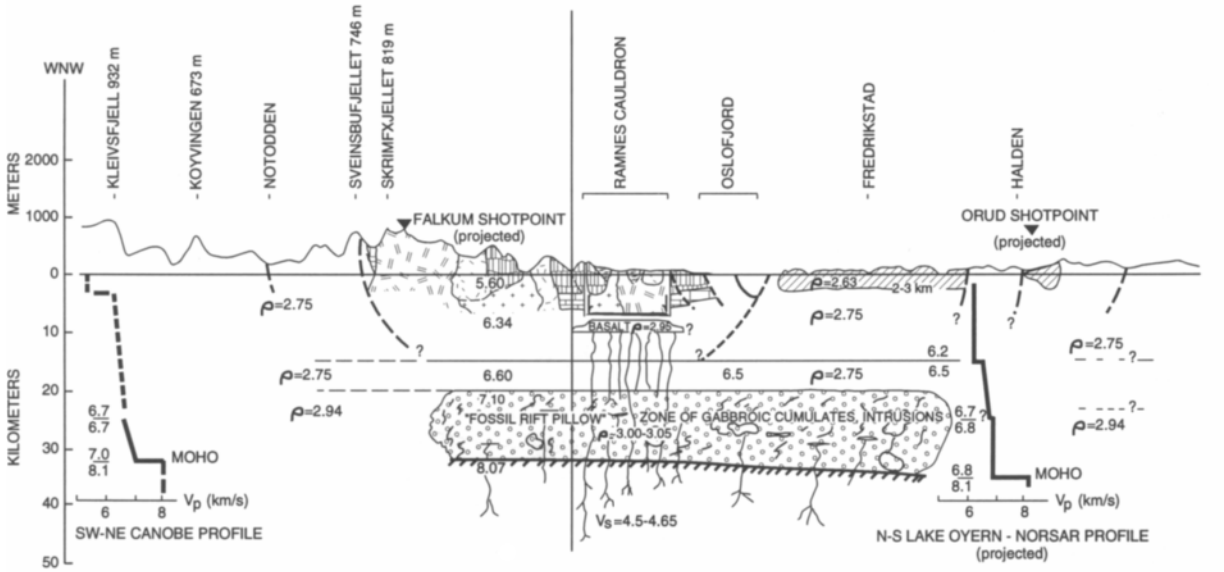
WNW
- KLEIVSFJELL 932 m
- KOYVINGEN 673 m
- NOTODDEN
- SVEINSBUFJELLET 746 m
- SKRIMFXJELLET 819 m
RAMNES CAULDRON
OSLOFJORD
- FREDRIKSTAD
- HALDEN
METERS
KILOMETERS
FALKUM SHOTPOINT
(projected)
ORUD SHOTPOINT
(projected)
ρ=2.75
5.60
6.34
ρ=2.63
2-3 km
ρ=2.75
BASALT ρ=2.95
6.2
6.5
6.60
6.5
ρ=2.75
ρ=2.94
7.10
"FOSSIL RIFT PILLOW"
ZONE OF GABBROIC CUMULATES, INTRUSIONS
ρ=3.00-3.05
8.07
6.7
6.8
6.8
8.1
MOHO
Vp (km/s)
6
8
Vs=4.5-4.65
SW-NE CANOBE PROFILE
N-S LAKE OYERN - NORSAR PROFILE
(projected)

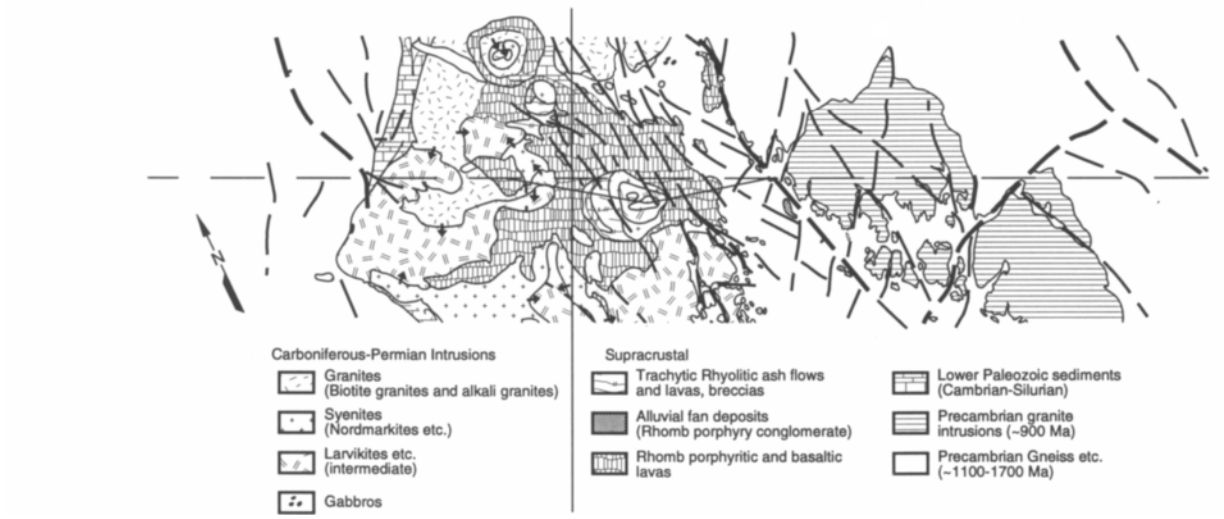
Carboniferous-Permian Intrusions
Granites
(Biotite granites and alkali granites)
Syenites
(Nordmarkites etc.)
Larvikites etc.
(intermediate)
Gabbros
Supracrustal
Trachytic Rhyolitic ash flows
and lavas, breccias
Alluvial fan deposits
(Rhomb porphyry conglomerate)
Rhomb porphyritic and basaltic
lavas
Lower Paleozoic sediments
(Cambrian-Silurian)
Precambrian granite
intrusions (~900 Ma)
Precambrian Gneiss etc.
(~1100-1700 Ma)

a moderate proportion of the total mass of mantle-derived magmas emplaced into the crust during the Oslo rifting event.

The storage of hot mantle-derived magmas in deep crustal magma-chambers also caused modifications of the Precambrian lower crust through contact metamorphism and anatexis. The silicic magmas which gave rise to the large granitic to syenitic batholiths represent anatectic (crustal) melts or mixing between mantle-derived and anatectic melts. Intrusions of anatectic magmas into the upper crust seem to have continued for 10–20 million years after the main period of emplacement of mantle-derived magmatic rocks. This suggests that the period of anomalous heating of the lithosphere was considerably shorter (10–20 million years) than the total period of magmatic activity (Neumann et al., 1992; Sundvoll et al., 1992).

However, the present day subcrustal lithosphere and the asthenosphere beneath southern Scandinavia do not appear to have obvious special structures or seismic properties uniquely associated with the crustal features of the Oslo-Skagerrak rift system.

9.6. Tectonic evolution

The tectonomagmatic evolution of the Oslo rift has been discussed in a number of papers (e.g. Ramberg, 1976; Ramberg and Larsen, 1978; Neumann et al., 1986; Wessel and Husebye, 1987; Sundvoll et al., 1990; Neumann et al., 1992). The models presented in these papers are based on the large amounts of data available for the northern, exposed part the rift, the Oslo Graben. Particularly important are the large number of age determinations by Sundvoll and Larsen (1990), Sundvoll et al. (1990, 1992) and Sundvoll and Larsen (1993). Information about the stress field has been inferred from the orientation and relative ages of different groups of structural elements (Ramberg and Larsen, 1978; Ramberg and Morgan, 1984; Buer, 1990). An updated review of the tectonomagmatic evolution of the Oslo Graben is presented below. The details of the tectonomagmatic evolution of the Skagerrak Graben are not yet known.

1: *Precursors or proto-rifting stage (>300 Ma).* The Oslo rifting event appears to have started in Upper Carboniferous time with formation of a depression in which sedimentary rocks and lavas were deposited (Ramberg and Spjeldnæs, 1976; Henningsmoen, 1978; Olaussen, 1981). This suggests that the rifting started with a period of stretching and thinning of the crust well before the onset of volcanism. Contemporaneous sills of intermediate to felsic composition (304–294 Ma) have been interpreted as a paleo-stress indicator which mark a stage of compression in the shallow crust prior to optimal extension (Ramberg and Larsen, 1978; Ramberg and Morgan, 1984; Sundvoll et al., 1992). No geological evidence of doming during the early stages of the Oslo rift has been found.

2: *Initial rifting stage and basalt volcanism (300–295 Ma).* The main magmatic period (extrusion of B1 basaltic rocks) and vertical movement along NNW–SSE to N–S trending faults, appears to have started about simultaneously in response to ENE–WSW to E–W crustal extension. The tectonic activity associated with the Permo-Carboniferous Oslo rift involved reactivation of a series of prominent Precambrian lineaments, this includes some of the large boundary faults (e.g. Ramberg and Larsen, 1978; Swensson, 1990; Neumann et al., 1992, and references therein).

3: *Main rifting and volcanic stage (295–275 Ma).* Large vertical displacements continued along major NNW–SSE to N–S trending faults. The total vertical displacement along the Oslofjorden fault zone (Fig. 9–3) is estimated to be about 3 km. It is likely that the Oslo Graben formed at this stage (Ramberg and Larsen, 1978; Sundvoll et al., 1990, 1990). Also the magmatism continued, but this period is dominated by the eruptions of RP lavas; basaltic flows from this period are relatively rare. During the later parts of this stage, block faulting within the main grabens created increasing topographic contrasts. The fault blocks are tilted so that the lavas now dip 10–30° (Oftedahl, 1952). The tectonic framework of the Oslo rift may, at least partially, be controlled by Precambrian structural elements (Ramberg and Larsen, 1978; Falkum and Petersen, 1980).

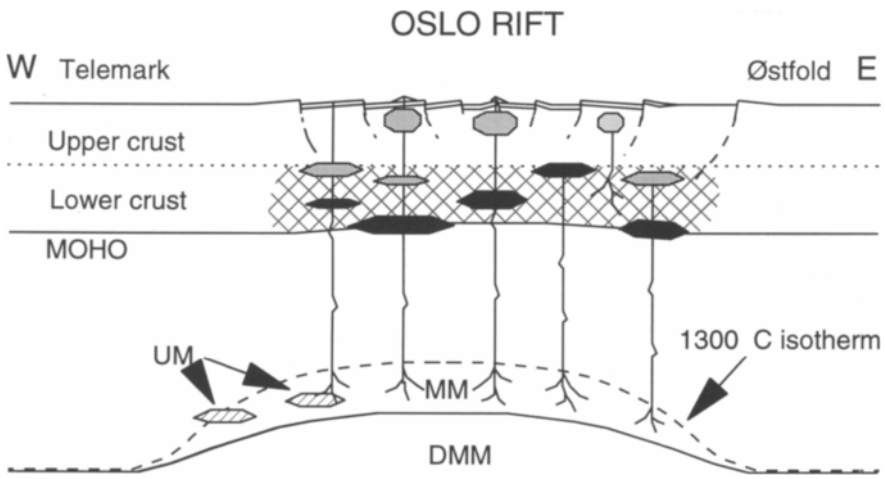

Fig. 9–12. A schematic model for the magmatic "plumbing system" at an early stage of the Oslo rifting event, about 300 to 240 Ma. Lithospheric thinning (indicated by the dotted line) is partly caused by conductive heating and passive transformation of lithosphere to asthenosphere. No attempt is made to draw this effect to scale. The lithospheric mantle represents the mildly depleted source MM, whereas the more enriched mantle source under the Skien area, UM, is indicated by hatched areas. Magma chambers are shown in black (mafic melts) and gray (intermediate to silicic melts); anatexis in the lower crust is indicated by the crosshatched region. See text for further explanation.

4: *Central volcano and composite intrusion stage (280–240 Ma).* The period of volcanism and terminated with the formation of central volcanoes, many of which developed into calderas (Fig. 9–3) (Ramberg and Larsen, 1978; Sundvoll et al., 1990). At the same time the magmatism became dominated by intrusions of monzonitic, and later syenitic and granitic, batholiths. Also large N–S trending RP dikes were emplaced inside the graben and on its flanks (< 40 m wide) during the early part of this period (Sundvoll and Larsen, 1993). The total period of magmatic activity lasted considerably longer in the northern (Akershus Graben Segment: about 300–240 Ma) than in the southern (Vestfold Graben Segment: about 300–265 Ma) part of the Oslo Graben (Sundvoll et al., 1990). The change in magmatic style was accompanied by a change in structural orientations from NNW–SSE, N–S and NNE–SSW, to NE–SW and NW–SE to W–E. The new directions clearly reflect a change in principal stress directions. The roundish shape of the silicic intrusions which characterize this stage was interpreted by Ramberg and Morgan (1984) as reflecting a period of mild compressional stress. Buer (1990) has proposed that the new directions result from doming along a NNE to NE axis, that is the rift axis. He associated the doming with thermal expansion caused by emplacement of large volumes of magma into the upper crust.

5: *Aftermath stage.* There have been suggestions that the magmatic activity in the Oslo rift may have continued into Triassic time. However, Rb-Sr and Sm-Nd isochron ages of a large number of dikes, including dikes cross-cutting all other Oslo rift features, give ages of 305–240 Ma, that is within the magmatic period for the lavas and batholiths (Sundvoll and Larsen, 1993). The area thus appear to have been unaffected, by the Mesozoic rifting of the North Sea and the North Danish Basin.

6: *Reactivation stage.* Only one intra-plate pre-Permian tectonic or magmatic event may with certainty be assigned to the general area of the Oslo rift, that is the formation of the Fen carbonatite complex near the SW corner of the Oslo Region (Fig. 9–1), 540 Ma ago (e.g. Brøgger, 1921; Andersen and

Sundvoll, 1987; Andersen and Taylor, 1988). It has also been proposed that the Late Precambrian (750 to 590 Ma) "Sparagmite Basin" north of the Oslo Region may represent a pre-Permian rifting episode (e.g. Bjørlykke, 1983). The "Sparagmite Basin" represents sedimentary deposits in a rifted basin; a few tholeiitic lava flows and mafic dikes reflect associated magmatic activity (e.g. Bjørlykke, 1983; Nystuen, 1987). An alternative model, proposed by Nystuen (1987), is that this rift formed 130–230 km NW of its present position, and was thrust into position during the Caledonian orogeny. Bjørlykke's (1983) model (the "Sparagmite Basin" formed *in situ*) implies that the Oslo rift formed along the same general trend as this Late Precambrian rift.

9.7. Conclusions

Available data suggest that the Oslo rift formed in response to a combination of regional stretching caused by dextral strike-slip movements along the Sorgenfrei-Tornquist Zone and a positive temperature anomaly in the asthenosphere. The earliest manifestation of the Oslo rifting event was the formation of a shallow depression in late Carboniferous time. Magmatism and graben formation started simultaneously about 300 million years ago, and lasted for about 60 million years. The main rifting stage lasted from about 295–275 Ma and coincide with the most active period of volcanism. Subsequent erosion has removed the upper 1–3 km of rift related and pre-rift rocks in the northern, exposed part of the rift, whereas in the southern, submerged part of the rift, rift-related deposits are buried under younger sediments.

Seismic, gravity and geochemical data imply that the rifting event caused significant modifications of the lithosphere. Both the crust and total lithosphere under the rift are thinned relative to the Precambrian basement on both sides. A 12 km thick high density and high velocity body occupies the lower crust along the rift axis and extends under the eastern and western rift-shoulder reflect magmatic processes which induced, or increased, stratification in the crust. Petrological and geochemical data suggest that this massive layer represents dense cumulates and gabbroic rocks formed by fractional crystallization of mantle-derived magmas in deep crustal (Fig. 9–12). The storage of hot, mafic magmas in the deep crust also caused anatexis of Permian gabbros and, to a lesser extent, Precambrian country-rocks, and transport of light, syenitic and granitic components to the upper crust, whereas dense residues were left in the deep crust together with the dense cumulates. The mafic magmatism associated with the rift appears to have originated in different parts of a heterogeneous upper mantle which, before the rifting event, belonged to the subcontinental lithosphere.

Important unsolved problems in the Oslo rift are the relative timing of tectonic activity and magmatism between the exposed Oslo Graben, and the submerged Skagerrak Graben, and the intensity of magmatism in the Skagerrak Graben as compared to the Oslo Graben.

Acknowledgments. We acknowledge the useful interaction with our colleagues in the CREST program during the preparation of this paper. We are also indebted to K. Bjørlykke, J. I. Faleide, A. M. Myhre, H. E. Ro, N. Spjeldnæs and B. Sundvoll for enlightening discussions and constructive criticism of earlier versions of this paper. Much of the data on which this paper have been collected through grants from the Norwegian Council for Sciences and Humanities (NAVF). Olsen thanks the Norwegian Council for Scientific and Industrial Research (NTNF) for a Senior Visiting Scientist Fellowship to NORSAR. Olsen and Baldridge acknowledge support from the Los Alamos branch of the Institute of Geophysics and Planetary Physics (IGPP) as well as partial travel support from NSF Grant EAR 86-17315 to the CREST Project.

9.8. References

Aki, K., Christoffersen, A., and Husebye, E.S., 1977. Determination of the three-dimensional seismic structure of the lithosphere. J. Geophys. Res., 82: 277–296.

Åm, K., 1973. Geophysical indications of Permian and Tertiary igneous activity in the Skagerrak. Norges Geol. Unders., 287: 1–25.

Andersen, T., and Sundvoll, B., 1987. Strontium and neodymium isotopic composition of an early tinguaite (nepheline microsyenite) in the Fen complex, Telemark (southeast Norway): Age and Petrogenetic implications. Norges Geol. Unders., 409: 29–34.

Andersen, T., and Taylor, P.N., 1988. Pb isotope chemistry of the Fen carbonatite complex, S.E. Norway: Age and petrological implications. Geochim. Cosmochim. Acta, 52: 209–216.

Anthony, E. Y., Segalstad, T. V., and Neumann, E.-R., 1989. An unusual mantle source region for nephelinites from the Oslo Region, Norway. Geochim. Cosmochim. Acta, 53: 1067–1076.

Aric, K., 1968. Reflexionsseismische Messungen in Skagerrak. J. Geophys., 34: 223–226.

Bannister, S.C., Ruud, B.O., and Husebye, E.S., 1991. Tomographic estimates of sub-Moho seismic velocities in Fennoscandia and structural implications. In: S. Bjørnsson, S. Gregerson, E.S. Husebye, H. Korhonen, and C.-E. Lund (Editors), Imaging and understanding the lithosphere of Scandinavia and Iceland. Tectonophysics, 189: 37–53.

Barth, T.F.W., 1945. Studies on the igneous rock complex of the Oslo Region. II. Systematic petrography of the plutonic rocks. Skr. Norske Vidensk.-Akad. Oslo I. Mat.-naturv. Kl. 1944, No 9, 104 pp, 1945.

Barton, P., and Wood, R., 1984. Tectonic evolution of the North Sea Basin: crustal stretching and subsidence. Geophys. J. Roy. astron. Soc., 79: 987–1,022.

Båth, M., 1984. A seismic refraction profile in Swedish Lapland. Report no. 2-84, Seismological Department, Univ. of Uppsala, 32 pp.

Berteussen, K.-A., 1975. Crustal structure and P-wave traveltime anomalies at NORSAR. Tectonophysics, 41: 71–84.

Berteussen, K.-A., 1977. Moho depth determinations based on spectral ratio analysis of NORSAR long period P-waves. Phys. Earth Planet. Int., 15: 13–27.

Berthelsen, A., 1980. Towards a palinspastic tectonic analysis of the Baltic Shield, Mem. B.R.G.M. 6th Colloq. Int. Geol. Congr., Paris, 108: 5–21.

Berthelsen, A., 1987. A tectonic model for the crustal evolution of the Baltic Shield. In: J.-P. Schaer and J. Rogers (Editors), The Anatomy of Mountain Ranges. Princeton University Press, Princeton, pp. 31–57.

Bjørlykke, K., 1974. Depositional history and composition of Lower Palaeozoic epicontinental sediments from the Oslo Region. Norges Geol. Unders., 305: 1–81.

Bjørlykke, K., 1983. Subsidence and tectonics in Late Precambrian and Paleozoic sedimentary basins of southern Norway. Norges Geol. Unders., 380: 159–172.

Blundell, D.J., and Gibbs, A.D. (Editors), 1990. Tectonic evolution of the North Sea Rifts. Clarendon, Oxford, 272 pp.

Bockelie, J.F., 1978. The Oslo Region during the Early Palaeozoic. In: I.B. Ramberg and E.-R. Neumann (Editors), Tectonics and Geophysics of Continental Rifts. D. Reidel, Dordrecht, pp. 195–202.

Brøgger, W.C., 1883. Spaltenverwerfungen in den Gegend Langesund-Skien. Nyt mag. f. Naturv., 28: 253–419.

Brøgger, W.C., 1886. Über die Bildungsgeschichte des Kristianiafjords. Nyt mag. f. Naturv., 30: 99–231.

Brøgger, W.C., 1890. Die Mineralien der Syenitpegmatitgange der sudnorwegischen Augit- und Nephelinsyenite. Zeitschr. Krystallogr. Mineral., 16: 663 pp.

Brøgger, W.C., 1900. Konglomerater i Kristianiafeltet: I. Om porfyrkonglomeratet paa ørækken Revlingen-Søstrene, en ny sedimentær formation fra Kristianiafeltet. Nyt. Mag. f. Naturv., 38: 29–64.

Brøgger, W.C., 1921. Die Eruptivgesteine des Kristianiagebietes. IV. Das Fengebiet in Telemark, Norwegen. Skr. Vidensk. Selsk., I. Mat.-naturv. Kl. 1920., No. 9: 408 pp.

Buch, L. von, 1810. Reise durch Norwegen und Lappland, vol. I and II, Berlin.

Buer, K.Y., 1990. Application of remote sensing data in geology, case studies - contribution to the understanding of the tectonomagmatic development of the Oslo Rift, Part A. Dr. Scient. thesis, University of Oslo, Norway (Unpublished).

Bungum, H., 1989. Earthquake occurrence and seismotectonics in Norway and surrounding areas. In: S. Gregersen and P.W. Basham (Editors), Earthquakes at North-Atlantic Passive Margins: Neotectonics and Postglacial Rebound. NATO ASI Series vol. 266, Kluwer, Dordrecht, pp. 501–519.

Bungum, H., and Fyen, J., 1979. Hypocentral distribution, focal mechanisms, and tectonic implications of Fennoscandian earthquakes, 1954–1978. Geol. Fören. Stockh. Förh., 101: 261–271.

Bungum, H., Havskov, J., Hokland, B.K., and Newmark, R., 1986. Contemporary seismicity of northwest Europe. Annales Geophys., 4B: 567–576.

Bungum, H., Husebye, E.S., and Ringdal, F., 1971. The NORSAR array and preliminary results of data analysis. Geophys. J. Roy. astron. Soc., 25: 115–126.

Bungum, H., Pirhonen, S., and Husebye, E.S., 1980. Crustal thickness in Fennoscandia. Geophys. J. R. Astron. Soc., 63: 759–774.

Calcagnile, G., 1982. The lithosphere-asthenosphere system in Fennoscandia. Tectonophysics, 90: 19–35.

Cassel, B.R., Mykkeltveit, S., Kanestrom, R., and Husebye, E.S., 1983. A North Sea-southern Norway seismic crustal profile. Geophys. J. Roy. astron. Soc., 72: 733–753.

Cloos, H., 1939. Hebung, Spaltung, Vulkanismus. Geol. Rundschau, 30: 405–527.

Clowes, R.M., Gens-Lenartowicz, E., Demartin, M., and Saxov, S., 1987. Lithospheric structure in southern Sweden - Results from FENNOLORA. Tectonophysics, 142: 1–14.

Dahl-Jensen, T., Dyrelius, D., Juhlin, C., Palm, H., and Pedersen, L.B., 1987. Deep reflection seismics in the Precambrian of Sweden. Geophys J. R. astron. Soc., 89: 371–389.

Dons, J.A., 1978. Terminology and history of investigations. In: J.A. Dons and B.T. Larsen (Editors) The Oslo Paleorift. A Review and Guide to Excursions. Norges Geol. Unders., 337: 9–16.

Dons, J.A., and Larsen, B.T., 1978. (Editors) The Oslo Paleorift. A Review and Guide to Excursions. Norges Geol. Unders., 337, 199 pp.

Egilson, T., and Husebye, E.S., 1991. An Oslo Graben experiment: Shooting at sea and recording on land. Tectonophysics, 189: 183–192.

EUGENO-S Working Group, 1988. Crustal structure and tectonic evolution of the transition between the Baltic Shield and the North German Caledonides (the EUGENO-S Project). Tectonophysics, 150: 253–348.

Falkum, T., and Petersen, J.S., 1980. The Sveconorwegian orogenic belt, a case of late Proterozoic plate collision. Geol. Rundschau, 69: 622–647.

Goldschmidt, V.M., 1911. Die Konttaktmetamorphose im Kristianiagebiet. Skr. Norske Vidensk.-Akad. Oslo, Mat.-naturv. Kl. 1911, No 11, 405 pp.

Gorbatschev, R., Lindh, A., Solyom, Z., Laitakari, I., Aro, K., Lobach-Zhuchenko; s.b., Markov, M.S., Ivliev, A.I., and Bryhni, I., 1987. Mafic dyke swarms of the Baltic Shield. In: H.C. Halls and W.F. Fahrig (Editors), Mafic Dyke Swarms. Geol. Ass. Canada, Spec. Pap., 34: 361–372.

Grønlie, G., Heier, K.S., and Swanberg, C.A., 1977. Terrestrial heat-flow determinations from Norway. Norsk Geol. Tidsskr., 57: 153–162.

Guggisberg, B., and Berthelsen, A., 1987. A two-dimensional velocity-model for the lithosphere beneath the Baltic Shield and its possible tectonic significance. Terra Cognita, 7: 631–638.

Gundem, M.B., 1984. 2-D seismic synthesis of the Oslo Graben. Candidatus Scientarum thesis, 164 pp., Univ. of Oslo, Norway.

Hageskov, B., 1981. The Sveconorwegian structures of the Norwegian part of the Kongsberg-Bamble-Østfold segment. Geol. Fören. Stockh. Förh., 102: 150–155.

Hänel, R., Grønlie, G., and Heier, K.S., 1974. Terrestrial heat flow determinations from lakes in southern Norway. Norsk Geol. Tidsskr., 54: 423–428.

Hänel, R., Grønlie, G., and Heier, K.S., 1979. Terrestrial heat flow determinations in Norway and an attempted interpretation. In: V. Chermak and L. Rybach (Editors), Terrestrial Heat Flow in Europe. Springer-Verlag, New York, pp. 232–239.

Hausmann, J.F., 1811–1818. Reise durch einen Theil von Dänemark, Norwegen und Schweden. Neue Jahrb. d. Berg- und Hüttenkunde, 1, Nürnberg.

Henningsmoen, G., 1978. Sedimentary rocks associated with the Oslo Region lavas, in The Oslo Paleorift. In: J.A. Dons and B.T. Larsen (Editors), A Review and Guide to Excursions. Norges Geol. Unders., 337: 17–24.

Hjelt, S.E., 1984. Deep electromagnetic studies of the Baltic Shield. J. Geophys., 48: 181–194.

Holtedahl, O., 1931. Jungpaläozoische Fossilien im Oslogebiete; ein vorläufige Mitteilung. Norsk geol. Tidsskr., 12: 323–339.

Husebye, E.S., Bungum, H., Fyen, J., and Gjøystdal, H., 1978. Earthquake activity in Fennoscandia between 1497 and 1975 and intraplate tectonics. Norsk Geol. Tidsskr., 58: 51–68.

Husebye, E.S., and Hovland, J., 1982. On upper mantle seismic heterogeneties beneath Scandinavia. Tectonophysics, 90: 1–17.

Husebye, E.S., Hovland, J., Christoffersson, A., Åstrøm, K., Slunga, R., and Lund, C.-E., 1986. Tomographical mapping of the lithosphere and asthenosphere beneath southern Scandinavia and adjacent areas. Tectonophysics, 128: 229–250.

Husebye, E.S., Ro, H.E., Kinck, J.J., and Larsson, F.R., 1988. Tectonic studies in the Skagerrak province: the 'Mobil Search' cruise. Norges Geol. Unders., Spec. Publ., 3: 14–20.

Ihlen, P.M., 1986. The geological evolution and metallogeny of the Oslo Paleorift. In: S. Olerud and P.M. Ihlen (Editors), Metallogeny associated with the Oslo Paleorift. Sveriges geol. unders. Ser. Ca, No 59: 6–17.

Ihlen P.M., and Martinsen, M., 1986. Ore deposits spatially related to the Drammen granite batholith. In: S. Olerud and P.M. Ihlen (Editors), Metallogeny associated with the Oslo Paleorift. Sveriges geol. unders. Ser. Ca, No 59: 38–42.

Ihlen, P.M., and Vokes, F.M., 1978. Metallogeny. In: J.A. Dons and B.T. Larsen (Editors), The Oslo Paleorift. A Review and Guide to Excursions. Norges Geol. Unders., 337: 75–90.

Johnston, A.C., 1989. The seismicity of 'stable continental interiors'. In: S. Gregersen and P.W. Basham (Editors), Earthquakes at North-Atlantic Passive Margins: Neotectonics and Postglacial Rebound, NATO ASI Series vol., 266, Kluwer, Dordrecht, pp. 299–327.

Johnston, A.C., and Kanter, L.R., 1990. Earthquakes in stable continental crust. Sci. Amer., 262: 68–75.

Kanestrøm, R., 1971. Seismic investigations of the crust and upper mantle in Norway. In: A. Vogel (Editors), Deep seismic sounding in Northern Europe. Swedish Natural Science Research Council (NFR), Stockholm, pp. 17–27.

Kanestrøm, R., 1973. A crust-mantle model for the NORSAR area. Pure Appl. Geophys., 87: 37–43.

Kanestrøm, R., 1977. Seismic investigations of the crust and Moho in southern Norway. In: K.S. Heier (Editor), The Norwegian Geotraverse Project, Unpublished Report, pp. 143–149.

Kanestrøm, R, and Haugland, K., 1971. Profile section 3–4. In: A. Vogel (Editor) Proceedings of the colloquium on Deep Seismic Sounding in Northern Europe. Swedish National Res. Council, Stockholm, pp. 76–91.

Keilhau, B.M., 1838. Christiania Uebergangs-Territorium. Gaea Norwegica I. Christiania, 126 pp.

Kinck, J.J., Husebye, E.S., and Lund, C.-E., 1991. The S. Scandinavian crust - structural complexities from seismic reflection and refraction profiling. Tectonophysics, 189: 117–133.

Kjerulf, T., 1855. Das Kristiania Silurbecken chemisch-geognostisch untersucht. Universitetsprogram, 68 pp.

Klemperer, S.L., 1988. Crustal thinning and nature of extension in the northern North Sea from deep seismic reflection profiling. Tectonics, 7: 803–821.

Klingspor, I., 1976. Radiometric age-determinations of basalts, dolerites and related syenites in Skåne, southern Sweden. Geol. För. Förh., 103: 285–289.

Kværna, T., 1984. Reinterpretation of seismic refraction profiles in the framework of Fennoscandian tectonic evolution. Candidatus Scientarum thesis, Univ. of Oslo, Norway, 135pp.

Larsen, B. T., 1975. Geology and tectonics of the Oslo rift zone (including tectonic map 1:250 000). Unpubl. report for the Norwegian Geotechnical Institute, Project nr. 74628.

Larsen, B. T., 1978. Krokskogen lava area. In: J.A. Dons and B.T. Larsen (Editors), The Oslo Paleorift. A Review and Guide to Excursions. Norges Geol. Unders., 337: 143–163.

Larsen, B. T., Ramberg, I. B., and Schou-Jensen, E., 1978. Central part of the Oslofjord. In: J.A. Dons and B. T. Larsen (Editors), The Oslo Paleorift. A Review and Guide to Excursions. Norges Geol. Unders., 337: 105–124.

Larsen, B. T., and Sundvoll, B., 1983. The Oslo rift, a high-volcanicity continental rift formed from a Hercynian continent - continent collision. IUGG XVIII General Assembly, Hamburg, Programme and Abstracts, vol 2: 594.

Larsson, F. R., and Husebye, E. S., 1990. Crustal reflectivity in the Skagerrak area. Tectonophysics, 189: 135–148.

Lie, J.E., and Husebye, E. S., 1993. Seismic imaging of upper crustal basement faults in the Skagerrak Sea. In: A. G. Green, A. Kröner, H.-J. Götze and N. Pavlenkova (Editors), Plate tectonic signatures in the continental lithosphere. Tectonophysics, 219: 119–128.

Lie, J. E., Pedersen, T., and Husebye, E. S., 1990. Observations of seismic reflectors in the lower lithosphere beneath the Skagerrak. Nature, 346: 165–168.

Lind, G., 1967. Gravity measurements over the Bohus granite in Sweden. Geol. Fören. Stockh. Förh., 88: 542–548.

Lund, C.-E., Roberts, R. G., Dahl-Jensen, T., and Lindgren, J., 1988. Deep crustal structure in the vicinity of the Siljan Ring. In: A. Boden and K.G. Eriksson (Editors), Deep Drilling in Crystalline Bedrock - Volume 1: The Deep Gas Drilling in the Siljan Impact Structure, Sweden. Springer-Verlag, Berlin, pp. 355–364.

Lund, C.-E., Roberts, R. G., and Juhlin, C., 1987. The reflectivity of the lower crust in southwestern Sweden. Annales Geophys., 5B: 375–380.

Lyell, C., 1835. Principles of geology. 4th ed. I–IV. London.

Mearns, E.W., 1986. Sm-Nd ages for Norwegian garnet peridotite. Lithos, 19: 269–278.

Mearns, E.W., Andersen, T., Mørk, M.B.E., and Morvik, R., 1986. $^{143}Nd/^{144}Nd$ evolution in depleted Baltoscandian mantle. Terra Cognita, 6: 247.

Mykkeltveit, S., 1980. A seismic profile in southern Norway. Pageoph., 118: 1310–1325.

Neumann, E.-R., 1980. Petrogenesis of the Oslo Region larvikites and associated rocks. J. Petrol., 21: 498–531.

Neumann, E.-R., 1988. Isotopic and petrological relations of the crust and upper mantle under the Oslo Graben, southeast Norway. Norges Geol. Unders. Special Publ., 3: 7–13.

Neumann, E.-R., 1994. The Oslo Rift: P-T-relations and lithospheric structure. Tectonophysics, 240: 159–172.

Neumann, E.-R., Andersen, T., and Mearns, E. W., 1988a. Olivine clinopyroxenite xenoliths in the Oslo rift, SE Norway. Contrib. Mineral. Petrol., 98: 184–193.

Neumann, E.-R., Larsen, B. T., and Sundvoll, B., 1985. Compositional variations among gabbroic intrusions in the Oslo rift. Lithos, 18: 35–59.

Neumann, E.-R., Olsen, K. H., Baldridge, W. S., and Sundvoll, B., 1992. The Oslo rift: A review. Tectonophysics, 208: 1–18.

Neumann, E.-R., Pallesen, S., and Andresen, P., 1986. Mass estimates of cumulates and residues after anatexis in the Oslo Graben. J. Geophys. Res., 91: 11,629–11,640.

Neumann, E.-R., Sundvoll, B., and Øverli, P. E., 1990. A mildly depleted upper mantle beneath southeast Norway: Nd-Sr isotopic and trace element evidence from basalts in the Permo-Carboniferous Oslo Rift. In: E.-R. Neumann (Editor), Rift Zones in the Continental Crust of Europe - Geophysical, Geological and geochemical Evidence: Oslo-Horn graben, Tectonophysics, 178: 89–107.

Neumann, E.-R., Tilton, G. R., and Tuen, E., 1988b. Sr, Nd, and Pb isotope geochemistry of the Oslo rift igneous province, southeast Norway. Geochim. Cosmochim. Acta, 52: 1997–2007.

Nystuen, J. P., 1975. Plutonic and subvolcanic intrusions in the Hurdal area, Oslo Region. Norges Geol. Unders., 317: 1–21.

Nystuen, J. P., 1987. Synthesis of the tectonic and sedimentological evolution of the late Proterozoic-early Cambrian Hedmark Basin, the Caledonian Thrust Belt, southern Norway. Norsk Geol. Tidsskr., 67: 395–418.

Oftedahl, C., 1952. Studies on the igneous rock complex of the Oslo Region. XII. The lavas. Norske Vidensk.-Akad. Skr. I. Mat.-naturv. Kl. 1952, No 3, 64 pp.

Oftedahl, C., 1953. Studies on the igneous rock complex of the Oslo Region. XIII. Norske Vidensk.-Akad. Skr. I. Mat.-naturv. Kl. 1953, No 3, 108 pp.

Olafsson, I., 1988. Deep crustal structure of the Møre margin from analysis of two ship multichannel seismic data. Dr. Scient. Thesis, University of bergen, Norway, 154 pp.

Olaussen, S., 1981. Marine incursion in Upper Paleozoic sedimentary rocks of the Oslo Region, southern Norway. Geol. Mag., 118: 281–288.

Olsen, K. H., Baldridge, W. S., Larsen, B. T., Neumann, E.-R., and Ramberg, I. B., 1987. A lithospheric transect across the Oslo paleorift (abs.). Eos, Trans. AGU 68: 1480.

Olsen, K. H., Larsen, B. T., Neumann, E.-R., and Baldridge, W. S., 1989. A lithospheric transect across the Oslo paleorift (abs.). TERRA Abstracts (EUG V) 1: 40.

Ramberg, I. B., 1972a. Crustal structure across the Permian Oslo Graben from gravity measurements. Nature Phys. Sci., 240: 149–153.

Ramberg, I. B., 1972b. Gravity measurements in the Oslo region - a catalogue of principal gravity station data. The University of Oslo, Oslo, Norway.

Ramberg, I. B., 1976. Gravity interpretation of the Oslo Graben and associated igneous rocks. Norges Geol. Unders., 325: 1–194.

Ramberg, I. B., Gabrielsen, R. H., Larsen, B. T., and Solli, A., 1977. Analysis of fracture patterns in southern Norway. Geologie en Mijnbouw, 56: 295–310.

Ramberg, I. B., and Larsen, B. T., 1978. Tectonomagmatic evolution. In: J.A. Dons and B.T. Larsen (Editors), The Oslo Paleorift. A Review and Guide to Excursions. Norges Geol. Unders., 337: 55–73.

Ramberg, I. B., and Morgan, P., 1984. Physical characteristics and evolutionary trends of continental rifts. Proceedings of the 27th Internat. Geol. Congress, 7: 165–216.

Ramberg, I. B., and Smithson, S. B., 1971. Gravity interpretation of the southern Oslo graben and adjacent Precambrian rocks. Tectonophysics, 11: 419–431.

Ramberg, I. B., and Spjeldnæs, N., 1978. The tectonic history of the Oslo region. In: I.B. Ramberg and E.-R. Neumann (Editors), Tectonics and Geophysics of Continental Rifts, Reidel, Dordrecht, pp. 167–194.

Rasmussen, E., Neumann, E.-R., Andersen, T., Sundvoll, B., Fjerdingstad, V., and Stabel, A., 1988. Petrogenetic processes associated with intermediate and silicic magmatism in the Oslo rift, southeast Norway. Min. Mag., 52: 293–307.

Ro, H. E., and Faleide, J. I., 1992. A stretching model for the Oslo rift. Tectonophysics, 208: 19–36.

Ro, H. E., Larsson, F. R., Kinck, J. J., and Husebye, E. S., 1990a. The Oslo Rift - its evolution on the basis of geological and geophysical observations. In: E.-R. Neumann (Editor), Rift Zones in the Continental Crust of Europe - Geophysical, Geological and geochemical Evidence: Oslo-Horn graben. Tectonophysics, 178: 11–28.

Ro, H. E., Stuevold, L. M., Faleide J. I., and Myhre, A. M., 1990b. Skagerrak Graben - the offshore continuation of the Oslo Graben. In: E.-R. Neumann (Editor), Rift Zones in the Continental Crust of Europe - Geophysical, Geological and geochemical Evidence: Oslo-Horn graben. Tectonophysics, 178: 1–10.

Rosendahl, B. R., 1987. Architecture of continental rifts with special reference to East Africa. Annu. Rev. Earth Planet. Sci., 15: 445–503.

Sæther, E., 1962. Studies on the igneous rock complex of the Oslo Region. XVIII. General investigation of the igneous rocks in the area north of Oslo. Norske Vidensk.-Akad. Skr. I. Mat.-naturv. Ny Serie, No 1, 184 pp.

Schønwandt, H. K., and Petersen, J. S., 1983. Continental rifting and porphyry-molybdenum occurrences in the Oslo region, Norway. Tectonophysics, 94: 609–631.

Schou-Jensen, E., and Neumann, E.-R., 1988. Volcanic rocks on Jeløya, central Oslo Region: the mafic lavas. Norsk Geol. Tidsskr., 68: 289–308.

Sellevoll, M. A., and Aalstad, I., 1971. Magnetic measurements and seismic profiling in the Skagerrak. Marine Geophys. Res., 1: 284–302.

Sellevoll, M. A., and Warrick, R. E., 1971. A refraction study of the crustal structure in Southern Norway. Bull. Seismol. Soc. Am., 61: 457–471.

Skjernaa, L., 1972. The discovery of a regional crush belt in the Ørje area, southeast Norway. Norsk Geol. Tidsskr., 52: 459–461.

Skjernaa, L., and Pedersen, S., 1982. The effect of penetrative Sveconorwegian deformation on the Rb-Sr isotopic systems in the Rømskog-Aurskog-Høland area, SE Norway. Precamb. Res., 17: 215–243.

Smithson, S. B., 1961. A regional gravity study over the Permian Bærum cauldron of the Oslo Region. Norsk Geol. Tidsskr., 41: 211– 222.

Smithson, S. B., 1963. Granite studies, I. A gravity investigation of two Precambrian granites in South Norway. Norges Geol. Unders., 214b: 53–140.

Starmer, I. C., 1972. The Sveconorwegian regeneration and earlier orogenetic events in the Bamble series, south Norway. Nor. Geol. Unders., 277: 37–52.

Starmer, I. C., 1985. The evolution of the south Norwegian Proterozoic as revealed by the major and mega-tectonics of the Kongsberg and Bamble sectors. In: A.C. Tobi and J.L.R. Touret (Editors), the Deep Proterozoic Crust in the North Atlantic Provinces, NATO ASI Series vol. 158, pp. 259–290.

Størmer, L., 1935. Contribution to the geology of the southern part of the Oslofjord: The rhomb-porphyry conglomerate with remarks on younger tectonics. Norsk geol. Tidsskr., 15: 43–113.

Størmer, L., 1967. Some aspects of the Caledonian geosyncline and foreland west of the Baltic Shield. Q. J. geol. Soc. London, 123: 183–214.

Sundvoll, B., and Larsen, B. T., 1990. Rb-Sr isotope systematics in the magmatic rocks of the Oslo Rift. Norges Geol. Unders., 418: 27–48.

Sundvoll, B., and Larsen, B. T., 1994. Rb-Sr and Sm-Nd relationship in dyke and sill intrusions in the Oslo Rift and related areas. Norges Geol. Unders. Bull., 425: 31–42.

Sundvoll, B., Larsen, B. T., and Wandaas, B., 1992. The age of the incipient magmatic phase in the Oslo Rift and its related stress regime. Tectonophysics, 208: 37–54.

Sundvoll, B., Neumann, E.-R., Larsen, B. T., and Tuen, E., 1990. Age relations among Oslo rift magmatic rocks: Implications for tectonic and magmatic modelling. In: E.-R. Neumann (Editor), Rift Zones in the Continental Crust of Europe - Geophysical, Geological and geochemical Evidence: Oslo-Horn Graben. Tectonophysics, 178: 67–87.

Swensson, E., 1990. Cataclastic rocks along the Nesodden Fault, Oslo Region: a reactivated Precambrian shear zone. In: E.-R. Neumann (Editor), Rift Zones in the Continental Crust of Europe - Geophysical, Geological and geochemical Evidence: Oslo-Horn graben. Tectonophysics, 178: 51–65.

Sykes, L. R., 1978. Intraplate seismicity, reactivation of preexisting zones of weakness, alkaline magmatism, and other tectonism postdating continental fragmentation. Rev. Geophys. Space Phys., 16: 621–688.

Trønnes, R. G., and Brandon, A. D., 1992. Mildly peraluminous high-silica granites in a continental rift: the drammen and Finnemarka batholiths, Oslo Rift, Norway. Contrib. Mineral. Petrol., 109: 275–294.

Tryti, J, and Sellevoll, M. A., 1977. A seismic crustal study of the Oslo rift. Pageoph., 115: 1061–1085.

Vogel, A., and Lund, C.-E., 1971. Profile section 2–3. In: A. Vogel (Editor), Deep seismic sounding in northern Europe. Swedish Natural Science Research Council (NFR), Stockholm, pp. 62–65.

Vogfjord, K. S., and Langston, C. A., 1990. Analysis of regional events recorded at NORESS. Bull. Seismol. Soc. Am., 88: 2,016–2,031.

Weigel, W., Hjelme, J., and Sellevoll, M., 1970. A refraction profile through the Skagerrak from northern Jutland to southern Norway. Geod. Inst. (Den.) Medd. 45, 26 pp.

Wessel, P., and Husebye, E. S., 1987. The Oslo Graben gravity high and taphrogenesis. Tectonophysics, 142: 15–26.

Wörner, G., Zindler, A. Staudigel, H. and Schmincke, H.-U., 1986. Sr, Nd, and Pb isotope geochemistry of Tertiary and Quaternary alkaline volcanics from West Germany. Earth Planet. Sci. Lett., 81: 151–162.

Worsley, D., Aarhus, N., Bassett, M. G., Howe, M. P. A., Mørk, A., and Olaussen, S., 1983. The Silurian succession of the Oslo Region. Norges Geol. Unders., 384: 1–57.

Ziegler, P. A., 1978. North Sea rift and basin development. In: I.B. Ramberg and E.-R. Neumann (Editors), Tectonics and Geophysics of Continental Rifts, D. Reidel, Dordrecht, pp. 249–277.

Ziegler, P. A., 1982. Geological Atlas of Western and Central Europe, Elsevier, Amsterdam, 130 pp and 40 plates.

This Page Intentionally Left Blank

Chapter 10

The Midcontinent rift system, U.S.A.: A major Proterozoic continental rift

D. J. Allen, L. W. Braile, W. J. Hinze, and J. Mariano

10.1. Introduction

Early regional geophysical studies in the central stable interior of the U.S.A. (Woollard, 1943; Lyons, 1950; Woollard and Joesting, 1964) showed the presence of an intense, curvilinear gravity anomaly extending from Kansas into Lake Superior (Plate 10–1). Except in the Lake Superior region, the surface rocks of this region are relatively flat-lying Phanerozoic sedimentary strata that provide no clue to the origin of the anomaly. This anomaly has come to be known as the 'midcontinent gravity high' or, more appropriately, the 'midcontinent geophysical anomaly', for it is both an intense gravity and magnetic anomaly (Plate 10–2; King and Zietz, 1971). Investigations by Thiel (1956) showed that this feature extends into an area of exposed mafic volcanic and clastic sedimentary rocks of the Middle Proterozoic Keweenawan sequence in the Lake Superior region, thereby providing an explanation for the anomaly. Subsequently, geological and geophysical studies in the mid-1960's in the Lake Superior region (e.g., Smith et al., 1966; White, 1972; Ocola and Meyer, 1973) supported existing evidence that suggested a possible rift origin for the Keweenawan rock package. This led Wold and Hinze (1982) to apply the genetic/location name of the Midcontinent Rift system (MCR) to the source of the anomaly. The MCR can be traced (Fig. 10–1) from Kansas into western Lake Superior, through the eastern portion of the Lake (Hinze et al., 1966), and beneath the Michigan basin into southeastern Michigan (Hinze et al., 1975). The associated gravity and magnetic anomalies extend for more than 2000 km and over most of their lengths are the most obvious and sharply-defined features of regional geophysical anomaly maps of North America (Plates 10–1 and 10–2).

Several lines of evidence have led to general acceptance of a rift origin for the geophysical anomaly. First, a great volume of mantle-derived magma was extruded and intruded within a relatively short time interval spanning a few tens of millions of years. The magmas were emplaced into and adjacent to a series of structural troughs related in part to normal faulting. Normal faults are not directly observable, however, because some have been modified by late stage reverse movement, whereas others may be deeply buried beneath the rift fill. Second, the MCR discordantly transects the structural patterns of older basement geological provinces (Fig. 10–1). There are notable exceptions, however, where the rift pattern was deflected by pre-existing zones of weakness. Third, the pre-rift crust has been thinned to less than one-third of its original thickness. The present crust, however, is generally thicker along the axis of the rift (up to 55 km in the Lake Superior region) due to the great thickness (up to 30 km) of the rift-rock package and underplating of the crust. Fourth, mafic dikes of Keweenawan age strike roughly parallel to the axis of the rift, testifying to the presence of tensional forces at the time of generation of the MCR.

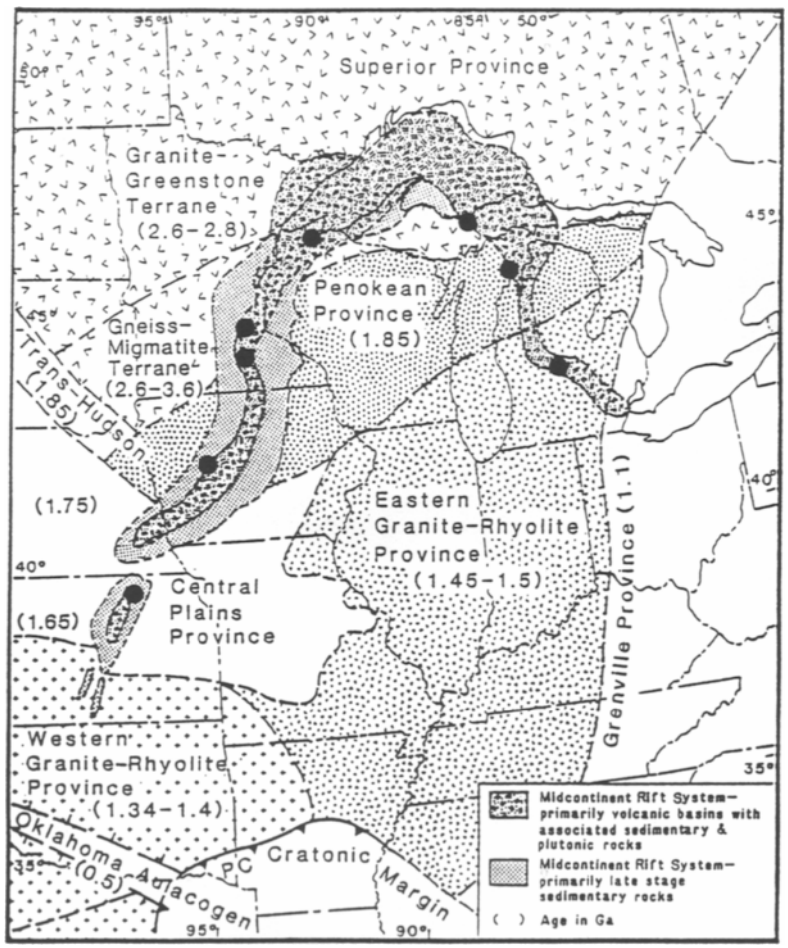

Fig. 10–1. Basement provinces of the midcontinent of North America (modified from Van Schmus et al., 1987) showing the position of the Midcontinent Rift system (after Hinze and Kelly, 1988). Filled circles are the locations of deep drill holes in the MCR that have penetrated through the late-stage clastic sedimentary strata of the MCR and/or into the igneous rocks of the rift.

Numerous journal and monograph articles have been written on specific geographic segments or geologic aspects of the MCR. Only a few, however, have attempted to present a comprehensive view of the entire rift (Halls, 1978; Green, 1983; Van Schmus and Hinze, 1985; Dickas, 1986a; Hinze et al., in press). In this paper we present a brief review of our current understanding of the structure of the MCR as revealed by geophysical investigations. Although much of this paper is derived from an earlier paper (Hinze et al., in press), we also report significant new information concerning the structure and evolution of this "world-class" rift.

10.2. Geologic framework

The rocks of the MCR in the Lake Superior region constitute the 1.1 Ga Keweenawan Supergroup (Morey and Van Schmus, 1988). They are divided into two major suites: a lower, predominantly volcanic sequence and an upper, overlying clastic sedi-

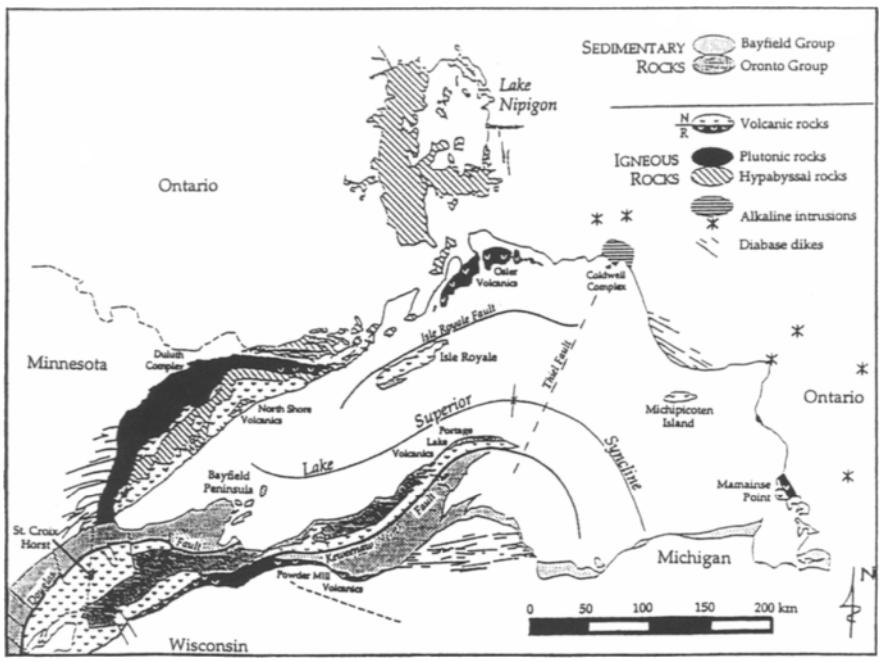

Fig. 10–2. Generalized basement geology of the Lake Superior basin (modified from Paces and Miller, 1993).

mentary package. Drillhole data (Fig. 10–1) and geophysical interpretations indicate that the rock sequence observed in the Lake Superior region is in general duplicated along the limbs of the rift extending southwest into Kansas and southeast across the Southern Peninsula of Michigan (Dickas, 1986a). Recent seismic reflection studies (e.g., Behrendt et al., 1988) show total maximum thicknesses of the order of 30 km in the Lake Superior region, whereas 15 km thicknesses are common in the limbs of the rift (e.g., Fox, 1988; Chandler et al., 1989; Woelk and Hinze, 1991). The present edges of both the volcanic and sedimentary units are erosional, indicating that the original extents of these rocks were greater than they are today.

10.2.1. Lower igneous sequence

The igneous sequence consists mainly of volcanic flows with lesser amounts of clastic sedimentary strata and plutonic rocks. The lavas were extruded contemporaneously with the rifting event, although some extension might have occurred prior to the onset of volcanism. The igneous sequence attains its maximum thickness along the Lake Superior syncline (Fig. 10–2).

Volcanism was preceded, at least locally, by early sedimentation. In the western Lake Superior region, for example, a thin basal clastic sedimentary unit lies beneath the earliest volcanic rocks. These clastic strata are relatively thin (~100 m) and consist mainly of quartzose sandstones with minor basal conglomerates (Ojakangas and Morey, 1982).

The volcanic flows are bimodal, ranging from picrite to rhyolite, although most of the rocks are basaltic. Rhyolites occur primarily as ignimbrites and also as low lava domes and widespread lavas (Green and Fitz, 1993). The high-alumina olivine tholeiites, which have the most primitive compositions, occur near the tops of the volcanic cycles in the Lake Superior region (Brannon, 1984; Green, 1987; Paces and Bell, 1989; Klewin and Shirey, 1992). The petrology and geochemistry of the vol-

canic flows have been reviewed in several recent publications (Green, 1982, 1983, 1987; Van Schmus and Hinze, 1985; Klewin and Shirey, 1992).

Individual flows show great continuity both along strike in outcrop and also across the basins as interpreted from seismic reflection sections. Many flows can be traced for distances exceeding 100 km. Measured thicknesses vary from a few meters to over 100 m (Green, 1989). Seismic data show reflections extending from surface exposures of volcanic rock to depths of 15 to 20 km (Hinze et al., 1990), testifying to the reflective nature of the volcanic section.

The volcanic flows are interbedded with red interflow clastic sedimentary rocks that range from muds to gravels (Merk and Jirsa, 1982; Wallace, 1981). These strata represent a small proportion (<5%) of the volcanic sequence (Wallace, 1981) and were derived primarily from the rift's volcanic rocks. Seismic impedance contrasts between the volcanic and interflow sedimentary rocks may be responsible for the strong reflections associated with the volcanic sequence. However, variations in velocity and density within the volcanic rocks could produce the observed seismic reflections (Halls, 1969; Lippus, 1988; Allen and Chandler, 1993).

The volcanic strata are locally intruded by plutonic rocks (Weiblen, 1982), although such intrusions represent a volumetrically minor proportion of the igneous sequence in the upper crust. These rocks occur as layered intrusions, sills, dikes, and isolated alkaline complexes. The layered intrusions, such as the Duluth Complex (Weiblen and Morey, 1980), are predominantly gabbroic with lesser granitic components. Keweenawan mafic sills and dikes occur throughout the Lake Superior region, but are concentrated in the Lake Nipigon area north of Lake Superior. Alkaline intrusions, such as the Coldwell Complex (Heaman and Machado, 1992), are smaller in volume than the Duluth Complex and display no intrusive relations to other rift rocks. Additional plutonic rocks may intrude the lower crust beneath the MCR. Such intrusions have been inferred on the basis of seismic and gravity data, although the volume of these rocks is not well known.

Recent studies of isotopic systematics of the rift's volcanic rocks (Brannon, 1984; Dosso, 1984; Klewin, 1989; Paces and Bell, 1989; Nicholson and Shirey, 1990; Klewin and Shirey, 1992; Van Schmus, 1992) have provided important information concerning the source of the rift's magmas. The consensus among current workers, based on both geochemical and physical evidence, is that magmas were derived from both lithospheric and mantle plume sources (e.g., Berg and Klewin, 1988; Klewin and Berg, 1991; Klewin and Shirey, 1992; Paces and Bell, 1989; Hutchinson et al., 1990; Nicholson and Shirey, 1990; Cannon, 1992; Klewin and Shirey, 1992; Van Schmus, 1992). The early magmas may have been derived from partial melting of the resident lithosphere due to the heat provided by a rising mantle plume, whereas the later magmas were most likely derived from partial melting of the plume head. Magmas derived from the undepleted plume head have e values near zero (Fig. 10–3), whereas magmas derived from lithospheric sources, such as the Type II rhyolites of Nicholson and Shirey (1990), have negative e values (Fig. 10–3).

10.2.2. Upper sedimentary sequence

As volcanism in the rift waned, sedimentary strata were deposited in a developing basin over the rift and in flanking basins. This sedimentary sequence is thickest along the Lake Superior syncline (Fig. 10–2) and consists mainly of clastic sedimentary strata that were derived from surrounding pre-Keweenawan rocks and syn-rift igneous rocks. The clastic rocks increase in both textural and compositional maturity upsection, from the relatively immature Oronto Group and lithostratigraphic equivalents (e.g., Solor Church Formation (Morey, 1977) of Minnesota) to the relatively mature Bayfield Group and lithostratigraphic equivalents (e.g., Jacobsville Sandstone of Michigan, Fond du Lac and Hinckley Sandstones of Minnesota).

The Oronto Group includes the Copper Harbor Conglomerate, the Nonesuch Shale, and the Freda Sandstone (Daniels, 1982; Suszek, 1991). The Copper Harbor Conglomerate is composed of conglomerates and sandstones made up largely of volcanic detritus. In addition, occasional thin basalt flows

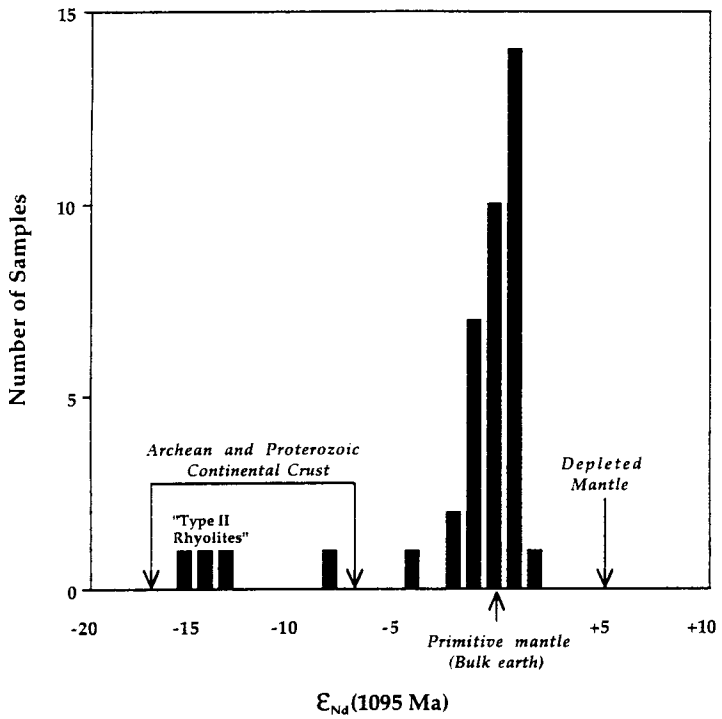

Fig. 10–3. Sm-Nd isotopic data for the Portage Lake Volcanics, Michigan. The e values of potential source regions are indicated. (Data are from Paces and Bell, 1989. and Nicholson and Shirey, 1990.)

have been encountered in this unit in the Lake Superior basin and in correlative units along the limbs of the rift in southern Michigan (McCallister et al., 1978) and in Kansas (Berendsen et al., 1988). The Nonesuch Shale, which lies conformably above the Copper Harbor Conglomerate, has traditionally been interpreted as lacustrine, although recent studies now suggest that it was deposited at least in part in a marine embayment (Hieshima and Pratt, 1991; Pratt et al., 1991). The upper formation of the Oronto Group is the Freda Sandstone, composed primarily of red-to-buff fluvial sandstones that are more mature than the sandstones lower in the group.

The Bayfield Group consists largely of fluvial sandstones that increase upward in textural and mineralogical maturity (Kalliokoski, 1982; Morey and Ojakangas, 1982). The rocks of this group are believed to have been deposited in broad sag basins encompassing both the rift basin and adjacent areas floored by pre-Keweenawan basement rocks. The contact between this group and earlier rift-rocks does not crop out, although seismic reflection studies in Lake Superior (Cannon et al., 1989) suggest an angular unconformity.

Lithostratigraphic equivalents of the Oronto and Bayfield Groups are presumably present along the limbs of the rift outside of the Lake Superior region (e.g., Fowler and Kuenzi, 1978; Dickas, 1986a; Berendsen et al., 1988; Witzke, 1990). Stratigraphic correlation has been tenuous, however, due to the lack of time markers in the units and limited paleomagnetic measurements.

10.2.3. Structural elements

The fundamental structure of the MCR in the Lake Superior region — an asymmetric basin containing a thick section of mafic volcanic rocks overlain by a thick sedimentary sequence — was established a century ago by geologists interested in the copper-

bearing Keweenawan rocks (e.g., Irving, 1883). We now recognize that this basin reaches a depth of ~30 km, with roughly 20 km of mafic volcanic flows overlain by 10 km of Keweenawan sedimentary strata. The pre-rift crust has been thinned to less than one-third of its original thickness during the rifting event. The present crust, however, is thickened along the rift (to in excess of 55 km) due to the massive addition of the igneous and sedimentary rocks.

Uplift has occurred along the ~2000 km length of the MCR. Early workers (e.g., Van Hise and Leith, 1911) discovered significant reverse movement at the base of the Portage Lake Volcanic sequence in the Northern Peninsula of Michigan (Fig. 10–2). This thrusting along the Keweenaw Fault was in part concurrent (Kalliokoski, 1989) with the deposition of the Bayfield Group and continued after the sedimentation ended. Similar uplift along reverse faults is evident from Kansas (Woelk and Hinze, 1991) to Lake Superior to the northern part of Michigan's Southern Peninsula (Fox, 1988). Many of these faults are interpreted as reactivated normal faults and have 5 km or more of stratigraphic displacement (Chandler et al., 1989; Cannon et al., 1989; Hinze et al., 1990). Other indications of vertical movement include anticlines within the rift-rock package (e.g., Fox, 1988; Allen et al., 1993; Mariano and Hinze, 1994a) and drag folding along reverse faults (Dickas, 1992; Mariano and Hinze, 1994a).

Several relatively minor cross-faults have been recognized along the MCR (e.g., Davidson, 1982; Mariano and Hinze, 1994a; Manson and Halls, 1992). These faults have relatively small displacements, do not transect the entire rift, and are probably late stage features.

10.3. Geophysical surveys

Geophysical surveys of the MCR, as is the case with many other paleorifts, have played a major role in defining and determining its nature (Hinze et al., 1992). Outcrops of the rift rocks are limited, and only a few, widely and poorly-distributed deep drill holes penetrate into the rift through the overlying sedimentary strata (Fig. 10–1). Even the rock exposures in the Lake Superior region have limitations because they represent the upper or marginal rocks of the rift.

10.3.1. Gravity and magnetic surveys

Gravity and magnetic surveys played an important role in the early definition and study of the MCR (Woollard, 1943; Thiel, 1956; Lyons, 1959, 1970; Craddock et al., 1963; Hinze, 1963; Hinze et al., 1966, 1975, 1982; White, 1966; King and Zietz, 1971; Oray et al., 1973; Halls, 1978; McSwiggen et al., 1987) because these methods readily detect the physical property contrasts among the igneous and sedimentary rocks of the rift and the surrounding country rocks. For example, strong density contrasts exist among the country rock (2.70-2.75 Mg/m^3), volcanic and plutonic rocks (2.90-2.95 Mg/m^3), Oronto Group (2.65-2.70 Mg/m^3), and Bayfield Group (2.35-2.45 Mg/m^3). As a result, intense gravity anomalies, both positive and negative, are associated with the rift (Plate 10–1). In Minnesota the central positive gravity anomaly attains values as much as 100 mGal above background level. In Iowa marginal, paralleling gravity minima on both sides of the maximum have values more than 80 mGal below the regional level. These intense gravity anomalies are the principal method for delineating the extent of the rift. The location of the rift as defined by its gravity anomaly has been corroborated by deep drill holes (Fig. 10–1) in the Southern Peninsula of Michigan (Sleep and Sloss, 1978), Wisconsin (Dickas, 1992), Minnesota (Morey, 1977; Allen and Chandler, 1993), Iowa (Anderson, 1990a), and Kansas (Berendsen et al., 1988) that have penetrated through the overlying Phanerozic formations into the MCR.

The related magnetic anomaly of the rift is more complex and less consistent over the interpreted length of the MCR (Plate 10–2). Problems in tracing the rift by means of the magnetic anomaly are the result of complicated magnetizations of the volcanic rocks. The remanent magnetization component of the volcanic rocks is of significantly greater magnitude than the induced magnetization component and is either normally or reversely polarized in a different direction from the induced magnetization.

Furthermore, the volcanic sequence is deformed, thereby rotating the remanent vector and complicating the magnitude and direction of the total magnetization.

Early modeling (e.g., Thiel, 1956; King and Zietz, 1971) ascribed the complex magnetic anomaly signature and the positive and negative gravity anomalies to upper crustal density and magnetization contrasts related to the rift-rock package. The central positive gravity and magnetic anomalies were interpreted as an uplifted block of mafic volcanic rocks, whereas the flanking anomaly minima were interpreted as originating from low-density, low-magnetization sedimentary strata related to a late-stage sag basin. More recently, models of these anomalies have included mafic intrusions beneath the volcanic rocks and a thickened crust. The mafic intrusions lead to a positive gravity effect along the rift axis, adding to the anomaly produced by the volcanic units, whereas the thickened crust produces a broad gravity minimum which complicates the interpretation of the negative anomalies associated with the bordering late-stage sag basins.

Gravity and magnetic coverage over the MCR is adequate for regional interpretations. Gridded data sets are publicly available for both gravity anomaly (4 km grid) and total magnetic intensity anomaly (2 km grid) data. Of particular importance are recent high-resolution aeromagnetic surveys of Lake Superior (Teskey et al., 1991) and Minnesota (Chandler, 1991). In Minnesota the high-resolution data permit detailed mapping of lithologic units within the Keweenawan volcanic sequence and their structural disturbances (Allen and Chandler, 1992, 1993).

10.3.2. Seismic surveys

Seismic refraction studies were an integral element of early investigations of the MCR. Seismic studies of the rift in Lake Superior (e.g., Steinhart and Smith, 1966) supported inferences from surface geology, but showed that the crustal structure was much more complicated than previously envisioned. These investigations revealed a complex crust consisting of low-velocity surface sedimentary rocks, an underlying thick section of high-velocity mafic volcanic rocks, a high-velocity layer (ranging from 6.63 to 6.90 km/s) beneath the volcanic rocks, and a crustal thickness in excess of 50 km. A rift origin for the structure was strongly suggested, but caution in acceptance of the rift hypothesis was expressed due to the lack of clear surface evidence for grabens and associated normal faults (White, 1966). Furthermore, it was at this time that the continuity of the structure as a series of segments from Kansas to Lake Superior and across the Michigan basin was established (Hinze et al., 1966, 1975; King and Zietz, 1971; Oray et al., 1973). Continued crustal seismic studies (Cohen and Meyer, 1966; Ocola and Meyer, 1973; Halls, 1982; Luetgert and Meyer, 1982; Wold et al., 1982) revealed more information on the regional structure of the Lake Superior basin and suggested a similar crustal structure in the western limb of the rift extending from Lake Superior to Kansas.

Seismic reflection studies of the rift ushered in a new era of understanding the nature of the MCR. COCORP deep seismic profiling across the rift beneath the Michigan basin and in northeastern Kansas revealed the presence of fault-bounded basins of mafic volcanic rocks overlain by thick upper sedimentary rock units (Brown et al., 1982; Serpa et al., 1984; Zhu and Brown, 1986; Woelk and Hinze, 1991). Increasing interest in the MCR as a frontier petroleum province, because of the presence of hydrocarbons in the Oronto Group, led to a number of seismic profiles by geophysical contractors. These profiles, with two-way-time (TWT) of 5 s or more, were collected over the western limb and Lake Superior segments of the rift. In general, the quality of these data are excellent; thus, those sections made available to the scientific community have been extremely useful for mapping the finer structures of the MCR not recognizable on seismic refraction profiles. Moreover, these data have been especially useful for constraining the interpretations of gravity and magnetic anomaly data. The interpretation of one or more of these profiles has been reported by Dickas (1986b), Nyquist and Wang (1988), Chandler et al. (1989), Mudrey et al. (1989), Hinze et al. (1990), Allen et al. (1993, 1994), and Mariano and Hinze (1994a). Additional seismic reflection surveys with TWT of 20 s were conducted by the Great Lakes International Multidisciplinary Program on Crustal Evolution (GLIMPCE) in 1986 over the western

Great Lakes (Green et al., 1989). These surveys have provided unprecedented images of the rift to sub-Moho depths. Results of these studies in Lake Superior and northern Lake Michigan have confirmed the regional structure interpreted from previous geologic and geophysical studies and have provided critical new details concerning the rift and underlying crust (Behrendt et al., 1988, 1990; Cannon and Green, 1989; Cannon et al., 1989, 1991; Hutchinson et al., 1990; Milkereit et al., 1990; Samson and West, 1992).

10.4. Structure of the Lake Superior basin

In the Lake Superior region, seismic reflection data, supported by other geophysical and geological data, confirm the existence of a deep fault-bounded axial basin filled with a thick volcanic sequence. This basin has been subdivided into individual segments, each of which is interpreted to have its own volcanic and sedimentological depositional patterns. The segments are commonly asymmetric, and it has been suggested that the asymmetry of the individual rift segments alternates within the basin (Mudrey and Dickas, 1988; Cannon et al., 1989; Dickas and Mudrey, 1989). Similar patterns of asymmetry have been observed in the western limb of the rift (Chandler et al., 1989) and in the East African Rift system (Bosworth et al., 1986; Rosendahl, 1987). This asymmetry is not universal along the MCR, however, as much of eastern Lake Superior is essentially symmetric (Cannon et al., 1989; Mariano and Hinze, 1994a; Samson and West, 1992). On the basis of contrasting rift structure and potential field anomaly signatures (Plates 10–3 and 10–4), the Lake Superior basin is divided into three distinct segments. These segments lie beneath the western, central, and eastern portions of Lake Superior. It is also appropriate that this discussion addresses the transition zones between the Lake Superior basin and the rift's western and eastern limbs.

10.4.1. Western Lake Superior

Recently released eight-second seismic reflection profiles from Lake Superior (McGinnis and Mudrey, 1991), together with proprietary data from northwestern Wisconsin, have resulted in a better understanding of the MCR in the western Lake Superior region. This portion of the rift is of particular interest because it encompasses the transition between the Lake Superior basin to the northeast and the rift's western limb to the southwest. Moreover, the Keweenawan rocks are exposed in northeast Minnesota, northern Wisconsin, and the western part of Michigan's Northern Peninsula. Therefore, seismic reflection, both onshore and beneath Lake Superior, is readily correlated with the outcropping geology. Combined interpretation of the seismic profiles with gravity and geologic data reveals several interesting structural and stratigraphic features, including two pre-Keweenawan ridges within the rift interior, the termination of major reverse faults, and, possibly, an Archean batholith buried beneath the rift.

Within the Lake Superior basin, seismic data image up to 9 km of sedimentary rocks (the majority of which are likely Oronto Group strata) and up to 18 km of volcanic flows beneath the Lake Superior syncline (Plates 10–3 and 10–4). These thicknesses are greater than those observed beneath the rift's western limb. At the northern termination of the western limb, for example, the Oronto Group is as thick as 4 km, and the underlying volcanic flows have a maximum thickness of 14 km. These maximum thicknesses occur beneath the Ashland syncline of Wisconsin which lies on top of the St. Croix Horst, an uplifted block of Keweenawan volcanic strata (Plates 10–3 and 10–4).

The western limb and Lake Superior basin segments of the MCR are separated by a prominent transverse ridge that was first hypothesized by White (1966) on the basis of gravity and magnetic data. Along White's Ridge, the volcanic strata are very thin (<2 km) and pinch out in northern Wisconsin, placing Oronto strata directly on top of the pre-rift basement (Fig. 10–4). Southeast of Grand Marais, Minnesota, the Lake Superior syncline is deflected around the southern end of a similar ridge (Fig. 10–4). Stratigraphic relations indicate that White's Ridge and the Grand Marais Ridge remained topographically positive as the adjacent volcanic basins subsided. The volcanic flows pinch out gradually onto

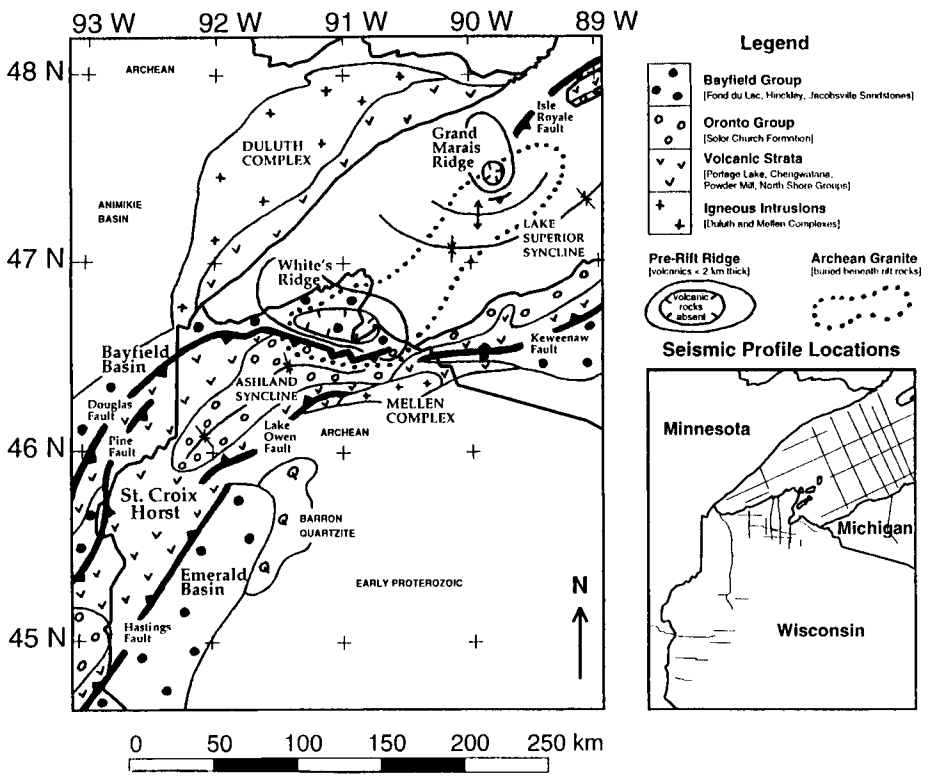

Fig. 10–4. Geologic map of the western Lake Superior region based on interpretation of seismic reflection profiles and gravity data. Smaller map shows the locations of the seismic profiles used in this study (after Allen et al., 1994).

the ridges, with no evidence for substantial normal faulting. Both ridges are characterized by intense, negative gravity anomalies (Plate 10–3).

The Douglas Fault defines the western margin of the St. Croix Horst (Plate 10–3, Plate 10–4, and Fig. 10–4). As this fault approaches Lake Superior, it bends east and follows the southern margin of White's Ridge. Displacement across the fault gradually decreases to the east until the fault is replaced by a fold near the eastern margin of White's Ridge. The seismic data also indicate that in western Lake Superior, the Isle Royale Fault gradually terminates ~40 km southwest of the Isle. Between the terminations of the Douglas and Isle Royale Faults, late-stage rift compressional forces resulted in folding rather than development of major reverse faulting. For example, the anticline north of the Lake Superior syncline (Fig. 10–4) trends parallel to the syncline and has a vertical relief of ~1 km.

In western Lake Superior, the rift's igneous and sedimentary rocks cannot fully account for the observed gravity signature. A northeast-striking, ~30 mGal negative anomaly (Fig. 10–5(c)) persists after the effect of the rift rocks (Fig. 10–5(b)) is removed from the observed gravity field (Fig. 10–5(a)). The trend, amplitude, and gradients of this anomaly suggest that it may be produced by a buried granite belt within the Archean greenstone-granite terrane that lies beneath the rift (Allen et al., 1993). As shown in Figure 10–4, the Douglas and Isle Royale Faults terminate as they approach the proposed granite belt, both pre-Keweenawan ridges occur above this structure, and the St. Croix Horst terminates at the southern margin of this feature. Therefore, this Archean

batholith might have acted as a buttress throughout the history of development of the rift, redirecting both the early tensional stresses and the late compressional stresses.

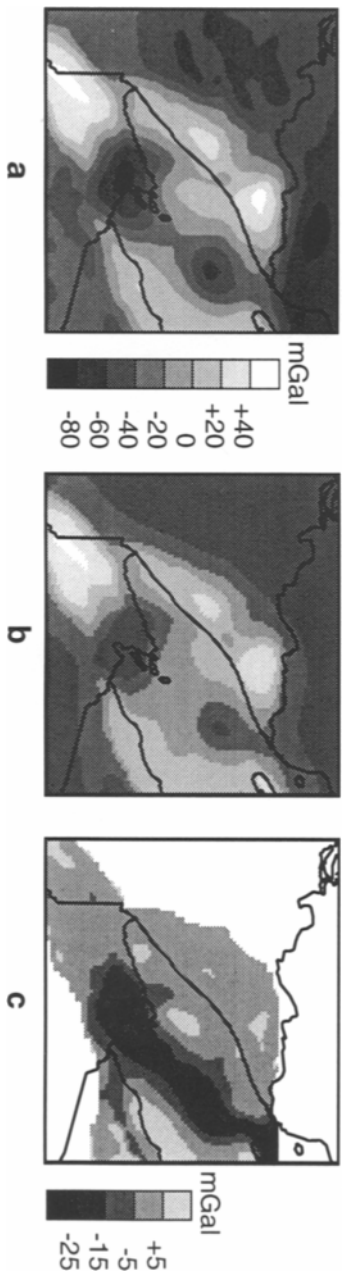

Fig. 10–5. Results of three-dimensional gravity modeling based on interpretation of seismic reflection data. Figs. 10–5a and 10–5b use the same gray scale. Values outside the Midcontinent Rift System are not shown. (a) Observed Bouguer gravity anomaly map. (b) Calculated gravity anomaly, based on the following densities (Mg/m^3): Bayfield Group: 2.40, Oronto Group: 2.65, Keweenawan volcanic rocks: 2.95, Pre-rift basement: 2.75. The assumed regional base level is -45 mGals. (c) Residual gravity anomaly map prepared by subtracting Fig. 10–5b from Fig. 10–5a. (After Allen et al., 1993.)

10.4.2. Central Lake Superior

Recent studies of wide-angle reflections and refractions obtained during the GLIMPCE seismic reflection experiments have provided information on the velocities and structure of the crust in central Lake Superior and confirm the current interpretations of the rift basin (Chan and Hajnal, 1989; Jefferson et al., 1989; Lutter et al., 1989; Meyer et al., 1989; Milkereit et al., 1990; Morel-a-l'Huisser and Green, 1989; Shay and Trehu, 1989; Trehu et al., 1991; Hamilton and Mereu, 1993). The subsidence required for the observed thickness of the Oronto Group and underlying volcanic flows has led Hutchinson et al. (1990) to suggest a stretching factor (b) of at least three. This estimate considers both thermal relaxation of the asthenosphere and removal of support from a mantle plume as it moved out of the region or dissipated.

The wide-angle data have also resulted in a major breakthrough in the study of deep-rift structures. Trehu et al. (1991) interpreted seismic data from GLIMPCE line A (Plates 10–3 and 10–4) using an iterative, forward modeling approach together with gravity modeling. Their interpretation shows a thickened crust and a lower crust of higher density and higher velocity beneath the rift. Hamilton and Mereu (1993) performed two-dimensional travel-time tomographic inversion on the same data from GLIMPCE line A and confirmed the presence of a thickened crust with a broad (~50 km wide) zone of high-velocity (7.0-7.2 km/s) lower crust beneath the axis of the rift. This zone, which is similar to the lower crustal model hypothesized for western Lake Superior, might be the result of high-velocity mantle derivatives in the lower crust.

The central and eastern Lake Superior segments of the MCR are separated by the Thiel Fault, a profound cross-structure that strikes NNE-SSW across Lake Superior from immediately east of the tip of the Keweenaw Peninsula (Plates 10–3 and 10–4). The fault occurs along the southeast edge of a buried

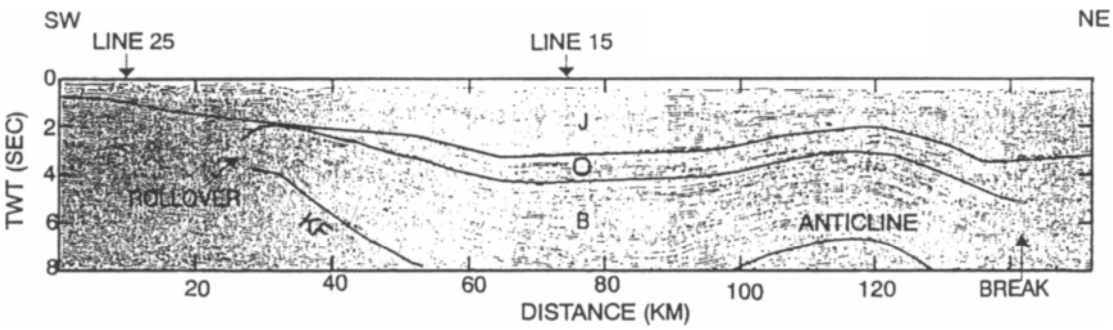

Fig. 10–6. Interpreted migrated seismic reflection record section of Grant-Norpac Inc./Argonne line 36. The Keweenawan units are identified as follows: J - Jacobsville sandstone or equivalents, O - Oronto Group, and B - Keweenawan basalts. KF - Keweenaw Fault (after Mariano and Hinze, 1994a).

Archean basement ridge which separates two volcanic basins in Lake Superior (Mariano and Hinze, 1994a). Cannon et al. (1989) interpret that the volcanic basin west of the fault is an asymmetric half-graben, whereas the basin on the east side of the fault is a symmetric graben. Gravity and magnetic modeling of the Thiel fault suggests that little if any thrusting occurred along it during the late-stage compressional event.

10.4.3. Eastern Lake Superior

A relatively symmetric cross-section of the MCR (Fig. 10–6) is interpreted along Grant-Norpac, Inc./ Argonne line 36 in eastern Lake Superior (Plates 10–3 and 10–4). Figure 10–7 shows the crustal section derived from combined seismic reflection interpretation and gravity modeling as well as modeling of the magnetic anomaly data (Fig. 10–8). The volcanic section is roughly 15 km thick with up to 10 km of overlying Oronto Group and Jacobsville Sandstone. The volcanic and sedimentary units are distinguished on the basis of their reflectivity (Fig. 10–6); there is no direct information to establish the contact between the units. An anticline, the Deer Park anticline, with a vertical relief of roughly 5 km, lies immediately east of the center of the basin (Plates 10–3 and 10–4). Stratigraphic relations, indicated in the seismic reflection data (Fig. 10–6), suggest that uplift of the anticline commenced during deposition of the Oronto Group sediments and was terminated before the completion of the Jacobsville Sandstone sedimentation. Presumably, the compression leading to the anticline was contemporaneous with the reverse movement along the southeastern extension of the Keweenaw fault; this fault represents the southwest margin of the volcanic basin in eastern Lake Superior. Reverse movement is also evident in the drag folding of the volcanic units (Fig. 10–6) at the western margin of the volcanic basin near kilometer 30. Additional structural complexity on this reverse fault has been observed farther northwest toward the Keweenaw Peninsula by Mariano and Hinze (1994a). They interpret the edge of the volcanic rocks as a low-angle splay off of the main reverse fault on the basis of the seismic reflection, gravity, and magnetic anomaly data. Previous investigators (Meshref and Hinze, 1970; Behrendt et al., 1988; Cannon et al., 1990) have also observed splays of the main reverse fault that merge with the main fault zone at depth in geophysical/geological models.

A fault is indicated at the eastern margin of the Deer Creek anticline, near kilometer 140 on Figure 10–7, by the disruption of the volcanic reflections. Mariano and Hinze (1994a) have interpreted this as a near-vertical fault, the Crisp Point fault, that developed late in Keweenawan time. Using seismic reflection profiles and gravity and magnetic anomaly

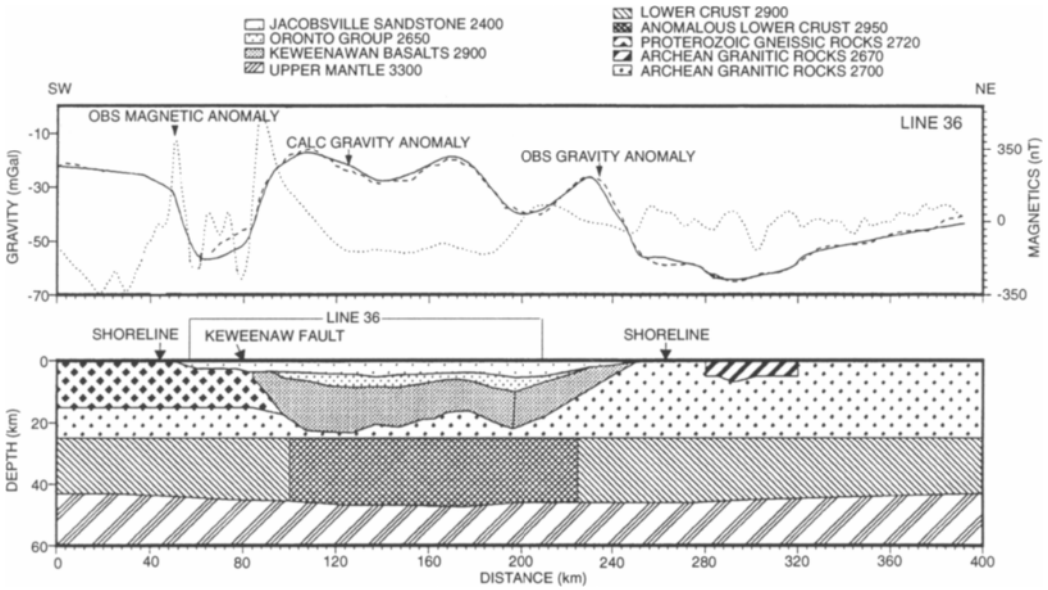

Fig. 10–7. Two-and-one-half-dimensional Bouguer gravity anomaly model of extended seismic reflection line shown in Fig. 10–6. Densities are indicated in kg/m^3 (after Mariano and Hinze, 1994b).

data, they have traced the fault northwesterly, parallel to the axis of the anticline to 50 km due south of Michipicoten Island (Fig. 10–2), where the fault turns sharply to the west and continues to the tip of the Keweenaw Peninsula (Plates 10–3 and 10–4).

As shown in Figure 10–8, only the upper 20% of the volcanic section is normally magnetically polarized. Similar values are modeled northwest to the Portage Lake Volcanics on the Keweenaw Peninsula. As a result, we infer that the normally polarized volcanic rocks are equivalent to the Portage Lake Volcanics and that the reversely polarized lower basalts are older than the reversal at ~1100 Ma. Modeling of the magnetic anomaly by Mariano and Hinze (1994b) indicates that the magnetization of the basalts extends to depths in excess of 20 km. Apparently the magnetization of these volcanic rocks has not been significantly altered by burial metamorphism or hydrothermal alteration.

South of Michipicoten Island in central eastern Lake Superior in the vicinity of the Crisp Point fault, the gravity and magnetic anomalies are inversely correlated (Plates 10–3 and 10–4), in contrast to their common direct correlation over much of Lake Superior. The inverse correlation coincides with the maximum thickness of a low-reflectivity zone on GLIMPCE line F (Fig. 10–9). This unit is interpreted by Mariano and Hinze (1994b) as a magnetic, low-density felsic volcanic unit that was extruded as the basaltic volcanism terminated.

Using gravity modeling constrained by seismic data, Mariano and Hinze (1994b) also interpreted a broad zone of high-density lower crust beneath eastern Lake Superior. This zone is similar to the lower crust imaged beneath central Lake Superior (Trehu et al., 1991; Hamilton and Mereu, 1993) and is believed to be a result of a combination of intrusion and underplating. In addition, Samson and West (1992) reprocessed the seismic reflection data of GLIMPCE line F in eastern Lake Superior and found a complex crust-mantle transition zone which they interpreted as being consistent with underplating of the crust during the rifting process.

Mariano and Hinze (1994a) note that there is virtually no attenuation of the rift structure in southeastern Lake Superior. Therefore, the transition be-

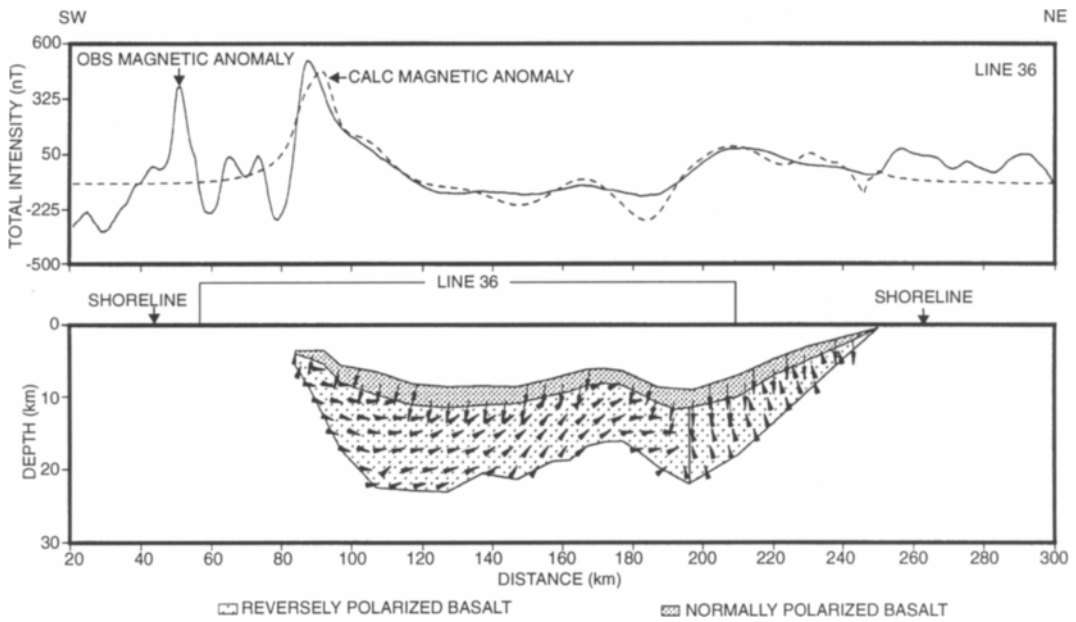

Fig. 10–8. Two-dimensional forward magnetic model of extended seismic reflection line shown in Fig. 10–6 and 10–7. Arrows indicate direction of total magnetization in the plane of the profile. The non-magnetic sedimentary strata are not shown (after Mariano and Hinze, 1994b).

tween the Lake Superior basin and the eastern limb of the MCR must occur south of Lake Superior. This transition is poorly understood due its burial beneath the Phanerozoic rocks of the Michigan basin and a lack of seismic reflection data in the eastern Northern Peninsula of Michigan. However, the rift narrows abruptly to the south in the eastern limb, to one-third of its width in eastern Lake Superior.

10.5. Structure of the western and eastern limbs of the rift

The structures of the eastern and western limbs of the MCR are not as well known as the Lake Superior segment due to a cover of Phanerozoic sedimentary strata and fewer deeply-penetrating seismic reflection profiles. Over the past decade, however, several new seismic profiles have become available over the limbs of the rift in the Southern Peninsula of Michigan, Wisconsin, Minnesota, Iowa, and Kansas. These data, together with gravity and magnetic modeling and direct information from an occasional deep drill hole (Fig. 10–1), have shown that the stratigraphic units and structure of the limbs of the MCR are essentially identical to those in the Lake Superior segment (Hinze et al., 1992).

10.5.1. Western limb

The interpretations of Chandler et al. (1989) in Minnesota and Wisconsin and Anderson (1990b) in Iowa have been particularly informative in understanding the nature of the western limb. These studies reveal that the rift structure consists of a central uplifted basaltic horst, bound by reverse faults and flanked by marginal clastic sedimentary basins (Fig. 10–10). On the basis of a combined seismic reflection and gravity investigation, Allen et al. (1994)

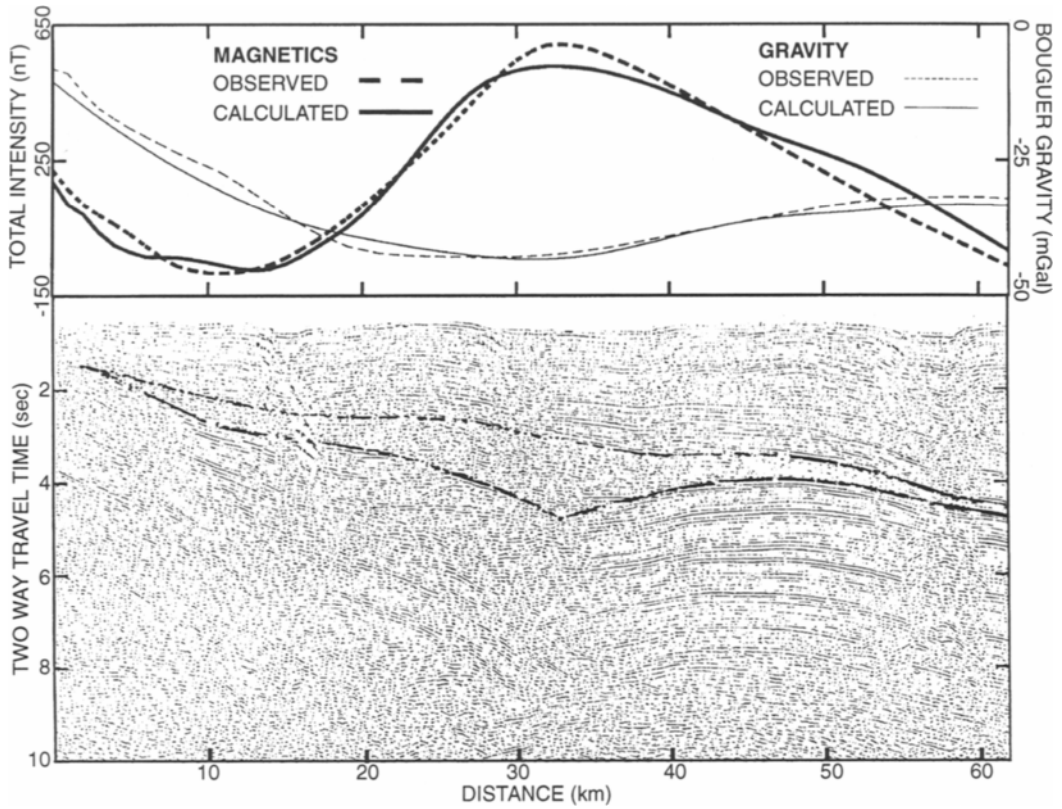

Fig. 10–9. Final stack seismic reflection record section detail of GLIMPCE line F in east-central Lake Superior showing the outline of the interpreted felsic flow used in the forward gravity and magnetic models. The observed and calculated Bouguer gravity and total intensity magnetic anomalies are shown (after Mariano and Hinze, 1994b).

suggest that the strata in the eastern marginal basin in Wisconsin, which attain a maximum thickness of 6 km, are most likely correlated with the Bayfield Group. Farther south along the western limb in Kansas, drilling has shown that Keweenawan igneous rocks (Berendsen et al., 1988; Van Schmus et al., 1990) occur above late-stage clastic sedimentary rocks that formed in sag basins over the rift. This inversion of the normal Keweenawan sequence was shown by Woelk and Hinze (1991), using reprocessed COCORP seismic reflection data and gravity and magnetic modeling, to be a result of high-angle reverse movement, along an originally normal fault (Fig. 10–11).

In Minnesota, a statewide high-resolution aeromagnetic survey (Chandler, 1991) was conducted by the Minnesota Geological Survey. These data, which were collected at a terrain clearance of 150-200 meters and a flight line separation of 400-500 meters, have provided a clearer image of the MCR in Minnesota. Figure 10–12(a) is a shaded relief magnetic map of the MCR, and Figure 10–12(b) is an interpretive map based on the aeromagnetic data. Areas underlain by (essentially non-magnetic) Keweenawan sedimentary rocks are characterized by subdued magnetic patterns, whereas (magnetic) Keweenawan volcanic rocks are often associated with intense short-wavelength anomalies. Of particular interest are a series of alternating positive and

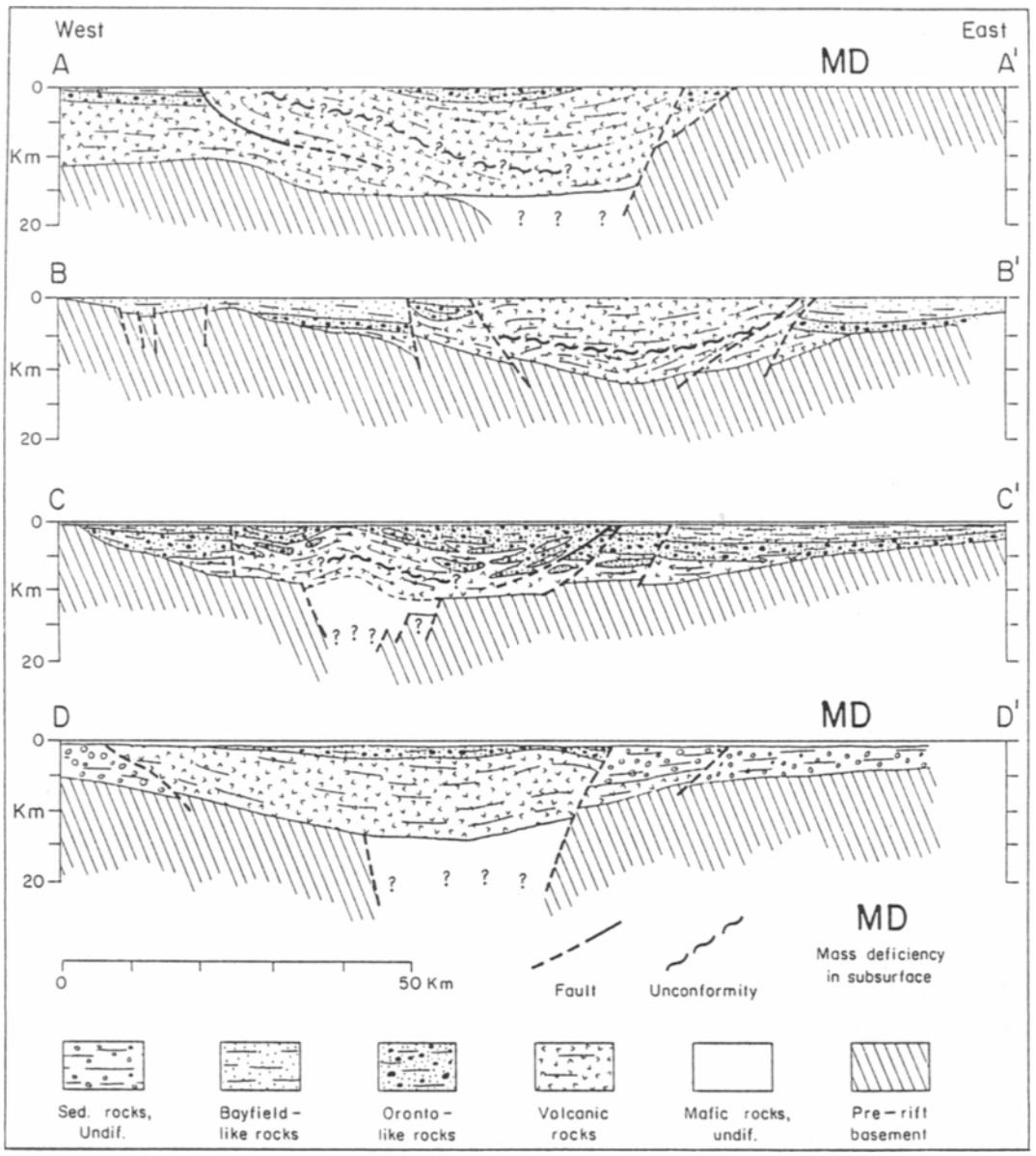

Fig. 10–10. Cross-sections of the MCR based on combined interpretation of seismic reflection, gravity, and magnetic data. A - Wisconsin, B - Minnesota and Wisconsin, C - Minnesota, D - Iowa (after Chandler et al., 1989).

negative high-frequency linear anomalies (Fig. 10–12(a)). These anomalies are continuous for up to 50 km and, where the volcanic rocks are exposed, trend parallel to the strike of the volcanic beds. This correlation has been useful for mapping packages of volcanic rocks in the subsurface and for identifying internal structures within the St. Croix Horst (Allen and Chandler, 1992). The most prominent magnetic anomalies are associated with reverse faults, such

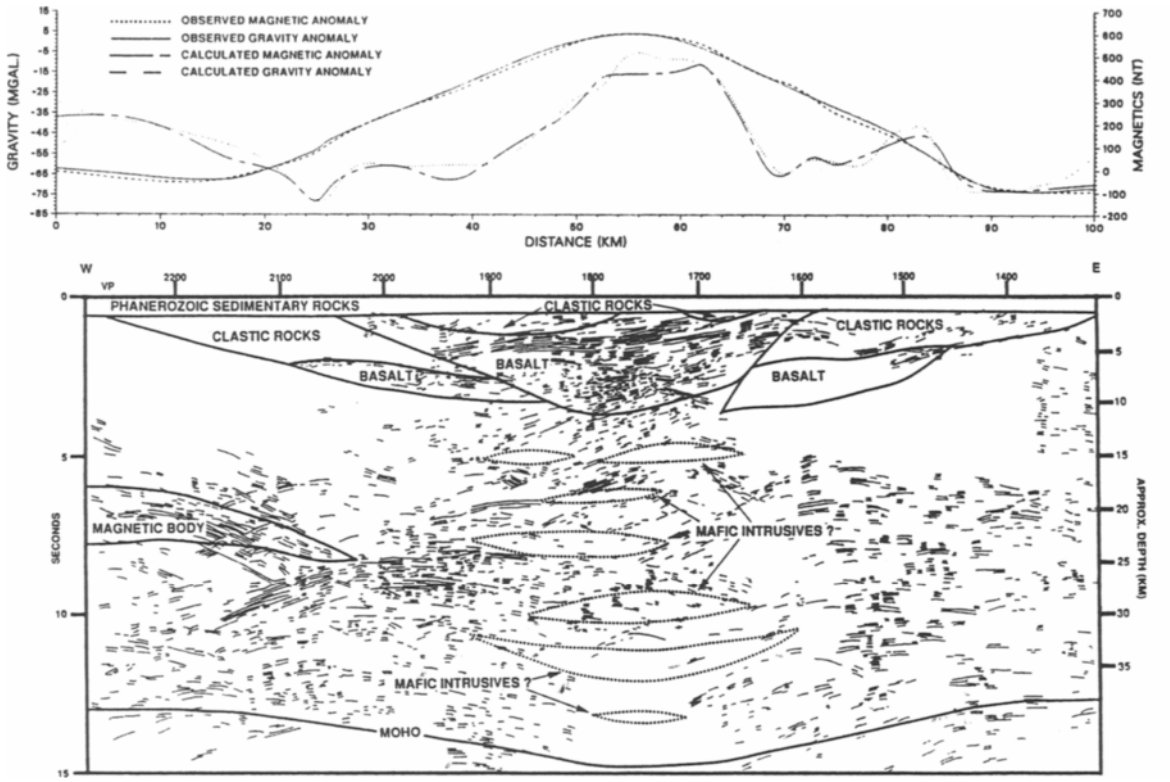

Fig. 10–11. Crustal cross-section (W-E) of the Midcontinent Rift in northeastern Kansas based on gravity modeling constrained by magnetic anomaly modeling and seismic reflection profiling (after Woelk and Hinze, 1991).

as the Douglas Fault (Fig. 10–12(b)), that juxtapose volcanic and sedimentary rocks along the margins of the St. Croix Horst. In addition, abrupt terminations of the linear anomalies are used to identify the Pine Fault (Fig. 10–12(b)), a fault within the St. Croix Horst that strikes parallel to the Douglas Fault.

A deep well just east of the Pine Fault (Fig. 10–12(b)) penetrated 0.98 km into the St. Croix Horst. With the exception of relatively minor interflow sedimentary units, the interval consists of basaltic volcanic rocks. The entire interval was cored, providing a unique opportunity to investigate the magnetic properties of the rift's volcanic rocks and therefore the origin of the short-wavelength linear magnetic anomalies. Figure 10–13 is a magnetic susceptibility log of the well, obtained by taking measurements on the core using a hand-held susceptibility meter. The log indicates two broad intervals of relatively high susceptibility separated by regions of low susceptibility, only one of which is produced by interflow sedimentary rocks. Measurements of remanent magnetization (NRM) indicate a similar pattern of alternating high and low NRM intensity. The volcanic rocks have intense remanent magnetizations, with an average Q (ratio of remanent to induced magnetization) of nearly 5. The variations in susceptibility and NRM intensity of the volcanic rocks are not correlated with obvious physical or chemical alteration, suggesting that they may be related to magma chemistry. Variations in magnetization such as those shown in Figure 10–13 are a likely candidate for the source of the observed short-wavelength linear aeromagnetic anomalies (Fig. 10–12(a)). Magnetic modeling indicates that the dipping

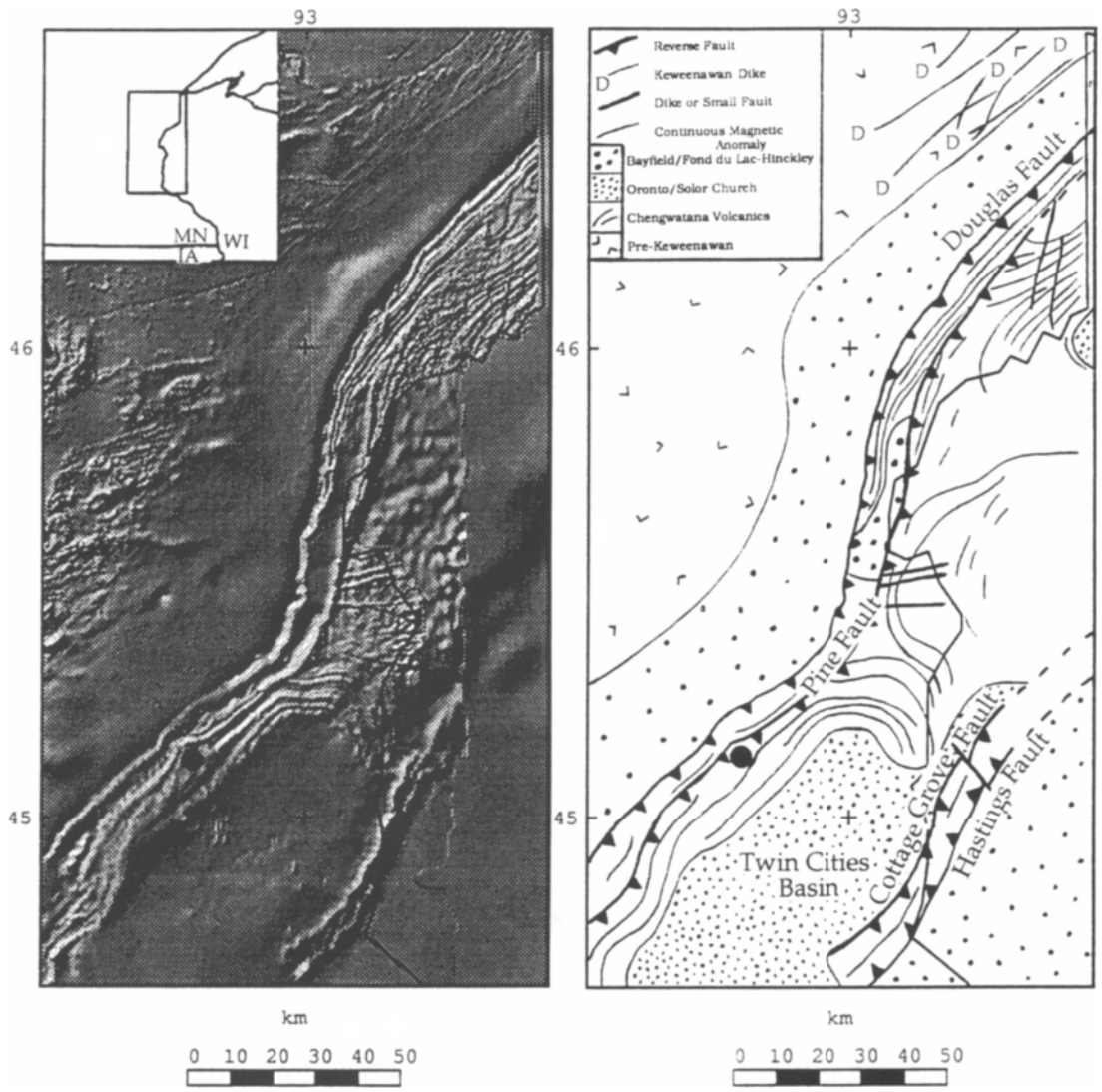

Fig. 10–12. Interpretation of aeromagnetic data in east-central Minnesota. (a-left) Shaded relief magnetic map. The sun illumination is from the northwest. (b-right) Interpretive map of the MCR based on aeromagnetic data. The location of the deep well is indicated. (After Allen and Chandler, 1992.)

layers of alternating strong and weak magnetization are capable of reproducing the observed magnetic anomaly signature.

Green (1991) has performed teleseismic tomographic inversion on the western limb of the rift in Wisconsin and Minnesota. He found that the lower crust in the range from 28-46 km depth shows higher velocities beneath that rift than in the adjacent crust. Beneath 46 km, he found a slightly lower velocity beneath the rift axis, which might be the result of a thickened crust beneath the MCR.

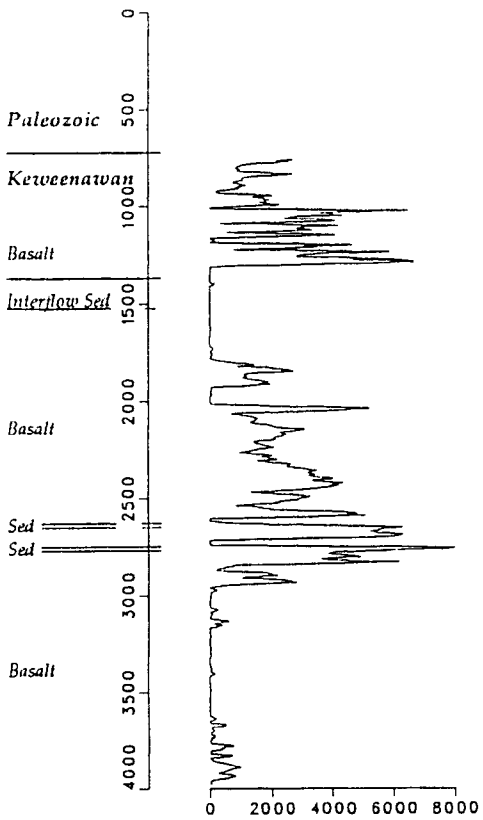

Fig. 10–13. Magnetic susceptibility (x10-6 emu/cc) vs. depth (ft) for the Northern Natural Gas well near Osseo, Minnesota (after Allen and Chandler, 1993).

The structure of the western limb of the rift has been traced by Yarger (1985) in magnetic data from central Kansas to the Oklahoma border. In a more speculative manner Nixon (1988) suggests that the rift extends into north-central Oklahoma on the basis of gravity modeling and geologic data. Based on isotopic dating of igneous rocks, surface geology, and geophysical anomalies, Keller and Adams (1992) suggest that the MCR may extend even farther into west Texas and New Mexico.

10.5.2. Eastern limb

The extension of the MCR from southeastern Lake Superior across the Northern Peninsula of Michigan and into the Southern Peninsula (Fox, 1988; Cannon et al., 1991) is evident in the continuity of the gravity anomaly (Oray et al., 1973; Hinze et al., 1975). However, the lack of negative gravity anomalies on either side of the positive anomaly, together with available basement drillhole data and seismic reflection profiling, suggests the absence of late-stage sedimentary basins along the margins of the central rift basin over much of its length in Michigan's Southern Peninsula. Furthermore, a significant length of the rift has no correlative magnetic anomaly, suggesting either destructive interference between normally and reversely polarized basalts within the rift basin or a lack of basalts. The latter scenario (i.e., lack of basalts) requires that the positive gravity anomaly is produced solely by deep intrusions which have a minimal magnetic signature.

Reverse faulting is equivocal in the Michigan segment of the rift. Seismic reflection profiling (Zhu and Brown, 1986; Fox, 1988), however, does indicate that the Keweenawan formations were folded. Although the age of the folding cannot be precisely determined from the seismic data (because of interference due to strong multiple reflections from the overlying Phanerozoic sedimentary strata of the Michigan basin), it is interpreted that folding is the result of the same late-stage compressional forces that produced reverse faulting elsewhere along the MCR. This compression may be associated with thrusting within the Grenville orogen to the east. The structural relations between the eastern extremity of the rift in southeastern Michigan and the western limit of the coeval (1.1 Ga) Grenville orogeny remain an open question, but the geophysical anomalies suggest that the extreme southeastern end of the rift, near the Canadian border (Fig. 10–1), is buried by Grenvillian rocks thrust to the west. Similar thrusting is observed elsewhere along the Grenville Front (Green et al., 1988, 1989; Pratt et al., 1989).

Gravity and magnetic anomalies have been used to postulate an extension of the eastern limb of the rift beyond the limit in southeastern Michigan that is shown in Figure 10–1. North-south striking positive gravity anomalies in southern Ohio, which continue south into Kentucky and Tennessee (Plate 10–1), have been interpreted as the indication of a possible continuation of the eastern limb of the MCR (e.g., Lyons, 1970; Keller et al., 1982; Dickas et al., 1992). This hypothesis recently has been promoted

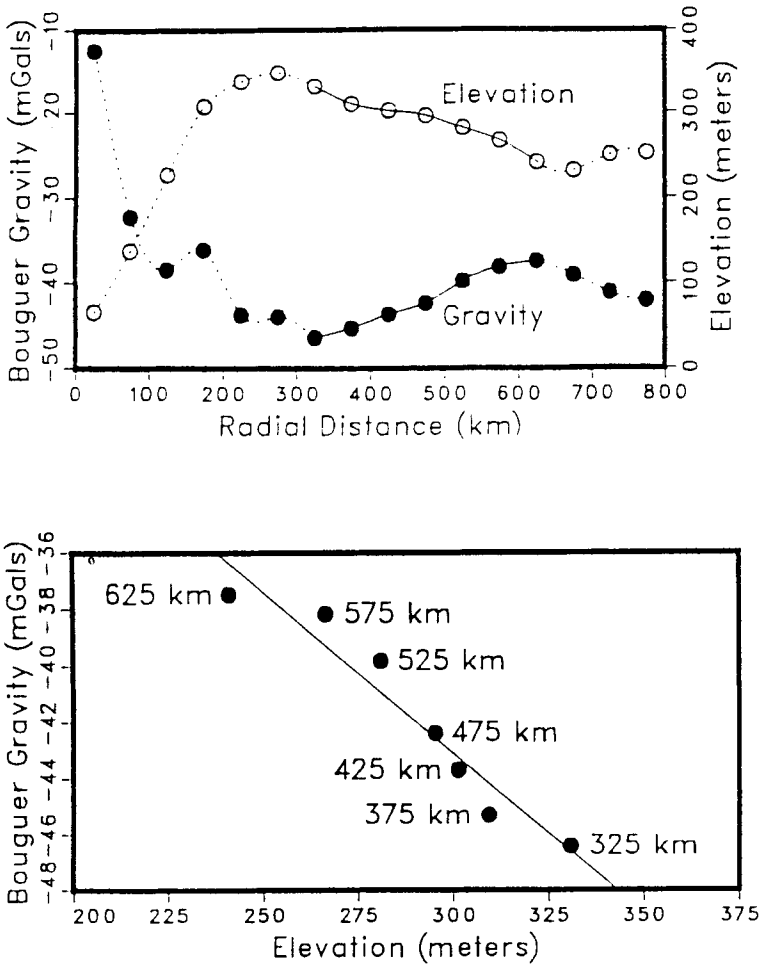

Fig. 10–14. Gravimetric and topographic relations in the Lake Superior region. (a) Average Bouguer gravity anomaly versus average elevation for radial distances between 300 and 650 km. Slope of line is -114 ± 29 mGals/km, compared to an expected value of -112 for isostatic equilibrium. (b) Average Bouguer gravity anomaly and elevation versus radial distance from a central point in Lake Superior. (After Allen et al., 1992.)

by drilling of Precambrian clastics in southwestern Ohio west of the interpreted position of the Grenville front (Shrake et al., 1991). However, these positive gravity anomalies lie within the Grenville Province, east of the Grenville Front (Fig. 10–1). Recent COCORP seismic reflection profiling and gravity modeling across a central Ohio profile (Pratt et al., 1989; Sunwoo, 1989) indicate that the positive gravity anomalies are actually associated with lower crustal rocks thrusted into place along the Grenville Front.

10.6. Regional rift structures

Combined analysis of gravity anomaly and topographic data by Allen et al. (1992) in the Lake Superior region suggests a broad-scale lithospheric feature that may be a remnant of the proposed Keweenaw hotspot (mantle plume) (Hutchinson et al., 1990). A broad, low-amplitude topographic high centered on Lake Superior, the so called Lake Superior Swell (Dutch, 1981b), is associated with a regional negative Bouguer gravity anomaly. Allen et

al. (1992) have shown that the average gravity anomaly value increases and the average elevation decreases in a linear manner over a radial distance of 300 to 650 km (Fig. 10–14(a)) from the approximate center of Lake Superior. The elevation/gravity anomaly relation suggests that the feature is in or approaches isostatic equilibrium (Fig. 10–14(b)). Allen et al. suggest that the correlated gravity and topographic anomalies are vestiges of the magmatic activity associated with the 1.1 Ga rifting event. The mass deficiency may represent a broad underplated region at the base of the crust, a modified upper mantle, or both. Underplating may result from either upper mantle or plume-derived magma that was trapped at the base of the crust. Alternatively, extraction of basaltic melts from either the lithospheric mantle or plume head, which subsequently became part of the lithosphere, may lead to a less dense upper mantle because the density of the depleted mantle may decrease due to an increased MgO/FeO ratio or loss of dense garnets (Boyd and McCallister, 1976; Oxburgh and Parmentier, 1977).

Evidence of an isolated Keweenawan uplift in northern Wisconsin and the Northern Peninsula of Michigan has been presented by Peterman and Sims (1988). They mapped a region of anomalously low (~1.1 Ga) Rb-Sr ages in the older Archean and Early Proterozoic rocks of the Wisconsin arch. They interpret these ages as representing closure of the Rb-Sr isotopic system as the region was arched upward, rapidly eroded, and cooled beneath the blocking temperature. They suggest that the uplift was a forebulge caused by loading of the crust by the dense igneous rocks of the MCR. However, flexural modeling of the rift (Peterman and Sims, 1988; Nyquist and Wang, 1989) does not satisfy the amount of uplift required by the model of Peterman and Sims.

10.7. Rock volumes, ages, and rates

An enormous volume of igneous material was added to the crust during the rifting episode. For example, seismic reflection data suggest that the present volume of volcanic rocks is approximately ~1 million km^3. In addition, Keweenawan feeder dikes occur at distances of up to 200 km from the rift axis (Green et al., 1987), indicating that additional volcanic rocks were once present and have been subsequently eroded from the margins of the MCR. As a result, Cannon (1992) estimates that the original volume of volcanic flows was at least 2 million km^3. Moreover, this volume does not consider the amount of mantle-derived magma that was trapped in the crust and never extruded.

Recent U-Pb age dating of the rift's igneous rocks indicates that this enormous volume of magma was emplaced during a relatively short period of time. The volcanic and plutonic rocks of the Lake Superior region have ages between 1109 and 1087 Ma (e.g., Van Schmus et al., 1982; Davis and Sutcliffe, 1985; Palmer and Davis, 1987; Davis and Paces, 1990; Heaman and Machado, 1992; Miller, 1992; Van Schmus, 1992; Paces and Miller, 1993). Moreover, Paces and Miller (1993) suggest that most of the magmatism in the Lake Superior region occurred during two major pulses from 1109 to 1106 Ma and from 1099 to 1094 Ma. A similar U-Pb age (1097.5±3 Ma) is reported for gabbro from a well in northeast Kansas (Van Schmus et al., 1990), suggesting that there is no major age progression along the length of the rift.

Using this information, magma production and lava accumulation rates can be crudely estimated. For example, assuming that a total of 2 million km^3 of volcanic rocks were erupted within 20 million years, an average magma production rate of 0.10 km^3/yr is suggested. Assuming a thickness of 20 km of volcanic strata beneath Lake Superior, an average accumulation rate of 1.0 mm/year is implied.

More precise estimates can be made using by combining high-precision U-Pb isotopic ages of specific volcanic units with measured stratigraphic intervals. For example, Davis and Paces (1990) calculated an average accumulation rate of 1.3 mm/yr and an average interflow repose period of 30 ka for the Portage Lake Volcanics of the Keweenaw Peninsula. In addition, they estimated a magma production rate of 0.02-0.05 km^3/yr, which is of the same order of magnitude as production rates for other rifts and hotspot regimes (e.g., Iceland, Hawaii, and Columbia River Basalts). Both the magma production rate and the average accumulation rate are consistent with the crude estimates presented above.

Davis and Paces (1990) also dated a basalt flow from within the Copper Harbor Conglomerate and estimated an accumulation rate of approximately 0.16 mm/yr for the lower-most Oronto Group (in contrast to a rate of 1.3 mm/yr for the underlying volcanic sequence), suggesting that the rate of subsidence of the rift depression decreased drastically concurrently with the cessation of the major volcanic pulse and the onset of sedimentation (Cannon, 1992). Assuming that this rate is representative of the Lake Superior basin, the implication is that the observed ~10 km thickness of rift sediments beneath Lake Superior accumulated over a period of ~62 million years (1087 to 1025 Ma). However, Cannon et al. (1990) analyzed Rb-Sr data from Michigan's Northern Peninsula and northern Wisconsin and interpreted that reverse movement occurred at ~1060±20 Ma along the Marenisco Fault, a fault which they interpreted as a splay off of the Keweenaw fault. Geological evidence indicates that the thrusting occurred near the end of sedimentation; therefore, a greater sedimentation rate, roughly 0.37 mm/yr (10 km / 27 m.y.), is required to account for the accumulation of the majority of the rift sediments prior to the reverse faulting. Perhaps the sedimentation rate was greater along the axis of the Lake Superior syncline than it was on the Keweenaw Peninsula where Davis and Paces (1990) made their estimate.

Paleomagnetic data are often useful for estimating relative ages of the rift's rocks (Van Schmus et al., 1982; Green, 1982; Halls and Pesonen, 1982; Palmer and Halls, 1986; Palmer and Davis, 1987). A change in polarity from reversed to normal that has been dated at ~1100 Ma (Davis and Paces, 1990; Paces and Miller, 1993) is widely observed in the Lake Superior region and, thus, is particularly useful as a stratigraphic correlation tool. However, evidence for another reversal period (Palmer, 1970; Robertson, 1973) of probable short duration in the Mamainse Point sequence (Klewin and Berg, 1991) and in the lower part of the Powder Mill Volcanics (Books, 1972) complicates the use of magnetic polarity as a stratigraphic correlation tool.

Mariano and Hinze (1992, 1994b) relied on magnetic polarity to estimate magma production rates in eastern Lake Superior. Their magnetic models, which were tightly constrained by seismic reflection and gravity data, suggest that the lower 15 km of the volcanic section is reversely magnetized and was therefore extruded during the reversed polarity epoch from ~1108 to 1100 Ma (Davis and Sutcliffe, 1985; Klewin and Shirey, 1992; Van Schmus, 1992). The resulting accumulation rate is similar to the rate obtained by Davis and Paces (1990) for the normally polarized, 1095 Ma Portage Lake Volcanics.

Allen and Chandler (1993) measured remanent magnetization for samples from the deep well (Fig. 10–12) into the St. Croix Horst in Minnesota, and determined that all of the samples were normally polarized. The volcanic strata penetrated by this well lie roughly in the middle of the volcanic section, implying that a substantial portion of the volcanic section is normally polarized. Subsequent magnetic modeling of the magnetic anomaly along a profile through the well, in addition to profiles elsewhere along the St. Croix Horst, suggests that the vast majority of the volcanic rocks of this segment of the rift's western limb are normally polarized. The implication is that the volcanic rocks along the St. Croix Horst may be slightly younger than those beneath eastern Lake Superior. Farther south along the western limb of the rift, however, Van Schmus et al. (1990) have found that the volcanic rocks obtained from a deep drill hole are reversely magnetized. Additional magnetic polarity measurements and magnetic modeling along the entire length of the rift are needed to resolve issues concerning the relative ages of the different segments of the MCR.

10.8. Origin of the Midcontinent Rift System

During the past decade, the acceptance of a rift origin for the Lake Superior basin and the midcontinent geophysical anomaly has been a critical step forward in understanding the tectonic evolution of the MCR. However, this recognition fails to clarify the mechanics of the causative process and the ultimate origin of the rift. Numerous processes have been suggested as the cause of continental rifts. In general, these processes fall into one of two categories. There are active mechanisms in which a thermal perturbation of the mantle (a plume) causes a disturbance within the overlying lithosphere, and

passive mechanisms, where plate interactions cause regional tension in the lithosphere (Baker and Morgan, 1981). Proposed origins of the MCR have invoked both mechanisms.

Numerous authors have suggested an active mechanism involving an upper mantle perturbation associated with an asthenospheric mantle plume or hotspot (e.g., Hinze et al., 1972; White, 1972; Green, 1983; Hutchinson et al., 1990; Cannon and Hinze, 1992). The early papers on this subject were largely speculative, without strong, quantitative support. This situation has changed, however, with the availability of improved deep seismic reflection data and intensive isotopic and geochemical analyses of the rift's volcanic rocks. These investigations suggest that the MCR is analogous to rifts associated with passive continental margins and mantle plumes (hotspots). The observed high volume (Behrendt et al., 1988; Cannon et al., 1989; Chandler et al., 1989; Hutchinson et al., 1990; Cannon, 1992) and rate (Davis and Paces, 1990; Cannon, 1992) of volcanism, the lack of an associated pervasive dike swarm with a consistent strike (Cannon and Hinze, 1992), the inferred extension (Chandler, 1983; Hutchinson et al., 1990), and the isotopic character of the Keweenawan volcanic rocks (Paces and Bell, 1989; Hutchinson et al., 1990; Nicholson and Shirey, 1990; Klewin and Shirey, 1992) support a mantle plume origin for the MCR. Hutchinson et al., (1990) discuss the geochemical and geophysical evidence for the origin of the MCR with a hot asthenospheric plume, which they term the 'Keweenaw hotspot', and the geologic implications of this interpretation. It is not clear, however, how this model can account for the necessary tension to produce the observed extension associated with the MCR.

Klewin and Shirey (1992) suggest that the lithospheric origin for the early basalts of the MCR, based on their isotopic and trace element geochemistry, indicate that a plume was not responsible for the initiation of the rifting event. Moreover, the overlap in time between the nearby Grenville orogeny and the 1100 Ma MCR has suggested a cause and effect relation related to a passive mechanism (e.g., Hinze and Wold, 1982; Van Schmus and Hinze, 1985; Gordon and Hempton, 1986). Cambray (1988) has suggested a passive origin wherein the opening and closing vectors of the MCR are restricted to an approximately north-south direction. However, the consistency of structures along the length of the rift and the lack of observed strike-slip motion on the limbs of the rift do not support the largely transtensional forces on the limbs of the rift predicted by this model. The significance of the relation between the MCR and the Grenville orogeny remains elusive, as does the source of the deviatoric tension that caused the MCR. None of the proposed mechanisms for tensional forces, such as bending or membrane stresses or drag on the base of the lithosphere, provides a satisfactory explanation for the available evidence. Resolution of this problem awaits further studies.

Uplifts appear anomalous in a rift regime, although they are observed in other continental rifts that have undergone regional compression (Milanovsky, 1981). The uplifts along the MCR are unusual in that they occur throughout the rift, regardless of rift orientation. We suggest that this origin is related to regional compressional forces associated with the east-to-west thrusting within the Grenville orogen immediately to the east of the MCR (Van Schmus and Hinze, 1985; Cannon, 1994). Van Schmus (1992) indicates that the peak of the Grenville orogeny was from 970 to 1030 Ma (Schärer and Gower, 1988). These regional forces, acting upon the thermally-weakened crust of the rift, could have reactivated the normal faults as high-angle reverse faults and also produced arching. Regional compression may also explain the sudden cessation of extension and the fact that the rift did not proceed to split divide the proto-North American continent, despite the nearly complete rupture of the crust.

10.9. Evolution of the Midcontinent Rift

10.9.1. Pre-Keweenawan influences upon the evolution of the MCR

Several lines of evidence suggest that pre-Keweenawan structures played an important role in shaping the evolution of the MCR. In western Lake Superior, for example, several structural anomalies of the rift are spatially correlated with the interpreted buried Archean granite belt (Fig. 10–4). The terminations of the Douglas and Isle Royale Faults, the

termination of the St. Croix Horst, and the presence of White's Ridge and the Grand Marais Ridge suggest that this ancestral feature played a significant role in the evolution of the MCR.

In eastern Lake Superior, Mariano and Hinze (1994a) note that transverse structures in the Lake Superior basin are parallel to the prevalent tectonic grain in the older rocks beyond the margins of the MCR. They suggest that these rift structures may have been in part controlled by pre-existing crustal features within the Archean basement. In addition, ancestral faults in the Archean rocks east of Lake Superior were reactivated as cross-faults to produce the anomalous structure associated with the basalt exposures on Mamainse Point (Fig. 10–2; Manson and Halls, 1992).

The evolution of the MCR may have been influenced by even broader structures. For example, the Lake Superior basin is both wider and deeper than the rift basins beneath the eastern and western limbs of the MCR. Interestingly, the Lake Superior basin formed in the Archean Superior Province, whereas the limbs formed in younger Proterozoic terranes to the south. Differences in crustal strength and thickness may be responsible for the contrasting rift structures that are observed in these two terranes (Klasner et al., 1982). It has also been suggested that the segmented pattern of grabens, which developed early in the history of the rift, may have been controlled by old zones of weakness that were reactivated by the rifting process (e.g., Weiblen and Morey, 1980; Mooney and Morey, 1981; Klasner et al., 1982).

10.9.2. Keweenawan evolution of the MCR

When discussing the evolution of the MCR, it is useful to portray the development in a series of cross-sections of the lithosphere through time (Hinze et al., in press). We present our current ideas of the evolution of the rift in Figure 10–15. These cross-sections are simplified, and no attempt is made to illustrate the plan view of the rift. The portrayed series of 'snapshots' of the lithosphere of the MCR region around 1.1 Ga is speculative and highly generalized; modifications to the sections are caused by local igneous events and structural disturbances, deflections of regional forces, and variations in the strength and other physical properties of the lithosphere. The diagrams generally represent the culmination of a particular episode in the development of the rift, and absolute ages are applied to the diagram to the extent possible. A brief description of these episodes follows.

As suggested by the model studies of mantle plumes by Griffiths and Campbell (1991), broad domal uplifts may occur at an early stage in the rifting process, when active rifting predominates as the ascending plume spreads out at the base of the lithosphere. Such a domal uplift is associated with, for example, the East African Rift. Although evidence for early regional upwarp is subtle in the MCR, we hypothesize that the rift was initiated with a broad, domal isostatic uplift over an ascending asthenospheric plume at ~1110 Ma (Fig. 10–15(a)). Convectional movements within the head of the mantle plume may have caused extensional forces, or they may have had an external origin.

Evidence indicates that the earliest rocks of the MCR were deposited in a broad sag basin on a positive topographic surface. Therefore, we propose that at ~1108 Ma (Fig. 10–15(b)), extensional forces reached a magnitude which, together with thermal weakening of the lithosphere, initiated a thinning or necking of the crust and upper mantle. As the head of the mantle plume approached the base of the lithosphere, it spread laterally, and the crest of the uplift subsided (forming the broad sag basin) while the distal portions continued to rise. Clastic sediments were deposited in this basin at ~1108 Ma. Shortly thereafter, portions of the upper mantle were melted by the thermal pulse of the rising plume. The resulting tholeiitic magmas rose through developing tensional cracks in the lithosphere. Evidence suggests that this early-stage volcanism and the associated feeder dikes were much more widespread than the present lateral extent of the rift (Green et al., 1987).

The head of the plume reached the base of the lithosphere (Fig. 10–15(c)) and continued to spread out laterally (~1100 Ma). Major extension led to additional thinning of the lithosphere, both crust and mantle, and the development of normal faults and associated grabens along the present axis of the rift. Extensional forces produced faulting in the brittle, upper crust which, in some segments of the MCR,

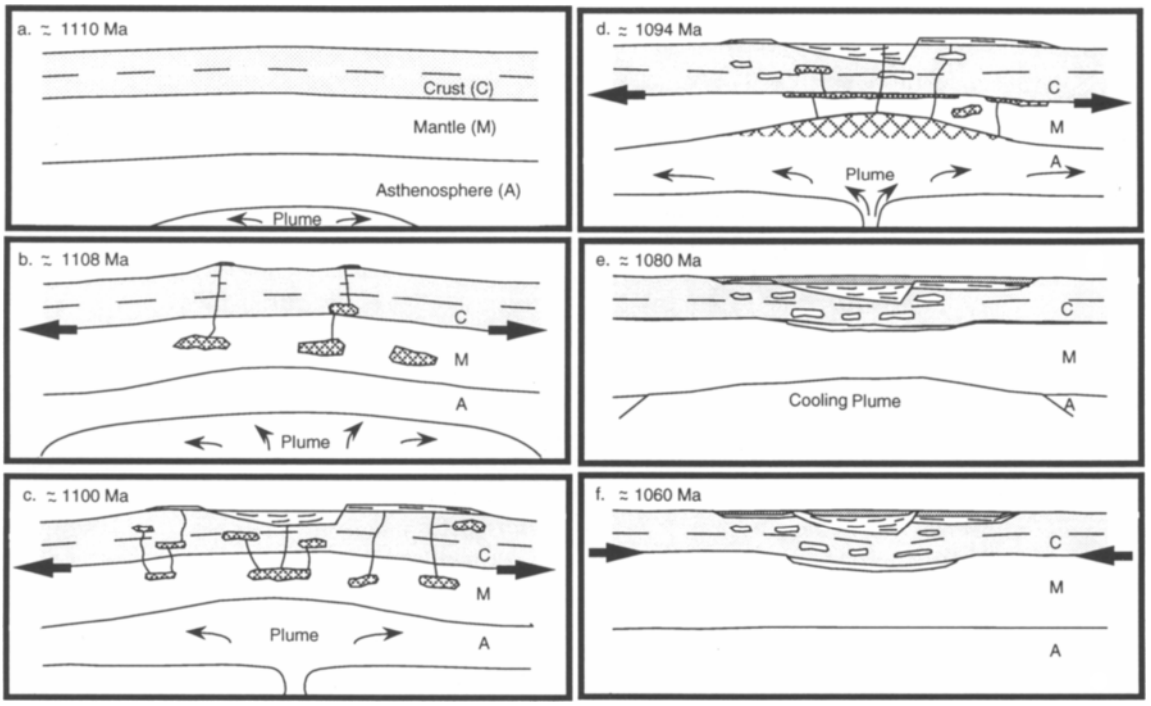

Fig. 10–15. Diagrammatic sketches of lithospheric cross-sections illustrating the magmatic/tectonic evolution of the Midcontinent Rift System from inception (a) to termination (f). Sketches are not to scale and mark different time intervals. Arrows indicate direction of principal horizontal stress. Cross-hatched areas are regions where magmas are present. Lined areas in and adjacent to the rift basin are volcanic rocks and overlying dotted patterns denote late-stage sedimentary rocks (after Hinze et al., in press).

was eventually completely removed. Faults penetrating the entire crust have not been observed in the seismic data; rather, deep reflections are parallel to the boundaries of the lower crust. These reflections may originate from ductile shear zones involved in the thinning of the lower crust during the extension process or from mantle intrusions. There is no evidence of a laterally displaced anomalous lower crust beneath the MCR as would be anticipated in rifts that involved simple shear (Wernicke, 1985).

Concurrent with the graben development, enormous volumes of basalt were extruded into the depression (Fig. 10–15(c)). The magmas were derived from lithospheric melting and an increasing amount of decompression melting within the plume (White and McKenzie, 1989). Subsidence generally kept pace with volcanism, with only the oldest of the flows being deposited subaqueously. This subsidence was due to a combination of extensional forces and mantle plume dynamics as the head of the plume rose to and spread out beneath the base of the lithosphere (e.g., Campbell and Griffiths, 1990; Griffiths and Campbell, 1991). The presence of a few major unconformities within the volcanic rock package and variations in the thickness of the rift rocks indicate that subsidence was neither continuous nor uniform and resulted to a significant degree from crustal sagging.

During the following roughly 6 m.y. (Fig. 10–15(d)), the plume continued to spread laterally, and melts from the plume became the predominant source of volcanic flows and intrusions. The melts intruded the crust and were extruded regionally over the rift, but primarily into the axial grabens and half-grabens which continued to develop in the colder, brittle crust over the continually-thinning lithosphere. Regional crustal underplating occurred with crystallization of melts ponded at the base of the crust and within the lower crust. With this last surge of magmatic/tectonic activity, the mantle plume became inactive, probably because of cooling below its solidus, extension terminated, and igneous activity sharply declined. However, volcanic activity did continue in a minor way to at least 1087 Ma.

Following the volcanism and the primarily extensional phase of the rifting, graben development ceased and broad sagging continued along the axis of the rift. As the head of the plume cooled (Fig. 10–15(e)), its upper portions were attached to the thinned lithosphere and the lithosphere continued to sag under the load of the massive extrusions and intrusions and due to thermal collapse in the underlying mantle. Sedimentation kept pace with subsidence, and sediments increased in maturity upward through the stratigraphic column during the history of the basins. Along the margins of the rift, the volcanic rocks were first eroded, giving rise to the Copper Harbor Conglomerate, but the volcanic rocks were soon covered by the conglomerate (which also covered the axial zones) and then by the more mature sediments of the Nonesuch Shale, Freda Sandstone, and the Bayfield Group in the expanding axial basins. These mature sedimentary units derived most of their material from pre-Keweenawan terranes bordering the basin. The presence of marine biogeochemical indicators in the Oronto Group (Hieshima and Pratt, 1991; Pratt et al., 1991) indicates that the water levels in the basins at least on occasion were at sea level.

Along the length of the MCR, the extensional forces were replaced by regional compression (Fig. 10–15(f)), probably from the Grenville orogen, that reactivated zones of weakness within the thermally-softened lithosphere of the rift zone. Most noticeably, the graben-normal faults were reactivated as high-angle reverse faults that were initiated during and following deposition of the Bayfield Group. In addition, regional and local drag folding of the rift rocks occurred at this time.

10.9.3. Post–Keweenawan evolution of the MCR

The lithospheric structures portrayed in Figure 10–15(f) are much as they are today in many segments of the MCR. Numerous observations, however, indicate that the rift continued to develop after 1.1 Ga. Subsequent uplift has led to partial, or in some regions complete, erosion of both the volcanic and clastic sedimentary rocks adjacent to the rift and the upper rift-rocks along the axis of the MCR. In addition, the MCR has played a role in the Phanerozoic evolution of the midcontinent.

Currently, the region centered around Lake Superior is a topographic high in isostatic response to the underplated crust or depleted upper mantle (Allen et al., 1992) associated with the rifting event. This topographic anomaly is believed to be a vestige of a broad domal uplift that was initiated during the 1100 Ma rifting process. In addition, continental deposits that may be of Cretaceous age are found in Minnesota, Wisconsin, Iowa, Illinois, and Ontario. Using this information, Dutch (1981a) reconstructed the late Cretaceous surface. His map (Fig. 10–16) implies that the Lake Superior region has been uplifted ~250 meters during the Cenozoic Era, suggesting that the Lake Superior Swell may have experienced isostatic adjustment during the Phanerozoic, long after its origination in Keweenawan time.

Reactivation of the rift's faults in post-Keweenawan time is documented by modern seismicity. Along most of its length, the MCR is not associated with major seismicity (Frantti, 1980; Mooney, 1981; Mooney and Morey, 1981; Mooney and Walton, 1986; Chandler and Morey, 1989; Steeples, 1980, 1981; Steeples et al., 1989). Recent microseismicity in Kansas and Nebraska, however, correlates with the Humboldt fault, a fault which parallels the eastern margin of the southern segment of the western limb of the MCR (Steeples, 1980). In addition, a concentration of microearthquakes occurs along a related hinge zone fault on the outward margin of the western flanking clastic sedimentary

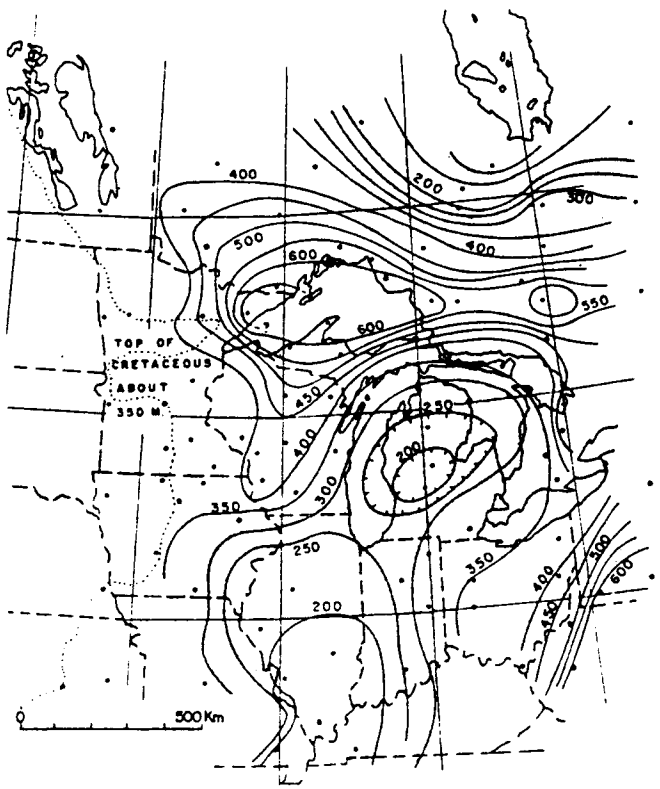

Fig. 10–16. Reconstructed late Cretaceous surface (elevations are in meters). Stipple pattern shows areas presently below 350 meters, the inferred late Cretaceous sea level (after Dutch, 1981a).

basin in Kansas. Steeples et al. (1989) also speculate that earthquakes occur near interpreted transform faults of the western limb of the rift.

Although evidence for present-day reactivation of rift structures is limited to Kansas and Nebraska, several structures and stratigraphic variations in the Phanerozoic sedimentary strata above the MCR document that many of the reverse faults along the entire length of the rift have been reactivated by post-Keweenawan forces (e.g., Middleton, 1991; Carlson, 1992; McGovern et al., 1993). Recent mapping in southeast Minnesota by Bloomgren (1993) reveals folding of the Cambrian and Ordovician strata. These folds occur directly above the Precambrian Belle Plaine Fault (Sloan and Danes, 1962), a profound cross-structure within the western limb of the MCR, suggesting post-Ordovician reactivation of the fault.

10.10. Conclusions

At 1100 Ma, a major disruption of the proto-North American continent led to a nearly complete rupture of the crust along the arcuate, ~2000 km length of the Midcontinent Rift system. The majority of the rift's igneous rocks were derived from a melting mantle plume and the overlying lithosphere over a short span of less than 20 m.y. The relation of the plume to the extensional forces causing the rift is presently unclear.

The MCR is a profound disruption of the crust, as indicated by its anomalous geophysical signatures. The geophysical data, together with limited outcrops of the rift rocks and a few deep drill holes, suggest a general consistency in structural style, tectonic evolution, and age along the length of the rift system. Although the pre-rift crust was thinned, in places, to less than one-third of its original thickness, the crust beneath the rift is anomalously thick due to the addition of up to 20 km of mantle-derived volcanic rocks and as much as 10 km of post-volcanic clastic sedimentary strata. In addition, the seismic velocity and density of the lower crust are increased, probably due to mantle-derived intrusions and crustal underplating.

The original rift grabens and their volcanic and sedimentary fill have been modified by regional compressional forces, perhaps associated with the roughly contemporaneous Grenville orogenic activity. The most profound of these modifications are the reactivation of the normal, graben faults as high-angle reverse faults with more than 5 km of stratigraphic displacement.

During the past decade, geophysical studies, particularly deeply-penetrating seismic reflection profiling, and isotopic analysis of the rift's volcanic rocks have provided much new insight into the MCR and its structural and magmatic evolution. Many problems, however, remain to be solved. For example, of special concern is the lack of information concerning the degree and form of modification of the lower crust beneath the rift. In addition, little is known about the manifestations of the rift in the upper mantle. Other significant questions concern the nature and source of the tensional forces. Were they generated entirely by the mantle plume head, or were other mechanisms involved? Was there a significant uplift produced by the head of the mantle plume? Also, is there evidence of a plume trail migrating to or from Lake Superior? Furthermore, what is the relation of the origin, development, and termination of the MCR to the evolution of the Grenville orogen?

Future research of the MCR should be directed at questions such as these. In addition, continued detailed investigations are needed to gain a more comprehensive knowledge of the geochemistry, magnetostratigraphy, and absolute ages of the rift rocks. Geochemical and isotopic studies should provide a clearer picture of the magmatic evolution of the rift and plume through both time and space. Additional isotopic dating and paleomagnetic measurements should result in a better understanding of the relative ages of the rift units along the entire length of the MCR. Also, efforts should be directed toward mapping the finer structures within the rift and expanding and refining the gross structural interpretations. Of particular interest are the transitional, transverse zones within the MCR, along which the rift structure changes abruptly and dramatically. Are these transition zones related to ancestral structures? How did the rift evolve along them?

During the next decade, detailed investigations of these topics, at specific sites along the rift, should provide a stronger framework for developing an integrated model of the entire rift. In the future, investigators will need to be more concerned with integrating information from individual locations along the rift and a variety of disciplines. Integrated models should consider the relative ages of the individual rift segments and their structural relations to one another which will lead to a better understanding of the spatial and temporal evolution of the MCR.

Acknowledgments. We acknowledge the useful interaction with our colleagues and the constructive criticism of numerous specialist working on the MCR. Special thanks are due to Albert B. Dickas and John C. Green who provided useful critiques of an earlier draft of this article. Financial support for this overview was provided in part by NSF Grant Number EAR-8617315.

10.11. References

Allen, D.J., and Chandler, V.W., 1992. The utility of high-resolution aeromagnetic data for investigating the Midcontinent Rift in East-Central Minnesota (abstract): Proceedings and Abstracts, 38th Institute on Lake Superior Geology, Hurley, Wisconsin, 3-5.

Allen, D.J., and Chandler, V.W., 1993. Magnetic properties of the Midcontinent Rift volcanics at Osseo, Minnesota: Clues to the origin of aeromagnetic anomalies (abstract): Proceedings and Abstracts, 39th Institute on Lake Superior Geology, Eveleth, Minnesota, 2-3.

Allen, D.J., Hinze, W.J., and Cannon, W.F., 1992. Drainage, topographic, and gravity anomalies in the Lake Superior region: Evidence for a 1100 Ma mantle plume: Geophys. Res. Lett., 19: 2119-2122.

Allen, D.J., Hinze, W.J., Dickas, A.B., and Mudrey, M.G., Jr., 1993. An integrated seismic reflection/three-dimensional gravity investigation of the Midcontinent Rift system, USA: western Lake Superior region: AAPG Hedberg Research Conference, Basement and Basins of Eastern North America, Ann Arbor, MI, 1993.

Allen, D.J., Hinze, W.J., Dickas, A.B., and Mudrey, M.G., Jr., 1994. Geophysical investigations of the Midcontinent Rift system: a new model for western Lake Superior and northern Wisconsin (abstract): Proceedings and Abstracts, 40th Institute on Lake Superior Geology, Houghton, Michigan.

Anderson, R.R. (Ed.), 1990a, The Amoco M.G. Eischeid #1 Deep Petroleum Test Carroll County, Iowa: Iowa Department of Natural Resources Special Report Series No. 2, 185 pp.

Anderson, R.R. (Editor), 1990b, Interpretation of geophysical data over the Midcontinent Rift system in the area of the M.G. Eischeid #1 Petroleum Test, Carroll County, Iowa, In: R.R. Anderson, ed., The Amoco M.G. Eischeid #1 Deep Petroleum Test Carroll County, Iowa: Iowa Department of Natural Resources Special Report Series No. 2, 27-38.

Baker, B.N., and Morgan, P., 1981. Continental rifting: Progress and outlook: EOS, American Geophysical Union Transactions, 62: 585-586.

Behrendt, J.C., Green, A.G., Cannon, W.F., Hutchinson, D.R., Lee, M., Milkereit, B., Agena, W.F., and Spencer, C., 1988. Crustal structure of the Midcontinent Rift system: Results from GLIMPCE deep seismic reflection profiles: Geology, 16: 81-85.

Behrendt, J.C., Hutchinson, D.R., Lee, M.W., Agena, W.F., Trehu, A., Thornber, C.R., Cannon, W.F., and Green, A., 1990. Seismic reflection (GLIMPCE) evidence of deep crustal and upper mantle intrusions and magmatic underplating associated with the Midcontinent Rift system of North America: Tectonophysics, 173: 617-626.

Berendsen, P., Borcherding, R.M., Doveton, J., Gerhard, L., Newell, K.D., Steeples, D., and Watney, W.L., 1988. Texaco Poersch #1, Washington County Kansas - Preliminary geologic report of the pre-Phanerozoic rocks: Kansas Geological Survey Open-File Report 88-22, 116 pp.

Berg, J.H., and Klewin, K.W., 1988. High-MgO lavas from the Keweenawan midcontinent near Mamainse Point, Ontario: Geology, 16: 1003-1006.

Bloomgren, B.A., 1993. Bedrock geology of Waseca County, Minnesota: Minnesota Geological Survey Miscellaneous Map Series M-73, scale 1:62500 and smaller.

Books, K.G., 1972. Paleomagnetism of some Lake Superior rocks: U.S. Geological Survey Professional Paper 760, 42 pp.

Bosworth, W., Lambiase, J., and Keisler, R., 1986. A new look at Gregory's Rift: The structural style of continental rifting: EOS, American Geophysical Union Transactions, 67: 577-583.

Boyd, F.R., and McCallister, R.H., 1976. Densities of fertile and sterile garnet peridotites: Geophys. Res. Lett., 15: 673-675.

Brannon, J., 1984. Geochemistry of successive lava flows of the Keweenawan North Shore Volcanic Group (Ph.D. dissertation): St. Louis, Missouri, Washington University, 312 pp.

Brown, L., Jensen, L., Oliver, J., Kaufman, S., and Steiner, D., 1982. Rift structure beneath the Michigan Basin from COCORP profiling: Geology, 10: 645-649.

Campbell, I.H., and Griffiths, R.W., 1990. Implications of mantle plume structure for the evolution of flood basalts: Earth and Planetary Science Letters., 99: 79-93.

Cambray, F.W., 1988. A tectonic model for the Mid-Continent Rift system (abstract): Proceedings and Abstracts, 34th Institute on Lake Superior Geology, Marquette, Michigan, 17.

Cannon, W.F., 1992. The Midcontinent rift in the Lake Superior region with emphasis on its geodynamic evolution: Tectonophysics, 213: 41-48.

Cannon, W.F., 1994. Closing of the Midcontinent rift - a far-field effect of Grenvillian compression: Geology, 22: 155-158.

Cannon, W.F., and Green, A.G., 1989. A model for development of the Midcontinent Rift in the Lake Superior Region (abstract): EOS, American Geophysical Union, 70: 272.

Cannon, W.F., and Hinze, W.J., 1992. Speculations on the origin of the North American Midcontinent Rift: Tectonophysics, 213: 49-55.

Cannon, W.F., Green, A.G., Hutchinson, D.R., Lee, M., Milkereit, B., Behrendt, J.C., Halls, H.C., Green, J.C., Dickas, A.B., Morey, G.B., Sutcliffe, R., and Spencer, C., 1989. The Midcontinent Rift beneath Lake Superior from GLIMPCE seismic reflection profiling: Tectonics, 8: 305-332.

Cannon, W.F., Peterman, Z.E., and Sims, P.K., 1990. Structural and isotopic evidence for Middle Proterozoic thrust faulting of Archean and Early Proterozoic rocks near the Gogebic Range, Michigan and Wisconsin (abstract): Proceedings and Abstracts, 36th Institute on Lake Superior Geology, Thunder Bay, Ontario, 11-12.

Cannon, W.F., Lee, M.W., Hinze, W.J., Schulz, K.J., and Green, A.G., 1991. Deep crustal structure of Precambrian crust beneath northern Lake Michigan, midcontinent North America: Geology, 19: 207-210.

Carlson, M.P., 1992. Tectonic implications and influence of the Midcontinent Rift system in Nebraska and adjoining areas (abstract): 10th Biennial International Conference on Basement Tectonics, Duluth, MN, 143-145.

Chan, W.K., and Hajnal, Z., 1989. Some features of the Midcontinent Rift from high density refraction signals (abstract): EOS, American Geophysical Union Transactions, 70: 274.

Chandler, V.W., 1983. Correlation of magnetic anomalies in east-central Minnesota and northwestern Wisconsin: Constraints on magnitude and direction of Keweenawan rifting: Geology, 11: 174-176.

Chandler, V.W., 1991. Aeromagnetic anomaly map of Minnesota: Minnesota Geological Survey State Map, Series 5-17, scale 1:500,000.

Chandler, V.W., and Morey, G.B., 1989. Seismic history of Minnesota and its geologic significance: An Update: Seismological Research Letters, 60: 79-86.

Chandler, V.W., McSwiggen, P.L., Morey, G.B., Hinze, W.J., and Anderson, R.L., 1989. Interpretation of seismic reflection, gravity and magnetic data across the Middle Proterozoic Midcontinent Rift System in western Wisconsin, eastern Minnesota, and central Iowa: American Association of Petroleum Geologists Bulletin, 73: 261-275.

Cohen, T.J., and Meyer, R.P., 1966. The Midcontinent Gravity High: Gross crustal structure, In: J.S. Steinhart, T.J. Smith, eds., The Earth Beneath the Continents: American Geophysical Union Monograph 10: 141-165.

Craddock, C., Thiel, E.C., and Gross, B., 1963. A gravity investigation of the Precambrian of southeastern Minnesota and western Michigan: J. Geophys. Res, 68: 6015-6032.

Daniels, P.A., Jr., 1982. Upper Precambrian sedimentary rocks: Oronto Group, *In:* R.J. Wold, W.J. Hinze, eds., Geology and Tectonics of the Lake Superior Basin: Geol. Soc. Am. Mem. 156: 107-133.

Davidson, D.M., Jr., 1982. Geological evidence relating to interpretations of the Lake Superior Basin structure, *In:* R.J. Wold, W.J. Hinze, eds., Geology and Tectonics of the Lake Superior Basin: Geol. Soc. Am. Mem. 156: 5-14.

Davis, D.W., and Sutcliffe, R.H., 1985, U-Pb ages from the Nipigon plate and northern Lake Superior: Geol. Soc. Am. Bull., 96: 1572-1579.

Davis, D.W., and Paces, J.B., 1990. Time resolution of geologic events on the Keweenaw Peninsula and implications for development of the Midcontinent Rift system: Earth and Planetary Science Letters, 97: 54-64.

Dickas, A.B., 1986a, Comparative Precambrian stratigraphy and structure along the Mid-Continent Rift: American Association of Petroleum Geologists Bulletin, 70: 225-238.

Dickas, A.B., 1986b, Seismologic analysis of arrested stage development of the Midcontinent rift, *In:* M.G. Mudrey, ed., Precambrian Petroleum Potential, Wisconsin and Michigan: Geoscience Wisconsin, 11, Wisconsin Geologic and Natural History Survey, 45-52.

Dickas, A.B., 1992. Preliminary report, geology and geophysics of the Terra/Patrick #7-22 Wildcat hydrocarbon test, Midcontinent Rift, Keystone Township, Bayfield County, Wisconsin (abstract): Proceedings and Abstracts, 38th Institute on Lake Superior Geology, Hurley, Wisconsin, 25-26.

Dickas, A.B., and Mudrey, M.G., Jr., 1989. Structural differentiation of the Midcontinent Rift System (abstract): EOS, American Geophysical Union Transactions, 70: 275.

Dickas, A.B., Mudrey, M.G. Jr., Ojakangas, R.W., and Shrake, D.L., 1992. A possible southeastern extension of the Midcontinent Rift System located in Ohio: Tectonics, 11: 1406-1414.

Dosso, L., 1984. The nature of the Precambrian subcontinental mantle: Isotopic study (Sr, Nd, Pb) of Keweenawan volcanism of the north shore of Lake Superior (Ph.D. dissertation): Minneapolis, Minnesota, University of Minnesota, 221 pp.

Dutch, S.I., 1981a, Post-Cretaceous vertical motions in the eastern midcontinent, U.S.A.: Zietschrift fur Geomorphologie Neue Folge Supplementbände 40: 13-25.

Dutch, S.I., 1981b, Isostasy, epeirogeny, and the highland rim of Lake Superior: Zietschrift fur Geomorphologie Neue Folge Supplementbände 40: 27-41.

Fowler, J.H., and Kunzi, W.D., 1978. Keweenawan turbidites in Michigan (deep borehole red beds): A founded basin sequence developed during evolution of a protoceanic rift systems: J. Geophys. Res, 83: 5833–5843.

Fox, A.J., 1988. An integrated geophysical study of the southeastern extension of the Midcontinent Rift System (M.S. thesis): West Lafayette, Indiana, Purdue University, 112 pp.

Frantti, G.G., 1980. Seismicity and crustal studies in the Lake Superior Precambrian province (abstract): EOS, American Geophysical Union Transactions, 61: 96.

Gordon, M.B., and Hempton, M.R., 1986. Collision-induced rifting: The Grenville Orogeny and the Keweenawan Rift of North America: Tectonophysics, 127: 1-25.

Green, A.G., Milkereit, B., Davidson, A., Spencer, C., Hutchinson, D.R., Cannon, W.F., Lee, M.W., Agena, W.F., Behrendt, J.C., and Hinze, W.J., 1988. Crustal structure of the Grenville Front and adjacent terranes: Geology, 16: 788-792.

Green, A.G., Cannon, W.F., Milkereit, B., Davidson, A., Behrendt, J.C., Spencer, C., Hutchinson, D.R., Lee, M.W., Agena, W.F., and Morel-a-l'Huisser, P., 1989. A GLIMPCE of the deep crust beneath the Great Lakes: American Geophysical Union Monograph 51: 65-80.

Green, J.C., 1982. Geology of Keweenawan extrusive rocks, In: R.J. Wold, W.J. Hinze, eds., Geology and Tectonics of the Lake Superior Basin: Geol. Soc. Am. Mem. 156: 47-55.

Green, J.C., 1983. Geologic and geochemical evidence for the nature and development of the middle Proterozoic (Keweenawan) Midcontinent Rift of North America: Tectonophysics, 94: 413-437.

Green, J.C., 1987. Plateau basalts of the Keweenawan North Shore Volcanic Group.: *Geol. Soc. Am. Centennial Field Guide - North-Central Section*, 59-62.

Green, J.C., 1989. Physical volcanology of mid-Proterozoic plateau lavas; the Keweenawan North Shore Volcanic Group, Minnesota: Geol. Soc. Am. Bull., 101: 486-500.

Green, J.C., and Fitz, T.J. III, 1993. Extensive felsic lavas and rhyoignimbrites in the Keweenawan Midcontinent Rift plateau volcanics, Minnesota: Petrographic and field recognition: Journal of Volcanology and Geothermal Research, 54: 177-196.

Green, J.C., Bornhorst, T.J., Chandler, V.W., Mudrey, M.G., Jr., Myers, P.R., Pesonen, L.V., and Wilband, J.T., 1987. Keweenawan dykes of the Lake Superior region: Evidence for the evolution of the Middle Proterozoic Midcontinent Rift of North America, In: H.C. Halls, W.F. Fahrig, eds., Mafic Dyke Swarms: Geological Association of Canada Special Paper 34: 289-302.

Green, W.V., 1991. Lithospheric seismic structure of the Cenozoic Kenya Rift and the Precambrian Midcontinent Rift from teleseismic tomography (Ph.D. dissertation): Madison, Wisconsin, University of Wisconsin-Madison, 179 pp.

Griffiths, R.W., and Campbell, I.H., 1991. Interaction of mantle plume heads with the Earth's surface and onset of small-scale convection: J. Geophys. Res, 96, 18,295-18,310.

Halls, H.C., 1969. Compressional wave velocities of Keweenawan rock specimens from the Lake Superior region: Canadian Journal of Earth Science, 6: 555-568.

Halls, H.C., 1978. The late Precambrian Central North America Rift System - A survey of recent geological and geophysical investigations, In: E.R. Neumann, I.B. Ramberg, eds., Tectonics and Geophysics of Continental Rifts: NATO Advanced Study Institute, Series C., Boston, Reidel, 37: 111-123.

Halls, H.C., 1982. Crustal thickness in the Lake Superior region, In: R.J. Wold, W.J. Hinze, eds., Geology and Tectonics of the Lake Superior Basin: Geol. Soc. Am. Mem. 156: 239-244.

Halls, H.C., and Pesonen, L.J., 1982. Paleomagnetism of Keweenawan rocks, in R.J. Wold, W.J. Hinze, eds., Geology and Tectonics of the Lake Superior Basin: Geol. Soc. Am. Mem. 156: 173-202.

Hamilton, D.A., and Mereu, R.F., 1993. 2-D tomographic imaging across the North American Midcontinent Rift system: Geophysical Journal International, 112: 344-358.

Heaman, L.M., and Machado, N., 1992. Timing and origin of the Midcontinent Rift alkaline magmatism, North America: Evidence from the Coldwell Complex. Contributions to Mineralogy and Petrology, 110: 289-303.

Hieshima, G.B., and Pratt, L.M., 1991. Sulfur/carbon ratios and extractable organic matter of the Middle Proterozoic Nonesuch formation, North American Midcontinent Rift: Precambrian Research, 54: 65-79.

Hinze, W.J., 1963. Regional gravity and magnetic anomaly maps of the Southern Peninsula of Michigan: Michigan Geological Survey Report of Investigation 1, 26 pp.

Hinze, W.J., O'Hara, N.W., Trow, J.W., and Secor, G.B., 1966. Aeromagnetic studies of eastern Lake Superior, In: J.S. Steinhart, T.J. Smith, eds., The Earth Beneath the Continents: American Geophysical Union Monograph 10: 95-110.

Hinze, W.J., Roy, R.F., and Davidson, D.M., Jr., 1972. The origin of late Precambrian rifts (abstract): Geol. Soc. Am., Abstracts with Program, 4: 723.

Hinze, W.J., Kellogg, R.L., and O'Hara, N.W., 1975. Geophysical studies of basement geology of southern peninsula of Michigan: American Association of Petroleum Geologists Bulletin, 59: 1562-1584.

Hinze, W.J., and Wold, R.J., 1982. Lake Superior geology and tectonics - overview and major unsolved problems, In: R.J. Wold, W.J. Hinze, eds., Geology and Tectonics of the Lake Superior Basin: Geol. Soc. Am. Mem. 156: 273-280.

Hinze, W.J., Wold, R.J., O'Hara, N.W., 1982. Gravity and magnetic anomaly studies of Lake Superior, *In:* R.J. Wold, W.J. Hinze, eds., Geology and Tectonics of the Lake Superior Basin: Geol. Soc. Am. Mem. 156: 203-222.

Hinze, W.J., and Kelly, W.C., 1988. Scientific drilling into the Midcontinent Rift System: EOS, American Geophysical Union Transactions, 69: 1649, 1656-1657.

Hinze, W.J., Braile, L.W., and Chandler, V.W., 1990. A geophysical profile of the southern margin of the Midcontinent Rift System in western Lake Superior: Tectonics, 9, 303-310.

Hinze, W.J., Allen, D.J., Fox, A.J., Sunwoo, D., Woelk, T., and Green, A.G., 1992. Geophysical investigations and crustal structure of the North American Midcontinent Rift system: Tectonophysics, 213: 17-32.

Hinze, W.J., Allen, D.J., Braile, L.W., and Mariano, J., 1993. Overview of the Midcontinent Rift system: Geol. Soc. Am. Special Paper, in press.

Hutchinson, D.R., White, R.S., Cannon, W.F., and Schulz, K.J., 1990. Keweenaw hot spot: Geophysical evidence for a 1.1 Ga mantle plume beneath the Midcontinent Rift System: J. Geophys. Res, 95: 10,869-10,884.

Irving, R.D., 1883, The copper-bearing rocks of Lake Superior: U.S. Geological Survey Monograph 5, 464 pp.

Jefferson, T.J., Karl, J.H., and Meyer, P.J., 1989. A model of the velocity distribution across the Midcontinent Rift: GLIMPCE Line A (abstract): EOS, American Geophysical Union Transactions, 70: 274.

Kalliokoski, J., 1982. Jacobsville Sandstone, *In:* R.J. Wold, W.J. Hinze, eds., Geology and Tectonics of the Lake Superior Basin: Geol. Soc. Am. Mem. 156: 147-155.

Kalliokoski, J., 1989. Jacobsville Sandstone and tectonic activity (abstract): Proceedings and Abstracts, 35th Institute on Lake Superior Geology, Duluth, Minnesota, 39-41.

Keller, G.R., and Adams, D.C., 1992. Thoughts on the nature and extent of Keweenawan rifting in North America based on recent results in other rift systems (abstract): EOS, American Geophysical Union Transactions, 73: 319.

Keller, G.R., Bland, A.E., and Greenberg, J.K., 1982. Evidence for a major late Precambrian tectonic event (rifting) in the eastern midcontinent region, United States: Tectonics, 1, 213-222.

King, E.R., and Zietz, I., 1971. Aeromagnetic study of the Midcontinent Gravity High of central United States: Geol. Soc. Am. Bull., 82: 2187-2208.

Klasner, J.S., Cannon, W.F., and Van Schmus, W.R., 1982. The pre-Keweenawan tectonic history of southern Canadian Shield and its influence on formation of the Midcontinent Rift, *In:* R.J. Wold, W.J. Hinze, eds., Geology and Tectonics of the Lake Superior Basin: Geol. Soc. Am. Mem. 156: 27-46.

Klewin, K.W., 1989. Polybaric fractionation in an evolving continental rift: Evidence from the Keweenawan Mid-continental Rift: Journal of Geology, 97: 65-76.

Klewin, K.W., and Berg, J.H., 1991. Petrology of the Keweenawan Mamainse Point lavas, Ontario: petrogenesis and continental rift evolution: J. Geophys. Res, 96, 457-474.

Klewin, K.W., and Shirey, S.B., 1992. The igneous petrology and magmatic evolution of the Midcontinent Rift system: Tectonophysics, 213: 33-40.

Lippus, C.S., 1988. The seismic properties of mafic volcanic rocks of the Keweenawan Supergroup and their implications (M.S. Thesis): West Lafayette, Indiana, Purdue University, 160 pp.

Luetgert, J.H., and Meyer, R.P., 1982. Structure of the western basin of Lake Superior from cross structure refraction profiles, *In:* R.J. Wold, W.J. Hinze, eds., Geology and Tectonics of the Lake Superior Basin: Geol. Soc. Am. Mem. 156: 245-255.

Lutter, W.J., Trehu, A.M., Nowack, R.L., and Shay, J.T., 1989. Inversion for crustal structure using first arrival refraction data from the 1986 Lake Superior GLIMPCE experiment (abstract): EOS, American Geophysical Union Transactions, 70: 274.

Lyons, P.L., 1950. A gravity map of the United States: Tulsa Geological Society Digest, 18: 33-43.

Lyons, P.L., 1959. The Greenleaf anomaly, a significant gravity feature, In: W.M. Hambleton, ed., Symposium on Geophysics in Kansas: Kansas Geological Survey Bulletin 137, 105-120.

Lyons, P.L., 1970. Continental and oceanic geophysics, *In:* H. Johnson, B.L. Smith, eds., The Megatectonics of Continents and Oceans: New Brunswick, Rutgers University Press, 147-166.

Manson, M.L., and Halls, H.C., 1992. The geometry and sense of post-Keweenawan faults in eastern Lake Superior: Implications for models of rift development (abstract): EOS, American Geophysical Union Transactions, 73: 320.

Mariano, J., and Hinze, W.J., 1992. Magnetic and seismic reflection interpretation of the Midcontinent Rift in eastern Lake Superior (abstract): EOS, American Geophysical Union Transactions, 73: 194.

Mariano, J., and Hinze, W.J., 1994a, Structural interpretation of the Midcontinent Rift in eastern Lake Superior from seismic reflection and potential-field studies: Canadian Journal of Earth Science, 31: 619–628.

Mariano, J., and Hinze, W.J., 1994b, Gravity and magnetic models of the Midcontinent Rift in eastern Lake Superior: Canadian Journal of Earth Science, 31: 661–674.

McCallister, R.H., Boctor, N.Z., and Hinze, W.J., 1978. Petrology of the spilitic rocks from the Michigan Basin drill hole, 1978: J. Geophys. Res, 83: 5825-5831.

McGinnis, L.D., and Mudrey, M.G., Jr., 1991. Seismic reflection profiling and tectonic evolution of the Midcontinent Rift in Lake Superior: Wisconsin Geological and Natural History Survey Miscellaneous Paper 91-2.

McGovern, M.G., Craddock, J.P., and Webers, G.F., 1993. Evidence for late Paleozoic displacement on the Keweenawan thrust fault from folded Paleozoic outliers in Michigan's upper peninsula (abstract): Proceedings and Abstracts, 39th Institute on Lake Superior Geology, Eveleth, Minnesota, 56-57.

McSwiggen, P.L., Morey, G.B., and Chandler, V.W., 1987. New model of Midcontinent Rift in eastern Minnesota and western Wisconsin: Tectonics, 6: 677-685.

Merk, G.P., and Jirsa, M.A., 1982. Provenance and tectonic significance of the Keweenawan interflow sedimentary rocks, *In:* R.J. Wold, W.J. Hinze, eds., Geology and Tectonics of the Lake Superior Basin: Geol. Soc. Am. Mem. 156: 97-106.

Meshref, W.M., and Hinze, W.J., 1970. Geologic interpretation of aeromagnetic data in western upper peninsula of Michigan: Michigan Department of Natural Resources, Geological Survey Report of Investigation 12, 25 pp.

Meyer, P.J., Karl, J.H., and Jefferson, T.J., 1989. Beamsteering applied to the GLIMPCE wide-angle data: Line A (abstract): EOS, American Geophysical Union Transactions, 70: 276.

Middleton, M.D., 1991. A preliminary study of rejuvenated movement along a Precambrian fault, St. Croix County, Wisconsin (abstract): Proceedings and Abstracts, 37th Institute on Lake Superior Geology, Eau Claire, Wisconsin, 70-71.

Milanovsky, E.E., 1981. Aulacogens of ancient platforms: problems of their origin and tectonic development: Tectonophysics, 73: 213-248.

Milkereit, B., Green, A.G., Lee, M.W., Agena, W.F., and Spencer, D., 1990. Pre- and post-stack migration of GLIMPCE reflection data: Tectonophysics, 173: 1-13.

Miller, J.D., Jr., 1992. The need for a new paradigm regarding the petrogenesis of the Duluth Complex (abstract): Proceedings and Abstracts, 38th Institute on Lake Superior Geology, Hurley, Wisconsin, 65-67.

Mooney, H.M., 1981. Minnesota earthquakes—1979: Earthquake Notes, 52: 57–58.

Mooney, H.M., and Morey, G.B., 1981. Seismic history of Minnesota and its geological significance: Seismological Society of America Bulletin, 71: 199-210.

Mooney, H.M., and Walton, M., 1986. Seismicity and tectonic relationships for Upper Great Lakes Precambrian Shield Province: U.S. Nuclear Regulatory Commission Final Report, July 1981-December 1982, NUREG/CR-3150, 47 pp.

Morel-a-l'Huissier, P., and Green, A.G., 1989. Modeling the GLIMPCE 1986 seismic refraction data recorded along seismic reflection Line A (abstract): EOS, American Geophysical Union Transactions, 70: 277.

Morey, G.B., 1977. Revised Keweenawan subsurface stratigraphy, southwestern, Minnesota: Minnesota Geological Survey Report of Investigation 16, 67 pp.

Morey, G.B., and Ojakangas, R.W., 1982. Keweenawan sedimentary rocks of eastern Minnesota and northwestern Wisconsin, *In:* R.J. Wold, W.J. Hinze, eds., Geology and Tectonics of the Lake Superior Basin: Geol. Soc. Am. Mem. 156: 135-146.

Morey, G.B., and Van Schmus, W.R., 1988. Correlation of Precambrian rocks of the Lake Superior region, United States: U.S. Geological Survey Professional Paper 1241-F, 31 pp.

Mudrey, M.G., Jr., and Dickas, A.B., 1988. Midcontinent rift model based upon Gregory Rift tectonic and sedimentation geometries (abstract): Proceedings and Abstracts, 34th Institute on Lake Superior Geology, Marquette, Michigan, 73-75.

Mudrey, M.G., Jr., McGinnis, L.D., Ervin, C.P., Nyquist, J., Dickas, A.B., Morey, G.B., Green, A.G., and Sexton, J.L., 1989. Structure of the Midcontinent Rift System in western

Lake Superior: Results from 8-sec reflection seismic data and gravity and magnetic anomalies (abstract): EOS, American Geophysical Union Transactions, 70: 278.

Nicholson, S.W., and Shirey, S.B., 1990. Evidence for a Precambrian mantle plume: A Sr, Nd, and Pb isotopic study of the Midcontinent Rift System in the Lake Superior region: J. Geophys. Res, 95: 10,851-10,868.

Nixon, G.A., 1988. An analysis of geophysical anomalies in north-central Oklahoma and their relationship to the Midcontinent Geophysical Anomaly (M.S. Thesis): Norman, Oklahoma, University of Oklahoma, 118 pp.

Nyquist, J.E., and Wang, H.F., 1988. Flexural modeling of the Midcontinent Rift: J. Geophys. Res, 93: 8852-8868.

Nyquist, J.E., and Wang, H.F., 1989. Flexural modeling of the Midcontinent Rift and the Goodman Swell (abstract): EOS, American Geophysical Union Transactions, 70: 275.

Ocola, L.C., and Meyer, R.P., 1973. Central North American rift system, 1. Structure of the axial zone from seismic and gravimetric data: J. Geophys. Res, 78, 5173-5194.

Ojakangas, R.W., and Morey, G.B., 1982. Keweenawan pre-volcanic quartz sandstones and related rocks of the Lake Superior region, *In:* R.J. Wold, W.J. Hinze, eds., Geology and Tectonics of the Lake Superior Basin: Geol. Soc. Am. Mem. 156: 85-96.

Oray, E., Hinze, W.J., and O'Hara, N.W., 1973. Gravity and magnetic evidence for the eastern termination of the Lake Superior syncline: Geol. Soc. Am. Bull., 84: 2763-2780.

Oxburgh, E.R., and Parmentier, E.M., 1977. Compositional and density stratification in oceanic lithosphere - causes and consequences: Journal of the Geological Society of London, 133: 343-355.

Paces, J.B., and Bell, K., 1989. Non-depleted sub-continental mantle beneath the Superior Province of the Canadian Shield: Nd-Sr isotopic and trace element evidence from Midcontinent Rift basalts: Geochimica et Cosmochimia Acta, 53: 2023-2035.

Paces, J.B., and Miller, J.D., Jr., 1993. Precise U-Pb ages of Duluth Complex and related mafic intrusions, northeastern Minnesota, U.S.A.: Geochronological insights to physical, petrogenetic, paleomagnetic and tectono-magmatic processes associated with the 1.1 Ga Midcontinent Rift system: J. Geophys. Res, 98: 13,997-14,013.

Palmer, H.C., 1970. Paleomagnetism and correlation of some Middle Keweenawan rocks, Lake Superior: Canadian Journal of Earth Science, 7: 1410-1436.

Palmer, H.C., and Halls, H.C., 1986. Paleomagnetism of the Powder Mill Group, Michigan and Wisconsin: A reassessment of the Logan Loop: J. Geophys. Res, 91: 11,571-11,580.

Palmer, H.C., and Davis, D.W., 1987. Paleomagnetism and U-Pb geochronology of volcanic rocks from Michipicoten Island, Lake Superior, Canada: Precise calibration of the Keweenawan polar wander track: Precambrian Research, 37: 157-171.

Peterman, Z.E., and Sims, P.K., 1988. The Goodman Swell: A lithospheric flexure caused by crustal loading along the Midcontinent Rift System: Tectonics, 7: 1077-1090.

Pratt, L.M., Summons, R.E., and Hieshima, G.B., 1991. Sterane and Triterpane biomarkers in the Precambrian Nonesuch formation, North American Midcontinent Rift: Geochimica et Cosmochimica Acta., 55: 911-916.

Pratt, T., Culotta, R., Hauser, E., Nelson, D., Brown, L., Kaufman, S., Oliver, J., and Hinze, W., 1989. Major Proterozoic basement features of the eastern midcontinent of North America revealed by recent COCORP profiling: Geology, 17: 505-509.

Robertson, W.A., 1973. Pole positions from the Mamainse Point lavas and their bearing on a Keweenawan pole path and polarity sequence: Canadian Journal of Earth Science, 10: 1541-1555.

Rosendahl, B.R., 1987. Architecture of continental rifts with special reference to East Africa: Annual Reviews of Earth and Planetary Science, 15: 445-503.

Samson, C., and West, G.F., 1992. Crustal structure of the Midcontinent Rift system in eastern Lake Superior from controlled-amplitude analysis of GLIMPCE deep reflection seismic data: Canadian Journal of Earth Science, 29: 636-649.

Schärer, U., and Gower, C.F., 1988. Crustal evolution in eastern Labrador: Constraints from precise U-Pb ages: Precambrian Research, 38: 405-421.

Serpa, L., Setzer, T., Farmer, H., Brown, L., Oliver, J., and others, 1984. Structure of the southern Keweenawan Rift from COCORP surveys across the Midcontinent Geophysical Anomaly in northeastern Kansas: Tectonics, 3: 367-384.

Shay, J.T., and Trehu, A.M., 1989. Structure of the Midcontinent Rift beneath Lake Superior (abstract): EOS, American Geophysical Union, 70: 274.

Shrake, D.L., Carlton, R.W., Wickstrom, L.H., Potter, P.L., Richard, B.H., Wolfe, P.J., and Sitler, G.W., 1991. A Pre-Mount Simon basin under the Cincinnati Arch: Geology, 19, 139-142.

Sleep, N.H., and Sloss, L.L., 1978. A deep borehole in the Michigan Basin: J. Geophys. Res, 83: 5815-5824.

Sloan, R.E., and Danes, Z.F., 1962. A geologic and gravity survey of the Belle Plaine area, Minnesota: Minnesota Academy of Science Proceedings, 30: 49-52.

Smith, T.J., Steinhart, J.S., and Aldrich, L.T., 1966. Crustal structure under Lake Superior, In: J.S. Steinhart, T.J. Smith, eds., The Earth Beneath the Continents. American Geophysical Union Monograph 10: 181-197.

Steeples, D.W., 1980. Microearthquakes recorded by the Kansas Geological Survey: Kansas Geological Survey Report Investigation 37, 25 pp.

Steeples, D.W., 1981. Kansas earthquakes—1979. Earthquake Notes, 52: 42-48.

Steeples, D.W., Hildebrand, G.M., Bennett, B.C., Miller, R.O., Chung, Y., and Knapp, R.W., 1989. Kansas-Nebraska seismicity studies using the Kansas-Nebraska microearthquake network: U.S. Nuclear Regulatory Commissions Final Report, NUREG/CR-5045, 71 pp.

Steinhart, J.S., and Smith, T.J. (Editors.), 1966. The Earth Beneath the Continents: American Geophysical Union Monograph 10, 663 pp.

Sunwoo, D., 1989. An integrated geophysical study of the Grenville Front in Ohio (M.S. Thesis): West Lafayette, Indiana, Purdue University, 94 pp.

Suszek, T.J., 1991. Petrography and sedimentation of the Middle Proterozoic (Keweenawan) Nonesuch Formation, western Lake Superior region, Midcontinent Rift System (M.S. Thesis): Duluth, Minnesota, University of Minnesota, Duluth, 198 pp.

Teskey, D.J., Thomas, M.D., Gibb, R.A., Dods, S.D., Kucks, R.P., Chandler, V.W., Fadaie, K., and Phillips, J.O., 1991. High resolution aeromagnetic survey of Lake Superior: EOS, American Geophysical Union Transactions, 72: 81, 85-86.

Thiel, E.C., 1956. Correlation of gravity anomalies with the Keweenawan geology of Wisconsin and Minnesota: Geol. Soc. Am. Bull., 67: 1079-1100.

Trehu, A., Morel-a-'l'Huissier, P., Meyer, R., Hajnal, Z., Karl, J., Mereu, R., Sexton, J., Shay, J., Chan, W.-K., Epili, D., Jefferson, T., Shih, X.-R., Wendling, S., Milkereit, B., Green, A., Hutchinson, D., 1991. Imaging the Midcontinent Rift beneath Lake Superior using large aperture seismic data: Geophys. Res. Lett., 18: 625-628.

Van Hise, C.R., and Leith, C.K., 1911, The geology of the Lake Superior region: U.S. Geological Survey Monograph 52, 641 pp.

Van Schmus, W.R., 1992. Tectonic setting of the Midcontinent Rift System: Tectonophysics, 213: 1-15.

Van Schmus, W. R., Green, J.C., and Halls, H.C., 1982. Geochronology of Keweenawan rocks of the Lake Superior region: A summary, In: R.J. Wold, W.J. Hinze, eds., Geology and Tectonics of the Lake Superior Basin: Geol. Soc. Am. Mem. 156: 165-171.

Van Schmus, W.R., and Hinze, W.J., 1985, The Midcontinent Rift System: Annual Reviews of Earth and Planetary Science, 13: 345-383.

Van Schmus, W.R., Bickford, M.E., and Zietz, I., 1987. Early and Middle Proterozoic provinces in the central United States, In: A. Kroner, ed., Proterozoic Lithospheric Evolution: Geodynamic Series, 17: 43-68.

Van Schmus, W.R., Martin, M.W., Sprowl, D.R., Geissman, J., and Berendsen, P., 1990. Age, Nd and Pb isotopic composition, and magnetic polarity for subsurface samples of the 1100 Ma Midcontinent Rift (abstract): Geol. Soc. Am., Abstracts with Program, 21: A174.

Wallace, H., 1981. Keweenawan geology of the Lake Superior Basin, In: F.H.A. Campbell, ed., Proterozoic Basins of Canada: Geological Survey of Canada, Paper 81-10: 399-417.

Weiblen, P.W., 1982. Keweenawan intrusive igneous rocks, In: R.J. Wold, W.J. Hinze, eds., Geology and Tectonics of the Lake Superior Basin: Geol. Soc. Am. Mem. 156: 57-82.

Weiblen, P.W., and Morey, G.B., 1980. A summary of the stratigraphy, petrology, and structure of the Duluth Complex: Am. J. Sci., 280A: 88-133.

Wernicke, B., 1985, Uniform-sense normal simple shear of the continental lithosphere: Canadian Journal of Earth Science, 22: 108-125.

White, W.S., 1966. Tectonics of the Keweenawan basin, western Lake Superior region: U.S. Geological Survey Professional Paper 524-E: E1-E23.

White, W.S., 1972. Keweenawan flood basalts and continental rifting (abstract): Geol. Soc. Am., Abstracts with Program, 4: 532-534.

White, R., and McKenzie D., 1989. Magmatism at rift zones: The generation of volcanic continental margins and flood basalts: J. Geophys. Res, 94: 7685-7729.

Witzke, B.J., 1990. General stratigraphy of the Phanerozoic and Keweenawan sequence, M.G. Eischeid #1 drillhole, Carroll Co., Iowa, In: R.R. Anderson, ed., The Amoco M.G. Eischeid #1 Deep Petroleum Test, Carroll County, Iowa: Iowa Geological Survey Special Report Series No. 2, 39-58.

Woelk, T.S., and Hinze, W.J., 1991. Model of the midcontinent rift system in northeastern Kansas: Geology, 19: 277-280.

Wold, R.J., and Hinze, W.J., 1982. Introduction, *in* R.J. Wold, W.J. Hinze, eds., Geology and Tectonics of the Lake Superior Basin: Geol. Soc. Am. Mem. 156: 1-4.

Wold, R.J., Hutchinson, D.R., and Johnson, T.C., 1982. Topography and surficial structure of Lake Superior bedrock as based on seismic reflection profiles, In: R.J. Wold, W.J. Hinze, eds., Geology and Tectonics of the Lake Superior Basin: Geol. Soc. Am. Mem. 156: 239-244.

Woollard, G.P., 1943. Transcontinental gravitational and magnetic profile of North America and its relation to geologic structure: Geol. Soc. Am. Bull., 54: 747-790.

Woollard, G.P., and Joesting, H.R., 1964. Bouguer Gravity Anomaly Map of the United States: U.S. Geological Survey, scale 1:25,000,000.

Yarger, H.L., 1985, Kansas basement study using spectrally filtered aeromagnetic data, In: W.J. Hinze, ed., The Utility of Regional Gravity and Magnetic Anomaly Maps: Society of Exploration Geophysicists, Tulsa, OK, 213-232.

Zhu, T., and Brown, L., 1986. Consortium for Continental Reflection Profiling Michigan surveys: reprocessing and results: J. Geophys. Res, 91: 11477-11495.

This Page Intentionally Left Blank

Chapter 11

Rifted passive margins

M. H. P. Bott

11.1. Introduction

Passive continental margins mark the juxtaposition of continental and oceanic lithosphere within plate interiors. They border most of the Atlantic, Indian and Arctic Oceans which are increasing in size by seafloor spreading as the continents drift apart. They are also located along the Antarctic edge of the closing Pacific Ocean and occur within some marginal seas such as the Mediterranean. Passive margins originate by the continental break-up process. At the time of their formation, they coincide with newly formed accretionary plate boundaries when they form a type of continental rift system. Subsequently, as the new ocean starts to open, the margins cease to be plate boundaries.

Passive margins are divisible into rifted and sheared (offset) types. Rifted margins form where the initial plate separation is approximately perpendicular to the rupture. They show a gradational transition, and their morphology can be subdivided into continental shelf, continental slope and continental rise. Sheared margins (Scrutton, 1982b) form when the initial split is along a transform fault; they generally show a much sharper transition and a much smaller thickness of sediments. They are not discussed here because of their limited relevance to continental rift structures.

Within the framework of the Wilson cycle, a typical passive margin would eventually be expected to become an active margin when the adjacent ocean cannot open any further and subduction develops at its edges. The ocean then starts to shrink, as the Pacific is now doing. Eventually the margin may become involved in collision orogeny, and may end up within a continental interior region which has suffered mountain building. In this way, remnants of ancient rift systems may occur within orogenic belts.

This contribution briefly discusses the salient features of passive margins with particular reference to the rift structures which develop during their formation. Examples are all taken from the Atlantic Ocean, particularly the North Atlantic, which has been studied in greatest detail. There are several recent compilations dealing with passive margins, and for further detail the reader is particularly referred to Scrutton (1982a) and Sheridan and Grow (1988).

11.2. Significance

Rifted passive margins are underlain by stretched continental crust formed prior to the final continental break-up. The stretched upper crust is rifted and often forms a region of highly extended terrain. Some segments of passive margins display intense flood basalt volcanism at about the time of the break-up and just before it. Passive margins thus show two of the major characteristics of continental rift structures, although most of them were not domed at the time of formation, rather the reverse. It has frequently been suggested or implied that a continental rift system such as that of East Africa may de-

velop into a future continental split (e.g. Burke and Whiteman, 1973). We thus need to compare the structures of the initial stages of passive margin formation with those of major continental rift systems.

Passive margins are of widespread economic importance as a source of oil and gas. The most detailed exploration of the sediment structure stems from the search for petroleum. However, geophysical and geological data from university and government research groups, as well as industry, has substantially contributed to our present knowledge of their structure and evolution.

11.3. Geological features

The sediments and igneous rocks of passive margins are discussed in this section. Commercial seismic reflection surveys in the 1960s indicated that normal passive margins are characterized by thick piles of sediment, and this became generally recognized in the 1970s (e.g. Sheridan, 1974). However, there are a few starved margins where sediments are thin or absent due to lack of supply during their development, such as the Biscay and Hatton margins, and these are important in enabling detailed investigation of the early development and of the crustal transition. Certain special regions suffered intense basaltic volcanism prior to continental break-up and these can be referred to as plume or hot spot passive margins. At inter-plume margins the associated igneous activity is more subdued and may be absent.

11.3.1. Sediments

The sediment structure at inter-plume passive margins is known as a result of commercial and other seismic reflection investigations (see section 11.4 below), supplemented by more sparse drill holes including a substantial number of DSDP sites. Specific examples are given in section 11.5 and here the main features are summarized.

In general, the sedimentary rocks found at passive margins have been formed during three successive stages. First, the continental basement may be overlain by sediments deposited prior to rifting, such as the Upper Jurassic strata of the North Biscay margin (Montadert et al., 1979). Second, syn-rift sediments of the rifting stage of margin development may be deposited at the time of initial rifting and continental stretching. They can be up to about 5 km thick but are usually rather thinner.

Third, post-rift sediments of the drifting stage are deposited subsequent to continental break-up and onset of seafloor spreading. They are separated from the underlying syn-rift sediments by the post-rift or break-up unconformity. Provided that there is an adequate supply of sediments, thicknesses of up to about 12 km of post-rift sediments can accumulate above the original base of the slope. If exceptional quantities of sediments are available near the mouth of a large river, these can build seawards over the original continental rise to form a delta. Early post-rift sediments may be deposited in deep water, but shelf sediments are typically shallow water marine clastics or carbonates depending on the environment of deposition. If there was restricted circulation in the early proto-ocean, salt deposits may form near the bottom of the post-rift sequence, with the possibility of subsequent diapirism into the overlying pile. The post-rift sediments are generally un-faulted (except for growth faults at the slope) indicating a quiet tectonic environment apart from slow but persistent subsidence at an exponentially decreasing rate.

11.3.2. Sediment structure

The structure of the syn-rift sediments is well imaged by seismic reflection lines over inter-plume margins such as the starved North Biscay margin (de Charpal et al., 1978) but is also seen at great depth beneath the post-rift sediments of the U. S. Atlantic margin (e.g. Sheridan, 1974; Klitgord et al., 1988). Syn-rift structures may extend into the adjacent continental borderlands. Special cases are discussed later in sections 11.5 and 11.6.

Syn-rift sediments are typically deposited in half grabens formed by intense stretching and thinning of the continental crust and lithosphere. The upper crust deforms by brittle extensional faulting which may include major sub-horizontal detachment surfaces as well as the fault wedges. The ductile lower crust and upper mantle deform by plastic stretching and thinning. The style of the upper crustal extensional deformation reflects a very low value of flex-

ural rigidity. Asymmetry within the underlying continental basement controls the polarity of the extensional wedges and the location of detachment surfaces. The region where

the lower crust and lithosphere are thinned, where break-up occurs, may be laterally offset from upper crustal stretching.

The two extreme models of the lithospheric stretching process are (1) *pure shear* (Fig. 11–1(a)) involving uniform and symmetrical stretching across the lithosphere (McKenzie, 1978), and (2) *simple shear* (Fig. 11–1(b)) whereby asymmetrical fault wedges in the upper crust are connected laterally by a detachment surface to offset stretching and thinning of the underlying lithosphere (Wernicke, 1985). As described by Lister et al. (1991), a wide variety of essentially asymmetric structures involving detachments can develop during the rift stage which are intermediate between these two models. Two of these are shown in Fig. 11–1. Fig. 11–1(c) shows asymmetrical faulting in the upper crust directly overlying a region of symmetrical ductile stretching. Fig. 11–1(d) shows a major offset connected by a detachment surface which separates lower and upper plates.

Characteristic asymmetrical syn-rift structures result from the prevalence of fault wedges and the occurrence of detachment surfaces. Additional asymmetry between complementary passive margins on opposite sides of an ocean such as the Atlantic arise as a result of offsets which occur between the zones of brittle upper crustal stretching and ductile stretching of the underlying lithosphere in relation to the location of the final break-up.

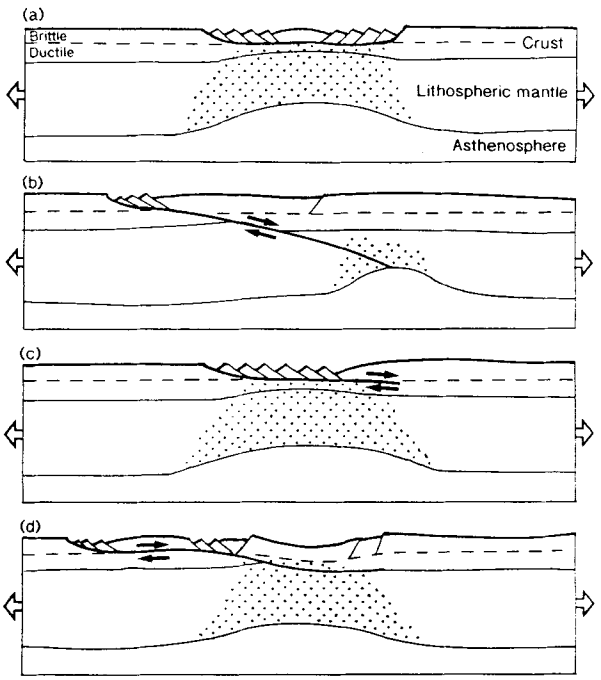

Fig. 11–1. Cartoons showing some of the simple models of extension of the continental lithosphere during the rifting stage of passive margin development given by Lister et al. (1991). (a) Pure shear extension producing symmetrical conjugate passive margins (ductile stretching indicated by stippling); (b) Simple shear (Wernicke) model; (c) Asymmetrical fault wedges underlain by symmetrical ductile stretching vertically beneath; (d) Delamination model with strongly asymmetrical stretching of the upper crust (fault wedges and detachment) and strongly offset pure shear ductile stretching of the underlying lithosphere. From Bott (1992a), reproduced by permission of the Geological Society of London.

11.3.3. Igneous activity

The continental borderlands adjacent to the so-called plume passive margin segments display extensive basaltic igneous activity at the time of continental break-up. By far the largest volumes of these igneous rocks are the predominantly tholeiitic flood basalts, which occupy local areas of the order of one thousand to one million km^2 with average aggregate thickness of about 1 km. Central intrusive complexes, sills and dike swarms also commonly occur. The most prominent occurrences are the early Tertiary volcanism of the North Atlantic region which was associated with the early Eocene break-up of Greenland and North Europe, and the Karroo, Parana and Deccan flood basalts which were associated with the break-up of Gondwanaland. Onshore volcanism may also affect inter-plume margin segments but it is much less intense. Here we discuss the plume margins, with particular reference to the early Tertiary North Atlantic province, recently described in Morton and Parson (1988). A further useful compilation used below is the Basaltic Volcanism Study Project (1981).

The North Atlantic province displays major igneous developments in central East Greenland and centered on the west Scotland - Faeroe region. The East Greenland lavas are quartz and olivine tholeiites with subordinate olivine basalts. Their total volume is estimated to be about 250,000 km^3 (Larsen et al., 1989). The Faeroe Islands are formed of quartz and olivine tholeiitic lavas with a thickness of about 5 km (Waagstein, 1988). Their estimated volume is probably about 4,000 km^3. The lavas of the British Isles province are alkali and tholeiitic basalts, with alkali and transitional types dominant; they occupy about 12,000 km^3. Central intrusive complexes and dike swarms occur in East Greenland and the British Isles, but are subordinate in volume to the lavas. Marine geophysical investigations indicate that perhaps even larger volumes of lava underlie the shelf regions of East Greenland, Faeroe Islands and Scotland, the subsided Rockall and Jan Mayen microcontinents and the earlier-formed Rockall Trough and Faeroe-Shetland Channel (see contributions in Morton and Parson, 1988).Taking the marine developments, erosion and ice cover into account, the total volume of lavas in this province is probably at least one million km^3.

The bulk of the early Tertiary igneous activity occurred between about 62 and 50 Ma, with the activity in North Scotland starting rather earlier than that of East Greenland (Mussett et al., 1988; Noble et al., 1988). Within each region, the flood basalts are the earliest phase. The onset of seafloor spreading was just prior to oceanic magnetic anomaly 24B, at about 54–52 Ma. Thus the main igneous activity took place over about 8–10 Ma prior to final break-up. A more precise sequence of events can be inferred from the East Greenland development (Bott, 1987). The main lava outpouring occurring over 2–3 Ma preceded the formation of the coastal flexure and dike swarm, which appears to have been contemporaneous with a short-lived episode of major stretching and thinning of the continental crust beneath the outer shelf, which is believed to precede the onset of seafloor spreading. This suggests that extensive melting may have resulted from decompression caused by local upwelling within the unstable hot upper mantle beneath the lithosphere prior to the syn-rift stage. Alternatively, White and McKenzie (1989) suggested that such flood basalts result from upwelling of the anomalously hot upper mantle as it rises passively beneath stretching and thinning lithosphere during the syn-rift stage.

A recently discovered type of igneous structure which occurs at most of the north-eastern North Atlantic margins is the downward fanning group of reflectors which extends along much of the continent-ocean crustal contact, as recently summarized by Parson et al. (1988). They are typically about 20 km wide, although if non-fanning reflectors are taken into account, the zone may be much wider. There has been controversy as to whether they overlie the edge of the disrupted continental crust (Hinz, 1981) or represent the earliest subaerial oceanic crust (Mutter et al., 1982), but DSDP drilling on the Voring Plateau which penetrated such a sequence indicates continental contamination of some of the lavas, suggesting that at least the inner part of the sequence is underlain by continental crust (Viereck et al., 1988).

11.4 Geophysical surveys and results

11.4.1. Seismic

(a) *Seismic refraction* was the earliest method of investigating the crustal thickness, layering and velocity structure at passive margins (e.g. Drake et al., 1959). This method reveals the broad transition from continental to oceanic crust and has been used very effectively in conjunction with gravity to model the broad structure across passive margins, using empirical velocity-density relationships such as Nafe-Drake (Nafe and Drake, 1963). However, the conventional seismic refraction method is limited in its resolution of the deep crustal transition. Recent developments which improve this resolution are described under (c) below.

(b) *Multi-channel seismic reflection profiling* has been instrumental in revealing the structure of the thick sediment piles, including the syn-rift and post-rift sediments and the break-up unconformity, as described above in section 11.3. This method also led to the discovery of the downward fanning dipping reflectors described briefly in section 11.3. Deep seismic reflection profiling has been used with some success to show up lower crustal reflections

and the reflection Moho across the Goban Spur margin west of U. K.(Peddy et al., 1989). Across the U. S. Atlantic margin, the Moho is observed over normal or slightly thinned continental crust and over oceanic crust, but not in the transitional region where the thick sediments obscure it (Klitgord et al., 1988).

(c) *Large aperture seismic experiments* using two or more ships have recently been used to extend the resolution of the deep crustal structure, particularly in the transitional region. Two methods are used (Stoffa and Buhl, 1979). In Common Depth Point profiling (CDP), two or more ships proceeding at constant offset all shoot and receive on arrays, thereby greatly increasing the seismic aperture enabling much better deep velocity information and lateral structural variation to be obtained at depth. In Expanding Spread Profiles (ESP), the two ships steam apart at the same speed, one shooting and one receiving, to yield an accurate velocity-depth profile through the crust. A series of ESPs parallel to the strike of the margin enables a crustal model across the transition between continental and oceanic crust to be determined with greatly improved resolution. Such surveys have revealed a region of high velocity (7.2–7.5 km/s) at the base of the transitional crust interpreted as igneous underplating at the Hatton margin (Fowler et al., 1989) and beneath the Baltimore and Carolina trough, U. S. Atlantic margin (Diebold et al., 1988; Tréhu et al., 1989).

11.4.2. Gravity

The gravity field across passive margins is generally well known from marine surveys (e.g. Featherstone et al, 1977; Sheridan et al., 1988). A free air gravity high which may exceed +100 mGal, but is more typically about +40 mGal, generally occurs along the outer shelf, and a low of similar amplitude occurs along the rise. These reflect approximate local isostatic equilibrium with compensation at the Moho, but there are smaller residual isostatic anomalies probably representing flexural effects associated with differential thermal subsidence and sediment loading. A review of the isostatic state of passive margins is given by Karner and Watts (1982).

Gravity profiles have been extensively used for modeling the crustal transition across passive margins in association with seismic data. Examples of such applications are given in section 11.5. The ambiguity associated with potential field modeling is greatly reduced in this way, although gravity still cannot give detailed resolution of the deep structure.

Satellite altimetry has directly determined the geoid on profiles across passive margins, as can be seen in the oceanic geoid map of Marsh et al. (1986). There is an abrupt change in the geoid height across these margins resulting from the dipolar nature of the isostatic compensation (Haxby and Turcotte, 1978). The geoid anomaly is more sensitive to deep isostatic compensation than gravity, and thus these profiles have the potential to yield information on the upper mantle density contrast between continents and oceans.

11.4.3. Magnetics

Most oceanic regions have been covered by magnetic profiling and surveying in sufficient detail to show the oceanic magnetic lineations which enable the ocean floor to be dated. In contrast, continental magnetic anomalies are generally less regular and of lower amplitude except where large anomalies are caused by lavas and igneous intrusions.

The edge of the oceanic magnetic anomalies can be used to map accurately and date the oldest oceanic crust adjacent to a margin, and thus to date the onset of seafloor spreading. As an example, the complementary margins of Rockall microcontinent and East Greenland can be dated at anomaly 24B (52–54 Ma) by this method (Montadert et al., 1979; Featherstone et al., 1977). This method fails when the oldest oceanic crust formed during a quiet magnetic period of prolonged single polarity such as occurs during the Late Jurassic and during the Late Cretaceous. However, the contrast in magnetization between the uniformly magnetic quiet zone oceanic crust and the more weakly magnetized continental crust may produce a strong edge effect magnetic anomaly. The East Coast Magnetic Anomaly of the U. S. Atlantic margin probably originates in this way (Klitgord et al., 1988). Magnetic anomalies are also useful at passive margins for estimating the depth to

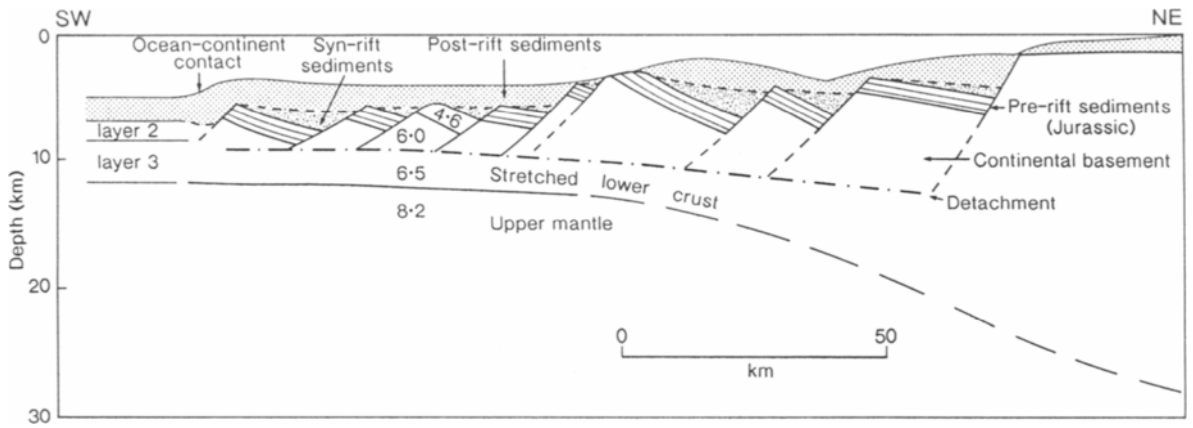

Fig. 11–2. Example of the structure of a starved inter-plume margin. Schematic crustal section through the northern continental margin of the Bay of Biscay, showing thin post-rift sediments (Late Aptian onwards), Early Cretaceous syn-rift sediments, tilted fault blocks of continental basement overlain by Jurassic pre-rift sediments, detachment surface separating lower and upper crust, continent-ocean contact beyond foot of slope and pattern of crustal thinning. Seismic velocities are shown in km/s. From Bott (1992a), reproduced by permission of the Geological Society of London.

magnetic basement, determining the fabric of the continental crust and mapping major igneous features beneath shelf and slope.

11.4.4. Heat flow and thermal state

There is practically no useful observational data on heat flow across passive margins, mainly because of the difficulty of making satisfactory measurements on the shelf and slope. An exception is the Red Sea, which is treated elsewhere in the book. The very limited data for the U. S. Atlantic margin is summarized by Sawyer (1988). However, considerable insight into the past and present temperature distributions can be obtained by thermal modeling based on assumed initial conditions and sedimentary history. The subsidence history of the margin indicates the cooling history of the underlying lithosphere and can be determined by backstripping (Watts and Ryan, 1976; Steckler et al., 1988).

11.4.5. Seismicity and state of stress

Passive margins display the lack of strong seismicity which is characteristic of plate interior regions. However, earthquakes do occur in certain regions reflecting local inhomogeneities and weaknesses, as in other plate interior regions. Passive margins have often been referred to as seismically inactive margins.

Observations of the present state of stress across passive margins depends on focal mechanism studies (oceans and continents) and in situ measurements (continents). Measurements are incorporated in the World Stress Map (Zoback et al., 1989). Oceanic lithosphere older than about 20 Ma is under horizontal deviatoric compression perpendicular to the ridges. Low lying continental regions are also found to be under horizontal compression approximately perpendicular to the adjacent ocean ridges, such as eastern North America and west Europe. The lack of tectonic activity except flexural subsidence indi-

cates that the lithosphere on both sides has been strong enough to withstand these stresses without failure during the whole of the drifting stage of development.

Theoretical stress modeling at passive margins (Bott and Dean, 1972) indicates that the continent may be in a state of deviatoric tension relative to the ocean. Combining this theoretical inference with the observational evidence above suggests that the adjacent oceanic regions are under moderately strong compression whereas the continents are affected by a weaker compression. On the other hand, if subcontinental lithosphere is denser than that beneath the adjacent ocean, this stress differential across a passive margin would be reduced or even annihilated.

The extensional structures and crustal thinning produced during the rifting stage indicate a quite different state of stress during the initial formation of the margin. A sufficiently strong deviatoric tension to give rise to whole lithospheric extensional failure applied at this time. An abrupt change in the state of stress evidently occurred at the time of the break-up unconformity when the a more neutral stress regime became rapidly established. This new state of stress was probably produced by ridge push from the newly formed ocean ridge.

11.5. Structure and development

Evidence is now presented of three well-studied examples from the North Atlantic illustrating the structure and evolution of a starved inter-plume margin (North Biscay), and fairly typical inter-plume margin (U. S. Atlantic margin) and a margin in a plume region (Hatton-Rockall).

11.5.1. North Biscay margin

At the North Biscay passive margin the rifting stage structures and the crustal transition are not deeply buried by post-rift sediments. It is the best known example of a starved margin. It has been studied by DSDP drilling (Montadert, Roberts et al., 1979) and by detailed seismic investigations (de Charpal et al., 1978; Le Pichon and Barbier, 1989). The results of these investigations have been crucial to our understanding of the general structure and evolution of passive margins.

A crustal section across this margin is shown in Figure 11–2. The transition from normal continental crust 30 km thick to oceanic crust 6 km thick occurs beneath the slope which is about 150 km wide. Thinned continental crust underlies the slope, and the continent-ocean contact occurs at the foot of the slope, where the extremely thinned continental crust is of similar thickness to the adjacent oceanic crust. There is no evidence of fan-shaped dipping igneous reflectors or of any other igneous activity prior to the oldest oceanic crust. The upper crust displays large extension by development of listric faulted wedges, with the faults facing seawards. Extreme thinning of the lower crust, which extends by ductile stretching, has occurred beneath the lower slope.

It is significant that the ductile stretching of the lower crust appears to be much greater than the brittle extension of the upper crust. Le Pichon and Barbier (1989) explained this by postulating a detachment fault separating the upper and lower crust. The missing part of the lower crust is thus now to be found on the complementary margin on the other side of the ocean. This emphasizes the asymmetry not only in the fault wedges but also between complementary margins.

The sedimentary succession, which reveals the evolutionary history of the margin, is well known from drilling and seismic reflection profiling. The continental basement is overlain by thin Upper Jurassic carbonates deposited in a shallow epicontinental sea, indicating that the region was underlain by fairly normal continental crust prior to the rifting stage. Syn-rift sediments were deposited in the half grabens as they formed, reaching maximum thicknesses of about 2 km. The syn-rift sediments appear to have been formed over about 25 Ma during the Lower Cretaceous although they may go back into the uppermost Jurassic. The post-rift unconformity is of Late Aptian age. The earliest drifting stage sediments are Late Aptian black shales deposited in about 2000 m of water at the foot of the slope, but shallowing towards the shelf. This indicates that the rifting stage resulted in overall subsidence. An additional 2300 m of thermal subsid-

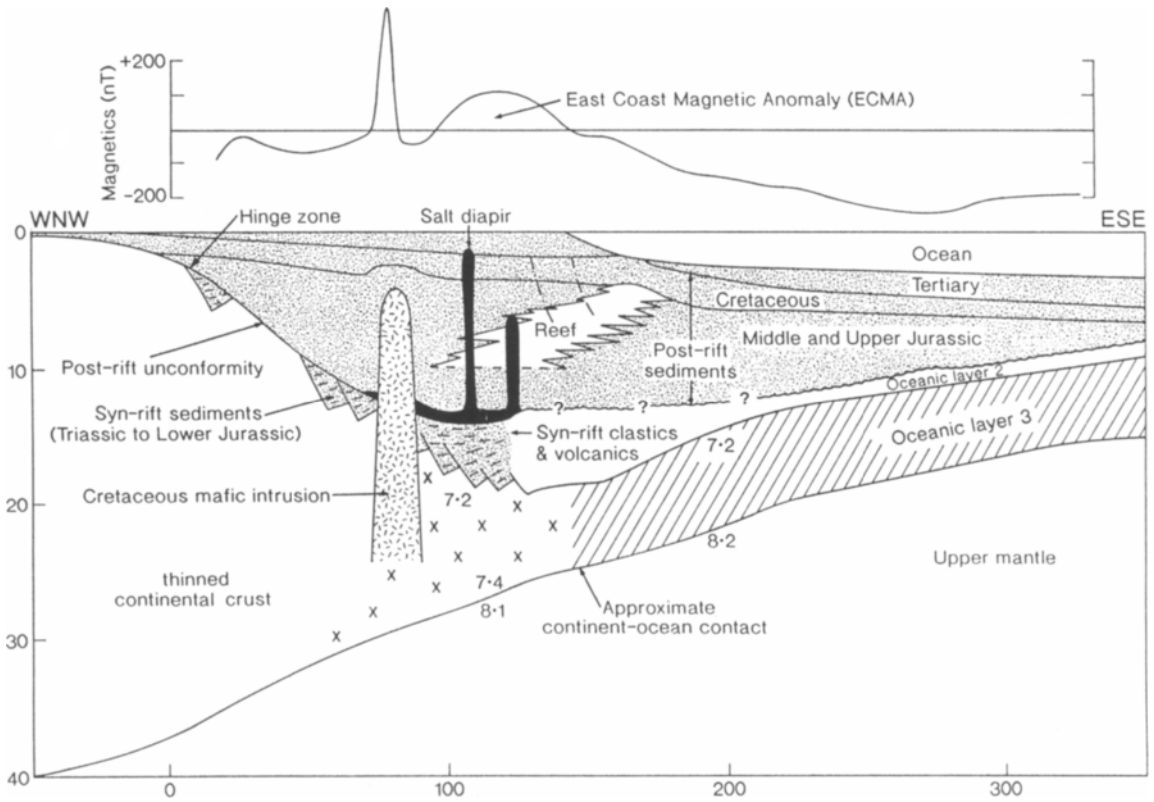

Fig. 11–3. A typical inter-plume passive margin. Crustal section through the U.S. Atlantic margin at Baltimore Canyon Trough. The section shows (1) the thick post-rift sediments with a prograding carbonate reef from Jurassic to Early Cretaceous, (2) syn-rift sediments deposited in half grabens with salt at the top, (3) the gradational crustal transition with the edge of true oceanic crust probably marked by the East Coast Magnetic Anomaly (ECMA), (4) the high velocity lower crust, and (5) salt diapirs and mafic intrusion penetrating post rift sediments. Redrawn from Grow and Sheridan (1988) and taken from Bott (1992a), reproduced by permission of the Geological Society of London.

ence of the margin has subsequently occurred at the foot of the slope, decreasing towards the shelf. The post-rift sediments are thin and include major hiatuses.

The results from the Biscay margin indicate that in absence of thick sediments, the margin developed in two stages. First, during the rifting stage lasting about 25 Ma the continental crust and lithosphere was stretched causing subsidence of 2000 m at the foot of the slope. There is no evidence for any doming or uplift during the rifting stage such as had previously been postulated for passive margins in general (Sleep, 1971). This suggests that the thermal anomaly at the onset of drifting was produced solely by the thinning of the lithosphere and the consequent upwelling of the underlying hot asthenosphere. There is no indication of any other underlying thermal anomaly. Second, during the drifting stage subsidence of up to 2300 m was caused by cooling of the lithosphere. Sediment loading had a relatively minor effect.

11.5.2. U. S. Atlantic continental margin

The Atlantic margin of eastern North America can be regarded as a fairly typical passive margin, with a good supply of sediment during its evolution. It has been studied in great detail by seismic, gravity and magnetic methods, and some drilling, as recently described in the DNAG volume (Sheridan and Grow, 1988). This and the complementary North African Atlantic margin are the oldest in the Atlantic Ocean, with seafloor spreading starting in the Early Jurassic. The crustal transition is buried beneath about 12 km of sediments.

A typical section across this margin, taken across the Baltimore Canyon trough at about 38°N, is shown in Figure 11–3 (Grow and Sheridan, 1988). The transition from 40 km thick continental crust to 7 km thick oceanic crust takes place over about 250 km. The pile of post-rift sediments is about 13 km thick, and the main seaward thickening starts abruptly at the hinge zone. The exact contact between disrupted continental crust and clear oceanic crust may be marked by the East Coast Magnetic anomaly, being located beneath the outer shelf. The post-rift unconformity is underlain by a series of half grabens with seaward facing bounding faults which are probably listric. Syn-rift deposits are locally up to about 5 km or more in thickness. The main region of stretched and modified continental crust extends over about 120 km from the hinge zone to the inferred continent-ocean crustal boundary. A region of 7.2–7.5 km/s lower crust underlies the outer part of the disrupted continental crust and may represent underplating, as has been suggested for the Carolina trough (Tréhu et al., 1989). A 25 km wide zone of seaward dipping downward fanning reflectors, which may mark the continent-ocean contact, has been observed on a USGS deep seismic reflection line east of Georges Bank (Klitgord et al., 1988). A local mafic intrusion penetrates the post-rift sediments of the Baltimore Canyon trough, giving rise to a sharp magnetic anomaly (Fig. 11–3).

The evolutionary history of the margin can be constructed from the evidence from numerous drill holes (e.g. Poag and Valentine, 1988) and from associated onshore syn-rift basins (Manspeizer and Cousminer, 1988). The onshore Newark basins are asymmetric half grabens filled with clastic Late Triassic sediments. The rifting stage probably included Late Triassic and most of the Early Jurassic, lasting about 50 Ma. This stage was accompanied by the Newark rift basalts and by the eastern North American dike swarms (de Boer et al., 1988). The rifting and associated igneous activity probably terminated at about 190–175 Ma, with the onset of seafloor spreading and salt deposition at the base of the post-rift sequence. An exponentially decaying thermal subsidence with sediment loading took place during the subsequent drifting stage, as inferred from backstripping and forward thermal modeling (Steckler et al., 1988).

An anomalous region of the U. S. Atlantic margin is the Blake Plateau (Dillon and Popenoe, 1988), a 250 km wide and fairly flat region with 800–1000 m water depth between the shelf edge and the slope between about 28° and 31° N. Geophysical investigations show that there are about 10 km of sediments in the Blake Plateau basin. The sediments are underlain by a crust which is about 20 km thick. The thin crust giving rise to the plateau was probably formed by stretching of normal continental crust during the Late Triassic to Early Jurassic rifting stage of formation, giving rise to a region of uniformly highly extended terrain. This is known as a marginal plateau, and such features occur at other passive margins, including some subsided microcontinental regions such as Rockall and Jan Mayen probably formed by the same process of fairly uniform extension of a region of continental crust during the rifting stage.

The U.S. Atlantic margin appears to differ from the North Biscay margin in two major ways. First, some significant igneous activity is in evidence during the rifting stage of development. Second, great thicknesses of sediment were deposited during the drifting stage. The 12 km thickness of post-rift sediments can readily be understood in terms of syn-rift lithospheric stretching followed by post-rift thermal subsidence as at Biscay, with the additional factors of (1) sediment loading which more than doubles the total amount of subsidence and (2) longer time span of development. There is no need to appeal to a major thermal anomaly during the rifting stage,

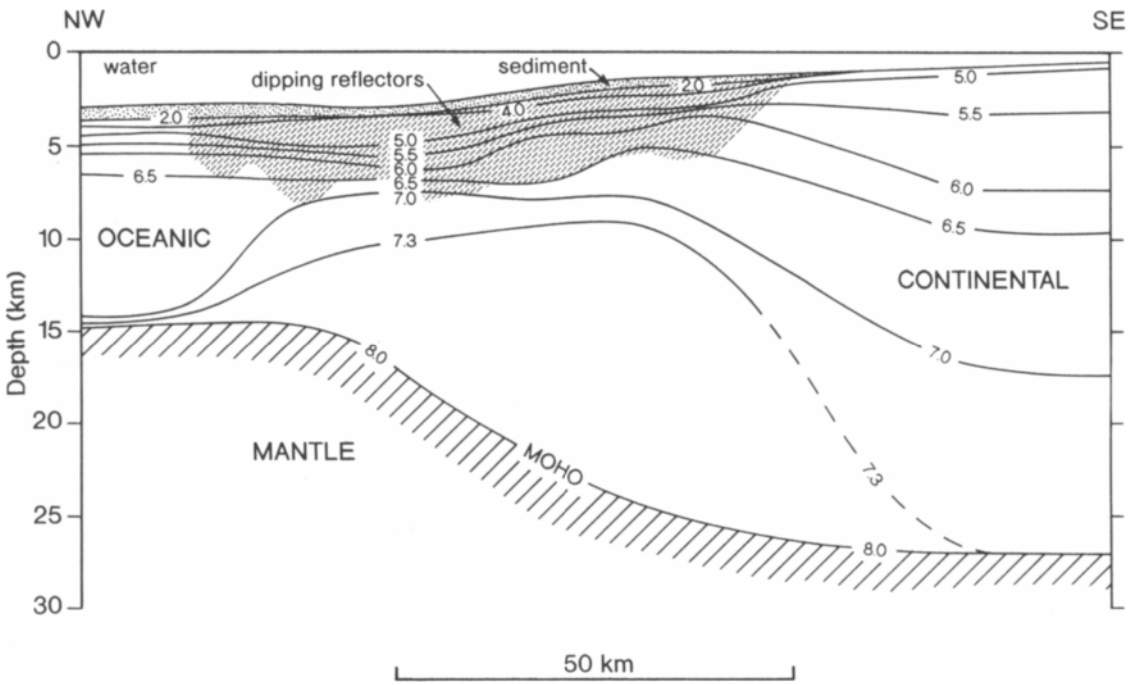

Fig. 11–4. Example of a plume passive margin. Section across the Hatton-Rockall margin at 59°N, showing the seismic velocity structure as obtained from a series of expanded spread profiles A to H. The section shows (1) the thick extrusive rocks including dipping reflectors which dominate the upper crust beneath the thin post rift sediments (shaded), (2) the gradational crustal transition with the lens of thick high velocity lower crust interpreted as underplated mafic material, and (3) the anomalously shallow oceanic region. Redrawn from Fowler et al. (1989).

apart from that produced by lithospheric stretching, although the syn-rift igneous activity does suggest hotter conditions than at North Biscay.

11.5.3. Hatton Rockall margin

The passive margin northwest of Hatton Bank (Rockall microcontinent) is probably the best-studied example of a highly magmatic plume margin. It is situated on the southern flank of the region affected by the intense early Tertiary volcanism of the northeastern North Atlantic. This margin has been studied by wide-angle two-ship multi-channel seismic investigations (White et al., 1987). Detailed gravity and magnetic data are also available. The nearby margin was drilled by DSDP (Montadert, Roberts et al., 1979). Seafloor spreading started in the early Eocene at anomaly 24B.

A crustal section across this margin based on a series of parallel along-strike expanding spread profiles is shown in Figure 11–4 (Fowler et al., 1989). The post-rift sediments are very thin and are underlain beneath the slope by a series of dipping reflectors which are interpreted as thick seaward dipping lavas. Any underlying syn-rift or pre-rift sediments are completely obscured by the thick lavas. The transition from 27 km thick continental crust to 7 km thick oceanic crust occurs beneath the gentle slope which is about 80 km wide. The increasing seaward thinning of the continental crust beneath the slope presumably results from stretching, although there

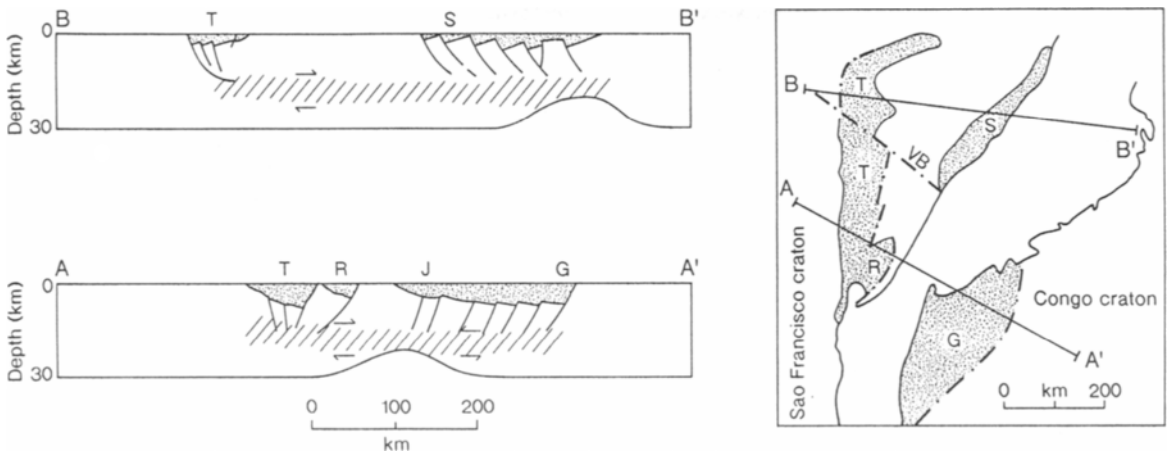

Fig. 11–5. Schematic cross sections across the Tucano-Gabon basin system bordering the South Atlantic Ocean at 10°–12° S, modified from Castro (1987). The locations of the two crustal sections AA and BB are shown on the sketch map of the continents prior to break-up. The following structural features are shown: G, Gabon basin, J, Jacuipe basin; R, Reconcavo basin; S, Sergipe-Alagoas basin, T, Tucano basin; Vb, Vaza-Barris transfer fault system. The upper crustal extensional faulting is separated from the ductile thinning of the lower crust by a postulated zone of mid-crustal weakness which is shaded diagonally. From Bott (1992a), reproduced by permission of the Geological Society of London.

is no direct evidence for this. There are two major anomalous features of the structure. First, there is a large lens of high velocity material (7.3–7.4 km/s) up to 14 km thick at the base of the crust beneath the margin, interpreted as underplated or intruded igneous material. The intense igneous activity which dominates upper and lower crust at this margin has been interpreted in terms of partial melting of upwelling asthenosphere as the lithosphere is stretched in a region near a pre-existing upper mantle hot spot (White et al., 1987). Second, the adjacent ocean floor is anomalously shallow for its age, and reflects the ongoing presence of an anomalously hot upper mantle in this region (Haigh, 1973).

The Hatton Bank margin is south of the region of greatest volcanism of the early Tertiary province. The maximum activity occurred in East Greenland and the region of the Faeroe Islands, which are located at opposite ends of the aseismic Icelandic transverse ridge, where the most intense activity has continued to form the thick oceanic crust of Icelandic type. It is difficult to explain the early Tertiary volcanism and the subsequent formation of the Icelandic transverse ridge except by an appeal to a hot spot in the upper mantle which preceded the continental breakup here, and has continued to affect a large region of the northeastern North Atlantic (Vogt, 1974; Bott, 1988).

11.6. Other rift structures near passive margins

Rift structures in the immediate vicinity of the passive margins have been considered above. Other rift type features associated with passive margins may extend further into the adjacent continents. Three examples of different type from the Atlantic region are described.

11.6.1. Tucano-Gabon graben system, South Atlantic

The north-south oriented Tucano graben is a conspicuous feature of northeastern Brazil. It is the largest of a series of deep sedimentary basins filled mainly by Early Cretaceous sediments on the complementary northeastern Brazil and Gabon mar-

gins. It is 400 km long, nearly 100 km wide and up to 7 km deep (Fig. 11–5). The Tucano basin is separated from the Atlantic margin by a triangular region of Precambrian basement. This and the other associated grabens are of particular interest because of their relationship to the formation of the complementary Brazilian and Gabon passive margins, as described by Ussami et al. (1986), Castro (1987) and de Matos (1992).

The great thickness of sediments in the Tucano basin were mainly formed over about 24 Ma in the Early Cretaceous, contemporaneous with the rifting stage of the adjacent passive margin. Significant subsidence terminated at the onset of seafloor spreading in the South Atlantic (Aptian/Albian boundary). The underlying crust appears to be unthinned and the evidence for significant thermal subsidence after this time is lacking. This suggested to Ussami et al. (1986) that the upper crustal stretching during formation of the Tucano basin was connected to lower lithospheric ductile thinning beneath the incipient passive margin to the east by a mid-crustal detachment surface and transfer faults, broadly according to the simple shear mechanism of Wernicke (1985). However, such a simple detachment surface is incompatible with the switching polarity of the Tucano basin, and a model along the lines of de Matos (1992) and Bott (1992a) involving a mid-crustal ductile shear zone as shown in Figure 11–5 better explains the observations.

The Tucano graben is an example of a rift formed on the continental borderland during the rifting stage of passive margin development. There are numerous examples of this type of rift in onshore regions adjacent to the Atlantic Ocean, including some failed-arms (Burke, 1976). The Tucano-Gabon is also a good example of asymmetrical development of a passive margin. Such asymmetry of conjugate margins is commonly seen elsewhere, although usually without such spectacular development. It originates from the combined effects of (1) asymmetrical rifting stage development with upper crustal extension laterally offset from the ductile stretching of the lower lithosphere, and/or (2) asymmetrical location of the line of continental splitting with respect to the stretched upper crust and/or the region of lithospheric thinning.

11.6.2. North Sea rift system

The Mesozoic North Sea rift system is deeply buried beneath thick Tertiary sediments but it has been studied in great detail by seismic reflection surveying and drilling because of the rich petroleum resources of the region. It exhibits very similar structural features to those of an inter-plume passive margin except that continental break-up did not occur. It can be regarded as a failed arm of the wider Mesozoic rifting along the North Atlantic borderlands. The dominant structures are the Viking Graben in the north and the Central Graben in the south. These join at a "triple junction" with the Moray Firth - Witch Ground Graben which extends westwards. The structure and evolution is described in Blundell and Gibbs (1990) and Hardman and Brooks (1990). A short summary review is given by Ziegler (1992) and sections across are shown in Figure 11–6.

North Sea rifting started with a Triassic to Early Jurassic rifting stage which was followed by Middle Jurassic doming. A second rifting stage dominated from Late Jurassic to Early Cretaceous, then waning and terminating in the Palaeocene.

The syn-rift sediments reach thicknesses of about 5 km within the grabens. The predominant dip of the faults on both sides is towards the center of the grabens, giving the overall structure some semblance of symmetry. Post-rift thermal subsidence without any conspicuous faulting occurred during the Tertiary. This is greatest along the line of the main grabens, reaching a maximum of 3.5 km over the Central Graben, and it extends laterally beyond the rift zone. The main associated igneous activity consists dominantly of mildly undersaturated alkali basalts of Middle Jurassic age (Ritchie et al., 1988; Latin and Waters, 1992).

The crustal structure is known from seismic refraction, seismic reflection and gravity observations (Barton and Wood, 1984; Hollinger and Klemperer, 1990). The Moho is slightly over 30 km deep in the adjacent regions and rises by about 9 km to 23 km beneath the Central Graben, where the sub-sedimentary crust is thinner by a factor of two, implying a 100 km extension of the continental crust. According the Ziegler (1992), upper crustal stretching by faulting is significantly less than the stretching re-

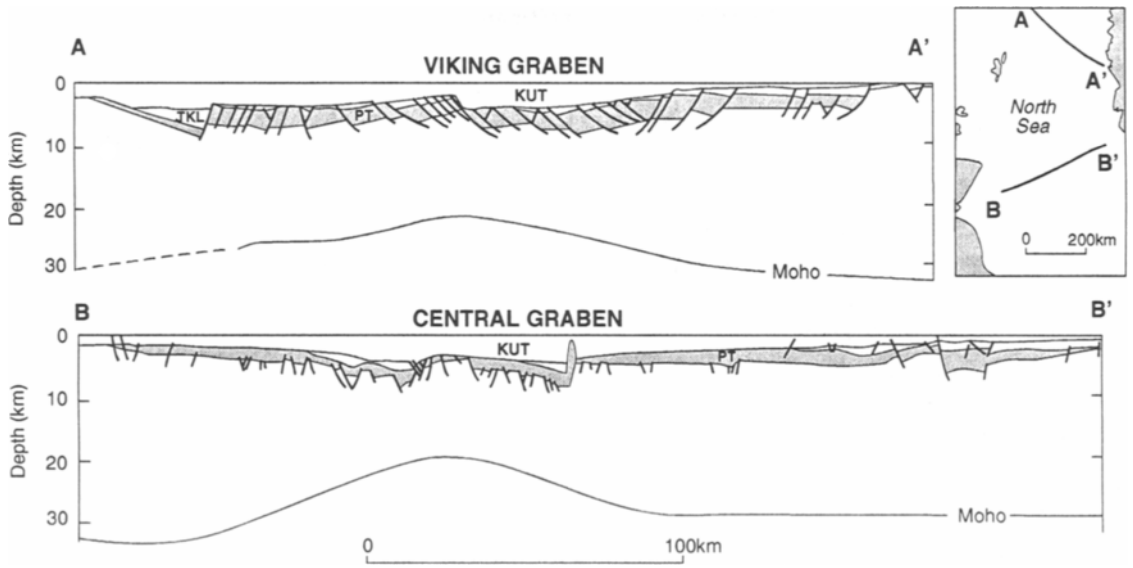

Fig. 11–6. Sections across the Viking Graben and the Central Graben (North Sea) to illustrate the relationship between rifting (Triassic to Upper Cretaceous), thermal subsidence (Upper Cretaceous to present) and crustal structure. PT = Permian and Triassic; JKL = Jurassic and Lower Cretaceous; KUT = Upper Cretaceous and Tertiary. Redrawn from Ziegler (1990).

quired to thin the underlying ductile crust. There is also related controversy as to whether the extension can be regarded as pure shear stretching or requires significant asymmetrical faulting.

The syn-rift and post-rift stages mimic those observed at a typical inter-plume passive margin. However, the North Sea rift system lacks the extreme stretching of the ductile crust typically observed at passive margins. Consequently the North Sea thermal subsidence is smaller by a factor of three or four. The rifting lasted 175 Ma and was complicated by a short doming between two stages of rifting, unlike that at a typical passive margin. This is a remarkably long duration for continental rifting of any type and may have resulted from the two separate stages. It contrasts with the more typical life time of rifting of about 50 Ma (see Chapter 1). The North Sea rift system also differs from the main Tertiary continental rift systems in that the doming was a much less significant factor.

11.6.3. Rockall Trough

Rockall Trough and its northern extension as the Faeroe-Shetland Channel is a major rift-like bathymetric depression which separates the Scottish and Irish shelf regions from the Rockall and Faeroes microcontinental region. The transverse Wyville-Thomson Ridge separates the Trough from the Channel. The Møre basin forms a buried northeastern extension of the Faeroe-Shetland Channel. Southern Rockall Trough is about 200 km wide with steep margins and it is about 3 km deep, with thick sediments beneath the seabed. The depression, which is about 1500 km long, narrows and shallows northwards towards the Møre basin. It has been referred to as the proto-North Atlantic.

The origin of the wide graben-like feature formed by the Rockall Trough and its northeastward extension remains controversial, as recently reviewed by Smythe (1989). One of the difficulties is the blanketing of much of the deep structure by thick Pale-

ocene and early Eocene volcanics. The most commonly held hypothesis is that it formed during the Cretaceous, possibly mid-late Cretaceous according to Roberts et al. (1981). The alternate hypothesis is that it formed earlier, possibly in the Late Carboniferous to Early Permian (see Smythe, 1989). As definitive magnetic anomalies are absent, it is disputable as to whether it formed by seafloor spreading or by extension of the continental crust or by a combination of these. It has been claimed that the crustal structure revealed by a comprehensive seismic experiment indicates stretched continental crust (Roberts et al., 1988), but Smythe (1989) considered the evidence to be ambiguous. The most recent two-ship seismic experiment (Joppen and White, 1990) indicated a 6 km thick crust which includes thick syn-rift intrusives. The nature of the crust remains uncertain although they favor a stretched continental origin.

The favored hypothesis is that Rockall Trough is underlain by continental crust which has been stretched by a factor of 6–10 during the Cretaceous. If this is correct, it must be underlain by a fairly uniform region of highly extended terrain. The symmetry of the structure is best fitted by the pure shear model shown in Figure 11–1(a).

11.7. Evolution

The broad evolution of passive margins as revealed by studies of Atlantic margins is summarized here, first by reference to weakly magmatic inter-plume margins, and second by reference to the highly magmatic plume segments.

11.7.1. Normal (inter-plume) margins

The evolution of normal passive margins, as inferred particularly from the evidence of North Biscay and U. S. Atlantic margins, follows the following stages:

(1) The margins have developed in continental interior regions having *pre-rifting stage* crust of typical continental thickness with elevation at or near sea level. However, the line of splitting is affected by basement weakness reflecting the alignment of earlier fold belts, such as the pan-African folding in the South Atlantic and the Caledonian-Appalachian fold belts of the North Atlantic. An exception is the early Eocene split of South Greenland from Rockall-Hatton Bank which broke through a Precambrian cratonic region (Bott, 1987).

(2) Continental break-up starts with a *rifting stage* of development, when a strip of continental lithosphere about 100 to 150 km wide becomes stretched to approaching twice its original width over a period of about 25–50 Ma. This suggests an average rate of separation of about 3 mm/yr. Stretching of the brittle upper crust gives rise to listrically faulted half-grabens and detachment faults. The lower crust responds by ductile stretching. The amount of stretching is broadly indicated by the resulting crustal thickness, with greatest stretching producing continental crust of similar thickness to oceanic crust in the central region. Thinning of the lithosphere proportionately raises the lithospheric isotherms accompanying upwelling of the underlying hot asthenosphere. Some volcanism extending into the onshore regions may occur as a result of the adiabatic decompression as the asthenospheric material upwells, but it is insufficient to swamp the incipient margin. The combined effect of the crustal thinning and the thermal anomaly is to produce a net subsidence of up to about 2 km. There is no requirement from the available evidence for a domal uplift affecting the stretched region and the adjacent borderlands, rather the reverse (but cf. Red Sea margins and the plume margins). It must be assumed that the continental crust was subjected to a substantial deviatoric tension during the rifting stage, and this may have originated from trench suction affecting opposite sides of a large continental mass such as Pangaea.

(3) The rifting stage abruptly terminates and the *drifting stage* starts with the onset of seafloor spreading. Extensional tectonics ceases and slow subsidence of the margin commences. Sediment piles of up to 12 km thickness may develop as a results of (1) the initial water depth after rifting, (2) exponentially decaying thermal subsidence as the lithosphere thickens and cools, and (3) subsidence due to sediment loading. The abrupt change in stress affecting the margin can be attributed to the ridge push plate boundary force at the newly formed ocean ridge.

As described in the preceding section, a variety of graben type basins can form in the onshore region during the rifting stage, and the final line of splitting may be asymmetrically located.

11.7.2. Plume passive margins

The evolution of the plume-dominated passive margins of the northeastern North Atlantic differs markedly from that of the more normal inter-plume passive margins discussed above, in the dominance of the associated magmatic activity. Tentatively, the evolution of this type of margin is summarized as follows:

(1) It is assumed that the first stage is the development of a hot spot in the upper mantle beneath, probably resulting from the break-through of a lower mantle plume of the type envisaged by Loper (1985) which carries hot material from the boundary layer at the base of the mantle into the upper mantle asthenosphere. The raised temperature lowers the density of the upper mantle and may give rise to some domal uplift, although detailed evidence is scanty.

(2) Eruption of large volumes of predominantly tholeiitic flood basalts, with intrusion of associated ring complexes and dikes, dominates the development over about 10 Ma prior to the onset of seafloor spreading. Stretching and thinning of the underlying continental crust may occur contemporaneously, but firm evidence on how this takes place is masked by the volcanics. However, subsidence during eruption, thinning of the continental crust beneath the slope, and plateau subsidence indicate that such rifting stage stretching has occurred. The intense magmatic activity originates by upwelling within an anomalously hot asthenosphere. This may accompany stretching of the lithosphere as advocated by White et al. (1987) It may occur prior to stretching as a result of local upwelling within the hot upper mantle as it develops from a plume.

(3) After onset of seafloor spreading, most of the continental volcanism dies out, with local activity in central complexes continuing for a further few million years. Thermal subsidence of the margins takes place as at inter-plume margins. The continental borderlands and the new oceanic region may be dominated by the upper mantle hot spot for well over 50 Ma as is still occurring in the northeastern North Atlantic where oceanic depths are anomalously shallow and continental borderlands are locally and regionally uplifted. A ridge of anomalously thick Icelandic type crust may be formed by the apex of the hot spot activity, forming a transverse ridge across the developing ocean.

11.7.3. Origin of passive margins

How do passive margins originate? The evidence suggests that they formed during a period of continent-wide extensional stress in the continental lithosphere, unlike the present-day situation with compression dominant in normal continental crust. A plausible suggestion is that their formation is triggered by development of an upper mantle hot spot above a lower mantle plume. The continental lithosphere above the plume would be weakened and subjected to additional local tension, initiating the continental split, which would then readily spread laterally into the inter-plume regions as a result of the continent wide tension. A new more compressional stress regime would be abruptly introduced once seafloor spreading started.

11.8. Passive margin rifting compared with present day continental rifting

The rifting stage of passive margin development has produced extensive ancient continental rift systems of a special type. Were these ancient rift systems identical to the present-day continental rift systems or is there a distinction? The difficulty in making this comparison is that the passive margin structures are almost all deeply buried and information about them is much less well resolved. There is sufficient evidence, however, to point out similarities and differences.

Both modern rift systems and ancient passive margin rift structures form long linear belts within original continental interior regions where the upper crust has been extended by faulting and graben formation, mainly half grabens. Both types have thus been formed as a result of horizontal deviatoric tension affecting the continental lithosphere. Both may be associated with syn-rift basaltic volcanic activ-

ity. Doming occurs in modern rift regions and also may occur along some passive margin segments. Both types of structure are possibly triggered by hot spot (plume) activity in the underlying upper mantle, and are to greater or lesser extent dependent on the state of ambient stress in the continental lithosphere.

There are, however, a number of major differences between modern rift systems and passive margin rift belts, summarized briefly as follows:

(1) Passive margin rift belts generally display much more extreme stretching than modern rifts and they may be rather wider.

(2) The lengthy inter-plume segments of passive margins appear not to have been affected by domal uplift, in strong contrast to most modern rift systems.

(3) The passive margin plume volcanism is predominantly tholeiitic whereas the modern rift system volcanism tends to be more alkalic, as exhibited in East Africa and Baikal but less so in Rio Grande.

The incipient passive margins formed a very extensive and interconnected series of rift systems during the Mesozoic. These differed significantly from modern uplifted rift systems. The simplest explanation for the difference is that the passive margin rifting occurred at a time when widespread tension affected the continental lithosphere, in contrast to the slight compression which is observed in the modern continental regions which are unelevated. The contrasting states of stress may depend on the nature of the plate boundary forces which affected continental regions at the time of continental break-up, with the possibility of subduction on opposite sides (Bott, 1992b). The trench suction plate boundary force thus probably dominated a supercontinent such as Pangaea at the time of break-up, giving rise to widespread tension. Ridge push dominates in the more fragmented modern continental regime.

11.9. References

Barton, P. and Wood, R., 1984. Tectonic evolution of the North Sea basin: crustal stretching and subsidence. Geophys. J. R. Astron. Soc., 79: 987–1022.

Basaltic Volcanism Study Project, 1981. Basaltic Volcanism on the Terrestrial Planets. Pergammon Press, New York, 1286 pp.

Blundell, D. J. and Gibbs, A. D.(Editors), 1990. Tectonic evolution of the North Sea rifts. Oxford University Press, Oxford, 272 pp.

Bott, M. H. P., 1987. The continental margin of central East Greenland in relation to North Atlantic plate tectonic evolution. J. Geol. Soc. London, 144: 561–568.

Bott, M. H. P., 1988. A new look at the causes and consequences of the Icelandic hot-spot. In: A. C. Morton and L. M. Parson (Editors), Early Tertiary volcanism and the opening of the NE Atlantic. Geol. Soc. London Spec. Publ., 39: 15–23.

Bott, M. H. P., 1992a. Passive margins and their subsidence. J. Geol. Soc. London, 149: 805–812.

Bott, M. H. P., 1992b. The stress regime associated with continental break-up. In: B. C. Storey, T. Alabaster and R. J. Pankhurst (Editors), Magmatism and the causes of continental break-up. Geol. Soc. London Spec. Publ., 68: 125–136.

Bott, M. H. P. and Dean, D. S., 1972. Stress systems at young continental margins. Nature, Phys. Sci., 235: 23–25.

Burke, K., 1976. Development of graben associated with the initial ruptures of the Atlantic Ocean. Tectonophysics, 36: 93–112.

Burke, K. and Whiteman, A. J., 1973. Uplift, rifting and the break-up of Africa. In: D. H. Tarling and S. K. Runcorn (Editors), Implications of continental drift to the Earth sciences, vol. 2. Academic Press, London, pp. 735–755.

Castro, A. C. M., Jr., 1987. The northeastern Brazil and Gabon basins: a double rifting system associated with multiple crustal detachment surfaces. Tectonics, 6: 727–738.

de Boer, J. Z., McHone, J. G., Puffer, J. H., Ragland, P.C. and Whittington, D., 1988. Mesozoic and Cenozoic magmatism. In: R. E. Sheridan and J. A. Grow (Editors), The Geology of North America, vol. I-2, The Atlantic continental margin: U. S. The Geological Society of America, Boulder, Colorado, pp. 217–241.

de Charpal, O., Guennoc, P., Montadert, L. and Roberts, D. G., 1978. Rifting, crustal attenuation and subsidence in the Bay of Biscay. Nature, 275: 706–711.

de Matos, R. M. D., 1992. The northeast Brazilian rift system. Tectonics, 11: 766–791.

Diebold, J. B., Stoffa, P. L. and the LASE Study Group, 1988. A large aperture seismic experiment in the Baltimore Canyon Trough. In: R. E. Sheridan and J. A. Grow, The Geology of North America, vol. I-2, The Atlantic continental margin: U. S. The Geological Society of America, Boulder, Colorado, pp. 387–398.

Dillon, W. P. and Popenoe, P., 1988. The Blake Plateau Basin and Carolina Trough. In: R. E. Sheridan and J. A. Grow, The Geology of North America, vol. I-2, The Atlantic continental margin: U. S. The Geological Society of America, Boulder, Colorado, pp. 291–328.

Drake, C. L., Ewing, M. and Sutton, G. H., 1959. Continental margins and geosynclines: the east coast of North America north of Cape Hatteras. Phys. Chem. Earth, 3: 110–198.

Featherstone, P. S., Bott, M. H. P. and Peacock, J. H., 1977. Structure of the continental margin of south-eastern Greenland. Geophys. J. R. Astron. Soc., 48: 15–27.

Fowler, S. R., White, R. S., Spence, G. D. and Westbrook, G. K., 1989. The Hatton Bank continental margin - II. Deep structure from two-ship expanding spread seismic profiles. Geophys. J., 96: 295–309.

Grow, J. A. and Sheridan, R. E., 1988. U. S. Atlantic continental margin; a typical Atlantic-type or passive continental margin. In: R. E. Sheridan and J. A. Grow (Editors) The Geology of North America, vol. I-2, The Atlantic continental margin: U. S. The Geological Society of America, Boulder, Colorado, pp. 1–7.

Haigh, B. I. R., 1973. North Atlantic oceanic topography and lateral variations in the upper mantle. Geophys. J. R. Astron. Soc., 33: 405–420.

Hardman, R. F. P. and Brooks, J. (Editors), 1990. Tectonic events responsible for Britain's oil and gas reserves. Geol. Soc. London Spec. Publ., 55, 404 pp.

Haxby, W.F. and Turcotte, D. L., 1978. On isostatic geoid anomalies. J. Geophys. Res., 83: 5473–5478.

Hinz, K., 1981. A hypothesis of terrestrial catastrophes. Wedges of very thick oceanward dipping layers beneath passive continental margins - their origin and palaeoenvironmental significance. Geologische Jahrbuch, E22: 3–28.

Holliger, K. and Klemperer, S. L., 1990. Gravity and deep seismic reflection profiles across the North Sea rifts. In: D. J. Blundell and A. D. Gibbs (Editors), Tectonic evolution of the North Sea rifts, Oxford University Press, Oxford, pp. 82–100.

Joppen, M. and White, R. S., 1990. The structure and subsidence of Rockall Trough from two-ship seismic experiments. J. Geophys. Res., 95: 19821–19837.

Karner, G. D. and Watts, A. B., 1982. On isostasy at Atlantic-type continental margins. J. Geophys. Res., 87: 2923–2948.

Klitgord, K. D., Hutchinson, D. R. and Schouten, H., 1988. U. S. Atlantic continental margin; structural and tectonic framework. In: R. E. Sheridan and J. A. Grow (Editors), The Geology of North America, vol. I-2, The Atlantic continental margin: U. S. The Geological Society of America, Boulder, Colorado, pp. 19–55.

Larsen, L. M., Watt, W. S. and Watt, M., 1989. Geology and petrology of the Lower Tertiary plateau basalts of the Scoresby Sund region, East Greenland. Bull. Grønlands Geol. Unders., 157: 1–164.

Latin, D. and Waters, F. G., 1992. Basaltic magmatism in the North Sea and its relationship to lithospheric extension. Tectonophysics, 208: 77–90.

Le Pichon, X. and Barbier, F., 1987. Passive margin formation by low-angle faulting within the upper crust: the northern Bay of Biscay margin. Tectonics, 6: 133–150.

Lister, G. S., Etheridge, M. A. and Symonds, P.A., 1991. Detachment models for the formation of passive continental margins. Tectonics, 10: 1038–1064.

Loper, D. E., 1985. A simple model of whole-mantle convection. J. Geophys. Res., 90: 1809–1836.

Manspeizer, W. and Cousminer, H. L., 1988. Late Triassic-Early Jurassic synrift basins of the U. S. Atlantic margin. In: R. E. Sheridan and J. A. Grow (Editors), The Geology of North America, vol. I-2, The Atlantic continental margin: U.S. The Geological Society of America, Boulder, Colorado, pp. 197–216.

Marsh, J. G., Brenner, A. C., Beckley, B. D. and Martin, T. V., 1986. Global mean sea surface based upon the Seasat altimeter data. J. Geophys. Res., 91: 3501–3506.

McKenzie, D., 1978. Some remarks on the development of sedimentary basins. Earth Planet. Sci. Lett., 40: 25–32.

Montadert, L., Roberts, D. G. et al., 1979. Initial reports of the Deep Sea Drilling Project, vol. 48. U. S. Government Printing Office, Washington, D. C., 1183 pp.

Montadert, L., Roberts, D. G., De Charpal, O. and Guennoc, P. 1979. Rifting and subsidence of the northern continental margin of the Bay of Biscay. *In:* L. Montadert, D. G. Roberts et al. (Editors), Initial reports of the Deep Sea Drilling Project, vol. 48. U. S. Government Printing Office, Washington, DC., pp. 1035–1060.

Morton, A. C. and Parson, L. M. (Editors), 1988. Early Tertiary volcanism and the opening of the NE Atlantic. Geol. Soc. London Spec. Publ., 39, 477 pp.

Mussett A. E., Dagley, P. and Skelhorn, R. R., 1988. Time and duration of activity in the British Tertiary igneous province. *In:* A. C. Morton and L. M. Parson (Editors), Early Tertiary volcanism and the opening of the NE Atlantic. Geol. Soc. London Spec. Publ., 39: 337–348.

Mutter, J. C., Talwani, M. and Stoffa, P. L., 1982. Origin of seaward-dipping reflectors in oceanic crust off the Norwegian margin by "subaerial sea-floor spreading". Geology, 10: 353–357.

Nafe, J. E. and Drake, C. L. 1963. Physical properties of marine sediments. *In:* M. N. Hill (Editor), The Sea, vol. 3. Interscience Publishers, New York, pp. 794–815.

Noble, R. H., Macintyre, R. M. and Brown, P. E., 1988. Age constraints on Atlantic evolution: timing of magmatic activity along the E Greenland continental margin. *In:* A. C. Morton and L. M. Parson (Editors), Early Tertiary volcanism and the opening of the NE Atlantic. Geol. Soc. London Spec. Publ., 39: 201–214.

Parson L. M. and the ODP Leg 104 Scientific Party, 1988. Dipping reflector styles in the NE Atlantic Ocean. In: A. C. Morton and L. M. Parson (Editors), Early Tertiary volcanism and the opening of the NE Atlantic. Geol. Soc. London Spec. Publ., 39: 57–68.

Peddy, C., Pinet, B., Masson, D., Scrutton, R., Sibuet, J. C., Warner, M. R., Lefort, J. P. and Shroeder, I. J. (BIRPS and ECORS), 1989. Crustal structure of the Goban Spur continental margin, Northeast Atlantic, from deep seismic reflection profiling. J. Geol. Soc. London, 146: 427–437.

Poag, C. W. and Valentine, P.C., 1988. Mesozoic and Cenozoic stratigraphy of the United States Atlantic continental shelf and slope. In: R. E. Sheridan and J. A. Grow (Editors), The Geology of North America, vol. I–2, The Atlantic continental margin: U. S. The Geological Society of America, Boulder, Colorado, pp. 67–85.

Ritchie, J. D., Swallow, J. L., Mitchell, J. G. and Morton, A. C., 1988. Jurassic ages from intrusives and extrusives within the Forties igneous province. Scott. J. Geol., 24: 81–88.

Roberts, D. G., Ginzberg, A., Nunn, K. and McQuillin, R., 1988. The structure of the Rockall Trough from seismic refraction and wide-angle reflection measurements. Nature, 332: 632–635.

Roberts, D. G., Masson, D. G. and Miles, P. R., 1981. Age and structure of the southern Rockall Trough: new evidence. Earth Planet. Sci. Lett., 52: 115–128.

Sawyer, D.S., 1988. Thermal evolution. *In:* R. E. Sheridan and J. A. Grow (Editors), The Geology of North America, vol. I-2, The Atlantic continental margin: U. S. The Geological Society of America, Boulder, Colorado, pp. 417–428.

Scrutton, R. A. (Editor), 1982a. Dynamics of passive margins. Geodynamics Series, vol. 6, American Geophysical Union, Washington, DC., 200 pp.

Scrutton, R. A., 1982b. Crustal structure and development of sheared passive continental margins. In: R. A. Scrutton (Editor), Dynamics of passive margins. Geodynamics Series., vol. 6, American Geophysical Union, Washington, DC., pp. 133–140.

Sheridan, R. E., 1974. Atlantic continental margin of North America. In: C.A. Burk and C. L. Drake (Editors), The Geology of continental margins. Springer-Verlag, New York, pp. 391–407.

Sheridan, R. E., and Grow, J. A. (Editors), 1988. The Geology of North America, vol. I-2, The Atlantic continental margin: U.S. The Geological Society of America, Boulder, Colorado, 610 pp.

Sheridan, R. E., Grow, J. A. and Klitgord, K. D., 1988. Geophysical data. In: R. E. Sheridan and J. A. Grow (Editors), The Geology of North America, vol. I-2, The Atlantic continental margin: The Geological Society of America, Boulder, Colorado, pp. 177–196.

Sleep, N. H., 1971. Thermal effects of the formation of Atlantic continental margins by continental break up. Geophys. J. R. Astron. Soc., 24: 325–350.

Smythe, D. K., 1989. Rockall Trough - Cretaceous or Late Paleozoic?. Scott. J. Geol., 25: 5–43.

Steckler, M. S., Watts, A. B. and Thorne, J. A., 1988. Subsidence and basin modeling at the U.S. Atlantic passive margin. In: R. E. Sheridan and J. A. Grow (Editors), The Geology of North America, vol. I-2, The Atlantic continental margin: U.S. The Geological Society of America, Boulder, Colorado, pp. 399–416.

Stoffa, P. L. and Buhl, P., 1979. Two-ship multichannel seismic experiments for deep crustal studies: expanded spread and constant offset profiles. J. Geophys. Res., 84: 7645–7660.

Tréhu, A.M., Ballard, A., Dorman, L. M., Gettrust, J. F., Klitgord, K. D. and Schreiner, A., 1989. Structure of the lower crust beneath the Carolina trough, U.S. Atlantic continental margin. J. Geophys. Res., 94: 10585–10600.

Ussami, N., Karner, G. D. and Bott, M. H. P., 1986. Crustal detachment during South Atlantic rifting and formation of Tucano-Gabon basin system. Nature, 322: 629–632.

Viereck, L. G., Taylor, P.N., Parson, L. M., Morton, A. C., Hertogen, J., Gibson, I. L. and the ODP Leg 104 Scientific Party, 1988. Origin of the Paleogene Voring Plateau volcanic sequence. *In:* A. C. Morton and L. M. Parson (Editors), Early Tertiary volcanism and the opening of the NE Atlantic. Geol. Soc. London Spec. Publ., 39: 69–83.

Vogt, P. R., 1974. The Iceland phenomenon: imprints of a hot spot on the ocean crust, and implications for flow below the plates. *In:* L. Kristjansson (Editor), Geodynamics of Iceland and the North Atlantic area. D. Reidel Publishing Company, Dordrecht-Holland, pp. 105–126.

Waagstein, R., 1988. Structure, composition and age of the Faeroe basalt plateau. In: A. C. Morton and L. M. Parson (Editors), Early Tertiary volcanism and the opening of the NE Atlantic. Geol. Soc. London Spec. Publ., 39: 225–238.

Watts, A. B. and Ryan, W. B. F., 1976. Flexure of the lithosphere and continental margin basins. Tectonophysics, 36: 25–44.

Wernicke, B., 1985. Uniform-sense normal simple shear of the continental lithosphere. Can. J. Earth Sci., 22: 108–125

White, R. and McKenzie, D., 1989. Magmatism at rift zones: the generation of volcanic continental margins and flood basalts. J. Geophys. Res., 94: 7685–7729.

White, R. S., Spence, G. D., Fowler, S. R., McKenzie, D. P., Westbrook, G. K. and Bowen, A. N., 1987. Magmatism at rifted continental margins. Nature, 330: 439–444.

Ziegler, P. A., 1990. Tectonic and paleogeographic development of the North Sea rift system. In: D. J. Blundell and A. D. Gibbs (Editors), Tectonic evolution of the North Sea rifts. Oxford University Press, Oxford, pp. 1–36.

Ziegler, P. A., 1992. North Sea rift system. Tectonophysics, 208: 55–75.

Zoback, M. L., Zoback, M. D., Adams, J., Assumpção, M., Bell, S., Bergman, E. A., Blümling, P., Brereton, N. R., Denham, D., Ding, J., Fuchs, K., Gay, N., Gregersen, S., Gupta, H. K., Gvishiani, A., Jacob, K., Klein, R., Knoll, P., Magee, M., Mercier, J. L., Müller, B. C., Paquin, C., Rajendran, K,

Chapter 12

The Southern Oklahoma Aulacogen

G. R. Keller and W. S. Baldridge

12.1 Introduction

The northwest trending structures which extend across southern Oklahoma and northwestern Texas include some of the largest in North America (Fig. 12–1). For example, the Anadarko basin contains more than 12 km of Cambrian through Permian sedimentary rocks (Ham and Wilson, 1967). In his definitive study, Shatski (1946) recognized the regional significance of these features and compared these North American structures to the Donets basin in the western portion of the USSR. He defined these compressively reactivated rifts as aulacogens. The aulacogen concept was put into a plate tectonic framework by Hoffman et al.(1974) and the structures extending across southern Oklahoma have been referred to as the Southern Oklahoma or Wichita aulacogen since that time. This set of structures begins at the early Paleozoic continental margin in northeastern most Texas (Kruger and Keller, 1986). Additional structures as far northwest as eastern Utah have Paleozoic tectonic histories which suggest they may be part of this aulacogen. (Larson et al., 1985). The rift phase of this feature formed as a result of a major continental breakup in latest Precambrian/earliest Paleozoic time which formed Paleozoic North America and a number of continental rifts. (e.g. Keller et al., 1983). The late Paleozoic deformation which formed the structures we see today occurred as a result of the Ouachita orogeny. These structures constitute one of North America's major petroleum provinces, and have been the subject of a recent overview by Perry (1989), and the igneous and tectonic evolution have been summarized by McConnell and Gilbert (1990) and Gilbert and Denison (1993).

12.2 Significance

The Southern Oklahoma aulacogen is significant because it is a classic example of such a feature. The early and middle Paleozoic post rift subsidence and late Paleozoic deformation produced the Anadarko basin which is one of the deepest basins in the world and is a major petroleum province (e.g. Feinstein, 1981). This aulacogen provides the structural framework for a major portion of the central U.S. and some related faults may have experienced recent movements (Meers fault, e.g. Luza et al., 1987) and could pose an earthquake hazard.

12.3. Geological information

The post rift history of the southern Oklahoma region is extremely well known because of extensive petroleum exploration (10,000's of wells have been drilled) and has been documented in detail by Ham et al. (1964) in a landmark paper. Our knowledge of the rifting is based primarily on many studies of the igneous rocks exposed in the Wichita uplift (see Gilbert, 1983 and Gilbert and Denison, 1993 for summaries), regional relationships (Keller et al., 1983), and the post rift subsidence (e.g. Feinstein,

1981; Garner and Turcotte, 1984). There is indirect evidence for actual rift faults (Ham et al., 1964; Gilbert, 1983) but none have actually been mapped. The pattern of distribution of the Carlton Rhyolite Group suggests these units were laid down in and overfilled a trough (Gilbert, 1983). The late Paleozoic event which formed the uplift resulted in erosion of much of the rock record of rifting and that which is presumably preserved is buried beneath about 12 km of younger rocks in the Anadarko basin. Perry (1989) reviewed the evidence for an early Paleozoic sedimentary trough coinciding with the rift. There is evidence for hinge-lines in the thickening of Silurian and Devonian units which suggest that the depocenter in this trough was in the vicinity of the Wichita uplift (Amsden, 1975; Cardott and Lambert, 1985). Control for thicknesses of Cambrian and Ordovician units is limited, but the interpreted isopachs of Gatewood (1978) place the depocenter in a similar position. As shown by Feinstein (1981), the rate of subsidence decreased from the Cambrian into the early Mississippian. The lack of deep water sediments indicates sedimentation kept pace with subsidence. Based on all of the considerations discussed above, Perry (1989) inferred the outline of the rifted area to be as shown in Figure 12–2.

Early igneous activity resulted in intrusion of a layered gabbroic complex, the Glen Mountains Layered Complex (GMLC), (Powell et al., 1980; Powell, 1986). These rocks are probably early Cambrian in age (577 ± 165 Ma, Lambert and Unruh, 1986). The GMLC may have an extrusive equivalent, the Navajoe Mountain Basalt-Spilite Group, a series of shallow submarine flows. Compositional data are limited for these units, partly because of pervasive alteration. However, both units are thought to be tholeiitic in composition. The GMLC is intruded by small, internally layered basaltic plutons, also of tholeiitic composition. One of these was dated at 552 Ma., which provides a younger limit on the age of the GMLC (Bowring and Hoppe, 1982). The total suite of basic rocks is referred to as the Raggedy Mountain Gabbro Group (Powell, 1986) and is known from drilling to have dimensions of ~40 km by ~175 km. The large (~ 100 mGal.) gravity maximum associated with these rocks indicates that their lateral extent is greater than this and that their vertical extent is about 10 km (Fig. 12–3).

Massive volumes (possibly up to 40,000 km^3) of peralkaline silicic magmas were generated about 525 m.y. ago, producing the Carleton Rhyolite Group and its possible intrusive equivalent, the Wichita Granite Group (Gilbert and Meyers, 1986; Weaver and Gilbert, 1986). Emplacement of these rocks occurred shortly after major uplift of the rift. The origin of these silicic magmas, which are characterized by high K_20 (K_20 = 4.2-5.3%; K_20/Na_20 = 1.1-1.5), enriched incompatible trace elements, and F-bearing alkali amphiboles, is uncertain. Associated tholeiitic basalts, occurring as late-stage dibase dikes, may be genetically related or may simply represent the heat source for melting of preexisting crust. High initial $^{87}Sr/^{86}Sr$ (0.707 ± 0.001) of the silicic rocks suggests that at least some crustal component is involved in their origin.

The Precambrian basement rock provinces in the region are well known (Denison et al., 1984) and suggest that an older boundary may extend through the area. Gilbert (1983) suggests that such a boundary may have played a role in controlling the location of the rifting.

12.4. Geophysical surveys and results

There is a considerable amount of geophysical data available in the southern Oklahoma aulacogen area. However, there is a paucity of published seismic reflection data. There are 1000's of kilometers of proprietary data which have been shown to researchers by various industry groups, and a few record sections have found their way into the literature (e. g. Jacobson, 1984). Thus, our knowledge of the post early Paleozoic history and structures is better than can be documented formally. The Consortium for Continental Reflection Profiling (COCORP) recorded several profiles in southwestern Oklahoma (Brewer et al., 1981, 1983) and a university consortium conducted a wide-angle reflection/ refraction experiment in the same area (Chang et al., 1989; Zhu and McMechan, 1989; Kang and McMechan, 1990; Hamilton, 1989; Hsueh, 1991).

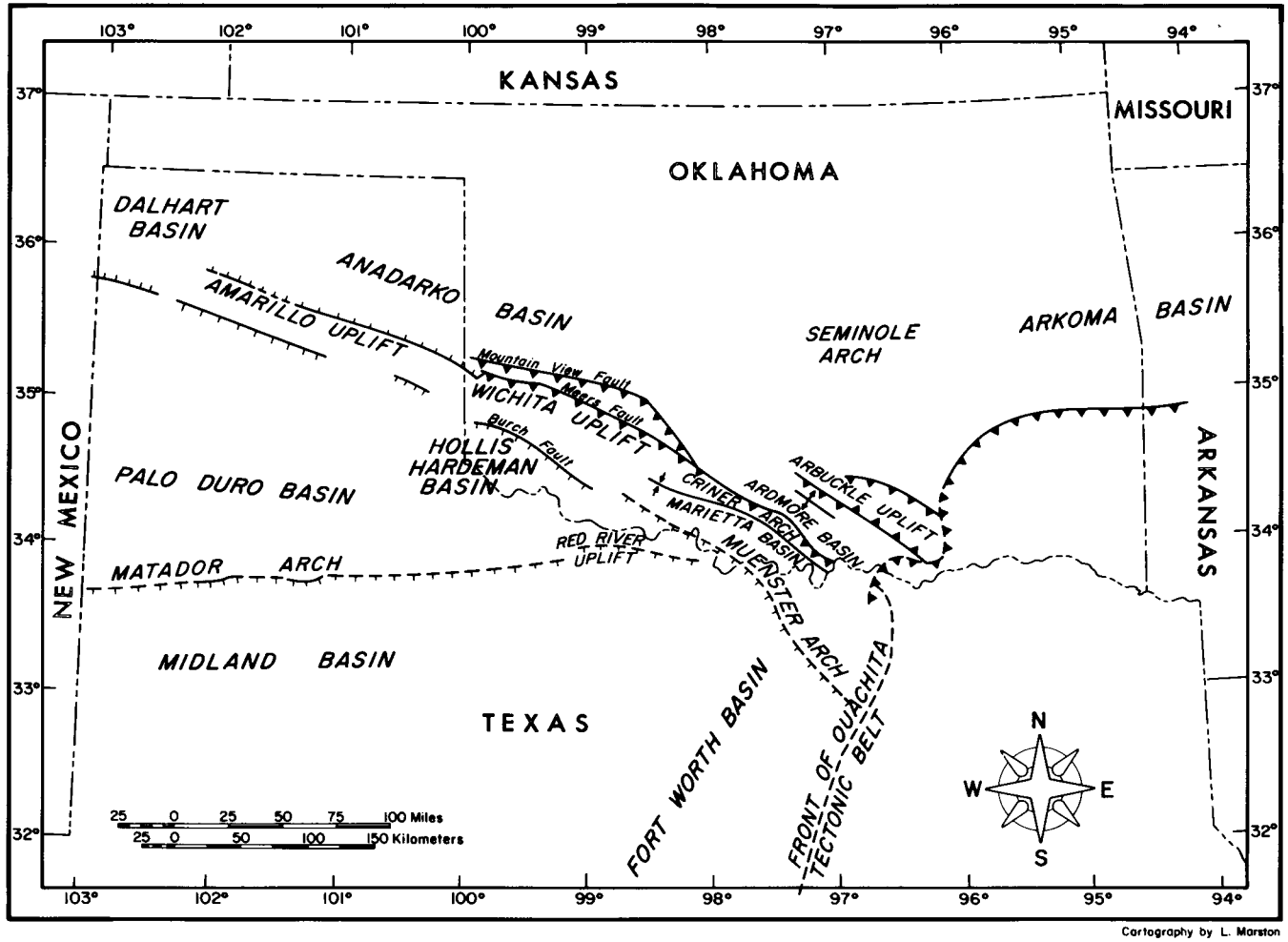

Fig. 12–1. Index map showing the major tectonic features associated with the southern Oklahoma aulacogen.

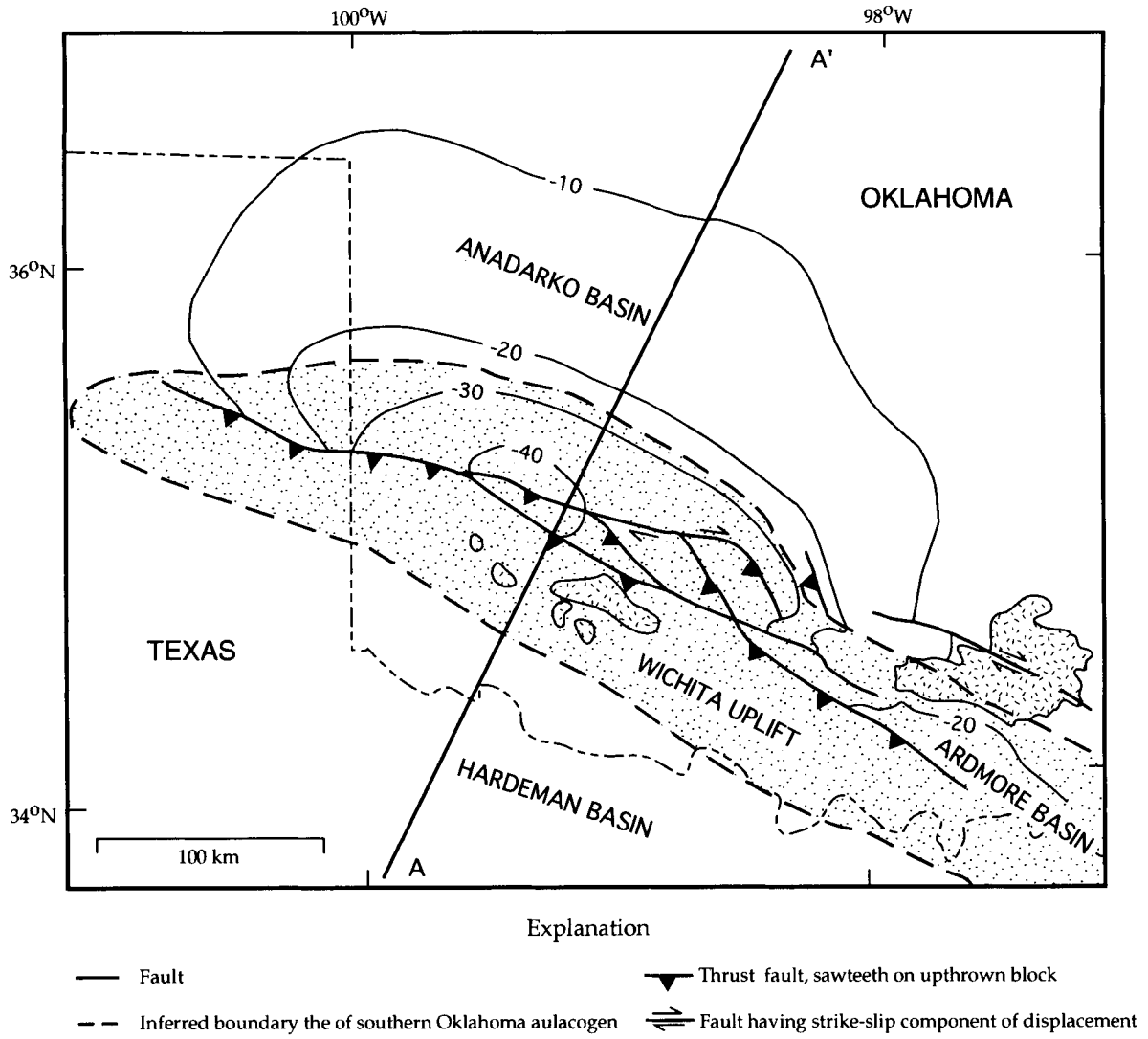

Fig. 12–2. Map showing inferred extent of the southern Oklahoma aulacogen and major faults. Contours are of depth (1000's of feet) to Proterozoic basement beneath the Anadarko basin. Modified from Parry (1989).

These results provide a good picture of the deep structure of the Wichita uplift, the Anadarko basin to the north, and the Hardeman basin area to the south (Fig. 12–2). The upper crust of this uplift is composed of high velocity (>6.5 km/s P-wave velocity) material, and it overthrusts the Anadarko basin in a complex zone (Brewer et al., 1983; Chang et al, 1989). To the north, the Precambrian basement cannot be unambiguously identified because of the great thicknesses of reflective sediments. However, these data indicate that total sedimentary rock thickness estimates of 12 km may even be conservative. To

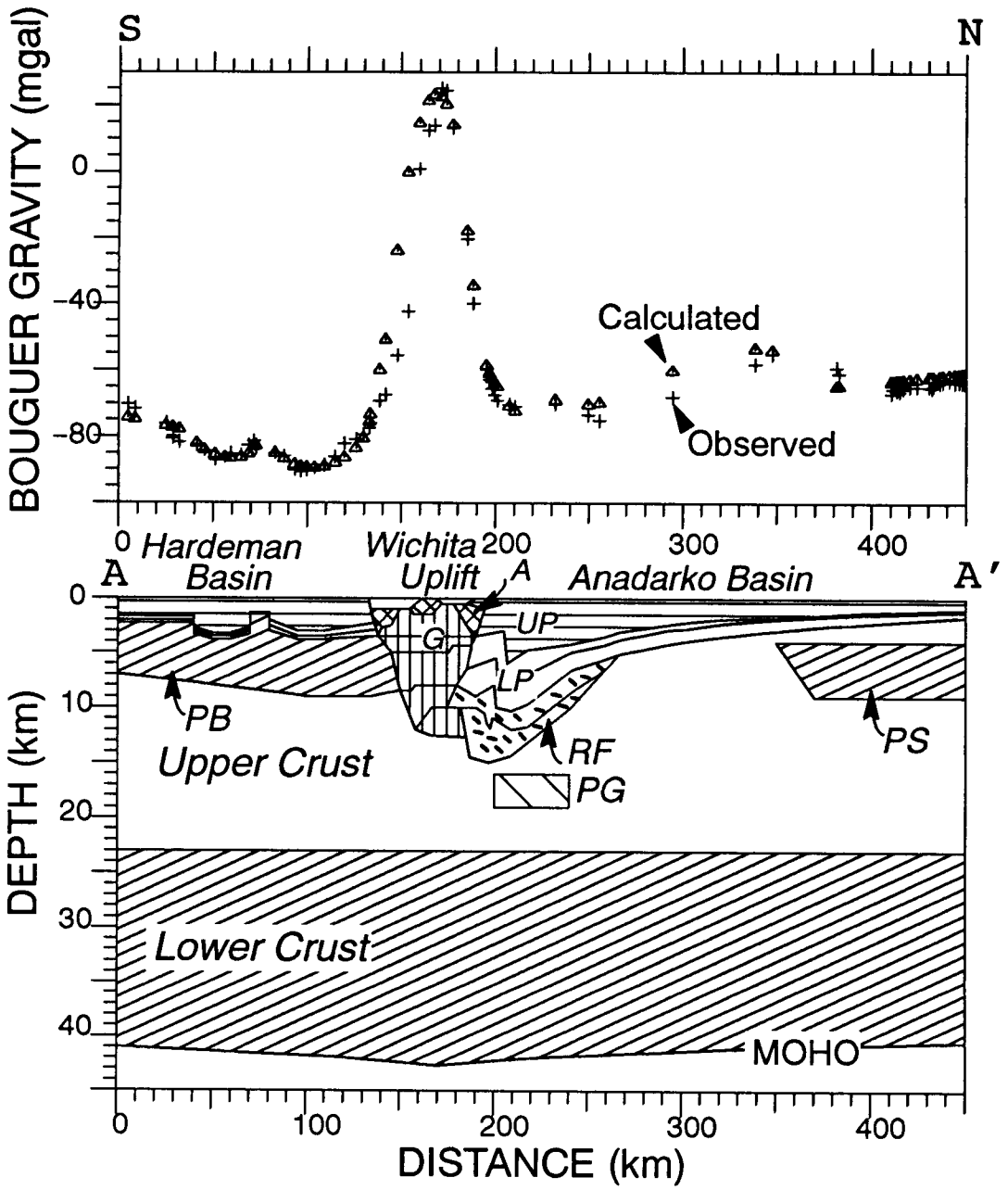

Fig. 12–3. Crustal model across the southern Oklahoma aulacogen based on an integrated analysis of seismic, gravity, and geologic data. UP-upper Paleozoic strata; LP - lower Paleozoic strata; A - granitic rocks; G - Gabbroic rocks; PB - Proterozoic basin; RF - Rift fill of sediments and volcanics; PS - Proterozoic sediments or intrusions probably associated with the Midcontinent rift system. PG - Proterozoic gabbro probably associated with the midcontinent rift system (Robbins and Keller, 1992).

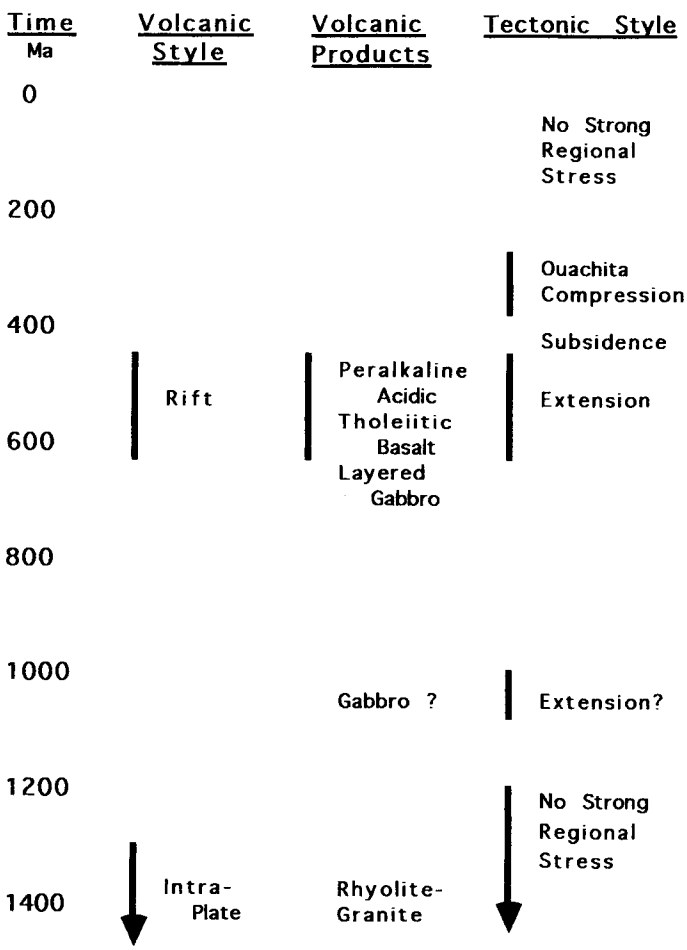

Fig. 12–4. Tectonic and magmatic evolution.

the south, Brewer et al., (1981) interpreted extensive layered reflectors within the Precambrian basement to indicate the presence of a late Proterozoic basin and Hamilton (1989) showed that a gravity low in this area is consistent with this interpretation.

The deep crustal structure of the region is only generally known. The studies discussed above produced limited data on deep structure, and the one long seismic refraction line in the area (Mitchell and Landisman, 1970) provides a low resolution picture because of the wide spacing of the recordings. However, enough control exists to conclude that the crust is approximately 40 km thick throughout the area. An excellent data base of gravity and magnetic readings exists for the area (e.g. Robbins and Keller, 1992). Magnetic anomalies in the Wichita uplift area trend parallel to the aulacogen and are complex as one would expect over shallow igneous rocks of varied composition.

The gravity data provide significant control on deep structure and show that the aulacogen is associated with a huge positive (>100 mGal) gravity

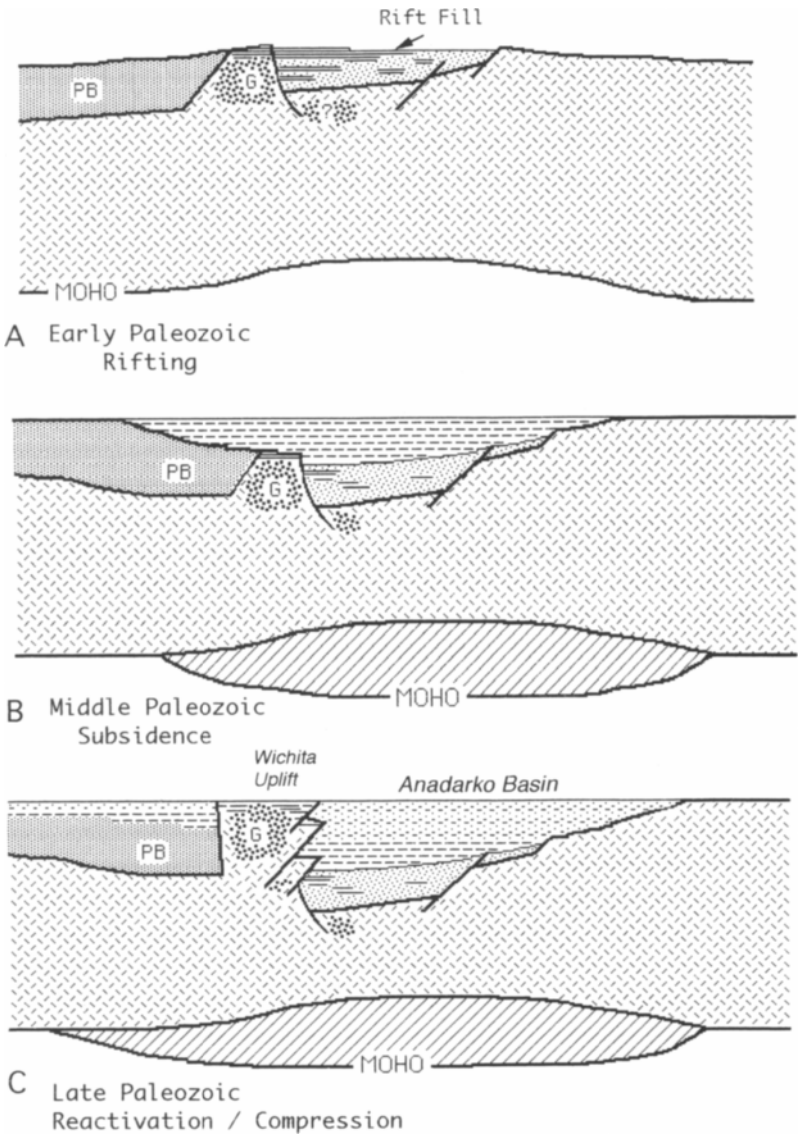

Fig. 12–5. Schematic evolution of lithospheric structure.

anomaly (Fig. 12–3) which requires the presence of a major crustal anomaly in the vicinity of the Wichita uplift. Hamilton (1989) showed that the gravity and seismic results over the uplift could be satisfied with an internally consistent model. Hsueh (1991) produced a seismic model of the Anadarko basin which was tied to Hamilton's (1989) model. A gravity model based on these studies is shown as Figure 12–3. This crustal model represents an integrated analysis of all available geophysical and geological data

and provides a generalized picture of crustal structure. It has generally been confirmed by studies of reflected phases from the Moho contained in the university consortium seismic data (Suleiman, 1993). Although resolution in the lower crust is limited, this may be the best picture of the deep structure of an aulacogen presently available.

12.5. Structure and interpretation

As discussed above, we can only infer the presence of rift structures from indirect evidence. In addition to the evidence mentioned above, the amount of modification of the crust is impressive. Little if any of the original upper continental crust remains beneath the Wichita uplift. Lack of control and subsequent deformation make it impossible to conclude anything about the nature of the lower crust and Moho at the time of rifting. There has been some debate about the source of the late Paleozoic uplift and deformation. The plate tectonic framework is one of collision (generally from the southeast). Sedimentary evidence clearly dates the main deformation as being Pennsylvanian in age. The folds and reverse faults present are evidence for northeast compression (e.g., Ham et al., 1964; Perry, 1989). Folding and basement involved thrusting progressed from southwest to northeast and the presence of strike-slip faults suggest transpressional tectonism. Many of the anticlines formed are asymmetrical and overturned to the northeast. The igneous rocks of the rift were exposed by the uplift, and their erosional debris exceeds 3 km in thickness adjacent to the Wichita uplift.

The presence of northwest trending strike-slip faults, has led to a difference of opinion about the relative importance of compression and shearing in forming the structures present. Budnick (1986) explains this entire period of deformation within the framework of a northwest trending megashear. However, Granath (1989), McConnell (1989), and Perry (1989) have recently analyzed subsurface data from drill holes and outcrop data and conclude that strike-slip movements greater than 20 km are unlikely. Geophysical data show that reverse faulting must be very important and indicate that the early Paleozoic continental margin to the southeast was not disrupted by major strike-slip movement (Kruger and Keller, 1986). In addition, most geologic evidence favors northeast directed compression as the main structural regime although small strike-slip movements certainly occurred implying an element of transpression (e.g., Perry, 1989). The reconciliation of this stress direction within the plate tectonic framework remains an open question From the standpoint of rifting, the important thing is that this postrift deformation obliterated most of the rock record which would reveal details of the rift history.

12.6. Tectonic evolution

The tectonic evolution of the Southern Oklahoma aulacogen has been discussed in detail by Gilbert (1983), Perry (1989), and Gilbert an Denison (1993). The general sequence of events in portrayed in Figure 12–4. Many details are in question, but the sequence includes: 1) possible formation of a Precambrian boundary which localized the later rifting; 2) Cambrian rifting and magmatism, 3) post rift subsidence; 4) late Paleozoic deformation, 5) stability. A series of block diagrams illustrating the major steps in the tectonic evolution are shown as Figure 12–5. The most distinctive aspects of this evolution are the scale of the post rift subsidence and deformation. The total structural relief shown in Figure 12–3 is 15 km over a lateral distance of no more that 10 km.

12.7. Conclusions

The Southern Oklahoma aulacogen is a major structural element of interior North America. As a rift, this feature involved extensive volcanism and modification of the crust. When reactivated by later events at the continental margin, vertical displacements alone were approximately 15 km.

Acknowledgements. The authors have benefited greatly by discussions with R.E. Denison, M.C. Gilbert, J.W. Granath, D.A. McConnel and W.J. Perry. R.E. Denison provided a critical review of the manuscript.

12.8. References

Amsden, T.W., 1975. Hunton Group (Late Ordovician, Silurian, and Early Devonian) in the Anadarko Basin of Oklahoma. Oklahoma Geol. Surv. Bull. 121, 214 pp.

Bowring, S.A. and W.J. Hoppe, 1982. U/Pb zircon ages from Mount Sheridan Gabbro, Wichita Mountains. Oklahoma Geol. Surv. Guidebook 21: 54-59.

Brewer, J.A., L.D. Brown, D. Steiner, J.E. Oliver, and S. Kaufman, 1981. Proterozoic basin in the southern Midcontinent of the United States revealed by COCORP deep seismic profiling. Geology, 9: 569-575.

Brewer, J.A., R. Good, J.E. Oliver, L.D. Brown, and S. Kaufman, 1983. COCORP profiling across the Southern Oklahoma aulacogen; overthrusting of the Wichita Mountains and compression within the Anadarko Basin. Geology, 11: 109-114.

Budnick, R.T., 1986. Left Lateral intraplate deformation along the Ancestral Rocky Mountains: implications for late Paleozoic plate motions. In: B. Johnson and A.W. Balley (Editors), Intraplate Deformation: Characteristics, Processes and Causes. Tectonophysics, 132: 195-214.

Cardott, B.J. and M.W. Lambert, 1985. Thermal maturation by vitrinite reflectance of Woodford Shale, Anadarko basin, Oklahoma. Am. Assoc. Petrol. Geol. Bull. 69: 1982-1998.

Chang, W.F., G.A. McMechan, and G.R. Keller, 1989. Wavefield processing of data from a large-aperture seismic experiment in southwestern Oklahoma. J. Geophys. Res., 94: 1803-1816.

Coffman, J.D., M.C. Gilbert, and D.A. McConnell, 1986. An interpretation of the crustal structure of the southern Oklahoma aulacogen satisfying gravity data. Oklahoma Geol. Surv. Guidebook 23: 1-10.

Denison, R.E., Lidiak, E.G., Bickford, M.E., and Kisvarsanyi, E.B., 1984. Geology and Geochronology of Precambrian Rocks in the Central Interior Region of the United States. Geol. Survey Professional Paper 1241-C, 20 pp.

Feinstein, S., 1981. Subsidence and thermal history of southern Oklahoma aulacogen; implications for petroleum exploration. Am. Assoc. Petrol. Geol. Bull. 65: 2521-2533.

Garner, D.L. and Turcotte, D.L., 1984. The thermal and mechanical evolution of the Anadarko basin. Tectonophysics, 107: 1-24.

Gatewood, L.E., 1978. Stratigraphic trap possibilities in the Arbuckle Group; general relationships. Shale Shaker, 28: 219-227.

Gilbert, M.C., and R.E. Denison, 1993. Late Proterozoic to Early Cambrian basement of Oklahoma. In: Reed, J.C., Jr., Bickford, M.W., Houston, R.S., Link, P.K., Ranking, D.W., Sims, P.K., and Van Schmus, W.R., editors, The Geology of North America, Geol. Soc. Am., Precambrian: Conterminous U.S., C - 2: 303-314.

Gilbert, M.C. and J.D. Myers, 1986. Overview of the Wichita Granite Group. Oklahoma Geol. Surv. Guidebook 23. 107-116.

Gilbert, M.C., 1983. Timing and chemistry of igneous events associated with the Southern Oklahoma aulacogen. In: Morgan, P., and Baker, B.H., editors. Processes of continental rifting. Tectonophysics, 94: 439-455.

Granath, J.W., 1989. Structural evolution of the Ardmore basin, Oklahoma: Progressive deformation in the foreland of the Ouachita collision, Tectonics, 8:1015-1036.

Ham, W.E., R.E. Denison, and C.A. Merritt, 1964. Basement rocks and structural evolution of southern Oklahoma. Oklahoma Geological Survey Bulletin 95: 302. pp.

Ham, W.E., and J.L. Wilson, 1967. Paleozoic epeirogeny and orogeny in the central United States. American Journal of Science, 265: 332-407.

Hamilton, L.S., 1989. Structure of the Wichita Uplift, Southern Oklahoma, from a Wide-Angle Seismic Experiment. M.S. thesis, Univ. of Texas at El Paso 69 pp.

Hanson, R.E., and Z. Al-Shaieb, 1980. Voluminous subalkaline silicic magmas related to intracontinental rifting in the southern Oklahoma aulacogen. Geology, 3: 180-184.

Hoffman, P., J.F. Dewey, and K. Burke, 1974. Aulacogens and their genetic relations to geosynclines, with a Proterozoic example from Great Slave Lake, Canada. In: Dott, R.J., Jr., and Shaver, R.H., editors, Modern and ancient geosynclinal sedimentation: Society of Economic Paleontologists and Mineralogists, Special Publication 19, p. 38-55.

Hsueh, Fu-Jen, 1991. Application of Ray Trace Modeling to a Large Scale Seismic Experiment in Oklahoma. M.S. thesis, Univ. of Texas at El Paso, 94 pp.

Jacobson, M.I., 1984. The Harrisburg trough, Stephens County, Oklahoma; an update. American Association of Petroleum Geologists Mid-continent Regional Meeting, Oklahoma City, 1981, Technical Proceedings, Oklahoma City Geological Society, p. 127-137.

Kang, I.B. and McMechan, G.A., 1990. Two-dimensional elastic pseudo-spectral modeling of wide-aperture seismic array data with application to the Wichita Uplift-Anadarko Basin region of southwestern Oklahoma: Bulletin of Seismological Society of American, 80: 1677-1695.

Keller, G.R., E.G. Lidiak, W.J. Hinze, and L.W. Braile, 1983. The role of rifting in the tectonic development of the midcontinent, U.S.A.. In: Morgan P., and Baker, B.H., editors., Processes of continental rifting Tectonophysics, 94: 391-412.

Kruger, J.M., and G.R Keller, 1986. Interpretation of crustal structure from regional gravity anomalies, Ouachita Mountains area and adjacent Gulf coastal plain. Am. Assoc. Petrol. Geol. Bull., 70: 667-689.

Lambert, D.D., D.M. Unruh, and M.C. Gilbert, 1988. Rb-Sr and Sm-Nd isotopic study of the Glen Mountains layered complex: Initiation of rifting within the southern Oklahoma aulacogen. Geology, 16: 13-17.

Larson, E.E., P.E. Patterson, G. Curtis, R. Drake, F.E. Mutschler, 1985. Petrologic, paleomagnetic, and structural evidence of a Paleozoic rift system in Oklahoma, New Mexico, Colorado, and Utah. Geol. Soc. Am. Bull., 96: 1364-1372.

McConnell, D.A. and M.C. Gilbert, 1990. Cambrian extensional tectonics and magmatism within the Southern Oklahoma Aulacogen: Tectonophysics, 174: 147-157.

McConnel, D.A., 1989. Determination of offset across the northern margin of the Wichita uplift, southwest Oklahoma, Geol. Soc. Am. Bull., 101: 1317-1332.

Mitchell, B.J., and M. Landisman, 1970. Interpretation of a crustal section across Oklahoma. Geol. Soc. Am. Bull., 81: 2647-2656.

Papesh, H., 1983. A regional geophysical study of the southern Oklahoma aulacogen. M.S. thesis, Univ. of Texas at El Paso, 68 pp.

Perry, W.J. Jr., 1989. Tectonic Evolution of the Anadarko Basin Region, Oklahoma, U.S. Geological Survey Bulletin 1866A, 19 pp.

Powell, B.N., M.C. Gilbert, and J.F. Fisher, 1980. Lithostratigraphic classification of basement rocks of the Wichita province, Oklahoma: Summary. Geol. Soc. Am. Bull., 91: 509-514.

Powell, B.N., 1986. The Raggedy Mountain Group. Oklahoma Geol. Surv. Guidebook 23: 21-52.

Robbins, S.L. and G.R. Keller, 1992. Complete Bouguer and isostatic residual gravity maps of the Anadarko basin, Wichita Mountains, and surroundings areas, Oklahoma, Kansas, Texas, and Colorado, U.S. Geological Survey Bulletin 1866G, 11 pp.

Shatski, N.S., 1946. The great Donets basin and the Wichita system; comparative tectonics of ancient platforms. Akademiya Nauk SSSR Izvestiya, Seriya Geologicheskaya, 6: 57-90.

Suleiman, A.S., 1993. Geophysics of the rifts associated with the Sirt basin (North Africa) and the Anadarko basin (North America), Ph.D. dissertation, Univ. of Texas at El Paso, 150 pp.

Weaver, B.L. and M.C. Gilbert, 1986. Reconnaissance geochemistry of silicic igneous rocks of the Wichita Mountains: The Wichita granite group and the Carlton Rhyolite Group. Oklahoma Geol. Surv. Guidebook 23: 117-125.

Zhu, X. and McMechan, G.A., 1989. 2-D tomographic imaging of velocities in the Wichita Uplift-Anadarko Basin region of southwestern Oklahoma: Bulletin of the Seismological Society of American, 79: 873-887.

Chapter 13

West and Central African rift system

G.R. Keller, R.F. Wendlandt, and M.H.P. Bott

13.1. Introduction

The separation of Africa and South America in the Early Cretaceous was a major event in the tectonic history of both continents which has been documented to extend well into their interiors. The Benue trough (Fig. 13–1) was the most prominent continental structure formed as these continents completed their separation during the Cretaceous and is associated with major reserves of hydrocarbons. The importance of rifting in the formation of this feature was recognized early (e.g., King, 1950; Cratchley and Jones, 1965), and it has been widely accepted as a classic example of a failed arm of a RRR triple junction (Burke et al., 1972; Burke and Whitman, 1973; Burke and Dewey, 1974). However, transtension was probably dominant during the formation of the Benue trough, due to the significance of strike-slip faulting which was also recognized early (e.g., Grant, 1971). More recent studies (e.g., Benkhelil and Robineau, 1983; Maurine et al., 1986; Benkhelil et al., 1988) in fact have established that such faulting played a major role in the tectonic evolution of the region at least from the Albian (~100 Ma) to the end of the Cretaceous.

From a larger perspective, the Benue trough is one element of an extensive rift system which can be studied on both sides of the equatorial Atlantic Ocean. The importance of viewing structures in this system from such a perspective has been appreciated for many years (e.g., Wright, 1968, 1981; Burke and Dewey, 1974). Several recent papers provide excellent overviews of this rift system which extends from northeast Brazil through the Benue trough and on across Africa (e.g., Chang et al., 1992; Castro, 1987; Popoff, 1988; Benkhelil, 1989; Fairhead and Green, 1989; Genik, 1992; Jorgensen and Bosworth, 1989; McHargue et al., 1994; Bosworth and Morley, 1994). The African portion of this rift system has several arms and may extend as far eastward as Kenya (Fig. 13–1), and the purpose of this chapter is to provide an overview of these features which have been named the West and Central African rift system (WCARS; Fairhead, 1986).

13.2. Significance

The Benue trough, east Niger rift basins, and Sudanese rift basins are major elements of the WCARS and are associated with major reserves of hydrocarbons (e.g., Petters and Ekweozor, 1982; Nwachukwu, 1985; Schull, 1986, 1988; Genik, 1992) and have helped focus the attention of the petroleum industry on Paleozoic and Mesozoic rifting in the African continent (e.g., Lambiase, 1989). The Niger delta which lies at the mouth of the Benue trough formed mostly subsequent to the rifting and is one of the World's great petroleum provinces (e.g., Doust and Omatsola, 1989). Even though Benue trough is often thought of as a classic example of a failed arm of a rift (Burke and Dewey, 1974), major strike-slip movements have also occurred (e.g. Popoff, 1988; Benkhelil, 1989; Fairhead and Green, 1989). These

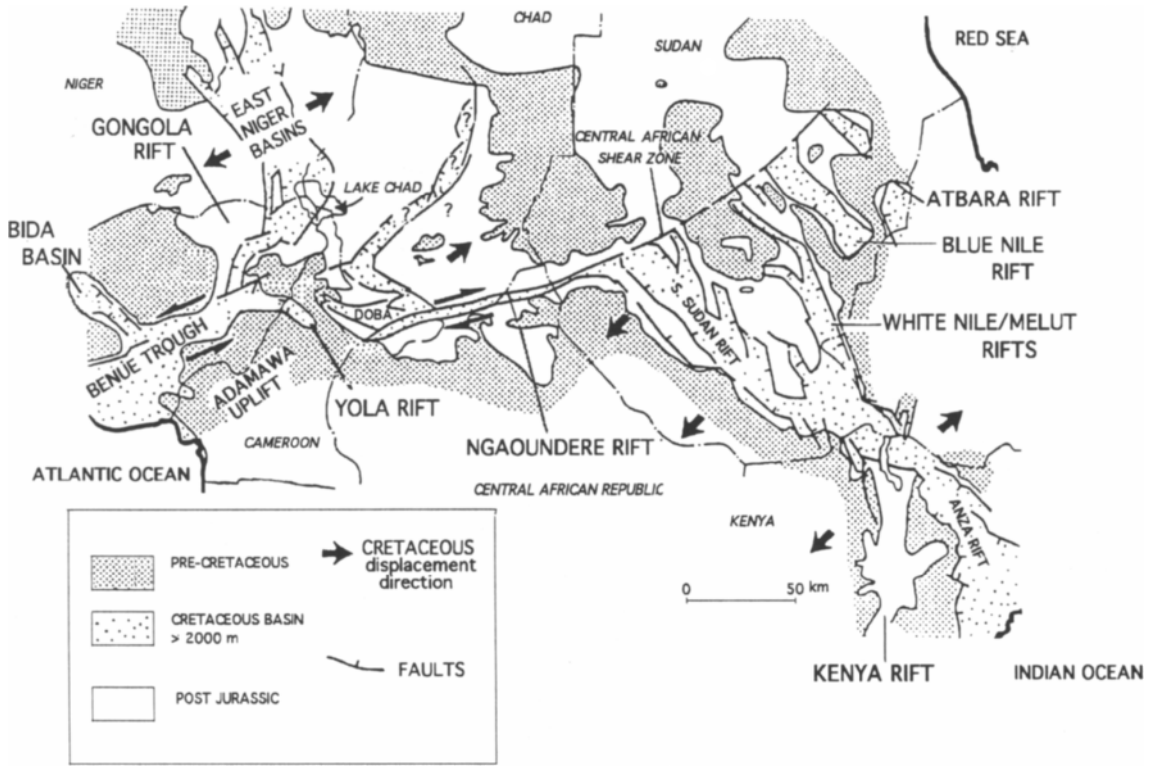

Fig. 13–1. Regional index map of the West and Central African rift system. Southern Sudan rift is also called the Muglad rift. The east Niger basins (Niger rift) are a complex rift zone whose major element is the Termit basin. Modified from Fairhead and Green (1989)

movements may have extended across the continent as it nearly split apart in the Cretaceous (e.g., Burke and Dewey, 1974; Fairhead, 1988 a, b). Thus, the region is an ideal place to investigate the interaction of extension and shear during major rifting events (e.g., Guiraud and Maurin, 1992).

13.3. Geologic Information

13.3.1. Overview

The West and Central African rift system (WCARS) is a large and complex feature whose elements have experienced distinct, usually multiphase geologic histories which in some cases are poorly documented. However, these elements all seem to have experienced a major phase of extension in the Cretaceous which is the basis for linking them to define the WCARS. The early history of many of these features is poorly known due to the thick cover of younger rocks and lack of deep drilling data, and in some cases, subsidence and presumably extension extended into the early Tertiary. Volcanism which could help tie down the timing of tectonic events is sparse in the central and eastern portions of the WCARS (Genik, 1992; McHargue et al., 1992; Bosworth and Morley, 1994).

The Benue trough (Fig. 13–2) is the most intensively studied portion of the WCARS. The early Cretaceous history of this feature is poorly known because of the great thickness of marine and continental middle and upper Cretaceous rocks it con-

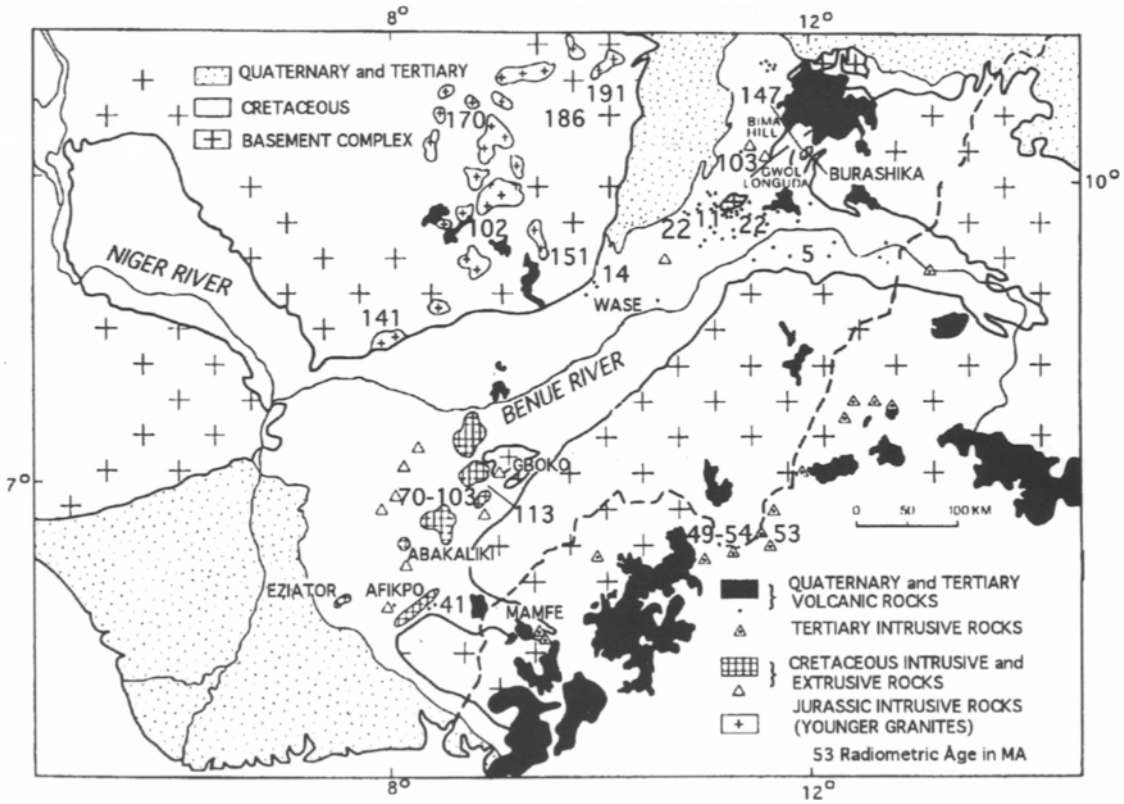

Fig. 13–2. Index map of the Benue trough region. Modified from Benkhelil (1989).

tains. Benkhelil et al. (1988) produced a contour map of the depth to crystalline basement in the Benue trough. The basement is over 5 km deep in many parts of the central portion of the trough, and even greater depths are reached to the southwest where the trough is overlain by the Niger delta. There is a complex basement ridge along the trough which separates a series of sub-basins which may be pull-apart structures that formed during strike-slip movements (Benkhelil et al., 1988; Benkhelil, 1989).

There have been many studies of the sedimentary rocks contained within the Benue trough (e.g., Carter et al., 1963; Burke et al., 1970; Petters, 1978; and Allix and Popoff, 1983). Popoff (1988) presents an extremely useful overview of the tectonic development of the trough from a regional perspective. Pre-Aptian exposures are rare, but recent syntheses by Popoff (1988), Benkhelil et al. (1988), and Benkhelil (1989) provide an interpreted history of the entire Cretaceous. Albian/Aptian rocks were deposited in the series of en échelon sub-basins discussed above. There was an episode of late Cretaceous (Santonian to Maastrichtian) folding in the trough which Benkhelil et al. (1988) document and interpret as being due to a combination of compression and strike-slip faulting.

Recent studies have shown that the Cretaceous extension was not limited to the Benue trough. As suggested by Cratchley et al. (1984), the rifting extended into the Chad basin area, and Fairhead and Green (1989) present geophysical data documenting the presence of a northwest trending arm they

refer to as the Niger rift (east Niger basins, Fig. 13–1). At the eastern end of the Benue trough, it splits into the Gongola and Yola rifts (Fig. 13–1). Further eastward, there is a series of east-west trending basins (e.g. Dobas, Fig. 13–1) in southern Chad (Genik, 1992).

Brown and Fairhead (1983) and Bermingham et al. (1983) introduced the idea of rifting and shearing extending eastward across Africa (Fig. 13–1) to connect with Cretaceous rifts in Sudan. The narrow zone of extension which extends across central Africa (Ngaoundere rift, Fig. 13–1) is a reactivation of the Central African shear zone which is probably of Pan-African age (e.g., Browne and Fairhead, 1983; Jorgensen and Bosworth, 1989). The rifting in Sudan is well documented due to the publication of data from petroleum exploration efforts in the region (Schull, 1986, 1988; Mann, 1989; Jorgensen and Bosworth, 1989; McHargue et al., 1992). The sequence of events here is complex, but rifting appears to have spanned the Mesozoic and extended into the early Tertiary (e.g., Lambiase, 1989). The rifting in Sudan may extend across northern Kenya (Fairhead, 1988a, b) to connect with a Mesozoic rift system (Anza rift) present in that area (Reeves et al., 1987; Bosworth, 1992). Bosworth and Morley (1994) and Dindi (1994) have recently conducted studies of the structure and evolution of the Anza rift (Fig. 13–1). The drilling and seismic data presented by Bosworth and Morley (1994) show that rifting may have occurred throughout the Mesozoic in Kenya but was widespread in the upper Cretaceous.

13.3.2. Igneous activity

Wilson and Guiraud (1992) reviewed the late Jurassic to Recent magmatic activity in western and central Africa and showed that the Benue trough region is the most magmatically active portion of the WCARS. Three temporarily and spatially distinct volcanic provinces occur in the vicinity of the Benue trough (Fig. 13–2). The oldest occurrences are the pre-rift alkaline ring complexes and volcanics of the Jos Plateau that are 100-200 km NW of the trough. Synrift volcanics occur within the Benue trough and are frequently interbedded with sediments. The youngest occurrences are the alkaline intrusives (66-30 Ma) and volcanics (35 Ma to Recent) of the Cameroon line. A temporal succession of younging from NW to SE, across the Benue trough, is indicated by these three provinces. However, only the Jos Plateau volcanics, show a systematic temporal distribution (Fig. 13–2) unto themselves as they generally increase in age to the northeast.

The alkaline complexes of the Jos Plateau consist primarily of alkaline silicic intrusives and volcanics that were erupted or emplaced between about 215 Ma and 140 Ma (Rahaman et al., 1984). Igneous occurrences are oldest in the NNE and youngest to the SSW. The distribution of volcanism, however, was strongly controlled by reactivation of Pan-African structures. Well-developed temporal progressions of chains of volcanoes along ENE-WSW and NNW-SSE transcurrent lineaments characterize the province (Bowden et al., 1987). The ENE-WSW structural control parallels the marginal faults of the Benue trough. The volcanic rocks are predominantly comenditic ignimbrites and lavas with minor amounts of intercalated intermediate and basic lavas (silica-saturated). Andesite compositions are inferred to be the result of mixing acidic and basic end members (Bowden and Karche, 1984). The plutonic rock occurrences are predominantly biotite granites (concentrated in the south) and peralkaline granites and granites (in the north).

Some latest Jurassic volcanism (147 ± 7) has been observed in the area of the northeast portion of the trough (Fig. 13–2) (e.g. Popoff et al., 1983), but this activity pre-dates the formation of the trough. Volcanics interbedded with sediments in this same region also have been dated (Popoff et al., 1983) yielding an age of 103 ± 5 Ma (Albian). Other Cretaceous igneous activity (transitional basalts and alkali rhyolites) (Fig. 13–2) has been dated to be in the range of 70 to 113 Ma (Benkhelil et al., 1988; Grant et al., 1972; Umeji and Caen-Vachette, 1983).

The Cameroon volcanic line, located 200-300 km southeast of the Benue trough (Fig. 13–2) is a long-lived feature which has been episodically active from 65 Ma to the present (Dunlop, 1983; Fairhead, 1988b). It extends some 1600 km in an approximately NE-SW direction that parallels the southern margin of the Benue trough. This feature does not appear to be a classic hotspot trace (Morgan, 1983)

because all of its volcanic centers have been active in the last 10 Ma (Dunlop, 1983). There is no evidence of a systematic age progression along the Cameroon line (Fitton, 1987), and the basalts of the oceanic and continental regions are geochemically and isotopically similar (Fitton and Dunlop, 1985). The last eruption was in 1982. Meyers and Rosendahl (1991) also argue against the hotspot hypothesis because their seismic reflection data indicate uplifts along the trend which were synchronous with the volcanism.

The earliest phase of igneous activity on the Cameroon line is represented by a series of intrusive ring complexes of predominantly granite and syenite composition but with lesser amounts of gabbro. These complexes (Fig. 13–2) range in age from 66-30 Ma (Cantagrel et al., 1978; Lasserre, 1978; Jacquemin et al., 1982). Younger volcanic activity occurred in the same region (Fig. 13–2) from about 35 Ma to Recent. The volcanoes occur in both continental and oceanic settings. Basalts are of alkalic affinity, ranging from nephelinite to transitional basalt. Evolved magmas range from phonolite to alkali rhyolite. In general, basalts in the oceanic setting tend to evolve toward phonolite while those in the continental setting evolve toward peralkaline rhyolite (Fitton, 1987).

The origin of the Cameroon line is believed to be related to that of the Benue trough (Fitton, 1980). Anticlockwise rotation and northward migration of the African plate approximately 12 (degrees) during the past 60 Ma (Smith et al., 1981) moved the rifted lithosphere relative to a thermal anomaly in the asthenosphere, in Fitton's interpretation. Moreau et al. (1987) and Fairhead (1988b) suggest that this volcanic line may be due to strike-slip faulting, and Okereke (1988) discusses the differences between the Benue trough and Cameroon line particularly the associated gravity anomalies. He concludes that the Cameroon line is associated with a mantle upwarp and active rifting.

Reports of rift-related igneous activity in the remainder of the WCARS are rare. It is unlikely that major occurrences of volcanism would not be documented in the published literature. However, minor indications of magmatism may not have yet been found or reported. Genik (1992) tabulated the scattered occurrences of igneous rocks in wells in eastern Niger and southern Chad. A number of Cretaceous ages were determined radiometrically, but the volume of magmatism appears small. McHargue et al. (1992) also reported that evidence of magmatism in the Sudan rifts is rare. Bosworth and Morley (1994) report that drilling in the Anza rift has encountered basalts which were dated by K-Ar whole rock analysis to be 130 ± 7 Ma (Neocomian) and 82.9 ± 4.1 Ma (Campanian) in age. Drilling in the area documents that the younger of these events was limited in extent. However, the older event may be more widespread, and they also found seismic evidence of a possible early Tertiary sill.

13.4. Geophysical surveys and results

The major type of geophysical data available for the Central and western African rift system is gravity readings. Many studies have been undertaken in Nigeria, Chad, and Cameroon (e.g., Cratchley and Jones, 1965; Cratchley et al., 1984; Hospers, 1965; Collingnon, 1968; Ajakaiye and Burke, 1973; Ojo and Ajakaiye, 1975; Adighije, 1981). Okereke and Fairhead (1984) and Fairhead and Okereke (1987) augmented and compiled these data and produced a summary interpretation of crustal structure in the western portion of the rift system.

Aeromagnetic data coverage is complete for the Benue trough area (Ofoegbu, 1984, 1988; Ajakaiye et al., 1985). These data have been used to outline intrusions, estimate the depth to basement (e.g., Benkhelil et al., 1988), and determine the extent of basement highs. Some of these highs outcrop and have been studied extensively (e.g., Ojo, 1988). Aeromagnetic data have also been used to trace oceanic fracture zones under the Niger delta (Babalola and Gipson, 1991).

Browne and Fairhead (1983) relied mainly on gravity data in their definitive study of the Central African rift system. This feature includes the Sudanese rifts which are of particular interest because of their petroleum reserves. Gravity studies

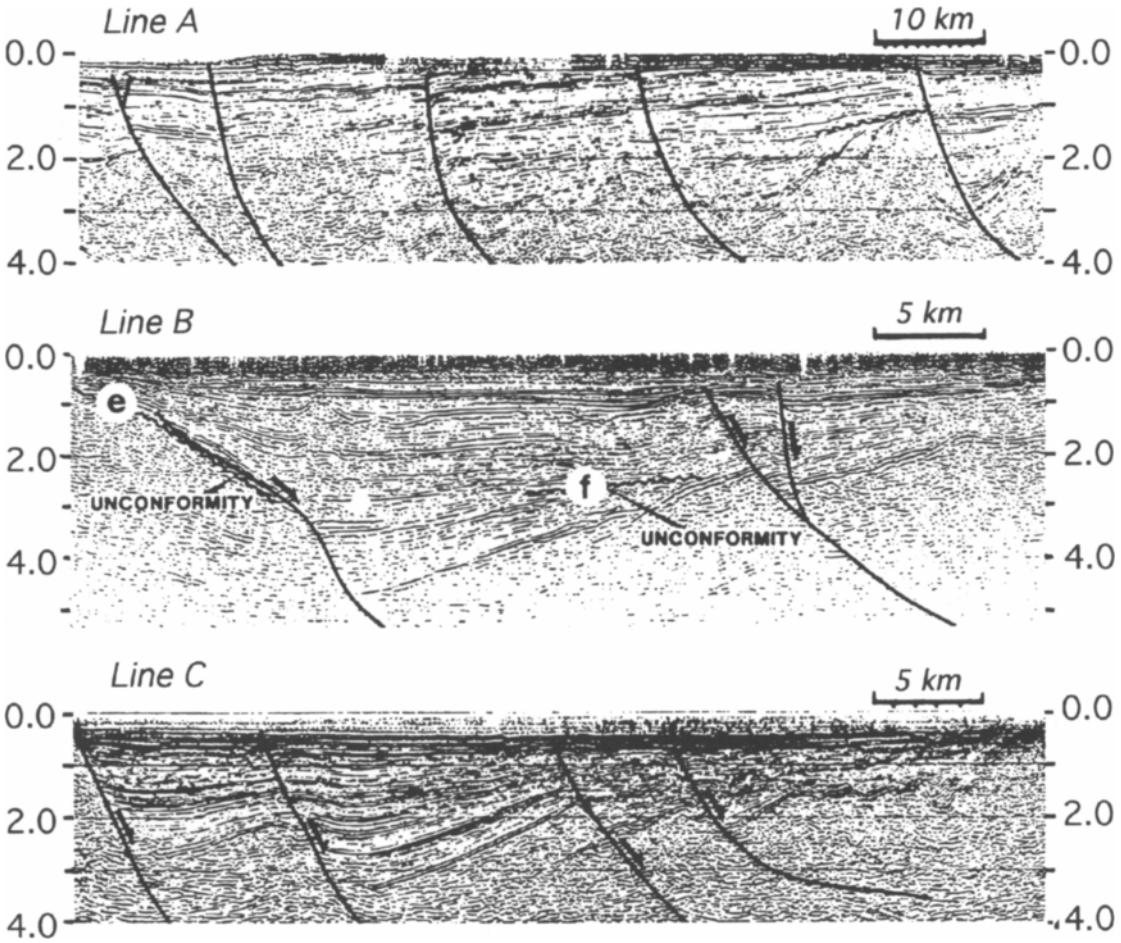

Fig. 13–3. Seismic reflection data from the Sudan rifts. Lines A and B are from the southern Sudan rift and Line C is from the Melut rift. e - eroded fault scarp. f - eroded updip basin edge. Modified from Mann (1989)

of Sudan have been completed by Browne et al. (1985) and Jorgensen and Bosworth (1989). Dindi (1994) recently analyzed gravity and aeromagnetic data in the Anza rift of Kenya.

Deep seismic results have been obtained in the Benue trough/Cameroon line area by Dorbath et al. (1986) and Stuart et al. (1985). Published seismic reflection data are sparse in the entire rift system. Avbovbo et al. (1986) present seismic data from the area just southwest of Lake Chad. These data document the structural style in this area which involves both normal faults and broad folds. Genik (1992) presented several seismic reflection profiles from the east Niger and southern Chad basins. These data document a complex geologic evolution which has resulted in extensional, transtensional, and transpressional structures. Mann (1989) and Bosworth (1992) presented seismic reflection data in Sudan showing the asymmetry of rifts basins there (Fig. 13–3). Also, Green et al. (1991) and Bosworth

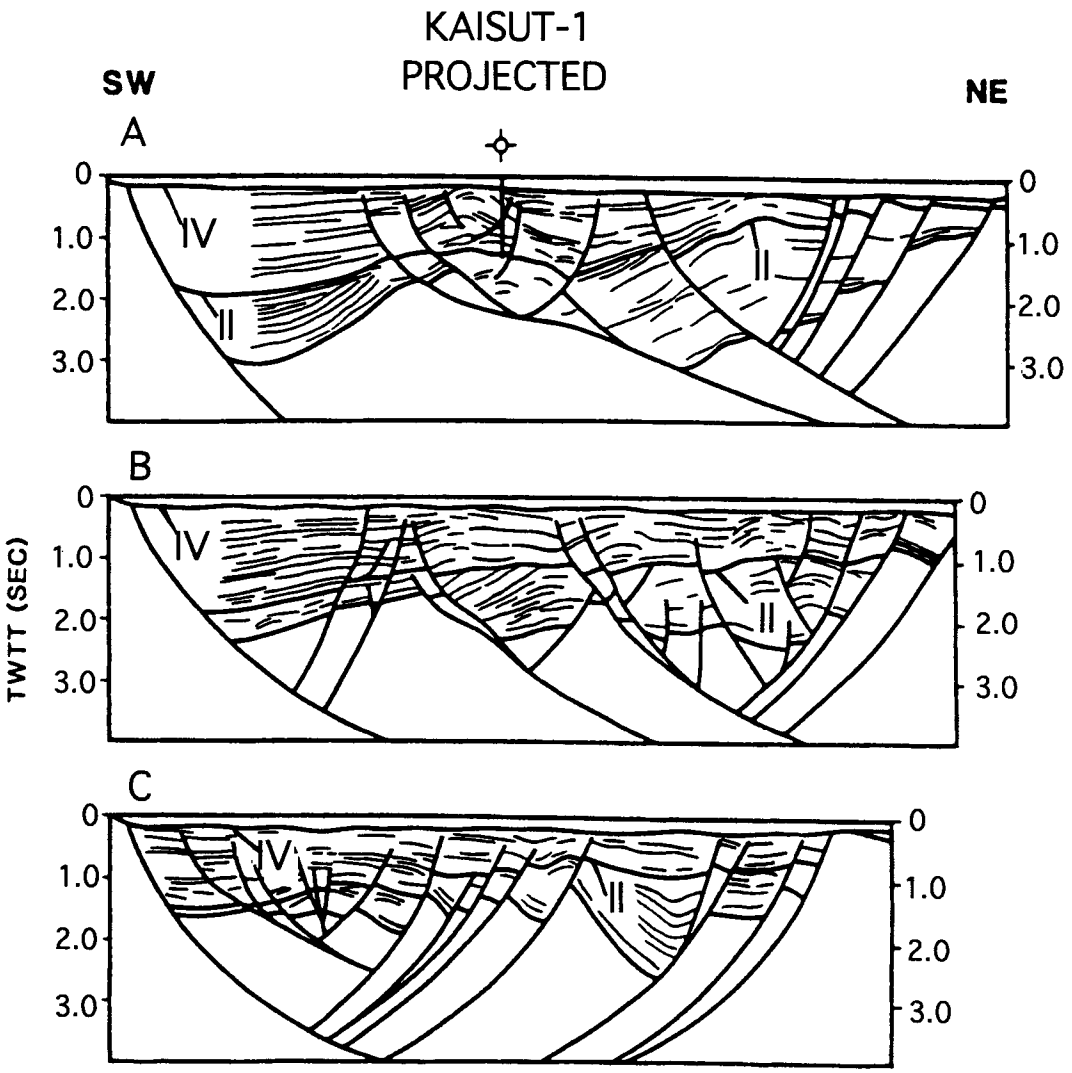

Fig. 13–4. Line drawings of seismic reflection data from the Anza rift. Bold, numbered lines are unconformities. II = approximately the Cretaceous-Tertiary boundary , IV = top of synrift section. Modified from Bosworth and Morley (1994).

and Morley (1994) present several seismic reflection profiles crossing the Anza rift which document the rift structures present there.

13.5. Structure and interpretation

It is difficult to generalize about structures in the Benue trough. Proprietary seismic reflection data must be extensive but have been unavailable to aca-

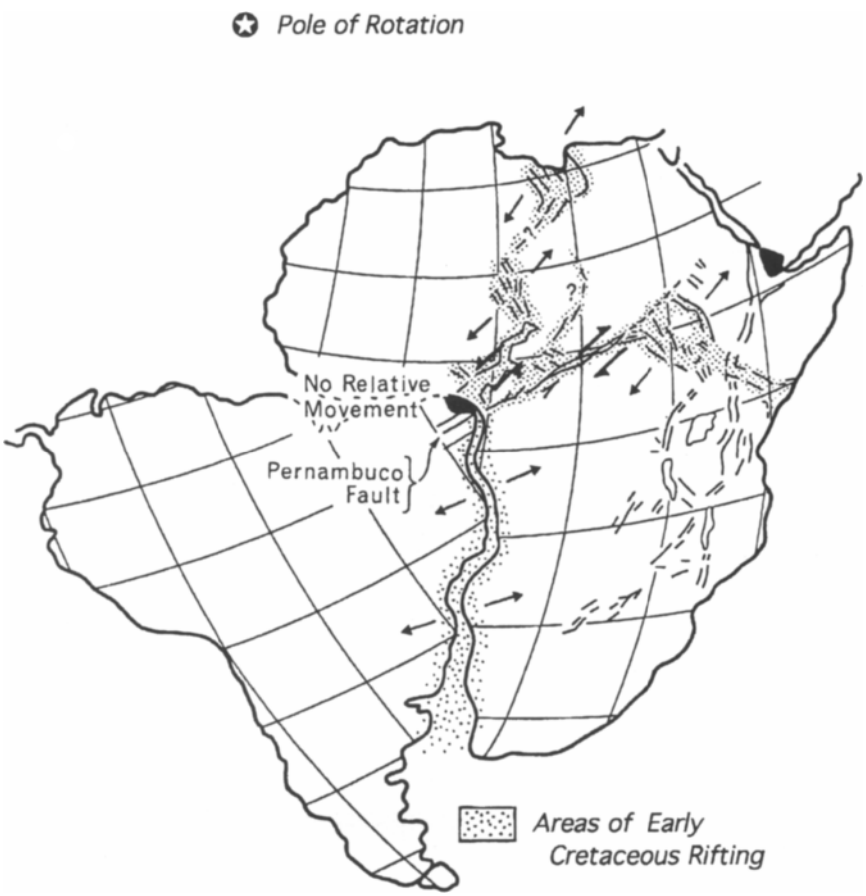

Fig. 13–5. Plate tectonic setting of the Western and Central African rift system in the Cretaceous. Modified from Fairhead and Green (1989).

demic researchers which have had to rely primarily on gravity and magnetic data. Models of basement structure which have been proposed attest to the structural complexity present and to the importance of strike-slip movements. There is structural evidence for a change in the direction of extension from N-S before the late Aptian (~115 Ma) to ENE during the late Aptian-Albian. At about 80 Ma, a variety of data document a short period of compression occurred which correlates with a period of rapid change in the direction of plate motion (Guiraud et al., 1992).

Although complicated by a local gravity low due to the thick Cretaceous sedimentary pile present, the Benue trough is associated with a regional gravity high due to crustal thinning. By removing the effects of the sedimentary section and tying to the only deep seismic data available (Dorbath et al., 1986; Stuart et al., 1985), Fairhead and Okereke (1987, 1990) were able to estimate crustal thickness in the lower Benue trough area to be about 20 km increasing to about 25 km to the northeast. Fairhead and Okereke (1987, 1990) estimated the amount of extension to be 95 km in the Benue trough, 65 km in the Gongola rift, and 55 km in the Yola rift (Fig.

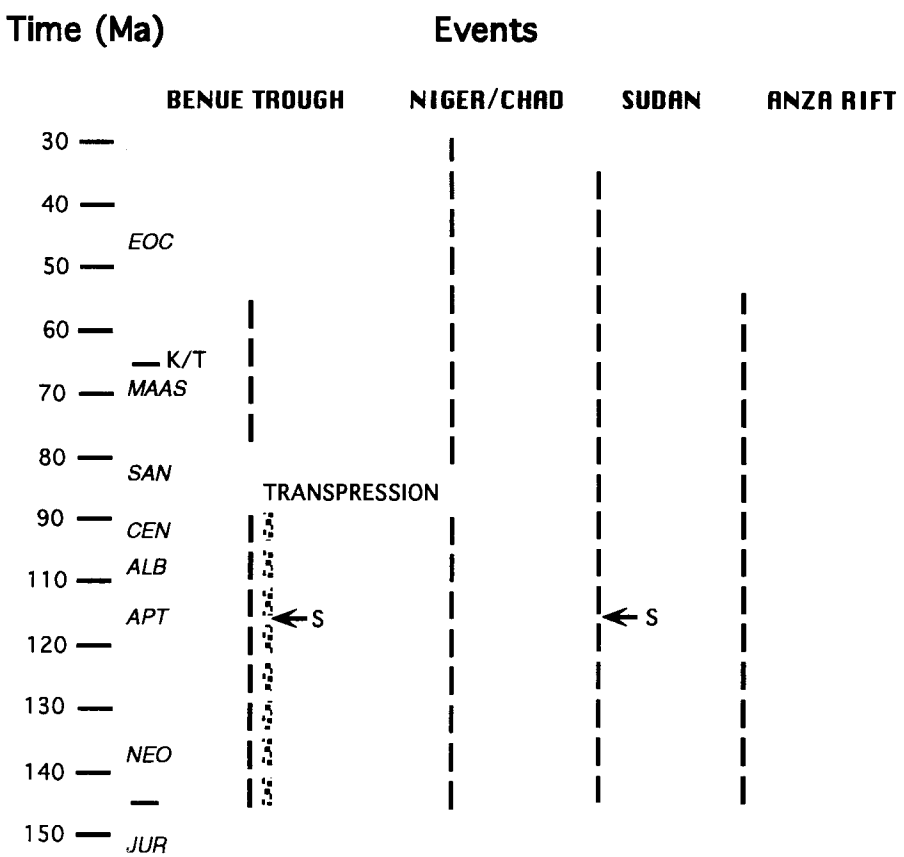

Fig. 13–6. Generalized evolution of the West and Central African rift system. Dashed lines indicate periods of rifting. Stippled line indicates a period of significant magmatism. S - change in stress orientation. Jur - Jurassic, Neo - Neocomian, Apt - Aptian, Alb - Albian, Cen - Cenomanian, Maas - Maastrictian, Eoc - Eocene.

13–1.). Fairhead and Green (1989) used a similar approach to study the Niger rift. Their gravity analysis indicated significant crustal thinning and up to 58 km of crustal extension. Genik (1992) presented evidence that the Termit basin in this area contains an unusual amount of sediment (~14 km).

Gravity (Fairhead and Okereke, 1987; Okereke, 1988) and teleseismic data (Dorbath et al., 1986) contain negative anomalies along the Cameroon line indicating the presence of anomalous mantle as suggested by Fitton (1987).

In Sudan, gravity (Browne et al. 1985; Jorgensen and Bosworth, 1989) and seismic reflection data provide a general picture of crustal structure. Sedimentary fill in the asymmetrical basins approaches 10 km in thickness (McHargue et al., 1992), and regional gravity anomalies indicate the presence of crustal thinning in rifted areas. Jorgensen and Bosworth (1989) have proposed a simple shear model for the development of the region. The structural style of the rift basins is documented in detail by Mann (1989) and Bosworth (1992) who presented a considerable amount of seismic reflection data (Fig. 13–3). These data show the region to be a typi-

cal extensional terrane with tilted fault blocks bounded by listric normal faults, and McHargue et al. (1992) and Bosworth (1992) document that there were several phases of structural evolution.

The work of Green et al. (1991), Bosworth and Morley (1994), and Dindi (1994) provide a detailed picture of the structure and history of the Anza rift. This feature has experienced several stages of evolution including a marine incursion in the upper Cretaceous (Cenomanian). The rifting may have began as early as the late Jurassic and may have extended into the early Tertiary. This feature is characterized by complex graben structures in which several unconformities can be recognized (Fig. 13–4.). The total sedimentary fill may approach 10 km in places, and gravity data indicate that the crust thins by about 5 km beneath the rifted region.

Bosworth and Morley (1994) interpret that a change in structural style from moderately-dipping to steeply-dipping faults had occurred in the Anza rift by the late Cretaceous. A similar change in style has been observed in the Rio Grande rift (Baldridge et al., this volume). It is also interesting to note that the younger Kenya rift displays no obvious evidence of control by the older Anza rift structures where the two features cross in the Lake Turkana area.

13.6. Evolution

The broad-scale setting of the WCARS was the rifting of Africa and South America to form the Atlantic Ocean (Fig. 13–5). This Cretaceous activity apparently tried to break Africa apart as it extended eastward to Sudan and then southeastward across northern Kenya (Fairhead, 1988 a, b). Binks and Fairhead (1992) and Guiraud and Maurin (1992) have taken this concept further to suggest that the continent can be divided into several large blocks and the complex structural development of the WCARS is due to the relative movement of these blocks. We have attempted to generalize recent ideas on the evolution of the WCARS as presented by Popoff (1988), Benkhelil (1989), Guiraud et al. (1992), Wilson and Guiraud (1992), Genik (1992), McHargue et al. (1992), Bosworth (1992), and Bosworth and Morley (1994) to produce Figure 13–6. The work of these authors shows that the sequence of events is undoubtedly not as simple and synchronous as shown. The change in rifting at about 115 Ma, the transpression at 80 Ma, and renewed rifting extending into the early Tertiary followed by sag basin development are events shared by at least several elements of the WCARS. Clearly there is still much to be learned about this complex rift system.

As pointed out by Fairhead (1986), the evolution of the WCARS is characterized primarily by subsidence which is in contrast to most other rifts. Gravity modeling shows that the area of crustal thinning is much wider than the zone of faulting in the upper crust and the amount of extension is at least 4 times greater than in the western and central Kenyan rifts (Fairhead, 1986). This appears to have resulted in an isostatic response that caused the rift shoulders as well as the main rift basins to subside.

13.7. Conclusions

The WCARS is a very large scale feature which is distinctive in that it traverses the entire continent. Its complex history involved extension, shearing, and compression over a period extending from the early Cretaceous into the early Tertiary. Portions of its history correlate with changes in plate movements, and the basins which formed contain major petroleum resources. It is characterized by an unusual amount of subsidence over most of its extent which has obscured many rift structures.

Acknowledgements. The authors have benefited from many discussions with J.D. Fairhead over the years. Michel Popoff was also kind enough to share his ideas.

13.8. References

Adighije, D.E., 1981. A gravity interpretation of the Benue Trough Nigeria, Tectonophysics, 79: 109-128.

Ajakaiye, D.E, 1981. Geophysical investigations in the Benue Trough - Review, Earth Evol. Sci., 2: 110-125.

Ajakaiye, D.E. and Burke, K.C., 1973. Bouguer gravity map of Nigeria. Tectonophysics, 16: 103-113.

Ajakaiye, D.E., Hall, D.H. and Millar, T.W., 1985. Interpretation of aeromagnetic data across the central crystalline shield area of Nigeria. Geophys. J.R. Astr. Soc., 83: 503-517.

Allix, P. and Popoff M., 1983. Le Crétacé inférieur de la partie nord-orientale du fossé de la Benoué (Nigéria): Un exemple de relation étroite entre tectonique et étroite . Bull. Cent. Rech. Explor.-Prod. Elf-Aquitaine, 7: 349-359.

Artsybassev, V.A. and Kogbe, C.A., 1974. Crustal structure of the Benue Valley area (Nigeria). Geol. Runds., 64: 324-329.

Avbovbo, A.A., Ayoola, E.O. and Osahon, G.A., 1986. Depositional and structural styles in Chad basin of northeastern Nigeria. Am. Assoc. Petrol. Geol. Bull., 70: 1787-1798.

Babalola, O.O. and Gipson, M., 1991. Aeromagnetic anomalies and discordant lineations beneath the Niger delta: Implications for new fracture zones and multiple sea-floor spreading directions in the "Meso-Atlantic" Gulf of Guinea cul-de-sac. Geophys. Res. Letters, 18: 1107-1110.

Benkhelil, J. and Robineau, B., 1983. Le fossé de la Bénoué est il un rift? Bull. Cent. Rech. Explor.-Prod. Elf-Aquitaine, 7: 315-321.

Benkhelil, J., Danielli, P., Ponsard J.F., Popoff, M., and Saugy, L., 1988. The Benue trough: Wrench-fault related basin on the border of the equatorial Atlantic. In: Manspeizer, W. (Editor), Triassic-Jurassic Rifting Continental Breakup and the Origin of Atlantic Ocean and Passive Margins. Dev. in Geotectonics (Elsevier, Amsterdam) 22: 787-819.

Benkhelil, J., 1989. The origin and evolution of the Cretaceous Benue trough (Nigeria). J. African Earth Sci., 8: 251-282.

Bermingham, P.M., Fairhead, J.D. and Stuart, G.W., 1983, Gravity study of the central African rift system: A model continental disruption 2. The Darfur domal uplift and associated Cainozoic volcanism. Tectonophysics, 94: 205-222.

Binks, R.M. and Fairhead, J.D., 1992. A plate tectonic setting for Mesozoic rifts of west and central Africa Tectonophysics, 213: 141-151.

Bosworth, W. and Morley, C.K., 1994. Structural and stratigraphic evolution of the Anza rift, Kenya. In, Crust and Upper Mantle Structure of the Kenya Rift. C.P. Prodehl, G.R. Keller, and M.A. Khan (Editors), Tectonophysics, 236: 93-115.

Bosworth, W., 1992. Mesozoic and early Tertiary rift tectonics in east Africa. Tectonophysics, 209: 115-137.

Bowden, P., Blach R., Martin, R.F., Ike, E.C., Kinnaird, J.A., and Batchelor, R.A. 1987. Niger-Nigerian alkaline ring complexes: A classic example of African Phanerozoic anorogenic mid-plate magmatism. In, Alkaline Igneous Rocks, eds. J.G. Fitton and B.G.J. Upton. Geological Society Special, Publication 30: 357-379.

Bowden, P. and Karche, J.P. 1984. Mid-plate A-type magmatism in the Niger-Nigeria anorogenic province: age variations and implications. In, African Geology. Eds., J. Klerkx and J. Michot, Musée Royal de l'Afrique Centrale, Tervuren, 167-177.

Browne, S.E. and Fairhead, J.D., 1983. Gravity study of the Central African Rift System: A model of continental disruption 1. The Ngaoundere and Abu Gabra rifts. Tectonophysics, 94: 187-203.

Browne, S.E., Fairhead, J.D. and Mohamed I.I., 1985. Gravity study of the White Nile Rift, Sudan, and its regional tectonic setting. Tectonophysics, 113: 123-137.

Burke, K.C., Dessauvagie, T.F.J. and Whiteman, A.J., 1972. Geological history of the Benue Valley and adjacent areas. In: T.F.J. Dessauvagie and A.J. Whiteman (Editors), African Geology. University of Ibadan, Ibadan, Nigera: pp. 187-205.

Burke, K. and Whiteman, A.J., 1973. Uplift rifting and the breakup of Africa. In: Tarling, D.H. and Runcorn, S.K. (Editors), Continental drift, sea-floor spreading and plate tectonics. New York, Academic Press, p. 735-755.

Burke, K.C. and Dewey, J.F., 1974. Two plates in Africa during the Cretaceous. Nature, 249: 313-316.

Cantagrel, J.M., Jamond, C. and Lasserre, M. 1978. Le magmatism alhalin de la ligne du Cameroun au Tertiaire inférieor: Donées géochronologiques K-Ar. C.R. Somm. Soc. Geol. Fr., 6: 300-303.

Carter, J.D., Barber, W., Taite, E.A. and Jones, G.P., 1963. The geology of parts of Adamawa, Bauchi and Bornu provinces in northeastern Nigeria. Geol. Surv. Nigeria, Bull. 30: 99 pp.

Castro, A.C.M., Jr., 1987. The northeastern Brazil and Gabon basins: A double rifting system associated with multiple crustal detachment surfaces. Tectonics, 6: 727-738.

Chang, H.K., Kowsmann, R.O., Figueiredo, A.M.F., and Bender, A.A., 1992. Tectonics and stratigraphy of the east Brazil rift system: An overview. Tectonophysics, 213: 97-138.

Colligno, F., 1968. Gravimétrie du Reconnaisance, Cameroun. ORSTOM, Paris, 35 pp.

Cratchley, C.R., Louis, P. and Ajakaiye, D.E., 1984. Geophysical and geological evidence for the Benue-Chad Basin Cretaceous rift valley system and its tectonic implications. J. African Earth Sci., 2: 141-150.

Cratchley, C.R. and Jones, J.P., 1965. An interpretation of the geology and gravity anomalies of the Benue Valley, Nigeria. Overseas Geol. Surv. Geophys. Paper 9: 1-28.

Dindi, E.W., 1994. Crustal structure of the Anza graben from gravity and magnetic investigations. In: G.R. Keller, and M.A. Khan (Editors), Crustal and Upper Mantle Structure of the Kenya Rift. Tectonophysics, 236: 359-371.

Dorbath, C., Dorbath, L., Fairhead, J.D. and Stuart, G.W., 1986. A teleseismic delay time study across the Central African Shear Zone in the Adamawa region of Cameroon, West Africa. Geophys. J.R. Astron. Soc., 86: 751-766.

Doust, H. and Omatsola, E., 1989. Niger delta: Am. Assoc. Petrol. Geol., Memoir 48: 201-238.

Dunlop, H., 1983. Strontium isotope geochemistry and potassium-argon studies on volcanic rocks from the Cameroon line, West Africa. Ph.D. Thesis, Univ. Edinburgh, Edinburgh, 347 pp.

Fairhead, J.D., 1979. A gravity link between the domally uplifted Cainozoic volcanic centres of North Africa and its similarity to the East African rift system anomaly. Earth Planet. Sci. Lett., 42: 109-113.

Fairhead, J.D., 1986. Geophysical controls on sedimentation within the African rift systems. In: L. Frostick et al. (Editors), Sedimentation in the African Rifts. Geol. Soc. London, Spec. Publ., 25: 19-27.

Fairhead, J.D., 1988a. Late Mesozoic rifting in Africa. In: Manspeizer, W. (Editor), Triassic-Jurassic Rifting, Continental Breakup and the Origin of Atlantic Ocean and Passive Margins. Dev. in Geotectonics (Elsevier, Amsterdam) 22: 821-831.

Fairhead, J.D., 1988b. Mesozoic plate tectonic reconstructions of the central South Atlantic Ocean: The role of the west and central African Rift system. Tectonophysics 155: 181-191.

Fairhead, J.D., 1992. A plate tectonic setting for Mesozoic rifts of west and central Africa. Tectonophysics, 213: 141-151.

Fairhead, J.D. and Green, C.M., 1989. Controls on rifting in Africa and the regional tectonic model for the Nigeria and East Niger rift basins. J. African Earth Sci., 8:231-249.

Fairhead, J.D. and Okereke, C.S., 1987. A regional gravity study of the West African Rift System in Nigeria and Cameroon and its tectonic interpretation. Tectonophysics 143: 141-159.

Fairhead, J.D. and Okereke, C.S., 1990. Crustal thinning and extension beneath the Benue trough based on gravity studies. Jour. African Earth Sciences, 11: 329-335.

Fitton, J.G., 1980. The Benue trough and the Cameroon line - A migrating rift system in west Africa. Earth and Planetary Sci. Letters, 51: 132-138.

Fitton, J.G. and Dunlop, H.M., 1985. The Cameroon line, West Africa, and its bearing on the origin of oceanic and continental alkali basalt; Earth and Planetary Sci. Letters, 72: 23-38.

Fitton, J.G., 1987. The Cameroon line, West Africa: A comparison between oceanic and continental volcanism. In, Alkaline Igneous Rocks, eds., J.G. Fitton and B.G.J. Upton. Geological Society, Special Publication 30: 273-291.

Genik, G.J., 1992. Regional framework, structural and petroleum aspects of rift basins in Niger, Chad and the Central African Republic (C.A.R.). Tectonophysics, 213: 169-185.

Grant, N.K., 1971. South Atlantic, Benue trough and Gulf of Guinea triple junction. Geol. Soc. Am. Bull., 82: 2295-2298.

Grant, N.K., Rex, D.C., and Freeth, S.J., 1972. Potassium-argon ages and strontium isotope ratio measurements from volcanic rocks in northeastern Nigeria. Contrib. Mineral. Petrol., 35: 277-292.

Green, L.C., Richards, D.R., and Johnson, R.A., 1991. Crustal structure and tectonic evolution of the Anza rift, northern Kenya. Tectonophysics, 197: 203-211.

Guiraud, R., Binks, R.M., Fairhead, J.D., and Wilson, M., 1992. Chronology and geodynamic setting of Cretaceous-Cenozoic rifting in west and central Africa. Tectonophysics, 213: 227-234.

Guiraud, R. and Maurin, J.-C., 1992. Early Cretaceous rifts of western and central Africa: An overview. Tectonophysics, 213: 153-168.

Gumati, Y.D. and Kanes. W.H., 1985. Early Tertiary subsidence and sedimentary facies - Northern Sirte basin, Libya. Am. Assoc. Petrol. Geol. Bull., 69: 39-52.

Hospers, J., 1965. Gravity field and structures of the Niger delta, Nigeria, West Africa. Geol. Soc. Am. Bull., 76: 407-422.

Jacquemin, H., Sheppard, S.M.F. and Vidal, P. 1982. Isotopic geochemistry (O, Sr, Pb) of the Golda Zuelva and Mboutou anorogenic complexes, North Cameroon: mantle origin with evidence for crustal contamination. Earth Planet, Sci. Lett. 61: 97-111.

Jorgensen, G.J. and Bosworth, W., 1989. Gravity modeling in the Central African rift system, Sudan: Rift geometries and tectonic significance. J. African Earth Sci., 8:283-306.

King, L.C., 1950. Outline and description of Gondwanaland. Geol. Mag., 87: 353-359.

Lambiase, J.J., 1989. The framework of African rifting during the Phanerozoic. J. African Earth Sci., 8: 183-190.

Lasserre, M., 1978. Mise au point sur les granitöides dits "ultimes" du Cameroun: gisement, pétrographic et géochronologie. Bull. Bur. Rech. géol. min., Paris, Ser. 2, Sect IV, no. 2, 143-59.

Maurine, J.C., Benkhelil, J. and Robineau, B., 1986. Fault rocks of the Kaltungo lineament (NE Nigeria) and their relationship with the Benue Trough. J. Geol. Soc. London, 143: 587-599.

Mann, D.C., 1989. Thick-skin and thin-skin detachment faults in continental Sudanese rift basins. J. African Earth Sci., 8:307-322.

McHargue, T.R., Heidrick, T.L., and Livingston, J.E., 1992. Tectonostratigraphic development of the interior Sudan rifts, central Africa. Tectonophysics, 213: 187-202.

Meyers, J.B. and Rosendahl, B.R., 1991. Seismic reflection character of the Cameroon volcanic line: Evidence for uplifted oceanic crust. Geology, 19: 1072-1076.

Moreau, C., Regnoult, J.-M., Déruelle, B., Robineau, B., 1987. A new tectonic model for the Cameroon line, Central Africa. Tectonophysics, 139: 317-334.

Morgan, W.J., 1983. Hotspot tracks and the early rifting of the Atlantic. Tectonophysics, 94: 123-139.

Nwachukwu, J.I., 1985. Petroleum prospects of Benue trough, Nigeria. Am. Assoc. Petrol. Geol. Bull., 69: 601-609.

Ofoegbu, C.O., 1984. Interpretation of aeromagnetic anomalies over the Lower and Middle Benue Trough of Nigeria. Geophys. J.R. Astron. Soc., 79: 813-823.

Ofoegbu, C.O., 1988. An aeromagnetic study of part of the Upper Benue Trough, Nigeria. J. African Earth Sci., 7: 77-90.

Ojo, O.M., 1988. Stream sediment geochemistry of Guberunde Horst, "Gongola Basin", Upper Benue trough Nigeria. Jour. African Earth Sci., 7: 91-101.

Ojo, S.B. and Ajakaiye, D.E., 1975. Preliminary interpretation of gravity measurements in the Middle Niger Basin Area, Nigeria. In: C.A. Kogbe (Editor), Geology of Nigeria. Elizabethan Publishing Co., Lagos, pp. 294-307.

Okereke, C.S. and Fairhead, J.D., 1984. A catalogue of gravity measurements for Nigeria and Cameroon. Depart. Earth Sci., Univ. Leeds, Leeds, 300 pp.

Okereke, C.S., 1988. Contrasting modes of rifting: The Benue trough and Cameroon volcanic line, West Africa. Tectonics, 7: 775-784.

Petters, S.W., 1978. Stratigraphic evolution of the Benue trough and its implications for the upper Cretaceous paleogeography of West Africa. Jour. Geol., 86: 311-322.

Petters, S.W. and Ekweozor, C.M., 1982. Petroleum geology of Benue trough and southeastern Chad basin, Nigeria. Am. Assoc. Petrol. Geol. Bull., 66: 1141-1149.

Popoff, M., Benkhelil, J., Simon, B. and Motte, J.J., 1983. Approche géodynamique du fosse de la Benoué (NE Nigeria) é partir des données de terrain et de téledétection. Bull. Cent. Rech. Explor. Prod. Elf-Aquitaine, Paris, 7: 323-337.

Popoff, M., 1988. Du Gondwana " l'Atlantique sud: les connexions du fassé de la Bénoué avec les bassins du Nord-Est brésilien jusqu' é l'ouverture du golfe de Guinée au Crétacé inférieur. In: The West African Connection (Sougy J. and Rodgers, J. editors), J. Afric. Earth Sci., Special publication, Oxford, G.B. 7, 2, pp. 409-431.

Rahaman, M.A., Van Breeman, O., Bowden, P. and Bennet, J.N., 1984. Detailed age study of the migration of younger granite ring complex in Nigeria. J. Geol., 92: 173-184.

Reeves, C.V., Karanja, F.M., and MacLeod, I.N., 1987. Geophysical evidence for a Jurassic triple-junction in Kenya. Earth Planet. Sci. Ltrs., 81: 299-311.

Schull, J.T., 1986. Oil exploration in non-marine rift basins of interior Sudan. Am. Assoc. Petrol. Geol. Bull., 70: 1762.

Schull, J.T., 1988, Rift basins of interior Sudan: petroleum exploration and discovery: Am. Assoc. Petrol. Geol. Bull., 72: 1128-1142.

Smith, A.G., Hurley, A.M. and Briden, J.C. 1981. Phanerozoic Paleocontinental World Maps. Cambridge University Press, Cambridge, 102 pp.

Stuart, G.W., Fairhead, J.D., Dorbath, L. and Dorbath, C., 1985. A seismic refraction study of the crustal structure associated with the Adamawa Plateau and Garoua Rift, Cameroon, West Africa. Geophys. J.R. Astron. Soc., 81: 1-12.

Umeji, A.C. and Caen-Vachette, N., 1983. Rb-Sr isochron from Gboko and Ikyuen rhyolites and its implications for the age and evolution of the Benue Trough, Nigeria. Geol. Mag., 120: 529-533.

Wilson, M., and Guiraud, R., 1992. Magmatism and rifting in western and central Africa, from Late Jurassic to Recent times. Tectonophysics, 213: 203-225.

Wright, J.B., 1968. South Atlantic continental drift and the Benue trough. Tectonophysics, 6: 301-309.

This Page Intentionally Left Blank

Part V.

Epilogue

This Page Intentionally Left Blank

Chapter 14

Continental rifting: A final perspective

W. S. Baldridge, G. R. Keller, and L. W. Braile

14.1. Introduction

Formation of extensional stresses in the Earth's lithosphere is a global tectonic phenomenon, occurring in all plate settings. When initiated in continental lithosphere, extension can give rise to a range of tectonic features, most commonly continental rifts as defined in Chapter 1 of this book. Whether the forces originate from processes operating at plate boundaries or from beneath plates, rifts reflect fundamental processes associated with plate tectonics that affect not only the entire thickness of the lithosphere over lateral distance of hundreds to thousands of kilometers but also the upper part of the sublithospheric mantle (Olsen, 1992). Nowhere is the relationship of continental rifting to fundamental plate-tectonic processes clearer than where extension has proceeded to the point of sea-floor spreading, such as in the Afar region of the East African rift system. Yet, in these locations, later stages of lithospheric extension have overprinted earlier stages, obscuring some of the initial processes of breakup. Thus, continental rifts preserve the most complete, and possibly the only, record of critical structures and of transient processes associated with the incipient stages of continental breakup.

14.2. Magmatism and mantle plumes

The relationship of continental rifts to plumes, especially the question of whether rifts are initiated by plumes, is still a matter of conjecture. Plumes imply upwelling of mantle from significant depths (several hundred km) along an adiabat, resulting in significant decompressive melting as mantle rocks are elevated above their solidus temperatures. Plume-driven rifting would comprise an "active" rift mechanism, as defined by Sengör and Burke (1978). Geophysical investigations, as documented in this book, seem to indicate that low-velocity, low-density upper mantle inferred to be at or very near its melting temperature is a universal feature of modern continental rifts. Recent long-offset seismic refraction and teleseismic investigations of the East African and Rio Grande rifts (Chapters 5, 6) yield particularly compelling evidence for buoyant mantle to depths of 100–200 kilometers or more.

Yet, while some upwelling undoubtedly occurs beneath continental rifts, the apparent lack of significant magmatism in many rifts seems to argue that upwelling is not an expression of mantle plumes, which necessarily generate large volumes of basaltic rocks. In fact, the very existence of mantle plumes is inferred from such large volumes of magmatic

rocks, with many volcanic provinces displaying age progressions which correlate with plate motions. Little other direct evidence for plumes exists. "Apparent lack" of magmatism refers to the fact that some rifts such as the European Cenozoic rift system (Chapter 4), Rio Grande rift (Chapter 6), and Baikal rift (Chapter 8) contain only small volumes of volcanic rocks. The possibility that magmatic rocks may have been generated in the mantle and emplaced into the crust without eruption to the surface must be evaluated by geophysical means. Large intrusions do not occur in the upper crust of these rifts, and seismic velocities of the lower crust do not seem as high as would be expected from emplacement of large volumes of mafic intrusions at or near the base of the crust (V_p = 6.9–7.2 km/s), rendering it unlikely that significant volumes of magma were ever generated in these rifts. This observation of little volcanism agrees with the small amount of extension sustained by continental rifts (generally less than 20%), which does not permit enough upwelling to cause significant melting of the underlying mantle. Thus, upwelling produces a detectable thermal anomaly but without substantial melting. Extension of more than 100% is required before significant decompression melting becomes important (McKenzie and Bickle, 1988; White and McKenzie, 1989). Perhaps the best information on the lower crust of continental rift zones is that available for parts of the East African rift, due largely to the KRISP experiments (Chapter 5). By comparison, seismic information on the lower crust in many other rift zones is limited. As a result, many published conclusions (including those herein) may be altered with better information.

Even the presence of large volumes of magmatic rocks, such as in the Afar and other parts of the East African rift system (Chapter 5) and in the Proterozoic Midcontinent rift system (Chapter 10), may not require an explanation involving plume activity. Instead, large volumes of basaltic melts may be generated by relatively shallow, secondary mantle convection driven by lateral temperature gradients at the base of the plate (Mutter et al., 1988). Also, the large volumes of magmatic rocks associated with early (Oligocene-early Miocene) extension in the region of the Basin and Range province and Rio Grande rift (Chapter 6) probably mirror upwelling of asthenosphere which was advected beneath the overriding North American plate as the subducting Farallon plate increased its dip (Cross and Pilger, 1978). But asthenospheric upwelling does not necessarily imply a deeply rooted plume. True plume-driven continental rifting may necessarily result in sea-floor spreading. The question of whether rifting is init*iated* by upwelling of mantle, though conceptually simple, is probably unanswerable for most rifts due to the complex history of most continental regions.

Despite these complexities, some melting does occur beneath all continental rifts. Basaltic magmas have geochemical signatures indicating their extraction from lithospheric mantle as well as from underlying asthenosphere. Data from several rift zones are interpreted to indicate a progression from early lithospheric magma sources to younger, mixed asthenospheric-lithospheric or asthenospheric sources (Anthony et al., 1990; Daley and DePaolo, 1992). A likely melting mechanism involves partial melting of those regions of mantle that are enriched in incompatible elements (particularly volatile components) or less mafic, lower-melting-point constituents (Harry and Leeman, 1995) compared with adjacent regions of relatively more "depleted" (but equally hot) mantle as temperatures are raised. Thus, partial melts may form in isolated pockets with different compositions that depend on local bulk composition, extent of partial melting (which itself reflects local bulk composition), interactions with surrounding depleted matrix, and ascent histories.

14.3. Short- and long-term effects on continental lithosphere

Continental rifts have existed at least since the Proterozoic Eon, and their effects on continental lithosphere are both short- and long term (> 10^9 years).

14.3.1. Crustal effects

The short-term effects of rifting on continental crust result mainly from elevated temperatures, which can partially or completely cancel out effects

of velocity and density increases due to intrusion of mafic rocks. In active rifts such as the Rio Grande and Baikal rifts (Chapters 6, 8), V_p of the middle and lower crust tends to be 0.1–0.2 km/s lower than laterally adjacent crust. These small differences in velocities are interpreted to indicate that the crustal compositions are similar to those of adjacent crust, typically inferred to be of intermediate composition, but that the rocks are at elevated temperatures. Lower crustal V_p beneath the Kenya portion of the East African rift is 6.9 km/s, suggesting that some higher velocity mafic component is present. In contrast to active rifts, available crustal velocities beneath paleorifts tend to be higher than adjacent unrifted crust (Chapter 3B). This velocity increase is attributed to densification of crust by magmatism during rifting, and to cooling to normal continental crustal temperatures after rifting, as discussed below.

Continental rifting strongly affects the long-term character of the crust, primarily through magmatism and extension. The primary effect of magmatism is to transfer partial melts (basaltic melts) from the mantle to the crust, thereby increasing the overall density (hence, seismic velocity) of the crust (Wendlandt et al., 1991). Because the relatively higher density basaltic magma may be unable to rise through the relatively more buoyant crust, it has been widely hypothesized that magma ponds at the base of the crust in a process referred to as "underplating" (Furlong and Fountain, 1986; Bergantz, 1989). Yet, with the prominent exception of several passive margins (e.g., North Atlantic, Hatton; Chapter 11) and possibly the Basin and Range province (Chapter 7), little or no evidence exists for substantial underplating beneath many extended regions. For the Kenya rift portion of the East African rift system, despite the large volume of volcanic rocks, lower crustal V_p is only about 6.9 km/s (Chapter 5), indicating a possibly substantial mafic component within or at the base of the lower crust but probably not of wholesale underplating. Rather, the lower crust has probably undergone extensive injection by mafic magma, creating a massively intruded layer that resembles underplating (Hay et al., 1995). Addition of large volumes of magmatic material to the lower crust may actually thicken the crust beyond its original, pre-rift thickness, overcompensating for crustal thinning due to extension. Such may have been the case for the Kenya rift near the Kenya dome. Large volumes of magmatic rocks within and beneath the crust of rift zones lead to significant sagging of the crust as the crustal density increases upon cooling (e.g., Midcontinent rift zone, Chapter 10).

In addition to density increases caused by addition of magmatic material from the mantle, crustal melting spawned by intrusion of mantle-derived magma tends to increase the density of the lower crust relative to the upper crust because mafic and ultramafic minerals are left behind as residua of fractional melting and crystallization (e.g., Oslo graben, Chapter 9), and fusible material is moved toward the surface (Kay and Mahlburg-Kay, 1991).

Modification of crust may also occur through deformational processes associated directly with rifting or associated with post-rifting stress regimes. In highly extended parts of the Basin and Range province, crystalline rocks ("core complexes"}, possibly from midcrustal depths, have risen to the surface beneath ductile shear zones as overlying upper crust was removed by extensional thinning (Chapter 7). Lateral flow of ductile lower crust in isostatic response to flank uplift may also partially compensate for ductile thinning caused by extension. Lateral flow of lower crust may be a contributing mechanism (in addition to underplating) by which crustal thickness of the Basin and Range province is maintained at a relatively constant 30 km and elevation of nearly 2 km despite extension ranging from <100% to about 250%. An additional mechanism for modifying crust in rift zones is illustrated by the Southern Oklahoma aulacogen, where subrift intrusive rocks may have been thrust into the upper crust by post-rift compressive deformation (Chapter 12).

The process of continental rifting has a long term and possibly permanent effect on continental crust. The New Madrid rift zone is seismically active along structures associated with the ancient rift, and both the Midcontinent and New Madrid rifts have undergone substantial crustal subsidence (Chapter 10). These long-lasting effects result from permanent compositional changes to the lithosphere, resulting in part in densification of the crust.

14.3.2. Long-term effects on mantle

Once the thermal anomaly beneath a continental rift has decayed away (the definition of a paleorift, see Chapter 1), asthenospheric mantle that was associated with the rift will be displaced relative to the overlying lithosphere by mantle convection and/or plate motion. Hence, paleorifts such as the Oslo rift (Chapter 9) and the Midcontinent rift (Chapter 10) apparently have no deep-seated (i.e., sublithospheric) signature. Lithospheric mantle, on the other hand, is irreversibly altered by several processes, including by the extraction of melts from it. Melt extraction depletes the mantle lithosphere in volatile and low-melting-point components, and by the removal of "incompatible" trace elements that preferentially partition into the melts. Partial melts of mantle peridotite are more iron-rich (compared to magnesium) than their source rocks. Thus, their extraction leaves behind a residue that is less dense than previously, hence is characterized by lower P-wave velocities (Wendlandt et al., 1991). In addition, new lithospheric mantle is probably created as upwelled asthenosphere cools and is converted to lithospheric mantle.

14.3.3. The Moho

Igneous processes (intrusion, fractionation, and crustal melting) associated with rifting may obscure both the physical and chemical distinctiveness of the Moho, which is defined as a seismic discontinuity at which V_p increases to greater than 7.5 km/s (depending on temperature and depth) consistent with the boundary between crustal and uppermost mantle rocks. The effect of an increase in density of the lower crust and decrease in density of the upper mantle, described above, is to result in a gradual transition in seismic velocities from crust to mantle. Much has been written about the possible effect of phase changes in altering the nature of the "petrologic Moho" as the lower crust undergoes cooling. Mafic intrusive rocks of the lower crust will invert from a dominantly plagioclase-pyroxene mineralogy to a higher density, though not significantly higher velocity, garnet-pyroxene (i.e., eclogitic) mineralogy as crustal temperatures decrease. If significant underplating occurs during rifting, rocks that were originally "crustal" in their composition and mineralogy could undergo phase transformation to a "mantle" mineralogy in terms of their densities, potentially creating a high density "root" at the base of the crust. However, even for the Midcontinent rift system such a high density lower crust is not observed (Chapter 10).

14.4. Timing

The timing of uplift, faulting, and magmatism, are of key importance in understanding processes of lithospheric extension. Many factors complicate and/or obscure the sequence of events which occur during rifting. First, the response of the lithosphere is very much a function of the state of the lithosphere at the time rifting begins. For example, the Baikal rift zone (Chapter 8) appears to have formed in cold, stable lithosphere, while the Rio Grande rift formed in a region that had experienced almost continuous deformation and magmatism for the previous 50 Ma (Chapter 6). Also, in the Rio Grande rift area, crustal thickening and uplift associated with Laramide deformation occurred prior to rifting. Differences in pre-existing conditions such as these may explain some of the differences among rifts. In addition to real differences, apparent differences in timing of events may stem from difficulties in interpreting the geologic record. For example, erosion driven by relative vertical movements erases parts of the record and buries other parts under basin sediments. Older faults may be buried or uplifted and eroded as the locus of faulting shifts, leading to the perception that faulting is younger than is actually the case. Also, the timing of magmatism may be misunderstood if not expressed at the surface as volcanism, where it is available for precise dating. Despite these difficulties, enough information exists to document important similarities and significant differences among different rift zones (Fig. 14–1).

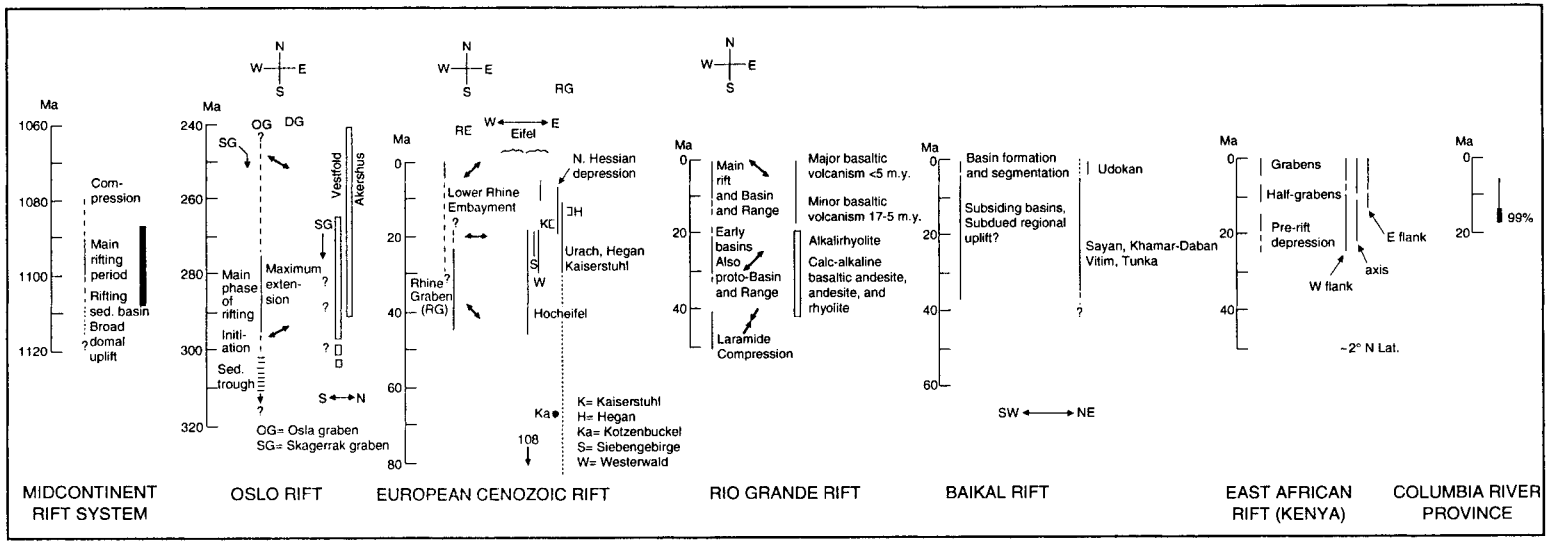

Fig. 14–1. Timing of tectonic deformation and magmatism for selected modern and paleorifts, Solid lines or heavy solid bars indicate periods of mafic magmatism; open bars denote intermediate and/or silicic magmatism. Heavy arrows show direction of extension (↔) or compression (→←) relative to cardinal directions shown above. Light arrows for Oslo rift, European Cenozoic rift system, and Baikal rift indicate south-to-north, west-to-east, and southwest-to-northeast geographic variations, respectively. Columbia River flood basalt province shown for comparison. Figure constructed by E.-R. Neumann, R. F. Wendlandt, and W. S. Baldridge.

14.5. Rupture of lithosphere

Recent debate has centered on whether lithosphere in continental rifts extends by simple or by pure shear (Wernicke, 1985). In detail, crust and mantle may deform by either strain mechanism. In the upper crust, extension occurs along planar, listric, and detachment brittle faults. Paradoxically, while geologic and seismic reflection data provide evidence for low-angle faults, earthquake focal mechanisms do not substantiate their role. In the middle and lower crust and lithospheric mantle, deformation occurs along ductile faults (including detachments) and by penetrative ductile flow, as shown in exposed middle and lower crustal sections. Considering the lithosphere as a whole, a variety of geophysical and geochemical data from several modern rifts seems to indicate that the region of greatest crustal thinning approximately overlies the region of greatest lithospheric thinning (Chapters 4–6). In addition, data from seismic refraction lines and from teleseismic observations indicate that the mantle anomalies underlying rifts are centered approximately beneath the axes of the rifts to a depth exceeding 200 km. The coincidence of the axes of crustal and mantle thinning suggests that extension of lithosphere during continental rifting occurs mainly by pure shear mechanisms, at least at the largest scale, rather than by simple shear along inclined shear zones cutting through the lithosphere. These arguments do not necessarily imply that simple shear on a lithospheric scale does not occur, but at the present time it does not appear to be a major process in continental rifts. In addition to simple and pure shear mechanisms, lithosphere may also be thinned by melting at its base above upwelling asthenosphere. This mechanism ("thermal thinning"), although perhaps not a major process overall, is likely to be important in rifts associated with large volumes of volcanic rocks, and provides a means of recycling compositionally enriched components of the continental lithosphere into the asthenosphere.

14.6. What's next?

Much progress has been gained in understanding the processes of continental rifting and on the long-term effects of rifts on the continental lithosphere. As the chapters of this book document, it now seems clear that, in addition to their different tectonic settings, continental rifts differ from each other in important elements of their crustal and lithospheric structure, magmatism, and evolution. Much remains to be learned, as well, especially as new tools and techniques are developed. Certain questions such as whether rifting of continental lithosphere proceeds by propagation of stresses from a rift tip, or by instantaneous development of new rift basins (Mutter, 1995), are yet to be satisfactorily resolved. Both of these mechanisms may be valid for oceanic rifts, but continental lithosphere is much more complex. For example, in most continental rifts the effect of pre-existing structures appears to have some, and possibly a major, control on the locations and types of structures that form in the upper crust. For both the Kenyan and Baikal rifts, the rifts themselves appear to be localized at the suture zones of Archean and Proterozoic lithospheric provinces. Thus, propagation mechanisms for oceanic lithosphere, which is much younger and therefore more homogeneous than continental lithosphere, may only be partially valid for continental rifts. Another potentially important area of study, which is not limited to rift zones, is that of mantle anisotropy. Anisotropy may provide an important techniques for understanding flow patterns in the mantle, and thus the relationship between rifts and plumes.

Great progress has been made over the last two decades in understanding rifts, allowing modern rifts to be contrasted and compared better, and to be compared to paleorifts with more confidence. Studies of continental rifts will continue to yield insights into fundamental processes of plates tectonics and of the dynamics and geochemistry of the deeper mantle.

14.7. References

Anthony, E. Y., Segalstad, T. V., and Neumann, E.-R., 1989. An unusual mantle source region for nephelinites from the Oslo rift, Norway. Geochim. Cosmochim. Acta, 53: 1067–1076.

Bergantz, G. W., 1989, Underplating and partial melting: Implications for melt generation and extraction. Science, 245: 1093–1095.

Cross, T. A., and Pilger, R. H., Jr., 1978. Constraints on absolute motion and plate interaction inferred from Cenozoic igneous activity in the western United States, Am. J. Sci., 278: 865–902.

Daley, E. E., and DePaolo, D. J., 1992. Isotopic evidence for lithospheric thinning during extension: southeastern Great Basin. Geology, 20: 104–108.

Furlong, K. P., and Fountain, D. M., 1986. Continental crustal underplating: Thermal considerations and seismic-petrologic consequences. J. Geophys. Res., 91: 8285–8294.

Hay, D. E., Wendlandt, R. F., and Keller, G. R., 1995. Origin of Kenya rift plateau-type flood phonolites: Integrated petrologic and geophysical constraints on the evolution of the crust and upper mantle beneath the Kenya rift. J. Geophys. Res., 100: 10,549–10.557.

Harry, D. L, and Leeman, W. P., 1995. Partial melting of melt metasomatized subcontinental mantle and the magma source potential of the lower lithosphere. J. Geophys. Res., 100: 10,255–10,269.

Kay, R. W., and Mahlburg-Kay, S., 1991. Creation and destruction of lower continental crust. Geologische Rundschau, 80/2: 259–278.

McKenzie, D., and Bickle, M. J., 1988. The volume and composition of melt generated by extension of the lithosphere, J. Petrol., 29: 625–679.

Mutter, J. C., 1995. Hot, fat and falling apart? Nature, 374: 499–500.

Mutter, J. C., Buck, W. R., and Zehnder, C. M., 1988. Convective partial melting 1. A model for the formation of thick basaltic sequences during the initiation of spreading. J. Geophys. Res., 93: 1031–1048.

Olsen, K. H., 1992. Continental rifting. In: W. A. Nierenberg (Editor), Encyclopedia of Earth System Science. Academic, San Diego. Vol. 1: 627–641.

Sengör, A. M. C., and Burke, K., 1978. Relative timing of rifting and volcanism on Earth and its tectonic implications. Geophys. Res. Lett,: 5: 419–421.

Wendlandt, R. F.., Baldridge, W. S., and Neumann, E.-R., 1991. Modification of lower crust by continental rifting. Geophys. Res. Lett., 18: 1759–1762.

Wernicke, B., 1985. Uniform-sense normal simple shear of the continental lithosphere. Canadian J. Earth Sci., 22: 108–125.

White, R., and McKenzie, D., 1989. Magmatism at rift zones: the generation of volcanic continental margins and flood basalts. J. Geophys. Res., 94: 7685–7729.

This Page Intentionally Left Blank

Subject Index

E

F

G

H

I

J

K

L

M

N

O

P

R

S

T

U

V

W

X

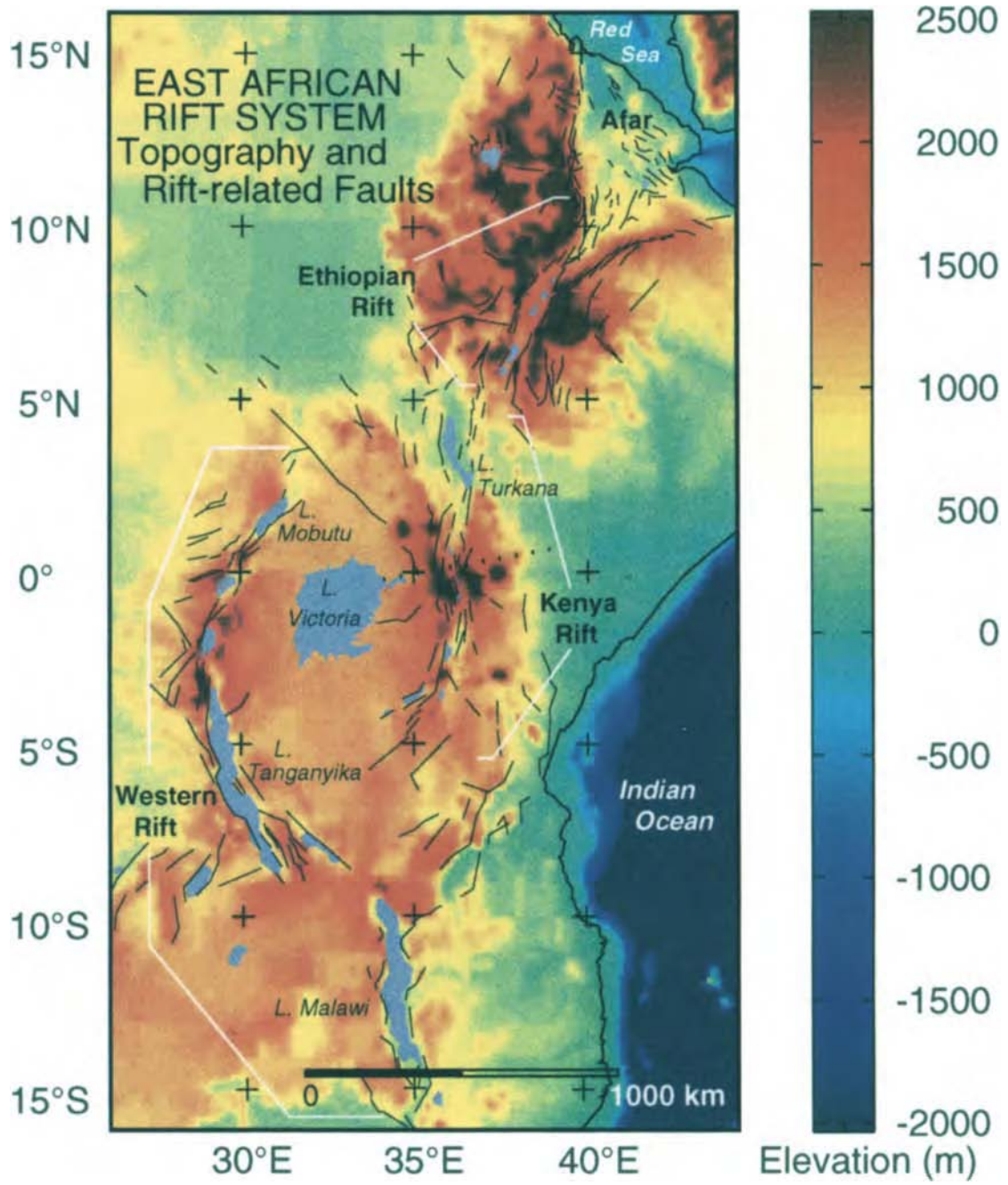

Plate 5–1. Topographic map of east Africa. Colors indicate elevation in meters. Elevations higher than 2500 m are shown as dark red. Elevations lower than –2000 m are shown as dark blue. Lakes, irrespective of their surface elevation, are colored light blue. Elevation data were obtained from the 5-minute world elevation grid ETPOPO5 from the Global Relief CD-ROM produced by the (US) National Geophysical Data Center. Major faults which appear to be associated with the East African rift system are shown as light lines and are from the International Geological Map of Africa (Choubert and Fauve-Muret, 1990). Major northwesterly trending lines northwest of Lake Malawi and north of Lake Victoria are the Tanganyika-Rukwa-Malawi fault zone (Rosendahl et al., 1986) and the Aswa shear belt (Rosendahl et al., 1987). These features have been interpreted to be related to the segmentation (Coussement et al., 1994) of the EARS although the Aswa shear belt is Precambrian in age. The dotted line near the center of the map indicates the location of a crustal and upper mantle velocity model derived from KRISP 85 and KRISP 90 seismic refraction and teleseismic data.

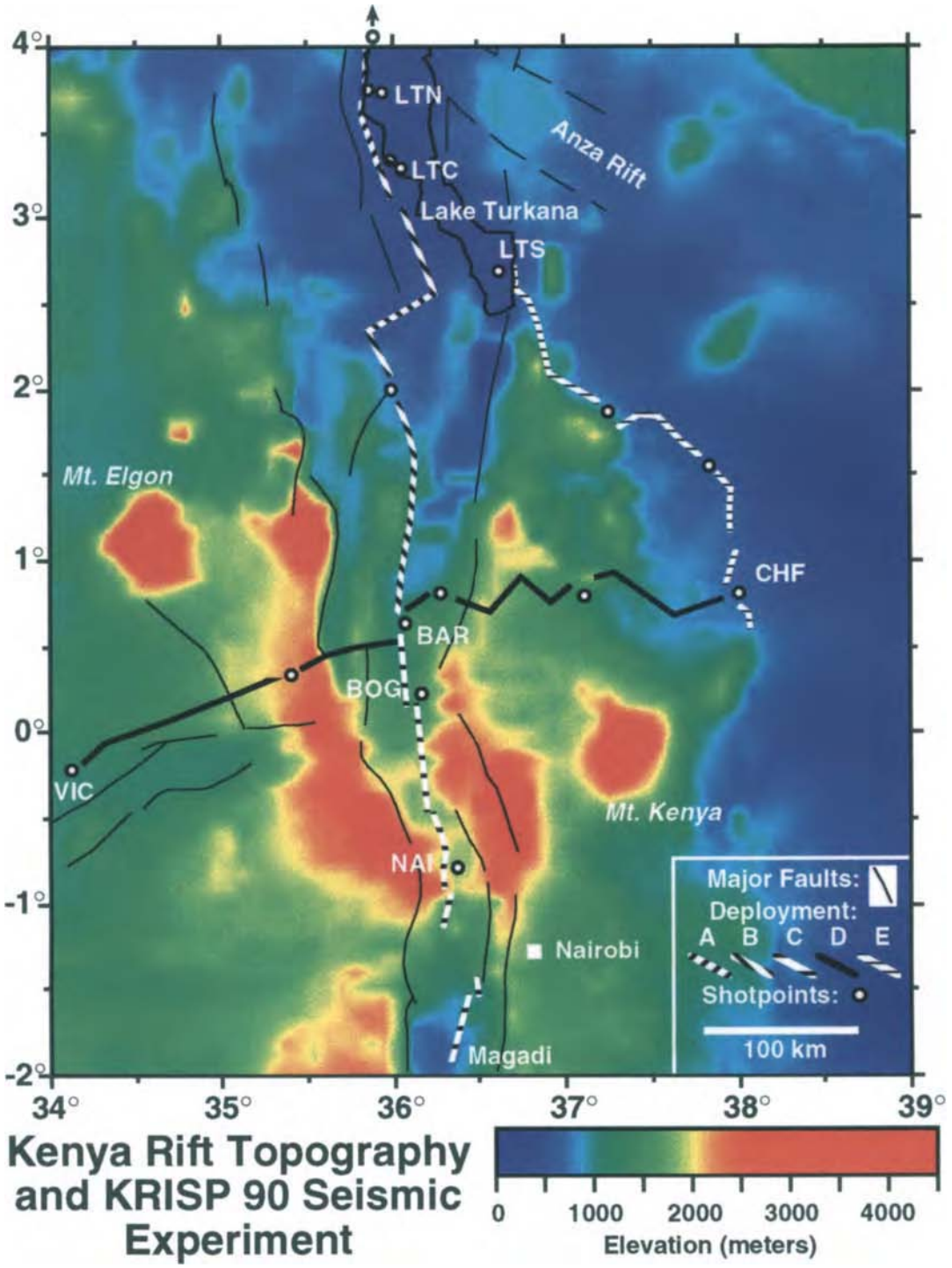

Plate 5–2. Topographic map of the central portion of the Kenya rift. Colors indicate elevations in meters. The topographically high region in the south-central portion of the map is known as the Kenya dome. Circles are shotpoints and heavy lines are seismograph deployment profiles for the KRISP 90 seismic refraction and wide-angle reflection project. Labeled shotpoints are: VIC = Lake Victoria; NAI = Lake Naivasha; BOG = Lake Bogoria; BAR = Lake Baringo; LTN, LTC and LTS are Lake Turkana North, Central and South; and CHF = Chanlers Falls. Light black lines are major faults.

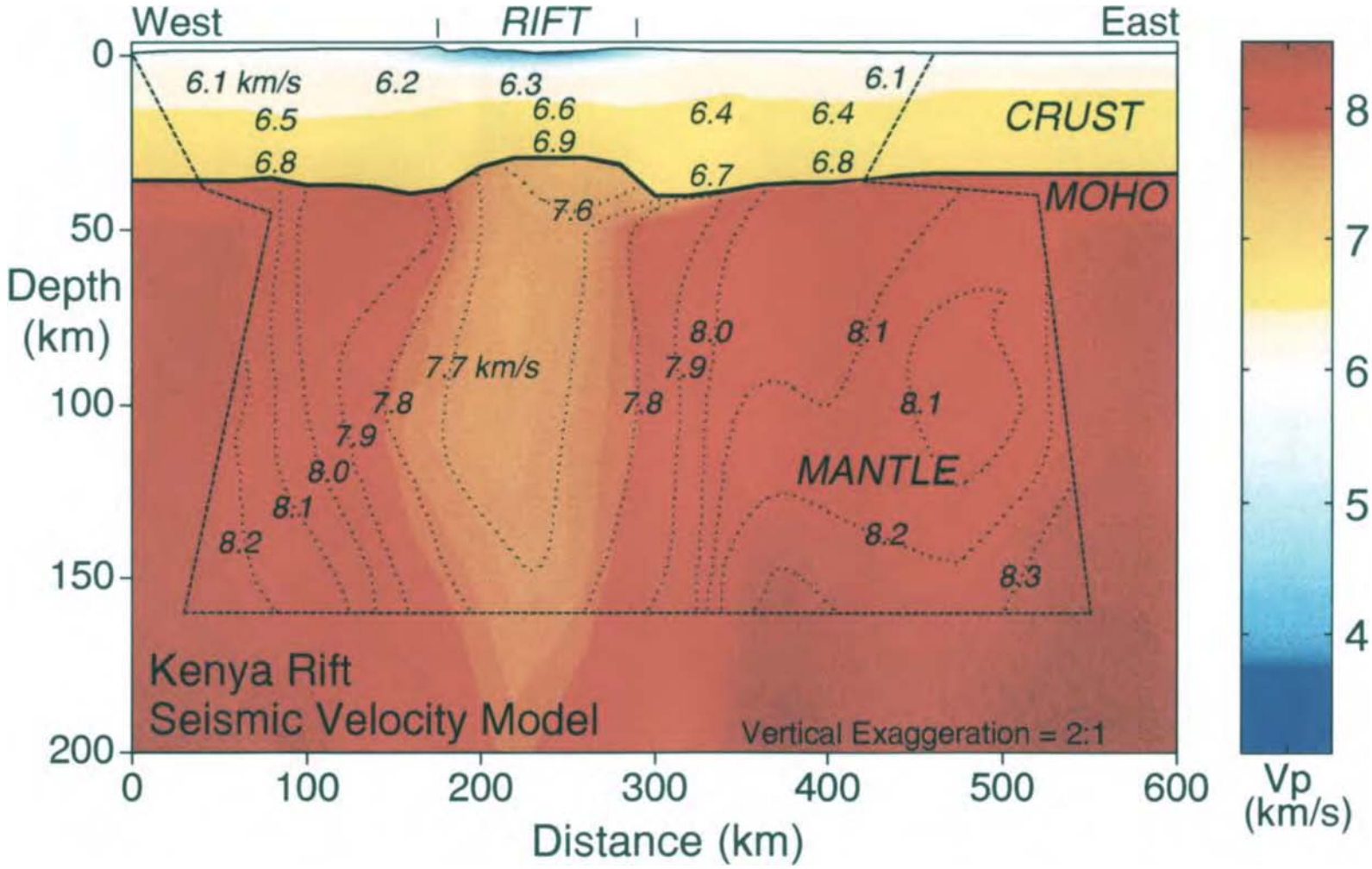

Plate 5–3. Compressional wave seismic velocity model of the crust and uppermost mantle beneath the Kenya rift and adjacent regions. Profile location is shown on Plate 5–1 (dotted line near equator) and corresponds (from 0 to 450 km distance range) to the cross-line refraction profile (Braile et al., 1994) from the KRISP 90 experiment (Plate 5–2). Velocities (in km/s) are shown by the color scale and by contours in the upper mantle. Crustal and P_n (just beneath the Moho which is shown by the heavy line) velocities were defined by the cross-line refraction and wide-angle reflection model of Braile et al. (1994). Upper mantle velocities were converted (see text) from velocity differences computed by Slack et al. (1994) from teleseismic arrival delay times. The dashed line outlines the region of significant raypath coverage for the refraction and teleseismic data.

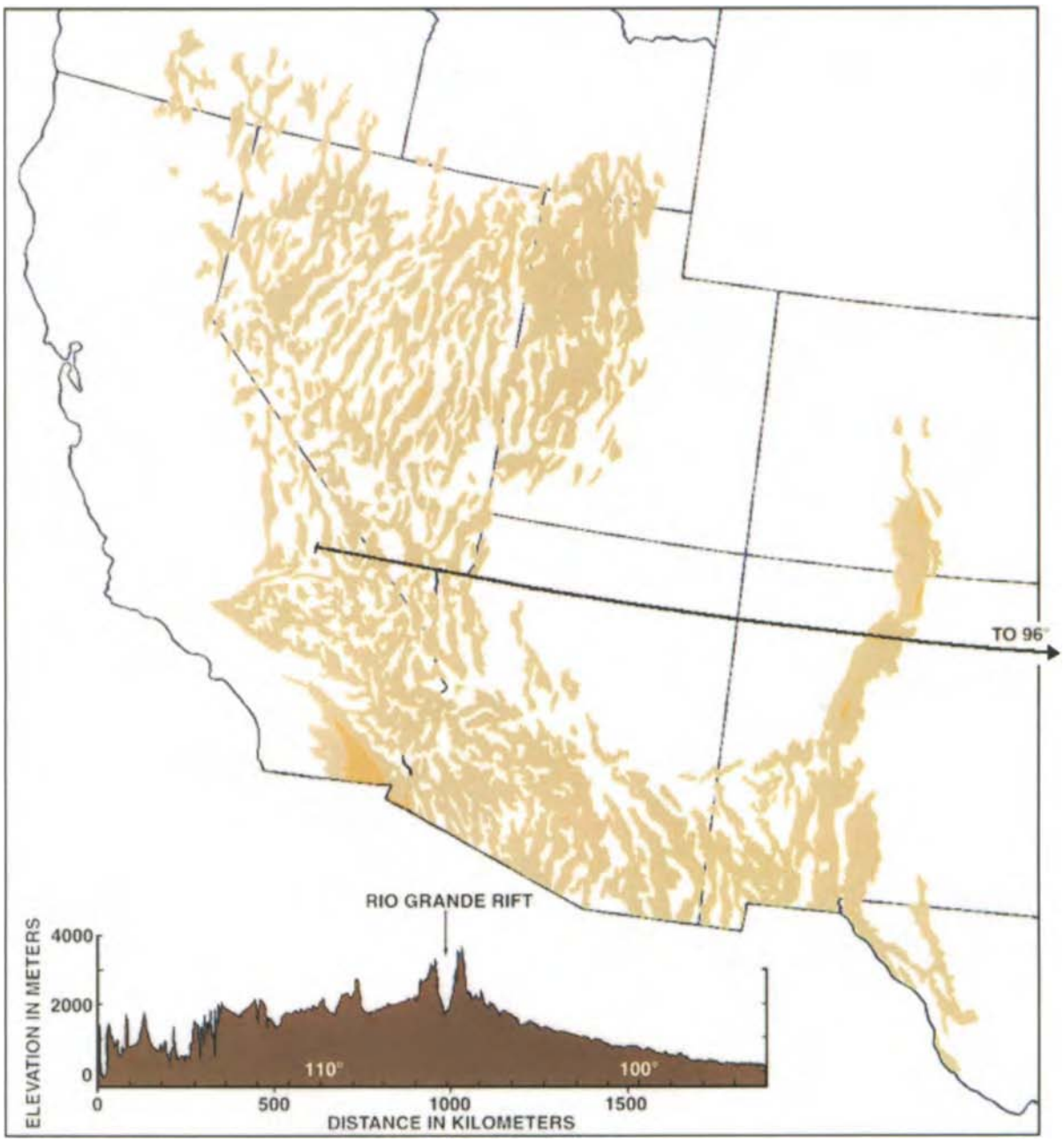

Plate 6–1. Physiographic map of the western U.S., indicating breadth of Cenozoic lithospheric extension in western U. S. Sediment-filled basins of the Basin and Range province and the Rio Grande rift are shown in light-brown; orange indicates basin depths >2500 m. Location of elevation profile from 96°W to 117°W (below) is shown by heavy line. Modified from Baldridge and Olsen (1989).

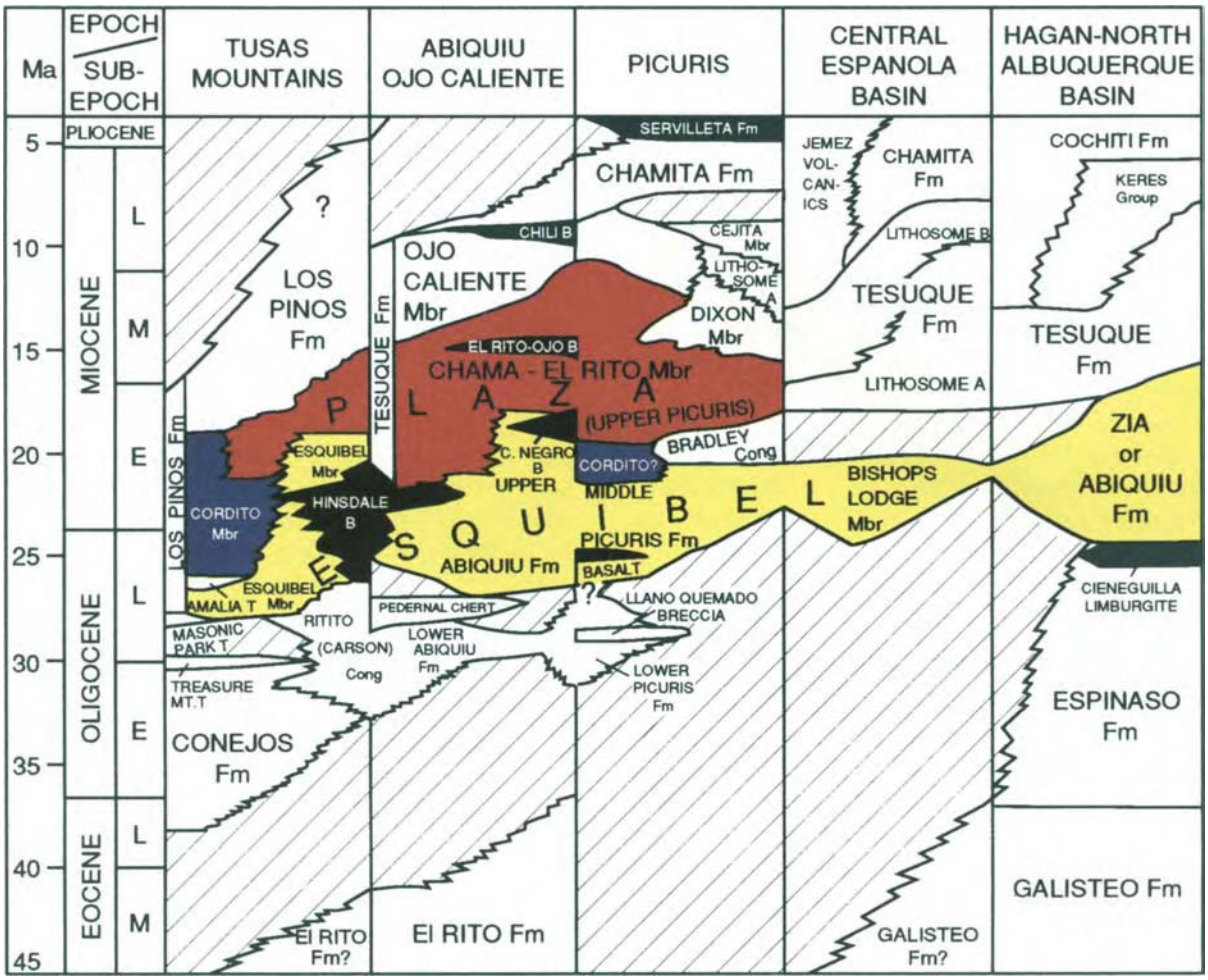

Plate 6–2. Chronostratigraphic chart of middle Eocene through lower Pliocene stratigraphic units in the Española and northeastern Albuquerque-Belen basins. Section is oriented approximately from north (left) to south. Solid black pattern indicates basaltic rocks. Much radiometric age control exists for volcanic and volcaniclastic units, but has been omitted for clarity. Modified from Ingersoll et al. (1990).

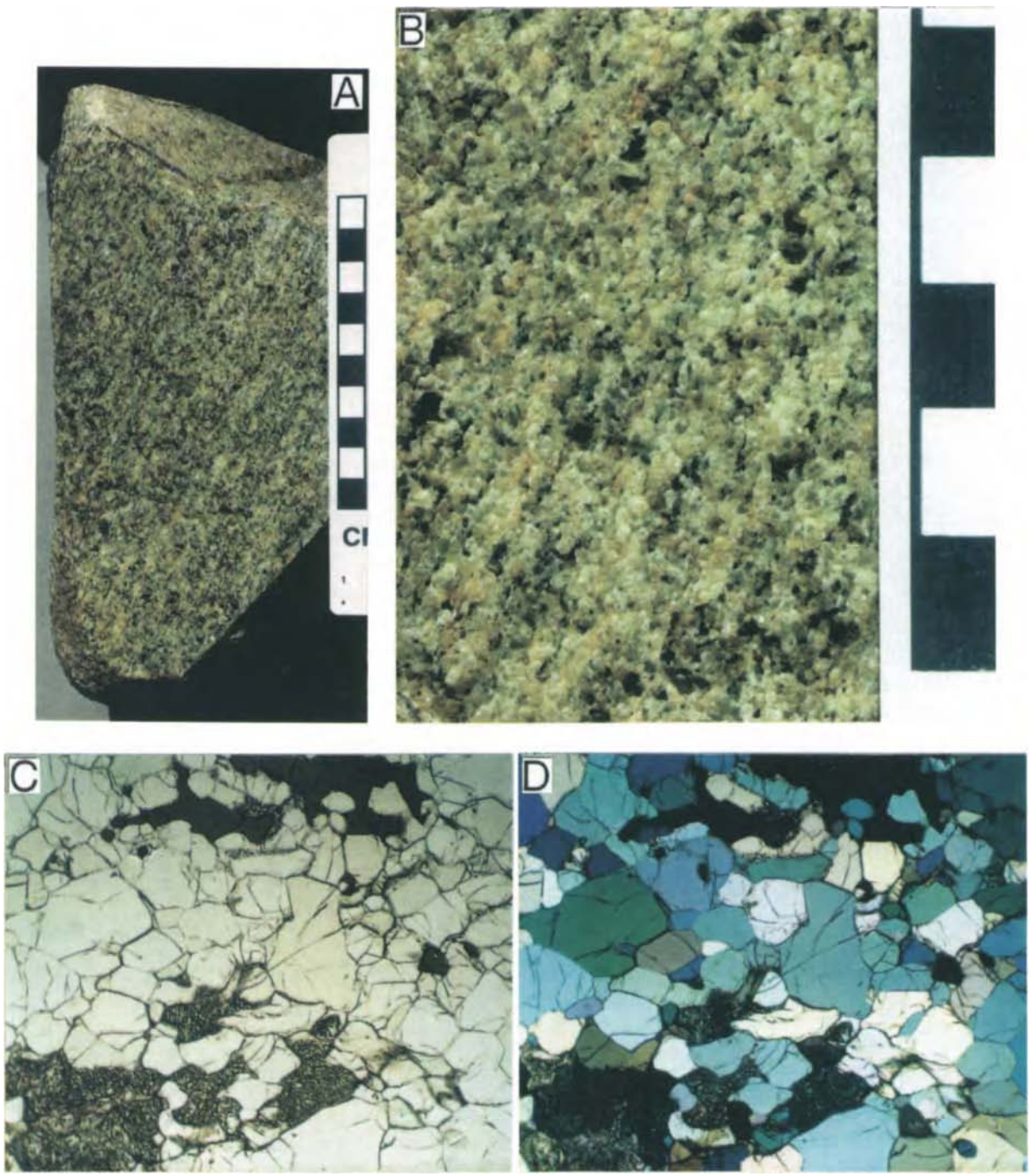

Plate 6–3. Xenolith of spinel lherzolite (olivine + enstatite + Cr–augite + spinel, in order of decreasing abundance) included in basalt from the Elephant Butte volcanic field in the central Rio Grande rift, New Mexico. A. Overall view showing granular texture and slight gneissic fabric. Black and white bars are each one cm long. B. Macroscopic view. Main green-colored mineral is olivine, dark green (nearly black) mineral is enstatite, and tiny bright green grains are Cr-rich diopside. Spinel is not readily apparent. Black and white bars are each one cm long. C. Photomicrograph, plane-polarized light. Dark, irregularly shaped mineral at top is spinel. Granular texture is reflected by numerous triple points, where grain boundaries intersect at approximately 120° angles. Width of photo is 7.6 mm. D. Same area as in C, crossed nicols.

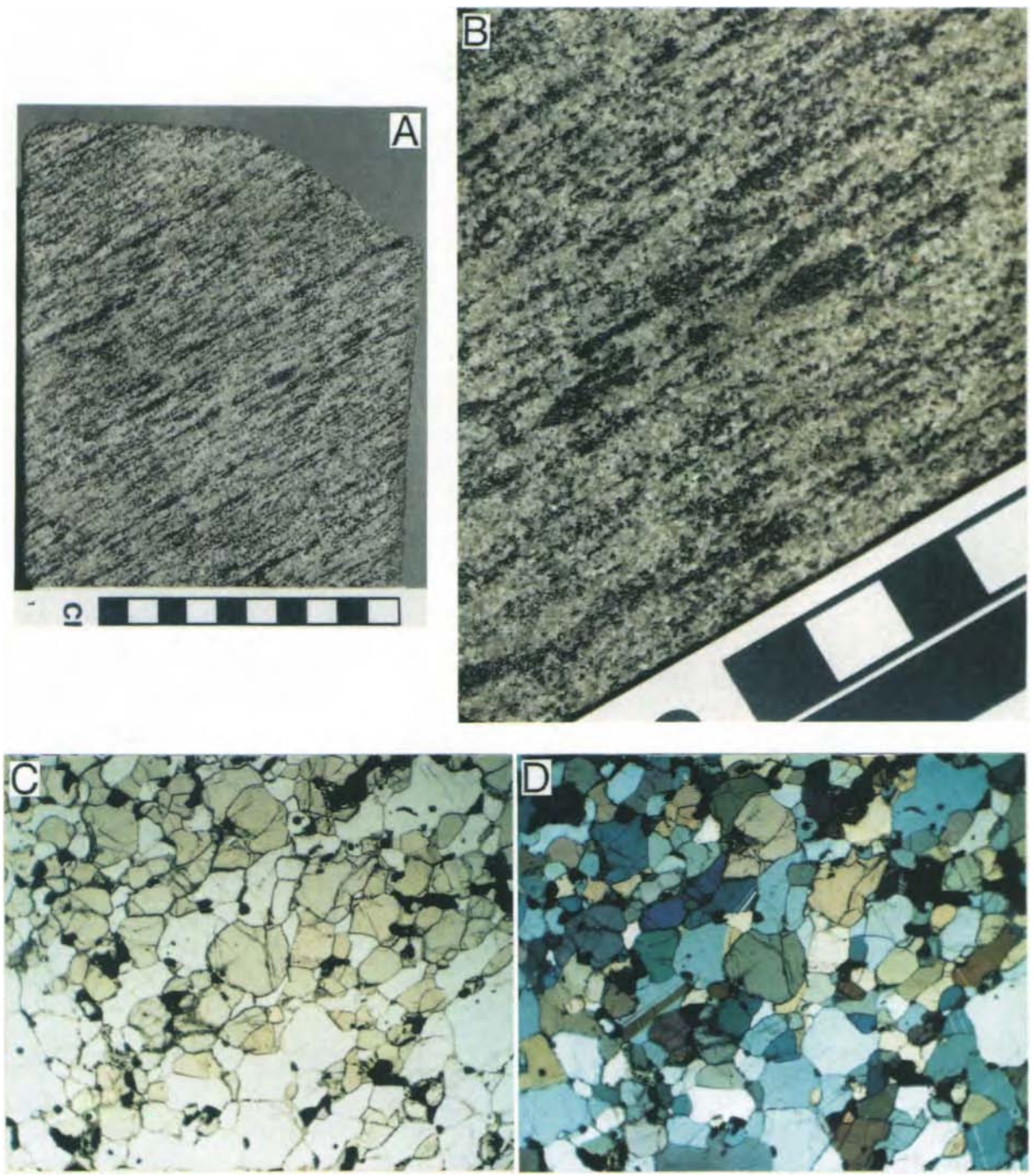

Plate 6–4. Xenolith of two-pyroxene granulite (clinopyroxene + orthopyroxene + plagioclase + spinel) included in basalt from the Elephant Butte volcanic field in the central Rio Grande rift, New Mexico. A. Overall view. Well developed gneissic fabric is readily apparent. The mineralogy and mineral compositions of this rock are consistent with a derivation from the lower crust. Black and white bars are each one cm long. B. Macroscopic view, showing mineral segrations which define the gneissic fabric. Plagioclase is white; pyroxenes are dark green (appear black). Black and white bars are each one cm long. C. Photomicrograph, plane-polarized light. Pyroxenes are pale green, plagioclase is white, spinel is black (small grains). Texture is granoblastic polygonal, characteristic of granulites. Width of photo is 7.6 mm. D. Same area as in C, crossed nicols.

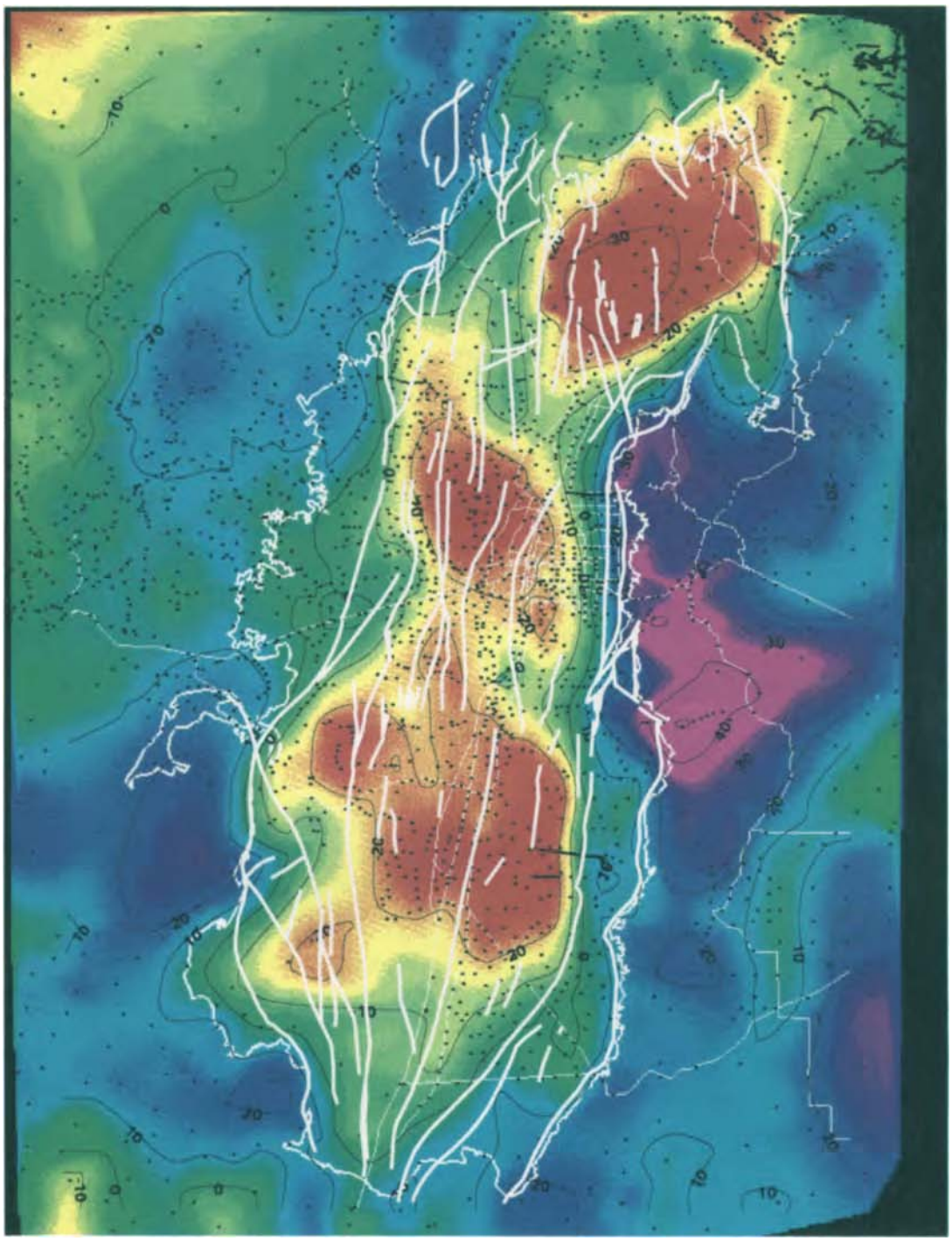

Plate 6–6. Isostatic residual gravity anomaly map of the Albuquerque-Belen basin. Contour interval is 10 mGal. Color scheme is as follows: yellow through red are low values, corresponding to thick basin-fill material; blue through magenta are high values, coinciding with flanking uplifts. Black dots are data points. Heavy white lines indicate major faults; medium white lines demarcate approximate edge of basin; light white lines are major roads. The city of Albuquerque, New Mexico, is located approximately in middle of figure. Plate modified and provided by C.E. Heywood, U. S. Geological Survey, Albuquerque, New Mexico, from Heywood (1992).

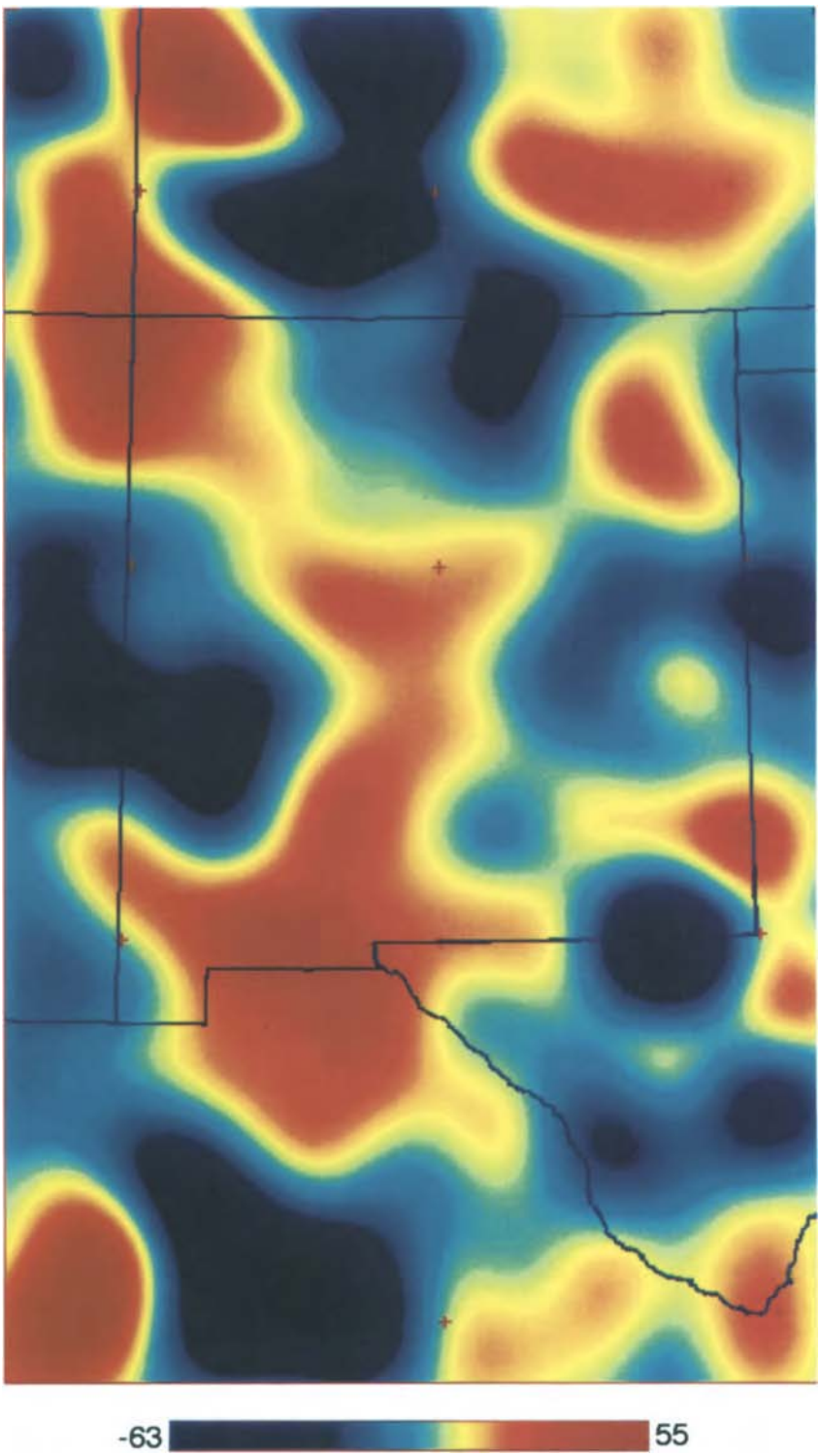

Plate 6–7. Low-pass filtered gravity map of the Rio Grande rift region. Wavelengths less than 125 km were attenuated.

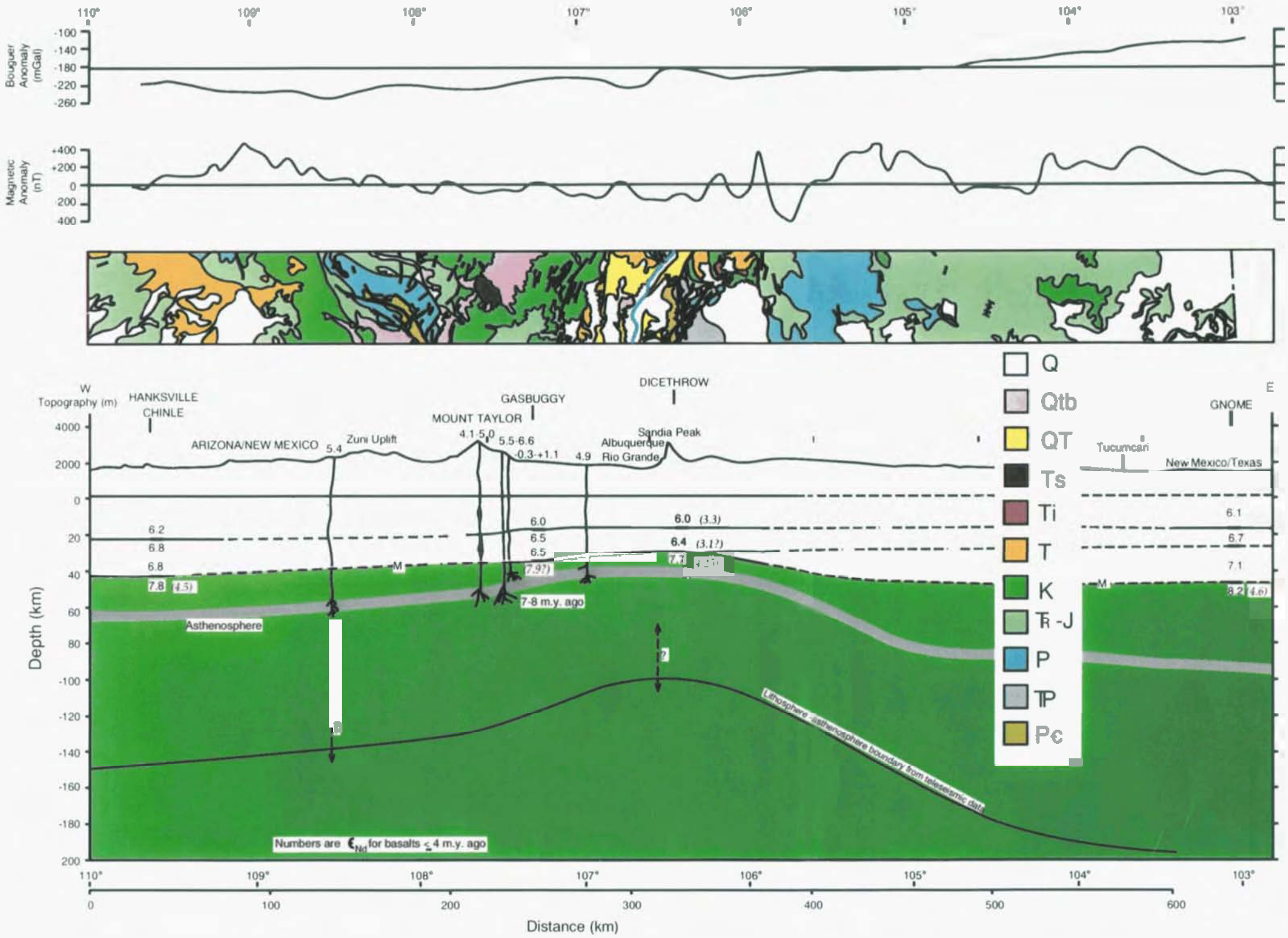

Plate 6–9. Gravity, magnetic, and heat flow profiles, geological strip map. and lithospheric transect through the Rio Grande rift at 35°10'N, near Albuquerque, New Mexico. Depth to asthenosphere is based on isotopic compositions of basaltic rocks (Perry et al., 1987, 1988). For comparison, depth to asthenosphere based on teleseismic data (see text) is also shown. Pe is Precambrian crystalline rocks, PP is Pennsylvanian sedimentary rocks, P is Permian sedimentary rocks, TR-J is Triassic and Jurassic (undifferentiated) sedimentary rocks, K is Cretaceous sedimentary rocks, T is Tertiary sediments and sedimentary rocks, Ti is Tertiary intrusive rocks, Ts is Tertiary intermediate and silicic volcanic rocks, QT is Tertiary and Quaternary (undifferentiated) sediments and sedimentary rocks, Qtb is Tertiary and Quaternary (undifferentiated) basaltic volcanic rocks, and Q is Quaternary sediments.

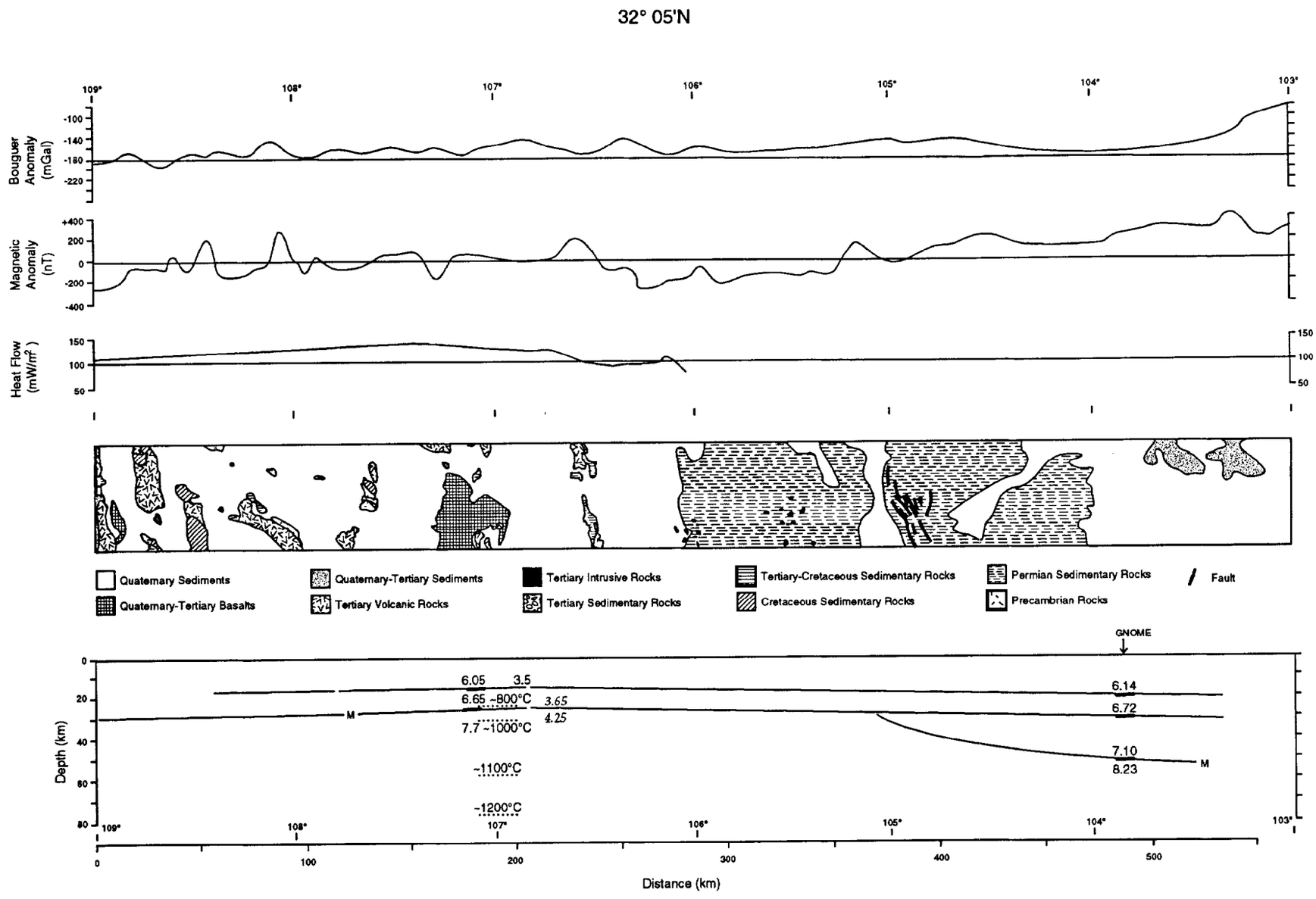

Plate 6–10. Gravity, magnetic, and heat flow profiles, geological strip map, and lithospheric transect through the Rio Grande rift at 32°05'N, near El Paso, Texas.

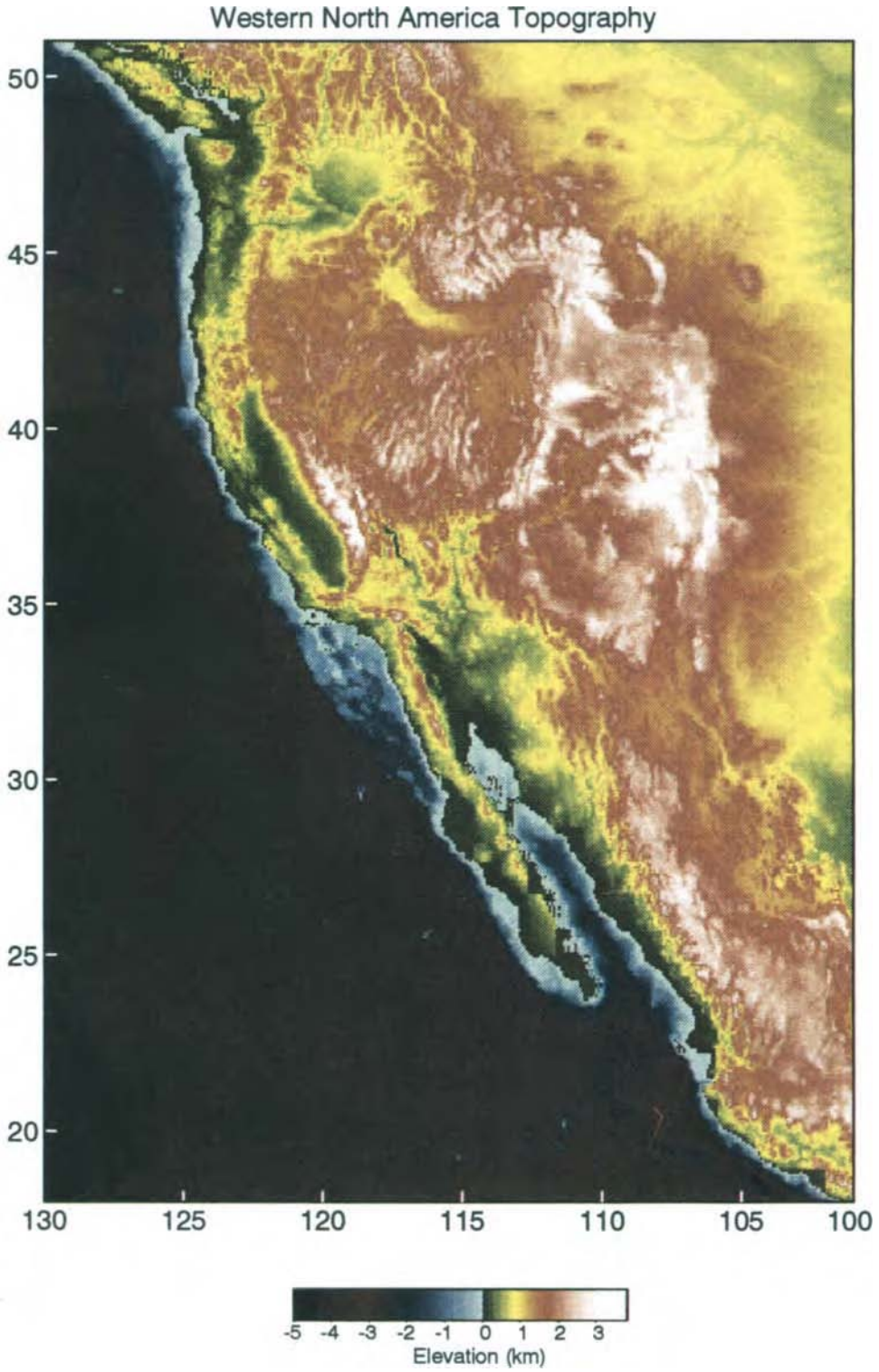

Plate 7–1. Topography of western North America. The northern Basin and Range province is higher on average than the southern Basin and Range, and the topographic boundary is quite distinct (located between the southern ends of the Sierra Nevada and Colorado Plateau).

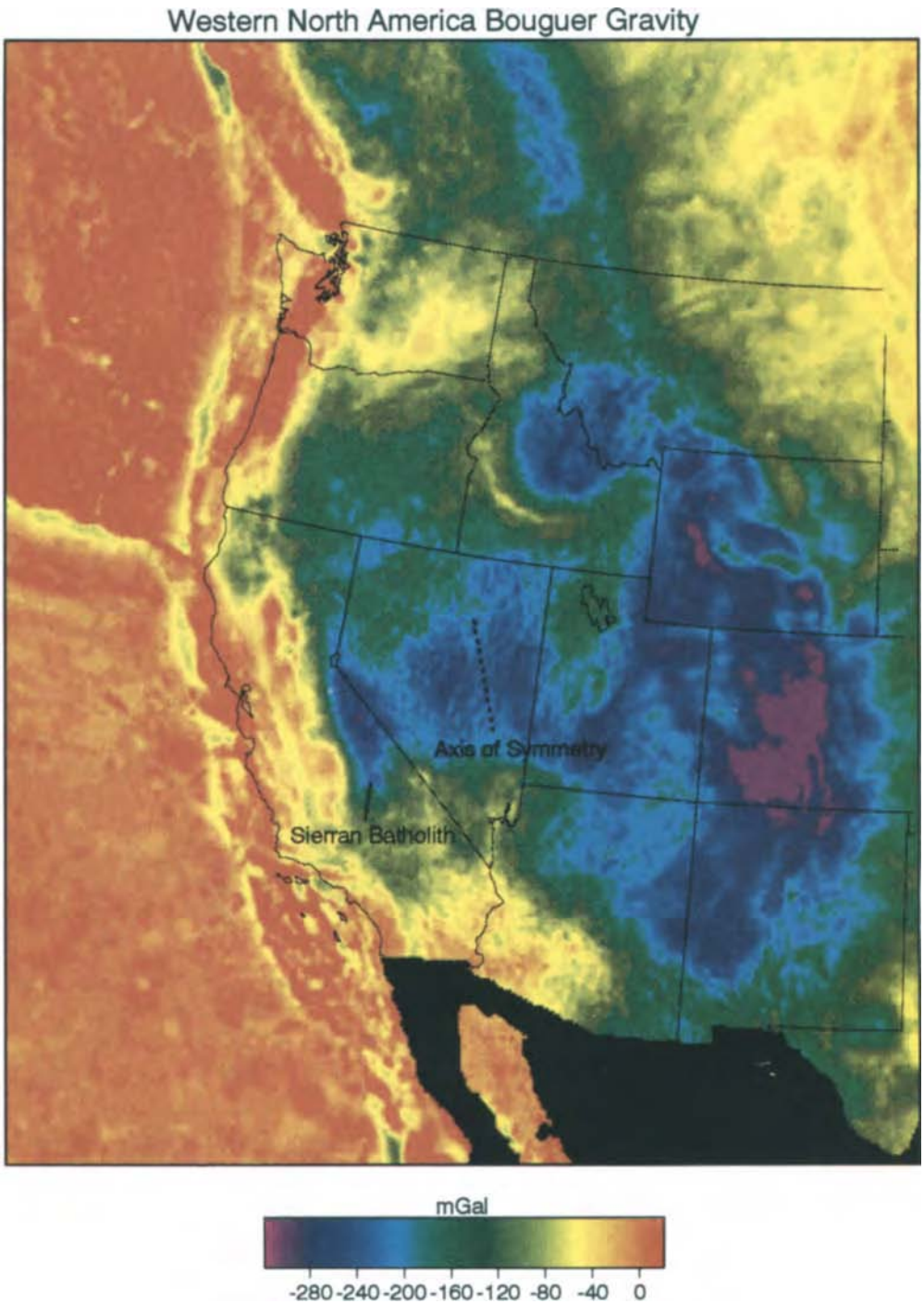

Plate 7–2. Bouguer gravity of western North America. The northern Basin and Range is a symmetric regional gravity low. See text for discussion.

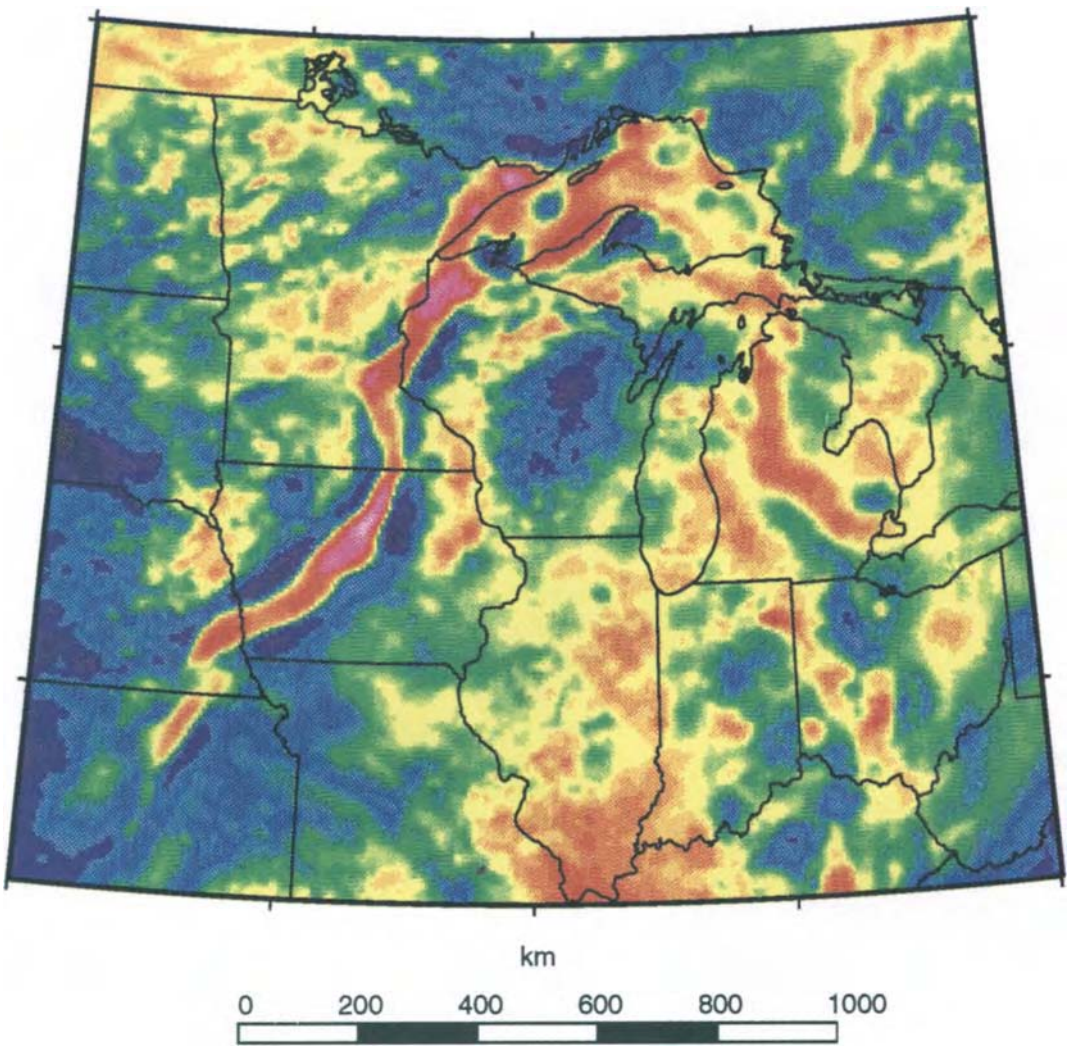

Plate 10–1. Bouguer gravity anomaly map of the midcontinent of North America.

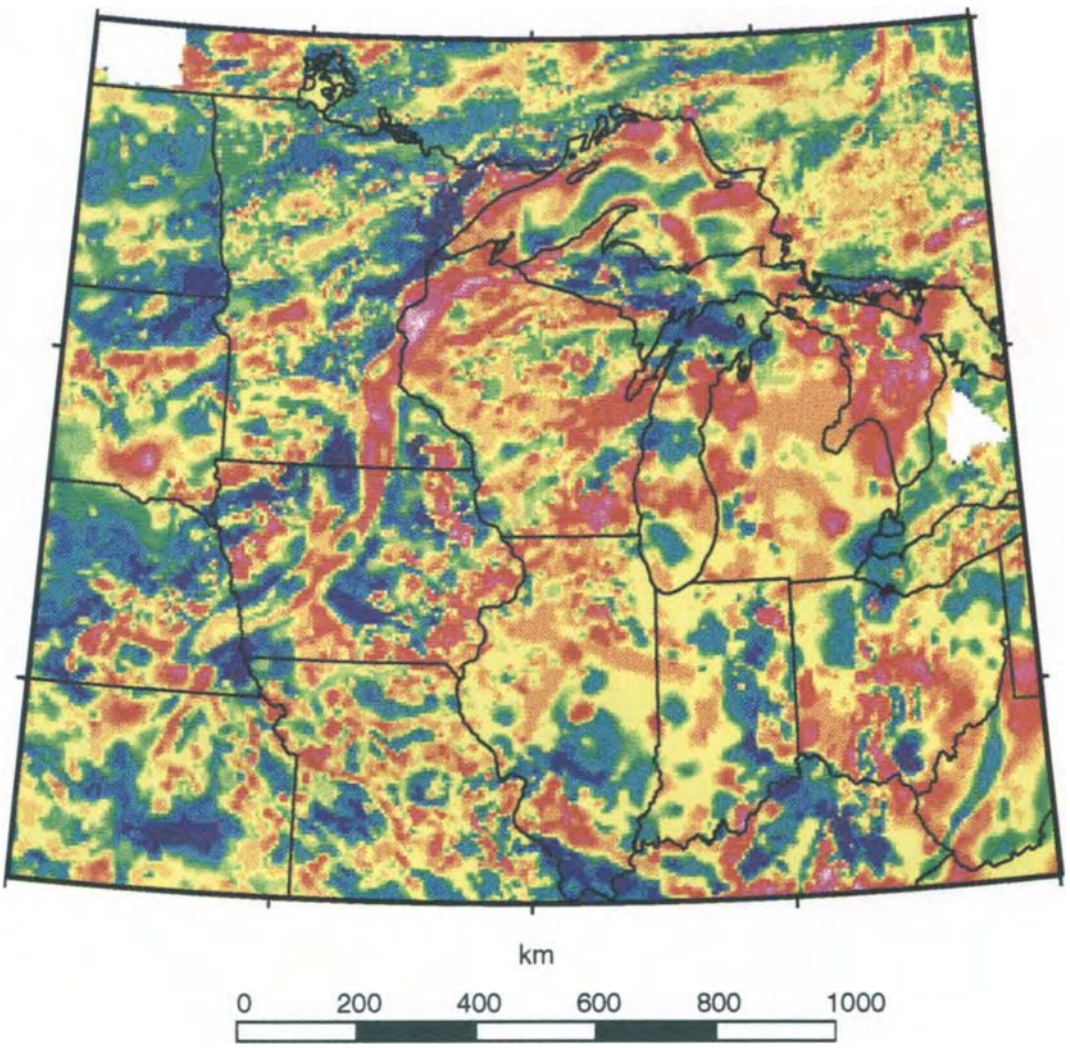

Plate 10–2. Total magnetic intensity anomaly map of the midcontinent of North America.

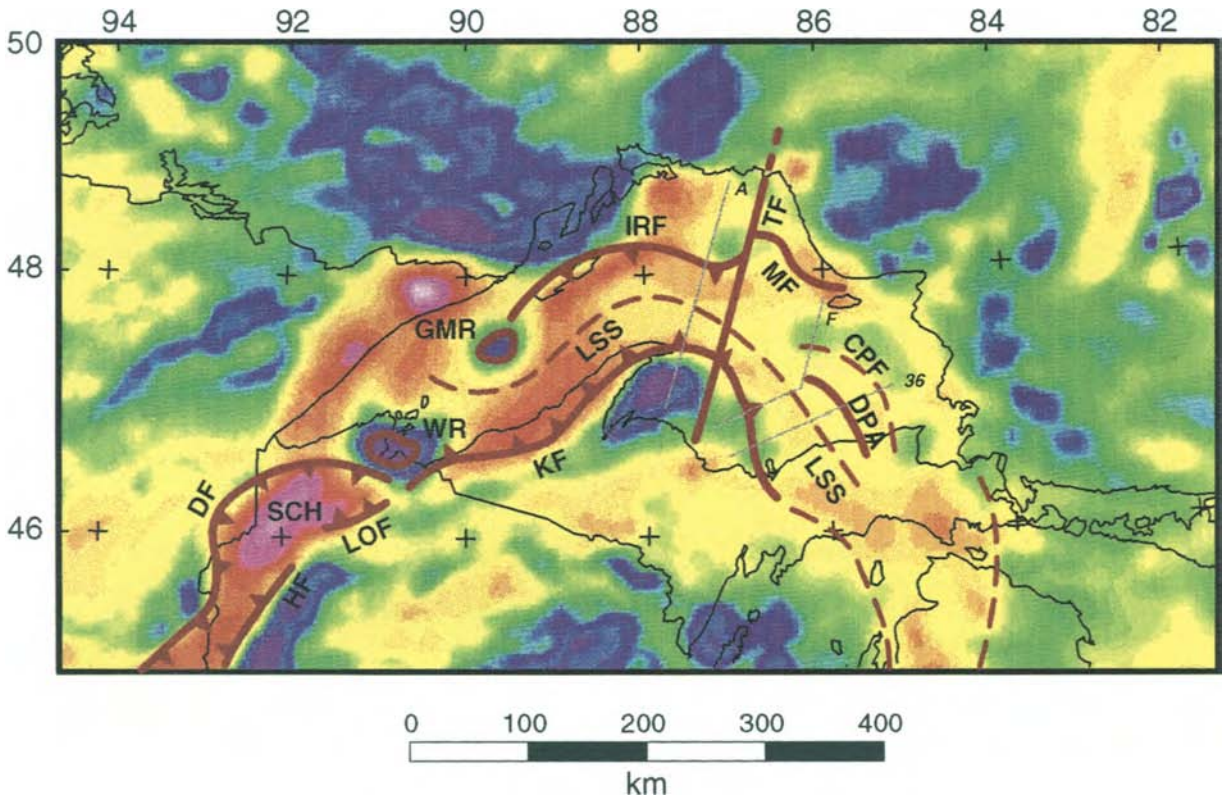

Plate 10–3. Bouguer gravity anomaly map of the Lake Superior region indicating major structural elements. Thin lines are seismic reflection profiles discussed in the text with their designation (e.g., A). LSS – Axis of Lake Superior syncline; SCH – St. Croix horst; WR – White's ridge; GMR – Grand Marais ridge; DPA – Deer Park anticline; DF – Douglas fault; HF – Hastings fault; LOF – Lake Owen fault; KF – Keweenaw fault; IRF – Isle Royale fault; TF – Thiel fault: MF – Michipocoten fault; CPF – Crisp Point fault.

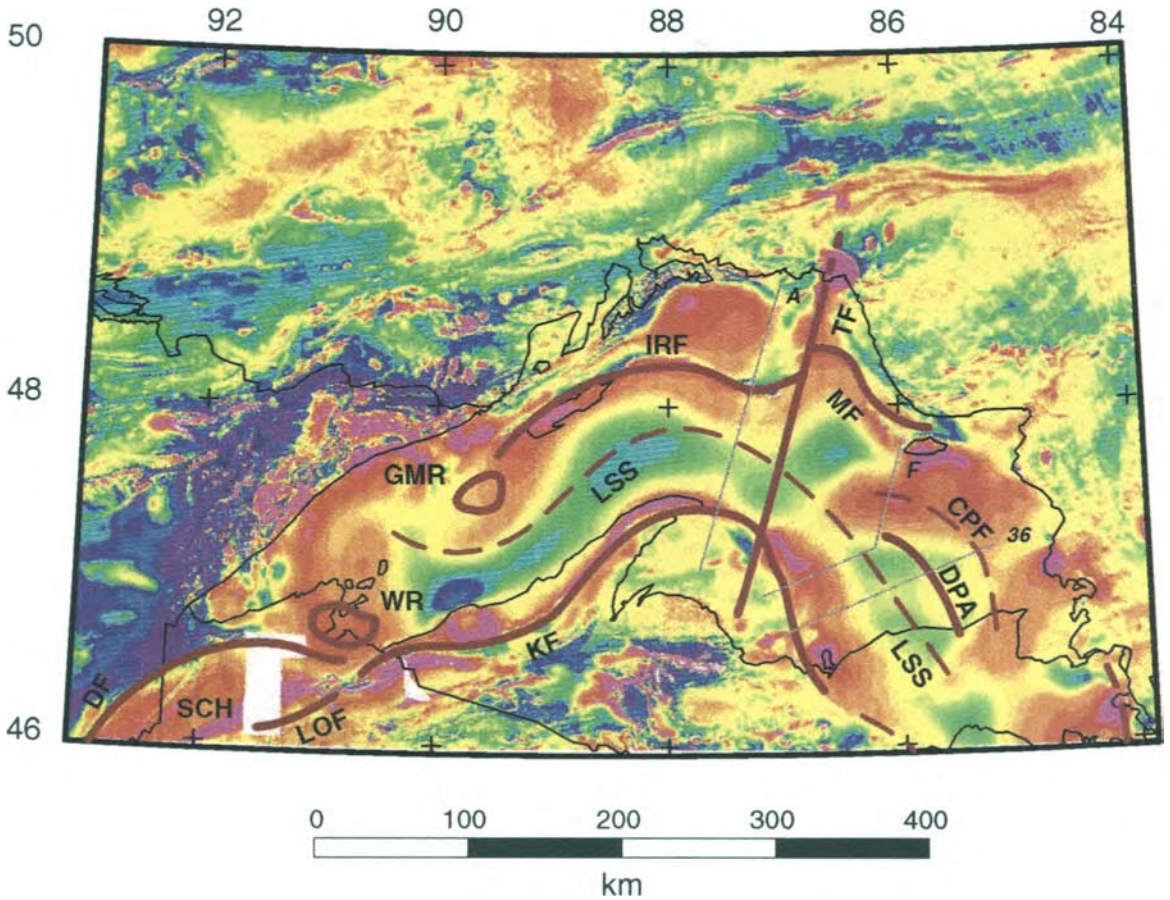

Plate 10–4. Total magnetic intensity anomaly map of the Lake Superior region indicating major structural elements. Thin lines are seismic reflection profiles discussed in the text with their designation (e.g., A). LSS – Axis of Lake Superior syncline; SCH – St. Croix horst; WR – White's ridge; GMR – Grand Marais ridge; DPA – Deer Park anticline; DF – Douglas fault; HF – Hastings fault; LOF – Lake Owen fault; KF – Keweenaw fault; IRF – Isle Royale fault; TF – Thiel fault: MF – Michipocoten fault; CPF – Crisp Point fault.

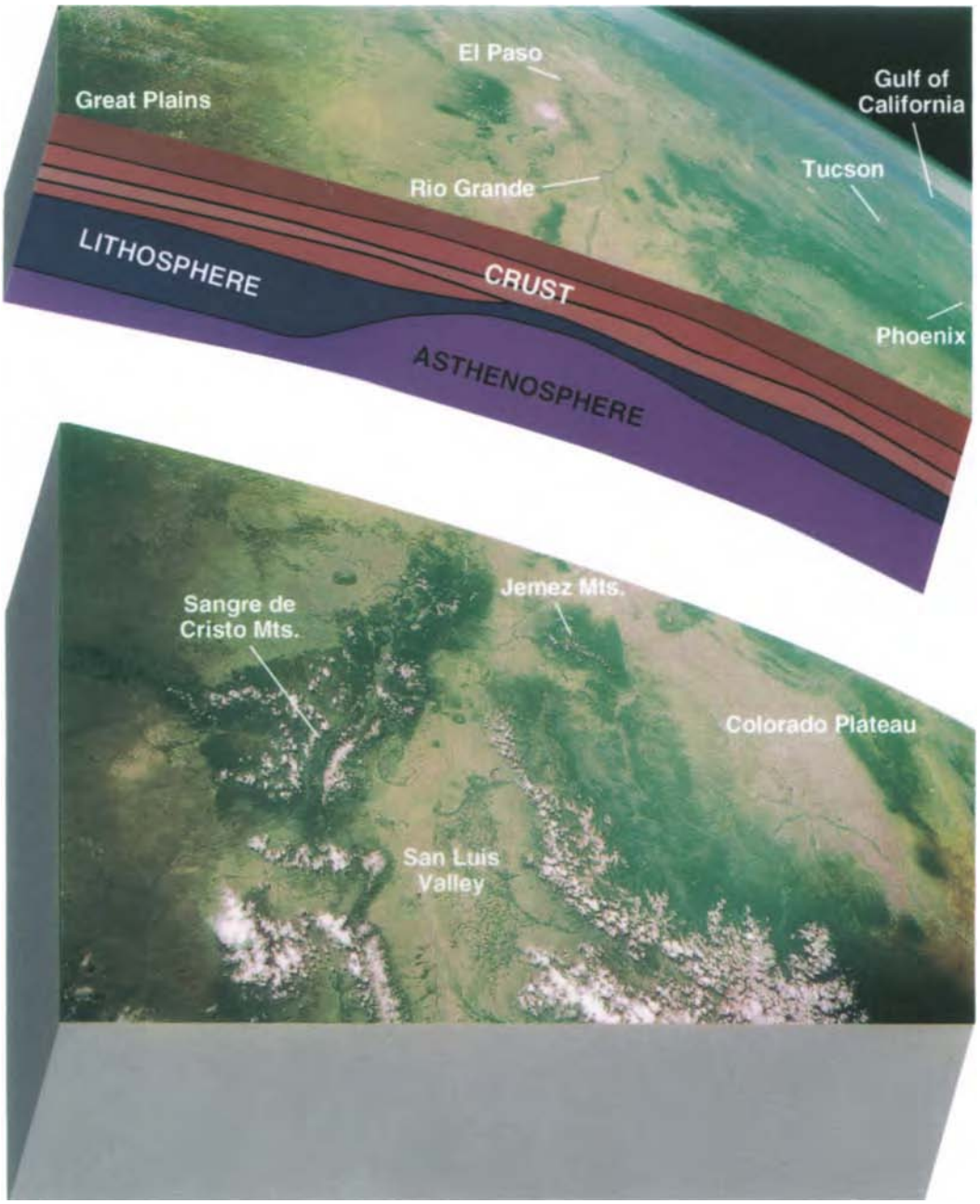

Frontispiece: This spectacular photograph shows a southward view of the Rio Grande rift from the southern San Luis Valley of Colorado to the bolsons of west Texas and Chihuahua (near top), a distance of over 700 km. The Sangre de Christo Mountains, part of the Southern Rocky Mountains, and the Great Plains lie east of the rift. The gypsum dunes of White Sands National Monument are prominent near the middle of the upper (southern) block. The Colorado Plateau lies west of the of the northern and central segments of the rift. Farther south and west, the Basin and Range Province stretches across southern New Mexico, southern Arizona and northern Mexico to the Gulf of California and Baja California, visible near the Earth's limb. The cross section showing crustal layers and upper mantle structure (see color Plate 6–9 of Chapter 6, "The Rio Grande Rift"), is constructed through Albuquerque, New Mexico. At this latitude (35°10'N), the vertical and horizontal scales are approximately the same. For conventional map views of the area see Figure 6–1 and Color Plate 7–1. This photograph is number STS40-151-23, taken with the Linhof camera from the Space Shuttle Columbia on 7 June 1991, at a nominal altitude of 287 km.

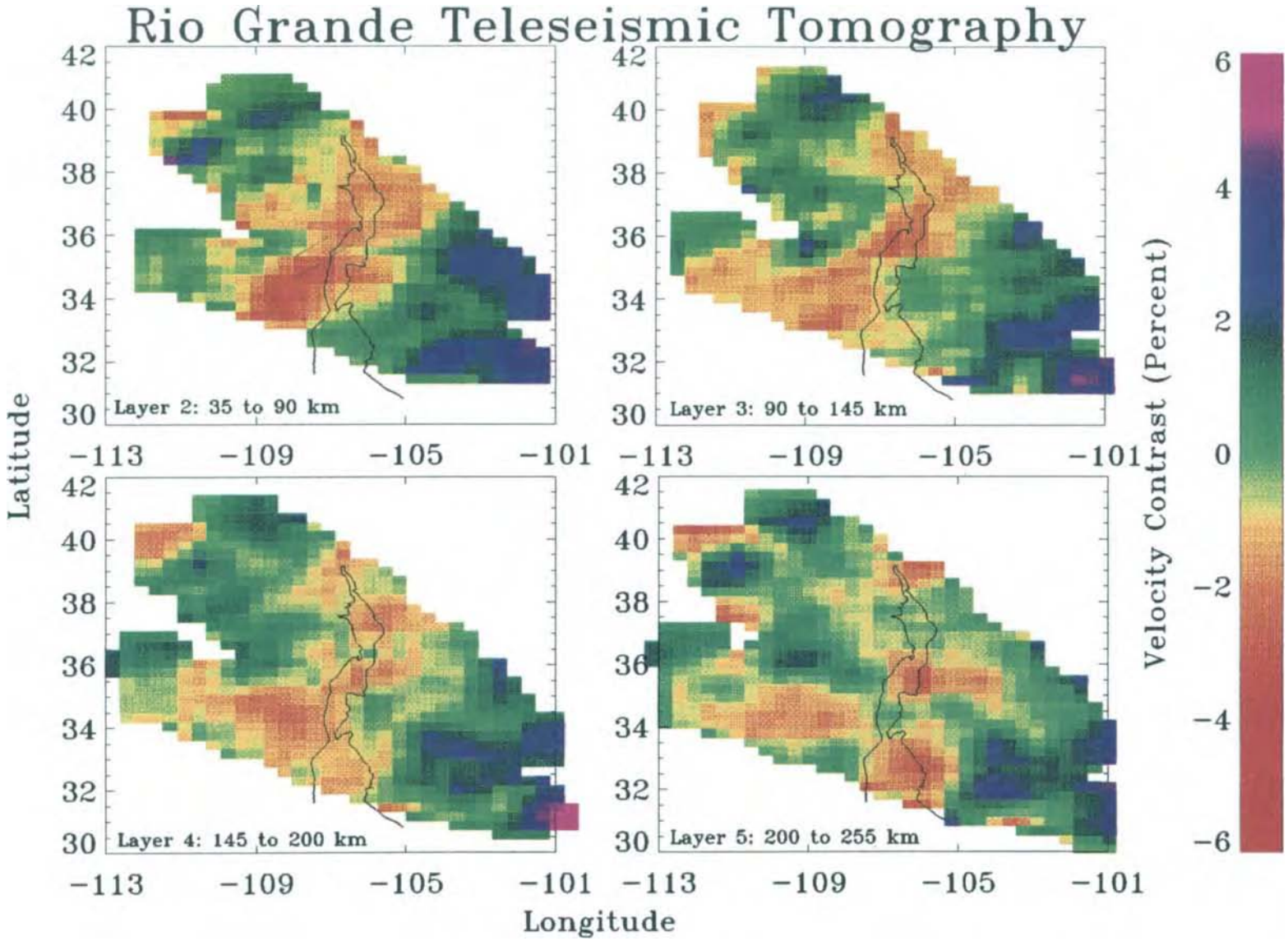

Plate 6–5. Teleseismic P-wave travel-time residuals resolved for four layers beneath the northern and central Rio Grande rift. Inversion is based on the Aki-Christofferson-Husebye method (from Slack, 1994).

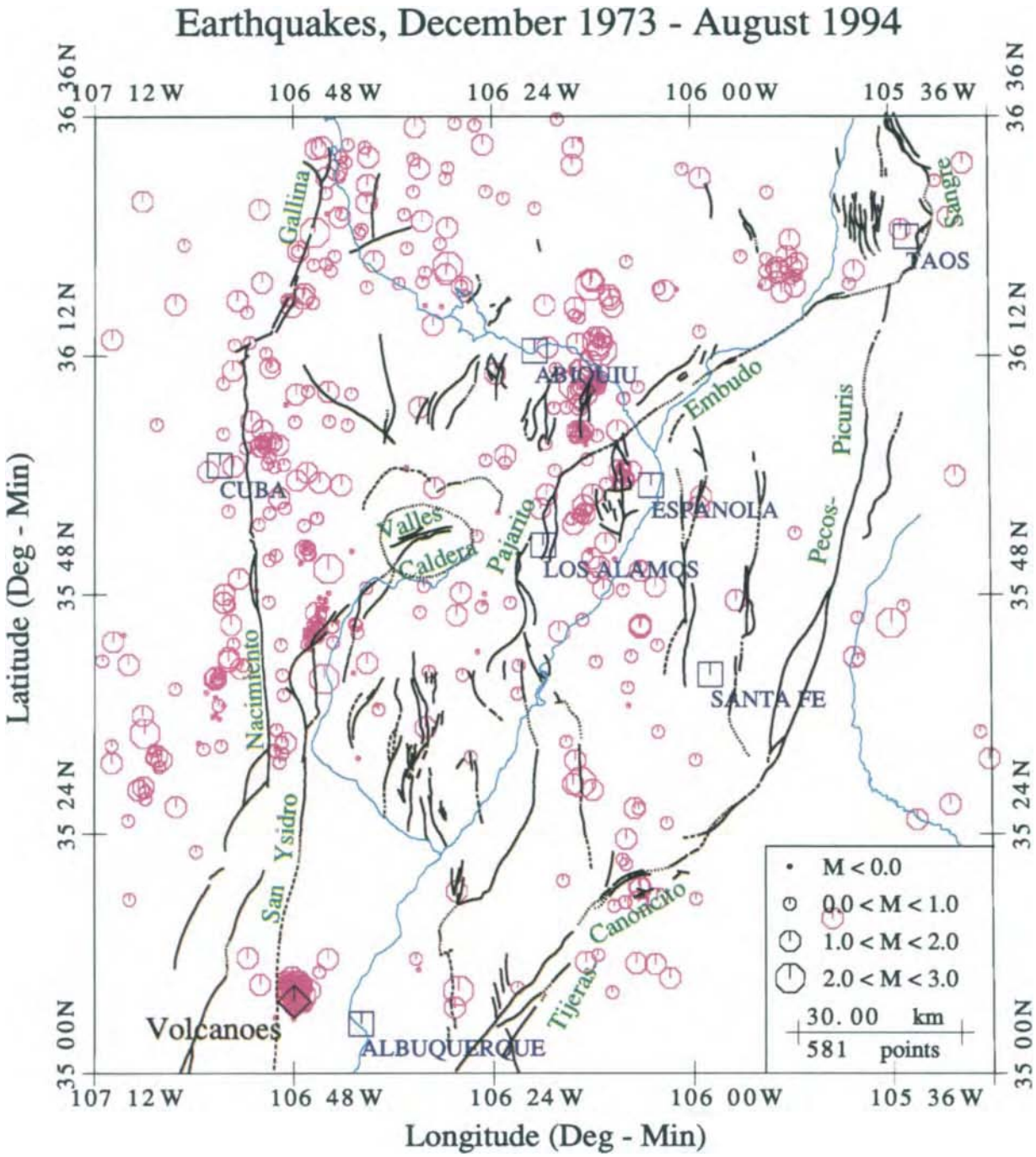

Plate 6–8. Map of relocated earthquake epicenters in the Jemez Mountains–Española basin area for the period December 1973 to August 1994.